CELEBRATING 40 YEARS OF THE CHILEAN SOCIETY OF PHARMACOLOGY

EDITED BY: Gonzalo E. Yevenes, Jorge Fuentealba, Javier A. Bravo, Guillermo Diaz-Araya, Ramón Sotomayor-Zárate, Jenny Lucy Fiedler and Miguel Reyes-Parada

PUBLISHED IN: Frontiers in Pharmacology

frontiers Research Topics

ISSN 1664-8714
ISBN 978-2-88966-398-9
DOI 10.3389/978-2-88966-398-9

About Frontiers

Frontiers is more than just an open-access publisher of scholarly articles: it is a pioneering approach to the world of academia, radically improving the way scholarly research is managed. The grand vision of Frontiers is a world where all people have an equal opportunity to seek, share and generate knowledge. Frontiers provides immediate and permanent online open access to all its publications, but this alone is not enough to realize our grand goals.

Frontiers Journal Series

The Frontiers Journal Series is a multi-tier and interdisciplinary set of open-access, online journals, promising a paradigm shift from the current review, selection and dissemination processes in academic publishing. All Frontiers journals are driven by researchers for researchers; therefore, they constitute a service to the scholarly community. At the same time, the Frontiers Journal Series operates on a revolutionary invention, the tiered publishing system, initially addressing specific communities of scholars, and gradually climbing up to broader public understanding, thus serving the interests of the lay society, too.

Dedication to Quality

Each Frontiers article is a landmark of the highest quality, thanks to genuinely collaborative interactions between authors and review editors, who include some of the world's best academicians. Research must be certified by peers before entering a stream of knowledge that may eventually reach the public - and shape society; therefore, Frontiers only applies the most rigorous and unbiased reviews.
Frontiers revolutionizes research publishing by freely delivering the most outstanding research, evaluated with no bias from both the academic and social point of view. By applying the most advanced information technologies, Frontiers is catapulting scholarly publishing into a new generation.

What are Frontiers Research Topics?

Frontiers Research Topics are very popular trademarks of the Frontiers Journals Series: they are collections of at least ten articles, all centered on a particular subject. With their unique mix of varied contributions from Original Research to Review Articles, Frontiers Research Topics unify the most influential researchers, the latest key findings and historical advances in a hot research area! Find out more on how to host your own Frontiers Research Topic or contribute to one as an author by contacting the Frontiers Editorial Office: researchtopics@frontiersin.org

CELEBRATING 40 YEARS OF THE CHILEAN SOCIETY OF PHARMACOLOGY

Topic Editors:
Gonzalo E. Yevenes, University of Concepcion, Chile
Jorge Fuentealba, University of Concepcion, Chile
Javier A. Bravo, Pontificia Universidad Católica de Valparaíso, Chile
Guillermo Diaz-Araya, University of Chile, Chile
Ramón Sotomayor-Zárate, Universidad de Valparaiso, Chile
Jenny Lucy Fiedler, University of Chile, Chile
Miguel Reyes-Parada, University of Chile, Chile

Citation: Yevenes, G. E., Fuentealba, J., Bravo, J. A., Diaz-Araya, G., Sotomayor-Zárate, R., Fiedler, J. L., Reyes-Parada, M., eds. (2021). Celebrating 40 Years of the Chilean Society of Pharmacology. Lausanne: Frontiers Media SA. doi: 10.3389/978-2-88966-398-9

Table of Contents

frontiers in Pharmacology

EDITORIAL
published: 17 December 2020
doi: 10.3389/fphar.2020.623195

Editorial: Celebrating 40 Years of the Chilean Society of Pharmacology

Gonzalo E. Yévenes[1], Javier A. Bravo[2], Guillermo Díaz-Araya[3], Ramón Sotomayor-Zárate[4], Jenny L. Fiedler[5], Miguel Reyes-Parada[6,7] and Jorge Fuentealba[1]**

[1]Department of Physiology, University of Concepcion, Concepción, Chile, [2]Instituto de Química, Facultad de Ciencias, Pontificia Universidad Católica de Valparaíso, Valparaíso, Chile, [3]Department of Pharmacological and Toxicological Chemistry, Faculty of Chemical and Pharmaceutical Sciences, University of Chile, Santiago, Chile, [4]Centro de Neurobiología y Fisiopatología Integrativa (CENFI), Instituto de Fisiología, Facultad de Ciencias, Universidad de Valparaíso, Valparaíso, Chile, [5]Department of Biochemistry and Molecular Biology, Faculty of Chemistry and Pharmaceutical Sciences, Universidad de Chile, Santiago, Chile, [6]Centro de Investigación Biomédica y Aplicada (CIBAP), Escuela de Medicina, Facultad de Ciencias Médicas, Universidad de Santiago de Chile, Santiago, Chile, [7]Facultad de Ciencias de la Salud, Universidad Autónoma de Chile, Talca, Chile

Keywords: pharmacology, addiction, pain, hypertension, receptor

Editorial on the Research Topic

Celebrating 40 Years of the Chilean Society of Pharmacology

Pharmacology can be defined as the study of the effects of chemical substances on the function of living organisms. Thus, pharmacology is essentially a translational discipline, bridging together biomedical and chemical sciences with the clinical practice. Therefore, the formation and growing of Pharmacological Societies around the world has been, and will continue to be, key in the development of integrated basic, experimental, and clinical sciences.

This Research Topic aimed to celebrate the Chilean Society of Pharmacology (SOFARCHI) 40th anniversary by providing a diverse collection of in-depth reviews and original articles coming from members of our Society and colleagues around the world. SOFARCHI is a non-profit scientific society whose main objective is the promotion of research in pharmacology, from theoretical to experimental, and to clinical points of view. SOFARCHI was founded in 1978 with about 60 members who carried out teaching and research in pharmacology mainly in the central (Santiago and Valparaíso) and in southern zone (Concepción, Valdivia, and Temuco) of Chile. Since 1978, SOFARCHI has held 41 annual congresses and currently has more than 140 members. In addition, SOFARCHI encourages the development and dissemination of pharmacology through promoting research among its members, sponsoring undergraduate and graduate courses, and fostering the creation of teaching books on different pharmacological topics. The Society also actively aids the Institute of Public Health, an agency of the Chilean state, in the technical evaluation of medicines that require sanitary registration. This highlights the commitment of SOFARCHI to promote the proper use of medicines in Chile, making known the main therapeutic and adverse effects of drugs to our fellow citizens. Lastly, the Society has developed a strong outreach program engaging our scientific work to high school students along the country.

Over the last 10 years SOFARCHI has experienced important growth. The annual congress, our main yearly scientific activity, brings together more than 250 attendees, where about 70% of them are undergraduate and graduate students. Thus, SOFARCHI as a young society is always poised to contribute to Chile's scientific and technological development, but also ready to collaborate with other partners in Latin America, and the world. Therefore, we believe that this research topic brings together many of the main lines of research carried out by Chilean pharmacologists. We are grateful to the Frontiers in Pharmacology Editorial team and many international experts from the field of

OPEN ACCESS

Edited and reviewed by:
Alastair George Stewart,
The University of Melbourne, Australia

****Correspondence:***
Jorge Fuentealba
jorgefuentealba@udec.cl
Gonzalo E. Yévenes
gyevenes@udec.cl

Specialty section:
This article was submitted to Translational Pharmacology, a section of the journal Frontiers in Pharmacology

Received: *29 October 2020*
Accepted: *09 November 2020*
Published: *17 December 2020*

Citation:
Yévenes GE, Bravo JA, Díaz-Araya G, Sotomayor-Zárate R, Fiedler JL, Reyes-Parada M and Fuentealba J (2020) Editorial: Celebrating 40 Years of the Chilean Society of Pharmacology. Front. Pharmacol. 11:623195. doi: 10.3389/fphar.2020.623195

pharmacology who have been able to support the research topic with their expertise, serving as editors and reviewers.

We are glad that our topic generated an important global impact, reaching more than 50,000 article views and more than 12,000 downloads. The articles published in our research topic include reviews, mini-reviews, perspectives, brief research reports and original research articles. Our topic is grateful to the 240 authors that made their scientific contributions by submitting work of excellence to the Topic.

We would like to first highlight the broad thematic spectrum of the reviews and mini-reviews published in the issue, covering from molecular and cellular to pre-clinical and clinical pharmacology. This group of articles includes in-depth reviews on the contribution of the kappa opioid system to dopamine-related compulsive behaviors (Escobar et al.), on the chemical properties of amphetamine analogs with activity as monoamine oxidase inhibitors (Reyes-Parada et al.), on the contribution and relevance of P_2X receptors in Alzheimer disease and in the toxicity of soluble Aβ peptide oligomers (Godoy et al.) and on novel strategies and perspectives for the treatment of dental pulp-derived pain (Schuh et al.). This group of contributions also included a detailed clinically-oriented review provided by Castillo et al., which summarizes the clinical experience of Chilean pharmacologists who have worked for more than 10 years with dexmedetomidine, a highly selective α2-adrenergic agonist with sedative and analgesic properties, with minimal respiratory effects. On the other hand, the Topic incorporated self-sustained minireviews summarizing and discussing the relevance of benzofurans as potential chemical scaffolds against Alzheimer disease (Cabrera-Pardo et al.), the effects of vitamin C on cancer cells and its therapeutic potential in cancer (Roa et al.), novel drugs targeting pentameric ligand-gated ion channels as potential novel analgesics (Lara et al.), the neurobiological basis of obsessive compulsive disorder (OCD) with focus on glutamate transporter 3 (EAAT3) (Escobar et al.), recent advances on therapies against non-infectious uveitis (Valenzuela et al.) and the beneficial effects of the mifepristone in metabolic syndromes (Diaz-Castro et al.).

The Topic also achieved to gather a significant number of brief research reports and original research articles of a wide thematic diversity. Aspects of molecular and cellular pharmacology on physiological and pathological states of different systems were covered by original articles offering new findings. At the drug-receptor level, Yarur et al. showed that type-2 β-corticotrophin releasing factor receptor forms a stable heteromeric protein complex with type-1 dopamine receptor, offering a new potential therapeutic target in tissues where both receptors are co-expressed, while San Martin et al., described the functional actions of serotonin type-3 receptor antagonists on glycine receptors associated with pain control. New studies focused on molecular and cellular neuropharmacology were also tackled. In the context of Alzheimer disease, Panes et al., demonstrated that soluble oligomers of Aβ peptide alter key proteins of mitochondrial dynamics and biogenesis in hippocampal neurons, contributing to neuronal dysfunction and death. In terms of potential side-effects of common drugs at the cellular level, Ampuero et al. showed that chronic administration of the fluoxetine reduces dendritic arborization in cortical and limbic areas of the rat brain, suggesting that the permanent SSRI consumption can go beyond the expected antidepressant effects. Furthermore, lines of research focused on cardiovascular and renal pharmacology also contributed to the topic by studying aspects of IFN-β and pro-renin signaling. In this context, Bolivar et al., showed that IFN-β exerts both pro-inflammatory and anti-inflammatory effects on non-stimulated rat cardiac fibroblasts through differential activation of STAT proteins, establishing a new framework for the complex effects of IFN-β on cells of the cardiovascular system, while Reyes-Martinez et al., showed that the pharmacological inhibition of COX-2 in the collecting duct cells might prevent tubular damage after the activation of the intratubular renin–angiotensin system, which may contribute to control renal failure in hypertension and diabetes.

Other original contributions to our topic covered relevant issues with impact on human health, such as chronic pain, cancer, addiction, hypertension, and chronic kidney disease. Regarding neural mechanisms underlying chronic pain, Retamal et al. presented original research showing that central sensitization in rat spinal cord occurs through BDNF release and an increased expression of glial BDNF and pTrkB. In terms of potential novel therapies and strategies against chronic pain, Garrido-Suárez et al. show that mangiferin, a glucosylxanthone broadly distributed in higher plants such as *Mangifera indica L.*, has an anti-allodynic effect in a model of chronic post-ischemia pain, while Gonzalez et al., have shown that the antinociceptive efficacy of the common opioid drug, methadone, is potentiated by the co-application of magnesium salts in the spared nerve injury mouse model of chronic pain. In the field of cancer research, two groups of researchers provide new insights. Using biopsies of gastric cancer, Hevia et al. have shown that several types of purinergic receptors, such as P_2Y_2R and P_2X_4R, are involved in gastric cancer. Interestingly, the authors found a correlation between the expression levels of specific purinergic receptors and the survival rates of patients. In parallel, Lavanderos et al., provide pharmacogenetic evidence as a potential tool to predict adverse drug reactions in Chilean patients diagnosed with testicular cancer. In another study, Robles-Planells et al., demonstrated that the organic extract of *Lithraea caustic*, an endemic stinging plant of central Chile, decreases melanoma tumor growth in a murine model. In addition, other scientific contributions have focused attention on addiction. Velasquez et al., demonstrated that a neonatal programming with estradiol enhances the pharmacological effects produced by morphine in rats, suggesting that early exposure to sex hormones may contribute to opioid addiction in adulthood; on the other hand, Quiroz et al., have shown that a competitive nAChR antagonist (UFR2709) significantly reduced the ethanol consumption of alcohol-preferring rats. Finally, and related to human hypertension, Gonzalez et al., elucidated a biochemical pathway which could underlie the antihypertensive effect of dietary potassium (K^+) observed in human studies. Interestingly, many of the blood pressure lowering actions of K^+ were seen in both hypertensive and normotensive rats, supporting a beneficial effect of dietary potassium in health and disease. Similarly, Vio et al., showed that a chronic high potassium diet down regulates key components of intratubular

renin-angiotensin system. This down regulation could be a novel mechanism involved in the potassium-induced natriuresis that is beneficial for blood pressure and cardiovascular health. In the same field, Mondaca-Ruff et al., demonstrated a relationship between autophagy, the AT1R/RhoA/Rho Kinase-dependent pathway and Ang II-induced hypertrophy of vascular smooth muscle cells. Last, but not least, Figueroa et al., demonstrated that the pro-inflammatory phase of unilateral ureteral obstruction, a model of Chronic Kidney Disease, involves tubular damage with cortical upregulation of juxtaglomerular renin and medullary (pro)renin receptor downregulation. This scenario suggests a differential iRAS modulation as part of the mechanisms involved in the early stages of chronic kidney disease.

The thematic diversity of our topic also includes articles focused on developmental aspects and on medicinal chemistry. The original research contributed by De La Fuente-Ortega et al., demonstrated that prenatal ethanol exposure affects iron homeostasis of specific brain areas (i.e., PFC and hippocampus), suggesting a critical role of iron homeostasis in maladaptive cognition observed in fetal alcohol spectrum disorder. In addition, Benavides-Rivas et al., described the role of enzymatic glutamate synthesis in the neurulation process using *Xenopus oocytes*. Finally, original research article of Sáez-Briones et al., studied the novel compound 2-Br-4,5-MDMA, a MDMA (3,4-methylenedioxy-methamphetamine, "Ecstasy") analog brominated at C(2) of the aromatic ring. Interestingly, 2-Br-4,5-MDMA maintains the effects of MDMA as a substrate of the serotonin transporter (SERT). However, the bromination of MDMA modified the expected behavioral responses in rats, showing an absence of the classical MDMA-elicited behavioral responses including hyperlocomotion, enhanced active avoidance conditioning responses and increased social interaction.

In conclusion, we believe that the diversity of articles incorporated in our Research Topic reflects the integrative spirit of our scientific society and the translational character of the pharmacological sciences. In addition, we think that the new findings published show the growing quality of the Chilean science and highlight the rising contribution of our scientists to the global knowledge. We look forward to celebrate many years more of the SOFARCHI.

AUTHOR CONTRIBUTIONS

All the authors have equally contributed to the work. The authors reviewed and approved the text for publication.

ACKNOWLEDGMENTS

We would like to thank all authors and reviewers for their valuable contribution. Also, we would like to acknowledge the support of FONDECYT 1170252, 1170425, 1200474, 1200908, 1170662 and 1190729.

Conflict of Interest: The authors declare that the research was conducted in the absence of any commercial or financial relationships that could be construed as a potential conflict of interest.

frontiers in Pharmacology

ORIGINAL RESEARCH
published: 02 October 2018
doi: 10.3389/fphar.2018.01119

Anti-allodynic Effect of Mangiferin in Rats With Chronic Post-ischemia Pain: A Model of Complex Regional Pain Syndrome Type I

Bárbara B. Garrido-Suárez[1], Gabino Garrido[2], Marian Castro-Labrada[1], Zenia Pardo-Ruíz[1], Addis Bellma Menéndez[1], Evelyn Spencer[1], Jozi Godoy-Figueiredo[3], Sergio H. Ferreira[3] and René Delgado-Hernández[4]*

[1] *Laboratorio de Farmacología y Toxicología, Centro de Investigación y Desarrollo de Medicamentos, Havana, Cuba,* [2] *Departamento de Ciencias Farmacéuticas, Facultad de Ciencias, Universidad Católica del Norte, Antofagasta, Chile,* [3] *Department of Pharmacology, Faculty of Medicine of Ribeirão Preto, University of São Paulo, São Paulo, Brazil,* [4] *Centro de Estudio para las Investigaciones y Evaluaciones Biológicas, Instituto de Farmacia y Alimentos, Universidad de La Habana, Havana, Cuba*

OPEN ACCESS

Edited by:
Ramón Sotomayor-Zárate, Universidad de Valparaíso, Chile

Reviewed by:
Gonzalo E. Yevenes, Universidad de Concepción, Chile
Luis Constandil, Universidad de Santiago de Chile, Chile
Edgar Pastene, Universidad de Concepción, Chile

***Correspondence:**
Gabino Garrido
gabino.garrido@gmail.com

Specialty section:
This article was submitted to Neuropharmacology, a section of the journal Frontiers in Pharmacology

Received: *09 June 2018*
Accepted: *13 September 2018*
Published: *02 October 2018*

Citation:
Garrido-Suárez BB, Garrido G, Castro-Labrada M, Pardo-Ruíz Z, Bellma Menéndez A, Spencer E, Godoy-Figueiredo J, Ferreira SH and Delgado-Hernández R (2018) Anti-allodynic Effect of Mangiferin in Rats With Chronic Post-ischemia Pain: A Model of Complex Regional Pain Syndrome Type I. Front. Pharmacol. 9:1119. doi: 10.3389/fphar.2018.01119

The present study reproduces chronic post-ischemia pain (CPIP), a model of complex regional pain syndrome type I (CRPS-I), in rats to examine the possible transient and long-term anti-allodynic effect of mangiferin (MG); as well as its potential beneficial interactions with some standard analgesic drugs and sympathetic-mediated vasoconstriction and vasodilator agents during the earlier stage of the pathology. A single dose of MG (50 and 100 mg/kg, p.o.) decreased mechanical allodynia 72 h post-ischemia-reperfusion (I/R). MG 100 mg/kg, i.p. (pre- vs. post-drug) increased von Frey thresholds in a yohimbine and naloxone-sensitive manner. Sub-effective doses of morphine, amitriptyline, prazosin, clonidine and a NO donor, SIN-1, in the presence of MG were found to be significantly anti-allodynic. A long-term anti-allodynic effect at 7 and 13 days post-I/R after repeated oral doses of MG (50 and 100 mg/kg) was also observed. Further, MG decreased spinal and muscle interleukin-1β concentration and restored muscle redox status. These results indicate that MG has a transient and long-term anti-allodynic effect in CPIP rats that appears to be at least partially attributable to the opioid and α_2 adrenergic receptors. Additionally, its anti-inflammatory and antioxidant mechanisms could also be implicated in this effect. The association of MG with sub-effective doses of these drugs enhances the anti-allodynic effect; however, an isobolographic analysis should be performed to define a functional interaction between them. These findings suggest the possible clinical use of MG in the treatment of CRPS-I in both early sympathetically maintained pain and long-term sympathetically independent pain.

Keywords: adrenergic receptor, chronic post-ischemia pain, complex regional pain syndrome, mangiferin, sympathetically maintained pain

Abbreviations: CPIP, chronic post-ischemia pain; CG, carbonyl protein groups concentration; GHS, reduced glutathione; HPLC, high-performance liquid chromatography; IL-1β, interleukin 1 *beta*; MDA, malondialdehyde; MG, mangiferin; NF-κB, transcription nuclear factor *kappa* B; NMDA, *N*-methyl-D-aspartate; NO, nitric oxide; Pr, protein; ROS, reactive oxygen species; SOD, superoxide dismutase; TNFα, tumor necrosis factor *alpha*.

INTRODUCTION

Complex regional pain syndrome (CRPS) is a disabling condition most often presenting after trauma affecting the distal part of an extremity. It is characterized by a continuing pain, which is disproportionate to the inciting event, in addition to sensory, autonomic, motor, and trophic disturbances (Bruehl et al., 2002; Beerthuizen et al., 2012). In the clinical setting, it is broadly accepted that the trauma-related differentiation of CRPS is by the absence (CRPS-I) and presence (CRPS-II) of evident nerve lesions. However, a more comprehensive pathophysiology-based classification regarding peripheral inflammatory and central neuroplasticity phenotypes has been proposed (Birklein and Schlereth, 2015). Particularly, the sympathetic activity would be contributory rather than causative and exacerbate ischemia, inflammation, and consequent pain in early-stage disease (Bonica, 1990; Coderre and Bennett, 2010). After trauma, nociceptors in the affected limb become sensitive to catecholamines. Direct or indirect coupling between the efferent sympathetic systems and the afferent systems may lead to sympathetic-maintained pain (SMP). Noradrenaline (NA) released by the sympathetic postganglionic neuron (SPGN) or adrenaline via the circulation are implicated in SMP. Which by means of G protein-coupled receptors (GPCRs) α- and β-adrenoceptors subtypes via distinct signaling pathways modifies the activity of ion channels and Ca^{2+} influx (Pertovaara, 2013). Hypothetical interactions between sympathetic noradrenergic nerve fibers, peptidergic afferent nerve fibers, blood vessels, and immune cells leading to vasoconstriction, further release of cytokines and sensitization, have been suggested. This, in turn, would amplify nociceptive impulse transmission in the spinal cord in CRPS-I patients (Jäning and Baron, 2003). The exaggerated inflammatory response to tissue injury has been suggested to be involved in the origin and maintenance of CRPS-I, since an imbalance between pro-inflammatory with respect to anti-inflammatory cytokine concentrations, elevated activity of mast cells, neurogenic inflammatory reactions, and markers of oxidative stress were found (Huygen et al., 2004; Alexander et al., 2005, 2007; Üçeyler et al., 2007; Birklein and Schmelz, 2008; Eisenberg et al., 2008). Subsequently, the anti-inflammatory treatment of CRPS-I patients may be beneficial and today is a novel tendency that must be investigated (Fischer et al., 2010). Many of the presumably sympathetic symptoms can be explained through inflammation. It has been suggested that the traditionally used sympathetic blocks should be an exception, rather than a rule for CRPS treatment (Birklein and Schlereth, 2015). In view of the positive results in clinical trials for both the ROS scavengers and corticosteroids, studies combining them are recommended (Zollinger et al., 1999; Pérez et al., 2003; Bianchi et al., 2006).

Chronic post-ischemia pain (CPIP) is a recognized model of CRPS-I, which reproduces peripheral pathophysiology after ischemia/reperfusion (I/R) of the hind paw of rodents (Coderre et al., 2004). After reperfusion, animals develop hyperemia and edema for only a few hours; however, the behaviors of spontaneous pain, long-term mechanical and cold hyperalgesia, which spreads to the uninjured contralateral hind paw are significant (Coderre et al., 2004). CPIP rats show a pharmacological profile similar to CRPS patients, which is refractory to most standard analgesic treatments, as well as nociceptive and vascular hypersensitivity to norepinephrine inhibited by anti-sympathetic treatments (Millecamps and Coderre, 2008; Xanthos and Coderre, 2008; Xanthos et al., 2008). In addition, several antioxidants show a long-term anti-allodynic effect in CPIP rats (Kwak et al., 2011; Schiller et al., 2015; Kim et al., 2017; Yeo et al., 2017). I/R leads to the massive appearance of ROS and pro-inflammatory cytokines, which induce microvascular spasms and capillary dysfunction (Coderre and Bennett, 2010). The underlying sex differences in inflammation and oxidative stress which are regulated by estrogens, as well as its impact I/R-evoked mechanical allodynia in CPIP has been reported (Tang et al., 2017). In particular, the NF-κB pathway which induces the transcription of genes implicated in the expression of proteins involved in inflammation, oxidative stress, synaptic plasticity, and neuron–glial interactions is also involved in the development of mechanical allodynia in a CPIP model (de Mos et al., 2009).

Mangiferin (MG) is a glucosylxanthone broadly distributed in higher plants such as *Mangifera indica* L. (Núñez-Sellés et al., 2002). Previous studies have documented the anti-inflammatory and antioxidant properties of MG (Garrido et al., 2004; Pardo-Andreu et al., 2008; Das et al., 2012) without toxic effects (Prado et al., 2015). Furthermore, we proposed its possible value to be investigated in neuropathic pain and CRPS (Garrido-Suárez et al., 2010), since neuroimmune activation and nitroxidative stress are recognized as new targets for its therapeutic intervention (De Leo et al., 2006; Üçeyler et al., 2007; Eisenberg et al., 2008; Salvemini et al., 2011). Additionally, its capacity to modulate endothelial dysfunction is an attractive attribute to the treatment of both early and late stages of CRPS (Song et al., 2015). Most of the biological activities of this compound are explained, at least in part, by inhibition of NF-κB pathway activation (Leiro et al., 2004). MG also shows the ability to decrease mast cell activity related to its anti-allergic properties, as well as neuroprotective and immunomodulatory effects (García et al., 2002; García-Rivera et al., 2006; Campos-Esparza et al., 2009; Pardo-Andreu et al., 2010). Concerning the analgesic profile of MG studied in acute inflammatory pain models, the participation of the endogenous opioid system and adenosine in its anti-nociceptive activity has been accepted (Dar et al., 2005; Lopes et al., 2013). This effect at the peripheral site involves the activation of δ, κ, and probably μ opioid receptors, as well as the L-arginine-nitric oxide (NO)-cGMP ATP-sensitive K^+ channel pathway (Izquierdo et al., 2013). Moreover, a transient activity of MG on nociceptive pathways mediated by α_2 adrenergic receptors in cooperation with the opioid system has also been reported (Garrido-Suárez et al., 2014). On the other hand, MG decreased mechano-hypernociception and allodynia in traumatic models of neuropathic pain, also considered as CRPS type II models (Garrido-Suárez et al., 2014; de los Monteros-Zuñiga et al., 2016). Likewise, some preliminary results in clinical CRPS case series treated with *M. indica* extract formulations show an improvement of average pain scores and sensory abnormalities (Garrido-Suárez et al., 2009). These facts make this molecule

an attractive multi-target compound with the potentiality to be introduced in CRPS treatment. Then, the aim of the present study was to evaluate the anti-allodynic effect of MG in the early and late stages of CPIP to clarify some underlying pharmacological mechanisms, as well as its potential beneficial interactions with other drugs with clinical relevance on abnormal pain sensations during the earlier stage of the pathology.

MATERIALS AND METHODS

Drugs and Chemicals

Mangiferin (2-β-D-glucopyranosyl-1,3,6,7-tetrahydroxy-9H-xanthen-9-one) was supplied by the Laboratory of Analytical Chemistry, Center of Pharmaceutical Chemistry (Cuba). It was isolated from the *M. indica* stem bark standardized extract by extraction with methanol yielding a yellow powder with 93.82 ± 3.35% purity as determined by liquid chromatographic methods, UV/VIS spectrophotometry and IR, NMR spectroscopic methods and capillary electrophoresis method (Núñez-Sellés et al., 2002). The remaining percentage has been shown to contain a mixture of an isomer, iso-MG (4-C-b-D-glucopyranosyl-1,3,6,7-tetrahydroxyxanthone), and MG monomethyl ether, homo-MG (2-C-b-D-glucopyranosyl-3-methoxy-1,6,7-trihydroxyxanthone) (Núñez Sellés et al., 2016). MG was suspended in DMSO (5% in saline solution) and carboxymethyl cellulose (CMC) 0.05% for intraperitoneal and oral administration, respectively. The solution DMSO + saline has no effects on nociception (Colucci et al., 2008).

Drugs as naloxone hydrochloride, morphine hydrochloride, prazosin hydrochloride, clonidine hydrochloride, yohimbine hydrochloride, 3-morpholinylsydnoneimine chloride (SIN-1), and amitriptyline were purchased from Sigma Chemical Co. (St. Louis, MO, United States). All these compounds were dissolved in saline 0.9%.

Superoxide dismutase was obtained from Randox Labs (Crumlin, United Kingdom), antibodies against rat interleukin-1β (IL-1β) from R&D Systems, Inc. (Minneapolis, MN, United States), Ellman's reagent [5,5'-dithiobis(2-nitrobenzoic acid)], bovine serum albumin (BSA), glutathione, and malondialdehyde bis(dimethyl acetal) from Sigma Chemical Co. (St. Louis, MO, United States), LPO-586 kit from Calbiochem (La Jolla, CA, United States), and nitrate reductase from Boehringer Mannheim (Milan, Italy). All other reagents were of analytical grade.

Experimental Animals

Experimental procedures were carried out in accordance with European regulations on animal protection (Directive 86/609), the Declaration of Helsinki, and the Guide for the Care and Use of Laboratory Animals as adopted and promulgated by the US National Institutes of Health (NIH Publication No. 85–23, revised 1996). All experimental protocols were approved by the Institutional Animal Care and Ethical Committee of the Center for Drugs Research and Development (CIDEM/SP00511). Male Sprague-Dawley (8–10 weeks) rats weighing 200–250 g were obtained from the Center for Experimental Animals Production (CENPALAB, La Habana, Cuba). They were kept in controlled conditions (22 ± 0.5°C, relative humidity 40–60%, a 7 a.m. to 7 p.m. alternate light-dark cycle, food, and water *ad libitum*). The experiments took place during the light period and animals belonging to the various treatment groups (n = 6–7 for each group) were tested in randomized order.

Animal Model of Complex Regional Pain Syndrome Type I (CRPS-I)

Chronic post-ischemia pain was induced by ischemia and reperfusion injury of the left hind paw (Coderre et al., 2004). Briefly, animals were anesthetized over a 3-h period with a bolus (55 mg/kg, i.p.) and chronic i.p. infusion of sodium pentobarbital for 2 h (27.5 mg/kg/h). After induction of anesthesia, a Nitrile 70 Durometer O-ring (O-rings West, Seattle, WA, United States) with a 5.5 mm internal diameter was placed around the rat's left ankle joint. After 3 h the O-ring was cut, allowing reperfusion of the hind limb. The sham rats received exactly the same treatment, with the exception that the O-ring was cut so that it only loosely surrounded the ankle and did not occlude blood flow to the hindpaw.

Study Design

Treatment With Single Oral Mangiferin on Mechanical Allodynia in the Early Phase of CPIP Model

The effect of single oral doses of MG on mechanical allodynia was studied 72 h post-I/R using four CPIP groups that received MG (10, 50, and 100 mg/kg, 10 mL/kg) or vehicle (CMC 0.05%) and a sham CPIP also treated with vehicle by oral route (n = 7 per group). Then five groups were constituted: CPIP-vehicle, CPIP-MG10, CPIP-MG50, CPIP-MG100, and sham-CPIP. Animals were tested in the ipsilateral hind paw at baseline (prior to I/R injury), before treatment, and at 60, 120, and 180 min after treatment.

Pre-treatment With α_1 and α_2 Antagonists, α_2 Agonist, Nitric Oxide Donor, Opioid Agonist and Monoamine Reuptake Inhibitor on the Anti-allodynic Effect of Mangiferin in the Early Phase CPIP Model

There were six experiments to examine the MG anti-allodynic mechanisms or its possible beneficial interactions on 72 h post-I/R with drugs utilized in these conditions. In each experiment, different groups of rats were pre-treated with one drug, respectively: prazosin (1–5 mg/kg) a selective α_1 adrenoceptor antagonist, yohimbine (1–5 mg/kg) a selective α_2 adrenoreceptor antagonist, clonidine (0.01–0.1 mg/kg) a α_2 agonist, SIN-1 (1–10 mg/kg) a NO donor, morphine (0.3–3 mg/kg) a preponderantly μ opioid agonist, and amitriptyline (3–10 mg/kg) a monoamine reuptake inhibitor or vehicle (SS). All drugs were administered intraperitoneally (1 mL/kg). Afterward, a single dose of MG (100 mg/kg, i.p.) or vehicle (DMSO 5%) was injected 15 min later. Following 20 min after MG injection and 35 min of the pre-treatment, mechanical allodynia was tested. Approximately 10 min before that, MG or highest doses of agonist drugs (morphine and clonidine) were injected; a group of animals was pre-treated with antagonist drugs naloxone

(1 mg/kg) or yohimbine (0.1 mg/kg), respectively. The agonist and antagonist drugs and the doses were selected according to the previous reports and pilot experiments in our laboratory, since all drug doses do not induce significant abnormalities in the rotarod test (Dar et al., 2005; Millecamps and Coderre, 2008; Xanthos et al., 2008).

Treatment With Repeated Oral Doses of Mangiferin on Mechanical Allodynia in the Latest Phase of CPIP Model

A medication protocol to evaluate some clinical effects of MG that could appear only after its repeated oral administration during 7 days after 72 h post-CPIP was also designed. The animals were divided in six CPIP rat groups (n = 6–7 each): CPIP-vehicle group that received CMC (0.05%); experimental CPIP-MG groups that received MG (10, 50, and 100 mg/kg, 10 mL/kg; CPIP-MG10, CPIP-MG50, CPIP-MG100); reference group that received prednisone (5 mg/kg; CPIP-P5); and sham CPIP (sham-CPIP) also treated with vehicle by oral route. The rats were evaluated on days 7 and 13 post-I/R injury during medication and after its discontinuation, respectively.

Mechanical Allodynia

Mechano-allodynia of the hindpaw was assessed by measuring the hindpaw withdrawal response to von Frey filament stimulation according to a modification of the up/down method (Chaplan et al., 1994). Briefly, rats were placed in Plexiglas cages (21 cm × 26 cm × 27 cm) with a wire grid bottom. Filaments (Stoelting, Wood Dale, IL, United States) were applied to the plantar surface of the hind paw for approximately 5 s in either ascending or descending strength, to determine the filament closest to the threshold of response. Each filament was applied five times; a response to three of the five applications was counted as positive. The minimum stimulus intensity was 0.25 g, and the maximum was 15 g. Based on the response pattern and the force of the final filament, the 50% response threshold (grams) was calculated. The resulting pattern of positive and negative responses was tabulated, and the 50% response threshold was interpolated using the formula:

$$50\%\ g\ threshold\ =\ \left(10^{[xf+\ k\delta]}\right)\ /10,000$$

where xf = the value (in log units) of the final von Frey hair used; k = tabular value 11 for pattern of positive/negative responses; and δ = mean difference (in log units) between stimuli (here, 0.224). CPIP rats that had not developed mechanical allodynia at 48 h post-IR injury (non-responders, 50% threshold >10 g) were excluded from further measurements of mechanical allodynia after treatments.

Tissue Sampling and Preparation

All rats including the control group were euthanized by cervical dislocation under anesthesia with diethyl ether. Each rat was put in a closed cylindrical jar and overdosed with diethyl ether until loss of the righting reflex. This step took approximately 75 s. Short exposure of rats to diethyl ether reported to have an insignificant effect on cytochrome P450 enzymes, which are known to play an important role in oxidative stress (Plate et al., 2005). Then the muscle samples of the superficial plantar layer (one each from the Flexor Hallucis Brevis, Flexor Digiti Minimi Brevis, and Flexor Digitorium Brevis, each weighing between 25 and 50 mg) and spinal cord samples at L5–L6 (each weighing about 20–25 mg) were obtained, cut into small pieces and homogenized using an Omni tissue homogenizer (Omni International, Gainesville, VA, United States) (de Mos et al., 2009). Tissues were homogenized in ice-cold lyses buffer (0.1 M phosphate, pH 7.4, 1 mM EDTA, 9 mL per gram of tissue using a tube pestle). Samples were centrifuged at 1500 × g for 15 min at 4°C. The supernatants were then stored at −80°C until further analysis.

Muscle and Spinal IL-1β Determination by Enzyme-Linked Immunosorbent Assay (ELISA)

Protein was estimated in all homogenates (Lowry et al., 1951). BSA 0.01–0.2 mg/mL was used as standard. Quantification of IL-1β secretion was measured by an in-house sandwich ELISA based on matched antibodies against rat IL-1β. Briefly, a 96-well ELISA plate that was pre-coated with anti-rat polyclonal IL-1β antibody and was incubated with a 100 μL sample or rat IL-1β standards at each well. Following incubation for 2 h at room temperature, the wells were washed three times using a washing buffer, after which biotinylated anti-rat IL-1β antibody was added and incubated for 2 h. Then, streptavidin-peroxidase was added, incubated for another 30 min and followed by three washes. Then a tetramethylbenzidine solution was added, incubated for 30 min in the dark, and the peroxidase-catalyzed color change was stopped by acidification with 1 N H_2SO_4. The absorbance was measured with the microplate reader at 450 nm with reference at 630 nm. Results were expressed as pg of cytokine/mg of protein.

Determination of Redox Biomarkers in Ipsilateral Muscles

Redox biomarkers were determined by spectrophotometric methods using a Pharmacia 1000 Spectrophotometer (Pharmacia, Uppsala, Sweden). Total protein content was measured by Bradford's method with BSA as standard (Bradford, 1976). SOD activity was determined by using a RANSOD kit, where xanthine and xanthine oxidase were used to generate superoxide anion radicals (O_2^-), which react with 2-(4-iodophenyl)-3-(4-nitrophenyl)-5-phenyltetrazolium chloride (INT) to form a red formazan dye. SOD activity was measured by the inhibition degree of this reaction (Boehringer Mannheim, 1987). After precipitation of thiol proteins, the glutathione (GSH) levels were measured according to the method of Sedlak and Lindsay (1968) with Ellman's reagent [5,5′-dithiobis(2-nitrobenzoic acid)], and the absorbance was measured at 412 nm. Purified GSH was used to generate standard curves. The concentration of MDA was determined using the LPO-586 kit. In the assay, the production of a stable chromophore after 40 min of incubation at 45°C was measured at 586 nm. For standards, freshly prepared solutions of MDA bis [dimethyl acetal] were employed (Erdelmeier et al., 1998). As a surrogate marker of protein damage, carbonyl protein groups were determined

as previously described using 2,4-dinitrophenylhydrazine as chromogen (Levine et al., 2000). In addition, nitrates/nitrites (NO_3^-/NO_2^-) level, as a surrogate marker of nitric oxide (NO), was determined by converting nitrates to nitrites using nitrate reductase. Then, Griess reagent [1% sulphanilamide, 0.1% *N*-(1-Naphthyl)ethylenediamine dihydrochloride in 0.25% phosphoric acid] was added (Granger et al., 1995). Samples were incubated at room temperature for 10 min, and absorbance was measured at 540 nm.

Statistical Analyses

Data were analyzed using the statistical program Graph Pad Prism 5 (GraphPad Software, Inc., La Jolla, CA, United States). Baseline mechanical allodynia test results were compared with one-way ANOVA followed by Dunnett *post hoc* test. Post-treatment differences between groups were analyzed using a 2-way repeated-measures ANOVA followed by the Bonferroni *post hoc* test. The results are presented as mean ± SEM. Baseline von Frey thresholds are included in the figures for each drug trial but are not included in these statistical analyses. Redox biomarkers and IL-1β were analyzed using one-way ANOVA followed by Dunnett *post hoc* test. The Spearman's rank correlation coefficient was used to calculate correlations between numerical spinal IL-1β protein data and the paw-withdrawal threshold data. $P \leq 0.05$ was considered statically significant.

RESULTS

Effect of Single Oral Mangiferin on Mechanical Allodynia in the Early Phase of CPIP Model

Paw-withdrawal thresholds of the ipsilateral hind paw at baseline did not differ between CPIP (n = 40) and sham (n = 7) rats (11.4 ± 0.2 and 12.1 ± 0.5 g, respectively, P = 0.599). At 72 h after I/R injury, CPIP rats developed a reduction in paw-withdrawal threshold (mean 50% von Frey threshold of 4.0 ± 0.3 g) compared to sham (mean 50% von Frey threshold of 11.5 ± 0.3 g) ($P < 0.001$) (**Figure 1**). Within the CPIP group, 33 rats (82.5%) displayed a 50% von Frey threshold <6 and were regarded as responders for mechanical allodynia, which were randomly allocated to different experimental groups. Two-way ANOVA reveals significant main effects of time (pre-post) ($F_{3,93}$ = 22.33, $P < 0.0001$) and dose ($F_{4,93}$ = 29.28, $P < 0.0001$) and a significant time × dose interaction ($F_{12,93}$ = 5.07, $P < 0.0001$). Compared with the vehicle group, the paw-withdrawal threshold only increased significantly at 60 min in CPIP rats treated with a high dose (100 mg/kg) of MG (CPIP-vehicle = 3.4 ± 0.6 g, CPIP-MG10 = 3.7 ± 0.5 g, CPIP-MG50 = 4.0 ± 0.4 g, CPIP-MG100 = 7.5 ± 1.7 g, $P < 0.05$, sham = 12.0 ± 0.4 g). However, at 120 min after its single administration, the anti-allodynic effect was observed in animals that received doses of 50 and 100 mg/kg (CPIP-vehicle = 3.1 ± 0.8 g, CPIP-MG10 = 5.6 ± 1.0 g, CPIP-MG50 = 10.0 ± 1.1 g, $P < 0.001$, CPIP-MG100 = 11.2 ± 1.4 g, $P < 0.001$, sham = 12.0 ± 0.8 g). Likewise, this effect remained at 180 min (CPIP-vehicle = 4.2 ± 0.8 g, CPIP-MG10 = 4.8 ± 0.8 g, CPIP-MG50 = 9.0 ± 1.0 g, $P < 0.001$, CPIP-MG100 = 11.0 ± 0.9 g, $P < 0.001$, sham-CPIP = 12.0 ± 0.8 g) (**Figure 1**).

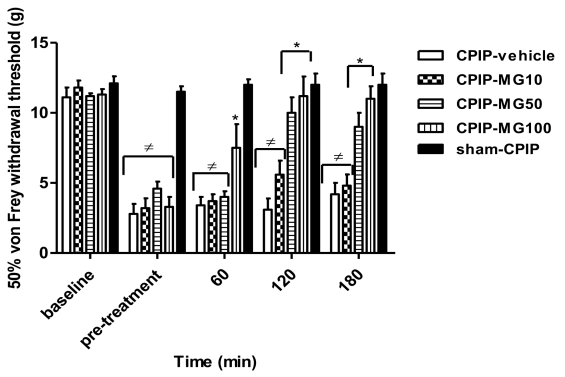

FIGURE 1 | Mechanical ipsilateral paw-withdrawal threshold (grams) determined by von Frey test prior to ischemia/reperfusion injury (baseline), pre-treatment and at 60, 120, and 180 min post-treatment in chronic post-ischemia pain (CPIP) and sham rats. The animals received a single oral dose of mangiferin (10–100 mg/kg, 10 mL/kg, p.o., MG) or vehicle (CMC 0.05%) at 72 h post-reperfusion. Each column represents the reactivity time of 6–7 animals per group as mean ± SEM. $^*P < 0.05$ represents the statistical difference between treated groups and control (CPIP-vehicle), while $^{\neq}P < 0.05$ represents the statistical difference between CPIP groups regarding sham-CPIP rats.

Effects of Pre-treatment With α_1 and α_2 Antagonists, α_2 Agonist and Nitric Oxide Donor on the Anti-allodynic Effect of Mangiferin in the Early Phase of CPIP Model

Figure 2 shows the mechanical (von Frey) thresholds (grams) of 72 h-CPIP rats at baseline, before, and 35 min after pre-treatment with the vehicle or anti-sympathetic agents (α_1 and α_2 antagonists, α_2 agonist) and a NO donor vasodilator in the presence or absence of MG 100 mg/kg. Two-way ANOVA reveals significant main effects of time (pre-post) ($F_{1,33}$ = 415.17, $P < 0.0001$) and treatment ($F_{5,33}$ = 14.62, $P < 0.0001$) and a significant time × treatment interaction ($F_{5,33}$ = 26.08, $P < 0.0001$). The I/R von Frey thresholds were significantly lower than baselines for all groups and the vehicle (SS – DMSO) injection did not result in a significant increase in paw-withdrawal threshold. MG (100 mg/kg) – SS (pre- vs. post-drug) was found to be significantly anti-allodynic ($P < 0.001$) with respect to vehicle administration (SS – DMSO = 3.2 ± 0.6 g vs. SS – MG100 = 10.7 ± 1.0 g, $P < 0.001$). Compared with pre-drug values, von Frey thresholds were significantly increased in all CPIP groups pre-treated with prazosin, except for its low dose (1 mg/kg) (prazosin 1 – DMSO = 6.4 ± 0.9 g, prazosin 5 – DMSO = 10.1 ± 0.6 g, $P < 0.001$, prazosin 1 – MG = 11.7 ± 0.4 g, $P < 0.001$, prazosin 5 – MG = 13.5 ± 0.3 g, $P < 0.001$). However, a sub-effective dose of prazosin in the presence of MG was found

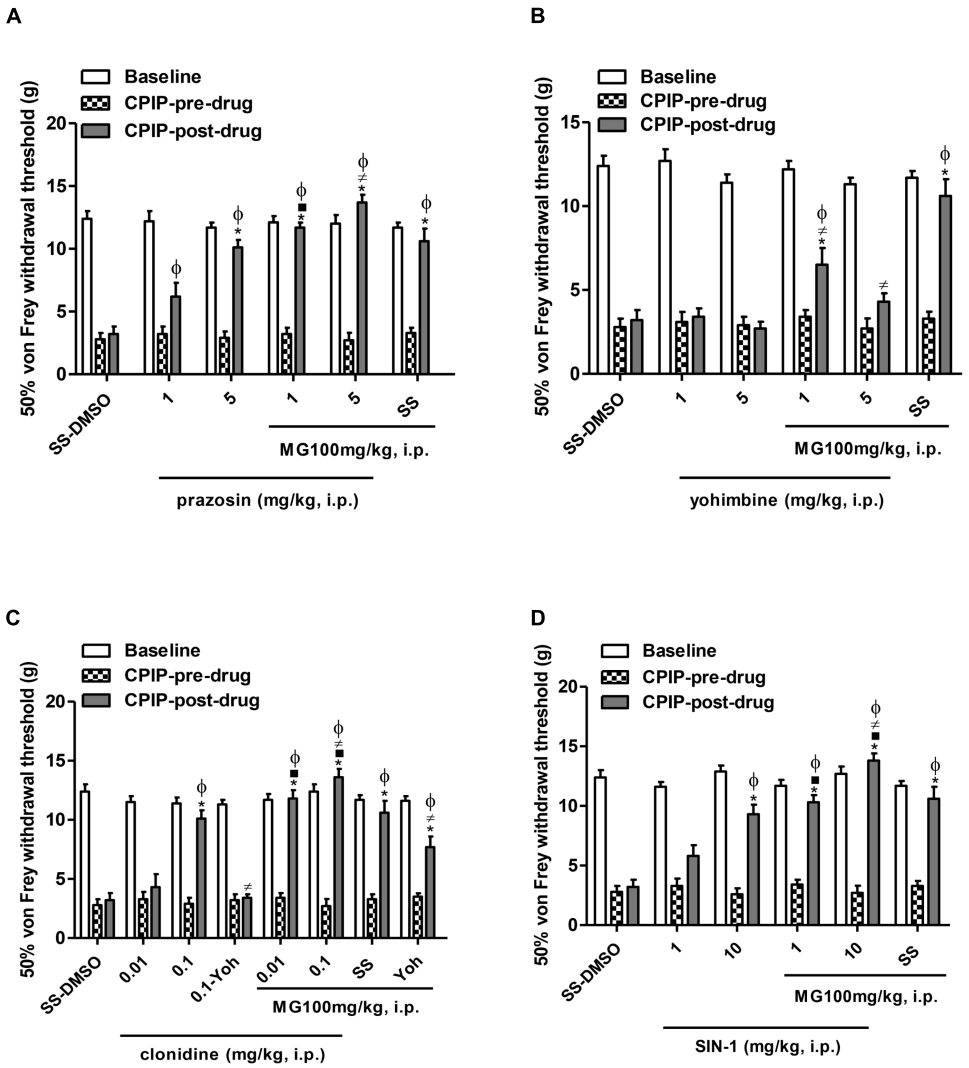

FIGURE 2 | Influence of the pre-treatment with sympathetic α_1-and α_2-adrenergic antagonists, prazosin and yohimbine, respectively, α_2-adrenergic agonist clonidine and nitric oxide donor, SIN-1 (1 mL/kg, i.p.) on the anti-allodynic effect of mangiferin (100 mg/kg, 1 mL/kg, i.p., MG) or vehicle (DMSO 5%) 72 h after the ischemia/reperfusion-injury. Animals received **(A)** saline or prazosin (1–5 mg/kg), **(B)** saline or yohimbine (1–5 mg/kg), **(C)** saline or clonidine (0.01–0.1 mg/kg), **(D)** saline or SIN-1 (1–10 mg/kg). The effect of MG and the highest dose of agonist drug clonidine were reversed by yohimbine (0.1 mg/kg). Each column represents the reactivity time of 6–7 animals per group as mean ± SEM. $^{*}P < 0.05$ represents the statistical difference between CPIP post-drug and CPIP pre-drug, while $^{\cdot}P < 0.05$ represents the statistical difference between CPIP post-drugs in the presence or absence of MG, $^{\neq}P < 0.05$ represents the statistical difference between CPIP post-drugs treated with MG or pre-treated with the highest dose of clonidine in presence or absence of yohimbine, $^{\phi}P < 0.05$ represents the statistical difference between treated groups regarding control vehicle (SS-DMSO).

to be significantly anti-allodynic ($P < 0.001$). Additionally, CPIP rats pre-treated with an effective dose of prazosin (5 mg/kg) and treated with MG show significantly increased von Frey thresholds compared to the SS – MG100 group ($P < 0.05$) (**Figure 2A**).

Figure 2B shows the (pre- vs. post-drug) comparison of 72 h-CPIP rats mechanical von Frey thresholds of animals pre-treated with yohimbine (1–5 mg/kg). Two-way ANOVA shows significant main effects of time (pre-post) ($F_{1,33} = 31.45$, $P < 0.0001$) and treatment ($F_{5,33} = 15.61$, $P < 0.0001$) and a significant time × treatment interaction ($F_{5,33} = 10.12$, $P < 0.0001$). Non-significant increases in thresholds of animals were observed (yohimbine 1 – DMSO = 3.4 ± 0.5 g, yohimbine 5 – DMSO = 2.7 ± 0.4 g). Nevertheless, in CPIP rats treated with mangiferin, yohimbine reversed its anti-allodynic effect dependently from dose (yohimbine 1 – MG = 6.5 ± 1.0 g, $P < 0.001$, yohimbine 5 – MG = 4.3 ± 0.5 g, $P < 0.001$ vs. SS – MG100 = 10.7 ± 1.0 g).

The results presented in **Figure 2C** show the (pre- vs. post-drug) comparison of 72 h-CPIP rats mechanical von Frey thresholds of animals pre-treated with clonidine (0.01–0.1 mg/kg). Two-way ANOVA shows significant main effects of time (pre-post) ($F_{1,43} = 244.54$, $P < 0.0001$) and treatment ($F_{7,43} = 25.72$, $P < 0.0001$) and a significant time × treatment interaction ($F_{7,43} = 23.05$, $P < 0.0001$).

Compared to pre-drug values, von Frey thresholds were significantly increased in all groups pre-treated with clonidine, except the group pre-treated with the low dose (clonidine 0.01 – DMSO = 4.3 ± 1.1 g, clonidine 0.1 – DMSO = 10.1 ± 0.7 g, $P < 0.001$, clonidine 0.01 – MG = 11.8 ± 0.7 g, $P < 0.001$, clonidine 0.1 – MG = 13.5 ± 0.3 g, $P < 0.001$). The particular interest was that a sub-effective dose of clonidine 0.01 mg/kg in the presence of MG was found to be significantly anti-allodynic ($P < 0.001$), this effect was also observed in CPIP rats pre-treated with clonidine 0.1 mg/kg ($P < 0.01$). Additionally, the clonidine 0.1 – MG group shows significantly increased von Frey thresholds compared with SS – MG group ($P < 0.05$). The selective α_2 antagonist yohimbine 0.1 mg/kg reversed the anti-allodynic effect of the high dose of clonidine ($P < 0.001$) and partially the effect of mangiferin ($P < 0.05$).

The (pre- vs. post-drug) comparison of von Frey thresholds in CPIP rats pre-treated with a donor of NO. Two-way ANOVA shows significant main effects of time (pre-post) ($F_{1,33} = 252.17$, $P < 0.0001$) and treatment ($F_{5,33} = 16.67$, $P < 0.0001$) and a significant time × treatment interaction ($F_{5,33} = 17.43$, $P < 0.0001$). SIN-1 (1–10 mg/kg) show a significant increase in all groups except for its low dose (SIN-1 1 – DMSO = 6.1 ± 0.9 g, SIN-1 10 – DMSO = 9.3 ± 0.8 g, $P < 0.001$, SIN-1 1 – MG = 10.3 ± 0.6 g, $P < 0.001$, SIN-1 10 – MG = 13.8 ± 0.6 g, $P < 0.001$). The sub-effective dose of SIN-1 in the presence of MG was found to be significantly anti-allodynic ($P < 0.001$), this effect was also observed in CPIP rats pre-treated with SIN-1 at a high dose ($P < 0.01$). In addition, the SIN-1 10 – MG group shows significantly increased von Frey thresholds in comparison to the SS – MG group ($P < 0.05$) (**Figure 2D**).

Effects of Pre-treatment With a μ Opioid Agonist or Monoamine Reuptake Inhibitor on the Anti-allodynic Effect of Mangiferin in the Early Phase of CPIP Model

Figure 3 shows the mechanical (von Frey) thresholds (grams) of 72 h-CPIP rats at baseline, before, and 35 min after pre-treatment with the vehicle or standard drugs utilized in CRPS patients (morphine or amitriptyline) in the presence or absence of MG 100 mg/kg, 20 min after its injection. Two-way ANOVA shows significant main effects of time (pre-post) ($F_{1,43} = 235.37$, $P < 0.0001$) and treatment ($F_{7,43} = 19.94$, $P < 0.0001$) and a significant time × treatment interaction ($F_{7,43} = 21.06$, $P < 0.0001$). The post-I/R von Frey thresholds were significantly lower than baseline for all groups, and the vehicle (SS – DMSO) injection did not result in a significant increase in paw-withdrawal threshold. SS – MG (100 mg/kg) (pre- vs. post-drug) was found to be significantly anti-allodynic ($P < 0.001$) with respect to vehicle post-drug administration (SS – DMSO = 3.2 ± 0.6 g vs. SS – MG100 = 10.7 ± 1.0 g, $P < 0.001$). The (pre- vs. post-drug) comparison of von Frey thresholds in CPIP rats pre-treated with morphine (0.3–3 mg/kg) show a significant increase in all groups except for its low dose (morphine 0.3 – DMSO = 6.1 ± 0.9 g, morphine 3 – DMSO = 9.3 ± 0.8 g, $P < 0.001$, morphine 0.3 – MG = 10.3 ± 0.6 g, $P < 0.001$, morphine 3 – MG = 13.8 ± 0.6 g, $P < 0.001$). The sub-effective dose of morphine in the presence of MG was found to be significantly anti-allodynic ($P < 0.001$), this effect was also observed in CPIP rats pre-treated with morphine at a high dose ($P < 0.001$). In addition, the morphine 3 – MG group shows significantly increased von Frey thresholds compared to the SS – MG100 group ($P < 0.05$). The non-selective μ opioid antagonist naloxone 1 mg/kg reversed the anti-allodynic effect of the high dose of morphine ($P < 0.01$) and partially the effect of mangiferin ($P < 0.01$) (**Figure 3A**).

Two-way ANOVA shows significant main effects of time (pre-post) ($F_{1,33} = 204.48$, $P < 0.0001$) and treatment ($F_{5,33} = 31.17$, $P < 0.0001$) and a significant time × treatment interaction ($F_{5,33} = 26.01$, $P < 0.0001$). The (pre- vs. post-drug) comparison of von Frey thresholds in CPIP rats pre-treated with amitriptyline (3–10 mg/kg) show a non-significant increase in thresholds of animals (amitriptyline 3 – DMSO = 4.2 ± 0.9 g, amitriptyline 10 – DMSO = 5.2 ± 0.4 g). Nevertheless, both doses of amitriptyline in the presence of MG where found to be significantly anti-allodynic (amitriptyline 3 – MG = 12.6 ± 0.3 g, $P < 0.001$, amitriptyline 10 – MG = 13.6 ± 0.5 g, $P < 0.001$). Additionally, the amitriptyline 10 – MG group shows significantly increased von Frey thresholds compared to the SS – MG100 – group ($P < 0.05$) (**Figure 3B**).

Effect of Repeated Oral Doses of Mangiferin on Redox Status and IL-1β Concentration in Ipsilateral Plantar Muscle in the Latest Phase of CPIP Model

Lipid peroxidation (as the concentration of MDA μM/mg Pr in the sample) measured 13 days post-I/R injury was increased significantly ($P < 0.001$) in CPIP rats treated with the vehicle, as compared to sham CPIP controls (**Table 1**). Likewise, a surrogate marker of protein damage (carbonyl protein groups) was increased ($P < 0.001$) in CPIP rats with respect to sham controls. The animals treated with MG 100 mg/kg and prednisone show a significant decrease of MDA formation ($P < 0.001$) and ($P < 0.01$), respectively, as well as CG ($P < 0.001$, $P < 0.001$). A significant increase of NO_3^-/NO_2^- levels, as an indicator of NO production in muscle tissue of CPIP rats, was observed ($P < 0.001$). Repeated doses of MG 100 mg/kg like prednisone reduces the NO oxidation products concentrations ($P < 0.001$, $P < 0.001$). GSH was inhibited significantly ($P < 0.001$) in CPIP rats when compared to sham controls. The amount of SOD increased significantly ($P < 0.001$) post-I/R in comparison with the sham CPIP ipsilateral muscle superficial layer. MG 100 mg/kg, like prednisone, significantly restores GSH ($P < 0.001$, $P < 0.01$) and SOD ($P < 0.001$, $P < 0.001$) close to more physiological concentrations. Additionally, IL-1β (pg/mg) in this injured peripheral tissue was also increased in CPIP rats compared with sham controls (CPIP – vehicle = 1565 ± 422 vs. sham – CPIP = 344 ± 17, $P < 0.001$). The experimental groups CPIP – MG100 and CPIP – MG50, as well as referential group prednisone 5, show a significant decrease of this pro-inflammatory cytokine (CPIP – MG50 = 676 ± 185, $P < 0.05$,

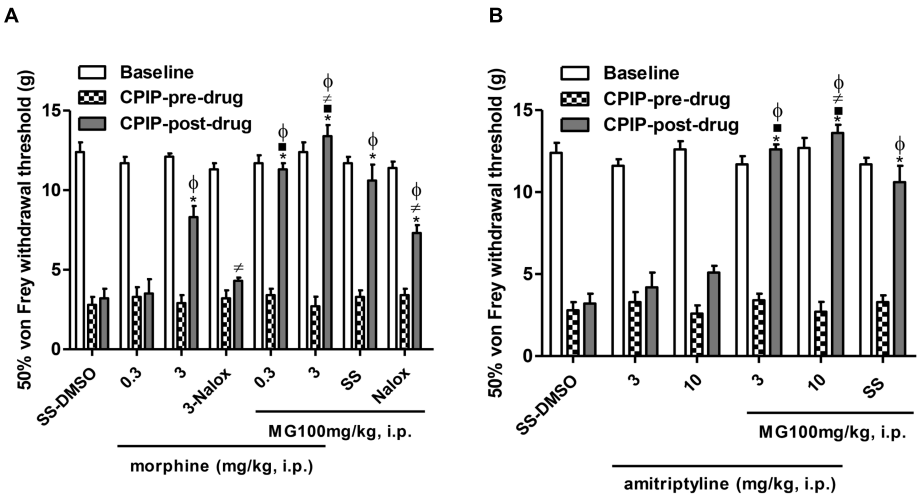

FIGURE 3 | Influence of the pre-treatment with morphine or amitriptyline on the anti-allodynic effect of mangiferin (100 mg/kg, 1 mL/kg, i.p., MG) or vehicle (DMSO 5%) 72 h after the ischemia/reperfusion-injury. Animals received **(A)** saline or morphine (0.3–3 mg/kg), **(B)** saline or amitriptyline (3–10 mg/kg). The effect of MG and the highest dose of agonist drug morphine were reversed by naloxone (1 mg/kg). Each column represents the reactivity time of 6–7 animals per group as mean ± SEM. $^{*}P < 0.05$ represents the statistical difference between CPIP post-drug and CPIP pre-drug, while $^{\cdot}P < 0.05$ represents the statistical difference between CPIP post-drugs in the presence or absence of MG, $^{\neq}P < 0.05$ represents the statistical difference between CPIP post-groups treated with MG or highest dose of morphine in the presence or absence of naloxone, $^{\Phi}P < 0.05$ represents the statistical difference between treated groups regarding control vehicle (SS-DMSO).

TABLE 1 | Redox biomarkers in ipsilateral muscles of sham and CPIP rats treated with repeated oral doses of mangiferin (MG), prednisone (P), or vehicle.

Group	Dose	MDA (μM/mg Pr)	CG (nM/mg Pr)	NO (μM/mg Pr)	GSH (μM/mg Pr)	SOD (U/L/mg Pr)
Sham-CPIP	10 mL/kg	2.10 ± 0.15	0.71 ± 0.02	14.26 ± 0.74	108.20 ± 5.36	26.33 ± 0.85
CPIP-vehicle	10 mL/kg	5.53 ± 0.32[c]	1.96 ± 0.05[c]	35.26 ± 1.38[c]	61.18 ± 2.38[c]	69.72 ± 1.55[c]
CPIP-P5	5 mg/kg	3.43 ± 0.30[b]	1.19 ± 0.04[a]	17.61 ± 0.51[a]	84.52 ± 3.03[b]	40.09 ± 2.93[a]
CPIP-MG100	100 mg/kg	3.20 ± 0.11[a]	0.94 ± 0.04[a]	24.37 ± 1.28[a]	81.97 ± 1.91[a]	38.91 ± 2.03[a]

Data are presented as mean ± SEM of n = 5–6 per group. [a]p ≤ 0.001, [b]p ≤ 0.01 represent the statistical difference between treated groups and control (CPIP – vehicle group), and [c]p ≤ 0.001 represent the statistical difference between treated groups and sham – CPIP group. CMC 0.05% was used as the vehicle by the oral route. CPIP, chronic post-ischemia pain; CG, carbonyl protein groups concentration; GSH, reduced glutathione; MDA, malondialdehyde; NO, nitric oxide; Pr, protein; SOD, superoxide dismutase.

CPIP – MG100 = 344 ± 21, $P < 0.001$, CPIP – prednisone 5 = 209 ± 39, $P < 0.001$) in ipsilateral muscle tissue 13 days after I/R injury (**Figure 4**).

Effect of Repeated Oral Doses of Mangiferin on Mechanical Allodynia in the Latest Phase of CPIP Model and Its Relation to IL-1β Spinal Concentration

At 7 days post-I/R injury and after repeated oral dairy similar doses of MG (10–100 mg/kg) for 5 days, CPIP rats treated with doses of 50 and 100 mg/kg showed an increase in ipsilateral paw-withdrawal threshold compared to vehicle CPIP animals. The group treated with prednisone 5 mg/kg (CPIP-P5) did not significantly increase its von Frey mechanical thresholds at this time (CPIP – vehicle = 4.3 ± 0.8, CPIP – MG10 = 7.7 ± 1.1, CPIP – MG50 = 10.5 ± 0.9, $P < 0.001$, CPIP – MG100 = 11.1 ± 1.1, $P < 0.001$, CPIP – P5 = 7.4 ± 1.2) (**Figure 5A**). Once finished the MG administration at 13 days post-I/R injury, the animals, even after 4 days of its discontinuation, showed significantly increased withdrawal thresholds as well as those treated with prednisone (CPIP – vehicle = 3.9 ± 1.0, CPIP – MG10 = 6.0 ± 0.8, CPIP – MG50 = 8.1 ± 1.1, $P < 0.05$, CPIP – MG100 = 9.0 ± 1.0, $P < 0.01$, CPIP – P5 = 9.0 ± 1.0, $P < 0.01$) (**Figure 5B**). At this time point, IL-1β (pg/mg) in the spinal cord tissue was increased in CPIP rats compared to the sham controls (CPIP – vehicle = 3614 ± 254 vs. sham – CPIP = 2091 ± 33, $P < 0.01$). The concentration of IL-1β in the CPIP-MG100 group (2082 ± 51, $P < 0.001$) decreased significantly, similar to its reference group treated with prednisone (2244 ± 138, $P < 0.01$), compared to the CPIP – vehicle animals, respectively (**Figure 5C**). A Spearman's correlation analysis for paw-withdrawal threshold data and numerical spinal protein IL-1β data was performed. This analysis included results from the vehicle, prednisone and MG 50 and 100 mg/kg treated CPIP rats ($n = 24$). Correlation analysis identified an association between reduced mechanical paw-withdrawal threshold and increased spinal protein concentration of IL-1β in CPIP rats ($r = -0.9216$; $P < 0.0001$) (**Figure 5D**).

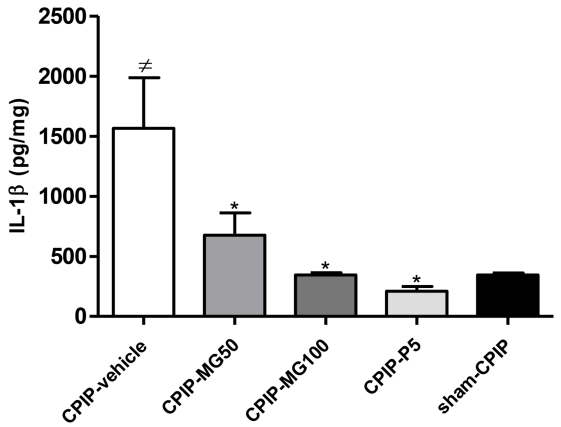

FIGURE 4 | IL-1β protein concentration in the muscle samples of the superficial plantar layer 13 days after post-ischemia/reperfusion and 4 days after mangiferin (10–100 mg/kg, 10 mL/kg, p.o., MG), vehicle (CMC 0.05%) or prednisone (5 mg/kg, P) discontinuation. IL-1β was measured by ELISA. Each bar represents the mean ± SEM (n = 6 animals). $^{\neq}P < 0.05$ represents the statistical difference regarding sham-CPIP rats, $^{*}P < 0.05$ represents the statistical difference regarding the CPIP-vehicle group.

DISCUSSION

The findings of the present study evidenced for the first time the anti-allodynic effect of MG in CPIP rats. However, the presence of a mixture of an isomer, iso-MG and MG monomethyl ether, homo-MG (Núñez Sellés et al., 2016) could facilitate the pharmacologic effect. This model mimics the CRPS-I-symptomatology made by persistent deep tissue (muscle, bone, and nerve) microvascular pathology that leads to a combination of inflammatory and neuropathic pain processes (Coderre et al., 2004; Coderre and Bennett, 2010). In this context hypoxia and acidosis, as well as the subsequent formation of ROS are robust nociceptive triggers implicated in acute inflammation and edema associated with microvascular endothelial cell I/R injury in the early phase of CPIP (Coderre and Bennett, 2010). These include vascular abnormalities such as persistent ischemia, dependent on either slow-flow no-reflow due to capillary blockage, or arterial vasospasms due to sympathetic vasoconstrictor hyper-responsiveness and/or endothelial cell dysfunction (Blaisdell, 2002). Prolonged deep tissue ischemia for a week following reperfusion may result in chronic inflammation leading to peripheral and central sensitization (Laferrière et al., 2008; Kwak et al., 2011). MG, after its repeated administration, also shows a long-term anti-allodynic effect in the late phase of CPIP related to the decrease of spinal and peripheral IL-β and restoration of redox status in the affected limb.

The sympathetic nervous system (SNS) in CRPS-I may have an important contributory role in early-stage of disease (Coderre and Bennett, 2010). Accordingly, mechanical allodynia in CPIP rats has been explicated in part by sympathetically maintained pain (SMP) mechanisms, particularly exaggerated sympathetically mediated vascular contractility and persistent tissue ischemia (Xanthos and Coderre, 2008; Xanthos et al., 2008). The nociceptive responses to NE in CPIP rats are paralleled by enhanced vasoconstrictive responses to NE and are relieved by α-adrenergic antagonists or vasodilators. Subsequently, an indirect sympathetic–sensory coupling has been proposed to explicate CPIP and CRPS-I hypersensitivity. This process may depend more on early upregulation of adrenoceptors on vascular smooth muscle cells of the rat hind limb than on primary afferents (Xanthos et al., 2008). MG does not affect NE induced vasoconstrictor responses in rat mesenteric resistance arteries, suggesting its inability for antagonized vascular smooth muscle cells α_1-adrenoceptors, which are pivotal in SMP (Raja et al., 1991; Beltran et al., 2004). However, the inhibition of NE induced vasoconstriction and Ca^{2+} influx in the rat thoracic aorta by its more bioavailable aglycone (norathyriol) and the endothelium-independent vasorelaxant actions of some xanthones have been reported (Ko et al., 1991; Jiang et al., 2004). Several differences between the distribution of sympathetic nerve fibers to the blood vessels have been recognized. For most tissues, all the vessels except the capillaries, precapillary sphincters, and metarterioles are innervated by SNS. Particularly, the smooth muscles in the arterioles of the nutritive capillaries are controlled by local factors, whereas the arterioles in the subpapillary plexus are predominantly sympathetically controlled (Groeneweg et al., 2009). A gradation from proximal to peripheral arteries toward denser innervation and greater neurogenic responses has been found in rats. Then vasoactive effects of individual α-adrenergic receptor subtypes can be strongly influenced by species and expression of subtypes in particular vascular beds. This may be particularly relevant to hindpaw vascular bed under I-R injury which has significant effects within the microvasculature (Nilsson et al., 1986; Xanthos and Coderre, 2008). Despite the fact that the vasoactive effect of MG was studied in large and intermediate arteries it may be an approach to infer its possible activity on vascular α-adrenergic receptors. Sympathetic blocking with systemic guanethidine, α_1 antagonist prazosin, α_2 agonist clonidine, and mixed α_1/α_2-adrenergic antagonist phentolamine each induce an anti-allodynic effect 2 days after I/R in CPIP rats (Xanthos et al., 2008). Additionally, α_2 antagonist yohimbine did not induce anti-allodynia, supporting the beneficial role of α_2–adrenoceptor agonists such as clonidine in CRPS patients (Ragavendran et al., 2016). The present results suggest the contribution of α_2–adrenoceptors in the anti-allodynic effect of MG as well as any favorable interaction between this xanthone and adrenergic agents. Most α_2–adrenoceptors are autoreceptors, mediating negative feedback on NE release from SPGNs leading to local vasodilation (Pertovaara, 2013). Nevertheless, spinal α_2 adrenergic receptors implicated in pre-synaptic and post-synaptic nociceptive inhibition or peripheral α_2 adrenergic receptors which are expressed by primary nociceptive sensory neurons and immune cells could also be involved in this effect. Previously, a transient effect of MG on nociceptive pathways mediated by spinal α_2 adrenergic receptors was reported (Garrido-Suárez et al., 2014). Furthermore, the contribution of the L-arginine-NO-cGMP-ATP-sensitive K^+ channel pathway to its mechanisms (Izquierdo et al., 2013) could have influenced this effect, considering the known reciprocal interplay between NO

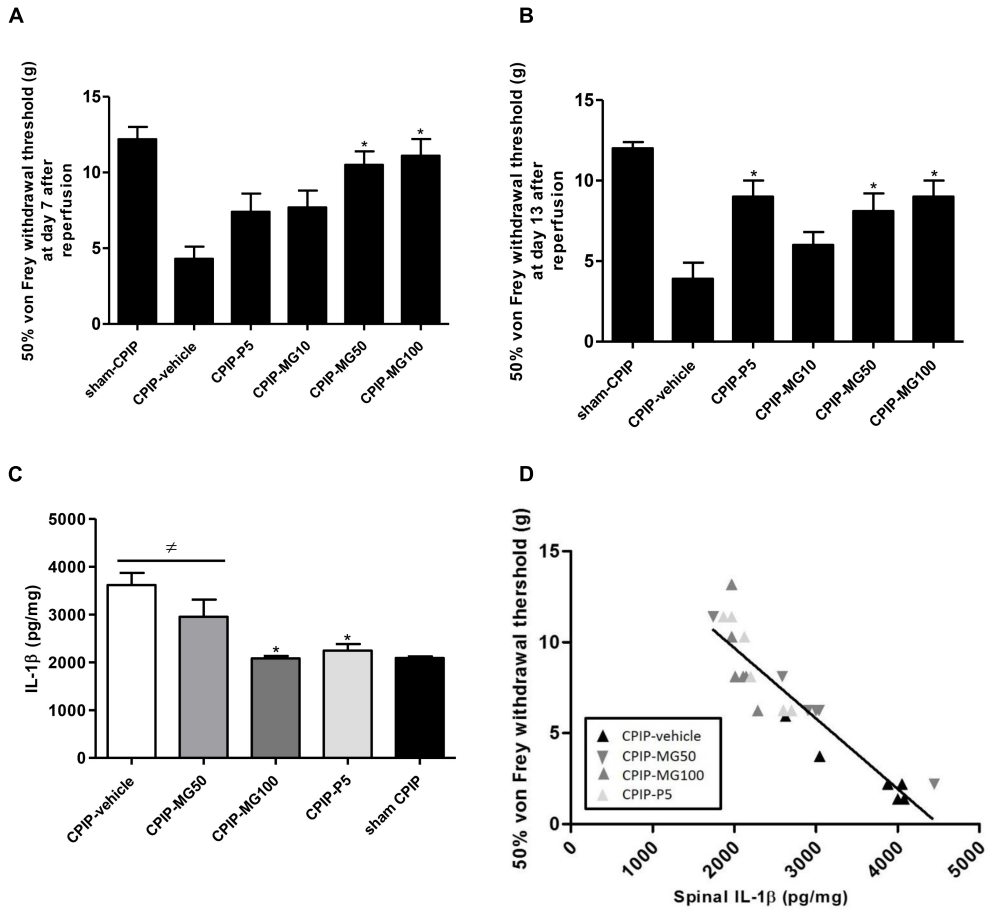

FIGURE 5 | Mechanical paw-withdrawal threshold (grams) determined by von Frey test in CPIP and sham CPIP rats after 7 repeated oral doses of mangiferin (10–100 mg/kg, 10 mL/kg, p.o., MG), vehicle (CMC 0.05%) or prednisone (5 mg/kg, P). **(A)** Effect of MG during the medication at 7 days after ischemia/reperfusion (I/R). **(B)** Effect of MG after its discontinuation 13 days post-I/R. The data are presented as mean ± SEM. $^{*}P < 0.05$ represents the statistical difference between treated groups and control CPIP-vehicle. **(C)** IL-1β protein concentration measured by ELISA in the spinal cord 13 days post-I/R and 4 days after MG discontinuation. Each bar represents the mean ± SEM ($n = 6$ animals). $^{\neq}P < 0.05$ represents the statistical difference regarding sham-CPIP rats, $^{*}P < 0.05$ represents the statistical difference with respect CPIP-vehicle group. **(D)** The relationship between mechanical paw-withdrawal threshold and the spinal IL-1β concentration 13 days post-I/R injury in CPIP rats that were treated with vehicle, MG 50 mg/kg, MG 100 mg/kg, and prednisone. Rats showed the significant inverse relationship between these variables ($r = –0.9216$; $P < 0.0001$).

and α_2-adrenoceptor in the induction of spinal antinociception (Cury et al., 2011).

The role of the endothelial nitric oxide synthase (eNOS)-NO-cGMP pathway in the regulation of local blood flow and endothelial homeostasis is recognized (Moncada et al., 1991). In the CPIP model, nociceptive behaviors are induced by intradermal injection of the eNOS inhibitor (L-NIO), besides the nociceptive hypersensitivity to NE are reduced by the NO donor (SIN-1) (Xanthos and Coderre, 2008; Xanthos et al., 2008). The current results also suggest a possible beneficial interaction between SIN-1 and MG. After I/R injury, there is both an upregulation and hyper-responsiveness of vascular adrenoceptors as well as a reduced production of NO (Xanthos et al., 2008). In cold CRPS patients, an imbalance between the vasodilator NO and the vasoconstrictor endothelin-1 (ET-1) in artificial blisters on the skin of the affected extremity has been demonstrated (Groeneweg et al., 2006); evidence that advised about the role of endothelial dysfunction linked to aberrant inflammatory responses in CRPS vasomotor disturbances (Groeneweg et al., 2008, 2009). CPIP mice show enhanced painful responses to intraplantar ET-1 injections and upregulation of ET-A receptors in hind paw muscle (Millecamps et al., 2010). Interestingly, a protective effect of xanthones against endothelial dysfunction by reducing the levels of endogenous NOS inhibitors could promote vasodilation in these conditions (Jiang et al., 2004). Congruently, MG dose-dependently enhances eNOS level in the gastric mucosa of an I/R model (Mahmoud-Awny et al., 2015). Likewise, its ability to inhibit smooth muscle spasms in tracheal rings have been linked with epithelium eNOS-NO-cGMP-dependent mechanisms (Vieira et al., 2013). Additonally, it was previously reported that MG inhibited ET-1 secretion and restored the loss of NO production when cells were exposed to high glucose under endoplasmic reticulum stress conditions (Song et al., 2015). An earlier study of the

CPIP model revealed that topical combinations including α_{2A} receptor agonists, phosphodiesterase four inhibitors, or NO donors improved both arterial and capillary blood flow associated with effective analgesia (Ragavendran et al., 2013; Laferrière et al., 2014). All these facts add support to our interpretation that MG relaxant properties may be closely related to the activation of the NO-cGMP pathway in CPIP.

Although currently there are no positive trials in CRPS for drugs such as tricyclic antidepressants (TCA) or opioids, both are often indicated (Birklein and Schlereth, 2015). Amitriptyline was ineffective in decreasing mechanical allodynia in CPIP rats and morphine had a slight, but significant anti-allodynic effect, early when tissues exhibit elevated local production of ROS and other inflammatory mediators (Millecamps and Coderre, 2008). This experiment showed that the anti-allodynic effect of MG was naloxone-sensitive. Other authors have described the participation of endogenous opioid peptides and the activation of peripheral opioid receptors in its analgesic mechanisms (Dar et al., 2005; Izquierdo et al., 2013; Lopes et al., 2013). Current results also suggest a beneficial interaction of MG with both drugs, probably related to its ability to modulate noradrenergic, serotonergic, and opioid systems (Garrido-Suárez et al., 2014; de los Monteros-Zuñiga et al., 2016), in addition to a potent antioxidant effect depending on its ROS scavenging (Garrido et al., 2008) and iron-complexing abilities (Pardo-Andreu et al., 2008). Particularly, hypoxia-inducible factor 1α (HIF-1α), which is regulated by ROS, has been implicated in CPIP pathogenesis and its inhibition produces anti-allodynia (Hsiao et al., 2016). MG shows the ability to down-regulate the expression of HIF-1α in ischemic mouse retina (Kim et al., 2016). On the other hand, peroxynitrite (PN; $ONOO^-$), may be involved in the mechanical allodynia and NMDA receptor-mediated central sensitization in the CPIP model (Kwak et al., 2014). Subsequently, *N*-acetyl-L-cysteine (NAC) or $ONOO^-$ decomposition catalysts prevent mechanical allodynia and decrease the phosphorylation of the NMDA spinal receptor (Kwak et al., 2011, 2014). In agreeing with the present result, a synergistic effect of the combination morphine and NAC, as well as potent analgesia by a bifunctional compound μ opioid agonist/antioxidant, have been demonstrated in CPIP rats (Schiller et al., 2015). In this regard, TCA has a large volume of pre-clinical and clinical evidence, which support the recommendation for its use as a first-line treatment for neuropathic pain (Finnerup et al., 2015). CPIP like CRPS-1 is characterized by the absence of evident nerve lesions (Coderre et al., 2004; Harden et al., 2010). However, the evaluation of anti-neuropathic drugs is rational since a reduced density of the sensory fiber terminal arbors in the epidermis similar to small-fiber neuropathy observed in CRPS-I patients has been described (Oaklander et al., 2006; Laferrière et al., 2008). Additionally, the ectopic discharge of sensory A-fibers and C-fibers traveling within ischemic and inflamed nerves in CPIP play a role in central sensitization (Coderre and Bennett, 2010). Interestingly, MG prevents sciatic nerve Wallerian degeneration, and in clinical settings, the association of *M. indica* extract formulations (containing 10–20% of MG) with amitriptyline improved dynamic mechanical allodynia in CRPS and zoster-associated pain patients (Garrido-Suárez et al., 2009, 2011, 2014).

It has been proposed that the progression from early to late stage CRPS-I reflects the evolving dominance of no-reflow over slow-flow in deep tissue capillaries. The same bases could underlie the transition from SMP to sympathetically independent pain (SIP) in CRPS-I (Coderre and Bennett, 2010). A long-term anti-allodynic effect of MG, even after its discontinuation was also observed, suggesting its utility for preventing the progression from early to late phases of CPIP. Possibly, protective effects against inflammation and vascular abnormalities by repeated treatment with MG from early stages could explicate this result. MG restored the redox balance and decreased IL-1β protein concentration in the ipsilateral paw muscles of CPIP rats. This ability of MG to increase the total antioxidant capacity and GSH, normalize MDA, and reduce a serum level of IL-1β was also previously reported in a gastric ulcer I/R model (Mahmoud-Awny et al., 2015). The rise of pro-inflammatory cytokines has been considered causative of the imbalance between endothelial NO and ET-1 in CRPS, which in turn inhibits eNOS activity and accelerates the transcription of preproendothelin-1 (Patel et al., 2002; Groeneweg et al., 2006). On the other hand, in smooth muscle, cytokines stimulate inducible nitric oxide synthase (iNOS) transcription, which promotes the formation of NO. Subsequently, its combination with superoxide form $ONOO^-$ increases oxidative damage and endothelial dysfunction (Alonso and Radomski, 2003). ET-1 and $ONOO^-$ also contribute to hyperalgesia in these conditions (Millecamps et al., 2010; Salvemini et al., 2011). In the present study, a reduction of local production of nitrites was observed. MG could restore the physiological balance between endothelial constitutive and inducible NOS in CPIP rats since this xanthone prevented tumor necrosis factor α (TNFα) or IL-1-induced NF-κB activation (Leiro et al., 2004). MG decreases iNOS mRNA and iNOS protein levels in inflammatory peritoneal macrophages, as well as TNFα, NO, and ROS production in several studies (García et al., 2002; Garrido et al., 2004). MG also inhibits IL-1β and iNOS expression in vascular smooth muscle cells (Beltran et al., 2004), besides enhanced eNOS, while reducing iNOS in the serum of rats under gastric I/R insult (Mahmoud-Awny et al., 2015). Inflammatory mechanisms associated with deep tissue nociceptor sensitization and ectopic discharge in sensory fibers could initiate and maintain central sensitization in CPIP (Coderre and Bennett, 2010). Several cytokines including IL-1, IL-6, and TNFα have been found in the spinal cord fluid, serum, and peripheral tissues of CRPS patients (Alexander et al., 2005). TNFα and IL-β have been implicated in mechanical hyperalgesia, as well as inducing long-term potentiation in the spinal dorsal horn via NF-κB in nerve-injured rats (Lin et al., 2007). Pro-inflammatory cytokines and ROS may induce glutamatergic dysfunction for inhibiting glial cells' ability to remove glutamate from the synaptic cleft (De Leo et al., 2006). Here, 13 days after I/R injury, an inversed correlation between paw-withdrawal threshold and spinal IL-1β protein was observed, while previously the role of muscle and spinal NF-κB in the development of mechanical allodynia in a CPIP model was demonstrated (de Mos et al., 2009). Further non-specific modulators of NF-κB including steroids used as a

reference in this study have been useful in animals and CRPS patients (Bianchi et al., 2006). Hence, the anti-allodynic effect of MG could be correlated with the inhibition of spinal IL-1β production.

CONCLUSION

The present results suggest that MG displays a transient anti-allodynic effect in CPIP model and any potential favorable interaction with agents that block sympathetic vasoconstriction or enhanced NO-dependent vasodilatation, opioids, and TCA, possibly by additive/or supra-additive mechanisms. However, an isobolographic analysis should be performed to define a functional interaction between them. This effect appears to be at least partially attributable to the opioid and α_2 adrenergic receptors. Its long-term anti-allodynic effect was related to the spinal and peripheral IL-1β decrease and resorting of redox status in the affected limb, suggesting that MG may be useful in CRPS-I patients with clinical relevance in both SMP and SIP.

AUTHOR CONTRIBUTIONS

BG-S provided ideas or concepts for the definition of intellectual context, particularly designed and performed the *in vivo* experiments in CPIP model, analyzed the data, wrote the paper, conceived and designed the project. GG revised the paper, contributed to writing and editing the manuscript, and the execution of project. MC-L performed the analgesic experiments. ZP-R performed the IL-1β determination by ELISA and wrote this method. ABM performed the analgesic experiments. ES performed the analgesic experiments. JG-F performed the redox biomarkers determination in ipsilateral muscles and contributed to execution of project. SF and RD-H supervised the study and contributed to execution of the project. All authors read and approved the final manuscript.

FUNDING

This study was financed by projects MINSAP No. 0808001 (Cuba), CAPES No. 120/2011 (Brazil), and FONDECYT No. 1130601 (Chile).

ACKNOWLEDGMENTS

The authors thank Prof. Fernando Cervero, Dr. André Laferrière, and Prof. Terence J. Coderre from the Department of Anesthesia, McGill University, Montreal, QC, Canada, who provided a Nitrile 70 Durometer O-ring and for their contribution to our knowledge about the CPIP model and other animal models of pain. Special thanks to Jorge Conde Garrido for the advice on the correct use of the English language.

REFERENCES

Alexander, G. M., Perreault, M. J., Reichenberger, E. R., and Schwartzman, R. J. (2007). Changes in immune and glial markers in the CSF of patients with Complex Regional Pain Syndrome. *Brain Behav. Immun.* 21, 668–676. doi: 10.1016/j.bbi.2006.10.009

Alexander, G. M., van Rijn, M. A., van Hilten, J. J., Perreault, M. J., and Schwartzman, R. J. (2005). Changes in cerebrospinal fluid levels of pro-inflammatory cytokines in CRPS. *Pain* 116, 213–219. doi: 10.1016/j.pain.2005.04.013

Alonso, D., and Radomski, M. W. (2003). The nitric oxide-endothelin-1 connection. *Heart Fail. Rev.* 8, 107–115. doi: 10.1023/A:1022155206928

Beerthuizen, A., Stronks, D. L., Van't Spijker, A., Yaksh, A., Hanraets, B. M., Klein, J., et al. (2012). Demographic and medical parameters in the development of Complex Regional Pain Syndrome type 1 (CRPS1): prospective study on 596 patients with a fracture. *Pain* 153, 1187–1192. doi: 10.1016/j.pain.2012.01.026

Beltran, A. E., Alvarez, Y., Xavier, F. E., Hernanz, R., Rodriguez, J., Núñez, A. J., et al. (2004). Vascular effects of the *Mangifera indica* L. extract (Vimang). *Eur. J. Pharmacol.* 499, 297–305. doi: 10.1016/j.ejphar.2004.07.073

Bianchi, C., Rossi, S., Turi, S., Brambilla, A., Felisari, G., and Mascheri, D. (2006). Long-term functional outcome measures in corticosteroid-treated Complex Regional Pain Syndrome. *Eura. Medicophys.* 42, 103–111.

Birklein, F., and Schlereth, T. (2015). Complex Regional Pain Syndrome—significant progress in understanding. *Pain* 156, S94–S103. doi: 10.1097/01.j.pain.0000460344.54470.20

Birklein, F., and Schmelz, M. (2008). Neuropeptides, neurogenic inflammation and Complex Regional Pain Syndrome (CRPS). *Neurosci. Lett.* 437, 199–202. doi: 10.1016/j.neulet.2008.03.081

Blaisdell, F. W. (2002). The pathophysiology of skeletal muscle ischemia and the reperfusion syndrome: a review. *Cardiovasc. Surg.* 10, 620–630. doi: 10.1016/S0967-2109(02)00070-4

Boehringer Mannheim (1987). Biochemica Information. A Revised Biochemical Reference Source. Enzymes for Routine. Berlin: Boehringer Mannheim.

Bonica, J. J. (ed.). (1990). "Causalgia and other reflex sympathetic dystrophies," in *The Management of Pain*, (Philadelphia, PA: Lea & Febiger), 220–243.

Bradford, M. M. (1976). A rapid and sensitive method for the quantitation of microgram quantities of protein utilizing the principle of protein dye binding. *Anal. Biochem.* 72, 248–254. doi: 10.1016/0003-2697(76)90527-3

Bruehl, S., Harden, R. N., Galer, B. S., Saltz, S., Backonja, M., and Stanton-Hicks, M. (2002). Complex Regional Pain Syndrome: are there distinct subtypes and sequential stages of the syndrome? *Pain* 95, 119–124. doi: 10.1016/S0304-3959(01)00387-6

Campos-Esparza, M. R., Sánchez-Gómez, M. V., and Matute, C. (2009). Molecular mechanisms of neuroprotection by two natural antioxidants polyphenols. *Cell Calcium* 45, 358–368. doi: 10.1016/j.ceca.2008.12.007

Chaplan, S. R., Bach, F. W., Progel, J. W., Chug, J. M., and Yaksh, T. L. (1994). Quantitative assessment of allodynia in the rat paw. *J. Neurosci. Methods* 53, 55–63. doi: 10.1016/0165-0270(94)90144-9

Coderre, T. J., and Bennett, G. J. (2010). A hypothesis for the cause of Complex Regional Pain Syndrome-type I (reflex sympathetic dystrophy): pain due to deep-tissue microvascular pathology. *Pain Med.* 11, 1224–1238. doi: 10.1111/j.1526-4637.2010.00911.x

Coderre, T. J., Xanthos, D. N., Francis, L., and Bennett, G. J. (2004). Chronic post-ischemia pain (CPIP): a novel animal model of Complex Regional Pain Syndrome -type I (CRPS-I; reflex sympathetic dystrophy) produced by prolonged hindpaw ischemia and reperfusion in the rat. *Pain* 112, 94–105. doi: 10.1016/j.pain.2004.08.001

Colucci, M., Maione, F., Bonito, M. C., Piscopo, A., Di Giannuario, A., and Pieretti, S. (2008). New insights of dimethyl sulphoxide effects (DMSO) on experimental *in vivo* models of nociception and inflammation. *Pharmacol. Res.* 57, 419–425. doi: 10.1016/j.phrs.2008.04.004

Cury, Y., Picolo, G., Gutierrez, V. P., and Ferreira, S. H. (2011). Pain and analgesia. The dual effect of nitric oxide in the nociceptive system. *Nitric Oxide* 25, 243–254. doi: 10.1016/j.niox.2011.06.004

Dar, A., Faizi, S., Naqvi, S., Roome, T., Zikr-ur-Rehman, S., Ali, M., et al. (2005). Analgesic and antioxidant activity of mangiferin and its derivatives: the

structure activity relationship. *Biol. Pharm. Bull.* 28, 596–600. doi: 10.1248/bpb.28.596

Das, J., Ghosh, J., Roy, A., and Sil, P. C. (2012). Mangiferin exerts hepatoprotective activity against D- galactosamine induced acute toxicity and oxidative/nitrosative stress *via* Nrf2-NFκB pathways. *Toxicol. Appl. Pharmacol.* 260, 35–47. doi: 10.1016/j.taap.2012.01.015

De Leo, J. A., Tawfik, V. L., and La Croix-Fralish, M. L. (2006). The tetrapartite synapse: path to CNS sensitization and chronic pain. *Pain* 122, 17–21. doi: 10.1016/j.pain.2006.02.034

de los Monteros-Zuñiga, A. E., Izquierdo, T., Quiñones-Bastidas, G. N., Rocha-González, H. I., and Godínez-Chaparrom, B. (2016). Anti-allodynic effect of mangiferin in neuropathic rats: involvement of nitric oxide-cyclic GMP-ATP sensitive K + channels pathway and serotoninergic system. *Pharmacol. Biochem. Behav.* 150–151, 190–197. doi: 10.1016/j.pbb.2016.10.007

de Mos, M., Laferrière, A., Millecamps, M., Pilkington, M., Sturkenboom, M. C. J. M., Huygen, F. J. P. M., et al. (2009). Role of NFκB in an animal model of Complex Regional Pain Syndrome–type I (CRPS-I). *J. Pain* 10, 1161–1169. doi: 10.1016/j.jpain.2009.04.012

Eisenberg, E., Shtahl, S., Geller, R., Reznick, A. Z., Sharf, O., Ravbinovich, M., et al. (2008). Serum and salivary oxidative analysis in Complex Regional Pain Syndrome. *Pain* 138, 226–232. doi: 10.1016/j.pain.2008.04.019

Erdelmeier, I., Gerard-Monnier, D., Yadan, J. C., and Chaudiere, J. (1998). Reactions of N-methyl-2-phenylindole with malondialdehyde and 4-hydroxyalkenals. Mechanistic aspects of the colorimetric assay of lipid peroxidation. *Chem. Res. Toxicol.* 11, 1184–1194. doi: 10.1021/tx970180z

Finnerup, N. B., Attal, N., Haroutounian, S., McNicol, E., Baron, R., Dworkin, R. H., et al. (2015). Pharmacotherapy for neuropathic pain in adults: a systematic review and meta-analysis. *Lancet Neurol.* 14, 162–173. doi: 10.1016/S1474-4422(14)70251-0

Fischer, S. G. L., Zuurmond, W. W. A., Birklein, F., Loer, S. A., and Perez, R. S. G. M. (2010). Anti-inflammatory treatment of Complex Regional Pain Syndrome. *Pain* 151, 251–256. doi: 10.1016/j.pain.2010.07.020

García, D., Delgado, R., Ubeira, F. M., and Leiro, J. (2002). Modulation of rat macrophage function by the *Mangifera indica* L. extract (Vimang) and mangiferin. *Int. Immunopharmacol.* 2, 797–806. doi: 10.1016/S1567-5769(02)00018-8

García-Rivera, D., Hernández-Balmaseda, I., Álvarez-León, A., Cancio-Hernández, B., Márquez-Montiel, L., Garrido-Garrido, G., et al. (2006). Anti-allergic properties of *Mangifera indica* L. extract (Vimang) and contribution of its glucosylxanthone mangiferin. *J. Pharm. Pharmacol.* 58, 385–392. doi: 10.1211/jpp.58.3.0014

Garrido, G., Delgado, R., Lemus, Y., Rodríguez, J., García, D., and Núñz-Selles, A. J. (2004). Protection against septic shock and suppression of tumor necrosis factor alpha and nitric oxide production on macrophages and microglia by a standard aqueous extract of *Mangifera indica* L. (Vimang®): role of mangiferin isolated from the extract. *Pharmacol. Res.* 50, 165–172. doi: 10.1016/j.phrs.2003.12.020

Garrido, G., González, D., Romay, C., Núñez-Selles, A. J., and Delgado, R. (2008). Scavenger effect of a mango (*Mangifera indica* L.) food supplement's active ingredient on free radicals produced by human polymorphonuclear cells and hypoxanthine–xanthine oxidase chemiluminescence systems. *Food Chem.* 107, 1008–1014. doi: 10.1016/j.foodchem.2007.09.012

Garrido-Suárez, B., Garrido, G., Delgado, R., Bosch, F., and Rabí, M. C. (2011). Case series in patients with zoster-associated pain using *Mangifera indica* L extract. *Forsch. Komplementmed.* 18, 345–350. doi: 10.1159/000335124

Garrido-Suárez, B., Rabí, M. C., Bosch, F., Garrido-Garrido, G., and Delgado-Hernández, R. (2009). Introducción de la suplementación con formulaciones vimang en el síndrome doloroso regional complejo: experiencia en 15 pacientes. *Rev. Soc. Esp. Dolor* 16, 87–96. doi: 10.1016/S1134-8046(09)70915-2

Garrido-Suárez, B. B., Garrido, G., Castro-Labrada, M., Merino, N., Valdés, O., Rodeiro, I., et al. (2014). Anti-hypernociceptive effect of mangiferin in persistent and neuropathic pain models in rats. *Pharmacol. Biochem. Behav.* 124, 311–319. doi: 10.1016/j.pbb.2014.06.019

Garrido-Suárez, B. B., Garrido, G., Delgado, R., Bosch, F., and Rabí, M. C. (2010). A *Mangifera indica* L. extract could be used to treat neuropathic pain and implication of mangiferin. *Molecules* 15, 9035–9045. doi: 10.3390/molecules15129035

Granger, D. L., Taintor, R. R., Boockvar, K. S., and Hibbs, J. B. Jr. (1995). Determination of nitrate and nitrite in biological samples using bacterial nitrate reductase coupled with the Griess reaction. *Methods* 7, 78–83. doi: 10.1006/meth.1995.1011

Groeneweg, G., Huygen, F. J. P. M., Coderre, T. J., and Zijlstra, F. J. (2009). Regulation of peripheral blood flow in Complex Regional Pain Syndrome: clinical implication for symptomatic relief and pain management. *BMC Musculoskelet. Disord.* 10:116. doi: 10.1186/1471-2474-10-116

Groeneweg, G., Huygen, F. J. P. M., Niehof, S. P., Wesseldijk, F., Bussmann, J. B. J., Schasfoort, F. C., et al. (2008). Effect of tadalafil on blood flow, pain, and function in chronic cold Complex Regional Pain Syndrome: a randomized controlled trial. *BMC Musculoskelet. Disord.* 9:143. doi: 10.1186/1471-2474-9-143

Groeneweg, J. G., Huygen, F. J. P. M., Heijmans-Antonissen, C., Niehof, S., and Zijlstra, F. J. (2006). Increased endothelin-1 and diminished nitric oxide levels in blister fluids of patients with intermediate cold type Complex Regional Pain Syndrome type 1. *BMC Musculoskelet. Disord.* 7:91. doi: 10.1186/1471-2474-7-91

Harden, R. N., Bruehl, S., Perez, R. S., Birklein, F., Marinus, J., Maihofner, C., et al. (2010). Validation of proposed diagnostic criteria (the "Budapest Criteria") for Complex Regional Pain Syndrome. *Pain* 150, 268–274. doi: 10.1016/j.pain.2010.04.030

Hsiao, H. T., Lin, Y. C., Wang, J. C., Tsai, Y. C., and Liu, Y. C. (2016). Hypoxia inducible factor-1α inhibition produced anti-allodynia effect and suppressed inflammatory cytokine production in early stage of mouse Complex Regional Pain Syndrome model. *Clin. Exp. Pharmacol. Physiol.* 43, 355–359. doi: 10.1111/1440-1681.12536

Huygen, F., Ramdhani, N., Van Toorenenbergen, A., Klein, J., and Zijlstra, F. J. (2004). Mast Cells are involved in inflammatory reactions during Complex Regional Pain Syndrome. *Immunol. Lett.* 91, 147–154. doi: 10.1016/j.imlet.2003.11.013

Izquierdo, T., de los Monteros-Zuñiga, A. E., Cervantes-Durán, C., Lozada, M. C., and Godínez-Chaparro, B. (2013). Mechanisms underlying the antinociceptive effect of mangiferin in the formalin test. *Eur. J. Pharmacol.* 718, 393–400. doi: 10.1016/j.ejphar.2013.08.004

Jäning, W., and Baron, R. (2003). Complex Regional Pain Syndrome: mystery explained? *Lancet Neurol.* 2, 687–697. doi: 10.1016/S1474-4422(03)00557-X

Jiang, D. J., Dai, Z., and Li, Y. J. (2004). Pharmacological effects of xanthones as cardiovascular protective agents. *Cardiovasc. Drug Rev.* 22, 91–102. doi: 10.1111/j.1527-3466.2004.tb00133.x

Kim, J. H., Kim, Y. C., Nahm, F. S., and Lee, P. B. (2017). The therapeutic effect of vitamin C in an animal model of Complex Regional Pain Syndrome produced by prolonged hindpaw ischemia-reperfusion in rats. *Int. J. Med. Sci.* 14, 97–101. doi: 10.7150/ijms.17681

Kim, S. J., Sung, M. S., Heo, H., Lee, J. H., and Park, S. W. (2016). Mangiferin protects retinal ganglion cells in ischemic mouse retina via SIRT1. *Curr. Eye Res.* 41, 844–855. doi: 10.3109/02713683.2015.1050736

Ko, F. N., Lin, C. N., Liou, S. S., Huang, T. F., and Teng, C. M. (1991). Vasorelaxation of rat thoracic aorta caused by norathyriol isolated from Gentianaceae. *Eur. J. Pharmacol.* 192, 133–139. doi: 10.1016/0014-2999(91)90079-6

Kwak, K.-H., Jung, H., Park, J. M., Yeo, J.-S., Kim, H., Lee, H. C., et al. (2014). A peroxynitrite decomposition catalyst prevents mechanical allodynia and NMDA receptor activation in the hind-paw ischemia reperfusion injury rats. *Exp. Ther. Med.* 7, 508–512. doi: 10.3892/etm.2013.1440

Kwak, K.-H., Lim, D. G., and Baek, W. Y. (2011). N-acetyl-L-cysteine attenuates ischemia/reperfusion injury–induced allodynia and N-methyl-D-aspartate receptor activation in rats. *Curr. Ther. Res. Clin. Exp.* 72, 216–227. doi: 10.1016/j.curtheres.2011.08.001

Laferrière, A., Abaji, R., Tsai, C.-Y., Ragavendran, J. V., and Coderre, T. J. (2014). Topical combinations to treat microvascular dysfunction of chronic postischemia pain. *Anesth. Analg.* 118, 830–840. doi: 10.1213/ANE.0000000000000141

Laferrière, A., Millecamps, M., Xanthos, D. N., Xiao, W. H., Siau, C., de Mos, M., et al. (2008). Cutaneous tactile allodynia associated with microvascular dysfunction in muscle. *Mol. Pain* 4:49. doi: 10.1186/1744-8069-4-49

Leiro, J., Arranz, J. A., Yáñez, M., Ubeira, F. M., Sanmartín, M. L., and Orallo, F. (2004). Expression profiles of genes involved in the mouse nuclear factor-kappa B signal transduction pathway are modulated by mangiferin. *Int. Immunopharmacol.* 4, 763–778. doi: 10.1016/j.intimp.2004.03.002

Levine, R. L., Wehr, N., Williams, J. A., Stadtman, E. R., and Shacter, E. (2000). Determination of carbonyl groups in oxidized proteins. *Methods Mol. Biol.* 99, 15–24.

Lin, Y. L., Zhou, L. J., Hu, N. W., Xu, J. T., Chang, Y. W., Zhang, T., et al. (2007). Tumor necrosis factor α induces long-term potentiation of C-fiber evoked field potentials in spinal dorsal horn in rats with nerve injury: the role of NF-kappa B, JNK and p38 MAPK. *Neuropharmacology* 52, 708–715. doi: 10.1016/j.neuropharm.2006.09.011

Lopes, S. C., da Silva, A. V., Rodriguez Arruda, B., Morais, T. C., Barros Rios, J., Trevisan, M. T., et al. (2013). Peripheral antinociceptive action of mangiferin in mouse models of experimental pain: role of endogenous opioids, KATP-channels and adenosine. *Pharmacol. Biochem. Behav.* 110, 19–26. doi: 10.1016/j.pbb.2013.05.016

Lowry, O., Rosebrough, N. J., Farr, A. L., and Randall, R. J. (1951). Protein measurement with the Folin phenol reagent. *J. Biol. Chem.* 193, 265–275.

Mahmoud-Awny, M., Attia, A. S., Abd-Ellah, M. F., and El-Abhar, H. S. (2015). Mangiferin mitigates gastric ulcer in ischemia/reperfused rats: involvement of PPAR-γ, NF-κB and Nrf2/HO-1 signaling pathways. *PLoS One* 10:e0132497. doi: 10.1371/journal.pone.0132497

Millecamps, M., and Coderre, T. J. (2008). Rats with chronic post-ischemia pain exhibit an analgesic sensitivity profile similar to human patients with Complex Regional Pain Syndrome-type I. *Eur. J. Pharmacol.* 583, 97–102. doi: 10.1016/j.ejphar.2008.01.006

Millecamps, M., Laferrière, A., Ragavendran, J. V., Stone, L. S., and Coderre, T. J. (2010). Role of peripheral endothelin receptors in an animal model of Complex Regional Pain Syndrome type 1 (CRPS-I). *Pain* 15, 174–183. doi: 10.1016/j.pain.2010.07.003

Moncada, S., Palmer, R. M., and Higgs, E. A. (1991). Nitric oxide: physiology, pathophysiology and pharmacology. *Pharmacol. Rev.* 43, 109–142.

Nilsson, H., Goldstein, M., and Nilsson, O. (1986). Adrenergic innervation and neurogenic response in large and small arteries and veins from the rat. *Acta Physiol. Scand.* 126, 121–133. doi: 10.1111/j.1748-1716.1986.tb07795.x

Núñez Sellés, A., Daglia, M., and Rastrelli, L. (2016). The potential role of mangiferin in cancer treatment through its immunomodulatory, anti-angiogenic, apoptopic, and gene regulatory effects. *Biofactors* 42, 475–491. doi: 10.1002/biof.1299

Núñez-Sellés, A., Velázquez-Castro, H., Agüero-Agüero, J., González-González, J., Naddeo, F., De Simone, F., et al. (2002). Isolation and quantitative analysis of phenolic antioxidants, free sugars, fatty acids and polyols from mango (*Mangifera indica* L.) stem bark aqueous decoction used in Cuba as nutritional supplement. *J. Agric. Food Chem.* 50, 762–766. doi: 10.1021/jf011064b

Oaklander, A. L., Rissmiller, J. G., Gelman, L. B., Zheng, L., Chang, Y., and Gott, R. (2006). Evidence of focal small-fiber axonal degeneration in Complex Regional Pain Syndrome-I (reflex sympathetic dystrophy). *Pain* 120, 235–243. doi: 10.1016/j.pain.2005.09.036

Pardo-Andreu, G. L., Barrios, M. F., Curti, C., Hernandez, I., Merino, N., Lemus, Y., et al. (2008). Protective effects of *Mangifera indica* L extract (Vimang), and its major component mangiferin, on iron-induced oxidative damage to rat serum and liver. *Pharmacol. Res.* 57, 79–86. doi: 10.1016/j.phrs.2007.12.004

Pardo-Andreu, G. L., Maurmann, N., Kellermann, G. R., de Farias, C. B., Schwartsmann, G., Delgado, R., et al. (2010). Mangiferin, a naturally glucoxilxanthone improves long-term object recognition memory in rats. *Eur. J. Pharmacol.* 635, 124–128. doi: 10.1016/j.ejphar.2010.03.011

Patel, J. N., Jager, A., Schalkwijk, C., Corder, R., Douthwaite, J. A., Yudkin, J. S., et al. (2002). Effects of tumour necrosis factor alpha in the human forearm: blood flow and endothelin-1 release. *Clin. Sci.* 103, 409–415. doi: 10.1042/cs1030409

Pérez, R. S. G. M., Zuurmond, W. W. A., Bezemer, P. D., Kuik, D. J., van Loenen, A. C., de Lange, J. J., et al. (2003). The treatment of complex regional syndrome type I with free radical scavengers: a randomized and controlled study. *Pain* 102, 297–307. doi: 10.1016/S0304-3959(02)00414-1

Pertovaara, A. (2013). The noradrenergic pain regulation system: a potential target for pain therapy. *Eur. J. Pharmacol.* 716, 2–7. doi: 10.1016/j.ejphar.2013.01.067

Plate, A. Y. A., Crankshaw, D. L., and Gallaher, D. D. (2005). The effect of anesthesia by diethyl ether or isoflurane on activity of cytochrome P4502E1 and P450 reductases in rat liver. *Anesth. Analg.* 101, 1063–1064. doi: 10.1213/01.ane.0000166791.30963.ef

Prado, Y., Merino, N., Acosta, J., Herrera, J. A., Luque, Y., Hernández, I., et al. (2015). Acute and 28-day subchronic toxicity studies of mangiferin, a glucosylxanthone isolated from *Mangifera indica* L. stem bark. *J. Pharm. Pharmacogn. Res.* 3, 13–23.

Ragavendran, J. V., Laferrière, A., Bennett, G. J., Ware, M. A., Gandhi, W., Bley, K., et al. (2016). Effects of topical combinations of clonidine and pentoxifylline on capsaicin-induced allodynia and postcapsaicin tourniquet-induced pain in healthy volunteers: a double-blind, randomized, controlled study. *Pain* 157, 2366–2374. doi: 10.1097/j.pain.0000000000000659

Ragavendran, J. V., Laferrière, A., Xiao, W. H., Bennett, G. J., Padi, S. S., Zhang, J., et al. (2013). Topical combinations aimed at treating microvascular dysfunction reduce allodynia in rat models of CRPS-I and neuropathic pain. *J. Pain* 14, 66–78. doi: 10.1016/j.jpain.2012.10.004

Raja, S. N., Treede, R. D., Davis, K. D., and Campbell, J. N. (1991). Systemic alpha-adrenergic blockade with phentolamine: a diagnostic test for sympathetically maintained pain. *Anesthesiology* 74, 691–698. doi: 10.1097/00000542-199104000-00012

Salvemini, D., Little, J. W., Doyle, T., and Neumann, W. L. (2011). Roles of reactive oxygen and nitrogen species in pain. *Free Radic. Biol. Med.* 51, 951–966. doi: 10.1016/j.freeradbiomed.2011.01.026

Schiller, P. W., Nguyen, T. M. D., Saray, A., Poon, A. W. H., Laferrière, A., and Coderre, T. J. (2015). The bifunctional μ opioid agonist/antioxidant [Dmt(1)] DALDA is a superior analgesic in an animal model of Complex Regional Pain Syndrome-type I. *ACS Chem. Neurosci.* 6, 1789–1793. doi: 10.1021/acschemneuro.5b00228

Sedlak, J., and Lindsay, R. H. (1968). Estimation of total, protein-bound, and non-protein sulfhydryl groups in tissue with Ellman's reagent. *Anal. Biochem.* 25, 192–205. doi: 10.1016/0003-2697(68)90092-4

Song, J., Li, J., Hou, F., Wang, X., and Liu, B. (2015). Mangiferin inhibits endoplasmic reticulum stress-associated thioredoxin-interacting protein/NLRP3 inflammasome activation with regulation of AMPK in endothelial cells. *Metabolism* 64, 428–437. doi: 10.1016/j.metabol.2014.11.008

Tang, C., Li, J., Tai, W. L., Yao, W., Zhao, B., Hong, J., et al. (2017). Sex differences in Complex Regional Pain Syndrome type I (CRPS-I) in mice. *J. Pain Res.* 10, 1811–1819. doi: 10.2147/JPR.S139365

Üçeyler, N., Eberle, T., Rolke, R., Birklein, T., and Sommer, C. (2007). Differential expression patterns of cytokines in Complex Regional Pain Syndrome. *Pain* 132, 195–205. doi: 10.1016/j.pain.2007.07.031

Vieira, A. B., Coelho, L. P., Insuela, D. B. R., Carvalho, V. F., dos Santos, M. H., Silva, P. M. R., et al. (2013). Mangiferin prevents guinea pig tracheal contraction via activation of the nitric oxide-cyclic GMP pathway. *PLoS One* 8:e71759. doi: 10.1371/journal.pone.0071759

Xanthos, D. N., Bennett, G. J., and Coderre, T. J. (2008). Norepinephrine-induced nociception and vasoconstrictor hypersensitivity in rats with chronic post-ischemia pain. *Pain* 137, 640–651. doi: 10.1016/j.pain.2007.10.031

Xanthos, D. N., and Coderre, T. J. (2008). Sympathetic vasoconstrictor antagonism and vasodilatation relieve mechanical allodynia in rats with chronic postischemia pain. *J. Pain* 9, 423–433. doi: 10.1016/j.jpain.2007.12.005

Yeo, J., Jung, H., and Lee, H. (2017). Effects of glutathione on mechanical allodynia and central sensitization in chronic postischemic pain rats. *Pain Res. Manag.* 2017:7394626. doi: 10.1155/2017/7394626

Zollinger, P. E., Tuinibreijer, W. E., Kreis, R. W., and Breederveld, R. S. (1999). Effects of vitamin C on frequency of reflex sympathetic dystrophy in wrist fractures: a randomised trial. *Lancet* 354, 2025–2028. doi: 10.1016/S0140-6736(99)03059-7

Conflict of Interest Statement: The authors declare that the research was conducted in the absence of any commercial or financial relationships that could be construed as a potential conflict of interest.

The handling Editor and reviewer GY declared their involvement as co-editors in the Research Topic, and confirm the absence of any other collaboration.

frontiers in Pharmacology

ORIGINAL RESEARCH
published: 10 October 2018
doi: 10.3389/fphar.2018.01143

Burst-Like Subcutaneous Electrical Stimulation Induces BDNF-Mediated, Cyclotraxin B-Sensitive Central Sensitization in Rat Spinal Cord

*Jeffri Retamal[1,2], Andrea Reyes[1], Paulina Ramirez[1,2], David Bravo[1,2], Alejandro Hernandez[1], Teresa Pelissier[3], Luis Villanueva[4] and Luis Constandil[1,2]**

[1] Laboratory of Neurobiology, Department of Biology, Faculty of Chemistry and Biology, University of Santiago de Chile, Santiago, Chile, [2] Center for the Development of Nanoscience and Nanotechnology (CEDENNA), Santiago, Chile, [3] Program of Molecular and Clinical Pharmacology, Institute of Biomedical Sciences, Faculty of Medicine, University of Chile, Santiago, Chile, [4] Centre de Psychiatrie et Neurosciences, INSERM UMR 894, Paris, France

Intrathecal administration of brain derived neurotrophic factor (BDNF) induces long-term potentiation (LTP) and generates long-lasting central sensitization in spinal cord thus mimicking chronic pain, but the relevance of these observations to chronic pain mechanisms is uncertain. Since C-fiber activation by a high-frequency subcutaneous electrical stimulation (SES) protocol causes spinal release of BDNF and induces spinal cord LTP, we propose that application of such protocol would be a sufficient condition for generating long-lasting BDNF-mediated central sensitization. Results showed that application of burst-like SES to rat toes produced (i) rapid induction of hyperalgesia that lasted for more than 3 weeks, (ii) early increase of C-reflex activity followed by increased wind-up scores lasting for more than 1 week, and (iii) early increase followed by late decrease in BDNF protein levels and phosphorylated TrkB that lasted for more than 1 week. These changes were prevented by the TrkB antagonist cyclotraxin-B administered shortly before SES, while hyperalgesia was reversed by cyclotraxin-B administered 3 days after SES. Results suggest that mechanisms underlying central sensitization first involve BDNF release of probably neuronal origin, followed by brief increased expression of likely glial BDNF and pTrkB that could switch early phase sensitization into late one.

Keywords: subcutaneous electrical stimulation, hyperalgesia, C-reflex, windup, brain-derived neurotrophic factor, cyclotraxin-B

OPEN ACCESS

Edited by:
Ramón Sotomayor-Zárate, Universidad de Valparaíso, Chile

Reviewed by:
James W. Grau, Texas A&M University, United States
Claudio Coddou, Universidad Católica del Norte, Chile

***Correspondence:**
Luis Constandil
luis.constandil@usach.cl

Specialty section:
This article was submitted to Translational Pharmacology, a section of the journal Frontiers in Pharmacology

Received: *28 June 2018*
Accepted: *21 September 2018*
Published: *10 October 2018*

Citation:
Retamal J, Reyes A, Ramirez P, Bravo D, Hernandez A, Pelissier T, Villanueva L and Constandil L (2018) Burst-Like Subcutaneous Electrical Stimulation Induces BDNF-Mediated, Cyclotraxin B-Sensitive Central Sensitization in Rat Spinal Cord. Front. Pharmacol. 9:1143. doi: 10.3389/fphar.2018.01143

INTRODUCTION

Chronic pain is characterized by its persistence in time even when the primary cause had already been resolved. It is causally related to a phenomenon called central sensitization characterized by hyperalgesia, allodynia, and expansion of receptive field, which mainly results, among other factors, from long-lasting increases in efficacy of synaptic communication between nociceptive afferent fibers and some specific dorsal neurons, termed long-term potentiation (LTP) (Latremoliere and Woolf, 2009; Sandkühler, 2009). LTP can typically be induced in some synapses of the hippocampus (Bliss and Lømo, 1973), cerebral cortex (Artola and Singer, 1987) or spinal cord

dorsal (Randic et al., 1993) horn by applying high-frequency electrical stimulation (e.g., 50–100 Hz) to corresponding presynaptic neurons. During persistent pain, LTP is assumed to be generated in dorsal horn synapses by a barrage of action potentials triggered from the injured peripheral tissue, which travels via nociceptive afferent C-fibers (Sandkühler, 2009). The increase in synaptic efficacy that defines the LTP process results from changes in phosphorylation and expression of some molecules in the spinal cord dorsal horn, as well as from the remodeling of specific neuronal circuits there (Latremoliere and Woolf, 2009; Sandkühler, 2009). In this context, inflammatory, neuropathic and other forms of chronic pain, are causally related to upregulation of a variety of pronociceptive mediators produced by neurons and glial cells in the spinal cord, i.e., glutamate (Kawamata and Omote, 1996; Andó and Sperlágh, 2013), ATP (Cui et al., 2014), cytokines (Whitehead et al., 2010), neurotrophins (Coull et al., 2005), which are accompanied by complex changes in dorsal horn expression of the corresponding receptors, i.e., glutamate, purinergic, cytokine, and BDNF receptors (Latremoliere and Woolf, 2009). In turn, intrathecal injection of these mediators to naïve animals can induce a behavioral pain response, but only the intrathecal injection of the neurotrophin BDNF and ATP has been found to produce a significant hyperalgesic status that is maintained for several weeks (Nakagawa et al., 2007; Constandil et al., 2011; Marcos et al., 2017).

The understanding of the specific role of each pronociceptive mediator in the initiation and maintenance of chronic pain is hindered by the fact that all the animal models used in chronic pain research produce variable degrees of peripheral tissue damage, which prevents the collection of reliable molecular, structural, functional, and behavioral information from the very beginning of pain elicitation, which is critical to differentiate the spinal mechanisms that initiate chronic pain (e.g., early LTP) from those involved in its maintenance (e.g., late LTP). Therefore, development of new experimental pain models of chronic pain devoid of peripheral lesion is a real need today. Here we propose the development of a new model of chronic pain in rat, devoid of peripheral lesion, based on the induction of spinal cord central sensitization by means of the application of a high-frequency subcutaneous electrical stimulation (SES) protocol to a rat hind paw, strong enough for activating nociceptive C-fibers, and to take advantage from this model to study the participation of BDNF in the initial stages of chronic pain. For this purpose, we conducted a long-term evaluation of the hyperalgesia developed in rats submitted to different burst-like SES protocols, as well as of the changes produced in nociceptive transmission properties in the spinal cord, using paw pressure testing and C-fiber-mediated reflex recording, respectively. By utilizing these experimental paradigms, we studied the effect of i.t. administration of the highly potent and selective allosteric TrkB antagonist cyclotraxin-B (CTX-B) (Cazorla et al., 2010), in order to give insights on the participation of the BDNF neurotrophin on the early and/or late neuroplastic mechanisms underlying spinal cord sensitization. Finally, the ability of burst-like SES to overexpress BDNF levels and to phosphorylate TrkB in lumbar spinal cord, as well as the susceptibility of these changes to CTX-B administration, were also studied using ELISA methods. The rats used were additionally studied regarding the potential capacity of high-frequency SES to produce peripheral lesion at the site of application, which is the main unwanted factor of experimental chronic pain models existing today during exploration of central sensitization mechanisms.

MATERIALS AND METHODS

Animals

Adult male Sprague–Dawley rats (200–220 g) were purchased from the Animal Facility Centre of the Faculty of Medicine, University of Chile, and maintained in a controlled environment (12 h light/dark cycles and ambient temperature of 22°C) with food and water freely available. The animals were housed 3 to 4 per cage on a wood chip litter. All efforts were made to minimize the number of animals used. The experiments were performed in agreement with the Guide for the Care and Use of Laboratory Animals of NIH (National Research Council, 2011), Pain and Laboratory Animals: Publication Practices for Better Data Reproducibility and Better Animal Welfare (Carbone and Austin, 2016), and were approved by the local institutional Bioethics Committee of the University of Santiago of Chile (C-589). To perform the determinations required in the study, all the investigators were blinded to the experimental conditions. To determine the number of required rats, we use G*Power 3 Software (Faul et al., 2007) for conducting sample size power analysis.

High-Frequency Subcutaneous Electrical Stimulation (SES)

The rats were anesthetized with 2.5% isoflurane/97.5% O_2 (Sigma, St. Louis, MO, United States) employing a latex diaphragm-modified rodent facemask, and stimulated electrically with high-frequency SES through a pair of steel electrodes subcutaneously placed in the fourth and fifth toes of the right hind paw. Three different high-frequency SES protocols were initially used: Protocol 1: 1-s pulse trains applied every 10 s during a 3-min period, each train composed by rectangular pulses of 1 ms and 7 mA intensity, at 100 Hz; this current intensity is slightly over the threshold current required for subcutaneous activation of C-fibers as calculated from the C-reflex study (see below); Protocol 2: similar to protocol 1, but applied during 20 min; Protocol 3: similar to protocol 1, but repeating the high-frequency SES after a 10-min interval. This last protocol produced reliable hyperalgesia beginning 1 h after SES application and lasting for more than 21 days, and was selected to be used for the remainder of the study (SES group). To explore the specificity of the hyperalgesic response to pulse frequency and current intensity used in protocol 3, two other pulse frequencies of 50 and 10 Hz were tested while maintaining the 7-mA current (50 Hz 7 mA and 10 Hz 7 mA groups); in addition, two other constant currents of 5 and 3 mA were tested but now maintaining the original 100 Hz frequency (100 Hz 5 mA and 100 Hz 3 mA groups). All the variants of the high-frequency SES utilized were generated with a S88

Grass stimulator, associated to a SIU5 Grass stimulus isolator unit and to a CCU1 Grass constant current unit (all from Astro-Med, Inc., West Warwick, RI, United States). Control rats were also anesthetized and the electrodes subcutaneously inserted into the toes, but no electrical stimulation was applied (SES-sham group). Once the different SES or SES-sham protocols were applied, the stimulating electrodes utilized for that purpose were removed.

Mechanical Nociception Test

The paw pressure test was used to evaluate the threshold for mechanical nociception in SES-treated and SES-sham rats. The test consisted of the progressive application of a uniformly increasing pressure over the right hind paw using an Analgesy Meter (Ugo Basile, Italy), until a withdrawal reflex come on. To avoid injury, a cut-off value of 480 g was used. The mechanical nociception was evaluated before applying the high-frequency SES protocol, and 1 h and 1, 3, 7, 14, and 21 days post-SES protocol. Because induction of hyperalgesia in one paw sometimes leads to bilateral hyperalgesia, the mechanical thresholds of the paw ipsilateral and contralateral to the SES protocol were initially evaluated. Because no significant changes were found in the mechanical threshold in the contralateral leg, only the ipsilateral leg was tested for the remaining of the study.

Protein Extraction and Quantification of BDNF and pTrk-B

L3–L5 spinal cord segments extracted were kept on ice, homogenized (Tissue Tearor model 985370, Biospec Products, Inc., United Kingdom) in lysis buffer (9803S, Cell Signaling Technology, Danvers, MA, United States) containing 1× sodium orthovanadate and 1× Roche complete protease inhibitor cocktail, and centrifuged at 7000 rpm (Hettich, universal model 320R, Tuttlingen, Germany) at 4°C for 15 min. The protein concentration was determined by the bicinchoninic acid method (BCA) using the kit BCA Protein Assay through a colorimetric reaction quantified in an FC multiskan ELISA reader (Thermo Fisher Scientific, Barrington, IL, United States). BSA curve was used as a standard to quantify the total protein concentration. Measurements were made at an absorbance of 562 nm.

Quantification of BDNF and pTrk-B was performed by ELISA according to manufacturer specifications. BDNF protein was quantified using the ELISA E_{max} Immunoassay System (Promega, Madison, WI, United States), while for quantifying pTrkB the ELISA test PathScan® Phospho-TrkB (panTyr) (Cell Signaling Technology, Danvers, MA, United States) was used. In our experience, BDNF concentrations determined with ELISA are in a similar range to those detected by Western blot method.

C-Reflex and Wind-Up Recording

The electromyographic (EMG) activity associated to the hind limb-flexion nociceptive reflex evoked by activation of C fibers of the sural nerve (C-reflex) was studied by using the method described by Falinower et al. (1994). All the procedures were performed on rats anesthetized with 0.8% isoflurane/99.2% O_2 and placed on a homoeothermic blanket system (37 ± 0.5°C). Briefly, a pair of uncoated platinum low profile needle electrodes was inserted subcutaneously into the lateral part of the third and fourth toes. The electrical stimuli, consisting of single rectangular shocks of 1-ms duration with 2-time the current intensity required to elicit a threshold C-reflex, were delivered at 0.1 Hz from a Grass stimulator S11 associated with a SIU5 Grass stimulus isolator unit and to a CCU1 Grass constant current unit. The EMG responses were recorded via another pair of platinum electrodes inserted through the skin into the ipsilateral biceps femoris muscle. The responses were amplified with a Grass P511 preamplifier (Astro-Med, Inc., West Warwick, RI, United States), and digitized at 4 KHz and integrated into a 150–450 ms post-stimulus time window using a PowerLab 2/20 (ADInstruments, Castle Hill, NSW, Australia) connected to a IMAC computer (Apple INC, CA, United States). Plotting integrated C-reflex responses versus increasing stimulus intensities allowed detecting the C-fiber threshold current intensity in naïve rats (6.5 ± 0.3 mA) by linear regression procedure. C-reflex data was recorded as averages of 15 consecutive windows of integrated C-reflex (stimulation at 0.1 Hz, 2 × threshold current intensity). To study the potentiation of C-reflexes to repetitive stimulation, known as wind-up, the stimulating frequency was incremented to 1 Hz while maintaining the 2 × threshold current intensity. The wind-up was evaluated by using data only from the first seven consecutive windows, which show incremental trend, and calculated as the slope of the regression line fitted to these seven-point data. CTX-B or saline was i.t. injected prior to applying the high-frequency SES or the sham protocol and the C-reflex and wind-up followed for 30, 60, 90, and 120 min. Afterward, the stimulating and recording electrodes were removed and the rat returned to its cage. Seven days after, C-reflex and wind-up studies were repeated on the same animals, and thereafter the rats were sacrificed by means of an overdose of isoflurane.

Inhibition of TrkB Receptor

CTX-B, manufactured as Tat-cyclotraxin-B (Bio S & T, Montreal, QC, Canada), was dissolved in saline and administered intrathecally as a single dose of 40 μg/kg, in a 10 μl volume. CTX-B was administered preventively, 90 min before the application of the high-frequency SES protocol (n = 6), and curatively 3 days after application of high-frequency SES (n = 6), according to Constandil et al. (2012). Both groups were evaluated daily for 7 days. On day 7, after the last algesimetric measurement, the animals were sacrificed by an overdose of anesthesia and the lumbar spinal cord (L3–L5 segments) was removed for proteins analysis.

Evaluation of Safety of the High-Frequency SES Protocols in Animals

To study whether the SES protocols produce or not inflammation in the rat's right hind paw, increase in volume, flushing, temperature were determined in the hind paw prior and 10

and 60 min after the application of the high-frequency SES protocols, by means of Vernier caliper, visual inspection and a contact thermistor thermometer applied on the skin surface of the paw, respectively. In addition, plasma extravasation of Evans blue dye in the stimulated hind paw was also determined using a modification of the technique described by Gonzalez et al. (2005). Briefly, 50 mg/kg of Evans blue dye was injected into a tail vein of the rat 10 min before application of SES to the hind paw, and serial images of the paw were recorded with a Sony WX500 digital camera prior and 10 and 60 min after the application of the high-frequency SES protocol. Extravasated dye was evaluated through change in light reflectance (8 bit 0–255 scale) by measuring the mean value of pixels included in a 5 mm × 5 mm square region of the dorsomedial part of the stimulated hind paw, by using the Fiji image processing package (Laboratory for Optical and Computational Instrumentation, University of Wisconsin–Madison, Madison, WI, United States).

Data Analysis

The results were expressed as means ± SEM and analyzed with the statistical software GraphPad Prism 6.0 (GraphPad Software Inc., San Diego, CA, United States). To assess the time-course of changes induced by the high-frequency SES protocol, analyses were performed by comparing pre and post-treatment scores using the Kruskal–Wallis test followed by the *post hoc* Dunn's multiple comparisons test. Non-parametric statistics was chosen because animal groups were composed by six rats, a sample size that usually not allows to demonstrate a Gaussian distribution of data group. The GraphPad Prism 6.0 was used to calculate area under curves and slopes of linear regression fitting in the wind-up study. In all comparisons, statistical significance was established at $p < 0.05$.

RESULTS

High-Frequency SES Induced Long-Lasting Hyperalgesia in the Rat

As shown in **Figure 1**, the SES-sham group exhibited no significant change in the paw pressure threshold during the 21 days of the study, indicating that the mere subcutaneous insertion of the stimulating electrodes under the skin of toes does not significantly modify the nociceptive threshold to subsequent mechanical nociceptive testing of rats. In contrast, all groups receiving high frequency SES showed a significant decrease of the paw pressure threshold during variable time intervals, depending on the protocol used. In the group receiving the SES protocol 1 (3-min stimulation, 7 mA, 100 Hz), the paw pressure threshold decreased on day 3 post-stimulation and remained significantly decreased until day 10, as compared to the basal value obtained prior to electrical stimulation (**Figure 1A**). In the group receiving the SES protocol 2 (20-min stimulation, 7 mA, 100 Hz), the paw pressure threshold remained significantly decreased since day 1 post-stimulation until day 3, compared to the basal value (**Figure 1A**); the experiment was stopped on day 3 and the rats ($n = 2$) euthanized because the paw showed an electrical burn injury. In the group stimulated with protocol 3 (2 × 3-min stimulation, 7 mA, 100 Hz), the paw pressure threshold decreased since 1 h post-SES until to the end of the experiment on day 21 post-SES (**Figure 1A**). Animals subjected to this protocol (SES group) showed no visible injury in the area stimulated. Furthermore, none of the signs associated with inflammation (increase in volume, flushing, increased temperature, and plasma extravasation) were observed in the hind paw of these animals 10 min or 1 h post-SES (**Table 1**). However, we cannot totally rule out that there has been some subtle alteration in the stimulated paw of the SES group that was not detected by our inflammatory assays.

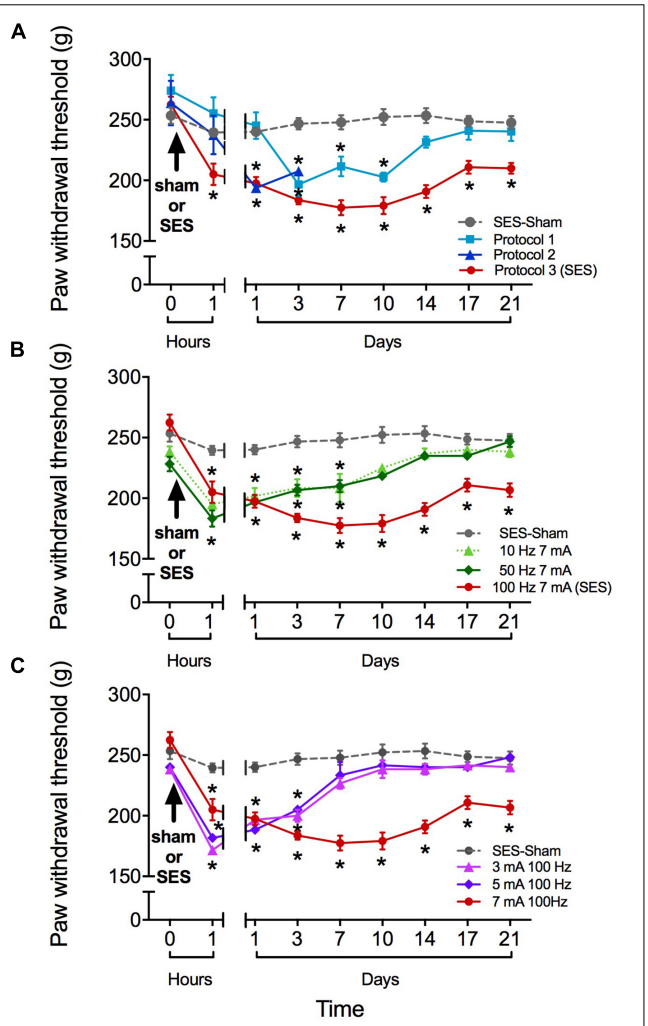

FIGURE 1 | Paw pressure threshold of rats submitted to different high-frequency SES protocols. **(A)** SES-sham protocol and three high frequency protocols. Protocol 1: 100 Hz, 7 mA, 3 min; Protocol 2: 100 Hz, 7 mA, 20 min; Protocol 3 (SES): 100 Hz, 7 mA, 3 min*2. **(B)** SES-sham protocol and 10 Hz, 7 mA; 100 Hz, 50 Hz, 7 mA and 7 mA (SES). **(C)** SES-sham protocol and 3 mA, 100 Hz; 5 mA, 100 Hz and 7 mA, 100 Hz (SES). Values are mean ± SEM ($n = 6$ rats per group). Asterisks indicate a significant intragroup difference (*$p < 0.05$) when post-SES values were compared with the pre-SES score at time zero (Kruskal–Wallis test followed by the *post hoc* Dunn's multiple comparisons test).

TABLE 1 | Inflammatory parameters measured in animals submitted to the high-frequency SES protocol.

Stimulated hind paw	Previous SES	Ten minutes post-SES	One hour post-SES
Temperature (°C)	31.1 ± 0.8	31.31 ± 0.6	31.5 ± 0.5
Skin color	Normal	Normal	Normal
Hind paw thickness (mm)	4.9 ± 1.0	4.8 ± 2.1	4.8 ± 2.6
Plasma extravasation	83.7 ± 6.3	92.1 ± 8.4	87.9 ± 8.3

Values are mean ± SEM (n = 6 rats per group). No significant differences between previous basal and 10 min or 1 h post-SES values were found (Kruskal–Wallis test).

Reduction in SES frequency to 50 or 10 Hz (but maintaining the 7-mA current intensity) resulted in a less lasting effect of SES, since in these conditions the decrease in mechanical nociceptive threshold only lasted for 7 days (**Figure 1B**). Alternatively, reduction of SES current intensity to 5 or 3 mA (but maintaining the 100-Hz frequency of stimulation) led to a decrease of the mechanical nociceptive threshold that lasted for only 3 days (**Figure 1C**).

High-Frequency SES Induced Biphasic Effects in BDNF Expression and TrkB Phosphorylation in Rat Lumbar Spinal Cord

The high-frequency SES applied to the hind paw modified in a biphasic manner the BDNF concentration in the lumbar spinal cord. Initially, at 6 h post-stimulation, the BDNF expression level increased by 42% with respect to the basal level. At 12 and 24 h post-SES the BDNF levels were similar to the basal one, whereas at days 3 and 7 post-stimulation the BDNF expression levels were significantly lower (around 50% decrease) than the basal level (**Figure 2A**). The concentration of pTrkB in lumbar segments of the spinal cord also presented a biphasic variation, but with a phase shift of the peak of 6 h. Indeed, pTrkB levels were significantly higher 12 h after SES stimuli, while showing a significant decrease 3 and 7 days after the electrical stimuli compared to the basal measure prior to SES (**Figure 2B**).

Intrathecal Cyclotraxin-B Prevented and Reversed Mechanical Hyperalgesia and the Late Decrease in Lumbar Spinal Cord Expression Levels of BDNF and pTrkB Induced by High-Frequency SES

CTX-B, administered i.t. 90 min before SES, prevented the decrease in paw pressure threshold produced by the SES while saline did not (**Figure 3A**). In agreement, in animals receiving pre-SES injection of CTX-B, the expression levels of BDNF (**Figure 4A**) and pTrk-B (**Figure 4B**) found in lumbar spinal segments on day 7 post-SES were not significantly different to those found in SES-sham animals. CTX-B administered i.t. 3 days post-SES significantly reverted the decrease in paw pressure threshold produced by the high-frequency SES protocol, the paw withdrawal threshold on day 7 being returned to the pre-SES score (**Figure 3B**). Intrathecal CTX-B, given on day 3 post-SES, prevented the late decrease in BDNF and pTrk-B expressions, as on day 7 post-SES these animals did not show significant differences in expression levels of the transcripts with respect to corresponding levels found in the SES-sham group (**Figures 4A,B**, respectively).

High-Frequency SES Induced Differential Short- and Long-Term Increments of Nociceptive Transmission in Rat Spinal Cord: Preventive Effect of CTX-B

Animals subjected to the high-frequency SES protocol showed increased integrated C-reflex activity 60 min following SES, as related to the pre-SES baseline value, which attained statistical significance upon 120 min post-SES (**Figure 5A**). In these animals, the integrated C-reflex responses returned to basal values 7 days after application of the SES protocol. No significant changes were observed in the time-course of the C-reflex response in animals subjected to the SES-sham protocol (**Figure 5A**). Since C-reflex responses, unlike

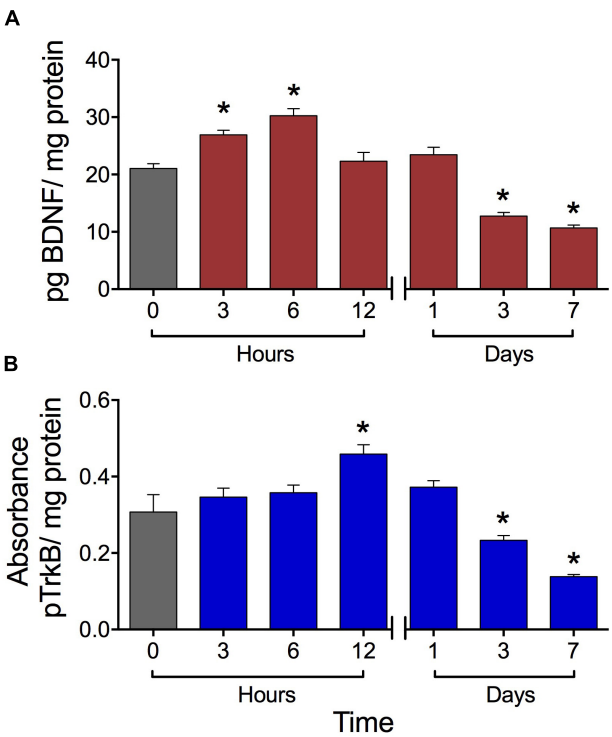

FIGURE 2 | Expression levels of BDNF **(A)** and pTrkB **(B)** in the L3–L5 laminae of dorsal lumbar spinal cord of rats submitted to the high-frequency SES protocol. Values are means ± SEM (n = 6 rats per group). BDNF and pTrkB were measured with ELISA test. The BDNF was expressed as pg BDNF/mg protein due to the absorbance was compared with a concentration reference curve, while that for pTrkB we have a not a reference curve. Asterisks show a significant difference (*$p < 0.05$) respect to time zero (black bar) (Kruskal–Wallis test followed by the *post hoc* Dunn's multiple comparisons test).

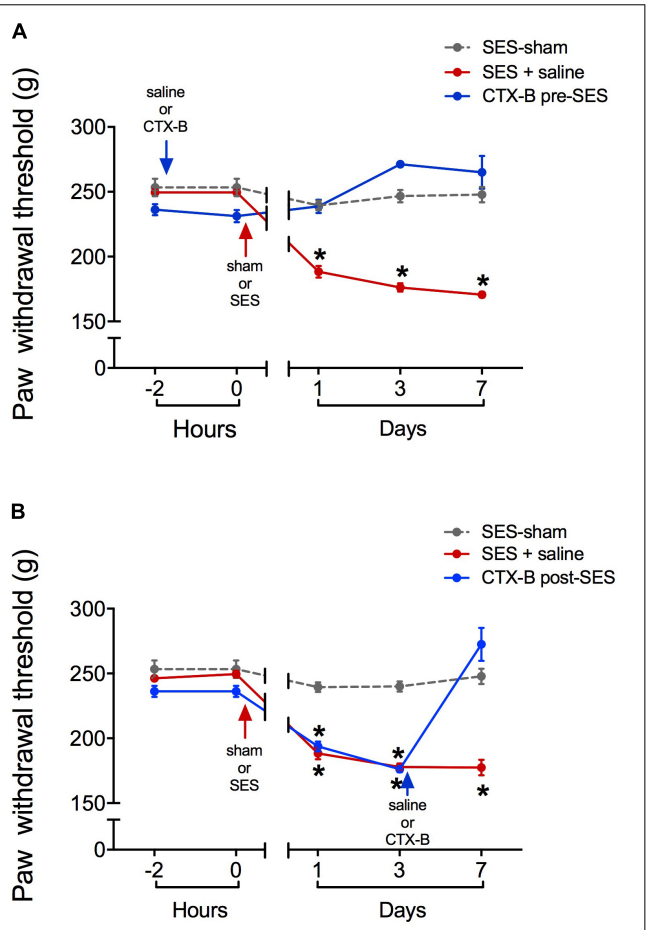

FIGURE 3 | Antagonistic effects of CTX-B upon high-frequency SES induced-hyperalgesia, as revealed by paw pressure thresholds. **(A)** CTX-B or saline was administered 90 min before SES (CTX-B SES-sham, CTX-B pre-SES), **(B)** CTX-B or saline was administered 3 days after SES (CTX-B SES-sham and CTX-B post-SES). Values are means ± SEM (n = 6 rats per group). Asterisks indicate a significant intragroup difference (*$p < 0.05$) when post-SES scores were compared with the pre-SES score (time 0) (Kruskal–Wallis test followed by the *post hoc* Dunn's multiple comparisons test).

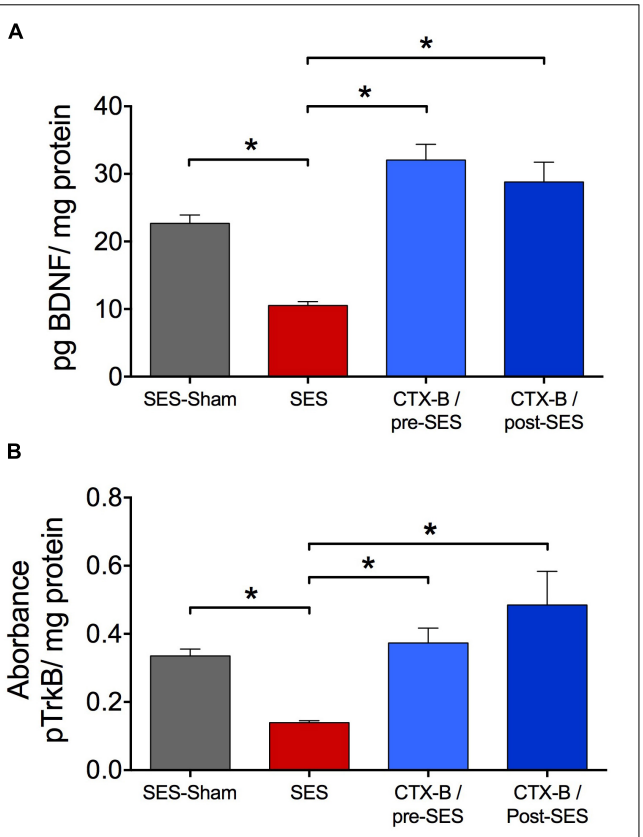

FIGURE 4 | Antagonistic effects of CTX-B upon high-frequency SES induced-decreased in the expression levels of both BDNF **(A)** and pTrkB **(B)** on day 7 after SES. Values are means ± SEM (n = 6 rats per group). Asterisks indicate a significant intergroup difference (*$p < 0.05$, Kruskal–Wallis test followed by the *post hoc* Dunn's multiple comparisons test).

mechanical hyperalgesia, returned spontaneously to basal values 7 days after application of the SES protocol, the antagonistic effect of CTX-B administered post-SES on the integrated C-reflex was not tested.

Wind-up scores did not change along the 210-min period of recording after applying the high-frequency SES protocol, as related to baseline scores obtained prior to SES application. However, on day 7 after SES, wind-up activity was significantly increased with respect to pre-SES scores (**Figure 5B**), which is indicative of a late neuroplastic event. No significant changes were observed throughout the experiment in C-reflex wind-up scores from animals subjected to the sham-SES protocol (**Figure 5B**).

Administration of CTX-B 90 min before the application of the high-frequency SES protocol prevented the increase in C-reflex activity elicited by SES (**Figure 5A**). CTX-B administered prior to SES also prevented the late increase of wind-up scores (**Figure 5B**).

DISCUSSION

We found that application of a high-frequency SES protocol, strong enough to activate C-fibers in the nociceptive afferent pathway, is a sufficient condition for generating long-lasting central sensitization in naïve animals, as revealed by (i) rapid induction of hyperalgesia that lasted for more than 3 weeks, (ii) early increase of integrated C-reflex activity followed by increased wind-up scores lasting for more than 1 week, and (iii) early increase in the levels of BDNF protein and phosphorylated TrkB, followed by late decreased levels of both molecular markers that lasted for more than 1 week. All these changes were prevented by intraperitoneal administration of CTX-B before SES, and intrathecal injection of CTX-B 3 days after SES also was effective to reverse the hyperalgesia induced. The SES protocol used did not generate noticeable injury in peripheral tissue, as revealed by unchanged values either in volume, flushing, temperature, or plasma extravasation of the stimulated hind paw.

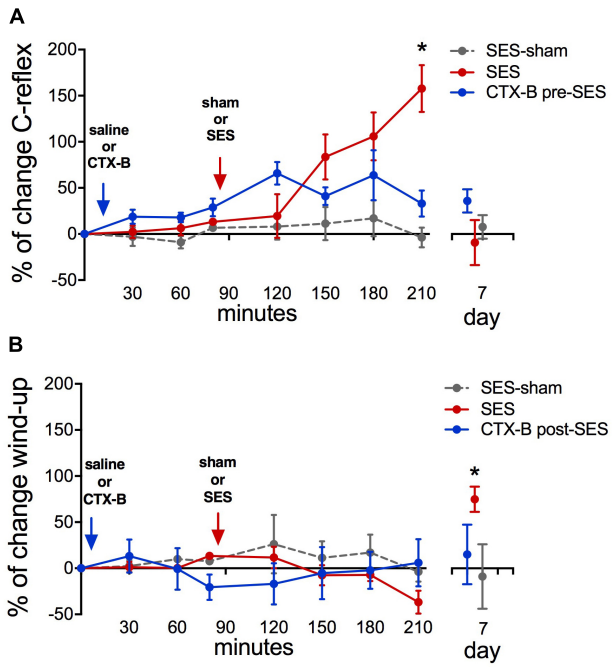

FIGURE 5 | Percent of change in C-reflex activity **(A)** and wind-up score **(B)** after applying the high-frequency SES protocol and the effects of CTX-B administered 90 min before SES. Values are means ± SEM (n = 6 rats per group). Asterisks indicate a significant intragroup difference when post-SES scores were compared with the pre-SES value (*$p < 0.05$, Kruskal–Wallis test followed by the *post hoc* Dunn's multiple comparisons test).

Nociceptive sensitization induced by peripheral electric stimulation was first demonstrated by Woolf and Wall (1986), who showed that low frequency (2 Hz) conditioning electrical stimuli at an intensity sufficient to activate C-afferent fibers result in a short-term (3 h) heterosynaptic facilitation of the flexor motoneuronal response in anesthetized decerebrate spinal rat. Later, other authors showed that low-frequency electric stimulation (10 Hz) of peripheral C-fibers evoked a longer (48 h) but still short, central sensitization to mechanical stimuli in awake behaving rats (Hathway et al., 2009). Thus, low-frequency stimulation of peripheral C-fibers does not mimic the temporal profile of pain observed in most animal models of chronic pain, which persists quite stable for more than 15 days. Here, we showed that a 3-min series of high-frequency electric stimulation at 100 Hz, applied at 7 mA to the rat hind paw, which is slightly over the threshold current required for subcutaneous activation of C-fibers, produced heterotopic mechanical hyperalgesia that persisted for 1 week. Moreover, upon repetition of the series 10 min after, the hyperalgesic status was prolonged for at least 3 weeks. Such an enduring hyperalgesia is quite similar to that found in preclinical models of chronic pain, at least in terms of time-course and stability of the central sensitization process. In humans, repeated electrical stimulation of the skin with trains of 100 Hz at 10–20 × individual detection threshold, which supposedly targeted peptidergic C-fibers, produced a gradual increase in both the homotopic and heterotopic pain, which persisted for about 200 min (Klein et al., 2004), thus providing a link between the present results and clinical observations concerning the hyperalgesic effect of high-frequency stimulation protocols. Central sensitization can also be triggered by natural stimuli applied to the skin such as mechanical, thermal, or by irritating reactive chemicals, but also by a variety of mediators released in injured tissue, such as ATP, cytokines, and neurotrophins (Sandkühler, 2009). However, the major advantages of electrical stimulation over any other types of stimulation are brevity and strict control in time of stimulus onset, cut-off, frequency, pulse pattern, and duty cycle, as well as the absence of peripheral injury and associated peripheral sensitization phenomena. It is worthy to note that in spite of no plasma extravasation and edema were observed in the stimulated hind paw during the course of the present experiments, there is older data showing that antidromically activated C afferents could lead to peripheral release of neuropeptides that could result in vasodilation and plasma extravasation in the skin (Gee et al., 1997; Hathway et al., 2009), which are key components of neurogenic inflammation. Nevertheless, it has been reported that unlike neurogenic inflammation produced by capsaicin, mustard oil or histamine, antidromic electrical stimulation of C-fibers did not evoke spontaneous activity in the polymodal fibers tested nor did it markedly affect their mechanical and thermal excitability in periods of up to 1 h after stimulation (Reeh et al., 1986), thereby indicating absence of peripheral sensitization. Further, the literature shows that the time-course of symptoms (vasodilation, plasma extravasation, or edema) for the electrically evoked, C-fiber mediated neurogenic inflammation did not last for more than 1 h (Gee et al., 1997; Nakagawa et al., 2007; Hathway et al., 2009) and, therefore, they can be ruled out as factors involved in the more lasting central effects produced by the SES protocol.

Ying et al. (2006) generated bilateral mechanical allodynia in the rat hind paw by using a pair of stainless-steel hooks for direct electrical stimulation of the exposed sciatic nerve with 30 Volt pulses (100 Hz, 20 trains of 2 s duration at 10 s intervals). Without proper control of the stimulating current intensity, this procedure may provide a very strong current that will flow through across the entire nerve and, as discussed by Ying et al. (2006), a slight degeneration of some myelinated and unmyelinated fibers in the sciatic nerve was observed under an electronic microscope which might lead to activate peri-sciatic immune cells. As reported elsewhere, bilateral allodynia can be created in rats by microinjection of immune activators around one healthy sciatic nerve, where intense immune activation produces bilateral allodynia, while low level immune activation produces allodynia only in the microinjected side (Milligan et al., 2003). In some initial experiments, we also included testing of the mechanical threshold of the hind paw contralateral to the applied SES. Unlike the ipsilateral hind paw, no hyperalgesia could be demonstrated in the contralateral one (results not shown).

Central sensitization in the spinal cord has been linked to immediate-onset, transcription-independent, NMDA receptor-mediated mechanisms, such as LTP (Sandkühler, 2009), and afterward maintained by a late-onset, transcription-dependent mechanism that include ERK signaling to the nucleus and

subsequent phosphorylation of CREB, with increased expression of early genes codifying for c-fos, COX_2 and the neurotrophin BDNF, as well as for other late response genes (Latremoliere and Woolf, 2009). In the spinal cord, early-phase LTP could be rapidly induced (within minutes) as an activity-dependent regulated process virtually by any type of high-frequency burst-like stimulation at C-fiber intensity, without requiring of protein synthesis (Sandkühler, 2009). The reduced paw pressure threshold and the increased C-reflex activity detected 1 to 2 h following SES, short before BDNF and pTrkB upregulation, are most likely the behavioral consequence of the development of an early-onset, activity-dependent, LTP-based, central sensitization process. Furthermore, since the changes induced by SES in paw pressure threshold and C-reflex activity were prevented by administration of CTX-B, a drug that is unable to modify the nociceptive thresholds in normal non-sensitized mice (Constandil et al., 2012), it is likely that the whole process was triggered by the release of BDNF from primary afferents due to SES. This interpretation is supported by the following observations: (i) high-frequency SES, but not low-frequency SES, of afferent sensory nerves at C-fiber intensity causes spinal release of BDNF (Lever et al., 2001); (ii) intrathecal injection of BDNF produces CTX-B-sensitive enduring mechanical hyperalgesia in rats, which imitates that induced by high-frequency SES (M'Dahoma et al., 2015); (iii) full-length TrkB receptors were present at somato-dendritic membranes of lamina II neurons in the rat and mouse dorsal horn (Salio et al., 2005); (iv) binding of BDNF to the TrkB receptor regulates neural response and synaptic function in the dorsal horn output neurons through a variety of neuroplasticity mechanisms, including increased phosphorylation of NMDA receptor subunits NR1 (Slack et al., 2004; Liu et al., 2015) and NR2B (Peng et al., 2012; Ding et al., 2015; Li et al., 2017); (v) activation of NMDA receptors downstream to TrkB signaling is essential for behavioral expression of the mechanical hyperalgesia induced by intrathecal BDNF (Marcos et al., 2017). It is then conceivable that BDNF released by C-fibers during SES application rapidly facilitates the induction of NMDA-dependent early-phase LTP in the spinal cord thereby leading to central sensitization, as reflected by the lower paw pressure threshold and the increased C-reflex activity. This effect in spinal cord parallels BDNF-dependent postsynaptic LTP induced in the hippocampus either by long-lasting high-frequency (Chen et al., 1999) or by repeated theta burst (Kang et al., 1997) presynaptic stimulation, but unlike spinal cord, in the hippocampus the origin of BDNF is most likely of postsynaptic origin (Edelmann et al., 2015).

Unlike paw pressure threshold and C-reflex activity, spinal wind-up was not modified soon after the administration of SES, perhaps because BDNF-mediated phosphorylation of NMDA receptors in the postsynaptic density did not provide the extra-calcium current required to significantly increase wind-up. Alternatively, failure of SES to rapidly potentiate wind-up could be intrinsic to the experimental design, since wind-up is a form of reversible homosynaptic potentiation, i.e., the synapses activated by the conditioning and test inputs should be the same (Jeftinija and Urban, 1994). In fact, because the high frequency SES (the conditioning stimulus) was applied with electrodes placed in the fourth and fifth toes while wind-up (the tested response) was induced by low-frequency stimulation of the third and fourth toes, it is likely that the SES-activated synapses (and the corresponding phosphorylated NMDA receptors by BDNF release) were different to those tested for wind-up responsiveness. Nevertheless, once late, transcription-dependent plasticity has likely been developed, which entails widespread trafficking of new proteins to specific targets in the whole neuron, thereby including synapses to be tested for wind-up, the wind-up scores increased (e.g., 1 week after SES stimulation), as occurs in monoarthritis (Constandil et al., 2009) and neuropathic (D'Mello et al., 2011) chronic pain models.

High-frequency SES increased the expression levels of BDNF protein and pTrkB in lumbar spinal cord tissue, an effect that lasted around 6 to 12 h. Previous work demonstrated that sciatic nerve electrical stimulation (20 Hz at C-fiber strength) led to increased BDNF mRNA and TrkB mRNA expressions in rat dorsal root ganglion and dorsal horn, respectively, 2 h after stimulation (Mannion et al., 1999). Because these changes in expression of BDNF and TrkB transcripts occurred a few hours after the triggering of the hyperalgesia, these signal pathways appear relevant to the maintenance of central sensitization rather than its induction. The higher expression of BDNF protein observed 3–6 h after applying the SES protocol probably represents induction of BDNF in microglia, as indeed occurs in neuropathic pain models (Coull et al., 2005). Actually, in the rat and mouse dorsal horn the neuronal BDNF expression is restricted to primary afferent terminals which occurs mainly in laminae I and II, where BDNF is stored in synaptic vesicles (Salio et al., 2005; Merighi et al., 2008), and therefore the large bulk of BDNF protein we measured in the dorsal horn likely correspond to microglial BDNF transcripts. This rather late production of BDNF in spinal cord microglia could result from microglial activators, such as ATP and fractalkine (CX3CL1), which are released from stimulated primary afferent neurons in naïve and hyperalgesic animals (for review see Taves et al., 2013) and activate microglia via the corresponding P2X, TrkB, and CX3CR1 receptors and the associated downstream p38 MAPK pathway (Gong et al., 2009; Trang et al., 2009; Zhuang et al., 2007). It has been shown that microglial derived BDNF contributes to pain hypersensitivity through phosphorylation of the NMDA receptor subunits NR1 via ERK and PKC (Slack et al., 2004) and NR2B via Fyn kinase (Li et al., 2017), and also through the disinhibition of nociceptive processing in the dorsal horn via downregulation of the K^+-Cl^- cotransporter KCC2 (Ferrini and De Koninck, 2013). Finally, BDNF also triggers long-term neuronal plasticity in the brain, and possibly in the spinal cord, via the activation of TrkB-ERK-CREB cascade, thereby signaling for a multitude of proteins involved in protein synthesis-dependent late-phase LTP (Minichiello, 2009). Thus, the activity-dependent increases of spinal BDNF and TrkB are temporally and functionally well positioned to switch early-phase LTP in the spinal cord into late-phase LTP.

Of note, 3 and 7 days after SES application, the expression levels of both BDNF protein and pTrkB in lumbar spinal cord tissue were found to be decreased below the pre-SES levels, as measured by ELISA method. Unexpectedly, i.t. CTX-B

administered 3 days after SES application, normalized the decreased expression of both transcripts, when tested by ELISA on the day 7 post-SES. This suggests that decreased BDNF and pTrkB expressions are the result of an active BDNF-mediated, negative feedback process, which can be removed by CTX-B. In this regard, BDNF-stimulated internalization of TrkB receptors via rapid ubiquitination and degradation has been recently shown (Proenca et al., 2016), but BDNF-mediated BDNF autoregulation has never been reported. Instead, BDNF-positive feedback loops mediating transcriptional BDNF upregulation in cortical neurons (Tuvikene et al., 2016) and in microglia (Zhang et al., 2014) have been proposed. Also intriguing is that CTX-B administered 3 days after SES, reverted the already established sensitization process despite the fact that at this time-point the spinal cord BDNF and pTrkB levels were lower than the baseline pre-SES levels. This argues for two complementary hypotheses: (i) once created, the central sensitization process is maintained by a BDNF-dependent mechanism, likely of microglial origin, and (ii) the reduced BDNF/TrkB signaling observed 3 days after SES is sufficient for maintaining the already installed sensitization process. Support for these assumptions could be found in the observation that during chronic pain BDNF can overexpress NR2B-containing spinal NMDA receptors either via non-genomic SHP2/PSD-95/NR2B signaling (Ding et al., 2015) or by promoting CREB-mediated transcription of NR2B subunit (Liang et al., 2016). In this context, it is conceivable that the normal (or even reduced) BDNF/TrkB signaling in spinal cord, which usually do not correlate with hyperalgesia in healthy animals, in sensitized ones could lead to significant phosphorylation of the overexpressed NR2B-containing NMDA receptor population, thereby contributing to the maintenance of the sensitization process. If so, the concomitant hyperalgesia should be sensitive to TrkB receptor blockade by CTX-B, in spite of the reduced level of BDNF/TrkB signaling at this time-point. An alternative, but not necessarily contradictory, explanation is that the relevant factor for BDNF-induced neuroplastic effects in spinal cord (like LTP or spinal sensitization) is not the level of BDNF/pTrkB-like immunoreactivity, as assessed by ELISA or Western blotting, but the amount of microglial released BDNF that may bound TrkB receptors. Unfortunately, detection of released BDNF in micro dialysates from animal brains has proven to be extremely difficult because of its low concentration, i.e., at the sub-nanogram/ml level (however, see Yoo et al., 2016).

Finally, we cannot discard that some degree of sensitization in primary afferents could be due to unknown modifications induced by the SES protocol within the DRG. Indeed, electrical activation of A delta and C-fibers has been shown to increase pERK in dorsal root ganglion neurons (Dai et al., 2002). However, whether enhanced ERK signaling in nociceptive afferents could be involved in the triggering of peripheral mechanical hyperalgesia/allodynia remains unexplored, in part because the mechanosensitive channel (or channels) that mediate mechanical pain has not been identified.

CONCLUSION

In summary, our findings demonstrate that a high-frequency SES protocol at intensity slightly over the C-fiber threshold is a sufficient condition for generating rapid and long-lasting sensitization of rat dorsal horn neurons that resembles chronic pain features, as assessed by either phasic mechanical or phasic/repetitive electric nociceptive stimuli that targeted C-fibers. The SES protocol used herein allowed for clear-cut dissection of early and late events underlying central sensitization in the spinal cord, because it admits immediate assessment of nociception and does not generate any noticeable injury in peripheral tissue that may constitute a confounding factor during nociceptive evaluation. Using CTX-B, a slowly reversible TrkB antagonist, we determined that the mechanisms underlying early sensitization are primarily mediated by activity and involve release of BDNF of probably neuronal origin, shortly followed by brief increased expression of likely glial BDNF that can switch early-phase sensitization into late one, thus substantiating CTX-B as a potential powerful tool for novel therapeutic strategies aimed to prevent or even treat some forms of chronic pain.

AUTHOR CONTRIBUTIONS

JR and LC provided ideas or concepts for definition of intellectual context, particularly designed and performed the experiments. JR, AR, PR, and TP performed the research. JR, PR, and DB contributed new reagents and analytic tools. JR, AH, TP, LV, and LC analyzed the data. AH and LC wrote the paper. All authors read and approved the final version of the manuscript.

FUNDING

This work was supported by the FONDECYT Project (Grants 1181622 and 1120952) and Centers of Excellence with BASAL/CONICYT financing, CEDENNA (Grant FB0807).

ACKNOWLEDGMENTS

We thank Ms. Cristina Arenas for technical support and animal care.

REFERENCES

Andó, R. D., and Sperlágh, B. (2013). The role of glutamate release mediated by extra synaptic P2X7 receptors in animal models of neuropathic pain. *Brain Res. Bull.* 93, 80–85. doi: 10.1016/j.brainresbull.2012.09.016

Artola, A., and Singer, W. (1987). Long-term potentiation and NMDA receptors in rat visual cortex. *Nature* 330, 649–652. doi: 10.1038/330649a0

Bliss, T., and Lømo, T. (1973). Long-lasting potentiation of synaptic transmission in the dentate area of the anaesthetized rabbit following stimulation of the perforant path. *J. Physiol.* 232, 331–356. doi: 10.1113/jphysiol.1973.sp010273

Carbone, L., and Austin, J. (2016). Pain and laboratory animals: publication practices for better data reproducibility and better animal welfare. *PLoS One* 11:e0155001. doi: 10.1371/journal.pone.0155001

Cazorla, M., Jouvenceau, A., Rose, C., Guilloux, J. P., Pilon, C., Dranovsky, A., et al. (2010). Cyclotraxin-B, the first highly potent and selective TrkB inhibitor, has anxiolytic properties in mice. *PLoS One* 5:e9777. doi: 10.1371/journal.pone.0009777

Chen, G., Kolbeck, R., Barde, Y. A., Bonhoeffer, T., and Kossel, A. (1999). Relative contribution of endogenous neurotrophins in hippocampal long-term potentiation. *J. Neurosci.* 19, 7983–7990. doi: 10.1523/JNEUROSCI.19-18-07983.1999

Constandil, L., Aguilera, R., Goich, M., Hernández, A., Alvarez, P., Infante, C., et al. (2011). Involvement of spinal cord BDNF in the generation and maintenance of chronic neuropathic pain in rats. *Brain Res. Bull.* 86, 454–459. doi: 10.1016/j.brainresbull.2011.08.008

Constandil, L., Goich, M., Hernández, A., Bourgeais, L., Cazorla, M., Hamon, M., et al. (2012). Cyclotraxin-B, a new TrkB antagonist, and glial blockade by propentofylline, equally prevent and reverse cold allodynia induced by BDNF or partial infraorbital nerve constriction in mice. *J. Pain* 13, 579–589. doi: 10.1016/j.jpain.2012.03.008

Constandil, L., Hernández, A., Pelissier, T., Arriagada, O., Espinoza, K., Burgos, H., et al. (2009). Effect of interleukin-1β on spinal cord nociceptive transmission of normal and monoarthritic rats after disruption of glial function. *Arthritis Res. Ther.* 11:R105. doi: 10.1186/ar2756

Coull, J. A., Beggs, S., Boudreau, D., Boivin, D., Tsuda, M., Inoue, K., et al. (2005). BDNF from microglia causes the shift in neuronal anion gradient underlying neuropathic pain. *Nature* 438, 1017–1021. doi: 10.1038/nature04223

Cui, J., He, W., Yi, B., Zhao, H., Lu, K., Ruan, H., et al. (2014). mTOR pathway is involved in ADP-evoked astrocyte activation and ATP release in the spinal dorsal horn in a rat neuropathic pain model. *Neuroscience* 275, 395–403. doi: 10.1016/j.neuroscience.2014.06.030

Dai, Y., Iwata, K., Fukuoka, T., Kondo, E., Tokunaga, A., Yamanaka, H., et al. (2002). Phosphorylation of extracellular signal-regulated kinase in primary afferent neurons by noxious stimuli and its involvement in peripheral sensitization. *J. Neurosci.* 22, 7737–7745. doi: 10.1523/JNEUROSCI.22-17-07737.2002

Ding, X., Cai, J., Li, S., Liu, X. D., Wan, Y., and Xing, G. G. (2015). BDNF contributes to the development of neuropathic pain by induction of spinal long-term potentiation via SHP2 associated GluN2B-containing NMDA receptors activation in rats with spinal nerve ligation. *Neurobiol. Dis.* 73, 428–451. doi: 10.1016/j.nbd.2014.10.025

D'Mello, R., Marchand, F., Pezet, S., McMahon, S. B., and Dickenson, A. H. (2011). Perturbing PSD-95 interactions with NR2B-subtype receptors attenuates spinal nociceptive plasticity and neuropathic pain. *Mol. Ther.* 19, 1780–1792. doi: 10.1038/mt.2011.42

Edelmann, E., Cepeda-Prado, E., Franck, M., Lichtenecker, P., Brigadski, T., and Leßmann, V. (2015). Theta burst firing recruits BDNF release and signaling in postsynaptic CA1 in spike-timing-dependent LTP. *Neuron* 86, 1041–1054. doi: 10.1016/j.neuron.2015.04.007

Falinower, S., Willer, J. C., Junien, J. L., and Le Bars, D. (1994). A C-fiber reflex modulated by heterotopic noxious somatic stimuli in the rat. *J. Neurophysiol.* 72, 194–213. doi: 10.1152/jn.1994.72.1.194

Faul, F., Erdfelder, E., Lang, A. G., and Buchner, A. (2007). G*Power 3: a flexible statistical power analysis program for the social, behavioral, and biomedical sciences. *Behav. Res. Methods* 39, 175–191. doi: 10.1038/srep33694

Ferrini, F., and De Koninck, Y. (2013). Microglia control neuronal network excitability via BDNF signalling. *Neural Plast.* 2013:429815. doi: 10.1155/2013/429815

Gee, M. D., Lynn, B., and Cotsell, B. (1997). The relationship between cutaneous C fibre type and antidromic vasodilatation in the rabbit and the rat. *J. Physiol.* 503, 31–44. doi: 10.1111/j.1469-7793.1997.031bi.x

Gong, Q. J., Li, Y. Y., Xin, W. J., Zang, Y., Ren, W. J., Wei, X. H., et al. (2009). ATP induces long-term potentiation of C-fiber-evoked field potentials in spinal dorsal horn: the roles of P2X4 receptors and p38 MAPK in microglia. *Glia* 57, 583–591. doi: 10.1002/glia.20786

Gonzalez, H. L., Carmichael, N., Dostrovsky, J. O., and Charlton, M. P. (2005). Evaluation of the time course of plasma extravasation in the skin by digital image analysis. *J. Pain* 6, 681–688. doi: 10.1016/j.jpain.2005.06.004

Hathway, G. J., Vega-Avelaira, D., Moss, A., Ingram, R., and Fitzgerald, M. (2009). Brief, low frequency stimulation of rat peripheral C-fibres evokes prolonged microglial-induced central sensitization in adults but not in neonates. *Pain* 144, 110–118. doi: 10.1016/j.pain.2009.03.022

Jeftinija, S., and Urban, L. (1994). Repetitive stimulation induced potentiation of excitatory transmission in the rat dorsal horn: an in vitro study. *J. Neurophysiol.* 71, 216–228. doi: 10.1152/jn.1994.71.1.216

Kang, H., Welcher, A. A., Shelton, D., and Schuman, E. M. (1997). Neurotrophins and time: different roles for TrkB signaling in hippocampal long-term potentiation. *Neuron* 19, 653–664. doi: 10.1016/S0896-6273(00)80378-5

Kawamata, M., and Omote, K. (1996). Involvement of increased excitatory amino acids and intracellular $Ca2^{+}$ concentration in the spinal dorsal horn in an animal model of neuropathic pain. *Pain* 68, 85–96. doi: 10.1016/S0304-3959(96)03222-8

Klein, T., Magerl, W., Hopf, H. C., Sandkühler, J., and Treede, R. D. (2004). Perceptual correlates of nociceptive long-term potentiation and long-term depression in humans. *J. Neurosci.* 24, 964–971. doi: 10.1523/JNEUROSCI.1222-03.2004

Latremoliere, A., and Woolf, C. J. (2009). Central sensitization: a generator of pain hypersensitivity by central neural plasticity. *J. Pain* 10, 895–926. doi: 10.1016/j.jpain.2009.06.012

Lever, I. J., Bradbury, E. J., Cunningham, J. R., Adelson, D. W., Jones, M. G., McMahon, S. B., et al. (2001). Brain-derived neurotrophic factor is released in the dorsal horn by distinctive patterns of afferent fiber stimulation. *J. Neurosci.* 21, 4469–4477. doi: 10.1523/JNEUROSCI.21-12-04469.2001

Li, S., Cai, J., Feng, Z. B., Jin, Z. R., Liu, B. H., Zhao, H. Y., et al. (2017). BDNF contributes to spinal long-term potentiation and mechanical hypersensitivity via Fyn-mediated phosphorylation of NMDA receptor GluN2B subunit at tyrosine 1472 in rats following spinal nerve ligation. *Neurochem. Res.* 42, 2712–2729. doi: 10.1007/s11064-017-2274-0

Liang, Y., Liu, Y., Hou, B., Zhang, W., Liu, M., Sun, Y. E., et al. (2016). CREB-regulated transcription coactivator 1 enhances CREB-dependent gene expression in spinal cord to maintain the bone cancer pain in mice. *Mol. Pain* 12, 1–11. doi: 10.1177/1744806916641679

Liu, M., Kay, J. C., Shen, S., and Qiao, L. Y. (2015). Endogenous BDNF augments NMDA receptor phosphorylation in the spinal cord via PLCγ, PKC, and PI3K/Akt pathways during colitis. *J. Neuroinflammation* 12:151. doi: 10.1186/s12974-015-0371-z

Mannion, R. J., Costigan, M., Decosterd, I., Amaya, F., Ma, Q. P., and Holstege, J. C. (1999). Neurotrophins: peripherally and centrally acting modulators of tactile stimulus-induced inflammatory pain hypersensitivity. *Proc. Natl. Acad. Sci. U.S.A.* 96, 9385–9390. doi: 10.1073/pnas.96.16.9385

Marcos, J. L., Galleguillos, D., Pelissier, T., Hernández, A., Velásquez, L., Villanueva, L., et al. (2017). Role of the spinal TrkB-NMDA receptor link in the BDNF-induced long-lasting mechanical hyperalgesia in the rat: a behavioural study. *Eur. J. Pain* 21, 1688–1696. doi: 10.1002/ejp.1075

M'Dahoma, S., Barthélemy, S., Tromilin, C., Jeanson, T., Viguier, F., Michot, B., et al. (2015). Respective pharmacological features of neuropathic-like pain evoked by intrathecal BDNF versus sciatic nerve ligation in rats. *Eur. Neuropsychopharmacol.* 25, 2118–2130. doi: 10.1016/j.euroneuro.2015.07.026

Merighi, A., Salio, C., Ghirri, A., Lossi, L., Ferrini, F., Betelli, C., et al. (2008). BDNF as a pain modulator. *Prog. Neurobiol.* 85, 297–317. doi: 10.1016/j.pneurobio.2008.04.004

Milligan, E. D., Twining, C., Chacur, M., Biedenkapp, J., O'Connor, K., Poole, S., et al. (2003). Spinal glia and proinflammatory cytokines mediate mirror-image neuropathic pain in rats. *J. Neurosci.* 23, 1026–1040. doi: 10.1523/JNEUROSCI.23-03-01026.2003

Minichiello, L. (2009). TrkB signalling pathways in LTP and learning. *Nat. Rev. Neurosci.* 10, 850–860. doi: 10.1038/nrn2738

Nakagawa, T., Wakamatsu, K., Zhang, N., Maeda, S., Minami, M., Satoh, M., et al. (2007). Intrathecal administration of ATP produces long-lasting allodynia in rats: differential mechanisms in the phase of the induction and maintenance. *Neuroscience* 147, 445–455. doi: 10.1016/j.neuroscience.2007.03.045

National Research Council (2011). *Guide for the Care, and Use of Laboratory Animals*, 8th Edn. Washington DC: The National Academies Press.

Peng, H. Y., Chen, G. D., Lai, C. Y., Hsieh, M. C., and Lin, T. B. (2012). Spinal SIRPα1-SHP2 interaction regulates spinal nerve ligation-induced neuropathic

pain via PSD-95-dependent NR2B activation in rats. *Pain* 153, 1042–1053. doi: 10.1016/j.pain.2012.02.006

Proenca, C. C., Song, M., and Lee, F. S. (2016). Differential effects of BDNF and neurotrophin 4 (NT4) on endocytic sorting of TrkB receptors. *J. Neurochem.* 138, 397–406. doi: 10.1111/jnc.13676

Randic, M., Jiang, M. C., and Cerne, R. (1993). Long-term potentiation and long-term depression of primary afferent neurotransmission in the rat spinal cord. *J. Neurosci.* 13, 5228–5241. doi: 10.1523/JNEUROSCI.13-12-05228.1993

Reeh, P. W., Kocher, L., and Jung, S. (1986). Does neurogenic inflammation alter the sensitivity of unmyelinated nociceptors in the rat? *Brain Res.* 384, 42–50.

Salio, C., Lossi, L., Ferrini, F., and Merighi, A. (2005). Ultrastructural evidence for a pre- and postsynaptic localization of full-length trkB receptors in substantia gelatinosa (lamina II) of rat and mouse spinal cord. *Eur. J. Neurosci.* 22, 1951–1966. doi: 10.1111/j.1460-9568.2005.04392.x

Sandkühler, J. (2009). Models and mechanisms of hyperalgesia and allodynia. *Physiol. Rev.* 89, 707–758. doi: 10.1152/physrev.00025.2008

Slack, S. E., Pezet, S., McMahon, S. B., Thompson, S. W., and Malcangio, M. (2004). Brain-derived neurotrophic factor induces NMDA receptor subunit one phosphorylation via ERK and PKC in the rat spinal cord. *Eur. J. Neurosci.* 20, 1769–1778. doi: 10.1111/j.1460-9568.2004.03656.x

Taves, S., Berta, T., Chen, G., and Ji, R.-R. (2013). Microglia and spinal cord synaptic plasticity in persistent pain. *Neural Plast.* 2013:753656. doi: 10.1155/2013/753656

Trang, T., Beggs, S., Wan, X., and Salter, M. W. (2009). P2X4-receptor-mediated synthesis and release of brain-derived neurotrophic factor in microglia is dependent on calcium and p38-mitogen-activated protein kinase activation. *J. Neurosci.* 29, 3518–3528. doi: 10.1523/JNEUROSCI.5714-08.2009

Tuvikene, J., Pruunsild, P., Orav, E., Esvald, E. E., and Timmusk, T. (2016). AP-1 Transcription factors mediate BDNF-positive feedback loop in cortical neurons. *J. Neurosci.* 36, 1290–1305. doi: 10.1523/JNEUROSCI.3360-15.2016

Whitehead, K. J., Smith, C. G., Delaney, S. A., Curnow, S. J., Salmon, M., Hughes, J. P., et al. (2010). Dynamic regulation of spinal pro-inflammatory cytokine release in the rat in vivo following peripheral nerve injury. *Brain Behav. Immun.* 24, 569–576. doi: 10.1016/j.bbi.2009.12.007

Woolf, C. J., and Wall, P. D. (1986). Relative effectiveness of C primary afferent fibers of different origins in evoking a prolonged facilitation of the flexor reflex in the rat. *J. Neurosci.* 6, 1433–1442. doi: 10.1523/JNEUROSCI.06-05-01433.1986

Ying, B., Lü, N., Zhang, Y. Q., and Zhao, Z. Q. (2006). Involvement of spinal glia in tetanically sciatic stimulation-induced bilateral mechanical allodynia in rats. *Biochem. Biophys. Res. Commun.* 340, 1264–1272. doi: 10.1016/j.bbrc.2005.12.139

Yoo, Y. K., Lee, J., Kim, J., Kim, G., Kim, S., Kim, J., et al. (2016). Ultra-sensitive detection of brain-derived neurotrophic factor (BDNF) in the brain of freely moving mice using an interdigitated microelectrode (IME) biosensor. *Sci. Rep.* 6:33694. doi: 10.1038/srep33694

Zhang, X., Zeng, L., Yu, T., Xu, Y., Pu, S., Du, D., et al. (2014). Positive feedback loop of autocrine BDNF from microglia causes prolonged microglia activation. *Cell Physiol. Biochem.* 34, 715–723. doi: 10.1159/000363036

Zhuang, Z. Y., Kawasaki, Y., Tan, P. H., Wen, Y. R., Huang, J., and Ji, R. R. (2007). Role of the CX3CR1/p38 MAPK pathway in spinal microglia for the development of neuropathic pain following nerve injury-induced cleavage of fractalkine. *Brain Behav. Immun.* 21, 642–651. doi: 10.1016/j.bbi.2006.11.003

Conflict of Interest Statement: The authors declare that the research was conducted in the absence of any commercial or financial relationships that could be construed as a potential conflict of interest.

frontiers in Pharmacology

ORIGINAL RESEARCH
published: 28 November 2018
doi: 10.3389/fphar.2018.01368

IFN-β Plays Both Pro- and Anti-inflammatory Roles in the Rat Cardiac Fibroblast Through Differential STAT Protein Activation

*Samir Bolívar[1,2], Renatto Anfossi[2], Claudio Humeres[2], Raúl Vivar[2], Pía Boza[2], Claudia Muñoz[2], Viviana Pardo-Jimenez[2], Francisco Olivares-Silva[2] and Guillermo Díaz-Araya[2,3]**

[1] Faculty of Chemistry and Pharmacy, Atlantic University, Barranquilla, Colombia, [2] Department of Chemical Pharmacology and Toxicology, Faculty of Chemical and Pharmaceutical Sciences, University of Chile, Santiago, Chile, [3] Advanced Center for Chronic Diseases, Faculty of Chemical and Pharmaceutical Sciences and Faculty of Medicine, University of Chile, Santiago, Chile

Cardiac fibroblasts (CFs) contribute to theinflammatory response to tissue damage, secreting both pro- and anti-inflammatory cytokines and chemokines. Interferon beta (IFN-β) induces the phosphorylation of signal transducer and activator of transcription (STAT) proteins through the activation of its own receptor, modulating the secretion of cytokines and chemokines which regulate inflammation. However, the role of IFN-β and STAT proteins in modulating the inflammatory response of CF remains unknown. CF were isolated from adult male rats and subsequently stimulated with IFN-β to evaluate the participation of STAT proteins in secreting chemokines, cytokines, cell adhesion proteins expression and in their capacity to recruit neutrophils. In addition, in CF in which the TRL4 receptor was pre-activated, the effect of INF-β on the aforementioned responses was also evaluated. Cardiac fibroblasts stimulation with IFN-β showed an increase in STAT1, STAT2, and STAT3 phosphorylation. IFN-β stimulation through STAT1 activation increased proinflammatory chemokines MCP-1 and IP-10 secretion, whereas IFN-β induced activation of STAT3 increased cytokine secretion of anti-inflammatory IL-10. Moreover, in TLR4-activated CF, IFN-β through STAT2 and/or STAT3, produced an anti-inflammatory effect, reducing pro-IL-1β, TNF-α, IL-6, MCP-1, and IP-10 secretion; and decreasing neutrophil recruitment by decreasing ICAM-1 and VCAM-1 expression. Altogether, our results indicate that IFN-β exerts both pro-inflammatory and anti-inflammatory effects in non-stimulated CF, through differential activation of STAT proteins. When CF were previously treated with an inflammatory agent such as TLR-4 activation, IFN-β effects were predominantly anti-inflammatory.

Keywords: IFN-β (interferon β), cardiac fibroblast, STAT, proinflammatory, anti-infammatory

OPEN ACCESS

Edited by:
Lei Xi,
Virginia Commonwealth University, United States

Reviewed by:
Zhi-Qing Zhao,
Mercer University, United States
Francisco Villarreal,
University of California, San Diego, United States

****Correspondence:***
Guillermo Díaz-Araya
gadiaz@ciq.uchile.cl

Specialty section:
This article was submitted to Translational Pharmacology, a section of the journal Frontiers in Pharmacology

Received: *25 August 2018*
Accepted: *07 November 2018*
Published: *28 November 2018*

Citation:
Bolívar S, Anfossi R, Humeres C, Vivar R, Boza P, Muñoz C, Pardo-Jimenez V, Olivares-Silva F and Díaz-Araya G (2018) IFN-β Plays Both Pro- and Anti-inflammatory Roles in the Rat Cardiac Fibroblast Through Differential STAT Protein Activation. Front. Pharmacol. 9:1368. doi: 10.3389/fphar.2018.01368

INTRODUCTION

The classical role of cardiac fibroblasts (CFs) is extracellular matrix (ECM) protein homeostasis. However, CF can also act as "sentinel" cells, detecting changes in chemical and mechanical signals in the heart and stimulating an appropriate response (Frangogiannis, 2007; Van Linthout et al., 2014; Díaz-Araya et al., 2015). Immediately after tissue damage, CF contribute to the inflammation

necessary for repair, secreting pro-inflammatory cytokines, such as tumor necrosis factor alpha (TNF-α) and interleukin 1 beta (IL-1β), as well as pro-inflammatory chemokines, such as monocyte chemoattractant protein 1 (MCP-1) and interleukin-8 (Kukielka et al., 1995). However, CF also secrete inhibitory mediators capable of suppressing pro-inflammatory signals, such as interleukin-10 (IL-10) and transforming growth factor beta (TGF-β) (Dewald et al., 2005; Nahrendorf et al., 2007; Turner et al., 2009, 2010). Finally, CF express intercellular and vascular adhesion molecules (ICAM-1, VCAM-1, and E-selectin) to recruit immune cells (Kacimi et al., 1998; Turner et al., 2011).

Interferon beta (IFN-β) is a cytokine produced by innate immune cells, including macrophages and dendritic cells, as well as non-immune cells, such as fibroblasts and epithelial cells (Ivashkiv and Donlin, 2014). IFN-β elicits a wide range of effects, including anti-inflammatory and pro-inflammatory responses, and also regulates the development and activation of virtually all innate and adaptive immune effector cells. IFN-β has a variety of documented effects on immune cells; for instance, IFN-β modulates TNF-α and IL-10 expression in peripheral blood mononuclear cells (Rudick et al., 1996; Coclet-Ninin et al., 1997), reduces TNF-α expression in monocytes (Jungo et al., 2001), and increases IL-10 expression in dendritic cells (Yen et al., 2015). However, the effects of IFN-β on non-immune cells such as CF remain unknown.

The cellular effects of IFN-β are mediated through the JAK/STAT signaling pathway and vary according to context and cell phenotype (Darnell et al., 1994; Ihle, 1995; Chen et al., 2004). Interferon type I receptor (IFNAR)activation by IFN-β induces signal transducer and activator of transcription (STAT) protein phosphorylation, and the canonical IFN-β signaling pathway can activate the formation of p-STAT1/p-STAT2 heterodimers that bind to interferon regulator factor 9. The activated proteins then translocate to the nucleus, activating the transcription of inflammatory genes known as interferon-stimulated response elements (Platanias, 2005). In contrast, the formation of p-STAT1 and/or p-STAT3 homodimers inhibits the activation of p-STAT1/p-STAT2 heterodimer-dependent genes, suppressing the inflammatory properties of IFN-β (Ivashkiv and Donlin, 2014; López de Padilla and Niewold, 2016). Whereas, recent studies have provided significant insight into the roles of activated STAT2 and STAT3 proteins in modulating inflammation, especially in immune and vascular cells (Szelag et al., 2016). STAT3 modulates proliferation, differentiation, survival, oxidative stress, and metabolism in cardiomyocytes, fibroblasts, endothelial cells, progenitor cells, and various inflammatory cells (O'Shea and Murray, 2008; Haghikia et al., 2014). However, the effects of STAT protein activation by IFN-β on modulation of inflammatory response in CF are unclear. In this work, we sought to study the effects of IFN-β on CF pro-inflammatory (MCP-1, IL-1β, TNF-α and IP-10 secretion; VCAM-1 and ICAM-1 expression) and anti-inflammatory effects (IL-10 secretion); and the involvement of STAT pathway in mediating these actions. Furthermore, we hypothesized that these effects could be greatly influenced by inflammatory activation of CF, for which we stimulated CF TLR4 receptor, a well-studied receptor involved in pro-inflammatory fibroblast functions, with lipopolysaccharide (LPS), a TLR4 specific agonist, to promote CF inflammatory environment.

MATERIALS AND METHODS

Materials

Fetal bovine serum (FBS), trypsin/EDTA and prestained molecular weight marker were purchased from Merck (Darmstadt, Germany). Enhanced chemiluminescence (ECL) reagent was acquired from PerkinElmer Life Sciences (Boston, MA, United States). Sterile plastic material was purchased from CoStar (Corning Costar, NJ, United States). Mouse primary antibodies for ICAM-1, and VCAM-1 were purchased from Abcam (Cambridge, MA, United States). Rabbit GAPDH was acquired from Calbiochem (Darmstadt, Germany). Anti-RP1 PE Mouse anti-rat granulocytes was purchased from BD Biosciences (Franklin Lakes, NJ, United States). Fluorescent-conjugated goat anti-mouse IgG (H+L) secondary antibodies, Alexa Fluor 488 and 555 and Opti-MEM® were purchased from Thermo Fisher Scientific (Waltham, MA, United States). HRP-conjugated antibodies were purchased from Santa Cruz Biotechnology (Santa Cruz, CA, United States). The primary antibodies for p-Stat1, p-Stat2, and p-Stat3 were purchased from Cell Signaling Technology (Boston, MA, United States). Anti- Stat1, Stat2 and Stat3 were obtained from Santa Cruz Biotechnology (Dallas, TX, United States). Ficoll Histopaque-1083 was purchased from Sigma-Aldrich (St. Louis, MO, United States). Multiplex kit (RECYTMAG 65K/MILLIPLEX MAP Rat Cytokine/Chemokine Magnetic Bead Panel) and TGF-β1 were purchased from Merck-Millipore (Tamecula, CA, United States). Lipofectamine® 2000 was purchased from Invitrogen (Carlsbad, CA, United States). Transwellfilename plates (#3422) were purchased from Corning (New York, NY, United States). The Silencer® against Stat1, Stat2, Stat3 and Scramble siRNA (negative control Silencer®) were obtained from Life Technologies. InvivoGen LPS-EB Ultrapure (InvivoGen tlrl-pelps, from *E. coli* O111:B4) was extracted through successive hydrolysis steps and purified by phenol-TEA-DOC extraction; according to InvivoGen, this LPS is specific for TLR4 activation. Collagenase type II was purchased from InvivoGen (San Diego, CA, United States).

Animals

Male adult Sprague Dawley rats were obtained from the animal breeding facility of the Faculty of Chemical and Pharmaceutical Sciences at the University of Chile. The animals were housed in cages (12-h light/dark cycles) with access to rat chow and water ad libitum. All studies were performed in compliance with the NIH Guide for the Care and Use of Laboratory Animals, updated in 2011[1], and experimental protocols were approved by our Institutional Ethics Review Committee.

[1]https://grants.nih.gov/grants/olaw/guide-for-the-care-and-use-of-laboratory-animals.pdf

Cell Culture and Treatments

Cardiac fibroblast were isolated from adult Sprague Dawley Rats (3–4 weeks old) using enzymatic digestion, as previously described (Humeres et al., 2016). Briefly, rats were anesthetized by ketamine/xylazine injection and their hearts extracted in an aseptic environment. Atria were removed and ventricles cut into small pieces (1–2 mm) for later collagenase II digestion. The digestion yield was separated by 10-min centrifugation at 1000 rpm. The pellet was resuspended in 10 ml of Dulbecco's Modified Eagle Medium/Nutrient Mixture F-12 (DMEM/F12) supplemented with 10% FBS and antibiotics (100 μg/ml streptomycin and 100 units/ml penicillin) and cultured in a humid atmosphere at 5% CO_2/95% O_2 and 37°C until confluence (5 days). The purity of the CF population was assessed with several markers. CF showed positive staining for vimentin (Santa Cruz Biotechnology, Santa Cruz, CA, United States) and were negative against sarcomeric actin and desmin (Sigma-Aldrich, St. Louis, MO, United States).

Cells from passage 1 were used for all experiments, and they were maintained in DMEM F12 for 18 h until experiments were performed. CF were pre-treated with IFN-β (500 U/mL) for 30 to 120 min, and LPS (1 μg/mL) was used as inflammatory stimulus. For experiments involved with JAK/STAT inhibition, CF were incubated with Ruxolitinib (JAK inhibitor, 500 nM), or transfected with Stat1, Stat2, and Stat3 siRNAs (100 ng/mL) for 8 h previous Ruxolitinib, IFN-β or LPS incubation.

Isolation of Neutrophils From Bone Marrow

For neutrophils isolation from bone marrow, we used cell sorting by flow cytometry fluorescence strategy (FACS) (BD FACSAria™ III, BD Biosciences) using RP-1 antibody as specific marker for rat neutrophils (Skrajnar et al., 2009). The femur and tibia were extracted from both extremities of the rats, and the epiphysis was excised at the level of the metaphysis of both bone types. The bone marrow is then removed by infusion of DMEM/F12 medium by means of a 25G-wide syringe onto a 100 mm Petri dish. The leukocyte and erythrocyte rich cell suspension was then centrifuged at 300 *g* for 10 min at room temperature. The erythrocytes present in the suspension were then lysed with 0.83% ammonium chloride (NH_4Cl) for 7 min and the remaining suspension was washed twice with tissue storage solution (MACS) (2 mM EDTA, 0.5% BSA) and incubated with phycoerythrin (PE) conjugated anti RP-1 antibody at a concentration of 0.5 μl anti-RP-1 per 1×10^6 cells in 100 μl of total volume for 30 min, avoiding light. The leukocyte suspension is then washed twice with MACS medium and assayed by Cell Sorting (Beckson-Dickinson FACS flow and sorting cytometer). Approximately 20% of cells isolated were identified as RP-1 + cells (neutrophils). The sorted population consisted of 98% RP-1 positive neutrophils (less than 1–2% monocytes/lymphocytes) and a 99% in viability. Purified neutrophils were centrifuged and pooled for further experiments.

STATs Knockdown

FC were plated in 35 mm to 80% confluency and serum starved overnight. A solution of 4 uL Lipofectamine® + 100 uL Opti-MEM® and 5 uL siRNA (Silencer®) + 100 uL Opti-MEM® was incubated for 15 min at room temperature, mixed and further incubated for 15 min. CF were treated with the siRNA preparation for 8 h at 37°C, media replaced DMEM F12 for additional 24 h and lastly cells were harvested for further analysis. The codes products used were: RefSeq Stat1 NM_001034164.1, RefSeq Stat2 NM_001011905.1, RefSeq Stat3 NM_012747.2.

Western Blot Analysis

After respective treatments, cells were lysed in 50 mM Tris, 300 mM NaCl, 1 mM $MgCl_2$, 0.5 mM ethylenediaminetetraacetic acid (EDTA), 0.1 mM EGTA, 20% glycerol, 1% NP40 cell lysis buffer, 0.5 mM 1,4-dithiothreitol (DTT), and inhibitor cocktail. Lysates were vigorously vortexed for 10 s and centrifuged at 15,000 rpm for 10 min, and total protein content was determined using Bradford assay. Equivalent amounts of protein were loaded to SDS PAGE. Western blotting was performed by transferring proteins to nitrocellulose membranes and blocking with 10% fat-free milk (w/v) in TBS-Tween for 1 h at room temperature. Membranes were probed with the appropriate primary antibody overnight at 4°C and then with peroxidase-conjugated secondary antibody for 2 h at room temperature. Finally, the ECL Advance Western Blotting Detection Kit was used for immunodetection. Protein levels were determined by densitometric analysis using Image J (NIH, Bethesda, MD, United States) and normalized to GAPDH and total STAT levels, according to the experiment.

Immunofluorescence Assay

Cardiac fibroblasts were fixed in 4% paraformaldehyde solution for 20 min at room temperature and permeabilized in 0.1% Triton X-100 for 10 min at room temperature. Non-specific proteins were blocked with 3% bovine serum albumin solution for 30 min at room temperature. Cells in coverslips were incubated with the appropriate primary antibody overnight at 4°C and an appropriate fluorophore-conjugated secondary antibody for 2 h at room temperature. Images were obtained using a spinning-disk microscope.

Luminex Immunobead Assay

Supernatant was collected and stored at −80°C prior to cytokine analysis. Depending on the experiment CF were previously transfected with Stat siRNA and treated with IFN-β or LPS, or both for 24 h. One h before analysis, samples were thawed and analyzed for cytokine and chemokine protein levels using the Milliplex MAP-Rat Cytokine/Chemokine Magnetic Bead Panel Immunology Multiplex Assay according to manufacturer instructions. The proinflammatory cytokines (Il-6, TNF-α) and chemokines (MCP-1 and IP-10); and also antinflammatory cytoquines (IL-10) were measured. Cytokine levels were read on Luminex 200 System, Multiplex Bio-Assay. Quantification was based on standard curves for each cytokine, in the concentration range of 1.5–10,000 pg/ml. Values were standardized by measuring total amounts of cells and expressed as pg/50.000 cells.

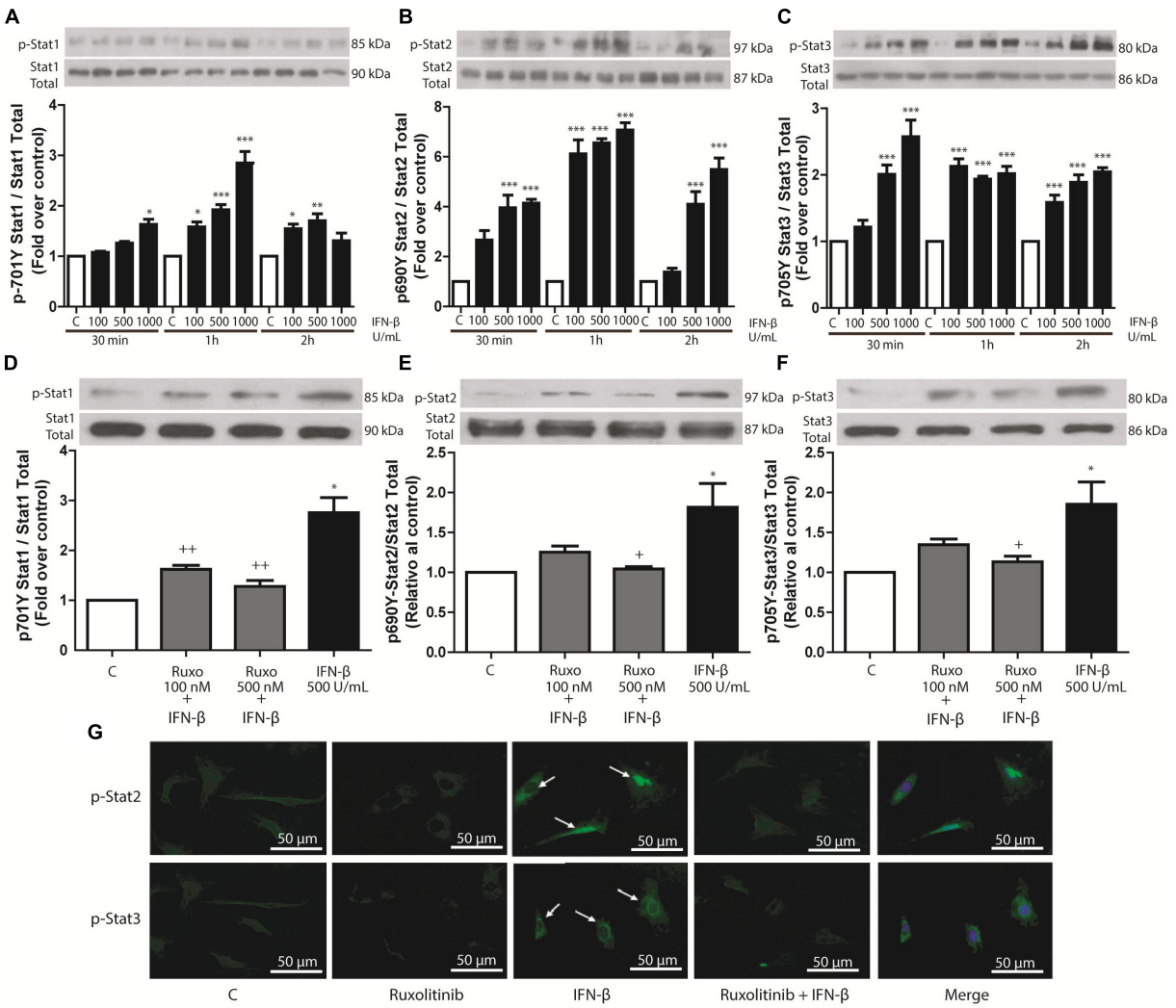

FIGURE 1 | IFN-β activates the JAK/STAT signaling pathway in CF. **(A–C)** The upper panelshows a Western blot image, indicating the INF-β-induced p-STAT1, p-STAT2, and p-STAT3 expression levels; STAT1, STAT2, and STAT3 were used as loading controls. The graphical analysis is presented at the bottom of each panel. Error bars indicate theSD for four independent experiments. $^{***}p < 0.001$, $^{**}p < 0.01$, $^{*}p < 0.05$ vs. control. **(D–F)** CF were pretreated with or without Ruxolitinib (100 and 500 nM) for 1 h and stimulated with IFN-β (500 U/ml) for 24 h. The upper panel of each figure corresponds to the representative image of p-STAT1, p-STAT2, and p-STAT3 expression levels; STAT1, STAT2, and STAT3 were used as loading controls. The graphical analysis is presented at the bottom of each panel. Error bars indicate the SD for four independent experiments. $^{***}p < 0.001$, $^{*}p < 0.05$ vs. control. $^{++}p < 0.01$, $^{+}p < 0.05$ vs. IFN-β. **(G)** CF were pretreated with or without Ruxolitinib (100 and 500 nM) for 1 h and stimulated with IFN-β (500 U/ml) for 24 h. p-STAT2 and p-STAT3 were detected by immunofluorescence using anti-p-STAT2 and anti-p-STAT3 antibodies and Alexa Fluor® 488-conjugated secondary antibody (green staining). Representative images of the immunocytochemistry for three independent experiments are shown, indicating the nuclear translocation of p-STAT2 and p-STAT3. $^{+}p < 0.05$ vs. IFN-β.

Migration Assays of Neutrophils

In vitro neutrophil migration assays were performed using Transwell® plates with porous polycarbonate membrane filters (6.5 mm diameter, 8.0 µm pore) between an upper and lower compartment. In the upper chamber, 4×10^5 neutrophils labeled with calcein were seeded in 200 µL of DMEM/F12. The lower chamber contained 500 µl of conditioned medium obtained from the treated CF with IFN-β and/or LPS in the presence or absence of anti-STAT siRNA. The neutrophils migrated for 3 h at 37°C and 5% CO_2/95% O_2. The fluorescently labeled neutrophils that migrated to the lower compartment were measured using a fluorescence spectrometer equipped with a microplate (Multi-Mode Reader Synergy 2, BioTek). DMEM/F12 (without CF supernatant) was used in the lower compartment as a negative control and DMEM/F12 + 50% FBS was used as a positive control. The percentage of neutrophil migration was calculated as follows; 100 x [fluorescence of migrated cells/fluorescence of total aggregated cells]. Prior to these studies, we performed neutrophil population identification tests. RP-1 protein expression results confirmed that 20% of the total leukocyte population was composed of neutrophils (**Supplementary Figure S1**).

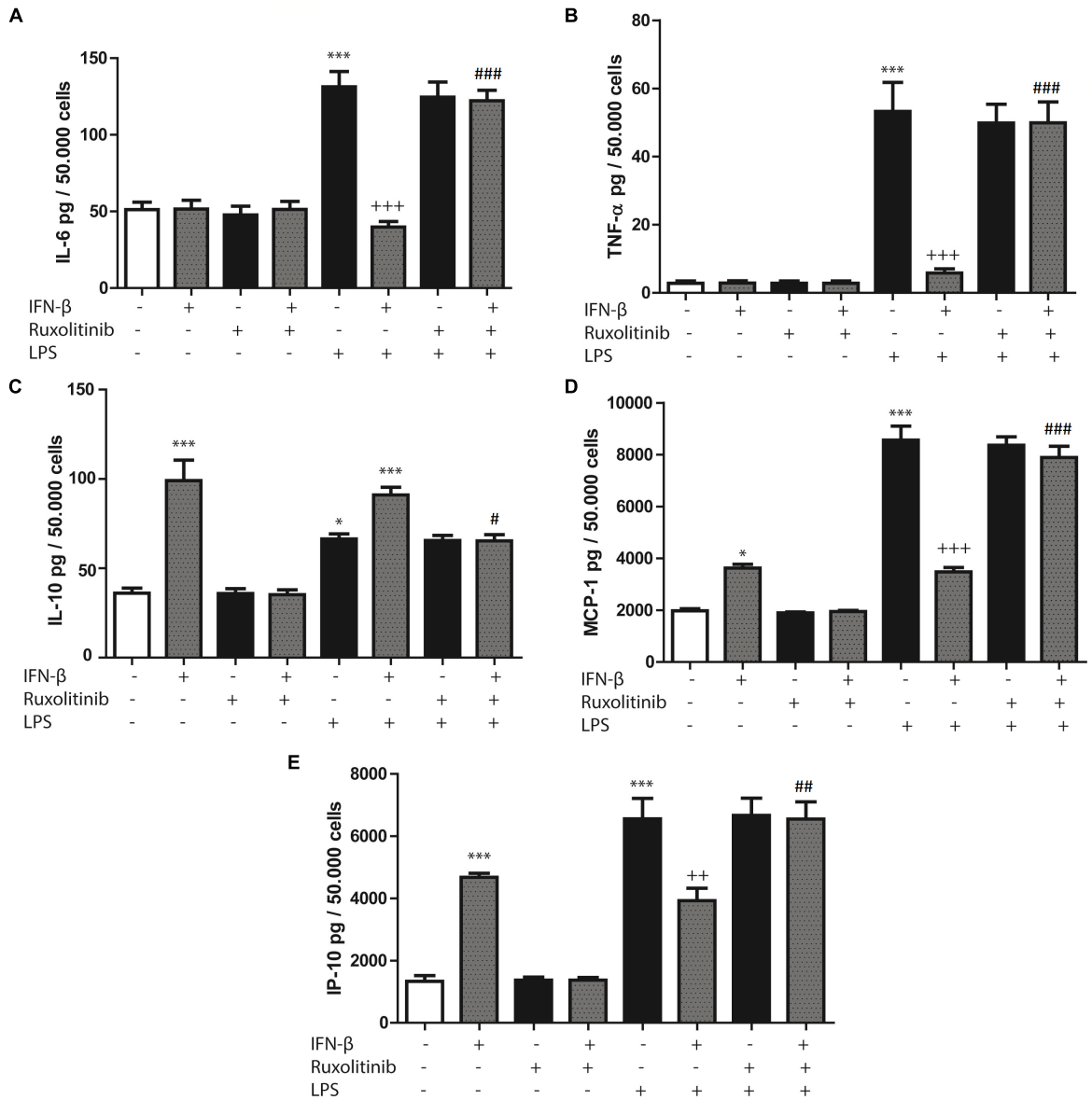

FIGURE 2 | Effects of IFN-β and STAT proteins on LPS-induced cytokine secretion: **(A–E)** CF were transfected with scramble or 200 ng of si-STAT1, si-STAT2, and si-STAT3 for 8 h, serum-deprived of for 24 h, pre-treated with IFN-β for 1 h, and stimulated with LPS for 24 h. **(A)** IL-6, **(B)** TNF-β, **(C)** IL-10, **(D)** MCP-1 and **(E)** IP-10 secretion to the culture medium was determined by LUMINEX assay. Error bars indicate the SD for three independent experiments. $^{***}p < 0.001$, $^{**}p < 0.01$, vs. scramble. $^{+++}p < 0.001$ vs. scramble + LPS. $^{###}p < 0.001$, $^{##}p < 0.01$ vs. scramble + IFN-β + LPS. $^{\&\&\&}p < 0.001$, $^{\&\&}p < 0.01$ vs. scramble + IFN-β.

Adhesion Assays of Neutrophils

Cell adhesion *in vitro* was analyzed by Cell Sorting (Beckson-Dickinson FACS flow and sorting cytometer). In brief, leukocytes obtained from rat bone marrow were resuspended in DMEM/F12 medium at a rate of 1.5×10^6 cells/100 μl, and then were added to 35 mm plates on a confluent monolayer of CF (15×10^4) previously transfected with and without Scramble, siRNA Stat1, siRNA Stat2, and siRNA Stat3, and treated in the presence or absence of LPS and IFN-β. After an incubation period of 2 h at 37°C, cell plates were washed with 1X sterile phosphate-buffered saline (PBS) and CF with adhered leukocytes were peeled off using 0.1% trypsin in 1X sterile PBS. The suspension of CF and adhered leukocytes were then washed with MACS medium for 5 min at room temperature and incubated with anti-RP-1/PE antibody at the rate of 0.5 μl of anti-RP-1 per 10^6 cells in 100 μl of total volume for 30 min, avoiding light. The cell suspension (CF and leukocyte), was then washed twice with MACS medium and assayed by Cell Sorting. Percentage of neutrophil adhesion was calculated as follows; 100 x (number of adherent RP-1 + cells/total number of aggregated RP-1 + cells). The analysis was performed using FlowJo 7.0 (TreeStar Software).

Statistical Analysis

Data are expressed as the mean ± SD of at least three independent experiments. Statistical analysis was performed using one-way ANOVA followed by Tukey's multiple comparison tests with GraphPad Prism Software. $p < 0.05$ was considered significant.

RESULTS

IFN-β Activates the JAK/STAT Signaling Pathway in CF

IFN-β (100, 500, or 1000 U/mL) induced concentration-dependent phosphorylation of STAT1, STAT2, and STAT3 in CF. Results were significant after 30 min and 1 and 2 h of IFN-β stimulation, respectively (**Figures 1A–C**). To assess whether STAT phosphorylation was dependent on the activation of JAK/STAT signaling pathway by IFN-β through activation of IFN-β receptor (IFNAR), CF were pretreated with 100 or 500 nM of JAK inhibitor Ruxolitinib, which inhibited IFN-β-induced STAT1, STAT2, and STAT3 protein phosphorylation (**Figures 1D–F**). Immunofluorescence results were consistent with this finding (**Figure 1G**); which showed that stimulation of CF with IFN-β (500 U/mL) for 1 h increased STAT2 and STAT3 nuclear localization (white arrows). Taken together, these results show that IFN-β activates the JAK/STAT signaling pathway through the IFNAR.

In TLR4-Activated CF, IFN-β Inhibits Cytokines and Chemokines Secretion

Cardiac fibroblasts are important cellular effectors of the inflammatory response in cardiac tissue, where TLR4 activation by LPS or heparan sulfate has been shown to induce cytokine and chemokine secretion. Therefore, we evaluated whether IFN-β stimulates cytokines and chemokines secretion by CF. CF treated with IFN-β (24 h) did not modify IL-6 or TNF-α secretion levels, whereas it increased IL-10 secretion (**Figures 2A–C**). Ruxolitinib significantly inhibited the increase of IL-10 secretion induced by IFN-β. In contrast, treating CF with LPS (24 h) significantly increased IL-6, TNF-α and IL-10 secretion, although LPS produced a smaller effect than IFN-β on IL-10 secretion. Pre-treating CF with IFN-β for 1 h and then LPS for 24 h significantly inhibited the LPS-induced increase in IL-6 and TNF-α secretion (**Figures 2A,B**). However, IL-10 secretion levels were similar to those for IFN-β, and Ruxolitinib inhibited the effects of IFN-β, in the presence of LPS (**Figure 2C**).

In regard to chemokines, treatment with either IFN-β or LPS increased MCP-1 and IP-10 secretion, although LPS produced a larger effect than IFN-β. However, pre-treating CF with IFN-β for 1 h and then LPS for 24 h resulted in lower MCP-1 and IP-10 secretion levels than those associated with LPS treatment. Pre-treatment with Ruxolitinib inhibited the effects of IFN-β in the presence or the absence of LPS (**Figures 2D,E**).

Collectively, these results suggest that in CF, IFN-β by itself stimulates IL-10, MCP-1 and IP-10 secretion; however, in the presence of a pro-inflammatory stimulus, such as LPS, INF-β dampens the secretion of inflammatory cytokines and chemokines triggered by this pro-inflammatory stimulus.

IFN-β Activates STAT2 and/or STAT3 to Inhibit LPS-Induced Cytokine and Chemokine Secretion in CF

STAT1, STAT2, and STAT3 siRNA (si-STAT1, si-STAT2, si-STAT3) were used to evaluate whether IFN-β-activated STAT proteins modulated cytokine or chemokine secretion, either alone or in the presence of LPS. Each siRNA was specific for its particular target (**Supplementary Figure S2**).

STAT3 activation modulated IFN-β-induced decrease of IL-6 in presence of LPS, since si-STAT3 prevented the decrease of IL-6 induced by IFN-β on LPS-treated CF. Both STAT2 and STAT3 activation were involved in IFN-β-induced decrease of TNF-α levels in LPS treated CF, as demonstrated by si-STAT2 and si-STAT3 prevention of TNF-α decrease. On the contrary, cytokine levels (IL-6 and TNF-α) induced by IFN-β on LPS-treated CF were unaffected by STAT1 knockdown (**Figures 3A,B**).

In addition, STAT3 (and not STAT1 or STAT2) was also crucial in IFN-β-induced IL-10 secretion, since STAT3 knockdown reverse IFN-β effects both in presence and absence of LPS (**Figure 3C**). In the case of MCP-1 and IP-10 secretion increased by IFN-β, it was observed that only STAT1 was necessary for such effect (**Figures 3D,E**). In contrast, STAT3 played an important role in modulating the IFN-β-induced MCP-1 secretion in the presence of LPS, since si-STAT3 reversed the effects of IFN-β on the LPS-induced activity. Neither STAT1 nor STAT2 modulated these effects of IFN-β (**Figure 3D**). Finally, in regard to IP-10 secretion, the effect of IFN-β in presence of LPS was dependent on both STAT2 and STAT3 activation, while being independent of STAT1 (**Figure 3E**).

IFN-β Activates STAT2 and STAT3 to Modulate LPS-Induced Pro-IL-1β Expression in CF

We have previously reported that LPS induces pro-IL-1β expression in CF. To evaluate the effects of IFN-β on expression of this cytokine, CF were treated with LPS for 8 h. LPS significantly increased pro-IL-1β expression, while IFN-β by itself had no effect. However, INF-β significantly decreased LPS-induced pro-IL-1β expression, which was completely abolished when CF were pretreated with Ruxolitinib (**Figure 4A**) As shown by the use of siRNA, both si-STAT2 and si-STAT3 were involved in IFN-β effects on pro-IL-1β expression on LPS-treated CF, whereas STAT1 was not involved (**Figure 4B**).

IFN-β Activates STAT3 to Inhibit LPS-Induced ICAM-1 and VCAM-1 Expression in CF

The aim of experiment was to evaluate whether IFN-β-activated STAT proteins could also regulate cell adhesion

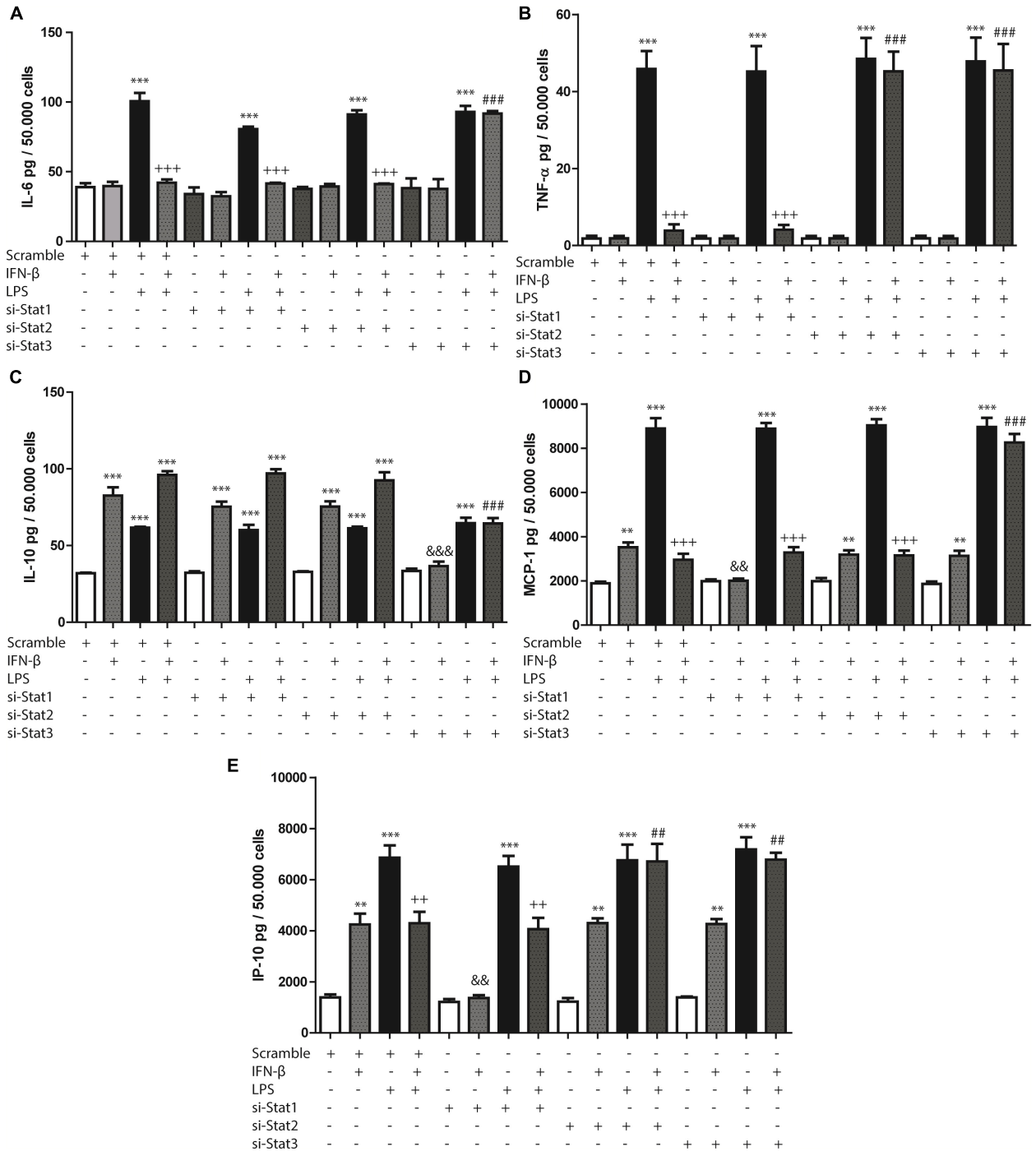

FIGURE 3 | Effects of IFN-β and STAT proteins on LPS-induced cytokine secretion: **(A–E)** CF were transfected with scramble or 200 ng of si-STAT1, si-STAT2, and si-STAT3 for 8 h, serum-deprived of for 24 h, pre-treated with IFN-β for 1 h, and stimulated with LPS for 24 h. **(A)** IL-6, **(B)** TNF-β, **(C)** IL-10, **(D)** MCP-1 and **(E)** IP-10 secretion to the culture medium was determined by LUMINEX assay. Error bars indicate the SD for three independent experiments. $^{***}p < 0.001$, $^{**}p < 0.01$, vs. scramble. $^{+++}p < 0.001$ vs. scramble + LPS. $^{\#\#\#}p < 0.001$, $^{\#\#}p < 0.01$ vs. scramble + IFN-β + LPS. $^{\&\&\&}p < 0.001$, $^{\&\&}pp < 0.01$ vs. scramble + IFN-β.

protein expression in CF (another important characteristic of inflammation). As shown by **Figures 5A,B**, LPS significantly increased ICAM-1 and VCAM-1 protein expression levels in CF, while prestimulation of IFN-β inhibited LPS-induced expression of ICAM-1 and VCAM-1, by activation of STAT3. On the contrary, neither STAT1 and STAT2 were involved in IFN-β inhibition of cell adhesion proteins expression in LPS-treated CF.

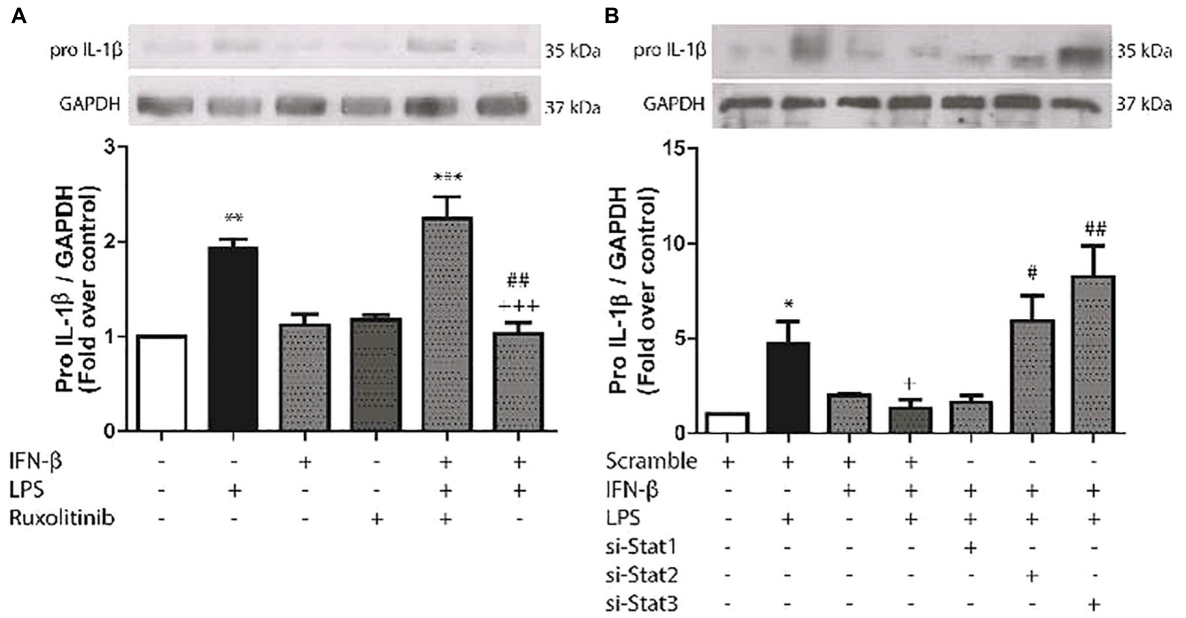

FIGURE 4 | Effects of IFN-β and STAT proteinson LPS-induced pro-IL-1β protein expression. **(A)** CF were pretreated with or without Ruxolitinib (500 nM) for 1 h and stimulated with IFN-β (500 U/ml) for 24 h. The upper panel shows a representative Western blot image, indicating expression levels of pro-IL-1β protein and GAPDH (used as charge control). The graphical analysis is presented at the bottom of the panel. Error bars indicate the SD for three independent experiments. $^{***}p < 0.001$, $^{**}p < 0.01$ vs. control. $^{\#\#}p < 0.01$ vs. LPS. $^{+++}p < 0.001$ vs. Ruxo + IFN-β + LPS). **(B)** CF were transfected with scramble or 200 ng of si-STAT1, si-STAT2, and si-STAT3 for 8 h, serum-deprived for 24 h, pretreated with IFN-β (500 U/ml) for 1 h, and stimulated with LPS (1 μg / ml) for 8 h. The upper panel shows a Western blot image, indicating expression levels of pro-IL-1β protein and GAPDH (used as charge control). The graphical analysis is presented at the bottom of the panel. Error bars indicate the SD for three independent experiments. $^{*}p < 0.05$ vs. scramble. $^{+}p < 0.05$ vs. scramble + LPS. $^{\#\#}p < 0.01$, $^{\#}p < 0.05$ vs. scramble + IFN-β + LPS.

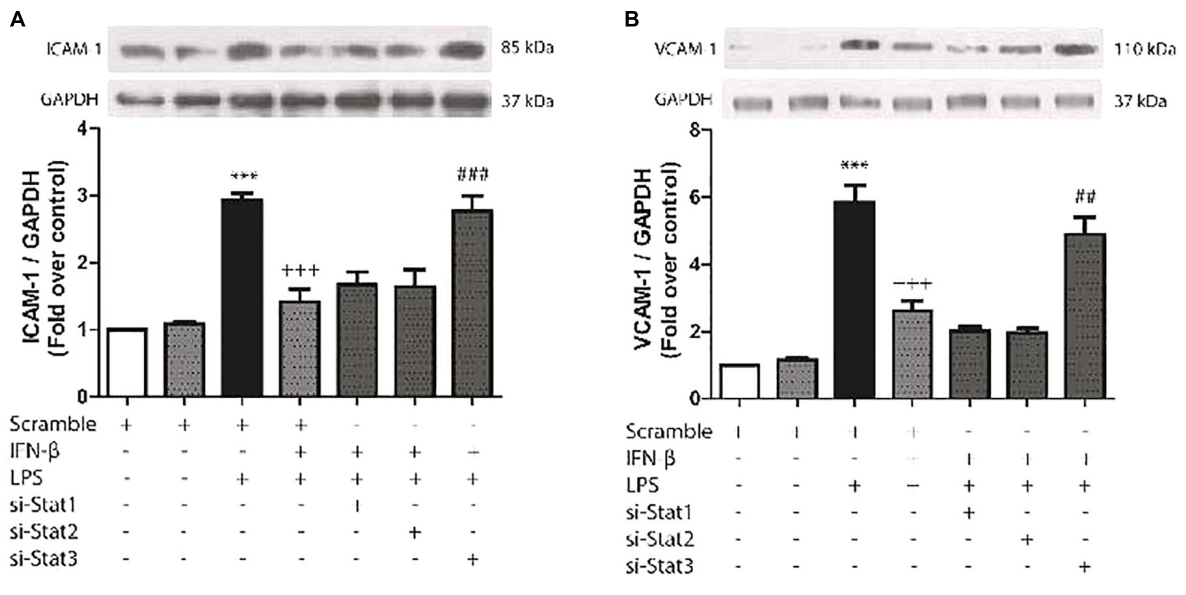

FIGURE 5 | IFN-β decreases LPS-induced ICAM-1/VCAM-1 expression through STAT3. **(A–B)** CF were transfected with scramble or 200 ng of si-STAT1, si-STAT2, and si-STAT3 for 8 h, serum-deprived for 24 h, pretreated with IFN-β (500 U/ml) for 1 h, and stimulated with LPS (1 μg/ml) for 8 h. **(A)** The upper panel shows a representative Western blot image, indicating expression levels of ICAM-1 and GAPDH (used as charge control). The graphical analysis is presented at the bottom of each panel. Error bars indicate the SD for three independent experiments. $^{***}p < 0.001$ vs. scramble. $^{+++}p < 0.001$ vs. scramble + LPS. $^{\#\#\#}p < 0.001$ vs. scramble + IFN-β + LPS. **(B)** The upper panel shows a representative Western blot image, indicating expression levels of VCAM-1 and GAPDH (used as charge control). The graphical analysis is presented at the bottom of each panel. Error bars indicate the SD for three independent experiments. $^{***}p < 0.001$ vs. scramble. $^{+++}p < 0.001$ vs. scramble + LPS. $^{\#\#}p < 0.01$ vs. scramble + IFN-β + LPS.

IFN-β Activates STAT3 to Inhibit LPS-Induced Neutrophil Recruitment by CF

Previous work from our laboratory has shown that CF are able to recruit immune system cells by secreting chemokines and increasing cell adhesion proteins on the surface of CF. In agreement with our previous findings, we observed that LPS induced IP-10 and MCP-1 secretion in CF, as well as ICAM-1 and VCAM-1 expression, and that IFN-β inhibited these effects. We then asked whether the changes in both cytokines/chemokines and cell adhesion molecules induced by IFN-β could modulate neutrophil recruitment to CF. Neutrophil migration toward conditioned medium obtained from CF treated with IFN-β was increased respect to media from untreated CF. The migration of neutrophils was also increased when moving toward culture media obtained from LPS-treated CF; however, when CF were pretreated with IFN-β before LPS stimulation a synergic effect was not observed and neutrophil migration was similar to that observed in IFN-β alone (**Figure 6**). Only STAT1 activation was involved in neutrophil migration to IFN-β-treated CF media, whereas STAT2 and STAT3 were necessary for the migration of neutrophils to culture media obtained from LPS-treated CF that were previously incubated with IFN-β (**Figure 6**).

For the adhesion assays, 34.3% of the neutrophils adhered to CF surface (**Figure 7A**). Adhesion increased to 40.3% for IFN-β-treated CF (**Figure 7B**) and to 68.3%for LPS-treated CF (**Figure 7C**). In a similar trend to our previous results, CF pretreatment with IFN-β before LPS, seems to exert a non-synergic antinflammatory effects since neutrophil adhesion was lower than LPS stimulation alone (42 versus 68.3%, respectively) (**Figure 7D**). Adhesion was not dependent on STAT1 nor STAT2; however, activation of STAT3 by IFN-β, was crucial for inhibiting the LPS-induced neutrophil adhesion (**Figures 7E,F**). si-STAT3 blocked the effect of IFN-β, boosting neutrophil adhesion to 62.6% (**Figure 7G**). **Figure 7H** shows a graphical analysis of the adhesion results.

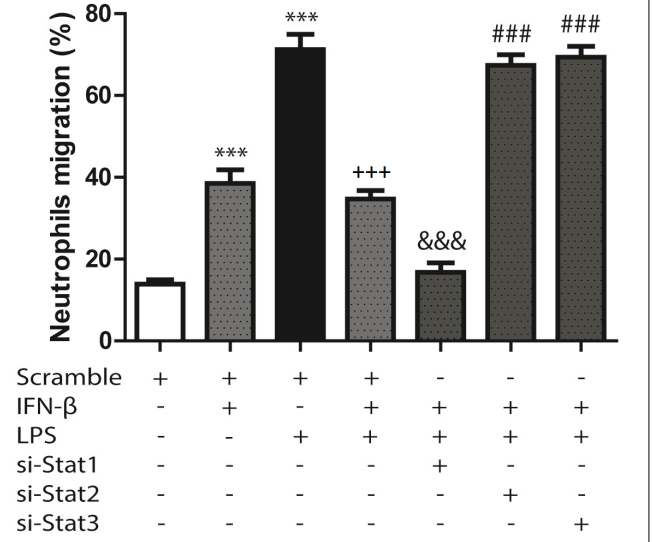

FIGURE 6 | Neutrophil migration induced by conditioned culture media derived from IFN-β- and LPS-treated CF: assays were performed in transwell chambers. Neutrophils charged with fluorescent calcein were seeded in the upper chamber and allowed to migrate at 37°C for 3 h to the lower chamber containing conditioned culture medium derived from CF that were transfected with scramble or 200 ng of STAT1 siRNA, STAT2, and STAT3 for 8 h, serum-deprived for 24 h, pretreated with IFN-β (500 U/ml) for 1 h, and stimulated with LPS (1 μg/ml) for 8 h. Fluorescent neutrophils that migrated to the lower compartment were measured using a fluorescence spectrometer, and the chemotactic activity was expressed as the percentage of fluorescent cells in the lower chamber as compared to the fluorescence of the total neutrophils added. Error bars indicate the SD for three independent experiments. $^{***}p < 0.001$ vs. scramble. $^{+++}p < 0.001$ vs. scramble + LPS. $^{\&\&\&}p < 0.001$ vs. scramble + IFN-β. $^{\#\#\#}p < 0.001$ vs. scramble + IFN-β + LPS.

DISCUSSION

IFN-β through differential STAT protein activation, either by itself or previous to a pro-inflammatory stimulus (in this case, LPS), acts as a key regulator of the cellular inflammatory response in CF. The proinflammatory actions of IFN-β are STAT1-dependent, while its anti-inflammatory activity is mediated by STAT2 and/or STAT3 activation.

IFN-β Activates the JAK/STAT Signaling Pathway in CF

Activation of different STAT proteins by IFN-β produces diverse effects in various cell types (van Boxel-Dezaire et al., 2006). In cardiac tissue some studies have shown that cardiomyocytes express higher levels of IFN-β than CF; however, CF express higher levels of IFNAR, making CF more sensitive than cardiomyocytes to stimulation by IFN-β (Zurney et al., 2007). Type I interferons such as IFN-β can activate all known STAT proteins, and in this study, IFN-β activated STAT1, STAT2, and STAT3 proteins in CF. These actions occurred through JAK, since the effects were inhibited by the JAK inhibitor Ruxolitinib. Zurney et al. (2007), demonstrated that IFN-β induces STAT1 and STAT2 phosphorylation in rat CF (Zurney et al., 2007); however, in CF STAT protein activation is not exclusive to IFN, as IL-6 and Angiotensin II also induce STAT3 activation (Tsai et al., 2008; Meléndez et al., 2010). Our findings show that IFN-β exerts its effects in CF in a time- and concentration-dependent manner. These results are consistent with Pertsovskaya et al. (2013), who demonstrated that IFN-β activates early STAT1 phosphorylation, although additional phosphorylation is observed at later times. Similar results have also been found in other cell types (van Boxel-Dezaire et al., 2006; Happold et al., 2014). Collectively, our results show that IFN-β triggers STAT1, STAT2, and STAT3 protein phosphorylation in CF, with comparable kinetics for all three STAT proteins, at similar IFN-β concentrations and with similar time courses.

IFN-β Through STAT1 Activation Induce a Pro-inflammatory Effect in CF

To date, there has been little published evidence regarding modulation of cytokine and chemokine secretion by IFN-β in

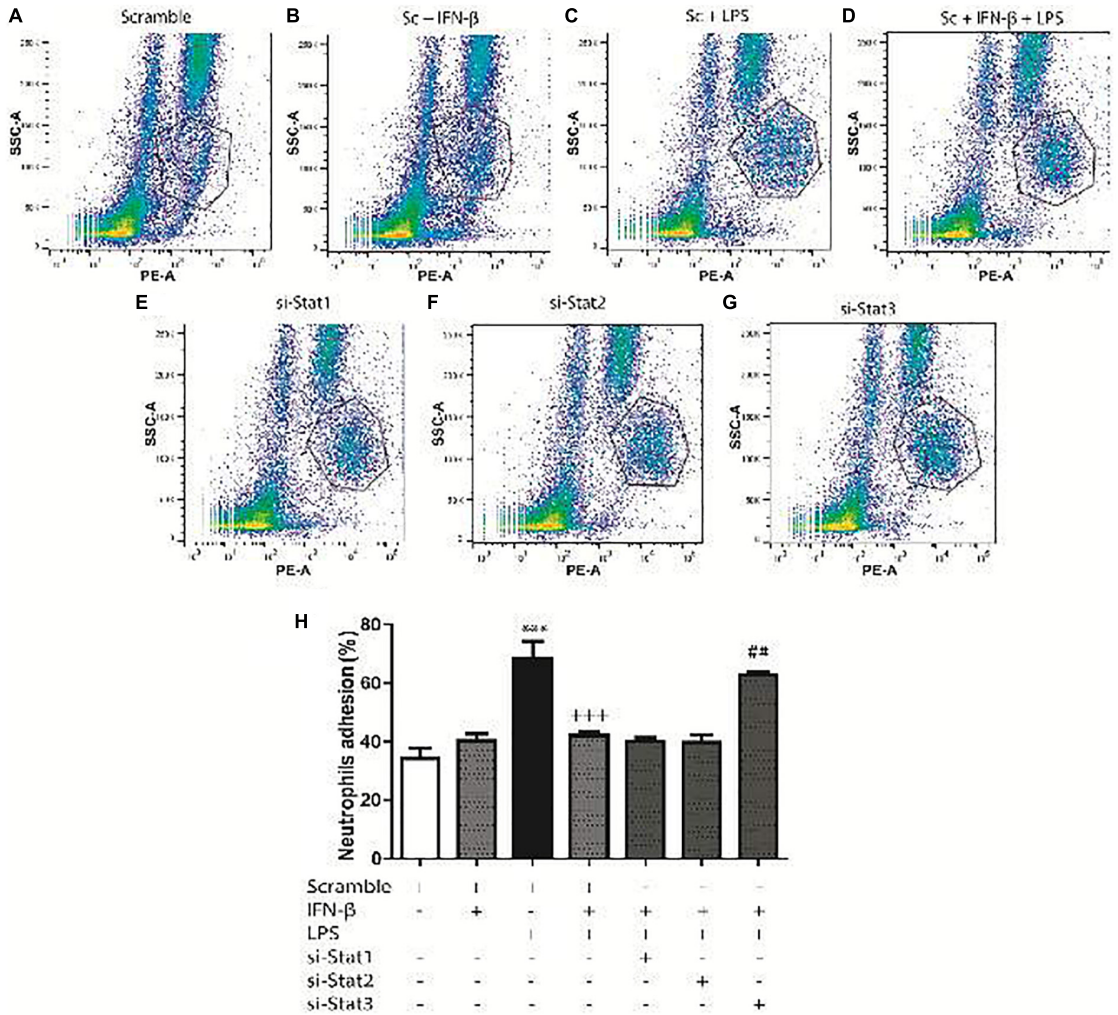

FIGURE 7 | IFN-β decreases neutrophil adhesion to CF. Leukocytes were labeled with anti-RP1/PE (neutrophil marker) and incubated for 2 h at 37°C with confluent monolayers of CF transfected with scramble or 200 ng si-STAT and treated with IFN-β and LPS. Cells were analyzed using flow cytometry. **(A–G)** FACS dots plots are representative images of the percentage of neutrophils adhered to CF. **(H)** Graphical analysis of the percentage of neutrophils in co-culture adhered to scramble-transfected CF with no treatment or treated with IFN-β or LPS. The neutrophil adhesion index was calculated was as follows: 100 x [no. cells (RP1 +) adhered/total number of cells (RP-1 +)]. Error bars indicate the SD for three independent experiments. $^{***}p < 0.001$ vs. scramble. $^{+++}p < 0.001$ vs. scramble + LPS. $^{\#\#}p < 0.01$ vs. scramble + IFN-β + LPS.

cultured CF. Our results demonstrate a dual action of IFN-β increasing proinflammatory and also anti-inflammatory cytokine secretion; however, previous to a pro-inflammatory environment (such as TLR4 activation by LPS), it behaves as an anti-inflammatory agent.

Chemokines, including MCP-1 and IP-10, are crucial for assembling the immune response, acting as chemoattractants for various immune cells (Frangogiannis, 2004). Our results show that IFN-β increased MCP-1 and IP-10 secretion by activating STAT1. Cumulative evidence suggests that STAT1 activation promotes the release of IP-10, in murine macrophages (Park et al., 2015), and it is well-known that increased STAT1 phosphorylation induces p65-NF-κβ phosphorylation and acetylation, promoting its activation and therefore increasing p65-NF-κβ-dependent proinflammatory response (Furrer et al., 2016). Whereas other studies have showed different results regarding the effect of STAT activation on chemokine and cytokine secretion. In human umbilical vein endothelial cells, MCP-1 mRNA expression was dependent on STAT3 activation (Wiejak et al., 2013). According to our results, we suggest that STAT1 activation by IFN-β plays a key role in the pro-inflammatory response of cultured CF.

In CF Previous to a Pro-inflammatory Stimulus, IFN-β Through STAT2 and/or STAT3 Activation Induces an Anti-inflammatory Effect

Our results show that IFN-ß by itself, produces a modest increase in secretion of cytokine IL-10. However, when CF are challenged

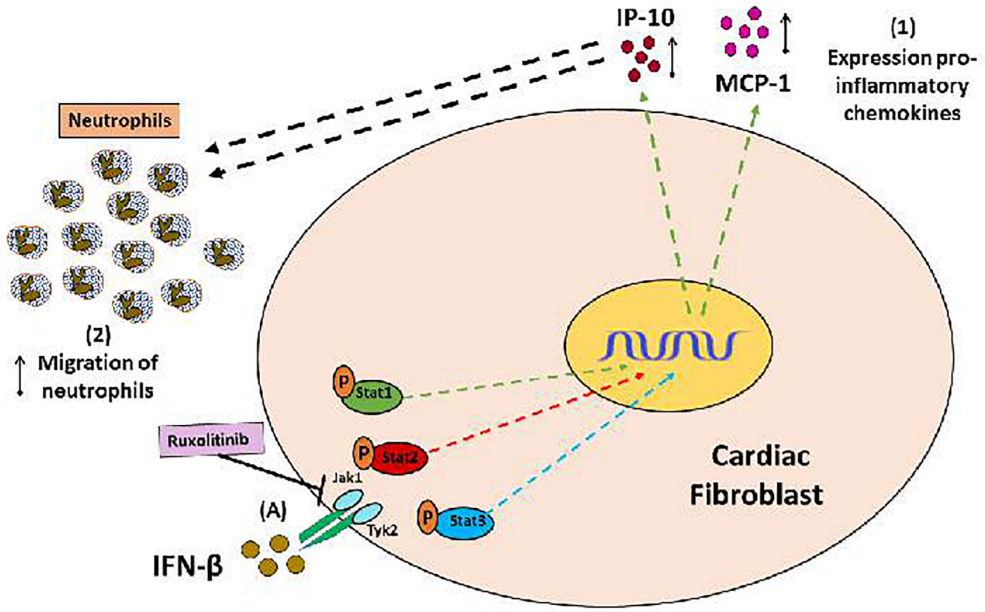

FIGURE 8 | Proinflammatory and anti-inflammatory effects of IFN-β in CF: (A) IFN-β triggers JAK/STATsignaling pathway activation (STAT1, STAT3, and STAT3 proteins). (1) IFN-β induces a pro-inflammatory response in the CF through STAT1 protein activation (green arrows), characterized by increased expression of the chemokines IP-10 and MCP-1, as well as (2) increased neutrophil migration, favored by chemokines released from CF.

with a potent pro-inflammatory stimulus like LPS, IFN-ß shows a stronger anti-inflammatory effect, as IFN-β inhibited LPS-induced IL-6 and TNF-α secretion. Our results suggest that STAT3 activation is crucial for IFN-β-induced IL-10 secretion, as well as its suppressive effect on the LPS-induced TNF-α and IL-6 secretion. Studies in other cell types partially coincide with our results. Ramgolam et al. (2009), suggested that IFN-β1 induces IL-10 secretion through STAT1 and STAT3 activation, and this effect inhibits Th17 cell differentiation (Ramgolam et al., 2009). However, other studies have found results contrary to ours. In murine dendritic cells, IFN-β-induced IL-10 secretion is mediated through the IFNAR in a STAT2-dependent manner (Yen et al., 2015), whereas STAT1 was also identified as a negative regulator of IL-10 expression in monocytes *in vivo* (VanDeusen et al., 2006). Our results suggest that in CF, IFN-β previous to a pro-inflammatory stimulus, provides a protective, anti-inflammatory effect increasing IL-10 levels and inhibiting LPS-induced IL-6 and TNF-α secretion.

Various studies have shown that CF are the main source of IL-1β in the infarcted myocardium (Long, 2001; Nian et al., 2004). Boza et al. (2016) demonstrated that in CF, LPS increases pro-IL-1β expression, which is dependent on the PI3K/Akt and NF-κβ signaling pathways. However, LPS does not activate the NLRP3 inflammasome and consequently does not triggers pro-IL-1β fragmentation and active IL-1β secretion. The same authors demonstrated that ATP is required for inflammasome assembly and activation, which triggers fragmentation of pro-IL-1β to its active form IL-1β and stimulates its secretion (Boza et al., 2016). Our results show that IFN-β inhibits LPS-induced pro-IL-1β expression through the JAK/STAT2 and/or STAT3 pathways. Although the exact mechanism remains unknown, there is evidence that IFN-β affects IL-1β secretion. Guarda et al. (2011), reported that IFN-I inhibits IL-1β production in bone marrow-derived murine macrophages through transcription of p-STAT1 dimers, repressing the activity of the inflammatory proteins NLRP1 and NLRP3 (Guarda et al., 2011). These interesting findings are consistent with our results, suggesting that IFN-I is capable of inhibiting pro-IL-1β production. The STAT-activated proteins implicated in the studies are different, likely attributable to the different cell types. However, other data from immune cell studies show contradictory results. Malireddi and Kanneganti (2013), demonstrated that IFN-I activates the inflammasome through upregulation of caspase-1 and expression of NLRP3, RIG-I, and AIM2, potentiating the inflammatory response. Given the importance of CF in IL-1β expression and secretion, our results suggest that in CF, the IFN-β through STAT2 and STAT3 activation negatively regulates the inflammatory response triggered by a pro-inflammatory stimulus.

IFN-β Activates STAT2 and STAT3 to Decrease Cell Adhesion Molecule Expression and Neutrophil Recruitment

Immune cell recruitment is a key step in the progression of inflammation-associated cardiovascular pathologies. This step depends initially on chemokine secretion and ICAM-1 and VCAM-1 expression at the inflammation site (Kukielka et al., 1993; Cook-Mills et al., 2011). Couture et al. (2009), have shown that TNF-α and PMA increase neutrophil recruitment by CF. Previous results from our laboratory have shown that in CF,

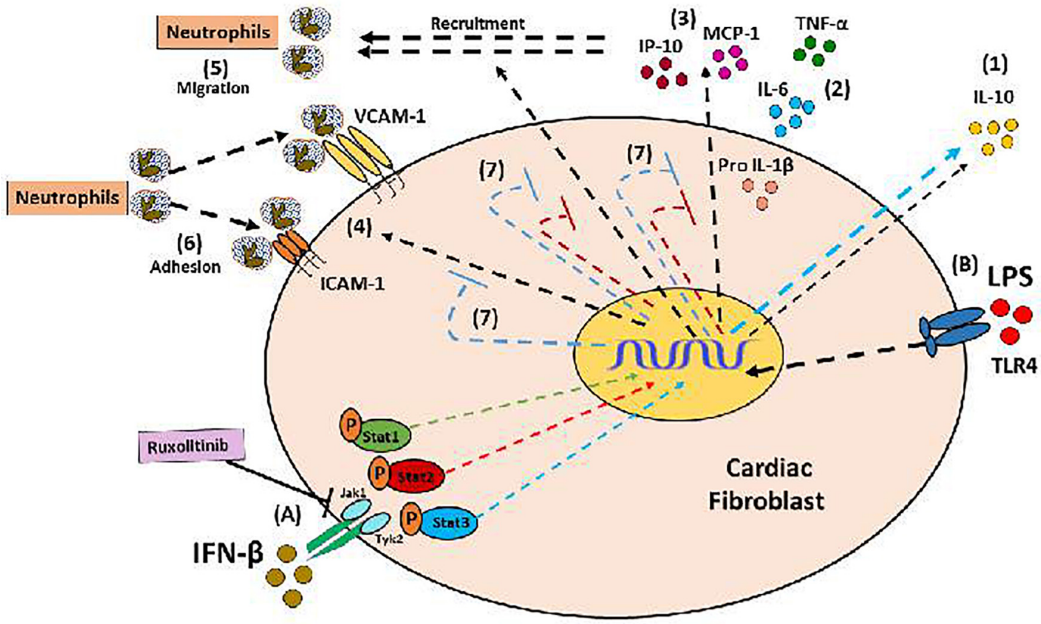

FIGURE 9 | Anti-inflammatory effect of IFN-β in CF: **(A)** IFN-β induces the activation of its JAK / STAT transduction pathway (proteins Stat1, Stat3, Stat3); and directly through Stat3 induces the secretion of IL-10 (1). **(B)** The LPS is a pro-inflammatory stimulus that favors the secretion of cytokines (2), chemokines (3), expression of adhesion molecules (4), which finally favors the recruitment of neutrophils by the FC (5 and 6) . (7) IFN-β through the activation of Stat2 and Stat3 proteins (red and blue STOP lines), inhibits the pro-inflammatory effects of LPS.

TLR4 activation by LPS, induces monocyte recruitment by CF themselves, due initially to the monocyte migration favored by MCP-1 secretion; whereas ICAM-1 and VCAM-1 expression in turn favors monocyte adhesion (Humeres et al., 2016). Our results show that in CF, IFN-β activates STAT3 to inhibit LPS-induced ICAM-1 and VCAM-1 expression. However, other studies have reported different results for the effect of IFN-β on adhesion protein expression. Combined treatment with TNF-α, IL-1β, and IFN-β has been shown to increase ICAM-1 and VCAM-1 expression in human umbilical vein endothelial cells (Shen et al., 1997; Dhib-Jalbut and Marks, 2010). Similarly, in the alveolar macrophages of rats with bleomycin-induced pulmonary fibrosis, STAT1 activation correlated significantly with increased ICAM-1 expression and severity of lung tissue inflammation (Fan and Wang, 2005). Collectively, our results reinforce the concept that STAT2 and/or STAT3 activation by IFN-β are essentials for triggering the anti-inflammatory response in CF.

Neutrophil infiltration occurs within the first few hours after tissue injury (Braunwald and Kloner, 1985), representing a crucial step for initiation of inflammatory repair (Kakkar and Lefer, 2004; Frangogiannis, 2006). Our results show that in CF, treatment with IFN-β alone increases neutrophil migration through STAT1 activation. There is abundant and contradictory data in the literature regarding the effects of IFN-β on cell migration. IFN-β prevents neutrophil infiltration in animal models of cerebral inflammation (Veldhuis et al., 2003a,b), and decreases serum-induced migration of polymorphonuclear cells (Aas et al., 1996). On the other hand, our results show that when CF are challenged by a pro-inflammatory stimulus such as LPS, IFN-β through STAT2 and STAT3 activation decreases both chemokine secretion and adhesion molecule expression. This effects decreases neutrophil recruitment, demonstrating the anti-inflammatory properties of IFN-β in CF.

To date, no other *in vitro* studies have elucidated the effect of IFN-β and/or STAT activation on neutrophil recruitment by CF. Our results allow us to conclude that previous to a pro-inflammatory environment induced by an inflammatory insult, IFN-β exerts an anti-inflammatory effect in CF, reducing neutrophil recruitment. It is well-known that neutrophil recruitment after cardiac injury is crucial for rapidly inducing the healing process; however, prolonged neutrophil recruitment may lead to chronic inflammation in the tissue and eventually cardiac fibrosis (Frangogiannis et al., 2002; Frangogiannis and Entman, 2005; Frangogiannis, 2006).

CONCLUSION

Collectively, our results help to understand the *in vitro* regulation of INF-β-mediated inflammatory response in CF. IFN-β plays a dual role in regulating inflammation, acting as a crucial player in modulating the pro- or anti-inflammatory behavior of CF depending of environment. IFN-β by itself, activates STAT1 to generate a pro-inflammatory response, characterized by increased chemokines MCP-1 and IP-10 expression, which increase neutrophil migration (see **Figure 8**). However, IFN-β also activates STAT3 to induce secretion of the anti-inflammatory cytokine IL-10 (see **Figure 9**, blue arrow). Nevertheless,

previous to a pro-inflammatory environment TLR4-activated, IFN-β triggers a marked anti-inflammatory effect in CF by activating STAT2 and/or STAT3. This anti-inflammatory effect is characterized by inhibition of LPS-induced IL-6, TNF-α, MCP-1, and IP-10 secretion and reduction of pro-IL-1β, ICAM-1, and VCAM-1 expression, decreasing neutrophil recruitment.

AUTHOR CONTRIBUTIONS

SB, RA, CH, RV, PB, and GD-A contributed to the conception and design of the study. CM and VP-J organized the database. SB, FO-S, and RV performed the statistical analysis. SB and GD-A wrote the first draft of the manuscript. CM, VP-J, PB, and CH wrote sections of the manuscript. All authors contributed to manuscript revision, read and approved the submitted version.

FUNDING

This work was supported by FONDECYT (Grant Nos. 1130300 and 1170425 to GD-A), CONICYT (Grant No. 63130233 to SB), and FONDAP ACCDiS (Grant No. 15130011).

SUPPLEMENTARY MATERIAL

The Supplementary Material for this article can be found online at: https://www.frontiersin.org/articles/10.3389/fphar.2018.01368/full#supplementary-material

FIGURE S1 | Identification of neutrophil population isolated from bone marrow.

FIGURE S2 | Effectiveness and selectivity of siRNA.

REFERENCES

Aas, V., Lappegård, K. T., Siebke, E. M., and Benestad, H. B. (1996). Modulation by interferons of human neutrophilic granulocyte migration. *J. Interferon Cytokine Res.* 16, 929–935. doi: 10.1089/jir.1996.16.929

Boza, P., Ayala, P., Vivar, R., Humeres, C., Tapia Cáceres, F., Muñoz, C., et al. (2016). Expression and function of toll-like receptor 4 and inflammasomes in cardiac fibroblasts and myofibroblasts: IL-1β synthesis, secretion, and degradation. *Mol. Immunol.* 74, 96–105. doi: 10.1016/j.molimm.2016.05.001

Braunwald, E., and Kloner, R. A. (1985). Myocardial reperfusion: a double-edged sword? *J. Clin. Invest.* 76, 1713–1719. doi: 10.1172/JCI112160

Chen, J., Baig, E., and Fis, E. N. (2004). Diversity and relatedness among the type I interferons. *J. Interferon Cytokine Res.* 24, 687–698. doi: 10.1089/jir.2004.24.687

Coclet-Ninin, J., Dayer, J. M., and Burger, D. (1997). Interferon-beta not only inhibits interleukin-1beta and tumor necrosis factor-alpha but stimulates interleukin-1 receptor antagonist production in human peripheral blood mononuclear cells. *Eur. Cytokine Netw.* 8, 345–349.

Cook-Mills, J. M., Marchese, M. E., and Abdala-Valencia, H. (2011). Vascular cell adhesion molecule-1 expression and signaling during disease: regulation by reactive oxygen species and antioxidants. *Antioxid. Redox Signal.* 15, 1607–1638. doi: 10.1089/ars.2010.3522

Couture, P., Paradis-Massie, J., Oualha, N., and Thibault, G. (2009). Adhesion and transcellular migration of neutrophils and B lymphocytes on fibroblasts. *Exp. Cell Res.* 315, 2192–2206. doi: 10.1016/j.yexcr.2009.04.013

Darnell, J. E., Kerr, I. M., and Stark, G. R. (1994). JAK-STAT pathways, and transcriptional activation in response to IFNs, and other extracellular proteins. *Science* 264, 1415–1421. doi: 10.1126/science.8197455

Dewald, O., Zymek, P., Winkelmann, K., Koerting, A., Ren, G., Abou-Khamis, T., et al. (2005). CCL2/monocyte chemoattractant protein-1 regulates inflammatory responses critical to healing myocardial infarcts. *Circ. Res.* 96, 881–889. doi: 10.1161/01.RES.0000163017.13772.3a

Dhib-Jalbut, S., and Marks, S. (2010). Interferon-beta mechanisms of action in multiple sclerosis. *Neurology* 74, S17–S24. doi: 10.1212/WNL.0b013e3181c97d99

Díaz-Araya, G., Vivar, R., Humeres, C., Boza, P., Bolívar, S., and Muñoz, C. (2015). Cardiac fibroblasts as sentinel cells in cardiac tissue: receptors, signaling pathways and cellular functions. *Pharmacol. Res.* 101, 30–40. doi: 10.1016/j.phrs.2015.07.001

Fan, X., and Wang, Z. (2005). STAT1 antisense oligonucleotides attenuate the proinflammatory cytokine release of alveolar macrophages in bleomycin-induced fibrosis. *Cell Mol. Immunol.* 2, 211–217.

Frangogiannis, N. G. (2004). Chemokines in the ischemic myocardium: from inflammation to fibrosis. *Inflamm. Res.* 53, 585–595. doi: 10.1007/s00011-004-1298-5

Frangogiannis, N. G. (2006). The mechanistic basis of infarct healing. *Antioxid. Redox Signal.* 8, 1907–1939. doi: 10.1089/ars.2006.8.1907

Frangogiannis, N. G. (2007). Chemokines in ischemia and reperfusion. *Thromb. Haemost.* 97, 738–747. doi: 10.1160/TH07-01-0022

Frangogiannis, N. G., and Entman, M. L. (2005). Chemokines in myocardial ischemia. *Trends Cardiovasc. Med.* 15, 163–169. doi: 10.1016/j.tcm.2005.06.005

Frangogiannis, N. G., Smith, C. W., and Entman, M. L. (2002). The inflammatory response in myocardial infarction. *Cardiovasc. Res.* 53, 31–47. doi: 10.1016/S0008-6363(01)00434-5

Furrer, A., Hottiger, M. O., and Valaperti, A. (2016). Absent in Melanoma 2 (AIM2) limits pro-inflammatory cytokine transcription in cardiomyocytes by inhibiting STAT1 phosphorylation. *Mol. Immunol.* 74, 47–58. doi: 10.1016/j.molimm.2016.04.009

Guarda, G., Braun, M., Staehli, F., Tardivel, A., Mattmann, C., and Förster, I. (2011). Type I interferon inhibits interleukin- 1 production and inflammasome activation. *Immunity* 34, 213–223. doi: 10.1016/j.immuni.2011.02.006

Haghikia, A., Ricke-Hoch, M., Stapel, B., Gorst, I., and Hilfiker-Kleiner, D. (2014). STAT3, akey regulator of cell-to-cell communication in the heart. *Cardiovasc. Res.* 102, 281–289. doi: 10.1093/cvr/cvu034

Happold, C., Roth, P., Silginer, M., Florea, A. M., Lamszus, K., Frei, K., et al. (2014). Interferon-β induces loss of spherogenicity and overcomes therapy resistance of glioblastoma, stem. *Cells Mol. Cancer Ther.* 13, 948–961. doi: 10.1158/1535-7163.MCT-13-0772

Humeres, C., Vivar, R., Boza, P., Muñoz, C., Bolivar, S., Anfossi, R., et al. (2016). Cardiac fibroblast cytokine profiles induced by proinflammatory or profibrotic stimuli promote monocyte recruitment and modulate macrophage M1/M2 balance in vitro. *J. Mol. Cell. Cardiol.* 101, 69–80. doi: 10.1016/j.yjmcc.2016.10.014

Ihle, J. N. (1995). The Janus protein tyrosine kinase family and its role in cytokine signaling. *Adv. Immunol.* 6, 1–35. doi: 10.1016/S0065-2776(08)60582-9

Ivashkiv, L. B., and Donlin, L. T. (2014). Regulation of type I interferon responses. *Immunology* 14, 36–49. doi: 10.1038/nri3581

Jungo, F., Dayer, J. M., Modoux, C., Hyka, N., and Burger, D. (2001). IFN-β inhibits the ability of T lymphocytes to induce TNF-α and IL-1β production in monocytes upon direct cell-cell contact. *Cytokine* 14, 272–282. doi: 10.1006/cyto.2001.0884

Kacimi, R., Karliner, J. S., Koudssi, F., and Long, C. S. (1998). Expression and regulation of adhesion molecules in cardiac cells by cytokines. *Circ. Res.* 82, 576–586. doi: 10.1161/01.RES.82.5.576

Kakkar, A. K., and Lefer, D. J. (2004). Leukocyte and endothelial adhesion molecule studies in knockout mice. *Curr. Opin. Pharmacol.* 4, 154–158. doi: 10.1016/j.coph.2004.01.003

Kukielka, G. L., Hawkins, H. K., Michael, L., Manning, A. M., Youker, K., Lane, C., et al. (1993). Regulation of intercelular adhesion molecule-1 (ICAM-1) expression in ischemic and reperfused myocardium. *J. Clin. Invest.* 92, 1504–1516. doi: 10.1172/JCI116729

Kukielka, G. L., Smith, C. W., LaRosa, G. J., Manning, A. M., Mendoza, L. H., Daly, T. J., et al. (1995). Interleukin-8 gene induction in the myocardium after

ischemia and reperfusion in vivo. *J. Clin. Invest.* 95, 89–103. doi: 10.1172/JCI117680

Long, C. S. (2001). The role of interleukin-1 in the failing heart, *Heart Fail. Rev.* 6, 81–94.

López de Padilla, C. M., and Niewold, T. B. (2016). The type I interferons: basic concepts and clinical relevance in immune-mediated inflammatory diseases. *Gene* 576, 14–21. doi: 10.1016/j.gene.2015.09.058

Malireddi, R. K., and Kanneganti, T. D. (2013). Role of type I interferons in inflammasome activation, cell death, and disease during microbial infection. *Front. Cell. Infect. Microbiol.* 3:77. doi: 10.3389/fcimb.2013.00077

Meléndez, G. C., McLarty, J. L., Levick, S. P., Du, Y., Janicki, J. S., and Browe, G. L. (2010). Interleukin 6 mediates myocardial fibrosis, concentric hypertrophy, and diastolic dysfunction in rats. *Hypertension* 56, 225–231. doi: 10.1161/HYPERTENSIONAHA.109.148635

Nahrendorf, M., Swirski, F. K., Aikawa, E., Stangenberg, L., Wurdinger, T., Figueiredo, J. L., et al. (2007). The healing myocardium sequentially mobilizes two monocyte subsets with divergent and complementary functions. *J. Exp. Med.* 204, 3037–3047. doi: 10.1084/jem.20070885

Nian, M., Lee, P., Khaper, N., and Liu, P. (2004). Inflammatory cytokines and postmyocardial infarction remodeling. *Cir. Res.* 94, 1543–1553. doi: 10.1161/01.RES.0000130526.20854.fa

O'Shea, J. J., and Murray, P. J. (2008). Cytokine signaling modules in inflammatory responses. *Immunity* 28, 477–487. doi: 10.1016/j.immuni.2008.03.002

Park, O. J., Cho, M. K., Yun, C. H., and Han, S. H. (2015). Lipopolysaccharide of *Aggregatibacter actinomycetemcomitans* induces the expression of chemokines MCP-1, MIP-1α, and IP-10 via similar but distinct signaling pathways in murine macrophages. *Immunobiology* 220, 1067–1074. doi: 10.1016/j.imbio.2015.05.008

Pertsovskaya, I., Abad, E., Domedel-Puig, N., Garcia-Ojalvo, J., and Villoslada, P. (2013). Transient oscillatory dynamics of interferon beta signaling in macrophages. *BMC Syst. Biol.* 7:59. doi: 10.1186/1752-0509-7-59

Platanias, L. C. (2005). Mechanisms of type-I and type-II-interferon-mediated signaling. *Nat. Rev. Immunol.* 5, 375–386. doi: 10.1038/nri1604

Ramgolam, V. S., Sha, Y., Jin, J., Zhang, X., and Markovic-Plese, S. (2009). IFN-beta inhibits human Th17 cell differentiation. *J. Immunol.* 183, 5418–5427. doi: 10.4049/jimmunol.0803227

Rudick, R. A., Ransohoff, R. M., Peppler, R., VanderBrug Medendorp, S., Lehmann, P., and Alam, J. (1996). Interferon beta induces interleukin-10 expression: relevance to multiple sclerosis. *Ann. Neurol.* 40, 618–627. doi: 10.1002/ana.410400412

Shen, J., T-To, S. S., Schrieber, L., and King, N. J. (1997). Early E-selectin, VCAM-1, ICAM-1, and late major histocompatibility complex antigen induction on human endothelial cells by flavivirus and comodulation of adhesion molecule expression by immune cytokines. *J. Virol.* 71, 9323–9332.

Skrajnar, S., Anzur-Lasnik, M., and Bedina-Zavec, A. (2009). A flow cytometric method for determination of the blood neutrophil fraction in rats. *J. Am. Assoc. Lab. Anim. Sci.* 48, 152–156.

Szelag, M., Piaszyk-Borychowska, A., Plens-Galaska, M., Wesoly, J., and Bluyssen, H. A. (2016). Targeted inhibition of STATs and IRFs as a potential treatment strategy in cardiovascular disease. *Oncotarget* 7, 48788–48812. doi: 10.18632/oncotarget.9195

Tsai, C. T., Lai, L. P., Kuo, K. T., Hwang, J. J., Hsieh, C. S., Hsu, K. L., et al. (2008). Angiotensin II activates signal transducer and activators of transcription 3 via Rac1 in atrial myocytes and fibroblasts: implication for the therapeutic effect of statin in atrial structural remodeling. *Circulation* 117, 344–355. doi: 10.1161/CIRCULATIONAHA.107.695346

Turner, N. A., Das, A., O'Regan, D. J., Ball, S. G., and Porter, K. E. (2011). Human cardiac fibroblasts express ICAM-1, E-selectin and CXC chemokines in response to proinflammatory cytokine stimulation, Int. *J. Biochem. Cell. Biol.* 43, 1450–1458. doi: 10.1016/j.biocel.2011.06.008

Turner, N. A., Das, A., Warburton, P., O'Regan, D. J., Ball, S. G., and Porter, K. E. (2009). Interleukin-1α stimulates pro-inflammatory cytokine expression in human cardiac myofibroblasts. *Am. J. Physiol. Heart Circ. Physiol.* 297, H1117–H1127. doi: 10.1152/ajpheart.00372.2009

Turner, N. A., Warburton, P., O'Regan, D. J., Ball, S. G., and Porter, K. E. (2010). Modulatory effect of interleukin-1α on expression of structural matrix proteins, MMPs and TIMPs in human cardiac myofibroblasts: role of p38 MAP kinase. *Matrix Bio.* 29, 613–620. doi: 10.1016/j.matbio.2010.06.007

van Boxel-Dezaire, A. H., Rani, M. R., and Stark, G. R. (2006). Complex modulation of cell type-specific signaling in response to type I interferons. *Immunity* 25, 361–372. doi: 10.1016/j.immuni.2006.08.014

Van Linthout, S., Miteva, K., and Tschoöpe, C. (2014). Crosstalk between fibroblasts and inflammatory cells. *Cardiovasc. Res.* 102, 258–269. doi: 10.1093/cvr/cvu062

VanDeusen, J. B., Shah, M. H., Becknell, B., Blaser, B. W., Ferketich, A. K., Nuovo, G. J., et al. (2006). STAT-1-mediated repression of monocyte interleukin-10 gene expression in vivo. *Eur. J. Immunol.* 36, 623–630. doi: 10.1002/eji.200535241

Veldhuis, W. B., Derksen, J. W., Floris, S., Van Der Meide, P. H., De Vries, H. E., Schepers, J., et al. (2003a). Interferon-beta blocks infiltration of inflammatory cells and reduces infarct volume after ischemic stroke in the rat. *J. Cereb. Blood Flow Metab.* 23, 1029–1039.

Veldhuis, W. B., Floris, S., Van der Meide, P. H., Vos, I. M., de Vries, H. E., Dijkstra, C. D., et al. (2003b). Interferon-beta prevents cytokine-induced neutrophil infiltration and attenuates blood-brain barrier disruption. *J. Cereb. Blood Flow Metab.* 23, 1060–1069.

Wiejak, J., Dunlop, J., Mackay, S. P., and Yarwood, S. J. (2013). Flavanoids induce expression of the suppressor of cytokine signalling 3 (SOCS3) gene and suppress IL-6-activated signal transducer and activator of transcription 3 (STAT3) activation in vascular endothelial cells. *Biochem. J.* 454, 283–293. doi: 10.1042/BJ20130481

Yen, J. H., Kong, W., Hooper, K. M., Emig, F., Rahbari, K. M., Kuo, P. C., et al. (2015). Differential effects of IFN-β on IL-12, IL-23, and IL-10 expression in TLR-stimulated dendritic cells. *J. Leukoc. Biol.* 98, 689–702. doi: 10.1189/jlb.3HI0914-453R

Zurney, J., Howard, K. E., and Sherry, B. (2007). Basal expression levels of IFNAR and Jak-STAT components are determinants of cell-type-specific differences in cardiac antiviral responses. *J. Virol.* 81, 13668–13680. doi: 10.1128/JVI.01172-07

Conflict of Interest Statement: The authors declare that the research was conducted in the absence of any commercial or financial relationships that could be construed as a potential conflict of interest.

frontiers in Pharmacology

ORIGINAL RESEARCH
published: 05 February 2019
doi: 10.3389/fphar.2018.01553

Angiotensin II-Regulated Autophagy Is Required for Vascular Smooth Muscle Cell Hypertrophy

*David Mondaca-Ruff[1], Jaime A. Riquelme[1], Clara Quiroga[2], Ignacio Norambuena-Soto[1], Fernanda Sanhueza-Olivares[1], Paulina Villar-Fincheira[1], Tomás Hernández-Díaz[1], Nicole Cancino-Arenas[1], Alejandra San Martin[3], Lorena García[1], Sergio Lavandero[1,4] and Mario Chiong[1]**

[1] Advanced Center for Chronic Diseases (ACCDiS), Centro de Estudios en Ejercicio, Metabolismo y Cáncer (CEMC), Departamento Bioquímica y Biología Molecular, Facultad Ciencias Químicas y Farmacéuticas, Universidad de Chile, Santiago, Chile, [2] Advanced Center for Chronic Diseases (ACCDiS), División de Enfermedades Cardiovasculares, Facultad de Medicina, Pontificia Universidad Católica de Chile, Santiago, Chile, [3] Division of Cardiology, Department of Medicine, Emory University, Atlanta, GA, United States, [4] Department of Internal Medicine (Cardiology Division), University of Texas Southwestern Medical Center, Dallas, TX, United States

Hypertension is a disease associated to increased plasma levels of angiotensin II (Ang II). Ang II can regulate proliferation, migration, ROS production and hypertrophy of vascular smooth muscle cells (VSMCs). However, the mechanisms by which Ang II can affect VSMCs remain to be fully elucidated. In this context, autophagy, a process involved in self-digestion of proteins and organelles, has been described to regulate vascular remodeling. Therefore, we sought to investigate if Ang II regulates VSMC hypertrophy through an autophagy-dependent mechanism. To test this, we stimulated A7r5 cell line and primary rat aortic smooth muscle cells with Ang II 100 nM and measured autophagic markers at 24 h by Western blot. Autophagosomes were quantified by visualizing fluorescently labeled LC3 using confocal microscopy. The results showed that treatment with Ang II increases Beclin-1, Vps34, Atg-12–Atg5, Atg4 and Atg7 protein levels, Beclin-1 phosphorylation, as well as the number of autophagic vesicles, suggesting that this peptide induces autophagy by activating phagophore initiation and elongation. These findings were confirmed by the assessment of autophagic flux by co-administering Ang II together with chloroquine (30 μM). Pharmacological antagonism of the angiotensin type 1 receptor (AT1R) with losartan and RhoA/Rho Kinase inhibition prevented Ang II-induced autophagy. Moreover, Ang II-induced A7r5 hypertrophy, evaluated by α-SMA expression and cell size, was prevented upon autophagy inhibition. Taking together, our results suggest that the induction of autophagy by an AT1R/RhoA/Rho Kinase-dependent mechanism contributes to Ang II-induced hypertrophy in VSMC.

Keywords: angiotensin II, VSMC, autophagy, hypertrophy, AT1R, ROCK, losartan

OPEN ACCESS

Edited by:
Jorge Fuentealba, Universidad de Concepción, Chile

Reviewed by:
Carlos F. Sánchez-Ferrer, Universidad Autónoma de Madrid, Spain
Marcelo González, Universidad de Concepción, Chile

****Correspondence:***
Mario Chiong
mchiong@ciq.uchile.cl

Specialty section:
This article was submitted to Translational Pharmacology, a section of the journal Frontiers in Pharmacology

Received: *02 October 2018*
Accepted: *20 December 2018*
Published: *05 February 2019*

Citation:
Mondaca-Ruff D, Riquelme JA, Quiroga C, Norambuena-Soto I, Sanhueza-Olivares F, Villar-Fincheira P, Hernández-Díaz T, Cancino-Arenas N, San Martin A, García L, Lavandero S and Chiong M (2019) Angiotensin II-Regulated Autophagy Is Required for Vascular Smooth Muscle Cell Hypertrophy. Front. Pharmacol. 9:1553. doi: 10.3389/fphar.2018.01553

INTRODUCTION

Cardiovascular diseases are a major cause of mortality around the world (Roth et al., 2017). Hypertension, which is generally characterized by high angiotensin II (Ang II) plasma levels, is a highly prevalent vascular disease, given that by 2015, 874 million people were reported to have a systolic blood pressure of 140 mm Hg or higher (Forouzanfar et al., 2017). Vascular smooth muscle

cells (VSMCs), a major component of the vessel wall, are responsible for the control of blood flow and arterial pressure by regulating the lumen's diameter of resistance vessels in response to Ang II (Rzucidlo et al., 2007; Gomez and Owens, 2012) through the activation of the AT1 receptor (AT1R) (Mehta and Griendling, 2007). In addition to this physiological response, sustain activation of the AT1R results in vascular remodeling that permanently increased vascular resistance (Taubman, 2003).

It has been well-established that Ang II induces VSMC hypertrophy, characterized by an increase in cell size. α-smooth muscle actin (α-SMA) and protein synthesis (Geisterfer et al., 1988; Andrawis et al., 1993). Moreover, the size of VSMCs of hypertensive patients is increased in comparison to normotensive ones (Owens, 1985; Gariepy et al., 1993). Besides VSMC hypertrophy and contraction, Ang II-mediated AT1R activation can also regulate cell proliferation, migration and reactive oxygen species production (Rosendorff, 1996; Touyz, 2005). Many of these processes are mediated by the activation of the RhoA/Rho Kinase (ROCK) signaling pathway (Seko et al., 2003). Pursuing new mechanisms involved in vascular remodeling, autophagy has been described to regulate VSMCs phenotype (Jia et al., 2006; Salabei and Hill, 2013). Autophagy, is a tightly regulated protein degradation mechanism that begins with the formation of a phagophore, then a double membrane vesicle called the autophagosome that fuses with the lysosome to promote the degradation and recycling of proteins and organelles (Gatica et al., 2015; Lavandero et al., 2015). Autophagy is a multistep process comprehended by an initiation complex conformed by Beclin 1 and Vps34 and two ubiquitin-like system formed by LC3 and the AuTophaGy-related (ATG) proteins. Beclin-1 induces autophagy by forming a complex with Vps34, a phosphatidyl inositol-3-kinase type III (PI3KCIII) that generates phosphatidylinositol-3-phosphate [PtdIns (3) P], which is necessary for the elongation of the autophagosome (Yin et al., 2016). Following the induction process, elongation is achieved by the activation of two parallel pathways: ATG proteins and the LC3 protein system (Yang and Klionsky, 2010). In this pathway, Atg7 presents activity similar to the E1 enzyme of the ubiquitin-proteasome system, which mediates the conjugation of Atg12 to Atg5, forming the Atg12-Atg5 complex, which subsequently is coupled with Atg16 forming the complex Atg12-Atg5-Atg16, which is required for the elongation of the autophagosome. In the other pathway, Atg4 can proteolyze the pro-LC3 to produce LC3 I. Then, LC3 I is conjugated to phosphatidyl ethanolamine (PE) by the action of Atg7 and Atg3 (ubiquitin-like E2 enzyme), generating LC3 II, which binds to the autophagosome membrane favoring its elongation (Mizushima et al., 1998). The final step is carried out by the fusion of the autophagosome with the lysosome, forming an autolysosome. The degradation of the content located within the autolysosome is carried out by lysosomal hydrolases, and the catabolized products are released into the cytosol and recycled to cover the nutrient and/or structural needs (Gatica et al., 2015; Lavandero et al., 2015). In line with this, it has been reported that TNF-α (Jia et al., 2006) and PDGF-BB (Salabei et al., 2013), which are increased in vascular pathologies, may also induce autophagy and dedifferentiation of VSMCs (Chen et al., 2013; Salabei et al., 2013). Nonetheless, the association between autophagy and phenotype switching of VSMCs, remains to be fully elucidated. Therefore, we sought to investigate whether Ang II induces VSMC hypertrophy through an autophagy dependent mechanism.

Here, we show that Ang II induces autophagy through the activation of phagophore initiation and elongation by an AT1R/RhoA/Rho Kinase-dependent mechanism. Moreover, autophagy inhibition completely prevents Ang II-induced hypertrophy in VSMC.

MATERIALS AND METHODS

Materials

Ang II (100 nM), losartan (1 μM), Y-27632 (10 μM), chloroquine (30 μM), siRNA scramble and siRNA against Beclin-1 were purchased from Sigma (Sigma-Aldrich, Corp., St. Louis, MO, United States). Spautin 1 (10 μM) was purchased from Cayman (Cayman Chemical Company, Ann Arbor, MI, United States). The following antibodies were used for the Western blot experiments: LC3 1:1000 (cat #2775 Cell Signaling, Danvers, MA, United States), Atg7 1:1000 (cat #8558 Cell Signaling, Danvers, MA, United States), Atg12–Atg5 1:500 (cat #2630 Cell Signaling, Danvers, MA, United States), Atg4 1:1000 (cat # 5299 Cell Signaling, Danvers, MA, United States), Beclin1 1:2000 (cat #3738 Cell Signaling, Danvers, MA, United States), p-Beclin1 Thr^{119} 1:500 (cat #ABC118 EMD Millipore, Darmstadt, Germany), Vps34/phosphatidylinositol 3-kinase class III (Vps34) 1:1000 (cat # 3811 Cell Signaling, Danvers, MA, United States), p-mTOR Ser^{2448} 1:1000 (cat # 2971 Cell Signaling, Danvers, MA, United States), p-TSC2 Thr^{1462} 1:1000 (cat # 3617 Cell Signaling, Danvers, MA, United States), p-p70s6k Thr^{389} 1:1000 (cat # 9205 Cell Signaling, Danvers, MA, United States), p-AMPKα Thr^{172} 1:1000 (cat # 50081 Cell Signaling, Danvers, MA, United States), p-4E-BP1 $Thr^{37/46}$ 1:1000 (cat # 2855 Cell Signaling, Danvers, MA, United States), MYPT1 (cat # 2634 Cell Signaling, Danvers, MA, United States), p-MYPT1 Thr^{853} 1:1000 (cat # 4563 Cell Signaling, Danvers, MA, United States), α-SMA 1:20000 (cat #ab7817 Abcam, Cambridge, MA, United States), calponin 1:5000 (cat # ab46794 Abcam, Cambridge, MA, United States), SM22 1:5000 (cat #ab14106 Abcam, Cambridge, MA, United States), GAPDH 1:50000 (cat #8795 Sigma-Aldrich, Corp., St. Louis, MO, United States), β-tubulin 1:5000 (cat # T0198, Sigma-Aldrich, Corp., St. Louis, MO, United States) and Horseradish peroxidase-linked secondary antibody 1:5000 anti-mouse and anti-rabbit from Calbiochem (Calbiochem, La Jolla, CA, United States).

Cell Culture

Primary rat aortic vascular smooth muscle cells (RASMCs) were prepared from Sprague-Dawley rats (200–250 g). All animal experiments were performed in accordance with the Guide for the Care and Use of Laboratory Animals (8th Edn, 2011) and were approved by the institutional bioethics Committee from the School of Medicine of Emory University. RASMCs were prepared by removing the thoracic aorta and cleaned it in Hanks'

balanced salt solution. Then vessels were incubated in Hanks' solution with 175 units/mL of collagenase at 37°C for 30 min. Then adventitia and endothelium were removed from the tissue and incubated overnight in Dulbecco's modified Eagle's medium (DMEM) with 10% fetal bovine serum (FBS) at 37°C with 95% O_2 and 5% CO_2. To complete the enzymatic digestion, aortas were incubated in Hanks' solution with collagenase 175 units/mL and elastase 0.5 mg/mL for 2 h. The digestion was terminated by addition of 10 mL of DMEM with 20% of calf serum. VSMCs were centrifuged and plated at 1×10^4 cells/cm^2 in DMEM with 10% fetal calf serum, 2 mM glutamine and antibiotics (penicillin and streptomycin). Cells were gradually weaned to 10% calf serum after three passages. Passages from 5 to 10 were used for experiments.

The A7r5 cell line, derived from embryonic rat aorta, was purchased from the American Type Culture Collection (ATCC, CRL-1444). A7r5 cells were cultured in DMEM supplemented with 10% FBS and 2 mM pyruvate and incubated at 37°C with 95% O_2 and 5% CO_2. Prior to stimulation, 80–90% confluent RASMCs and A7r5 were partially serum-starved overnight by incubating them in DMEM 2% FBS. Experiments were performed between passages 6 to 8.

Western Blot

Vascular smooth muscle cells were lysed using the RIPA lysis buffer (Tris-HCl 10 mmol/L, EDTA 5 mmol/L, NaCl 50 mmol/L, 1% deoxycholic acid and 1% Triton X-100, pH 7.4). Protein concentration was determined in A7r5 line by Bradford method (BioRad protein assay) while in RASMCs, protein concentration was determined by the bicinchoninic acid assay (Pierce BCA protein assay, Thermo Scientific). Equal amounts of protein from cells were separated by 7–15% SDS polyacrylamide gel electrophoresis and electrotransferred to PVDF membranes and blocked with 5% defatted milk in Tris-buffered saline pH 7.6, containing 0.1% (v/v) Tween 20 (TBS-T). Membranes were incubated with the primary antibodies at 4°C overnight. Membranes were then incubated with horseradish peroxidase-linked secondary antibody in 1% (w/v) defatted milk in TBST. The bands were detected using ECL (cat # NEL103001EA, Perkin Elmer, Waltham, MA, United States) luminescence was assessed using a digital imaging system (Syngene). Quantification of the bands by densitometry was performed using UN-SCAN-IT gel software. Protein content was normalized by β-tubulin or GAPDH.

Autophagy

Autophagy was evaluated by measuring LC3 II content by Western blotting and by the quantitation of autophagosome vesicles. Autophagic flux were evaluated in A7r5 and RASMCs using chloroquine (CQ) 30 μM during the last 4 h of the stimulation with Ang II (1–100 nM for dose response and 100 nM for rest of the experiments). Autophagosome vesicles were visualized in the A7r5 cell line seeded in 12 well plates with glass coverslips (18 mm) containing 3×10^5 cells per well. Cells were incubated in DMEM, 2% FBS for 24 h and transduced with the adenovirus LC3-GFP (Ad LC3-GFP) for 24 h using a multiplicity of infection (MOI) of 180. After transduction, cells were stimulated with Ang II 100 nM for 24 h in the presence or absence of CQ and losartan. Cells were washed with cold PBS and fixed with 4% paraformaldehyde and the nuclei was stained with Hoechst (1:1000). The images were analyzed using a Carl Zeiss Pascal 5 confocal microscopy. Inhibition of autophagy were performed using autophagy inhibitor spautin-1 (Liu et al., 2011) and siRNA against Beclin-1. Cells were pretreated with spautin 1, 10 μM, 1 h prior to stimulation with Ang II. For genetic inhibition of autophagy, cells were transfected with 100 nmol/L of siRNA scrambled or siRNA against Beclin-1 using oligofectamine (Life Technologies) in Optimem medium (Life Technologies) for 6 h, following the manufacturer's instructions and then stimulated with Ang II.

VSMCs Hypertrophy

A7r5 cells were seeded in 12 well plates with glass coverslips (18 mm) containing 3×10^5 cells per well. Cells were incubated in DMEM, 2% FBS for 24 h and then stimulated with Ang II 100 nM for 24 h in the presence or absence of CQ. Cells were washed with cold PBS and permeabilized with Triton X-100. Cells then were stained with phalloidin–Rhodamine (1:500; F-actin staining) and fixed with 4% paraformaldehyde, the nuclei was stained with Hoechst (1:1000). The images were analyzed using a Carl Zeiss Pascal 5 confocal microscopy. At least 30 cells from randomly fields were selected and the area was measured using the ImageJ software (NIH).

Statistical Analysis

All data are shown as mean ± standard error (SEM) of independent experiments. Data were analyzed by one-way ANOVA or Student's *t*-test, according to the experiment. Statistical significance was defined as $p < 0.05$. Newman–Keuls was used as *post hoc* test.

RESULTS

Ang II Induces Autophagy in VSMCs

In order to evaluate if Ang II promotes autophagy, we stimulated A7r5 cells with Ang II 100 nM for 0, 0.5, 1, 3, 6, 12, 24, and 48 h and measured LC3 II levels by western blot. We observed that Ang II treatment gradually increased the expression of LC3 II peaking at 24 h (**Figure 1A**). The LC3 II increase triggered by Ang II occurs in a dose-dependent manner (**Figure 1A**). Then, we assess autophagic flux by concomitant administration of CQ (30 μM) during the last 4 h of a 24 h treatment with Ang II 100 nM. The further accumulation of LC3 II in the CQ-treated A7r5 and RASMCs suggest that Ang II increased the autophagic flux (**Figures 1A,B**). The accumulation of LC3-containing autophagic vesicles (punctuated pattern, **Figure 1C**) induced by Ang II in the presence of CQ (**Figure 1C**) further confirms that Ang II induces autophagic flux.

Ang II Induces the Initiation and Elongation of Phagophore in VSMCs

Considering that autophagy is a multi-step process, we evaluated if Ang II promotes the initiation of this process in VSMCs.

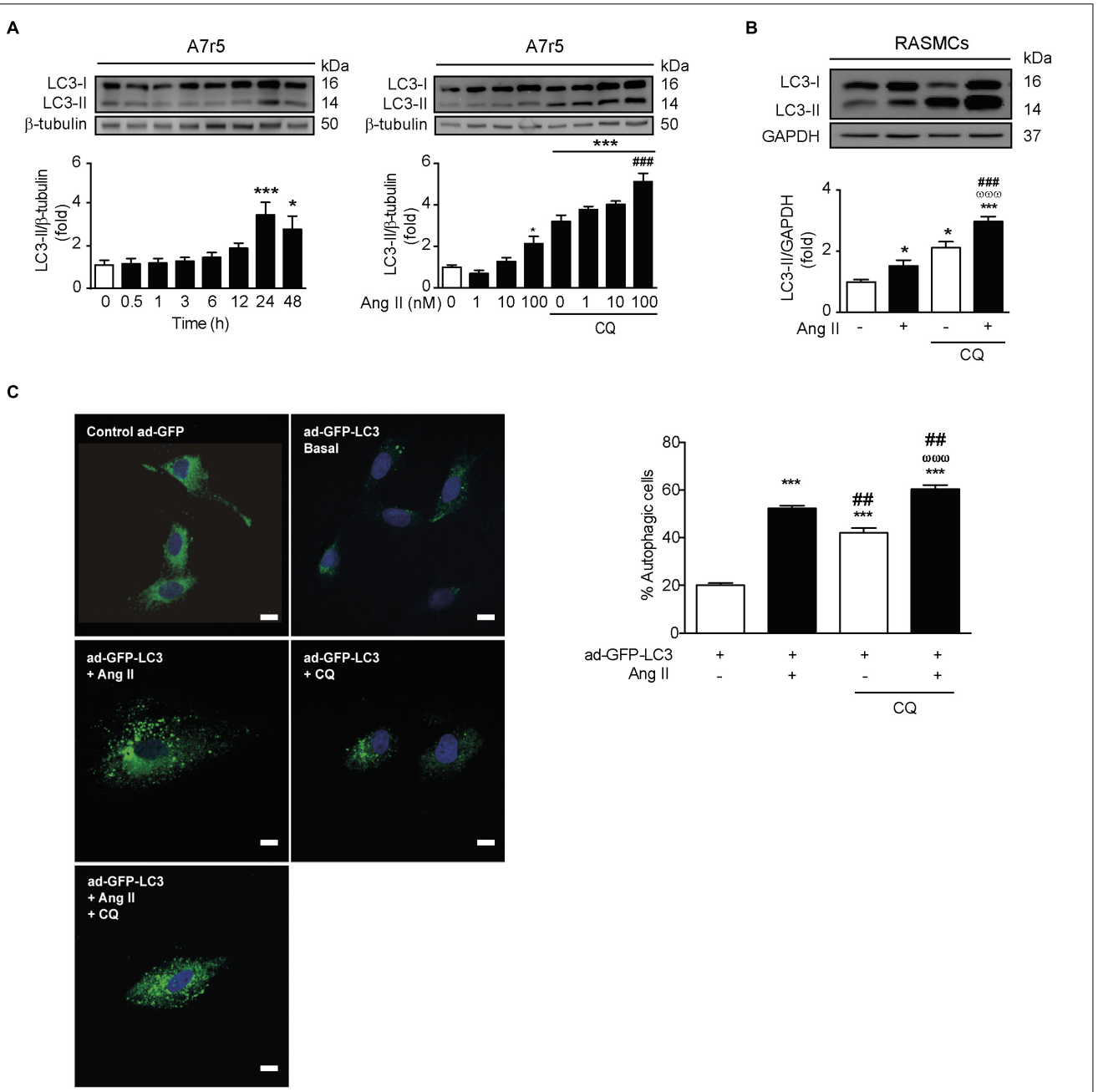

FIGURE 1 | Ang II induces autophagy in A7r5 and RASMCs. **(A)** A7r5 cells were stimulated with Ang II 100 nM for 0, 0.5, 1, 3, 6, 12, 24, and 48 h (left panel) and with 1, 10, and 100 nM for 24 h, in presence and absence of CQ 30 μM, added for the last 4 h of stimulus (right panel). The LC3 II levels were determined by Western blot. The upper panels show the representative Western blots, whereas lower panels show the quantification of the LC3 II levels. β-Tubulin was used as loading control (n = 4–5). **(B)** Primary cultures of rat aortic VSMCs (RASMCs) were stimulated with 100 nM of Ang II for 24 h in the presence and absence of CQ 30 μM, added during the last 4 h of stimulus. LC3 II levels and autophagic flux were determined by Western blot. β-Tubulin was used as loading control (n = 4). **(C)** A7r5 cells were transduced with an adenovirus overexpressing LC3-GFP (ad-LC3-GFP), using a MOI of 180 and Hoechst as nuclear stain. After 24 h of incubation, cells were stimulated with 100 nM of Ang II for 24 h. During the last 4 h of stimulus, cells were then incubated in the presence or absence of 30 μM CQ. Representative images were obtained with a confocal microscope using a 40x lens and data are expressed percentage of autophagic cells (n = 3, 30 cells per n). Scale bar = 25 μm. The results are shown as mean ± SEM. Data were analyzed using ANOVA. Newman–Keuls was used as *post hoc* test. $^{*}p < 0.05$, $^{***}p < 0.001$ vs. control; $^{\#\#}p < 0.01$, $^{\#\#\#}p < 0.001$ vs. Ang II 100 nM, $^{\omega\omega\omega}p < 0.001$ vs. CQ.

To assess this, we quantified the expression of the initiation protein Beclin-1 in A7r5 and RASMCs stimulated with Ang II. We observed that Ang II significantly increased the expression of this protein in both cell types (**Figure 2A**). Moreover, Vps34 protein expression, a class III phosphatidylinositol 3-kinase type involved in phagophore initiation (Gatica et al., 2015;

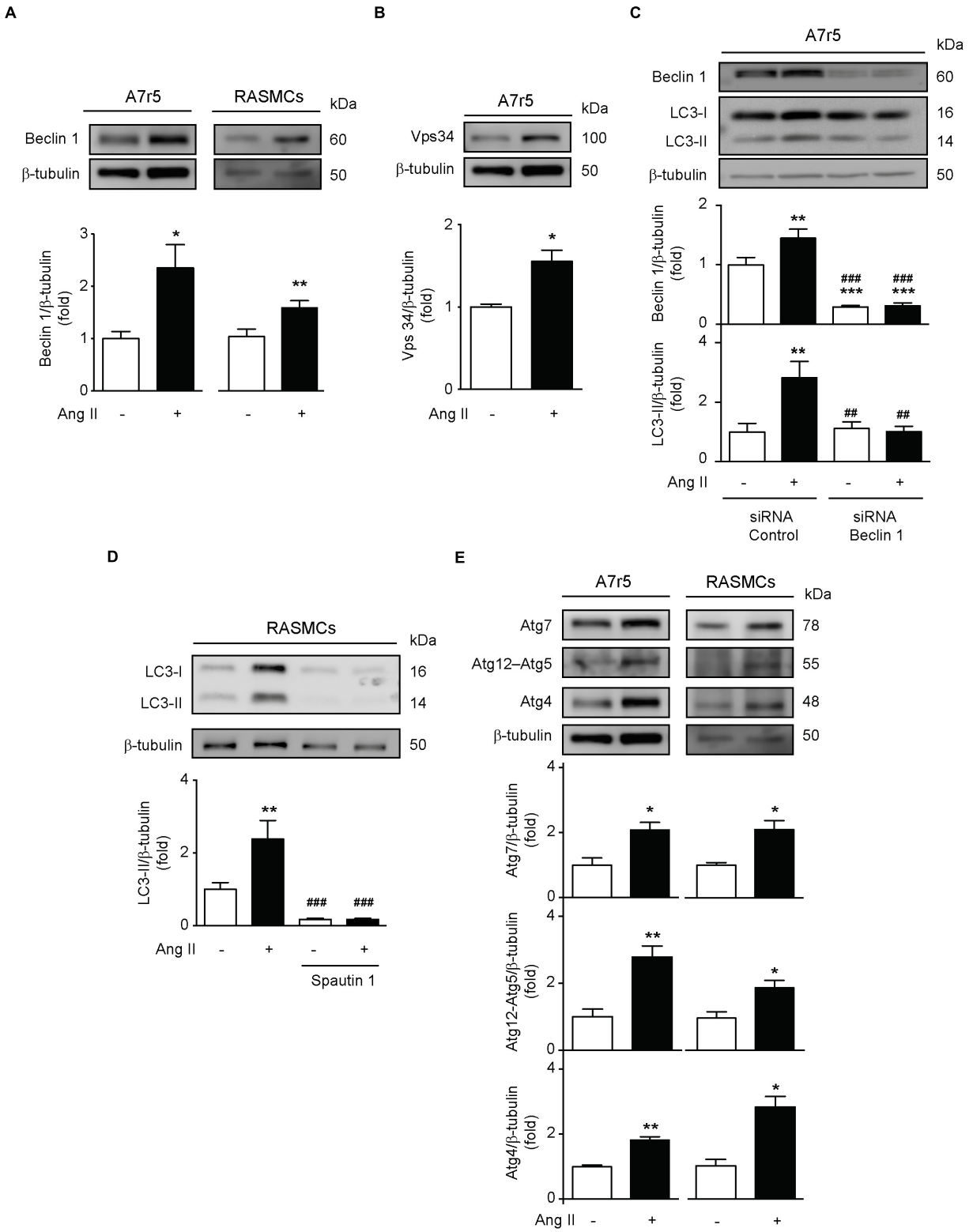

FIGURE 2 | Ang induces phagophore initiation and elongation in A7r5 and RASMCs. **(A)** A7r5 and RASMCs cells were stimulated with Ang II 100 nM for 24 h. Protein levels of Beclin 1 were determined by Western blot in A7r5 and RASMCs and were normalized by β-tubulin (n = 4–5). **(B)** A7r5 cells were stimulated with Ang II 100 nM for 24 h and Vps34 levels were measured by Western blot and normalized to β-tubulin (n = 3). **(C)** A7r5 cells were transfected with 100 nM of siRNA against Beclin 1 for 6 h and incubated in DMEM with 2% of FBS for 16 h. Then, cells were stimulated with Ang II 100 nM for 24 h and protein levels of Beclin 1

(Continued)

FIGURE 2 | Continued
and LC3 II were evaluated by Western blot and normalized by β-tubulin (n = 5). **(D)** Primary culture of RASMCs were pre-treated with Spautin 1, 10 μM, 1 h before the stimulation with Ang II 100 nM for 24 h. LC3 II levels were determined by Western blot and normalized by β-tubulin (n = 4). **(E)** A7r5 and RASMCs cells were stimulated with Ang II 100 nM for 24 h and protein levels of Atg7, Atg12–Atg5, and Atg4 were determined by Western blot and normalized by β-tubulin. Data were analyzed using Student's t-test or one way ANOVA followed by Newman–Keuls *post hoc* test. Results are shown as mean ± SEM, n = 3–5. $^{*}p < 0.05$, $^{**}p < 0.01$, $^{***}p < 0.001$ vs. control; $^{\#\#}p < 0.01$, $^{\#\#\#}p < 0.001$ vs. Ang II.

Lavandero et al., 2015), was also increased in response to Ang II in A7r5 (**Figure 2B**). These findings were further confirmed by showing that Ang II was unable to increase LC3 II levels when Beclin-1 was knocked down using a siRNA in A7r5 cells (**Figure 2C**). Additionally, when Ang II was co-administered with spautin-1, which promotes Vps34 degradation (Liu et al., 2011), LC3 II protein content was not augmented (**Figure 2D**). Furthermore, to evaluate the effects of this peptide in the autophagosome elongation, we treated both A7r5 and primary RASMCs with Ang II and we observed an increment in Atg7, Atg12–5, and Atg4 protein levels (**Figure 2E**). These results suggests that Ang II increases autophagy initiation and elongation in A7r5 and RASMCs.

AT1R Activation Mediates Ang II-Induced Autophagy

In order to investigate the participation of the AT1R in Ang II-mediated autophagy, we pre-treated A7r5 cells with losartan (1 μM) for 1 h before Ang II treatment. We observed that the increase in LC3 II levels triggered by Ang II was prevented upon pre-treatment with the AT1R antagonist (**Figure 3A**). This result was confirmed by quantification of the autophagic flux in the presence of CQ, followed by the assessment of LC3 II protein levels (**Figure 3A**) and the formation of autophagic vesicles (**Figure 3B**). In addition, losartan also prevented Ang II-induced initiation and elongation of the phagophore by abolishing Ang II-induced Beclin-1 phosphorylation in Thr^{119}, as well as the expression of Beclin-1 (**Figure 3C**), Vps34 (**Figure 3D**), Atg7, Atg12–5, and Atg4 (**Figure 3E**).

Ang II Induces Autophagy Through a ROCK-Dependent Mechanism

Since mTOR inhibition is the canonical autophagy activation mechanism (Gatica et al., 2015; Lavandero et al., 2015), we first evaluated the activity of this signaling pathway. The results show that Ang II triggers the phosphorylation of the mTOR Ser^{2448} and the mTOR downstream targets p70s6k and 4E-BP1 (**Figure 4A**). Moreover, Ang II also promotes TSC2 Thr^{1462} phosphorylation, as well as the inhibition of AMPK-α Thr^{172} phosphorylation (**Figure 4B**). Phosphorylation of Thr^{1462} inhibits TSC2 activity and induces mTOR activation (Huang and Manning, 2008). On the other hand, reduction of AMPK activity facilitates the activation of mTOR (Jeon, 2016). Thereby, our results suggest that mTOR is active after stimulation with Ang II.

Then, we investigated whether ROCK, a downstream component of the AT1R pathway, is required for the induction of autophagy triggered by Ang II. To test this, we stimulated A7r5 cells with Ang II and we determined the MYPT1 phosphorylation (a downstream target of ROCK). Ang II increased phospho-MYPT1 as compared to untreated cells, but this effect was lost upon co-administration of this peptide with the ROCK inhibitor, Y-27632 10 μM (**Figure 4C**). Moreover, to evaluate the role of the ROCK signaling pathway in autophagy, we measured LC3 II levels in response to Ang II. As expected, pre-treatment with Y-27632 completely abolished Ang II-dependent increase in LC3 II protein levels (**Figure 4D**). Additionally, ROCK inhibition also prevented Ang II-mediated increase in Beclin-1 protein content (**Figure 4E**).

Ang II-Induced VSMC Hypertrophy Requires ROCK-Dependent Induction of Autophagy

It is well-stablished that Ang II induces hypertrophy in VSMC and that α-SMA expression is a major component of this hypertrophic response (Geisterfer et al., 1988; Andrawis et al., 1993; Yoshida et al., 2004). To evaluate this, we stimulated A7r5 cells with Ang II and measured cell area and α-SMA protein levels. Ang II increased VSMCs area and fluorescence intensity, effect that was prevented by autophagy inhibition with CQ (**Figure 5A**). Ang II also increased α-SMA protein levels (**Figure 5B**). Moreover, AT1R antagonism (**Figure 5B**), ROCK inhibition (**Figure 5C**), as well as blockage of autophagy with CQ (**Figure 5D**) and knock down of Beclin 1 with siRNA (**Figure 5E**) prevented the α-SMA increase after Ang II stimulation.

DISCUSSION

The main findings of this study were: (i) Ang II induced autophagy in VSMCs, (ii) this peptide participated in the initiation and elongation of the phagophore, (iii) Ang II-induced autophagy is mediated by AT1R/ROCK signaling pathway and not by mTOR, and (iv) Ang II induced VSMC hypertrophy, as determined by an increase in cell area and α-SMA protein levels, through an autophagy-dependent mechanism.

Our findings show that 100 nM of Ang II activated autophagy with a maximum at 24 h of stimulus. In this context, Zhang et al. (2016), reported that this concentration of Ang II increased proliferation, migration and protein content of pro-inflammatory factors, such as MCP-1, VCAM-1, and IL-β1 in VSMCs. Moreover, cells treated with Ang II showed increased NAPDH oxidase activity and ROS production via a mechanisms involving MAPKs and PI3K/Akt signaling pathways, but these effects were lost in the presence of losartan and Ang-(1–7) (Zhang et al., 2016). In line with this, Hu et al. (2002) showed that Ang II 100 nM increased COX-2 mRNA and protein levels in VSMCs. PPAR α and γ activators abolish Ang II-dependent increase in

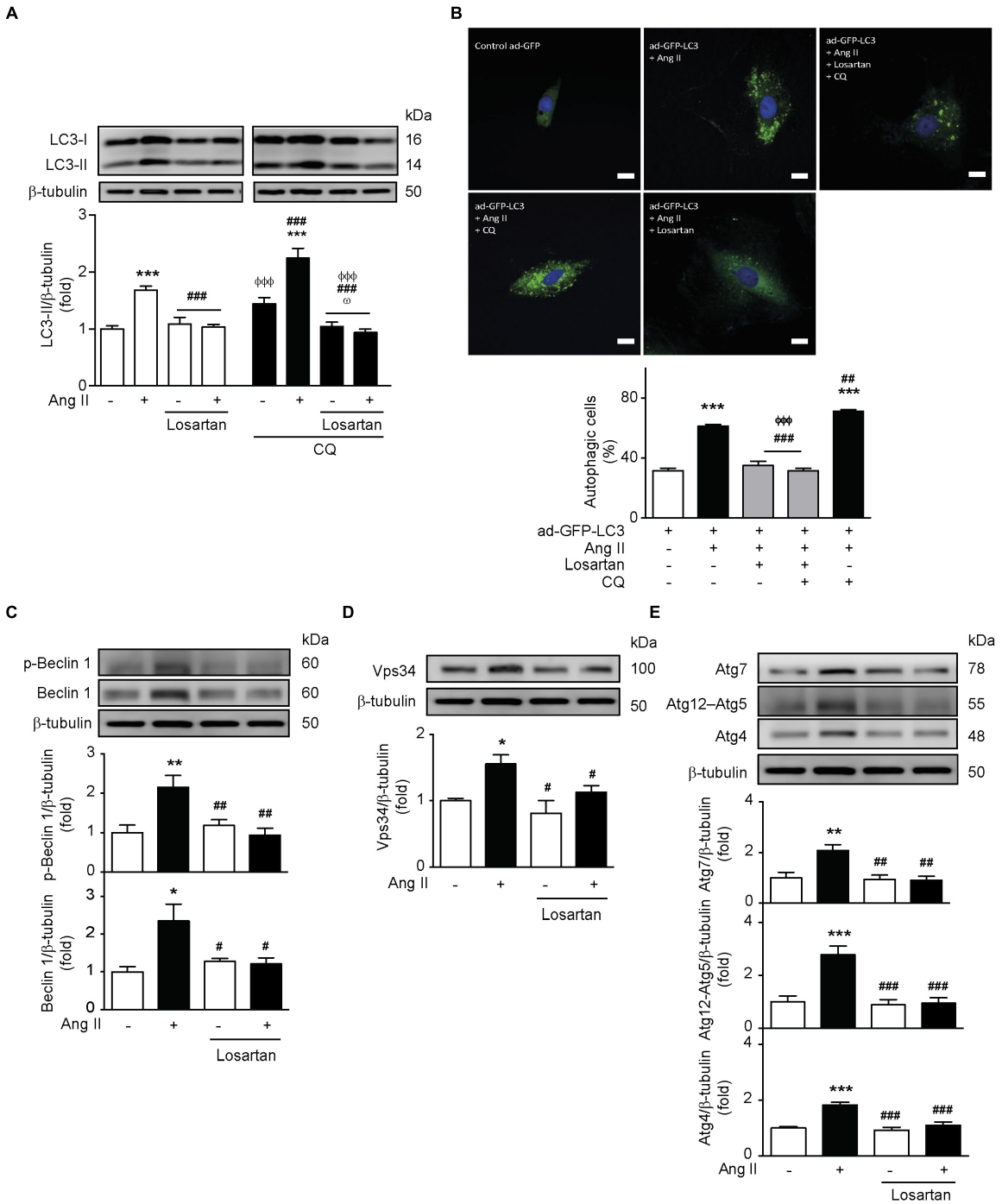

FIGURE 3 | Ang II induces autophagy through an AT1R-dependent mechanism. **(A)** A7r5 cells were pre-treated with Losartan 1 μM 1 h before stimulation with Ang II 100 nM for 24 h. During the last 4 h of stimulus, cells were also treated in the presence and absence of CQ 30 μM. LC3-II levels were determined by Western blot and normalized by β-tubulin ($n = 5$). **(B)** A7r5 cells were transduced with an adenovirus overexpressing LC3-GFP (ad-LC3-GFP), using an MOI of 180. After 24 h of incubation, cells were pretreated with losartan 1 μM, 1 h before stimulation with Ang II 100 nM for 24 h. During the last 4 h of stimulus with Ang II, cells were incubated in the presence or absence of CQ 30 μM. The nucleus were stained with Hoechst. Cells were visualized by confocal microscopy. The images are representative of $n = 3$, 30 cells per n. Scale bar = 25 μm. **(C)** A7r5 cells were pre-treated with losartan 1 μM, 1 h before stimulation with Ang II 100 nM for 24 h. Levels of Beclin 1 and its phosphorylation in Thr^{119} (p-Beclin 1) were determined by Western blot and normalized by β-tubulin ($n = 4$). **(D)** A7r5 cells were pretreated with losartan 1 μM, 1 h before stimulation with Ang II 100 nM for 24 h. Vps34 levels were determined by Western blot and normalized by β-tubulin ($n = 3$). **(E)** A7r5 cells were pretreated with losartan 1 μM, 1 h before stimulation with Ang II 100 nM for 24 h. Levels of Atg7, Atg12–Atg5, and Atg4 were determined by Western blot and normalized by β-tubulin ($n = 4$–5). The results are shown as mean ± SEM. Data were analyzed using one way ANOVA followed by Newman–Keuls *post hoc* test. $^{*}p < 0.05$, $^{**}p < 0.01$, $^{***}p < 0.001$ vs. control; $^{\#}p < 0.05$, $^{\#\#}p < 0.01$, $^{\#\#\#}p < 0.001$ vs. Ang II; $^{\Phi\Phi\Phi}p < 0.001$ vs. Ang II + CQ; $^{\omega}p < 0.05$ vs. CQ.

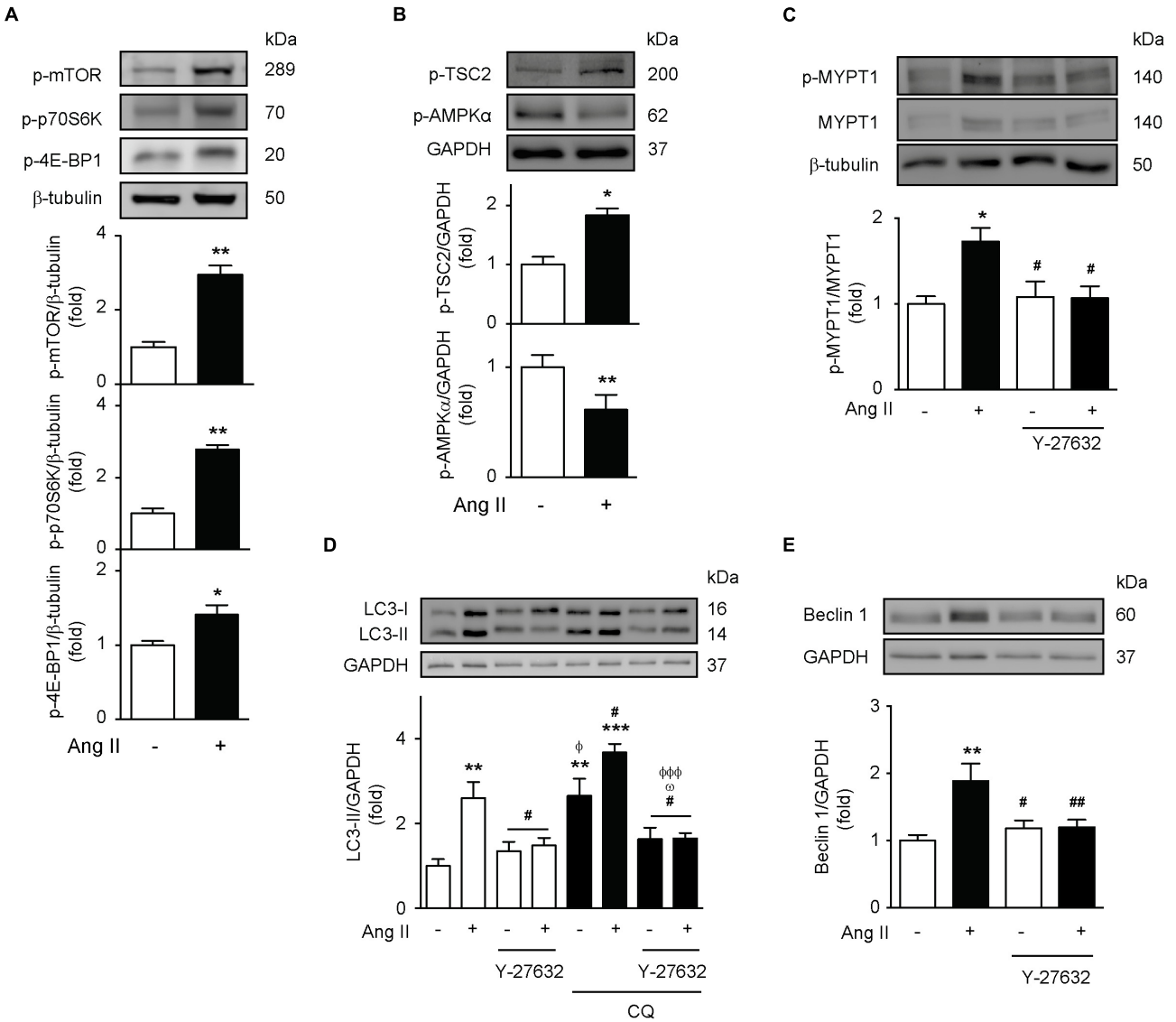

FIGURE 4 | Ang II induces autophagy through a ROCK-dependent mechanism. **(A,B)** A7r5 cells were stimulated with 100 nM of Ang II for 24 h. Levels of p-mTOR Ser^{2448}, p-p70S6K Thr^{389}, p-4E-BP1 Thr$^{37/46}$, p-TSC2 Thr^{1462}, and p-AMPKα Thr^{172} were determined by Western blot and normalized by β-tubulin or GAPDH (n = 4–5). **(C)** A7r5 cells were pre-treated with Y-27632 (ROCK inhibitor, 10 μM), 1 h before stimulation with Ang II 100 nM for 24 h. ROCK activation levels were evaluated by MYPT1 phosphorylation in Thr^{853} assessed by Western blot. Protein levels were normalized by β-tubulin (n = 3). **(D)** A7r5 cells were pre-treated with 10 μM of Y-27632, 1 h before stimulation with Ang II 100 nM for 24 h. During the last 4 h of stimulus, cells were treated in the presence and absence of CQ 30 μM. LC3 II levels were determined by Western blot and normalized by GAPDH (n = 5). **(E)** A7r5 cells were pretreated with 10 μM of Y-27632, 1 h before stimulation with Ang II 100 nM for 24 h. Beclin 1 levels were determined by Western blot and normalized by GAPDH (n = 5). Results are shown as mean ± SEM. Data were analyzed using Student's t-test or one way ANOVA followed by Newman–Keuls *post hoc* test. $^{*}p < 0.05$, $^{**}p < 0.01$, $^{***}p < 0.001$ vs. control; $^{\#}p < 0.05$, $^{\#\#}p < 0.01$ vs. Ang II; $^{\Phi}p < 0.05$, $^{\Phi\Phi\Phi}p < 0.001$ vs. Ang II + CQ; $^{\omega}p < 0.05$ vs. CQ.

migration and COX-2 levels (Hu et al., 2002). These alterations play an important role in the development and progression of hypertension (Oparil et al., 2018). Our results supports that autophagy may be a potential mechanism mediating the deleterious effects of Ang II in VSMCs in the context of vascular diseases. However, cause-effect experiments are required to further explore this possibility.

The link between Ang II and autophagy has been previously explored by Yu et al. (2014). The authors of this study evaluated the role of mitochondrial K_{ATP} channels in autophagy induced by Ang II in rat aortic smooth muscle cells (Yu et al., 2014). While the authors showed increased LC3 II levels in response to Ang II 100 nM, their autophagic flux experiments with bafilomycin did not produce accumulation of this protein, which indicates that autophagy was not activated. Moreover, they also evaluated formation of autophagic vesicles by immunofluorescence, but measurement of autophagic flux was not performed (Yu et al., 2014).

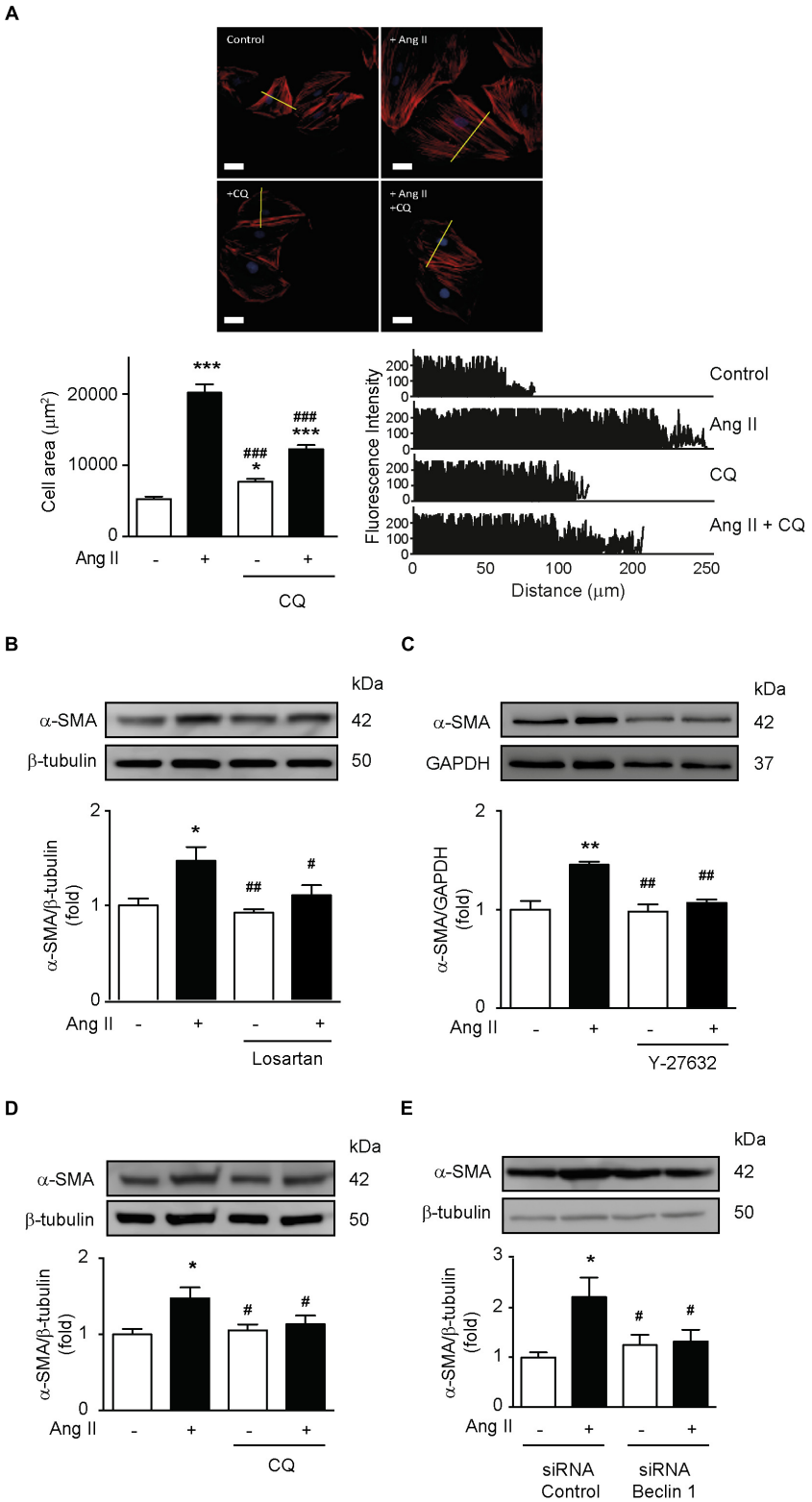

FIGURE 5 | Ang II-dependent autophagy elicits hypertrophy in VSMCs. **(A)** A7r5 cells were treated with or without Ang II 100 nM. During the last 4 h of stimulus, cells were treated in the presence and absence of CQ 30 μM. Then cells were stained with phalloidin–rhodamine and nuclei were stained with Hoechst. Images were captured using a confocal microscope using 40x lens. Cell area and fluorescence intensity were measured using the ImageJ software. *n* = 3,30 cells per condition. Scale bar = 25 μm. A7r5 cells were pre-treated with **(B)** Losartan 1 μM or **(C)** Y-27632 10 μM, 1 h before stimulation with Ang II 100 nM for 24 h.

(Continued)

FIGURE 5 | Continued
During the last 4 h of stimulus, cells were treated in the presence and absence of CQ 30 μM **(D)**. **(E)** A7r5 cells were transfected with a control siRNA or siRNA against Beclin 1 100 nM for 6 h and incubated in DMEM with 2% of FBS for 16 h. Cells were then stimulated with Ang II 100 nM for 24 h. α-SMA levels were evaluated by Western blot and normalized by β-tubulin ($n = 5$). α-SMA levels were determined by Western blot and normalized by GAPDH ($n = 5$). Data were analyzed using Student's *t*-test or one way ANOVA followed by Newman–Keuls *post hoc* test. The results are shown as mean ± SEM. $^{*}p < 0.05$, $^{**}p < 0.01$, $^{***}p < 0.001$ vs. control; $^{\#}p < 0.05$, $^{\#\#}p < 0.01$, $^{\#\#\#}p < 0.001$ vs. Ang II.

Our experiments with CQ confirmed that Ang II indeed triggered autophagy. However, this process requires different stages to be completed (Lavandero et al., 2015). Our data suggest that Ang II is involved in the initiation of autophagy, which was evidenced by an increase in Beclin-1 protein content and its phosphorylation in Thr^{119}, along with the increased Vps34 protein levels. In order to interact with Vps34 and initiate autophagy, Beclin-1 is first dissociated from its inhibitory complex with Bcl-2 (Pattingre et al., 2005). In HeLa cells that, Beclin-1 can be phosphorylated in Thr^{119} by ROCK, thereby promoting its release from the inhibitory union with Bcl-2 (Gurkar et al., 2013). The next step in autophagy is the elongation of the phagophore (Gatica et al., 2015). Yu et al. (2014) found that knocking down Atg5 significantly reduced LC3 II levels in VSMCs treated with Ang II. However, there are no studies evaluating whether Ang II can regulate Atg7 or Atg4 in VSMCs. Our findings show that Ang II promoted an increase in the levels of Atg12–Atg5, Atg7 and Atg4, suggesting that this peptide can stimulate the elongation of the phagophore, which was confirmed by the increase in the percentage of cells with punctuated pattern. Nonetheless, while it has been thoroughly described that ATGs participate in the autophagic process (Mizushima et al., 1998; Mizushima et al., 2011), the mechanisms by which they are regulated, remains to be fully understood. It has been reported that the transcriptional factor FOXO1 can induce the expression of Atg7, Atg5 and Atg12, thus eliciting the induction autophagy (Zhao et al., 2010; Xu et al., 2011). Moreover, Qi et al. (2014) showed that in liver-specific FOXO1 knockout mice, blood pressure, as well as plasma levels of angiotensinogen and Ang II were reduced. Although this study was performed in liver tissue, the link between FOXO1 and Ang II further suggest this transcriptional factor may be responsible for the modulation of ATGs in the autophagy induced by Ang II in VSMCs, but future experiments should clarify this point.

The classic pathway to induce autophagy requires mTOR inhibition (Gatica et al., 2015). Nevertheless, our results showed that Ang II activated mTOR signaling pathway. Accordingly, it has been previously described that Ang II can activate the mTOR pathway by increasing the phosphorylation of its downstream targets, p70S6K and 4E-BP1 and that may be associated with higher vascular damage and hypertrophy (Haider et al., 2002; Yamakawa et al., 2003; Hafizi et al., 2004; Li et al., 2004; Zhu et al., 2012). mTOR is a key regulator of protein synthesis (Fonseca et al., 2014). Consistent with the role of mTOR as key determinant of the rate of protein synthesis, our findings indicate that Ang-induced VSMC hypertrophy requires mTOR activation. It's important to note that while we do not show mTOR activation elicited by Ang II in RASMCs, the activation of the mTOR signaling pathway by Ang II has been described in primary cultures of aortic and coronary smooth muscle cells of rats and humans, respectively (Haider et al., 2002; Hafizi et al., 2004).

Under nutrient deprivation conditions, mTOR is inhibited and autophagy is activated (Jung et al., 2010). Under this setting, there is a decrease in the AMP/ATP ratio, thus triggering AMPK activation, which in turn, can inhibit mTOR by phosphorylating raptor and TSC2 (Gwinn et al., 2008; Jung et al., 2010). On the other hand, in the presence of nutrients, mTOR inhibits autophagy by a mechanism that involves ULK1 and AMBRA1 phosphorylations (Ganley et al., 2009; Nazio et al., 2013). Our findings suggest that Ang II-induced autophagy does not inhibit mTOR or activates AMPK. Therefore, we sought to explore the potential mechanism by which Ang II can promote autophagy by assessing the role of the AT1R in this effect. Our results indicated that pre-treatment with losartan prevented the Ang II-mediated increase in LC3 II, Vps34 and Beclin-1 levels, as well as Beclin 1 phosphorylation in Thr^{119}. In addition autophagic flux and formation of autophagic vesicles were also decreased. Accordingly, Yu et al. (2014) found that pre-treatment with olmesartan and candesartan abolished the increase in LC3 II levels, although this study does not show autophagic flux experiments in the presence of AT1R antagonists.

Interestingly, Porrello et al. (2009) reported that Ang II administration in neonatal rat ventricular myocytes overexpressing AT1R, showed increased hypertrophy and higher autophagic activity, thereby increasing the number of autophagosomes. Moreover, autophagy was diminished in the presence of candesartan. In addition, they observed that AT2R overexpression reduced Ang II-induced autophagy even in presence of AT1R overexpression. Therefore, their results suggest that Ang II induces autophagy in cardiomyocytes by an AT1R dependent mechanism and that AT2R may antagonize this effect (Porrello et al., 2009). Moreover, Lin et al. (2014) showed that mechanical stress induced an increase in hypertrophy and autophagy in cardiomyocytes. However, these effects were reduced by losartan, but not with PD123319, which antagonizes AT2R, treatment (Lin et al., 2014).

The role of AT1R in the elongation of the phagophore has been only partially studied. Zhang et al. (2014) described that in a porcine model of renovascular hypertension, autophagy was activated in the myocardium, which was evidenced by an increase in LC3 II, Beclin-1 and Atg12–Atg5 (which is involved in phagophore elongation). This effect was prevented upon AT1R antagonism with valsartan. Our results further support these findings, given that losartan abolished the Ang II-induced increase in Atg7, Atg12–5 and Atg4 protein levels.

Pursuing AT1R downstream targets, we assessed the role of RhoA/ROCK in the Ang II-induced autophagy. This pathway is active in hypertension, given that, this disease is characterized

by high levels of Ang II. Moreover, the RhoA/ROCK signaling pathway is a key regulator of vascular tone and remodeling induced by AT1R activation (Noma et al., 2006). ROCK has 2 isoforms; ROCK1 is expressed in lung, liver, spleen, testicles and kidney, whereas ROCK2 is mainly present in brain and heart (Wirth, 2010; Satoh et al., 2011). Thus, we used Y-27632, a ROCK inhibitor, which can inhibit both isoforms by binding to their catalytic site (Ishizaki et al., 2000). ROCK inhibition by Y-27632 was confirmed by assessing a reduction in the phosphorylation of MYPT1 in Thr^{853}, which is the gold standard to evaluate the ROCK activity (Kitazawa et al., 2003; Dimopoulos et al., 2007; Khromov et al., 2009). Our data showed that increased autophagy in response to Ang II is lost upon pre-treatment with Y-27632. These findings are in agreement with the study performed by Gurkar et al. (2013) which described that ROCK phosphorylates Beclin-1 in Thr^{119} to activate autophagy.

Our data show that Ang II-dependent autophagy induced an increase in cell area and α-SMA protein levels in VSMCs. In hypertension, which involves remodeling of the vascular wall, α-SMA is increased in comparison to healthy blood vessels (Schildmeyer et al., 2000; Rzucidlo et al., 2007; Goulopoulou and Webb, 2014; Liu et al., 2015). Inhibition of ROCK-induced autophagy should be explored as a selective mechanism to reduce vascular damage during hypertension.

From a translational perspective, it's important to highlight that *in vivo* studies linking autophagy to vascular hypertrophy are scarce. Martinet and De Meyer (2009) described that autophagy was increased in atherosclerotic plaques, suggesting its relevance in vascular diseases and therefore, this may be extrapolated to hypertension, but a potential effect in hypertrophy remains to be explored. Moreover, given that autophagy is a ubiquitous process that occurs in virtually all cells (Yin et al., 2016), it can be induced in an *in vivo* setting using starvation models (Mizushima et al., 2004). Nonetheless, there are no selective inhibitors of autophagy and therefore, there are still multiple obstacles to overcome in the road to a translational approach of the therapeutic targeting of autophagy in vascular diseases.

One of the main limitations of our study is that, although key findings were observed with RASMCs, not all experiments were performed using primary cells and future research should thoroughly address the role of autophagy in angiotensin II-induced hypertrophy using animal models in order to further confirm our results. In addition, we used CQ to block autophagy, but interestingly, it has been recently reported that its mechanism of action may involve defective fusion of the lysosome with the autophagosome, instead of modulating the acidity of lysosomes (Mauthe et al., 2018). Moreover, CQ was found to induce disorganization of the endo-lysosomal system and the Golgi apparatus via a mechanism that is independent of autophagy, which could be involved in the blockade of the fusion process (Mauthe et al., 2018). Given the off-target effects of CQ, a comparison with another compound to evaluate autophagic flux, such as Bafilomycin A1 may be needed in order to thoroughly confirm our findings.

Taken together, our results indicate that Ang II induces VSMC hypertrophy through a mechanism that involves autophagy activation via AT1R/ROCK-dependent signaling pathway. Therefore, autophagy may be a novel therapeutic target to prevent VSMC hypertrophy during Ang II-induced hypertension.

AUTHOR CONTRIBUTIONS

DM-R, ASM, CQ, LG, SL, and MC contributed to conception and design of the study. DM-R, IN-S, FS-O, PV-F, TH-D, and NC-A performed the experiments. DM-R performed the statistical analysis. DM-R and JR wrote the first draft of the manuscript. MC and ASM wrote the sections of the manuscript. All authors contributed to manuscript revision, read and approved the submitted version.

FUNDING

This work was supported by Fondecyt grants 1140329 (MC) and 1180157 (MC), FONDAP ACCDiS 15130011 (SL, MC, and LG) and HL113167 and HL095070 from the National Institute of Health (ASM). DM-R was supported by CONICYT Ph.D. fellowship (21130337). JR was supported by FONDECYT postdoctoral fellowship (3160298).

ACKNOWLEDGMENTS

The authors wish to thank Fidel Albornoz and Gindra Latorre for their excellent technical assistance.

SUPPLEMENTARY MATERIAL

The Supplementary Material for this article can be found online at: https://www.frontiersin.org/articles/10.3389/fphar.2018.01553/full#supplementary-material

FIGURES S1–S5 | File containing all the original uncropped western blot images depicted in the **Figures 1(A,B)**, **2(A–E)**, **3(A,C–E)**, **4(A–E)**, and **5(B–E)**.

REFERENCES

Andrawis, N. S., Ruley, E. H., and Abernethy, D. R. (1993). Angiotensin II regulates human vascular smooth muscle alpha-actin gene expression. *Biochem. Biophys. Res. Commun.* 196, 962–968. doi: 10.1006/bbrc.1993.2343

Chen, P. H., Chen, X., and He, X. (2013). Platelet-derived growth factors and their receptors: structural and functional perspectives. *Biochim. Biophys. Acta* 1834, 2176–2186. doi: 10.1016/j.bbapap.2012.10.015

Dimopoulos, G. J., Semba, S., Kitazawa, K., Eto, M., and Kitazawa, T. (2007). Ca^{2+}-dependent rapid Ca^{2+} sensitization of contraction in arterial smooth muscle. *Circ. Res.* 100, 121–129. doi: 10.1161/01.RES.0000253902.90489.df

Fonseca, B. D., Smith, E. M., Yelle, N., Alain, T., Bushell, M., and Pause, A. (2014). The ever-evolving role of mTOR in translation. *Semin. Cell Dev. Biol.* 36, 102–112. doi: 10.1016/j.semcdb.2014.09.014

Forouzanfar, M. H., Liu, P., Roth, G. A., Ng, M., Biryukov, S., Marczak, L., et al. (2017). Global Burden of hypertension and systolic blood pressure of at least 110 to 115 mm Hg, 1990-2015. *JAMA* 317, 165–182. doi: 10.1001/jama.2016.19043

Ganley, I. G., Lam du, H., Wang, J., Ding, X., Chen, S., and Jiang, X. (2009). ULK1.A*TG*13.FIP200 complex mediates mTOR signaling and is essential for autophagy. *J. Biol. Chem.* 284, 12297–12305. doi: 10.1074/jbc.M900573200

Gariepy, J., Massonneau, M., Levenson, J., Heudes, D., and Simon, A. (1993). Evidence for *in vivo* carotid and femoral wall thickening in human hypertension. Groupe de prevention cardio-vasculaire en medecine du travail. *Hypertension* 22, 111–118. doi: 10.1161/01.HYP.22.1.111

Gatica, D., Chiong, M., Lavandero, S., and Klionsky, D. J. (2015). Molecular mechanisms of autophagy in the cardiovascular system. *Circ. Res.* 116, 456–467. doi: 10.1161/CIRCRESAHA.114.303788

Geisterfer, A. A., Peach, M. J., and Owens, G. K. (1988). Angiotensin II induces hypertrophy, not hyperplasia, of cultured rat aortic smooth muscle cells. *Circ. Res.* 62, 749–756. doi: 10.1161/01.RES.62.4.749

Gomez, D., and Owens, G. K. (2012). Smooth muscle cell phenotypic switching in atherosclerosis. *Cardiovasc. Res.* 95, 156–164. doi: 10.1093/cvr/cvs115

Goulopoulou, S., and Webb, R. C. (2014). Symphony of vascular contraction: how smooth muscle cells lose harmony to signal increased vascular resistance in hypertension. *Hypertension* 63, e33–e39. doi: 10.1161/HYPERTENSIONAHA.113.02444

Gurkar, A. U., Chu, K., Raj, L., Bouley, R., Lee, S. H., Kim, Y. B., et al. (2013). Identification of ROCK1 kinase as a critical regulator of Beclin1-mediated autophagy during metabolic stress. *Nat. Commun.* 4:2189. doi: 10.1038/ncomms3189

Gwinn, D. M., Shackelford, D. B., Egan, D. F., Mihaylova, M. M., Mery, A., Vasquez, D. S., et al. (2008). AMPK phosphorylation of raptor mediates a metabolic checkpoint. *Mol. Cell.* 30, 214–226. doi: 10.1016/j.molcel.2008.03.003

Hafizi, S., Wang, X., Chester, A. H., Yacoub, M. H., and Proud, C. G. (2004). ANG II activates effectors of mTOR via PI3-K signaling in human coronary smooth muscle cells. *Am. J. Physiol. Heart Circ. Physiol.* 287, H1232–H1238. doi: 10.1152/ajpheart.00040.2004

Haider, U. G., Sorescu, D., Griendling, K. K., Vollmar, A. M., and Dirsch, V. M. (2002). Resveratrol suppresses angiotensin II-induced Akt/protein kinase B and p70 S6 kinase phosphorylation and subsequent hypertrophy in rat aortic smooth muscle cells. *Mol. Pharmacol.* 62, 772–777. doi: 10.1124/mol.62.4.772

Hu, Z. W., Kerb, R., Shi, X. Y., Wei-Lavery, T., and Hoffman, B. B. (2002). Angiotensin II increases expression of cyclooxygenase-2: implications for the function of vascular smooth muscle cells. *J. Pharmacol. Exp. Ther.* 303, 563–573. doi: 10.1124/jpet.102.037705

Huang, J., and Manning, B. D. (2008). The TSC1-TSC2 complex: a molecular switchboard controlling cell growth. *Biochem. J.* 412, 179–190. doi: 10.1042/BJ20080281

Ishizaki, T., Uehata, M., Tamechika, I., Keel, J., Nonomura, K., Maekawa, M., et al. (2000). Pharmacological properties of Y-27632, a specific inhibitor of rho-associated kinases. *Mol. Pharmacol.* 57, 976–983.

Jeon, S. M. (2016). Regulation and function of AMPK in physiology and diseases. *Exp. Mol. Med.* 48:e245. doi: 10.1038/emm.2016.81

Jia, G., Cheng, G., Gangahar, D. M., and Agrawal, D. K. (2006). Insulin-like growth factor-1 and TNF-alpha regulate autophagy through c-jun N-terminal kinase and Akt pathways in human atherosclerotic vascular smooth cells. *Immunol. Cell Biol.* 84, 448–454. doi: 10.1111/j.1440-1711.2006.01454.x

Jung, C. H., Ro, S. H., Cao, J., Otto, N. M., and Kim, D. H. (2010). mTOR regulation of autophagy. *FEBS Lett.* 584, 1287–1295. doi: 10.1016/j.febslet.2010.01.017

Khromov, A., Choudhury, N., Stevenson, A. S., Somlyo, A. V., and Eto, M. (2009). Phosphorylation-dependent autoinhibition of myosin light chain phosphatase accounts for Ca^{2+} sensitization force of smooth muscle contraction. *J. Biol. Chem.* 284, 21569–21579. doi: 10.1074/jbc.M109.019729

Kitazawa, T., Eto, M., Woodsome, T. P., and Khalequzzaman, M. (2003). Phosphorylation of the myosin phosphatase targeting subunit and CPI-17 during Ca^{2+} sensitization in rabbit smooth muscle. *J. Physiol.* 546, 879–889. doi: 10.1113/jphysiol.2002.029306

Lavandero, S., Chiong, M., Rothermel, B. A., and Hill, J. A. (2015). Autophagy in cardiovascular biology. *J. Clin. Invest.* 125, 55–64. doi: 10.1172/JCI73943

Li, N., Wu, K. G., Wang, X. Y., Xie, L. D., Xu, C. S., and Wang, H. J. (2004). Angiotensin II stimulates phosphorylation of 4E-binding protein 1 and p70 S6 kinase in cultured vascular smooth muscle cells. *Acta Pharmacol. Sin.* 25, 593–596.

Lin, L., Tang, C., Xu, J., Ye, Y., Weng, L., Wei, W., et al. (2014). Mechanical stress triggers cardiomyocyte autophagy through angiotensin II type 1 receptor-mediated p38MAP kinase independently of angiotensin II. *PLoS One* 9:e89629. doi: 10.1371/journal.pone.0089629

Liu, C. F., Zhang, J., Shen, K., Gao, P. J., Wang, H. Y., Jin, X., et al. (2015). Adventitial gene transfer of catalase attenuates angiotensin II-induced vascular remodeling. *Mol. Med. Rep.* 11, 2608–2614. doi: 10.3892/mmr.2014.3069

Liu, J., Xia, H., Kim, M., Xu, L., Li, Y., Zhang, L., et al. (2011). Beclin1 controls the levels of p53 by regulating the deubiquitination activity of USP10 and USP13. *Cell* 147, 223–234. doi: 10.1016/j.cell.2011.08.037

Martinet, W., and De Meyer, G. R. (2009). Autophagy in atherosclerosis: a cell survival and death phenomenon with therapeutic potential. *Circ. Res.* 104, 304–317. doi: 10.1161/CIRCRESAHA.108.188318

Mauthe, M., Orhon, I., Rocchi, C., Zhou, X., Luhr, M., Hijlkema, K. J., et al. (2018). Chloroquine inhibits autophagic flux by decreasing autophagosome-lysosome fusion. *Autophagy* 14, 1435–1455. doi: 10.1080/15548627.2018.1474314

Mehta, P. K., and Griendling, K. K. (2007). Angiotensin II cell signaling: physiological and pathological effects in the cardiovascular system. *Am. J. Physiol. Cell Physiol.* 292, C82–C97. doi: 10.1152/ajpcell.00287.2006

Mizushima, N., Noda, T., Yoshimori, T., Tanaka, Y., Ishii, T., George, M. D., et al. (1998). A protein conjugation system essential for autophagy. *Nature* 395, 395–398. doi: 10.1038/26506

Mizushima, N., Yamamoto, A., Matsui, M., Yoshimori, T., and Ohsumi, Y. (2004). *In vivo* analysis of autophagy in response to nutrient starvation using transgenic mice expressing a fluorescent autophagosome marker. *Mol. Biol. Cell.* 15, 1101–1111. doi: 10.1091/mbc.e03-09-0704

Mizushima, N., Yoshimori, T., and Ohsumi, Y. (2011). The role of Atg proteins in autophagosome formation. *Annu. Rev. Cell Dev. Biol.* 27, 107–132. doi: 10.1146/annurev-cellbio-092910-154005

Nazio, F., Strappazzon, F., Antonioli, M., Bielli, P., Cianfanelli, V., Bordi, M., et al. (2013). mTOR inhibits autophagy by controlling ULK1 ubiquitylation, self-association and function through AMBRA1 and TRAF6. *Nat. Cell Biol.* 15, 406–416. doi: 10.1038/ncb2708

Noma, K., Oyama, N., and Liao, J. K. (2006). Physiological role of ROCKs in the cardiovascular system. *Am. J. Physiol. Cell Physiol.* 290, C661–C668. doi: 10.1152/ajpcell.00459.2005

Oparil, S., Acelajado, M. C., Bakris, G. L., Berlowitz, D. R., Cifkova, R., Dominiczak, A. F., et al. (2018). Hypertension. *Nat. Rev. Dis. Primers* 4:18014. doi: 10.1038/nrdp.2018.14

Owens, G. K. (1985). Differential effects of antihypertensive drug therapy on vascular smooth muscle cell hypertrophy, hyperploidy, and hyperplasia in the spontaneously hypertensive rat. *Circ. Res.* 56, 525–536. doi: 10.1161/01.RES.56.4.525

Pattingre, S., Tassa, A., Qu, X., Garuti, R., Liang, X. H., Mizushima, N., et al. (2005). Bcl-2 antiapoptotic proteins inhibit Beclin 1-dependent autophagy. *Cell* 122, 927–939. doi: 10.1016/j.cell.2005.07.002

Porrello, E. R., D'Amore, A., Curl, C. L., Allen, A. M., Harrap, S. B., Thomas, W. G., et al. (2009). Angiotensin II type 2 receptor antagonizes angiotensin II type 1 receptor-mediated cardiomyocyte autophagy. *Hypertension* 53, 1032–1040. doi: 10.1161/HYPERTENSIONAHA.108.128488

Qi, Y., Zhang, K., Wu, Y., Xu, Z., Yong, Q. C., Kumar, R., et al. (2014). Novel mechanism of blood pressure regulation by forkhead box class O1-mediated transcriptional control of hepatic angiotensinogen. *Hypertension* 64, 1131–1140. doi: 10.1161/HYPERTENSIONAHA.114.03970

Rosendorff, C. (1996). The renin-angiotensin system and vascular hypertrophy. *J. Am. Coll. Cardiol.* 28, 803–812. doi: 10.1016/S0735-1097(96)00251-3

Roth, G. A., Johnson, C., Abajobir, A., Abd-Allah, F., Abera, S. F., Abyu, G., et al. (2017). Global, Regional, and national burden of cardiovascular diseases for 10 causes, 1990 to 2015. *J. Am. Coll. Cardiol.* 70, 1–25. doi: 10.1016/j.jacc.2017.04.052

Rzucidlo, E. M., Martin, K. A., and Powell, R. J. (2007). Regulation of vascular smooth muscle cell differentiation. *J. Vasc. Surg.* 45(Suppl. A), A25–A32. doi: 10.1016/j.jvs.2007.03.001

Salabei, J. K., Cummins, T. D., Singh, M., Jones, S. P., Bhatnagar, A., and Hill, B. G. (2013). PDGF-mediated autophagy regulates vascular smooth muscle

cell phenotype and resistance to oxidative stress. *Biochem. J.* 451, 375–388. doi: 10.1042/BJ20121344

Salabei, J. K., and Hill, B. G. (2013). Implications of autophagy for vascular smooth muscle cell function and plasticity. *Free Radic. Biol. Med.* 65, 693–703. doi: 10.1016/j.freeradbiomed.2013.08.003

Satoh, K., Fukumoto, Y., and Shimokawa, H. (2011). Rho-kinase: important new therapeutic target in cardiovascular diseases. *Am. J. Physiol. Heart Circ. Physiol.* 301, H287–H296. doi: 10.1152/ajpheart.00327.2011

Schildmeyer, L. A., Braun, R., Taffet, G., Debiasi, M., Burns, A. E., Bradley, A., et al. (2000). Impaired vascular contractility and blood pressure homeostasis in the smooth muscle alpha-actin null mouse. *FASEB J.* 14, 2213–2220. doi: 10.1096/fj.99-0927com

Seko, T., Ito, M., Kureishi, Y., Okamoto, R., Moriki, N., Onishi, K., et al. (2003). Activation of RhoA and inhibition of myosin phosphatase as important components in hypertension in vascular smooth muscle. *Circ. Res.* 92, 411–418. doi: 10.1161/01.RES.0000059987.90200.44

Taubman, M. B. (2003). Angiotensin II: a vasoactive hormone with ever-increasing biological roles. *Circ. Res.* 92, 9–11. doi: 10.1161/01.RES.0000052920.70316.AE

Touyz, R. M. (2005). Intracellular mechanisms involved in vascular remodelling of resistance arteries in hypertension: role of angiotensin II. *Exp. Physiol.* 90, 449–455. doi: 10.1113/expphysiol.2005.030080

Wirth, A. (2010). Rho kinase and hypertension. *Biochim. Biophys. Acta* 1802, 1276–1284. doi: 10.1016/j.bbadis.2010.05.002

Xu, P., Das, M., Reilly, J., and Davis, R. J. (2011). JNK regulates FoxO-dependent autophagy in neurons. *Genes Dev.* 25, 310–322. doi: 10.1101/gad.1984311

Yamakawa, T., Tanaka, S., Kamei, J., Kadonosono, K., and Okuda, K. (2003). Phosphatidylinositol 3-kinase in angiotensin II-induced hypertrophy of vascular smooth muscle cells. *Eur. J. Pharmacol.* 478, 39–46. doi: 10.1016/j.ejphar.2003.08.044

Yang, Z., and Klionsky, D. J. (2010). Mammalian autophagy: core molecular machinery and signaling regulation. *Curr. Opin. Cell Biol.* 22, 124–131. doi: 10.1016/j.ceb.2009.11.014

Yin, Z., Pascual, C., and Klionsky, D. J. (2016). Autophagy: machinery and regulation. *Microb. Cell* 3, 588–596. doi: 10.15698/mic2016.12.546

Yoshida, T., Hoofnagle, M. H., and Owens, G. K. (2004). Myocardin and Prx1 contribute to angiotensin II-induced expression of smooth muscle alpha-actin. *Circ. Res.* 94, 1075–1082. doi: 10.1161/01.RES.0000125622.46280.95

Yu, K. Y., Wang, Y. P., Wang, L. H., Jian, Y., Zhao, X. D., Chen, J. W., et al. (2014). Mitochondrial KATP channel involvement in angiotensin II-induced autophagy in vascular smooth muscle cells. *Basic Res. Cardiol.* 109:416. doi: 10.1007/s00395-014-0416-y

Zhang, F., Ren, X., Zhao, M., Zhou, B., and Han, Y. (2016). Angiotensin-(1-7) abrogates angiotensin II-induced proliferation, migration and inflammation in VSMCs through inactivation of ROS-mediated PI3K/Akt and MAPK/ERK signaling pathways. *Sci. Rep.* 6:34621. doi: 10.1038/srep34621

Zhang, X., Li, Z. L., Crane, J. A., Jordan, K. L., Pawar, A. S., Textor, S. C., et al. (2014). Valsartan regulates myocardial autophagy and mitochondrial turnover in experimental hypertension. *Hypertension* 64, 87–93. doi: 10.1161/HYPERTENSIONAHA.113.02151

Zhao, Y., Yang, J., Liao, W., Liu, X., Zhang, H., Wang, S., et al. (2010). Cytosolic FoxO1 is essential for the induction of autophagy and tumour suppressor activity. *Nat. Cell Biol.* 12, 665–675. doi: 10.1038/ncb2069

Zhu, B., Zhou, Y., Xu, F., Shuai, J., Li, X., and Fang, W. (2012). Porcine circovirus type 2 induces autophagy via the AMPK/ERK/TSC2/mTOR signaling pathway in PK-15 cells. *J. Virol.* 86, 12003–12012. doi: 10.1128/JVI.01434-12

Conflict of Interest Statement: The authors declare that the research was conducted in the absence of any commercial or financial relationships that could be construed as a potential conflict of interest.

The reviewer MG and handling Editor declared their shared affiliation.

frontiers in Pharmacology

ORIGINAL RESEARCH
published: 28 February 2019
doi: 10.3389/fphar.2019.00157

Aromatic Bromination Abolishes the Psychomotor Features and Pro-social Responses of MDMA ("Ecstasy") in Rats and Preserves Affinity for the Serotonin Transporter (SERT)

Patricio Sáez-Briones[1], Vicente Castro-Castillo[2], Gabriela Díaz-Véliz[3], Luis Valladares[4], Rafael Barra[1], Alejandro Hernández[5] and Bruce K. Cassels[6]*

[1] Laboratory of Neuropharmacology and Behavior, Faculty of Medical Sciences, School of Medicine, Universidad de Santiago de Chile, Santiago, Chile, [2] Department of Organic Chemistry and Physical Chemistry, Faculty of Chemical and Pharmaceutical Sciences, Universidad de Chile, Santiago, Chile, [3] Faculty of Medicine, Institute for Biomedical Sciences, University of Chile, Santiago, Chile, [4] Laboratory of Hormones and Receptors, Instituto de Nutrición y Tecnología de los Alimentos (INTA), Universidad de Chile, Santiago, Chile, [5] Laboratory of Neurobiology, Department of Biology, Faculty of Chemistry and Biology, Universidad de Santiago de Chile, Santiago, Chile, [6] Chemobiodynamics Laboratory, Department of Chemistry, Faculty of Sciences, Universidad de Chile, Santiago, Chile

OPEN ACCESS

Edited by:
Ramón Sotomayor-Zárate, Universidad de Valparaíso, Chile

Reviewed by:
Cecilia Scorza, Instituto de Investigaciones Biológicas Clemente Estable (IIBCE), Uruguay
Romana Šlamberová, Charles University, Czechia

***Correspondence:**
Patricio Sáez-Briones
patricio.saez@usach.cl

Specialty section:
This article was submitted to Neuropharmacology, a section of the journal Frontiers in Pharmacology

Received: *05 January 2019*
Accepted: *11 February 2019*
Published: *28 February 2019*

Citation:
Sáez-Briones P, Castro-Castillo V, Díaz-Véliz G, Valladares L, Barra R, Hernández A and Cassels BK (2019) Aromatic Bromination Abolishes the Psychomotor Features and Pro-social Responses of MDMA ("Ecstasy") in Rats and Preserves Affinity for the Serotonin Transporter (SERT). Front. Pharmacol. 10:157. doi: 10.3389/fphar.2019.00157

The entactogen MDMA (3,4-methylenedioxy-methamphetamine, "Ecstasy") exerts its psychotropic effects acting primarily as a substrate of the serotonin transporter (SERT) to induce a non-exocytotic release of serotonin. Nevertheless, the roles of specific positions of the aromatic ring of MDMA associated with the modulation of typical entactogenic effects, using analogs derived from the MDMA template, are still not fully understood. Among many possibilities, aromatic halogenation of the phenylalkylamine moiety may favor distribution to the brain due to increased lipophilicity, and sometimes renders psychotropic substances of high affinity for their molecular targets and high potency in humans. In the present work, a new MDMA analog brominated at C(2) of the aromatic ring (2-Br-4,5-MDMA) has been synthesized and pharmacologically characterized *in vitro* and *in vivo*. First, binding competition experiments against the SERT-blocker citalopram were carried out in human platelets and compared with MDMA. Besides, its effects on platelet aggregation were performed in platelet enriched human plasma using collagen as aggregation inductor. Second, as platelets are considered an appropriate peripheral model for estimating central serotonin availability, the functional effects of 2-Br-4,5-MDMA and MDMA on ATP release during human platelet aggregation were evaluated. The results obtained showed that 2-Br-4,5-MDMA exhibits higher affinity for SERT than MDMA and fully abolishes both platelet aggregation and ATP release, resembling the pharmacological profile of citalopram. Subsequent *in vivo* evaluation in rats at three dose levels showed that 2-Br-4,5-MDMA lacks all key

MDMA-like behavioral responses in rats, including hyperlocomotion, enhanced active avoidance conditioning responses and increased social interaction. Taken together, the results obtained are consistent with the notion that 2-Br-4,5-MDMA should not be expected to be an MDMA-like substrate of SERT, indicating that aromatic bromination at C(2) modulates the pharmacodynamic properties of the substrate MDMA, yielding a citalopram-like compound.

Keywords: MDMA (3,4-methylenedioxymethamphetamine), 2-Br-4,5-MDMA (2-bromo-4,5-methylenedioxymethamphetamine), rat behavior, human platelet aggregation, ATP release, serotonin transporter

INTRODUCTION

The entactogen MDMA (3,4-methylenedioxymethamphetamine, **Figure 1A**), also known as "Ecstasy," engenders in humans an altered state of consciousness described as a feeling of heightened self-acceptance and empathy with other persons without impairing cognitive or orientation capabilities, while decreasing fear responses (Green et al., 2003). Due to these properties, evidence has accumulated regarding the potential applications of MDMA in psychotherapy (Parrott, 2007; Mithoefer et al., 2011, 2013; Feduccia and Mithoefer, 2018), as an adjunct in the treatment of neuropsychiatric disorders (Riedlinger and Riedlinger, 1994; Doblin, 2002; Bouso et al., 2008; Danforth et al., 2016) and alcoholism (Sessa, 2018).

MDMA is known to exert its acute psychotropic effects acting mainly as a special type of substrate of the serotonin transporter (SERT) (Crespi et al., 1997; Rothman et al., 2001) that induces non-exocytotic serotonin (5-HT) release by triggering a reversal of the normal transporter flux (Sitte and Freissmuth, 2010). As the basis of MDMA-like activity deserves to be explored for therapeutic purposes, efforts to develop MDMA analogs included mainly classical derivatives (Shulgin and Shulgin, 1991) and more recently synthetic cathinones (Morris, 2010) and benzofurans (Liechti, 2015). The group of "classical" analogs (some of them viewed as true MDMA substitutes), included the recreationally popular *N*-demethylated MDMA analog (and primary metabolite) MDA (Gouzoulis-Mayfrank and Hermle, 1998; Baylen and Rosenberg, 2006). As for the newer synthetic cathinones and benzofurans, modifications were focused on the aminoalkyl side chain, replacing the α- and the *N*-methyl by an α- (MBDB) or *N*-ethyl group (MDEA) or by locking its conformation in a 2-aminoindan ring structure (Nichols et al., 1986). Interestingly, it was further found that the ring-methylated MDA derivatives 1-(2-methyl-3,4-methylenedioxyphenyl)- and 1-(3-methyl-4,5-methylenedioxyphenyl)-2-aminopropane are not only fairly potent 5-HT releasers in rats but also substitute, at low doses, for the entactogen-like MBDB and MMAI in the drug discrimination paradigm, whereas the positional isomer 1-(2-methyl-4,5-methylenedioxyphenyl)-2-aminopropane is four times less potent than MMAI and only substitutes partially for MBDB (Parker et al., 1998). This evidence suggests that rational modifications of the benzene ring of MDMA can lead to potentially new analogs sharing some of the distinctive MDMA-like effects. As bromine can be considered as bio-isosteric to the methyl group, one should expect that appropriately brominated analogs of MDMA could exhibit similar MDMA-like properties. In addition, because halogenation has been described to modulate the interactions of a drug with its molecular target by establishing so-called "halogen bonds" (Hardegger et al., 2010), bromination might be a useful tool to reveal some valuable hints about the modulation of MDMA activity as a consequence of its interaction with SERT. Nevertheless, and despite its relevance, the pharmacological characterization of the effects of aromatic halogenation on the mode of binding at SERT referred to MDMA remains fragmentary and incomplete. For instance, aromatic bromination at C(2) to afford 1-(2-bromo-4,5-methylendioxyphenyl)-2-methylaminopropane (2-Br-4,5-MDMA) has been proposed as an approach to an analog that might exhibit entactogenic-like properties (Sáez-Briones and Hernández, 2013). This notion is supported by some members of the heterogenous group of psychotropic phenylalkylamines, including MDMA. Indeed, aromatic halogenation of structurally-related phenylalkylamine molecules can render hallucinogens of high potency *in vivo* (Barfknecht and Nichols, 1971; Shulgin and Shulgin, 1991) and high affinity for their corresponding molecular targets (e.g., 5-$HT_{2A/2C}$ receptors; Nichols, 2016, 2018), though only when the halogen is located at C(4). The *N*-unmethylated analog of 2-Br-4,5-MDMA, 1-(2-bromo-4,5-methylendioxyphenyl)-2-aminopropane (2-Br-4,5-MDA) was prepared long ago and tested in humans, and the subjective effect of an oral dose in excess of 300 mg was considered "amphetamine-like" (Sepúlveda et al., 1972). Regardless of the fact that the latter evidence should not necessarily extend to monoamine transporters, one could expect that aromatic bromination might induce similar effects on the mode of binding of MDMA. Consequently, we hypothesize that bromine substitution may increase the pharmacological features of MDMA, including SERT affinity, the ability to act as a SERT substrate and the distinctive behavioral effects already known for Ecstasy.

To verify this hypothesis, 2-Br-4,5-MDMA has been synthesized and pharmacologically evaluated in order to determine its binding affinity at human SERT. For this purpose, binding competition experiments against the SERT blocker citalopram were carried out in human platelets and compared with MDMA. In addition, the effects on platelet aggregation were performed in platelet enriched human plasma using collagen as aggregation inductor. As platelets also possess a high SERT density, they are considered a suitable peripheral model to

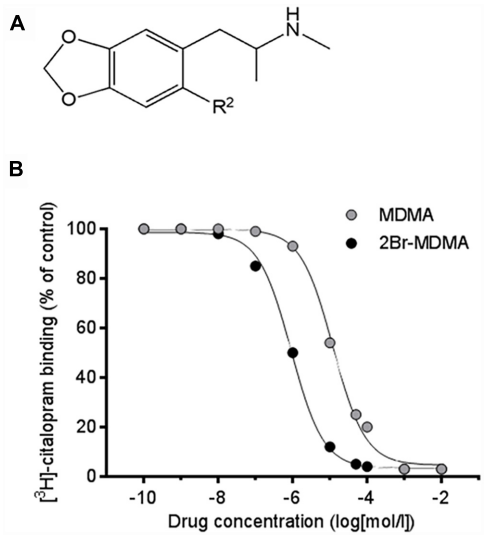

FIGURE 1 | (A) Chemical structures illustrating the MDMA moiety. For MDMA, the substituent located at the R^2 aromatic position is a hydrogen atom (R^2 = H). For 2-Br-4,5-MDMA, the substituent located at the R^2 aromatic position is a bromine atom (R^2 = Br). **(B)** Inhibition of specific [^{3}H]-citalopram binding to human platelet membranes by MDMA and 2-Br-4,5-MDMA, allowing the calculation of inhibition constant (K_i) values (means ± SEM) from three separate experiments. For MDMA, K_i = 9880 ± 1231 nM; for 2-Br-4,5-MDMA, K_i = 1060 ± 50.2 nM ($p < 0.002$, two-tailed unpaired Student's *t*-test). Reference values of K_i for serotonin and citalopram were 870 and 0.42 nM, respectively (curves not shown).

estimate central serotonin availability from the periphery and the amount of ATP released during platelet aggregation may be used as an indirect estimate of the activation level of SERT (Maurer-Spurej, 2005; Mercado and Kilic, 2010). Therefore, the functional features of 2-Br-4,5-MDMA on SERT were also determined evaluating the effects of the analog on platelet ATP release.

Finally, 2-Br-4,5-MDMA was evaluated *in vivo* at different doses using a sequence of behavioral paradigms in rats already used to construct the distinctive behavioral profile of MDMA (Quinteros-Muñoz et al., 2010): spontaneous behaviors (motor activity, locomotion, rearing, grooming, head shakes), evaluation in the elevated plus-maze, determination of active avoidance conditioning responses and assessment of social interaction (Sáez-Briones and Díaz-Véliz, 2012). Both drugs were tested as racemic mixtures, considering that this is the form commonly used in clinical and recreational settings. The results obtained support the notion that aromatic bromination at C(2) changes the mode of binding at SERT and the distinctive behavioral effects of MDMA.

MATERIALS AND METHODS

General Procedures

All reagents and solvents were commercially available from Sigma-Aldrich (St. Louis, MO, United States) or Merck (Darmstadt, Germany) and were used without further purification. Melting points are uncorrected and were determined with a Reichert Galen III hot plate microscope equipped with a DUAL JTEK Dig–Sense thermocouple thermometer. ^{1}H NMR spectra were recorded at 400 MHz on a Bruker AMX 400 spectrometer, using D_2O as solvent. The chemical shifts are reported as δ (ppm) downfield from TMS for ^{1}H NMR. Coupling constants (*J*) are given in Hz.

Organic Synthesis of MDMA and 2-Br-4,5-MDMA

3,4-Methylenedioxybenzaldehyde was converted to the β-nitrostyrene (Henry-Knoevenagel condensation with nitroethane) in an ionic liquid (2-hydroxyethylammonium formate) (Bicak, 2005; Alizadeh et al., 2010). After purification by crystallization, the reaction product was reduced to the amine with $LiAlH_4$. Then, 1.0 g of the 4,5-methylenedioxyamphetamine MDA (5.6 mmol) obtained was dissolved in THF (5.0 mL) and added dropwise with stirring to a solution of formic acetic anhydride (44.8 mmol) in THF (15 mL). The reaction was held at room temperature for 6 h. All volatile components were removed under vacuum affording a red colored oil, that was treated without purification with $LiAlH_4$ (1.0 g) in THF (10 mL). Then, 500 mg of the MDMA (**Figure 1A**) obtained was dissolved in AcOH (2.0 mL) and a 4 mol/L solution of Br_2 in AcOH (2.8 mmol) was added dropwise with stirring. The reaction was kept at room temperature for 24 h. The precipitate formed was collected by filtration to afford 2-Br-4,5-MDMA.HBr (**Figure 1A**), which was obtained as white crystals (1.2 g, 63%); mp 196–197°C. ^{1}H NMR (400 MHz, D_2O): δ 1.21 (d, J = 6.6 Hz, 3H, CH_3), 2.66 (s, 3H, CH_3), 2.93 (m, 2H, CH_2), 3.48 (m, 1H, CH), 5.92 (s, 2H, CH_2), 6.78 (s, 1H, ArH), 7.04 (s, 1H, ArH).

Binding of MDMA and 2-Br-4,5-MDMA at 5-HT Transporters (SERT)

Binding of MDMA and 2-Br-4,5-MDMA at SERT was determined from competition curves of the drugs against the high affinity ligand [^{3}H]-citalopram, using a modification of the assay in platelet membranes as described (Plenge and Mellerup, 1991). Blood from healthy donors was collected by venipucture into acid-citrate-dextrose (9:1) and centrifuged at 200 × *g* for 20 min to prepare platelet rich plasma (PRP). PRP (5 mL) was diluted in 20 mL buffer A (50 mM Tris–HCl buffer pH 7.4 containing 120 mM NaCl and 5 mM KCl) and centrifuged at 1700 × *g* for 20 min. The supernatant was discarded and the final membrane pellet was homogenized in 10 mL of buffer A and centrifuged twice at 27,000 × *g* for 20 min. It was then resuspended in 10 mL buffer A to yield a final protein concentration of about 0.8–1.2 mg/mL. [^{3}H]-citalopram binding was determined in 200 μL of platelet membranes loaded with 100 μL [^{3}H]-citalopram (2 nM). This concentration is in the range of the dissociation constant (K_D) value for citalopram binding at SERT in PRP (Plenge and Mellerup, 1991). Fifty micro liter of buffer (50 mM Tris-HCl, pH 7.4) containing increased concentrations (0.1 nmol/L to 10 mmol/L) of the unlabeled drugs (i.e., MDMA, 2-Br-4,5-MDMA), serotonin or citalopram was then added. After 60 min incubation at 25°C, homogenates

were diluted in 3 mL ice-cold buffer and filtered through Whatman GF/C glass fiber filters. The total time taken for the filtration/washing procedure was less 30 s. Filters were washed three times with 3 mL ice-cold buffer, and the radioactivity was measured by liquid scintillation spectrometry at 55% efficiency. Specific binding was defined as the difference between total labeled [^{3}H]-citalopram binding (triplicate samples) and the binding in the presence of 10 μM unlabeled citalopram (duplicate samples). The inhibitory constants (K_i), defined as the drug concentration displacing 50% of the specifically bound [^{3}H]-citalopram, were calculated from one-site competitive binding data using the Prism 5.0 program (GraphPad Inc., San Diego, CA, United States) according to Cheng and Prusoff (1973), and considering a K_D = 1.7 nM for [^{3}H]-citalopram binding in human platelets (Plenge and Mellerup, 1991).

Effects of MDMA and 2-Br-4,5-MDMA on Platelet Aggregation and SERT Functionality

The effects of MDMA and 2-Br-4,5-MDMA on SERT functionality were indirectly determined by studying the release of ATP during platelet aggregation induced by collagen, which is a process associated with 5-HT uptake at SERT. PRP were prepared from blood collected from human healthy donors as described above, and platelets were pelleted by centrifugation at 500 × *g* for 10 min and washed and re-suspended as described (Kim et al., 2013). Both platelet aggregation and ATP release from platelets were simultaneously measured using a lumi-aggregometer (Chrono-Log, United States). PRP were incubated and stabilized at 37°C in an aggregometry sample tube. Each sample was stirred at 1000 rpm for 1 min before testing. Samples were further pretreated in the presence of different concentrations (12.5, 25, 50, or 100 μM) of 2-Br-4,5-MDMA or MDMA for 10 min. Platelet aggregation was then induced by addition of collagen (1 μg/mL) as previously described (Muñoz et al., 2012). The resulting aggregations were measured as changes of light transmission that were recorded for 8 min. The extent of platelet aggregation was expressed as percentage of light transmission in a platelet-free medium. The ATP released from platelets was detected by a luciferin-luciferase detection system, ATP Bioluminescent Assay Kit (Sigma-Aldrich), according to the manufacturer's directions, and expressed as percentage.

Behavioral Evaluation

Animals

A total of 80 adult male Sprague-Dawley rats, weighing 200–230 g, were purchased from the rearing facility of the Pontifical Catholic University of Chile, and housed eight per cage in a temperature-controlled vivarium under a 12:12 h light-dark cycle (lights on from 0800 to 2000 h), with free access to standard rodent pellet diet and tap water. Behavioral observations took place in a sound-proof room at the same time of day to reduce the confounding influence of diurnal variation on spontaneous behavior. Each animal was tested only once, and the minimum number of animals and duration of observations required to obtain consistent data were employed. Experimental protocols were conducted in accordance with international standards of animal welfare and following the Guide for Care and Use of Laboratory Animals, National Research Council, United States, and were approved by the Bioethics Committee of the University of Santiago de Chile.

Drug Administration

Each drug was freshly dissolved in saline (0.9% NaCl) and administered intraperitoneally (i.p.) in a volume of 1 mL/kg body weight. MDMA and 2-Br-4,5-MDMA were administered at dose levels of 1, 5, and 10 mg/kg (i.p.), 30 min before the behavioral tests. Each experimental group consisted of 6–8 animals. Saline was used as control treatment. Certificate No 120, Institutional Ethics Committee, Universidad de Santiago de Chile.

Spontaneous Motor Activity

Each rat was placed individually in a Plexiglas cage (30 × 30 × 30 cm) located inside a soundproof chamber. The floor of the cage was an activity platform (Lafayette Instrument Co., Lafayette, IN, United States) connected to an amplifier and an electromechanical counter to monitor total spontaneous motor activity (Lafayette Instrument Co., United States). Locomotor activity was also recorded with an infrared photocell activity monitor (Columbus Instruments, United States), provided with an array of 15 infrared photocells spaced 1 in. (2.54 cm) apart. Total motility and locomotor activity were monitored every 5 min during a 30 min period. Simultaneously, the number of rearings, head shakes and the time (in seconds) spent in grooming behavior were manually recorded. Global spontaneous motor activity measures the total motor activity of the animal, including grooming, head shakes, rearing and locomotion. In contrast, locomotor behavior measures the horizontal displacement of the animal only. One head shake was scored when the animal exhibited a rapid up-and-down and/or rotating motion of the head, sometimes affecting the trunk as in "wet-dog shakes." One spontaneous grooming episode was scored as time spent by the animal in wiping and/or licking different body parts. All the observations were recorded in real time using a digital camera connected to a PC, and video sequences were used for later reanalysis when necessary.

Elevated Plus-Maze

This test has been widely validated to measure anxiety in rodents (Pellow and File, 1986). The apparatus consisted of two black Plexiglas open arms (50 × 10 cm each), two closed arms (50 × 10 × 20 cm each) and a central platform (10 × 10 cm). The maze was elevated 70 cm above the floor. Each animal was placed at the center of the maze, facing one of the closed arms. During a test period of 5 min, an observer recorded: (a) the number of open-arm entries; (b) the number of closed-arm entries; (c) the time spent in open arms; and (d) the time spent in closed arms. Arm entries were counted when the animal placed all four paws in an arm. Because illumination seems to play a crucial role in the plus-maze behavior of rats (Mora et al., 1996), the test was conducted under low artificial illumination conditions (approximately 10 lux). After the test, the maze was carefully cleaned with a wet tissue paper (70%

ethanol solution). The results were expressed as percentages of open-arm entries and of time spent in open arms, with regard to the total number of arm entries and the total time spent in both open and closed arms, respectively. Since, in this test, anxiety is reflected in the unconditioned aversion to heights and open spaces, the percentage of entries and time spent in open arms provide measures of fear-induced inhibition of exploratory activity. This ratio is increased by anxiolytic and reduced by anxiogenic compounds (Pellow et al., 1985).

Active Avoidance Conditioning

Each rat was individually placed into a two-way shuttle box (Lafayette Instrument Co., Lafayette, IN, United States) composed of two stainless steel modular testing units. Each unit was equipped with an 18-bar insulated shock grid floor, two 28 V DC lights and a tone generator (Mallory Sonalert 2800 Hz, Lafayette Instrument Co., Lafayette, IN, United States). Electric shocks were delivered to the grid floor by a master shock supply (Lafayette Instrument Co., Lafayette, IN, United States). The rats were trained over 50 trials, after a 5 min period of habituation. Each trial consisted of the presentation of a tone that after 5 s was overlapped with a 0.20 mA foot-shock until the animal escaped to the opposite chamber (maximum shock duration of 10 s). Between trials, the animal was allowed to rest for at least 15 s. A conditioned avoidance response (CAR) was defined as a crossing to the opposite chamber within the first 5 s (tone alone). If the rat did not escape by crossing to the opposite chamber during the foot-shock, this was considered as an escape failure (EF).

Assessment of Social Interaction

To evaluate social interaction, a modification of the method described by File (1980) was employed. A pair of Sprague Dawley rats (220–250 g) coming from different cages (i.e., without previous interaction) were marked on the tail with two different non-permanent dye colors and injected with a single dose (2.5 mg/kg or 5 mg/kg, i.p.) of either MDMA or 2-Br-4,5-MDMA. Rat pairs injected with saline i.p. served as controls. Thirty minutes after the injection, the rat pair was placed in an open black box (50 × 50 × 40 cm) with high walls made of acrylic polymer, and the spontaneous interaction in the test arena was observed and scored during 10 min. To do this, the time (in seconds) spent on diverse behaviors related to social interaction (approach and remaining side-by-side with the partner, general and anogenital sniffing of the partner) and the number of rearings and times lying belly down were scored independently for the two rats by two experienced persons. The test was conducted under low artificial illumination conditions (approximately 10 lux), and all observations were recorded in real time using a digital camera connected to a PC. After running the test, the box was carefully cleaned with a tissue paper wet with 70% ethanol solution.

Statistical Analysis

Data are presented as mean ± SEM, and all statistical analyses were performed with GraphPad Prism software (GraphPad Software, Inc., San Diego, CA, United States). For binding assays, each inhibitory constant (K_i) obtained was compared to that calculated for citalopram, a prototypical inhibitor of SERT, using two-tailed unpaired Student's *t*-test. For the effects on platelet aggregation, ATP release from platelets and rat behavior, data were analyzed by two-way ANOVA followed by the Dunnett (intragroup comparisons against saline control) or the Bonferroni (intergroup comparisons at similar concentrations or doses) multiple comparison *post hoc* tests. A probability level of 0.05 or less was accepted as significant.

RESULTS

Effects of MDMA and 2-Br-4,5-MDMA on [^{3}H]-Citalopram Binding to Platelet Membranes

Drug competition curves for [^{3}H]-citalopram binding (**Figure 1B**) allowed the inhibition constants (K_i) of MDMA and 2-Br-4,5-MDMA to be calculated for the site that is labeled by [^{3}H]-citalopram, which most likely is SERT. The K_i for MDMA at SERT was 9880 ± 1231 nM, while for 2-Br-4,5-MDMA it amounted to 1060 ± 50.2 nM ($p < 0.002$, two-tailed unpaired Student's *t*-test). Thus, the K_i value for 2-Br-4,5-MDMA was closely similar to that calculated for serotonin (879 nM), but it is three orders of magnitude higher than that of the classical SERT inhibitor citalopram (0.42 nM). Therefore, $K_{i.MDMA} > K_{i.2BrMDMA} = K_{i.5-HT} >> K_{i.citalopram}$.

Effects of MDMA and 2-Br-4,5-MDMA on Platelet Aggregation and ATP Release

Figure 2A shows that at 25 μM or higher, 2-Br-4,5-MDMA significantly inhibited collagen-induced platelet aggregation as compared to saline, whereas full inhibition was observed at 100 μM ($^{**}p < 0.01$, $^{***}p < 0.001$, intragroup Dunnett's multiple comparisons test). In contrast, MDMA induced only marginal (but significant) inhibition of platelet aggregation at 50 and 100 μM, an effect which was significantly weaker than that produced by 2-Br-4,5-MDMA ($^{\#\#\#}p < 0.01$, intergroup Bonferroni multiple comparisons test). Additionally, as seen in **Figure 2B**, both drugs exerted inhibitory effects upon the amount of ATP released from platelets (strong effect for 2-Br-4,5-MDMA and mild effect for MDMA, as compared to saline), in close parallelism to the effects of similar concentrations of the drugs on platelet aggregation ($^{***}p < 0.01$, for intragroup Dunnett's multiple comparisons test; $^{\#\#}p < 0.01$ and $^{\#\#\#}p < 0.001$, for intergroup Bonferroni multiple comparisons test).

Behavioral Evaluation

Effects of MDMA and 2-Br-4,5-MDMA on Spontaneous Motor Activity

Figures 3A,B show that MDMA (5, 10 mg/kg) induced a significant increase in locomotor behavior and global motor activity compared to saline controls ($^{**}p < 0.01$, $^{***}p < 0.001$, intragroup Dunnett's multiple comparisons test), whereas 2-Br-4,5-MDMA did not induce changes in these motor parameters at any of the concentrations used. Differential sensitivity of

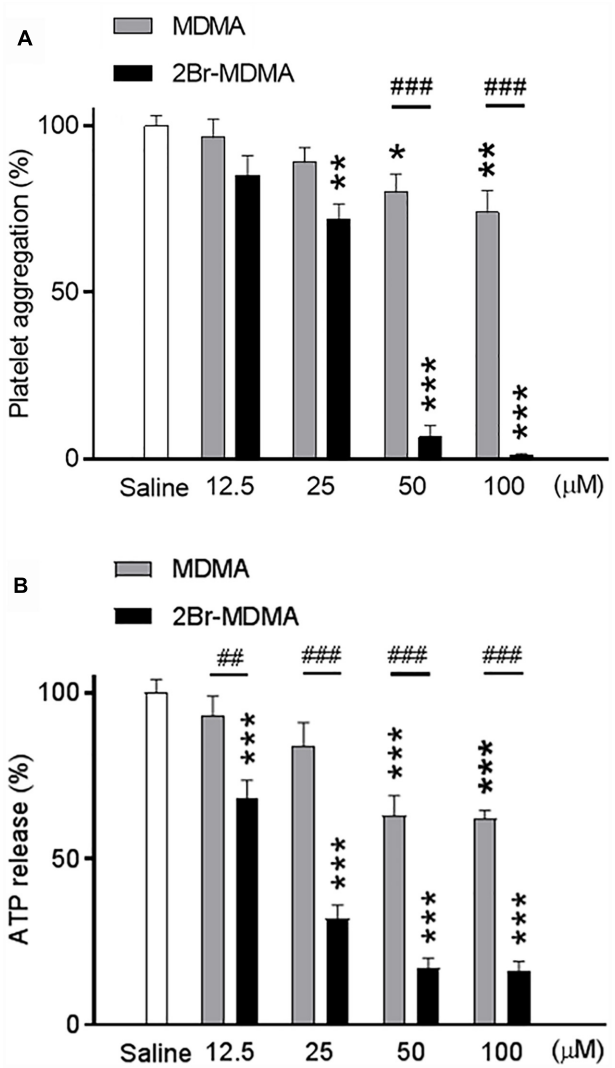

FIGURE 2 | Concentration-response relationships for the effects of MDMA and 2-Br-4,5-MDMA (12.5, 25, 50, and 100 μM) on: **(A)** collagen-induced platelet aggregation (platelet aggregation under saline without any drug was considered 100% aggregation), and **(B)** ATP released during collagen-induced platelet aggregation (ATP detected under saline without any drug was considered 100% release). Each bar represents a mean ± SEM ($n = 3$). Two-way ANOVA was used to identify the treatment (drug used) and/or the concentration (concentration used) as significant factors in the effect examined [for platelet aggregation, $F_{drug(1,\ 20)} = 146$ and $F_{concentration(4,\ 20)} = 76.56$; for ATP release, $F_{drug(1,\ 20)} = 127.8$ and $F_{concentration(4,\ 20)} = 62.73$]. Significance symbols arising from *post hoc* tests indicate either intragroup differences after 12.5, 25, 50, and 100 μM of drug concentration referred to saline controls ($^{*}p < 0.05$, $^{**}p < 0.01$, $^{***}p < 0.001$, Dunnett's multiple comparisons test) or intergroup differences between the same concentrations of MDMA or 2-Br-4,5-MDMA ($^{\#\#}p < 0.01$, $^{\#\#\#}p < 0.001$, Bonferroni multiple comparisons test).

locomotor and global motor behaviors to MDMA and 2-Br-4,5-MDMA administration was also detected upon comparison of the effects of both drugs at similar dosages ($^{\#}p < 0.05$, $^{\#\#}p < 0.01$, $^{\#\#\#}p < 0.001$, intergroup Bonferroni multiple comparisons test). Intragroup Dunnett's *post hoc* comparisons showed a significant reduction in the number of head-shakes in MDMA-injected rats (5 and 10 mg/kg; $^{***}p < 0.0001$) and also for those treated with any of the doses of the brominated analog ($^{***}p < 0.001$) (**Figure 3C**). Additionally, intragroup Dunnett's comparisons indicated that MDMA (5 and 10 mg/kg) significantly reduced the grooming behavior ($^{***}p < 0.0001$), while at these doses 2-Br-4,5-MDMA did not induce any change in grooming activity (**Figure 3D**). In addition, neither MDMA nor 2-Br-4,5-MDMA altered rearing behavior, both being indistinguishable from controls (data not shown). Thus, as a whole, the foregoing experimental series indicate that except for head-shakes, 2-Br-4,5-MDMA lacks the distinctive psychomotor features of MDMA.

Effects of MDMA and 2-Br-4,5-MDMA in the Elevated Plus-Maze

As seen on **Figure 4**, MDMA (10 mg/kg) induced a significant increase in the percentage of entries into the open arms ($^{**}p < 0.01$, intragroup Dunnett's multiple comparisons test) and an increased percentage of time spent in the open arms as well ($^{***}p < 0.001$, intragroup Dunnett's multiple comparisons test). In contrast, 2-Br-4,5-MDMA was unable to increase plus-maze open arms exploration at any of the doses used. On the other hand, the total number of entries into closed and open arms were not statistically different between 2Br-4,5-MDMA and MDMA, both being indistinguishable from controls (data not shown).

Effects of MDMA and 2-Br-4,5-MDMA on Active Avoidance Conditioning

As seen in **Figure 5A**, intragroup Dunnett's *post hoc* test reveals that whereas CAR was significantly improved after the administration of both higher doses of MDMA ($^{*}p < 0.05$), but it was significantly impaired by the same doses of 2-Br-4,5-MDMA ($^{*}p < 0.05$, $^{**}p < 0.01$). On the other hand, **Figure 5B** shows that escape failures were not affected by MDMA, but they were increased in rats injected with 1 and 5 mg/kg of 2-Br-4,5-MDMA ($^{***}p < 0.001$, Dunnett's multiple comparisons test). These results indicate that bromination of MDMA impairs the ability of the drug to improve acquisition in rats subjected to an active avoidance conditioning paradigm, together with producing an increase in escape failures.

Effects of MDMA and 2-Br-4,5-MDMA on Social Interaction

Dunnett's *post hoc* test revealed that both MDMA and 2-Br-4,5-MDMA equally promoted closeness to the partner ($^{*}p < 0.05$, $^{***}p < 0.001$) (**Figure 6A**), reduced anal-genital ($^{**}p < 0.01$, $^{***}p < 0.001$) (**Figure 6E**) and general sniffing of the partner $^{*}p < 0.05$, $^{**}p < 0.01$, $^{***}p < 0.001$) (**Figure 6F**), while both drugs produced no effect in the number of rearing episodes (**Figure 6C**). Nevertheless, MDMA administration significantly increased the time spent by rats lying next to each other and the lying belly down counts ($^{***}p < 0.001$) (**Figures 6B,D**), effects that were almost absent in rats receiving the brominated MDMA analog. Thus, the foregoing experimental series indicate that 2-Br-4,5-MDMA is almost unable to promote either the lying next to the partner response nor the lying belly down

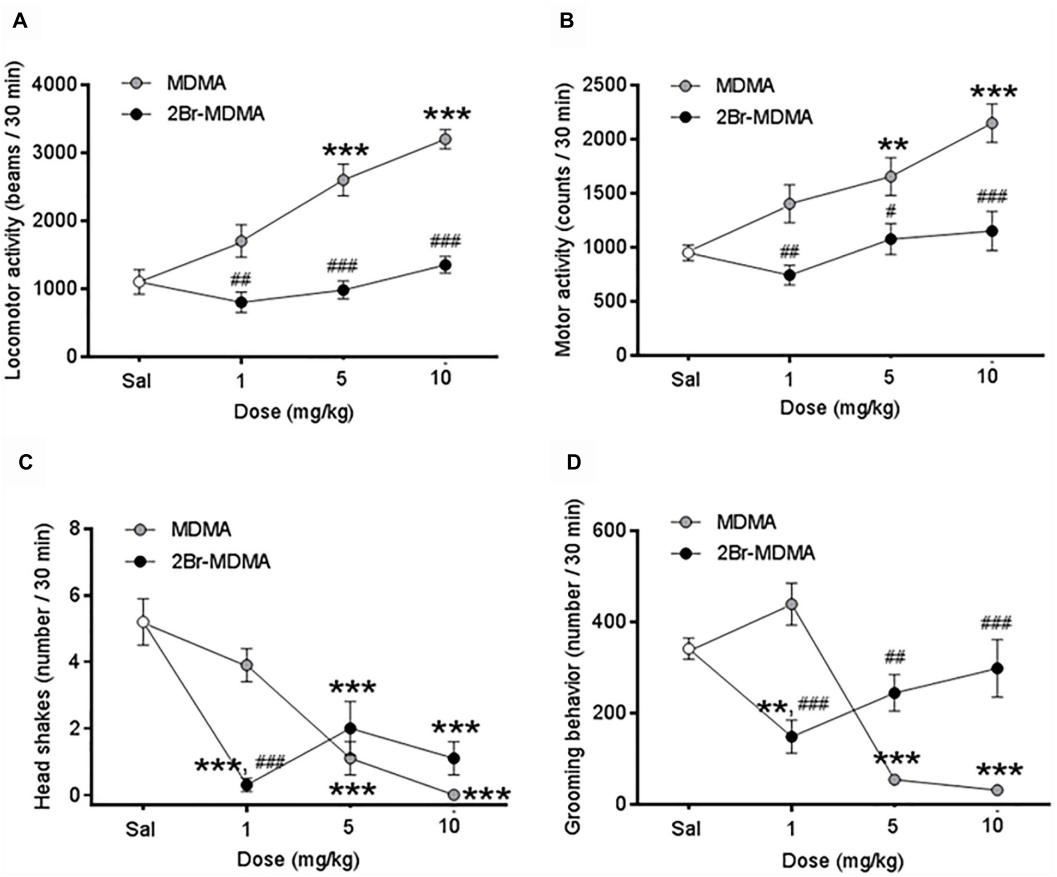

FIGURE 3 | Dose-response curves for the effects of MDMA and 2-Br-4,5-MDMA on spontaneous motor behaviors of rats: **(A)** locomotor activity, **(B)** total motor activity, **(C)** head shakes, **(D)** grooming behavior. Saline (Sal) was used as control. Drugs (1, 5, and 10 mg/kg) or saline were injected i.p. in a total volume of 1 mL/kg body weight. Behaviors were scored during 30 min, starting 30 min after drug or saline administration. Each point represents a mean ± SEM (n = 8). Two-way ANOVA was used to identify the treatment (drug used) and/or the dose (dose used) as significant factors in the effect examined [for locomotor activity, $F_{drug(1, 56)}$ = 75.71 and $F_{dose(2, 56)}$ = 18.27; for total motor activity, $F_{drug(1, 56)}$ = 29.97 and $F_{dose(2, 56)}$ = 9.402; for head shakes, $F_{drug(1, 56)}$ = 1.062 and $F_{dose(2, 56)}$ = 26.70; for grooming behavior, $F_{drug(1, 56)}$ = 2.689 and $F_{dose(2, 56)}$ = 14.06]. Significance symbols coming from *post hoc* tests indicate either intragroup differences after 1, 5, or 10 mg/kg of drug referred to Sal controls ($^{**}p < 0.01$, $^{***}p < 0.001$, Dunnett's multiple comparisons test) or intergroup differences between the same doses of MDMA or 2-Br-4,5-MDMA ($^{\#}p < 0.05$, $^{\#\#}p < 0.01$, $^{\#\#\#}p < 0.001$, Bonferroni multiple comparisons test).

behavior, and did not significantly alter the other indexes of social interaction evaluated.

DISCUSSION

The central aim of the present work was to determine the affinity and activity at SERT of the brominated ecstasy analog 2-Br-4,5-MDMA, as well as its effects on the distinctive acute behavioral hallmarks of MDMA in classical spontaneous psychomotor models and social interaction in rats. The results obtained point to three major facts: first, aromatic bromination at C(2) preserves SERT affinity, increasing it about 10-fold compared to MDMA; second, 2-Br-4,5-MDMA fully inhibits platelet aggregation and ATP release during this process; third, 2-Br-4,5-MDMA lacks most of the typical MDMA-like effects in classical psychomotor models in rats. Indeed, none of the most relevant psychomotor responses for MDMA (increased locomotion, enhanced acquisition in active avoidance experiments, exploration in the plus-maze) are present (Quinteros-Muñoz et al., 2010). Moreover, and most interestingly, 2-Br-4,5-MDMA did not promote specific social behaviors (lying next to the partner, lying belly down behavior) that might be considered as the pharmacological signature of MDMA in the social interaction paradigm (Sáez-Briones and Díaz-Véliz, 2012). In contrast, for other behavioral responses that have been described as non-MDMA distinctive hallmarks (e.g., rearing, grooming, head shakes; Quinteros-Muñoz et al., 2010) no differences were observed between 2Br-4,5-MDMA and MDMA.

Seminal work carried out decades ago identified the vesicular and membrane-bound SERTs as major targets of non-exocytotic MDMA-mediated 5-HT release *in vitro*, as neurotransmitter efflux required Na^+ on both sides of the membrane and was blocked by imipramine. Moreover, because these effects were reported to be different compared to those expected for

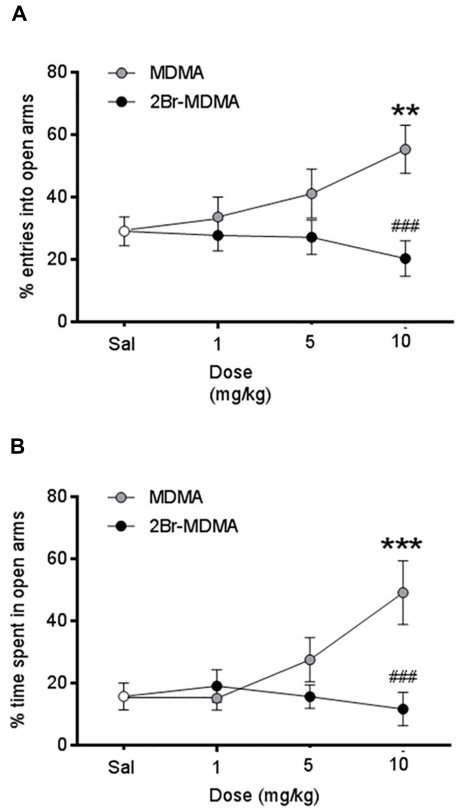

FIGURE 4 | Dose-response curves for the effects of MDMA and 2-Br-4,5-MDMA on behavior of rats in the elevated plus maze: **(A)** % entries into open arms, **(B)** % time spent in open arms. Saline (Sal) was used as control. Drugs (1, 5, and 10 mg/kg) or saline were injected i.p. in a total volume of 1 mL/kg body weight. Behaviors were scored during 30 min, starting 30 min after drug or saline administration. Each point represents a mean ± SEM (n = 8). Two-way ANOVA was used to identify the treatment (drug used) and/or the dose (dose used) as significant factors in the effect examined [for % entries into open arms, $F_{drug(1,\ 56)}$ = 10.33 and $F_{dose(2,\ 56)}$ = 0.8359; for % time spent in open arms, $F_{drug(1,\ 56)}$ = 7.432 and $F_{dose(2,\ 56)}$ = 2.514]. Significance symbols arising from *post hoc* tests indicate either intragroup differences after 1, 5, or 10 mg/kg of drug referred to Sal controls (**$p < 0.01$, ***$p < 0.001$, Dunnett's multiple comparisons test) or intergroup differences between the same doses of MDMA or 2-Br-4,5-MDMA ($^{###}p < 0.001$, Bonferroni multiple comparisons test).

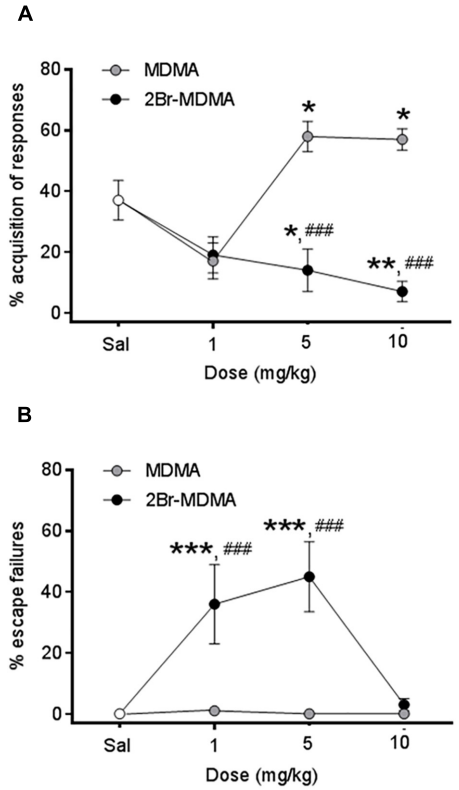

FIGURE 5 | Dose-response curves for the effects of MDMA and 2-Br-4,5-MDMA on active avoidance conditioning behavior of rats: **(A)** % acquisition of responses, **(B)** % escape failures. Saline (Sal) was used as control. Drugs (1, 5, and 10 mg/kg) or saline were injected i.p. in a total volume of 1 mL/kg body weight. Behaviors were scored during 30 min, starting 30 min after drug or saline administration. Each point represents a mean ± SEM (n = 8). Two-way ANOVA was used to identify the treatment (drug used) and/or the dose (dose used) as significant factors in the effect examined [for conditioned avoidance responses, $F_{drug(1,\ 56)}$ = 4.588 and $F_{dose(2,\ 56)}$ = 11.96; for escape failures, $F_{drug(1,\ 56)}$ = 22.55 and $F_{dose(2,\ 56)}$ = 6.707]. Significance symbols arising from *post hoc* tests indicate either intragroup differences after 1, 5, or 10 mg/kg of drug referred to Sal controls (*$p < 0.05$, **$p < 0.01$, ***$p < 0.001$, Dunnett's multiple comparisons test) or intergroup differences between the same doses of MDMA or 2-Br-4,5-MDMA ($^{###}p < 0.001$, Bonferroni multiple comparisons test).

structurally related psychedelics (Nichols and Glennon, 1984), it was proposed that the unique behavioral effects of MDMA might be mediated through its actions at SERT (Rudnick and Wall, 1992). Indeed, more recent evidence further elaborated that the acute psychotropic effects elicited by MDMA could be explained by means of a presynaptic mechanism that involves a reversal of the direction of transport of 5-HT through SERT elicited by the drug acting as a substrate (Sitte and Freissmuth, 2010; Dunlap et al., 2018).

The binding data for 2-Br-4,5-MDMA reported in the present work are in agreement with early *in silico* findings indicating that bromination at C(2) might not alter the binding capacity of MDMA (Núñez et al., 2009). Most interestingly, platelet aggregation inhibition data show that 2-Br-4,5-MDMA (but not MDMA) induced a fast and complete inhibition of platelet aggregation. Further, a mechanistic evaluation of the inhibition effects induced is consistent with the notion that 2-Br-4,5-MDMA might inhibit platelet aggregation by blocking the platelet serotonin resorption processes only, as also seems to be the case for the partial inhibition induced by MDMA (data not shown). A similar effect has already been reported for the SERT blocker citalopram at the same concentration using a similar experimental approach (Tseng et al., 2010). Nevertheless, considering the large differences among affinities at SERT, one may suggest that 2-Br-4,5-MDMA is a more potent blocker of serotonin influx than citalopram. The results obtained suggest that aromatic bromination at C(2) might modify the pharmacological profile of MDMA, favoring the establishment of blocking-like interactions at SERT that may account for the

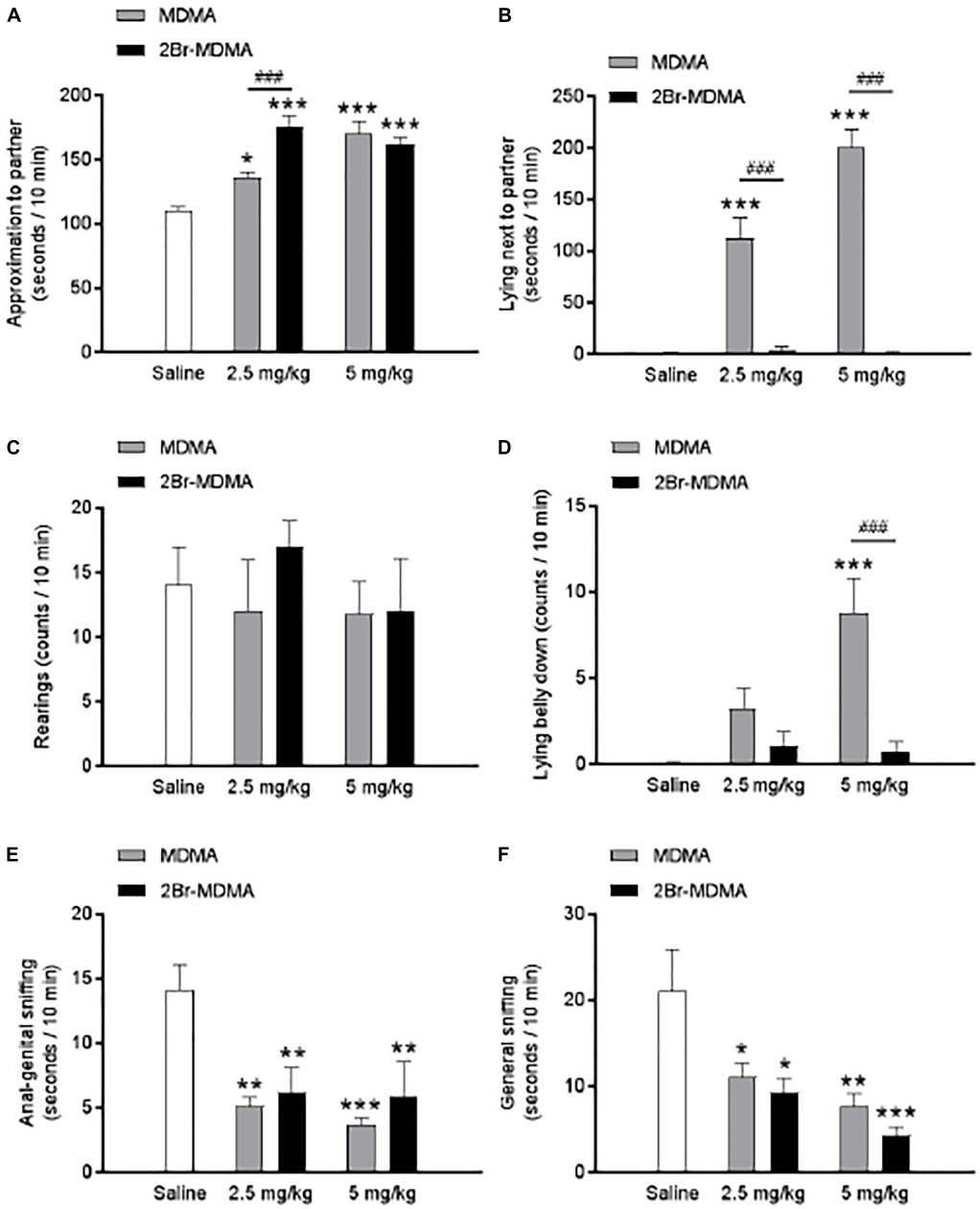

FIGURE 6 | Dose-response relationships for the effects of MDMA and 2-Br-4,5-MDMA on social behavior of rats: **(A)** approaching the partner, **(B)** lying next to the partner, **(C)** standing on hindlimbs (rearing), **(D)** lying belly down, **(E)** anal-genital sniffing, **(F)** general sniffing. Saline was used as control. Drugs (1, 5, and 10 mg/kg) or saline were injected i.p. in a total volume of 1 mL/kg body weight. Behaviors were scored during 30 min, starting 30 min after drug or saline administration. Each bar represents a mean ± SEM (n = 8). Two-way ANOVA was used to identify the treatment (drug used) and/or the dose (dose used) as significant factors in the effect examined [for approaching the partner, $F_{drug(1,\ 42)} = 4.004$ and $F_{dose(2,\ 42)} = 44.3$; for lying next to the partner, $F_{drug(1,\ 42)} = 127.7$ and $F_{dose(2,\ 42)} = 40.33$; for standing on hindlimbs, $F_{drug(1,\ 42)} = 0.4428$ and $F_{dose(2,\ 42)} = 0.3741$; for lying belly down, $F_{drug(1,\ 42)} = 16.04$ and $F_{dose(2,\ 42)} = 9.87$; for anal-genital sniffing, $F_{drug(1,\ 42)} = 0.5545$ and $F_{dose(2,\ 42)} = 16.15$; for general sniffing, $F_{drug(1,\ 42)} = 0.4586$ and $F_{dose(2,\ 42)} = 12.69$]. Significance symbols arising from *post hoc* tests indicate either intragroup differences after 1, 5, or 10 mg/kg of drug referred to Sal controls (*$p < 0.05$, **$p < 0.01$, ***$p < 0.001$, Dunnett's multiple comparisons test) or intergroup differences between the same doses of MDMA or 2-Br-4,5-MDMA ($^{\#\#\#}p < 0.001$, Bonferroni multiple comparisons test).

inhibition of platelet aggregation observed. In addition, although alterations in ATP release in the platelet model should be considered as an indirect measurement of possible differential functional activities at SERT (Tseng et al., 2010), these functional results for 2-Br-4,5-MDMA reinforce the idea of an apparent pharmacological similarity to citalopram. Indeed, aside from the concentration range considered, the inhibition of ATP release elicited by 2-Br-4,5-MDMA and citalopram reached almost the

same maximum (Tseng et al., 2010). In contrast, the SERT substrate MDMA (which inhibits platelet aggregation by around 15% only) shows a modest inhibitory activity on ATP release in the same concentration range. Despite the latter, as ATP release inhibition should be considered as an indirect evidence of alterations in SERT functionality, experiments evaluating 5-HT release are required to characterize these effects further.

Until recently, it was proposed that SERT should possess different binding sites for substrates and inhibitors (Gabrielsen et al., 2012). Nevertheless, the X-ray structure of the human SERT bound to citalopram and paroxetine published recently differs in some extent from this model (Coleman et al., 2016). Indeed, the structure shows two binding sites: S1 (thought to be the common binding site for blockers) and S2 (allosteric or vestibular binding site), but crystallographic data indicate that citalopram may bind to both binding sites as part of a complex, stereospecific interaction process that accounts for its antidepressive effects that may be mechanistically different from other selective serotonin reuptake inhibitors such as paroxetine (Topiol et al., 2017). Interestingly, a similar mode of binding was proposed earlier for 5-HT and MDMA as well (Field et al., 2010). In this scenario, MDMA is proposed to share a binding pocket with 5-HT and to induce 5-HT efflux by a translocation process that is not fully understood (Sitte and Freissmuth, 2015). On the other hand, because citalopram binds at both S1 and S2, an interesting question to address might be if this mode of binding is shared by 2-Br-4,5-MDMA. If this were the case, a modified "binding site preference" might be associated with the alterations in the behavioral profiles compared to MDMA, possibly as a result of conformational changes associated with the transport process along the transporter passage. In this regard, an interesting possibility associated with the preference for S2 might be the occurrence of halogen bonding (Zhou et al., 2007) in addition to or as an alternative to steric and hydrophobic interactions. Further research is needed to consider these possibilities.

In order to address the complexity of the relationship between a presynaptic mechanism and its behavioral implications, most efforts have been focused on the elucidation of the molecular mechanism associated with transport reversal, mainly at human SERT. This critical event has been proposed to be responsible for the psychotropic effects elicited not only by MDMA at SERT but also by structurally related stimulants such as amphetamine and methamphetamine at the dopamine transporter (Sitte and Freissmuth, 2010, 2015). Moreover, a substrate-mediated neurotransmitter efflux is considered to be a distinctive pharmacological property of amphetamines, which differ in this regard from other non-amphetamine substrates (Hilber et al., 2005). The efflux is believed to be part of a more complex mechanism that includes a supplemental carrier trafficking induction associated with the alteration of presynaptic second messenger pathways. Therefore, critical interactions at SERT could be expected to be correlated with the differences among psychotropic amphetamines evidenced at the behavioral level. The results obtained in the present work agree with this assumption, as shown by the differences between MDMA and 2-Br-4,5-MDMA in key ecstasy-like behavioral paradigms. Regarding the latter, it should be noted that the behavioral characterization of ecstasy has been attempted in different animal models, producing heterogeneous results that depend on several factors, such as dosage regimen, animal species or administration routes (Sáez-Briones and Hernández, 2013; Dunlap et al., 2018). Nevertheless, and for the purpose of the present work, a behavioral profile of MDMA in rats after acute administration based on complete dose-effect curves under the same experimental conditions has been used to evaluate the influence of aromatic bromination (Quinteros-Muñoz et al., 2010).

Dose-dependent hyperlocomotion is one key classical behavior in the rat allowing MDMA and possible MDMA-like molecules to be distinguished from their stimulant and psychedelic congeners (Quinteros-Muñoz et al., 2010). Interestingly, in the present study bromine substitution abolished the ability of acutely administered MDMA to increase locomotion (already described by McCreary et al., 1999; Baumann et al., 2008), to enhance acquisition in active avoidance experiments (already described by Galizio et al., 2009) and exploration in the plus-maze (already described by Lin et al., 1999; Navarro and Maldonado, 2002), and to promote some specific social behaviors (already described by Morley and McGregor, 2000), suggesting that 2-Br-4,5-MDMA might be classified as non-MDMA-like. The latter might be supported indirectly, at least in part, by the pharmacological effects reported for synthetic cathinones (e.g., MDPV) that, acting as blockers of monoamine transporters, still exhibit psychomotor activity (Marusich et al., 2014).

In particular, it has already been proposed that the unique locomotion activity pattern induced by MDMA in rodents seems to be strongly dependent on the differential activation of central D_1, D_2, and D_3 receptors (Risbrough et al., 2006). Therefore, one could speculate that the differences observed between MDMA and 2-Br-4,5-MDMA might be related to a differential activation rate of central dopaminergic receptors, as well as with the SERT and/or other monoamine transporters. The latter might be expressed as different availability ratios for dopamine and serotonin, as already reported for MDMA (Baumann et al., 2008). Interestingly, this effect seems to be dependent on the ability of MDMA to activate postsynaptic 5-$HT_{1B/1D}$ and presynaptic 5-HT_{2B} receptors (Bankson and Cunningham, 2001; Doly et al., 2008) when administered acutely. As bromine substitution can be expected to modulate ligand affinity (Hardegger et al., 2010), binding experiments at 5-HT_1 and 5-HT_2 receptors with 2-Br-4,5-MDMA are required to correlate the absence of hyperlocomotion with a modulation of receptor affinity/activity induced by the presence of bromine. The latter may arise as a result of functional selectivity favoring alternative transduction pathways (Moya et al., 2007), a pharmacological property exhibited by structurally related halogenated hallucinogens that do not enhance locomotion (Quinteros-Muñoz et al., 2010).

Active avoidance conditioning responses represent another key model for the evaluation of MDMA-like molecules, because the behavioral profile of MDMA in this protocol may be differentiated from those of structurally related stimulants and psychedelics. Notably, as bromine substitution exhibits a new behavioral profile, not altering (at low doses) and disrupting

(at 10 mg/kg) acquisition (together with an increase of the escape failures), one might classify these effects as mixed and/or psychedelic-like responses (Quinteros-Muñoz et al., 2010). As 2-Br-4,5-MDMA does not enhance the head shake response, one might speculate about the possibility that it might exhibit some hallucinogenic-like properties, as is the case of MMDA-2 that, by analogy with our naming of 2-Br-4,5-MDMA could be designated as 2-MeO-4,5-MDA (Shulgin and Shulgin, 1991; Quinteros-Muñoz et al., 2010). Interestingly, 2C-B (4-bromo-2,5-dimethoxyphenylethylamine), an entactogenic psychedelic (González et al., 2015) that does not enhance the head-shake response in rats and possesses low affinity for the 5-HT_{2A} receptor (Nelson et al., 1999) has been shown to be a low-affinity, non-competitive selective SERT blocker (Montgomery et al., 2007). The binding and functional data reported in the present work support this notion.

MDMA doses ranging from 2.5 to 5 mg/kg elevate "adjacent lying" in rats, a specific passive physical contact parameter measured in the social interaction model (Morley and McGregor, 2000; Ando et al., 2006). Pro-social behavior is mediated by the activation of serotonergic 5-HT_{1A} receptors elicited indirectly by acute doses of MDMA after massive 5-HT release in the hypothalamus (Morley et al., 2005) that elicits further the release of the neuropeptide oxytocin that, in turn, should be the direct effector of the pro-social behaviors induced by MDMA (Thompson et al., 2007). Interestingly, 2-Br-4,5-MDMA sustained almost all the pro-social behaviors typically enhanced by MDMA, with the only exception of the "adjacent lying" response. In this regard, one may speculate about a possible link between the amount of 5-HT released and the occurrence of specific pro-social behaviors. As 5-HT release should be modulated when affinity and/or activity at SERT changes, one might assume that bromine substitution diminished non-exocytotic 5-HT efflux, avoiding social interaction to be completed.

It should be noted that the entactogenic effects of MDMA in humans comprise a behavioral syndrome that may not be completely emulated in animal models. Nevertheless, social behavior has been used as a valuable tool in the preclinical testing of new drugs in laboratory animals. Indeed, an increase in social interaction has been shown to provide an index of potential anxiolytic activity (Cutier, 1993). This, in turn, establishes a link between social behavior and anxiety, highlighting the usefulness of this behavioral hallmark to estimate entactogenic-like effects (Sáez-Briones and Díaz-Véliz, 2012). Consequently, any disruption of basal anxiety may be expected to affect social behavior. As 2-Br-4,5-MDMA has been shown to be neither anxiolytic nor anxiogenic (**Figure 4**), one might propose that the selective abolishment of the "adjacent lying" response may not be related to an anxiety-related effect.

The question arises as to how bromination could disrupt the ability of MDMA to produce some specific behavioral effects while preserving (and even increasing) the capacity of the molecule to bind at SERT, as revealed by the nearly 10-fold lower K_i value of 2-Br-4,5-MDMA compared to MDMA. Two possible explanations may account for this apparent discrepancy: (i) firstly, bromination may have affected the ability of MDMA to cross the blood-brain barrier, thereby preventing 2-Br-4,5-MDMA from entering the brain, and (ii) secondly, bromination preserves the interaction of MDMA at SERT but may have altered the ability of MDMA to act as a substrate of the transporter (i.e., the ability to induce non-exocytotic 5-HT release). The first alternative seems to be unlikely considering that the bromine atom should increase the compound's lipophilicity without greatly affecting its molecular bulk and weight and thus favor brain penetration. Instead, the second alternative is more plausible. The behavioral effects of a SERT substrate may be produced by a non-exocytotic 5-HT release that could induce the activation of serotonergic receptors in the brain. Therefore, the *in vivo* effects of MDMA bromination should be explained by a change in the molecular mechanism associated with transport reversal at SERT, eventually transforming 2-Br-4,5-MDMA into a SERT blocker. Further experiments to fully characterize this qualitative change in the mode of binding at SERT are needed to confirm this possibility.

Finally, and most interestingly, the results obtained in the present work indicate that the similarities between 2-Br-4,5-MDMA and citalopram offer some hints about the therapeutic potential of this new MDMA analog: on the one hand, its ability to act as a citalopram-like blocker of SERT suggests that it may act as an antidepressant; on the other hand, its strong inhibition of platelet aggregation might be consistent with an anticoagulant drug profile. These open possibilities deserve to be addressed further.

CONCLUSION

In conclusion, and in contrast to our original hypothesis regarding the preservation or reinforcement of entactogenic qualities of MDMA, the results obtained in the present work are consistent with the notion that aromatic bromination of MDMA to give 2-Br-4,5-MDMA modulates its pharmacological features in a manner that resembles the effects of the SERT blocker citalopram, highlighting the relevance of this position on the aromatic ring as a key site to determine the mode of binding at SERT.

DATA AVAILABILITY

The datasets generated for this study are available on request to the corresponding author.

AUTHOR CONTRIBUTIONS

PS-B provided ideas or concepts for definition of intellectual context, particularly designed, and supervised the experiments. VC-C and BC performed the organic synthesis of compounds. PS-B and GD-V performed the behavioral experiments. LV performed binding studies and experiments at SERT. RB and AH analyzed the data. PS-B wrote the manuscript. All authors read and approved the final version of the manuscript.

FUNDING

This work was supported by DICYT-USACH (Grant No. 021701SB) and FONDECYT (Grant No. 1150868).

ACKNOWLEDGMENTS

We thank Mr. Fernando Marchant for technical support and animal care.

REFERENCES

Alizadeh, A., Kjodaci, M. M., and Eshghi, A. (2010). Ambiphilic dual activation role of a task-specific ionic liquid: 2-hydroxyethylammonium formate as a recyclable promoter and medium for the green synthesis of β-nitrostyrenes. *J. Org. Chem.* 75, 8295–8298. doi: 10.1021/jo101696z

Ando, R. D., Benko, A., Ferrington, L., Kirilly, E., Kelly, P. A., Bagdy, G., et al. (2006). Partial lesion of the serotonergic system by a single dose of MDMA results in behavioural desinhibition and enhances acute MDMA-induced social behavior on the social interaction test. *Neuropharmacology* 50, 884–896. doi: 10.1016/j.neuropharm.2005.12.010

Bankson, M. G., and Cunningham, K. A. (2001). 3,4-Methylenedioxymethamphetamine (MDMA) as a unique model of serotonin receptor function and serotonin-dopamine interactions. *J. Pharmacol. Exp. Ther.* 297, 846–852.

Barfknecht, C. F., and Nichols, D. E. (1971). Potential psychotomimetics. Bromomethoxyamphetamines. *J. Med. Chem.* 14, 370–372. doi: 10.1021/jm00286a026

Baumann, M. H., Clark, R. D., and Rothman, R. B. (2008). Locomotor stimulation produced by 3,4-methylenedioxymethamphetamine (MDMA) is correlated with dialysate levels of serotonin and dopamine in rat brain. *Pharmacol. Biochem. Behav.* 90, 208–217. doi: 10.1016/j.pbb.2008.02.018

Baylen, C. A., and Rosenberg, H. (2006). A review of the acute subjective effects of MDMA/ecstasy. *Addiction* 101, 933–947. doi: 10.1111/j.1360-0443.2006.01423.x

Bicak, N. (2005). A new ionic liquid: 2-hydroxyethylammonium. *J. Mol. Liquids* 116, 15–18. doi: 10.1016/j.molliq.2004.03.006

Bouso, J. C., Doblin, R., Farré, M., Alcázar, M. A., and Gómez-Jarabo, G. (2008). MDMA-assisted psychotherapy using low doses in a small sample of women with chronic posttraumatic stress disorder. *J. Psychoactive Drugs* 40, 225–236. doi: 10.1080/02791072.2008.10400637

Cheng, Y., and Prusoff, W. H. (1973). Relationship between the inhibition constant (K1) and the concentration of inhibitor which causes 50 per cent inhibition (I50) of an enzymatic reaction. *Biochem. Pharmacol.* 22, 3099–3108. doi: 10.1016/0006-2952(73)90196-2

Coleman, J. A., Green, E. M., and Gouaux, E. (2016). X-ray structures and mechanism of the human serotonin transporter. *Nature* 532, 334–338. doi: 10.1038/nature17629

Crespi, D., Mennini, T., and Gobbi, M. (1997). Carrier-dependent and Ca2+-dependent 5-HT and dopamine release induced by (+)-amphetamine, 3,4-methylenedioxyamphetamine, p-chloroamphetamine and (+)-fenfluramine. *Br. J. Pharmacol.* 121, 1735–1743. doi: 10.1038/sj.bjp.0701325

Cutier, M. G. (1993). Measure of social interactions. *Methods Neurosci.* 14, 101–110. doi: 10.1016/B978-0-12-185277-1.50011-3

Danforth, A. L., Struble, C. M., Yazar-Klosinski, B., and Grob, C. S. (2016). MDMA-assisted therapy: a new treatment model for social anxiety in autistic adults. *Prog. Neuropsychopharmacol. Biol. Psychiatry* 64, 237–249. doi: 10.1016/j.pnpbp.2015.03.011

Doblin, R. (2002). A clinical plan for MDMA (Ecstasy) in the treatment of posttraumatic stress disorder (PTSD): partnering with the FDA. *J. Psychoactive Drugs* 34, 185–194. doi: 10.1080/02791072.2002.10399952

Doly, S., Valjent, E., Setola, V., Callebert, J., Hervé, D., Launay, J. M., et al. (2008). Serotonin 5-HT2B receptors are required for 3,4methylenedioxymethamphetamine-induced hyperlocomotion and 5-HT release in vivo and in vitro. *J. Neurosci.* 28, 2933–2940. doi: 10.1523/JNEUROSCI.5723-07.2008

Dunlap, L. E., Andrews, A. M., and Olson, D. E. (2018). Dark classics in chemical neuroscience: 3,4-methylenedioxymetamphetamine. *ACS Chem. Neurosci.* 9, 2408–2427. doi: 10.1021/acschemneuro.8b00155

Feduccia, A. A., and Mithoefer, M. C. (2018). MDMA-assisted psychotherapy for PTSD: are memory reconsolidation and fear extinction underlying mechanisms? *Prog. Neuropsychopharmacol. Biol. Psychiatry* 84, 221–228. doi: 10.1016/j.pnpbp.2018.03.003

Field, J. R., Henry, L. K., and Blakely, R. D. (2010). Transmembrane domain 6 of the human serotonin transporter contributes to an aqueously accessible binding pocket for serotonin and the psychostimulant 3,4-methylenedioxymethamphetamine. *J. Biol. Chem.* 285, 11270–11280. doi: 10.1074/jbc.M109.093658

File, S. E. (1980). The use of social interaction as a method for detecting anxiolytic activity of chlordiazepoxide-like drugs. *J. Neurosci. Methods* 2, 219–238. doi: 10.1016/0165-0270(80)90012-6

Gabrielsen, M., Ravna, A. W., Kristiansen, K., and Sylte, I. (2012). Substrate binding and translocation of the serotonin transporter studies by docking and molecular dynamics simulations. *J. Mol. Model.* 18, 1073–1085. doi: 10.1002/minf.201600094

Galizio, M., McKinney, P., Cerutti, D. T., and Pitts, R. C. (2009). Effects of MDMA, methamphetamine and methylphenidate on repeated acquisition and performance in rats. *Pharmacol. Biochem. Behav.* 94, 305–311. doi: 10.1016/j.pbb.2009.09.010

González, D., Torrens, M., and Farré, M. (2015). Acute effects of the novel psychoactive drug 2C-B on emotions. *Biomed. Res. Int.* 2015:643878. doi: 10.1155/2015/643878

Gouzoulis-Mayfrank, E., and Hermle, L. (1998). 6. Are the "entactogens" a distinct psychoactive substance class? The contribution of human experimental studies to the classification of MDMA and other chemically related methylenedioxyamphetamine derivatives. *Heffter Rev. Psychedelic Res.* 1, 46–51.

Green, R. A., Mechan, A. O., Elliott, J. M., O'Shea, E., and Colado, M. I. (2003). The pharmacology and clinical pharmacology of 3,4-methylenedioxymethamphetamine (MDMA, "Ecstasy"). *Pharmacol. Rev.* 55, 463–508. doi: 10.1124/pr.55.3.3

Hardegger, L. A., Kuhn, B., Spinnler, B., Anselm, L., Ecabert, R., Stihle, M., et al. (2010). Systematic investigation of halogen bonding in protein–ligand interactions. *Angew. Chem.* 50, 314–318. doi: 10.1002/anie.201006781

Hilber, B., Scholze, P., Dorostkar, M. M., Sandtner, W., Holy, M., Boehm, S., et al. (2005). Serotonin-transporter mediated efflux: a pharmacological analysis of amphetamines and non-amphetamines. *Neuropharmacology* 49, 811–819. doi: 10.1016/j.neuropharm.2005.08.008

Kim, K., Lim, K. M., Shin, H. J., Seo, D. B., Noh, J. Y., Kang, S., et al. (2013). Inhibitory effects of black soybean on platelet activation mediated through its active component of adenosine. *Thromb. Res.* 131, 254–261. doi: 10.1016/j.thromres.2013.01.002

Liechti, M. E. (2015). Novel psychoactive substances (designer drugs): overview and pharmacology of modulators of monoamine signalling". *Swiss Med. Wkly.* 145, w14043. doi: 10.4414/smw.2015.14043

Lin, H. Q., Burden, P. M., Christie, M. J., and Johnston, G. A. (1999). The anxiogenic-like and anxiolytic-like effects of MDMA on mice in the elevated plus-maze: a comparison with amphetamine. *Pharmacol. Biochem. Behav.* 62, 403–408. doi: 10.1016/S0091-3057(98)00191-9

Marusich, J. A., Antonazzo, K. R., Wiley, J. L., Blough, B. E., Partilla, J. S., and Baumann, M. H. (2014). Pharmacoloy of novel synthetic sitmulants structurally related to the "bath salts" constituent 3,4-methylenedioxypyrovalerone (MDPV). *Neuropharmacology* 87, 206–213. doi: 10.1016/j.neuropharm.2014.02.016

Maurer-Spurej, E. (2005). Serotonin reuptake inhibitors and cardiovascular diseases: a platelet connection. *Cell. Mol. Life Sci.* 62, 159–170. doi: 10.1007/s00018-004-4262-1

McCreary, A. C., Bankson, M. G., and Cunningham, K. A. (1999). Pharmacological studies of the acute and chronic effects of (+)-3,4-methylenedioxymethamphetamine on locomotor activity: role of 5-hydroxytryptamine1A and 5-hydroxytryptamine1B/1D receptors. *J. Pharmacol. Exp. Ther.* 290, 965–973.

Mercado, C. P., and Kilic, F. (2010). Molecular mechanisms of SERT in platelets: regulation of plasma serotonin levels. *Mol. Interv.* 10, 231–241. doi: 10.1124/mi.10.4.6

Mithoefer, M. C., Wagner, M. T., Mithoefer, A. T., Jerome, L., and Doblin, R. (2011). The safety and efficacy of ±3,4-methylenedioxymethamphetamine-assisted psychotherapy in subjects with chronic, treatment-resistant posttraumatic stress disorder: the first randomized controlled pilot study. *J. Psychopharmacol.* 25, 439–452. doi: 10.1177/0269881110378371

Mithoefer, M. C., Wagner, M. T., Mithoefer, A. T., Jerome, L., Martin, S. F., Yazar-Klosinski, B., et al. (2013). Durability of improvement in post-traumatic stress disorder symptoms and absence of harmful effects or drug dependency after 3,4-methylenedioxymethamphetamine-assisted psychotherapy: a prospective long-term follow-up study. *J. Psychopharmacol.* 27, 28–39. doi: 10.1177/0269881112456611

Montgomery, T., Buon, C., Eibauer, S., Guiry, P. J., Keenan, A. K., and McBean, G. J. (2007). Comparative potencies of 3,4-methylenedioxymethamphetamine (MDMA) analogues as inhibitors of [3H]noradrenaline and [3H]5-HT transport in mammalian cell lines. *Br. J. Pharmacol.* 152, 1121–1130. doi: 10.1038/sj.bjp.0707473

Mora, S., Dussaubat, N., and Díaz-Véliz, G. (1996). Effects of the estrous cycle and ovarian hormones on behavioral indices of anxiety in female rats. *Psychoneuroendocrinology* 21, 609–620. doi: 10.1016/S0306-4530(96)00015-7

Morley, K. C., Arnold, J. C., and McGregor, I. S. (2005). Serotonin (1A) receptor involvement in acute 3,4-methylenedioxymethamphetamine (MDMA) facilitation of the social interaction in the rat. *Prog. Neuropsychopharmacol. Biol. Psychiatry* 29, 648–657.

Morley, K. C., and McGregor, I. S. (2000). (±)-3,4-Methylenedioxymethamphetamine (MDMA, ecstasy) increases social interaction in rats. *Eur. J. Pharmacol.* 408, 41–49. doi: 10.1016/S0014-2999(00)00749-4

Morris, K. (2010). UK places generic ban on mephedrone drug family. *Lancet* 375, 1333–1334. doi: 10.1016/S0140-6736(10)60559-4

Moya, P. R., Berg, K. A., Gutiérrez-Hernández, M., Sáez-Briones, P., Reyes-Parada, M., Cassels, B. K., et al. (2007). Functional selectivity of hallucinogenic phenethylamine and phenylisopropylamine derivatives at human 5-hydroxytryptamine (5-HT)2A and 5-HT2C receptors. *J. Pharmacol. Exp. Ther.* 321, 1054–1061. doi: 10.1124/jpet.106.117507

Muñoz, Y. C., Gómez, G. I., Moreno, M., Solis, C. L., Valladares, L., and Velarde, V. (2012). Dehydroepiandrosterone prevents then aggregation of platelets obtained from postmenopausal women with type 2 diabetes mellitus through the activation of the PKC/eNOS/NO pathway. *Horm. Metab. Res.* 44, 625–631. doi: 10.1055/s-0032-1309056

Navarro, J. F., and Maldonado, E. (2002). Acute and subchronic effects of MDMA ("ecstasy") on anxiety in male mice tested in the elevated plus-maze. *Prog. Neuropsychopharmacol. Biol. Psychiatry* 26, 1151–1154.

Nelson, D. L., Lucaites, V. L., Wainscott, D. B., and Glennon, R. A. (1999). Comparison of hallucinogenic phenylisopropylamine binding affinities at cloned human 5-HT(2A), 5-HT(2B) and 5-HT(2C) receptors. *Naunyn Schmiedebergs Arch. Pharmacol.* 359, 1–6. doi: 10.1007/PL00005315

Nichols, D. E. (2016). Psychedelics. *Pharmacol. Rev.* 68, 264–355. doi: 10.1124/pr.115.011478

Nichols, D. E. (2018). Chemistry and structure-activity relationships of psychedelics. *Curr. Top. Behav. Neurosci.* 36, 1–43. doi: 10.1007/7854_2017_475

Nichols, D. E., and Glennon, R. A. (1984). "Medicinal chemistry and structure activity relationships of hallucinogenic agents," in *Hallucinogens: Neurochemical, Behavioral and Clinical Perspectives*, ed. B. Jacobs (New York, NY: Raven Press), 95–112.

Nichols, D. E., Hoffmann, A. J., Oberlender, R. A., Jacob, P. III, and Shulgin, A. T. (1986). Derivatives of 1-(1,3-benzodioxol-5-yl)-2-butanamine: representative of a novel therapeutic class. *J. Med. Chem.* 29, 2009–2015. doi: 10.1021/jm00160a035

Núñez, G., Fierro, A., Sáez-Briones, P., Reyes-Parada, M., Zapata-Torres, G., and Cassels, B. K. (2009). Comparative study of the interactions of amphetamine derivatives with rat and human serotonin transporters through molecular modeling. *Rev. Farmacol. Chile* 2:75.

Parker, M. A., Marona-Lewicka, D., Kurrasch, D., Shulgin, A. T., and Nichols, D. E. (1998). Synthesis and pharmacological evaluation of ring-methylated derivatives of 3,4-(methylenedioxy)-amphetamine (MDA). *J. Med. Chem.* 41, 1001–1005. doi: 10.1021/jm9705925

Parrott, A. C. (2007). The psychotherapeutic potential of MDMA (3,4-methylenedioxy-methamphetamine): an evidence-based review. *Psychopharmacology* 191, 181–193. doi: 10.1007/s00213-007-0703-5

Pellow, S., Chopin, P., File, S. E., and Briley, M. (1985). Validation of open:closed arm entries in an elevated plus-maze as a measure of anxiety in the rat. *J. Neurosci. Methods* 14, 149–167. doi: 10.1016/0165-0270(85)90031-7

Pellow, S., and File, S. E. (1986). Anxiolytic and anxiogenic drug effects on exploratory activity in an elevated plus-maze: a novel test of anxiety in the rat. *Pharmacol. Biochem. Behav.* 24, 525–529. doi: 10.1016/0091-3057(86)90552-6

Plenge, P., and Mellerup, E. T. (1991). [3H]Citalopram binding to brain and platelet membranes of human and rat. *J. Neurochem.* 56, 248–252. doi: 10.1111/j.1471-4159.1991.tb02588.x

Quinteros-Muñoz, D., Sáez-Briones, P., Díaz-Véliz, G., Mora-Gutiérrez, S., Rebolledo-Fuentes, M., and Cassels, B. K. (2010). Behavioral profiles in rats distinguish among "Ecstasy", methamphetamine and 2,5-dimethoxy-4-iodo-amphetamine: mixed effects for ecstasy analogues. *Behav. Neurosci.* 124, 662–676. doi: 10.1037/a0020827

Riedlinger, T. J., and Riedlinger, J. E. (1994). Psychedelic and entactogenic drugs in the treatment of depression. *J. Psychoactive Drugs* 26, 41–55. doi: 10.1080/02791072.1994.10472600

Risbrough, V. B., Masten, V. L., Caldwell, S., Paulus, M. P., Low, M. J., and Geyer, M. A. (2006). Differential contributions of dopamine D1, D2, and D3 receptors to MDMA-induced effects on locomotor behavior patterns in mice. *Neuropsychopharmacology* 3, 2348–2358. doi: 10.1038/sj.npp.1301161

Rothman, R. B., Baumann, M. H., Dersch, C. M., Romero, D. V., Rice, K. C., Carroll, F. I., et al. (2001). Amphetamine-type central nervous system stimulants release norepinephrine more potently than they release dopamine and serotonin. *Synapse* 39, 32–41. doi: 10.1002/1098-2396(20010101)39:1<32::AID-SYN5>3.0.CO;2-3

Rudnick, G., and Wall, S. C. (1992). The molecular mechanism of "ecstasy" [3,4-methylenedioxymethamphetamine (MDMA)]: serotonin transporters are targets for MDMA-induced serotonin release. *Proc. Nat. Acad. Sci. U.S.A.* 89, 1817–1821. doi: 10.1073/pnas.89.5.1817

Sáez-Briones, P., and Díaz-Véliz, G. (2012). Social interaction in rats as behavioral model for studying entactogenicity. *Rev. Farmacol. Chile* 5, 33–41.

Sáez-Briones, P., and Hernández, A. (2013). MDMA (3,4-methylenedioxymethamphetamine) analogues as tools to characterize MDMA-like effects: an approach to understand entactogen pharmacology. *Curr. Neuropharmacol.* 11, 521–534. doi: 10.2174/1570159X11311050007

Sepúlveda, S., Valenzuela, R., and Cassels, B. K. (1972). Potential psychotomimetics. New bromoalkoxyamphetamines. *J. Med. Chem.* 15, 413–415. doi: 10.1021/jm00274a022

Sessa, B. (2018). Why MDMA therapy for alcohol use disorder? And why now? *Neuropharmacology* 142, 83–88. doi: 10.1016/j.neuropharm.2017.11.004

Shulgin, A. T., and Shulgin, A. (1991). *PIHKAL – A Chemical Love Story*. Berkeley, CA: Transform Press.

Sitte, H. H., and Freissmuth, M. (2010). The reverse operation of Na+/Cl- -coupled neurotransmitter transporters – why amphetamines take two to tango. *J. Neurochem.* 112, 340–355. doi: 10.1111/j.1471-4159.2009.06474.x

Sitte, H. H., and Freissmuth, M. (2015). Amphetamine, new psychoactive drugs and the monoamine transporter cycle. *Trends Pharmacol. Sci.* 36, 41–50. doi: 10.1016/j.tips.2014.11.006

Thompson, M. R., Callaghan, P. D., Hunt, G. E., Cornish, J. L., and McGregor, I. S. (2007). A role for oxytocin and 5-HT1A receptors in the prosocial effects of 3,4 methylenedioxymethamphetamine (MDMA; "Ecstasy"). *Neuroscience* 146, 509–514. doi: 10.1016/j.neuroscience.2007.02.032

Topiol, S., Bang-Andersen, B., Sanchez, C., Plenge, P., Loland, C. J., Juhl, K., et al. (2017). X-ray structure based evaluation of analogs of citalopram: compounds with increased affinity and selectivity compared with R-citalopram for the

allosteric site (S2) on SERT. *Bioorg. Med. Chem. Lett.* 27, 470–478. doi: 10.1016/j.bmcl.2016.12.037

Tseng, Y. L., Chiang, M. L., Huang, T. F., Su, K. P., Lane, H. Y., and Lai, C. (2010). A selective serotonin reuptake inhibitor, citalopram, inhibits collagen-induced platelet aggregation and activation. *Thromb. Res.* 126, 517–523. doi: 10.1016/j.thromres.2010.09.017

Zhou, Z., Zhen, J., Karpowich, N. K., Goetz, R. M., Law, C. J., Reith, M. E., et al. (2007). LeuT-desipramine structure reveals how antidepressants block neurotransmitter reuptake. *Science* 317, 1390–1393. doi: 10.1126/science.1147614

Conflict of Interest Statement: The authors declare that the research was conducted in the absence of any commercial or financial relationships that could be construed as a potential conflict of interest.

frontiers in Pharmacology

ORIGINAL RESEARCH
published: 08 March 2019
doi: 10.3389/fphar.2019.00206

Association Study Among Candidate Genetic Polymorphisms and Chemotherapy-Related Severe Toxicity in Testicular Cancer Patients

María A. Lavanderos[1], Juan P. Cayún[1], Ángela Roco[1,2], Christopher Sandoval[1], Leslie Cerpa[1], Juan C. Rubilar[1], Roberto Cerro[1], Sebastián Molina-Mellico[1], Cesar Celedón[1], Berta Cerda[3], Elena García-Martín[4], José A. G. Agúndez[4], Cristián Acevedo[1,5], Karina Peña[6], Dante D. Cáceres[1,7], Nelson M. Varela[1] and Luis A. Quiñones[1]**

[1] Laboratory of Chemical Carcinogenesis and Pharmacogenetics, Department of Basic and Clinical Oncology, Faculty of Medicine, University of Chile, Santiago, Chile, [2] Servicio Metropolitano de Salud Occidente, Santiago, Chile, [3] Instituto Nacional del Cáncer, Santiago, Chile, [4] Institute of Molecular Pathology Biomarkers, ARADyAL, University of Extremadura, Cáceres, Spain, [5] Clinical Hospital University of Chile, Santiago, Chile, [6] Department of Oncology, Hospital San Juan de Dios, Santiago, Chile, [7] Instituto de Salud Poblacional, Facultad de Medicina, Universidad de Chile, Santiago, Chile

OPEN ACCESS

Edited by:
Jorge Fuentealba,
Universidad de Concepción, Chile

Reviewed by:
Sujit Nair,
SVKM's Narsee Monjee Institute of Management Studies, India
Nathalie K. Zgheib,
American University of Beirut, Lebanon

***Correspondence:**
Luis A. Quiñones
lquinone@med.uchile.cl
Nelson M. Varela
nvarela@med.uchile.cl

Specialty section:
This article was submitted to Translational Pharmacology, a section of the journal Frontiers in Pharmacology

Received: 28 December 2018
Accepted: 19 February 2019
Published: 08 March 2019

Citation:
Lavanderos MA, Cayún JP, Roco Á, Sandoval C, Cerpa L, Rubilar JC, Cerro R, Molina-Mellico S, Celedón C, Cerda B, García-Martín E, Agúndez JAG, Acevedo C, Peña K, Cáceres DD, Varela NM and Quiñones LA (2019) Association Study Among Candidate Genetic Polymorphisms and Chemotherapy-Related Severe Toxicity in Testicular Cancer Patients. Front. Pharmacol. 10:206. doi: 10.3389/fphar.2019.00206

Testicular cancer is one of the most commonly occurring malignant tumors in young men with fourfold higher rate of incidence and threefold higher mortality rates in Chile than the average global rates. Surgery is the initial line of treatment for testicular cancers, and is generally followed by chemotherapy, usually with combinations of bleomycin, etoposide, and cisplatin (BEP). However, the adverse effects of chemotherapy vary significantly among individuals; therefore, the present study explored the association of functionally significant allelic variations in genes related to the pharmacokinetics/pharmacodynamics of BEP and DNA repair enzymes with chemotherapy-induced toxicity in BEP-treated testicular cancer patients. We prospectively recruited 119 patients diagnosed with testicular cancer from 2010 to 2017. Genetic polymorphisms were analyzed using PCR and/or qPCR with *TaqMan*® probes. Toxicity was evaluated based on the Common Terminology Criteria for Adverse Events, v4.03. After univariate analyses to define more relevant genetic variants ($p < 0.2$) and clinical conditions in relation to severe (III–IV) adverse drug reactions (ADRs), stepwise forward multivariate logistic regression analyses were performed. As expected, the main severe ADRs associated with the non-genetic variables were hematological (neutropenia and leukopenia). Univariate statistical analyses revealed that patients with *ERCC2* rs13181 T/G and/or *CYP3A4* rs2740574 A/G genotypes are more likely to develop alopecia; patients with *ERCC2* rs238406 C/C genotype may develop leukopenia, and patients with *GSTT1*-null genotype could develop lymphocytopenia (III–IV). Patients with *ERCC2* rs1799793 A/A were at risk of developing severe anemia. The *BLMH* rs1050565 G/G genotype was found to be associated with pain, and the *GSTP1* G/G genotype was linked infection ($p < 0.05$). Multivariate analysis showed an association between specific *ERCC1/2* genotypes and

cumulative dose of BEP drugs with the appearance of severe leukopenia and/or febrile neutropenia. Grades III–IV vomiting, nausea, and alopecia could be partly explained by the presence of specific *ERCC1/2*, *MDR1*, *GSTP1,* and *BLMH* genotypes ($p < 0.05$). Hence, we provide evidence for the usefulness of pharmacogenetics as a tool for predicting severe ADRs in testicular cancer patients treated with BEP chemotherapy.

Keywords: pharmacogenetics, polymorphisms, toxicity, testicular cancer, ADRs

INTRODUCTION

Testicular cancers are malignant cancers that mainly affect young men. Cisplatin-based chemotherapy has been routinely used as the standard therapy for the treatment of metastatic testicular cancers. The standard treatment scheme for patients with low-risk testicular cancers involves three cycles of bleomycin, etoposide, and cisplatin (BEP) or four cycles of etoposide and cisplatin. Patients with intermediate-risk or high-risk disease are routinely treated with up to four cycles of BEP or four cycles of etoposide, ifosfamide, and cisplatin. Chemotherapy for rescuing the relapse of testicular cancers includes a standard dose of vinblastine, cisplatin and ifosfamide (Pizzocaro et al., 1985; Mezvrishvili and Managadze, 2006).

However, chemotherapy represents a significant challenge in the day-to-day management of the patients, since the inter-individual variations in response to the chemotherapy drugs are a major cause of concern. A drug that is well-tolerated and causes a strong response in some patients could prove to be ineffective, toxic or cause adverse drug reactions (ADRs) in others; therefore, research is required to analyze the effects of genetic variations on the pharmacokinetics and/or pharmacodynamics of these drugs. Statistics indicate that 1 in 15 hospital admissions for testicular cancer in the United Kingdom was due to ADRs (Pirmohamed et al., 2004), and adverse drug effects in hospitalized patients were identified to be the fifth leading cause of death in the United States (Mancinelli et al., 2000). Other evidence suggests that the annual number of reported cases of adverse reactions is around two millions which has been reported to cost US $100 billion (Ross et al., 2011). The antineoplastic drugs have often been shown to exhibit toxicity at therapeutic concentrations; therefore, ADRs are frequently observed during chemotherapy, which has reportedly increased the total medical costs by 1.9%, and the costs of medicines by 15% (Huang and Ratain, 2009).

Response to chemotherapy may be determined by gene polymorphisms, which eventually govern the metabolism of cytotoxic drugs. The allelic variants of genes related with pharmacokinetics/pharmacodynamics processes can alter the enzyme activity of the metabolic proteins leading to changes in drug metabolism (Agundez, 2004; Quiñones et al., 2017). Therefore, the response to chemotherapy in patients may be partly determined by gene polymorphisms involved in the metabolism of these cytotoxic drugs. Most of the chemotherapeutic drugs are metabolized by phase I polymorphic Cytochrome P450 enzymes, whose variant alleles commonly affect drug effectiveness and toxicity (Kivistö et al., 1995; Quiñones et al., 2008; Božina et al., 2009; Ingelman-Sundberg and Sim, 2010; Deenen et al., 2011). Cytochrome P450 isoforms 3A4 and 3A5 (CYP3A4/5) play a role in etoposide metabolism (Zhuo et al., 2004). The *CYP3A4*1B* rs2740574 genotype is associated with an increased risk of leukemia following treatment with etoposide and teniposide. This variant has been reported to contribute to higher risk of secondary cancers (Felix et al., 1998). Moreover, two studies have also suggested that *CYP3A4*1B* is a risk factor allele for prostate cancer (Keshava et al., 2004).

On the other hand, polymorphisms in phase II enzymes have been reported to affect the resistance and adverse reactions to several chemotherapy regimens (Jain et al., 2007; Mazerska et al., 2016; Marchewka et al., 2017). Previous reports have shown that Glutathione-*S*-transferases (GSTs) are associated with resistance to cisplatin-based chemotherapy (Roco et al., 2014; Nissar et al., 2017). *GSTM1*-null and/or *GSTT1*-null genotypes are associated with the development of grades III–IV thrombocytopenia (Cho et al., 2010) upon combined chemotherapy with rituximab and cyclophosphamide/doxorubicin/vincristine/prednisone or R-CHOP. Grade $\geq$ III toxicity and grade $\geq$ III neurotoxicity has been observed in children with medulloblastoma treated with cycles of cisplatin, cyclophosphamide, and vincristine (Barahmani et al., 2009). Besides, the *GSTP1* Ile105Val polymorphism has been strongly associated with progression-free survival. The T/T genotype of the −69 C > T *GSTA1* polymorphism correlates with overall survival. Thrombocytopenia, anemia, and neuropathy were less frequent among patients with the *GSTM1*-null or *GSTM3* intron 6 AGG/AGG genotypes (Khrunin et al., 2010). Moreover, the presence of UDP-Glucuronosyl-transferase Family 1 Member A1 (*UGT1A1*) polymorphic variants has also been associated with chemotherapy response and Gilbert Syndrome after chemotherapy (Ha et al., 2017; Negoro et al., 2018). The most studied *UGT1A1* allele is *UGT1A1*28*, which has mainly been associated with an increased risk of irinotecan toxicity (Lyer et al., 2002). In line with this evidence, the FDA recommended tests to detect the presence of *UGT1A1*28*, to predict patients at risk of irinotecan poisoning[1].

ABC-drug transporters are also implicated in the metabolic response to chemotherapy (Domenichini et al., 2019). P-glycoprotein 1 (P-gp1), also known as multidrug resistance protein 1 (MDR1) or ATP- binding cassette sub-family B member 1, is highly polymorphic and several studies have reported that carriers of the T-allele for the genetic variation *C3435T* (rs1045642) have an increased risk of colon, breast, and renal cancer (Phuthong et al., 2017). However, Cizmarikova et al. (2010), found no significant differences in hematological

[1]https://www.fda.gov/drugs/scienceresearch/ucm572698.htm

toxicities in the groups with the *MDR1 C3435T* polymorphism in breast cancer.

On the other hand, bleomycin (BLM) is metabolically inactivated by the action of cysteine peptidase bleomycin hydrolase (BLMH) (Schwartz et al., 1999; Deenen et al., 2011). de Haas et al. (2008), showed that *BLMH* A/G genotype was related with reduced survival and higher prevalence of early relapses in testicular cancer patients. Recently, Jóna et al. (2016), showed lower rate of pulmonary complications in the A/A genotype group than those in the group containing the mutated allele: A/G+G/G in ABVD (doxorubicin, bleomycin, vinblastine, and dacarbazine)-treated Hodgkin lymphoma patients.

Several antineoplastic drugs have been reported to cause DNA damage. Numerous studies have investigated the association between single nucleotide polymorphisms (SNPs) in DNA repair enzymes, clinical outcomes, and resistance to chemotherapy (Zamble and Lippard, 1995; Gossage and Madhusudan, 2007; Frosina, 2009; Zhang et al., 2017) indicating that reduced activity of DNA repair enzymes may lead to an improved response to chemotherapy. However, compromised repair may also lead to accumulation of DNA damage in normal cells, leading to adverse side effects in normal tissues, thereby predisposing them toward secondary cancers. Due to these side effects, commonly used chemotherapeutic agents, including alkylating agents (cisplatin), inhibitors of DNA topoisomerase II (etoposide), and BLM have proven to be toxic to the patients.

Excision repair cross-complementary 1 (ERCC1) is a key protein involved in nucleotide excision repair (NER), and ERCC1-Xeroderma pigmentosum (ERCC1-XPF) catalyzes the incision on the site of DNA damage (Park et al., 1995). Elevated ERCC1 expression in cancers is associated with resistance to DNA damage-based chemotherapy (Chiu et al., 2011; Tsai et al., 2011). On the other hand, Xeroderma pigmentosum complementary group D (*XPD/ERCC2*) encodes a helicase which participates in both NER and basal transcription as part of the transcription factor IIH. Mutations abolishing the enzymatic function of the ERCC2 protein are manifested clinically in combinations of three severe syndromes, including Xeroderma pigmentosum (Lehmann, 2001; Clarkson and Wood, 2005). Polymorphisms in these enzymes further affect DNA repair and are involved in resistance to chemotherapy, survival, and cancer manifestation (Benhamou and Sarasin, 2002; Giovannetti et al., 2011).

Based on the accumulated scientific evidence about BEP chemotherapy, we here focused on functionally significant gene polymorphisms in proteins that control metabolism, uptake, and response to BEP drugs ([2]Roco et al., 2014; Chen et al., 2017). Mainly, the allelic variants of *CYP3A4* rs2740574 *(*1B)*, *CYP3A4* rs35599367 *(*22)*, *CYP3A5* rs776746 *(*3)*, *GSTM1*-null, *GSTP1* rs1695, *GSTT1*- null, *UGT1A1* rs8175347 *(*28)*, *BLMH* rs1050565, *ERCC1* rs11615, *ERCC1* rs3212986, *ERCC2* rs13181, *ERCC2* rs1799793, *ERCC2* rs238406, and *MDR1* rs1045642 were analyzed with non-genetic factors to validate their association with ADRs in testicular cancer patients treated with BEP schedule.

[2]https://www.pharmgkb.org/pathway/PA2025

MATERIALS AND METHODS

Patients

One hundred nineteen (119) patients with germinal (seminoma or non-seminoma) testicular cancer confirmed histologically, >18 years old, without chronic unbalanced or systemic pathology or other active cancers and without being included in the interventional study conducted 3 months before, were enrolled prospectively in this study. The enrollment was carried out from December 2010 – December 2017 at the Polyclinic of Hematology-oncology of Hospital San Juan de Dios, and the Polyclinic of Oncology of the National institute of Cancer. All the patients signed a written consent and an agreement to be included in this study. The study was carried out under strict ethical procedures recommended by the Ethics Committee of the University of Chile (August 17, 2010), and the Northern Metropolitan Health Service, National Cancer Institute (April 4, 2015), in accordance with the procedures suggested in the Declaration of Helsinki (Declaration of Helsinki, 1964), and according to Chilean Laws 20.120, 20.584, and 19.628, and the guidelines of the Good Clinical Practices. Chemotherapy regimen for all patients involved the administration of cisplatin and etoposide in combination with bleomycin for up to four cycles (BEP schedule), which is the standard treatment for patients with low or intermediate risk testicular cancers, all over the world (Pizzocaro et al., 1985; Mezvrishvili and Managadze, 2006).

This regimen was applied in conjunction with a rigorous and standardized hydration regimen for all the patients. The clinical variables were obtained from patients' clinical files and recorded in proper case report forms (CRFs). Laboratory assessment was performed after each cycle of chemotherapy. Treatment-related toxicity was graded according to the terminological common criteria for adverse reactions (v4.03), of the U.S. Department of Health and Human Services with a follow-up after 6 months of the last cycle of chemotherapy. The association study included age, height, weight, body surface area, and cumulative doses for the statistical analyses. **Table 1** shows the general characteristics of the studied patients.

Genotyping Analysis

Potentially functional SNPs encoding the proteins related to BEP response were obtained from the NCBI dbSNP database[3], and the SNPinfo Web Server[4] based on the level of evidence for each SNP (**Supplementary Table S1**). Genomic DNA was isolated from the peripheral blood samples of the subjects using High Pure PCR Template Preparation Kit (Catalog Number, 11796828001; Roche Diagnostics GmbH, Mannheim, Germany). *CYP3A4*1B* rs2740574, *CYP3A4*22* rs35599367, *CYP3A5*3* rs776746, *UGT1A1*28* rs8175347, *BLMH* rs1050565, *GSTP1* rs1695, *ERCC1* rs11615, *ERCC1* rs321986, *ERCC2* rs13181, *ERCC2* rs238406, *ERCC2* rs1799793, and *MDR1* rs1045642 were analyzed using *TaqMan*® SNP Genotyping Assay (Catalog number, 4362691; Thermo Fisher Scientific, Waltham, MA, United States), in an Stratagene Mx3000p real-time PCR system

[3]https://www.ncbi.nlm.nih.gov/snp

[4]https://snpinfo.niehs.nih.gov

TABLE 1 | Baseline characteristics of patients.

	n = 119	%
Age, years		
Average ± SD (range)	28.05 ± 8.29 (16–56)	
Median	27	
BSA, m^2		
Average ± SD (range)	1.89 ± 0.19 (1.5–2.8)	
Median	1.86	
Histologic type		
Seminoma	16	13.45
No seminoma	103	86.55
Number of cycles		
2 cycles	31	26.05
3 cycles	49	41.18
4 cycles	38	31.93
5 cycles	1	0.84
Cisplatin dose per cycle day		
Mg per BSA	100	
Etoposide dose per cycle day		
Mg per BSA	120	
Bleomycin dose per cycle day		
UI	30	

BSA, body surface area; SD, standard deviation.

(Agilent Technologies, Santa Clara, CA, United States). The presence of the *GSTM1*-null genotype was determined by the absence of a 273 bp fragment product in a 2% agarose gel (Bio-Rad Laboratories, Hercules, CA, United States). The presence of the *GSTT1*-null genotype was determined by the absence of a 268 bp fragment. Amplification fragment for β-globin was used as the internal control (Quiñones et al., 1999; Roco et al., 2012). Heterozygous and homozygous non-null individuals could not be differentiated, therefore double null genotypes (−/−) are the null genotypes reported. For Quality Assurance purposes we randomly choose 20% of the samples for (a) repetition of the analysis and (b) PCR-RFLP analysis for coincidence. When analyses were not coincident we excluded the samples. The sequences for *TaqMan*® probes and primers for PCR are listed in **Supplementary Tables S2**, **S3** enlists the description of each polymorphism.

Statistical Analyses

We performed a logistic regression analysis using Stata software, version 12.0 (Copyright 1985–2011 StataCorp., LP, College Station, TX, United States). A p-value of ≤ 0.05 was considered statistically significant. The odds ratio (OR) and 95% confidence intervals (CI) were reported in the univariate and multivariate logistic regression models. The logistic multivariate models were adjusted stepwise using a forward procedure with p-value ≤ 0.2 to include potentially relevant variables in order to derive statistical association models, characterized by Pseudo R^2. All association studies were assayed by testing three genetic models of inheritance, i.e., dominant, codominant and recessive models, and choosing parameters with better statistical association for each analysis.

For the univariate and multivariate analyses, we define several alternatives for dosage: *Ranges for dose*: to get the ranges we used quartiles (Q) to divide data in four groups, with lower range comprising Q_0 to the average between Q_1 and Q_2, intermediate range comprising of the average between Q_1 and Q_2 to the average between Q_2 and Q_3 and the largest range comprising of the average between Q_2 and Q_3 to Q_4. *Cumulative dose* was defined as the total dose administered to the patient during all the cycles of chemotherapy. *Cumulative dose by average*: the patients were divided in two groups according to their were lower/equal in relation the average cumulative dose ($\leq$average) or higher than the average cumulative dose (>average). Similar procedure was performed for weight, height, body surface and age and for chemotherapy cycles with frequency of 1–2, 3 and 4–5 cycles, getting dummy variables for the statistical analyses.

We did not check Hardy–Weinberg equilibrium (HWE) of our sample because it does not accomplish the conditions for HWE. This is not a random sampling in a random-mating population, a control or general population (Namipashaki et al., 2015) and is a group with a selection bias by the disease (i.e., SNPs can also be related to the cancer).

RESULTS

Patient Characteristics

The baseline characteristics of patients are shown in **Table 1**. A total of 119 Chilean patients from two hospitals in Chile were included and analyzed. Most patients were young (average age: 28.05 years), and were administered 2–5 cycles of BEP and predominantly showed no seminoma (86.55%). The genotypic and allelic frequencies for the analyzed polymorphisms are shown in **Supplementary Table S4**.

Toxicity to Chemotherapy

Adverse drug reactions represented in **Table 2** were recorded to determine the acute toxicity in patients with testicular cancer treated with BEP chemotherapy. The ADRs are shown in two columns, any grades (I–IV) column and severe or high-grade toxicities (III–IV) column. The most frequent toxicities observed included vomiting (82.35%), nausea (79.83%), anemia (60.68%), neutropenia (53.45%), and alopecia (52.94%). Most frequently observed high-grade toxicities included neutropenia (39.66%), leukopenia (12.71%), febrile neutropenia (12.61%), and vomiting (9.24%).

Association Between Genotypes and Toxicities

We performed univariate logistic regression of risk for severe (III–IV) ADRs in association with genotypes, in three models of inheritance namely, recessive, codominant, and dominant. The results are shown in **Supplementary Table S5** where only results with p-value ≤ 0.2 are included for the stepwise forward procedure for multivariate analysis. In **Table 3**, only statistically significant results for the univariate logistic regression analysis of risk of severe ADRs (III–IV), according to genotypes

TABLE 2 | Adverse drug reactions (ADRs) according degree of severity*.

	Any grades (I–IV)		Severe (grades III–IV)	
	No.	**%**	**No.**	**%**
Toxicity				
Vomiting	98	82.35	11	9.24
Nausea	95	79.83	8	6.72
Anemia	71	60.68	3	2.56
Neutropenia	62	53.45	46	39.66
Alopecia	63	52.94	5	4.20
Leukopenia	49	41.53	15	12.71
Pain	44	36.97	5	4.20
Mucositis	26	21.85	1	0.84
Diarrhea	24	20.17	0	0.00
Dermatological reaction	23	19.33	1	0.84
Thrombocytopenia	21	17.95	2	1.71
Hypotension	19	15.97	0	0.00
Lymphocytopenia	13	11.21	3	2.59
Neurotoxicity	10	8.40	2	1.68
Constipation	8	6.72	0	0.00
Pyrosis	5	4.20	0	0.00
Ototoxicity	4	3.36	0	0.00
Febrile Neutropenia	–	–	15	12.61

**ADR, adverse drug reaction, evaluated with Common Terminology Criteria for Adverse Events [CTCAE], 2017.*

are shown. These results show that *ERCC2* rs1799793 A/A genotype was associated with anemia in a recessive model of inheritance, *ERCC2* rs13181 T/G and *CYP3A4* rs2740574 A/G genotypes were associated with alopecia in a codominant model of inheritance, and *ERCC2* rs238406 A/A genotype was associated with leukopenia, both in codominant and recessive models of inheritance. *GSTT1*-null genotype was associated with lymphocytopenia, *BLMH* rs1050565 G/G genotype was linked with pain in a recessive model of inheritance and *GSTP1* rs1695 G/G genotype was associated with infections in a recessive model of inheritance.

The same analysis was performed for non-genetic factors (e.g., age, sex, weight, height, body surface, cycles, and cumulative dose) (**Supplementary Table S6**). **Table 4** shows only the statistically significant results obtained from the univariate logistic regression analysis of risk of severe ADRs (III–IV), analyzed according to non-genetic factors. We observed that the cumulative dose of bleomycin; bleomycin dose by average or bleomycin cycles by range were associate with febrile neutropenia as well as cisplatin dose by range. Similarly, cumulative total etoposide dose or dose by average were associated with leukopenia as well as the cumulative dose of cisplatin. Besides, neutropenia was associated with both, cumulative or cumulative by average dose of cisplatin or etoposide, and cumulative bleomycin. Finally, alopecia was significantly associated only with cumulative and cumulative by average dose of bleomycin.

After stepwise forward procedure, using associations with a $p \leq 0.2$, multivariate logistic regression analyses for the risk of severe ADRs, including genetic and non-genetic factors, were performed. **Table 5** show only statistically significant association models for severe ADRs. We obtained significant models for febrile neutropenia, leukopenia, vomiting, nausea, and alopecia.

TABLE 3 | Univariate logistic regression analysis of risk of severe ADRs (III–IV) according to genotypes.

ADR*	*n*	OR**	95% IC***	*p*-value****
Anemia				
ERCC2 (rs1799793)				
G/G + G/A	110	1.00		Reference
A/A	3	27.00	1.68–434.44	0.020
Leukopenia				
ERCC2 (rs238406)				
C/C	58	1.00		Reference
C/A	29	3.82	0.84–17.28	0.082
A/A	26	5.50	1.26–24.10	0.024
ERCC2 (rs238406)				
C/C	58	1.00		Reference
C/A + A/A	55	4.58	1.20–17.45	0.026
Lymphocytopenia				
GSTT1				
No null	108	1.00		Reference
Null	4	17.67	1.23–252.73	0.034
Alopecia				
CYP3A4*1B (rs2740574)				
A/A	106	1.00		Reference
A/G	12	6.87	1.02–46.06	0.047
G/G	1	–		
ERCC2 (rs13181)				
T/T	77	1.00		Reference
T/G	32	10.86	1.16–101.35	0.036
G/G	6	–		
Pain				
BLMH (rs1050565)				
A/A + A/G	93	1.00		Reference
G/G	26	16.73	1.78–157.15	0.014
Infections				
GSTP1 (rs1695)				
A/A + A/G	99	1.00		Reference
G/G	18	12.25	1.05–143.09	0.046

**ADR, adverse drug reaction, evaluated with CTCAE4.03.*
***OR, odds ratio.*
****95% CI, 95% confidence interval.*
*****Only statistical significant associations are shown ($p \leq 0.05$).*

DISCUSSION

Patient response to chemotherapy has been investigated for long, and ADR after chemotherapy is a substantial clinical problem. For testicular cancers, this is particularly relevant since besides surgery (inguinal orchiectomy) chemotherapy is routinely administered with combination of three cytostatic drugs, bleomycin, etoposide, and cisplatin. Even though chemotherapy is quite successful in the treatment for patients with seminoma and the success rates exceed 90%, adverse reactions are frequently

TABLE 4 | Univariate logistic regression analysis of risk of severe ADRs (III–IV) according to non-genetic factors.

ADR*	*n*	OR**	95% IC***	*p*-value****
Febrile neutropenia				
Bleomycin cumulative dose	117	1.01	1.00–1.02	0.014
Bleomycin cumulative dose by average				
≤Average	81	1.00		Reference
>Average	36	3.02	1.00–9.11	0.050
Chemotherapy cycles				
1–2	31	1.00		Reference
3	49	3.41	0.38–30.66	0.274
4–5	39	9.00	1.07–75.51	0.043
Leukopenia				
Cisplatin cumulative dose	116	1.00	1.00–1.01	0.017
Etoposide cumulative dose	116	1.00	1.00–1.00	0.006
Etoposide cumulative dose by average				
≤Average	62	1.00		Reference
>Average	54	5.62	1.49–21.15	0.011
Neutropenia				
Cisplatin cumulative dose	114	1.00	1.00–1.00	0.037
Etoposide cumulative dose	114	1.00	1.00–1.00	0.041
Cisplatin cumulative dose by average				
≤Average	58	1.00		Reference
>Average	56	2.82	1.29–6.14	0.009
Etoposide cumulative dose by average				
≤Average	60	1.00		Reference
>Average	54	2.72	1.26–5.91	0.011
Alopecia				
Bleomycin cumulative dose	117	1.02	1.00–1.03	0.046
Bleomycin cumulative dose by average				
≤Average	81	1.00		Reference
>Average	36	10.00	1.08–92.94	0.043

ADR, adverse drug reaction, evaluated with CTCAE4.03.
***OR, odds ratio.*
****95% CI, 95% confidence interval.*
*****Only statistical significant associations are shown ($p \leq 0.05$).*

TABLE 5 | Multivariate logistic regression analysis and risk of severe ADRs (grades III–IV), after stepwise forward procedure (cut-off $p < 0.2$).

ADR*	OR**	95% IC***	*p*-value****	Model data
Febrile neutropenia				
ERCC1 (rs11615)				Number of obs: 106 *p*-value: 0.0231 Pseudo R^2: 0.0956
C/C + C/T	1.00		Reference	
T/T	4.89	1.06–22.56	0.042	
Bleomycin cumulative dose	1.01	1.00–1.02	0.028	
Leukopenia				
ERCC2 (rs238406)				Number of obs: 111 *p*-value: 0.0031 Pseudo R^2: 0.1372
C/C	1.00		Reference	
C/A + A/A	4.09	1.04–15.99	0.043	
Etoposide cumulative dose by average				
≤Average	1.00		Reference	
>Average	4.48	1.15–17.48	0.031	
Vomiting				
MDR1 (rs1045642)				Number of obs: 111 *p*-value: 0.0121 Pseudo R^2: 0.1231
CC + CT	1.00		Reference	
TT	4.90	11.14–21.09	0.033	
ERCC1 (rs 3212986)				
C/C	1.00		Reference	
C/A + A/A	0.20	0.04–0.85	0.030	
Nausea				
GSTP1 (rs1695)				Number of obs: 115 *p*-value: 0.0344 Pseudo R^2: 0.1278
A/A + A/G	1.00		Reference	
G/G	5.43	1.04–28.42	0.045	
Cisplatin cumulative dose	1.00	1.00–1.01	0.047	
Alopecia				
BLMH (rs 1050565)				Number of obs: 115 *p*-value: 0.0124 Pseudo R^2: 0.2135
A/A + A/G	1.00		Reference	
G/G	6.95	1.00–48.23	0.050	
ERCC2 (rs13181)				
T/T	1.00		Reference	
T/G + G/G	10.57	1.07–104.02	0.043	

ADR, adverse drug reaction, evaluated with CTCAE4.03.
***OR, odds ratio.*
****95% CI, 95% confidence interval.*
*****Only statistical significant association models are shown ($p \leq 0.05$).*
Resulting significant equations:

$$Febr.Neutropenia = \frac{p}{1-p} = e^{-5.97+1.59[ERCC1\ rs11615\ C>T]+0.012[BLM\ C.\ DOSE]}$$

$$Leukopenia = \frac{p}{1-p} = e^{-3.74+1.41[ERCC2\ rs238406\ C>A]+1.50[ETOP\ C.\ DOSE\ BY\ AV]}$$

$$Vomiting = \frac{p}{1-p} = e^{-1.88+1.59[MDR1\ rs1045642\ C>T]-1.61[ERCC1\ rs3212986C>A]}$$

$$Nausea = \frac{p}{1-p} = e^{5.01+1.69[GSTP1\ rs1695A>G]+0.003[CISP\ C.\ DOSE]}$$

$$Alopecia = \frac{p}{1-p} = e^{-5.19+1.94[BLMH\ rs1050565\ A>G]+2.36[ERCC2\ rs13181T>G]}.$$

observed in response to one of the drugs or the drug combination. Therefore, in the present study, we have evaluated the role of genetic polymorphisms and other non-genetic factors as potential modifying risk factors for ADRs.

In the univariate analyses (**Table 3**), we found interesting association between *BLMH* rs1050565 G/G genotype and severe pain in patients (OR = 16.73, CI = 1.78–157.15, *p*-value = 0.014). Our observation is in line with the report from White and coworkers who showed an association between acute chest pain and bleomycin infusion (White et al., 1987). Considering that G allele of *BLMH* leads to the incorporation of 443Val in the enzyme, reducing its biochemical activity, this association supports our finding and high bleomycin plasma levels in patients can be expected.

On the other hand, patients with *CYP3A4* rs2740574 A/G genotypes are more likely to develop alopecia (OR = 6.87, CI = 1.02–46.06, *p*-value = 0.047). This gene encodes for the main enzyme involved in etoposide metabolism[2], and metabolizes cisplatin or bleomycin. The presence of G allele leads to reduced transcription of the enzyme, suggesting a relationship between dose and increased plasma levels of etoposide and alopecia.

Cisplatin mainly reacts with N-7 of guanine and adenine to form adducts with the DNA (Kelland, 2007) resulting in the formation of intra and inter strands crosslinks, causing potential errors in DNA repair, resulting in accumulation of damaged DNA, and activation of apoptotic pathway in neoplastic and normal cells. Therefore, it was important to analyze both, the drug-metabolizing enzymes (GSTs) and the DNA damage repair proteins. We observed that *GSTT1*-null genotype is associated with lymphocytopenia (OR = 17.67, CI = 1.23–252.73, *p*-value = 0.034) and *GSTP1* rs1695 G/G genotype is associated with increased infections (OR = 12.25, CI = 1.05–143.09, *p*-value = 0.046). Similarly, *ERCC2* rs1799793 A/A genotype showed association with anemia (OR = 27.00, CI = 1.68–434.44, *p*-value = 0.020), *ERCC2* rs238406 A/A genotype was associated with leukopenia (OR = 5.5, CI = 1.26–24.10, *p*-value = 0.024) and *ERCC2* rs13181 T/G genotype was linked with alopecia (OR = 10.86, CI = 1.16–101.35, *p*-value = 0.036), indicating that defects in the metabolism and/or the response to cisplatin could lead to the specific severe ADRs (**Table 3**). This is in agreement with studies that report that G allele of *GSTP1* rs1695 has been associated with an increased risk of myelosuppression, polyneuropathy, and toxicity (Joerger et al., 2012). Conversely, it has been found that the genotype *GSTP1* A/A is predicted to show a suboptimal response to chemotherapy with fluorouracil/cisplatin, and a lower survival rate in patients with advanced gastric cancer (Ruzzo et al., 2006). Studies on *GSTM1* and *GSTT1* have shown that high expression levels of both enzymes result in a low response to chemotherapy, and deletion of these genes shows high degrees of toxicity (Bai et al., 1996; Ambrosone et al., 2001). In ovarian cancer patients, severe emesis grades III–IV were associated with *GSTT1*-null genotype (Khrunin et al., 2010). In contrast, in patients with *GSTM1*-null genotype the risk of thrombocytopenia and anemia was lower (Khrunin et al., 2010). For *GSTP1*, the G/G genotype seems to decrease the susceptibility to grade III neuropathy when compared to that in patients with A/G and/or A/A genotypes (recessive model of inheritance) in ovarian cancer (Khrunin et al., 2010). In this study, however, we did not find an association of these polymorphic enzymes with the above-mentioned adverse

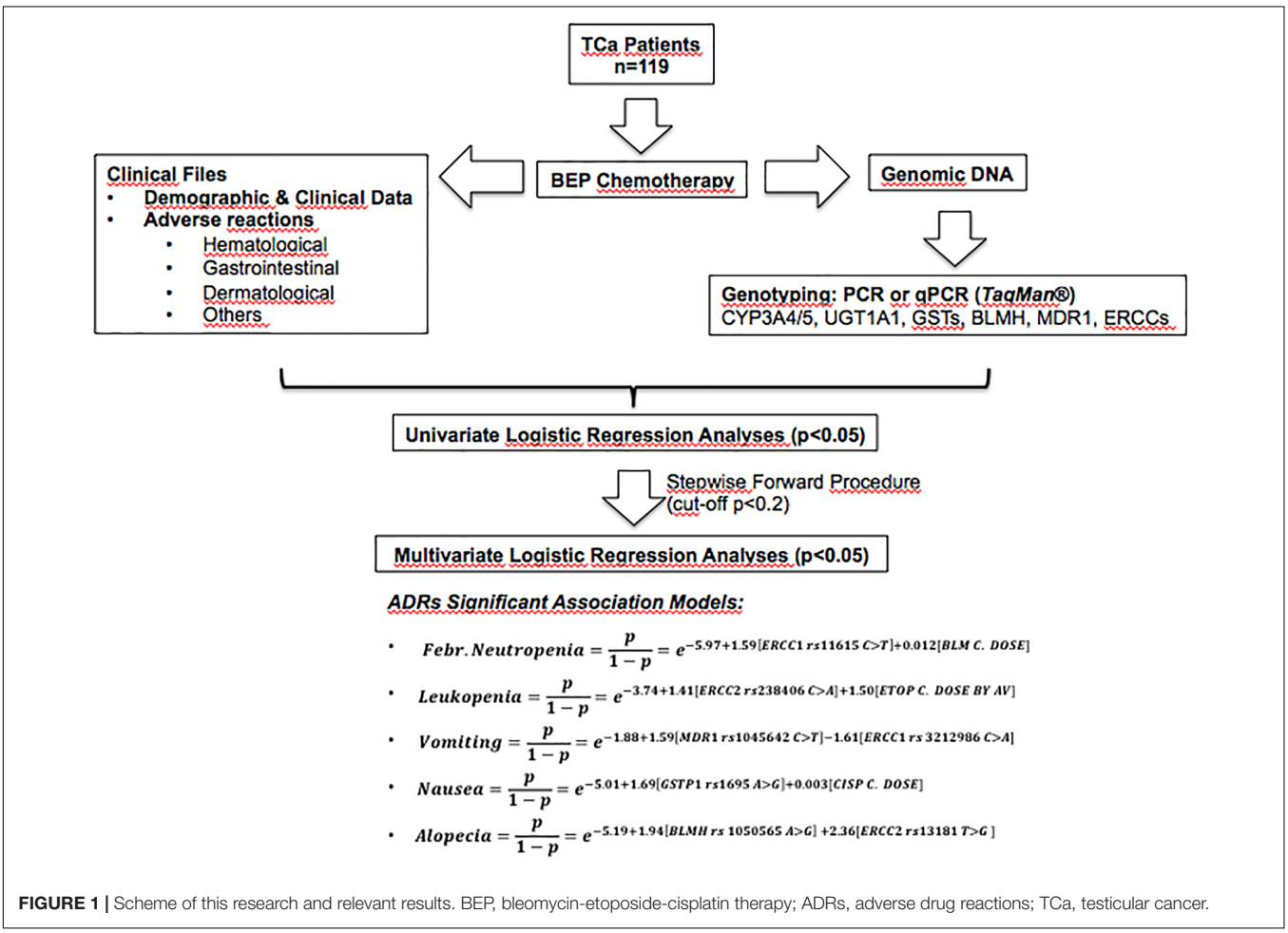

FIGURE 1 | Scheme of this research and relevant results. BEP, bleomycin-etoposide-cisplatin therapy; ADRs, adverse drug reactions; TCa, testicular cancer.

reactions. However, the effect of GST in hematological toxicity is reasonable, since GSTs are responsible for etoposide breakdown and elimination[2].

The analysis of univariate associations among severe ADRs and non-genetic factors (**Table 4**) showed an association between cumulative dose of bleomycin, bleomycin dose by average and bleomycin cycles by range; and that these parameters are associated with febrile neutropenia, as well as cisplatin dose by range. Similarly, cumulative dose of etoposide (total or by average) is associated with leukopenia as well as the cumulative dose of cisplatin. Besides, neutropenia is associated with both, cumulative or cumulative by average dose of cisplatin or etoposide. These results are consistent with the studies that report the relationship between hematological ADRs and BEP drugs, particularly etoposide and cisplatin[5][6]. Moreover, alopecia was significantly associated only with dose of bleomycin (cumulative and by average).

Multivariate analyses to obtain risk association models of severe ADRs, including polymorphisms and non-genetic variables (**Table 5**) yielded good models to partly explain febrile neutropenia (Pseudo R^2: 0.0956), leukopenia (Pseudo R^2: 0.1372), vomiting (Pseudo R^2: 0.1231), nausea (Pseudo R^2: 0.1278), and alopecia (Pseudo R^2: 0.2135). Interestingly, in these models, only dosage but not the demographic variables were relevant for severe ADRs.

For better understanding **Figure 1** shows a scheme of this research and relevant results. After recruitment, genotyping and data collection from patients, genetic and non-genetic factors were submitted to logistic univariate statistical analyses. Then, logistic multivariate models were adjusted using a stepwise forward procedure with a cut-off p-value ≤ 0.2. The multivariate models are described by pseudo R^2 values and equations for the obtained significant ADRs association models (febrile neutropenia, leukopenia, vomiting, nausea, and alopecia).

Despite our analysis, the study has some shortcomings. Although we had a relatively appropriate sample size for combinatorial analyses, fewer number of patients examined could mask potential associations, especially for low frequency polymorphisms, particularly in the multivariate analyses. Some other potentially candidate genes/polymorphisms were not evaluated in this study (based in level of evidence), which could be still relevant. Besides, the cumulative doses were obtained at the end of the therapy, which could limit our conclusions about this factor in relation to ADRs. We were not able to analyze additional potential toxicities such as hepatotoxicity and nephrotoxicity due to incomplete clinical data. These, and others missing clinical values, could be relevant, giving rise to a possible differential misclassification bias affecting estimated associations between potentially relevant combinations of risk factors and adverse reactions. Finally, we did not adjust p-values for multiple tests (Bonferroni's adjustment), which could generate direct implications in α and the p-value. However, it has been proposed that the adjustment is not always recommended, especially when high number of comparison are performed and multiple false negatives need to be avoided, which is the case (Goldman, 2008; Kim and Bang, 2016).

[5]http://chemocare.com/chemotherapy/drug-info/etoposide.aspx

[6]http://chemocare.com/chemotherapy/drug-info/cisplatin.aspx

CONCLUSION

Our findings from the univariate analyses suggest that patients with *ERCC2* rs13181 T/G and/or *CYP3A4* rs2740574 A/G genotypes are more likely to develop grades III–IV alopecia; patients with *ERCC2* rs238406 C/C genotype may develop severe leukopenia; and patients with *GSTT1*-null genotype could develop lymphocytopenia. Patients with *ERCC2* rs1799793 A/A genotype were at higher risk of developing anemia. Patients with *BLMH* rs1050565 G/G genotype experienced severe pain, and patients with *GSTP1* G/G genotype were susceptible to severe infections. As expected, severe ADRs associated with non-genetic variables were hematological (neutropenia and leukopenia). The multivariate analyses showed an association between specific *ERCC1/2* genotypes and cumulative dose of BEP drugs with the appearance of severe leukopenia and/or febrile neutropenia. Grades III–IV vomiting, nausea and alopecia could also be partly explained by the presence of specific *ERCC1*/2, *MDR1*, *GSTP1*, and *BLMH* genotypes. Our study provides additional evidence for the use of pharmacogenetics as a useful tool for potential prediction of severe ADRs in testicular patients treated with BEP chemotherapy.

AUTHOR CONTRIBUTIONS

ML, JC, and NV: experimental analyses, analysis of data, and writing the manuscript. AR: experimental analyses and writing the manuscript. CS, LC, JR, RC, SM-M, and CC: experimental analyses. BC and KP: enrolment of patients. EG-M and JA: conception of the research. CA: analysis of data and enrolment of patients. DC: analysis of data. LQ: conception of the research, analysis of data, and writing the manuscript.

FUNDING

This work was supported by grant FONDECYT #1140434.

ACKNOWLEDGMENTS

The authors wish to thank the testicular cancer patients from the "Instituto Nacional del Cáncer" and "San Juan de Dios" hospital for their altruistic collaboration in pursuit of the common welfare. They also thank the Latin American Society of Pharmacogenomics and Personalized Medicine (SOLFAGEM) by sponsoring this article.

SUPPLEMENTARY MATERIAL

The Supplementary Material for this article can be found online at: https://www.frontiersin.org/articles/10.3389/fphar.2019.00206/full#supplementary-material

REFERENCES

Agundez, J. A. G. (2004). Cytochrome P450 gene polymorphism and cancer. *Curr. Drug Metab.* 5, 211–224. doi: 10.2174/1389200043335621

Ambrosone, C. B., Sweeney, C., Coles, B. F., Thompson, P. A., McClure, G. Y., Korourian, S., et al. (2001). Polymorphisms in glutathione S-transferases (GSTM1 and GSTT1) and survival after treatment for breast cancer. *Cancer Res.* 61, 7130–7135.

Bai, F., Nakanishi, Y., Kawasaki, M., Takayama, K., Yatsunami, J., Pei, X. H., et al. (1996). Immunohistochemical expression of glutathione S-transferase-Pi can predict chemotherapy response in patients with nonsmall cell lung carcinoma. *Cancer* 78, 416–421. doi: 10.1002/(SICI)1097-0142(19960801)78:3<416::AID-CNCR6>3.0.CO;2-H

Barahmani, N., Carpentieri, S., Li, X. N., Wang, T., Cao, Y., Howe, L., et al. (2009). Glutathione S-transferase M1 and T1 polymorphisms may predict adverse effects after therapy in children with medulloblastoma. *Neuro Oncol.* 11, 292–300. doi: 10.1215/15228517-2008-089

Benhamou, S., and Sarasin, A. (2002). ERCC2/XPD gene polymorphisms and cancer risk. *Mutagenesis* 17, 463–469. doi: 10.1093/mutage/17.6.463

Božina, N., Bradamante, V., and Lovrić, M. (2009). Genetic polymorphism of metabolic enzymes P450 (CYP) as a susceptibility factor for drug response, toxicity, and cancer risk. *Arh. Hig. Rada Toksikol.* 60, 217–242. doi: 10.2478/10004-1254-60-2009-1885

Chen, Y., Zhang, H., and He, Q. (2017). Involvement of bleomycin hydrolase and poly(ADP-ribose) polymerase-1 in Ubc9-mediated resistance to chemotherapy agents. *Int. J. Oncol.* 50, 223–231. doi: 10.3892/ijo.2016.3777

Chiu, T. J., Chen, C. H., Chien, C. Y., Li, S. H., Tsai, H. T., and Chen, Y. J. (2011). High ERCC1 expression predicts cisplatin-based chemotherapy resistance and poor outcome in unresectable squamous cell carcinoma of head and neck in a betel-chewing area. *J. Transl. Med.* 9:31. doi: 10.1186/1479-5876-9-31

Cho, H. J., Eom, H. S., Kim, H. J., Kim, I. S., Lee, G. W., and Kong, S. Y. (2010). Glutathione-S-transferase genotypes influence the risk of chemotherapy-related toxicities and prognosis in Korean patients with diffuse large B-cell lymphoma. *Cancer Genet. Cytogenet.* 198, 40–46. doi: 10.1016/j.cancergencyto.2009.12.004

Cizmarikova, M., Wagnerova, M., Schonova, L., Habalova, V., Kohut, A., Linkova, A., et al. (2010). MDR1 (C3435T) polymorphism: relation to the risk of breast cancer and therapeutic outcome. *Pharmacogenomics J.* 10, 62–69. doi: 10.1038/tpj.2009.41

Clarkson, S. G., and Wood, R. D. (2005). Polymorphisms in the human XPD (ERCC2) gene, DNA repair capacity and cancer susceptibility: an appraisal. *DNA Repair* 4, 1068–1074. doi: 10.1016/j.dnarep.2005.07.001

Common Terminology Criteria for Adverse Events [CTCAE] (2017). *Cancer Therapy Evaluation Program, Common Terminology Criteria for Adverse Events, Version 3.0, DCTD, NCI, NIH, DHHS March 31, 2003*. Available at: http://ctep.cancer.gov

de Haas, E. C., Zwart, N., Meijer, C., Nuver, J., Boezen, H. M., Suurmeijer, A. J., et al. (2008). Variation in bleomycin hydrolase gene is associated with reduced survival after chemotherapy for testicular germ cell cancer. *J. Clin. Oncol.* 26, 1817–1823. doi: 10.1200/JCO.2007.14.1606

Deenen, M. J., Cats, A., Beijnen, J. H., and Schellens, J. H. (2011). Part 2: pharmacogenetic variability in drug transport and phase I anticancer drug metabolism. *Oncologist* 16, 820–834. doi: 10.1634/theoncologist.2010-0259

Domenichini, A., Adamska, A., and Falasca, M. (2019). ABC transporters as cancer drivers: potential functions in cancer development. *Biochim. Biophys. Acta. Gen. Subj.* 1863, 52–60. doi: 10.1016/j.bbagen.2018.09.019

Felix, C., Walker, A., Lange, B., Williams, T., Winicki, N., Cheung, N., et al. (1998). Association of CYP3A4 genotype with treatment-related leukemia. *Proc. Natl. Acad. Sci.* 95, 13176–13181. doi: 10.1073/pnas.95.22.13176

Frosina, G. (2009). DNA repair in normal and cancer stem cells, with special reference to the central nervous system. *Curr. Med. Chem.* 16, 854–866. doi: 10.2174/092986709787549253

Giovannetti, E., Pacetti, P., Reni, M., Leon, L. G., Mambrini, A., Vasile, E., et al. (2011). Association between DNA-repair polymorphisms and survival in pancreatic cancer patients treated with combination chemotherapy. *Pharmacogenomics* 12, 1641–1652. doi: 10.2217/pgs.11.109

Goldman, M. (2008). *Why is Multiple Testing a Problem?* Available at: https://www.stat.berkeley.edu/~mgoldman/Section0402.pdf

Gossage, L., and Madhusudan, S. (2007). Cancer pharmacogenomics: role of DNA repair genetic polymorphisms in individualizing cancer therapy. *Mol. Diagn. Ther.* 11, 361–380. doi: 10.1007/BF03256260

Ha, V. H., Jupp, J., and Tsang, R. Y. (2017). Oncology drug dosing in gilbert syndrome associated with UGT1A1: a summary of the literature. *Pharmacotherapy* 37, 956–972. doi: 10.1002/phar.1946

Huang, R. S., and Ratain, M. J. (2009). Pharmacogenetics and pharmacogenomics of anticancer agents. *Cancer J. Clin.* 59, 42–55. doi: 10.3322/caac.20002

Ingelman-Sundberg, M., and Sim, S. C. (2010). Pharmacogenetic biomarkers as tools for improved drug therapy; emphasis on the cytochrome P450 system. *Biochem. Biophys. Res. Commun.* 396, 90–94. doi: 10.1016/j.bbrc.2010.02.162

Jain, A. K., Jain, S., and Rana, A. C. (2007). Metabolic enzyme considerations in cancer therapy. *Malays J. Med. Sci.* 14, 10–17.

Joerger, M., Burgers, J. A., Baas, P., Doodeman, V. D., Smits, P. H., Jansen, R. S., et al. (2012). Gene polymorphisms, pharmacokinetics, and hematological toxicity in advanced non-small-cell lung cancer patients receiving cisplatin/gemcitabine. *Cancer Chemother. Pharmacol.* 69, 25–33. doi: 10.1007/s00280-011-1670-4

Jóna, Á, Miltényi, Z., Póliska, S., Bálint, B. L., and Illés, Á (2016). Effect of Bleomycin Hydrolase gene polymorphism on late pulmonary complications of treatment for Hodgkin Lymphoma. *PLoS One* 11:e0157651. doi: 10.1371/journal.pone.0157651

Kelland, L. (2007). The resurgence of platinum-based cancer chemotherapy. *Nat. Rev. Cancer* 7, 573–584. doi: 10.1038/nrc2167

Keshava, C. H., McCanlies, E., and Weston, A. (2004). CYP3A4 polymorphism-potential risk factor for breast and prostate cancer: a HuGE review. *Am. J. Epidemiol.* 160, 825–841. doi: 10.1093/aje/kwh294

Khrunin, A. V., Moisseev, A., Gorbunova, V., and Limborska, S. (2010). Genetic polymorphisms and the efficacy and toxicity of cisplatin-based chemotherapy in ovarian cancer patients. *Pharmacogenomics J.* 10, 54–61. doi: 10.1038/tpj.2009.45

Kim, J., and Bang, H. (2016). Three common misuses of P values. *Dent. Hypotheses* 7, 73–80. doi: 10.4103/2155-8213.190481

Kivistö, K. T., Kroemer, H. K., and Eichelbaum, M. (1995). The role of human cytochrome P450 enzymes in the metabolism of anticancer agents: implications for drug interactions. *Br. J. Clin. Pharmacol.* 40, 523–530. doi: 10.1111/j.1365-2125.1995.tb05796.x

Lehmann, A. R. (2001). The Xeroderma pigmentosum group D (XPD) gene: one gene, two functions, three diseases. *Genes Dev.* 15, 15–23. doi: 10.1101/gad.859501

Lyer, L., Das, S., Janisch, L., Wen, M., Ramirez, J., Karrison, T., et al. (2002). UGT1A1*28 polymorphism as a determinant of irinotecan disposition and toxicity. *Pharmacogenomics J.* 2, 43–47. doi: 10.1038/sj.tpj.6500072

Mancinelli, L., Cronin, M., and Sadée, W. (2000). Pharmacogenomics: the promise of personalized medicine. *AAPS PharmSci.* 2:E4. doi: 10.1208/ps020104

Marchewka, Z., Piwowar, A., Ruzik, S., and Długosz, A. (2017). Glutathione S -transferases class Pi and Mi and their significance in oncology. *Postepy Hig. Med. Dosw.* 71, 541–550. doi: 10.5604/01.3001.0010.3835

Mazerska, Z., Mróz, A., Pawłowska, M., and Augustin, E. (2016). The role of glucuronidation in drug resistance. *Pharmacol. Ther.* 159, 35–55. doi: 10.1016/j.pharmthera.2016.01.009

Mezvrishvili, Z., and Managadze, L. (2006). Three cycles of etoposide and cisplatin chemotherapy in clinical stage IS nonseminomatous testicular cancer. *Int. Urol. Nephrol.* 38, 621–624. doi: 10.1007/s11255-006-0038-x

Namipashaki, A., Razaghi-Moghadam, Z., and Ansari-Pour, N. (2015). The essentiality of reporting hardy-weinberg equilibrium calculations in population-based genetic association studies. *Cell J.* 17, 187–192. doi: 10.22074/cellj.2016.3711

Negoro, Y., Yano, R., Yoshimura, M., Suehiro, Y., Yamashita, S., Kodawara, T., et al. (2018). Influence of UGT1A1 polymorphism on etoposide plus platinum-induced neutropenia in Japanese patients with small-cell lung cancer. *Int. J. Clin. Oncol.* doi: 10.1007/s10147-018-1358-4 [Epub ahead of print].

Nissar, S., Syed-Sameer, A., Rasool, R., Chowdri, N. A., and Rashid, F. (2017). Glutathione S-transferase: biochemistry, polymorphism and role in colorectal carcinogenesis. *J. Carcinog. Mutagen.* 8, 1–9. doi: 10.4172/2157-2518.1000287

Park, C. H., Bessho, T., Matsunaga, T., and Sancar, A. (1995). Purification, and characterization of the XPF-ERCC1 complex of human DNA repair excision nuclease. *J. Biol. Chem.* 270, 22657–22660. doi: 10.1074/jbc.270.39.22657

Phuthong, S., Settheetham-Ishida, W., Natphopsuk, S., Settheetham, D., and Ishida, T. (2017). Haplotype analysis of MDR1 and risk for cervical cancer in Northeasterns Thailand. *Asian Pac. J. Cancer. Prev.* 18, 1815–1819. doi: 10.22034/APJCP.2017.18.7.1815

Pirmohamed, M., James, S., Meakin, S., Green, C., Scott, A. K., Walley, T. J., et al. (2004). Adverse drug reactions as cause of admission to hospital: prospective analysis of 18 820 patients. *BMJ* 329, 15–19. doi: 10.1136/bmj.329.7456.15

Pizzocaro, G., Piva, L., Salvioni, R., Zanoni, F., and Milani, A. (1985). Cisplatin, etoposide, bleomycin first-line therapy and early resection of residual tumor in far-advanced germinal testis cancer. *Cancer* 56, 2411–2415. doi: 10.1002/1097-0142(19851115)56:10<2411::AID-CNCR2820561012>3.0.CO;2-H

Quiñones, L., Berthou, F., Varela, N., Simon, B., Gil, L., and Lucas, D. (1999). Ethnic susceptibility to lung cancer: differences in CYP2E1, CYP1A1 and GSTM1 genetic polymorphisms between french caucasian and chilean populations. *Cancer Lett.* 141, 167–171. doi: 10.1016/S0304-3835(99)00099-3

Quiñones, L., Rosero, M., Roco, A., Moreno, I., Varela, F., Caceres, D., et al. (2008). Role of Cytochrome P450 enzymes in the metabolism of antineoplasic drugs: present situation and future perspectives. *Rev. Med. Chil.* 136, 1327–1335.

Quiñones, L. A., Roco, A. M., Cayún, J. P., Escalante, P., Miranda, C., Varela, N., et al. (2017). Clinical applications of pharmacogenomics. *Rev. Med. Chil.* 145, 483–500. doi: 10.4067/S0034-98872017000400009

Roco, A., Cayún, J. P., Contreras, S., Stojanova, J., and Quiñones, L. (2014). Can pharmacogenetics explain efficacy and safety of cisplatin pharmacotherapy? *Rev. Front. Genet.* 5:391. doi: 10.3389/fgene.2014.00391

Roco, A., Quiñones, L., Agúndez, J., García-Martín, E., Squicciarini, V., Miranda, C., et al. (2012). Allele frequencies of 23 functionally significant variant alleles related with metabolism of antineoplastic drugs in the Chilean population: comparison with Caucasian and Asian populations. *Front. Genet.* 3:229. doi: 10.3389/fgene.2012.00229

Ross, C. J., Visscher, H., Rassekh, S. R., Castro-Pastrana, L. I., Shereck, E., Carleton, B., et al. (2011). Pharmacogenomics of serious adverse drug reactions in pediatric oncology. *J. Popul. Ther. Clin. Pharmacol.* 18, e134–e151.

Ruzzo, A., Graziano, F., Kawakami, K., Watanabe, G., Santini, D., Catalano, V., et al. (2006). Pharmacogenetic profiling and clinical outcome of patients with advanced gastric cancer treated with palliative chemotherapy. *J. Clin. Oncol.* 24, 1883–1891. doi: 10.1200/JCO.2005.04.8322

Schwartz, D. R., Homanics, G. E., Hoyt, D. G., Klein, E., Abernethy, J., and Lazo, J. S. (1999). The neutral cysteine protease bleomycin hydrolase is essential for epidermal integrity and bleomycin resistance. *Proc. Natl. Acad. Sci. U.S.A.* 96, 4680–4685. doi: 10.1073/pnas.96.8.4680

Tsai, M. S., Weng, S. H., Kuo, Y. H., Chiu, Y. F., and Lin, Y. W. (2011). Synergistic effect of curcumin and cisplatin via down-regulation of thymidine phosphorylase and excision repair cross-complementary 1 (ERCC1). *Mol. Pharmacol.* 80, 136–146. doi: 10.1124/mol.111.071316

White, D. A., Schwartzberg, L. S., Kris, M. G., and Bosl, G. J. (1987). Acute chest pain syndrome during bleomycin infusions. *Cancer* 59, 1582–1585. doi: 10.1002/1097-0142(19870501)59:9<1582::AID-CNCR2820590909>3.0.CO;2-#

Zamble, D. B., and Lippard, S. J. (1995). Cisplatin and DNA repair in cancer chemotherapy. *Trends Biochem. Sci.* 20, 435–439. doi: 10.1016/S0968-0004(00)89095-7

Zhang, Y., Chang, D., and Zhang, J. (2017). Research advances in resistance to platinum-based chemotherapy in lung cancer. *Zhongguo Yi Xue Ke Xue Yuan Xue Bao* 39, 150–155. doi: 10.3881/j.issn.1000-503X.2017.01.025

Zhuo, X., Zheng, N., Felix, C., and Blair, I. (2004). Kinetics and regulation of cytochrome P450-mediated etoposide metabolism. *Drug Metab. Disp.* 32, 993–1000.

Conflict of Interest Statement: The authors declare that the research was conducted in the absence of any commercial or financial relationships that could be construed as a potential conflict of interest.

frontiers in Pharmacology

ORIGINAL RESEARCH
published: 26 March 2019
doi: 10.3389/fphar.2019.00295

Programming of Dopaminergic Neurons by Early Exposure to Sex Hormones: Effects on Morphine-Induced Accumbens Dopamine Release, Reward, and Locomotor Behavior in Male and Female Rats

*Victoria B. Velásquez[1], Gabriel A. Zamorano[1], Jonathan Martínez-Pinto[1], Christian Bonansco[2], Pablo Jara[3], Gonzalo E. Torres[4], Georgina M. Renard[5] and Ramón Sotomayor-Zárate[1]**

[1] Laboratorio de Neuroquímica y Neurofarmacología, Valparaíso, Chile, [2] Laboratorio de Neurofisiología, Instituto de Fisiología, Facultad de Ciencias, Universidad de Valparaíso, Valparaíso, Chile, [3] Facultad de Ciencias de la Salud, Universidad Autónoma de Chile, Santiago, Chile, [4] Department of Pharmacology and Therapeutics, College of Medicine, University of Florida, Gainesville, FL, United States, [5] Centro de Investigación Biomédica y Aplicada (CIBAP), Escuela de Medicina, Facultad de Ciencias Médicas, Universidad de Santiago de Chile, Santiago, Chile

OPEN ACCESS

Edited by:
Tod Edward Kippin, University of California, Santa Barbara, United States

Reviewed by:
Juan M. Dominguez, The University of Texas at Austin, United States
Wendy J. Lynch, University of Virginia, United States

***Correspondence:**
Ramón Sotomayor-Zárate
ramon.sotomayor@uv.cl;
rsotomayorz@gmail.com

Specialty section:
This article was submitted to Neuropharmacology, a section of the journal Frontiers in Pharmacology

Received: *06 November 2018*
Accepted: *11 March 2019*
Published: *26 March 2019*

Citation:
Velásquez VB, Zamorano GA, Martínez-Pinto J, Bonansco C, Jara P, Torres GE, Renard GM and Sotomayor-Zárate R (2019) Programming of Dopaminergic Neurons by Early Exposure to Sex Hormones: Effects on Morphine-Induced Accumbens Dopamine Release, Reward, and Locomotor Behavior in Male and Female Rats. Front. Pharmacol. 10:295. doi: 10.3389/fphar.2019.00295

Neonatal programming with sex hormones produces long-term functional changes in various tissues, including the brain. Previously, we demonstrated a higher content of dopamine and an increase in potassium-induced dopamine release in the nucleus accumbens of adult rats exposed to estradiol valerate. On the other hand, sex hormones also affect the opioid system increasing the expression of the μ opioid receptor and β-endorphins. Here, we investigated if neonatal programming with sex hormones alters the response to morphine during adulthood in rats and predispose them to neurochemical, rewarding and behavioral activating effects. We examined the effects of neonatal exposure to a single dose of estradiol valerate or testosterone propionate on morphine-induced (5 mg/kg, i.v.) dopamine release in the nucleus accumbens and morphine-induced (3 mg/kg, s.c.) locomotor activity and conditioned place preference when these rats were adults. Our results showed a significant increase in morphine-induced dopamine release in the nucleus accumbens of rats that were exposed neonatally to estradiol compared with control rats. This effect was correlated with higher place preference and locomotor activity induced by morphine in adult rats neonatally exposed to estradiol valerate. However, the effect of morphine on dopamine release and behaviors was similar in rats treated with testosterone compared to control rats. Additionally, the expression of mu (μ) opioid receptor, dopamine receptor type 1 (D_1) and dopamine receptor type 2 (D_2) in the nucleus accumbens of adult rats was not different after treatment with sex hormones. Taken together, our results demonstrated

an enhancement of pharmacological effects produced by morphine in rats neonatally programmed with estradiol valerate, suggesting that early exposure to sex hormones could represent a vulnerability factor in the development of addiction to opioid drugs such as morphine and heroin in adulthood.

Keywords: dopamine, morphine, microdialysis, estradiol, testosterone, programming, nucleus accumbens

INTRODUCTION

Drug addiction is defined as a chronic brain disease characterized by compulsive use of the drug, loss of control in drug intake and the emergence of a negative emotional state that is exacerbated by abstinence. In this context, opioids are highly addictive drugs of abuse linked with potent positive (pleasure/gratification) and negative (anxiety/stress) reinforcing effects (Koob et al., 2014). Preclinical studies also indicate that sex plays a critical role in drug addiction. In this sense, it has been shown that female rats have higher cocaine choice than males and the ovariectomization of rats reduces the cocaine choice (Kerstetter et al., 2012). On the other hand, fluctuations in sex hormone levels during the estrous cycle may or may not affect the self-administration of drugs of abuse. For example, cocaine choice is not affected during estrous cycle (Kerstetter et al., 2012), while heroin choice (an opioid most commonly used as a recreational drug for its euphoric effects) is reduced during proestrus phase of estrous cycle (Lacy et al., 2016). In addition, clinical studies have been shown prevalence that the abuse for opioid analgesics and tranquilizers is higher in women than men (UNODC, 2012), women increase drug intake and develop dependence more quickly than men (Becker and Hu, 2008) and when levels of estrogens are high and progesterone is low (follicular phase) the rewarding effects of cocaine are greater than the effects observed during luteal phase (progesterone is high) (Sofuoglu et al., 1999). These sex differences are associated with a modulation of the reward system (mesolimbic pathway) by sex hormones (Cummings et al., 2014; Becker and Koob, 2016; Becker et al., 2016). The mesolimbic pathway is comprised of dopamine (DA) neurons from the ventral tegmental area (VTA) projecting primarily to the nucleus accumbens (NAcc). This circuit is activated by natural rewards (Pfaus et al., 1990; Bassareo and Di Chiara, 1997) or drugs of abuse such as morphine (Di Chiara and Imperato, 1988), through an increase in NAcc DA release. It is known that DA neurons express androgen, estrogen and progesterone receptors (Kuppers et al., 2001; Ravizza et al., 2003; Creutz and Kritzer, 2004), so sex differences observed in human and animals studies could be explained in part by the activation of these receptors by sex hormones and the concomitant regulation in the expression of key proteins involved in DA neurotransmission (for review see Sotomayor-Zarate et al., 2014; Becker and Koob, 2016). The search for factors that can explain sex differences in vulnerability to drugs of abuse has led to the study of sensitive periods of development where various organs are immature. Accordingly, fetal and neonatal stages are periods highly sensitive to deleterious stimuli that can reprogram the normal physiology of different organs such as the brain. Our group has shown that neonatal exposure to estradiol affects dopaminergic brain areas involved in prolactin release (tuberoinfundibular pathway) (Sotomayor-Zarate et al., 2011), movement (nigrostriatal pathway) (Cruz et al., 2014) and reward (mesolimbic pathway) (Bonansco et al., 2018) in adulthood. We observed that neonatal administration of estradiol valerate (EV) increased DA levels and tyrosine hydroxylase (TH) expression in midbrain dopamine neurons of adult rats (Cruz et al., 2014; Espinosa et al., 2016; Bonansco et al., 2018). The increase in DA content is functionally associated with greater NAcc DA release induced by chemical depolarization with K^+ (Espinosa et al., 2016) or by electrical stimulation (Bonansco et al., 2018). However, it has not been evaluated whether neonatal exposure to estradiol favors greater reward effects induced by morphine in adulthood. The aim of the present study was to investigate the influence of neonatal administration of EV and testosterone propionate (TP) on morphine-induced NAcc DA release, conditioned place preference (CPP) and locomotor stimulation in adult male and female rats. In addition, in accordance with The National Institutes of Health (NIH) guidelines (McCullough et al., 2014; Miller et al., 2017), this study was focused in the effects of neonatal sex hormones administration in male and female rats. We postulate that neonatal EV and TP administration will increase morphine activating effects such as NAcc DA release, CPP and locomotor activity in adult male and female rats.

MATERIALS AND METHODS

Animals

105 males and 97 females Sprague Dawley pups from 16 litters were considered for the experiments. However, we excluded 14 rats (9 males and 5 females) that showed obvious signs of stress such as weight loss, porphyric secretions, piloerection and aggression behaviors, between others. The analyses were performed using 188 rats (96 males and 92 females) that showed a good state of health and they were assigned to the following experimental groups: female control (n = 29), male control (n = 34), female EV (n = 34), male EV (n = 33), female TP (n = 29) and male TP (n = 29). All rats were kept under the same conditions of temperature (21 ± 2°C), 12-h light-dark cycle (lights on at 08:00 h), food and water *ad libitum*. All experimental procedures were approved by the Ethics and Biosafety Committee from the Universidad de Valparaíso, and the Institutional Animal Experimentation Ethics Board and the Science Council (FONDECYT) of Chile. Efforts were made to minimize the number of rats used and their suffering.

Drugs and Reagents

EV, TP, sesame oil, DA standard, EDTA, and 1-octanesulfonic acid were purchased from Sigma-Aldrich, Inc. (St. Louis, MO, United States). Morphine hydrochloride was obtained from Laboratorio Sanderson S.A. (ISPCH N° F-10903/16, Santiago, Chile). All other reagents were of analytical and molecular grade.

Experimental Procedure

Male and female pups were single-injected at postnatal day (PND) 1 with EV (0.1 mg/50 μL of sesame oil s.c.), TP (0.1 mg/50 μL of sesame oil s.c.) or vehicle (control group: 50 μL of sesame oil s.c.). The doses of EV and TP used were previously published and produce long-term effects in reproductive and non-reproductive tissues such as the brain (Sotomayor-Zarate et al., 2011; Cruz et al., 2014; Espinosa et al., 2016). All pups were raised with a nursing mother until weaning age (PND21). After weaning, rats were housed in standard cages by experimental group and sex under the aforementioned vivarium conditions until PND60 for male and PND60-62 for female rats. Control females were tested in the diestrus phase of their cycles because both the EV and TP exposed rats treated rats are constantly arrested in this stage of the estrous (by action of the neonatal administration of hormones) (Cruz et al., 2014). The stage of estrous cycle was daily recorded from PND40 to the end of the study (PND60-62). The estrous cycle was assessed by analyzing the relative proportion of leukocytes, epithelial cells, and cornified cells in daily vaginal lavages, which characteristically change during the various stages of the estrous cycle. All the experimental groups were randomly assigned for the following experimental protocols.

Determination of NAcc DA Release

We used *in vivo* brain microdialysis in anesthetized rats following a general protocol previously published (Sotomayor-Zarate et al., 2013, 2015). Basal and morphine-induced DA extracellular levels were measured through high performance liquid chromatography (HPLC) coupled to electrochemical detection (ED). Rats used for microdialysis experiments were 9 (4 females and 5 males), 10 (5 females and 5 males), and 9 (4 females and 5 males) for control, EV and TP groups, respectively.

In vivo Brain Microdialysis

At PND60, rats were deeply anesthetized with isoflurane (5% in 0.6 L/min air flow) in an induction chamber and placed in a stereotaxic apparatus (model 68002, RWD Life Science Co. Ltd., Shenzhen, China) with a mask to maintain anesthesia for all the experiment (isoflurane 2% in 0.6 L/min air flow), using an animal anesthesia system (model 510, RWD Life Science Co. Ltd., Shenzhen, China). Body temperature was maintained at 37°C with an electrical blanket controlled by a thermostat. Concentric brain microdialysis probes (2 mm membrane length, model MAB 2.4.12, 35 kDa cut-off, Microbiotech AB, Stockholm, Sweden) were implanted in the NAcc using the coordinates from the Rat Brain Atlas (Paxinos and Watson, 2009) (NAcc: 1.50 mm posterior, 1.50 mm lateral, and 7.8 mm ventral to brain surface). Microdialysis probes were perfused with artificial cerebrospinal fluid (aCSF in mM: NaCl 147; KCl 2.7; $CaCl_2$ 1.2; $MgCl_2$ 0.85; pH 7.4) at a rate of 1 μL/min using an infusion pump (model RWD 210, RWD Life Science Co. Ltd., Shenzhen, China). After a stabilization period of 90 min, three perfusion samples were collected every 20 min in 3 μL of 0.2 M perchloric acid. At 60 min, an intravenous (i.v.) morphine injection (5 mg/kg) was administered to the rats. The dose of morphine has been previously published and injected by the same route of administration (Sotomayor et al., 2005). Seven perfusion samples were collected after morphine injection and all the perfusion samples were maintained on ice during the experiment and stored at −80°C until analysis. At the end of each experiment, rats were euthanized by decapitation with a guillotine (model 51330, Stoelting™ Co., Wood Dale, IL, United States) and brains were quickly removed and stored in formalin. Brain sections of 50 μm were stained with Leishman's eosin methylene blue solution (Cat. #1.05387.0500, Merck KGaA, Darmstadt, Germany) to verify probe location. Placement of the microdialysis probe was examined microscopically.

DA Quantification

Ten microliters of each dialysate sample were injected to the HPLC-ED system with the following equipment: An isocratic pump, (model PU-2080 Plus, Jasco Co. Ltd., Tokyo, Japan), a C18 column (model Kromasil 100-3.5-C18, AkzoNobel, Bohus, Sweden) and an electrochemical detector (set at 650 mV, 0.5 nA; model LC-4C, BAS, West Lafayette, IN, United States). The mobile phase, containing 0.1 M NaH_2PO_4, 1.0 mM 1-octanesulfonic acid, 1.0 mM EDTA and 8.0% (v/v) CH_3CN (pH 3.4) was pumped at a flow rate of 125 μL/min. DA extracellular levels were assessed by comparing the respective peak area and elution time of the sample with a reference standard and the quantification was performed using a calibration curve for each neurotransmitter (Program ChromPass, Jasco Co. Ltd., Tokyo, Japan).

Behavioral Studies

One hundred and sixty rats were used for CPP (n = 90) and locomotor activity (n = 70) experiments.

Conditioned Place Preference

Rats used for CPP were assigned to the following experimental groups: female control (n = 15), male control (n = 16), female EV (n = 16), male EV (n = 15), female TP (n = 14) and male TP (n = 14).

The CPP apparatus and the protocol used were previously described (Bonansco et al., 2018). Briefly, the conditioning protocol consisted of three parts: pre-test (one day before the conditioning period), the conditioning period and the test (24 h after the last injection). For the pre-test and the test, rats were placed in the neutral-gray center compartment with the two guillotine doors open and were allowed to explore the entire apparatus (two outer compartments) for 15 min. The time spent in each compartment was measured by analyzing the recordings obtained by internet protocol (IP) cameras (LX-C202 model; Lynx Security, China) fixed above each place preference apparatus and connected to a computer in another room. During the conditioning period (3 days) the non-preferred compartment

(the white side) was associated with the reward induced by morphine (3 mg/kg s.c., once per day). The morphine dose and conditioning period used in this work it was previously published (Michaels and Holtzman, 2008).

The time difference (ΔT) in seconds between the time spent in the white compartment on the test day and the pre-test day was used to determine the grade of conditioning in the rats.

Locomotor Activity

Rats used for measure distance traveled were assigned to the following experimental groups: female control (n = 10), male control (n = 13), female EV (n = 13), male EV (n = 13), female TP (n = 11) and male TP (n = 10).

The protocol used for locomotor activity experiments was previously described (Cruz et al., 2014; Dib et al., 2018). Briefly, rats were habituated to the test room for 1 h before starting the experimental protocol. Basal and morphine-induced horizontal locomotor activity was measured using an acrylic box (22 × 44 × 28 cm). Basal locomotor activity was registered for 30 min and then rats were injected with physiological saline solution (1 mL/kg, s.c.) or morphine (3 mg/kg, s.c.), recording the locomotor activity for 180 min. The dose of morphine used in our behavioral experiments was chosen to produce selective locomotor hyperactivity (Neisewander and Bardo, 1987; Di Chiara and Imperato, 1988). Higher doses of morphine (between 10 and 30 mg/kg) produce sedation and thus, reduce locomotor activity (Magnus-Ellenbroek and Havemann-Reinecke, 1993; Spanagel et al., 1993). Each complete session of locomotor activity (210 min) was recorded with an IP camera (LX-C202 model; Lynx Security, China) and the total traveled distance (m) was analyzed using ANY-Maze software (Stoelting Co., Wood Dale, IL, United States). Test cages were wiped and cleaned with 5% ethanol solution between trials.

qRT-PCR

Rats of the experimental groups injected with saline and used to measure locomotor activity were decapitated with a guillotine and the brain was removed. The NAcc was microdissected at 4°C using micro-punch, weighed on an analytical balance and stored at −80°C for further analysis. Real-time qRT-PCR was used to determine whether the mRNA encoding μ, D_1 and D_2 receptors changed in NAcc and VTA of adult female and male rats exposed to sex hormones at PND1. Total RNA was extracted using the E.Z.N.A.® Total RNA Kit I (Cat. #R6834-02; Omega Biotek) according to the manufacturer's instructions. RNA was quantified using the microplate Spectrophotometer Epoch (BioTek Inc., Winooski, VT, United States), and RNA integrity was assessed through agarose gel electrophoresis. Total RNA from each sample were reverse transcribed with PrimeScript RT reagent Kit (Cat. #RR047A; TaKaRa, Bio Inc., CA, United States), according to the manufacturer's instructions. Real-time RT-PCR was performed using Taqman assays for the following genes purchased from Thermo Fisher Scientific: *Drd1* (Cat: Rn03062203_s1, FAM dye-labeled), *Drd2* (Cat: Rn00561126_m1, VIC dye-labeled) and *Oprm1* (Cat: Rn01430371_m1, FAM dye-labeled). The cycle conditions were 50°C for 2 min, 95°C for 2 min, 40 cycles for 95°C for 3 s and 60°C for 30 s. The relative quantification method was performed using Rn45s (Cat: Rn03928990_g1, VIC dye labeled) as an endogenous control. Results were expressed as fold change by the $2^{-\Delta\Delta CT}$ method (Livak and Schmittgen, 2001).

Statistical Analysis

Data were expressed as mean ± SEM. Two-way ANOVA followed by Newman–Keuls *post hoc* test analysis were performed for all experiments to determine a significant interaction of treatment by sex. The statistical analyses were carried out with GraphPad Prism v6.0 (GraphPad Software, San Diego, CA, United States) and $P < 0.05$ was considered statistically significant.

RESULTS

Our data show that neonatal exposure to EV increases the rewarding effects of morphine and it represents a vulnerability factor that may enhance the development of opioid dependence.

Long-Lasting Effects of Neonatal Sex Hormones Administration on Morphine-Induced NAcc DA Release in Adult Rats

Figures 1A,B show time course of basal and morphine-induced extracellular levels of DA in NAcc. **Figure 1C** shows the area under the curve (AUC) that represents morphine-induced DA extracellular levels in control, EV and TP adult rats. In this context, neonatal exposure to EV in female and male rats increases morphine-induced NAcc DA release in the adulthood respect to control rats injected with vehicle (Two-way ANOVA followed by Newman–Keuls *post hoc* analysis; Interaction [$F_{(2,22)}$ = 0.4001, P = 0.6751]; Sex [$F_{(1,22)}$ = 3.328, P = 0.0817]; treatment [$F_{(2,22)}$ = 10.17, P = 0.0007]).

Long-Lasting Effects of Neonatal Sex Hormones Administration on Morphine-Induced CPP in Adult Rats

Figure 2 shows morphine-induced conditioned behavior in female and male adult rats exposed during the first 12 h of postnatal life to a single dose of EV or TP. As expected, morphine administration (3 mg/kg, s.c.) produced a significant increase in the time spent in the chamber paired to morphine injection vs. saline injection in female and male rats in all experimental groups (****$P < 0.0001$). (Two-way ANOVA followed by Newman–Keuls *post hoc* analysis; Interaction [$F_{(5,78)}$ = 0.5782, P = 0.7166]; Sex [$F_{(1,78)}$ = 11.64, P = 0.0010]; treatment [$F_{(5,78)}$ = 71.88, $P < 0.0001$]).

Long-Lasting Effects of Neonatal Sex Hormones Administration on Morphine-Induced Locomotor Activity in Adult Rats

Figures 3A,C show the temporal course of locomotor activity in the experimental groups that received only the saline

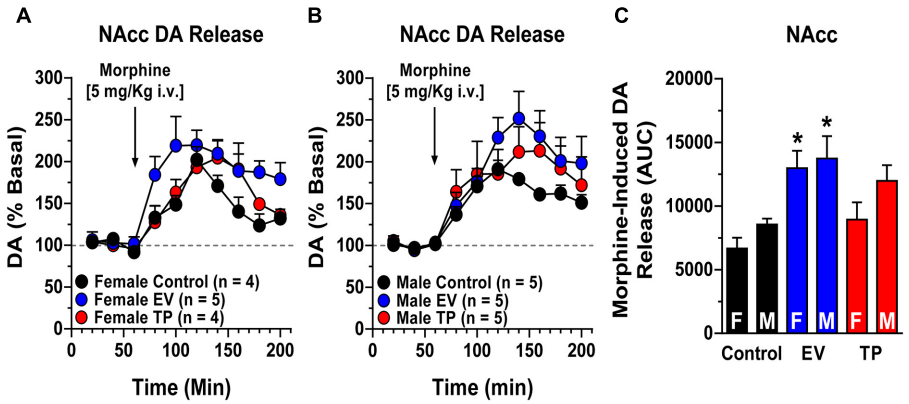

FIGURE 1 | Morphine-induced NAcc DA release using *in vivo* brain microdialysis. Panels **A** and **B** Time course of NAcc DA release expressed as percentage of baseline (mean ± SEM) in female **(A)** and male **(B)** adult rats exposed to neonatal administration to estradiol valerate (EV) or testosterone propionate (TP). At postnatal day (PND) 60 microdialysis experiments were performed and after a stabilization period, three perfusion samples were collected. At 60 min a dose of morphine (5 mg/kg, i.v.) was injected. **(C)** shows an increase in the area under the curve (AUC) of morphine-induced NAcc DA release in female (F) and male (M) adult rats. $^{*}P < 0.05$ for EV female rats vs. control female rats and for EV male rats vs. control male rats.

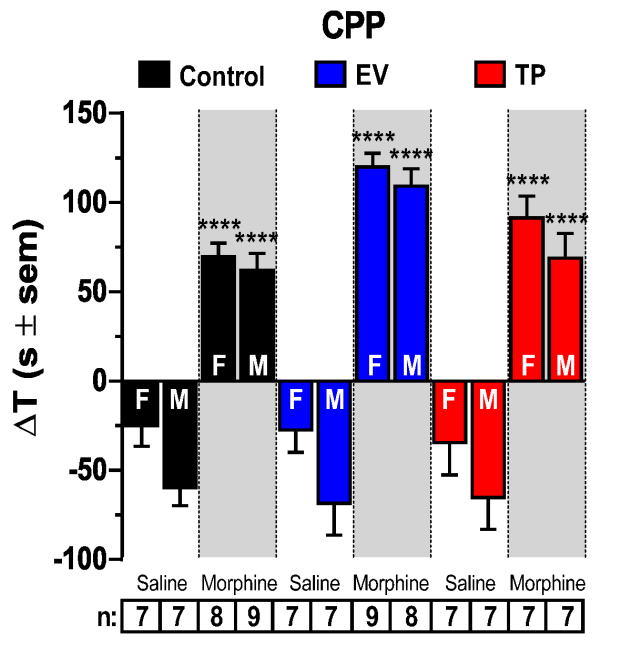

FIGURE 2 | Conditioned place preference (CPP) to saline or morphine of adult female (F) and male (M) rats exposed to estradiol valerate (EV) and testosterone propionate (TP) at postnatal day (PND) 1. Data are shown as the time difference (ΔT) in seconds between the time spent in the white compartment in the test day and the pre-test day. Neonatal exposure to EV in female and male rats increases CPP induced by morphine (3 mg/kg, s.c.) respect neonatal injection of vehicle in female and male rats at PND 60 ($^{****}P < 0.0001$).

(1 mL/kg, s.c.) injection. Morphine-induced locomotor activity was measured in adult female (**Figure 3B**) and male (**Figure 3D**) rats exposed during the first hours of postnatal life to EV or TP. **Figure 4** shows basal (4A: 0–30 min) and post-injection (4B: 30–210 min) cumulative locomotor activities between experimental groups. Basal cumulative locomotor activity (**Figure 4A**) was not different in our experimental groups (Two-way ANOVA followed by Newman–Keuls *post hoc* analysis; Interaction [$F_{(5,58)} = 1.012$, $P = 0.4192$]; Sex [$F_{(1,58)} = 3.424$, $P = 0.0694$]; treatment [$F_{(5,58)} = 1.102$, $P = 0.3695$]). **Figure 4B** shows that cumulative locomotor activity induced by morphine (30 to 210 min) was significantly higher than cumulative locomotor activity produced by saline injection ($^{*}P < 0.05$, $^{***}P < 0.001$, $^{****}P < 0.0001$). On the other hand, control and EV female rats have a greater cumulative locomotor activity induced by morphine than control and EV male rats induced by morphine ($^{\$}P < 0.05$) (Two-way ANOVA followed by Newman–Keuls *post hoc* analysis; Interaction [$F_{(5,58)} = 2.140$, $P = 0.0733$]; Sex [$F_{(1,58)} = 9.909$, $P = 0.0026$]; treatment [$F_{(5,58)} = 32.48$, $P < 0.0001$]).

Neonatal Exposure to Sex Hormones Does Not Affect the mRNA Expression of DA and μ Opioid Receptors in NAcc in Adulthood

mRNA expression for *Drd1* (**Figure 5A**), *Drd2* (**Figure 5B**), and μ opioid receptors (**Figure 5C**) were measured in NAcc of adult rats exposed during the first hours of post-natal life to a single dose of sex hormones. We did not observed a significant increase in *Drd1* (Two-way ANOVA followed by Newman–Keuls *post hoc* analysis; Interaction [$F_{(2,30)} = 0.1006$, $P = 0.9046$]; Sex [$F_{(1,30)} = 0.08264$, $P = 0.7757$]; treatment [$F_{(2,30)} = 1.988$, $P = 0.1546$]), *Drd2* (Two-way ANOVA followed by Newman–Keuls *post hoc* analysis; Interaction [$F_{(2,30)} = 0.1482$, $P = 0.8629$]; Sex [$F_{(1,30)} = 0.1634$, $P = 0.6889$]; treatment [$F_{(2,30)} = 3.076$, $P = 0.0609$]) and *Oprm1* (Two-way ANOVA followed by Newman–Keuls *post hoc* analysis; Interaction [$F_{(2,30)} = 1.040$, $P = 0.3659$]; Sex [$F_{(1,30)} = 3.757$, $P = 0.0620$]; treatment [$F_{(2,30)} = 0.1506$, $P = 0.8608$]), expressions in NAcc.

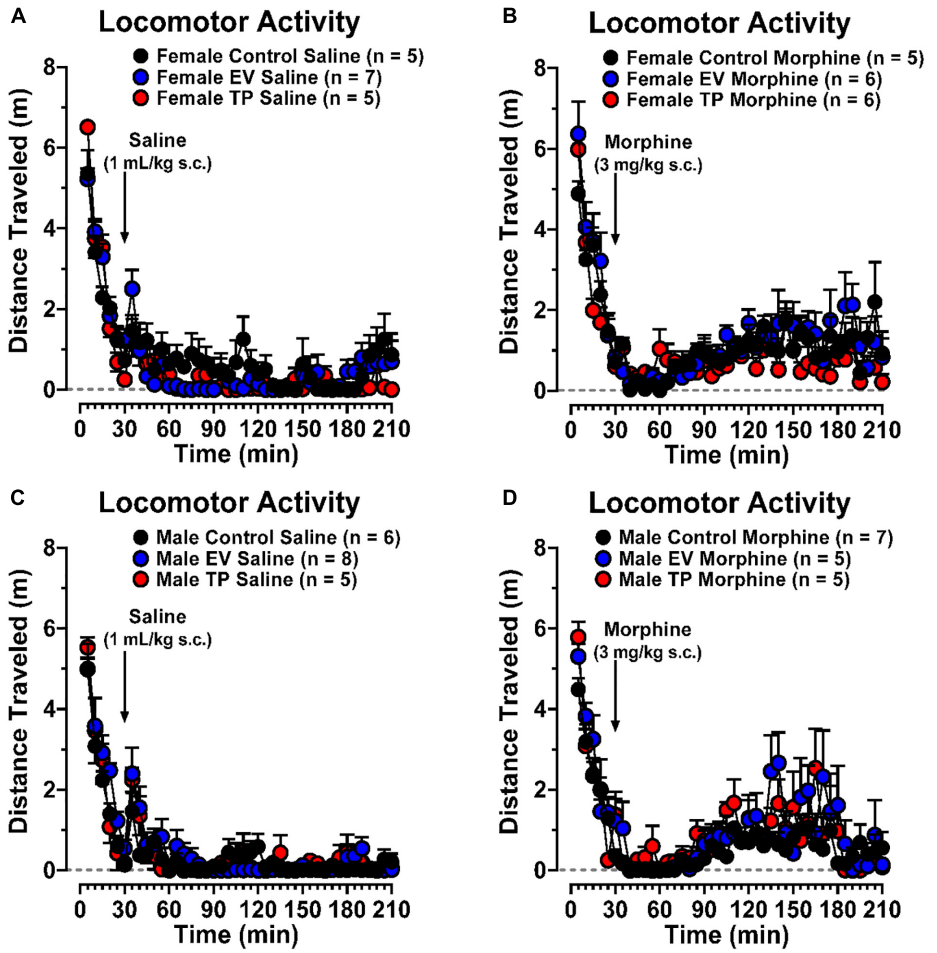

FIGURE 3 | Time course of basal, saline-induced and morphine-induced locomotor activity in female **(A,B)** and male **(C,D)** control, EV and TP rats expressed in distance traveled (m).

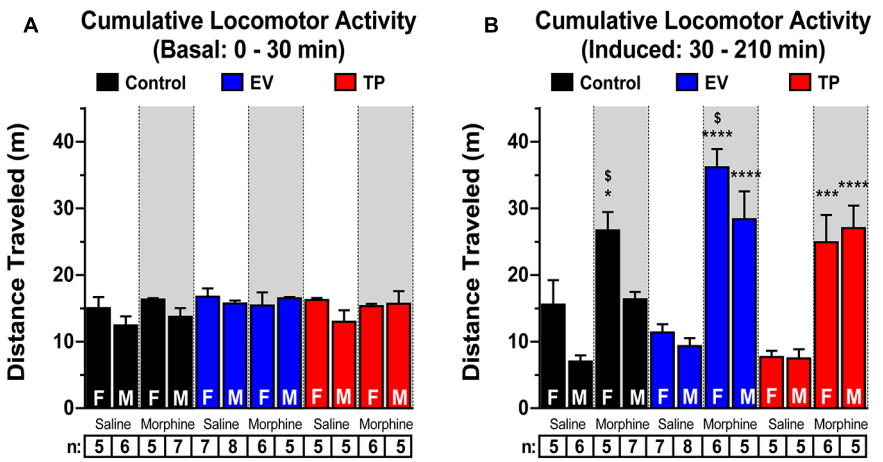

FIGURE 4 | Morphine-induced locomotor activity in adult female (F) and male (M) rats exposed to estradiol valerate (EV) or testosterone propionate (TP) at PND 1. Cumulative locomotor activity from 0 to 30 min (basal) **(A)** and from 30 to 210 min (**B**, induced by saline or morphine injection) in female (F) and male (M) control, EV and TP rats $^{*}P < 0.05$, $^{***}P < 0.001$ and $^{****}P < 0.0001$ versus saline female or saline male rats, respectively. $^{\$}P < 0.05$ versus respective male rats.

DISCUSSION

We have shown that neonatal EV administration produces a higher increase in morphine-induced NAcc DA release in both female and male adult rats compared to control rats. This effect correlates with a higher increase in morphine-induced CPP and locomotor activity in EV treated rats compared to controls. These findings indicate that neonatal exposure to sex hormones, especially estradiol, could reprogram the reward system and consequently alter to neurochemical, rewarding and behavioral activating effects of morphine in adult female and male rats.

Neonatal Administration of Sex Hormones Increases Morphine-Induced NAcc DA Release in Adult Male and Female Rats

Morphine injection produces an increase in NAcc DA release in adult rats exposed during the first hours of postnatal life to EV compared to control and TP rats. Morphine is an opiate found naturally in the opium poppy plant and it is used therapeutically as a narcotic analgesic. One of the most important adverse effects of morphine is the highly addictive potential (similar to heroin). At the neurochemical level, morphine increases extracellular levels of DA in the NAcc (Di Chiara and Imperato, 1988; Tanda et al., 1997). In our experiments, neonatal EV exposure in rats produced an increase in NAcc DA release (**Figure 1**), CPP (**Figure 2**), and locomotor activity (**Figures 3**, **4**) induced by morphine compared to control or TP-treated rats. In this context, several studies have shown that estradiol facilitates the motivation for drugs of abuse by interacting with reward system (Yoest et al., 2014). For example, estradiol increases cocaine self-administration, cocaine intake and motivation in ovariectomized rats (OVX) (Hu and Becker, 2008; Ramoa et al., 2013). On the other hand, locomotor activity induced by cocaine is lower in OVX than control (intact) rats (Walker et al., 2001). The neural and behavioral effects of estradiol on DA neurons have been associated with changes in expression levels of DA key proteins such as TH (rate-limiting enzyme of catecholamine biosynthesis), DAT (protein responsible for regulating DA levels through the uptake of DA) and DA receptors. In this sense, in OVX rats have been observed a reduction in levels of VTA TH and NAcc DAT that are restores after hormone replacement therapy (Chavez et al., 2010; Johnson et al., 2010). However, D_2 levels are increased in NAcc and dorsolateral striatum (DLS) of OVX rats to compare controls rats and the estradiol replacement reduced D_2 levels in NAcc and DLS of OVX rats (Chavez et al., 2010). The estradiol effects on these proteins are mediated by the activation of specific receptor such as estrogen receptor α (ERα) and estrogen receptor β (ERβ) expressed in reward system resulting in up- or down-regulation of gene expression (Simerly et al., 1990; Shughrue et al., 1997; Creutz and Kritzer, 2004). On the other hand, G protein-coupled estrogen receptor (GPER) produces rapid pharmacological response to estradiol (Gaudet et al., 2015). In NAcc and DLS the activation of GPER increases DA release induced by psychostimulant drugs in female rats (Becker, 1990; Cummings et al., 2014).

Regard our data, we previously demonstrated that neonatal exposure to EV during the first hours of postnatal life results in higher DA content in the mesolimbic pathway (VTA and NAcc) (Cruz et al., 2014; Espinosa et al., 2016) and increased NAcc DA release induced be a depolarizing stimulus (70 nM K^+) (Espinosa et al., 2016; Bonansco et al., 2018). In addition, neonatal exposure to EV reprograms the electrophysiological properties of VTA DA neurons, favoring a higher firing frequency compared to control rats (Bonansco et al., 2018). All of these alterations in the dopaminergic system induced by neonatal EV administration may contribute to the increased morphine-induced NAcc DA release in EV rats.

Another possible mechanism involved in the increased morphine-induced NAcc DA release in adult rats exposed to EV during the first hours of life (**Figure 1**) might be a decrease in the inhibitory effect of GABAergic neurons on midbrain DA neurons. It has been shown that neonatal estradiol benzoate administration results in an enhanced PFC DA release in adult female rats and a decrease in brain levels of allopregnanolone (a potent neurosteroid that is a positive modulator of $GABA_A$ receptors) when compared to control rats (Porcu et al., 2017).

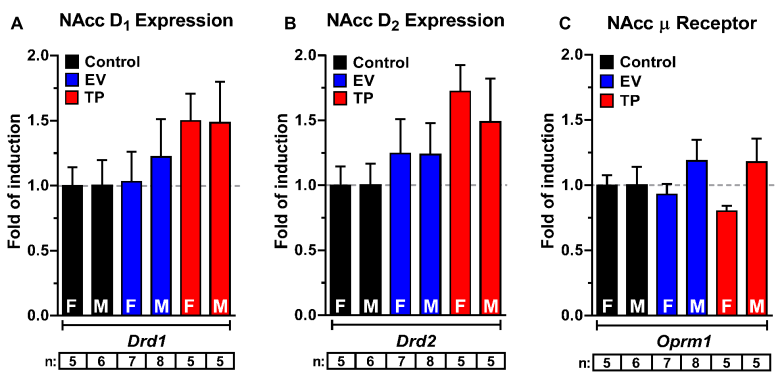

FIGURE 5 | Neonatal exposure to estradiol valerate (EV) and testosterone propionate (TP) does not affect the expressions of *Drd1* **(A)**, *Drd2* **(B)**, and *Oprm1* **(C)** in nucleus accumbens (NAcc) of adult female (F) and male (M) rats. All data have been normalized for levels of 18S expression within the same sample. Results are expressed as fold of induction regard control group and represent the mean ± SEM.

In addition, we showed that EV female adult rats have a decrease in GABA content in tuberal hypothalamus (Sotomayor-Zarate et al., 2011). Therefore, it is possible that this decrease in GABA content could also occur in the VTA, reducing the tonic inhibition of VTA DA neurons. Furthermore, the hyperpolarizing effect of morphine on VTA GABA neurons (Gysling and Wang, 1983; Johnson and North, 1992) in EV rats may favors a greater NAcc DA release than control rats. Interestingly, it has been shown that estradiol also stimulates VTA DA neurons through the inhibition of GABAergic afferents from medial preoptic area (anterior hypothalamus) to VTA, producing an increase in firing of DA neurons (Tobiansky et al., 2016).

Neonatal Administration of Sex Hormones Increases Morphine-Induced CPP and Locomotor Activity in Adult Male and Female Rats

The repeated administration of morphine (3 mg/kg s.c.) results in conditioning in rats of both sexes. Interestingly, the degree of conditioning induced by morphine was higher in adult EV rats compared to control rats (**Figure 2**), reflecting the development of a more intense reward that could be associated to the increased NAcc DA release induced by morphine in EV rats (**Figure 1**). The neonatal exposure to EV not only produced an increase in CPP behavior associated to repeated morphine administration in adult rats (**Figure 2**), but also an increase in locomotor activity in response to an acute administration of morphine (see **Figure 3**). The dose of morphine used in this work was effective to induce locomotor activity when compared to saline injection in all experimental groups. Interestingly, although the basal locomotor activity (**Figure 3**) measured during first 30 min (in the absence of injection of saline or morphine) in all experimental groups were not different, we observed an increase in the locomotor activity induced by morphine regard to saline injection (30 to 210 min) (**Figure 3**).

In female EV rats the morphine-induced locomotor activity was higher compared to female control rats, while in the case of male rats, administration of both EV and TP resulted in an enhanced locomotor activity after acute morphine compared to control male rats (**Figure 4**). These neurochemical and behavioral results demonstrate that DA neurons programmed with sex hormones are susceptible to greater activation by opioids such as morphine. In this context, the effect observed in TP male rats on morphine-induced locomotor activity might result from partial aromatization of testosterone (T) to estradiol (E_2) through cytochrome P450 aromatase, which is highly expressed in the midbrain (Raab et al., 1995). In previous work, we observed an increase in TH expression and DA levels in the substantia nigra and VTA in TP and EV male rats compared to controls. But, males treated with dihydrotestosterone (DHT), a non-aromatizable androgen at postnatal day 1 did not show changes in those parameters compared with controls, suggesting an estrogenic mechanism (Espinosa et al., 2016). On the other hand, published studies in intact female rats in diestrous phase of estrous cycle have a self-administration to drugs of abuse similar to males (Kerstetter et al., 2012; Lacy et al., 2016), in this work we observed that the neonatal administration of EV increases morphine-induced behaviors compared to control rats also in diestrous phase. Our results could suggest that the long-term effects observed on dopaminergic neurons by neonatal exposure to sex hormones could be due to permanent epigenetic changes. However, future studies would be needed.

Our results do not show changes in NAcc *Drd1* and *Drd2* expressions in female and male rats treated with EV and TP (**Figure 5**). In addition, we did not observe changes in NAcc μ opioid receptor expression, which suggests that the increase in the rewarding properties of morphine in EV rats might be due to an increase in DA synthesis (Bonansco et al., 2018) and DA release rather than changes in receptor expressions. However, the expression of proteins downstream of the activation of DA receptors should be explored, especially changes in the expression of the regulators of G-protein signaling (RGS) that are involved in locomotor responses to drugs of abuse (Gross et al., 2018) and modulated by estrogens (Silverman and Koenig, 2007).

CONCLUSION

In conclusion, the alteration of sex hormones homeostasis during the early stages of development, either by a supra-physiological exposure to these hormones or by persistent exposure to endocrine disruptors (environmental pollutants) with estrogenic activity produce long-term effects not only in reproductive tissues, but also in non-reproductive tissues such as the brain. In this context, neonatal exposure to sex hormones can be considered a factor of vulnerability for substance use disorders such as morphine addiction and abuse. Finally, our experimental model of neonatal reprogramming allows exploration of the epigenetic mechanisms involved in DA neurons that may be responsible for the long-term effects observed in this work.

DATA AVAILABILITY

All datasets generated for this study are included in the manuscript and/or the supplementary files.

AUTHOR CONTRIBUTIONS

VV performed microdialysis and conditioned place preference experiments. GZ performed the locomotor activity experiments. JM-P performed the qPCR experiments. CB, PJ, GT, GR, and RS-Z designed the experiments and interpreted the results. GR and RS-Z performed the statistical analysis of data and wrote the manuscript. RS-Z received funding for all experiments.

FUNDING

This work was supported by FONDECYT Grant N°116-0398 to RS-Z. In addition, the international cooperation established with GT (United States) has been possible thanks to the CONICYT Grant N°PAI80160020.

REFERENCES

Bassareo, V., and Di Chiara, G. (1997). Differential influence of associative and nonassociative learning mechanisms on the responsiveness of prefrontal and accumbal dopamine transmission to food stimuli in rats fed ad libitum. *J. Neurosci.* 17, 851–861. doi: 10.1523/JNEUROSCI.17-02-00851.1997

Becker, J. B. (1990). Estrogen rapidly potentiates amphetamine-induced striatal dopamine release and rotational behavior during microdialysis. *Neurosci. Lett.* 118, 169–171. doi: 10.1016/0304-3940(90)90618-J

Becker, J. B., and Hu, M. (2008). Sex differences in drug abuse. *Front. Neuroendocrinol.* 29:36–47. doi: 10.1016/j.yfrne.2007.07.003

Becker, J. B., and Koob, G. F. (2016). Sex differences in animal models: focus on addiction. *Pharmacol. Rev.* 68, 242–263. doi: 10.1124/pr.115.011163

Becker, J. B., Mcclellan, M., and Reed, B. G. (2016). Sociocultural context for sex differences in addiction. *Addict. Biol.* 21, 1052–1059. doi: 10.1111/adb.12383

Bonansco, C., Martinez-Pinto, J., Silva, R. A., Velasquez, V. B., Martorell, A., Selva, M. V., et al. (2018). Neonatal exposure to oestradiol increases dopaminergic transmission in nucleus accumbens and morphine-induced conditioned place preference in adult female rats. *J. Neuroendocrinol.* 30:e12574. doi: 10.1111/jne.12574

Chavez, C., Hollaus, M., Scarr, E., Pavey, G., Gogos, A., and Van Den Buuse, M. (2010). The effect of estrogen on dopamine and serotonin receptor and transporter levels in the brain: an autoradiography study. *Brain Res.* 1321, 51–59. doi: 10.1016/j.brainres.2009.12.093

Creutz, L. M., and Kritzer, M. F. (2004). Mesostriatal and mesolimbic projections of midbrain neurons immunoreactive for estrogen receptor beta or androgen receptors in rats. *J. Comp. Neurol.* 476, 348–362. doi: 10.1002/cne.20229

Cruz, G., Riquelme, R., Espinosa, P., Jara, P., Dagnino-Subiabre, A., Renard, G. M., et al. (2014). Neonatal exposure to estradiol valerate increases dopamine content in nigrostriatal pathway during adulthood in the rat. *Horm. Metab. Res.* 46, 322–327. doi: 10.1055/s-0033-1361159

Cummings, J. A., Jagannathan, L., Jackson, L. R., and Becker, J. B. (2014). Sex differences in the effects of estradiol in the nucleus accumbens and striatum on the response to cocaine: neurochemistry and behavior. *Drug Alcohol Depend.* 135, 22–28. doi: 10.1016/j.drugalcdep.2013.09.009

Di Chiara, G., and Imperato, A. (1988). Drugs abused by humans preferentially increase synaptic dopamine concentrations in the mesolimbic system of freely moving rats. *Proc. Natl. Acad. Sci. U.S.A.* 85, 5274–5278. doi: 10.1073/pnas.85.14.5274

Dib, T., Martinez-Pinto, J., Reyes-Parada, M., Torres, G. E., and Sotomayor-Zarate, R. (2018). Neonatal programming with testosterone propionate reduces dopamine transporter expression in nucleus accumbens and methylphenidate-induced locomotor activity in adult female rats. *Behav. Brain. Res.* 346, 80–85. doi: 10.1016/j.bbr.2017.12.001

Espinosa, P., Silva, R. A., Sanguinetti, N. K., Venegas, F. C., Riquelme, R., Gonzalez, L. F., et al. (2016). Programming of dopaminergic neurons by neonatal sex hormone exposure: effects on dopamine content and tyrosine hydroxylase expression in adult male rats. *Neural. Plast.* 2016:4569785. doi: 10.1155/2016/4569785

Gaudet, H. M., Cheng, S. B., Christensen, E. M., and Filardo, E. J. (2015). The G-protein coupled estrogen receptor, GPER: the inside and inside-out story. *Mol. Cell Endocrinol.* 418(Pt 3), 207–219. doi: 10.1016/j.mce.2015.07.016

Gross, J. D., Kaski, S. W., Schroer, A. B., Wix, K. A., Siderovski, D. P., and Setola, V. (2018). Regulator of G protein signaling-12 modulates the dopamine transporter in ventral striatum and locomotor responses to psychostimulants. *J. Psychopharmacol.* 32, 191–203. doi: 10.1177/0269881117742100

Gysling, K., and Wang, R. Y. (1983). Morphine-induced activation of A10 dopamine neurons in the rat. *Brain Res.* 277, 119–127. doi: 10.1016/0006-8993(83)90913-7

Hu, M., and Becker, J. B. (2008). Acquisition of cocaine self-administration in ovariectomized female rats: effect of estradiol dose or chronic estradiol administration. *Drug Alcohol Depend.* 94, 56–62. doi: 10.1016/j.drugalcdep.2007.10.005

Johnson, M. L., Ho, C. C., Day, A. E., Walker, Q. D., Francis, R., and Kuhn, C. M. (2010). Oestrogen receptors enhance dopamine neurone survival in rat midbrain. *J. Neuroendocrinol.* 22, 226–237. doi: 10.1111/j.1365-2826.2010.01964.x

Johnson, S. W., and North, R. A. (1992). Opioids excite dopamine neurons by hyperpolarization of local interneurons. *J. Neurosci.* 12, 483–488. doi: 10.1523/JNEUROSCI.12-02-00483.1992

Kerstetter, K. A., Ballis, M. A., Duffin-Lutgen, S., Carr, A. E., Behrens, A. M., and Kippin, T. E. (2012). Sex differences in selecting between food and cocaine reinforcement are mediated by estrogen. *Neuropsychopharmacology* 37, 2605–2614. doi: 10.1038/npp.2012.99

Koob, G. F., Arends, M. A., and Le Moal, M. (2014). *Drugs, Addiction, and the Brain*. Amsterdam: Elsevier.

Kuppers, E., Ivanova, T., Karolczak, M., Lazarov, N., Fohr, K., and Beyer, C. (2001). Classical and nonclassical estrogen action in the developing midbrain. *Horm. Behav.* 40, 196–202. doi: 10.1006/hbeh.2001.1671

Lacy, R. T., Strickland, J. C., Feinstein, M. A., Robinson, A. M., and Smith, M. A. (2016). The effects of sex, estrous cycle, and social contact on cocaine and heroin self-administration in rats. *Psychopharmacology* 233, 3201–3210. doi: 10.1007/s00213-016-4368-9

Livak, K. J., and Schmittgen, T. D. (2001). Analysis of relative gene expression data using real-time quantitative PCR and the 2(-Delta Delta C(T)) Method. *Methods* 25, 402–408. doi: 10.1006/meth.2001.1262

Magnus-Ellenbroek, B., and Havemann-Reinecke, U. (1993). Morphine-induced hyperactivity in rats–a rebound effect? *Naunyn Schmiedebergs Arch. Pharmacol.* 347, 635–642.

McCullough, L. D., De Vries, G. J., Miller, V. M., Becker, J. B., Sandberg, K., and Mccarthy, M. M. (2014). NIH initiative to balance sex of animals in preclinical studies: generative questions to guide policy, implementation, and metrics. *Biol. Sex Differ.* 5:15. doi: 10.1186/s13293-014-0015-5

Michaels, C. C., and Holtzman, S. G. (2008). Early postnatal stress alters place conditioning to both mu- and kappa-opioid agonists. *J. Pharmacol. Exp. Ther.* 325, 313–318. doi: 10.1124/jpet.107.129908

Miller, L. R., Marks, C., Becker, J. B., Hurn, P. D., Chen, W. J., Woodruff, T., et al. (2017). Considering sex as a biological variable in preclinical research. *Faseb. J.* 31, 29–34. doi: 10.1096/fj.201600781R

Neisewander, J. L., and Bardo, M. T. (1987). Expression of morphine-conditioned hyperactivity is attenuated by naloxone and pimozide. *Psychopharmacology* 93, 314–319. doi: 10.1007/BF00187249

Paxinos, G., and Watson, C. (2009). *The Rat Brain in Stereotaxic Coordinates. Compact Sixth Edition*. Cambridge,MA: Academic Press.

Pfaus, J. G., Damsma, G., Nomikos, G. G., Wenkstern, D. G., Blaha, C. D., Phillips, A. G., et al. (1990). Sexual behavior enhances central dopamine transmission in the male rat. *Brain Res.* 530, 345–348. doi: 10.1016/0006-8993(90)91309-5

Porcu, P., Lallai, V., Locci, A., Catzeddu, S., Serra, V., Pisu, M. G., et al. (2017). Changes in stress-stimulated allopregnanolone levels induced by neonatal estradiol treatment are associated with enhanced dopamine release in adult female rats: reversal by progesterone administration. *Psychopharmacology* 234, 749–760. doi: 10.1007/s00213-016-4511-7

Raab, H., Beyer, C., Wozniak, A., Hutchison, J. B., Pilgrim, C., and Reisert, I. (1995). Ontogeny of aromatase messenger ribonucleic acid and aromatase activity in the rat midbrain. *Brain Res. Mol. Brain Res.* 34, 333–336. doi: 10.1016/0169-328X(95)00196-Y

Ramoa, C. P., Doyle, S. E., Naim, D. W., and Lynch, W. J. (2013). Estradiol as a mechanism for sex differences in the development of an addicted phenotype following extended access cocaine self-administration. *Neuropsychopharmacology* 38, 1698–1705. doi: 10.1038/npp.2013.68

Ravizza, T., Veliskova, J., and Moshe, S. L. (2003). Testosterone regulates androgen and estrogen receptor immunoreactivity in rat substantia nigra pars reticulata. *Neurosci. Lett.* 338, 57–61. doi: 10.1016/S0304-3940(02)01317-4

Shughrue, P. J., Lane, M. V., and Merchenthaler, I. (1997). Comparative distribution of estrogen receptor-alpha and -beta mRNA in the rat central nervous system. *J. Comp. Neurol.* 388, 507–525. doi: 10.1002/(SICI)1096-9861(19971201)388:4<507::AID-CNE1>3.0.CO;2-6

Silverman, J. L., and Koenig, J. I. (2007). Evidence for the involvement of ERbeta and RGS9-2 in 17-beta estradiol enhancement of amphetamine-induced place preference behavior. *Horm. Behav.* 52, 146–155. doi: 10.1016/j.yhbeh.2007.03.017

Simerly, R. B., Chang, C., Muramatsu, M., and Swanson, L. W. (1990). Distribution of androgen and estrogen receptor mRNA-containing cells in the rat brain: an in situ hybridization study. *J. Comp. Neurol.* 294, 76–95. doi: 10.1002/cne.902940107

Sofuoglu, M., Dudish-Poulsen, S., Nelson, D., Pentel, P. R., and Hatsukami, D. K. (1999). Sex and menstrual cycle differences in the subjective effects from smoked cocaine in humans. *Exp. Clin. Psychopharmacol.* 7, 274–283. doi: 10.1037/1064-1297.7.3.274

Sotomayor, R., Forray, M. I., and Gysling, K. (2005). Acute morphine administration increases extracellular DA levels in the rat lateral septum by decreasing the GABAergic inhibitory tone in the ventral tegmental area. *J. Neurosci. Res.* 81, 132–139. doi: 10.1002/jnr.20537

Sotomayor-Zarate, R., Abarca, J., Araya, K. A., Renard, G. M., Andres, M. E., and Gysling, K. (2015). Exposure to repeated immobilization stress inhibits cocaine-induced increase in dopamine extracellular levels in the rat ventral tegmental area. *Pharmacol. Res.* 101, 116–123. doi: 10.1016/j.phrs.2015.08.015

Sotomayor-Zarate, R., Cruz, G., Renard, G. M., Espinosa, P., and Ramirez, V. D. (2014). Sex hormones and brain dopamine functions. *Cent. Nerv. Syst. Agents Med. Chem.* 14, 62–71. doi: 10.2174/1871524914666141226105137

Sotomayor-Zarate, R., Renard, G. M., Araya, K. A., Carreno, P., Fuentealba, J. A., Andres, M. E., et al. (2013). Long-term loss of dopamine release mediated by CRF-1 receptors in the rat lateral septum after repeated cocaine administration. *Behav. Brain Res.* 250, 206–210. doi: 10.1016/j.bbr.2013.05.012

Sotomayor-Zarate, R., Tiszavari, M., Cruz, G., and Lara, H. E. (2011). Neonatal exposure to single doses of estradiol or testosterone programs ovarian follicular development-modified hypothalamic neurotransmitters and causes polycystic ovary during adulthood in the rat. *Fertil. Steril.* 96, 1490–1496. doi: 10.1016/j.fertnstert.2011.09.011

Spanagel, R., Almeida, O. F., and Shippenberg, T. S. (1993). Long lasting changes in morphine-induced mesolimbic dopamine release after chronic morphine exposure. *Synapse* 14, 243–245. doi: 10.1002/syn.890140307

Tanda, G., Pontieri, F. E., and Di Chiara, G. (1997). Cannabinoid and heroin activation of mesolimbic dopamine transmission by a common mu1 opioid receptor mechanism. *Science* 276, 2048–2050. doi: 10.1126/science.276.5321.2048

Tobiansky, D. J., Will, R. G., Lominac, K. D., Turner, J. M., Hattori, T., Krishnan, K., et al. (2016). Estradiol in the preoptic area regulates the dopaminergic response to cocaine in the nucleus accumbens. *Neuropsychopharmacology* 41, 1897–1906. doi: 10.1038/npp.2015.360

UNODC (2012). *Informe Mundial Sobre las Drogas*. Viena: Naciones Unidas.

Walker, Q. D., Cabassa, J., Kaplan, K. A., Li, S. T., Haroon, J., Spohr, H. A., et al. (2001). Sex differences in cocaine-stimulated motor behavior: disparate effects of gonadectomy. *Neuropsychopharmacology* 25, 118–130. doi: 10.1016/S0893-133X(00)00248-7

Yoest, K. E., Cummings, J. A., and Becker, J. B. (2014). Estradiol, dopamine and motivation. *Cent. Nerv. Syst. Agents Med. Chem.* 14, 83–89. doi: 10.2174/1871524914666141226103135

Conflict of Interest Statement: The authors declare that the research was conducted in the absence of any commercial or financial relationships that could be construed as a potential conflict of interest.

frontiers in Pharmacology

BRIEF RESEARCH REPORT
published: 08 April 2019
doi: 10.3389/fphar.2019.00331

Inhibitory Actions of Tropeines on the α3 Glycine Receptor Function

Victoria P. San Martín, Carlos F. Burgos, Ana M. Marileo, Cesar O. Lara, Anggelo Sazo, Jorge Fuentealba, Leonardo Guzmán, Patricio A. Castro, Luis G. Aguayo, Gustavo Moraga-Cid and Gonzalo E. Yévenes**

Department of Physiology, Faculty of Biological Sciences, University of Concepción, Concepción, Chile

Glycine receptors (GlyRs) are chloride-permeable pentameric ligand-gated ion channels. The inhibitory activity of GlyRs is essential for many physiological processes, such as motor control and respiration. In addition, several pathological states, such as hyperekplexia, epilepsy, and chronic pain, are associated with abnormal glycinergic inhibition. Recent studies have pointed out that positive allosteric modulators targeting the GlyR α3 subunit (α3GlyR) displayed beneficial effects in chronic pain models. Interestingly, previous electrophysiological studies have shown that tropeines, which are a family of synthetic antagonists of the serotonin type 3 receptors (5-HT_3Rs), potentiate the activity of GlyRs conformed by α1 subunits. However, despite its importance as a pharmacological target in chronic pain, it is currently unknown whether the α3GlyR function is modulated by tropeines. Using electrophysiological techniques and molecular docking simulations, here we show that tropeines are inhibitors of the α3GlyR function. Tropisetron, a prototypical tropeine, exerted concentration-dependent inhibitory effects on α3GlyRs at the low micromolar range. In addition, three other tropeines showed similar effects. Single-channel recordings show that tropisetron inhibition is associated with a decrease in the open probability of the ion channel. Molecular docking assays suggest that tropeines preferentially bind to an agonist-free, closed state of the ion channel. The tropeine binding occurs in a discrete pocket around the vicinity of the orthosteric site within the extracellular domain of α3GlyR. Thus, our results describe the pharmacological modulation of tropeines on α3GlyRs. These findings may contribute to the development of GlyR-selective tropeine derivatives for basic and/or clinical applications.

Keywords: glycine receptor, tropeines, modulation, ligand-gated ion channels, electrophysiology, molecular docking

OPEN ACCESS

Edited by:
Milica S. Prostran, University of Belgrade, Serbia

Reviewed by:
Gillian Grafton, University of Birmingham, United Kingdom
Thomas Heinbockel, Howard University, United States

****Correspondence:***
Gustavo Moraga-Cid
gumoraga@udec.cl
Gonzalo E. Yévenes
gyevenes@udec.cl

Specialty section:
This article was submitted to Neuropharmacology, a section of the journal Frontiers in Pharmacology

Received: *16 October 2018*
Accepted: *19 March 2019*
Published: *08 April 2019*

Citation:
San Martín VP, Burgos CF, Marileo AM, Lara CO, Sazo A, Fuentealba J, Guzmán L, Castro PA, Aguayo LG, Moraga-Cid G and Yévenes GE (2019) Inhibitory Actions of Tropeines on the α3 Glycine Receptor Function. Front. Pharmacol. 10:331. doi: 10.3389/fphar.2019.00331

INTRODUCTION

Strychnine-sensitive glycine receptors (GlyRs) are anion-selective neurotransmitter-gated inhibitory ion channels. GlyRs belong to the pentameric ligand-gated ion channel superfamily, together with the inhibitory $GABA_A$ receptor and the excitatory nicotinic acetylcholine receptor (nAchR) and serotonin type 3 receptors (5-HT3Rs) (Lynch, 2004; Lynch, 2009; Zeilhofer et al., 2012). In the mammalian CNS, the enhancement of the chloride conductance through GlyR activation results in a transient hyperpolarization of the membrane potential, which contributes to the control of neuronal excitability. The GlyR-mediated inhibition controls critical

neurophysiological functions, such as motor coordination, respiratory control, muscle tone, as well as pain processing. Interestingly, several pathological states, such as hyperekplexia, epilepsy, autism, and chronic pain, have been associated with alterations on glycinergic inhibition (Harvey et al., 2004, 2008; Eichler et al., 2008; Pilorge et al., 2016).

Glycine receptors are pentameric complexes composed of α and β subunits, which can form receptors composed exclusively of α subunits (i.e., homomeric) or of α and β subunits (i.e., heteromeric) (Lynch, 2004; Corringer et al., 2012). Up until now, four α subunits (α1–4) and a single β subunit have been described. Although the α subunits share a high degree of sequence homology, they also exhibit important differences in their biophysical and pharmacological properties as well as in their expression patterns. These specific features are possibly linked to their proposed roles in physiological and pathological states (Lynch, 2009). A single GlyR subunit possesses an extracellular domain (ECD), four transmembrane domains (TM1-4) and an intracellular domain between the TM3 and TM4 domains (ICD). The binding of the neurotransmitter glycine to the ECD triggers the process of receptor activation, which results in the opening of the ion channel pore.

Despite the importance of GlyRs in physiological processes and in disease states, the present state of GlyR pharmacology is still limited (Yévenes and Zeilhofer, 2011; Zeilhofer et al., 2018). To date, only few agonists and antagonists of GlyRs have been characterized. Fortunately, recent studies have significantly expanded the GlyR pharmacology with the characterization of novel glycinergic positive allosteric modulators with analgesic actions in behavioral models of chronic pain (Zeilhofer et al., 2018). These studies pointed out that the potentiation of GlyRs composed of the α3 subunit is required for their *in vivo* analgesic actions. In this context, previous studies have shown that low nanomolar concentrations of several tropeines, which are a family of synthetic antagonists of the 5-HT_3Rs (Haus et al., 2004), potentiate GlyRs composed of α1 subunits (Chesnoy-Marchais, 1996; Supplisson and Chesnoy-Marchais, 2000; Yang et al., 2007; Maksay et al., 2009). However, despite its importance as a pharmacological target in chronic pain, it is currently unknown whether the α3GlyR function is modulated by tropeines in a similar fashion. Defining the actions of this class of ligands on α3GlyRs will elucidate their pharmacological potential as chemical templates for the development of novel glycinergic modulators. Using electrophysiological techniques and molecular docking simulations, here we show that tropeines exerted inhibitory actions on α3GlyRs. In addition, our molecular docking studies suggest that tropeines likely bind to a discrete site near the glycine-binding site, preferentially in an agonist-free closed state of the ion channel.

MATERIALS AND METHODS

Cell Culture and Transfection

HEK 293 cells (CRL-1573; American Type Culture Collection, Manassas, VA, United States) were cultured using standard methods (Lara et al., 2016). The cells were transfected using XfectTM Transfection Reagent (Clontech, United States) using 1.0 μg of cDNA plasmid encoding the α3GlyR subunit and 0.5 μg of EGFP. All recordings were made 24–36 h after transfection.

Electrophysiology

Glycine-evoked currents were recorded from transfected HEK 293 cells in the whole-cell voltage-clamp configuration at room temperature (20–24°C) at a holding potential of −60 mV (Lara et al., 2016). Patch electrodes (3–4 mΩ) were pulled from borosilicate glass and were filled with (in mM): 120 CsCl, 8 EGTA, 10 HEPES (pH 7.4), 4 $MgCl_2$, 0.5 GTP and 2 ATP. The external solution contained (in mM) 140 NaCl, 5.4 KCl, 2.0 $CaCl_2$, 1.0 $MgCl_2$, 10 HEPES (pH 7.4), and 10 glucose. Whole-cell recordings were performed with an Axoclamp 200B amplifier (Molecular Devices, United States) and acquired using Clampex 10.1 software. Data analysis was performed off-line using Clampfit 10.1 (Axon Instruments, Sunnyvale, CA, United States). Exogenous glycine-evoked currents were obtained using a manually applied pulse (3–4 s) of the agonist and an outlet tube (200 μm ID) of a custom-designed gravity-fed microperfusion system (flow rate ≈0.3–0.4 ml/min; exchange rate ≈50–80 ms) positioned 50–100 μm from the recorded cell. The methodologies employed for the single channel recordings of α3GlyRs in cell-attached configuration have been previously published (Marabelli et al., 2013; Lara et al., 2016). The patch pipettes (non-sylgard-coated) had tip resistances of 10–20 mΩ and were manually fire polished in a microforge (Narishige, Japan). The data were filtered (1-kHz low-pass 8-pole Butterworth) and acquired at 5–20 kHz using an Axopatch 200B amplifier and a 1322A Digidata (Axon Instruments, Union City, CA, United States). Data was acquired using pClamp software and analyzed off-line with Clampfit 10.1 (Axon Instruments, Union City, CA, United States). Tropeine stocks were prepared in high purity distilled water and subsequently diluted into the recording solution on the day of the experiment. Tropeines were obtained from AK Science (CA, United States). All other reagents were from Sigma-Aldrich (St. Louis, MO, United States).

Molecular Docking Procedures

Protein-ligand docking was performed using the structures of α3 and α1GlyRs obtained from the Protein DataBank (PDB ID: 5CFB, 5TIO, 3JAD, and 3JAE) (Du et al., 2015; Huang et al., 2015). The structures of tropisetron, granisetron, dolasetron, and ondansetron are available in the PubChem database (CID: 656665, 3510, 3033818, and 4595) and were prepared using LigPrep before docking simulations. All complexes were created with Glide (Schrödinger, LLC, New York, NY, 2016) using a receptor grid centered on the amino acids that form the orthosteric binding site for glycine [(+)F159,Y202,T204,F207, (−)R65,S129, on α3GlyR], and an extra-precision (XP) configuration. Analysis of the interface GlyR-tropeines included structural and energetic parameters performed by the same software. To estimate ligand-binding affinity, a theoretical Gibbs free energy of binding, ΔG_{bind}, was calculated by an energy calculation MM-GBSA using Prime (Schrödinger, LLC, New York, NY, 2016). All images were created using PyMol (v1.5, DeLano Scientific LLC, United States).

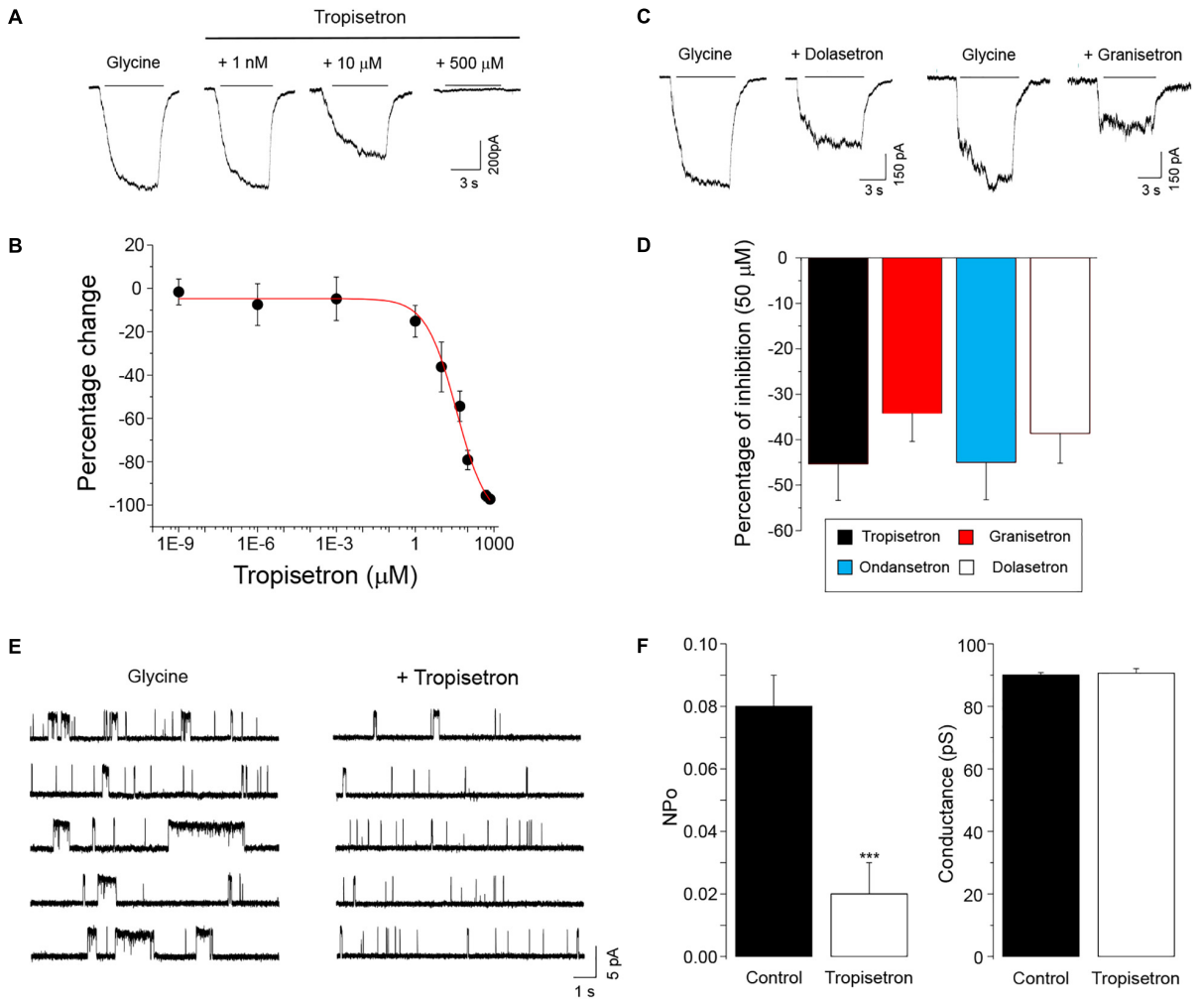

FIGURE 1 | Functional modulation of homomeric α3GlyRs by tropeines. **(A)** Whole-cell current traces evoked by 30–60 μM glycine before and during the application of tropisetron (1 nM, 10 μM, and 500 μM) from a single HEK293 cell expressing α3GlyRs. **(B)** The graph summarizes the effect of different tropisetron concentrations (1 fM–700 μM) on the glycine-activated currents (n = 8). **(C)** Current traces evoked by 30–60 μM glycine before and after the application of 50 μM granisetron and dolasetron from two different HEK293 cells expressing α3GlyRs **(D)** The plot summarizes the effects of 50 μM granisetron (n = 6), ondansetron (n = 8), dolasetron (n = 7) and tropisetron (n = 6) on the glycine-activated currents of α3GlyRs. Differences were not significant (ANOVA followed by Bonferroni *post hoc* test, $F(3,26) = 0.50$). **(E)** Single-channel recordings in the cell-attached configuration from a cell expressing α3GlyRs before and in the presence of 50 μM of tropisetron. **(F)** The graphs show that tropisetron significantly decreased the open probability of α3GlyRs, but did not modify the main conductance (***$P < 0.001$, paired Student t-test; n = 4).

Data Analysis

All values were expressed as mean ± s.e.m of normalized agonist-activated currents. $P < 0.05$ was considered statistically significant. Multiple comparisons were analyzed with ANOVA followed by a Bonferroni *post hoc* test. All the statistical analyses and plots were performed with MicroCal Origin 8.0 (Northampton, MA, United States).

RESULTS

We first examined the sensitivity of the homomeric α3GlyR to different concentrations of tropisetron (also known as ICS-205,930), a prototypical tropeine which is widely used as an anti-emetic drug. Application of tropisetron alone to cells expressing α3GlyRs did not elicit any detectable change in the holding currents, suggesting the absence of agonistic activity (not shown). Using a sub-saturating concentration of glycine (EC_{5-10}) to activate GlyRs, we found that nanomolar concentrations of tropisetron did not modify the amplitude of the chloride currents through α3GlyRs (**Figure 1A**). On the other hand, concentrations of tropisetron above 1 μM exerted a significant inhibitory effect on the α3GlyR activity (**Figures 1A,B**). The concentration-response curve analysis displayed an IC_{50} of 37 ± 11 μM (n = 8), with a maximal inhibition of −97.2 ± 2.1% with 700 μM of tropisetron (n = 8). To obtain additional insights on the chemical determinants associated with the inhibition of

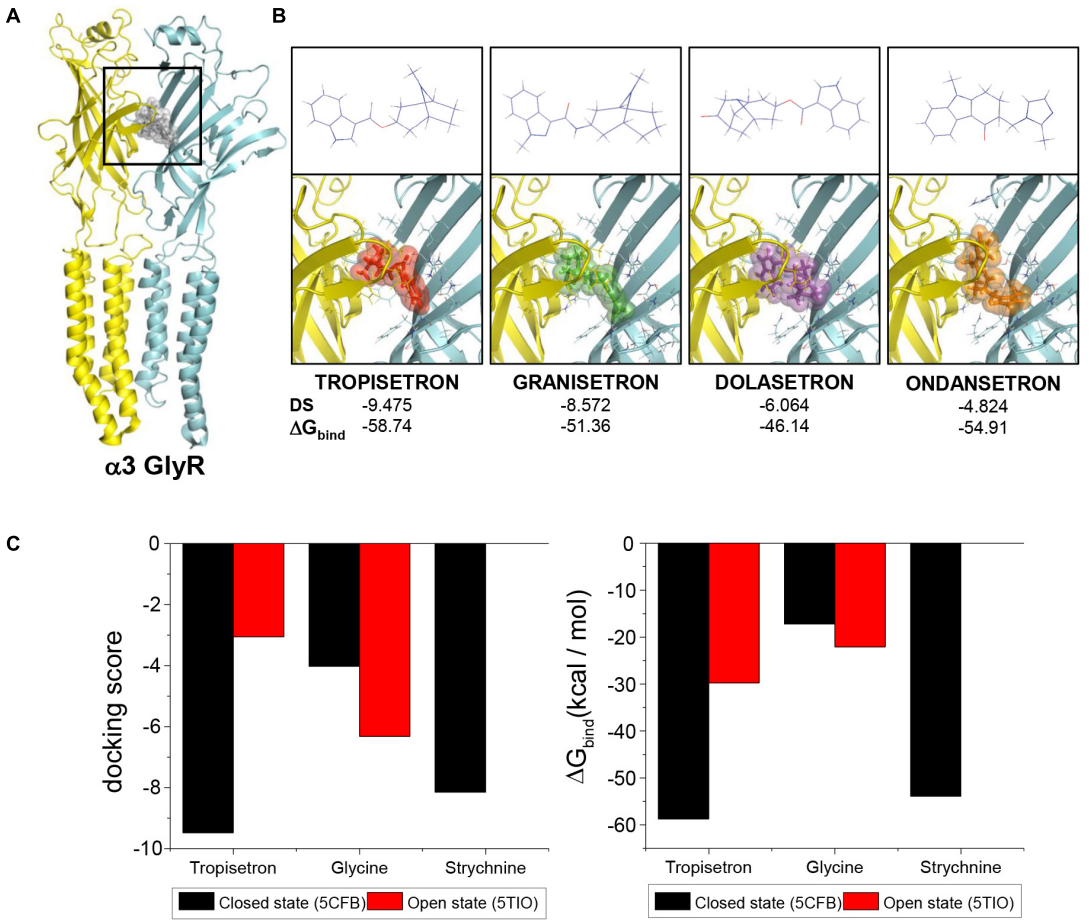

FIGURE 2 | Putative binding sites of tropeines on the extracellular domain of α3GlyRs. **(A)** The α3/α3 dimer in closed conformation (from the 5CFB structure) shows the predicted binding site of the tropeines experimentally tested (gray spheres). Both protein chains are identical and were colored in cyan and yellow. **(B)** 2D structures (upper panels) and binding site on α3GlyR for tropisetron, granisetron, dolasetron, and ondansetron (lower panels). For all complexes, the side chains of the amino acids at 5Å around the modulator and forming part of the binding site are shown. Docking score and ΔG_{bind} values are presented for each compound. **(C)** The graphs compare the docking scores and the theoretical ΔG_{bind} of tropisetron interaction with α3GlyRs in the closed and in the open state. The values obtained from the docking procedures with glycine and strychnine under similar conditions has been added as references.

α3GlyR by tropeines, we next analyzed the effects of three other tropeines on the α3GlyR function. We found that the application of 50 μM of granisetron, ondansetron, and dolasetron exerted a significant inhibition of the glycine-activated currents (**Figures 1C,D**). The extent of inhibition elicited by these compounds was not significantly different to those obtained with an equivalent concentration of tropisetron (**Figure 1D**), suggesting a conserved mechanism of inhibition. To investigate further the mechanism underlying the ion channel modulation, we next studied the tropeine modulation of α3GlyRs by performing single-channel recordings in the cell-attached configuration (**Figures 1E,F**). In agreement with our data obtained using whole-cell currents, the application of 50 μM of tropisetron to membrane patches expressing α3GlyRs significantly decreased the normalized open probability (nPo) by −76 ± 5.5%. On the other hand, tropeine did not elicit any significant change in the ion channel mean amplitude (Control = 5.40 ± 0.05 pA vs. tropisetron = 5.43 ± 0.09 pA, p = 0.65, paired t-test) or main conductance (Control = 90.0 ± 0.7 pS vs. tropisetron = 90.6 ± 1.5 pS, p = 0.59, paired t-test). Collectively, these results are consistent with a mechanism of ion channel inhibition resulting from the direct binding of tropisetron to the α3GlyR structure.

In order to explore the molecular and structural determinants of the tropeine inhibition, we next performed molecular docking assays using the crystal structures of α3GlyR as templates (Huang et al., 2015, 2017). All the tropeines tested were able to interact with the receptor in a favorable and stable manner (**Figures 2A,B**). A more detailed analysis of the binding site for tropeines showed that the amino acids S129, T204, and N42 of α3GlyR can form H-bonds with the modulators, while R65, F159, and F207 generate pi-cation interactions, and E157 forms a salt bridge with tropisetron (**Supplementary Figure S1**). Interestingly, the comparison between closed and open states suggests a significant preference of tropisetron to bind to the

closed conformation of the ion channel (Docking scores, closed state: −9.475; open state: −3.055) (**Figures 2B,C**). In addition, an increase in the theoretical ΔG_{bind} was predicted for the open state complex (−58.74 to −29.75 kcal/mol) (**Figures 2B,C**). The results obtained with tropisetron were similar for the other tropeines examined (**Supplementary Table S1**).

DISCUSSION

The traditional view of GlyR pharmacology comprises a limited number of agonists, antagonists and allosteric modulators (Yévenes and Zeilhofer, 2011; Zeilhofer et al., 2018). An important part of these investigations centered their attention on the α1 subunit of GlyRs, which is widely expressed in the mammalian spinal cord and brainstem. However, due to its relevance in chronic inflammatory pain, the α3GlyR has attracted recent attention as a target for the development of novel analgesics. Several studies have demonstrated that novel compounds such as the propofol analog 2,6-di-tert-butyl phenol (2,6-DTBP), the phytocannabinoid cannabidiol (CBD), the natural alkaloid gelsemine, and the synthetic tricyclic sulfonamide AM-1488 are able to modulate glycine-activated currents through α3GlyRs (Xiong et al., 2012; Acuña et al., 2016; Lara et al., 2016; Huang et al., 2017; Zeilhofer et al., 2018). Interestingly, although none of these modulators possesses a significant GlyR subunit-selectivity, they were able to reduce chronic pain symptoms in behavioral models. The tropeines examined in our study, similar to many of these modulators, have also been characterized as modulators of other GlyR subunits. Several electrophysiological studies showed that tropisetron potentiated α1GlyR currents at nanomolar concentrations, while higher micromolar concentrations produced inhibition (Chesnoy-Marchais, 1996; Supplisson and Chesnoy-Marchais, 2000; Yang et al., 2007; Maksay et al., 2009). On the other hand, tropisetron only showed inhibitory effects on α2 GlyR activity (Supplisson and Chesnoy-Marchais, 2000). The results of the present work with α3GlyRs are similar to those obtained in studies with α2GlyRs and suggest that tropeines have a conserved mechanism of action on α2 and α3GlyRs. Interestingly, additional molecular modeling and docking simulations showed that the putative binding site of tropisetron is highly conserved between α1 and α3 GlyR subunits (**Supplementary Figure S2**), suggesting a similar drug-receptor interaction at least in a certain concentration range. Considering all of the above, it appears that the mechanisms underlying the divergence on the functional modulation elicited by tropisetron in α1GlyRs versus α2/α3GlyRs are linked to the allosteric transitions associated to the ion channel gating rather than differential binding modes of tropeines. Although the presence of more than one binding site of tropeines to GlyRs cannot be ruled out without further experimental evidence, we speculate that some GlyR configurations with very similar tropeine binding modes may trigger differential allosteric transitions, favoring a tropeine-dependent potentiation or a tropeine inhibition. Future studies may help to define a more comprehensive view of the mechanisms underlying the differential effects of tropeines on GlyRs of diverse composition.

CONCLUSION

The present work describes the sensitivity of homomeric α3GlyRs to tropeines. Our results provide additional insights on the molecular mechanisms associated with the modulation of GlyRs by tropeines. A better understanding of the structural basis involved in the tropeine-GlyR interactions may contribute to the design of novel tropeine-based derivatives for basic and/or clinical applications.

AUTHOR CONTRIBUTIONS

VSM, CB, CL, AM, AS, and GM-C performed the research. JF, LG, PC, LA, GM-C, and GY designed the research and contributed with analytical tools. VSM, CB, CL, AM, GM-C, and GY analyzed the data. GM-C and GY wrote the manuscript. All authors read and approved the final version of the manuscript.

FUNDING

This work was supported by grant FONDECYT 1170252 (to GY), FONDECYT 1160851 (to GM-C), and FONDECYT 3170108 (to CB). CL and AM were supported by CONICYT doctoral fellowships 21171549 and 21181287, respectively. VSM and AS were supported by the University of Concepción postgraduate fellowships (Ph.D. Program in Biological Sciences and Master Program in Neurobiology, respectively).

ACKNOWLEDGMENTS

The authors thank L. Aguayo, I. Cid, and J. Gavilán for their outstanding technical assistance.

SUPPLEMENTARY MATERIAL

The Supplementary Material for this article can be found online at: https://www.frontiersin.org/articles/10.3389/fphar.2019.00331/full#supplementary-material

FIGURE S1 | Ligand interaction diagrams of tropeines with the extracellular domain of α3GlyR. A detailed analysis of the amino acids involved in the formation and stabilization of α3GlyR complexes with **(A)** tropisetron, **(B)** granisetron, **(C)** dolasetron, and **(D)** ondansetron. All detected interactions are described in the inner box. All detected interactions between α3GlyR and each molecule are described in the inner box with a cutoff of 4Å from the receptor. Hydrogen bonds are partially electrostatic interactions between a hydrogen atom bound to an electronegative group and an atom or a group of atoms, which acts an acceptor. In the tropeine-α3GlyR interaction, S129, T204 act as hydrogen-bond donors, while the N42 acts as an acceptor. Pi-cation interactions are non-covalent interactions that occurs between a charged group with an electron-rich π group, like aromatic rings. Pi-cation interactions were obserbed between R65, F159, and

F207 with tropisetron and granisetron. A salt bridge combines hydrogen bonds and ionic pairing. A salt bridge between the negative charged side chain of E157 with the NH2+ of several tropeines was observed. All analysis was performed using Maestro (Schrödinger, LLC, New York, NY, 2016).

FIGURE S2 | Putative binding sites of tropeines on the extracellular domain of α1GlyRs. **(A)** The α1/α1 dimer in closed conformation (from the 3JAD structure) shows the predicted binding site for all tropeines tested (in gray spheres). Both chains are identical and were colored in light blue and pale yellow for representative purposes **(B)** 2D structure and binding sites of tropisetron, granisetron, dolasetron and ondansetron on α1GlyR. For all complexes, the side chains of the amino acids at 5Å around the modulator and forming part of the binding site are shown. Docking score and ΔG_{bind} are presented for each compound. ΔG_{bind} values were calculated using the equation $G = E_{bond} + E_{electrostic} + E_{vdW} + G_{pol} + G_{np} - TS$, where G_{pol} corresponds to the solvation free energy obtained by using the generalized Born (GB) model, and Gnp is an estimation from solvent accessible surface area (SASA).

TABLE S1 | Characterization of the complexes generated between the tropeines and α3GlyRs in closed / open state. Docking score and ΔG_{bind} calculated for complexes generated using the 5CFB (closed) and 5TIO (open) structures of α3GlyR. Values for glycine and strychnine obtained using a protocol similar to tropeines have been added as references.

REFERENCES

Acuña, M. A., Yévenes, G. E., Ralvenius, W. T., Benke, D., Di Lio, A., Lara, C. O., et al. (2016). Phosphorylation state–dependent modulation of spinal glycine receptors alleviates inflammatory pain. *J. Clin. Invest.* 126, 2547–2560. doi: 10.1172/JCI83817

Chesnoy-Marchais, D. (1996). Potentiation of chloride responses to glycine by three 5-HT3 antagonists in rat spinal neurones. *Br. J. Pharmacol.* 118, 2115–2125. doi: 10.1111/j.1476-5381.1996.tb15651.x

Corringer, P. J., Poitevin, F., Prevost, M. S., Sauguet, L., Delarue, M., and Changeux, J. P. (2012). Structure and pharmacology of pentameric receptor channels: from bacteria to brain. *Structure* 20, 941–956. doi: 10.1016/j.str.2012.05.003

Du, J., Lü, W., Wu, S., Cheng, Y., and Gouaux, E. (2015). Glycine receptor mechanism elucidated by electron cryo-microscopy. *Nature* 526, 224–229. doi: 10.1038/nature14853

Eichler, S. A., Kirischuk, S., Jüttner, R., Schafermeier, P. K., Legendre, P., Lehmann, T. N., et al. (2008). Glycinergic tonic inhibition of hippocampal neurons with depolarizing GABAergic transmission elicits histopathological signs of temporal lobe epilepsy. *J. Cell. Mol. Med.* 12, 2848–2866. doi: 10.1111/j.1582-4934.2008.00357.x

Harvey, R. J., Depner, U. B., Wässle, H., Ahmadi, S., Heindl, C., Reinold, H., et al. (2004). GlyR α3: an essential target for spinal PGE2-mediated inflammatory pain sensitization. *Science* 304, 884–887. doi: 10.1126/science.1094925

Harvey, R. J., Topf, M., Harvey, K., and Rees, M. I. (2008). The genetics of hyperekplexia: more than startle! *Trends Genet.* 24, 439–447. doi: 10.1016/j.tig.2008.06.005

Haus, U., Späth, M., and Färber, L. (2004). Spectrum of use and tolerability of 5-HT3 receptor antagonists. *Scand. J. Rheumatol. Suppl.* 199, 12–18. doi: 10.1080/03009740410006961

Huang, X., Chen, H., Michelsen, K., Schneider, S., and Shaffer, P. L. (2015). Crystal structure of human glycine receptor-alpha3 bound to antagonist strychnine. *Nature* 526, 277–280. doi: 10.1038/nature14972

Huang, X., Shaffer, P. L., Ayube, S., Bregman, H., Chen, H., Lehto, S. G., et al. (2017). Crystal structures of human glycine receptor α3 bound to a novel class of analgesic potentiators. *Nat. Struct. Mol. Biol.* 24:108. doi: 10.1038/nsmb.3329

Lara, C. O., Murath, P., Muñoz, B., Marileo, A. M., San Martín, L., San Martín, V. P., et al. (2016). Functional modulation of glycine receptors by the alkaloid gelsemine. *Br. J. Pharmacol.* 173, 2263–2277. doi: 10.1111/bph.13507

Lynch, J. W. (2004). Molecular structure and function of the glycine receptor chloride channel. *Physiol. Rev.* 84, 1051–1095. doi: 10.1152/physrev.00042.2003

Lynch, J. W. (2009). Native glycine receptor subtypes and their physiological roles. *Neuropharmacology* 56, 303–309. doi: 10.1016/j.neuropharm.2008.07.034

Maksay, G., Laube, B., Schemm, R., Grudzinska, J., Drwal, M., and Betz, H. (2009). Different binding modes of tropeines mediating inhibition and potentiation of α1 glycine receptors. *J. Neurochem.* 109, 1725–1732. doi: 10.1111/j.1471-4159.2009.06083.x

Marabelli, A., Moroni, M., Lape, R., and Sivilotti, L. G. (2013). The kinetic properties of the α3 rat glycine receptor make it suitable for mediating fast synaptic inhibition. *J. Physiol.* 591, 3289–3308. doi: 10.1113/jphysiol.2013.252189

Pilorge, M., Fassier, C., Le Corronc, H., Potey, A., Bai, J., De Gois, S., et al. (2016). Genetic and functional analyses demonstrate a role for abnormal glycinergic signaling in autism. *Mol. Psychiatry* 21:936. doi: 10.1038/mp.2015.139

Supplisson, S., and Chesnoy-Marchais, D. (2000). Glycine receptor β subunits play a critical role in potentiation of glycine responses by ICS-205,930. *Mol. Pharmacol.* 58, 763–770. doi: 10.1124/mol.58.4.763

Xiong, W., Cui, T., Cheng, K., Yang, F., Chen, S. R., Willenbring, D., et al. (2012). Cannabinoids suppress inflammatory and neuropathic pain by targeting α3 glycine receptors. *J. Exp. Med.* 209, 1121–1134. doi: 10.1084/jem.20120242

Yang, Z., Ney, A., Cromer, B. A., Ng, H. L., Parker, M. W., and Lynch, J. W. (2007). Tropisetron modulation of the glycine receptor: femtomolar potentiation and a molecular determinant of inhibition. *J. Neurochem.* 100, 758–769. doi: 10.1111/j.1471-4159.2006.04242.x-

Yévenes, G. E., and Zeilhofer, H. U. (2011). Allosteric modulation of glycine receptors. *Br. J. Pharmacol.* 164, 224–236. doi: 10.1111/j.1476-5381.2011.01471.x

Zeilhofer, H. U., Acuña, M. A., Gingras, J., and Yévenes, G. E. (2018). Glycine receptors and glycine transporters: targets for novel analgesics? *Cell. Mol. Life Sci.* 75, 447–465. doi: 10.1007/s00018-017-2622-x

Zeilhofer, H. U., Wildner, H., and Yévenes, G. E. (2012). Fast synaptic inhibition in spinal sensory processing and pain control. *Physiol. Rev.* 92, 193–235. doi: 10.1152/physrev.00043.2010

Conflict of Interest Statement: The authors declare that the research was conducted in the absence of any commercial or financial relationships that could be construed as a potential conflict of interest.

frontiers in Pharmacology

ORIGINAL RESEARCH
published: 13 June 2019
doi: 10.3389/fphar.2019.00612

Differential Effects of Purinergic Signaling in Gastric Cancer-Derived Cells Through P2Y and P2X Receptors

*María José Hevia[1†], Patricio Castro[1,2†], Katherine Pinto[1], Mauricio Reyna-Jeldes[1], Felipe Rodríguez-Tirado[3], Claudia Robles-Planells[3], Sebastián Ramírez-Rivera[1], Juan Andrés Madariaga[1,4], Felipe Gutierrez[4], Javier López[1,4], Marcelo Barra[1,4], Erwin De la Fuente-Ortega[1], Giuliano Bernal[1] and Claudio Coddou[1]**

[1] Departamento de Ciencias Biomédicas, Facultad de Medicina, Universidad Católica del Norte, Coquimbo, Chile, [2] Departamento de Fisiología, Facultad de Ciencias Biológicas, Universidad de Concepción, Concepción, Chile, [3] Departamento de Biología, Facultad de Ciencias, Universidad de Chile, Santiago, Chile, [4] Hospital San Pablo, Coquimbo, Chile

OPEN ACCESS

Edited by:
Ramón Sotomayor-Zárate, University of Valparaíso, Chile

Reviewed by:
Philippe Séguéla, McGill University, Canada
Pablo R. Moya, University of Valparaíso, Chile

***Correspondence:**
Claudio Coddou
ccoddou@ucn.cl

[†]These authors have contributed equally to this work.

Specialty section:
This article was submitted to Translational Pharmacology, a section of the journal Frontiers in Pharmacology

Received: *14 March 2019*
Accepted: *15 May 2019*
Published: *13 June 2019*

Citation:
Hevia MJ, Castro P, Pinto K, Reyna-Jeldes M, Rodríguez-Tirado F, Robles-Planells C, Ramírez-Rivera S, Madariaga JA, Gutierrez F, López J, Barra M, De la Fuente-Ortega E, Bernal G and Coddou C (2019) Differential Effects of Purinergic Signaling in Gastric Cancer-Derived Cells Through P2Y and P2X Receptors. Front. Pharmacol. 10:612. doi: 10.3389/fphar.2019.00612

Gastric cancer (GC) is the one of the most prevalent cancers and one of the leading causes of cancer-induced deaths. Previously, we found that the expression of purinergic $P2Y_2$ receptor ($P2Y_2R$) is increased in GC samples as compared to adjacent healthy mucosa taken from GC-diagnosed patients. In this work, we studied in detail purinergic signaling in the gastric adenocarcinoma-derived cell lines: AGS, MKN-45, and MKN-74, and compared them to a nontumoral epithelial cell line: GES-1. In GC-derived cells, we detected the expression of several purinergic receptors, and found important differences as compared to GES-1 cells. Functional studies revealed a strong contribution of $P2Y_2$Rs in intracellular calcium increases, elicited by adenosine-triphosphate (ATP), uridine-triphosphate (UTP), and the $P2Y_2R$ agonist MRS2768. Responses were preserved in the absence of extracellular calcium and inhibited by $P2Y_2R$ antagonists. In GES-1 cells, ATP and UTP induced similar responses and the combination of P2X and P2Y receptor antagonists was able to block them. Proliferation studies showed that ATP regulates AGS and MKN-74 cells in a biphasic manner, increasing cell proliferation at 10–100 μM, but inhibiting at 300 μM ATP. On the other hand, 1–300 μM UTP, a $P2Y_2R$ agonist, increased concentration-dependent cell proliferation. The effects of UTP and ATP were prevented by both wide-range and specific purinergic antagonists. In contrast, in GES-1 cells ATP only decreased cell proliferation in a concentration-dependent manner, and UTP had no effect. Notably, the isolated application of purinergic antagonists was sufficient to change the basal proliferation of AGS cells, indicating that nucleotides released by the cells can act as paracrine/autocrine signals. Finally, in tumor-derived biopsies, we found an increase of $P2Y_2R$ and a decrease in P2X4R expression; however, we found high variability between seven different biopsies and their respective adjacent healthy gastric mucosa. Even so, we found a correlation between the expression levels of $P2Y_2R$ and P2X4R and survival rates of GC patients. Taken together, these results demonstrate the involvement of different purinergic receptors and signaling in GC, and the pattern of expression changes in tumoral cells, and this change likely directs ATP and nucleotide signaling from antiproliferative effects in healthy tissues to proliferative effects in cancer.

Keywords: gastric cancer, P2Y receptor, P2X receptor, ATP, uridine triphosphate (UTP), paracrine action

INTRODUCTION

Cancer, or malignant tumors, comprises a group of diseases that involve abnormal cell growth and proliferation and is a leading cause of death worldwide. Several factors can trigger the development and spread of malignant tumors, including tobacco use, obesity, alcohol consumption, infectious pathogens, exposure to ionizing radiation, and genetic factors, resulting in a complex pathophysiology and treatment. This pathology can be developed in various tissues and cell types, and among these, gastric cancer (GC) is the leading cause of cancer-induced deaths in Chile with an estimated mortality of 20/100,000 inhabitants (25.1/100,000 males and 13.2/100,000 females) for the last 10 years (Heise et al., 2009). Patients with early GC manifest symptoms that are indistinguishable from patients suffering from other benign diseases. These symptoms include anemia, dysphagia, or/and weight loss. Correspondingly, the majority of patients with advanced GC show symptoms including recurrent abdominal pain, anemia, weight loss, vomiting, and anorexia (Minsal, 2014). For this reason, it is desirable to develop therapeutic strategies to treat GC, as well as techniques that can predict risk of disease.

Nucleoside triphosphates such as adenosine-triphosphate (ATP) and uridine-triphosphate (UTP) are crucial for several metabolic processes and provide the energy necessary to carry all cellular processes. In addition to their crucial roles in cell metabolism, these molecules are also released into the extracellular space where they act as signaling molecules, activating various types of membrane receptors, which are termed purinergic receptors. These receptors include P2Y receptors (P2YRs), which are G-protein coupled (Abbracchio et al., 2006; Coddou et al., 2011; Jacobson et al., 2012) and P2X receptors (P2XRs), which are ATP-gated ionic channels that promote rapid depolarization as a consequence of cation influx through their cationic-selective pore (Coddou et al., 2011). Eight P2YR and seven P2XR subtypes have been identified (Abbracchio et al., 2006; Coddou et al., 2011; Jacobson et al., 2012). There is also a family of P1 G-protein coupled receptors that is activated by the purine nucleoside adenosine, the final product of ATP degradation by ectonucleotidases (Abbracchio et al., 2006; Jacobson et al., 2012).

Purinergic signaling is involved in several physiological and pathophysiological processes; ATP and other nucleotides can be released from most cell types in response to different stimuli and act as a paracrine or autocrine signal, or can be stored and released by vesicles which contain ATP together with other transmitters such as noradrenaline, neuropeptide Y, or acetylcholine in the peripheral nervous system, or with dopamine, gamma-aminobutyric acid (GABA) or glutamate in the central nervous system (Burnstock, 2013). Consistently, the actions of ATP as an extracellular signaling molecule can have short-term effects, for example in synaptic transmission, neuromodulation, and secretion, or long-term or trophic effects that include cell proliferation, differentiation, and death. Purinergic signaling and its receptors are present in several pathologies, including cancer, and there is a renewed effort to explore and develop therapies that affect purinergic signaling cascades. Nucleotides are abundant in the tumor microenvironment, especially ATP and adenosine, and this is in concordance with the proposed role of ATP as a danger signal and its participation in inflammatory processes (Di Virgilio, 2012). It has been shown in tumors that ATP accumulates in the extracellular space: the source of ATP can be either by leakage through damaged membranes or mediated by specific ATP transport across the plasma membrane. Moreover, recent studies have established that ATP is not only released by inflammatory-related processes, but also by processes directly related to cancer cell metabolism and antitumor immunity (Ghiringhelli et al., 2009). The final effect of extracellular ATP accumulation results in either increased or decreased tumor growth. The final response depends on several factors including the final concentration of ATP, degradation rate to adenosine, and the specific subtypes of purinergic receptors expressed in each particular type of tumor, and by its associated inflammatory cells (Di Virgilio, 2012). Purinergic signaling also controls the proliferation, growth, differentiation, and possibly metastasis of tumors due to its long-term or trophic effects. These effects are consequences of the activation of different signal transduction pathways that can lead to the generation of second messengers or activation of protein kinases or phosphatases which activate specific genes that are responsible for long-term effects (Burnstock and Verkhratsky, 2010). There is abundant evidence of the role of long-term purinergic signaling regulating proliferation. This evidence includes tumors from prostate, bladder, melanoma, and breast, among other organs (White and Burnstock, 2006). In most cases, but not all, P2YRs receptors are involved in proliferation-related events, while P2XRs mediate differentiation and cell death (White and Burnstock, 2006). In addition, purinergic signaling has been postulated to play an important role in the tumor microenvironment, participating in processes such as immunosuppression and in other normal/tumor cells interactions (Di Virgilio et al., 2018). High amounts of ATP are present in the tumor microenvironment and cancer cells have developed several strategies to use this ATP and the purinergic receptors involved to promote tumor growth and propagation, and to even suppress immune responses against cancer cells (Di Virgilio et al., 2018).

However, there is no information about the potential role of purinergic signaling in GC. A recent study from our group reported a significant increase in the expression of the $P2Y_2R$ in tumor biopsies from GC patients (Aquea et al., 2014). The results shown here not only indicate that there is a dramatic change in the expression profile of purinergic receptors in GC cells, but also suggest that purinergic signaling could be an important player in the pathophysiology of GC, reflected in the changes in proliferation of GC cells when purinergic signaling is pharmacologically manipulated. Thus, purinergic signaling could constitute a novel target for GC treatment.

MATERIALS AND METHODS

Cell Culture

HEK293 and AGS cells were obtained from ATCC (Manassas, VA, United States); MKN-45 and MKN-74 cells were obtained from Riken Bank (Tsukuba, Ibaraki, Japan); GES-1 cells were kindly donated by Dr. Dawit Kidane (University of Texas at Austin, USA). Cell lines were maintained under regular cell culture conditions:

Dulbecco's modified Eagle's medium (DMEM)-High-glucose for human embryonic kidney 293 cells (HEK293) and GES-1 (Gibco, NY, United States); F-12K for AGS cells (Corning, NY, United States); and RPMI 1640 for MKN-45 and MKN-74 cells (Corning, NY, United States). All cellular media was supplemented with 10% fetal bovine serum (Biological Industries, Kibbutz Beit-Haemek, Israel), 100 IU/mL penicillin G, and 100 µg/mL streptomycin sulfate (Sigma-Aldrich, St. Louis, MO, United States) and antibiotics. Cell lines were routinely subcultured after 4 days, and experiments were performed between the 8th and 30th passage. Transfection of AGS cells with P2X4R complementary DNA (cDNA) was conducted 24 h after plating the cells using 2 µg of deoxyribonucleic acid (DNA) and 5 µl of LipofectAMINE 2000 reagent (Invitrogen) in 2 ml of serum-free Opti-MEM. After 4.5 h of incubation, the transfection mixture was replaced with normal culture medium. Experiments were performed 24–48 h after transfection.

Polymerase Chain Reaction

Total RNA was isolated from HEK293, AGS, and GES cells using TRIsure (Bioline, USA) following the manufacturer's specifications. Briefly, cell samples were resuspended with 1 mL of TRIsure in RNase-free sterile tubes on ice and 200 µL of chloroform was added to each tube. The mixtures were vortexed for 30 s and centrifuged at 15,000 g for 15 min at 4°C. The aqueous phase was recovered and total RNA was precipitated with cold isopropanol (Merck, Darmstadt, Germany). Samples were centrifuged, and pellets were washed with 75% v/v ethanol–water diethyl pyrocarbonate (DEPC). Finally, RNA pellets were dried and dissolved in RNAse/DNAse free ultrapure water. Concentration was measured by ultraviolet–visible (UV-vis) spectrophotometry [Nanoquant Infinite M200 pro (TECAN, Männedorf, Switzerland)], and integrity was analyzed by electrophoresis on agarose gels. RNA (2 µg) was treated with RQ1 RNase-free DNase (Promega Corporation, Madison, WI, USA) in a final volume of 20 µl, and cDNA synthesis was performed using Moloney Murine Leukemia Virus (M-MLV) reverse transcriptase and oligo dT (Promega, Madison, WI, USA) according to the manufacturer's protocol in a final volume of 40 µl.

Polymerase chain reactions (PCRs) were carried out using GoTaq Green Master Mix (Promega) in Stratagene Mx 3000p equipment (Agilent Technologies, Santa Clara, CA, USA). PCR primer sequences are listed in **Table 1**. Reactions were performed using 7.5 µL of GoTaq Green Master Mix, 0.5 µL of forward and reverse primer (10 µM), 1 µL of cDNA (200 ng), and 5.5 µL of ultrapure water (Gibco). Cycling conditions were: 95°C for 2 min, followed by 35 cycles consisting of 95°C for 35 s, 53–55°C for 35 s and 72°C for 1 min, with a final extension step of 72°C for 2 min. PCR product was confirmed on agarose gels with Gel Red (Biotium, Freemont, CA, USA).

TABLE 1 | Primers for conventional polymerase chain reaction (PCR).

Gene	Sequence	Amplicon size
P2X1R	FP- 5′ -CCCACCATGGCACGGCGGT- 3′	767
	RP- 5′ -CCAACCACTCCACCCTTCTCA- 3′	
P2X2R	FP- 5′ -TCCACTTCTCCAAGGGCAAC- 3′	633
	RP- 5′ -AGTTGATAATGACCCCGATGAC- 3′	
P2X3R	FP- 5′ -TACGGGACACAGCCATTG- 3′	733
	RP- 5′ -CGGTACTCACTGCCATTT- 3′	
P2X4R	FP- 5′ -CACCCACAGCAACGGAGTCT- 3′	793
	RP- 5′ -TTTGATGGGGCTGTGGAGAG- 3′	
P2X5R	FP- 5′ -AACGTCTGTGCTGAGAATGAAG- 3′	280
	RP- 5′ -TCACATTGCTTTTGGAGAAGTTGA- 3′	
P2X6R	FP- 5′ -GGTCTATGTGGTAGGGTGGG- 3′	209
	RP- 5′ -GCGTCACAAGGAAGTTGGTC- 3′	
P2X7R	FP- 5′ -CTGCTGTCGCTCCCATATT- 3′	217
	RP- 5′ -CGCAGGTCTTGGGACTTCTT- 3′	
$P2Y_1R$	FP- 5′ -CTGTATCAGCGTGCTGGTGT- 3′	517
	RP- 5′ -TTTCCTTGTGGCTCGGGAGA- 3′	
$P2Y_2R$	FP- 5′ -TCCTGTTTCCCGCAGAGTTC- 3′	306
	RP- 5′ -CCATCCCAGGTGCCATTGAT- 3′	
$P2Y_4R$	FP- 5′ -CGTGCCCAACCTGTTCTTTG- 3′	537
	RP- 5′ -CAGCTGCTATCCTCAGGCAG- 3′	
$P2Y_6R$	FP- 5′ -ACACTCCTGATATGTCTCTCGG- 3′	616
	RP- 5′ -GCATAGAAGAGGAAGCGGACC- 3′	
$P2Y_{11}R$	FP- 5′ -CATCACCTGCATCAGCCTCA- 3′	195
	RP- 5′ -CTGGCCACGCTGCAGTT- 3′	
$P2Y_{12}R$	FP- 5′ -TTACACCCTGAGCCAAACCC- 3′	184
	RP- 5′ -TGCAGAATTGGGGCACTTCA- 3′	
$P2Y_{13}R$	FP- 5′ -TCCTAATGCTTGTGTTTTATGTGGT- 3′	160
	RP- 5′ -CTGGCAAAATGAAATGGAGCA- 3′	
$P2Y_{14}R$	FP- 5′ -TGCCAGAATCCCCTACACAA- 3′	163
	RP- 5′ -GATTTCCCTAAACGGCTGGC- 3′	

Real-Time qPCR

Analysis by real-time quantitative PCR (RT-qPCR) was performed to compare the level of gene expression of $P2Y_2R$ and P2X4R receptor from gastric mucosa from patients diagnosed with GC, obtained from the Hospital San Pablo, Coquimbo. Biopsies from both tumoral and adjacent healthy mucosa were obtained from each patient, and protocols were approved by the Ethical-Scientific Committee of the Faculty of Medicine of the Universidad Católica del Norte (CECFAMED-UCN). Patients voluntarily signed the respective informed consent form. Additionally we performed RT-qPCR analyses for P2X4R, P2X7R, $P2Y_1R$, $P2Y_2R$, and $P2Y_4R$ for the GC-derived cell lines AGS, MKN-45, and MKN-74 and compared expression levels to the gastric mucosa-derived cell line GES-1. Total RNA was extracted using RNeasy Mini Kit (Qiagen), and each experiment was performed in triplicate. First-strand cDNA was synthesized from 500 ng of total RNA with Affinity Script QPCR cDNA Synthesis Kit (Agilent Technologies). Gene-specific primers for purinergic receptors were designed using Primer 3 software (http://bioinfo.ut.ee/primer3-0.4.0/) to have melting temperatures of 60°C and to generate PCR products of approximately 100–200 bp. β2-Microglobulin gene (B2M) was used as an endogenous control to normalize experimental results. We chose B2M as our housekeeping gene because although variations in B2M have been observed in other cancer types, in our GC biopsies their expression has not been affected like in other housekeeping genes such as β-actin (Aquea et al., 2014). Information about the primer sequences is shown in **Table 2**. Primers were designed using Primer-Blast software from National Center for Biotechnology Information (NCBI), and efficiency was calculated from the slope of each standard curve, finding efficiency values between 90% and 101% obtained for all genes evaluated. Each qPCR contained 12.5 µL of 2× Brilliant II SYBR Green QPCR Master Mix (Agilent Technologies), 10 ng cDNA, and 0.45 µM (final concentration) of

TABLE 2 | Primers for real-time quantitative PCR (qPCR).

Gene	Sequence	Amplicon size
P2X4R	FP- 5′ -ACTATGATCAACATCGGCTCTG- 3′ RP- 5′ -CTAGCAAGACCCTGCTCGTAAT- 3′	149
P2X7R	FP- 5′ -CCAGTCACCAAACATGAGAGAG- 3′ RP- 5′ -GTTCCAGTTACCTGTTGCTGTG- 3′	180
$P2Y_1R$	FP- 5′ -TCGGTTACTGCTGCTTAGTTCTAC- 3′ RP- 5′ -TGAACTCGCTGGTAGTGTGTTAC- 3′	118
$P2Y_2R$	FP- 5′ -CTGGTAGCGAGAACACTAAGGAC- 3′ RP- 5′ -TTTGATGGGGCTGTGGAGAG- 3′	190
$P2Y_4R$	FP- 5′ -TTCATCTTCCGCCTCCGACC- 3′ RP- 5′ -GGCAGCGACAGCACATACAA- 3′	89
B2M	FP- 5′ -AGATGAGTATGCCTGCCGTG- 3′ RP- 5′ -TCATCCAATCCAAATGCGGC- 3′	120

each primer, in a final volume of 25 µl. RT-qPCR reactions were run at the Applied Biosystems StepOne™ (Applied Biosystems). QPCR conditions were as follows: initial denaturing for 10 min at 95°C, followed by 35 cycles of 10 s at 95°C, 45 s at 60°C, 60 s at 95°C, followed by 30 s at 60°C and 30 s at 95°C. The comparative 2(-ΔΔCT) method was used to quantify the relative abundance of transcripts (Livak and Schmittgen, 2001).

Protein Extraction and Western Blot Analysis

AGS or GES-1 cells were washed twice with phosphate-buffered saline (PBS) at 4°C and lysis buffer containing 50 mM Tris-HCl (pH 7.5), 0.1 M NaCl, 50 mM $MgCl_2$, and 1% Triton X-100 with complete protease inhibitors (Thermo Scientific™, Waltham, MA, United States). Protein concentrations were determined using a bicinchoninic acid (BCA) protein assay (Thermo Scientific™). Equal amounts of total protein were loaded and separated by sodium dodecyl sulfate–polyacrylamide gel electrophoresis (SDS-PAGE) gel electrophoresis, and then were transferred to polyvinylidene fluoride (PVDF) membranes (Thermo Scientific™). Membranes were blocked with buffer [5% nonfat dry milk in Tris-buffered saline (TBS) with 0.05% Tween-20 (TBS-T)] at room temperature for 1 h. Blots were incubated with primary antibodies against P2X4R, P2X7R, $P2Y_2R$, $P2Y_1R$ (Alomone Labs, Jerusalem, Israel), and β-actin (Sigma-Aldrich, St. Louis, MO, USA) at 4°C overnight. The blots were washed with TBS-T five times and incubated for 1 h at room temperature with corresponding secondary antibodies diluted in 1% nonfat dry milk blocking buffer. The immunoreactive bands were visualized by enhanced chemiluminescence detection using SuperSignal West Pico (Thermo Scientific™) and imaged with a C-DiGit scanner.

Immunofluorescence Microscopy

Human AGS, GES-1, MKN-45, and MKN75 cells were cultured on glass coverslips in 24-well dishes in their respective culture medium at 37°C (as described above). After cells reached 70–90% confluence, the cells were washed three times with phosphate-buffered saline containing 0.1 mM $CaCl_2$ and 1 mM $MgCl_2$ (PBS-CM), fixed for 20 min at room temperature with 3.7% paraformaldehyde, and quenched for 10 min with 50 mM NH_4Cl. Cells were permeabilized with 0.2% Triton X-100 in PBS-CM for 10 min at room temperature (RT) and blocked with PBS–1% bis(trimethylsilyl)acetamide (BSA) for 30 min. Then cells were incubated with primary antibodies against P2X4R, P2X7R, or $P2Y_2R$ (1:100) (Alomone Labs, Jerusalem, Israel) in a humidified chamber overnight at 4°C. Following incubation, cells were washed three times with PBS and incubated with respective secondary antibodies, Alexa Fluor 488-conjugated goat anti-mouse (or anti-rabbit) antibody (1:500) (Thermofisher Scientific™, Waltham, MA), together with nuclei stain Hoechst 33342 (1:2,000) (Sigma-Aldrich) for 1 h at RT. After washing with PBS, the coverslips were mounted with Prolong (Thermofisher Scientific™, Waltham, MA). Single focal images were taken using Zeiss LSM 800 confocal microscope (Carl Zeiss, Heidelberg, Germany) plan-apochromat 63x/1.46 oil objective. All images for each antibody were acquired under identical condition settings: 16-bit, 1,024 × 1,024 pixels, avoiding signal saturation, pinhole adjusted to 1 Airy unit, gain between 650 and 700 V and laser power ranging from 0.2 to 0.8%. The acquired images were processed generating regions of interest (ROIs) using Zen image software, and figure composition was performed using Adobe Photoshop (CS, Adobe Systems).

Intracellular Calcium Measurements

Cultured AGS or GES-1 cells at 70–85% confluence were loaded with Fluo4-AM (3 µM in dimethyl sulfoxide (DMSO), Molecular Probes, Eugene, OR) for 30 min at 37°C. Cells were washed twice with PBS and incubated for 30 min at 37°C and then mounted in a perfusion chamber that was placed on the stage of a confocal microscope (Zeiss LSM800) at 22–24°C. Purinergic agonists [ATP, UTP, benzoylbenzoyl ATP (BzATP), MRS2768, or α,β methylene ATP (α,β-meATP)] were added at the corresponding time at a final concentration of 100 µM in a bath solution. Cultured cells were briefly illuminated adjusting laser power (≤0.5%) and scan speed (6–7), using the ZEN 2.1 software (Zeiss). ROIs were simultaneously selected on cell somata containing Fuo4 fluorescence (laser excitation 480 nm, emission 510 nm) in a field with more than 150 cells. Images were collected at 2-s intervals during a continuous 12–15 min period. Imaging was carried out in 16-bit (0–65,000 units of fluorescence scale) with highly sensitive GaAsP detector (Zeiss). The Ca^{2+} transients, defined by an amplitude greater than two times the noise level, were acquired and analyzed offline using ZEN blue 2.1 software.

Cell Proliferation Studies

Studies were performed using a Vybrant® 3-(4,5-dimethylthiazol-2-yl)-2,5-diphenyltetrazolium bromide (MTT) Cell Proliferation Assay Kit (Thermo Scientific™, Waltham, MA) in AGS, MKN-45, MKN-74, and GES-1 cells. The MTT assay demonstrates several changes in mitochondrial activity, which are measured by the enzymatic reduction of MTT to formazan (Mosmann, 1983). Measuring the reductive capacity of mitochondria is widely used as evidence of cell metabolic functionality because formazan production is associated with several enzymes including peroxidases, oxidases, and dehydrogenases, which are essential for sustaining life. Therefore, cell proliferation assays are one of the main approaches for assessing cell viability (Prabst et al., 2017). Cells were incubated with 5,000 cells/well in 96-well plates for 24 h.

After this period, conditions were changed by adding purinergic agonists ATP, UTP, ADP (Sigma-Aldrich, St. Louis, MO), MRS2768 (Tocris, Minneapolis, MN) and/or antagonists suramin, pyridoxal phosphate-6-azo(benzene-2,4-disulfonic acid) (PPADS), AR-C 118925XX, BX430, and AZ10606120 dihydrochloride (Tocris, Minneapolis, MN). After an additional 24 h, proliferation was measured by MTT according the provider's protocol. In brief, culture media was replaced with an MTT-containing solution. After a 4-h incubation, 50 μL DMSO was added to the cells and mixed with a pipette. This mix was incubated for 10 min, and absorbance was measured at 540 nm in a NOVOSTAR multiplate reader. Cell viability was determined as a parameter of proliferation using the formula: % cell viability = (OD treatment/OD control) × 100.

Data Analysis

Data was presented as mean ± standard error of at least three different experiments using GraphPad Prism 5.01 software (GraphPad, San Diego, CA). Statistical analyses included nonparametric Mann–Whitney tests and Kruskall–Wallis test followed by the Dunn's multiple comparison test using GraphPad software. Statistical significance was set when $p < 0.05$.

RESULTS

Expression of Purinergic Receptors in Tumoral and Nontumoral Cell Lines

We assessed the expression of purinergic receptors in AGS, a cell line derived from a gastric adenocarcinoma, and GES-1, a cell line derived from normal gastric epithelium cells. In a first approach, we used PCR to evaluate the expression of several purinergic receptors. We found that both cell lines express several purinergic receptors; with the most remarkable difference being that GES-1 cells express more P2X receptors subtypes than AGS cells, which in general express more P2Y receptors (**Figure 1A**). The main purinergic receptors expressed by AGS cells were P2X2R, P2X4R, $P2Y_1R$, $P2Y_2R$, $P2Y_6R$, $P2Y_{11}R$, and $P2Y_{12}R$. Meanwhile, GES-1 cells expressed P2X2R, P2X4R, P2X5R, P2X7R, $P2Y_2R$, $P2Y_4R$, $P2Y_6R$, and $P2Y_{11}R$ (**Figure 1A**). Next, we compared the RNA levels of some P2XRs and P2YRs by qPCR to compare the changes between GES-1 cells, derived from healthy gastric mucosa and the GC cell lines AGS, MKN-45, and MKN-74. **Figure 1B** shows the decrease in expression of P2X4R and P2X7R in GC cell lines, as compared to GES-1 cells. In the case of the $P2Y_2R$, we found an increase in the expression in AGS and MKN-74 cells, but not in MKN-45, whereas the $P2Y_1R$ expression was increased in MKN-74 cells, as compared to GES-1 cells (**Figure 1B**). However, levels of $P2Y_4R$ RNA were relatively similar in all cell lines tested (**Figure 1B**). Then, we directly measured protein expression by Western blot, showing the presence of $P2Y_1R$, $P2Y_2R$, and P2X4R, and the absence of P2X7 in AGS cells (**Figure 1C**). Interestingly, in GES-1 cells, expression of P2X4R was strongly increased when cells were allowed to form a confluent monolayer, resembling the "normal" state of epithelium, whereas the expression of the other purinergic receptors was not affected by cell confluence (**Supplemental Figure 1**). To confirm these results, we performed immunofluorescence experiments as shown in **Figure 2**; these experiments confirmed the expression of the $P2Y_2R$ and the P2X4R in GES-1 and AGS cells; and the expression of P2X7R in GES-1 but not in AGS cells (**Figure 2A**). In addition, we confirmed a strong expression of $P2Y_2R$ and P2X4R in MKN-74 cells as compared to MKN-45 cells that exhibited a very low expression of both receptors (**Figure 2B**). Altogether, these experiments confirmed the expression of purinergic receptors in tumor-derived and healthy mucosa-derived gastric cell lines.

Purinergic Agonists Induce Intracellular Calcium Increases

In order to characterize the functional responses of purinergic receptors, we measured the increase of intracellular calcium ($[Ca^{2+}]_i$) in AGS and GES-1 cells evoked by purinergic agonists. Both ATP and UTP elicited robust increases of $[Ca^{2+}]_i$ in both cell lines. **Figure 3A** shows 2.5D images of a group of AGS and GES-1 cells and the responses evoked by 100 μM ATP, UTP, or BzATP. The percentage of responding AGS cells was 57 ± 4% and 48 ± 6% for ATP and UTP, respectively, whereas in GES-1 the percentage of responding cells was 95 ± 2% and 73 ± 12% for the same agonists (**Figure 3C**). We compared the total response, evoked by purinergic agonists we found that the effects of ATP and UTP were very similar in amplitude, with the difference that ATP induced longer-lasting responses as compared to UTP in both cell lines (**Figure 3B**). When we analyzed individual cell responses we found that ATP and UTP evoked responses with comparable relative amplitudes for the first peak of each spike (**Figure 3D** and **E**); however, the maximum fluorescence of these peaks was higher in AGS as compared to GES-1 cells (**Figure 3E**). In addition, we found a small but significant spontaneous activity in AGS but not in GES-1 cells (**Figure 3A** and **C**); this activity disappeared after removing calcium from the recording extracellular solution (**Figures 4A** and **B**). Interestingly the amplitudes of ATP and UTP evoked very similar responses in AGS cells in the presence or absence of extracellular calcium. However, the number of events was approximately one spike every 5 min in the presence of ATP and calcium, and was reduced to a single spike when extracellular calcium was removed (**Figure 4B**). To test the specific contribution of $P2Y_2R$ in AGS cells we used the specific agonist MRS2768, which evoked robust increases in $[Ca^{2+}]_i$ (**Supplemental Figure 2A**). Other purinergic agonists like α,β-meATP (P2X1 and P2X3 preferring) or BzATP (P2X7 preferring) did not elicit significant effects (**Supplemental Figures 2B** and **C**). These results strongly suggest that these experiments are mainly reflecting the activity of the $P2Y_2R$ and do not reflect potential contributions of P2XRs, such as P2X4R. To corroborate this, we performed recordings in GES-1 cells stimulated with only 100 μM ATP, or preincubated with the P2X4R specific antagonist BX430 (Ase et al., 2015); alone or with the $P2Y_2R$-antagoinist AR-C118925XX. Whereas the application of BX430 has a modest inhibitory effect on the ATP induced increase of $[Ca^{2+}]_i$, the joint application of both BX430 and AR-C118925XX completely inhibited the increase of $[Ca^{2+}]_i$, induced by ATP (**Figure 4C**).

Proliferation Studies in Cell Lines

To determine whether activation of purinergic receptors has consequences in cell proliferation of GC-derived and healthy

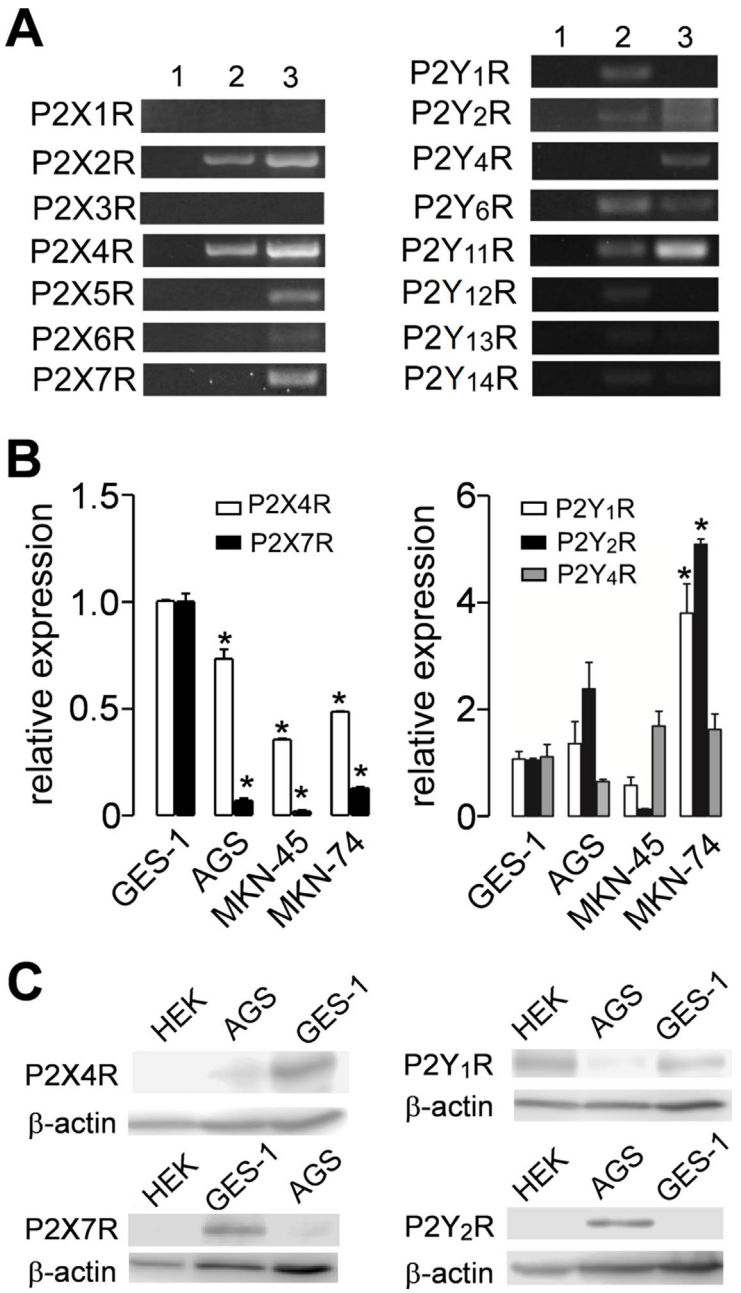

FIGURE 1 | Purinergic receptor pattern expression in normal and cancer-derived cell lines. **(A)** Representative polymerase chain reaction (PCR) from total RNA obtained from AGS (2) or GES-1 (3) cells for P2X receptors (P2XRs) (left) and P2Y receptors (P2YRs) (right). Lane 1 represents a blank control; the data shown is representative of at least three separate experiments. **(B)** Summary of quantitative PCR (qPCR) experiments showing RNA levels of P2X4R and P2X7R (left graph) or $P2Y_1R$, $P2Y_2R$, and P2Y4R (right graph) in control GES-1 cells or in gastric cancer (GC)-derived AGS, MKN-45, or MKN-74 cells. *$p < 0.05$, Kruskal–Wallis and Dunn´s tests. **(C)** Western blot analysis for the expression of P2X4R, P2X7R, $P2Y_1R$, $P2Y_2R$, and β-actin in HEK293, AGS, and GES-1 cells. Blots are representative of three different experiments.

gastric cell lines, we performed MTT cell viability assays. We first evaluated the effects of ATP, the endogenous ligand of purinergic receptors, and measured the changes in cell proliferation. In AGS and MKN-74 cells, ATP induced a biphasic response; whereas 1–100 μM increased cell viability, 300 μM ATP caused a 25% decrease in cell viability, as compared to their respective untreated control cells (**Figure 5A**). On the other hand, MKN-45 and GES-1 cells were only inhibited by 10–300 μM ATP in a concentration-dependent manner (**Figure 5A**). In another set of experiments, we evaluated the effects of UTP, a specific agonist for $P2Y_2R$ and $P2Y_4R$. With this agonist no inhibition was observed, only an increase of cell viability at 1–300 μM UTP in

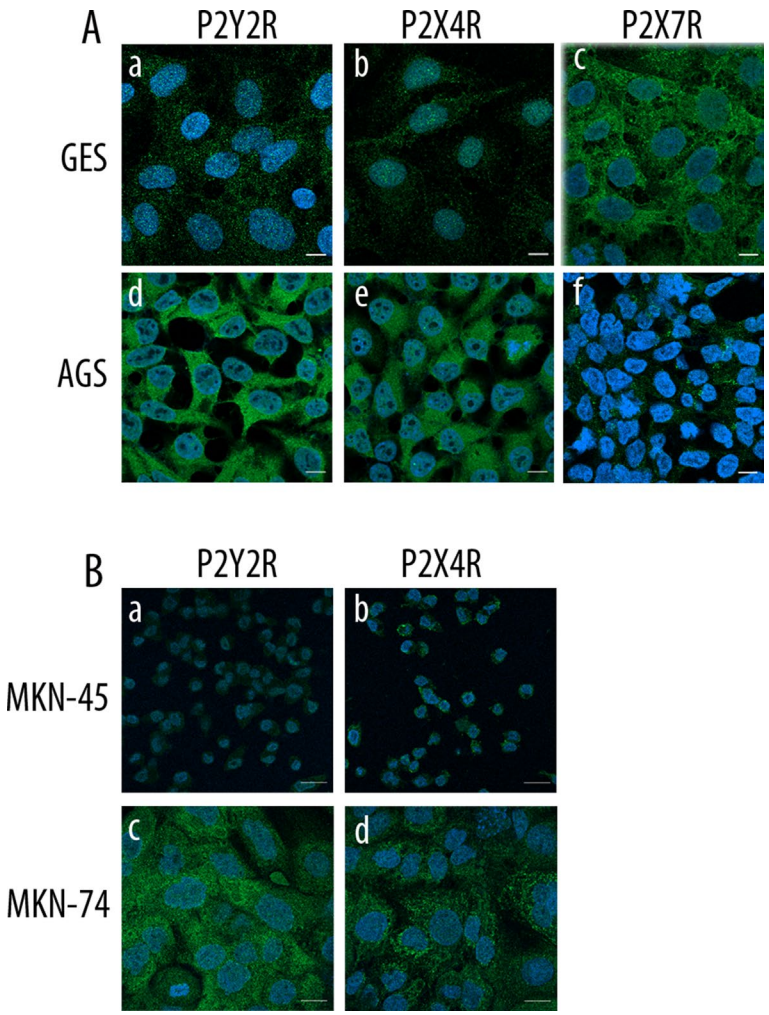

FIGURE 2 | Protein expression of purinergic receptors in normal and cancer-derived cell lines. **(A)** Confocal images from GES-1 and AGS cells showing immunofluorescence for $P2Y_2R$, P2X4R, and P2X7R; scale bar 10 μm. **(B)** Confocal images from MKN-45 and MKN-74 cells showing immunofluorescence for $P2Y_2R$ and P2X4R; scale bar 10 μm. In all cases the images shown are representative of three different samples.

AGS and MKN-74 cells (**Figure 5B**). In the case of MKN-45 and GES-1 cells, no effect of UTP was observed at the concentrations tested (**Figure 5B**). We also tested the effects of ADP, a selective agonist for $P2Y_1R$ and $P2Y_{11}R$, finding no significant changes in AGS cell proliferation (**Supplemental Figure 3**). These results not only confirmed that different receptor subtypes are mediating the purinergic responses, but also suggest that these receptors could have different roles in cell proliferation. To test this, we performed additional experiments using purinergic agonists and antagonists and evaluated their effects on AGS and GES-1 cells proliferation. **Figure 6** shows the conclusion of these experiments. In the first series of experiments, we used the $P2Y_2R$ and $P2Y_4R$ agonist UTP. The increase in cell proliferation induced by 100 μM UTP was significantly prevented by the wide range antagonist suramin but not by the P2X-preferring PPADS (**Figure 6A**, left graph). Suramin also inhibited the increase in cell proliferation induced by 100 μM ATP, and interestingly after this treatment cell viability decreased, as compared to untreated control cells; PPADS did not significantly affect AGS cell proliferation induced by ATP (**Figure 6A**, middle graph). We confirmed the pivotal role of the $P2Y_2R$ in cell proliferation using the specific agonist MRS2768, which increased AGS cell viability similarly to UTP (**Figure 6A**, right graph) and the specific $P2Y_2R$ antagonist AR-C118925XX which prevented the UTP increase in cell viability (**Figure 6A**, right graph). On the other hand, in GES-1 cells, the decrease in cell viability induced by ATP was prevented by wide range P2X antagonist PPADS but not by suramin, which does not inhibit P2X4R or P2X7R (**Figure 6B**). Seeing as ATP and related nucleotides have been postulated as paracrine and/or autocrine signaling molecules, we evaluated the effect of applying purinergic antagonists to control cells (with no exogenous ATP). In these experiments, AGS cell viability was significantly decreased with suramin and AR-C118925XX (**Figure 6C**) but was increased by PPADS and by the P2X4R-specific antagonist BX430, whereas the P2X7R antagonist AZ10606120 had no effect (**Figure 6C**). In GES-1 cells,

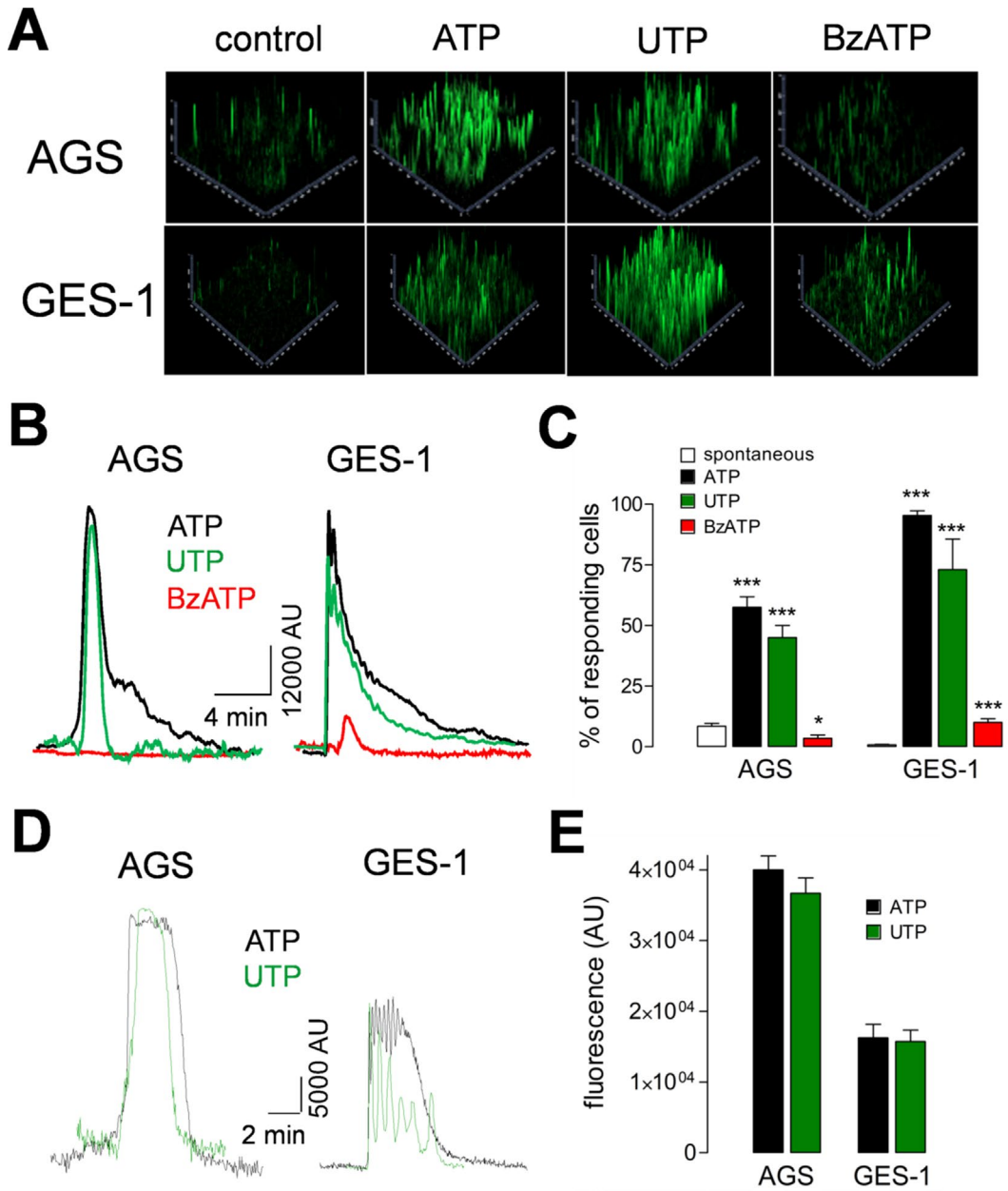

FIGURE 3 | Purinergic receptor induced increases of intracellular calcium. **(A)** Representative 2.5D representation of ATP, UTP, or BzATP (100 μM) induced increases of $[Ca^{2+}]_i$ in AGS and GES-1 cells. **(B)** Total increase of $[Ca^{2+}]_i$ induced by ATP (black traces), UTP (green traces), and BzATP (red traces) in AGS and GES-1 cells, in four to six fields. **(C)** Percentage of responding cells for spontaneous activity (open bars), ATP (black bars), UTP (green bars), and BzATP (red bars). $^*p < 0.05$; $^{***}p < 0.001$, ANOVA test, $n = 4–11$. **(D)** Representative recordings from single AGS or GES-1 cells showing the increase of $[Ca^{2+}]_i$ induced by 100 μM ATP (black traces) or UTP (green traces). **(E)** Summary of the maximal relative fluorescence, measured in arbitrary units (AU) induced by ATP (black bars) or UTP (green bars) in AGS and GES-1 cells, $n = 21–24$.

P2Y-preferring antagonists did not induce any effect on basal cell proliferation and only the application of BX430 induced a significant increase in cell viability (**Figure 6C**). Contrary to what was observed in AGS cells, AZ10606120 also increased basal proliferation in GES-1 cells (**Figure 6C**). Altogether, our results indicate that the P2X4R, not P2X7R, is the purinergic receptor that decreases cell proliferation in GC-derived cell lines. To confirm this, we performed additional experiments using a high ATP concentration (300 μM), which decreases cell proliferation. This decrease was completely inhibited in AGS cells when ATP was coapplied with the P2X4R antagonist BX430, but not with the P2X7R antagonist AZ10606120 (**Figure 6D**, left). However, in GES-1 cells AZ10606120 prevented the decrease in cell viability induced by 300 μM ATP (**Figure 6D**, right). Since P2X4R plays an

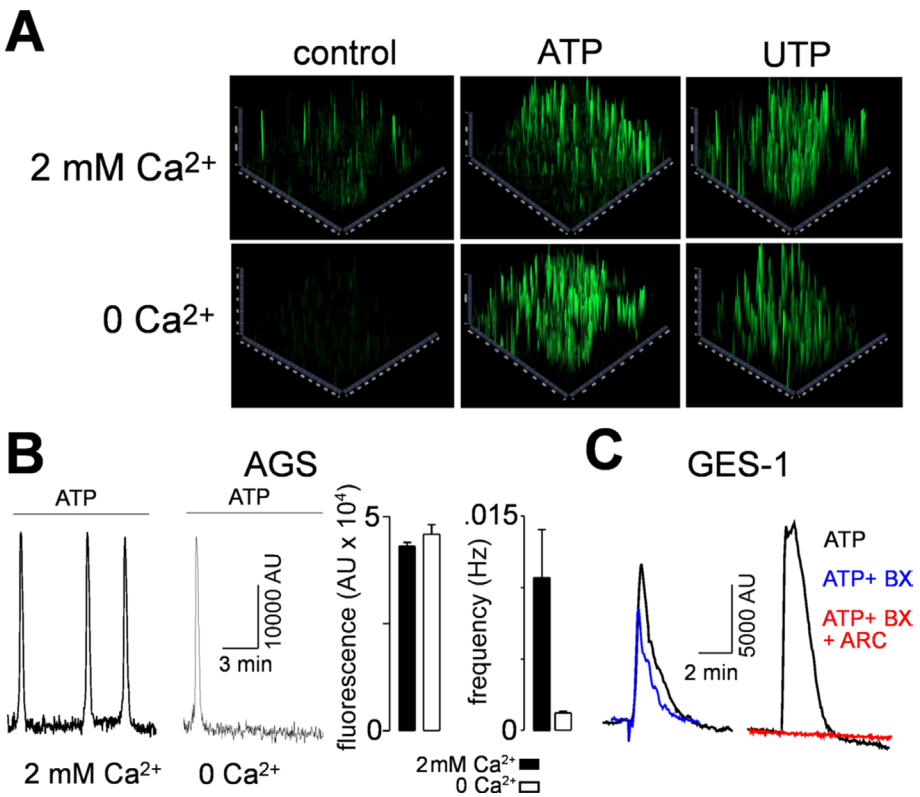

FIGURE 4 | Contribution of P2YRs and P2XRs to increases in $[Ca^{2+}]_i$. **(A)** 2.5D representations of AGS cells showing spontaneous (control) activity after the application of 100 μM ATP in the presence (upper images) or absence (lower images) of extracellular calcium. **(B)** Left, representative recordings from AGS cells showing the 100 μM ATP-induced spikes in the presence or in the absence of extracellular calcium. Right, summary of the maximal relative fluorescence and frequency of the ATP-induced spikes in the presence (black bars) or absence (open bars) of 2 mM extracellular Ca^{2+}. **(C)** Representative recordings showing $[Ca^{2+}]_i$ increases induced by 100 μM ATP alone (black traces) or together with BX430 (blue traces) or BX430 and ARC-118925XX (red trace).

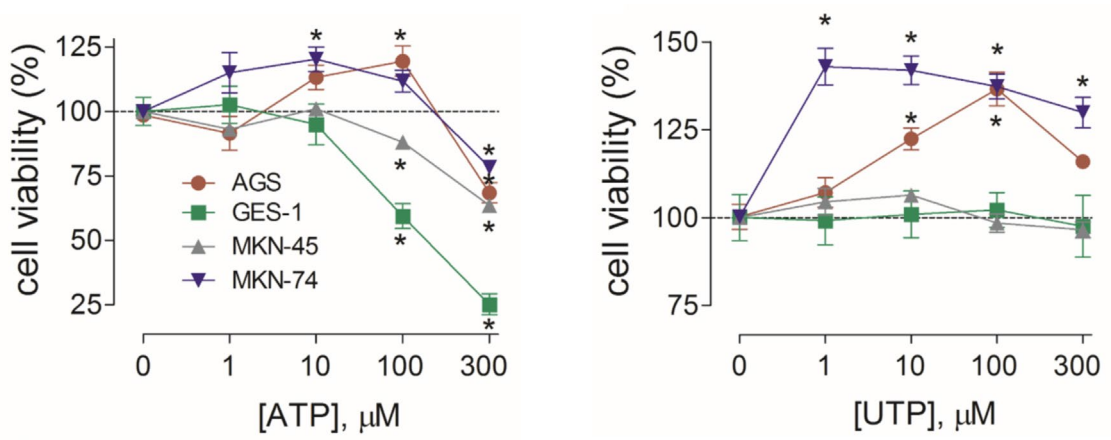

FIGURE 5 | Summary of the effects of ATP and UTP in the proliferation of gastric cell lines. Changes in cell proliferation assessed by cell viability in the absence or presence of 1–300 μM ATP (left graph) or UTP (right graph) for the AGS (red), GES-1 (green), MKN-45 (gray), or MKN-74 (purple) cells. *$p < 0.05$, Kruskal–Wallis and Dunn's tests, $n = 4–6$.

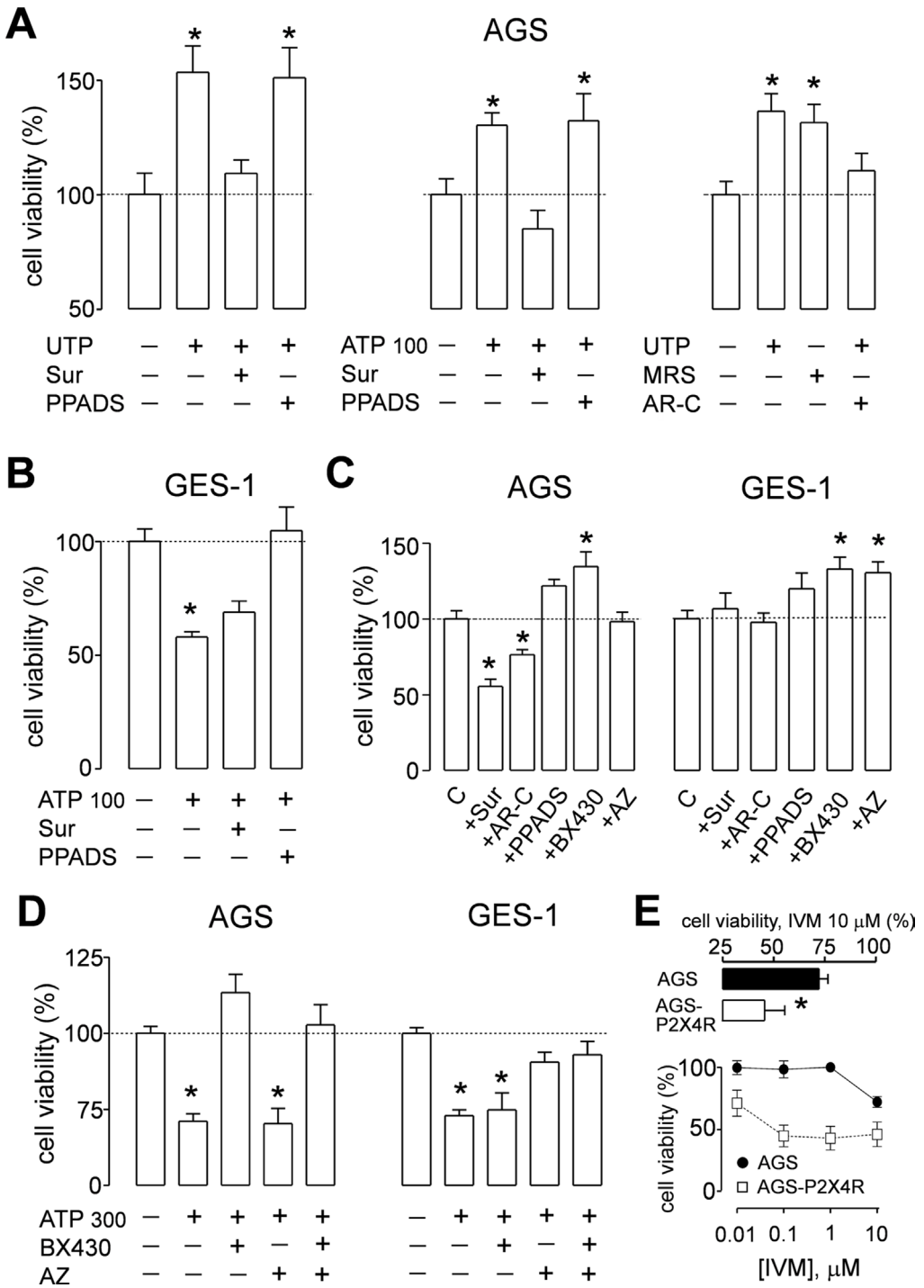

FIGURE 6 | Effects of purinergic agonists and antagonist on the proliferation of AGS and GES-1 cells. **(A)** Summary of cell viability experiments on AGS cells showing the effect of: *left graph*, 100 μM UTP alone, or coapplied with 100 μM suramin (Sur) or 100 μM PPADS; *middle graph*, 100 μM ATP alone, or coapplied with 100 μM suramin (Sur) or 100 μM pyridoxal phospate-6-azo(benzene-2,4-disulfonic acid) (PPADS); *right graph*, effects of 100 μM UTP alone, 10 μM MRS2768 alone, or 100 μM UTP plus 10 μM ARC-118925XX, n = 4–7. **(B)** Summary of cell viability experiments in GES-1 cells showing the effect of 100 μM ATP alone, and coapplied with 100 μM suramin (Sur) or 100 μM PPADS, n = 3–5. **(C)** Summary of the effects of purinergic antagonists alone on cell viability applied to AGS (left) and GES-1 cells (right). The antagonists used were suramin (Sur) (100 μM), PPADS (100 μM), ARC-118925XX (AR-C) (10 μM), BX430 (10 μM), and AZ10606120 (AZ) (3 μM), n = 4–6. **(D)** Summary of cell viability experiments on AGS (left) and GES-1 (right) cells showing the effect of 300 μM ATP alone, and coapplied with 10 μM BX430 or 3 μM AZ10606120 (AZ), n = 3–4. **(E)** Effects of ivermectin (IVM) in AGS cell proliferation; *lower graph*: concentration–response curve for 1 nm–10 μM IVM and its effect on cell viability on control (closed circles) or P2X4R-overexpressing (open squares) AGS cells; *upper graph*: detail of cell viability in control (black bar) or P2X4R-overexpressing (open bar) AGS cells treated with 10 μM IVM, n = 3–4 in all cases *$p < 0.05$, Kruskal–Wallis and Dunn´s tests.

important role mediating the protective effects of nucleotides, we tested the effect of the positive allosteric modulator ivermectin (Khakh et al., 1999), finding that the isolated application of 10 μM ivermectin was able to decrease basal proliferation of AGS cells, and when P2X4R was overexpressed in these cells the effects of IVM were more pronounced and started at 0.1 μM (**Figure 6E**).

Changes in the Expression of $P2Y_2$ and P2X4 Receptors in Gastric Cancer-Derived Biopsies and Gastric Cell Lines

We evaluated the changes in $P2Y_2R$ and P2X4R expression in tumors from patients diagnosed with GC and compared the results to their respective adjacent nontumoral gastric mucosa by qPCR. We analyzed seven GC tumors and their respective healthy gastric and we found a high degree of variation between the different tumors analyzed. The tumors were in both early and advanced adenocarcinomas, from five males and two females, with no metastasis. In general, $P2Y_2R$ RNA was increased 8.0 ± 3.9 fold in tumors as compared to normal tissue, whereas the P2X4R RNA decreased by half, 0.5 ± 0.2 fold (**Figure 7A**). However, as mentioned above, we found a high degree of variation between the different samples; in the case of $P2Y_2R$ we found a high (more than 10-fold) overexpression in T1, T2, and T3 and an important decrease in expression in T6 and T7 (**Figure 7B**). For P2X4R we found an important decrease of expression in T1, T2, T3, and T6 and no significant changes in T4, T5, and T7 (**Figure 7B**). We did not find any correlation between the expression of purinergic receptors and the tumor phenotype, probably because of the limited size of our sample.

Expression Levels of $P2Y_2$ Receptor and P2X4 Receptor Are Related to Gastric Cancer Patient Survival

Finally, we analyzed if high or low expression of $P2Y_2R$ and P2X4R is related to survival for 593 patients, taken from the Kaplan–Meier Plotter Database (kmplot.com) (Lanczky et al., 2016). Interestingly, we found that patients with high $P2Y_2R$ expression have a significantly lower survival rate as compared to patients with

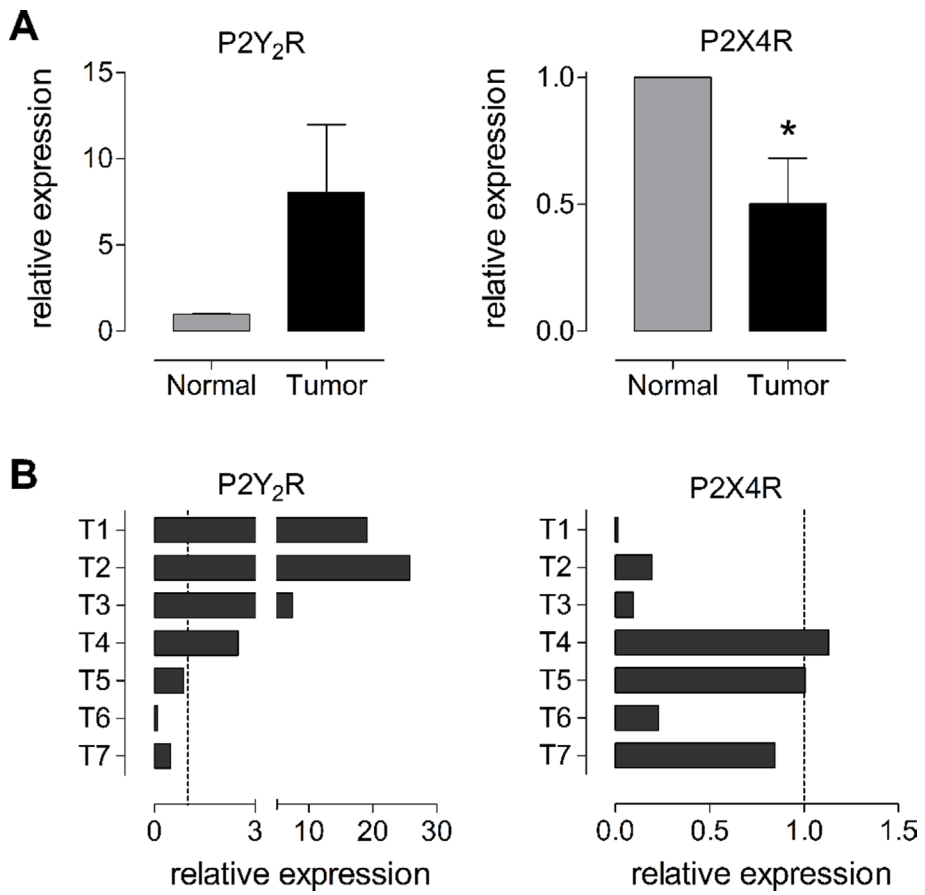

FIGURE 7 | Changes in RNA levels of $P2Y_2R$ and P2X4R in human biopsies from normal and tumoral gastric tissues. **(A)** Summary of the changes of RNA measured by qPCR for $P2Y_2R$ (left graph) or P2X4R (right graph) taken from seven different patients diagnosed with GC. Changes in RNA levels were measured comparing the expression of the purinergic receptor in the tumor with its levels in the adjacent healthy gastric mucosa. *$p < 0.05$, paired *t*-test. **(B)** Individual changes in $P2Y_2R$ (left) and P2X4R (right) RNA levels in the seven different tumor biopsies analyzed. Dotted line represents the basal expression in adjacent healthy gastric mucosa.

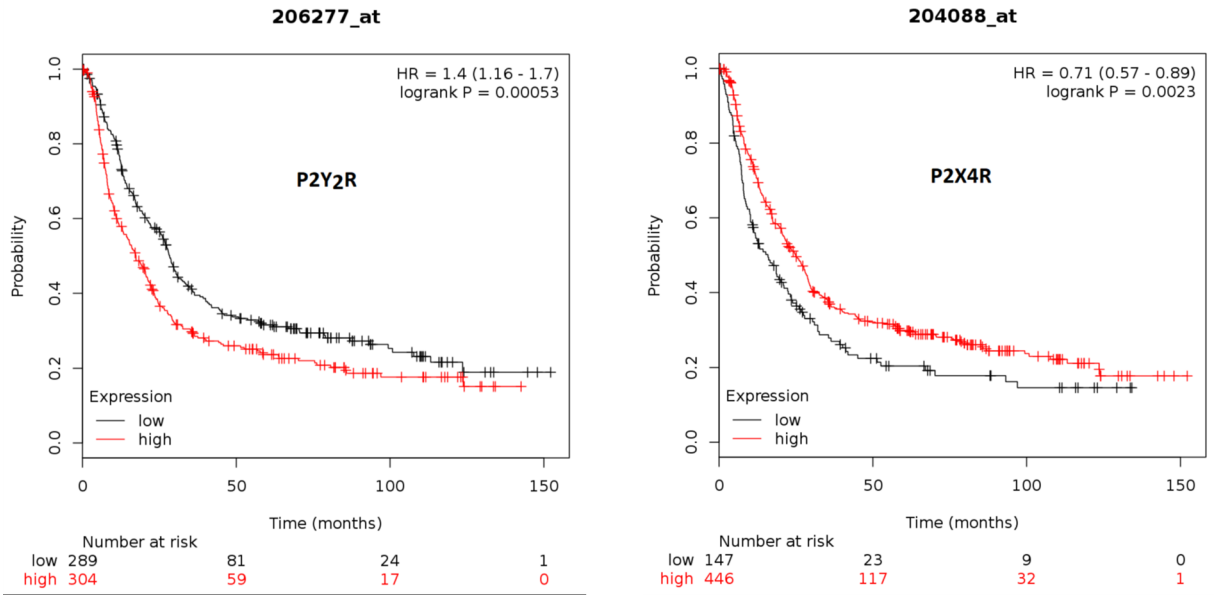

FIGURE 8 | Kaplan–Meier survival plots for high or low expression of $P2Y_2R$ and P2X4R in GC patients. Database was taken from the Kaplan–Meier Plotter Database (kmplot.com), from a total of 593 patients diagnosed with GC. Plots show the survival of patients with low (black line) and high (red line) expression of the $P2Y_2R$ (left plot) or the P2X4R (right plot)—number indicates surviving patients at 0, 50, 100, and 150 months.

low $P2Y_2R$ expression (**Figure 8**). On the other hand, patients with high P2X4R expression have significantly higher survival rates as compared to patients with low P2X4R expression (**Figure 8**).

DISCUSSION

Gastric cancer (GC) is one of the leading causes of cancer-induced deaths in the world. Although purinergic signaling has been studied in different cancer types, there is not abundant evidence about its role in GC. In the present work we have identified purinergic receptors present in several GC-derived cell lines and also in biopsies from patients diagnosed with GC, finding that the expression pattern varies between the different cell lines, and between healthy and tumor cells, and biopsies. In a first series of experiments, we evaluated the expression of purinergic receptors in three different GC-derived cell lines and in a cell line derived from healthy gastric mucosa. Although the expression varies among the cell lines, we find that healthy mucosa-derived GES-1 expresses more P2XRs as compared to GC-derived cells. In particular, we found that P2X7R and P2X4R are downregulated in GC-derived cell lines; on the other hand, in some GC-derived cell lines, namely, AGS and MKN-74, there is a consistent increase in the expression of P2YRs, especially $P2Y_2R$. Consistent with this, we observed in MTT proliferation studies that the activation of $P2Y_2R$ increases cell viability and proliferation, whereas P2X4R activation decreases it. In our experiments we consistently observed that the P2XR subtype responsible for decreases in GC-derived cell proliferation is P2X4R and not P2X7R, because firstly, we found that P2X7R is almost completely downregulated in AGS and MKN cell lines, and secondly, in cell proliferation studies the P2X7R antagonist AZ10602120 had no effect in preventing the activation of P2XRs by high concentrations of ATP, although we observed an effect of the P2X4R antagonist BX430. Moreover, the P2X4R positive allosteric modulator ivermectin was able to decrease the basal proliferation in AGS cells, and this effect was enhanced in P2X4R-overexpressing AGS cells. We cannot discard the contribution of P2X2R in the ATP-mediated decrease in GC-derived cell proliferation, seeing as we detected the expression of this receptor in AGS and GES-1 cells, but currently there are no reliable antagonists commercially available to test its specific contribution. In addition, we found that the sole application of $P2Y_2R$ and P2X4R antagonists can change the basal proliferation of these cells, indicating that nucleotides acting as paracrine and/or autocrine signaling molecules can produce an effect. This is especially relevant taking into account that the tumor microenvironment has increased ATP levels (Di Virgilio and Adinolfi, 2017), and this could contribute to tumor progression. We additionally performed calcium imaging experiments to directly asses the activation of P2 receptors and found P2-mediated responses in both AGS and GES-1 cells. In both cell lines the major contribution of intracellular calcium increases was consequence of the activation of $P2Y_2R$, although there is also a contribution of P2XRs in GES-1 cells. Three observations support this conclusion: 1) ATP and UTP evoked similar responses that match with the $P2Y_2R$ pharmacological profile; 2) in AGS cells the ATP or UTP increases in intracellular calcium are comparable in the absence or presence of extracellular calcium suggesting a major contribution of metabotropic receptors; and 3) the responses are sensitive to $P2Y_2R$ agonist MRS2678 and blocked by $P2Y_2R$ antagonist ARC-118925XX. All these results highlight the role of purinergic signaling in GC-derived cells and suggest that

its pharmacological manipulation could constitute an alternative treatment strategy.

Purinergic signaling plays a role in different types of cancer. For example, studies in a melanoma-derived cell line have shown the presence of P2Y and P2X receptors; in this particular cell line the stimulation of $P2Y_1R$ decreases the number of cells, whereas stimulation of the $P2Y_2R$ increases it. Conversely, P2X7R is also present in these cells and its specific activation induces apoptosis (White et al., 2005a; White et al., 2005b). Regarding lung cancer, the derived cell line A549 expresses functional $P2Y_2Rs$ and $P2Y_6Rs$, which mediate cell proliferation after specific activation by purinergic agonists (Schafer et al., 2003). Brain tumors such as gliomas and astrocytomas express $P2Y_1Rs$ and $P2Y_12Rs$, which in general mediate increases in cell number, but in some cell lines can also induce apoptosis (Sellers et al., 2001; Morrone et al., 2003). In the case of cervical cancer, studies with primary cultures from tumors and cell lines have demonstrated the functional expression of the P2X7R that mediates apoptosis with an expression increase of caspase-3 and caspase-9 (Wang et al., 2004). Proliferation of the breast cancer-derived cell line MCF-7 is decreased with high doses of ATP (over 100 μM), but lower doses of specific activation of $P2Y_2R$ increase cell proliferation, probably reflecting the action of different P2 receptor subtypes (Slater et al., 2004). More recently, it has been suggested that activation of $P2Y_2Rs$ also increases MCF-7 cell migration through the MEK-ERK1/2 signaling pathway (Chadet et al., 2014). In ovarian cancer, there are also conflicting studies: one group has reported an increase in cell proliferation on the OVCAR-3 cell line mediated by $P2Y_2R$ (Popper and Batra, 1993), whereas another group has found opposite effects mediated by this receptor in the EFO-21 and EFO-27 cell lines (Schultze-Mosgau et al., 2000). More recent works have addressed a role of purinergic signaling and $P2Y_2R$ in the regulation of cell migration and epithelium to mesenchymal transition in ovarian carcinoma-derived cells (Martinez-Ramirez et al., 2016). In leukemia, the roles of functional P2X7Rs and $P2Y_{11}Rs$ in lymphocytes from patients suffering this disease have been demonstrated, and it has been proposed that P2X7R mediates cell death, while $P2Y_{11}R$ mediates cell differentiation (Conigrave et al., 2000; Zhang et al., 2004). As in other cancers, conclusions about the role of purinergic signaling in colorectal cancer are not uniform. In one study, cell proliferation was increased by the activation of $P2Y_2R$ in primary cultures from colorectal tumors and in the HT29 cell line (Hopfner et al., 1998). However, another study showed an increase of proliferation mediated by the $P2Y_2R$ and a decrease in cell number mediated by $P2Y_1Rs$ and P2X7Rs in HCT8 and Caco-2 cell lines (Coutinho-Silva et al., 2005). In cells derived from human esophageal cancer, it has been shown that the expression of $P2Y_2Rs$ and P2X4Rs and the activation of the former leads to a decrease in cell number (Maaser et al., 2002). In human cancerous pancreatic duct epithelial cells, it has been also reported that the activation of $P2Y_2R$ by UTP increases cell proliferation and this process is mediated by the PI3K/Akt pathway (Choi et al., 2013). In prostate cancer, it has been shown that $P2Y_2R$ cooperates with EGFR to promote cell invasion and metastasis through the ERK1/2 pathway, suggesting a therapeutic possibility using purinergic blockers to treat this type of cancer (Li et al., 2015). Recently it has also been reported that platelet-derived nucleotides that activate an endothelial $P2Y_2R$, is a mechanism that allows metastasis of tumor cells by transendothelial migration (Schumacher et al., 2013). However, in GC there is not much information available regarding purinergic signaling. The first studies in this field have reported that adenosine and ATP could inhibit cell growth and induce apoptosis in GC-derived cell lines GT3-TKB and HGC-27, acting mainly through P1 receptors (Saitoh et al., 2004; Wang and Ren, 2006).

As in other types of cancer, in GC a change in the expression of several genes has been observed. One example is the overexpression of the gene encoding the human epidermal growth factor receptor 2 (HER2) found not only in GC, but also in other cancers such as colorectal, lung, and ovarian cancer (Gravalos and Jimeno, 2008). Other genes that are overexpressed in GC are ones that codify for the epidermal growth factor receptor (EGFR), vascular endothelial growth factor A (VEGFA) and its respective receptor, fibroblast growth factor receptor (FGFR), and hepatocyte growth factor receptor (Carcas, 2014). In addition, a variety of molecules that participate in events such as cell cycle or control of cell adhesion have been proposed as early biomarkers for GC and can be detected from tissues of fluids using molecular biology techniques (Yasui et al., 2011). These biomarkers include ADAM17 (Shou et al., 2012), MMP2, MMP9, and MMP11 (Sampieri et al., 2010; Zhao et al., 2010), survivin and CK19 (Bertazza et al., 2009), vimentin (Iwatsuki et al., 2010), CXCR4 (Ingold et al., 2010), ING5 (Xing et al., 2011), and Stanniocalcin2 (Yokobori et al., 2010); in all of these examples, these molecules are overexpressed in tumoral GC tissues. However, these changes are not uniform, and therapy effectiveness will depend on the degree of overexpression of the target gene. Although several pharmacological therapies for the treatment of GC have been studied, only two targeted treatments have been approved in the United States after positive clinical trials. One of these treatments is an HER2 inhibitor and has been studied as a therapy for several cancers. This drug, which has been termed trastuzumab, is a monoclonal antibody that binds to HER2 inhibiting signaling and preventing the cleavage of its extracellular domain (Hudis, 2007). However, trastuzumab treatment is only effective in patients with scores of IHC 2+ (equivocal) or IHC 3+ (positive) of HER2 overexpression (Hofmann et al., 2008). For that reason it is relevant to find new therapeutic targets, especially for patients with low HER2 scores.

In our GC experiments, we found that purinergic signaling exerts different effects that depend in the expression profile of purinergic receptors of the cell lines; for example UTP induces proliferation of AGS and MKN-74 cells, and both cell lines show a strong expression of the $P2Y_2R$, while the same agonist has no effect on MKN-45 cells that show a low expression of this receptor. This reflects the high variability among cancer and highlights the importance of a detailed disease characterization for each patient. Concordantly, in a last series of experiments we evaluated purinergic receptors in human GC biopsies and compared their expression of the tumor and their nearby healthy gastric mucosa. Although in general we

found that the expression of $P2Y_2R$ is increased and P2X4R is decreased in GC, when we compared the results of seven different patients, we found that these changes are not uniform. We infer that similarly to what has been observed with HER2 overexpression, patients with a high purinergic component will be more sensitive to a purinergic treatment. Interestingly, when we analyzed the survival of GC patients in terms of the expression of $P2Y_2R$ and P2X4R, we observed a positive correlation between their high or low expression and the survival rates; whereas high expression of $P2Y_2R$ decreased the survival of GC patients, high expression of P2X4R increased their survival. In this context, the grade of expression of some purinergic receptors, such as $P2Y_2R$ or P2X4R, could constitute a potential biomarker for GC.

In summary, we have described for the first time the purinergic signaling in GC-derived cell lines and found that purinergic signaling is a complex event that depends on the expression profile of specific purinergic receptors and on the nucleotide concentration present in the extracellular environment. The inhibition of some key purinergic receptors, for example $P2Y_2R$, plus the activation or other subtypes, for example P2X4R, could constitute a future strategy for GC treatment.

DATA AVAILABILITY STATEMENT

All datasets generated for this study are included in the manuscript and the supplementary files.

ETHICS STATEMENT

The protocols were approved by the Ethical-Scientific Committee of the Faculty of Medicine of the Universidad Católica del Norte (CECFAMED-UCN) and patients voluntarily signed their consent, document F.M. Nº 17.

AUTHOR CONTRIBUTIONS

CC, PC, MH, EF-O, and GB designed research; MH, PC, FR-T, CR-P, SR-R, FG, and EF-O performed experiments; MJH, PC, and CC analyzed data; JAM, FG, JL, and MB provided human biopsies; and CC, PC, and MH wrote the manuscript. KP-I and MR-J performed experiments and analyzed data.

FUNDING

This work was funded by Fondo Nacional de Desarrollo Científico y Tecnológico (FONDECYT) Regular Grant # 1161490, CONICYT Ph.D. Fellowship #21181885 and FONDEQUIP EQM140100. The funders had no role in the study design, data collection and analysis, decision to publish, or preparation of the article.

SUPPLEMENTARY MATERIAL

The Supplementary Material for this article can be found online at: https://www.frontiersin.org/articles/10.3389/fphar.2019.00612/full#supplementary-material

REFERENCES

Abbracchio, M. P., Burnstock, G., Boeynaems, J. M., Barnard, E. A., Boyer, J. L., Kennedy, C., et al. (2006). International Union of Pharmacology LVIII: update on the P2Y G protein-coupled nucleotide receptors: from molecular mechanisms and pathophysiology to therapy. *Pharmacol. Rev.* 58, 281–341. doi: 10.1124/pr.58.3.3

Aquea, G., Bresky, G., Lancellotti, D., Madariaga, J. A., Zaffiri, V., Urzua, U., et al. (2014). Increased expression of P2RY2, CD248 and EphB1 in gastric cancers from Chilean patients. *Asian Pac. J. Cancer Prev.* 15, 1931–1936. doi: 10.7314/APJCP.2014.15.5.1931

Ase, A. R., Honson, N. S., Zaghdane, H., Pfeifer, T. A., and Seguela, P. (2015). Identification and characterization of a selective allosteric antagonist of human P2X4 receptor channels. *Mol. Pharmacol.* 87, 606–616. doi: 10.1124/mol.114.096222

Bertazza, L., Mocellin, S., Marchet, A., Pilati, P., Gabrieli, J., Scalerta, R., et al. (2009). Survivin gene levels in the peripheral blood of patients with gastric cancer independently predict survival. *J. Transl. Med.* 7, 111. doi: 10.1186/1479-5876-7-111

Burnstock, G. (2013). Purinergic signalling: pathophysiology and therapeutic potential. *Keio J. Med.* 62, 63–73. doi: 10.2302/kjm.2013-0003-RE

Burnstock, G., and Verkhratsky, A. (2010). Long-term (trophic) purinergic signalling: purinoceptors control cell proliferation, differentiation and death. *Cell Death Dis.* 1, e9. doi: 10.1038/cddis.2009.11

Carcas, L. P. (2014). Gastric cancer review. *J. Carcinog.* 13, 14. doi: 10.4103/1477-3163.146506

Chadet, S., Jelassi, B., Wannous, R., Angoulvant, D., Chevalier, S., Besson, P., et al. (2014). The activation of P2Y2 receptors increases MCF-7 breast cancer cells migration through the MEK-ERK1/2 signalling pathway. *Carcinogenesis* 35, 1238–1247. doi: 10.1093/carcin/bgt493

Choi, J. H., Ji, Y. G., and Lee, D. H. (2013). Uridine triphosphate increases proliferation of human cancerous pancreatic duct epithelial cells by activating P2Y2 receptor. *Pancreas* 42, 680–686. doi: 10.1097/MPA.0b013e318271bb4b

Coddou, C., Yan, Z., Obsil, T., Huidobro-Toro, J. P., and Stojilkovic, S. S. (2011). Activation and regulation of purinergic P2X receptor channels. *Pharmacol. Rev.* 63, 641–683. doi: 10.1124/pr.110.003129

Conigrave, A. D., Van Der Weyden, L., Holt, L., Jiang, L., Wilson, P., Christopherson, R. I., et al. (2000). Extracellular ATP-dependent suppression of proliferation and induction of differentiation of human HL-60 leukemia cells by distinct mechanisms. *Biochem. Pharmacol.* 60, 1585–1591. doi: 10.1016/S0006-2952(00)00465-2

Coutinho-Silva, R., Stahl, L., Cheung, K. K., De Campos, N. E., De Oliveira Souza, C., Ojcius, D. M., et al. (2005). P2X and P2Y purinergic receptors on human intestinal epithelial carcinoma cells: effects of extracellular nucleotides on apoptosis and cell proliferation. *Am. J. Physiol. Gastrointest. Liver Physiol.* 288, G1024–G1035. doi: 10.1152/ajpgi.00211.2004

Di Virgilio, F. (2012). Purines, purinergic receptors, and cancer. *Cancer Res.* 72, 5441–5447. doi: 10.1158/0008-5472.CAN-12-1600

Di Virgilio, F., and Adinolfi, E. (2017). Extracellular purines, purinergic receptors and tumor growth. *Oncogene* 36, 293–303. doi: 10.1038/onc.2016.206

Di Virgilio, F., Sarti, A. C., Falzoni, S., De Marchi, E., and Adinolfi, E. (2018). Extracellular ATP and P2 purinergic signalling in the tumour microenvironment. *Nat. Rev. Cancer* 18, 601–618. doi: 10.1038/s41568-018-0037-0

Ghiringhelli, F., Apetoh, L., Tesniere, A., Aymeric, L., Ma, Y., Ortiz, C., et al. (2009). Activation of the NLRP3 inflammasome in dendritic cells induces IL-1beta-dependent adaptive immunity against tumors. *Nat. Med.* 15, 1170–1178. doi: 10.1038/nm.2028

Gravalos, C., and Jimeno, A. (2008). HER2 in gastric cancer: a new prognostic factor and a novel therapeutic target. *Ann. Oncol.* 19, 1523–1529. doi: 10.1093/annonc/mdn169

Heise, K., Bertran, E., Andia, M. E., and Ferreccio, C. (2009). Incidence and survival of stomach cancer in a high-risk population of Chile. *World J. Gastroenterol.* 15, 1854–1862. doi: 10.3748/wjg.15.1854

Hofmann, M., Stoss, O., Shi, D., Buttner, R., Van De Vijver, M., Kim, W., et al. (2008). Assessment of a HER2 scoring system for gastric cancer: results from a validation study. *Histopathology* 52, 797–805. doi: 10.1111/j.1365-2559.2008.03028.x

Hopfner, M., Lemmer, K., Jansen, A., Hanski, C., Riecken, E. O., Gavish, M., et al. (1998). Expression of functional P2-purinergic receptors in primary cultures of human colorectal carcinoma cells. *Biochem. Biophys. Res. Commun.* 251, 811–817. doi: 10.1006/bbrc.1998.9555

Hudis, C. A. (2007). Trastuzumab—mechanism of action and use in clinical practice. *N. Engl. J. Med.* 357, 39–51. doi: 10.1056/NEJMra043186

Ingold, B., Simon, E., Ungethum, U., Kuban, R. J., Muller, B. M., Lupp, A., et al. (2010). Vascular CXCR4 expression—a novel antiangiogenic target in gastric cancer? *PLoS One* 5, e10087. doi: 10.1371/journal.pone.0010087

Iwatsuki, M., Mimori, K., Fukagawa, T., Ishii, H., Yokobori, T., Sasako, M., et al. (2010). The clinical significance of vimentin-expressing gastric cancer cells in bone marrow. *Ann. Surg. Oncol.* 17, 2526–2533. doi: 10.1245/s10434-010-1041-0

Jacobson, K. A., Balasubramanian, R., Deflorian, F., and Gao, Z. G. (2012). G protein-coupled adenosine (P1) and P2Y receptors: ligand design and receptor interactions. *Purinergic Signal.* 8, 419–436. doi: 10.1007/s11302-012-9294-7

Khakh, B. S., Proctor, W. R., Dunwiddie, T. V., Labarca, C., and Lester, H. A. (1999). Allosteric control of gating and kinetics at P2X(4) receptor channels. *J. Neurosci.* 19, 7289–7299. doi: 10.1523/JNEUROSCI.19-17-07289.1999

Lanczky, A., Nagy, A., Bottai, G., Munkacsy, G., Szabo, A., Santarpia, L., et al. (2016). miRpower: a web-tool to validate survival-associated miRNAs utilizing expression data from 2178 breast cancer patients. *Breast Cancer Res. Treat.* 160, 439–446. doi: 10.1007/s10549-016-4013-7

Li, W. H., Qiu, Y., Zhang, H. Q., Tian, X. X., and Fang, W. G. (2015). P2Y2 receptor and EGFR cooperate to promote prostate cancer cell invasion *via* ERK1/2 pathway. *PLoS One* 10, e0133165. doi: 10.1371/journal.pone.0133165

Livak, K. J., and Schmittgen, T. D. (2001). Analysis of relative gene expression data using real-time quantitative PCR and the 2(-Delta Delta C(T)) Method. *Methods* 25 (4), 402–408.

Maaser, K., Hopfner, M., Kap, H., Sutter, A. P., Barthel, B., Von Lampe, B., et al. (2002). Extracellular nucleotides inhibit growth of human oesophageal cancer cells *via* P2Y(2)-receptors. *Br. J. Cancer* 86, 636–644. doi: 10.1038/sj.bjc.6600100

Martinez-Ramirez, A. S., Garay, E., Garcia-Carranca, A., and Vazquez-Cuevas, F. G. (2016). The P2RY2 receptor induces carcinoma cell migration and EMT through cross-talk with epidermal growth factor receptor. *J. Cell. Biochem.* 117, 1016–1026. doi: 10.1002/jcb.25390

Minsal (2014). "Guías Clínicas AUGE Cáncer Gástrico," in *Ministerio de Salud*.

Morrone, F. B., Jacques-Silva, M. C., Horn, A. P., Bernardi, A., Schwartsmann, G., Rodnight, R., et al. (2003). Extracellular nucleotides and nucleosides induce proliferation and increase nucleoside transport in human glioma cell lines. *J. Neurooncol.* 64, 211–218. doi: 10.1023/A:1025699932270

Mosmann, T. (1983). Rapid colorimetric assay for cellular growth and survival: application to proliferation and cytotoxicity assays. *J. Immunol. Methods* 65, 55–63. doi: 10.1016/0022-1759(83)90303-4

Popper, L. D., and Batra, S. (1993). Calcium mobilization and cell proliferation activated by extracellular ATP in human ovarian tumour cells. *Cell Calcium* 14, 209–218. doi: 10.1016/0143-4160(93)90068-H

Prabst, K., Engelhardt, H., Ringgeler, S., and Hubner, H. (2017). Basic colorimetric proliferation assays: MTT, WST, and resazurin. *Methods Mol. Biol.* 1601, 1–17. doi: 10.1007/978-1-4939-6960-9_1

Saitoh, M., Nagai, K., Nakagawa, K., Yamamura, T., Yamamoto, S., and Nishizaki, T. (2004). Adenosine induces apoptosis in the human gastric cancer cells *via an* intrinsic pathway relevant to activation of AMP-activated protein kinase. *Biochem. Pharmacol.* 67, 2005–2011. doi: 10.1016/j.bcp.2004.01.020

Sampieri, C. L., De La Pena, S., Ochoa-Lara, M., Zenteno-Cuevas, R., and Leon-Cordoba, K. (2010). Expression of matrix metalloproteinases 2 and 9 in human gastric cancer and superficial gastritis. *World J. Gastroenterol.* 16, 1500–1505. doi: 10.3748/wjg.v16.i12.1500

Schafer, R., Sedehizade, F., Welte, T., and Reiser, G. (2003). ATP- and UTP-activated P2Y receptors differently regulate proliferation of human lung epithelial tumor cells. *Am. J. Physiol. Lung Cell Mol. Physiol.* 285, L376–L385. doi: 10.1152/ajplung.00447.2002

Schultze-Mosgau, A., Katzur, A. C., Arora, K. K., Stojilkovic, S. S., Diedrich, K., and Ortmann, O. (2000). Characterization of calcium-mobilizing, purinergic P2Y(2) receptors in human ovarian cancer cells. *Mol. Hum. Reprod.* 6, 435–442. doi: 10.1093/molehr/6.5.435

Schumacher, D., Strilic, B., Sivaraj, K. K., Wettschureck, N., and Offermanns, S. (2013). Platelet-derived nucleotides promote tumor-cell transendothelial migration and metastasis *via* P2Y2 receptor. *Cancer Cell* 24, 130–137. doi: 10.1016/j.ccr.2013.05.008

Sellers, L. A., Simon, J., Lundahl, T. S., Cousens, D. J., Humphrey, P. P., and Barnard, E. A. (2001). Adenosine nucleotides acting at the human P2Y1 receptor stimulate mitogen-activated protein kinases and induce apoptosis. *J. Biol. Chem.* 276, 16379–16390. doi: 10.1074/jbc.M006617200

Shou, Z. X., Jin, X., and Zhao, Z. S. (2012). Upregulated expression of ADAM17 is a prognostic marker for patients with gastric cancer. *Ann. Surg.* 256, 1014–1022. doi: 10.1097/SLA.0b013e3182592f56

Slater, M., Danieletto, S., Pooley, M., Cheng Teh, L., Gidley-Baird, A., and Barden, J. A. (2004). Differentiation between cancerous and normal hyperplastic lobules in breast lesions. *Breast Cancer Res. Treat.* 83, 1–10. doi: 10.1023/B:BREA.0000010670.85915.0f

Wang, M. X., and Ren, L. M. (2006). Growth inhibitory effect and apoptosis induced by extracellular ATP and adenosine on human gastric carcinoma cells: involvement of intracellular uptake of adenosine. *Acta Pharmacol. Sin.* 27, 1085–1092. doi: 10.1111/j.1745-7254.2006.00342.x

Wang, Q., Wang, L., Feng, Y. H., Li, X., Zeng, R., and Gorodeski, G. I. (2004). P2X7 receptor-mediated apoptosis of human cervical epithelial cells. *Am. J. Physiol., Cell Physiol.* 287, C1349–C1358. doi: 10.1152/ajpcell.00256.2004

White, N., and Burnstock, G. (2006). P2 receptors and cancer. *Trends Pharmacol. Sci.* 27, 211–217. doi: 10.1016/j.tips.2006.02.004

White, N., Butler, P. E., and Burnstock, G. (2005a). Human melanomas express functional P2 X(7) receptors. *Cell Tissue Res.* 321, 411–418. doi: 10.1007/s00441-005-1149-x

White, N., Ryten, M., Clayton, E., Butler, P., and Burnstock, G. (2005b). P2Y purinergic receptors regulate the growth of human melanomas. *Cancer Lett.* 224, 81–91. doi: 10.1016/j.canlet.2004.11.027

Xing, Y. N., Yang, X., Xu, X. Y., Zheng, Y., Xu, H. M., Takano, Y., et al. (2011). The altered expression of ING5 protein is involved in gastric carcinogenesis and subsequent progression. *Hum. Pathol.* 42, 25–35. doi: 10.1016/j.humpath.2010.05.024

Yasui, W., Sentani, K., Sakamoto, N., Anami, K., Naito, Y., and Oue, N. (2011). Molecular pathology of gastric cancer: research and practice. *Pathol. Res. Pract.* 207, 608–612. doi: 10.1016/j.prp.2011.09.006

Yokobori, T., Mimori, K., Ishii, H., Iwatsuki, M., Tanaka, F., Kamohara, Y., et al. (2010). Clinical significance of stanniocalcin 2 as a prognostic marker in gastric cancer. *Ann. Surg. Oncol.* 17, 2601–2607. doi: 10.1245/s10434-010-1086-0

Zhang, X. J., Zheng, G. G., Ma, X. T., Yang, Y. H., Li, G., Rao, Q., et al. (2004). Expression of P2X7 in human hematopoietic cell lines and leukemia patients. *Leuk. Res.* 28, 1313–1322. doi: 10.1016/j.leukres.2004.04.001

Zhao, Z. S., Chu, Y. Q., Ye, Z. Y., Wang, Y. Y., and Tao, H. Q. (2010). Overexpression of matrix metalloproteinase 11 in human gastric carcinoma and its clinicopathologic significance. *Hum. Pathol.* 41, 686–696. doi: 10.1016/j.humpath.2009.10.010

Conflict of Interest Statement: The authors declare that the research was conducted in the absence of any commercial or financial relationships that could be construed as a potential conflict of interest.

frontiers in Pharmacology

ORIGINAL RESEARCH
published: 17 July 2019
doi: 10.3389/fphar.2019.00804

Chronic Fluoxetine Treatment Induces Maturation-Compatible Changes in the Dendritic Arbor and in Synaptic Responses in the Auditory Cortex

Estibaliz Ampuero[1], Mauricio Cerda[2], Steffen Härtel[2,3], Francisco Javier Rubio[4†], Solange Massa[4], Paula Cubillos[1], Lorena Abarzúa-Catalán[1], Rodrigo Sandoval[5], Albert M. Galaburda[6] and Ursula Wyneken[4]**

[1] Instituto de Ciencias Biomédicas, Facultad de Ciencias de la Salud, Universidad Autónoma de Chile, Santiago, Chile, [2] SCIAN-Lab, CIMT, Biomedical Neuroscience Institute (BNI), ICBM, Faculty of Medicine, University of Chile, Santiago, Chile, [3] Centro Nacional de Sistemas de Información en Salud (CENS), Faculty of Medicine, University of Chile, Santiago, Chile, [4] Laboratorio de Neurociencias, Universidad de los Andes, Santiago, Chile, [5] Departamento de Ciencias Biomédicas, Facultad de Medicina, Universidad Católica del Norte, Coquimbo, Chile, [6] Department of Neurology, Harvard Medical School and Beth Israel Deaconess Medical Center, Boston, MA, United States

Fluoxetine is a selective serotonin reuptake inhibitor (SSRI) used to treat mood and anxiety disorders. Chronic treatment with this antidepressant drug is thought to favor functional recovery by promoting structural and molecular changes in several forebrain areas. At the synaptic level, chronic fluoxetine induces an increased size and density of dendritic spines and an increased ratio of GluN2A over GluN2B N-methyl-D-aspartate (NMDA) receptor subunits. The "maturation"-promoting molecular changes observed after chronic fluoxetine should also induce structural remodeling of the neuronal dendritic arbor and changes in the synaptic responses. We treated adult rats with fluoxetine (0.7 mg/kg i.p. for 28 days) and performed a morphometric analysis using Golgi stain in limbic and nonlimbic cortical areas. Then, we focused especially on the auditory cortex, where we evaluated the dendritic morphology of pyramidal neurons using a 3-dimensional reconstruction of neurons expressing mRFP after *in utero* electroporation. With both methodologies, a shortening and decreased complexity of the dendritic arbors was observed, which is compatible with an increased GluN2A over GluN2B ratio. Recordings of extracellular excitatory postsynaptic potentials in the auditory cortex revealed an increased synaptic response after fluoxetine and were consistent with an enrichment of GluN2A-containing NMDA receptors. Our results confirm that fluoxetine favors maturation and refinement of extensive cortical networks, including the auditory cortex. The fluoxetine-induced receptor switch may decrease GluN2B-dependent toxicity and thus could be applied in the future to treat neurodegenerative brain disorders characterized by glutamate toxicity and/or by an aberrant network connectivity.

Keywords: dendritic architecture, auditory cortex, neuronal segmentation, antidepressant, NMDA receptors

OPEN ACCESS

Edited by:
Javier A. Bravo, Pontificia Universidad Católica de Valparaíso, Chile

Reviewed by:
Luigia Trabace, University of Foggia, Italy
Camila González Arancibia, University of Valparaíso, Chile

****Correspondence:***
Estibaliz Ampuero
estibaliz.ampuero@uautonoma.cl
Ursula Wyneken
uwyneken@uandes.cl

†Present Address:
Francisco Javier Rubio
National Institute on Drug Abuse Intramural Research Program, National Institutes of Health, Baltimore, MA, United States

Specialty section:
This article was submitted to Translational Pharmacology, a section of the journal Frontiers in Pharmacology

Received: *09 February 2019*
Accepted: *21 June 2019*
Published: *17 July 2019*

Citation:
Ampuero E, Cerda M, Härtel S, Rubio FJ, Massa S, Cubillos P, Abarzúa-Catalán L,Sandoval R, Galaburda AM, and Wyneken U (2019) Chronic Fluoxetine Treatment Induces Maturation-Compatible Changes in the Dendritic Arbor and in Synaptic Responses in the Auditory Cortex. Front. Pharmacol. 10:804. doi: 10.3389/fphar.2019.00804

INTRODUCTION

Selective serotonin reuptake inhibitors (SSRI) such as fluoxetine, used in chronic antidepressant treatment, induce adaptive rearrangements in the central nervous system that are not fully characterized. At the structural level, fluoxetine induces an enlargement of dendritic spines and increased spine density in several forebrain regions (Hajszan et al., 2005; Guirado et al., 2009; Ampuero et al., 2010; Kitahara et al., 2016). In adult rats, this is associated with a switch of synaptic glutamate receptor subunits favoring an enrichment of NMDA receptors (NMDA-Rs) containing preferentially GluN2A over GluN2B subunits (Ampuero et al., 2010; Rubio et al., 2013; Beshara et al., 2016), a switch consistent with synaptic maturation (Paoletti et al., 2013). NMDA-Rs are hetero-tetramers composed obligatorily of two GluN1 and two GluN2 subunits, which, in the majority of forebrain neurons, correspond to GluN2A and GluN2B. During development, GluN2B expression decreases dramatically. This goes along with increases in GluN2A-containing NMDA-Rs, which are mainly located in mature synapses and mediate cell survival. Conversely, GluN2B-containing NMDA-Rs are located in less stable (i.e., plastic) synapses, as well as at extrasynaptic sites, where they favor cell death (Paoletti et al., 2013). The developmental switch towards higher GluN2A expression, as well as experimental introduction of GluN2A subunits, produces a reduction in the dendritic length and branching that depends on different, C-terminal specific, intracellular signaling capacities (Kannangara et al., 2014; Bustos et al., 2017; Keith et al., 2019). In contrast, introduction of GluN2B subunits increase the number of dendritic branches and dendritic length (Sepulveda et al., 2010; Bustos et al., 2014). Considering the widespread increase in GluN2A subunits following fluoxetine, we examined structural and synaptic adaptations in cortical areas that are not directly involved in the modulation of mood, such as sensory (including auditory) and motor cortices, which are impaired in depression and might be affected by fluoxetine treatment (Zwanzger et al., 2012; Frodl, 2017; Yin et al., 2018). We specifically evaluated the dendritic architecture and the synaptic properties of pyramidal neurons in the auditory cortex after fluoxetine treatment, an area that is disturbed in depression (Zweerings et al., 2019). Our results indicate that fluoxetine induces structural and functional adaptations compatible with increased network maturation. These properties of fluoxetine could be useful in the treatment of diseases characterized by altered GluN2B over GluN2A ratios and the associated growth of aberrant dendritic arbors and/or of diseases characterized by NMDA-R-dependent toxicity due to GluN2B-dependent calcium overload.

MATERIALS AND METHODS

Materials

All chemical reagents were purchased from Sigma (St Louis, MO), unless otherwise stated.

Animals

Male Sprague–Dawley rats were housed in groups of three to four animals in their home cages and kept under a 12-h light/dark cycle (light on at 7 AM) cycle at 22 ± 1°C. Food and water were available *ad libitum*. At the beginning of the experiment, rats were 78 days old, and their average weight was 266.5 ± 42 g (control group) and 269 ± 40 g (fluoxetine group). At the end of the treatment period, rats were 106 days old and weighted 392 ± 51 and 372 ± 53 g on average, respectively.

As in our previous studies, fluoxetine at a dose of 0.7 mg/kg (Ely-Lilly Co., Indianapolis, USA) or saline solution (control) was administered by intraperitoneal (i.p.) injection once daily between 9 and 10 AM for 28 days. This dose induces increased BDNF expression and TrkB-dependent signaling at synapses, as well as remodeling glutamate neurotransmission and GluN2A over GluN2B switch of NMDA-R subunits (Wyneken et al., 2006; Ampuero et al., 2010; Rubio et al., 2013). This study was carried out in accordance with the Guide for the Care and the Use of Laboratory Animals from the National Institutes of Health (Ed 8; http://grants.nih.gov/grants/olaw/Guide-for-the-Care-and-Use-of-Laboratory-Animals.pdf) and the Bioethical Guidelines for the Use of Laboratory Animals from Universidad de los Andes Bioethical Committee. The protocol was supervised by the Universidad de los Andes Bioethical Committee.

Golgi Staining and Morphometric Analysis

To perform Golgi staining, the adult rats were sacrificed under ketamine (50 mg/kg) and xylazine (5 mg/kg) anesthesia, 24 h following the last fluoxetine or saline dose (n = 10–11 per group). The rats were perfused intracardially with saline solution followed by 300 ml of 4% buffered paraformaldehyde solution. Immediately after perfusion, the brains were removed and processed for Golgi staining using GolgiStainTM kit as previously described (Ampuero et al., 2007).

Coronal sectioning at 150 μm was performed to analyze dendritic morphology. The morphometric analysis of pyramidal neurons was restricted to stereotaxic coordinates (in mm): for the prelimbic (PrL) cortex to: interaural 13.20 and Bregma −4.20, for the secondary motor cortex (M2) to: interaural 5.86 and Bregma −3.14, for retrosplenial granular b cortex (RSGb) to: interaural 5.20 and Bregma −3.8 mm and for primary auditory cortex (AUD1) to: interaural 4.70 and Bregma −4.30 (Paxinos and Watson, 1998).

Golgi-stained images were obtained with a Nikon Eclipse TE2000-U inverted epifluorescence microscope with a Plan Fluor 20x/1.25 numeric aperture attached to a cooled monochrome camera DS-2MBWc.

Pyramidal neurons were defined by the presence of basilar dendrites, a distinctive, single apical dendrite, and dendritic spines (Spruston, 2008). The observer, blind to experimental conditions, selected randomly at least 10 neurons from each animal that fulfilled the following selection criteria: 1) absence of truncated dendrites, 2) consistent and dark impregnation along the entire dendritic field, and 3) spatial separation from neighboring impregnated neurons to avoid overlap. Camera lucida tracings from selected neurons (500×, BH-2, Olympus Co., Tokyo, Japan) were performed and then scanned (eight-bit grayscale TIFF images with 1,200 dpi resolution; EPSON ES-1000C) along with a calibrated scale for subsequent computerized image analysis. For morphometric analysis of digitized images, we used Image J

software (National Institutes of Health). In each selected neuron, the total, basal, and apical dendritic lengths were determined.

In Utero Electroporation

For *in utero* electroporation, five pregnant young female rats at embryonic day 16.5 were anesthetized with xylazine (5 mg/kg) and ketamine (50 mg/kg). After shaving the rat's belly at the location of the desired incision and disinfecting the abdominal skin with povidone solution, an approximately 2-cm midline skin incision was made followed by another incision along the linea alba. Then, both uterine horns were drawn out through the incision. To inject the plasmid, glass capillaries (pulled with the P97 Pipet Puller, Sutter Instruments, USA) were filled with the plasmid solution (1 μg/μl), mixed with Fast Green (<0.75 mg/ml, Sigma Aldrich, USA), and delivered into the left lateral ventricle with a pressure Pico pump (PV830, World Precision Instruments, USA). The plasmid containing the CAG promoter (i.e., driven by the strong ubiquitous promoter cytomegalovirus early enhancer and chicken beta actin) and the monomeric red fluorescent protein (mRFP) sequence, kindly shared by Joseph LoTurco, was used (LoTurco et al., 2009) (**Supplementary Figure 1**).

Electric pulses were applied with an electroporation system built with a power supply, a resistor, pulse/charge power switch, capacitor, and a foot pedal for providing the pulse. To introduce the plasmid into a larger region of the cortex, the cathode was placed on the location corresponding to the left temporal lobe, and the anode was placed on the location corresponding to the right temporal lobe. Voltage pulses were adjusted to the developing stage of the fetuses (65 mV for E16). Only one pulse lasting 3 s was applied. The embryos closest to the cervix were not injected nor electroporated because the possible death of these animals could block the delivery. After the procedure was completed, the two horns were reinserted into the abdominal cavity with an additional 5 ml of isotonic saline solution, and then, the abdominal wall and skin were closed with nylon and silk sutures, respectively. After surgery, the rats gave birth normally. Only male pups (n = 18) underwent further induction and treatment to circumvent hormonal differences influencing the results. At 78 days of age rats began fluoxetine treatment. Overall, the effectiveness of the electroporation procedure was 41%, and from these, 30% expressed mRFP in the primary auditory cortex (AUD1) resulting in six rats for 3-dimensional analysis.

3D Analysis

Image Acquisition

The images from mRFP-electroporated animals were obtained using a Leica LSI Macro-Zoom confocal laser scanning microscope with a 5× air objective (NA = 0.12) plus optical zoom 1.7×, excitation with solid state laser at 488 nm, and spectral detection. TIFF images (8 bits) of 1,024 × 1,024 pixels were acquired with 0.1 μm between z-sections and then projected into one 2D image (maximum intensity projection). To obtain a broad field of acquisition, the mosaic function in LAS-AF software (Leica Microsystems, Bannockburn, IL, USA) was used. At least 50–70 focal planes of 0.1 μm were obtained.

Image Segmentation

Semi-automatic segmentation was applied to the neuron stacks. The automatic part was implemented in FIJI software (Schindelin et al., 2012), sequentially using a normalization step to reduce variability among samples (using the full histogram), applying an anisotropic diffusion filter (parameters 0.1 and 0.99) to smooth neuron processes without blurring edges, highlighting elongated areas associated with processes with the Frangi filter (default parameters), and finally with a manual threshold to binarize the stack. A manual check verified that close neurons were at least separated by 1 voxel and the 3D connectivity of the object, so a simple 3D binary object was in the stack.

Skeleton Estimation

The segmented neuron was simplified into a graph, or skeleton, where segments represent processes, and branching points represent nodes. The skeleton estimation algorithm used as input a surface triangle-mesh geometrical representation that was computed in IDL (Lorensen and Cline, 1987). In brief, the skeleton computation is an optimization algorithm that searches for the best graph making a balance between two terms: a good representation of the original volume and use of as few segments as possible as proposed initially by Au et al. (2008) and implemented by Lavado (2018).

Parameter Computation

The parameters retrieved from the neurons were total dendritic length, apical dendritic length, basal dendritic length, and number and length of processes per category (primary, secondary, or higher). To obtain those parameters, a single segment was manually identified as the soma, as to orient the graph generating a tree-like structure. To define apical/basal length, a single process starting from the soma, which contains the segments defined as the apical reference, defined the apical process. To identify primary processes, the longest paths of each of the segments starting from the soma were computed, and recursively, the same algorithm repeated along the branches to identify higher order processes.

Slice Preparation and Extracellular Field Recording in Auditory Cortical Synapses

To prepare brain slices, animals were quickly decapitated and brains removed, immersed in ice-cold dissection buffer (in mM; 212.7 sucrose; 5 KCl; 1.25 NaH_2PO_4; 3 $MgSO_4$; 1 $CaCl_2$; 26 $NaHCO_3$; 10 glucose; pH 7.4), and coronal slices (400 μm thickness) were obtained using a vibratome (Ted Pella Inc., USA). Slices were transferred to an interface chamber containing artificial cerebrospinal fluid (aCSF) saturated with 95% O_2–5% CO_2 at 36°C, left at these conditions for 45 min, and then maintained at 24°C for 1 h.

Field excitatory postsynaptic potentials (fEPSP) recorded from auditory cortex were evoked as described in Hefti and Smith (Hefti and Smith, 2000). Briefly, electrical stimulation (biphasic, constant current, 200 ms stimuli) was delivered every 15 s to the layer I in the primary auditory cortex of control and fluoxetine-injected rat brain slices, using a concentric bipolar electrode (FHC Corporate

and Manufacturing, Bowdoin, ME, USA) and recorded in layers II–III. Recording electrodes comprised glass micropipettes (1–3 MΩ) filled with aCSF. Baseline recordings were performed using oxygenated (5% CO_2–95% O_2) Mg^{2+}-free aCSF at 32°C on the recording chamber continually perfused at a flow of 2 ml/min. After 10 min, the recording solution was replaced by Mg^{2+}-free aCSF containing 20 μM 6-cyano-7-nitroquinoxaline-2,3-dione (CNQX) and 10 μM Picrotoxin, to block α-amino-3-hydroxy-5-methyl-4-isoxazolepropionic acid (AMPA) and gamma-aminobutyric acid receptors ($GABA_A$) receptors. After incubation of 20 min, the NMDA-R-mediated component of the fEPSP was recorded for 10 additional minutes. Finally, the recording chamber solution was replaced a second time by an aCSF containing 20 μM CNQX, 10 μM Picrotoxin, and 150 nM ifenprodil, to block GluN2B-containing NMDA receptors, and incubated again for 20 min to record the remaining GluN2A-mediated NMDA-R component for 10 additional minutes. Data recorded from pharmacological experiments were acquired using an extracellular amplifier (Model EX 4-400 Differential Extracellular Amplifier, Dagan Corporation, USA) and a data acquisition board (National Instruments, USA) controlled through Igor Pro software (WaveMetrics Inc, Lake Oswego, Oregon, USA). All the electrophysiological experiments were performed using tissues from at least eight different animals for each condition.

Analysis of Field Excitatory Postsynaptic Potentials Obtained From the Auditory Cortex

To determine differences between fEPSP obtained from control and fluoxetine-treated slices, acquired data were transferred to the scientific graphing and data analysis software Origin 9.0. Thereafter, the rising and decay portions of each curve were independently adjusted to a Boltzmann curve, obtaining from the fitted rising part the peak and rise time parameters, whereas decay time was obtained from the latter. The area under curve was calculated using the first 30 ms of the curve, taking as time 0 the beginning of the fEPSP curve.

Statistical Analysis

The values are shown as the means ± SEM. Statistical significance was evaluated by Mann–Whitney *U*-test for morphological data (Golgi staining and 3D reconstruction) and two way-ANOVA followed by *post hoc* Bonferroni correction for electrophysiological data (GraphPad Prism software, San Diego, USA), as indicated in the figure legends. A probability level of 0.05 or less was considered significant.

RESULTS

Repetitive Fluoxetine Administration Induces Shortening of the Dendritic Arbor of Pyramidal Neurons

We had previously shown that repetitive fluoxetine treatment augmented the spine density and the number of mature, mushroom-type spines and favored GluN2A-containing NMDARs and GluA2-containing α-amino-3-hydroxy-5-methylisoxazole-4-propionate receptors (AMPA-Rs) (Ampuero et al., 2010; Ampuero et al., 2013; Rubio et al., 2013). Consistently, this switch in glutamate receptor subunits was associated with decreased calcium influx, synaptic plasticity, and hippocampus-dependent learning (Ampuero et al., 2013; Rubio et al., 2013; Beshara et al., 2016). Taking into consideration that glutamate receptor subunits determine dendritic morphology in neurons, we then examined morphological changes in dendritic length and complexity (Bustos et al., 2017; Keith et al., 2019). Using the Golgi staining method, we measured the dendritic length of apical and basal branches of pyramidal neurons in several cortical areas. In two limbic cortices, e.g., the prelimbic cortex (PrL) and retrosplenial granular b cortex (RSGb), a decrease in the total dendritic length after fluoxetine treatment was observed, and this resulted from a reduction in the basal dendritic lengths in layer II–III neurons of the PrL cortex (in μm, control = 998 ± 53; fluoxetine = 802 ± 108, $p = 0.045$) and in layer V neurons (in μm, control = 986 ± 204; fluoxetine = 624 ± 72, $p = 0.038$). Similarly, the basal dendritic length decreased in layer V neurons of the RSGb cortex (in μm, control = 821 ± 134; fluoxetine = 499 ± 54, $p = 0.020$) (**Figure 1** and **Supplementary Table 1**). In the RSGb, we did not obtain reliable staining of layer II–III neurons. Similarly, in cortical areas not directly involved in antidepressant action, e.g., pyramidal neurons of the II–III layer of the secondary motor cortex (M2) and primary auditory cortex (AUD1), a reduction in the dendritic length was shown: in M2, apical branches were reduced (in μm, control = 1,043 ± 129; fluoxetine = 598 ± 60, $p = 0.014$), while in AUD1, the basal dendritic length was affected (in μm, control = 1,661 ± 138; fluoxetine = 1,086 ± 99, $p = 0.0025$) (**Figure 2** and **Supplementary Table 1**).

Although the Golgi method has been used for decades to assess dendritic arbor morphology, this technique does not allow a 3-dimensional reconstruction. We thus used mRFP expression in cortical neurons to analyze the dendritic arbor of pyramidal neurons from layer V of AUD1 (**Figure 3** and **Supplementary Table 2**). In **Figure 3A**, an overview of the electroporation procedure, including expression of the fluorescent protein in isolated neurons, is shown. In **Figure 3B**, a representative image of the 3-dimensional reconstructed branches of neurons obtained from control or repetitive fluoxetine-treated animals is shown. Representative images at different levels of analysis are indicated, showing the raw data in the upper panel, the skeletonized data in the middle panel, and the reduced skeleton in the lower panel. The analysis of the reduced skeleton revealed a significant reduction in both the apical (in μm, control = 2,739 ± 272; fluoxetine = 1,460 ± 315, $p = 0.008$) and the basal (in μm, control = 3,178 ± 302; fluoxetine = 1,786 ± 242, $p = 0.008$) dendritic length after fluoxetine (**Figure 3C**). When comparing both experimental approaches to assess the dendritic length, we found (as expected) greater dendritic length when the 3-dimensional reconstruction was performed, as well as a significant reduction of basal dendrites lengths after fluoxetine, in contrast to the Golgi method with which this difference was not significant and thus was not detectable with the 2-dimensional analysis. Similarly, decreased complexity of the dendritic tree was detected after fluoxetine when using the 3-dimensional method but not the Golgi method (**Figure 3D**). This resulted from a decrease in the number of secondary and tertiary processes, while primary processes were not affected.

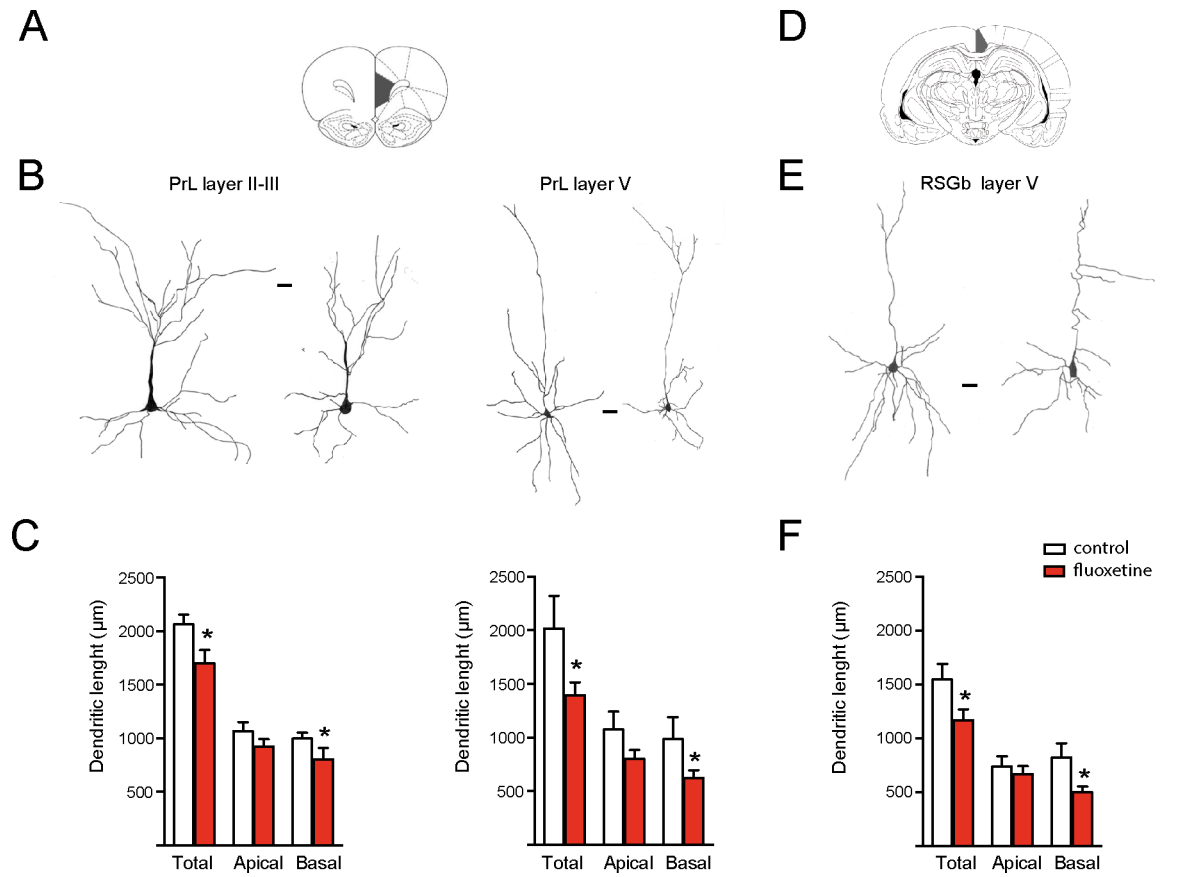

FIGURE 1 | Chronic fluoxetine treatment (28 days) decreased the dendritic length of pyramidal neurons in limbic cortices. Golgi staining was performed to analyze the prelimbic (PrL) and retrosplenial granular b (RSGb) cortices. Neurons were drawn with camera lucida and digitally scanned to visualize the morphology. **(A)** and **(D)** The analyzed areas are schematically shown (Paxinos and Watson, 1998). **(B)** and **(E)** Representative drawing of pyramidal neurons obtained from vehicle treated (control) or fluoxetine-treated rats. In the PrL cortex, layer II–III and V neurons were analyzed, while in the RSGb cortex, the analysis was restricted to layer V neurons. In each case, the neuron at the left is from the control (vehicle treated), while the neuron at the right is from the fluoxetine-treated animal. Scale bar: 20 µm. **(C)** and **(F)** Quantifications of the total, apical, and basal dendritic lengths of neurons in the PrL cortex (layers II/III in the left panel and layer V in the right panel) and RSGb cortices. Values represent the mean ± SEM. For each condition, we analyzed at least 10 neurons obtained from four animals per condition for the PrL cortex and three animals per condition for the RSGb cortex. *$p \leq 0.05$, Mann–Whitney *U*-test.

This result is consistent with the morphological consequences observed in neuronal cultures in which GluN2A/GluN2B ratios are manipulated (Bustos et al., 2014; Bustos et al., 2017). Now, we also show that repetitive fluoxetine treatment induces a general reduction in the dendritic arbor in limbic and nonlimbic cortical areas, which is indicative of increased maturation. These results are also consistent with previous observations of increased dendritic spine density and of mushroom-type synapses after fluoxetine (Ampuero et al., 2010; Rubio et al., 2013).

Electrophysiological Recordings in the Auditory Cortex Suggest Increased Synaptic GluN2A Subunit Levels

To assess whether the evoked field potentials in the auditory cortex are consistent with increased synaptic GluN2A levels (Ampuero et al., 2010), we evaluated the NMDA-mediated responses by blocking AMPA receptors with CNQX. Additionally, we blocked GluN2B-containing NMDA-Rs with ifenprodil in a sequential manner, using slices obtained from control and fluoxetine-treated animals (**Supplementary Table 3**). **Figure 4A** shows representative traces of these experimental conditions, while in **Figure 4B–E**, different parameters of the fEPSP are evaluated. The peak amplitude of the total or NMDA-mediated response did not change (**Figure 4B**). However, ifenprodil was ineffective in reducing the peak amplitude of the field excitatory postsynaptic potential (fEPSP) after fluoxetine treatment (in mV, control = −0.247 ± 0.066; fluoxetine = −0.499 ± 0.087, p = 0.038 in the condition CNQX plus ifenprodil), consistent with a GluN2B-to-GluN2A switch. In the same line, control responses were blocked by CNQX plus ifenprodil (in mV, aCSF = −0.758 ± 0.019; CNQX + ifen = −0.247 ± 0.066; p = 0.017), while in slices of fluoxetine-treated rats, CNQX plus ifenprodil did not block the response with respect to aCSF. Moreover, **Figure 4C** shows a significant decrease in the rise time when the AMPA and GluN2B components of the fEPSP were removed (i.e., in the presence of

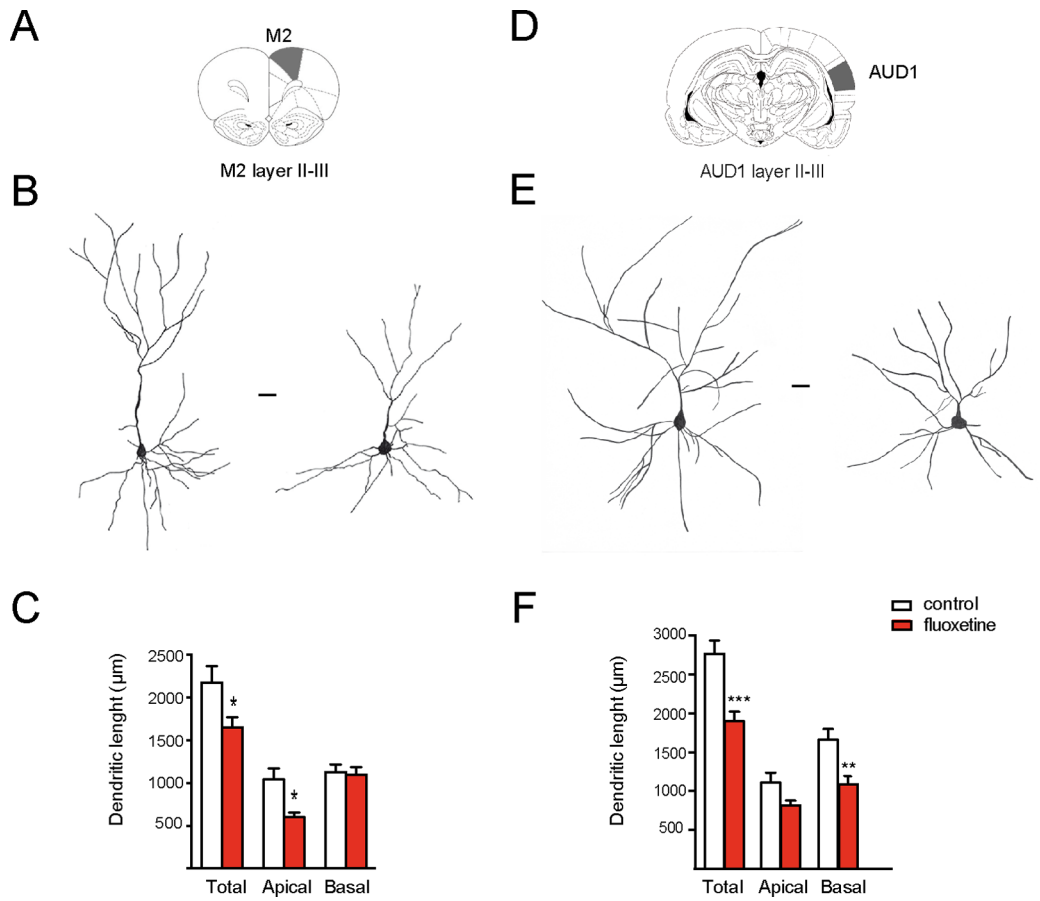

FIGURE 2 | Chronic fluoxetine treatment (28 days) decreased the dendritic length of pyramidal neurons in the motor and auditory cortices (layer II–III). Golgi-stained neurons of the II–III layer of the secondary motor cortex (M2) and the primary auditory cortex (AUD1) were drawn with camera lucida and digitally scanned. **(A)** and **(D)** Scheme of the analyzed areas (Paxinos and Watson, 1998). **(B)** and **(E)** Representative drawings of neurons obtained from vehicle or fluoxetine-treated animals. In each case, the neuron at the left is from the control (vehicle-treated), while the neuron at the right is from the fluoxetine-treated animal. Scale bar: 20 µm. **(C)** and **(F)** Quantifications of the total, apical, and basal dendritic lengths. For each condition, we analyzed at least 10 neurons obtained from three animals per group (in the case of M2) and from three (control) and four (fluoxetine-treated) animals in the case of AUD1. Values represent mean ± SEM. $^{*}p \leq 0.05$; $^{**}p < 0.01$ $^{***}p < 0.001$ Mann–Whitney *U*-test.

CNQX plus ifenprodil) (in ms, control = 0.264 ± 0.02; fluoxetine = 0.17 ± 0.02, $p = 0.008$), consistent with an increase in GluN2A receptor subtypes, which are known to present faster rise time kinetics than other GluN2 subunits (Hansen et al., 2018). Interestingly, the integrated response over 30 ms (area under the curve, mV*ms) increased in all conditions after fluoxetine compared to control animals (**Figure 4D**). In this case, the total aCSF response was control = 3.4 ± 0.3; fluoxetine = 5.0 ± 0.6 ($p = 0.029$); the NMDA-mediated response after AMPA-R blockade was of control = 1.2 ± 0.2; fluoxetine = 3.0 ± 0.5 ($p = 0.029$); and the GluN2A-mediated response was of control = 0.80 ± 0.1; fluoxetine = 1.5 ± 0.3 ($p = 0.031$). These results are consistent with previous data showing a larger proportion of mushroom-like spines and increased spine density after fluoxetine administration (Ampuero et al., 2010). In addition, the percentage of blockade of the integrated NMDA-mediated response (i.e., in the presence of CNQX) after ifenprodil decreased in treated animals, revealing a relative reduction in the GluN2B-mediated response (**Figure 4E**). The following percentages of blockade were observed: in control slices, the blockade by CNQX was of 37.93 ± 4.9% and increased to 72.86 ± 14% when ifenprodil was added ($p = 0.035$). In contrast, in slices from fluoxetine-treated rats, blockade by CNQX was 57.68 ± 3.8%, and after ifenprodil, it was only 50.79 ± 4.5%, revealing (as in **Figure 4B**) a failure of ifenprodil to block the synaptic response; this is consistent with a reduction in the GluN2B-mediated response after fluoxetine treatment.

DISCUSSION

The morphological and electrophysiological data obtained in the present work show that the treatment of adult rats with fluoxetine during 4 weeks induced a reduction in the dendritic arbor in cortical pyramidal neurons and a gain of GluN2A over GluN2B mediated fEPSPs in the auditory cortex. The 3-dimensional reconstruction of neurons from serial microscopic images provided an advantageous

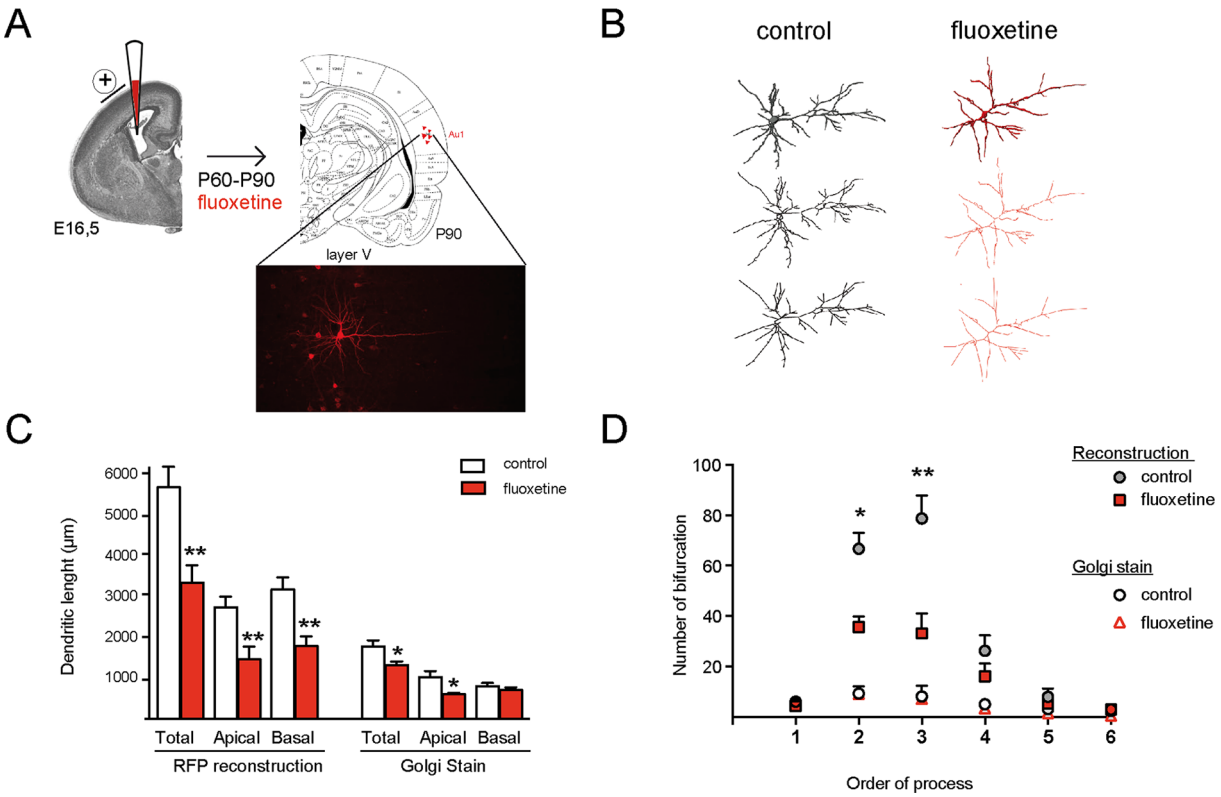

FIGURE 3 | Repetitive flx treatment decreases the dendritic length of pyramidal neurons in the primary auditory cortex of rats. **(A)** Schematic representation of in utero electroporation to target gene delivery into neurons in the auditory cortex. The inset shows mRFP electroporated pyramidal neurons selected for analysis in layer V of the primary auditory cortex in coronal slices of 150 µm. **(B)** The 3-dimensional reconstruction of confocal images is shown for isolated neurons obtained from vehicle and fluoxetine-treated animals. Upper panel: raw image; middle panel: skeletonized form; and lower panel: the reduced skeletonized form. **(C)** Quantifications (mean ± SEM) of the total, apical, and basal dendrites, measured in the skeletonized form of neurons after 3-dimensional reconstruction (left grouped bars) or measured after Golgi staining of the same area (right grouped bars). **(D)** Quantification of the number of bifurcations according to increasing orders of processes. Value represent mean ± SEM. For 3-dimensional reconstruction, eight control neurons obtained from three animals and seven neurons obtained from three animals were analyzed. *$p \leq 0.05$; **$p < 0.01$ Mann–Whitney *U*-test.

and powerful strategy for better visualizing changes in dendritic morphology. We propose that the fluoxetine-induced sculpting of neuronal circuits could be useful in the treatment of brain disorders characterized by a shift towards pathologically increased neuronal sprouting and altered synaptic transmission, such as in some forms of epilepsy.

Morphological Changes in Pyramidal Neurons After Fluoxetine

We and several other groups had previously reported that fluoxetine increased spine density as well as the proportion of mushroom-type (i.e., mature) spines in several forebrain regions (Hajszan et al., 2005; Guirado et al., 2009; Ampuero et al., 2010; Kitahara et al., 2016). A spine increment in the somatosensory cortex with the use of the rapid acting antidepressant ketamine has been proposed as a common and necessary mechanism involved in effective antidepressant treatment (Pryazhnikov et al., 2018). However, the functional consequences of such changes for neuronal network activity remain uncertain. In our experiments, we also observed increased spine density but decreased dendritic length. To estimate whether fluoxetine changes the total number of synapses, we calculated whether a mean increase of 21.4 ± 3.4% in spine density (Ampuero et al., 2010; Rubio et al., 2013) and a mean decrease in the dendritic length of 25.7 or 41.3% (Golgi method or 3-dimensional reconstruction, respectively) affects the total synapse number. With both estimations, it could be concluded that the number of total synapses does not change (Golgi method or 3-dimensional reconstruction, respectively). Note that as spine density varies along primary and higher order dendrites, these estimations are simple approximations based on the mean percentage of spine increase. However, as reported by us and by others, the synaptic contacts shift to a more stable type (i.e., mushroom type), putatively affecting in a positive manner the strength of certain synaptic connections but causing the pruning of others.

Synaptic Responses in the Auditory Cortex

In patients, it has been shown that auditory cortex activation and auditory perception and processing are impaired in

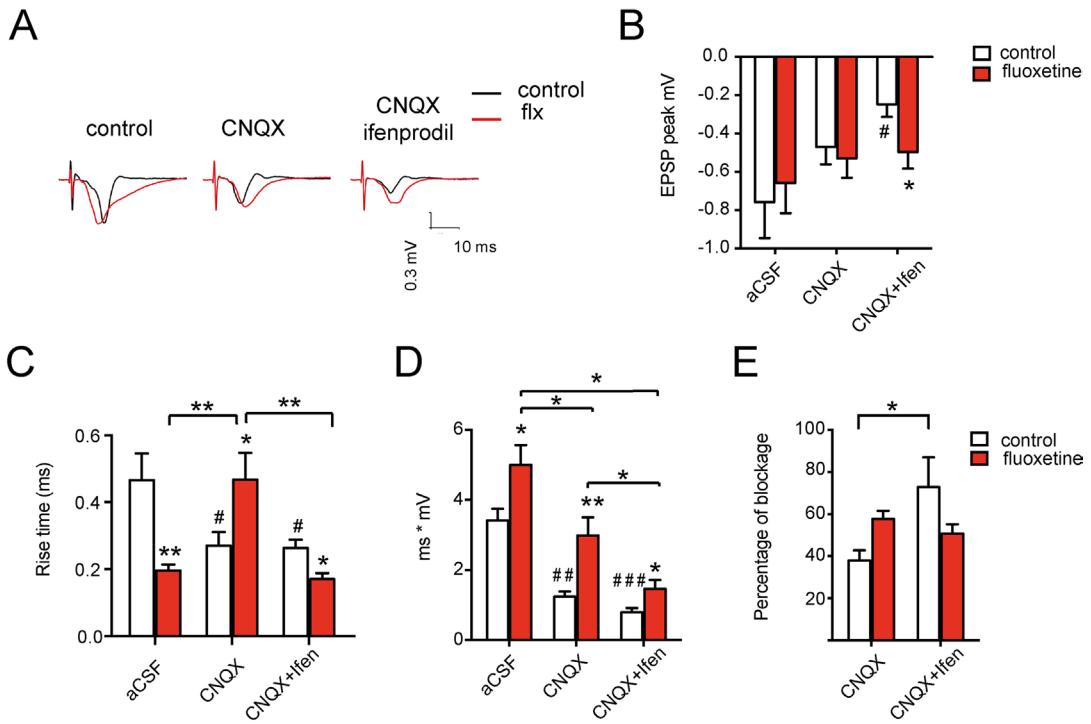

FIGURE 4 | Chronic fluoxetine treatment modifies the postsynaptic response in the auditory cortex of rats. Different parameters of the fEPSPs were measured after stimulation in layer I and recording in layer II–III: **(A)** Representative recordings in slices from vehicle or fluoxetine-treated animals (left) followed by the NMDA-mediated response (in the presence of CNQX to block AMPA receptors) (middle) and of the GluN2A-mediated response (in the presence of CNQX + ifenprodil to block AMPA and GluN2B-containing receptors) (right). **(B)** Peak fEPSPs, **(C)** rise time (or the time at which the 67% of the peak potential is achieved), **(D)** total postsynaptic potential (area under the curve), and **(E)** percentage of blockade of the total fEPSP by CNQX (NMDA component) or by CNQX + ifenprodil (GluN2A component). Slices were perfused with Mg-free aCSF (control recording) or with aCSF in the presence of CNQX and then in the presence of CNQX + ifenprodil. For each condition, at least 32 slices were recorded, obtained from 16 animals (n = 8 control and n = 8 fluoxetine). Figures show the mean ± SEM. One way-ANOVA followed by *post hoc* Bonferroni test was used. $^{*}p \leq 0.05$; $^{**}p < 0.01$ relative to the control within each drug condition (i.e., within each pair of red vs. white bar). For indicated comparisons among groups, unpaired t-tests were used $^{\#}p \leq 0.05$; $^{\#\#}p < 0.01$, $^{\#\#\#}p < 0.001$ relative to the first bar (aCSF-control without drug addition).

depression (Zwanzger et al., 2012; Bonetti et al., 2017; Zweerings et al., 2019). Moreover, age-related hearing loss has been associated with late life depression (Husain et al., 2014; Rutherford et al., 2018; Scinicariello et al., 2019), and in animals, chronic restraint stress decreased glucose metabolism in the auditory cortex (Wei et al., 2018). It would be relevant to know whether antidepressant medication reverts auditory dysfunction. In our study, we addressed the effects of fluoxetine in naïve (nondepressed) rats.

The electrophysiological recordings of fEPSPs in the auditory cortex were compatible with increased glutamatergic synaptic response and increased GluN2A levels in synapses (Ampuero et al., 2010; Rubio et al., 2013). In fact, the amplitude of the evoked and integrated response increased in all the examined conditions (total, NMDA-mediated and GluN2A-mediated), revealing that, independent of the postsynaptic glutamate receptor composition, the glutamatergic response increased. In addition, the ineffectiveness of ifenprodil in reducing the NMDA-mediated response after fluoxetine administration indicated a loss in the contribution of GluN2B receptors to synaptic fEPSPs, and the fEPSP rise time decreased when the GluN2B component was removed with ifenprodil, unmasking in such a way the characteristic GluN2A fast rise time kinetics, as reported previously (Amico-Ruvio et al., 2012).

Consistent with the idea of more mature and less plastic synapses at AUD1 intracortical synapses, the field postsynaptic potential augmented after fluoxetine while long-term potentiation (LTP) was impaired (Dringenberg et al., 2014). Similar effects of fluoxetine were observed by us and others in the hippocampal CA1 region (Rubio et al., 2013; Van Dyke et al., 2019). These changes, indicating more mature but less plastic synapses, were corroborated using glutamatergic markers which also extended to GABAergic markers of synaptic maturation in the visual cortex (Beshara et al., 2016). We postulate that the plasticity-inducing effect of fluoxetine described by others (Maya Vetencourt et al., 2008; Kobayashi et al., 2010; Guirado et al., 2014; Ruiz-Perera et al., 2015) might be compatible, at different time points, with the synaptic stabilization and dendritic pruning observed in our rat model. However, it is not yet known which temporal changes during the treatment period may sequentially induce a plasticity period, followed by a stabilization period characterized by a "mature" network. The time course of these changes might

be related to region-specific differences in serotonin receptor expression types and/or levels (Charnay and Leger, 2010). Auditory processing is impaired in major depression, and this is reverted by SSRIs (Frodl, 2017). We have focused here on the auditory cortex because the participation of serotonin in the auditory processing is well documented, and it can be modulated after repetitive administration of the SSRI fluoxetine (Ji and Suga, 2007; Hurley and Hall, 2011).

Therapeutic Potential Associated to Selective Reduction of GluN2B Subunits and of Dendritic Tree Length

Our results indicate that the SSRI fluoxetine induced dendritic and synaptic pruning in areas of the cerebral cortex not directly implicated in the main symptoms of depression. In principle, these pro-maturational effects could be useful for restoring stable synaptic networks in pathologies where a shift towards immature circuits and/or to GluN2B-dependent neurotoxicity occurs. Thus, in animal models of temporal lobe epilepsy, the GluN2B/GluN2A ratio increased in several forebrain regions (Amakhin et al., 2017; Zubareva et al., 2018), and synapses enriched in GluN2B subunits favored seizure susceptibility (Okuda et al., 2017), whereas blockade of GluN2B receptors during experimental status epilepticus with compounds that included the rapid acting antidepressant ketamine (a non-selective NMDA-R antagonist) reduced neuronal damage (Loss et al., 2019). Moreover, fluoxetine and other SSRIs are considered to be safe in the treatment of depression in epileptic patients, although exceptions (e.g., in some epilepsy subtypes) to this general rule might exist (Kanner, 2016a; Kanner, 2016b). However, the use of fluoxetine to favor GluN2A-associated structural and functional synaptic changes in nondepressed epileptic patients or even in preventing oxidative stress associated to neurological disorders is open to discussion and additional experimental work (Zhu et al., 2018).

Interestingly, the neuroprotective potential of direct and selective GluN2B blockade has extensively been addressed in several brain disorders (Gielen et al., 2009; Mony et al., 2009). Moreover, uncoupling of GluN2B C-terminal-dependent signaling or selective GluN2B blockade has antidepressant effects (Li et al., 2018) and might exert neuroprotective properties in Alzheimer's disease, Huntington's disease, and after stroke (Dau et al., 2014; Wu and Tymianski, 2018; Xu et al., 2019). In all these cases, fluoxetine could complement therapeutic strategies aimed at preventing or reducing neurotoxicity. In additional observations, fluoxetine reduces β-amyloid levels and toxicity, an effect that may depend on subunit-specific NMDA-R blockade and increased GluN2A-dependent brain-derived neurotrophic factor (BDNF) and transforming-growth-factor-β1 (TGF-β1) signaling (Tucci et al., 2014; Schiavone et al., 2017; Caraci et al., 2018). Moreover, fluoxetine displays direct GluN2B antagonism, an effect that results convergent with the GluN2B to GluN2A subunit switch and the morphological consequences described by us (Kiss et al., 2012). This selectivity would be advantageous over the nonselective NMDA-R antagonist ketamine, a promising novel antidepressant drug with unwanted side effects that have yet to be overcome (Duman, 2018; Orhurhu et al., 2019). Interestingly, several mechanisms underlying the therapeutic action of ketamine are shared with fluoxetine, but with a different time scales. In such a way, GluN2B subunits are essential for the antidepressant effect of ketamine and the downstream activation of mTOR signaling (Wang et al., 2011; Miller et al., 2014) and ketamine regulates positively spinogenesis (Moda-Sava et al., 2019).

Taken together, the morphological changes observed by us after repetitive fluoxetine administration, consistent with a GluN2B subunit reduction in several forebrain areas, may have promising applications in brain disorders beyond depression.

AUTHOR CONTRIBUTIONS

EA and UW designed experiments and wrote the manuscript; AG participated and instructed in *in utero* electroporation experiments and revised the manuscript; MC, EA, and SH did 3-dimensional reconstruction and quantifications; FR and SM did *in utero* electroporation and drug treatments; PC, EA, and LA-C did Golgi staining and analysis blind to the experimental condition; FR and RS critically reviewed the manuscript; and RS did electrophysiological recordings.

FUNDING

This work was supported by Fondecyt 1140108 (to UW), 1181823 (to SH) and 11161033 (to MC), Conicyt (to EA), CONICYT PIA ACT1402, ICM P09-015-F, and DAAD 57220037 and 57168868 (to SH and MC), and CORFO 16CTTS-66390 (to SH).

SUPPLEMENTARY MATERIAL

The Supplementary Material for this article can be found online at: https://www.frontiersin.org/articles/10.3389/fphar.2019.00804/full#supplementary-material

REFERENCES

Amakhin, D. V., Malkin, S. L., Ergina, J. L., Kryukov, K. A., Veniaminova, E. A., Zubareva, O. E., et al. (2017). Alterations in properties of glutamatergic transmission in the temporal cortex and hippocampus following pilocarpine-induced acute seizures in Wistar rats. *Front. Cell Neurosci.* 11, 264. doi: 10.3389/fncel.2017.00264

Amico-Ruvio, S. A., Paganelli, M. A., Myers, J. M., and Popescu, G. K. (2012). Ifenprodil effects on GluN2B-containing glutamate receptors. *Mol. Pharmacol.* 82, 1074–1081. doi: 10.1124/mol.112.078998

Ampuero, E., Dagnino-Subiabre, A., Sandoval, R., Zepeda-Carreno, R., Sandoval, S., Viedma, A., et al. (2007). Status epilepticus induces region-specific changes in dendritic spines, dendritic length and TrkB protein content of rat brain cortex. *Brain Res.* 1150, 225–238. doi: 10.1016/j.brainres.2007.02.089

Ampuero, E., Rubio, F. J., Falcon, R., Sandoval, M., Diaz-Veliz, G., Gonzalez, R. E., et al. (2010). Chronic fluoxetine treatment induces structural plasticity and selective changes in glutamate receptor subunits in the rat cerebral cortex. *Neuroscience* 169, 98–108. doi: 10.1016/j.neuroscience.2010.04.035

Ampuero, E., Stehberg, J., Gonzalez, D., Besser, N., Ferrero, M., Diaz-Veliz, G., et al. (2013). Repetitive fluoxetine treatment affects long-term memories but not learning. *Behav. Brain Res.* 247, 92–100. doi: 10.1016/j.bbr.2013.03.011

Au, O. K., Tai, C. L., Chu, H. K., Cohen-Or, D., and Lee, T. (2008). Skeleton extraction by mesh contraction. *ACM Trans.* 27, 1–10. doi: 10.1145/1360612.1360643

Beshara, S., Beston, B. R., Pinto, J. G., and Murphy, K. M. (2016). Effects of fluoxetine and visual experience on glutamatergic and GABAergic synaptic proteins in adult rat visual cortex. *eNeuro* 2, 1–13. doi: 10.1523/ENEURO.0126-15.2015

Bonetti, L., Haumann, N. T., Vuust, P., Kliuchko, M., and Brattico, E. (2017). Risk of depression enhances auditory Pitch discrimination in the brain as indexed by the mismatch negativity. *Clin. Neurophysiol.* 128, 1923–1936. doi: 10.1016/j.clinph.2017.07.004

Bustos, F. J., Jury, N., Martinez, P., Ampuero, E., Campos, M., Abarzua, S., et al. (2017). NMDA receptor subunit composition controls dendritogenesis of hippocampal neurons through CAMKII, CREB-P, and H3K27ac. *J. Cell Physiol.* 232, 3677–3692. doi: 10.1002/jcp.25843

Bustos, F. J., Varela-Nallar, L., Campos, M., Henriquez, B., Phillips, M., Opazo, C., et al. (2014). PSD95 suppresses dendritic arbor development in mature hippocampal neurons by occluding the clustering of NR2B-NMDA receptors. *PLoS One* 9, e94037. doi: 10.1371/journal.pone.0094037

Caraci, F., Spampinato, S. F., Morgese, M. G., Tascedda, F., Salluzzo, M. G., Giambirtone, M. C., et al. (2018). Neurobiological links between depression and AD: the role of TGF-beta1 signaling as a new pharmacological target. *Pharmacol. Res.* 130, 374–384. doi: 10.1016/j.phrs.2018.02.007

Charnay, Y., and Leger, L. (2010). Brain serotonergic circuitries. *Dialogues Clin. Neurosci.* 12, 471–487.

Dau, A., Gladding, C. M., Sepers, M. D., and Raymond, L. A. (2014). Chronic blockade of extrasynaptic NMDA receptors ameliorates synaptic dysfunction and pro-death signaling in Huntington disease transgenic mice. *Neurobiol. Dis.* 62, 533–542. doi: 10.1016/j.nbd.2013.11.013

Dringenberg, H. C., Branfield Day, L. R., and Choi, D. H. (2014). Chronic fluoxetine treatment suppresses plasticity (long-term potentiation) in the mature rodent primary auditory cortex *in vivo*. *Neural Plast.* 2014, 571285. doi: 10.1155/2014/571285

Duman, R. S. (2018). Ketamine and rapid-acting antidepressants: a new era in the battle against depression and suicide. *F1000Res* 7, 1–10. doi: 10.12688/f1000research.14344.1

Frodl, T. (2017). Recent advances in predicting responses to antidepressant treatment. *F1000Res* 6, 1–6. doi: 10.12688/f1000research.10300.1

Gielen, M., Siegler Retchless, B., Mony, L., Johnson, J. W., and Paoletti, P. (2009). Mechanism of differential control of NMDA receptor activity by NR2 subunits. *Nature* 459, 703–707. doi: 10.1038/nature07993

Guirado, R., Perez-Rando, M., Sanchez-Matarredona, D., Castren, E., and Nacher, J. (2014). Chronic fluoxetine treatment alters the structure, connectivity and plasticity of cortical interneurons. *Int. J. Neuropsychopharmacol.* 17, 1635–1646. doi: 10.1017/S1461145714000406

Guirado, R., Varea, E., Castillo-Gomez, E., Gomez-Climent, M. A., Rovira-Esteban, L., Blasco-Ibanez, J. M., et al. (2009). Effects of chronic fluoxetine treatment on the rat somatosensory cortex: activation and induction of neuronal structural plasticity. *Neurosci. Lett.* 457, 12–15. doi: 10.1016/j.neulet.2009.03.104

Hajszan, T., Maclusky, N. J., and Leranth, C. (2005). Short-term treatment with the antidepressant fluoxetine triggers pyramidal dendritic spine synapse formation in rat hippocampus. *Eur. J. Neurosci.* 21, 1299–1303. doi: 10.1111/j.1460-9568.2005.03968.x

Hansen, K. B., Yi, F., Perszyk, R. E., Furukawa, H., Wollmuth, L. P., Gibb, A. J., et al. (2018). Structure, function, and allosteric modulation of NMDA receptors. *J. Gen. Physiol.* 150, 1081–1105. doi: 10.1085/jgp.201812032

Hefti, B. J., and Smith, P. H. (2000). Anatomy, physiology, and synaptic responses of rat layer V auditory cortical cells and effects of intracellular GABA(A) blockade. *J Neurophysiol* 83, 2626–2638. doi: 10.1152/jn.2000.83.5.2626

Hurley, L. M., and Hall, I. C. (2011). Context-dependent modulation of auditory processing by serotonin. *Hear. Res.* 279, 74–84. doi: 10.1016/j.heares.2010.12.015

Husain, F. T., Carpenter-Thompson, J. R., and Schmidt, S. A. (2014). The effect of mild-to-moderate hearing loss on auditory and emotion processing networks. *Front. Syst. Neurosci.* 8, 10. doi: 10.3389/fnsys.2014.00010

Ji, W., and Suga, N. (2007). Serotonergic modulation of plasticity of the auditory cortex elicited by fear conditioning. *J. Neurosci.* 27, 4910–4918. doi: 10.1523/JNEUROSCI.5528-06.2007

Kannangara, T. S., Bostrom, C. A., Ratzlaff, A., Thompson, L., Cater, R. M., Gil-Mohapel, J., et al. (2014). Deletion of the NMDA receptor GluN2A subunit significantly decreases dendritic growth in maturing dentate granule neurons. *PLoS One* 9, e103155. doi: 10.1371/journal.pone.0103155

Kanner, A. M. (2016b). Most antidepressant drugs are safe for patients with epilepsy at therapeutic doses: a review of the evidence. *Epilepsy Behav.* 61, 282–286. doi: 10.1016/j.yebeh.2016.03.022

Keith, R. E., Azcarate, J. M., Keith, M. J., Hung, C. W., Badakhsh, M. F., and Dumas, T. C. (2019). Direct intracellular signaling by the carboxy terminus of NMDA receptor GluN2 subunits regulates dendritic morphology in hippocampal CA1 pyramidal neurons. *Neuroscience* 396, 138–153. doi: 10.1016/j.neuroscience.2018.11.021

Kiss, J. P., Szasz, B. K., Fodor, L., Mike, A., Lenkey, N., Kurko, D., et al. (2012). GluN2B-containing NMDA receptors as possible targets for the neuroprotective and antidepressant effects of fluoxetine. *Neurochem. Int.* 60, 170–176. doi: 10.1016/j.neuint.2011.12.005

Kitahara, Y., Ohta, K., Hasuo, H., Shuto, T., Kuroiwa, M., Sotogaku, N., et al. (2016). Chronic fluoxetine induces the enlargement of perforant path-granule cell synapses in the mouse dentate gyrus. *PLoS One* 11, e0147307. doi: 10.1371/journal.pone.0147307

Kobayashi, K., Ikeda, Y., Sakai, A., Yamasaki, N., Haneda, E., Miyakawa, T., et al. (2010). Reversal of hippocampal neuronal maturation by serotonergic antidepressants. *Proc. Natl. Acad. Sci. U.S.A.* 107, 8434–8439. doi: 10.1073/pnas.0912690107

Lavado, A. (2018). *Comparación de algoritmos de cálculo del Skeleton y su aplicación en biología. Memoria Ingeniero Civil en Computación*. Santiago, Chile: Universidad de Chile.

Li, S. X., Han, Y., Xu, L. Z., Yuan, K., Zhang, R. X., Sun, C. Y., et al. (2018). Uncoupling DAPK1 from NMDA receptor GluN2B subunit exerts rapid antidepressant-like effects. *Mol. Psychiatry* 23, 597–608. doi: 10.1038/mp.2017.85

Lorensen, W. E., and Cline, H. E. (1987). A high resolution 3D surface reconstruction algorithm. *Comp. Graph.* 21, 163–169. doi: 10.1145/37402.37422

Loss, C. M., Da Rosa, N. S., Mestriner, R. G., Xavier, L. L., and Oliveira, D. L. (2019). Blockade of GluN2B-containing NMDA receptors reduces short-term brain damage induced by early-life status epilepticus. *Neurotoxicology* 71, 138–149. doi: 10.1016/j.neuro.2019.01.002

LoTurco, J., Manent, J. B., and Sidiqi, F. (2009). New and improved tools for in utero electroporation studies of developing cerebral cortex. *Cereb. Cortex* 19 Suppl 1, i120–125. doi: 10.1093/cercor/bhp033

Maya Vetencourt, J. F., Sale, A., Viegi, A., Baroncelli, L., De Pasquale, R., O'leary, O. F., et al. (2008). The antidepressant fluoxetine restores plasticity in the adult visual cortex. *Science* 320, 385–388. doi: 10.1126/science.1150516

Miller, O. H., Yang, L., Wang, C. C., Hargroder, E. A., Zhang, Y., Delpire, E., et al. (2014). GluN2B-containing NMDA receptors regulate depression-like behavior and are critical for the rapid antidepressant actions of ketamine. *eLife* 3, e03581. doi: 10.7554/eLife.03581

Moda-Sava, R. N., Murdock, M. H., Parekh, P. K., Fetcho, R. N., Huang, B. S., Huynh, T. N., et al. (2019). Sustained rescue of prefrontal circuit dysfunction by antidepressant-induced spine formation. *Science* 364. , 1–11. doi: 10.1126/science.aat80788

Mony, L., Kew, J. N., Gunthorpe, M. J., and Paoletti, P. (2009). Allosteric modulators of NR2B-containing NMDA receptors: molecular mechanisms and therapeutic potential. *Br. J. Pharmacol.* 157, 1301–1317. doi: 10.1111/j.1476-5381.2009.00304.x

Okuda, K., Kobayashi, S., Fukaya, M., Watanabe, A., Murakami, T., Hagiwara, M., et al. (2017). CDKL5 controls postsynaptic localization of GluN2B-containing NMDA receptors in the hippocampus and regulates seizure susceptibility. *Neurobiol. Dis.* 106, 158–170. doi: 10.1016/j.nbd.2017.07.002

Orhurhu, V. J., Claus, L. E., and Cohen, S. P. (2019). "Ketamine toxicity," in *StatPearls* (FL: Treasure Island).

Paoletti, P., Bellone, C., and Zhou, Q. (2013). NMDA receptor subunit diversity: impact on receptor properties, synaptic plasticity and disease. *Nat. Rev. Neurosci.* 14, 383–400. doi: 10.1038/nrn3504

Paxinos, G., and Watson, C. (1998). *The rat brain in stereotaxic coordinates*. San Diego: Academic Press.

Pryazhnikov, E., Mugantseva, E., Casarotto, P., Kolikova, J., Fred, S. M., Toptunov, D., et al. (2018). Longitudinal two-photon imaging in somatosensory cortex of behaving mice reveals dendritic spine formation enhancement by subchronic administration of low-dose ketamine. *Sci. Rep.* 8, 6464. doi: 10.1038/s41598-018-24933-8

Rubio, F. J., Ampuero, E., Sandoval, R., Toledo, J., Pancetti, F., and Wyneken, U. (2013). Long-term fluoxetine treatment induces input-specific LTP and LTD impairment and structural plasticity in the CA1 hippocampal subfield. *Front. Cell. Neurosci.* 7, 66. doi: 10.3389/fncel.2013.00066

Ruiz-Perera, L., Muniz, M., Vierci, G., Bornia, N., Baroncelli, L., Sale, A., et al. (2015). Fluoxetine increases plasticity and modulates the proteomic profile in the adult mouse visual cortex. *Sci. Rep.* 5, 12517. doi: 10.1038/srep12517

Rutherford, B. R., Brewster, K., Golub, J. S., Kim, A. H., and Roose, S. P. (2018). Sensation and psychiatry: linking age-related hearing loss to late-life depression and cognitive decline. *Am. J. Psychiatry* 175, 215–224. doi: 10.1176/appi.ajp.2017.17040423

Scinicariello, F., Przybyla, J., Carroll, Y., Eichwald, J., Decker, J., and Breysse, P. N. (2019). Age and sex differences in hearing loss association with depressive symptoms: analyses of NHANES 2011–2012. *Psychol. Med.* 49, 962–968. doi: 10.1017/S0033291718001617

Schiavone, S., Tucci, P., Mhillaj, E., Bove, M., Trabace, L., and Morgese, M. G. (2017). Antidepressant drugs for beta amyloid-induced depression: a new standpoint? *Prog. Neuropsychopharmacol. Biol. Psychiatry* 78, 114–122. doi: 10.1016/j.pnpbp.2017.05.004

Schindelin, J., Arganda-Carreras, I., Frise, E., Kaynig, V., Longair, M., Pietzsch, T., et al. (2012). Fiji: an open-source platform for biological-image analysis. *Nat. Methods* 9, 676–682. doi: 10.1038/nmeth.2019

Sepulveda, F. J., Bustos, F. J., Inostroza, E., Zuniga, F. A., Neve, R. L., Montecino, M., et al. (2010). Differential roles of NMDA receptor subtypes NR2A and NR2B in dendritic branch development and requirement of RasGRF1. *J. Neurophysiol.* 103, 1758–1770. doi: 10.1152/jn.00823.2009

Spruston, N. (2008). Pyramidal neurons: dendritic structure and synaptic integration. *Nat. Rev. Neurosci.* 9, 206–221. doi: 10.1038/nrn2286

Tucci, P., Mhillaj, E., Morgese, M. G., Colaianna, M., Zotti, M., Schiavone, S., et al. (2014). Memantine prevents memory consolidation failure induced by soluble beta amyloid in rats. *Front. Behav. Neurosci.* 8, 332. doi: 10.3389/fnbeh.2014.00332

Van Dyke, A. M., Francis, T. C., Chen, H., Bailey, A. M., and Thompson, S. M. (2019). Chronic fluoxetine treatment *in vivo* enhances excitatory synaptic transmission in the hippocampus. *Neuropharmacology* 150, 38–45. doi: 10.1016/j.neuropharm.2019.03.005

Wang, C. C., Held, R. G., Chang, S. C., Yang, L., Delpire, E., Ghosh, A., et al. (2011). A critical role for GluN2B-containing NMDA receptors in cortical development and function. *Neuron* 72, 789–805. doi: 10.1016/j.neuron.2011.09.023

Wei, K., Bao, W., Zhao, Z., Zhou, W., Liu, J., Wei, Y., et al. (2018). Changes of the brain activities after chronic restraint stress in rats: a study based on (18)F-FDG PET. *Neurosci. Lett.* 665, 104–109. doi: 10.1016/j.neulet.2017.11.047

Wu, Q. J., and Tymianski, M. (2018). Targeting NMDA receptors in stroke: new hope in neuroprotection. *Mol. Brain* 11, 15. doi: 10.1186/s13041-018-0357-8

Wyneken, U., Sandoval, M., Sandoval, S., Jorquera, F., Gonzalez, I., Vargas, F., et al. (2006). Clinically relevant doses of fluoxetine and reboxetine induce changes in the TrkB content of central excitatory synapses. *Neuropsychopharmacology* 31, 2415–2423. doi: 10.1038/sj.npp.1301052

Xu, L. Z., Li, B. Q., and Jia, J. P. (2019). DAPK1: a novel pathology and treatment target for Alzheimer's disease. *Mol. Neurobiol.* 56, 2838–2844. doi: 10.1007/s12035-018-1242-2

Yin, Y., Wang, M., Wang, Z., Xie, C., Zhang, H., Zhang, H., et al. (2018). Decreased cerebral blood flow in the primary motor cortex in major depressive disorder with psychomotor retardation. *Prog. Neuropsychopharmacol. Biol. Psychiatry* 81, 438–444. doi: 10.1016/j.pnpbp.2017.08.013

Zhu, J., Xu, S., Li, S., Yang, X., Yu, X., and Zhang, X. (2018). Up-regulation of GluN2A-containing NMDA receptor protects cultured cortical neuron cells from oxidative stress. *Heliyon* 4, e00976. doi: 10.1016/j.heliyon.2018.e00976

Zubareva, O. E., Kovalenko, A. A., Kalemenev, S. V., Schwarz, A. P., Karyakin, V. B., and Zaitsev, A. V. (2018). Alterations in mRNA expression of glutamate receptor subunits and excitatory amino acid transporters following pilocarpine-induced seizures in rats. *Neurosci. Lett.* 686, 94–100. doi: 10.1016/j.neulet.2018.08.047

Zwanzger, P., Zavorotnyy, M., Diemer, J., Ruland, T., Domschke, K., Christ, M., et al. (2012). Auditory processing in remitted major depression: a long-term follow-up investigation using 3T-fMRI. *J. Neural Transm.* 119, 1565–1573. doi: 10.1007/s00702-012-0871-2

Zweerings, J., Zvyagintsev, M., Turetsky, B. I., Klasen, M., Konig, A. A., Roecher, E., et al. (2019). Fronto-parietal and temporal brain dysfunction in depression: a fMRI investigation of auditory mismatch processing. *Hum. Brain Mapp.* doi: 10.1002/hbm.24623. [Epub ahead of print].

Conflict of Interest Statement: The authors declare that the research was conducted in the absence of any commercial or financial relationships that could be construed as a potential conflict of interest.

frontiers in Pharmacology

ORIGINAL RESEARCH
published: 23 July 2019
doi: 10.3389/fphar.2019.00803

(Pro)renin Receptor-Dependent Induction of Profibrotic Factors Is Mediated by COX-2/EP4/NOX-4/Smad Pathway in Collecting Duct Cells

*Cristian Reyes-Martinez[1], Quynh My Nguyen[2], Modar Kassan[3] and Alexis A. Gonzalez[1]**

[1] Instituto de Química, Pontificia Universidad Católica de Valparaíso, Valparaiso, Chile, [2] Skaggs School of Pharmacy and Pharmaceutical Sciences, University of California, San Diego, San Diego, CA, United States, [3] Cardiovascular Division, Department of Medicine, Abboud Cardiovascular Research Center, University of Iowa Carver College of Medicine, Iowa City, IA, United States

The binding of prorenin to the (pro)renin receptor (PRR) triggers the activation of MAPK/ERK1/2 pathway, induction of cyclooxygenase-2 (COX-2), NOX-4-dependent production of reactive oxygen species (ROS), and the induction of transforming growth factor β (TGF-β) and profibrotic factors connecting tissue growth factor (CTGF) and plasminogen activator inhibitor (PAI-I) in collecting duct (CD) cells. However, the role of COX-2 and the intracellular pathways involved are not clear. We hypothesized that the PRR activation increases profibrotic factors through COX-2-mediated PGE2 activation of E prostanoid receptor 4 (EP4), upregulation of NOX-4/ROS production, and activation of Smad pathway in mouse CD cells. Recombinant prorenin increased ROS production and protein levels of CTGF, PAI-I, and TGF-β in M-1 CD cell line. Inhibition of MAPK, NOX-4, and COX-2 prevented this effect. Inhibition of MEK, COX-2, and EP4 also prevented the upregulation of NOX-4. Because TGF-β activates Smad pathway, we evaluate the phosphorylation of Smad2 and 3. COX-2 inhibition or EP4 antagonism significantly prevented phosphorylation of Smad 2/3. Mice that were infused with recombinant prorenin showed an induction in the expression of CTGF, PAI-I, TGF-β, fibronectin, and collagen I in isolated collecting ducts as well as the expression of alpha smooth muscle actin (α-SMA) in renal tissues. COX-2 inhibition prevented this induction. These results indicate that the induction of TGF-β, CTGF, PAI-I, and ROS occurs through PRR-dependent activation of MAPK and NOX-4; however, this mechanism depends on COX-2-derived PGE2 production and the activation of EP4 and Smad pathway.

Keywords: (Pro)renin receptor, cyclooxygenase inhibition, reactive oxygen species, intrarenal renin–angiotensin system, collecting duct renin

OPEN ACCESS

Edited by:
Javier A. Bravo, Pontificia Universidad Católica de Valparaíso, Chile

Reviewed by:
Nazareno Paolocci, Johns Hopkins University, United States
Zhiping Liu, Augusta University, United States

****Correspondence:***
Alexis A. Gonzalez
alexis.gonzalez@pucv.cl

Specialty section:
This article was submitted to Translational Pharmacology, a section of the journal Frontiers in Pharmacology

Received: *10 October 2018*
Accepted: *21 June 2019*
Published: *23 July 2019*

Citation:
Reyes-Martinez C, Nguyen QM, Kassan M and Gonzalez AA (2019) (Pro)renin Receptor-Dependent Induction of Profibrotic Factors Is Mediated by COX-2/EP4/NOX-4/Smad Pathway in Collecting Duct Cells. Front. Pharmacol. 10:803. doi: 10.3389/fphar.2019.00803

INTRODUCTION

The binding of prorenin to the (pro)renin receptor (PRR) triggers the phosphorylation of mitogen-activated protein kinases/extracellular regulated kinases 1/2 (MAPK/ERK1/2) (Batenburg et al., 2007; Feldt et al., 2008; Muller et al., 2008; Ballarin-Gonzalez et al., 2013) and upregulates cyclooxygenase-2 (COX-2) in kidney tissues (Kaneshiro et al., 2006). We have reported that PRR

activation by recombinant prorenin increases COX-2 expression independently of angiotensin (ANG) II in cultured renal collecting duct (CD) cells (Gonzalez et al., 2013). Both activation and upregulation of PRR have been associated with renal tissue damage (Kaneshiro et al., 2006; Kaneshiro et al., 2007; Ichihara et al., 2008). Liu showed that proximal tubular cells treated with prorenin show upregulation of transforming growth factor beta (TGF-b1) and alpha-smooth muscle actin (α-SMA) (Yisireyili et al., 2014). In human kidney embryonic (HEK) cells, augmentation of reactive oxygen species (ROS) is observed after PRR stimulation. This effect is mediated by a NOX-4-dependent mechanism (Clavreul et al., 2011).

We recently showed that cultured CD cells treated with nanomolar concentrations of recombinant prorenin undergo to epithelial–mesenchymal transition and have increased levels of intracellular ROS, activation of MAPK pathway, and upregulation of profibrotic factors including CTGF, plasminogen activator inhibitor-1 (PAI-I) and TGF-β, fibronectin, and collagen I (Gonzalez et al., 2017). Although there are still a discrepancy between the plasma levels of prorenin and the effective physiological concentrations for PRR activation in the kidney (Campbell et al., 2009), it has been shown that high plasma prorenin is present in patients with diabetic nephropathy (Franken et al., 1992), a condition that is associated with microvascular pathologies (Chiarelli et al., 2001). PRR contributes to development of diabetic kidney disease through TGF-β and connective tissue growth factor (CGTF) signaling cascade (Huang et al., 2011). Yoshida et al. demonstrated that high plasma prorenin plays a role in the development of coronary artery disease (Yoshida et al., 2015). Interestingly, it has been shown that African-Americans who have known susceptibility to high blood pressure showed disproportionately high levels of prorenin (Tu et al., 2012).

In diabetic animal models, there is an increase in prorenin and renin expression in the CD (Kang et al., 2008). Because PRR is expressed in the neighbor CD intercalated cell (Gonzalez et al., 2013), prorenin or renin coming from the principal cells of the CD might stimulate PRR, leading to activation of signaling pathways such as MAPK/ERK 1/2 and induction of COX-2. Although the events that follow the activation of PRR on ROS generation, MAPK pathway activation, and upregulation of profibrotic genes have been partially described (Clavreul et al., 2011; Gonzalez et al., 2017), the role of COX-2 in this regulation is not fully understood. It has been shown that the ERK1/2 pathway and cAMP/PKA pathway increase the expression of NOX-4 (Clavreul et al., 2011; Muzaffar et al., 2012). Activation of the Gs (cAMP/PKA) coupled prostaglandin receptor EP4 increases NOX-4 expression in liver cells. In addition, overexpression of COX-2 shows higher NOX4 levels and ROS content, while the presence of a COX-2 inhibitor decreases these effects (Sancho et al., 2011). Reactive oxygen species (ROS) are involved in TGF-β and Smad signaling (Lafon et al., 1996; Hong et al., 1997; Chiu et al., 2001), which are known to be activators of fibrotic factors such as CTGF and PAI-I (Clarkson et al., 1999; Kilari et al., 2018). The ERK pathway can enhance Smad activity. Additionally, ERK inhibition reduces TGF-β1-stimulated Smad phosphorylation as well as collagen production and promoter activities, suggesting that ERK activity is necessary for an optimal response to TGF-β1 (Hayashida et al., 2003).

In the present study, we aimed to demonstrate that the activation of PRR increases profibrotic factors through COX-2-mediated PGE_2 activation of E prostanoid receptor 4 (EP4), the upregulation of NOX-4/ROS production, and activation of Smad pathway in mouse CD cells. To test this, M-1 CD cell line was treated with recombinant prorenin with and without inhibition of MAPK pathway, NOX-4 and COX-2. Specific pharmacological blockade of EP4 receptor was also tested in M-1 cells incubated with hrPR. Since Smad 2 and 3 are considered as downstream mediators of TGF-β signaling (Meng et al., 2015) and because TGF-β is induced by ROS, we evaluated the phosphorylation of Smad2 and 3, which are activated by TGF-β receptor in the presence of EP4 antagonist. Additionally, we performed *in vivo* experiments in mice infused with human recombinant prorenin (100 ng/min) *via* an osmotic minipump for 36 h with and without selective COX-2 inhibitor. The expression of profibrotic factors was analyzed in isolated CDs and renal medullary tissues.

MATERIALS AND METHODS

M-1 Cell Culture

M-1 cells (ATCC, VA) are a CD cell line with phenotypic characteristics of cortical CD cells (Stoos et al., 1991). M-1 cells are composed of principal cells and intercalated cells constitutively expressing COX-2 (Nasrallah et al., 2001), prorenin–renin, and PRR constitutively (Gonzalez et al., 2015; Gonzalez et al., 2017; Gonzalez et al., 2017). The M-1 cells were cultured as previously described (Gonzalez et al., 2015; Gonzalez et al., 2016; Gonzalez et al., 2017). Cells were harvested after 6 h of treatments with human recombinant prorenin (hrPR) (Cayman Chemical, EE.UU). at 10^{-8} mol/l according to its described range of affinity in nanomolar range (Batenburg et al., 2007; Wilkinson-Berka, 2008)

Pharmacological Blockers in M-1 Cells

Treatment with NOX-4 inhibitor GKT 137831 was performed at three different concentrations (10, 20, and 30 μM) to explore the effect on ROS production according to the literature (Sedeek et al., 2013a). GKT 137831 was then used at 30 μM for protein expression analysis. Similarly, we tested the effects of PD98059, a potent and selective inhibitor of MAP kinase kinases (MAPKK), MEK1 and MEK2 (Alessi et al., 1995) at two concentrations (30 and 50 μM) (Gonzalez et al., 2017), to explore the effects on ROS production and induction of profibrotic proteins mediated by hrPR. NS-398 was used at 10^{-5} mol/l (Ferguson et al., 1999) to determine COX-2 inhibition effect on ROS and profibrotic protein expression. CD cells show high expression of EP4 receptors (Gonzalez et al., 2013; Wang et al., 2016). We used L-161982 (Cayman Chemical), a potent and selective EP4 receptor antagonist that demonstrates selective binding to human EP4 receptors with a Ki value of 0.024 M. We used a fourfold higher concentration (100 nM) (Takayama et al., 2002). All pharmacological inhibitors

were added 30 min before incubations with hrPR. M-1 CD cells were harvested after 6 h. Controls were performed with vehicle (DMSO, 0.06% vol/vol).

Measurement of Reactive Oxygen Species in M-1 Cells

M-1 cells were seeded in 96-well black polystyrene plates and treated with MEK, COX-2, or NOX-4 inhibitors during 15 min at 37°C. Then, all groups were treated with probe carboxy-2′, 7′-dichloro-dihydro-fluorescein diacetate (DCFHDA, Sigma Chemical Co, St. Louis, MO, USA) at 25 μM for 30 min at 37°C. Fluorescence measurements of DCF (the product of H2DCFDA oxidation: excitation, 495 nm; emission, 529 nm) were performed on a plate reader (Appliskan; Thermo Fisher Scientific, Waltham, MA, USA). To normalize results, total protein from each well was quantified by the bicinchoninic acid (BCA) method. A positive control was conducted using 50 μM H_2O_2.

In Vivo Treatments

The Institutional Animal Care and Use Committees approved all animal protocols. Male CF-1 mice (18–20 g, $n = 5$) were cage housed and maintained in a temperature-controlled room with 12-h light/dark cycles with free access to tap water and standard rat chow. Experiments with chronic infusions of prorenin have been performed previously in rhesus monkeys at 400 ng/min, causing three- to fourfold increases in normal plasma prorenin concentrations from ∼70 to ∼250 ng/ml/h (Lenz et al., 1990). High plasma prorenin, as high as ∼1,000 pg/ml, has been found in patients with cardiovascular risk (Yoshida et al., 2015). Human recombinant prorenin (Cayman Chemicals) was infused at a rate of 100 ng/min *via* osmotic minipump for 36 h. Selective COX-2 inhibitor NS-398 attenuates myocardial fibrosis in mice at 5 mg kg (Chi et al., 2017) and is able to block the LPS-induced increase in PGE_2 in rats at same dose (Lugarini et al., 2002). NS-398 (Cayman Chemicals, EE.UU). was administered in 5% aqueous methylcellulose solution by oral gavage every 6 h. Sham-operated mice were used as controls and administered methylcellulose solution. For physiological parameters presented in **Table 1**, four mice were placed in cages for urine collections. Urine osmolality was measured by vapor pressure osmometry (Vapro Osmometer, model 5600, Wescor). Creatinine measurements in plasma and urine were used to calculate the estimated creatinine clearance over 16 h as an approach to determine renal function. Urinary sodium and potassium were measured as described previously (Gonzalez et al., 2014).

Immunofluorescence in Freshly Isolated Collecting Ducts

At the end of the study, mice were euthanized by conscious decapitation, and renal tissues were collected to perform immunofluorescence and Western blots in freshly isolated inner medullary collecting ducts. Freshly isolated collecting ducts were prepared as previously described (Gonzalez et al., 2011), with variations in digestion time and wash steps. Briefly, inner medullary tissues were digested in 10 ml of DMEM-Ham F-12, 20 mg of collagenase B, 7 mg of hyaluronidase, 80 mmol/l of urea, and 130 mmol/l of NaCl and incubated at 37°C under continuous agitation for 30 mi. After centrifugation, the pellet was washed in prewarmed culture medium without enzymes. The resulting IMCD cell suspension was seeded in six-well chambers (Nalge Nunc, Rochester, NY, USA) and fixed in cold methanol for 20 min, blocked with PBS-Tween (0.1%) plus BSA (3%) for 1 h, and stained with anti-fibronectin (Cat. No. sc-8422; Santa Cruz Biotechnology) or anti-collagen I antibody (Cat. No. 34710, Abcam) at 1:200 dilutions and detected with secondary antibody Alexa Fluor 488 conjugated to anti-rabbit IgG (Invitrogen) at 1:500 dilutions. Negative controls were obtained by omission of the specific primary antibody. Measurements of fluorescence intensity were performed with NIS Elements software (Nikon) in 10 fields from each processed kidney and expressed as fluorescence intensity versus total number of collecting duct in each field previously counted in light field (**Figure 5B**).

Tissue Immunofluorescence

Kidney sections (3 μm) were stained with rabbit anti-PRR (Cat. No. HPA003156, Sigma Chemical Co, St. Louis, MO, USA) at 1:200 dilutions or α-SMA antibody from Abcam (ab5694, Abcam, Cambridge, MA, USA) followed by the incubation of the corresponding immunofluorescent secondary antibody (1:1,000, Alexa Fluor® 594, Invitrogen, Carlsbad, CA, USA). Negative controls were obtained by omission of the specific primary antibody. Samples were counterstained with 4′,6-diamidino-2-phenylindole (DAPI, Invitrogen, Carlsbad, CA, USA) for nuclei staining.

TABLE 1 | Physiological parameters in mice after 36 h of subcutaneous infusions with saline, human recombinant prorenin (hrRP), and hrPR plus COX-2 inhibitor NS-398.

	Saline	hrPR	NS398	hrPR+NS398
Body weight, g	22 ± 3	20 ± 3	18 ± 4	19 ± 4
Kidney weight, g	0.29 ± 0.01	0.30 ± 0.02	0.28 ± 0.03	0.29 ± 0.01
Urine osmolality, mosmol/kgH2O	345 ± 8	375 ± 9*	348 ± 8	380 ± 8*
Urine flow, ml/16 h	6.02 ± 0.02	5.35 ± 0.05	4.91 ± 0.06	4.21 ± 0.10*
Estimated GFR, ml·min^{-1}	0.92 ± 0.03	0.89 ± 0.04	0.86 ± 0.05	0.84 ± 0.05*
FENa %	0.91 ± 0.02	0.88 ± 0.02	0.87 ± 0.02	0.87 ± 0.03
FEK %	1.4 ± 0.2	1.3 ± 0.3	1.4 ± 0.4	1.3 ± 0.2

$p < 0.05$ versus Saline group.

Protein Expression Analysis

Forty micrograms of total protein were used for Western blot analysis. Protein expression levels were quantified after immunoblotting using a 1:1,000 dilution of the following specific antibodies: connecting tissue growth factor (CTGF; Cat. No. sc-25440, Santa Cruz Biotechnology), PAI-1 (Cat. No. SC-8979, Santa Cruz Biotechnology), TGF-β (Cat. No. SC-130348, Santa Cruz Biotechnology), COX-2 antibody (Cayman, Ann Arbor, MI, USA), mouse anti-phospho-p44/42 ERK1/2 (Thr202/Tyr204), and a rabbit anti-total ERK antibody (Cell Signaling Technology, Beverly, MA, USA). NOX-4 antibody was purchased from Santa Cruz (sc-21860). Antibodies against Anti-Smad2/3 antibody and anti p-Smad2/3 were obtained from Abcam (Abcam, Cambridge, MA, USA). Primary antibodies were followed by incubation with either donkey anti-rabbit or anti-mouse IgG IRDye 800 CW (Santa Cruz Biotechnology) at 1:3,000 dilutions. Resulting bands were compared to molecular weight standards (M. Biosources, San Diego, CA, USA). Densitometry was performed with ImageJ software and normalized to monoclonal anti-β-actin antibody (Cat. A2228, Sigma Chemical Co, St. Louis, MO, USA).

Statistical Analyses

For Western blot, an average number of three to six independent observations was performed for each treatment and represented as fold change versus controls. For *in vivo* studies, five mice were used in each group. Data were evaluated by the Grubb test, followed when appropriate by paired and unpaired Student's *t*-test or by one-way ANOVA with Tukey post-test. Significance was defined as $p < 0.05$. No significant differences are expressed as "ns". Results are expressed as mean ± SEM.

RESULTS

Recombinant Prorenin Causes ERK1/2 Phosphorylation and Increases COX-2 and NOX-2 Expression in M-1 Cells

As previously described, treatment with recombinant prorenin induced ERK1/2 phosphorylation over the time of incubations, reaching a peak after 10 min of incubation. It subsequently decreased after 1 h (**Figure 1A**). After 6 h, COX-2 and NOX-4 were augmented (ratio protein/β-actin densitometric values: 1.67 ± 0.16 vs. 0.66 ± 0.08 for COX-2 and 1.48 ± 0.08 vs. 0.70 ± 0.19, for NOX4 $p < 0.05$); however, inhibition of MAPK pathway with PD98059 prevented this effect.

MAPK Inhibition Impairs ROS Formation and the Upregulation of CTGF, TGF-β, and PAI-I Caused by Recombinant Prorenin Incubations

Inhibition of MAPK pathway prevented ROS formation (**Figure 2A**). We tested two concentrations of PD98059:

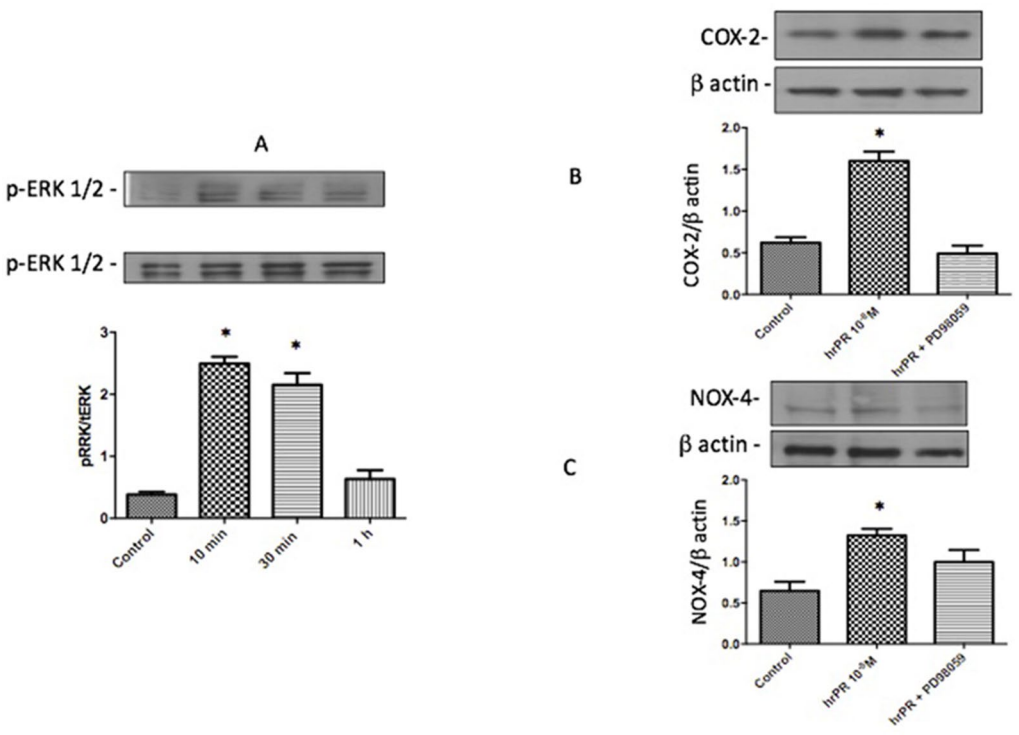

FIGURE 1 | Incubations with recombinant prorenin increase the abundance of COX-2 and NOX-4 *via* MAPK pathway in M-1 cells. **(A)**. Time response of ERK1/2 phosphorylation after incubations with 10^{-8} M human recombinant prorenin (hrPR). MAPK inhibition impairs hrPR-dependent upregulation of COX-2 **(B)** and NOX-4 **(C)**. *$p < 0.05$, $n = 4$.

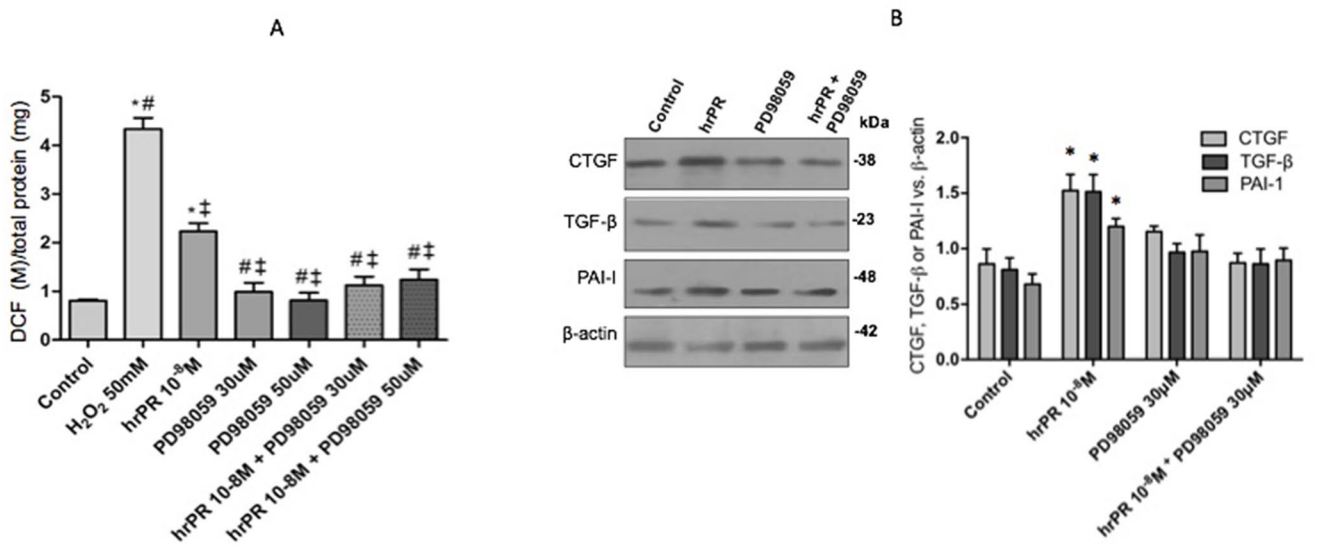

FIGURE 2 | MAPK pathway inhibition by PD98059 prevented the induction of ROS levels and profibrotic markers CTGF, TGF-β, and PAI-I. **(A)**. For ROS quantification, M-1 cells were treated with PD98059 at 30 and 50 μM during 15 min, incubated with DCFH-DA probe for 30 min, and treated with hrPR for 15 min. Results are expressed as DCF probe fluorescence intensity versus total protein (mean ± SEM) **(B)**. Protein levels of CTGF, TGF-β, and PAI-I represented by Western blot analysis (left) and quantitation (right) in M-1 cells incubated during 6 h with hrPR, PD98059, or hrPR plus PD98059, $^{*}p < 0.05$ versus control, $^{\#}p < 0,05$ versus hrPR group, $^{\ddagger}p < 0,05$ versus positive control, $n = 5$.

30 and 50 mmol/l. No differences were found between both concentrations in the blunted effect on hrPR-dependent induction of ROS (control: 0.80 ± 0.01; hrPR: 2.22 ± 0.21, $p <$ 0.05 vs. control; PD98059 30 mmol/l: 1.24 ± 0.17, p = ns vs. control; PD98059 50 mmol/l: 1.12 ± 0.12, p = ns vs. control). Induction of CTGF, TGF-β, and PAI-I was prevented by MAPK inhibition (ratio protein/β-actin densitometric values: 0.87 ± 0.18, 0.86 ± 0.22, 0.90 ± 0.19, respectively, p = ns); see **Figure 2B** for immunoblot analysis.

Induction of ROS and Profibrotic Protein Expression Is Prevented by Inhibition of NOX-4

Figure 3A shows the effect of NOX-4 inhibition in M-1 CD cells incubated with human recombinant prorenin (hrPR) at 10^{-8} mol/l. Treatment with hrPR increased DCF/protein ratio (2.15 ± 0.23 vs. 0.68 ± 0.09, $p < 0.05$); however, pre-treatment with GTK 137831 prevented this effect at doses of 30 mmol/l (0.62 ± 0.01 vs. 0.68 ± 0.09, p = ns) and to a lesser extent at doses of 10 and 20 mmol/l (1.04 ± 0.15, p = ns vs. control and 1.45 ± 0.19, $p < 0.05$ vs. control). Afterward, the following experiments evaluating protein expression were done using 30 mmol/l GTK 137831. **Figure 3B** shows the effects of NOX-4 inhibition on the expression of CTGF, PAI-I, and TGF-β in M-1 cells incubated with hrPR. As observed, hrPR causes a significant increase in protein levels of all three markers analyzed (ratio protein vs. β-actin densitometric values: CTGF, 1.52 ±0.07 vs. 0.50 ± 0.01, $p < 0.05$; TGF-β, 1.51 ± 0.08 vs. 0.49 ± 0.02, $p < 0.05$; PAI-I, 1.21 ± 0.02 vs. 0.50 ± 0.02, $p < 0.05$).

COX-2 Inhibition Impairs the Induction of ROS NOX-4 and Profibrotic Genes in M-1 CD Cells Treated With Recombinant Prorenin

We performed new experiments incubating M-1 cells with hrPR or hrPR plus pre-incubations with specific COX-2 inhibitor NS-398. As shown in **Figure 4A**, NS-398 completely blunted the induction of NOOX-4 protein expression at 10^{-5} M. The increases in intracellular ROS caused by hrPR were also blunted by NS-398 (control: 0.51 ± 0.01; hrPR: 2.15 ± 0.18, $p <$ 0.05 vs. control; hrPR+NS-398: 0.64 ± 0.08, p = ns vs. control, **Figure 4B**). Similarly, the induction of CTGF, TGF-β, and PAI-I was prevented by MAPK inhibition (ratio protein/β-actin densitometric values: 0.87 ± 0.18, 0.86 ± 0.22, 0.90 ± 0.19, p = ns vs. control group, **Figure 4C**).

EP4 Receptor Antagonism Decreases ROS Production, NOX-4 Expression, Induction of TGF-β, CTGF, and PAI-I, and Activation of the Smad Pathway in M-1 Cells Incubated With hrPR

We next tested if pharmacological blockade of the EP4 receptor would be able to prevent ROS formation and the induction of TGF-β, CTGF, and PAI-I in M-1 cells incubated with hrPR. As shown in **Figure 5A**, ROS production was ameliorated in M-1 cells that were treated with hrPR and pre-incubated with L-161982 at 10^{-7} M. The EP4 receptor antagonist partially prevented the induction of TGF-β, CTGF, and PAI-I (**Figure 5B**). This was also associated with a reduction in the protein expression of NOX-4 (**Figure 5C**). EP4 receptor antagonism prevented the

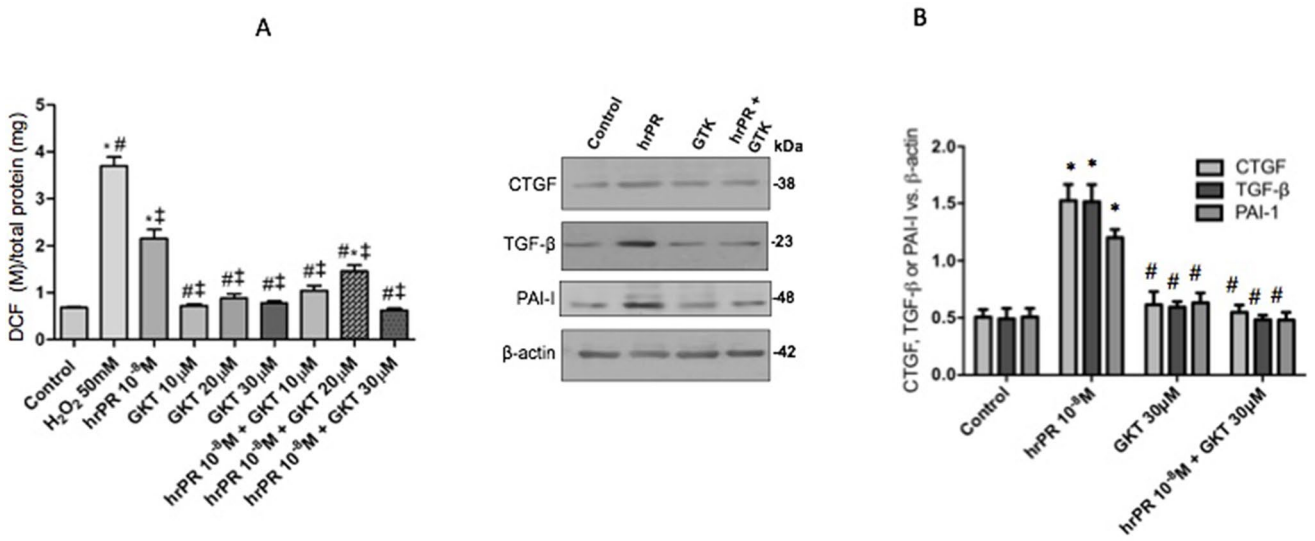

FIGURE 3 | NOX-4 inhibition by pharmacological agent GKT 137831 prevented the induction of ROS and profibrotic markers CTGF, TGF-β, and PAI-I. **(A)**. For ROS quantification, M-1 cells were treated with GKT at 10, 20, and 30 μM during 15 min, incubated with DCFH-DA probe for 30 min, and treated with human recombinant prorenin (hrPR) for 15 min. Results are expressed as DCF probe fluorescence intensity versus total protein (mean ± SEM) **(B)**. Protein levels of CTGF, TGF-β, and PAI-I represented by Western blot analysis (left) and quantitation (right) in M-1 cells incubated during 6 h with hrPR, GTK, or hrPR plus GTK. $^{*}p < 0.05$ versus control, $^{\#}p < 0.05$ versus hrPR group, $^{\ddagger}p < 0.05$ versus positive control, $n = 5$.

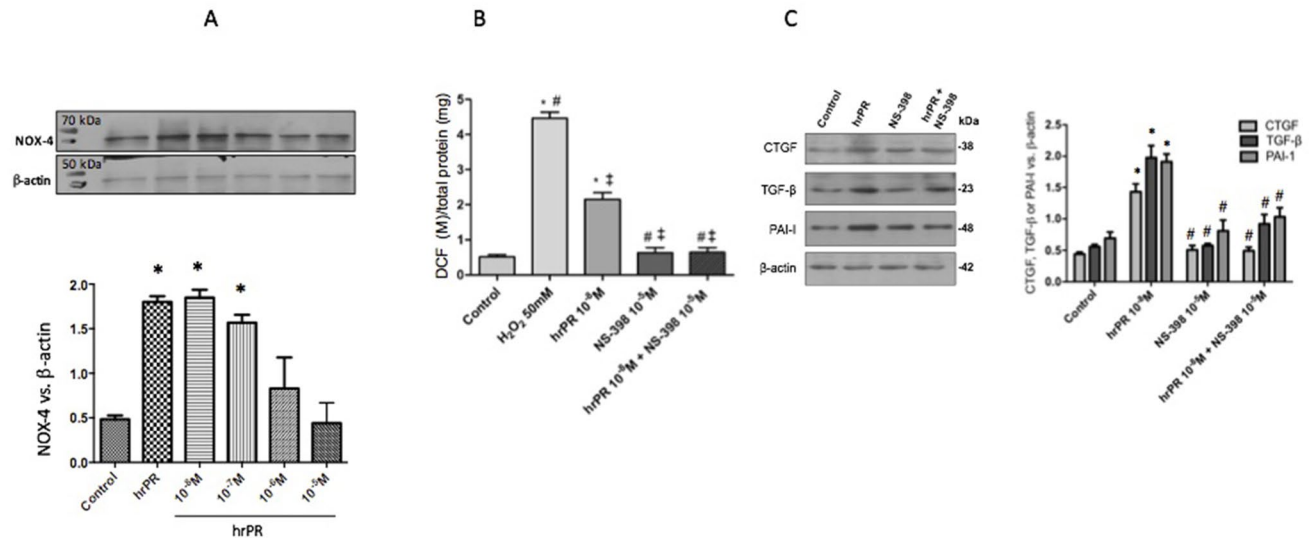

FIGURE 4 | Selective COX-2 inhibitor NS-398 prevented NOX-4 upregulation, the induction of ROS, and the increase in profibrotic markers CTGF, TGF-β, and PAI-I. **(A)**. A dose response effect of COX-2 inhibitor NS-398 on NOX-4 protein expression in M-1 cells incubated with hrPR. **(B)**. For ROS quantification, M-1 cells were treated with NS-398 (10^{-5} M) during 15 min, incubated with DCFH-DA probe for 30 min, and treated with hrPR for 15 min. Results are expressed as DCF probe fluorescence intensity versus total protein (mean ± SEM) **(C)**. Protein levels of CTGF, TGF-β, and PAI-I represented by Western blot analysis (left) and quantitation (right) in M-1 cells incubated during 6 h with hrPR, NS-398, or hrPR plus NS-398, $^{*}p < 0.05$ versus control, $^{\#}p < 0.05$ versus hrPR group, $^{\ddagger}p < 0.05$ versus positive control, $n = 5$.

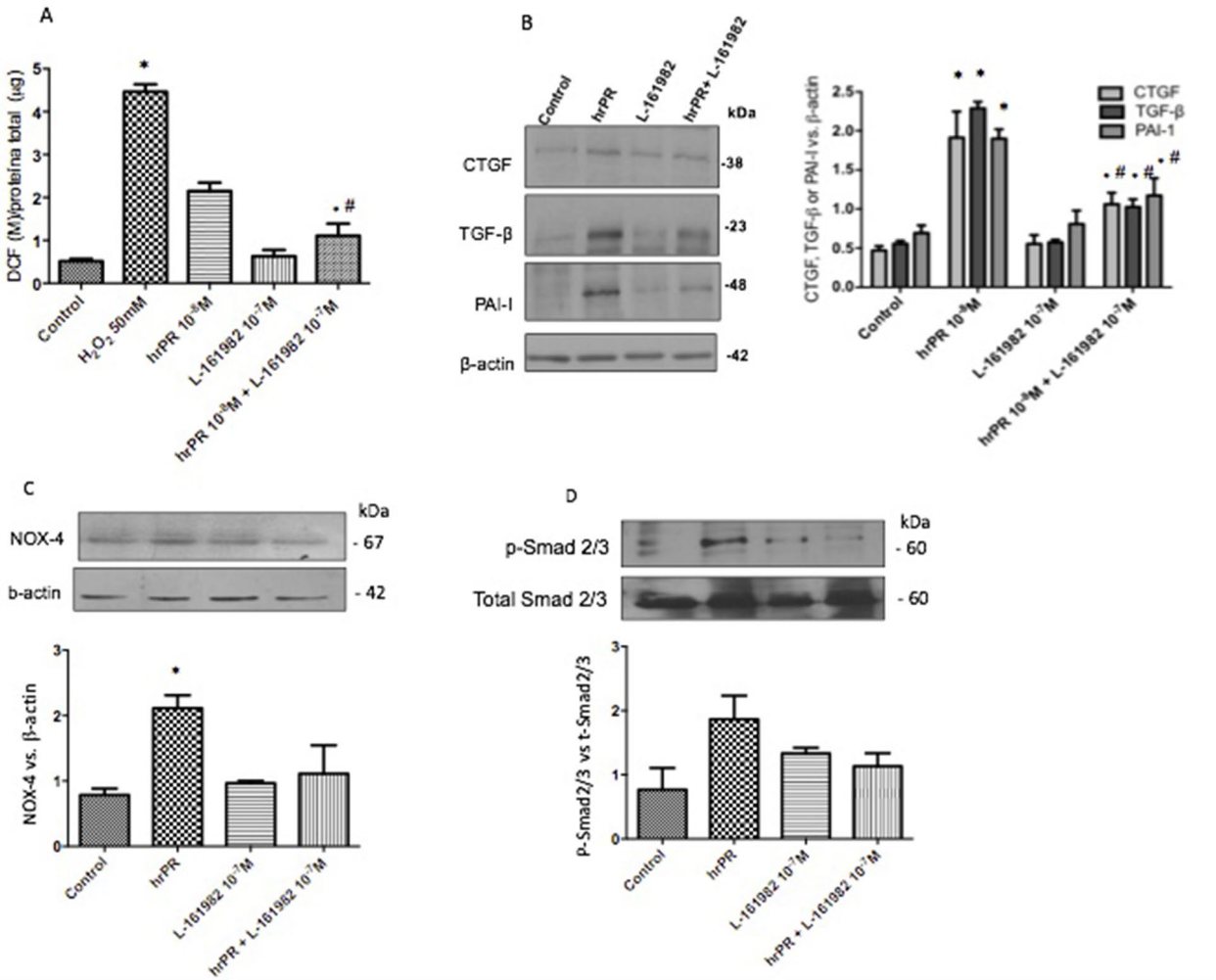

FIGURE 5 | E-Prostanoid receptor 4 blockade prevents hrPR-induced ROS accumulation, NOX-4 upregulation, and induction of profibrotic factors CTGF, TGF-β, and PAI-I. Another set of M-1 cells was tested for ROS production and protein expression of NOX-4, CTGF, TGF-β, and PAI-I. Pre-incubations with 10^7 M of L-161982 partially prevented ROS induction **(A)** and upregulation of profibrotic factors **(B)**. NOX-4 induction was prevented by EP4 L-161982 **(C)**. Because NOX-4 is responsible for ROS production and TGF-β synthesis, we tested the activation of Smad pathway by examining phosphorylation of Smad2 and 3. Preincubations with EP4 inhibitor prevented Smad2 and 3 phosphorylation levels in response to hrPR incubations **(D)**.

phosphorylation of Smad 2/3 (**Figure 5D**), indicating that the activation of TGF-β receptor is involved in the induction of profibrotic factors.

Chronic Infusion of Recombinant Prorenin Increases the Expression of CTGF, PAI-I, and TGF-β Proteins in Medullary CDs; COX-2 Inhibition Prevents This Effect

We tested the effect of chronic infusion of hrPR at a rate of 100 ng/min, *via* an osmotic minipump for 36 h on normal and treated plasma prorenin levels. Using renin enzymatic activity, prorenin was measured in kidney homogenates as the difference between renin activity before and after trypsin activation of prorenin. Estimated plasma prorenin levels were 1,564 ± 109 in controls and 3,514 ± 201 in hrPR-infused groups ($p < 0.05$, $n = 4$). Although PRR has been described at the apical aspect of intercalated CD cells (Gonzalez et al., 2011; Gonzalez et al., 2013), it has also been described at the basolateral membrane (Wang et al., 2016). Physiological parameters such as body weight, kidney weight, urine osmolality, urine flow, Na+ and K+, and estimated GFR are shown in **Table 1**. Prorenin infusion during 36 h slightly reduced Na+ excretion and significantly increased urine osmolality. As shown in **Figure 6,** immunofluorescence studies in kidney slides from control mice showed mostly apical distribution of PRR (in red color and arrows) surrounding the luminal aspect of the CD. Then, we expect that the actions of hrPR might be mediated through blood and filtered hrPR-dependent activation of PRR. **Figure 6E** shows the protocols in mice and the extractions of inner medullary CDs to perform immunoblots and immunofluorescence. Freshly isolated inner medullary CDs

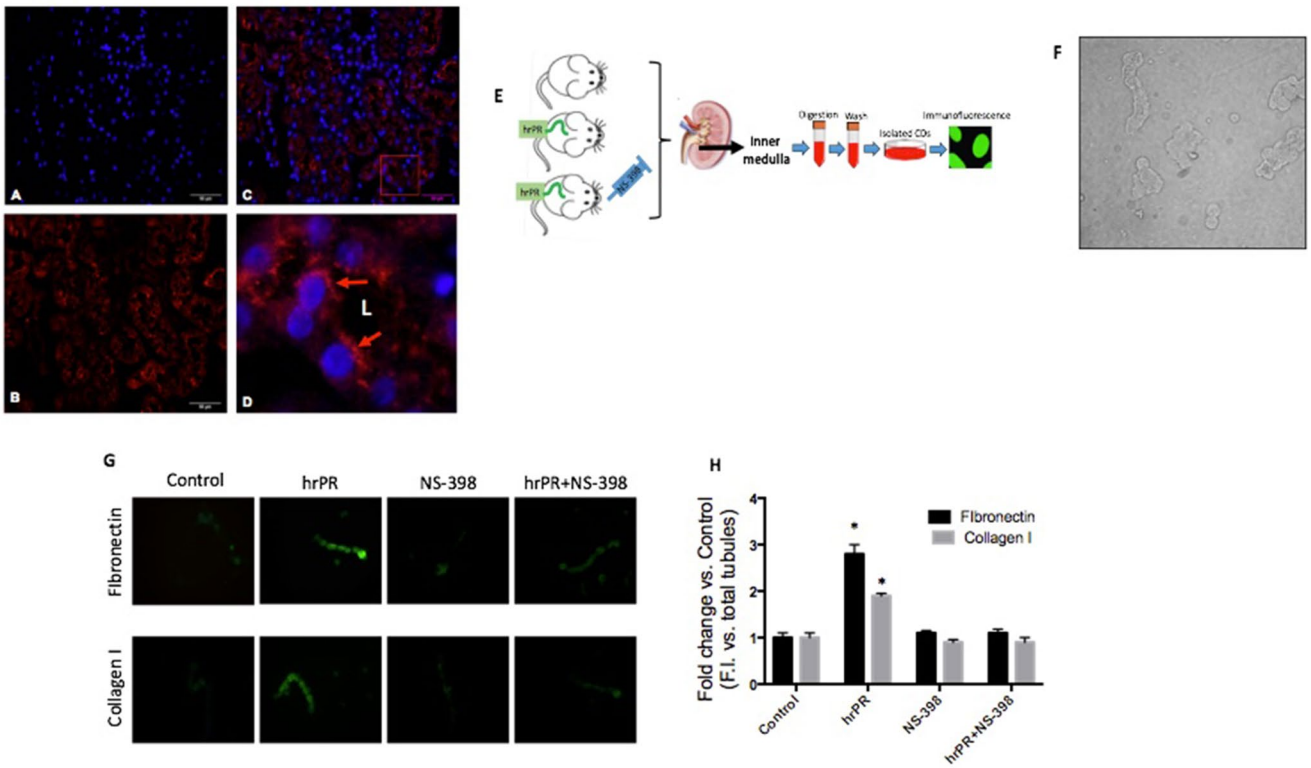

FIGURE 6 | *In vivo* approach to evaluate the effect of chronic hrPR infusion with or without COX-2 inhibition on the expression of collagen I, fibronectin, CTGF, TGF-β, and PAI-I in inner medullary CDs. Immunofluorescence performed in mouse kidney sections showing specific labeling of (Pro)renin receptor in the CDs. **(A)**. DAPI staining for nuclei. **(B)**. Anti-PRR. **(C)** Merge image. **(D)**. 10× digital zoom of merged image showing apical distribution of PRR (red arrows). L indicates tubular lumen. **(E)**. *In vivo* methodology. Human recombinant prorenin was infused at a rate of 100 ng/min *via* an osmotic minipump for 36 h. COX-2 inhibitor NS-398 was administered at 10 mg/kg by oral gavage every 6 h. Sham-operated mice and administered methyl cellulose solution were used as controls. At the end of the study, mice were euthanized by conscious decapitation and renal tissues collected to perform immunofluorescence and Western blots in freshly isolated inner medullary CDs. **(F)**. Representative image of the resulting suspension of freshly isolated inner medullary CDs. **(G)**. Inner medullary CDs were fixed, blocked, and stained with anti-fibronectin or anti-collagen I antibody and detected with secondary antibody Alexa Fluor 488 conjugated to anti-rabbit IgG. **(H)**. Measurements of fluorescence intensity in 10 fields from each processed kidney and expressed as fluorescence intensity versus total number of CD in each field.

(**Figure 6F**) from chronically infused hrPR mice showed augmented fibronectin and collagen I immunofluorescence intensity as compared to controls. NS-398-treated mice did not show changes in immunofluorescence intensity when compared to controls. Mice with COX-2 inhibition treatment and hrPR infusions did not show increase in fibronectin or collagen I staining (**Figures 6G, H**). We next examined the expression profile of phosphorylated and total ERK1/2 and profibrotic genes in renal tissues from mice. As shown in **Figure 7**, the changes in CTGF, PAI-I, and TGF-β expression in inner medullary tissues caused by hrPR infusion were accompanied by increased ERK1/2 phosphorylation (ratio protein/β-actin densitometric values: controls, 0.67 ± 0.01 vs. hrPR, 1.76 ± 0.02, $p < 0.05$). However, despite ERK phosphorylation, the expression of CTGF, PAI-I, and TGF-β was not different from controls in mice infused with hrPR and treated with NS-398. Positive staining for α-SMA was present in some tubular cells but not in interstitial renal cells from mice infused with hrPR. A reduction in the staining was evidenced in mice infused with NS-398 (**Figure 7C**). Finally, we determined levels of IL-1β mRNA relative to 18S mRNA as indicative of inflammatory damage. **Figure 7D** shows a small but significant increase in IL-1β (IL-1β/18S mRNA, hrPR: 2.06 ± 0.09 vs. control: 1.21 ± 0.11, $p < 0.05$) that was partially prevented by COX-2 inhibition (hrPR+NS398: 1.67 ± 0.04 vs. hrPR: 2.06 ± 0.09, $p < 0.05$).

DISCUSSION

The possible pathological role of PRR has been under intense investigation during the last two decades. Seminal experiments showing that PRR is able to activate prorenin and renin catalytic activity (Nguyen and Burckle, 2004; Nguyen et al., 2004) pointed out its possible role in intratubular and intrarenal Ang I formation with the consequent increase in Ang II levels, contributing to the deleterious effects of Ang II such as vasoconstriction (Nguyen and Contrepas, 2008), antinatriuresis (Nguyen et al., 2002), and profibrotic signals (Clavreul et al., 2011). All these effects are especially relevant in hypertension and kidney disease. The activation of PRR by its agonists is relevant, given the evidence that shows that in diabetes, there are high levels of circulating prorenin (Franken et al., 1992;

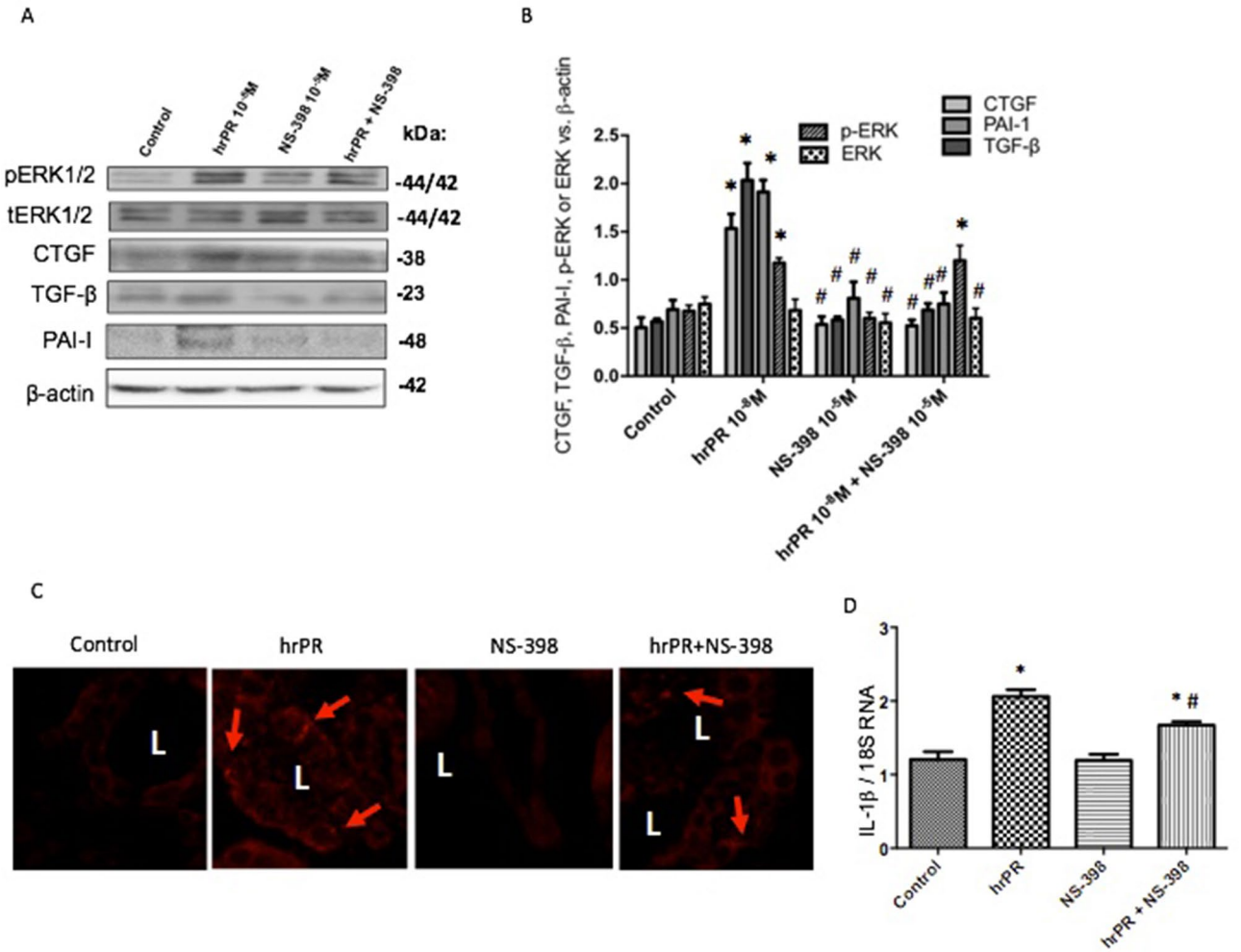

FIGURE 7 | Representative Western blot images **(A)** and quantitation **(B)** of phospho-ERK, total ERK, CTGF, TGF-β, and PAI-I in inner medullary tissues ($n = 5$). $^{*}p < 0.05$ versus control, $^{\#}p < 0.05$ versus hrPR group. **(C)**. Immunofluorescence of alpha smooth muscle actin (α-SMA), a fibrosis-related marker in kidney sections from control mice, saline-infused mice, and mice infused with hrPR. Staining is present in some tubular cells but not in the interstitial cells in renal slides of mice infused with hrPR. A reduced α-SMA staining was evidenced in mice infused with NS-398. **(D)**. IL-1β mRNA relative to 18S mRNA as indicative of inflammatory damage. $p < 0.05$ versus control, $^{\#}p < 0.05$ versus hrPR group.

Chiarelli et al., 2001) and upregulation of the PRR (Huang and Siragy, 2009; Huang and Siragy, 2010). Similarly, it is suggested that high plasma prorenin concentration plays a role in the development of coronary artery disease (Yoshida et al., 2015). Transgenic rats overexpressing PRR show renal tissue damage (Kaneshiro et al., 2006) and elevated blood pressure (Burckle et al., 2006). Additionally, in animal models of diabetes and hypertension, the synthesis and secretion of prorenin and renin are greatly augmented in the principal cells of the CD (Prieto-Carrasquero et al., 2004; Kang et al., 2008; Prieto-Carrasquero et al., 2008), supporting the concept of a local activation of a tubular renin–angiotensin system. Thus, the mechanisms by which PRR may influence local renin–angiotensin system and tissue damage need to be clarified.

We have previously shown that the activation of PRR increases ROS and profibrotic genes in cultured M-1 CD cell line, which supports the hypothesis that the activation of this receptor may generate renal tissue damage (Gonzalez et al., 2017). However, the exact mechanisms are still unclear. By using PRR's natural ligand prorenin (recombinant human prorenin) at nanomolar concentrations, we demonstrated that the activation of PRR activates MAPK pathway and upregulates COX-2 and NOX-4. PRR activation also promotes intracellular ROS accumulation and the upregulation of CTGF, TGF-β, and PAI-1. These effects are blunted by pharmacological inhibition of MAPK, NOX-4, and COX-2 enzymatic activities. Importantly, we showed that the antagonism of the E-prostanoid receptor EP4, which is a Gs-coupled receptor (Gs/cAMP/PKA pathway activator), also prevented the upregulation of NOX-4 and profibrotic factors. Interestingly, the phosphorylation of Smad2/3 was prevented by EP4 antagonist, indicating that TGF-β receptor

may be not activated due to the impairment of the autocrine actions of TGF-β (**Figure 8**). We also demonstrated that prorenin infusions increase the expression of profibrotic genes and fibronectin and collagen I positive staining in mice isolated CDs. Importantly, the co-treatment with a selective COX-2 inhibitor NS-398 prevented this effect, despite the activation of MAPK pathway (**Figure 7**). This indicates that COX-2 activity, and probably EP4 activation, is necessary for the PRR-dependent upregulation of profibrotic factors and cellular ROS generation.

At micromolar concentrations, PD98059 is a highly selective *in vitro* inhibitor of MEK1 activation and MAPK cascade (Alessi et al., 1995). In our experiment, two different concentrations of the inhibitor were used, based on the IC50 described with respect to the inhibition it generates in ERK 1 (4 μM) and in ERK 2 (50 μM) and in the evidence obtained by different authors previously (Gonzalez et al., 2017). **Figure 2** shows that there is no significant difference between levels of ROS obtained for two concentrations tested; as a result, we continued working with the concentration that was previously established by our group (30 μM). As shown in **Figure 2**, we confirmed our previous studies, which showed that ERK inhibition impairs ROS generation and profibrotic gene expression mediated by PRR stimulation. Next, we proceeded with studying the effects of NOX-4 inhibition in CD cells.

Clavreul et al. demonstrated that in HEK cells that were transfected with a siRNA targeting the PRR, the expression of NOX-4 was prevented as well as the increase in superoxide production, TGF-β, fibronectin, and PAI-1expression (Clavreul et al., 2011). Due to this evidence, we decided to use a pharmacological inhibitor of NOX-4, which is the main isoform with physiological actions in CD cells (Lu et al., 2016). The pharmacological inhibitor GKT 137831 has been described as a dual inhibitor of both NOX-4 and NOX-1 (Green et al., 2012). The effectiveness of GKT 137831 has been demonstrated in cells of the pulmonary vascular wall and cardiac fibroblasts, where it blocks the action of NOX-4 and, thereby, prevents an increase in ROS production (Green et al., 2012). To evaluate its effects on ROS generation in the M-1 CD cell line, we tested three different concentrations, based on concentrations used in the studies of Green et al. (Green et al., 2012). These concentrations were 10, 20, and 30 μM. As seen in **Figure 2**, the addition of this inhibitor prevents ROS induction in the M-1 CD cells at all three concentrations. However, we decided to work with 30 μM, since at this concentration, ROS generation was much closer to the control (**Figure 2**). NOX-4 inhibition was able to prevent the increase in ROS with respect to the basal condition, which indicates in the first instance that the main source of ROS is effectively NOX-4, which is consistent with Clavreul's evidence (Clavreul et al., 2011). GTK 137831 also prevented the increase in the synthesis of profibrotic proteins **(Figure 3)**, indicating that the activation of NOX-4 can directly activate the production of profibrotic factors.

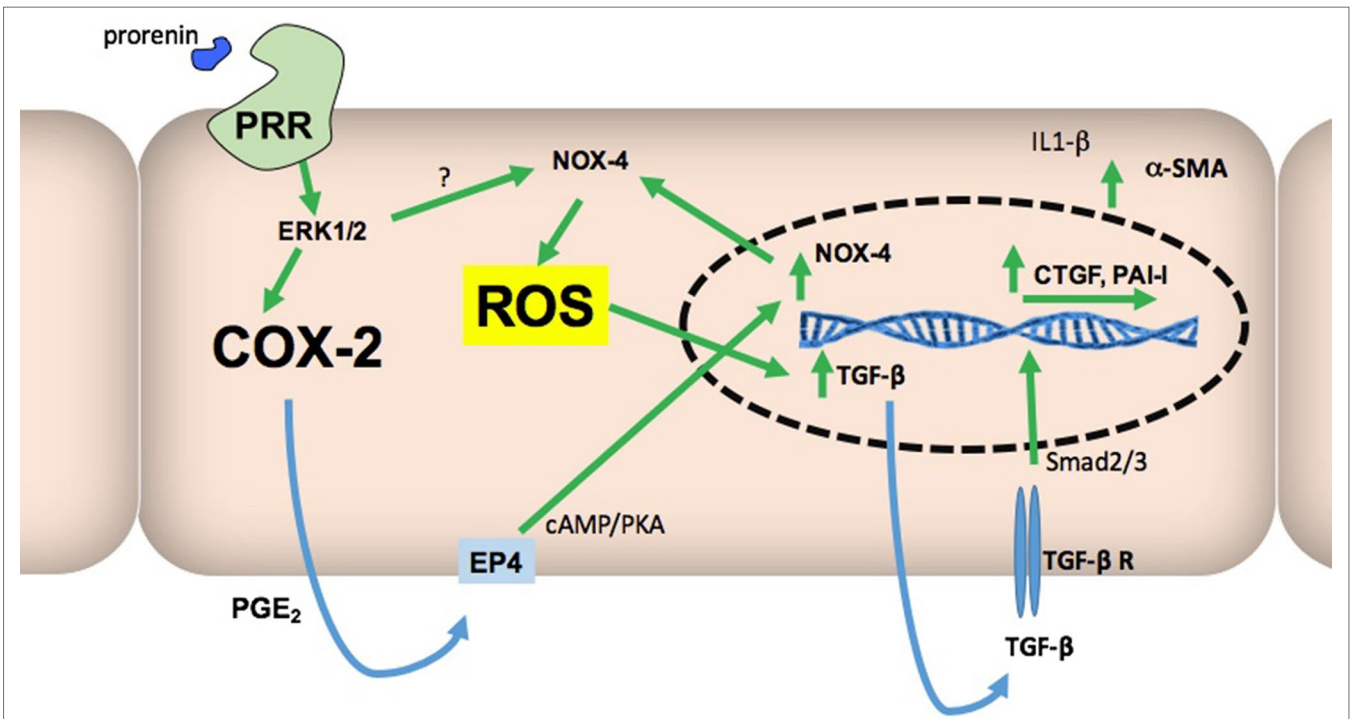

FIGURE 8 | Proposed model to explain how COX-2 might be essential in the stimulatory pathway for ROS production and increased expression of profibrotic genes mediated by PRR activation. Stimulation of PRR by prorenin or renin activates ERK1/2 phosphorylation leading to COX-2 and NOX-4 upregulation. Our data also suggest that upregulation of NOX-4 depends on both the MAPK pathway and activation of EP4 receptor. ROS formation also depends on NOX-4 activity and EP4 signaling, and ROS is responsible for TGF-β upregulation and activation of Smad pathway through TGF-β receptor. This would then lead to CTGF and PAI-I upregulation. Targeting COX-2-mediated prostaglandin E2 (PGE_2) synthesis may reduce NOX-4 activity and ROS production.

Activation of the prostaglandin receptor EP4 increases NOX-4 expression in liver cells. In addition, overexpression of COX-2 leads to higher NOX-4 levels and ROS content, while inhibition of the enzyme leads to decreased NOX-4 levels and ROS content (Sancho et al., 2011). In turn, ROS are involved in TGF-β and Smad signaling (Lafon et al., 1996; Chiu et al., 2001), which induces fibrotic factors CTGF and PAI-I (Clarkson et al., 1999; Kilari et al., 2018). The ERK pathway can enhance Smad activity. On the other hand, ERK inhibition reduces TGF-β1-stimulated Smad phosphorylation as well as collagen production and promoter activities, suggesting that ERK activity is necessary for an optimal response to TGF-β1 (Hayashida et al., 2003). Although we observed a reduction in ROS production and profibrotic factors in hrPR-treated cells, the suppression was not complete. This incomplete suppression indicates that the activity of endogenous NOX-4 may be induced by MAPK pathway independent of COX-2-mediated PGE_2 and EP4 activation. Furthermore, it is possible that low levels of ROS might function in various pathophysiological processes, contributing to the activation of transcription factors leading to induction of profibrotic factors as well (Sedeek et al., 2013a; Sedeek et al., 2013b). We have reported that antioxidants prevented the increase in profibrotic factors, indicating an evident role of ROS as a signaling agent in a pathophysiological process (Gonzalez et al., 2017).

Our data were corroborated *in vivo* using chronic infusions of human recombinant prorenin during 36 h. We observed an increased expression of profibrotic genes in isolated CDs from treated mice through Western blot analysis of pERK and total ERK, CTGF, TGF-β, and PAI-I and by immunofluorescence analysis of fibronectin and collagen I expression (**Figures 6** and **7**) We also observed α-SMA staining in mice with hrPR infusions, which was less evident in mice treated with COX-2 inhibitor. It is possible that recombinant prorenin infusion increased profibrotic protein expression through direct interactions with apical PRR by filtration from plasma and having access to the distal tubular lumen or by having access to basolateral PRR through the blood.

Despite the evidence of the role of NOX-4 and ERK pathway in renal fibrosis, little is known about their interactions with COX-2. PRR and COX-2 are co-located in CD cells (Gonzalez et al., 2013), which suggests that they could be functionally related. Kaneshiro et al. demonstrated in 2006 that the overexpression of human PRR in rats resulted in an over-regulation of COX-2 in renal cortex, which contributed to the generation of tubular damage, due to the inflammation mediated by prostaglandins (Kaneshiro et al., 2006). In addition to this evidence, it is known that the activation of MAPK activates COX-2, which consequently leads to production of PGE_2 in the CD. Furthermore, we have recently published evidence of the participation of PGE_2, synthesized by COX-2, in the regulation of prorenin. Prorenin causes further increases in COX-2 expression, generating transient COX-2-prorenin positive feedback (Salinas-Parra et al., 2017). As mentioned before, the relationship between COX-2 and NOX-4 observed in hepatocytes (Sancho et al., 2011) suggests that a similar system regulated by positive feedback may be present in CD cells (**Figure 8**).

In summary, our results indicate that the induction of ROS, TGF-β, and profibrotic factors CTGF and PAI-I occurs through PRR-dependent activation of MAPK and NOX-4. Additionally, it depends on intact COX-2 activity that leads to PGE_2-dependent activation of EP4 receptor and TGF-β receptor-dependent Smad pathway activation. Site-specific pharmacological inhibition of COX-2 in the CD may help to prevent tubular damage during states of activation of intratubular renin–angiotensin system, such as hypertension and diabetes.

ETHICS STATEMENT

The Institutional Animal Care and Use Committees of the Pontificia Universidad Catolica de Valparaiso approved all animal protocols.

AUTHOR CONTRIBUTIONS

AG, CR-M, MK, and QMN performed the experiments, analyzed the data and provided the final version of the manuscript.

FUNDING

This study was funded by DI Grant Nº 0.39.307/2018 Pontificia Universidad Católica de Valparaíso, Chile and Fondo Nacional de Desarrollo Científico y Tecnológico (FONDECYT) 1191006.

REFERENCES

Alessi, D. R., Cuenda, A., Cohen, P., Dudley, D. T., and Saltiel, A. R. (1995). PD 098059 is a specific inhibitor of the activation of mitogen-activated protein kinase kinase *in vitro* and *in vivo*. *J. Biol. Chem.* 270, 27489–27494. doi: 10.1074/jbc.270.46.27489

Ballarin-Gonzalez, B., Dagnaes-Hansen, F., Fenton, R. A., Gao, S., Hein, S., Dong, M. D., et al. (2013). Protection and systemic translocation of siRNA following oral administration of chitosan/siRNA nanoparticles. *Mol. Ther. Nucleic Acids* 2, e76. doi: 10.1038/mtna.2013.2

Batenburg, W. W., Krop, M., Garrelds, I. M., de Vries, R., de Bruin, R. J. A., Burckle, C. A., et al. (2007). Prorenin is the endogenous agonist of the (pro) renin receptor. Binding kinetics of renin and prorenin in rat vascular smooth muscle cells overexpressing the human (pro)renin receptor. *J. Hypertens.* 25, 2441–2453. doi: 10.1097/HJH.0b013e3282f05bae

Burckle, C. A., Danser, A. H. J., Muller, D. N., Garrelds, I. M., Gasc, J. M., Popova, E., et al. (2006). Elevated blood pressure and heart rate in human renin receptor transgenic rats. *Hypertension* 47, 552–556. doi: 10.1161/01.HYP.0000199912.47657.04

Campbell, D. J., Nussberger, J., Stowasser, M., Danser, A. H. J., Morganti, A., Frandsen, E., et al. (2009). Activity assays and immunoassays for plasma renin and prorenin: information provided and precautions necessary for accurate measurement. *Clin. Chem.* 55, 867–877. doi: 10.1373/clinchem.2008.118000

Chi, Y. C., Shi, C. L., Zhou, M., Liu, Y., Zhang, G., and Hou, S. A. (2017). Selective cyclooxygenase-2 inhibitor NS-398 attenuates myocardial fibrosis in mice after myocardial infarction *via* Snail signaling pathway. *Eur. Rev. Med. Pharmacol. Sci.* 21, 5805–5812. doi: 10.26355/eurrev_201712_14028

Chiarelli, F., Pomilio, M., De Luca, F. A., Vecchiet, J., and Verrotti, A. (2001). Plasma prorenin levels may predict persistent microalbuminuria in children with diabetes. *Pediatr. Nephrol.* 16, 116–120. doi: 10.1007/s004670000514

Chiu, C., Maddock, D. A., Zhang, Q., Souza, K. P., Townsend, A. R., and Wan, Y. (2001). TGF-beta-induced p38 activation is mediated by Rac1-regulated generation of reactive oxygen species in cultured human keratinocytes. *Int. J. Mol. Med.* 8, 251–255. doi: 10.3892/ijmm.8.3.251

Clarkson, M. R., Gupta, S., Murphy, M., Martin, F., Godson, C., and Brady, H. R. (1999). Connective tissue growth factor: a potential stimulus for glomerulosclerosis and tubulointerstitial fibrosis in progressive renal disease. *Curr. Opin. Nephrol. Hypertens.* 8, 543–548. doi: 10.1097/00041552-199909000-00002

Clavreul, N., Sansilvestri-Morel, P., Magard, D., Verbeuren, T. J., and Rupin, A. (2011). (Pro)renin promotes fibrosis gene expression in HEK cells through a Nox4-dependent mechanism. *Am. J. Physiol. Renal.* 300, F1310–F1318. doi: 10.1152/ajprenal.00119.2010

Feldt, S., Batenburg, W. W., Mazak, I., Maschke, U., Wellner, M., Kvakan, H., et al. (2008). Prorenin and renin-induced extracellular signal-regulated kinase 1/2 activation in monocytes is not blocked by aliskiren or the handle-region peptide. *Hypertension* 51, 682–688. doi: 10.1161/HYPERTENSIONAHA.107.101444

Ferguson, S., Hebert, R. L., and Laneuville, O. (1999). NS-398 upregulates constitutive cyclooxygenase-2 expression in the M-1 cortical collecting duct cell line. *J. Am. Soc. Nephrol.* 10, 2261–2271.

Franken, A. A. M., Derkx, F. H. M., Blankestijn, P. J., Janssen, J.A.M.J.L., Mannesse, C. K., Hop, W., et al. (1992). Plasma prorenin as an early marker of microvascular disease in patients with diabetes-mellitus. *Diabetes Metab.* 18, 137–143.

Gonzalez, A. A., Cifuentes-Araneda, F., Ibaceta-Gonzalez, C., Gonzalez-Vergara, A., Zamora, L., Henriquez, R., et al. (2016). Vasopressin/V2 receptor stimulates renin synthesis in the collecting duct. *Am. J. Physiol. Renal.* 310, F284–F293. doi: 10.1152/ajprenal.00360.2015

Gonzalez, A. A., Green, T., Luffman, C., Bourgeois, C. R., Gabriel Navar, L., and Prieto, M. C. (2014). Renal medullary cyclooxygenase-2 and (pro)renin receptor expression during angiotensin II-dependent hypertension. *Am. J. Physiol. Renal Physiol.* 307, F962–F970. doi: 10.1152/ajprenal.00267.2014

Gonzalez, A. A., Lara, L. S., Luffman, C., Seth, D. M., and Prieto, M. C. (2011). Soluble form of the (pro) renin receptor is augmented in the collecting duct and urine of chronic angiotensin ii-dependent hypertensive rats. *Hypertension* 57, 859–864. doi: 10.1161/HYPERTENSIONAHA.110.167957

Gonzalez, A. A., Liu, L., Lara, L. S., Bourgeois, C. R., Ibaceta-Gonzalez, C., Salinas-Parra, N., et al. (2015). PKC-alpha-dependent augmentation of cAMP and CREB phosphorylation mediates the angiotensin II stimulation of renin in the collecting duct. *Am. J. Physiol. Renal Physiol.* 309, F880–F888. doi: 10.1152/ajprenal.00155.2015

Gonzalez, A. A., Liu, L., Lara, L. S., Seth, D. M., Navar, L. G., and Prieto, M. C. (2011). Angiotensin II stimulates renin in inner medullary collecting duct cells *via* protein kinase C and independent of epithelial sodium channel and mineralocorticoid receptor activity. *Hypertension* 57, 594–599. doi: 10.1161/HYPERTENSIONAHA.110.165902

Gonzalez, A. A., Luffman, C., Bourgeois, C. R., Vio, C. P., and Prieto, M. C. (2013). Angiotensin II-independent upregulation of cyclooxygenase-2 by activation of the (Pro)renin receptor in rat renal inner medullary cells. *Hypertension* 61, 443–449. doi: 10.1161/HYPERTENSIONAHA.112.196303

Gonzalez, A. A., Salinas-Parra, N., Leach, D., Navar, L. G., and Prieto, M. C. (2017). PGE2 upregulates renin through E-prostanoid receptor 1 *via* PKC/cAMP/CREB pathway in M-1 cells. *Am. J. Physiol. Renal.* 313, F1038–F1049. doi: 10.1152/ajprenal.00194.2017

Gonzalez, A. A., Zamora, L., Reyes-Martinez, C., Salinas-Parra, N., Roldan, N., Cuevas, C. A., et al. (2017). (Pro)renin receptor activation increases profibrotic markers and fibroblast-like phenotype through MAPK-dependent ROS formation in mouse renal collecting duct cells. *Clin. Exp. Pharmacol. Physiol.* 1134–1144. doi: 10.1111/1440-1681.12813

Green, D. E., Murphy, T. C., Kang, B. Y., Kleinhenz, J. M., Szyndralewiez, C., Page, P., et al. (2012). The Nox4 inhibitor GKT137831 attenuates hypoxia-induced pulmonary vascular cell proliferation. *Am. J. Respir. Cell Mol. Biol.* 47, 718–726. doi: 10.1165/rcmb.2011-0418OC

Hayashida, T., Decaestecker, M., and Schnaper, H. W. (2003). Cross-talk between ERK MAP kinase and Smad signaling pathways enhances TGF-beta-dependent responses in human mesangial cells. *FASEB J.* 17, 1576–1578. doi: 10.1096/fj.03-0037fje

Hong, Y. H., Peng, H. B., La Fata, V., and Liao, J. K. (1997). Hydrogen peroxide-mediated transcriptional induction of macrophage colony-stimulating factor by TGF-beta1. *J. Immunol.* 159, 2418–2423.

Huang, J. Q., and Siragy, H. M. (2009). Glucose Promotes the production of interleukine-1 beta and cyclooxygenase-2 in mesangial cells *via* enhanced (pro)renin receptor expression. *Endocrinology* 150, 5557–5565. doi: 10.1210/en.2009-0442

Huang, J. Q., and Siragy, H. M. (2010). Regulation of (pro) renin receptor expression by glucose-induced mitogen-activated protein kinase, nuclear factor-kappa B, and activator protein-1 signaling pathways. *Endocrinology* 151, 3317–3325. doi: 10.1210/en.2009-1368

Huang, J. Q., Matavelli, L. C., and Siragy, H. M. (2011). Renal (pro)renin receptor contributes to development of diabetic kidney disease through transforming growth factor-beta 1-connective tissue growth factor signalling cascade. *Clin. Exp. Pharmacol.* P 38, 215–221. doi: 10.1111/j.1440-1681.2011.05486.x

Ichihara, A., Sakoda, M., Kurauchi-Mito, A., Nishiyama, A., and Itoh, H. (2008). Involvement of receptor-bound prorenin in development of nephropathy in diabetic db/db mice. *J. Am. Soc. Hypertens.* 2, 332–340. doi: 10.1016/j.jash.2008.04.009

Kaneshiro, Y., Ichihara, A., Sakoda, M., Takemitsu, T., Nabi, A. H. M. N., Uddin, M. N., et al. (2007). Slowly progressive, angiotensin II-independent glomerulosclerosis in human (pro)renin receptor-transgenic rats. *J. Am. Soc. Nephrol.* 18, 1789–1795. doi: 10.1681/ASN.2006091062

Kaneshiro, Y., Ichihara, A., Takemitsu, T., Sakoda, M., Suzuki, F., Nakagawa, T., et al. (2006). Increased expression of cyclooxygenase-2 in the renal cortex of human prorenin receptor gene-transgenic rats. *Kidney Int.* 70, 641–646. doi: 10.1038/sj.ki.5001627

Kang, J. J., Toma, I., Sipos, A., Meer, E. J., Vargas, S. L., and Peti-Peterdi, J. (2008). The collecting duct is the major source of prorenin in diabetes. *Hypertension* 51, 1597–1604. doi: 10.1161/HYPERTENSIONAHA.107.107268

Kilari, S., Yang, B., Sharma, A., McCall, D. L., and Misra, S. (2018). Increased transforming growth factor beta (TGF-beta) and pSMAD3 signaling in a murine model for contrast induced kidney injury. *Sci. Rep.* 8, 6630. doi: 10.1038/s41598-018-24340-z

Lafon, C., Mathieu, C., Guerrin, M., Pierre, O., Vidal, S., and Valette, A. (1996). Transforming growth factor beta 1-induced apoptosis in human ovarian carcinoma cells: protection by the antioxidant N-acetylcysteine and bcl-2. *Cell Growth Differ.* 7, 1095–1104.

Lenz, T., Sealey, J. E., Lappe, R. W., Carilli, C., Oshiro, G. T., Baxter, J. D., et al. (1990). Infusion of recombinant human prorenin into rhesus monkeys. Effects on hemodynamics, renin–angiotensin–aldosterone axis and plasma testosterone. *Am. J. Hypertens.* 3, 257–261. doi: 10.1093/ajh/3.4.257

Lu, X., Wang, F., Liu, M., Yang, K. T., Nau, A., Kohan, D. E., et al. (2016). Activation of ENaC in collecting duct cells by prorenin and its receptor PRR: involvement of Nox4-derived hydrogen peroxide. *Am. J. Physiol. Renal Physiol.* 310, F1243–F1250. doi: 10.1152/ajprenal.00492.2015

Lugarini, F., Hrupka, B. J., Schwartz, G. J., Plata-Salaman, C. R., and Langhans, W. (2002). A role for cyclooxygenase-2 in lipopolysaccharide-induced anorexia in rats. *Am. J. Physiol. Regul. Integr. Comp. Physiol.* 283, R862–R868. doi: 10.1152/ajpregu.00200.2002

Meng, X. M., Tang, P. M., Li, J., and Lan, H. Y. (2015). TGF-beta/Smad signaling in renal fibrosis. *Front. Physiol.* 6, 82. doi: 10.3389/fphys.2015.00082

Muller, D. N., Klanke, B., Feldt, S., Cordasic, N., Hartner, A., Schmieder, R. E., et al. (2008). (Pro) renin receptor peptide inhibitor "handle-region" peptide does not affect hypertensive nephrosclerosis in Goldblatt rats. *Hypertension* 51, 676–681. doi: 10.1161/HYPERTENSIONAHA.107.101493

Muzaffar, S., Jeremy, J. Y., Angelini, G. D., and Shukla, N. (2012). NADPH oxidase 4 mediates upregulation of type 4 phosphodiesterases in human endothelial cells. *J. Cell. Physiol.* 227, 1941–1950. doi: 10.1002/jcp.22922

Nasrallah, R., Laneuville, O., Ferguson, S., and Hebert, R. L. (2001). Effect of COX-2 inhibitor NS-398 on expression of PGE(2) receptor subtypes in M-1 mouse CCD cells. *Am. J. Physiol. Renal.* 281, F123–F132. doi: 10.1152/ajprenal.2001.281.1.F123

Nguyen, G., and Burckle, C. A. (2004). The (pro)renin receptor: biology and functional significance. *B. Acad. Nat. Med. Paris* 188, 621–628.

Nguyen, G., and Contrepas, A. (2008). Physiology and pharmacology of the (pro)renin receptor. *Curr. Opin. Pharmacol.* 8, 127–132. doi: 10.1016/j.coph.2007.12.009

Nguyen, G., Burckle, C. A., and Sraer, J. D. (2004). Renin/prorenin-receptor biochemistry and functional significance. *Curr. Hypertens. Rep.* 6, 129–132. doi: 10.1007/s11906-004-0088-3

Nguyen, G., Delarue, F., Burckle, C., Bouzhir, L., Giller, T., and Sraer, J. D. (2002). Pivotal role of the renin/prorenin receptor in angiotensin II production and cellular responses to renin. *J. Clin. Invest.* 109, 1417–1427. doi: 10.1172/JCI0214276

Prieto-Carrasquero, M. C., Botros, F. T., Pagan, J., Kobori, H., Seth, D. M., Casarini, D. E., et al. (2008). Collecting duct renin is upregulated in both kidneys of 2-kidney, 1-clip Goldblatt hypertensive rats. *Hypertension* 51, 1590–1596. doi: 10.1161/HYPERTENSIONAHA.108.110916

Prieto-Carrasquero, M. C., Harrison-Bernard, L. M., Kobori, H., Ozawa, Y., Hering-Smith, K. S., Hamm, L. L., et al. (2004). Enhancement of collecting duct renin in angiotensin II-dependent hypertensive rats. *Hypertension* 44, 223–229. doi: 10.1161/01.HYP.0000135678.20725.54

Salinas-Parra, N., Reyes-Martinez, C., Prieto, M. C., and Gonzalez, A. A. (2017). Prostaglandin E2 induces prorenin-dependent activation of (pro)renin receptor and upregulation of cyclooxygenase-2 in collecting duct cells. *Am. J. Med. Sci.* 354, 310–318. doi: 10.1016/j.amjms.2017.05.018

Sancho, P., Martin-Sanz, P., and Fabregat, I. (2011). Reciprocal regulation of NADPH oxidases and the cyclooxygenase-2 pathway. *Free Radic. Biol. Med.* 51, 1789–1798. doi: 10.1016/j.freeradbiomed.2011.08.011

Sedeek, M., Gutsol, A., Montezano, A. C., Burger, D., Nguyen Dinh Cat, A., Kennedy, C. R., et al. (2013a). Renoprotective effects of a novel Nox1/4 inhibitor in a mouse model of Type 2 diabetes. *Clin. Sci. (Lond.)* 124, 191–202. doi: 10.1042/CS20120330

Sedeek, M., Nasrallah, R., Touyz, R. M., and Hebert, R. L. (2013b). NADPH oxidases, reactive oxygen species, and the kidney: friend and foe. *J. Am. Soc. Nephrol.* 24, 1512–1518. doi: 10.1681/ASN.2012111112

Stoos, B. A., Narayfejestoth, A., Carretero, O. A., Ito, S., and Fejestoth, G. (1991). Characterization of a mouse cortical collecting duct cell-line. *Kidney Int.* 39, 1168–1175. doi: 10.1038/ki.1991.148

Takayama, K., Garcia-Cardena, G., Sukhova, G. K., Comander, J., Gimbrone, M. A., and Libby, P. (2002). Prostaglandin E-2 suppresses chemokine production in human macrophages through the EP4 receptor. *J. Biol. Chem.* 277, 44147–44154. doi: 10.1074/jbc.M204810200

Tu, W., Eckert, G. J., Pratt, J. H., and Jan Danser, A. H. (2012). Plasma levels of prorenin and renin in blacks and whites: their relative abundance and associations with plasma aldosterone concentration. *Am. J. Hypertens.* 25, 1030–1034. doi: 10.1038/ajh.2012.83

Wang, F., Lu, X., Peng, K., Fang, H., Zhou, L., Su, J., et al. (2016). Antidiuretic action of collecting duct (pro)renin receptor downstream of vasopressin and PGE2 receptor EP4. *J. Am. Soc. Nephrol.* 27, 3022–3034. doi: 10.1681/ASN.2015050592

Wilkinson-Berka, J. L. (2008). Prorenin and the (pro)renin receptor in ocular pathology. *Am. J. Pathol.* 173, 1591–1594. doi: 10.2353/ajpath.2008.080757

Yisireyili, M., Saito, S., Abudureyimu, S., Adelibieke, Y., Ng, H. Y., Nishijima, F., et al. (2014). Indoxyl sulfate-induced activation of (pro)renin receptor promotes cell proliferation and tissue factor expression in vascular smooth muscle cells. *PLoS One* 9 (10), e109268. doi: 10.1371/journal.pone.0109268

Yoshida, G., Kawasaki, M., Murata, I., Hayakawa, Y., Aoyama, T., Miyazaki, N., et al. (2015). Higher plasma prorenin concentration plays a role in the development of coronary artery disease. *Biomark. Res.* 3, 18. doi: 10.1186/s40364-015-0044-1

Conflict of Interest Statement: The authors declare that the research was conducted in the absence of any commercial or financial relationships that could be construed as a potential conflict of interest.

The handling editor declared a shared affiliation, though no other collaboration, with the authors CR-M and AG, at the time of review.

frontiers in Pharmacology

REVIEW
published: 18 September 2019
doi: 10.3389/fphar.2019.01068

Potential Novel Strategies for the Treatment of Dental Pulp-Derived Pain: Pharmacological Approaches and Beyond

Christina M. A. P. Schuh[1†], Bruna Benso[2,3†] and Sebastian Aguayo[2]*

[1] Centro de Medicina Regenerativa, Facultad de Medicina Clínica Alemana-Universidad del Desarrollo, Santiago, Chile, [2] School of Dentistry, Faculty of Medicine, Pontificia Universidad Catolica de Chile, Santiago, Chile, [3] Department of Physiology, Faculty of Medicine, Universidad Austral de Chile, Millennium Nucleus of Ion Channels Associated Diseases (MiNICAD), Valdivia, Chile

The diagnosis and management of pain is an everyday occurrence in dentistry, and its effective control is essential to ensure the wellbeing of patients. Most tooth-associated pain originates from the dental pulp, a highly vascularized and innervated tissue, which is encased within mineralized dentin. It plays a crucial role in the sensing of stimuli from the local environment, such as infections (i.e. dental caries) and traumatic injury, leading to a local inflammatory response and subsequently to an increase in intra-pulp pressure, activating nerve endings. However, thermal, chemical, and mechanical stimuli also have the ability to generate dental pulp pain, which presents mechanisms highly specific to this tissue and which have to be considered in pain management. Traditionally, the management of dental pulp pain has mostly been pharmacological, using non-steroidal anti-inflammatory drugs (NSAIDs) and opioids, or restorative (i.e. removal of dental caries), or a combination of both. Both research areas continuously present novel and creative approaches. This includes the modulation of thermo-sensitive *transient receptor potential cation channels* (TRP) by newly designed drugs in pharmacological research, as well as the use of novel biomaterials, stem cells, exosomes and physical stimulation to obtain pulp regeneration in regenerative medicine. Therefore, the aim of this review is to present an up-to-date account of causes underlying dental pain, novel treatments involving the control of pain and inflammation and the induction of pulp regeneration, as well as insights in pain in dentistry from the physiological, pharmacological, regenerative and clinical perspectives.

Keywords: dentistry, pain, dentin, dental caries, regenerative medicine, pharmacology, collagen, endodontics

OPEN ACCESS

Edited by:
Ramón Sotomayor-Zárate, University of Valparaíso, Chile

Reviewed by:
Hugo F. Miranda, University of Chile, Chile
Teresa Pelissier, University of Chile, Chile

***Correspondence:**
Sebastian Aguayo
sebastian.aguayo@uc.cl

†These authors have contributed equally to this work

Specialty section:
This article was submitted to Translational Pharmacology, a section of the journal Frontiers in Pharmacology

Received: *05 July 2019*
Accepted: *22 August 2019*
Published: *18 September 2019*

Citation:
Schuh CMAP, Benso B and Aguayo S (2019) Potential Novel Strategies for the Treatment of Dental Pulp-Derived Pain: Pharmacological Approaches and Beyond. Front. Pharmacol. 10:1068. doi: 10.3389/fphar.2019.01068

INTRODUCTION

Despite many advances in the fields of diagnosis, material sciences and therapeutics, oral diseases continue to burden millions of people worldwide, causing a significant impact on both health costs and patient quality of life (Hall-Stoodley et al., 2004; Logan and Brett, 2013; Römling et al., 2014). According to the Global Burden of Disease Study 2016, it is estimated that more than 3.5 billion people worldwide suffer from oral diseases, with 2.4 billion of those cases being dental caries (Vos et al., 2017). Furthermore, it is also estimated that 743 million people are affected by periodontal

disease, a chronic progressive weakening of the supporting structures of the tooth that leads to tooth loss and dysfunction (Tonetti et al., 2017). Despite the fact that these oral diseases display a wide variety of symptoms, many patients seek dental advice due to the presence of pain in the mouth and/or facial region. Therefore, the diagnosis and management of orofacial pain is an essential need for dentists to ensure the wellbeing of patients, as well as to determine the most appropriate treatment plan for each clinical situation.

In general terms, pain can be defined as an "unpleasant sensory and emotional experience that is associated with actual or potential tissue damage or described in such terms" (Gebhart, 2000). Thus, it is a subjective appreciation that varies between individuals, which can make its clinical diagnosis challenging. In dentistry, pain is a multifactorial experience that also includes strong emotional and previous-experience components (Sessle, 1986). There are many origins of pain in the orofacial region; however, the most frequent pain is the one initiating from within the tooth and dental pulp (Estrela et al., 2011), which can be triggered by a wide and diverse range of stimuli including hot and cold temperatures, air puffs, sugar consumption, and mechanical pressure. Orofacial pain originating from structures surrounding the tooth (such as periodontal tissue, oral mucosa and alveolar bone) will not be covered in this review.

Tooth Anatomy and Its Relevance in Dental Pain Perception

Teeth are highly complex organs located within the oral cavity. They are constituted by three mineralized tissues known as enamel, dentin, and cement, which surround the un-mineralized tissue known as dental pulp (**Figure 1A**). Mineralized tissues of the tooth are mostly comprised of hydroxyapatite crystals with varying amounts of organic content (e.g. type-I collagen, other proteins), and their main functions are to provide structural integrity to the tooth and to protect the pulp from environmental injury (Shahmoradi et al., 2014). Enamel is the most mineralized tissue in the body; therefore, it plays a central role in mastication and in protecting dentin and pulp from environmental injury. Cement, on the other hand, is present on the surface of the root, and is involved in the anchoring of the tooth to the alveolar bone by means of the periodontal ligament.

Dentin is a mineralized dental tissue contained within enamel and cementum, constituted by hydroxyapatite (70% weight), organic material (20% weight) and water (10% weight) (Goldberg, 2011). The organic material is mostly comprised of a matrix of type-I collagen, and its presence is crucial for the structural stability as well as the elasticity of the tooth (Butler and Ritchie, 1995; Bertinetti et al., 2015). Dentin is maintained by the cellular prolongations of odontoblasts, which are nested within dentinal tubules- channels extending from the dental pulp until the enamel-dentin junction (Arana-Chavez and Massa, 2004) (**Figure 1B**). These tubules are flooded with dentinal (interstitial) fluid; thus, dentin receives nutrients by direct perfusion from the dental pulp. Most importantly, as dentin is strongly interconnected with the dental pulp and its innervation, it is crucial in the process of dental pain perception.

Interestingly, the initial portion of the dentinal tubules contains pulp nerve endings and thus dentin exposed to the oral cavity (i.e. by caries or trauma) can actively respond to environmental stimuli and trigger nociception (**Figure 1B**). Stimulatory sources that can directly or indirectly affect the dental pulp include chemical irritation, dental caries, infiltration of bonding materials, trauma and orthodontic movements, among others (Tikhonova et al., 2018). This phenomenon is also known as *dentinal hypersensitivity*, as seemingly innocuous stimuli can generate an exaggerated pain response in patients (Miglani et al., 2010). Nerve endings located in the initial portion of dentinal tubules and dental pulp are mainly constituted of A-delta and C fibers—afferent endings of the trigeminal nerve—that can be triggered by both mechanical and thermal stimuli (Jain et al., 2013).

There are three main hypotheses regarding the mechanisms behind dentinal hypersensitivity. The first hypothesis, also

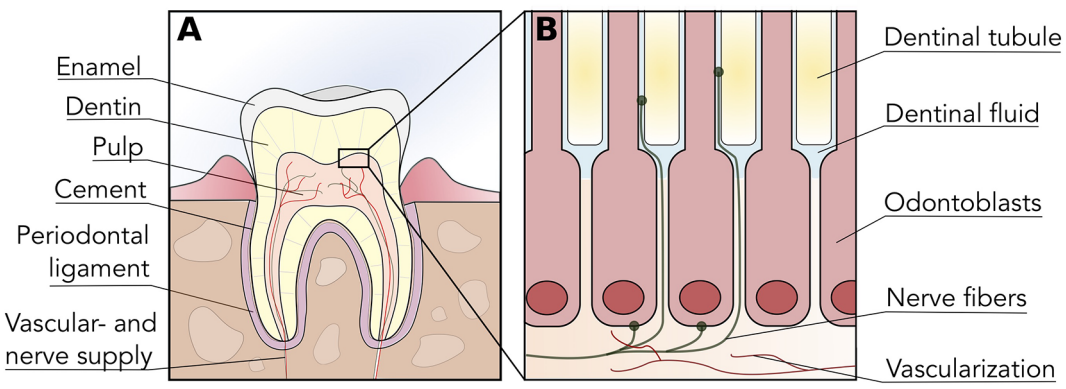

FIGURE 1 | Tooth and dental pulp anatomy. **(A)** Diagrammatic representation of a tooth cross-section illustrating the organization of enamel, dentin, cement and dental pulp within the tooth structure. The dental pulp is vascularized and innervated through the root apex, which provides nociception *via* afferent trigeminal nerves. **(B)** The odontoblast layer is located in the interphase between dentin and dental pulp, with prolongations extending into dentin *via* dentinal tubules. Sensory nerve fibers penetrate the odontoblast layer and enter the initial portion of dentinal tubules, thus permeability or alterations in dentin can trigger nociception.

known as the *neural theory*, states that nerve endings within dentinal tubules are directly able to respond to external stimuli. Nociceptive temperature-sensitive receptors such as TRPV1 and TRPA1 are believed to be involved in pain transduction from hot and cold thermal stimuli (Chung et al., 2013). The second hypothesis or *hydrodynamic theory* proposes that thermal and mechanical stimuli, such as air spraying, can exert pressure changes that cause fluid movement within the dentinal tubules (Andrew and Matthews, 2000; Shibukawa et al., 2015). This movement is believed to trigger A-delta and C fibers, although the presence of specialized mechanoreceptors in these fibers is still debatable. Finally, the *odontoblast transducer theory* states that odontoblast cells themselves are responsible for pain perception. Expression of TRPV channels in odontoblasts as well as their direct excitability support this theory (Won et al., 2018).

Additional to dentinal hypersensitivity, dental pain can also be a consequence of localized inflammation within the dental pulp. This response is at times exacerbated due to the lack of compliance given by the surrounding mineralized tissues, and therefore minor inflammatory changes can result in exaggerated pain perception. Known pro-inflammatory mediators involved in pulpal pain include substance P, calcitonin gene-related peptide, histamine, and cytokines (Caviedes-Bucheli et al., 2008, Caviedes-Bucheli et al., 2011; Sessle, 2011). These molecules are responsible for sensitizing nerve endings as well as increasing intra-pulp pressure by virtue of increasing vascular supply to the dental pulp (Rechenberg et al., 2016). Furthermore, inflammatory mediators released as part of the response system act in the production of vascularized alterations mediated by different receptors such as those from toll-like receptor (TLR) variants 2 and 4 (Nakanishi et al., 2011). It is believed that TLR-2 positive cells are present in the early phases of regulation (including the first 3 h after stimulus), which recognize different pathogen-derived molecules such as triacyl lipopeptides from bacteria and mycobacteria, peptidoglycan, and lipoteichoic acid of gram-positive bacteria and zymosan from fungi (Park et al., 2015; Rechenberg et al., 2016). On the other hand, TLR4 has a central role in the response to co-stimulatory molecules originating from gram-negative bacteria, such as lipopolysaccharides (LPS) (Nakanishi et al., 2011; Park et al., 2015). Considering TLR and the release of pro-inflammatory cytokines like IL-8, IL-6 and chemokines, the succession of stimulatory events can lead to a painful and hyperalgesic process within the dental pulp (ElSalhy et al., 2013). The wide range of factors and stimuli involved leads many to describe the dental pulp as an innervated tissue associated with pain transduction mechanisms that have yet to be fully explained (Mutoh et al., 2007).

Dental Caries and Its Relevance in Dental Pain

There are several known causes responsible for the onset of dental pain including infection, trauma, dental treatment and chemical injury (Alonso-Ezpeleta et al., 2012; Jain et al., 2013; Khan et al., 2019). These situations share the common factor of either exposing dentin or dental pulp to the environment and/or generating an inflammatory process within the dental pulp, initiating dentinal hypersensitivity, and/or inflammatory pain. Nevertheless, in the clinical setting, the most common source of dental pain is due to dental caries.

Dental caries (also known as tooth decay) affects the vast majority of the population and is one of the main causes of tooth loss in patients of all ages (Petersen et al., 2005; Kassebaum et al., 2014; Dye et al., 2015). Worldwide, recent data shows that most adults have been affected by dental caries, and therefore this pathology represents a large economic burden to individuals and healthcare providers. The Global Burden of Disease Study 2013, reporting data on 301 diseases and injuries, concluded that tooth pain resulting from caries affected over 200 million worldwide, and was the fifth commonest acute condition observed overall (Global Burden of Disease Study, 2013; Rice et al., 2016).

Caries is a biofilm-mediated multifactorial infectious disease characterized by the loss of mineral from the tooth surface due to bacterial colonization, which can affect all mineralized tissues in teeth (Pitts et al., 2017). Although caries pathogenesis is highly complex and multifactorial, it is believed to be initiated by species such as *Streptococcus mutans* and *lactobacilli,* which induce surface demineralization by the production of extracellular acids that destroy the mineralized matrix of the tooth (Beighton et al., 2010; Krzyściak et al., 2014; Wassel and Khattab, 2017). The process of caries formation starts on the surface of the outer layers of the tooth, and if not treated it progresses into the underlying dentin layer (Pitts et al., 2017). Caries can also affect the root portion of teeth once this area becomes exposed to the oral environment. This is common in elderly people suffering from gingival recession, and thus these patients are at higher risk of developing root caries lesions (Wierichs and Meyer-Lueckel, 2015). Therefore, dental caries can trigger dental pain in a two-fold manner: by exposing dentin to the environment with subsequent onset of dentinal hypersensitivity, and by generating a localized pulp inflammation in response to bacterial invasion and bacterial molecules (such as bacterial peptides and LPS).

Pain as a consequence of dental caries is a known occurrence in the clinics, which is also supported by many investigations demonstrating the association between caries and pain in children and adults (Reid et al., 2003; Nomura et al., 2005; Bastos et al., 2006). In children, pain generated by caries has also been associated to reduced child weight, growth, and quality of life (Sheiham, 2006). Several studies have provided insight into the mechanisms behind how caries can trigger dental pain within the dental pulp. Firstly, the progressive demineralization generated by caries dissolves the outer layers of the tooth and exposes dental pulp nerve endings to environmental stimuli, triggering dentinal hypersensitivity. However, there is also evidence suggesting bacterial toxins are able to permeate into the dental pulp *via* dentinal tubules and initiate an inflammatory response within odontoblasts and the surrounding tissue (Farges et al., 2015). Durand et al. (2006) showed that lipoteichoic acid (LTA), an important bacterial wall molecule, increased the expression of chemokines in odontoblasts *via* upregulation of TLR 2. Similarly, Farges et al. (2011) observed increase in pro-inflammatory IL-6 production in odontoblasts upon LTA stimulation. Furthermore, cyclooxygenase (COX) has been shown to be associated to tissue inflammation on several levels. In inflamed tissues there

is an increase in the biosynthesis of prostaglandins, which are generated by COX isoenzimes metabolizing arachidonic acid (Ricciotti and FitzGerald, 2011). Also, while COX-1 is constitutively expressed in many tissues, COX-2 is promoted by inflammatory stimuli and is directly involved with inflammatory pain generation (Dubois et al., 1998). Within this context, Petrini et al. (2012) demonstrated an increase of prostaglandin E2 in teeth with reversible dental pulp inflammation compared to normal controls. In addition, the penetration of bacterial cells into the dental pulp may also be an important stimulus for nociception, as Chiu et al. (2013) demonstrated that bacteria can directly activate nociceptors in a mice model. Therefore, it is necessary to remove all caries-infected dental tissue as a previous step before beginning tooth restoration, in order to completely resolve inflammation in the dental pulp. However, in cases of extreme pulpal inflammation or when the caries lesion enters into the pulp chamber, dental pulp necrosis may occur. In these cases, the dental pulp must be completely removed by means of a root canal procedure (pulpectomy) and replaced by thermoplastic material.

Furthermore, Rodd and Boissonade (2000) demonstrated an increase of substance P in carious teeth compared to healthy samples, and its expression was further increased in painful samples compared to asymptomatic teeth. The levels of another neuropeptide, neuropeptide Y, was also found to be elevated in teeth affected by caries compared to controls (El Karim et al., 2006) TRPV-1 expression was also increased in carious teeth compared to controls, and vascular expression of TRPV-1 within the dental pulp was associated to increased dental pain (Morgan et al., 2005). Recently, Hall et al. (2016) demonstrated an upregulation of TNF-α in patients with caries, which was even more pronounced in patients with dental pain.

CURRENT PHARMACOLOGICAL APPROACHES FOR DENTAL PAIN TREATMENT

The therapeutic management of sensitive and painful regions is one of the most relevant aspects in the dental practice due to its direct influence on patient quality of life (Murray et al., 1996). Current management of pain deriving from inflammation utilizes several approaches including local intervention and adjuvant pharmacological treatments (Ward, 1974; Dal Secco et al., 2006). Local interventions, particularly dental restorations, aim to isolate the dental pulp and dentin from environmental stimuli triggering hypersensitivity as well as remove caries lesions to resolve underlying pulpal inflammatory process. On the other hand, pharmacological treatment contributes to the promotion of analgesia, with frequently used drugs being nonsteroidal anti-inflammatories (NSAIDs), opioids and NMDA receptor blockers (Chou and Huffman, 2007). Considering that the origin of pulpal pain can occur at different points during treatment (i.e. preoperative, perioperative, and postoperative), the drug strategy must be chosen according to the individual conditions of each clinical case (Primosch et al., 1993; Vanegas et al., 2010). For example, analgesic drug treatment can begin before intervention (known as pre-emptive analgesia) with the aim of inhibiting the inflammatory process prior to dental restoration in asymptomatic patients (Ong et al., 2005). As several investigations have discussed conventional pharmacological management of dental pain in the past (Hargreaves and Abbott, 2005; Becker, 2010; Moore and Hersh, 2014; Berlin et al., 2018), this review will only provide a brief summary of current treatment options utilized in clinics.

Currently, the first line of drugs for the treatment of dental-derived pain are acetaminophen and NSAIDs (Moore et al., 2018). Both have been shown to be essential in the management of minor to moderate post-operative pain in dentistry (Bailey et al., 2013) and proven to be safe and effective, having them as the most favored options among treatments available in the market (Ong et al., 2005). NSAIDs have been demonstrated to inhibit the action of COX-1 and COX 2, thus are important in controlling inflammatory pain in a wide range of tissues (Brune and Patrignani, 2015). On the other hand, the exact mechanism of action for acetaminophen in humans remains unclear, although some authors believe it has an effect on a splice variant of COX-1 (previously believed to be the COX-3 isoenzyme) (Graham and Scott, 2005; Bertolini et al., 2006; Sharma and Mehta, 2013). In conjunction with opioids, acetaminophen and NSAIDs such as ibuprofen have been demonstrated to alleviate moderate to severe postoperative pain (Ashley et al., 2016) as well as acute dental pain (Chang et al., 2001; Bailey et al., 2013). Pain treatment of vulnerable patient groups such as elderly or patients with gastrointestinal issues is challenging, however there is supportive evidence for the use of acetaminophen alone or in combination with codeine (Ong et al., 2007; Ganzberg, 2018). Studies show that associating NSAIDs with opioids may have the additional benefit of controlling post-operative pain (**Table 1**), however, selective COX-2 inhibitors have been proven to be more effective (Chang et al., 2001; Korn et al., 2004). Additionally, special considerations should be taken to reduce opioid overprescribing and abuse, especially with young patients and patients that can be managed solely with NSAIDs (Noble et al., 2010).

Multimodal drug therapy is achieved by combining drugs with complementary mechanisms of action with the aim of reducing postoperative pain (Brooks et al., 2017; Matute Crespo and Montero Matamala, 2017). When treating moderate to severe pain, combination pharmacotherapy may be an effective alternative to treat pain and improve patient recovery times (Ganda, 2008). Originally, multimodal analgesia was advocated for use in ambulatory anesthesia combining NSAIDs and opioid analgesics, with or without anesthetic infiltration (Devin and McGirt, 2015). Combining oral or IV acetaminophen with selective or non-selective cyclooxygenase-2 inhibitors (COXIBs) has also demonstrated to be a safe option for pain treatment (Ong et al., 2007). These drugs can be administered *via* different routes, however special considerations must be taken into account when treating high-risk patient groups such as the elderly (Becker, 2010), as there are still conflicting reports in the literature regarding their safety and tolerability in these patients (Ganda, 2008). Overall, dental practitioners should make clinical decisions based on optimal described dosages, with non-opioid drugs as the primary treatment option (Becker, 2010).

TABLE 1 | Pharmacological treatment possibilities to control post-operative pain in dentistry with opioids alone and in different combinations.

		Authors*	Study design	Sample size	Pharmacological treatment groups	Outcome instrument	Postoperative measurement	Postoperative assessment of pain	Study conclusions
Opioid alone	**Tramadol**	(Mehrvarzfar et al., 2012)	Randomized clinical trial, double-blind and placebo-controlled	100	Placebo Tramadol 100 mg Acetaminophen 325 mg +Ibuprofen 200 mg+ Caffeine 40 mg (Novafen) Naproxen 500 mg	10-point VAS	Placebo 3.2 (2.6–3.9) Tramadol 2.2 (1.2–3.1) Novafen 0.4 (0.1–0.8) Naproxen 0.7 (0.3–1.1)	24 h	A single oral dose of Naproxen, Novafen and Tramadol taken immediately after dental treatment reduced postoperative pain following pulpectomy.
	Codeine	(Sunshine et al., 1983)	Randomized clinical trial, double-blind and placebo-controlled	120	Placebo Propiram Fumarate 50 mg Codeine Sulfate 60 mg	4-point rate scale none = 0; mild = 1; moderate = 2, severe = 3	Placebo 1.27 (0.25) Propiram Fumarate 2.11 (0.22) Codeine 1.72 (0.23)	6 h	Propiram fumarate 50 mg is an effective oral analgesic similar to codeine sulfate 60 mg, with the possibility of a longer effect.
Opioid combination	**Tramadol/ Acetaminophen**	(Edwards et al., 2002)	Systematic- review with meta-analysis	1376	Acetaminophen 650 mg Ibuprofen 400 mg Tramadol 75 mg Tramadol 75mg/ acetaminophen 650 mg	NNT (95% CI) PGE**	4.5 (3.6–6.1) 2.7 (2.3–3.3) 11 (6.9–26) 3.0 (2.5–3.7)	8 h	Overall, this meta-analysis demonstrated analgesic superiority of the combination drug over its components, without additional toxicity.
	Codeine/ Acetaminophen	(Chang et al., 2001)	Randomized clinical trial, double-blind and placebo-active controlled	393	Placebo (1:6:6, respectively) Rofecoxib 50 mg Codeine 60 mg/ Acetaminophen 600 mg	TOPAR6***	Placebo 3.4 (1.0–5.8) Rofecoxib 12.4 (11.3–13.4) Codeine/ Acetaminophen 7.0 (5.9/8.0)	6 h	In this study of moderate to severe postoperative dental pain, the analgesic efficacy of Rofecoxib 50 mg was greater than that of codeine/ acetaminophen, with a lower incidence of adverse events and nausea.
	Oxycodone/ Acetaminophen	(Korn et al., 2004)	Randomized clinical trial, double-blind and placebo-active controlled	212	Placebo (1:3:3, respectively) Rofecoxib 50 mg Oxycodone 5mg/ Acetaminophen 325 mg	GLOBAL24#	Placebo 0.3 (0.2) Rofecoxib 2.1 (0.2) Oxycodone/ Acetaminophen 1.3 (0.2)	24 h	The superior efficacy of Rofecoxib 50 mg compared to oxycodone/acetaminophen 5/325 mg support the use of Rofecoxib for the treatment of acute post-surgical pain.

**All studies included in this summarized tables were checked for GRADE criteria; **PGE- Patient Global Evidence; ***TOPAR6- pain relief over 6 h; #GLOBAL24 - Global assessment of treatment at 24 h.*

Nevertheless, in the case of persistent acute pain, short-acting opioid drugs may be an interesting alternative for treating this group of patients (Becker and Phero, 2005).

Despite the widespread use of acetaminophen, NSAIDs and opioids, and the benefits they provide for dental pain management, it is important to address several limitations of these drugs. Drug selection criteria is directly related to patient treatment needs and potential risk factors (such as cardiovascular disease), as there is a high number of potential interactions between commonly used NSAIDs and other medications (Ganzberg, 2018). As a general recommendation, patients must be evaluated for safety and possible adverse effects before taking NSAID treatment into consideration, especially in high-risk groups such as medically compromised patients (Wongrakpanich et al., 2018). A number of side effects for NSAIDs and opioids have been reported, such as gastrointestinal problems, nausea, and constipation (Benyamin et al., 2008; Nagi et al., 2015; Ganzberg, 2018). Furthermore, dependence to some of these drugs is currently a critical issue for public health in the US and worldwide, particularly opioid addiction due to misuse and excessive prescription (Nack et al., 2017; Jones et al., 2018). Therefore, several innovative approaches are currently being pursued as alternatives to conventional pharmacological pain management therapy in dentistry, including novel drug targets and regenerative and non-invasive medical approaches.

FUTURE TRENDS AND NOVEL INSIGHTS INTO THE PHARMACOLOGICAL TREATMENT OF PAIN IN DENTISTRY: UNVEILING TRPV1 AS A DRUG TARGET

As previously stated, dental pulp pain has its origin in the stimulation of the nerve fibers acting as a complex defense mechanism against external factors (Magloire et al., 2010; Solé-Magdalena et al., 2018). When dental pulp suffers an injury, the nociceptive neurons initiate and increase a process known as neurogenic inflammation (Chung et al., 2013; Mizumura and Murase, 2015). Within this context, transient receptor potential (TRP) proteins are known to play an important role in dental nociception. TRP proteins are a large family of cation-permeable ion channels (Latorre et al., 2007; Nilius and Owsianik, 2010) sensitive to electrical, chemical, mechanical, and thermal stimuli, and many of them act as cell receptors involved in environmental detection (Morales-Lázaro et al., 2013). Current research links TRP proteins to hereditary neuropathies, neuronal disorders, and other TRP channel-associated channelopathies (Rosenbaum and Simon, 2007). The group of temperature-activated TRP channels (thermoTRPs) is composed of different sub-families (i.e. vanilloid, melastatin, ankiryn, and canonical) which are important for the detection and integration of peripheral sensory input (Caterina, 2007). Therefore, the understanding of how certain ligands modulate close-open configurations of thermoTRP channels could significantly facilitate the pharmaceutical design and elaboration of TRP drug modulators (Rosenbaum and Simon, 2007; Steinberg et al., 2014; Yang and Zheng, 2017).

The discovery of TRPV1 channels and their role in the signaling process and temperature-mediated nociception has enabled progress in strategies for managing and treating pain (Caterina et al., 1997; Rosenbaum and Simon, 2007; Julius, 2013). TRPV 1-4 thermal detectors are expressed in sensory nerves, transducing both proprioceptive and nociceptive information and providing information about environmental as well as body temperature to the central nervous system (Baez et al., 2014). Agonist-induced activation of TRPV1 channels has been critical to their identification and functional description (Matta and Ahern, 2007; Gao et al., 2016). At the molecular level, the canonical agonist capsaicin binds to the channel with high affinity (< 0.7 interaction score) and enables discrimination of TRPV1 from other vanilloid subtype channels (Yang and Zheng, 2017). Several vanilloid-related compounds are also able to induce transition to the open state with high affinity; interestingly, most of them are compounds of natural origin or minor derivatives of the natural chemical structure (Norman et al., 2007; Cui et al., 2016). Moreover, the gating mechanism in TRP channels as well as traffic to the plasma membrane is strongly regulated by phosphoinositides and their sub-products [diacylglycerol (DAG), inositol triphosphate (IP3)], polyunsaturated fatty acids (PUFAs) as well as metabolites generated by COX, LOX and CYP enzymes (Rosenbaum and Simon, 2007). To date, many compounds capable of inhibiting TRPV1 have been discovered such as resiniferatoxin (agonist), GRC6211 (antagonist), and QX-314 (TRPV1 permeable Na+ channel blocker); however, none of them is available yet for clinical therapeutics (Meotti et al., 2014). As allosteric control by lipid binding adds pharmacological properties to TRPV1, here the intention is to discuss the modulation of TRPV1 cellular activity by antagonists in the context of the pharmacological basis of oral pain sensation caused by inflammatory conditions (Steinberg et al., 2014).

The study and development of composites capable of acting on TRPV1 receptors have evolved greatly over time and capsaicin has been identified as the selective agonist ligand (Cheung et al., 2008; Gregorio-Teruel et al., 2014). The mechanism through which capsaicin exerts its function is known as tachyphylaxis, a rapid desensitization phenomenon associated to pore opening of cation channels permeable to sodium and potassium (Gavva et al., 2004; Ohbuchi et al., 2016). It is dependent on the exposure of the ligand to the channel, i.e., that the influx of Ca2+ ions has a protective feedback mechanism that presents a reduced response to repeated exposure (Brauchi and Orio, 2011; Yang and Zheng, 2017). The reversible effect of channel desensitization was also observed in situations of overdose and epidermal degeneration of nerve fibers (Rosenbaum and Simon, 2007; Cheung et al., 2008).

In clinics, capsaicin-derived formulations to treat severe and chronic pain are available in a drug delivery system known as transdermal patches (Carnevale and Rohacs, 2016). Formulations with a stable release of 8% capsaicin (80 mg per gram of adhesive) as a dermal patch have been approved for use on neuropathic pain in the US and Europe, and can be used at multiple sites according to patient needs (Trevisani and Szallasi, 2010). Randomized clinical trials in diseases like diabetes, traumatic tissue injuries, herpes zoster infections, and cancer among others, have proven

the clinical safety and efficacy of the formulation in terms of improving patient quality of life (Kulkantrakorn et al., 2013).

Capsaicin has also been tested in association with other drugs such as local anesthetics (Gerner et al., 2008). Among these is the quaternary lidocaine derivate QX-314, which displays the therapeutic advantage of prolonging the anesthetic effect 10-times when compared to lidocaine hydrochloride (Nakagawa and Hiura, 2013). Ries et al. (2009) utilized capsaicin as a V1 agonist, enabling QX-314 to reach its intracellular binding site in the sodium channel. This scenario suggests that QX-314 in the presence of capsaicin can produce selective blocking mediated by TRPV1 (Binshtok et al., 2007). This pharmacological association was tested *in vivo* for an inferior alveolar nerve block, where a selective, long-lasting effect on sensory perception was noted without affecting motor areas (Lim et al., 2007). The above-described selective and long-lasting activity could be ideal in future formulations for the treatment of odontalgias caused by inflammatory processes, as well as in painful episodes caused by temporomandibular joint disorders (Kim et al., 2010a). Also, it demonstrates the potential of capsaicin and vanilloid-1 derivatives in the clinical management of pain associated with frequent episodes of pulpal inflammation in dentistry (Hossain et al., 2019). Due to the strong involvement of TRPV1 in the transmission of pain processes, structure-activity studies allowed for modifications in the structure of capsaicin and the development of analogous compounds in the attempt to eliminate the undesired irritation effect and pungency (Baskaran et al., 2018).

In this context, numerous specific TRPV1 antagonists have been developed with the aim of inhibiting nociceptive sensitization and the resulting transduction of the pain signaling process (Norman et al., 2007). Capsazepine was described as the first competitive antagonist of the channel, but its poorly selective binding capacity made it fail in clinical trials (Bevan et al., 1992). In models applied to the treatment of dental pain, examples of clinical records of compounds and their respective laboratories include AMG 517 (Amgen), AZD1386 (AstraZeneza), MK2295 (Merck/Neurogen) and SB705498 (GSK) (Trevisani and Szallasi, 2010). The clinical trial coordinated for SB705498 described it primarily as a powerful *in vitro* TRPV1 antagonist with the ability to reverse inflammation and pain *in vivo* (Gunthorpe et al., 2007). The controlled clinical trial was a multicenter (Korea, Italy, and UK), single-blind and placebo randomized study with a total of 145 patients, and the evaluated outcome corresponded to postoperative pain during third molar extraction surgery (Gunthorpe et al., 2007; De Petrocellis and Moriello, 2013). The experimental groups consisted of the treatments: SB705498 (400 mg and 1,000 mg), placebo and co-codamol (2 capsules of 500 mg paracetamol, 12.8 mg phosphatized codeine and 2 placebo capsules) (Cairns, 2009). In January 2019, the phase II results concluded in 2008 were published and no serious adverse effects were found; however, reported effects of SB705498 included headaches (n = 5) and heat sensation (n = 2) for the highest dose of 1,000 mg (Gunthorpe et al., 2007). The pharmaceutical industry has made a concerted effort to generate potent and selective compounds for TRPV1, in particular due to its attractive mechanism of action, which differs from the nonsteroidal anti-inflammatories, and also in the attempt to find a drug with a wide therapeutic window (Cheung et al., 2008; Trevisani and Szallasi, 2010).

NOVEL APPROACHES FOR DENTAL PAIN TREATMENT AND BEYOND: REGENERATIVE MEDICINE AND OTHERS

Regenerative medicine, and more specifically cell and tissue engineering approaches, have become increasingly popular in dental research over the last years. The key concept underlying these approaches is to develop a causative treatment aiming for long-term regeneration rather than immediate pain control. Due to its complex structure, regeneration of dentin and dental pulp has been proven a difficult and versatile task, which can be firstly categorized according to the primary clinical problem tackled (antibacterial treatment or pulp restoration) and subsequently into the following strategies: a) bio(active)materials, b) stem cells and cell-based approaches, c) exosomes, and d) physical stimuli, as well as combinations of the above approaches (**Figure 2**).

Bioactive Materials

The use of active materials to control inflammation, infection and pain has been described since ancient times. Ancient Egyptians utilized pastes of ochre, honey, and willow extract (containing salicin) to treat loosening teeth as well as dental pain (Leek, 1967; Forshaw, 2009). The activity attributed to the materials used is mostly antibacterial, with salicin also displaying anti-inflammatory properties. Utilizing bioactive materials is a strategy pursued until today, currently aiming to ensure bio- and cyto-compatibility as well as reliable mechanic properties. Bioactive materials extensively used for pulp capping have been *calcium hydroxide* (causing mineralization by reduction of pyrophosphate) (Farhad and Mohammadi, 2005), *mineral trioxide aggregate* (MTA) (Torabinejad and Chivian, 1999) (a Portland cement-based substrate stimulating proliferation, migration, and differentiation of dental pulp stem cells into odontoblast-like cells to produce a collagen matrix) (Parirokh and Torabinejad, 2010; Paranjpe et al., 2011) and *biodentine* (a tricalcium-silicate based susbtrate with similar properties as mineral trioxide aggregate in terms of dental pulp stem cell differentiation) (Luo et al., 2014; Malkondu et al., 2014). Newer materials based on bioglass derivates are aiming to improve overall results of pulp capping, however, so far have only demonstrated decreased setting times and increased compressive strength as main favourable characteristics (Long et al., 2018; Hanada et al., 2019). Addressing the issue of biofilm formation, Yang et al. added the antimicrobial quaternary ammonium salt monomer 2-methacryloxylethyl dodecyl methyl ammonium bromide to Portland cement, and could demonstrate a *Streptococcus mutans*-inhibiting effect for up to 6 months (Yang et al., 2014). Kwon et al. (2019) used 2-methacryloyloxyethyl phosphorylcholine in combination with mineral trioxide aggregate and found a two-fold effect: on the one hand the composite demonstrated protein-repellent properties and prevented adhesion of *Enterococcus*

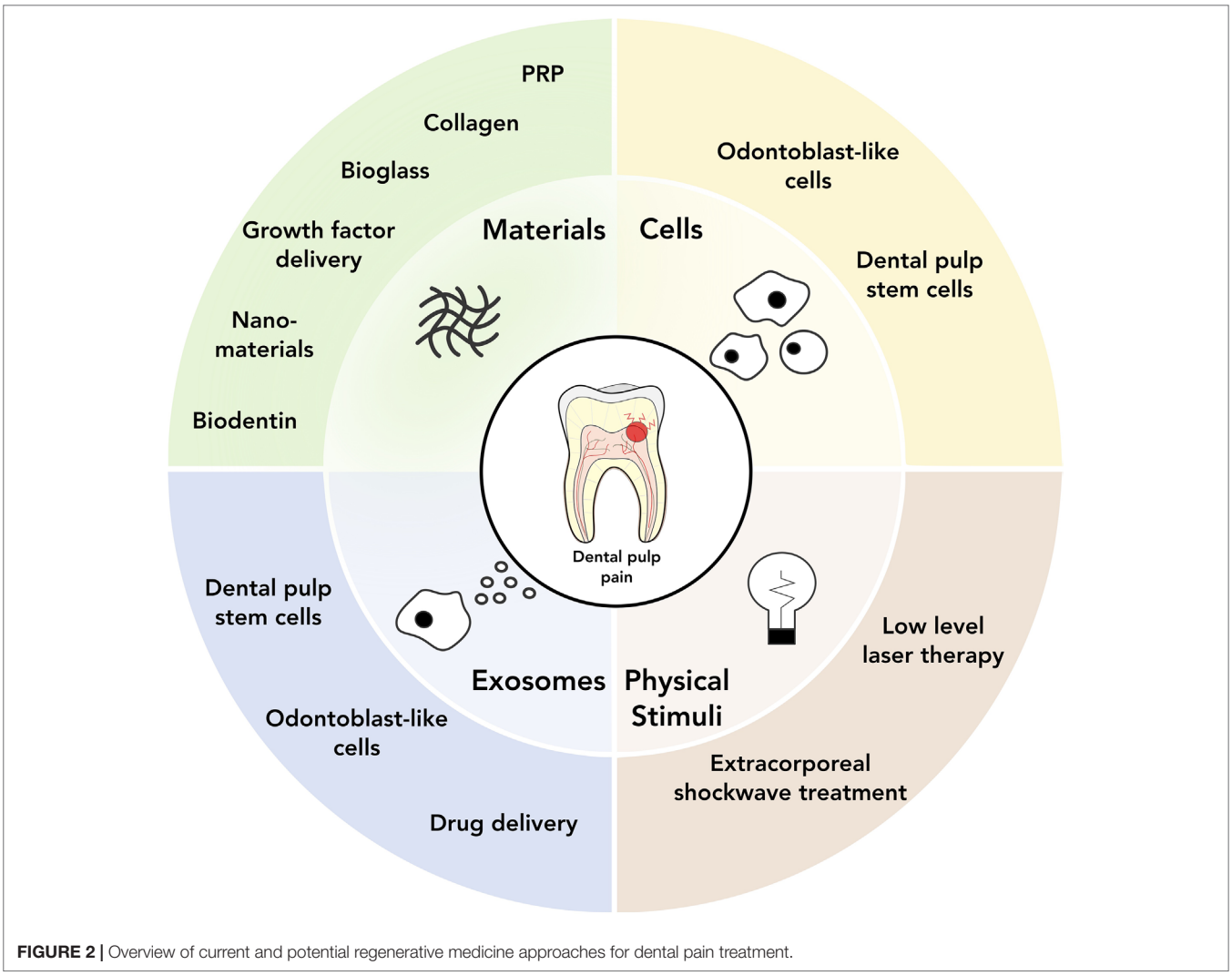

FIGURE 2 | Overview of current and potential regenerative medicine approaches for dental pain treatment.

faecalis, and on the other hand increased calcium ion deposition on the surface compared to mineral trioxide aggregate alone.

With recent advances in nanoscale manufacturing, an increased number of approaches have utilized the opportunities given by nano-structured materials to effectively deliver drugs into the dental pulp. Cuppini et al. (2019) developed a tricalcium-phosphate based paste containing amoxicillin microspheres, calcium tungstate and indomethacin nanocapsules to deliver antimicrobial and anti-inflammatory compounds to the defect site. Zhu et al. (2017) designed calcium silicate nanoparticles in combination with silver and zinc as a nano-disinfectant for dentin tubules and root canals. However, Ji et al. (2018) pointed out a limitation of this approach as insufficient amounts of nanoparticles are transported reliably through dentinal tubules; thus, they designed magnetic nanoparticles for directed transport through the dental pulp. Iron nanoparticles coated with prednisolone were applied onto the dental pulp and directed through dentinal tubules using external magnets, and authors hypothesized that this approach can serve to transport medications to reduce dental pulp inflammation, as well as enhance bond strength of composite resin to dentin (Ji et al., 2018).

Another potential way of controlling pain related to dentinal hypersensitivity is to develop materials that promote dentinal regeneration. As type-I collagen is the most abundant structural protein in the extracellular matrix, collagen-derived scaffolds have been of interest to promote homing and differentiation of cells for dental pulp regenerative purposes (Prescott et al., 2008). To induce reparative dentinogenesis, Rutherford et al. (1993) utilized osteogenic protein 1 and bone morphogenic factor 7 in a collagen matrix, as a chemo-attractive layer on dental pulp sealed with temporary dental cement. In the case of osteogenic protein 1, a higher amount of dentin deposition was observed while bone morphogenic factor 7 did not induce reparative dentinogenesis (Rutherford and Gu, 2000). Using a similar approach involving a combination of growth factors (bFGF, VEGF, or PDGF with a basal set of NGF and BMP7), Kim et al. (2010b) highlighted a beneficial effect of applying growth factor cocktails to stimulate cell homing and subsequent expression of van Willebrand factor, dentin sialoprotein, and NGF. Also, Rosa et al. (2013) found that

an injectable type I collagen scaffold in combination with stem cells from human exfoliated deciduous teeth (SHED) was able to express odontoblastic differentiation markers when implanted into root canals. The resulting pulp-like tissue presented similar vascularization and cellularity compared to control dental pulps, and formation of new dentin was observed throughout the root. Furthermore, Jiang et al. (2017) induced root canal regeneration of immature teeth by using a resorbable collagen membrane paired with MTA, and observed complete resolution of signs and symptoms in all patients. However, no statistically significant improvement in regeneration was observed compared to the MTA-only control group. Besides collagen, other materials have also been of interest for promoting pulp regeneration, such as platelet rich derivates such as platelet rich plasma (PRP) or platelet rich fibrin (PRF). These materials are known for their richness in growth factors, which makes them a popular biomaterial in several areas of regenerative medicine (De Pascale et al., 2015). Regarding dental pulp regeneration, several groups have utilized the strategy of autologous PRP/PRF with varying results. While Torabinejad et al. (2015) and Rodríguez-Benítez et al. (2015) reported improved rates of bone formation and re-vascularization, Bezgin et al. (2015) found no advantages in using PRP for pulpal repair. Overall, further research is necessary in order to clarify the potential effectiveness of PRP and PRF for dental pulp regeneration.

It is important to note that these material-based approaches rely mainly on the regenerative capacity of the dental pulp, augmenting the formation of new dentin by stimulating tissue-resident dental pulp stem cells and controlling inflammation as well as infection. In aging teeth however, dentinal regeneration with material-based approaches has significantly lower success rates (Lipski et al., 2018), creating a demand for combined cell-material approaches.

Cell-Based Approaches

The dental pulp is a tissue rich in vasculature and different cell types such as fibroblasts, dental pulp stem cells (DPSC), and odontoblasts. The latter are capable of forming dentin by production of collagenous and non-collagenous mineralizing proteins (known as secondary dentin). Furthermore, the odontoblast layer is located at the interface between dental pulp and dentin, protruding their processes into the dentinal tubules (**Figure 1B**). The dental pulp is crucial for tooth homeostasis and presents stimulus-dependent strategies for self-repair known as reactive dentinogenesis, where stimuli such as dental caries can induce odontoblasts to deposit tertiary dentin (Smith et al., 1995). Reparative dentinogenesis involves the dental pulp and its cellular components in response to a severe insult. When the odontoblast layer is disrupted, DPSC migrate into the site of injury and differentiate into odontoblast-like cells, forming new but irregular and less tubular dentin (Mitsiadis and Rahiotis, 2004; Tziafas, 2010). The presence of DPSC therefore is crucial for reparative dentinogenesis to occur. However, with age the dentin layer becomes thicker and the pulp chamber decreases in size, limiting the amount of DPSC available for regeneration. Furthermore, the resident DPSC are subjected to senescence through the p16INK4a/Rb pathway, driving the otherwise highly proliferative cells into cell cycle arrest (Feng et al., 2014). Hence, the main goals in pulpal cell therapy are to deliver DPSC to the damaged, resected or retracted pulp chamber, and/or to transplant odontoblasts to obtain dentin restoration.

DPSC display common features to mesenchymal stem cells such as ability to differentiate into several mesenchymal lineages, as well as a low immunogenicity. The latter makes them suitable for allogeneic stem cell therapies (Pierdomenico et al., 2005). Several studies speculate whether odontoblast-like cells differentiated from DPSC display the same characteristics as native odontoblasts (Shi et al., 2005; Huang et al., 2009). In the early 2000s, proof-of-concept studies demonstrated a high potential of dental-derived stem cells to differentiate into a functional pulp-like complex, using hydroxyapatite in ectopic rat models (Gronthos et al., 2002; Miura et al., 2003). Interestingly, in a similar model using 3D printed hydroxyapatite and DPSC or apical papilla stem cells, Hilkens et al. (2017) could not find significant differences between the stem cell- and cell free-groups in terms of angiogenesis. However, it was shown by Huang et al. (2010) that apical papilla stem cells and DPSC are capable of producing pulp-like tissue *de novo*, differentiating into odontoblast-like cells producing dentin-like tissue on existing dentinal walls.

One of the key questions in cell therapy is the route of delivery through which cells are administered to the site of interest, with approaches ranging from free cell transplantation to scaffold-free cell sheets and natural or synthetic scaffolds. Collagen and atelocollagen served as scaffolds to deliver mesenchymal stem cells in several studies (Iohara et al., 2011; Iohara et al., 2013; Hayashi et al., 2015), improving the formation of pulp-like tissue and secondary dentin in dog models (Iohara et al., 2011; Iohara et al., 2013). In a pilot clinical study, functional dentin formation was observed with no adverse effects (Nakashima et al., 2017). Interestingly, DPSC transplantation with platelet-rich fibrin did not show superior results compared to controls and was found to produce mainly periodontal tissue and not pulp (Hausner et al., 2007). Chitosan-hydrogel scaffolds seeded with DPSC in combination with growth factors formed pulp-like tissue and a layer of regenerative dentin in a necrotic-tooth dog model (El Ashiry et al., 2018). Decellularized swine dental pulp seeded with DPSC was found to induce the formation of pulp-like tissue and a layer of odontoblast-like cells in a subcutaneous mouse model (Hu et al., 2017). Also, Zhang et al. (2017) analysed decellularized tooth bud scaffolds seeded with porcine dental epithelial cells, human dental pulp cells, and human umbilical vein endothelial cells in combination with BMP-2, and discovered formation of organized dentin in a mini-pig model. Furthermore, in a scaffold-free approach, Itoh et al. (2018) designed a dual-celltype sheet containing undifferentiated DPSCs and differentiated odontoblast-like cells, reporting pulp regeneration in an ectopic mouse model. Xuan et al. (2018) demonstrated in a minipig–pulpectomy-model that pelleted DPSC are capable of regenerating whole pulp tissue, including the odontoblast layer. In a subsequent clinical trial, they observed similar effects in patients and furthermore sensory nerve regeneration.

Exosome Therapies

One of the main recurrent issues in cell therapy is promoting the survival of transplanted cells in the recipient tissue over time. Factors like mechanical and nutritional stress, hypoxia, or detachment from the extracellular matrix as well as immune responses limit cell survival during and after the transplantation process. Many attempts have been made to increase cell homing and design long-term active cells therapies including biomaterial- or growth factor co-administration, reactive oxygen species protected hydrogels or preconditioning of the cells, among others (reviewed by Baldari et al., 2017). Within this context, exosomes have been proposed as an interesting alternative to cell transplantation and have gained popularity over the last decade, avoiding the challenge of cellular homing. Exosomes were first described in mammalian cell culture in 1981 as the cargo of microvesicles being shed from cells (Trams et al., 1981). They were believed to be a cellular "waste" system, mainly involved in the removal of obsolete molecules from the cell and cell wall (Pan and Johnstone, 1983). Due to key findings such as their role in expression of antigens (Raposo, 1996) and ability to transfer mRNA/miRNA (Valadi et al., 2007), they are now established as one of the main factors in inter-cellular communication. By definition, exosomes are vesicles between 30 and 150 nm in size, and their cell surface markers and cargo can be associated to the phenotype, metabolic status, and biological role of their cell of origin (Ratajczak et al., 2006; Valadi et al., 2007; Alcayaga-Miranda, 2016).

Exosomes have been harvested from several types mesenchymal stem cells and have demonstrated immune-modulatory and pro-angiogenic properties, amongst others (Liang et al., 2016; Cosenza et al., 2018). Within the analysed sources, DPSC have been demonstrated to produce exosomes with the capacity of regulating acute inflammation by suppressing activities of cathepsin B and matrix metalloproteinases in a carrageenan-induced inflammation model (Pivoraitė et al., 2015). As mentioned above, exosomes are a tool for cellular communication, representing the cell's current state. Huang et al. (2016) utilized this characteristic and hypothesized that cell-type specific exosomes can trigger lineage-specific differentiation of stem cells. They differentiated DPSCs into odontoblast-like cells to subsequently isolate the exosomes and could verify a superior odontoblast differentiation *in vitro* as well as regeneration of pulp-like tissue in an *in vivo* tooth slice model. Hu et al. (2019) confirmed these findings and analysed underlying mechanisms, finding an activation of the TGFβ1/smads signalling pathway *via* transfer of microRNAs.

Aside from active native cargo, exosomes have shown to be promising system for bio-inspired and targeted drug delivery (reviewed by Zhang et al., 2019). Despite a lack of studies reporting the use of drug-loaded exosomes for the treatment of dental pain, there are several likely possibilities originating from experiences in other tissues. One potential avenue could be the local delivery of anti-inflammatory drugs into the pulp, as curcumin-loaded stem cell or macrophage exosomes have shown to display anti-inflammatory properties (Sun et al., 2010; Kalani et al., 2016). Also, delivery of liposome-encapsulated superoxide dismutase and catalase has demonstrated to locally suppress periodontal inflammation in a dog model (Petelin et al., 2000). Alternative approaches, originating from advances in nano-engineering, have demonstrated that exosomes can also be directed to specific tissues, making them an attractive option for targeted therapy (Gomari et al., 2018; Tian et al., 2018). Furthermore, several groups have designed artificial ion channels using DNA origami (reviewed by Shen et al., 2014). These channels could potentially resemble the biologic function of channels (i.e. TRP channel) and could be inserted as "mock-channels" into cell membranes. Overall, exosomes appear to be a promising alternative to cell therapy for dental pulp pain treatment; however, their efficacy relies strongly on recipient cells, which could be an issue in cases where the dental pulp is necrotic or a pulpectomy has been performed.

Physical Therapies

Aside from pharmacological pain treatment or causative tissue engineering approaches such as biomaterials and cell-based therapies, physical therapies such as photo-biomodulation or shockwave treatment are an upcoming field in dentistry. Some studies have tried to modulate pain and inflammation with these approaches, including treatment of dental pain.

Low level laser therapy (LLLT) was invented in the 1960s, and in an attempt to identify cancer risks of laser it was found to induce hair growth in mice (Mester et al., 1968). It utilizes wavelengths between 600 nm and 1,000 nm and has been found to trigger many effects at the cellular and tissue levels. For example, cytochrome C oxidase absorbs near-infrared light, triggering downstream events such as changes in ATP, reactive oxygen species and nitric oxide (reviewed by Farivar et al., 2014). Regarding dental pain management, LLLT has been reported to reduce pain in several situations such as postoperatively after root canal retreatment (Arslan et al., 2017) or in cases of dentinal hypersensitivity (Gerschman et al., 1994; Orhan et al., 2011). However, several studies also demonstrate a regenerative effect of LLLT. In an *in vitro* tooth-slice model, LLLT increased odontogenic and angiogenic gene expression (El Nawam et al., 2019). Kim et al. (2018) also reported increased dentinogenic differentiation of DPSC *in vitro* using pulsing LLLT, proposing high production of reactive oxygen species and activation of the TGF-β1 signalling pathway as potential mechanisms. In rat models it was shown that LLLT increased the density of odontoblasts and induced formation of more regular dentin after mechanical pulp damage (de Santana et al., 2017) and furthermore, stimulated cell proliferation as well as dentin formation after pulpal apoptosis (Shigetani et al., 2011). These results suggest LLLT as a promising non-invasive approach for dental pain management in diverse clinical situations, although further studies are needed to confirm its clinical reproducibility.

Extracorporeal shockwave treatment (ESWT) has demonstrated beneficial effects in several areas of regenerative medicine [e.g. bone regeneration (Schaden et al., 2001) or ischemia-induced tissue necrosis (Mittermayr et al., 2011)]. Shockwaves are sonic pulses characterized by an initial rise in pressure, reaching a positive peak of up to 100 MPa within 10 ns, followed by a negative amplitude of up to 10 MPa and a total life cycle of less than 10 μs (Ogden et al., 2001). The underlying effect on cells and tissues has been attributed to increased ATP secretion and subsequent activation of the extracellular-signal-regulated kinase pathway (ERK) (Weihs et al., 2014). For DPSC it has been demonstrated

that extracellular ATP activates P2 receptors and downstream signaling events that induce odontogenic differentiation, with ESWT suggested as one of the triggering factors (Wang et al., 2016). Furthermore, it has been shown that ESWT increases efficacy of desensitizing agents for dentine hypersensitivity (Datey et al., 2016). Despite these promising initial studies, there remains a lack of animal and clinical studies associating ESWT to dental pain control, and future research is needed to strengthen these initial observations.

CONCLUSIONS AND FUTURE PERSPECTIVES

Although significant improvements have been made in dental care, dental pain remains a frequent source for patient poor quality of life. Current treatment is mainly centered around a combination of the pharmacological management of symptoms and restorative treatment, nonetheless drugs such as NSAIDs or opioids can potentially present significant side effects and addiction in limited patients. Thus, there are many novel approaches for dental pain management being explored in hopes of improving treatment outcomes in the long-term. Approaches such as TRPV1-targeting drugs have shown promising results so far, although further clinical research is needed in order to demonstrate their efficacy in dental pain management. Furthermore, causative treatment approaches originating from regenerative medicine have the potential to significantly improve the resolution of dental pain. Cell-based and exosome therapies are already being used in other fields, and introduction into clinics could provide long-term solutions for the modulation of local pulp inflammation and nociception. Material-based therapies that promote tooth remineralization have been used in the past, and current advances improving bioactivity and antibacterial effect of materials could provide clinicians with novel approaches for the treatment of dental caries and subsequent dental pain.

Interestingly, physical therapies such as LLLT and ESWT have been widely used for the treatment of inflammation and pain in a range of tissues in humans (Cotler et al., 2015; Lee et al., 2017; Moya et al., 2018). One of the main advantages of these approaches is their non-invasiveness, generating a biological effect in deep tissues without the need of surgery of restorative treatment. Initial studies regarding use of LLLT and ESWT for dentinal hypersensitivity showed promising results (Gerschman et al., 1994; Datey et al., 2016), as well as the use of ESWT for controlling inflammation in other areas of the mouth. However, there is still a lack of clarity regarding the biological mechanism of ESWT in tissues. Further studies elucidating the mechanisms underlying ESWT as well as effectiveness to resolve dental pulp inflammation and pain are necessary.

As discussed throughout this review, teeth are highly specialized organs with a quite particular nociception mechanism. Nerve fibers within the dental pulp are triggered either by environmental factors (dentinal hypersensitivity) or by the release of pro-inflammatory and bacterial molecules. Thus, the ultimate goal of any therapy should be to reduce local inflammation while restoring protection to dentin and the dental pulp, in order to provide causative treatment and long-term success to patients. Current research should therefore focus on developing novel and causative treatments against dental pain, with limited adverse effects and clinically reproducible results.

AUTHOR CONTRIBUTIONS

CS and BB contributed equally to this manuscript. CS, BB and SA participated in the conception of the review. SA drafted the initial full manuscript. CS, BB and SA wrote and edited the manuscript.

FUNDING

This work was sponsored by Fondo Nacional de Desarrollo Científico y Tecnológico (FONDECYT) grant #11180101. CS is supported by FONDECYT grant #11180406. BB is supported by FONDECYT grant #3170518. SA is supported by FONDECYT grant #11180101. MiNICAD is supported by Iniciativa Científica Milenio, Ministry of Economy, Development and Tourism, Chile.

REFERENCES

Alcayaga-Miranda, F., Varas-Godoy, M., and Khoury, M. (2016). Harnessing the Angiogenic potential of stem cell-derived exosomes for vascular regeneration. *Stem Cells Int.* 2016, 3409169. doi: 10.1155/2016/3409169

Alonso-Ezpeleta, L. O., Gasco-Garcia, C., Castellanos-Cosano, L., Martín-González, J., López-Frías, F. J., and Segura-Egea, J. J. (2012). Postoperative pain after one-visit root-canal treatment on teeth with vital pulps: comparison of three different obturation techniques. *Med. Oral Patol. Oral Cir. Bucal.* 17 (4), e721–e727. doi: 10.4317/medoral.17898

Andrew, D., and Matthews, B. (2000). Displacement of the contents of dentinal tubules and sensory transduction in intradental nerves of the cat. *J. Physiol.* 529, 791–802. doi: 10.1111/j.1469-7793.2000.00791.x

Arana-Chavez, V. E., and Massa, L. F. (2004). Odontoblasts: the cells forming and maintaining dentine. *Int. J. Biochem. Cell Biol.* 36, 1367–1373. doi: 10.1016/j.biocel.2004.01.006

Arslan, H., Doğanay, E., Karataş, E., Ünlü, M. A., and Ahmed, H. M. A. (2017). Effect of low-level laser therapy on postoperative pain after root canal retreatment: a preliminary placebo-controlled, triple-blind, randomized clinical trial. *J. Endod.* 43, 1765–1769. doi: 10.1016/j.joen.2017.06.028

Ashley, P. F., Parekh, S., Moles, D. R., Anand, P., and MacDonald, L. C. (2016). Preoperative analgesics for additional pain relief in children and adolescents having dental treatment. *Cochrane Database Syst. Rev.* CD008392. doi: 10.1002/14651858.CD008392.pub3

Baez, D., Raddatz, N., Ferreira, G., Gonzalez, C., and Latorre, R. (2014). "Gating of thermally activated channels," in Current topics in membranes (Elsevier), 51–87. doi: 10.1016/B978-0-12-800181-3.00003-8

Bailey, E., Worthington, H. V., van Wijk, A., Yates, J. M., Coulthard, P., and Afzal, Z. (2013). Ibuprofen and/or paracetamol (acetaminophen) for pain relief after surgical removal of lower wisdom teeth. *Cochrane Database Syst. Rev.* (12), CD004624. doi: 10.1002/14651858.CD004624.pub2

Baldari, S., Di Rocco, G., Piccoli, M., Pozzobon, M., Muraca, M., and Toietta, G. (2017). Challenges and strategies for improving the regenerative effects of mesenchymal stromal cell-based therapies. *Int. J. Mol. Sci.* 18, E2087. doi: 10.3390/ijms18102087

Baskaran, P., Covington, K., Bennis, J., Mohandass, A., Lehmann, T., and Thyagarajan, B. (2018). Binding efficacy and thermogenic efficiency of pungent

and nonpungent analogs of capsaicin. *Molecules* 23, E3198. doi: 10.3390/molecules23123198

Bastos, J. L. D., Nomura, L. H., and Peres, M. A. (2006). Dental pain, socioeconomic status, and dental caries in young male adults from southern Brazil. *Cad. Saude Publica* 21, 1416–1423. doi: 10.1590/S0102-311X2005000500014

Becker, D. E. (2010). Pain management: Part 1: managing acute and postoperative dental pain. *Anesth. Prog.* 57, 67–79. doi: 10.2344/0003-3006-57.2.67

Becker, D. E., and Phero, J. C. (2005). Drug therapy in dental practice: nonopioid and opioid analgesics. *Anesth. Prog.* 52, 140–149. doi: 10.2344/0003-3006(2005)52[140:DTD]2.0.CO;2

Beighton, D., Al-Haboubi, M., Mantzourani, M., Gilbert, S. C., Clark, D., Zoitopoulos, L., et al. (2010). Oral bifidobacteria: caries-associated bacteria in older adults. *J. Dent. Res.* 89, 970–974. doi: 10.1177/0022034510369319

Benyamin, R., Trescot, A. M., Datta, S., Buenaventura, R., Adlaka, R., Sehgal, N., et al. (2008). Opioid complications and side effects. *Pain Physician* 11, 105–120.

Berlin, H., List, T., Ridell, K., and Klingberg, G. (2018). Dentists' attitudes towards acute pharmacological pain management in children and adolescents. *Int. J. Paediatr. Dent.* 28, 152–160. doi: 10.1111/ipd.12316

Bertinetti, L., Masic, A., Schuetz, R., Barbetta, A., Seidt, B., Wagermaier, W., et al. (2015). Osmotically driven tensile stress in collagen-based mineralized tissues. *J. Mech. Behav. Biomed. Mater.* 52, 14–21. doi: 10.1016/j.jmbbm.2015.03.010

Bertolini, A., Ferrari, A., Ottani, A., Guerzoni, S., Tacchi, R., and Leone, S. (2006). Paracetamol: new vistas of an old drug. *CNS Drug Rev.* 12, 250–275. doi: 10.1111/j.1527-3458.2006.00250.x

Bevan, S., Hothi, S., Hughes, G., James, I. F., Rang, H. P., Shah, K., et al. (1992). Capsazepine: a competitive antagonist of the sensory neurone excitant capsaicin. *Br. J. Pharmacol.* 107, 544–552. doi: 10.1111/j.1476-5381.1992.tb12781.x

Bezgin, T., Yilmaz, A. D., Celik, B. N., Kolsuz, M. E., and Sonmez, H. (2015). Efficacy of platelet-rich plasma as a scaffold in regenerative endodontic treatment. *J. Endod.* 41, 36–44. doi: 10.1016/j.joen.2014.10.004

Binshtok, A. M., Bean, B. P., and Woolf, C. J. (2007). Inhibition of nociceptors by TRPV1-mediated entry of impermeant sodium channel blockers. *Nature* 449, 607–610. doi: 10.1038/nature06191

Brauchi, S., and Orio, P. (2011). Voltage sensing in thermo-TRP channels. *Adv. Exp. Med. Biol.* 704, 517–530. doi: 10.1007/978-94-007-0265-3_28

Brooks, E., Freter, S. H., Bowles, S. K., and Amirault, D. (2017). Multimodal pain management in older elective arthroplasty patients. *Geriatr. Orthop. Surg. Rehabil.* 8, 151–154. doi: 10.1177/2151458517720297

Brune, K., and Patrignani, P. (2015). New insights into the use of currently available non-steroidal anti-inflammatory drugs. *J. Pain Res.* 8, 105–118. doi: 10.2147/JPR.S75160

Butler, W. T., and Ritchie, H. (1995). The nature and functional significance of dentin extracellular matrix proteins. *Int. J. Dev. Biol.* 39 (1), 169–179.

Cairns, B. E. (2009). *Peripheral receptor targets for analgesia : novel approaches to pain treatment*. Hoboken, New Jersey: John Wiley & Sons. doi: 10.1002/9780470522226

Carnevale, V., and Rohacs, T. (2016). TRPV1: a target for rational drug design. *Pharmaceut. (Basel).* 9, E52. doi: 10.3390/ph9030052

Caterina, M. J. (2007). Transient receptor potential ion channels as participants in thermosensation and thermoregulation. *Am. J. Physiol. Regul. Integr. Comp. Physiol.* 292, R64–R76. doi: 10.1152/ajpregu.00446.2006

Caterina, M. J., Schumacher, M. A., Tominaga, M., Rosen, T. A., Levine, J. D., and Julius, D. (1997). The capsaicin receptor: a heat-activated ion channel in the pain pathway. *Nature* 389, 816–824. doi: 10.1038/39807

Caviedes-Bucheli, J., Azuero-Holguin, M. M., Correa-Ortiz, J. A., Aguilar-Mora, M. V., Pedroza-Flores, J. D., Ulate, E., et al. (2011). Effect of experimentally induced occlusal trauma on substance P expression in human dental pulp and periodontal ligament. *J. Endod.* 37, 627–630. doi: 10.1016/j.joen.2011.02.013

Caviedes-Bucheli, J., Muñoz, H. R., Azuero-Holguín, M. M., and Ulate, E. (2008). Neuropeptides in dental pulp: the silent protagonists. *J. Endod.* 34, 773–788. doi: 10.1016/j.joen.2008.03.010

Chang, D. J., Fricke, J. R., Bird, S. R., Bohidar, N. R., Dobbins, T. W., and Geba, G. P. (2001). Rofecoxib versus codeine/acetaminophen in postoperative dental pain: a double-blind, randomized, placebo- and active comparator-controlled clinical trial. *Clin. Ther.* 23, 1446–1455. doi: 10.1016/S0149-2918(01)80119-3

Cheung, W. S., Calvo, R. R., Tounge, B. A., Zhang, S.-P., Stone, D. R., Brandt, M. R., et al. (2008). Discovery of piperidine carboxamide TRPV1 antagonists. *Bioorg. Med. Chem. Lett.* 18, 4569–4572. doi: 10.1016/j.bmcl.2008.07.035

Chiu, I. M., Heesters, B. A., Ghasemlou, N., Von Hehn, C. A., Zhao, F., Tran, J., et al. (2013). Bacteria activate sensory neurons that modulate pain and inflammation. *Nature* 501, 52–57. doi: 10.1038/nature12479

Chou, R., and Huffman, L. H. (2007). Medications for acute and chronic low back pain: a review of the evidence for an American Pain Society/American College of Physicians Clinical Practice Guideline. *Ann. Intern. Med.* 147, 505. doi: 10.7326/0003-4819-147-7-200710020-00008

Chung, G., Jung, S. J., and Oh, S. B. (2013). Cellular and molecular mechanisms of dental nociception. *J. Dent. Res.* 92 (11), 948–955. doi: 10.1177/0022034513501877

Cosenza, S., Toupet, K., Maumus, M., Luz-Crawford, P., Blanc-Brude, O., Jorgensen, C., et al. (2018). Mesenchymal stem cells-derived exosomes are more immunosuppressive than microparticles in inflammatory arthritis. *Theranostics* 8, 1399–1410. doi: 10.7150/thno.21072

Cotler, H. B., Chow, R. T., Hamblin, M. R., and Carroll, J. (2015). The use of low level laser therapy (LLLT) for musculoskeletal pain. *MOJ Orthop. Rheumatol.* 2, 68. doi: 10.15406/mojor.2015.02.00068

Cui, M., Gosu, V., Basith, S., Hong, S., and Choi, S. (2016). "Chapter three – polymodal transient receptor potential vanilloid type 1 nocisensor: structure, modulators, and therapeutic applications," in *Advances in Protein Chemistry and Structural Biology*, (Netherlands: Elsevier), 81–125. doi: 10.1016/bs.apcsb.2015.11.005

Cuppini, M., Zatta, K. C., Mestieri, L. B., Grecca, F. S., Leitune, V. C. B., Guterres, S. S., et al. (2019). Antimicrobial and anti-inflammatory drug-delivery systems at endodontic reparative material: synthesis and characterization. *Dent. Mater.* 35, 457–467. doi: 10.1016/j.dental.2019.01.002

Dal Secco, D., Moreira, A. P., Freitas, A., Silva, J. S., Rossi, M. A., Ferreira, S. H., et al. (2006). Nitric oxide inhibits neutrophil migration by a mechanism dependent on ICAM-1: role of soluble guanylate cyclase. *Nitric Oxide* 15, 77–86. doi: 10.1016/j.niox.2006.02.004

Datey, A., Adeeb Thaha, C. S., Patil, S. R., Gopalan, J., and Chakravortty, D. (2016). Enhancing the efficiency of desensitizing agents with shockwave treatment-a new paradigm in dentinal hypersensitivity management. *RSC Adv.* 6, 68973–68978. doi: 10.1039/C6RA12342B

De Pascale, M. R., Sommese, L., Casamassimi, A., and Napoli, C. (2015). Platelet derivatives in regenerative medicine: an update. *Transfus. Med. Rev.* 29, 52–61. doi: 10.1016/j.tmrv.2014.11.001

De Petrocellis, L., and Moriello, A. S. (2013). Modulation of the TRPV1 channel: current clinical trials and recent patents with focus on neurological conditions. *Recent Pat. CNS Drug Discov.* 8, 180–204. doi: 10.2174/157488980866613120 9124012

de Santana, D. A., Fonseca, G. F., Ramalho, L. M. P., Rodriguez, T. T., and Aguiar, M. C. (2017). Effect of low-level laser therapy (λ780 nm) on the mechanically damaged dentin-pulp complex in a model of extrusive luxation in rat incisors. *Lasers Med. Sci.* 32, 1995–2004. doi: 10.1007/s10103-017-2295-6

Devin, C. J., and McGirt, M. J. (2015). Best evidence in multimodal pain management in spine surgery and means of assessing postoperative pain and functional outcomes. *J. Clin. Neurosci.* 22, 930–938. doi: 10.1016/j.jocn.2015.01.003

Dubois, R. N., Abramson, S. B., Crofford, L., Gupta, R. A., Simon, L. S., A. Van De Putte, L. B., et al. (1998). Cyclooxygenase in biology and disease. *FASEB J.* 12, 1063–1073. doi: 10.1096/fasebj.12.12.1063

Durand, S. H., Flacher, V., Romeas, A., Carrouel, F., Colomb, E., Vincent, C., et al. (2006). Lipoteichoic acid increases TLR and functional chemokine expression while reducing dentin formation in in vitro differentiated human odontoblasts. *J. Immunol.* 176, 2880–2887. doi: 10.4049/jimmunol.176.5.2880

Dye, B. A., Thornton-Evans, G., Li, X., and Iafolla, T. J. (2015). Dental caries and tooth loss in adults in the United States, 2011–2012. *NCHS Data Brief*, (197), 1–8. doi: 10.1080/713604647

Edwards, J. E., McQuay, H. J., and Moore, R. A. (2002). Combination analgesic efficacy: individual patient data meta-analysis of single-dose oral tramadol plus acetaminophen in acute postoperative pain. *J. Pain Symptom Manage.* 23, 121–130. doi: 10.1016/S0885-3924(01)00404-3

El Ashiry, E. A., Alamoudi, N. M., El Ashiry, M. K., Bastawy, H. A., El Derwi, D. A., and Atta, H. M. (2018). Tissue engineering of necrotic dental pulp of immature teeth with apical periodontitis in dogs: radiographic and histological evaluation. *J. Clin. Pediatr. Dent.* 42, 373–382. doi: 10.17796/1053-4625-42.5.9

El Karim, I. A., Lamey, P. J., Linden, G. J., Awawdeh, L. A., and Lundy, F. T. (2006). Caries-induced changes in the expression of pulpal neuropeptide Y. *Eur. J. Oral Sci.* 114 (2), 133–137. doi: 10.1111/j.1600-0722.2006.00343.x

El Nawam, H., El Backly, R., Zaky, A., and Abdallah, A. (2019). Low-level laser therapy affects dentinogenesis and angiogenesis of in vitro 3D cultures of dentin-pulp complex. *Lasers Med. Sci.* doi: 10.1007/s10103-019-02804-6

ElSalhy, M., Azizieh, F., and Raghupathy, R. (2013). Cytokines as diagnostic markers of pulpal inflammation. *Int. Endod. J.* 46, 573–580. doi: 10.1111/iej.12030

Estrela, C., Guedes, O. A., Silva, J. A., Leles, C. R., Estrela, C. R., de, A., et al. (2011). Diagnostic and clinical factors associated with pulpal and periapical pain. *Braz. Dent. J.* 22, 306–311. doi: 10.1590/S0103-64402011000400008

Farges, J. C., Alliot-Licht, B., Renard, E., Ducret, M., Gaudin, A., Smith, A. J., et al. (2015). Dental pulp defence and repair mechanisms in dental caries. *Mediators Inflamm.* 2015, 230251. doi: 10.1155/2015/230251

Farges, J. C., Carrouel, F., Keller, J. F., Baudouin, C., Msika, P., Bleicher, F., et al. (2011). Cytokine production by human odontoblast-like cells upon Toll-like receptor-2 engagement. *Immunobiology* 216, 513–517. doi: 10.1016/j.imbio.2010.08.006

Farhad, A., and Mohammadi, Z. (2005). Calcium hydroxide: a review. *Int. Dent. J.* 55, 293–301. doi: 10.1111/j.1875-595X.2005.tb00326.x

Farivar, S., Malekshahabi, T., and Shiari, R. (2014). Biological effects of low level laser therapy. *J. lasers Med. Sci.* 5, 58–62.

Feng, X., Xing, J., Feng, G., Huang, D., Lu, X., Liu, S., et al. (2014). P16 INK4A mediates age-related changes in mesenchymal stem cells derived from human dental pulp through the DNA damage and stress response. *Mech. Ageing Dev.* 141–142, 46–55. doi: 10.1016/j.mad.2014.09.004

Forshaw, R. J. (2009). The practice of dentistry in ancient Egypt. *Br. Dent. J.* 206, 481–486. doi: 10.1038/sj.bdj.2009.355

Ganda, K. M. (2008). Dentist's guide to medical conditions, medications, and complications.

Ganzberg, S. (2018). Concerns about NSAIDs. *J. Am. Dent. Assoc.* 149, 667. doi: 10.1016/j.adaj.2018.06.008

Gao, Y., Cao, E., Julius, D., and Cheng, Y. (2016). TRPV1 structures in nanodiscs reveal mechanisms of ligand and lipid action. *Nature* 534, 347–351. doi: 10.1038/nature17964

Gavva, N. R., Klionsky, L., Qu, Y., Shi, L., Tamir, R., Edenson, S., et al. (2004). Molecular determinants of vanilloid sensitivity in TRPV1. *J. Biol. Chem.* 279, 20283–20295. doi: 10.1074/jbc.M312577200

Gebhart, G. F. (2000). "Scientific issues of pain and distress," in *National Research Council (US) Committee on Regulatory Issues in Animal Care and Use. Definition of pain and distress and reporting requirements for laboratory animals: Proceedings of the workshop held June 22, 2000*. Washington (DC): National Academies Press (US), (2000). doi: 10.17226/10035

Gerner, P., Binshtok, A. M., Wang, C.-F., Hevelone, N. D., Bean, B. P., Woolf, C. J., et al. (2008). Capsaicin combined with local anesthetics preferentially prolongs sensory/nociceptive block in rat sciatic nerve. *Anesthesiology* 109, 872–878. doi: 10.1097/ALN.0b013e31818958f7

Gerschman, J. A., Ruben, J., and Gebart-Eaglemont, J. (1994). Low level laser therapy for dentinal tooth hypersensitivity. *Aust. Dent. J.* 39, 353–357. doi: 10.1111/j.1834-7819.1994.tb03105.x

Global Burden of Disease Study, C (2013). Global Burden of Disease: 2013. *Lancet* 2015 386, 743–800. doi: 10.1016/S0140-6736(15)60692-4

Goldberg, M. (2011). Dentin structure composition and mineralization. *Front. Biosci.* E3, 281. doi: 10.2741/e281

Gomari, H., Moghadam, M. F., and Soleimani, M. (2018). Targeted cancer therapy using engineered exosome as a natural drug delivery vehicle. *Onco. Targets. Ther.* 11, 5753–5762. doi: 10.2147/OTT.S173110

Graham, G. G., and Scott, K. F. (2005). Mechanism of action of paracetamol. *Am. J. Ther.* 12, 46–55. doi: 10.1097/00045391-200501000-00008

Gregorio-Teruel, L., Valente, P., González-Ros, J. M., Fernández-Ballester, G., and Ferrer-Montiel, A. (2014). Mutation of I696 and W697 in the TRP box of vanilloid receptor subtype I modulates allosteric channel activation. *J. Gen. Physiol.* 143, 361–375. doi: 10.1085/jgp.201311070

Gronthos, S., Brahim, J., Li, W., Fisher, L. W., Cherman, N., Boyde, A., et al. (2002). Stem cell properties of human dental pulp stem cells. *J. Dent. Res.* 81, 531–535. doi: 10.1177/154405910208100806

Gunthorpe, M. J., Hannan, S. L., Smart, D., Jerman, J. C., Arpino, S., Smith, G. D., et al. (2007). Characterization of SB-705498, a potent and selective vanilloid receptor-1 (VR1/TRPV1) antagonist that inhibits the capsaicin-, acid-, and heat-mediated activation of the receptor. *J. Pharmacol. Exp. Ther.* 321, 1183–1192. doi: 10.1124/jpet.106.116657

Hall-Stoodley, L., Costerton, J., and Stoodley, P. (2004). Bacterial biofilms: from the natural environment to infectious diseases. *Nat. Rev. Microbiol.* 2, 95–108. doi: 10.1038/nrmicro821

Hall, B. E., Zhang, L., Sun, Z. J., Utreras, E., Prochazkova, M., Cho, A., et al. (2016). Conditional TNF-α overexpression in the tooth and alveolar bone results in painful pulpitis and osteitis. *J. Dent. Res.* 95, 188–195. doi: 10.1177/0022034515612022

Hanada, K., Morotomi, T., Washio, A., Yada, N., Matsuo, K., Teshima, H., et al. (2019). In vitro and in vivo effects of a novel bioactive glass-based cement used as a direct pulp capping agent. *J. Biomed. Mater. Res. - Part B Appl. Biomater.* 107, 161–168. doi: 10.1002/jbm.b.34107

Hargreaves, K., and Abbott, P. V. (2005). Drugs for pain management in dentistry. *Aust. Dent. J.* 50, S14–S22. doi: 10.1111/j.1834-7819.2005.tb00378.x

Hausner, T., Schmidhammer, R., Zandieh, S., Hopf, R., Schultz, A., Gogolewski, S., et al. (2007). Nerve regeneration using tubular scaffolds from biodegradable polyurethane. *Acta Neurochir.* Suppl. 100, 69–72. doi: 10.1007/978-3-211-72958-8_15

Hayashi, Y., Murakami, M., Kawamura, R., Ishizaka, R., Fukuta, O., and Nakashima, M. (2015). CXCL14 and MCP1 are potent trophic factors associated with cell migration and angiogenesis leading to higher regenerative potential of dental pulp side population cells. *Stem Cell Res. Ther.* 6, 111. doi: 10.1186/s13287-015-0088-z

Hilkens, P., Bronckaers, A., Ratajczak, J., Gervois, P., Wolfs, E., and Lambrichts, I. (2017). The angiogenic potential of DPSCs and SCAPs in an in vivo model of dental pulp regeneration. *Stem Cells Int.* 2017, 2582080. doi: 10.1155/2017/2582080

Hossain, M. Z., Bakri, M. M., Yahya, F., Ando, H., Unno, S., and Kitagawa, J. (2019). The role of transient receptor potential (TRP) channels in the transduction of dental pain. *Int. J. Mol. Sci.* 20 (3), 526. doi: 10.3390/ijms20030526

Hu, L., Gao, Z., Xu, J., Zhu, Z., Fan, Z., Zhang, C., et al. (2017). Decellularized swine dental pulp as a bioscaffold for pulp regeneration. *Biomed Res. Int.* 2017, 9342714. doi: 10.1155/2017/9342714

Hu, X., Zhong, Y., Kong, Y., Chen, Y., Feng, J., and Zheng, J. (2019). Lineage-specific exosomes promote the odontogenic differentiation of human dental pulp stem cells (DPSCs) through TGFβ1/smads signaling pathway via transfer of microRNAs. *Stem Cell Res. Ther.* 10, 170. doi: 10.1186/s13287-019-1278-x

Huang, C. C., Narayanan, R., Alapati, S., and Ravindran, S. (2016). Exosomes as biomimetic tools for stem cell differentiation: applications in dental pulp tissue regeneration. *Biomaterials* 111, 103–115. doi: 10.1016/j.biomaterials.2016.09.029

Huang, G. T.-J., Gronthos, S., and Shi, S. (2009). Mesenchymal stem cells derived from dental tissues vs. those from other sources: their biology and role in regenerative medicine. *J. Dent. Res.* 88, 792–806. doi: 10.1177/0022034509340867

Huang, G. T.-J., Yamaza, T., Shea, L. D., Djouad, F., Kuhn, N. Z., Tuan, R. S., et al. (2010). Stem/progenitor cell-mediated de novo regeneration of dental pulp with newly deposited continuous layer of dentin in an in vivo model. *Tissue Eng. Part A* 16, 605–615. doi: 10.1089/ten.tea.2009.0518

Iohara, K., Imabayashi, K., Ishizaka, R., Watanabe, A., Nabekura, J., Ito, M., et al. (2011). Complete pulp regeneration after pulpectomy by transplantation of CD105 + stem cells with stromal cell-derived factor-1. *Tissue Eng. Part A* 17, 1911–1920. doi: 10.1089/ten.tea.2010.0615

Iohara, K., Murakami, M., Takeuchi, N., Osako, Y., Ito, M., Ishizaka, R., et al. (2013). A novel combinatorial therapy with pulp stem cells and granulocyte colony-stimulating factor for total pulp regeneration. *Stem Cells Transl. Med.* 2, 818. doi: 10.5966/sctm.2012-0132

Itoh, Y., Sasaki, J. I., Hashimoto, M., Katata, C., Hayashi, M., and Imazato, S. (2018). Pulp regeneration by 3-dimensional dental pulp stem cell constructs. *J. Dent. Res.* 97, 1137–1143. doi: 10.1177/0022034518772260

Jain, N., Gupta, A., and Meena, N. (2013). An insight into neurophysiology of pulpal pain: facts and hypotheses. *Korean J. Pain*. 26 (4), 347-355. doi: 10.3344/kjp.2013.26.4.347

Ji, Y., Choi, S. K., Sultan, A. S., Chuncai, K., Lin, X., Dashtimoghadam, E., et al. (2018). Nanomagnetic-mediated drug delivery for the treatment of dental disease. *Nanomedicine* 14, 919–927. doi: 10.1016/j.nano.2018.01.013

Jiang, X., Liu, H., and Peng, C. (2017). Clinical and radiographic assessment of the efficacy of a collagen membrane in regenerative endodontics: a randomized, controlled clinical trial. *J. Endod.* 43, 1465–1471. doi: 10.1016/j.joen.2017.04.011

Jones, M. R., Viswanath, O., Peck, J., Kaye, A. D., Gill, J. S., and Simopoulos, T. T. (2018). A brief history of the opioid epidemic and strategies for pain medicine. *Pain Ther.* 7, 13–21. doi: 10.1007/s40122-018-0097-6

Julius, D. (2013). TRP channels and pain. *Annu. Rev. Cell Dev. Biol.* 29, 355–384. doi: 10.1146/annurev-cellbio-101011-155833

Kalani, A., Chaturvedi, P., Kamat, P. K., Maldonado, C., Bauer, P., Joshua, I. G., et al. (2016). Curcumin-loaded embryonic stem cell exosomes restored neurovascular unit following ischemia-reperfusion injury. *Int. J. Biochem. Cell Biol.* 79, 360–369. doi: 10.1016/j.biocel.2016.09.002

Kassebaum, N. J., Bernabé, E., Dahiya, M., Bhandari, B., Murray, C. J. L., and Marcenes, W. (2014). Global burden of severe tooth loss. *J. Dent. Res.* 93, 20S–28S. doi: 10.1177/0022034514537828

Khan, J., Zusman, T., Wang, Q., and Eliav, E. (2019). Acute and chronic pain in orofacial trauma patients. *Dent. Traumatol.* 2019. doi: 10.1111/edt.12493.

Kim, H. B., Baik, K. Y., Seonwoo, H., Jang, K. J., Lee, M. C., Choung, P. H., et al. (2018). Effects of pulsing of light on the dentinogenesis of dental pulp stem cells in vitro. *Sci. Rep.* 8, 2057. doi: 10.1038/s41598-018-19395-x

Kim, H. Y., Kim, K., Li, H. Y., Chung, G., Park, C.-K., Kim, J. S., et al. (2010a). Selectively targeting pain in the trigeminal system. *Pain* 150, 29–40. doi: 10.1016/j.pain.2010.02.016

Kim, J. Y., Xin, X., Moioli, E. K., Chung, J., Lee, C. H., Chen, M., et al. (2010b). Regeneration of dental-pulp-like tissue by chemotaxis-induced cell homing. *Tissue Eng. Part A* 16, 3023–3031. doi: 10.1089/ten.tea.2010.0181

Korn, S., Vassil, T. C., Kotey, P. N.-A., and Fricke, J. R. (2004). Comparison of rofecoxib and oxycodone plus acetaminophen in the treatment of acute pain: a randomized, double-blind, placebo-controlled study in patients with moderate to severe postoperative pain in the third molar extraction model. *Clin. Ther.* 26, 769–778. doi: 10.1016/S0149-2918(04)90076-8

Krzyściak, W., Jurczak, A., Kościelniak, D., Bystrowska, B., and Skalniak, A. (2014). The virulence of Streptococcus mutans and the ability to form biofilms. *Eur. J. Clin. Microbiol. Infect. Dis.* 33, 499–515. doi: 10.1007/s10096-013-1993-7

Kulkantrakorn, K., Lorsuwansiri, C., and Meesawatsom, P. (2013). 0.025% Capsaicin gel for the treatment of painful diabetic neuropathy: a randomized, double-blind, crossover, placebo-controlled trial. *Pain Pract.* 13, 497–503. doi: 10.1111/papr.12013

Kwon, J.-S., Lee, M.-J., Kim, J.-Y., Kim, D., Ryu, J.-H., Jang, S., et al. (2019). Novel anti-biofouling bioactive calcium silicate-based cement containing 2-methacryloyloxyethyl phosphorylcholine. *PLoS One* 14, e0211007. doi: 10.1371/journal.pone.0211007

Latorre, R., Brauchi, S., Orta, G., Zaelzer, C., and Vargas, G. (2007). ThermoTRP channels as modular proteins with allosteric gating. *Cell Calcium* 42, 427–438. doi: 10.1016/j.ceca.2007.04.004

Lee, S., Lee, S., Jeong, M., Oh, H., and Lee, K. (2017). The effects of extracorporeal shock wave therapy on pain and range of motion in patients with adhesive capsulitis. *J. Phys. Ther. Sci.* 29, 1907–1909. doi: 10.1589/jpts.29.1907

Leek, F. F. (1967). The practice of dentistry in ancient Egypt. *J. Egypt. Archaeol.* 53, 51–58. doi: 10.1177/030751336705300109

Liang, X., Zhang, L., Wang, S., Han, Q., and Zhao, R. C. (2016). Exosomes secreted by mesenchymal stem cells promote endothelial cell angiogenesis by transferring miR-125a. *J. Cell Sci.* 129, 2182–2189. doi: 10.1242/jcs.170373

Lim, T. K. Y., MacLeod, B. A., Ries, C. R., and Schwarz, S. K. W. (2007). The quaternary lidocaine derivative, QX-314, produces long-lasting local anesthesia in animal models in vivo. *Anesthesiology* 107, 305–311. doi: 10.1097/01.anes.0000270758.77314.b4

Lipski, M., Nowicka, A., Kot, K., Postek-Stefańska, L., Wysoczańska-Jankowicz, I., Borkowski, L., et al. (2018). Factors affecting the outcomes of direct pulp capping using Biodentine. *Clin. Oral Investig.* 22, 2021–2029. doi: 10.1007/s00784-017-2296-7

Logan, N., and Brett, P. (2013). The control of mesenchymal stromal cell osteogenic differentiation through modified surfaces. *Stem Cells Int*. 2013, 10. doi: 10.1155/2013/361637

Long, Y. Z., Liu, S. Y., Li, W., and Dong, Y. M. (2018). [Physical and chemical properties of pulp capping materials based on bioactive glass]. *Beijing Da Xue Xue Bao.* 50, 887–891. doi: 10.19723/j.issn.1671-167X.2018.05.021

Luo, Z., Kohli, M. R., Yu, Q., Kim, S., Qu, T., and He, W. X. (2014). Biodentine induces human dental pulp stem cell differentiation through mitogen-activated protein kinase and calcium-/calmodulin-dependent protein kinase II pathways. *J. Endod.* 40, 937–942. doi: 10.1016/j.joen.2013.11.022

Magloire, H., Maurin, J. C., Couble, M. L., Shibukawa, Y., Tsumura, M., Thivichon-Prince, B., et al. (2010). Topical review. Dental pain and odontoblasts: facts and hypotheses. *J. Orofac. Pain* 24, 335–349.

Malkondu, Ö., Kazandağ, M. K., and Kazazoğlu, E. (2014). A review on biodentine, a contemporary dentine replacement and repair material. *Biomed Res. Int.* 2014, 1160951. doi: 10.1155/2014/160951

Matta, J. A., and Ahern, G. P. (2007). Voltage is a partial activator of rat thermosensitive TRP channels. *J. Physiol.* 585, 469–482. doi: 10.1113/jphysiol.2007.144287

Matute Crespo, M., and Montero Matamala, A. (2017). Avances farmacológicos en el manejo multimodal de la analgesia perioperatoria. *Rev. Esp. Anestesiol. Reanim.* 64, 467–471. doi: 10.1016/j.redar.2017.03.006

Mehrvarzfar, P., Abbott, P. V., Saghiri, M. A., Delvarani, A., Asgar, K., Lotfi, M., et al. (2012). Effects of three oral analgesics on postoperative pain following root canal preparation: a controlled clinical trial. *Int. Endod. J.* 45, 76–82. doi: 10.1111/j.1365-2591.2011.01950.x

Meotti, F. C., Lemos de Andrade, E., and Calixto, J. B. (2014). "TRP modulation by 1553 natural compounds," in *Handbook of experimental pharmacology*, (GER Elsevier) 1177–1238. doi: 10.1007/978-3-319-05161-1_19

Mester, E., Szende, B., and Gärtner, P. (1968). The effect of laser beams on the growth of hair in mice. *Radiobiol. Radiother. (Berl).* 9, 621–626.

Miglani, S., Aggarwal, V., and Ahuja, B. (2010). Dentin hypersensitivity: recent trends in management. *J. Conserv. Dent.* 13, 218–224. doi: 10.4103/0972-0707.73385

Mitsiadis, T. A., and Rahiotis, C. (2004). Parallels between tooth development and repair: conserved molecular mechanisms following carious and dental injury. *J. Dent. Res.* 83, 896–902. doi: 10.1177/154405910408301202

Mittermayr, R., Hartinger, J., Antonic, V., Meinl, A., Pfeifer, S., Stojadinovic, A., et al. (2011). Extracorporeal shock wave therapy (ESWT) minimizes ischemic tissue necrosis irrespective of application time and promotes tissue revascularization by stimulating angiogenesis. *Ann. Surg.* 253, 1024–1032. doi: 10.1097/SLA.0b013e3182121d6e

Miura, M., Gronthos, S., Zhao, M., Lu, B., Fisher, L. W., Robey, P. G., et al. (2003). SHED: stem cells from human exfoliated deciduous teeth. *Proc. Natl. Acad. Sci.* 100, 5807–5812. doi: 10.1073/pnas.0937635100

Mizumura, K., and Murase, S. (2015). "Role of nerve growth factor in pain," in *Handbook of experimental pharmacology*, (GER Elsevier). 57–77. doi: 10.1007/978-3-662-46450-2_4

Moore, P. A., and Hersh, E. V. (2014). Combining ibuprofen and acetaminophen for acute pain management after third-molar extractions. *J. Am. Dent. Assoc.* 144, 898–908. doi: 10.14219/jada.archive.2013.0207

Moore, P. A., Ziegler, K. M., Lipman, R. D., Aminoshariae, A., Carrasco-Labra, A., and Mariotti, A. (2018). Benefits and harms associated with analgesic medications used in the management of acute dental pain. *J. Am. Dent. Assoc.* 149, 256–265.e3. doi: 10.1016/j.adaj.2018.02.012

Morales-Lázaro, S. L., Simon, S. A., and Rosenbaum, T. (2013). The role of endogenous molecules in modulating pain through transient receptor potential vanilloid 1 (TRPV1). *J. Physiol.* 591, 3109–3121. doi: 10.1113/jphysiol.2013.251751

Morgan, C. R., Rodd, H. D., Clayton, N., Davis, J. B., and Boissonade, F. M. (2005). Vanilloid receptor 1 expression in human tooth pulp in relation to caries and pain. *J. Orofac. Pain* 19, 248–260.

Moya, D., Ramón, S., Schaden, W., Wang, C. J., Guiloff, L., and Cheng, J. H. (2018). The role of extracorporeal shockwave treatment in musculoskeletal disorders. *J. Bone Jt. Surg. – Am.* 100, 251–263. doi: 10.2106/JBJS.17.00661

Murray, H., Locker, D., Mock, D., and Tenenbaum, H. C. (1996). Pain and the quality of life in patients referred to a craniofacial pain unit. *J. Orofac. Pain* 10, 316–323.

Mutoh, N., Tani-Ishii, N., Tsukinoki, K., Chieda, K., and Watanabe, K. (2007). Expression of toll-like receptor 2 and 4 in dental pulp. *J. Endod.* 33, 1183–1186. doi: 10.1016/j.joen.2007.05.018

Nack, B., Haas, S. E., and Portnof, J. (2017). Opioid use disorder in dental patients: the latest on how to identify, treat, refer and apply laws and regulations in your practice. *Anesth. Prog.* 64, 178–187. doi: 10.2344/anpr-64-03-09

Nagi, R., Yashoda Devi, B. K., Rakesh, N., Reddy, S. S., and Patil, D. J. (2015). Clinical implications of prescribing nonsteroidal anti-inflammatory drugs in oral health care — A review. *Oral Surg. Oral Med. Oral Pathol. Oral Radiol.* 119, 264–271. doi: 10.1016/j.oooo.2014.12.002

Nakagawa, H., and Hiura, A. (2013). Comparison of the transport of QX-314 through TRPA1, TRPM8, and TRPV1 channels. *J. Pain Res.* 6, 223–230. doi: 10.2147/JPR.S41614

Nakanishi, T., Takegawa, D., Hirao, K., Takahashi, K., Yumoto, H., and Matsuo, T. (2011). Roles of dental pulp fibroblasts in the recognition of bacterium-related factors and subsequent development of pulpitis. *Jpn. Dent. Sci. Rev.* 47, 161–166. doi: 10.1016/j.jdsr.2011.02.001

Nakashima, M., Iohara, K., Murakami, M., Nakamura, H., Sato, Y., Ariji, Y., et al. (2017). Pulp regeneration by transplantation of dental pulp stem cells in pulpitis: a pilot clinical study. *Stem Cell Res. Ther.* 8, 61. doi: 10.1186/s13287-017-0506-5

Nilius, B., and Owsianik, G. (2010). Transient receptor potential channelopathies. *Pflügers Arch. - Eur. J. Physiol.* 460, 437–450. doi: 10.1007/s00424-010-0788-2

Noble, M., Treadwell, J. R., Tregear, S. J., Coates, V. H., Wiffen, P. J., Akafomo, C., et al. (2010). Long-term opioid management for chronic noncancer pain. *Cochrane Database Syst. Rev.* 2010 (1), CD006605. doi: 10.1002/14651858.CD006605.pub2

Nomura, L. H., Bastos, J. L. D., and Peres, M. A. (2005). Dental pain prevalence and association with dental caries and socioeconomic status in schoolchildren, Southern Brazil, 2002. *Braz. Oral Res.* 18, 134–140. doi: 10.1590/S1806-83242004000200008

Norman, M. H., Zhu, J., Fotsch, C., Bo, Y., Chen, N., Chakrabarti, P., et al. (2007). Novel vanilloid receptor-1 antagonists: 1. Conformationally restricted analogues of trans-cinnamides †. *J. Med. Chem.* 50, 3497–3514. doi: 10.1021/jm070189q

Ogden, J. A., Tóth-Kischkat, A., and Schultheiss, R. (2001). Principles of shock wave therapy. *Clin. Orthop. Relat. Res.* (387), 8–17. doi: 10.1097/00003086-200106000-00003

Ohbuchi, K., Mori, Y., Ogawa, K., Warabi, E., Yamamoto, M., and Hirokawa, T. (2016). Detailed analysis of the binding mode of vanilloids to transient receptor potential vanilloid type I (TRPV1) by a mutational and computational study. *PLoS One* 11, e0162543. doi: 10.1371/journal.pone.0162543

Ong, C. K.-S., Lirk, P., Seymour, R. A., and Jenkins, B. J. (2005). The efficacy of preemptive analgesia for acute postoperative pain management: a meta-analysis. *Anesth. Analg.* 100, 757–773. doi: 10.1213/01.ANE.0000144428.98767.0E

Ong, C. K. S., Lirk, P., Tan, C. H., and Seymour, R. A. (2007). An evidence-based update on nonsteroidal anti-inflammatory drugs. *Clin. Med. Res.* 5, 19–34. doi: 10.3121/cmr.2007.698

Orhan, K., Aksoy, U., Can-Karabulut, D. C., and Kalender, A. (2011). Low-level laser therapy of dentin hypersensitivity: a short-term clinical trial. *Lasers Med. Sci.* 26, 591–598. doi: 10.1007/s10103-010-0794-9

Pan, B. T., and Johnstone, R. M. (1983). Fate of the transferrin receptor during maturation of sheep reticulocytes in vitro: selective externalization of the receptor. *Cell* 33, 967–978. doi: 10.1016/0092-8674(83)90040-5

Paranjpe, A., Smoot, T., Zhang, H., and Johnson, J. D. (2011). Direct contact with mineral trioxide aggregate activates and differentiates human dental pulp cells. *J. Endod.* 37, 1691–1695. doi: 10.1016/j.joen.2011.09.012

Parirokh, M., and Torabinejad, M. (2010). Mineral trioxide aggregate: a comprehensive literature review-part III: clinical applications, drawbacks, and mechanism of action. *J. Endod.* 36, 400–413. doi: 10.1016/j.joen.2009.09.009

Park, S. H., Ye, L., Love, R. M., Farges, J.-C., and Yumoto, H. (2015). Inflammation of the dental pulp. *Mediators Inflamm.* 2015, 980196. doi: 10.1155/2015/980196

Petelin, M., Pavlica, Z., Ivanuša, T., Šentjurc, M., and Skalerič, U. (2000). Local delivery of liposome-encapsulated superoxide dismutase and catalase suppress periodontal inflammation in beagles. *J. Clin. Periodontol.* 27, 918–925. doi: 10.1034/j.1600-051x.2000.027012918.x

Petersen, P. E., Bourgeois, D., Ogawa, H., Estupinan-Day, S., and Ndiaye, C. (2005). The global burden of oral diseases and risks to oral health. *Bull. World Health Organ.* 83, 661–669. doi: /S0042-96862005000900011

Petrini, M., Ferrante, M., Ciavarelli, L., Ceccarini, A., Brunetti, L., Vacca, M., et al. (2012). Prostaglandin E2 to diagnose between reversible and irreversible pulpitis. *Int. J. Immunopathol. Pharmacol.* 25, 157–163. doi: 10.1177/039463201202500118

Pierdomenico, L., Bonsi, L., Calvitti, M., Rondelli, D., Arpinati, M., Chirumbolo, G., et al. (2005). Multipotent mesenchymal stem cells with immunosuppressive activity can be easily isolated from dental pulp. *Transplantation* 80, 836–842. doi: 10.1097/01.tp.0000173794.72151.88

Pitts, N. B., Zero, D. T., Marsh, P. D., Ekstrand, K., Weintraub, J. A., Ramos-Gomez, F ., et al. (2017). Dental caries. *Nat. Rev. Dis. Prim.* 3. doi: 10.1038/nrdp.2017.30

Pivoraitė, U., Jarmalavičiūtė, A., Tunaitis, V., Ramanauskaitė, G., Vaitkuvienė, A., Kašėta, V., et al. (2015). Exosomes from human dental pulp stem cells suppress carrageenan-induced acute inflammation in mice. *Inflammation* 38, 1933–1941. doi: 10.1007/s10753-015-0173-6

Prescott, R. S., Alsanea, R., Fayad, M. I., Johnson, B. R., Wenckus, C. S., Hao, J., et al. (2008). In vivo generation of dental pulp-like tissue by using dental pulp stem cells, a collagen scaffold, and dentin matrix protein 1 after subcutaneous transplantation in mice. *J. Endod.* 34, 421–426. doi: 10.1016/j.joen.2008.02.005

Primosch, R. E., Antony, S. J., and Courts, F. J. (1993). The efficacy of preoperative analgesic administration for postoperative pain management of pediatric dental patients. *Anesth. Pain Control Dent.* 2, 102–106.

Raposo, G. (1996). B lymphocytes secrete antigen-presenting vesicles. *J. Exp. Med.* 183, 1161–1172. doi: 10.1084/jem.183.3.1161

Ratajczak, J., Miekus, K., Kucia, M., Zhang, J., Reca, R., Dvorak, P., et al. (2006). Embryonic stem cell-derived microvesicles reprogram hematopoietic progenitors: evidence for horizontal transfer of mRNA and protein delivery. *Leukemia* 20, 847–856. doi: 10.1038/sj.leu.2404132

Rechenberg, D. K., Galicia, J. C., and Peters, O. A. (2016). Biological markers for pulpal inflammation: a systematic review. *PLoS One* 11, e0167289. doi: 10.1371/journal.pone.0167289

Reid, B. C., Chenette, R., and Macek, M. D. (2003). Prevalence and predictors of untreated caries and oral pain among special olympic athletes. *Spec. Care Dent.* 23 (4), 139–142. doi: 10.1111/j.1754-4505.2003.tb00300.x

Ricciotti, E., and FitzGerald, G. A. (2011). Prostaglandins and inflammation. *Arterioscler. Thromb. Vasc. Biol.* 31, 986–1000. doi: 10.1161/ATVBAHA.110.207449

Rice, A. S. C., Smith, B. H., and Blyth, F. M. (2016). Pain and the global burden of disease. *Pain* 157 (4), 791–796. doi: 10.1097/j.pain.0000000000000454

Ries, C. R., Pillai, R., Chung, C. C. W., Wang, J. T. C., MacLeod, B. A., and Schwarz, S. K. W. (2009). QX-314 produces long-lasting local anesthesia modulated by transient receptor potential vanilloid receptors in mice. *Anesthesiology* 111, 122–126. doi: 10.1097/ALN.0b013e3181a9160e

Rodd, H. D., and Boissonade, F. M. (2000). Substance P expression in human tooth pulp in relation to caries and pain experience. *Eur. J. Oral Sci.* 108, 467–474. doi: 10.1034/j.1600-0722.2000.00924.x

Rodríguez-Benítez, S., Stambolsky, C., Gutiérrez-Pérez, J. L., Torres Lagares, D., and Segura-Egea, J. J. (2015). Pulp revascularization of immature dog teeth with apical periodontitis using triantibiotic paste and platelet-rich plasma: a radiographic study. *J. Endod.* 41, 1299–1304. doi: 10.1016/j.joen.2015.05.002

Römling, U., Kjelleberg, S., Normark, S., Nyman, L., Uhlin, B. E., and Åkerlund, B. (2014). Microbial biofilm formation: a need to act. *J. Intern. Med.* 276, 98–110. doi: 10.1111/joim.12242

Rosa, V., Zhang, Z., Grande, R. H. M., and Nör, J. E. (2013). Dental pulp tissue engineering in full-length human root canals. *J. Dent. Res.* 92, 970–975. doi: 10.1177/0022034513505772

Rosenbaum, T., and Simon, S. A. (2007). *TRPV1 Receptors and Signal Transduction*. Boca Raton (FL): CRC Press/Taylor & Francis. doi: 10.1201/9781420005844.ch5

Rutherford, R. B., and Gu, K. (2000). Treatment of inflamed ferret dental pulps with recombinant bone morphogenetic protein-7. *Eur. J. Oral Sci.* 108, 202–206. doi: 10.1034/j.1600-0722.2000.108003202.x

Rutherford, R. B., Wahle, J., Tucker, M., Rueger, D., and Charette, M. (1993). Induction of reparative dentine formation in monkeys by recombinant human osteogenic Protein-1. *Arch. Oral Biol.* 38, 571–576. doi: 10.1016/0003-9969(93)90121-2

Schaden, W., Fischer, A., and Sailler, A. (2001). Extracorporeal shock wave therapy of nonunion or delayed osseous union. *Clin. Orthop. Relat. Res.* (387): 90–4. doi: 10.1097/00003086-200106000-00012

Sessle, B. J. (1986). Recent developments in pain research: central mechanisms of orofacial pain and its control. *J. Endod.* 12, 435–444. doi: 10.1016/S0099-2399(86)80196-0

Sessle, B. J. (2011). "Peripheral and central mechanisms of orofacial inflammatory pain," in *International Review of Neurobiology*. 97, 179–206. doi: 10.1016/B978-0-12-385198-7.00007-2

Shahmoradi, M., Bertassoni, L. E., Elfallah, H. M., and Swain, M. (2014). "Fundamental structure and properties of enamel, dentin and cementum BT — Advances in calcium phosphate biomaterials,". Ed. B. Ben-Nissan (Berlin, Heidelberg: Springer Berlin Heidelberg), 511–547. doi: 10.1007/978-3-642-53980-0_17

Sharma, C. V., and Mehta, V. (2013). Paracetamol: mechanisms and updates. *BJA Educ.* 14, 153–158. doi: 10.1093/bjaceaccp/mkt049

Sheiham, A. (2006). Dental caries affects body weight, growth and quality of life in pre-school children. *Br. Dent. J.* 201, 625–626. doi: 10.1038/sj.bdj.4814259

Shen, Y., Saboe, P. O., Sines, I. T., Erbakan, M., and Kumar, M. (2014). Biomimetic membranes: a review. *J. Memb. Sci.* 454, 359–381. doi: 10.1016/j.memsci.2013.12.019

Shi, S., Miura, M., Seo, B. M., Robey, P. G., Bartold, P. M., and Gronthos, S. (2005). The efficacy of mesenchymal stem cells to regenerate and repair dental structures. *Orthod. Craniofacial Res.* 8, 191–199. doi: 10.1111/j.1601-6343.2005.00331.x

Shibukawa, Y., Sato, M., Kimura, M., Sobhan, U., Shimada, M., Nishiyama, A., et al. (2015). Odontoblasts as sensory receptors: transient receptor potential channels, pannexin-1, and ionotropic ATP receptors mediate intercellular odontoblast-neuron signal transduction. *Pflugers Arch. Eur. J. Physiol.* 467, 843–863. doi: 10.1007/s00424-014-1551-x

Shigetani, Y., Sasa, N., Suzuki, H., Okiji, T., and Ohshima, H. (2011). GaAlAs laser irradiation induces active tertiary dentin formation after pulpal apoptosis and cell proliferation in rat molars. *J. Endod.* 37, 1086–1091. doi: 10.1016/j.joen.2011.05.020

Smith, A. J., Cassidy, N., Perry, H., Begue-Kirn, C., Ruch, J. V., and Lesot, H. (1995). Reactionary dentinogenesis. *Int. J. Dev. Biol.* 39, 273–280.

Solé-Magdalena, A., Martínez-Alonso, M., Coronado, C. A., Junquera, L. M., Cobo, J., and Vega, J. A. (2018). Molecular basis of dental sensitivity: the odontoblasts are multisensory cells and express multifunctional ion channels. *Ann. Anat. - Anat. Anzeiger* 215, 20–29. doi: 10.1016/j.aanat.2017.09.006

Steinberg, X., Lespay-Rebolledo, C., and Brauchi, S. (2014). A structural view of ligand-dependent activation in thermoTRP channels. *Front. Physiol.* 5, 171. doi: 10.3389/fphys.2014.00171

Sun, D., Zhuang, X., Xiang, X., Liu, Y., Zhang, S., Liu, C., et al. (2010). A novel nanoparticle drug delivery system: the anti-inflammatory activity of curcumin is enhanced when encapsulated in exosomes. *Mol. Ther.* 18, 1606–1614. doi: 10.1038/mt.2010.105

Sunshine, A., Laska, E. M., Olson, N. Z., Colon, A., Gonzalez, L., and Tirado, S. (1983). Analgesic effects of oral propiram fumarate, codeine sulfate and placebo in postoperative pain. *Pharmacother. J. Hum. Pharmacol. Drug Ther.* 3, 299–303. doi: 10.1002/j.1875-9114.1983.tb03281.x

Tian, T., Zhang, H. X., He, C. P., Fan, S., Zhu, Y. L., Qi, C., et al. (2018). Surface functionalized exosomes as targeted drug delivery vehicles for cerebral ischemia therapy. *Biomaterials* 150, 137–149. doi: 10.1016/j.biomaterials.2017.10.012

Tikhonova, S., Booij, L., D'Souza, V., Crosara, K. T. B., Siqueira, W. L., and Emami, E. (2018). Investigating the association between stress, saliva and dental caries: a scoping review. *BMC Oral Health* 18, 41. doi: 10.1186/s12903-018-0500-z

Tonetti, M. S., Jepsen, S., Jin, L., and Otomo-Corgel, J. (2017). Impact of the global burden of periodontal diseases on health, nutrition and wellbeing of mankind: a call for global action. *J. Clin. Periodontol.* 44, 456–462. doi: 10.1111/jcpe.12732

Torabinejad, M., and Chivian, N. (1999). Clinical applications of mineral trioxide aggregate. *J. Endod.* 25, 197–205. doi: 10.1016/S0099-2399(99)80142-3

Torabinejad, M., Milan, M., Shabahang, S., Wright, K. R., and Faras, H. (2015). Histologic examination of teeth with necrotic pulps and periapical lesions treated with 2 scaffolds: an animal investigation. *J. Endod.* 41, 846–852. doi: 10.1016/j.joen.2015.01.026

Trams, E. G., Lauter, C. J., Norman Salem, J., and Heine, U. (1981). Exfoliation of membrane ecto-enzymes in the form of micro-vesicles. *BBA - Biomembr.* 645, 63–70. doi: 10.1016/0005-2736(81)90512-5

Trevisani, M., and Szallasi, A. (2010). Targeting TRPV1: Challenges and issues in pain management. *Open Drug Discov. J.* 2, 37–49. Ferrara Italy. Bentham Open. doi: 10.2174/1877381801002010037

Tziafas, D. (2010). Dentinogenic potential of the dental pulp: facts and hypotheses. *Endod. Top.* 17, 42–64. doi: 10.1111/j.1601-1546.2010.00248.x

Valadi, H., Ekström, K., Bossios, A., Sjöstrand, M., Lee, J. J., and Lötvall, J. O. (2007). Exosome-mediated transfer of mRNAs and microRNAs is a novel mechanism of genetic exchange between cells. *Nat. Cell Biol.* 9, 654–659. doi: 10.1038/ncb1596

Vanegas, H., Vazquez, E., and Tortorici, V. (2010). NSAIDs, opioids, cannabinoids and the control of pain by the central nervous system. *Pharmaceut. (Basel).* 3, 1335–1347. doi: 10.3390/ph3051335

Vos, T., Abajobir, A. A., Abbafati, C., Abbas, K. M., Abate, K. H., Abd-Allah, F., et al. (2017). Global, regional, and national incidence, prevalence, and years lived with disability for 328 diseases and injuries for 195 countries, 1990-2016: a systematic analysis for the Global Burden of Disease Study 2016. *Lancet* 390, 1211–1259. doi: 10.1016/S0140-6736(17)32154-2

Wang, W., Yi, X., Ren, Y., and Xie, Q. (2016). Effects of adenosine triphosphate on proliferation and odontoblastic differentiation of human dental pulp cells. *J. Endod.* 42, 1483–1489. doi: 10.1016/j.joen.2016.07.013

Ward, P. A. (1974). The inflammatory mediators. *Ann. N. Y. Acad. Sci.* 221, 290–298. doi: 10.1111/j.1749-6632.1974.tb28228.x

Wassel, M. O., and Khattab, M. A. (2017). Antibacterial activity against Streptococcus mutans and inhibition of bacterial induced enamel demineralization of propolis, miswak, and chitosan nanoparticles based dental varnishes. *J. Adv. Res.* 8, 387–392. doi: 10.1016/j.jare.2017.05.006

Weihs, A., Fuchs, C., Teuschl, A., Hartinger, J., Slezak, P., Mittermayr, R., et al. (2014). Shock wave treatment enhances cell proliferation and improves wound healing by ATP release-coupled extracellular signal-regulated kinase (ERK) activation. *J. Biol. Chem. Sep* 26, 27090–27104. doi: 10.1074/jbc.M114.580936

Wierichs, R. J., and Meyer-Lueckel, H. (2015). Systematic review on noninvasive treatment of root caries lesions. *J. Dent. Res.* 94, 261–271. doi: 10.1177/0022034514557330

Won, J., Vang, H., Kim, J. H., Lee, P. R., Kang, Y., and Oh, S. B. (2018). TRPM7 mediates mechanosensitivity in adult rat odontoblasts. *J. Dent. Res.* 97, 1039–1046. doi: 10.1177/0022034518759947

Wongrakpanich, S., Wongrakpanich, A., Melhado, K., and Rangaswami, J. (2018). A comprehensive review of non-steroidal anti-inflammatory drug use in the elderly. *Aging Dis.* 9, 143–150. doi: 10.14336/AD.2017.0306

Xuan, K., Li, B., Guo, H., Sun, W., Kou, X., He, X., et al. (2018). Deciduous autologous tooth stem cells regenerate dental pulp after implantation into injured teeth. *Sci. Transl. Med.* 10, eaaf3227. doi: 10.1126/scitranslmed.aaf3227

Yang, F., and Zheng, J. (2017). Understand spiciness: mechanism of TRPV1 channel activation by capsaicin. *Protein Cell* 8, 169–177. doi: 10.1007/s13238-016-0353-7

Yang, Y., Huang, L., Dong, Y., Zhang, H., Zhou, W., Ban, J., et al. (2014). In vitro antibacterial activity of a novel resin-based pulp capping material containing the quaternary ammonium salt MAE-DB and Portland cement. *PLoS One* 9, e112549. doi: 10.1371/journal.pone.0112549

Zhang, M., Zang, X., Wang, M., Li, Z., Qiao, M., Hu, H., et al. (2019). Exosome-based nanocarriers as bio-inspired and versatile vehicles for drug delivery: recent advances and challenges. *J. Mater. Chem. B* 7, 2421–2433. doi: 10.1039/C9TB00170K

Zhang, W., Vazquez, B., Oreadi, D., and Yelick, P. C. (2017). Decellularized tooth bud scaffolds for tooth regeneration. *J. Dent. Res.* 96, 516–523. doi: 10.1177/0022034516689082

Zhu, J., Liang, R., Sun, C., Xie, L., Wang, J., Leng, D., et al. (2017). Effects of nanosilver and nanozinc incorporated mesoporous calcium-silicate nanoparticles on the mechanical properties of dentin. *PLoS One* 12, e0182583. doi: 10.1371/journal.pone.0182583

Conflict of Interest Statement: The authors declare that the research was conducted in the absence of any commercial or financial relationships that could be construed as a potential conflict of interest.

frontiers in Pharmacology

ORIGINAL RESEARCH
published: 15 October 2019
doi: 10.3389/fphar.2019.01212

Potassium Intake Prevents the Induction of the Renin-Angiotensin System and Increases Medullary ACE2 and COX-2 in the Kidneys of Angiotensin II-Dependent Hypertensive Rats

Alexis A. Gonzalez[1], Matias Gallardo[1], Carlos Cespedes[2,3] and Carlos P. Vio[2,3]*

[1] Institute of Chemistry, Pontificia Universidad Católica de Valparaíso, Valparaíso, Chile, [2] Department of Physiology, Center for Aging and Regeneration CARE UC, Pontificia Universidad Católica de Chile, Santiago, Chile, [3] Facultad de Medicina y Ciencia, Universidad San Sebastián, Santiago, Chile

OPEN ACCESS

Edited by:
Miguel Reyes-Parada, University of Chile, Chile

Reviewed by:
Kazem Zibara, Lebanese University, Lebanon
Mohammed A. Nayeem, West Virginia University, United States

***Correspondence:**
Alexis A. Gonzalez
alexis.gonzalez@pucv.cl

Specialty section:
This article was submitted to Translational Pharmacology, a section of the journal Frontiers in Pharmacology

Received: *24 June 2019*
Accepted: *20 September 2019*
Published: *15 October 2019*

Citation:
Gonzalez AA, Gallardo M, Cespedes C and Vio CP (2019) Potassium Intake Prevents the Induction of the Renin-Angiotensin System and Increases Medullary ACE2 and COX-2 in the Kidneys of Angiotensin II-Dependent Hypertensive Rats. Front. Pharmacol. 10:1212. doi: 10.3389/fphar.2019.01212

In angiotensin II (Ang II)-dependent hypertensive rats there is an increased expression of proximal tubule angiotensinogen (AGT), collecting duct renin and angiotensin converting enzyme (ACE), which contributes to intratubular Ang II formation. Ang II acts on Ang II type 1 receptors promoting sodium retention and vasoconstriction. However concurrently, the ACE2-Ang-(1–7) axis and the expression of kallikrein and medullary prostaglandins counteract the effects of Ang II, promoting natriuresis and vasodilation. Human studies demonstrate that dietary potassium (K^+) intake lowers blood pressure. In this report we evaluate the expression of AGT, ACE, medullary prorenin/renin, ACE2, kallikrein and cyclooxygenase-2 (COX-2) in Ang II-infused rats fed with high K^+ diet (2%) for 14 days. Dietary K^+ enhances diuresis in non-infused and in Ang II-infused rats. The rise in systolic blood pressure in Ang II-infused rats was attenuated by dietary K^+. Ang II-infused rats showed increased renal protein levels of AGT, ACE and medullary prorenin and renin. This effect was attenuated in the Ang II + K^+ group. Ang II infusion decreased ACE2 compared to the control group; however, K^+ diet prevented this effect in the renal medulla. Furthermore, medullary COX-2 was dramatically induced by K^+ diet in non-infused and in Ang II infused rats. Dietary K^+ greatly increased kallikrein immunostaining in normotensive rats and in Ang II-hypertensive rats. These results indicate that a high K^+ diet attenuates Ang II-dependent hypertension by preventing the induction of ACE, AGT and collecting duct renin and by enhancing medullary COX-2 and ACE2 protein expression in the kidney.

Keywords: potassium, blood pressure, renin, angiotensin, hypertension, kallikrein, sodium, cyclooxygenase

INTRODUCTION

The activity of the systemic renin-angiotensin system (RAS) promotes vasoconstriction and sodium reabsorption primarily by angiotensin II (Ang II)-dependent stimulation of aldosterone release and by activation of distal nephron sodium channels (Masilamani et al., 1999; Chaszczewska-Markowska et al., 2016). Sodium reabsorption in the collecting duct (CD) also occurs *via* direct

activation of epithelial sodium channels (ENaC) by Ang II type 1 receptor (AT1R) independent of aldosterone (Mamenko et al., 2012; Zaika et al., 2013). The amount of sodium reabsorbed by the CD impacts sodium balance and blood pressure (Kim et al., 2007) and the availability of intrarenal and intratubular Ang II is crucial for sodium entry and global sodium balance. Accumulated evidence demonstrated the presence of an intrarenal RAS (Navar et al., 2011) whose activity is stimulated in Ang II-dependent hypertension (Liu et al., 2011) and in salt induced renal injury (Kobori et al., 2001; Prieto-Carrasquero et al., 2004; Susic et al., 2009). mRNA angiotensinogen (AGT) expression can be detected in the proximal tubules and is augmented in Ang II-infused rats (Kobori et al., 2004). Renin is expressed in the CD and is upregulated in Ang II-dependent hypertension (Prieto-Carrasquero et al., 2004). This evidence, along with the augmented expression of angiotensin converting enzyme (ACE) in animal models of hypertension (Gonzalez-Villalobos et al., 2009), indicates that intrarenal RAS activation has a role in intratubular Ang II formation. Furthermore in Ang II-infused rats the concentrations of intratubular Ang II are much higher than expected by plasma accumulation (Vonthun et al., 1994; Navar et al., 2001) suggesting a critical role of the newly formed intratubular Ang II on sodium reabsorption and blood pressure.

On the other hand, the angiotensin converting enzyme 2 (ACE2) plays an important role in counteracting the effects of RAS activation (Bader, 2013). ACE2 cleaves Ang II to produce Ang-(1-7), promoting natriuresis and vasodilation *via* nitric oxide (NO) production in renal tissues through the actions of the Mas receptor (Ferrario and Varagic, 2010). Along with this axis, the Ang II infusion also promotes the induction of cyclooxygenase-2 (COX-2) in the renal medulla leading to the production of natriuretic and vasodilatory prostaglandins (PGs) counteracting the anti-natriuretic effects of Ang II.

Evidence demonstrates that K^+ supplementation lowers blood pressure (Geleijnse et al., 2003; Rodrigues et al., 2014). This fact is relevant in light of evidence of reduced K^+ consumption by modern society (Noubiap et al., 2015; Jung et al., 2019). Research into this matter could lead to public health interventions to prevent cardiovascular disease linked to hypertension and renal disease. Despite growing evidence showing the augmented intrarenal expression of most of the components of the RAS in Ang II-dependent hypertension (Navar et al., 2011), little is known about the effect of K^+ diet supplementation in this model and its impact on the expression of AGT, ACE, CD renin and ACE2. Here, we investigate the effect of K^+ dietary supplementation on systolic blood pressure, natriuresis, and protein levels of intrarenal RAS and on ACE2 and COX-2 in Ang II-dependent hypertensive rats.

MATERIALS AND METHODS

Animals

Animal protocols were approved by the Animal Care and Use Committee of *Pontificia Universidad Católica de Chile* (Animal Welfare Assurance no. A5848-01) and conducted in accordance with the National Institutes of Health *Guide for the Care and Use of Laboratory Animals*. Six male Sprague-Dawley rats were used for each experimental group with a total number of 24 rats for this study. By the completion of the experimental protocols (14 days training on systolic blood pressure measurements, K^+ diet, osmotic minipump implantation and 14 days of Ang II infusion), no signs of disease or mortality were observed.

Potassium Diet

Male Sprague-Dawley rats were divided into four groups, Control group: sham-operated with normal K^+ diet (0.9% KCl in food); Normal K^+ diet plus chronic Ang II infusions for 14 days; High K^+ diet with sham surgery (2% KCl in food); High K^+ diet with chronic Ang II infusion for 14 days. Rats receiving high K^+ diet were adapted 1 week before the beginning of treatment with 1% KCl in the drinking water.

Ang II Infusion and Systolic Blood Pressure

Male Sprague-Dawley rats were infused subcutaneously with Ang II (Sigma, Cat # A9525, St. Louis, MO) by osmotic minipumps (Alzet model 2002, infusion rate of 0.5 mL/h) at a concentration of 400 ng/kg/min for 14 days, as previously described (Gonzalez et al., 2011). Minipump implantation was performed under ketamine/xylazyne anesthesia (25/2.5 mg/kg ip). Systolic blood pressures were monitored by the CODA tail-cuff blood pressure system (Kent Scientific Corporation, Torrington, CT) on days −7, −1, 7, and 14. At the end of the study, rats were placed during 18 h in metabolic cages (Tecniplast, Buguggiate, VA, Italy) for urine collection with the purpose of determining sodium and K^+ concentrations and creatinine levels. After 14 days rats were euthanized by anesthetic overdose and blood samples were collected from the vena cava for electrolytes and creatinine measurements to calculate fractional Na^+ and K^+ excretions. Kidneys were processed to obtain samples for immunohistochemistry and Western blotting. All physiological values were normalized by body weight.

Immunohistochemistry

Immunolocalization studies were performed using an indirect immunoperoxidase technique. Briefly, the renal tissue samples, 3–4 mm thick, were fixed by immersion in Bouin's solution for 18–24 h at 21–24°C. Then the samples were dehydrated, embedded in Paraplast Plus, sectioned at 5–7 μm thickness with a rotatory microtome (Leica Biosystems, Germany), and mounted on glass slides. Kidney sections were dewaxed, hydrated and washed in Tris–phosphate buffer, pH 7.6 and incubated overnight with anti-COX-2 at 1:500 (SC-1747, Santa Cruz, CA), at room temperature. This was followed by incubation with the corresponding secondary antibody and with the peroxidase-antiperoxidase complex (MP Biomedicals, Santa Ana, CA). Peroxidase activity was detected by incubation of the sections with 0.1% (wt/vol) 3,3′-diaminobenzidine and 0.03% (vol/vol) hydrogen peroxide. Kidney sections were analyzed as previously described (Villanueva et al., 2008) using Nikon Eclipse E600 microscopy and Nikon DS-Ri1 camera (Nikon Corp., Tokyo, Japan). Four representative fields for each section were used

and an average of six rats quantified. Images were quantified by Simple PCI 6.0 software (Hamamatsu Corporation, Sewickley, PA) and average values of stained areas were expressed as fold change of controls.

Biochemical Parameters

Serum and urine electrolytes were assayed using an ion selective electrolyte analyzer model 9180 (Roche Diagnostic, Mannheim, Germany).

Western Blot

Kidneys were stored at −80°C and then were defrosted. Fifty mg of medullary or cortical kidney tissues were homogenated in lysis RIPA buffer (50 mM Tris-HCl pH 8.0; 150 mM NaCl; 1% NP-40; 0.5% sodium deoxycolate; 0.1% SDS) and centrifuged at 14,000 rpm during 10 min at 4°C. Protein concentrations was determined by Bradford method using Protein Assay (Bio-Rad, Hercules, CA). Total protein content was denatured in SDS-PAGE sample buffer for 20 min at 60°C. To assess consistency of protein loading, 15 µg of protein from each sample were resolved by SDS-PAGE. For immunoblot, each sample was run at 40 µg/lane. Proteins were transferred to PVDF membranes (Bio-Rad, Hercules, CA) blocked with 5% non-fat milk and blotted with each antibody. Primary antibodies used included the following: mouse anti renin/prorenin (B-12 133145, Santa Cruz, CA) at 1:2,000; mouse anti AGT (IBL-20101 OG-922, Japan) at 1:10,000; mouse anti ACE (CD 143, Chemicon Millipore, Warford, UK); rabbit anti ACE2 (H-175 SC-20998, Santa Cruz, CA) at 1:1,000; rabbit anti COX-2 (Cayman 160126, Ann Arbor, MI) at 1:2,000, incubates for 2 h at room temperature. Rabbit anti-cathepsin G antibody (ab197354, Abcam, Cambridge, UK), rabbit anti-chymase (ab233103 Abcam, Cambridge, UK)) and rabbit anti AT1 receptor (sc-515884, Santa Cruz, CA) were used at 1:200 and incubated 24 h at room temperature. Secondary antibodies were tagged with horseradish peroxidase (Santa Cruz, CA, USA). Immunoreactivity was assessed by chemioluminiscence kit (Perkin-Elmer, Life Sciences, Boston, MA, USA). Arbitrary density units were normalized to the mean intensity of control group, defined as 1.0. Values were averaged and mean values compiled for statistical analysis.

Statistical Analysis

Results are expressed as mean ± SEM. Grubb's test was used to detect outliers in univariate data assumed to come from a normally distributed population. Comparisons between groups were performed using One-Way ANOVA when appropriate with Tukey's post-test. $P \leq 0.05$ values were considered statistically significant, P = NS is not significant.

RESULTS

Potassium Diet Attenuates the Increase in Systolic Blood Pressure in Ang II Infused Rats

Systolic blood pressure was recorded starting 1 week before minipump implantation. Dietary K^+ supplementation with 1% KCl started one before Ang II infusion; however, a slight but not significant reduction was observed at day −1. Systolic blood pressure increased in Ang II-infused rats starting at day 7 (153 ± 7 mmHg vs. control group, 128 ± 4 mmHg, P = 0.032) and progressively increased up to 209 ± 13 mmHg vs. 133 ± 3 mmHg, P = 0.0008) by day 14. The Ang II + K^+ group showed similar increase at day 7 (159 ± 6 mmHg); however, at day 14, the increases in systolic blood pressure were attenuated and significantly reduced as compared to Ang II-infused rats with regular K^+ diet (156 ± 4 mmHg vs. 209 ± 13 mmHg, P = 0.012, **Figure 1A**).

Diuretic Responses and Na^+, K^+ Balance With High Potassium Diet

Urinary flow was greatly increased in rats supplemented with dietary K^+ (20.37 ± 2.03 vs. 1.19 ± 0.04 mL/kg/h, P = 0.022). As reported before, Ang II infusion induces pressure diuresis (6.54 ± 1.74 vs. 1.19 ± 0.04 mL/kg/h, P = 0.011), and this effect seems to be enhanced by K^+ supplementation (8.82 ± 2.52 vs. 1.19 ± 0.04 mL/kg/h, P = 0.010). Sodium balance after 14 days of treatment was close to 0 in control groups, decreased in K^+ and Ang II groups and slightly decreased in K^+ group (**Figure 1B)**. However, K^+ balance was reduced in K^+ group. Combined Ang II infusion plus K^+ showed no differences with control in K^+ and Na^+ balance (**Figures 1B**, **C**). No differences were found in U_v Na^+ among groups (**Figure 1D**). However, U_V K^+ was induced by K^+ diet as well as by Ang II infusion (**Figure 1E**).

Potassium Intake Prevented the Induction of AGT, Tubular Renin and ACE in Ang II-Infused Rats

The expression of AGT protein and mRNA are expressed in proximal tubules and can be detected in cortical renal tissues. We performed semi-quantitative immunoblots using homogenates from micro-dissected cortical tissues of control rats, K^+ supplemented, Ang II infused + regular K^+ diet and Ang II + high dietary K^+ (**Figure 2**). No changes in AGT protein abundances were found in rats with high K^+ diet vs. those treated with regular diet in the renal cortex (0.6 ± 0.3 vs. 1.0 ± 0.2, P = 0.34, **Figure 1A**) or in the renal medulla (0.9 ± 0.2 vs. 1.0 ± 0.2, P = 0.44, **Figure 1B**). AGT protein abundance was increased in Ang II-infused rats in the renal cortex (6.0 ± 0.2 vs. 1.0 ± 0.2, P = 0.0003). K^+ supplementation partially prevented the induction of AGT in Ang II-infused rats (2.7 ± 0.4 vs. 6.0 ± 0.2, P = 0.033). Similar results were observed by analyzing the stained area of cortical AGT showing no changes with K^+ diet (0.64 ± 0.06 vs. 1.00 ± 0.04, P = 0.48) but increased staining in the Ang II group (2.42 ± 0.16 vs. 1.00 ± 0.04, P = 0.031). As observed in Western blot results, Ang II + K^+ prevented AGT induction when compared to Ang II rats (1.17 ± 0.13 vs. 2.42 ± 0.16, P = 0.013), see **Figures 2C**, **D**. Prorenin and renin are expressed in the CD, and their abundances are increased in chronic Ang II-infused rats (Prieto-Carrasquero et al., 2004). To avoid contamination of the juxtaglomerular renin component, we used micro-dissected tissues exclusively from renal inner medullary tissues to measure renin as source of CD. Prorenin plus renin protein levels did not show changes in the renal cortex (**Figure 3A**), however, both

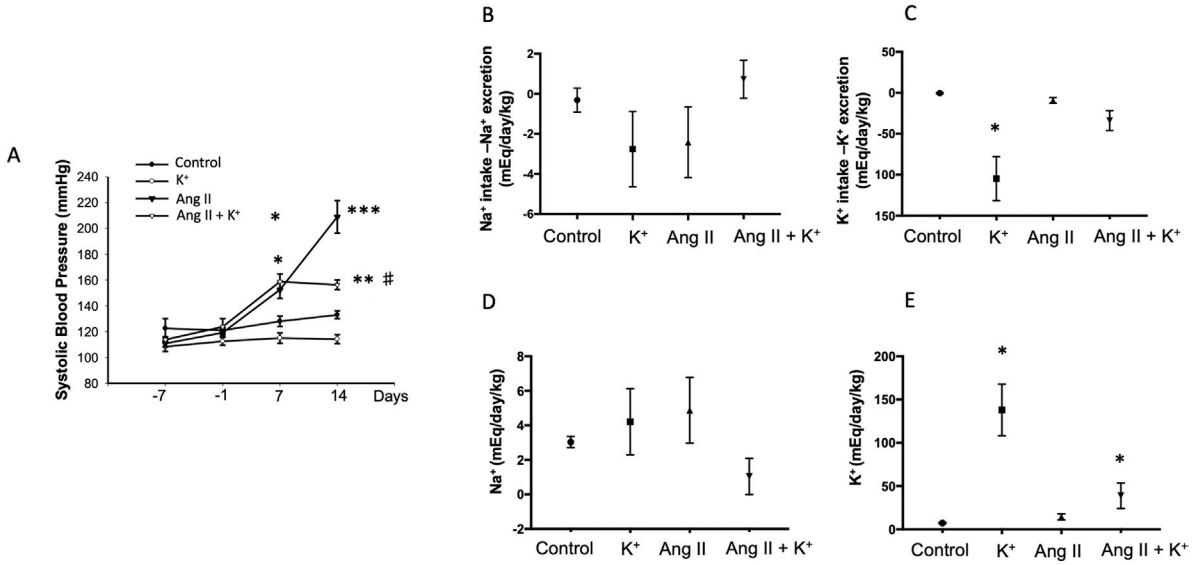

FIGURE 1 | Systolic blood pressure (SBP, tail cuff method) and Na^+, K^+ balance in response to chronic Ang II infusion (400 ng/kg/min during 14 days) with or without K^+ dietary supplementation. **(A)** No changes in basal SBP were observed at day –7. K^+ dietary supplementation was started at day –7 and SBP was recorded at day 7. After 2 weeks of treatment K^+ caused a reduction in SBP as compared to controls (black circles), the significant differences were maintained until day 14. SBP was increased by day 7 in Ang II infused rats, as well as in Ang II + K^+ group. By day 14 Ang II group reached 209 ± 13 mmHg, while Ang II + K^+ group reached 153 ± 4 mmHg, *P < 0.05, **P < 0.01, ***P < 0.001 vs. control group (normal K^+ diet, sham operated); #P < 0.05 vs. Ang II group, n = 6. **(B)** Na^+ and K^+ **(C)** balance in mEq/day/body mass. **(D)** and **(E)** show U_v Na^+ and K^+ in mEq/day/kg.

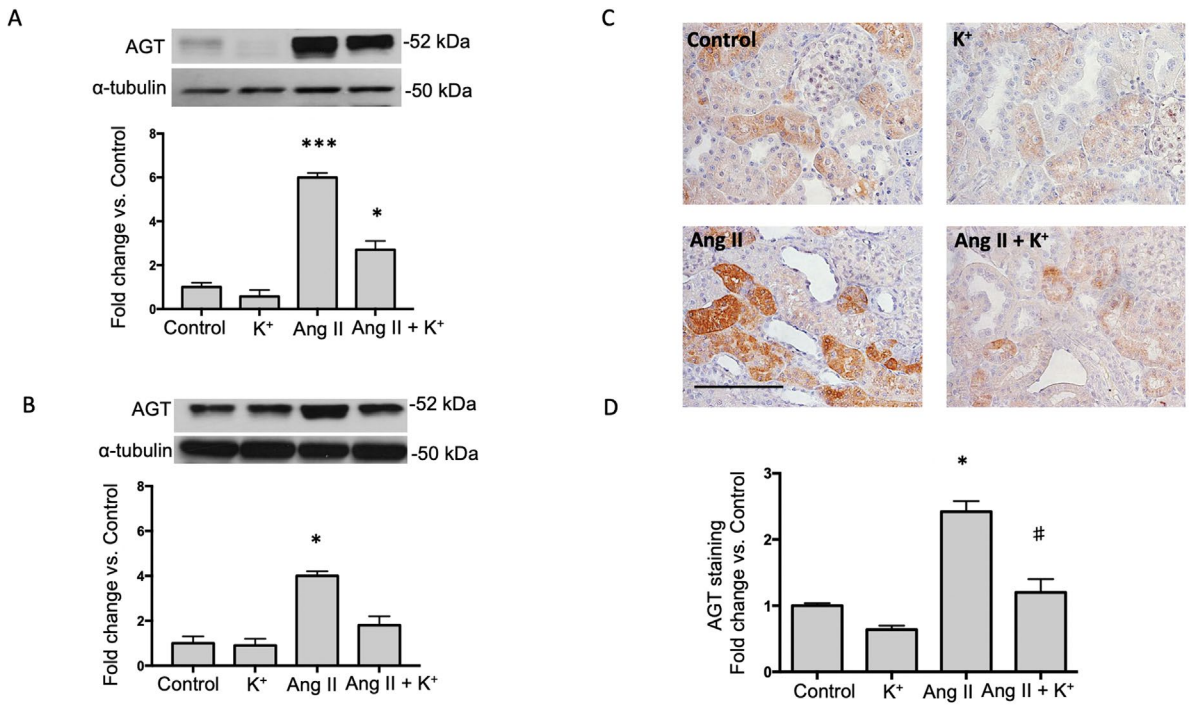

FIGURE 2 | Potassium intake attenuates the induction of angiotensinogen (AGT) expression in Ang II-infused rats. Representative immunoblot and densitometric analysis of AGT protein in renal cortex **(A)** and medulla **(B)** of control rats, K^+ supplemented, Ang II infused and Ang II-infused + K^+ supplementation. α-tubulin was used to correct variation in sample loading. Values are expressed as fold change of control group. **(C)** A representative image of AGT immunostaining showing the typically proximal tubule specific staining, which is increased by Ang II infused rats. KCl supplementation prevented this effect. **(D)** Quantification of stained areas in four representative fields for each section from six rats. Images were quantified by Simple PCI 6.0 software and the average values of stained areas were expressed as fold change of controls. *P < 0.05, ***P < 0.001 vs. control group (normal K^+ diet, sham operated); #P < 0.05 vs. Ang II group, n = 6. Scale bar: 100 μm.

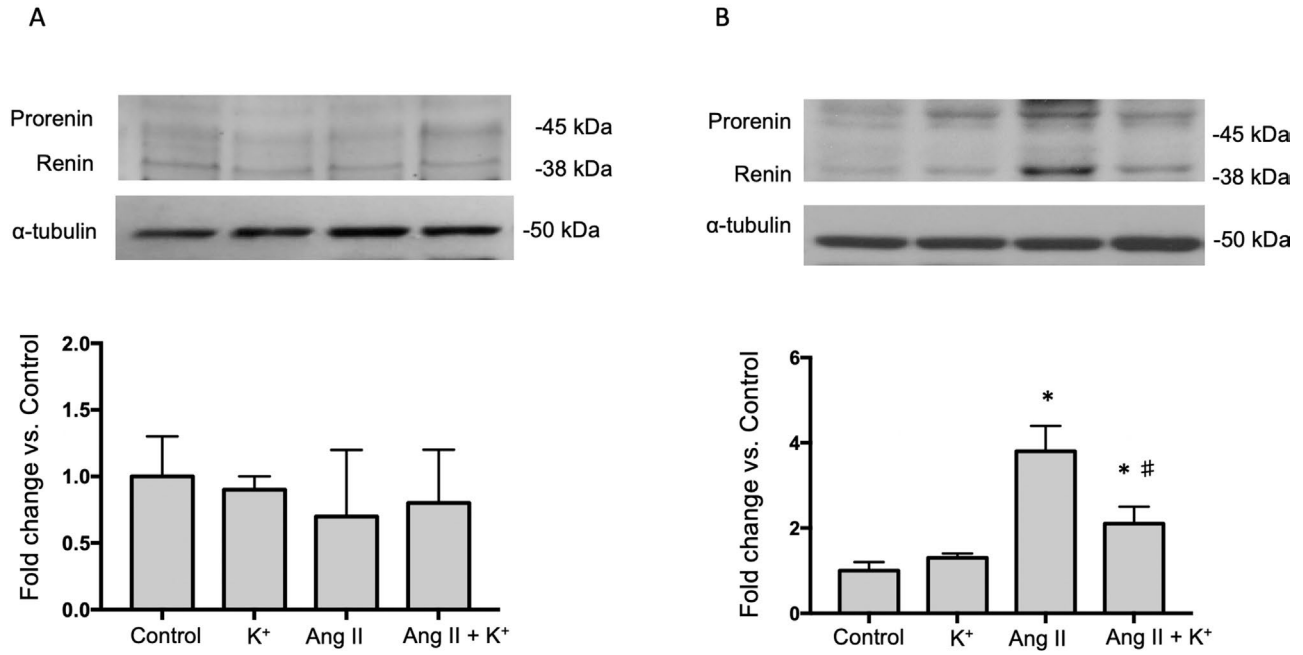

FIGURE 3 | Representative immunoblot and densitometric analysis of prorenin and renin bands in renal cortex **(A)** and medullary tissues **(B)** of control rats, K^+ supplemented, Ang II infused and Ang II infused + K^+ dietary supplementation. Ang II infusion enhances prorenin and renin protein abundances in renal medulla and K^+ intake partially prevented this effect. Micro-dissected inner medullas were used as source of collecting duct renin to avoid juxtaglomerular renin derived. Note that in cortical tissue renin band is more prevalent than prorenin band (data not shown). *$P < 0.001$ vs. control group (normal K^+ diet, sham operated); #$P < 0.05$ vs. Ang II group, n = 6. α-tubulin was used to correct variation in sample loading (same cortical α-tubulin was used for AGT and renin). Values are expressed as fold change of control group.

bands were augmented in medullary tissues of Ang II-infused rats compared to control group (3.8 ± 0.6 vs. 1.0 ± 0.2, $P < 0.0009$). Although K^+ supplementation increases renin plus prorenin protein expression in Ang II-infused rats (2.1 +/- 0.4 vs. 1.0 ± 0.2, $P < 0.033$), it was significantly less that of the Ang II group (2.1 ± 0.4 vs. 3.8 ± 0.6, P = 0.011, (**Figure 3B**).

Potassium Intake Prevents Ang II-Dependent Upregulation of ACE and Increases the Expression of ACE2 in the Renal Medulla

AGT can be cleaved by CD renin to form Ang I. It is expected that ACE expressed in the luminal side of the proximal tubule or CD promote its conversion to Ang II. We analyzed the expression of ACE in both, cortical and medullary tissues and compared them to control tissues as a fold change defined as 1.0 in controls. K^+ dietary supplementation did not alter ACE expression in renal cortical **(Figure 4A)** or medullary **(Figure 4B)** renal tissues. ACE protein levels were augmented in cortical (5.87 ± 1.10 vs. 1.00 ± 0.21, P = 0.008) and medullary tissues (1.68 ± 0.19 vs. 1.00 ± 0.18, P = 0.009) of Ang II infused rats. K^+ dietary supplementation completely prevented the induction of ACE in the renal medulla (1.02 ± 0.11 vs. 1.00 ± 0.18, P = 0.89) but not in the cortex (4.63 ± 0.54 vs. 1.00 ± 0.21, P = 0.0084). We next investigated the effect of Ang II infusions and K^+ diet on ACE2 expression in cortical and medullary tissues. As shown in **Figures 4C**, **D**, K^+ diet causes a reduction in ACE2 expression in normotensive rats (non-infused), this effect was evident in the cortex (0.14 ± 0.01 vs. 1.00 ± 0.13, P = 0.0004) but not in the medulla (0.71 ± 0.11 vs. 1.00 ± 0.14, P = 0.34). In Ang II infused + normal K^+ diet ACE2 was also reduced in both the cortex and in the medulla. The reduction of ACE2 protein expression caused by Ang II infusion in medullary tissues (Ang II: 0.44 ± 0.06, P = 0.00023 vs. control) was partially reversed in the Ang II + K^+ diet (0.65 ± 0.09, P = 0.08 vs. control).

COX-2 Protein Expression is Induced by Dietary K^+ Intake in the Renal Medulla

Because activation of bradykinin B2 receptor enhances COX-2 in the kidney, we investigated if high K^+ diet might involve the induction of medullary COX-2. In the renal medulla COX-2 mediated PGE_2 production stimulates vasodilation and natriuresis (Gonzalez et al., 2009) contributing to the benefic effects of K^+ diet. As shown in **Figure 5A**, K^+ diet downregulates cortical COX-2 (0.23 ± 0.09 vs. 1.00 ± 0.21, P = 0.007), but greatly induces medullary COX-2 (6.8 ± 1.4 vs. 1.0 ± 0.2, P = 0.007, **Figure 5B**). No additional changes of COX-2 expression were detected in cortical COX-2. Ang II infusions did not change COX-2 expression (0.8 ± 0.6-fold change of control, P = 0.42). However, Ang II infused rats with high K^+ diet showed a 12-fold increase in COX-2 expression in medullary tissues (12.2 ± 1.1 vs. 1.0 ± 0.2, $P < 0.001$). COX-2 immunostainings showed a significant decrease in rats with K^+ diet (0.29 ± 0.04, P = 0.0033), Ang II (0.26 ± 0.04, P = 0.0024) and Ang II + K^+ group (0.23 ± 0.02, P = 0.010) when compared to control rats (1.00 ± 0.19), see **Figures 5C**, **D**.

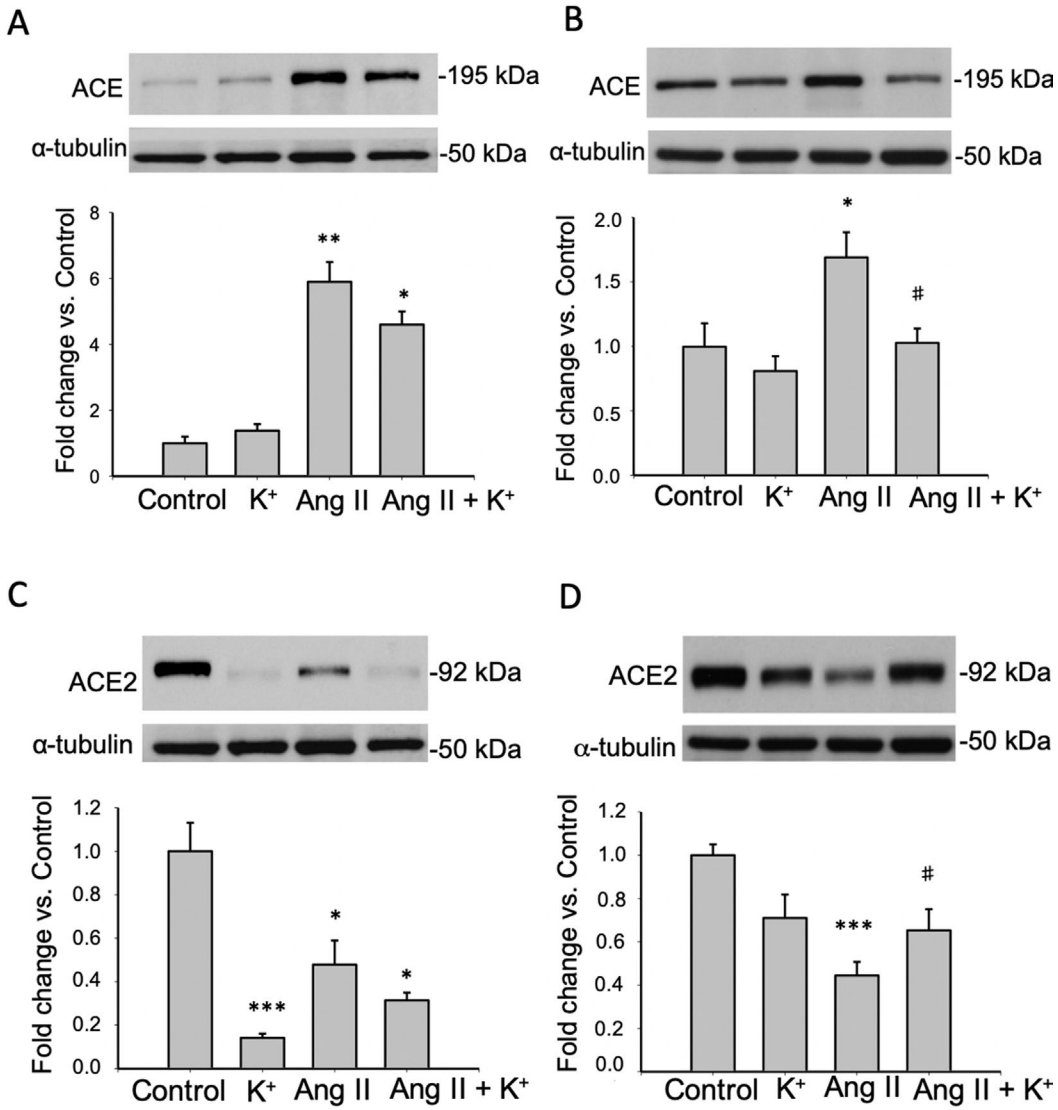

FIGURE 4 | Reciprocal changes in ACE and ACE2 in response to K^+ intake in rats infused with Ang II. ACE protein expression is shown in cortex **(A)** and medulla **(B)**. ACE2 protein abundances are shown in cortex **(C)** and medulla **(D)**. *P < 0.05, **P < 0.01, ***P < 0.001 vs. control group, #P < 0.05 vs. Ang II group, n = 6. α-tubulin was used to correct variation in sample loading. Values are expressed as fold change of control group.

Potassium Intake Increases Kallikrein Protein Expression in Normotensive and in Ang II-Dependent Hypertensive Rats

To explore the effect of high K^+ diet on kallikrein expression we performed immunolocalization studies using an indirect immunoperoxidase technique in kidney slides. **Figure 6A** shows representative images of all groups while **Figure 6B** shows the quantification expressed as fold change of control (normal K^+ diet non infused-sham operated). As observed, K^+ caused a sixfold increase in the staining area as compared to controls, while Ang II infusion dramatically reduced kallikrein staining (0.19 ± 0.02, P = 0.02 vs. control). Importantly, K^+ diet reversed this effect increasing kallikrein expression (2.5 ± 0.2 vs. 1.0 ± 0.3, P = 0.0031).

Expression of Chymase and Cathepsin G During High Potassium Intake in Normotensive and in Ang II-Dependent Hypertensive Rats

Since it has been described that the kidney expresses alternative Ang II-producing enzymes such as chymase and cathepsin G, we evaluated protein levels of these two enzymes by immunoblot (**Figure 7A**) upon Ang II and K^+ treatments. We did not detect changes in protein levels by immunoblots.

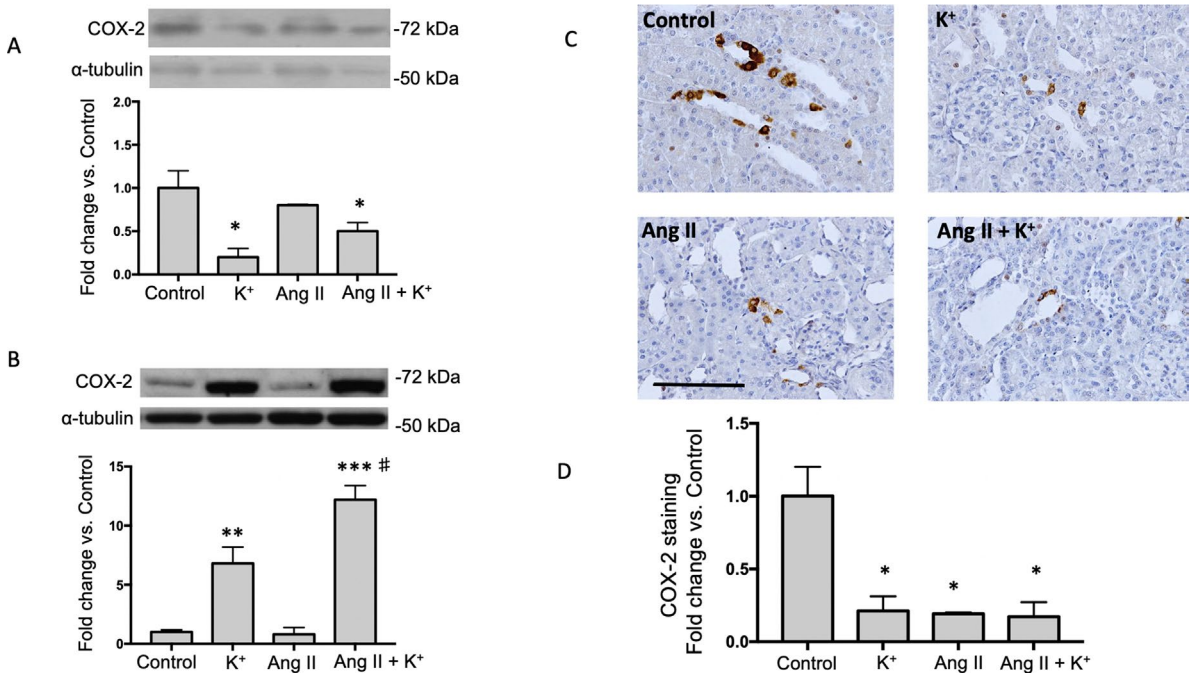

FIGURE 5 | COX-2 is induced in the renal medulla of non-infused and Ang II infused rats supplemented with high K^+ diet but not in cortex. Representative immunoblot and densitometric analysis showing fold change vs. controls in cortex **(A)** and medulla **(B)**. Representative images of immunohistochemistry showing positive cells (brown color) for COX-2 in **(C) (D)** Quantification of stained areas in four representative fields for each section from six rats. Images were quantified by Simple PCI 6.0 software and the average values of stained areas were expressed as fold change of controls. *P < 0.05, **P < 0.01, ***P < 0.001 vs. control group (normal K^+ diet, sham operated); #P < 0.05 vs. Ang II group, n = 6. α-tubulin was used to correct variation in sample loading. Values are expressed as fold change of control group. Scale bar: 100 μm.

Immunohistochemistry images showed a few chymase positive cells and did not show significant changes in cell number or intensity (data not shown) (**Figure 7B**).

DISCUSSION

In this study we demonstrated that Ang II-dependent blood pressure responses at day 14 of treatment are partially prevented by dietary supplementation of K^+. We also showed that Ang II-dependent induction of CD renin, AGT and ACE was prevented by K^+ diet. Dietary K^+ supplementation also increased the expression of ACE2 and COX-2 in the renal medulla. This was paralleled with enhanced K^+ excretion. Pressure diuresis observed in Ang II-infused rats was slightly but non-significantly increased by high K^+ diet. Similarly, urine flow was augmented in normotensive (non-infused) and in Ang II-dependent hypertensive rats with high K^+ diet. These findings indicate that the reciprocal changes caused by high K^+ in intrarenal RAS and in medullary COX-2 and ACE2 promote vasodilation and diuretic effects, buffering the effects of Ang II.

Induction of intrarenal RAS in the Ang II-dependent hypertensive model has been widely reported in rats (Yang and Xu, 2017). Expression of AGT has been described in proximal tubules and its synthesis and secretion to luminal fluid is stimulated by chronic Ang II *via* the AT1R mechanism (Kobori et al., 2001). AGT can be detected in urine samples of hypertensive humans (Kobori et al., 2009) and in animal models of hypertension (Gonzalez-Villalobos et al., 2008) and renal disease (Kobori et al., 2003). AGT is the only source for renin enzyme to produce Ang I (Chaszczewska-Markowska et al., 2016). Cumulated evidence demonstrates that renin expression is enhanced in the CD during chronic Ang II infusion (Prieto-Carrasquero et al., 2004) and diabetic disease (Kang et al., 2008). CD renin is regulated by activation of AT1R and independently of blood pressure (Prieto-Carrasquero et al., 2008). Its cardinal role in the development of hypertension is evidenced by the increases in blood pressure in mice with renin overexpression (Ramkumar et al., 2013). Expression of ACE is induced along with the induction of renin synthesis in the CD during Ang II-dependent hypertension (Gonzalez-Villalobos et al., 2010). Knockout models of renal ACE, have demonstrated the absence of hypertension in response to chronic Ang II infusions (Gonzalez-Villalobos et al., 2013). Thus, intrarenal Ang II formation stimulated by the induction of AGT, renin and ACE may contribute to sodium and water retention and high blood pressure. Here we show that induction of AGT and collecting duct renin from Ang II infused rats is prevented by K^+ dietary supplementation. Although AGT was still high in the cortex the induction was less evident (**Figure 2**). It is possible that the reduced expression of intrarenal RAS components may impact the availability of the distal nephron to produce intratubular Ang II. Ang II causes aldosterone release from adrenals and mineralocorticoid receptor (MR)-mediated Na^+ reabsorption through ENaC in the CD (Beutler et al., 2003). In addition, AT1R in the apical side of the CD cells

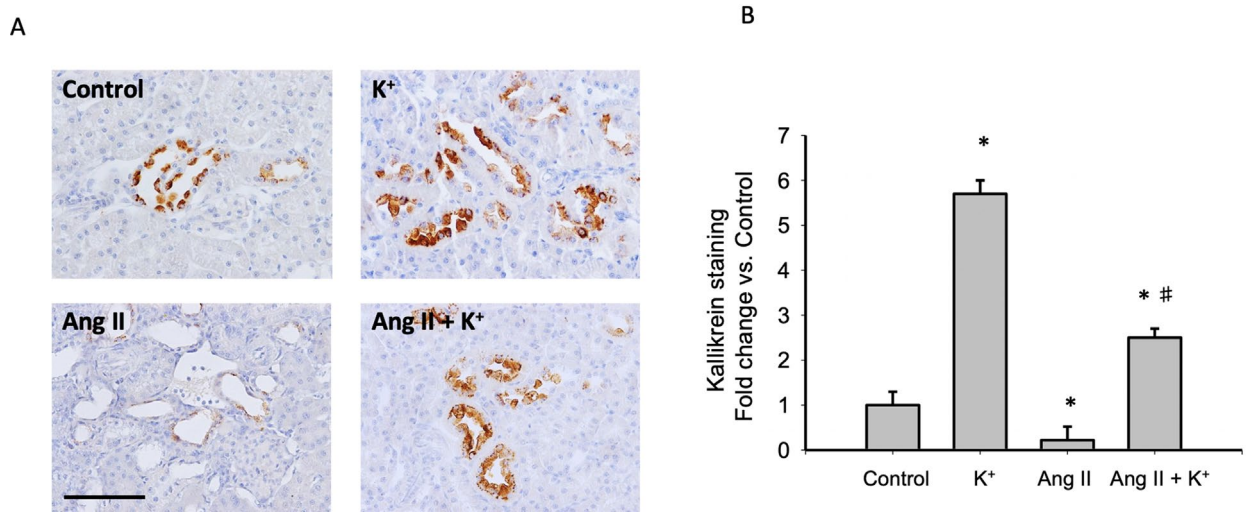

FIGURE 6 | (A) Representative images of immunohistochemistry showing positive cells (brown color) for kallikrein protein. **(B)** Quantification of stained areas in four representative fields for each section from six rats. Images were quantified by Simple PCI 6.0 software and the average values of stained areas were expressed as fold change of controls. *P < 0.05 vs. control group (normal K+ diet, sham operated); #P < 0.05 vs. Ang II group, n = 6. Scale bar: 100 μm.

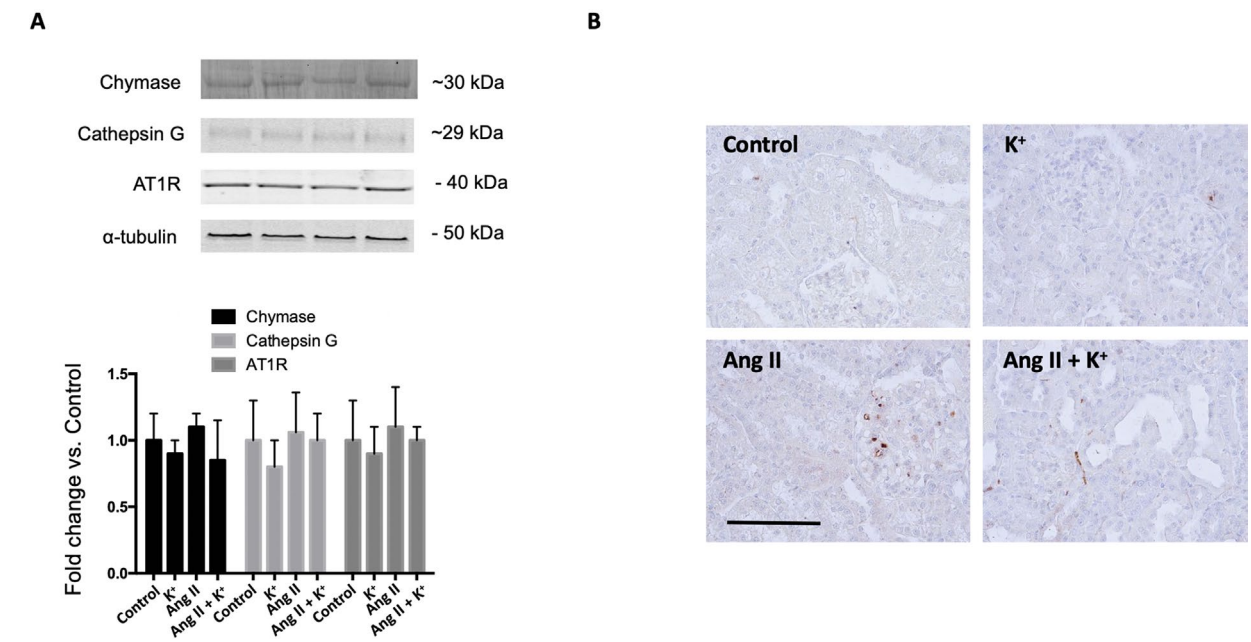

FIGURE 7 | (A) Expression of chymase, cathepsin G and the angiotensin II type 1 receptor (AT1) during high potassium intake in normotensive and Ang II-dependent hypertensive rats assessed by immunoblot. No significant changes were observed in protein abundances. **(B)** Immunohistochemical detection of chymase. Scale bar: 100 μm, n = 6.

(Harrison-Bernard et al., 2002) directly stimulates the activity of ENaC leading to increased sodium reabsorption (Mamenko et al., 2013). Furthermore, treatment with amiloride (ENaC inhibitor) reduces blood pressure in Ang II infused rats (Gonzalez et al., 2011). This suggests a major role of luminal Ang II and apical AT1R in the stimulation of apical sodium transport in connecting tubules and in the CD. Indeed, it has been shown that K^+ decreased the abundance of NCC expression (Wang et al., 2018). Van der Lubbe et al. showed that K^+-induced natriuresis was accompanied by inhibition of the Na^+-Cl^- cotransporter (van der Lubbe et al., 2013). Although we did not explore the exact mechanisms by which K^+ diet decreases intrarenal RAS components, we believe that the absence of intraluminal Ang II formation contributes to lower Ang II-dependent activation of distal sodium transporters. Proteinases

such as chymase, and cathepsin G, have been demonstrated to be an alternative pathway for Ang II formation in renal and in heart tissues (DellÌtalia et al., 2018). We observed that the expression of chymase was slightly but not significantly reduced by K^+ diet or by Ang II infusion. The same pattern was observed for cathepsin G (**Figure 7A**). We were unable to detect cathepsin G by using immunohistochemistry. We detected a few cells stained for chymase, mostly in interstitial cells; however, no significant changes in the intensity of labeling or cell number was evidenced (**Figure 7B**). An increase in Ang II levels might not lead to a significant effect if the AT1 receptor is already fully expressed. Our results show a positive correlation between renin and AGT expression which are supported by the atlas of tissue RAS created by (Nehme et al. 2015) This fact, along with the evidence of the high expression of AT1R in the kidneys (Nehme et al. 2019) may eventually lead to a bottleneck if the AT1 receptor is not altered. However, evidence shows that AT1 receptor expression is not modified by Ang II induced hypertension (Harrison et al. 1997). We did not find changes in AT1 receptor expression (**Figure 7A**); thus, we believe that changes in intratubular Ang II instead of changes in AT1 receptor levels are responsible for intratubular actions of Ang II.

Despite these observations, the natriuretic effect seen by the balance between Na^+ intake and excretion was only partially stimulated by K^+ diet. This was also similar to the pressure natriuretic effect observed in Ang II infused rats (**Figure 1B**). Dietary K^+ caused an increased K^+ excretion with a negative balance between K^+ intake and excretion, and Ang II infused animals did not show altered K^+ excretion. Interestingly, Ang II + K^+ group showed a significant K^+ excretion as compared to control group.

It has been shown that K^+ diet increased the expression of kallikrein, in the connecting tubule41. Kallikrein cleaves kininogen to form bradykinin, which in turn binds to bradykinin B2 receptor (Rodriguez et al. 2004). ACE inhibition also potentiates bradykinin effects (Kaplan et al. 2002), thus the decrease in ACE expression may explain the increase in the kinin-kallikrein system. Activation of the B2 receptor induces the synthesis of COX-2. Our findings demonstrate that K^+ diet induces the expression of kallikrein which is mainly expressed in connecting tubules (Kaplan et al. 2002) as well as COX-2 expression in the renal medulla of normotensive and Ang II-dependent hypertensive rats. COX-2 induction promotes synthesis of vasodilatory PGs, which may cross the interstitial tissue reaching intratubular fluid to decrease the activity and expression of

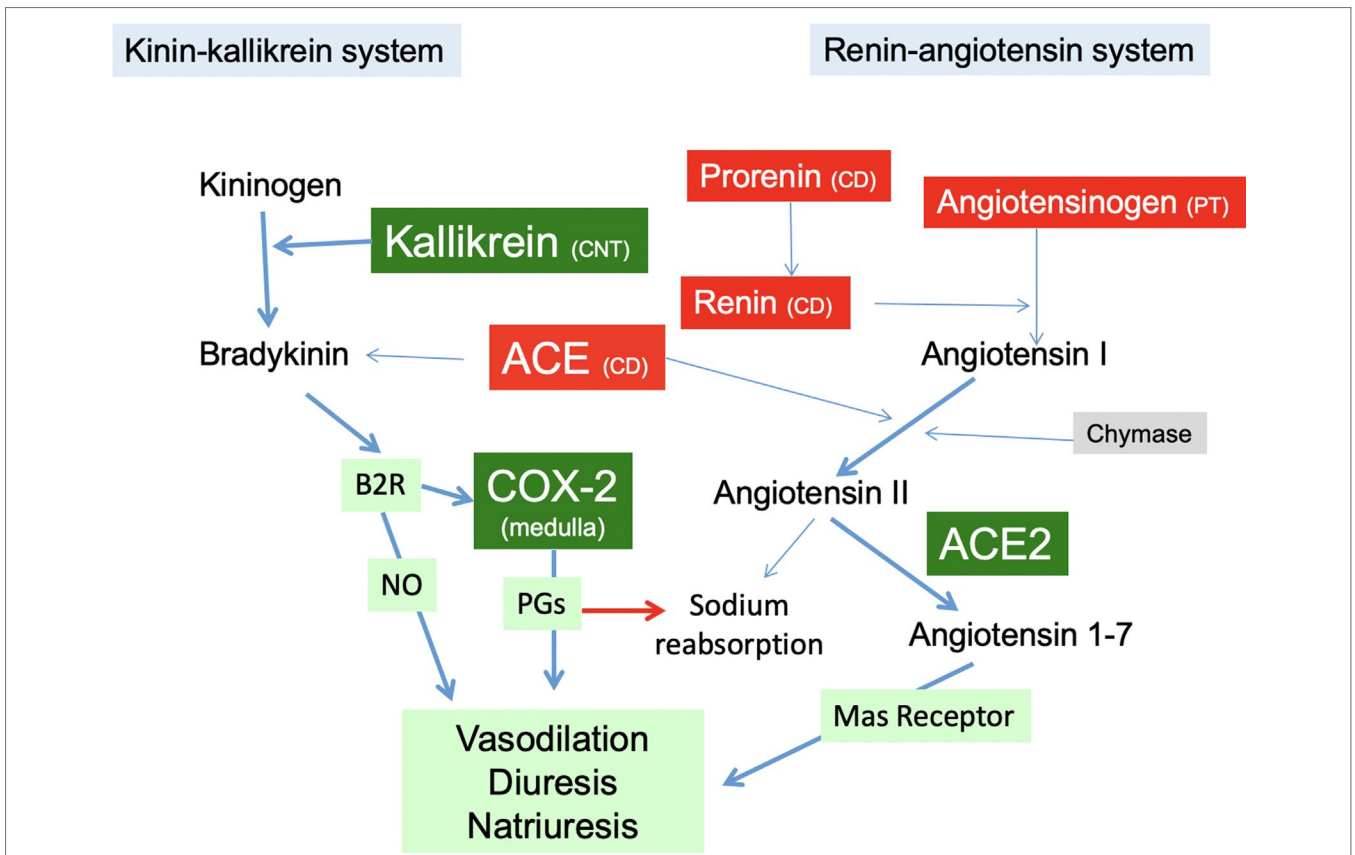

FIGURE 8 | The RAS in the kidney in Ang II-infused rats with high K^+ diet. Green boxes represent proteins induced by high K^+ intake in Ang II infused rats (kallikrein, COX-2, ACE2) promoting vasodilatory, diuretic and natriuretic actions through PGs. High K^+ diet impairs upregulation of the components of the intrarenal RAS (red boxes), reducing the capacity for intratubular Ang II formation. PT, proximal tubule; CD, collecting duct; CNT, connecting tubule; NO, nitric oxide; B2R, bradykinin B2 receptor; COX-2, cyclooxygenase-2; ACE, angiotensin converting enzyme.

ENaC (Gonzalez et al., 2009) thereby reducing sodium reabsorption and contributing to lower blood pressure (**Figure 8**).

A recent meta-analyses study of 22 randomized controlled trials in adults demonstrated that increased K^+ intake reduces systolic blood pressure (Aburto et al. 2013). Systematic review of the literature also showed that increased K^+ has no adverse effect on blood lipid concentrations, catecholamine concentrations, or renal function. Furthermore, higher K^+ intake lowers the risk of incident of stroke (Aburto et al. 2013). It is likely that the beneficial effects of high K^+ diet might be due to the modulation of the expression of the intrarenal RAS and the enhanced expression of peptides with vasodilator effects. Our data indicate that high K^+ diet causes reciprocal changes in the regulation of vasoactive hormones through the upregulation of natriuretic COX-2, ACE2 and by preventing the upregulation of intratubular/intrarenal RAS during Ang II-dependent hypertension.

DATA AVAILABILITY STATEMENT

The raw data supporting the conclusions of this manuscript will be made available by the authors, without undue reservation, to any qualified researcher.

ETHICS STATEMENT

The animal study was reviewed and approved by Animal Care and Use Committee of Pontificia Universidad Católica de Chile (Animal Welfare Assurance no. A5848-01) and conducted in accordance with the National Institutes of Health Guide for the Care and Use of Laboratory Animals.

AUTHOR CONTRIBUTIONS

AG and CV designed the experiments. CC and MG conducted most of the experiments, collected and analyzed the data. AG and CC wrote the manuscript, and CV contributed to its final revision.

FUNDING

This work was supported by: Proyecto de Financiamiento Basal, AFB 170005 and Fondo Nacional de Investigación Científica y Tecnológica FONDECYT 1130741 (CV) and 1191006 (AG).

ACKNOWLEDGMENTS

We would like to thank Maria Alcoholado for technical assistance.

SUPPLEMENTARY MATERIAL

The Supplementary Material for this article can be found online at: https://www.frontiersin.org/articles/10.3389/fphar.2019.01212/full#supplementary-material

REFERENCES

Aburto, N. J., Hanson S., Gutierrez H., Hooper L., Elliott P., Cappuccio, F. P., et al. (2013). Effect of increased potassium intake on cardiovascular risk factors and disease: systematic review and meta-analyses. *BMJ* 346, f1378. doi: 10.1136/bmj.f1378

Bader, M. (2013). ACE2, angiotensin-(1-7), and Mas: the other side of the coin. *Pflugers Arch.* 465, 79–85. doi: 10.1007/s00424-012-1120-0

Beutler, K. T., Masilamani S., Turban S., Nielsen J., Brooks H. L., Ageloff S., et al. (2003). Long-term regulation of ENaC expression in kidney by angiotensin II. *Hypertension* 41, 1143–1150. doi: 10.1161/01.HYP.0000066129.12106.E2

Chaszczewska-Markowska, M., Sagan, M., and Bogunia-Kubik, K. (2016). The renin-angiotensin-aldosterone system (RAAS) - physiology and molecular mechanisms of functioning. *Postepy Hig. Med. Dosw. (Online)* 70, 917–927. doi: 10.5604/17322693.1218180

DellÌtalia, L. J., Collawn, J. and Ferrario C. M. (2018) Multifunctional role of chymase in acute and chronic tissue injury and remodeling. *Circ. Res.* 19; 122 (2), 319–336.

Ferrario, C. M., and Varagic, J. (2010). The ANG-(1-7)/ACE2/mas axis in the regulation of nephron function. *Am. J. Physiol. Renal Physiol.* 298, F1297–F1305. doi: 10.1152/ajprenal.00110.2010

Figueroa, C. D., Caorsi, I., Subiabre, J., and Vio, C. P. (1984). Immunoreactive Kallikrein Localization in the Rat-Kidney - an Immuno-Electron-Microscopic Study. *J. Histochem. Cytochem.* 32, 117–121. doi: 10.1177/32.1.6558105

Geleijnse, J. M., Kok, F. J., and Grobbee, D. E. (2003). Blood pressure response to changes in sodium and potassium intake: a metaregression analysis of randomised trials. *J. Hum. Hypertens.* 17, 471–480. doi: 10.1038/sj.jhh.1001575

Gonzalez, A. A., Cespedes, C., Villanueva, S., Michea, L., and Vio, C. P. E. (2009). Prostanoid-1 receptor regulates renal medullary alpha ENaC in rats infused with angiotensin II. *Biochem. Bioph. Res. Co.* 389, 372–377. doi: 10.1016/j.bbrc.2009.08.157

Gonzalez, A. A., Liu, L., Lara, L. S., Seth, D. M., Navar, L. G., Prieto, M. C., et al. (2011). Angiotensin II Stimulates Renin in Inner Medullary Collecting Duct Cells *via* Protein Kinase C and Independent of Epithelial Sodium Channel and Mineralocorticoid Receptor Activity. *Hypertension* 57, 594–599. doi: 10.1161/HYPERTENSIONAHA.110.165902

Gonzalez-Villalobos, R. A., et al. (2013). The absence of intrarenal ACE protects against hypertension. *J. Clin. Invest.* 123, 2011–2023. doi: 10.1172/JCI65460

Gonzalez-Villalobos, R. A., Seth, D. M., Satou, R., Horton, H., Ohashi, N., Miyata, K., et al. (2008). Intrarenal angiotensin II and angiotensinogen augmentation in chronic angiotensin II-infused mice. *Am. J. Physiol. Renal* 295, F772–F779. doi: 10.1152/ajprenal.00019.2008

Gonzalez-Villalobos, R. A., Satou, R., Seth, D. M., Semprun-Prieto, L. C., Katsurada, A., Kobori, H., et al. (2009). Angiotensin-Converting Enzyme-Derived Angiotensin II Formation During Angiotensin II-Induced Hypertension. *Hypertension* 53, 351–355. doi: 10.1161/HYPERTENSIONAHA.108.124511

Gonzalez-Villalobos, R. A., Satou, R., Ohashi, N., Semprun-Prieto, L. C., Katsurada, A., Kim, C., et al. (2010). Intrarenal mouse renin-angiotensin system during ANG II-induced hypertension and ACE inhibition. *Am. J. Physiol. Renal* 298, F150–F157. doi: 10.1152/ajprenal.00477.2009

Harrison-Bernard, L. M., Navar, L. G., Ho, M. M., Vinson, G. P., and el-Dahr, S. S., (1997). Immunohistochemical localization of ANG II AT1 receptor in adult rat kidney using a monoclonal antibody. doi: 10.1152/ajprenal.1997.273.1.F170

Harrison-Bernard, L. M., Zhuo, J. L., Kobori, H., Ohishi, M., and Navar, L. G. (2002). Intrarenal AT(1) receptor and ACE binding in ANG II-induced

hypertensive rats. Am. J. Physiol. Renal 282, F19–F25. doi: 10.1152/ajprenal.0335.2000

Jung, S., Kim, M. K., Shin, J., Choi, B. Y., Lee, Y. H., Shin, D., et al. (2019). High sodium intake and sodium to potassium ratio may be linked to subsequent increase in vascular damage in adults aged 40 years and older: the Korean multi-rural communities cohort (MRCohort). *Eur. J. Nutr.* 58 (4), 1659-1671. doi: 10.1007/s00394-018-1712-3

Kang, J. J., Toma, I., Sipos, A., Meer, E. J., Vargas, S. L., Peti-Peterdi, J. et al. (2008). The collecting duct is the major source of prorenin in diabetes. *Hypertension* 51, 1597–1604. doi: 10.1161/hypertensionaha.107.107268

Kaplan, A. P., Joseph, K., and Silverberg, M. (2002). Pathways for bradykinin formation and inflammatory disease. *J. Allergy Clin. Immunol.* 109, 195–209. doi: 10.1067/mai.2002.121316

Kim, Y. H., Spencer, K. B., Beierwaltes, W. H., Everett, L. A., Green, E. D., Shin, W., et al. (2007). Reduced ENaC protein abundance contributes to the lower blood pressure observed in pendrin-null mice. *Am. J. Physiol. Renal Physiol.* 293, F1314–F1324. doi: 10.1152/ajprenal.00155.2007

Kobori, H., Harrison-Bernard, L. M., and Navar L. G. (2001). Enhancement of Angiotensinogen Expression in Angiotensin II–Dependent Hypertension. 37, 1329–1335. doi: 10.1161/01.HYP.37.5.1329

Kobori, H., Nishiyama, A., Harrison-Bernard, L. M., and Navar, L. G. (2003). Urinary angiotensinogen as an indicator of intrarenal angiotensin status in hypertension. *Hypertension* 41, 42–49. doi: 10.1161/01.HYP.0000050102.90932.CF

Kobori, H., Prieto-Carrasquero, M. C., Ozawa, Y., and Navar, L. G. (2004). AT1 receptor mediated augmentation of intrarenal angiotensinogen in angiotensin II-dependent hypertension. *Hypertension* 43, 1126–1132. doi: 10.1161/01.HYP.0000122875.91100.28

Kobori, H., AlperJr, A. B., Shenava, P., Katsurada, A., Saito, T., Ohashi, N., et al. (2009). Urinary Angiotensinogen as a Novel Biomarker of the Intrarenal Renin-Angiotensin System Status in Hypertensive Patients. *Hypertension* 53, 344–U407. doi: 10.1161/HYPERTENSIONAHA.108.123802

Liu, L., McCormack, M., Seth, D. M., Kobori, H., Navar, L. G., Prieto, M. C., et al. (2011). Increased renin excretion is associated with augmented urinary angiotensin II levels in chronic angiotensin II-infused hypertensive rats. *Am. J. Physiol. Renal* 301, F1195–F1201. doi: 10.1152/ajprenal.00339.2011

Mamenko, M., Zaika, O., Prieto, M. C., Jensen, V. B., Doris, P. A., Navar, L. G., et al. (2012). Angiotensin II Increases Activity of the Epithelial Na+ Channel (ENaC) in Distal Nephron Additively to Aldosterone. *J. Biol. Chem.* 287, 660–671. doi: 10.1074/jbc.M111.298919

Mamenko, M., et al. (2013). Chronic Angiotensin II Infusion Drives Extensive Aldosterone-Independent Epithelial Na+ Channel Activation. *Hypertension* 62, 1111–1122. doi: 10.1161/HYPERTENSIONAHA.113.01797

Masilamani, S., Kim, G. H., Mitchell, C., Wade, J. B., and Knepper, M. A. (1999). Aldosterone-mediated regulation of ENaC alpha, beta, and gamma subunit proteins in rat kidney. *J. Clin. Invest.* 104, R19–R23. doi: 10.1172/JCI7840

Navar, L. G., Mitchell, K. D., Harrison-Bernard, L. M., Kobori, H., and Nishiyama, A. (2001). Intrarenal angiotensin II levels in normal and hypertensive states. *J. Renin-Angio-Aldo S.* 2, S176–S184. doi: 10.1177/14703203010020013001

Navar, L. G., Kobori, H., Prieto, M. C., and Gonzalez-Villalobos, R. A. (2011). Intratubular Renin-Angiotensin System in Hypertension. *Hypertension* 57, 355–362. doi: 10.1161/HYPERTENSIONAHA.110.163519

Nehme, A., Cerutti, C., Dhaouadi, N., Gustin, M. P., Courand, P. Y., Zibara, K., et al. (2015). Atlas of tissue renin-angiotensin-aldosterone system in human: A transcriptomic meta-analysis. *Sci. Rep.* 5, 10035. 1–14. doi: 10.1038/srep10035

Nehme, A., Zouein, F. A., Zayeri, Z. D., and Zibara, K. (2019). An Update on the Tissue Renin Angiotensin System and Its Role in Physiology and Pathology. *J. Cardiovasc. Dev. Dis.* 6. doi: 10.3390/jcdd6020014

Noubiap, J. J., Bigna, J. J., and Nansseu, J. R. (2015). Low sodium and high potassium intake for cardiovascular prevention: evidence revisited with emphasis on challenges in sub-Saharan Africa. *J. Clin. Hypertens. (Greenwich)* 17, 81–83. doi: 10.1111/jch.12439

Prieto-Carrasquero, M. C., Harrison-Bernard, L. M., Kobori, H., Ozawa, Y., Hering-Smith, K. S., Hamm, L. L., et al. (2004). Enhancement of collecting duct renin in angiotensin II-dependent hypertensive rats. *Hypertension* 44, 223–229. doi: 10.1161/01.HYP.0000135678.20725.54

Prieto-Carrasquero, M. C., Botros, F. T., Pagan, J., Kobori, H., Seth, D. M., Casarini, D. E., et al. (2008). Collecting duct renin is upregulated in both kidneys of 2-kidney, 1-clip Goldblatt hypertensive rats. *Hypertension* 51, 1590–1596. doi: 10.1161/HYPERTENSIONAHA.108.110916

Ramkumar, N., Ying, J., Stuart, D., and Kohan, D. E. (2013). Overexpression of Renin in the Collecting Duct Causes Elevated Blood Pressure. *Am. J. Hypertens.* 26, 965–972. doi: 10.1093/ajh/hpt071

Rodrigues, S. L., Baldo, M. P., Machado, R. C., Forechi, L., Molina, M. C., Mill, J. G., et al. (2014). High potassium intake blunts the effect of elevated sodium intake on blood pressure levels. *J. Am. Soc. Hypertens.* 8, 232–238. doi: 10.1016/j.jash.2014.01.001

Rodriguez, J. A., Vio, C. P., Pedraza, P. L., McGiff, J. C., and Ferreri, N. R. (2004). Bradykinin regulates cyclooxygenase-2 in rat renal thick ascending limb cells. *Hypertension* 44, 230–235. doi: 10.1161/01.HYP.0000136751.04336.e9

Susic, D., Frohlich, E., Kobori, H., Shao, W., Seth, D. M., Navar, L. G., et al. (2009). Augmented Tubular Renin-Angiotensin System in Salt-Induced Renal Injury and Prevention by Angiotensin II Receptor Blockade. *Hypertension* 54, E48–E49. doi: 10.1097/HJH.0b013e3283440683

van der Lubbe, N., Moes, A. D., Rosenbaek, L. L., Schoep, S., Meima, M. E., Danser, A. H., et al. (2013). K+-induced natriuresis is preserved during Na+ depletion and accompanied by inhibition of the Na+-Cl- cotransporter. *Am. J. Physiol. Renal* 305, F1177–F1188. doi: 10.1152/ajprenal.00201.2013

Villanueva, S., Cespedes, C., Gonzalez, A. A., Roessler, E., and Vio, C. P. (2008). Inhibition of bFGF-receptor type 2 increases kidney damage and suppresses nephrogenic protein expression after ischemic acute renal failure. *Am. J. Physiol. Reg. I* 294, R819–R828. doi: 10.1152/ajpregu.00273.2007

Vio, C. P., and Figueroa, C. D. (1987). Evidence for a stimulatory effect of high potassium diet on renal kallikrein. *Kidney Int.* 31, 1327–1334. doi: 10.1038/ki.1987.146

Vonthun, A. M., Vari, R. C., Eldahr, S. S., and Navar, L. G. (1994). Augmentation of Intrarenal Angiotensin-Ii Levels by Chronic Angiotensin-Ii Infusion. *Am. J. Physiol.* 266, F120–F128. doi: 10.1152/ajprenal.1994.266.1.F120

Wang, M. X., Cuevas, C. A., Su, X. T., Wu, P., Gao, Z. X., Lin, D. H., et al. (2018). Potassium intake modulates the thiazide-sensitive sodium-chloride cotransporter (NCC) activity *via the* Kir4.1 potassium channel. *Kidney Int.* 93, 893–902. doi: 10.1016/j.kint.2017.10.023

Yang, T., and Xu, C. (2017). Physiology and Pathophysiology of the Intrarenal Renin-Angiotensin System: An Update. *J. Am. Soc. Nephrol.* 28, 1040–1049. doi: 10.1681/ASN.2016070734

Zaika, O., Mamenko, M., Staruschenko, A., and Pochynyuk, O. (2013). Direct Activation of ENaC by Angiotensin II: Recent Advances and New Insights. *Curr. Hypertens. Rep.* 15, 17–24. doi: 10.1007/s11906-012-0316-1

Conflict of Interest: The authors declare that the research was conducted in the absence of any commercial or financial relationships that could be construed as a potential conflict of interest.

frontiers in Pharmacology

ORIGINAL RESEARCH
published: 22 October 2019
doi: 10.3389/fphar.2019.01201

Lithraea caustic (Litre) Extract Promotes an Antitumor Response Against B16 Melanoma

*Claudia Robles-Planells[1,2†], Sofia A. Michelson[1†], Javier Mena[1], Daniela Escrig[1], Juan L. Rojas[3], Giselle Sanchez-Guerrero[1], Ronny Hernández[1], Carlos Barrera-Avalos[1,2], Leonel E. Rojo[1,2], Daniela Sauma[4], Alexis M. Kalergis[5], Mónica Imarai[1,2], Ricardo Fernández[6], Carolina A. Robles[1], Elías Leiva-Salcedo[1], Rocio Santander[7], Alejandro Escobar[8] and Claudio Acuña-Castillo[1,2]**

[1] Departamento de Biología, Facultad de Química y Biología, Universidad de Santiago de Chile, Santiago, Chile, [2] Centro de Biotecnología Acuícola, Universidad de Santiago de Chile, Santiago, Chile, [3] Escuela de Medicina, Facultad de Ciencias Médicas, Universidad de Santiago de Chile, Santiago, Chile [4] Departamento de Biología, Facultad de Ciencias, Universidad de Chile, Santiago, Chile, [5] Millennium Institute Immunology and Immunotherapy, FOCIS Center of Excellence, Facultad de Ciencias Biológicas, Facultad de Medicina, Pontificia Universidad Católica de Chile, Santiago, Chile, [6] Departamento de Salud, Universidad de Los Lagos, Osorno, Chile, [7] Departamento de Ciencias del Ambiente, Facultad de Química y Biología, Universidad de Santiago de Chile, Santiago, Chile, [8] Laboratorio Biología Celular y Molecular, Instituto de Investigación en Ciencias Odontológicas, Facultad de Odontología, Universidad de Chile, Santiago, Chile

OPEN ACCESS

Edited by:
Javier A. Bravo, Pontificia Universidad Católica de Valparaíso, Chile

Reviewed by:
Walter J. Storkus, University of Pittsburgh, United States
Shankar Munusamy, Drake University, United States

***Correspondence:**
Claudio Acuña-Castillo
claudio.acuna@usach.cl

†These authors have contributed equally to this work

Specialty section:
This article was submitted to Translational Pharmacology, a section of the journal Frontiers in Pharmacology

Received: *27 December 2018*
Accepted: *17 September 2019*
Published: *22 October 2019*

Citation:
Robles-Planells C, Michelson SA, Mena J, Escrig D, Rojas JL, Sanchez-Guerrero G, Hernández R, Barrera-Avalos C, Rojo LE, Sauma D, Kalergis AM, Imarai M, Fernández R, Robles CA, Leiva-Salcedo E, Santander R, Escobar A and Acuña-Castillo C (2019) Lithraea caustic (Litre) Extract Promotes an Antitumor Response Against B16 Melanoma. Front. Pharmacol. 10:1201. doi: 10.3389/fphar.2019.01201

Melanoma immunotherapy, specifically the autotransplant of dendritic cells charged with tumors antigens, has shown promising results in clinical trials. The positive clinical effects of this therapy have been associated to increased Th17 response and delayed-type hypersensitivity (DTH) against to tumor antigens. Some synthetic compounds, such as diphenylcyclopropenone (DPCP), are capable of triggering a DTH response in cutaneous malignancies and also to induce clinically relevant effects against melanoma. In this work, we evaluated Litre extract (LExT), a standardized extract of a Chilean stinging plant, *Lithraea caustic* (Litre). As Litre plant is known to induce DTH, we used a murine B16 melanoma model to compare the topical and intratumor efficacy of LExT with synthetic DTH inducers (DPCP and 2,4-dinitrochlorobenzene [DNCB]). LExt contained mainly long chain catechols and sesquiterpenes. The intratumor injection of LExT induced a significant delay in tumor growth, similarly topical treatment of an established tumor with 0.1% LExT ointment induced a growth delay and even tumor regression in 15% of treated animals. No significant changes were observed on the T-cell populations associated to LExT treatment, and neither DNCB nor DPCP were capable to induce none of the LExT-induced antitumoral effects. Interestingly, our results indicate that LExT induces an antitumor response against melanoma in a mouse model and could bring a new –and affordable- treatment for melanoma in humans.

Keywords: cancer, topic treatment, *Lithraea caustic*, DTH response, immunotherapy

INTRODUCTION

Melanoma is a type of skin cancer derived from melanocytes and is the most lethal form of malignant skin tumors. Meanwhile, melanoma shows a lower-population prevalence; its incidence has doubled in the last decade (Matthews et al., 2017); this increase has a significant impact on public health, considering that conventional therapies have limited efficacy in advanced stages of the

disease. Interestingly, the treatments based on immunotherapy have shown promising results in contrast to conventional chemotherapeutic approaches (George et al., 2016). The use of high doses of IL-2 was the first anti-cancer immunotherapeutic approach, and while its use has been capable of inducing tumor remissions in patients with advanced melanoma, its effect is limited to a small fraction of patients and also associated with elevated cytotoxicity (Smith et al., 2009).

On the other hand, it has been reported that blocking antibodies against specific targets, such as the Programmed Cell Death protein 1 (PD-1) and/or against cytotoxic T-lymphocyte antigen 4 (CTLA-4), promote tumor rejection, suggesting therapeutic alternatives against this type of cancer(Curran et al., 2010). Another promising immunotherapy is the use of auto-transplant of autologous dendritic cells (DCs), which are generated from precursors cells present on peripheral blood monocytes. DCs need to be loaded with tumor antigens and then activated *in vitro*, before being auto-transplanted to the cancer patients. Previous studies on the vaccination of melanoma patients with melanoma peptides (Nestle et al., 1998; Tel et al., 2013; Schreibelt et al., 2015) or DCs cell lysate (Escobar et al., 2005; Durán-Aniotz et al., 2013; Lo et al., 2019) provided evidence of significant clinical and immunological anti-tumor responses at cancer stages III and IV. These approaches increased short-term survival and progression-free survival related to a functional tumor-specific T-cell response, with a predominant T cytotoxic(Nestle et al., 1998; Tel et al., 2013; Schreibelt et al., 2015) and helper profiles (IFNγ, Th1, and IL-17, Th17 cells) (Escobar et al., 2005; Durán-Aniotz et al., 2013; Lo et al., 2019) and a marked reduction in the proportion of CD4 transforming growth factor (TGF) β+ regulatory T cells(Lo et al., 2019). Interestingly, these immunological profiles were similar to those of delayed-type hypersensitivity response (DTH)-positive reactions against the melanoma peptides (Nestle et al., 1998) or cell lysates (Escobar et al., 2005; Durán-Aniotz et al., 2013; Lo et al., 2019), suggesting a potential role of DTH in an antitumor response against melanoma tumors.

DTH is an overreaction against a specific antigen, and it is executed in two phases. First, the sensitization phase, in which the primary contact with the antigen occurs followed by the generation of memory T cells, and second, the effector phase, in which a subsequent second-time exposure to the antigen induces macrophages attraction to the contact zone to further trigger innate and adaptive immune responses (Kobayashi et al., 2001). Allergic contact dermatitis (ACD) corresponds to a type of delayed-type hypersensitivity response to small reactive molecules (haptens), which triggers skin inflammation mediated by stimulated T cells (Nosbaum et al., 2009). ACD has been used as a tool to develop immunotherapy against cutaneous warts, based on two molecules, 2,4-dinitrochlorobenzene (DNCB) and diphenylcyclopropenone (diphencyprone; DPCP) (Holzer et al., 2006). These latter compounds have been successfully tested in the treatment of recalcitrant viral warts, alopecia, basilioma, and spinocellular carcinoma (Buckley and du Vivier, 1999). In view that DTH induction is a crucial process in those patients exhibiting an antitumor response, the induction of DTH against different forms of cancers has been clinically evaluated since 1970. As a result, DNCB has been successfully used in the treatment of cutaneous cancerous lesions, including melanoma, in which DNCB showed efficacy in reverting and decreasing metastasis (Berd et al., 2001; Von Nida and Quirk, 2003). Recent studies demonstrated that treatments with DPCP produce a inhibition of melanoma tumor growth (Damian et al., 2009), suggesting its use as a feasible option to treat melanoma cutaneous lesions ineligible/refractory to surgery (Yeung et al., 2017). There are a variety of molecules, present in insect saliva, nickel, latex, and natural compounds of plants, which have been associated to DTH responses in humans, with a high prevalence on ACD induction (Erkes and Selvan, 2014). For instance, the natural oil from the North American plant poison ivy, poison oak or poison sumac are potent DTH inductors and have been suggested to affect between 60% and 80% of the exposed population. Unfortunately, 10% to 20% of these cases display severe, dangerous responses in exposed patients. However, despite the known potential to induce strong DTH, these type molecules have limited evidence as a potential treatment against skin malignancies (Baldwin et al., 1982; Novick and Bosniak, 1986). Therefore, basic and clinical research on new DTH-inducing compounds against melanoma is interesting and newfangled.

Plants associated with DTH response produce stinging molecules from the urushiols family. For instance, *Lithraea caustica* (Litre) is an endemic Chilean tree distributed from Coquimbo (Latitude 29°57′S) to Cautin (Latitude 39°38′S) which produces high levels of an urushiol-type compound called litreol. The organics extracts of this tree induce a potent DTH response, and its direct application on cultured tumor cells induces cell death (Kalergis et al., 1997; Russo et al., 2009). However, its effect against tumors *in vivo* has not yet been evaluated. In the present study we evaluated the antitumor effect of Litre extract (LExT), a proprietary LExT of *L. caustica*. For this this aim, we used a B16 murine melanoma model. The antitumor effect of LExT was compared with those of DNCB and DPCP, two compounds previously used in human skin malignancies. LExT induced a marked delay in the growth of melanoma tumors. The antitumor effect of LExT was not associated with specific changes on T-cell infiltration, but with an increase in inflammatory damage at late stages of tumor growth. This effect of LExT is highly relevant considering that neither DNCB nor DPCP are capable of inducing a potent antitumor response in mice. The present study is, to our knowledge, the first report describing the effects of a topical formulation based on LExT as a treatment against melanoma. Given our results, we suggest that LExT could be further studied as a topic immunotherapy against melanoma in humans.

Abbreviations: CD, Cluster of differentiation; FOXp3, Forkhead box p3; Tbet, T-box expressed in T-cells; RORγ(t), RAR-related orphan receptor gamma; DPCP, Diphenylcyclopropenone; DNCB, Dinitrochlorobencene; LexT, Litre Extract; DTH, Delayed-type hypersensitivity; Th, Lymphocyte T helper; CTLA, Cytotoxic T Lymphocyte-Associated; APC, Antigen presenting cell; DC, Dendritic cell; ACD, Allergy contact dermatitis.

METHODS

Tumor Cell Line Culture and Animals

Murine melanoma B16 cells were cultured in DMEM (Gibco) supplemented with 10% fetal bovine serum (FBS) (Invitrogen,

Grand Island, NY) and incubated at 37°C, 5% CO_2. Six-to-eight-weeks old C57BL/6 ($H2^b$) mice were obtained from the Universidad de Santiago de Chile animal facility. Mice were fed *ad libitum*, with a 12/12-h light/dark cycle. All procedures were conducted in accord to guidelines on the recognition of pain, distress and discomfort in experimental animals described by Morton and Griffiths, except for temperature evaluation (Morton and Griffiths, 1985). Protocols were reviewed and approved by the Ethics Committee of the Universidad de Santiago de Chile. LExT was prepared by organic extraction. Briefly, fresh leaves of *L. caustica* were collected and dried at room temperature by seven days. Once dried, 40 g of leaves were mixed with 1-L petroleum ether for 20 min. After filtration, the solvent was concentrated in a rotary evaporator under vacuum until complete solvent evaporation, the extract was then recovered, and the purity was evaluated by layer chromatography using a mobile phase composed of hexane/ethyl acetate (95:5). All the reagents used were analytical grade from Merck Co.

Sensitization and Treatment With DPCP, DNCB, and Lext

The effect of topical treatment with LExT was evaluated in mice bearing tumor previously sensitized. To do so, mice were shaved in the dorsal area and sensitized by skin application with vehicle or for each compound independently (20 µl of DPCP 2% in acetone, 20 µl of DNCB 2% in acetone or an ointment containing 0.1% LExT). Sensitization was done at 1- to 2-cm away from area where the tumor was later injected. Then, 3 days after, mice were subcutaneously injected in the lumbar zone with 100 µl of 2×10^6 tumor cells/ml in PBS, with a tumor cell suspension obtained by trypsinization from cells cultured at 80% confluence. Once the tumor was detectable (0.3 mm^3 approximately), animals were treated with the same ointment (0.1% DPCP or 0.1% DNCB or 0.1% LExT) or vehicle every other day. The effect of LExT as an intratumor treatment was also evaluated to determine the effects that mice were sensitized and then injected with tumor cells, under the same conditions aforementioned. Once a volume of approximately 2 mm^3 has been reached, one injected dose of 50 ul of excipient or 0.1% LExT was applied to each tumor. In all cases, tumor emergence and size measurements were checked daily with a caliper. The tumor volume (mm^3) was calculated by measuring tumor diameter with a caliper and using the expression for calculating the hemisphere volume, $V(\mathrm{mm}^3) = \frac{1}{12} \times \pi \times d^3$, where r = tumor radius; d = tumor diameter. The control group was not sensitized (non-treated). For the treatment, the mice were sensitized with an ointment containing 0.1% LExT under one armpit.

T-Cell Population Analysis

For both treatment protocols, the end-point criterion was when the tumor volume reached 250 mm^3 or a maximum period of 60 days without tumor. Afterward, mice were sacrificed by cervical dislocation, and the spleen and the tumor were removed. Spleen was disaggregated using a stainless-steel mesh (100 µm), erythrocytes were removed by differential lysis using an ACK buffer (NH_4Cl 155 mM, $KHCO_3$ 10 mM, Na_2EDTA 1 mM, pH 7.3) with gentle agitation for 5 min (Leiva-Salcedo et al., 2011), then centrifuged at 1200*g* for 10 min and discarded the supernatant. In C57BL/6 wild-type mice, splenocytes were suspended at 2×10^6 cells/ml in 1 ml of cold blocking buffer (2% FBS in PBS, IF buffer) and incubated at 4°C per 30 min. Cells were stained with antibodies against the cell surface markers CD4, CD8, and CD25, with anti-mouse CD4-FITC (eBioscience), anti-mouse CD8-PE (eBioscience), and anti-mouse CD25-PE (eBioscience), respectively. Then resuspended in a fixation/permeabilization solution (Fix/Perm; eBioscience) and incubated with anti-Foxp3-PerCP (eBioscience) antibody for Treg population, anti-human/mouse RORγ(t)-PE (eBioscience) antibody for Th17 population and anti-human/mouse T-bet, PerCP-Cy5.5 (eBioscience) antibody for Th1 population, simultaneously to anti-CD4-FITC antibody labeling (eBioscience, USA). All samples were analyzed by flow cytometry using a BD Accuri C6 cytometer (BD Bioscience, San Jose, CA), and data were analyzed by FlowJo 7.6.1 software (Tree Star, Inc.). For details on these methods, please see Morales et al. (2017).

Histopathological Procedures

Tumors were removed and fixed in 10% buffered formalin for 24 h and then dehydrated with an increasing sequential concentration of ethanol (Histoprocesser, Leica ASP300). Then tumors were included in paraffin and cut at 5-µm thick with a rotatory microtome (Leica RM 2235). The samples were stained with hematoxylin-eosin (HE) using a tissue stainer (Leica ST5020). Histological samples were observed in a light microscope (Olympus CX41) coupled with a digital camera and using an achromatic wide field objective. Images were acquired at 4×, 10×, 40×, and 100×. Ten fields were examined per sample to evaluate necrosis, hemorrhage, inflammatory infiltrate, vascularization, and the level of tissue perfusion (expressed as the number of blood vessels). In all samples, we defined absence (−), low (+), high (++), and extremely high level (+++). The levels of necrosis indicate the destruction of the neoplastic cells in response to a direct cytotoxic action mediated by the inflammatory infiltration. Neoplastic cells viability was expressed as melanin levels (i.e., low melanin, low cell viability). The less populated tissue areas containing a high accumulation of cell debris were defined as necrosis. The hemorrhage was defined as the interstitial tissue areas with erythrocytes extravasation. The inflammatory infiltration was characterized by the presence of leucocytes, monocytes, and polymorph nuclear cells. The vascularization was defined as the number of capillary vessels present in the samples. Tumor cell viability was determined by the intensity of nuclear chromaticism, the presence of defined cell limits, and melanin production.

Chemical Analysis

A Thermo Scientific GC–MS system (GC: model: Trace 1300 and MS: model TSQ8000Evo) was used to analyze the sample. The separation was performed on a 60 m× 0.25 mm internal diameter fused silica capillary column coated with 0.25-µm film DB-5MS. The injector and the detector temperatures were, respectively, 200°C and 250°C. Oven temperature was held at 40°C for 5 min,

then programmed from 40°C to 300°C at 5°C/min and finally maintained at 300°C for 90 min. The mode used was splitless injection; helium was used as carrier gas; and flow rate was 1.3 ml/min. Mass spectra were recorded over a range of 40- to 400 atomic mass units at 0.2 s/scan. Solvent cut time was 11 min. Ionization energy was 70 eV. The chemical composition of the oil was identified by comparing its spectra with those of a NIST14 library and confirmed by contrasting their retention indices with data published in other studies.

Statistics

Tumor onset was ere analyzed using Kaplan–Meir curves and the log-rank test. Tumor-onset growth and size were analyzed by Kruskal–Wallis one-way ANOVA, two-way ANOVA followed by the Sidak post-test, and linear regression fitting and comparison. Th1, Th17, and Treg subpopulations were analyzed by the Mann–Whitney test. Analyses and graphs were performed using GraphPad Prism 5.01 software. Results are expressed as means ± standard error of means (SEMs). Statistical differences were considered significant when $p < 0.05$.

RESULTS

The use of epifocal DTH inductors against unresectable cutaneous melanoma lesions has reached clinical relevance, as they are efficacious chemotherapies for the type of malignancies. In this work, we evaluated the effect of LExT, an urushiols-containing extract from Litre described has a potent DTH inducer on a mouse (López et al., 1998), in a model of melanoma. Catechol analysis was performed as described elsewhere (Urzúa et al, 2011) and the results are shown in **Table 1**. Our first approach was to evaluate whether LExT induces *in vivo* antitumor response. For this purpose, after a sensibilization phase, we intratumorally applied either vehicle or LExT to animals when the tumor size reached 2 mm^3 average (**Figure 1A**), which normally occurred between days 10 and 13 after the injection of tumor B16 cells (**Figure 1B**). We observed that it took 4 days for the mice intratumorally injected with a vehicle to show significant tumor growth, and maximal tumor volume was reached at day 9 after vehicle treatment (**Figure 1C**). Whereas in the LExT-treated animals, it took 8 days after treatment to reach significant tumor growth, and the maximal volume was reached at day 15 after LExT treatment. The average tumor volume in LExT-treated animals was significantly lower than that of vehicle-treated counterparts at day 5 after challenge (**Figure 1C**). These data demonstrated the robust inhibitory effect of LExT on tumor development. Our next aim was to evaluate whether the epifocal application of LExT would induce similar results as the intratumor injected LExT therapy (**Figure 2A**), because epifocal therapies are significantly less toxic than systemic therapies. Animals were challenged with alive tumor cells, once the tumor was established, the animals received topical treatment with either placebo or 0.1% LExT ointment every other day (**Figure 2A**). Tumors were detectable between 8 and 17 days after tumor cells challenge, then the animals were grouped to avoid differences in tumor size among both groups (Control and LExT-treated mice). Placebo-treated animals showed an increase in the tumor volume from day 5, reaching a maximum tumor volume at day 12 (**Figure 2B**). Similar to intratumor treatment the epifocal treatment induced a delay in the time to maximal tumor growth, as in the Control group it took 11 to 12 days to reach the maximal volume,

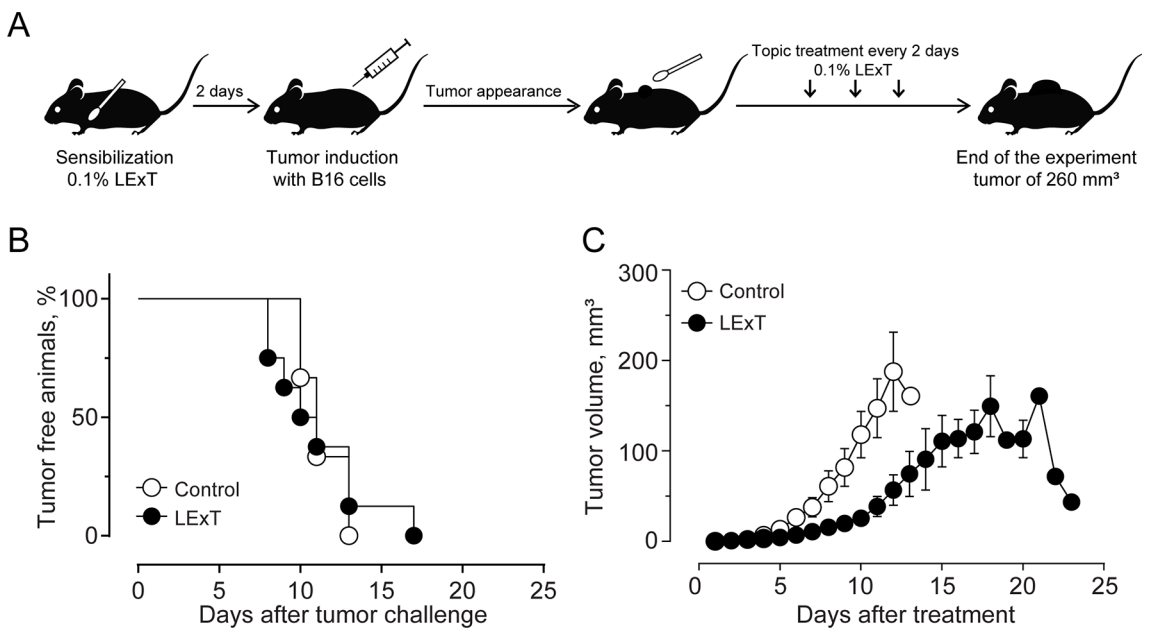

FIGURE 1 | Effect of Litre extract (LExT) as a topical treatment on tumor volume in C57BL/6 mice. (A) Treatment diagram. Animals were sensitized and then topically treated with an excipient or 0.1% LExT every two days until the end of the experiment; (B) Kaplan-Meier analysis for tumor onset and (C) Kinetics of tumor growth on control excipient-treated and LExT-treated mice. The abrupt decrease in tumor volume at day 21 in the LExT group indicates a tumor regression in 17% of treated mice. Values are mean ± SEM of 8-12 animals per group.

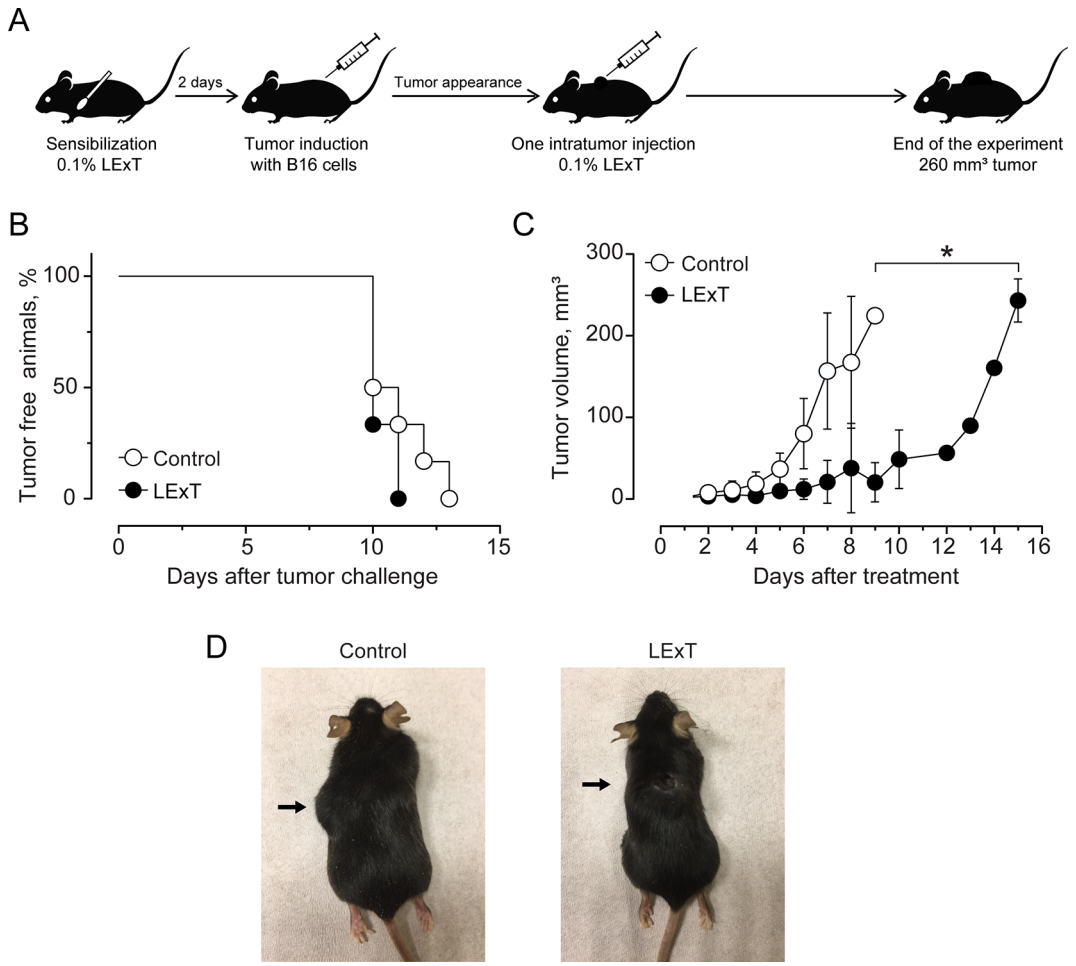

FIGURE 2 | Effect of Litre extract (LExT) intra-tumor treatment in tumor volume in C57BL/6 mice. (A) Treatment diagram. Animals were sensitized and then intratumorally injected with one dose of 50 μL of excipient or 0.1% LExT; (B) Kaplan-Meier analysis for tumor onset and (C) Kinetics of tumor growth on excipient-treated (control) and LExT-treated mice; Values are mean ± SEM of 8 animals per group. (D) Representative images of the tumor in LExT-treated and non-treated animals at the end of the experiment. Values are mean ± SEM of 8-12 animals per group. *p<0.05, Assessed by Kruskal–Wallis one-way ANOVA.

while the LExT-treated animals reached this stage at 18-20 day. Also, in the LExT-treated group, 17% of tumor regression was observed (**Figure 2C**). Altogether these results suggest that LExT (intratumor or topical) has a robust antitumor effect in melanoma tumors.

To further characterize the LExT mode of action, we analyzed whether LExT induces changes of T-cells populations and subpopulations that could suggest an immune response against the tumor. This effect was evaluated both in the tumor and in the spleen at the end of the tumor growth period. We detected a significant decrease in CD4+ tumor infiltrated cells, without significant changes in CD8+ cells (**Figure 3A**) compared with controls, whereas in the spleen, neither CD4+ nor CD8+ showed any changes respect to controls (**Figure 3B**). Similarly, LExT treatment did not induce significant changes in CD4+ subpopulation expressing markers for Th1, T-bet+CD4+ (**Figure 4A**), Th17, RORγ(τ)+CD4+ T cells (**Figure 4B**) nor in Treg, Foxp3-CD25+CD4+ (**Figure 4C**) positive cells in the spleen. These results suggest at the in our experimental conditions, no significant changes in populations and subpopulations of T cells were observed in response to LExT, except for a significant decrease in CD4+ infiltrating cells.

Although changes on CD4+ and CD8+ T-cell populations were not observed in response to LExT in our model of melanoma, the fact that *L. caustic* is known to induce inflammation led us to evaluate the presence of inflammatory markers in the tumors of LExT-treated animals. To do so, we studied histological parameters of focal necrosis, and inflammatory leukocytes infiltrate inside the tumors. We found that more inflammatory cells infiltrates in LExT-treated tumors (right column) than in the tumors of vehicle-treated animals (**Figure 5**) as shown in 5× (**Figure 5A**) and 40× (**Figure 5B**) images (**Table 2**). We also found evidence of necrosis in tumors of LExT-treated animals. These results indicate that LExT induced a marked inflammation in the tumors.

Finally, we compared the effects elicited by epifocal LExT against melanoma with those of clinically validated contact sensitizers (DNCB, DPCP) previously used as an epifocal

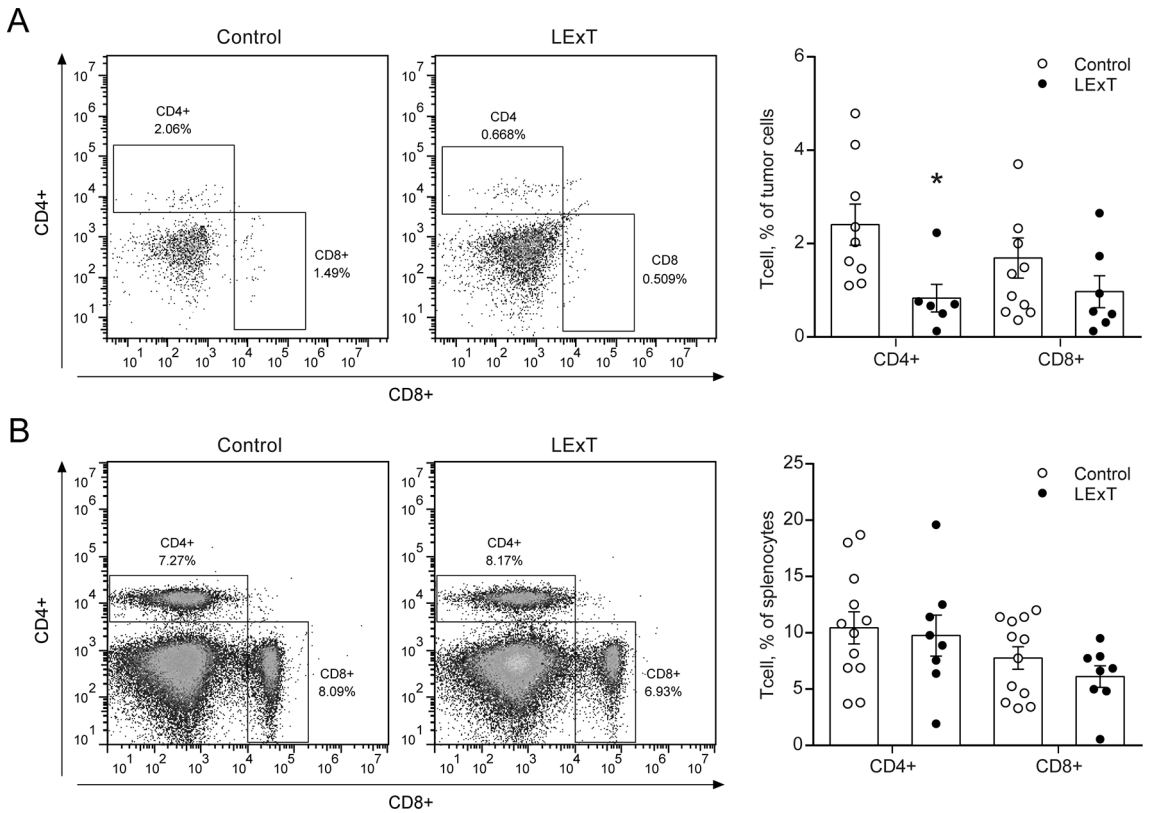

FIGURE 3 | Effect of topical Litre extract (LExT) treatment in splenic and tumor-infiltrating CD4+ and CD8+ T cells in C57BL/6 mice. Representative dot plots (left panel) and quantification of $CD4^+$ and $CD8^+$ T cells identified in **(A)** total tumor-infiltrating and **(B)** splenocytes cells excised from LExT-treated and non-treated mice. Values are mean ± SEM, *p<0.05 *vs.* excipients, assessed by the Mann–Whitney test.

treatment in the same skin cancer. Initially, we evaluated the effect of the DNCB treatment, a well-studied DTH inducer (Wack et al., 2002). To evaluate the effects of DNCB on tumor growth, we set a tumor on C57/BL6 mice, injecting tumor cells, as described in the *Methods* section of this work. Mice developed detectable tumors between 10 and 21 days post-tumor cell challenge (**Figure 6A**). In agreement with previous reports, systemic DNCB induced a mild inhibitory effect on tumor growth (**Figure 6B**), associated with an increase in CD4+ and CD8+ T-cell levels in the tumor infiltrates (**Figure 6C**), without significant changes in these population in the spleen (**Figure 6D**). These results suggest that increases in the specific T-cell population in the tumor might be responsible for the delay in tumor growth for DNCB. We further evaluated the current gold standard hapten used to treat melanoma, DPCP (Wack et al., 2002; Damian et al., 2013; Yeung et al., 2017). Strikingly, DPCP treatment did not induce antitumor effects in our murine model of melanoma (**Figure 7**), nor any change in conventional populations of cells in the spleen or the tumor tissue (data not shown). Altogether, these results indicate that LexT induces an antitumoral response and deserves further investigations to develop a new anti-melanoma immunotherapy expanding the currently limited therapeutic options for this disease.

DISCUSSION

In this study, we reported that epifocal treatment with LExT decreases melanoma tumor growth in B16 mice model. Intriguingly, we observed that the gold standard epifocal treatments used against melanoma in humans, DNCB and DPCP, were not effective against melanoma in mice, as only DNCB was able to induce a mild antitumor effect in our murine model of melanoma.

DNCB and DPCP are the most commonly used compounds in immunotherapy against recalcitrant viral warts, basilioma and spinocellular carcinoma. Unfortunately, DNCB has shown mutagenic effects in the "Ames Test." Although no clinical evidence has yet shown carcinogenesis susceptibility in patients treated with DNCB (Buckley and du Vivier, 1999), this potential mutagenic toxicity has restricted DNCB use in humans. Current evidence suggests that DPCP has been characterized as an efficacious antitumor contact sensitizer with no mutagenic risk, opening a new avenue for anticancer therapeutic strategies based on DTH induction (Singh and Lavanya, 2010). On this regard, both DPCP and DNCB, have been used in the treatment of several cutaneous lesions in humans (Von Nida and Quirk, 2003; Damian et al., 2009; Harper et al., 2014; Trowbridge et al., 2014). Interestingly, no studies are describing comparable effects

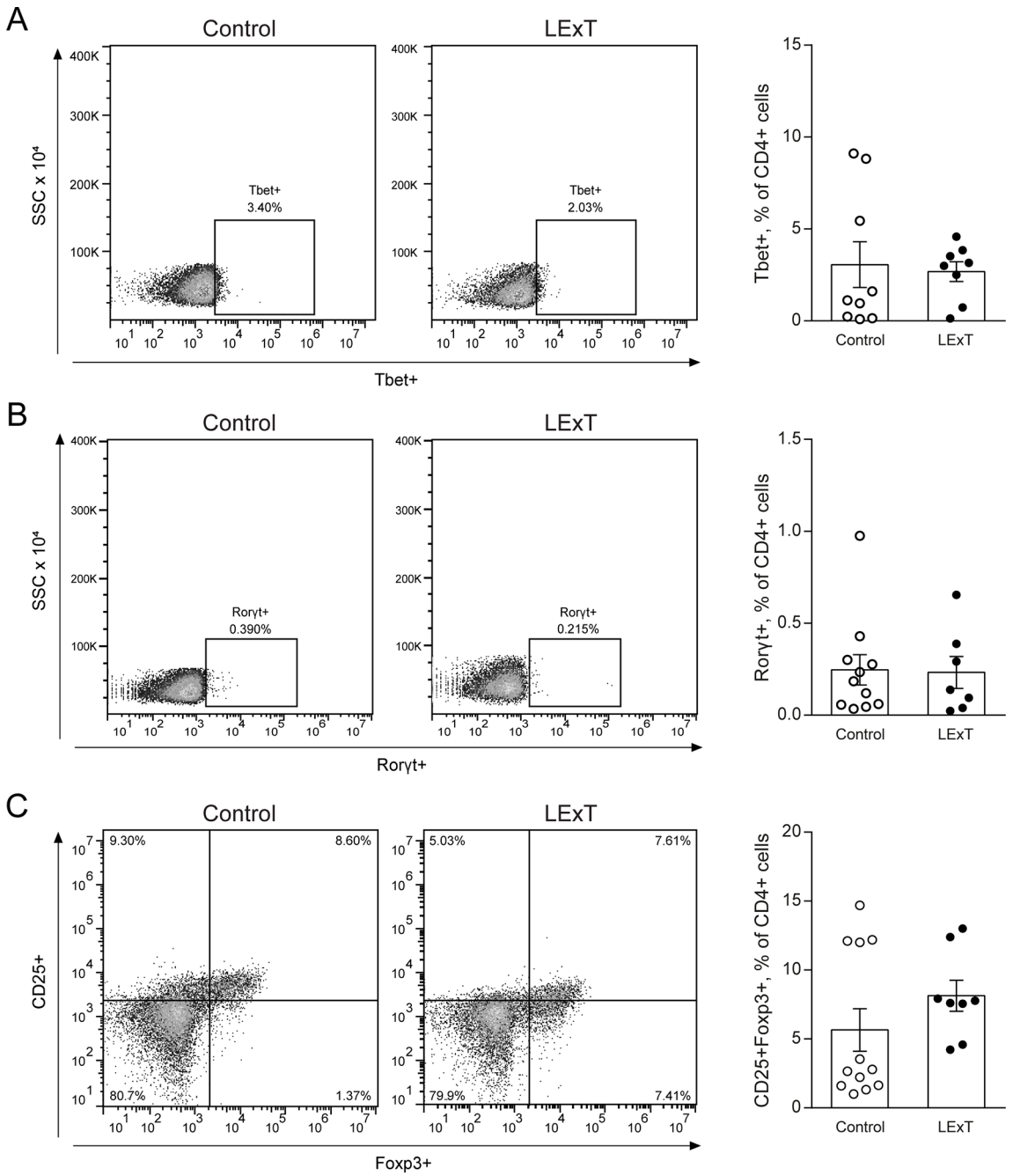

FIGURE 4 | Effects of Litre extract (LExT) as a topical treatment on spleen levels of Th1, Th17, and T regulatory (Treg) cells in C57BL/6 mice. Representative dot plots (left panel) and quantification of **(A)** Th1 (CD4+ Tbet+), **(B)** Th17 (CD4+ RORγ(t)+) and **(C)** Treg cells (CD4+ CD25+ FoxP3+) in LExT-treated and non-treated mice. Values are Means ± SEMs.

of these drugs in mouse models of melanoma. Probably, the differences observed comparing both models can be explained by different experimental designs, particularly in the duration of the treatments. In murine experiments, for example, the treatments typically last for three weeks, whereas the human treatments last up to 18 weeks (Damian et al., 2013; Yeung et al., 2017). On this regard, Sutmuller et al. inoculated low amounts of B16 cells (two orders of magnitude lower), it allowed them to follow up the tumor emergence for up to 12 weeks (Sutmuller et al., 2001). This strategy seemingly offers the possibility to improve the comparisons by increasing the duration of the treatments for up to 10 weeks.

Further research on the potential side effects of LExT is necessary to evaluate its safety as an anticancer therapy since aerial

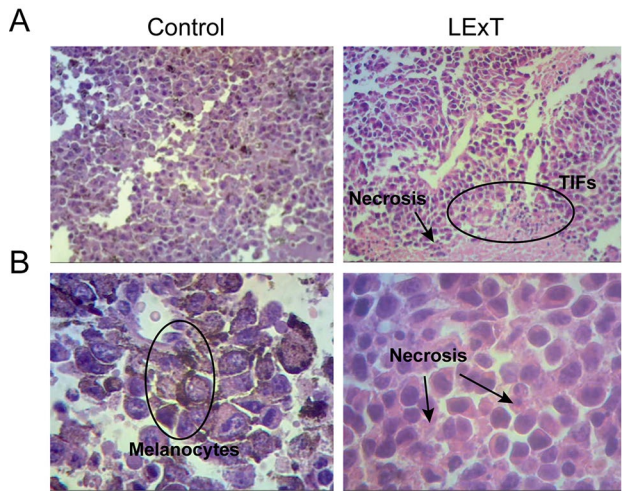

FIGURE 5 | Histological characterization of tumors derived from Litre extract (LExT)-treated C56BL/6 mice. Representative images of tumor obtained from Control-treated (left column) and LExT-treated (right column) mice. **(A)** and **(B)** show representative images for 5X and 40X magnifications, respectively. Each image is representative of 7-10 tumors obtained from each treatment. TIFs, tumor-infiltrating lymphocytes.

parts of *L. caustic* is known to induce allergic reactions, dermatitis, and skin inflammation including in mice (López et al., 1998). Unfortunately, there are no reliable epidemiological data on the prevalence of the Litre-induced DTH, or even more important, the percentage of the population that displays highly severe reactions when they come in contact with urushiols-congaing plants. An estimation based on the statistics for other urushiol-containing plants suggests that the population sensitive to Litre would be around 75% to 90%. Unlike other urushiols, litreol's effect was studied on cancer cells viability, which demonstrated a direct impact on cells viability (Russo et al., 2009). Urushiols are lipid-soluble immunogenic molecules, composed by a catechol nucleus substituted on C4 with a C15 hydrophobic chain, in the case of poison ivy, or with a C17 hydrophobic chain, in poison oak (Kalish et al., 1994), or substituted on C3 with a C15 hydrophobic chain, in the case of litreol (Russo et al., 2009). Several mechanisms by which urushiols act as immunogens have been suggested, such as intracellular hapten processed by the endogenous pathway to be presented to CD8+ T cells, extracellular haptens processed by the exogenous way to activate CD4+ T cells; and finally, urushiol could be also recognized by CD8+ T cells without processing, possibly by direct conjugation with class I MHC (Kalish et al., 1994).

Regarding the latter suggested urushiol-mediated immunogenic mechanisms, isolated CD8+ T cells from skin lesions of urushiol sensitized human subjects favor their role in the effector phase of contact dermatitis produced by poison ivy (Kalish and Johnson, 1990). Current studies indicate that IL-4 is an important downregulator during the elicitation phase of contact sensitivity (CS), demonstrated by the presence of high levels of IL-4 mRNA in the dermis and epidermis following skin challenge with trinitrochlorobenzene (TNCB) (Asada et al., 1997; Arakawa et al., 2018). Also, mice treated with anti-IL-4 mAb shortly before ear challenge showed increased ear swelling responses, this being accompanied by enhanced IFNγ, IL-2, and IL-12 mRNA signals in the dermis. These findings suggest that IL-4 blunts CS by regulating local production of proinflammatory cytokines (Asada et al., 1997), which could explain the increase in inflammation detected in our histological sections of melanoma tumors. The hapten urushiol can bind to epidermal cells, both keratinocytes and Langerhans cells, which may then migrate through lymphatics vessels to lymph nodes, where they present the antigen to T cells, allowing the recruitment of immune cell to the tumor area. Another feasible alternative is that the keratinocytes

TABLE 1 | Identity of the chemical compounds of LExT identified by GC/ MS/MS.

N°	Compound	RI_{exp}	Relative abundance (%)	Identification
1	Caryophyllene	1436.73	0.68	RI, MS
2	Aromandendrene	1463.90	0.17	RI, MS
3	Humulene	1467.29	0.62	RI, MS
4	γ-Muurolene	1487.00	0.06	RI, MS
5	β-Ionone	1493.52	0.11	RI, MS
6	α-Muurolene	1512.03	0.14	RI, MS
7	Cuparene	1523.96	0.19	RI, MS
8	γ-Muurolene	1528.62	0.12	RI, MS
9	β-Cadinene	1535.37	0.15	RI, MS
10	Calamenene	1537.47	0.12	RI, MS
11	Dihydroactinidiolide	1552.52	0.34	RI, MS
12	α-Calacorene	1559.58	0.12	RI, MS
13	Caryophyllene oxide	1605.44	1.08	RI, MS
14	Humulene-1,2-epoxide	1632.83	1.56	RI, MS
15	Cadalene	1693.15	0.35	RI, MS
16	Neophytadiene	1833.88	0.72	RI, MS
17	Perhydrofarnesyl acetone	1841.28	0.34	RI, MS
18	Phytol	2110.86	5.12	RI, MS
19	4,8,12,16-Tetramethylheptadecan-4-olide	2360.75	0.44	RI, MS
20	Ginkgol	2493.72	2.79	RI, MS
21	Tetracosanal	2629.24	1.87	RI, MS
22	3-(Pentadec-10-enyl)-catechol	2678.84	12.48	RI, MS
23	Hexacosanal	2832.25	4.41	RI, MS
24	1-Hexacosanol	2895.97	12.52	RI, MS
25	Octacosanal	3036.18	6.35	RI, MS
26	Octacosanol	3098.95	7.09	RI, MS
27	γ-Sitosterol	3366.40	7.61	RI, MS
	Total sesquiterpenes		**5.8%**	
	Long chain catechols		**9.6%**	
	Total catechols		**22.1%**	

TABLE 2 | Quantification of tumor histopathological features from control and LExT-treated mice.

	Control			LExT		
	low	high		low	high	
Necrosis	5	10	ns	1	8	*
Inflammation	4	11	ns	3	6	ns
Vascularization	4	8	ns	5	4	ns
Melanin	7	8	ns	7	2	*

*ns: non-significant difference, Low: mild response, High: severe response, *p < 0.05, assessed by Kruskal–Wallis one-way ANOVA.*

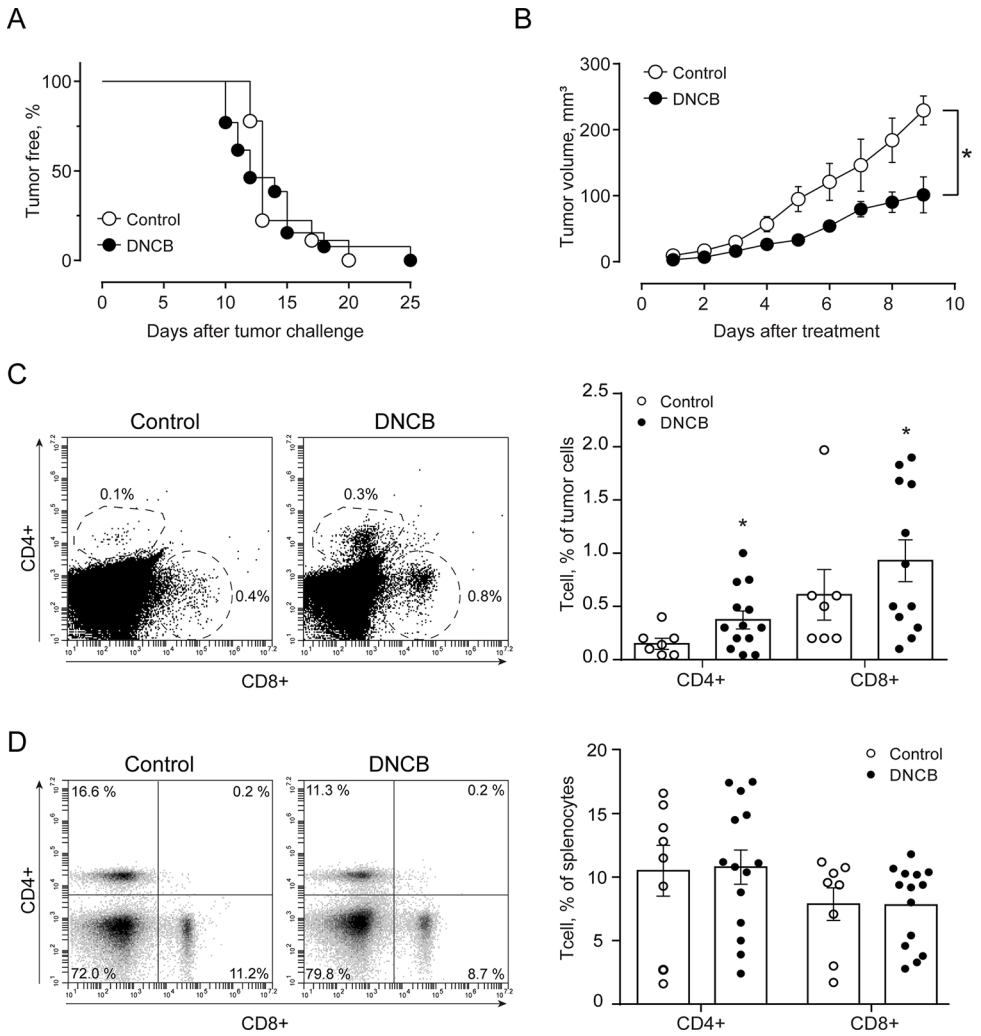

FIGURE 6 | Effect of DNCB treatment on B16 tumor onset and growth (volume) and CD4+ and CD8+ cells in the tumor and spleen in C57BL/6 mice. **(A)** Kaplan-Meier analysis for tumor onset on excipient-treated (control) and DNCB-treated mice; **(B)** Kinetics of tumor growth in DNCB-treated and non-treated animals. * $p < 0.05$, assessed by Kruskal–Wallis one-way ANOVA. Representative dot plots of $CD4^+$ and $CD8^+$ cells identified in **(C)** total tumor-infiltrating cell and **(D)** splenocytes cells excised from DNCB-treated and non-treated mice. Values are mean ± SEM, *$p < 0.0$ vs. excipients, assessed by the Mann–Whitney test.

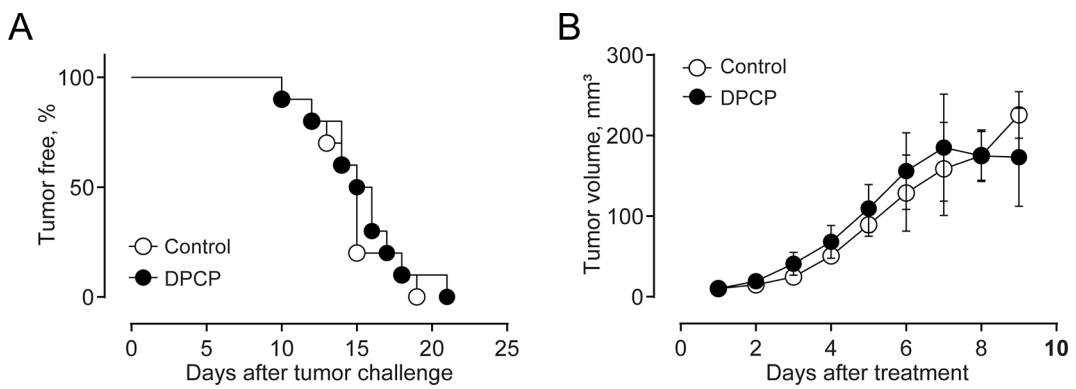

FIGURE 7 | Effect of DPCP treatment on B16 tumor onset and growth (volume) and CD4+ and CD8+ cells in the tumor and spleen in C57BL/6 mice. **(A)** Kaplan-Meier analysis for tumor onset on excipient-treated (control) and DPCP-treated mice; **(B)** Kinetics of tumor growth in DPCP-treated and non-treated animals. Values are Means ± SEMs.

may have an initial recognition of the antigen that produces its activation, which then causes the recruitment of leukocytes and production of cytokines, including IL-1, IL-6, and GM-CSF (Kalish, 1990). This way, keratinocytes would participate in antigen presentation process, as well as in T-cell activation. The close relationship between melanocytes and keratinocytes may play a key role in the anti-tumor response mediated by litreol treatment, because the keratinocytes can mediate melanocyte functions via several pathways, including cell-cell adhesion, cell-matrix adhesion, and paracrine signaling (Chung et al., 2011).

While we did not corroborate the described effects of *Litre* on the induction of DTH response (López et al., 1998), we cannot rule out the participation of DTH response in the effect of LExT against melanoma. In our experiments, the mode of action for the efficacious anticancer response of LExT remain to be elucidated, specifically the molecular mechanisms of the immune response. Altogether it is feasible to propose that a LExT-induced DTH (López et al., 1998) response could partially explain the antitumor we have observed. The fact that IL-17–mediated DTH is crucial for antitumor response in melanoma supports this idea (Escobar et al., 2005). On this regard, Muranski et al. described that adoptive transfer of Th17 lymphocytes in mice challenged with B16 cells generate a complete regression of the tumor, inducing up to 100% survival after 60 days post tumor challenge (Muranski et al., 2008). Intriguingly, in our study, T cells positive for Th1 and Th17 markers at a systemic level did not show measurable changes at the end of the experiment. A possible explanation for this result is that changes in the levels of Th1- and Th17-positive cells occurred during the early stages of the tumor development in animals treated with LExT.

Meanwhile, in late stages, the increased tumor mass at the end of the experiment could mask possible changes on T-cell population. Even more, at the end of the treatment, the tumor could have overcome the immunological restrictions occurred during the equilibrium phase, leading to fully developed tumor (Finn, 2012). For the litreol specifically, Lopez et al. demonstrated that the contact dermatitis induced by litreol has two components: a primary T CD4+ cell independent and a secondary CD8+ T dependent and regulated by CD4+ T cells (López et al., 1998). Regardless, while no significant changes or apparently inconclusive changes (associated to a decrease of CD4+ cells) were observed in our experiments, tumor-infiltrating specific CD4+ and CD8+ T-cell population could be a small fraction of the total T cells. To characterize whether our treatment induces a specific antitumor response, and to describe the role of T-cell subpopulations on the antitumor mediated effects, it is necessary to perform new experiments, e.g., using the B16-OVA cell model that will allow the study of specific OVA T-cell induction, among other parameters. Similarly, the exact role of the subpopulations and the immune mechanism remain to be elucidated.

Finally, we conclude that easy-to-use contact allergens applied topically, such as LExT, provide advantages over other therapies requiring specialized equipment and laboratory facilities to generate vaccines for cancer. In some cases, only the sensitization without direct challenge over the tumor was enough to achieve the antitumor efficacy of a complete treatment with LExT. Our results on the inhibition of tumor development suggest that LExT could be of great help in the development of new therapies for local melanoma.

AUTHOR CONTRIBUTIONS

SM and CR-P: Both authors equally contributed to this work, CR performed the LExT preparation, DE, AE, JM, DS, JR, MI: Performed DPCP and DNCB experiments, SM, GS-G, CB-A, RH CR-P, DS: performed LExT experiments, CR-P, CB-A, RF, EL-S, DS, LR, AK, MI, CA-C participated in experimental design, outlined and wrote the manuscript, RS: performed LExT GC/MS//MS analyses.

FUNDING

This work was funded by FONDECYT 1110734 and 1161015 (MI), 11140731 (EL-S) PAI 79140059 (EL-S), 11140915 (LR), 1180666 (AE), DICYT and DGT s/n (CA-C), CONICYT fellowship (CR-P, CB-A), CONICYT FONDEQUIP/GC MS/MS EQM 150084.

REFERENCES

Arakawa, T., Sugiyama, T., Matsuura, H., Okuno, T., Ogino, H., Sakazaki, F., et al. (2018). Effects of Supplementary Seleno-L-methionine on Atopic Dermatitis-Like Skin Lesions in Mice. *Biol. Pharm. Bull.* 41, 1456–1462. doi: 10.1248/bpb.b18-00349

Asada, H., Linton, J., and Katz, S. I. (1997). Cytokine gene expression during the elicitation phase of contact sensitivity: Regulation by endogenous IL-4. *J. Invest. Dermatol.* 108, 406–411. doi: 10.1111/1523-1747.ep12289700

Baldwin, R. W., Byers, V. S., Hannant, D., Jones, J. A., Pimm, M. V., and Price, M. R. (1982). Cellular interactions modulating host resistance to tumours. *Recent Results Cancer Res.* 80, 338–345. doi: 10.1007/978-3-642-81685-7_55

Berd, D., Sato, T., Cohn, H., Maguire, H. C., and Mastrangelo, M. J. (2001). Treatment of metastatic melanoma with autologous, hapten-modified melanoma vaccine: regression of pulmonary metastases. *Int. J. Cancer* 94, 531–539. doi: 10.1002/ijc.1506.abs

Buckley, D. A., and du Vivier, A. W. (1999). Topical immunotherapy in dermatology. *Int. J. Clin. Pract.* 53, 130–137.

Chung, H., Suh, E. K., Han, I. O., and Oh, E. S. (2011). Keratinocyte-derived laminin-332 promotes adhesion and migration in melanocytes and melanoma. *J. Biol. Chem.* 286, 13438–13447. doi: 10.1074/jbc.M110.166751

Curran, M. A., Montalvo, W., Yagita, H., and Allison, J. P. (2010). PD-1 and CTLA-4 combination blockade expands infiltrating T cells and reduces regulatory T and myeloid cells within B16 melanoma tumors. *Proc. Natl. Acad. Sci.* 107, 4275–4280. doi: 10.1073/pnas.0915174107

Damian, D. L., Saw, R. P. M., and Thompson, J. F. (2013). Topical immunotherapy with diphencyprone for in transit and cutaneously metastatic melanoma. *J. Surg. Oncol.* 109 (4), 308–313. doi: 10.1002/jso.23506

Damian, D. L., Shannon, K. F., Saw, R. P., and Thompson, J. F. (2009). Topical diphencyprone immunotherapy for cutaneous metastatic melanoma. *Australas. J. Dermatol.* 50, 266–271. doi: 10.1111/j.1440-0960.2009.00556.x

Durán-Aniotz, C., Segal, G., Salazar, L., Pereda, C., Falcón, C., Tempio, F., et al. (2013). The immunological response and post-treatment survival of DC-vaccinated melanoma patients are associated with increased Th1/Th17 and

reduced Th3 cytokine responses. *Cancer Immunol. Immunother.* 62, 761–772. doi: 10.1007/s00262-012-1377-3

Erkes, D. A., and Selvan, S. R. (2014). Hapten-induced contact hypersensitivity, autoimmune reactions, and tumor regression: plausibility of mediating antitumor immunity. *J. Immunol. Res.* 2014, 1–28. doi: 10.1155/2014/175265

Escobar, A., López, M., Serrano, A., Ramirez, M., Pérez, C., Aguirre, A., et al. (2005). Dendritic cell immunizations alone or combined with low doses of interleukin-2 induce specific immune responses in melanoma patients. *Clin. Exp. Immunol.* 142, 555–568. doi: 10.1111/j.1365-2249.2005.02948.x

Finn, O. J. (2012). Immuno-oncology: understanding the function and dysfunction of the immune system in cancer. *Ann. Oncol.* 23, 8–11. doi: 10.1093/annonc/ mds256

George, D. D., Armenio, V. A., and Katz, S. C. (2016). Combinatorial immunotherapy for melanoma. *Cancer Gene Ther*. 24 (3), 141–127. doi: 10.1038/cgt.2016.56

Harper, F., Worsnop, F., Powel, B., and Akhras, V. (2014). Topical diphencyprone immunotherapy as a treatment for cutaneous metastatic malignant melanoma, squamous cell carcinoma and eccrine porocarcinoma: a report of 15 cases. *Br. J. Dermatol.* 171, 4–5.

Holzer, A. M., Kaplan, L. L., and Levis, W. R. (2006). Haptens as drugs: contact allergens are powerful topical immunomodulators. *J. Drugs Dermatol.* 5, 410–416.

Kalergis, A. M., Lopez, C. B., Becker, M. I., Diaz, M. I., Sein, J., Garbarino, J. A., et al. (1997). Modulation of fatty acid oxidation alters contact hypersensitivity to urushiols: role of aliphatic chain beta-oxidation in processing and activation of urushiols. *J. Invest. Dermatol.* 108, 57–61. doi: 10.1111/1523-1747.ep12285632

Kalish, R. S. (1990). The use of human T-lymphocyte clones to study T-cell function in allergic contact dermatitis to urushiol. *J. Invest. Dermatol.* 94 (6), s108–s111. doi: 10.1111/1523-1747.ep12876061

Kalish, R. S., and Johnson, K. L. (1990). Enrichment and function of urushiol (poison ivy)-specific T lymphocytes in lesions of allergic contact dermatitis to urushiol. *J. Immunol.* 145.

Kalish, R. S., Wood, J. A., and LaPorte, A. (1994). Processing of urushiol (poison ivy) hapten by both endogenous and exogenous pathways for presentation to T cells in vitro. *J. Clin. Invest.* 93, 2039–2047. doi: 10.1172/JCI117198

Kobayashi, K., Kaneda, K., and Kasama, T. (2001). Immunopathogenesis of delayed-type hypersensitivity. *Microsc. Res. Tech.* 53, 241–245. doi: 10.1002/jemt.1090

Leiva-Salcedo, E., Coddou, C., Rodriguez, F. E., Penna, A., Lopez, X., Neira, T., et al. (2011). Lipopolysaccharide inhibits the channel activity of the P2X7 Receptor. *Mediat. Inflamm.* 2011, 152625. doi: 10.1155/2011/152625

Lo, M. N., Escobar, A., Ginesta, A., Reyes, D., and Gonza, R. (2019). Prolonged survival of dendritic cell – vaccinated melanoma patients correlates with tumor-specific delayed type IV hypersensitivity response and reduction of tumor growth factor-expressing T cells. *J. Clin. Oncol.* 27, 945–952. doi: 10.1200/JCO.2008.18.0794

López, C. B., Kalergis, A. M., Becker, M. I., Garbarino, J. a, and De Ioannes, a E. (1998). CD8+ T cells are the effectors of the contact dermatitis induced by urushiol in mice and are regulated by CD4+ T cells. *Int. Arch. Allergy Immunol.* 117, 194–201. doi: 10.1159/000024010

Matthews, N. H., Li, W.-Q., Qureshi, A. A., Weinstock, M. A., and Cho, E., (2017). "Epidemiology of Melanoma," in *Cutaneous Melanoma: Etiology and Therapy* Codon Publications, Australian. 3–22. doi: 10.15586/codon.cutaneousmelanoma.2017.ch1

Morales, J., Barrera-Avalos, C., Castro, C., Castillo, S., Barrientos, C., Robles-Planells, C., et al. (2017). Dead tumor cells expressing infectious salmon anemia virus fusogenic protein favor antigen cross-priming in vitro. *Front. Immunol.* 8, 1170. doi: 10.3389/fimmu.2017.01170

Morton, D., and Griffiths, P. (1985). Guidelines on the recognition of pain, distress and discomfort in experimental animals and an hypothesis for assessment. *Vet. Rec.* 116, 431–436. doi: 10.1136/vr.116.16.431

Muranski, P., Boni, A., Antony, P. A., Cassard, L., Irvine, K. R., Kaiser, A., et al. (2008). Tumor-specific Th17-polarized cells eradicate large established melanoma. *Blood* 112, 362–373. doi: 10.1182/blood-2007-11-120998

Nestle, F. O., Alijagic, S., Gilliet, M., Sun, Y., Grabbe, S., Dummer, R., et al. (1998). Vaccination of melanoma patients with peptide- or tumor lysate-pulsed dendritic cells. *Naz`t. Med.* 4, 328–332. doi: 10.1038/nm0398-328

Nosbaum, A., Vocanson, M., Rozieres, A., Hennino, A., and Nicolas, J. F. (2009). Allergic and irritant contact dermatitis. *Eur. J. Dermatol.* 19, 325–332. doi: 10.1684/ejd.2009.0686

Novick, N. L., and Bosniak, S. L. (1986). The failure of immunotherapy with dinitrochlorobenzene and Rhus extract for recurrent conjunctival squamous papillomas. *J. Dermatol. Surg. Oncol.* 12, 602–605. doi: 10.1111/j.1524-4725.1986.tb01958.x

Russo, A., Cardile, V., De Ioannes, A., and Garbarino, J. (2009). Effect of litreol on the viability of human cancer cells. *Chem. Biol. Interact.* 179, 178–184. doi: 10.1016/j.cbi.2008.10.013

Schreibelt, G., Bol, K. F., Westdorp, H., Florian, W., Figdor, C. G., and de Vries, I. J. M. (2015). Effective clinical responses in metastatic melanoma patients after vaccination with primary myeloid dendritic cells. *Clin. Cancer Res.* 22 (9), 1–5. doi: 10.1158/1078-0432.CCR-15-2205

Singh, G., and Lavanya, M. (2010). Topical immunotherapy in alopecia areata. *Int. J. Trichology* 2, 36. doi: 10.4103/0974-7753.66911

Smith, F. O., Downey, S. G., Klapper, J. A., Yang, J. C., Richard, M., Royal, R. E. et al., (2008). Treatment of metastatic melanoma using interleukin-2 alone or in conjunction with vaccines. *J. Surg. Oncol.* 14, 5610–5618. doi: 10.1158/1078-0432.CCR-08-0116

Sutmuller, R. P. M. P., van Duivenvoorde, L. M. M., van Elsas, A., Schumacher, T. N. M. N., Wildenberg, M. E. E., Allison, J. P. P., et al. (2001). Synergism of cytotoxic T lymphocyte-associated antigen 4 blockade and depletion of CD25(+) regulatory T cells in antitumor therapy reveals alternative pathways for suppression of autoreactive cytotoxic T lymphocyte responses. *J. Exp. Med.* 194, 823–832. doi: 10.1084/jem.194.6.823

Tel, J., Erik, H. J. G. A., Baba, T., Schreibelt, G., Schulte, B. M., Benitez-Ribas, D., et al. (2013). Natural human plasmacytoid dendritic cells induce antigen-specific T-cell responses in melanoma patients. *Cancer Res.* 73, 1063–1075. doi: 10.1158/0008-5472.CAN-12-2583

Trowbridge, R. M., Mitkov, M. V., Pittelkow, M. R., and Agrawal, D. K. (2014). Immunomodulation of malignant melanoma by contact sensitizing agents. *Expert Rev. Clin. Immunol.* 10, 63–76. doi: 10.1586/1744666X.2014.850415

Urzúa, A., Sotes, G., and Echeverría, J. (2011). Presence of 3-(pentadec-10-enyl)-catechol allergen in the epicuticular components of *Lithrea caustica* (Anacardiaceae). *Bol. Latinoam. y del Caribe Plantas Med. y Aromat.* 10 (6), 590–594.

Von Nida, J., and Quirk, C. (2003). Successful treatment of in-transit melanoma metastases using topical 2-4 dinitrochlorobenzene. *Australas. J. Dermatol.* 44, 277–280. doi: 10.1046/j.1440-0960.2003.00009.x

Wack, C., Kirst, A., Becker, J. C. J., Lutz, W. K., Bröcker, E. B., Fischer, W. H., et al. (2002). Chemoimmunotherapy for melanoma with dacarbazine and 2,4-dinitrochlorobenzene elicits a specific T cell-dependent immune response. *Cancer Immunol. Immunother.* 51, 431–439. doi: 10.1007/s00262-002-0292-4

Yeung, C., Petrella, T. M., Wright, F. C., Abadir, W., and Look Hong, N. J. (2017). Topical immunotherapy with diphencyprone (DPCP) for in-transit and unresectable cutaneous melanoma lesions: an inaugural Canadian series. *Expert Rev. Clin. Immunol.* 13, 383–388. doi: 10.1080/1744666X.2017.1286984

Conflict of Interest: The authors declare that the research was conducted in the absence of any commercial or financial relationships that could be construed as a potential conflict of interest.

frontiers in Pharmacology

REVIEW
published: 07 November 2019
doi: 10.3389/fphar.2019.01330

Exploring the Role of P2X Receptors in Alzheimer's Disease

*Pamela Andrea Godoy, Oscar Ramírez-Molina and Jorge Fuentealba**

Neuroactive Compounds Screening Laboratory,Departamento de Fisiología, Facultad de Cs. Biológicas, Universidad de Concepción, Concepción, Chile

Several studies have pointed to soluble oligomers of beta amyloid peptide (SOAβ) as the principal neurotoxic agents responsible for the generation of synaptotoxic events that can explain the main symptoms of Alzheimer's disease (AD). Among the toxic features associated with SOAβ, one of the most notorious is the formation of a non-selective pore-like structure in the plasma membrane, which may partly explain the overload of intracellular Ca^{2+}. There is evidence that the pore causes leakage of key intracellular compounds, such as adenosine triphosphate (ATP), to the extracellular milieu. Extracellular ATP activates P2X receptors (P2XR), which are ligand-gated ion channels (LGICs) widely expressed in both neuron and glial cells and act as neuromodulators of synaptic activity by promoting Ca^{2+} entry and facilitating neurotransmitter release. There is abundant evidence correlating the overexpression of these receptors to neurodegenerative diseases, including AD, thus opening the possibility that P2XR could potentiate the toxic mechanisms induced by SOAβ and contribute to intracellular Ca^{2+} overload in neurons and other mechanisms related to glial activation and inflammation. In this review, we correlate scientific evidence related to the main toxic effects induced by SOAβ and those that are mediated by purinergic P2XR. The data suggest that these purinergic receptors participate in the deleterious cellular and molecular effects of SOAβ that lead to the pathogenesis of AD. This information sheds light on the participation of new components in SOAβ toxicity that could be interesting as pharmacological targets for the development of molecular or chemical compounds able to modulate them.

Keywords: purinergic receptors, P2X receptors, amyloid beta, Alzheimer's disease, adenosine triphosphate

OPEN ACCESS

Edited by:
Francisco Ciruela, University of Barcelona, Spain

Reviewed by:
Thomas Grutter, Université de Strasbourg, France
Samuel J. Fountain, University of East Anglia, United Kingdom

****Correspondence:***
Jorge Fuentealba
jorgefuentealba@udec.cl

Specialty section:
This article was submitted to Neuropharmacology, a section of the journal Frontiers in Pharmacology

Received: *09 September 2019*
Accepted: *18 October 2019*
Published: *07 November 2019*

Citation:
Godoy PA, Ramírez-Molina O and Fuentealba J (2019) Exploring the Role of P2X Receptors in Alzheimer's Disease. Front. Pharmacol. 10:1330. doi: 10.3389/fphar.2019.01330

INTRODUCTION

Alzheimer's Disease and Aβ Peptide

Alzheimer's disease (AD) is a neurodegenerative disorder characterized by the progressive loss of memory and decline in other cognitive skills. AD is the main cause of dementia that affect the elderly and it is expected that by the year 2050 152 million people around the world will be affected (Philip Scheltens et al., 2016; Patterson, 2018). Sadly, there are no effective treatments despite efforts to find different therapeutic approaches (Patterson, 2018). There are two classical histopathological hallmarks in AD: amyloid plaques and neurofibrillary tangles (Ballard et al., 2011). Amyloid plaques are composed of insoluble aggregates of Aβ peptide, while neurofibrillary tangles are formed by hyperphosphorylated tau protein (Kocahan and Doğan, 2017). The pathogenesis of AD has not been completely elucidated yet, but one of the theories that tries to explain the origin of this disease is the amyloid hypothesis (Hardy and Higgins, 1992; Selkoe, 2000; Karran et al., 2011), a theory that has changed and evolved over time. Today, it is proposed that increased levels and aggregation of

Aβ are important to the development of AD (Ballard et al., 2011), and that soluble oligomers of Aβ are the pathogenic form of this peptide (Lal et al., 2007; Cline et al., 2018).

Amyloid-β Peptide: Pore Formation and Leakage of Adenosine Triphosphate (ATP)

It is now largely accepted that the beta-amyloid peptide (Aβ) is the main toxic agent in Alzheimer's disease. Aβ aggregation generates small soluble oligomers, larger insoluble oligomers, fibrils, and finally, one of the hallmarks of this disorder, the senile plaques (Mudher and Lovestone, 2002). Aβ peptide is generated by the cleavage of the Amyloid Precursor Protein (APP), a transmembrane protein that can be proteolytically processed through two pathways: the non-amyloidogenic that involves the participation of the α and γ secretases, and the amyloidogenic in which the β and γ secretases produce the Aβ peptide (Thinakaran and Koo, 2008). Different studies suggest that the soluble oligomers (SOAβ) are the main form of aggregated Aβ that generates synaptotoxic events (Lal et al., 2007; Shankar et al., 2007; Krafft and Klein, 2010). Several toxic events induced by SOAβ have been described such as acute cytosolic Ca^{2+} increase (in a concentration-dependent manner), reduced synaptic vesicle recycling and depletion of these vesicles (Parodi et al., 2010), impairment in mitochondrial dynamics and mitochondrial dysfunction (Wang et al., 2007), increment in oxidative stress, and inflammation (Varadarajan et al., 2000; Ballard et al., 2011). Furthermore, a direct interaction of the Aβ peptide with some membrane receptors such as α7 nicotinic receptor and the cellular prion protein has been described (Wang et al., 2000; Peters et al., 2015). Also, the excitotoxicity effect of Aβ peptide with NMDA receptors has been widely studied and correlated (Zhang et al., 2016). This peptide impairs LTP through NMDA receptors, and this impairment can be ameliorated by decreasing glutamate levels (Zhang et al., 2016). Under chronic conditions, the Aβ peptide decreases NMDA levels and its presence in the membrane thereby reducing glutamatergic transmission (Zhang et al., 2016). On the other hand, memantine, an NMDA antagonist, is used to treat some stages of AD because it helps to modulate the high calcium levels that are potentiated by NMDA receptors (Wang and Reddy, 2017). It seems that Aβ peptide impairs glutamate uptake allowing its increased availability in the extracellular milieu (Wang and Reddy, 2017), and this can contribute to the excitotoxicity observed in acute stages of AD, and chronic depletion that is characteristic in advanced stages (Sáez-Orellana et al., 2016). Another remarkable toxic effect that has been described is the capacity of the Aβ peptide to generate pore-like structures in the plasma membrane (Arispe et al., 1993; Mobley et al., 2004; Parodi et al., 2010). Although the mechanism for this pore formation is still under discussion, several studies suggest that the pore allows the passage of different molecules through a non-selective channel, and that soluble oligomers are the species responsible for its formation (Lal et al., 2007; Fuentealba et al., 2011; Sáez-Orellana et al., 2016; Kandel et al., 2017; Lee et al., 2017). This pore formation in the plasma membrane can explain some of the classic toxic events seen after treatment with SOAβ, such as the non-controlled increase in intracellular calcium [$(Ca^{2+})_i$] levels that generate an overload of this cation in the cytosol (Mattson et al., 1992; Berridge, 2010; Parodi et al., 2010; Sepulveda et al., 2010), which could lead to the observed mitochondrial dysfunction and neuronal death (Kruman and Mattson, 1999). It has been proposed that the pore generated by the Aβ peptide starts as a cationic selective channel and later transitions to a non-selective pore that allows the passage of molecules up to 900Da of weight such as EtBr and 6-NBDG, a glucose fluorescent analog (Sepúlveda et al., 2014). Besides the entry of some molecules into the cell, this pore can produce a leakage of some relevant intracellular compounds such as ATP. Indeed, several studies showed an increment in the extracellular levels of this molecule induced by Aβ peptide treatment (Kim et al., 2007; Fuentealba et al., 2011; Sáez-Orellana et al., 2016). The extracellular increase in ATP (by leakage through the pore or some other mechanism such as co-secretion of ATP with other neurotransmitter) could be associated with a reactive glia response. ATP can generate calcium transients in glial cells, and it appears to contribute to astrocytic hyperactivity in a mouse AD model (Delekate et al., 2014). Therefore, some authors have proposed that ATP participates in the inflammation process widely described in this neurodegenerative disease (Heppner et al., 2015; McGeer et al., 2016), while others propose that ATP, through some P2X receptors (P2XR), could participate directly in some of the toxic SOAβ effects observed in neurons (Sáez-Orellana et al., 2016; Sáez-Orellana et al., 2018).

ATP and Purinergic Receptors

Purinergic receptors are activated by purine molecules, and the two main families are P2Y and P2X receptors. P2Y are G protein-coupled receptors composed of 8 different subunits, whereas P2XR are from the ligand gated ion channel (LGIC) family and 7 different subunits have been described in mammals (Burnstock, 2006; Kaczmarek-Hájek et al., 2012; Khakh and North, 2012). When P2XR are activated by ATP, they allow the passage of cations and have a high Ca^{2+} permeability (Khakh and North, 2012). To see a more extensive review on P2XR and their role in neurological disorders see Sáez-Orellana et al. (2015). ATP has been described to play an important role in inflammation because it is present in the extracellular environment in inflammatory processes where purinergic receptors can be activated (Molz et al., 2015). ATP can be released through traumatic processes

Abbreviations: AD, Alzheimer's disease; APP, Amyloid Precursor Protein; ATP, Adenosine triphosphate; BBG, Brilliant Blue G; BzATP, 2,3′-O-(4-Benzoylbenzoyl) ATP; [Ca^{2+}]i, Intracellular calcium; CNS, Central nervous system; EC_{50}, Half maximal effective concentration; EGFP, Enhanced green fluorescent protein; EtBr, Ethidium bromide; KO, Knockout; LGIC, Ligand gated ion channel; LPS, Lipopolysaccharides; mRNA, Messenger RNA; NMDA, N-methyl-D-aspartate; NSAIDs, Nonsteroidal anti-inflammatory drugs; oATP, Oxidized ATP; P2XR, Ionotropic purinergic receptors; P2X2R, Ionotropic purinergic P2X2 receptor; P2X4R, Ionotropic purinergic P2X4 receptor; P2X7R, Ionotropic purinergic P2X7 receptor; P2Y, Purinergic G protein-coupled receptors; PC12, Rat adrenal gland pheochromocytoma; PGE2, Prostaglandin E2; PPADS, Pyridoxal phosphate-6-azo(benzene-2,4-disulfonic acid) tetrasodium salt Hydrate; PSD95, Post synaptic density protein 95; qRT-PCR, Real time reverse transcription polymerase chain reaction; ROS, Reactive oxygen species; SOAβ, Soluble oligomers of beta amyloid peptide; SV2, Synaptic vesicle protein 2; 6-NBDG, 6-(N-(7-Nitrobenz-2-oxa-1,3-diazol-4-yl)amino)-6-Deoxyglucose.

such as necrosis and also by controlled release through other mechanisms like hemichannels (Idzko et al., 2014) and co-secretion with neurotransmitters like catecholamine (Gandía et al., 1987; Xu et al., 1991; Estévez-Herrera et al., 2016). Once in the extracellular milieu, ATP can activate P2 receptors and subsequent activation of several different signaling cascades. The upregulation of some P2XR, such as P2X7, have been reported on immune cells, where several evidence demonstrate their involvement in different inflammation processes (Burnstock, 2016). In this cell type ATP triggers the release of inflammatory mediators as cytokines and prostaglandin E2 (PGE2) (Burnstock, 2016). P2X7 appears to be the most important P2XR on inflammation, this receptor is expressed on immune cells such as mast cells, neutrophils, macrophages and microglia, where it has a proinflammatory role, by causing the inflammasome assembly and secretion of IL1β (Idzko et al., 2014; Karmakar et al., 2016). In this review, we discuss in more depth the role of some ionotropic purinergic receptors (P2XR) in the Aβ peptide related toxicity and Alzheimer's disease, a neurodegenerative disorder where inflammation is a central mechanism.

ALZHEIMER'S DISEASE AND PURINERGIC IONOTROPIC RECEPTORS

P2X7 and Inflammation

The P2X7 coding sequence was obtained from brain and peripheral ganglion, and later it was described that this purinergic receptor is expressed in microglia and ependymal cells from the central nervous system (CNS) (Collo et al., 1997). High concentrations of ATP (in the low millimolar range) are needed to activate P2X7R (EC_{50} 100 μM for the rat receptor) (Khakh and North, 2012; Di Virgilio et al., 2018). It has been widely described that the P2X7 purinergic receptor participates in different inflammatory processes (Di Virgilio et al., 2017), and therefore, could play a key role in chronic inflammation and neuropathic pain. Indeed, a study done in P2X7 knockout (KO) mice found that these animals did not present inflammation or neuropathic pain (Chessell et al., 2005). This purinergic receptor has been found in all immune cells and is upregulated in inflammatory processes; and it has also been related to most neurodegenerative diseases (Di Virgilio et al., 2018). Therefore, the most studied P2XR in the context of AD is P2X7, and some light has been shed on its possible participation in the pathogenesis mechanism of this neurodegenerative disorder. A study using Tg2567 transgenic mice that overexpress APP with the Swedish mutation found an overexpression of P2X7 in 24 month old mice when compared to age match controls, with most of the staining surrounding amyloid plaques (Parvathenani et al., 2003). Furthermore, it has been described the overexpression of P2X7 in microglia and astrocytes from patients with AD (McLarnon et al., 2006; Martin et al., 2019). It has also been found that this receptor was overexpressed in cultured fetal human microglia exposed to Aβ, and that the cells treated with the peptide elicited a larger calcium influx by the agonist BzATP, which suggests a functional overexpression of this purinergic receptor. The same overexpression was observed in hippocampus from rats injected with Aβ, where the immunostaining was associated mainly with microglia (McLarnon et al., 2006). Results from another study showed that Aβ induced ROS production in a primary microglia culture that was mediated by the increment in intracellular calcium through P2X7R activation by extracellular ATP (Kim et al., 2007). Other studies demonstrated that microglia cells lacking P2X7R did not show an increment in intracellular calcium and ATP release after exposure to Aβ, but wild type cells expressing P2X7 did (Sanz et al., 2009). Furthermore, the use of oATP (a P2XR blocker) in wild type cells also inhibited the ATP release after Aβ exposure (Sanz et al., 2009). Finally, it was found that Aβ induced the release of IL-1β from a primary microglia culture and this effect was blocked by apyrase, while microglia from a KO mouse for P2X7 did not release IL-1β after Aβ exposure (Sanz et al., 2009). Also, intrahippocampal injection of Aβ in mice produced an accumulation of IL-1β, but in P2X7 KO mice the release of this cytokine was significantly lower (Sanz et al., 2009). Microglia not only release inflammatory cytokines, they also phagocytize the Aβ peptide. It has been described that silencing of P2X7 or the use of Brilliant Blue G (BBG), a non-competitive antagonist of P2X7 with a nanomolar affinity, and over 1,000-fold more potent than at P2X4 (Jiang et al., 2000), on microglia cells not only inhibited the release of pro-inflammatory cytokines such as IL-1β and TNF-α, but also increased Aβ phagocytosis by these cells (Ni et al., 2013). The results from this work suggested that the increment in IL-1β mediated by the activation of P2X7 produced an impairment in Aβ phagocytosis. Moreover, the administration of BBG to mice injected intrahippocampally with Aβ showed an improvement in cognitive and spatial learning function (Fan et al., 2014). This same study observed that BBG prevented the reduction in dendritic filopodia and density of spines induced by Aβ in hippocampal primary cultures (Fan et al., 2014). Recently, a more in-depth study of P2X7 expression was performed in a transgenic mouse model produced by breeding the J20AD mouse model (which overexpresses APP with the Swedish and Indiana mutations) and ^{P2X7R}EGFP reporter mice, which expresses this fluorescent protein under the control of the P2X7 promoter (Martinez-Frailes et al., 2019). In this model, they observed that in advanced stages of the disease, once microgliosis could be detected, the expression of P2X7 increased in microglial cells, and the number of microglial cells that expressed P2X7 also increased and were mainly localized on senile plaques. The data suggested that this effect was caused by the neuroinflammation produced in these mice, and that ATP could act as a chemotaxis signal for microglial cells through the activation of P2X7, which lead the microglial cells to the senile plaques. Interestingly, they also found that P2X7R activation reduced the phagocytic capacity of these cells (Martinez-Frailes et al., 2019). Recently, it has been described that in the APPPS1 transgenic mice P2X7R deficiency reduces the cognitive impairment and the number of Aβ plaques and soluble species, although they did not observed significantly differences in the Aβ phagocytosis and the activation state of microglia (Martin et al., 2019). Despite the fact that they did not observe changes in the expression of cytokines, such as IL-1β and TNFα, they demonstrated that APPPS1 mice deficient for P2X7 present lower cerebral levels of chemokines (CCL3, CCL4,

and CCL5) than in the APPPS1 transgenic mice (Martin et al., 2019), together with this they observed a reduced $CD8^+$ T cell recruitment in the choroid plexus and hippocampus. Therefore, P2X7 appears to be involved in the chemokine production and T cell recruitment induced by Aβ in the APPPS1 transgenic mice (Martin et al., 2019).

The inflammatory process is an important feature in the pathology of AD; therefore some reports have suggested a protective role for nonsteroidal anti-inflammatory drugs (NSAIDs) (Vlad et al., 2008; Zurita et al., 2013). All of these results suggest an important role for ATP and P2X7 in the inflammatory response of the microglia cells in AD through the release of cytokines such as IL-1β and the impairment of Aβ phagocytosis.

P2X4 in Inflammation and Neuronal Death

The P2X4 receptor was cloned from rat brain where it was found to be expressed in neurons and blood vessels (Soto et al., 1996). The gene that codes for P2X4 in humans is located on chromosome 12, close to the P2X7 gene, and they were likely produced by local gene duplication (Suurväli et al., 2017). It was found that P2X4 increased its expression in P2X7 KO mice suggesting that these receptors could complement their function (Suurväli et al., 2017). The crystal structure of P2X4 from zebrafish was the first P2X receptor to be observed revealing that these are trimeric receptors (Kawate et al., 2009). P2X4 has also been correlated with some inflammation processes. For instance, P2X4R appears to participate in joint inflammation and osteoarthritis, where it induces the expression of IL-1β, TNFα and participates in the inflammasome formation (Fan et al., 2014; Li et al., 2014). Also, it has been described that in human monocyte-derived macrophages P2X4R activated by ATP and through Ca^{2+} influx modulates the expression and secretion of the chemokine CXCL5, therefore, this receptor could participate in the neutrophils recruitment (Layhadi et al., 2018). In the CNS, it has been demonstrated that P2X4 increased its expression in microglial cells after exposure to LPS, which enhanced the sensitivity and the response to low ATP concentrations (Raouf et al., 2007). Furthermore, an upregulation of P2X4 in activated microglial cells after brain ischemic injury was also observed and was related to the increase in extracellular ATP levels (Cheng et al., 2014). Surprisingly, it was found that P2X4 protein levels were decreased in the middle frontal gyrus and middle temporal gyrus from AD patients with severe cognitive impairment (Varma et al., 2009). On the other hand, in hippocampal neurons exposed to the Aβ peptide, P2X4 levels were increased after 6 h of treatment, and this receptor expression was observed in cell bodies; while after 12 h of exposure to Aβ, P2X4 was observed in cell bodies and neurites (Varma et al., 2009). Also, an accumulation of a smaller P2X4 fragment was found after exposure to Aβ, and this was prevented by using a caspase inhibitor suggesting that this cleavage of P2X4 by caspase impaired the trafficking induced by ATP exposure (Varma et al., 2009). This cleavage could change some properties of these channels, generating a bigger amplitude response and a slower closure time in response to ATP (Varma et al., 2009). Finally, overexpression of P2X4 in neurons enhanced the toxic effect of Aβ, while silencing of this purinergic receptor decreased cellular death after exposure to Aβ indicating that this purinergic receptor contributed to the neuronal cell death induced by Aβ (Varma et al., 2009).

Hence, P2X4R could participate in some inflammatory processes in AD, together with P2X7R, since similarities between these two subtypes have been described; and potentiating the toxic effects of Aβ peptide and increasing neuronal death. Additionally, it seems interesting the recently advances discussed in the literature (Stokes et al., 2017), about the inhibition of these receptors. It has been described that some antidepressants such as paroxetine, inhibits P2X4 (Abdelrahman et al., 2017), but this molecule is not selective for P2X4, being more potent inhibiting the reuptake of serotonin (Stokes et al., 2017). Recent research have led to the discovery of for more selective antagonist for this receptor, like the benzodiazepine derivative 5-BDBD and compounds derived from N-substituted phenoxazine (Stokes et al., 2017). This opens a new space for the pharmacological developing of new drugs capable to modulate the P2X4R.

P2X2 Upregulation

The P2X2 receptor was first described in rat pheochromocytoma PC12 cells (Brake et al., 1994). Later, it was demonstrated to have a wide expression in the central nervous system. For example, its immunoreactivity was dense in some important areas such as the olfactory bulb, cerebral cortex, amygdala and hippocampus (Kanjhan et al., 1999). Hippocampal pyramidal cells from CA1 to CA4 and granular cells of the dentate gyrus express high levels of P2X2 and the immunostaining is mostly confined to the soma and dendrites (Kanjhan et al., 1999). In general, a strong P2X2 expression was associated to neurons in different CNS areas. Its presence in dendritic spines supports the idea that ATP can act as a fast excitatory neurotransmitter, whereas the presynaptic localization is consistent with the report of purinergic receptors acting as neurotransmitter release modulators (Kanjhan et al., 1999). The expression of heteromeric P2X2/3 receptors in neurons from the dorsal root ganglion and their involvement in neuropathic pain has been described (Ueno et al., 2003). It was found that P2X2 and P2X3 mRNA increased in mouse models of neuropathic pain, and results suggested that this heteromeric receptor was involved in mechanical allodynia in this mouse model (Ueno et al., 2003). This upregulation could be in the presynapse of dorsal root ganglion neurons facilitating the mechanical stimuli transmission that could cause mechanical allodynia (Ueno et al., 2003). The upregulation of P2X2 (along with P2X4) has also been described in an *in vitro* ischemic model (Cavaliere et al., 2003). The addition of suramin (a P2 antagonist) during the ischemic insult prevented cell death, and moreover, the silencing of P2X2 decreased the ischemic damage (Cavaliere et al., 2003). The same increase in P2X2 was also observed in the CA1–CA2 pyramidal cell layer, strata oriens and radiatum using immunostaining in an *in vivo* animal model of ischemia (Cavaliere et al., 2003). P2X2 colocalized with neuronal markers, but not with glial markers, confirming the neuronal expression of P2X2, while P2X4 was mainly observed in glial cells (Cavaliere et al., 2003). The P2X2 overexpression in neurons and the

prevention of cellular damage by silencing P2X2 suggest a role for this purinergic receptor in neuronal degeneration. Our group and others have described that after exposure to Aβ there was a consistent increment in intracellular calcium, but we found that co-treatment with apyrase or PPADS significantly reduced this increment (Sáez-Orellana et al., 2016). The same could be observed for the increment in frequency and amplitude of excitatory activity by acute exposure to Aβ (Sáez-Orellana et al., 2016). Therefore, this data supports the idea that Aβ induces excitotoxic events and P2XR would be contributing to this effect

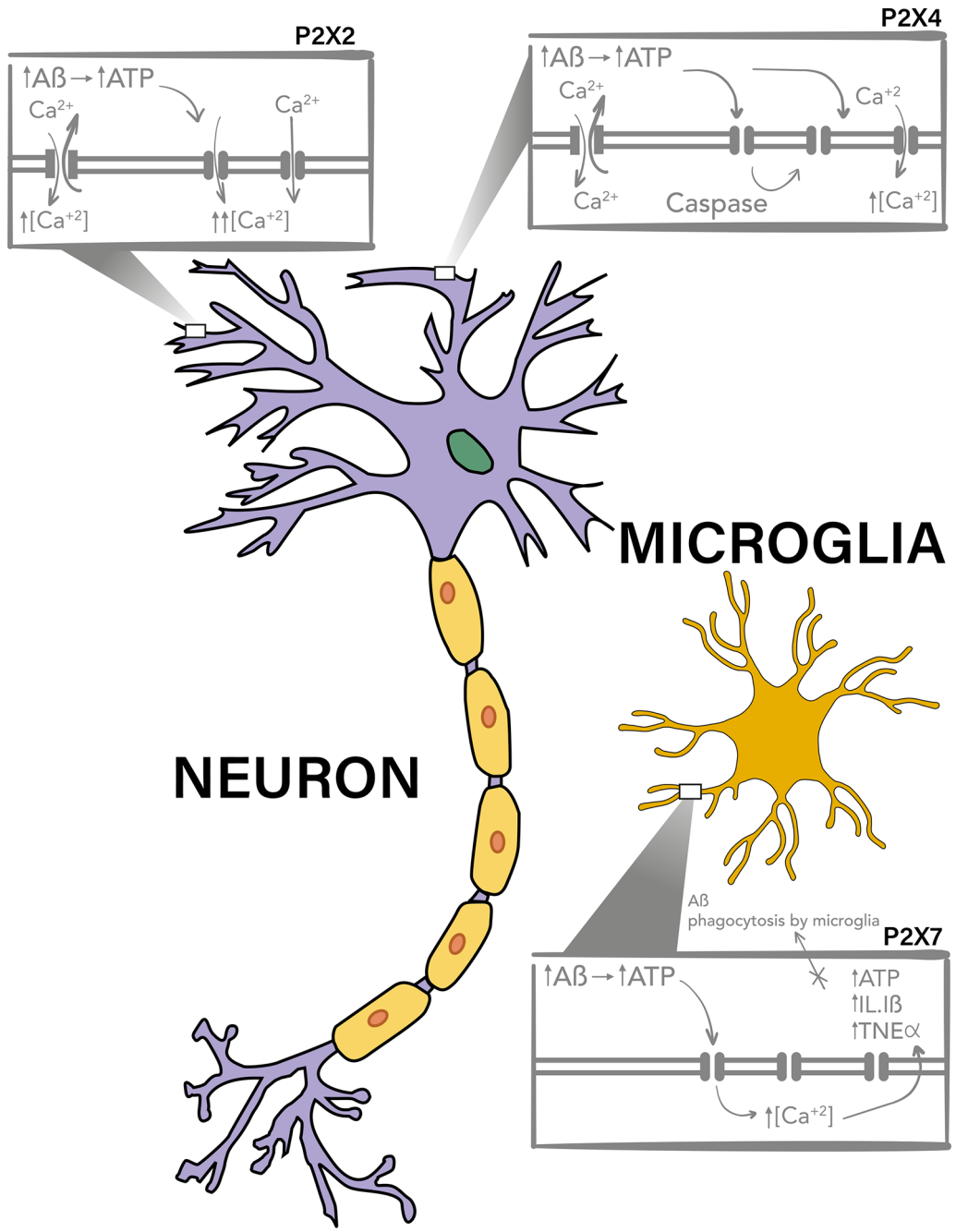

FIGURE 1 | P2X7, P2X4, and P2X2 purinergic receptors are involved in Aβ toxicity. P2X4 and P2X2 have a neuronal expression and have been described to be upregulated and to participate in the toxic mechanisms of Aβ peptide, probably due to the potentiation of the increment on intracellular calcium levels after activation by ATP, which is increased in the extracellular milieu. It has been described that after Aβ treatments there is a P2X4 fragment produced by caspase which is accumulated in the plasma membrane and have different channel properties, allowing the activation of this receptor for longer periods of time. On the other hand P2X7 has a mainly microglial expression, and it has also been reported to overexpresses on Aβ toxicity models and AD. This purinergic receptor, also through increase in intracellular calcium levels, potentiate the release of pro-inflammatory cytokines and participates in the impairment of Aβ phagocytosis by the microglia.

by facilitating the increment in intracellular calcium and synaptic facilitation (Sáez-Orellana et al., 2016). Chronic exposure to Aβ decreased SV2 and PSD95 proteins and this effect was prevented by PPADS, a P2XR antagonist. Furthermore, PPADS was able to prevent the decrease in cell viability observed with Aβ (Sáez-Orellana et al., 2018). Using qRT-PCR, a significant increase in mRNA for P2X1, 2, 5, and 7 was found after 12 h of exposure to Aβ, but after 24 h only P2X2 remained increased (Sáez-Orellana et al., 2018). The levels of P2X2 were analyzed with immunocytochemistry and western blot and the results also demonstrated an increment in P2X2 after 24 h of exposure to Aβ (Sáez-Orellana et al., 2018). Taken together, these results suggest that excitotoxic effects induced by Aβ are associated to changes in the purinergic tone, where an increase in extracellular ATP by leakage through the amyloid pore could cause an overexpression of purinergic receptors, as observed for P2X2, potentiating the acute and chronic toxic effects of Aβ.

DISCUSSION

Extracellular ATP and P2XR play an important role in several inflammatory processes, where the upregulation of some subunits have been described in different immune cells and they mediate the secretion of some inflammatory mediators. Therefore, ATP and ionotropic purinergic P2X receptors could play an important role in the pathogenesis of Alzheimer's disease, a neurodegenerative disorder that exhibits a sustained inflammatory response.

P2X7 is the P2XR most studied on the pathogenesis of AD. This purinergic receptor has a prominent expression in glial cells and it appears to participate in the inflammatory response of microglia through the release of cytokines, chemokines and the impairment of Aβ phagocytosis (**Figure 1**, Lower box).

P2X4 is expressed in both microglia and neurons, and therefore it could participate in some inflammatory processes in AD, (**Figure 1**, upper right box), together with P2X7R, and in neuronal death.

Finally, some evidence show that purinergic receptors participate in the excitotoxic effects induced by Aβ, where their upregulation, as that observed for P2X2, could potentiate the toxic effects of the Aβ peptide (**Figure 1**, upper left box).

In conclusion, all the literature discussed in this review points to the P2XR family as potential therapeutic targets in the development of new treatments for Alzheimer's disease.

AUTHOR CONTRIBUTIONS

PG and OR-M made the full literature recompilation and initial revision. PG and JF discussed the literature and wrote the text and OR-M designed the initial scheme.

FUNDING

This work was funded by FONDECYT 1161078 (JF). PG is a PhD student of CONICYT (21160392).

ACKNOWLEDGMENTS

We thank Laurie Aguayo for edition of this manuscript.

REFERENCES

Abdelrahman, A., Namasivayam, V., Hinz, S., Schiedel, A. C., Köse, M., Burton, M., et al. (2017). Characterization of P2X4 receptor agonists and antagonists by calcium influx and radioligand binding studies. *Biochem. Pharmacol.* 125, 41–54. doi: 10.1016/j.bcp.2016.11.016

Arispe, N., Rojas, E., and Pollard, H. B. (1993). Alzheimer disease amyloid beta protein forms calcium channels in bilayer membranes: blockade by tromethamine and aluminum. *Proc. Natl. Acad. Sci.* 90 (2), 567–571. doi: 10.1073/pnas.90.2.567

Ballard, C. G., Serge, Corbett, Anne, Brayne, Carol, Aarsland, Dag, and Jones, Emma. (2011). Alzheimer's disease. *Lancet* 377, 9770. doi: 10.1016/S0140-6736(10)61349-9

Berridge, M. J. (2010). Calcium hypothesis of Alzheimer's disease. *Pflügers Archiv. Eur. J. Physiol.* 459 (3), 441–449. doi: 10.1007/s00424-009-0736-1

Brake, A. J., Wagenbach, M. J., and Julius, D. (1994). New structural motif for ligand-gated ion channels defined by an ionotropic ATP receptor. *Nature* 371 (6497), 519. doi: 10.1038/371519a0

Burnstock, G. (2006). Historical review: ATP as a neurotransmitter. *Trends Pharmacol. Sci.* 27 (3), 166–176. doi: 10.1016/j.tips.2006.01.005

Burnstock, G. (2016). P2X ion channel receptors and inflammation. *Purinergic Signal.* 12 (1), 59–67. doi: 10.1007/s11302-015-9493-0

Cavaliere, F., Florenzano, F., Amadio, S., Fusco, F., Viscomi, M., D'Ambrosi, N., et al. (2003). Up-regulation of P2X2, P2X4 receptor and ischemic cell death: prevention by P2 antagonists. *Neuroscience* 120 (1), 85–98. doi: 10.1016/S0306-4522(03)00228-8

Cline, E. N., Bicca, M. A., Viola, K. L., and Klein, W. L. (2018). The amyloid-β oligomer hypothesis: Beginning of the third decade. *J. Alzheimer's Dis.* 64 (s1), S567–S610. doi: 10.3233/JAD-179941

Collo, G., Neidhart, S., Kawashima, E., Kosco-Vilbois, M., North, R., and Buell, G. (1997). Tissue distribution of the P2X7 receptor. *Neuropharmacology* 36 (9), 1277–1283. doi: 10.1016/S0028-3908(97)00140-8

Cheng, R.-d., Ren, J.-j., Zhang, Y.-y., and Ye, X.-m. (2014). P2X4 receptors expressed on microglial cells in post-ischemic inflammation of brain ischemic injury. *Neurochem. Int.* 67, 9–13. doi: 10.1016/j.neuint.2014.01.011

Chessell, I. P., Hatcher, J. P., Bountra, C., Michel, A. D., Hughes, J. P., Green, P., et al. (2005). Disruption of the P2X7 purinoceptor gene abolishes chronic inflammatory and neuropathic pain. *Pain* 114 (3), 386–396. doi: 10.1016/j.pain.2005.01.002

Delekate, A., Füchtemeier, M., Schumacher, T., Ulbrich, C., Foddis, M., and Petzold, G. C. (2014). Metabotropic P2Y1 receptor signalling mediates astrocytic hyperactivity in vivo in an Alzheimer's disease mouse model. *Nat. Commun.* 5, 5422. doi: 10.1038/ncomms6422

Di Virgilio, F., Dal Ben, D., Sarti, A. C., Giuliani, A. L., and Falzoni, S. (2017). The P2X7 receptor in infection and inflammation. *Immunity* 47 (1), 15–31. doi: 10.1016/j.immuni.2017.06.020

Di Virgilio, F., Schmalzing, G., and Markwardt, F. (2018). The elusive P2X7 macropore. *Trends Cell Biol.* 28 (5), 392–404. doi: 10.1016/j.tcb.2018.01.005

Estévez-Herrera, J., Domínguez, N., Pardo, M. R., González-Santana, A., Westhead, E. W., Borges, R., et al. (2016). ATP: The crucial component of secretory vesicles. *Proc. Natl. Acad. Sci.* 113 (28), E4098–E4106. doi: 10.1073/pnas.1600690113

Fan, C., Zhao, X., Guo, X., Cao, X., and Cai, J. (2014). P2X4 promotes interleukin-1β production in osteoarthritis via NLRP1. *Mol. Med. Rep.* 9 (1), 340–344. doi: 10.3892/mmr.2013.1748

Fuentealba, J., Dibarrart, A. J., Fuentes-Fuentes, M. C., Saez-Orellana, F., Quinones, K., Guzman, L., et al. (2011). Synaptic failure and adenosine triphosphate imbalance induced by amyloid-beta aggregates are prevented by

blueberry-enriched polyphenols extract. *J. Neurosci. Res.* 89 (9), 1499–1508. doi: 10.1002/jnr.22679

Gandía, L., López, M. G., Fonteríz, R. I., Artalejo, C. R., and García, A. G. (1987). Relative sensitivities of chromaffin cell calcium channels to organic and inorganic calcium antagonists. *Neurosci. Lett.* 77 (3), 333–338. doi: 10.1016/0304-3940(87)90523-4

Hardy, J. A., and Higgins, G. A. (1992). Alzheimer's disease: the amyloid cascade hypothesis. *Science* 256 (5054), 184–186. doi: 10.1126/science.1566067

Heppner, F. L., Ransohoff, R. M., and Becher, B. (2015). Immune attack: the role of inflammation in Alzheimer disease. *Nat. Rev. Neurosci.* 16 (6), 358. doi: 10.1038/nrn3880

Idzko, M., Ferrari, D., and Eltzschig, H. K. (2014). Nucleotide signalling during inflammation. *Nature* 509 (7500), 310. doi: 10.1038/nature13085

Jiang, L.-H., Mackenzie, A. B., North, R. A., and Surprenant, A. (2000). Brilliant blue G selectively blocks ATP-gated rat P2X7 receptors. *Mol. Pharmacol.* 58 (1), 82–88. doi: 10.1124/mol.58.1.82

Kaczmarek-Hájek, K., Lörinczi, É., Hausmann, R., and Nicke, A. (2012). Molecular and functional properties of P2X receptors—recent progress and persisting challenges. *Purinergic Signal.* 8 (3), 375–417. doi: 10.1007/s11302-012-9314-7

Kandel, N., Zheng, T., Huo, Q., and Tatulian, S. A. (2017). Membrane Binding and Pore Formation by a Cytotoxic Fragment of Amyloid β Peptide. *J. Phys. Chem. B.* 121 (45), 10293–10305. doi: 10.1021/acs.jpcb.7b07002

Kanjhan, R., Housley, G. D., Burton, L. D., Christie, D. L., Kippenberger, A., Thorne, P. R., et al. (1999). Distribution of the P2X2 receptor subunit of the ATP-gated ion channels in the rat central nervous system. *J. Comp. Neurol.* 407 (1), 11–32. doi: 10.1002/(SICI)1096-9861(19990428)407:1<11::AID-CNE2>3.0.CO;2-R

Karmakar, M., Katsnelson, M. A., Dubyak, G. R., and Pearlman, E. (2016). Neutrophil P2X 7 receptors mediate NLRP3 inflammasome-dependent IL-1β secretion in response to ATP. *Nat. Commun.* 7, 10555. doi: 10.1038/ncomms10555

Karran, E., Mercken, M., and De Strooper, B. (2011). The amyloid cascade hypothesis for Alzheimer's disease: an appraisal for the development of therapeutics. *Nat. Rev. Drug Discovery* 10 (9), 698. doi: 10.1038/nrd3505

Kawate, T., Michel, J. C., Birdsong, W. T., and Gouaux, E. (2009). Crystal structure of the ATP-gated P2X 4 ion channel in the closed state. *Nature* 460 (7255), 592. doi: 10.1038/nature08198

Khakh, B. S., and North, R. A. (2012). Neuromodulation by extracellular ATP and P2X receptors in the CNS. *Neuron* 76 (1), 51–69. doi: 10.1016/j.neuron.2012.09.024

Kim, S. Y., Moon, J. H., Lee, H. G., Kim, S. U., and Lee, Y. B. (2007). ATP released from [beta]-amyloid-stimulated microglia induces reactive oxygen species production in an autocrine fashion. *Exp. Mol. Med.* 39 (6), 820. doi: 10.1038/emm.2007.89

Kocahan, S., and Doğan, Z. (2017). Mechanisms of Alzheimer's disease pathogenesis and prevention: the brain, neural pathology, N-methyl-D-aspartate receptors, tau protein and other risk factors. *Clin. Psychopharmacol. Neurosci.* 15 (1), 1. doi: 10.9758/cpn.2017.15.1.1

Krafft, G. A., and Klein, W. L. (2010). ADDLs and the signaling web that leads to Alzheimer's disease. *Neuropharmacology* 59 (4–5), 230–242. doi: 10.1016/j.neuropharm.2010.07.012

Kruman, I. I., and Mattson, M. P. (1999). Pivotal role of mitochondrial calcium uptake in neural cell apoptosis and necrosis. *J. Neurochem.* 72 (2), 529–540. doi: 10.1046/j.1471-4159.1999.0720529.x

Lal, R., Lin, H., and Quist, A. P. (2007). Amyloid beta ion channel: 3D structure and relevance to amyloid channel paradigm. *Biochim. Biophys. Acta (BBA)-Biomembranes* 1768 (8), 1966–1975. doi: 10.1016/j.bbamem.2007.04.021

Layhadi, J. A., Turner, J., Crossman, D., and Fountain, S. J. (2018). ATP evokes Ca2+ responses and CXCL5 secretion via P2X4 receptor activation in human monocyte-derived macrophages. *J. Immunol.* 200 (3), 1159–1168. doi: 10.4049/jimmunol.1700965

Lee, J., Kim, Y. H., T. Arce, F., Gillman, A. L., Jang, H., Kagan, B. L., et al (2017). Amyloid β Ion Channels in a Membrane Comprising Brain Total Lipid Extracts. *ACS Chem. Neurosci.* 8 (6), 1348–1357. doi: 10.1021/acschemneuro.7b00006

Li, F., Guo, N., Ma, Y., Ning, B., Wang, Y., and Kou, L. (2014). Inhibition of P2X4 suppresses joint inflammation and damage in collagen-induced arthritis. *Inflammation* 37 (1), 146–153. doi: 10.1007/s10753-013-9723-y

Martin, E., Amar, M., Dalle, C., Youssef, I., Boucher, C., Le Duigou, C., et al (2019). New role of P2X7 receptor in an Alzheimer's disease mouse model. *Mol. Psychiatry* 24 (1), 108. doi: 10.1038/s41380-018-0108-3

Martinez-Frailes, C., Di Lauro, C., Bianchi, C., de Diego-García, L., Sebastian-Serrano, A., Bosca, L., et al. (2019). Amyloid peptide induced neuroinflammation increases the P2X7 receptor expression in microglial cells, impacting on its functionality. *Front. Cell. Neurosci.* 13, 1–15. doi: 10.3389/fncel.2019.00143.

Mattson, M. P., Cheng, B., Davis, D., Bryant, K., Lieberburg, I., and Rydel, R. E. (1992). beta-Amyloid peptides destabilize calcium homeostasis and render human cortical neurons vulnerable to excitotoxicity. *J. Neurosci.* 12 (2), 376–389. doi: 10.1523/JNEUROSCI.12-02-00376.1992

McGeer, P. L., Rogers, J., and McGeer, E. G. (2016). Inflammation, antiinflammatory agents, and Alzheimer's disease: the last 22 years. *J. Alzheimer's Dis.* 54 (3), 853–857. doi: 10.3233/JAD-160488

McLarnon, J. G., Ryu, J. K., Walker, D. G., and Choi, H. B. (2006). Upregulated expression of purinergic P2X7 receptor in Alzheimer disease and amyloid-β peptide-treated microglia and in peptide-injected rat hippocampus. *J. Neuropathol. Exp. Neurol.* 65 (11), 1090–1097. doi: 10.1097/01.jnen.0000240470.97295.d3

Mobley, D. L., Cox, D. L., Singh, R. R., Maddox, M. W., and Longo, M. L. (2004). Modeling Amyloid< i> β-Peptide Insertion into Lipid Bilayers. *Biophys. J.* 86 (6), 3585–3597. doi: 10.1529/biophysj.103.032342

Molz, S., Olescowicz, G., Kraus, J. R., Ludka, F. K., and Tasca, C. I. (2015). Purine receptors are required for DHA-mediated neuroprotection against oxygen and glucose deprivation in hippocampal slices. *Purinergic Signal.* 11 (1), 117–126. doi: 10.1007/s11302-014-9438-z

Mudher, A., and Lovestone, S. (2002) doi: 10.1016/S0166-2236(00)02031-2

Ni, J., Wang, P., Zhang, J., Chen, W., and Gu, L. (2013). Silencing of the P2X7 receptor enhances amyloid-β phagocytosis by microglia. *Biochem. Biophys. Res. Commun.* 434 (2), 363–369. doi: 10.1016/j.bbrc.2013.03.079

Parodi, J., Sepúlveda, F. J., Roa, J., Opazo, C., Inestrosa, N. C., and Aguayo, L. G. (2010). β-amyloid causes depletion of synaptic vesicles leading to neurotransmission failure. *J. Biol. Chem.* 285 (4), 2506–2514. doi: 10.1074/jbc.M109.030023

Parvathenani, L. K., Tertyshnikova, S., Greco, C. R., Roberts, S. B., Robertson, B., and Posmantur, R. (2003). P2X7 mediates superoxide production in primary microglia and is up-regulated in a transgenic mouse model of Alzheimer's disease. *J. Biol. Chem.* 278 (15), 13309–13317. doi: 10.1074/jbc.M209478200

Patterson, C. (2018). *World Alzheimer Report 2018—The state of the art of dementia research: New frontiers.* Alzheimer's Disease International (ADI): London, UK. .

Peters, C., Espinoza, M. P., Gallegos, S., Opazo, C., and Aguayo, L. G. (2015). Alzheimer's Aβ interacts with cellular prion protein inducing neuronal membrane damage and synaptotoxicity. *Neurobiol. Aging* 36 (3), 1369–1377. doi: 10.1016/j.neurobiolaging.2014.11.019

Philip Scheltens, K. B., Breteler, Monique M B, de Strooper, Bart, Giovanni B, Frisoni, Stephen, Salloway, Wiesje, Maria, et al. (2016). Alzheimer's disease. *Lancet* 388 (10043), 505–517. doi: 10.1016/S0140-6736(15)01124-1

Raouf, R., Chabot-Doré, A.-J., Ase, A. R., Blais, D., and Séguéla, P. (2007). Differential regulation of microglial P2X4 and P2X7 ATP receptors following LPS-induced activation. *Neuropharmacology* 53 (4), 496–504. doi: 10.1016/j.neuropharm.2007.06.010

Sáez-Orellana, F., Fuentes-Fuentes, M. C., Godoy, P. A., Silva-Grecchi, T., Panes, J. D., Guzmán, L., et al. (2018). P2X receptor overexpression induced by soluble oligomers of amyloid beta peptide potentiates synaptic failure and neuronal dyshomeostasis in cellular models of Alzheimer's disease. *Neuropharmacology* 128, 366–378. doi: 10.1016/j.neuropharm.2017.10.027

Sáez-Orellana, F., Godoy, P., Bastidas, C., Silva-Grecchi, T., Guzmán, L., Aguayo, L., et al. (2016). ATP leakage induces P2XR activation and contributes to acute synaptic excitotoxicity induced by soluble oligomers of β-amyloid peptide in hippocampal neurons. *Neuropharmacology* 100, 116–123. doi: 10.1016/j.neuropharm.2015.04.005

Sáez-Orellana, F., Godoy, P. A., Silva-Grecchi, T., Barra, K. M., and Fuentealba, J. (2015). Modulation of the neuronal network activity by P2X receptors and their involvement in neurological disorders. *Pharmacol. Res.* 101, 109–115. doi: 10.1016/j.phrs.2015.06.009

Sanz, J. M., Chiozzi, P., Ferrari, D., Colaianna, M., Idzko, M., Falzoni, S., et al. (2009). Activation of microglia by amyloid β requires P2X7 receptor expression. *J. Immunol.* 182 (7), 4378–4385. doi: 10.4049/jimmunol.0803612

Selkoe, D. J. (2000). Toward a comprehensive theory for Alzheimer's disease. Hypothesis: Alzheimer's disease is caused by the cerebral accumulation and cytotoxicity of amyloid β-protein. *Ann. New York Acad. Sci.* 924 (1), 17–25. doi: 10.1111/j.1749-6632.2000.tb05554.x

Sepúlveda, F. J., Fierro, H., Fernandez, E., Castillo, C., Peoples, R. W., Opazo, C., et al. (2014). Nature of the neurotoxic membrane actions of amyloid-b on

hippocampal neurons in Alzheimer's disease. *Neurobiol. Aging* 35, 472e481. doi: 10.1016/j.neurobiolaging.2013.08.035

Sepulveda, F. J., Parodi, J., Peoples, R. W., Opazo, C., and Aguayo, L. G. (2010). Synaptotoxicity of Alzheimer beta amyloid can be explained by its membrane perforating property. *PloS One* 5 (7), e11820. doi: 10.1371/journal.pone.0011820

Shankar, G. M., Bloodgood, B. L., Townsend, M., Walsh, D. M., Selkoe, D. J., and Sabatini, B. L. (2007). Natural oligomers of the Alzheimer amyloid-β protein induce reversible synapse loss by modulating an NMDA-type glutamate receptor-dependent signaling pathway. *J. Neurosci.* 27 (11), 2866–2875. doi: 10.1523/JNEUROSCI.4970-06.2007

Soto, F., Garcia-Guzman, M., Gomez-Hernandez, J. M., Hollmann, M., Karschin, C., and Stühmer, W. (1996). P2X4: an ATP-activated ionotropic receptor cloned from rat brain. *Proc. Natl. Acad. Sci.* 93 (8), 3684–3688. doi: 10.1073/pnas.93.8.3684

Stokes, L., Layhadi, J. A., Bibic, L., Dhuna, K., and Fountain, S. J. (2017). P2X4 receptor function in the nervous system and current breakthroughs in pharmacology. *Front. Pharmacol.* 8, 291. doi: 10.3389/fphar.2017.00291

Suurväli, J., Boudinot, P., Kanellopoulos, J., and Boudinot, S. R. (2017). P2X4: A fast and sensitive purinergic receptor. *Biomed. J.* 40 (5), 245–256. doi: 10.1016/j.bj.2017.06.010

Thinakaran, G., and Koo, E. H. (2008). Amyloid precursor protein trafficking, processing, and function. *J. Biol. Chem.* 283 (44), 29615–29619. doi: 10.1074/jbc.R800019200

Ueno, S., Moriyama, T., Honda, K., Kamiya, H.o., Sakurada, T., and Katsuragi, T. (2003). Involvement of P2X2 and P2X3 receptors in neuropathic pain in a mouse model of chronic constriction injury. *Drug Dev. Res.* 59 (1), 104–111. doi: 10.1002/ddr.10208

Varadarajan, S., Yatin, S., Aksenova, M., and Butterfield, D. A. (2000). Review: Alzheimer's amyloid β-peptide-associated free radical oxidative stress and neurotoxicity. *J. Struct. Biol.* 130 (2), 184–208. doi: 10.1006/jsbi.2000.4274

Varma, R., Chai, Y., Troncoso, J., Gu, J., Xing, H., Stojilkovic, S., et al. (2009). Amyloid-β induces a caspase-mediated cleavage of P2X4 to promote purinotoxicity. *Neuromol. Med.* 11 (2), 63–75. doi: 10.1007/s12017-009-8073-2

Vlad, S. C., Miller, D. R., Kowall, N. W., and Felson, D. T. (2008). Protective effects of NSAIDs on the development of Alzheimer disease. *Neurology* 70 (19), 1672–1677. doi: 10.1212/01.wnl.0000311269.57716.63

Wang, H.-Y., Lee, D. H., D'Andrea, M. R., Peterson, P. A., Shank, R. P., and Reitz, A. B. (2000). β-Amyloid1–42 Binds to α7 Nicotinic Acetylcholine Receptor with High Affinity implications for alzheimer's disease pathology. *J. Biol. Chem.* 275 (8), 5626–5632. doi: 10.1074/jbc.275.8.5626

Wang, R., and Reddy, P. H. (2017). Role of glutamate and NMDA receptors in Alzheimer's disease. *J. Alzheimer's Dis.* 57 (4), 1041–1048. doi: 10.3233/JAD-160763

Wang, X., Su, B., Perry, G., Smith, M. A., and Zhu, X. (2007). Insights into amyloid-β-induced mitochondrial dysfunction in Alzheimer disease. *Free Radical Biol. Med.* 43 (12), 1569–1573. doi: 10.1016/j.freeradbiomed.2007.09.007

Xu, Y., Duarte, E. P., and Forsberg, E. J. (1991). Calcium dependency of muscarinic and nicotinic agonist-induced ATP and catecholamine secretion from porcine adrenal chromaffin cells. *J. Neurochem.* 56 (6), 1889–1896. doi: 10.1111/j.1471-4159.1991.tb03445.x

Zhang, Y., Li, P., Feng, J., and Wu, M. (2016). Dysfunction of NMDA receptors in Alzheimer's disease. *Neurol. Sci.* 37 (7), 1039–1047. doi: 10.1007/s10072-016-2546-5

Zurita, M. P., Muñoz, G., Sepúlveda, F. J., Gómez, P., Castillo, C., Burgos, C. F., et al. (2013). Ibuprofen inhibits the synaptic failure induced by the amyloid-β peptide in hippocampal neurons. *J. Alzheimer's Dis.* 35 (3), 463–473. doi: 10.3233/JAD-122314

Conflict of Interest: The authors declare that the research was conducted in the absence of any commercial or financial relationships that could be construed as a potential conflict of interest.

frontiers in Pharmacology

ORIGINAL RESEARCH
published: 07 November 2019
doi: 10.3389/fphar.2019.01312

Prenatal Ethanol Exposure Misregulates Genes Involved in Iron Homeostasis Promoting a Maladaptation of Iron Dependent Hippocampal Synaptic Transmission and Plasticity

Erwin De La Fuente-Ortega, Wladimir Plaza-Briceño, Sofía Vargas-Robert and Paola Haeger**

Departamento de Ciencias Biomédicas, Facultad de Medicina, Universidad Católica del Norte, Coquimbo, Chile

OPEN ACCESS

Edited by:
Miguel Reyes-Parada, University of Chile, Chile

Reviewed by:
Enrico Sanna, University of Cagliari, Italy
Mariela Fernanda Perez, Universidad Nacional de Córdoba, Argentina

***Correspondence:**
Erwin De La Fuente-Ortega
edelafuente@ucn.cl
Paola Haeger
phaeger@ucn.cl

Specialty section:
This article was submitted to Neuropharmacology, a section of the journal Frontiers in Pharmacology

Received: *11 June 2019*
Accepted: *15 October 2019*
Published: *07 November 2019*

Citation:
De La Fuente-Ortega E, Plaza-Briceño W, Vargas-Robert S and Haeger P (2019) Prenatal Ethanol Exposure Misregulates Genes Involved in Iron Homeostasis Promoting a Maladaptation of Iron Dependent Hippocampal Synaptic Transmission and Plasticity. Front. Pharmacol. 10:1312. doi: 10.3389/fphar.2019.01312

Prenatal ethanol exposure (PAE) induces behavioral maladptations in offspring, including a deficit in memory formation which is part of the umbrella sign of fetal alcohol spectrum disorder. Clinical and preclinical studies have shown that iron depletion exacerbates cognitive problems in offspring exposed to ethanol *in utero* and that PAE promotes dysregulation in brain iron homeostasis. However, the mechanisms underlying brain iron dysregulation and neuronal activity defects in adolescent offspring of PAE are unclear and poorly understand. Here, we used a PAE rat model to analyze messenger RNA (mRNA) and protein expression of iron homeostasis genes such as transferrin receptor (TfR), divalent metal transporter (DMT1), ferroportin (FPN1), and ferritin (FT) in brain areas associated with memory formation such as the prefrontal cortex (PFC), ventral tegmental area, and hippocampus. Interestingly, we found that 21 day old PAE rats have higher mRNA expression of DMT1 in the PFC, and TfR in the hippocampus, compared to control animals. In contrast FPN has lower mRNA expression in the PFC, and FT and FPN1 have lower expression in the hippocampus. In agreement with these results, we found a 1.5–2 fold increase of TfR and DMT1 protein levels both in the hippocampus and the PFC. Additionally, using an electrophysiological approach, we found that in hippocampal slices from PAE rats, iron treatment decreased long-term potentiation (LTP), but not AMPAR basal transmission (AMPAR fEPSP). In contrast, in control slices Fe-NTA did not affect LTP but decreased significantly the AMPAR fEPSP. Meanwhile, iron chelation with deferiprone decreased AMPAR transmission in PAE and control slices and decreased LTP only in controls slices. These results suggest that PAE affects iron homeostasis of specific brain areas—PFC and hippocampus—which could be involved in maladaptive cognition observed in this animal model.

Keywords: fetal alcohol syndrome, iron homeostasis, glutamatergic transmission, long term potentiation, adolescence, fetal brain programming

Abbreviations: VTA, ventral tegmental area; PFC, prefrontal cortex; TfR, transferrin receptor; DMT1, divalent metal transporter; FT, ferritin; FPN, ferroportin; P21, postnatal day 21; P70–78, postnatal day 70–78.

INTRODUCTION

The consumption of alcohol during pregnancy significantly alters fetal development and growth (Cuzon et al., 2008), and also affects cognitive processes throughout the child's life (Ramsay, 2010; Skorput et al., 2015). Several clinical and preclinical studies have shown that prenatal ethanol exposure (PAE) can trigger cognitive disability and/or promote drug addiction during adolescence and adulthood (Bond and di Giusto, 1976; Phillips and Whitlock, 1976; Fabio et al., 2015) (Contreras et al., 2017). According to the World Health Organization, Chile has the highest alcohol consumption per capita within Latin America, with men consuming 13.9 L and women consuming 5.5 L of pure alcohol annually (Aros et al., 2009). It has been reported that out of 9,600 women interviewed in a study regarding prenatal exposure to ethanol, 57.4% admitted to have ingested alcohol at some point during pregnancy (Aros et al., 2009).

Interestingly, some studies using PAE mice models have shown that this condition triggers an imbalance in brain iron homeostasis (Miller et al., 1995; Carter et al., 2007; Huebner et al., 2016; Carter et al., 2017). However, these studies have focused on iron homeostasis in the whole brain during the gestational stage (Huebner et al., 2016), and in midbrain and subcortical areas during the postnatal (P17) stage of the offspring (Miller et al., 1995). However, it is unknown whether PAE affects iron homeostasis and/or neuronal activity in brain areas related with cognitive processes such as the prefrontal cortex (PFC) (Eichenbaum, 2017), the hippocampus (Burgess et al., 2002) and the ventral tegmental area (VTA) (Lisman and Grace, 2005) in adolescent animals.

Brain iron homeostasis plays important functions that require the expression of several genes which are important to maintain adequate intracellular iron levels. Iron is involved in fundamental processes such as cellular metabolism, cognitive processes, and memory formation (Aisen et al., 1999; Hidalgo et al., 2007; Carlson et al., 2009; Haeger et al., 2010). In the brain, iron is necessary for several steps involved in neurotransmitter production such as metabolic synthesis, packaging, uptake as well as degradation (Beard and Connor, 2003). In addition, iron contributes to synaptic plasticity through the catalytic production of reactive oxygen species (ROS) by the Fenton reaction; increasing intracellular calcium levels through ryanodine receptor activation (Hidalgo et al., 2007; Muñoz et al., 2011).

For neurons to comply with all their functions, they must maintain appropriate iron levels by regulating the expression of several iron homeostasis proteins which mediate ion uptake, storage, and release from neurons (Beard and Connor, 2003). Iron uptake is mediated by the TfR, which binds the iron (Fe^{3+})–transferrin complex at the cell surface and internalizes it towards endosomes for iron reduction (Fe^{2+}), which then translocates to the cytosol by divalent metal transporter 1 (DMT1) (Núñez et al., 1990; Bogdan et al., 2016). DMT1 can also can be expressed at the cell surface allowing direct translocation of Fe^{2+} to the cytosol (Pelizzoni et al., 2012). Once in the cytosol, Fe^{2+} can be stored by the cytosolic protein FT, used by mitochondria, or constitute a free or labile iron fraction (Kruszewski, 2003; Valko et al., 2005; Mackenzie et al., 2008). Excess of intracellular Fe^{2+} is exported from the neurons through ferroportin 1 (FPN) (Wu et al., 2004; Boserup et al., 2011). In response to iron level fluctuation, neurons can regulate the expression of genes involved in iron homeostasis (e.g. TfR, DMT1, FPN, or FT) mainly by a posttranscriptional mechanism involving the iron-response element (IRE)/iron regulatory protein (IRP) system (Wang and Pantopoulos, 2011; Singh et al., 2014). Moreover, the systemic iron metabolism can be regulated by hepcidin (gene HAMP), an hormone released by liver that regulate iron by interacting with its receptor FPN (Collins et al., 2008). HAMP also can be expressed by glia in the brain (Urrutia et al., 2013).

The effect of PAE together with iron depletion or a supplementation diet have been studied mainly during gestation until G20 or until the early postnatal (P14/P30) development of rats by assessing the expression of some brain iron homeostasis proteins, and morphological alterations (apoptosis and myelination) (Rufer et al., 2012; Huebner et al., 2016). Particularly, it has been described that PAE reduced postnatal iron levels and increases the expression of FT and transferrin (Tf) at whole cerebral cortex (Miller et al., 1995), meanwhile iron deficient PAE rats exacerbate the reduction of iron levels at gestational day 20–10 in total brain and reduce the expression of iron homeostasis proteins (e.g. Tf/TfR, and FT) without changes to others (e.g. FPN and DMT1) (Rufer et al., 2012; Huebner et al., 2016). However, these studies have not evaluated the effects of PAE on the hippocampus and neuronal activity of adolescent offspring.

How PAE could affect iron homeostasis genes in specific brain areas related with cognitive behaviors in adolescent offspring and how iron fluctuations can affect neuronal activity were the main aims of this study. To this end, we used a PAE rat model to analyze the messenger RNA (mRNA) and protein expression of iron homeostasis genes (TfR, DMT1, FPN1, and FT) at three different brain areas associated with cognitive impairment of FASD: the PFC, the VTA, and hippocampus. Interestingly, we found that P21 rats with PAE presented increased expression of TFR in the PFC, and DMT1 in the hippocampus, meanwhile FPN in the PFC, FT and FPN in the hippocampus, decreased their mRNA expression. In agreement with this, we found a 1.5–2 fold increase of TfR and DMT1 protein levels in the PFC and hippocampus by Western-blot. Additionally, using an electrophysiological approach on hippocampal slices of P21 rats, we found that iron supplementation decreased long-term potentiation (LTP), but not the AMPAR synaptic transmission, of PAE rats compared to control slices. Meanwhile, iron chelation with deferiprone (DFP) produced a significant decrease of LTP in controls rats, but not in PAE rats. These results suggest that PAE affects the iron homeostasis in specific brain areas associated with memory and learning, the PFC and the hippocampus. These alterations may underlie the maladaptive behavior observed in the PAE animal model.

MATERIAL AND METHODS

Animals and Prenatal Alcohol Exposure Treatment

We followed the protocol described previously by Contreras et al., 2017. Pregnant Sprague–Dawley rats were exposed to ethanol (10% v/v) and 64 mg/l of sucralose (daily). Ethanol

consumption was initiated on day 5 ± 2 days of gestation until 1 week after the offspring were born (P7). The consumption of liquid and food was monitored during the consumption period. After the ethanol protocol, rats were left with food and water *ad libitum*. Offspring were weaned at 21 days after birth (P21) and separated by sex. Protocols for rat handling were carried out in accordance with the recommendations of the Assessor Committee in Bioethical guidelines from the National Fund for Scientific and Technological Development (FONDECYT, Chile) and approved by the Bioethic, Scientific, and Animal Care and Use Committee of the Universidad Católica del Norte, Chile.

Brain Sample Extraction

Different brain samples were extracted by microdissection. The brain region enriched of PFC and VTA was extracted from limited slices approximately from 4.2 to 2.7 mm and −5.2 to −6.8 mm from bregma, respectively, according to the Paxinos and Watson (1998). From the same brain, whole hippocampus was also removed. Samples were extracted from P21 and P70–78 offspring, which were exposed or not to ethanol in utero. Samples were collected on dry ice and stored at −80°C until processed.

Tissue Homogenization and Western-Blot

We used the protocol described by Contreras (Contreras et al., 2017). Briefly, 100 mg of brain tissues (PFC, hippocampus, or VTA) were homogenized with 300 µl lysis buffer (20 mM MOPS/Tris pH 7, 0.3 M sucrose, 2 mM EDTA, 2 mM EGTA, 1% NP-40, and 0.1% sodium dodecyl sulfate), plus protease inhibitors. 10–30 µg of proteins was suspended in 3X loading buffer and denatured for 10 min at 70–80°C. Proteins were separated by 10% sodium dodecyl sulfate polyacrylamide gel electrophoresis (Minigel-BioRad), and transferred to 0.2 µm nitrocellulose membranes (Whatman-Protran #10401396, Merck). The membranes were blocked with 5% nonfat milk in phosphate-buffered saline (PBS) for 1 h at room temperature and incubated for 18 h at 4°C with the following primary antibodies, anti-β-actin (Sigma-Aldrich, 1:10,000), anti-TfR (Thermofisher Scientific, H68.4, 1:500), anti-DMT1 (Gift from Dr Marco Tulio Nuñez, 1:1,000 (Haeger et al., 2010). The membranes were washed three times with 0.2% Tween 20 in PBS at room temperature and incubated with secondary antibodies conjugated to horseradish peroxidase (HRP) (antirabbit HRP or antimouse HRP, both from Cell Signaling Tech. Danvers, USA) dissolved in 3% albumin-PBS 1X for 1 h at room temperature. After washing the blots three times with 0.2% Tween-PBS, they were exposed to chemiluminescent substrates (p-coumaric acid/luminol) for 1 min and scanned with a C-digit blot scanner (LI-COR). The bands were quantified with the ImageJ software (National Institutes of Health, USA) and normalized to β-actin.

Quantitative Reverse Transcription PCR

We performed quantitative reverse transcription PCR (RT-qPCR) analysis for DMT1-1B (+IRE and −IRE isoforms), TfR, FT, FPN, and HAMP in the PFC, hippocampus, and VTA of PAE rats, comparing them with controls using the method previously described by Contreras 2017 (Contreras et al., 2017). Brain tissues samples (50–100 mg) were homogenized with TRIzol (TRIzol^{R} Reagent, Invitrogen ™ Life Technologies, USA) to extract total RNA, treated with DNase (1 U, Turbo DNA-free™ Kit, Life-Technologies) to eliminate contaminant DNA. First strand complementary DNA was synthesized with the Improm II ™ kit (Promega, USA), the reaction tube contained 10 µg RNA, 3 mM $MgCl_2$, 0.5 mM dNTPs, reaction buffer [50 mM Tris–HCl (pH 8.3 at 25°C), 75 mM KCl, and 10 mM DTT], 20 U (1 µl) of reverse transcriptase (Improm II TM, Promega, USA), and nuclease-free water, reaching 5 µl of final reaction volume. For qPCR, specific primers for genes involved in iron homeostasis and housekeeping genes (β-actin or GAPDH) with melting temperatures (Tm) of 60°C and amplicons of approximately 100–200 bp are shown in **Table 1**. The qPCR reaction contained 5 µl of 2X SYBR green master mix (kapa sybr®fast, biosystems, USA), complementary DNA (5 µl), 50 nM of each primer, and nuclease-free water until the final reaction volume reached 10 µl. Real-time PCR reactions were run with the Applied Biosystems StepOne™ system (Applied Biosystems) using the following amplification conditions: initial denaturation for 10 min at 95°C followed by 40 cycles of

TABLE 1 | Nucleotide sequences of the forward (F) and reverse (R) primers used for qRT-PCR of genes involved in iron homeostasis and housekeeping genes in *Rattus norvegicus*.

Gene	Sequences (5'-3')	Amplicon (bp)	Reference
ratDMT1 (+) IRE	F: GCCTGTCTGTCTGTCTTTGC R: CCCAGTGTTTCCCAACTAACA	134	(Pelizzoni et al., 2012)
ratDMT1 (-) IRE	F: AAGGCGAAGAAAGATCTGGAG R: CCACAGGCCGCTGTTTG	113	(Andersen et al., 2007)
ratTFR1	F: ATACGTTCCCCGTTGTTGAGG R: GGCGGAAACTGAGTATGGTTGA	111	(Naz et al., 2012)
ratFPN1	F: TCGGTTCCTCTCACTCCTGT R: GTGGAGAGAGAGTGGCCAAG	198	(Urrutia et al., 2013)
ratHAMP	F: GAAGGCAAGATGGCACTAAGCA R: TCTCGTCTGTTGCCGGAGATAG	102	(Moriconi et al., 2009)
ratBeta-actin	R: TCTACAATGAGCTGCGTGTG R: TACATGGCTGGGGTGTTGAA	130	(Haeger et al., 2010)
ratGAPDH	F: AACGACCCCTTCATTGAC R: TCCACGACATACTCAGCAC	191	(Dong et al., 2010)

denaturation at 95°C for 15 s, and annealing/extension at 60°C for 30 s. Gene expression levels were normalized to housekeeping genes, β-actin or GAPDH, according to the PCR efficiency similarity. To determine differences between the expression of iron homeostasis gene (fold changes) in the PAE rat groups and the control group (**Figures 1** and **2**, and **Supplementary Tables 2** and **3**), the expression of iron homeostasis genes were quantified in both groups using 2−ΔCt as previously described (Schmittgen and Livak, 2008). Briefly, the mRNA expression of iron homeostasis genes in each group was calculated:

$$\text{Formula 1, mRNA expression of control group} = 2^{-\Delta Ct,\text{control}} / 2^{-\Delta Ct,\text{Mean control}}$$

$$\text{Where, } \Delta Ct, \text{ control} = \left(\text{Ct gene of interest} - \text{Ct internal housekeeping}\right) \text{control}$$

$$\text{and } 2^{-\Delta Ct,\text{Mean control}} = \left(\sum 2^{-\Delta Ct,\text{control}}\right) / \text{n litters}$$

$$\text{Formula 2, mRNA expression of PAE group} = 2^{-\Delta Ct,\text{PAE}} / 2^{-\Delta Ct,\text{Mean control}}$$

$$\text{Where, } \Delta Ct, \text{ PAE} = \left(\text{Ct gene of interest} - \text{Ct internal housekeeping}\right) \text{PAE}$$

$$\text{and } 2^{-\Delta Ct,\text{Mean control}} = \left(\sum 2^{-\Delta Ct,\text{control}}\right) / \text{n litters}$$

In addition, to determine the relative mRNA levels between PAE and control animals were calculated using the $2^{-\Delta\Delta Ct}$ method, where ΔΔCt = (Ct gene of interest − Ct internal housekeeping)$_{PAE}$ − (Ct gene of interest − Ct internal housekeeping)$_{Control}$

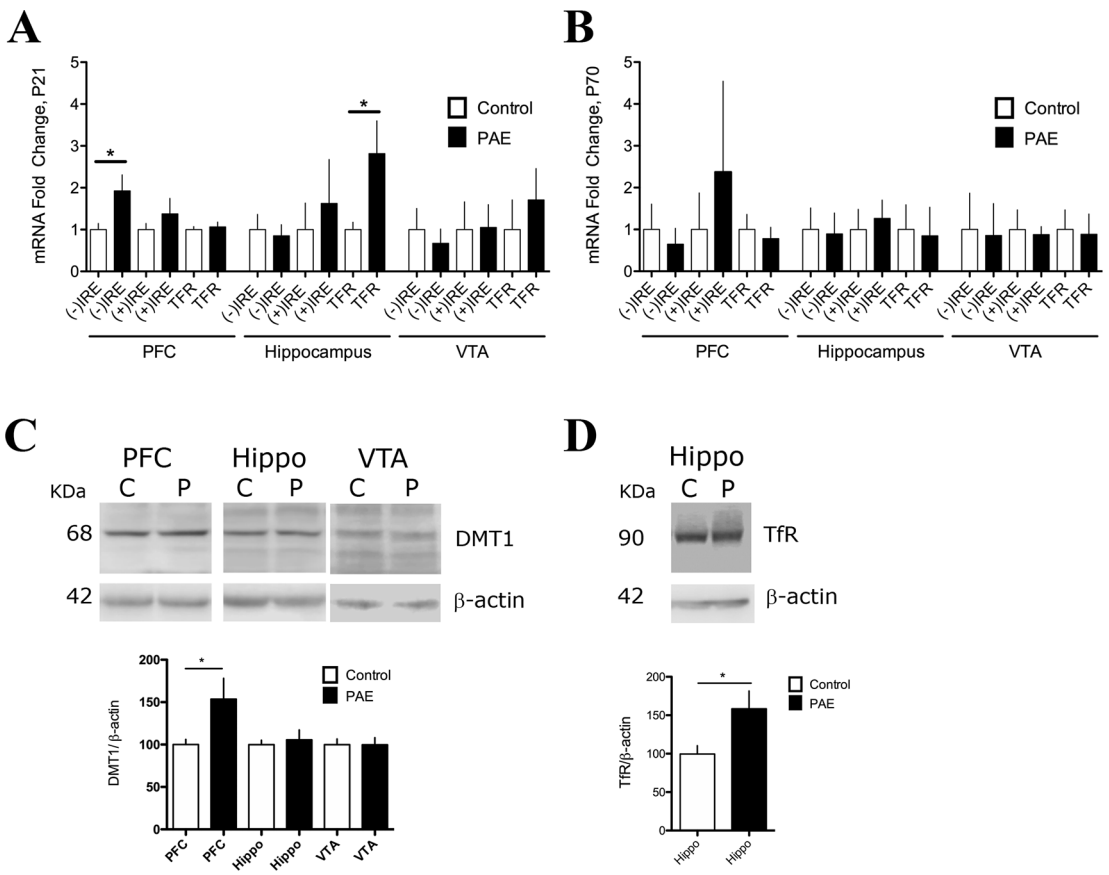

FIGURE 1 | Prenatal ethanol exposure (PAE) affected messenger RNA (mRNA) and protein expression of iron transporters divalent metal transporter (DMT1) and transferrin receptor (TfR) in rat brain. **(A)** Relative mRNA expression of DMT1 isoforms [(–) IRE and (+) IRE], and TFR in the prefrontal cortex (PFC), hippocampus, and ventral tegmental area (VTA) of P21 PAE rats compared to respective brain areas of P21 controls rats. Graph A shows mRNA expression (fold change) in controls and PAE calculated using formula 1 and 2 (*Material and methods*) with means ± SEM. *p < 0.05 for comparison by Mann–Whitney. N 5. **(B)** Relative mRNA expression of the same genes and brain areas of PAE and control rats as A, but for ages P70–78. Graph B shows mRNA expression (fold) in controls and PAE, calculated using formula 1 and 2 (*Material and methods*) with means ± SEM. *p < 0.05 for comparison by Mann–Whitney. N 5 litters. **(C)** Western blot analysis of DMT1 expression in control (C) and PAE (P) P70–78 rats in the PFC, hippocampus (Hippo), and VTA. N = 10 litters. **(D)** Western blot analysis of TfR expression in control (C) and PAE (P) of P21. N = 6 litters. DMT1 and TfR proteins were immuno-detected using specific antibodies and normalized to β-actin (42 kDa). Graphs in C and D show means ± SEM, and *p < 0.05 for the indicated comparisons by Mann–Whitney test.

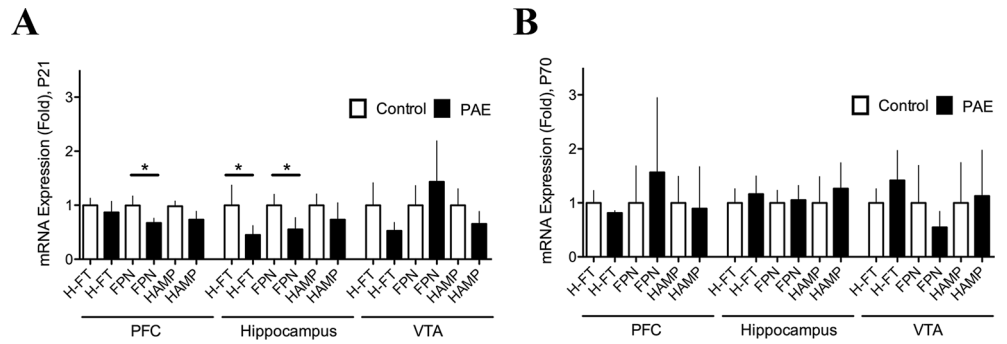

FIGURE 2 | Prenatal ethanol exposure (PAE) affected ferritin and ferroportin messenger RNA (mRNA) expression in rat brain. **(A)** Relative mRNA expression of ferritin (H-FT), ferroportin (FPN), and hepcidin (HAMP) in brain areas of P21 PAE rats—prefrontal cortex (PFC), hippocampus, and ventral tegmental area (VTA)—compared to respective brain areas in control rats at P21 days old. **(B)** Relative mRNA expression of the same genes and brain areas of PAE rats as A, but for day P70–78 compared to the respective brain areas in P70–78 control rats. Graphs A and B show mRNA expression (fold change) in controls and PAE calculated using formulas 1 and 2 (*Material and methods*) with means ± SEM. *p < 0.05 for comparison by Mann–Whitney. N 8 litters.

(Livak and Schmittgen, 2001; Pfaffl, 2001). At least three animals from each litter were analyzed and values were averaged per group, a minimum of three independent litters were analyzed.

Hippocampal Slice Electrophysiology

We followed the protocol described by Nguyen and Kandel, 1997. Acute transverse hippocampal slices with a thickness of 400 mm were prepared from 17 to 30 days old Sprague–Dawley rats using a DTK-1000 Microslicer (Ted Pella, Inc.) in ice cold dissection buffer (in mM: 215 sucrose, 2.5 KCl, 1.6 NaH_2PO_4, 26 $NaHCO_3$, 4 $MgSO_4 \times 7H_2O$, 4 $MgCl_2$, 1 $CaCl_2$, and 20 glucose, bubbled with a mixture of 5% CO_2 and 95% O_2). Slices were incubated for 30 min to 1 h at room temperature in artificial cerebrospinal fluid (ACSF, in mM: 124 NaCl, 2.5 KCl, 26 $NaHCO_3$, 1 NaH_2PO_4, 2.5 $CaCl_2$, 1.3 $MgSO_4$, and 10 glucose, bubbled with a mixture of 5% CO_2 and 95% O_2). Hippocampal slices were visualized using a Nikon Eclipse FN1 microscope. All experiments were performed at 28 ± 1°C in a submersion-type recording chamber perfused at 2 ml/min with ACSF supplemented with the GABAA receptor antagonist picrotoxin (PTX 100 μM). fEPSPs were evoked by stimulating Schaffer collaterals with a glass microelectrode (3–4 MΩ, filled with NaCl 1 M) positioned in the stratum radiatum of the CA1 area at 100 μm further than recording electrode located in the same region. Stimulation intensity was adjusted to elicit fEPSP amplitudes that were around 40% of the maximum size. For basal AMPAR transmission analysis, after 10–15 min of a stable baseline, slices from control or PAE rats were incubated with 20 μM Fe-NTA (a donor of Fe^{3+} as the complex $FeCl_3$–sodium nitrilotriacetate, Fe-NTA, 1:2.2, mol:mol), 100 μM DFP, or saline solution (vehicle) in an ACSF buffer. Slices that showed maximal fEPSPs >2 mV were rejected. Then basal transmission was measured for 40–45 min compared to the baseline average.

Paired-pulse ratio (PPR) was calculated by delivering two pulses at 100-ms inter stimulus interval and was defined as the ratio of the amplitude of the second fEPSP to the amplitude of the first fEPSP (fEPSP2/fEPSP1). Fiber Volley (Fv) amplitude was calculated using the peak, and amplitude of the descending phase of the FV curve was measured by recording the magnitude of the fEPSP as a function of stimulus intensity.

For LTP analysis, slices from control or PAE rats were preincubated with 20 μM Fe-NTA, 100 μM DFP, or vehicle (saline solution) in ACSF during 40 min and were continually perfused during the experiment. Plasticity was induced by high frequency stimulation (HFS) (100 Hz, 1 s). In all experiments the difference and comparison between the averaged-baseline and the responses after the induction was determined. All recordings were performed using a MultiClamp 700B amplifier (Molecular Devices), elicited at 15–20 s intervals, filtered at 2.4 kHz, and acquired at 10 kHz, using custom-made software written in Igor Pro 6.36 (Wavemetrics). Unless otherwise indicated, all electrophysiological values are provided as mean ± SEM and illustrated traces are the average of 30–40 responses.

All the experiments were repeated at least three times with different litters. For electrophysiological recordings, three to five acute hippocampal slices per subject were used and pooled to count as one litter.

Statistical Analysis

Data from groups, control and PAE, are presented as means ± SEM. For relative mRNA expression of iron homeostasis genes between PAE group and controls (**Figures 1A**, **B** and **Figures 2A**, **B**), the means ± SEM were analyzed by nonparametric Mann–Whitney. The comparison of mRNA expression between brain areas—PFC, hippocampus, and VTA—at P21 or P70–78 (in **Supplementary Figure 1**, and **Supplementary Table 1**), was analyzed by nonparametric Kruskal–Wallis, Dunn's multiple comparison test. The comparison of mRNA expression between different ages, P21 and P70–78, at specific areas was analyzed by Mann–Whitney test. For relative mRNA expression of genes involved in iron homeostasis between different ages (P21, P70–70) (**Supplementary Figure 2**), was calculated using the $2^{-\Delta\Delta CT}$ and statistical analysis by one-sample t-test, indicating significance ($^*p < 0.05$, $^{**}p < 0.05$). For protein expression the differences in mean values between two conditions were compared by a Mann–Whitney test. The electrophysiological

data were analysed with two way ANOVA repeated measures, followed by Tukey's *post-hoc*. In some particular cases, we also conducted planned comparation to analyze the effect of iron before and after treatment (paired t test) or iron effect of PAE LTP (unpaired t test). The partial eta squared (η^2p) or Cohen's d were used to inform effect size and the alpha level was kept at 0.05 across tests. Was calculated using the following formula: sum of square (SS)/(SS + error of SS).

RESULTS

PAE Altered the Expression of Iron Homeostasis Genes in Brain Regions Involved in Learning and Memory Processes

Brain iron homeostasis is a complex processes modulated by several proteins which are expressed in the brain, including DMT1 isoforms, TfR, FT, FPN, and the HAMP (Hentze et al., 2004; Ke et al., 2005; Singh et al., 2014). DMT1-1B isoforms (+IRE and −IRE) are expressed exclusively in the brain (Ke et al., 2005). First we evaluated the basal expression of these genes in control littermates. We evaluated gene expression in different brain regions (PFC, hippocampus, and VTA) and ages (P21 respect to P70–78) by RT-PCR and normalized to β-actin ($2^{-\Delta CT)}$ (**Supplementary Figures 1A–F**, and **Supplementary Table 1A**). The analysis showed that some genes presented significant differences between the PFC, hippocampus, and VTA at P21 or P70–78 (using nonparametric Kruskal–Wallis test following Dunn's multiple comparison test, **Supplementary Table 1A**). At P21 the isoform DMT1 (−) IRE and (+) IRE are expressed at higher levels in the VTA compared to the hippocampus (p = 0.0009, p = 0.0005, respectively); HAMP mRNA are expressed in higher levels in the VTA compared to the hippocampus (p = 0.00001); FPN are expressed in higher levels in the hippocampus compared to the PFC (p = 0.0235). While at P70–78 we did not find significant changes in iron homeostasis genes between the brain areas (**Supplementary Figure 1**). In addition, we analyzed whether iron homeostasis genes in specific brain areas present differences in expression levels between ages P21 and P70–78 (**Supplementary Table 1B**). We found that FPN expression decreased in the hippocampus in P70 compared to P21 (p = 0.0159, Mann–Whitney test). Meanwhile, HAMP mRNA expression increased in the PFC in P70 compared to P21 (p = 0.00375 Mann–Whitney test).

Next, we evaluated the effects of PAE on DMT1 and TFR gene expression at the mRNA and protein levels (**Figures 1A–C**). Using RT-qPCR and ($2^{-\Delta Ct\ PAE}/2^{-\Delta Ct\ Control}$, formula 1 and 2, *Material and Methods*), we found that the DMT1 (−) IRE mRNA isoform was increased by 1.925 ± 0.38 fold in the PFC (p = 0.0415, Mann–Whitney test), but it was not affected in the hippocampus and VTA of P21 PAE rats (**Figure 1A**, **Supplementary Table 2A**). In addition, P70–78 PAE rats did not present significant difference in DMT1 mRNA isoforms in P70–78 rats in these three areas analyzed (**Figure 1B**, **Supplementary Table 2B**). The comparative expression of these genes in different ages and brain regions can be observed in **Supplementary Figure 2A**. Consistent with the qRT-PCR analysis, we found that the PFC of PAE rats, but not hippocampus and VTA, presented a significant increased expression of DMT1 isoform proteins (bands of 68 kDa) immuno-detected with an antibody against the N-terminal domain (**Figure 1C**) (PAE 153.5 ± 24.54 N = 6, vs. controls 100 ± 6.05 N = 6, p = 0.0315, Mann–Whitney test). Additionally, we found that adolescent P21 PAE rats presented a significant increase in TFR mRNA (2.818 ± 0.7804 N = 9, p = 0.0071, Mann–Whitney test) in the hippocampus, but not in the PFC and VTA, compared to P21 control rats (**Figure 1A**, **Supplementary Table 2A**). Meanwhile in P70–78 PAE rats, TFR mRNA expression was unaffected (**Figure 1B**, **Supplementary Table 2B**). Consistent with the high expression of TFR mRNA in the hippocampus, Western blot analysis confirmed a significant increase of TfR protein expression (PAE 158 ± 23.17 versus controls 99.63 ± 10.80, p = 0.0043, Mann–Whitney test) at the hippocampus in P21 PAE rats compared to control rats (**Figure 1D**). Altogether, these results indicated that prenatal ethanol exposure changed the expression of proteins involved in iron uptake in a tissue-selective manner in P21 rats. Overexpression of the DMT-1B/(−)IRE isoform occurred in the PFC, meanwhile TfR overexpression was observed in the hippocampal region, and no changes occurred in the VTA of P21 PAE rats. Furthermore, cellular misregulation of DMT1 and TFR also suggest that additional genes involved in iron homeostasis can be misregulated in PAE rats.

PAE Altered the Expression of the Cellular Iron Storage Protein (Ferritin) and Iron Release Protein (Ferroportin) in Brain Regions Involved in Learning and Memory Processes

In order to test whether additional genes involved in iron homeostasis were altered by PAE we analyzed relative mRNA expression of FT and/or FPN by RT-qPCR (**Figures 2A**, **B**, **Supplementary Tables 3A**, **B**). We found that P21 PAE rats presented a significantly decreased expression of FPN mRNA (PAE 0.6738 ± 0.08506 N = 8 versus control 0.9963 ± 0.1759 N = 8, p = 0.0415, Mann–Whitney test) in the PFC, and both the heavy chain-ferritin (H-FT) (PAE rats 0.4513 ± 0.1710 N = 9 versus control 0.9997 ± 0.3728 N = 9, p = 0.0122, Mann–Whitney test) and FPN mRNA (PAE rats 0.5541 ± 0.2172, N = 8, versus control rats 0.9996 ± 0.2025 N = 8, p = 0.019, Mann–Whitney test) were significantly decreased in the hippocampus compared to P21 control rats (**Figure 2**, **Supplementary Table 3A**). While P70–80 PAE and control rats did not present significant changes in mRNA expression of these genes (**Figure 3B**, **Supplementary Table 3B**). In addition, we analyzed gene expression of HAMP, a hormone that regulates iron homeostasis by inflammatory stimuli in the brain (Urrutia et al., 2013), however we did not find significant variation of HAMP mRNA in PAE rats both at P21 and P70–78 (**Figure 2A**, **Supplementary Tables 3A**, **B**). The comparative expression of these genes at different ages and brain regions can be observed

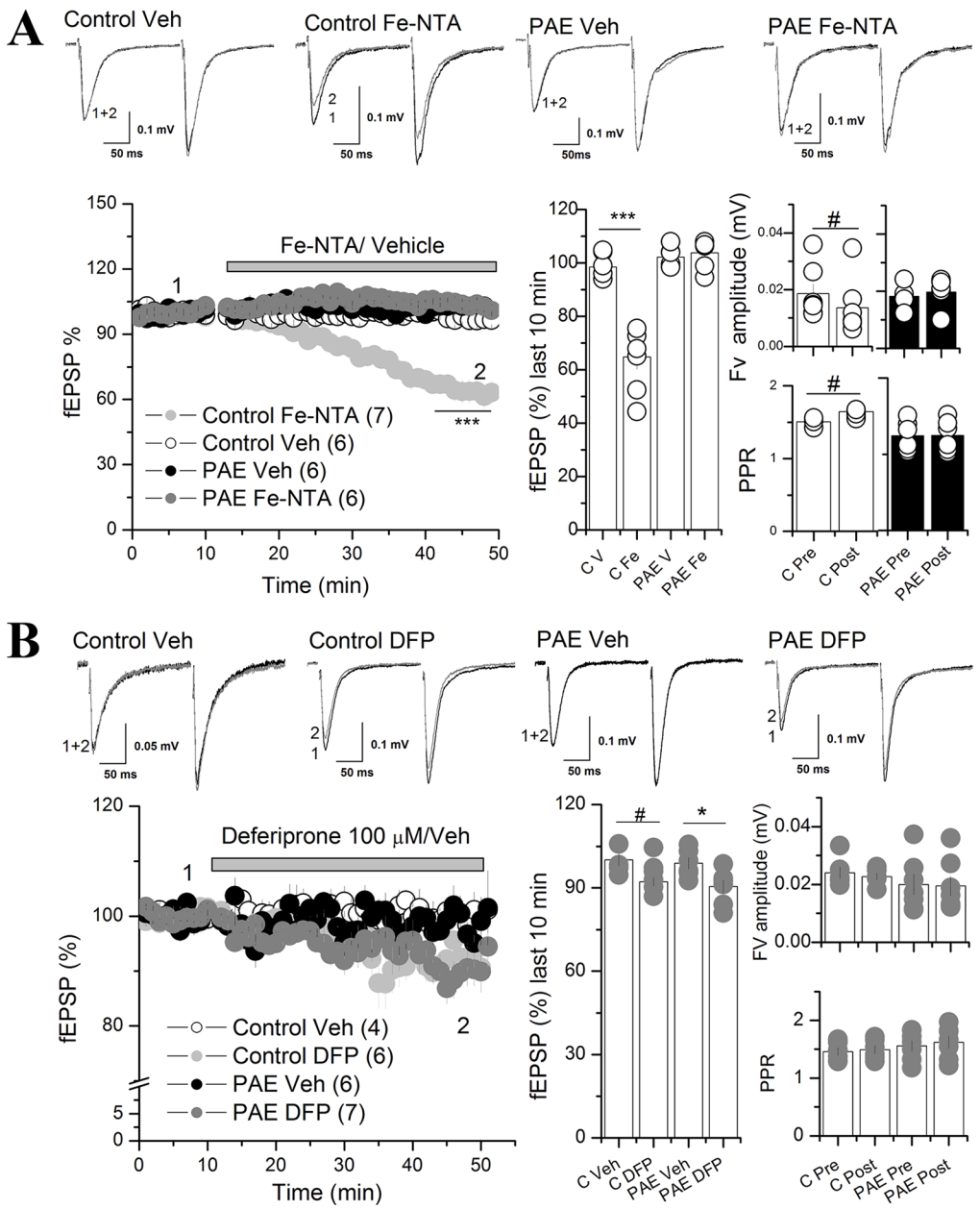

FIGURE 3 | Iron addition (Fe-NTA) and iron chelator (DFP) affects AMPAR synaptic transmission at the CA1 of the hippocampus of PAE rats compared to control rats. **(A)** Effect of Fe-NTA on basal transmission of PAE and control rats. Basal transmission (% fEPSP) was recorded on slices from control and PAE rats and 20 μM Fe-NTA or vehicle (Veh, V) was bath applied as is indicated in the graph. Bar graphs represent the average % fEPSP during the last 10 min, the fiber volley (Fv) amplitude and PPR pre HFS (Pre) and last 10 min of recording (Post) was represented in bar graphs. Note that FeNTA reduced basal transmission in control but not in PAE rats. Fv was decreased meanwhile PPR was larger (fEPSP2/fEPSP1) in control rats and not in PAE. **(B)** The effect of deferiprone (DFP) on basal transmission of PAE and control rats. After baseline, 100 μM DFP or vehicle (Veh, V) was bath applied as is indicated in the graph. Note that DFP incubation reduced basal transmission in PAE rats and controls. Fiber volley (Fv) amplitude and paired-pulse ratio (PPR) were not affected in PAE or control rats. In all panels, sample traces were taken at the times indicated by numbers on the summary plot; the number of litter is indicated in parentheses. ***p < value 0.0001, *p < value 0.05, repeated measured two way ANOVA followed Tukey's *post-hoc* test. #p < 0.01 paired t test **(A)** and unpaired t test **(B)**.

in **Supplementary Figure 2B**. Thus, these results show that PAE altered the expression of genes involved in cellular iron storage (FT) and iron release (FPN) in a tissue specific manner and in an inverse manner than that of DMT1 and TFR. While in PAE rats the H-FT and FPN genes were downregulated, the iron homeostasis genes involved in iron-uptake such as DMT1 and TfR were upregulated in brain areas involved with learning and memory process. These evidences suggest that the neuronal activity of the PFC and hippocampus could be affected by iron homeostasis dysregulation in PAE rats.

Iron Addition Decreased Basal Excitatory Transmission in the Scha-CA1 Region of the Hippocampus in Control But Not in PAE Rats

To evaluate whether altered iron homeostasis protein expression has any effects on synaptic transmission, we focused on glutamatergic neuronal activity in the hippocampal CA1 area, amply related with learning and memory processes (Eccles, 1986). We incubated hippocampal slices with Fe-NTA or DFP, in order to increase or deplete neuronal iron, respectively. Fe-NTA is a membrane impermeable iron complex, which can be uptake by cells in a transferrin-dependent or transferrin-independent manner (Matsuura, 1983; Chitambar and Sax, 1992). Meanwhile, DFP is a membrane permeable chelator for labile intracellular iron conforming the labile iron pool (LIP) (Glickstein et al., 2006).

First we evaluated basal excitatory synaptic transmission in hippocampal slices by measuring AMPAR field excitatory postsynaptic potentials (fEPSPs) in the CA1 region elicited by stimulation of Schaffer collateral fibers (Scha) before and after bath application of 20 μM Fe-NTA (**Figure 3A**). The two ANOVA anaysis revels a significant main effect between iron vs vehicle treatment [$F_{(1,5)}$ = 20.72, p = 0.0061, η^2p = 0.8] and an interaction between prenatal and iron treatment [$F_{(1,5)}$ = 63.21, *p* = 0.0005, η^2p = 0.98]. Analysis of the 10 last minutes of recording with Tukey's *post-hoc* test reveled that Fe-NTA did not affect excitatory basal transmission in PAE animals (**Figure 3A**), meanwhile in control slices, Fe-NTA reduced significantly the AMPAR fEPSP compared with vehicle treatment (64.8 ± 4.5% C Fe vs 89.56 ± 2.1% C Veh) (p = 0.00046). We also analyzed the fiber volley (Fv) amplitude and PPR. The two way ANOVA analysis of Fv and PPR, reveled a significant main interaction between prenatal conditions with iron treatment for Fv: $F_{(1,5)}$ = 13.013, p = 0.01542, η^2p = 0.72, and for PPR: $F_{(1,5)}$ = 20.10045, p = 0.0065, η^2p = 0.8. Tukey's *post-hoc* test was not able to show significantly differences, however, since the data are recolected before and after treatment, we performed a paired t test, which showed significant reduction in FV (0.014 ± 0.004, p = 0.00272 paired t test) together with a significant increased PPR (1.5 ± 0.029, p = 0.008 paired t test pre vs post application of Fe-NTA in control slices). These results showed that excitatory basal transmission was dysregulated in the hippocampal CA1 of PAE rats, since it was unaffected by Fe-NTA when transmission was reduced, most likely affecting presynaptic function.

Next we tested the efficacy of the glutamatergic synapse of PAE slices in presence of Fe-NTA. We measured AMPAR fEPSP at different stimulation intensities. No differences were detected in the fEPSP AMPAR responses (**Supplementary Figure 3**).

Additionally, we evaluated the effect of labile iron depletion on excitatory basal transmission in PAE and control rats with 100 μM DFP (**Figure 3B**). The two way ANOVA analysis showed a significant main differences between vehicle vs DFP treatment [$F_{(1,4)}$ = 10.319, p = 0.003252, η^2p = 0.72]. The Tukey analysis of the 10 last minutes of recording showed that DFP significant decreased AMPAR fEPSP in PAE rats (90.46 ± 2.27% PAE DFN vs 98.84 ± 2.03% PAE Veh (p = 0.03605), a pattern that was very similar, but not significant, to found in slices from control animals bathed with DFP (100.1 ± 2.16% C Veh; 92.18 ± 1.6% C DFN; p = 0.077). Because the trens obseved in the bar graph 3B we conducted a planned analysis between C Veh and C DFN. We found that DFN reduced AMPAR fEPSP in control slices (p = 0.015 unpaired t test). In addition, no significant differences were found in the Fv and PPR in PAE or controls before and after DFP application. We used vehicle (saline or DMSO) as a control of recording, demonstrating the stable recording during the whole experiment. These results suggest that a regulated LIP concentration is necessary to maintain AMPAR fEPSP in both conditions, PAE and control rats.

Iron Addition Exacerbated the Decreasing Long-Term Potentiation in PAE Rats Compared to Control Rats

Previous studies have shown that intracellular iron participates in signaling mediated by ROS, which can modulate LTP in a dose-dependent manner (Massaad and Klann, 2011)(Beckhauser et al., 2016). Our results show that the hippocampus from PAE rats presented a misregulation in genes involved in iron homeostasis (TFR, FPN, and FT), predicting that LTP will be much more affected by incubation with iron than the control. To evaluate this we evoked LTP using HFS in the Sha-CA1 region from slices preincubated 40 min with 20 μM Fe-NTA or vehicle (saline) (**Figure 4A**).The two way ANOVA analysis showed a significant main differences between AMPAR fEPSP in slices from control vs PAE animals [$F_{(1,5)}$ = 11.48 p = 0.01949, η^2p = 0.69), as previously described (Marquardt and Brigman, 2016) (**Figure 4A**). Also is showed a significant difference between vehicle and Fe-NTA treatment [$F_{(1,5)}$ = 4.767, p = 0.008076 η^2p = 0.48). However, the Tukey analysis showed that iron incubation slighly decreased LTP in PAE rats compared to vehicle incubation (108.52 ± 3.48% PAE Fe; 119.99 ± 2.50% PAE Veh, Tukey p = 0.05706). We also conduced a planned comparision between both groups and found that Fe-NTA treatment significant reduced LTP in PAE animals (p = 0.0202 unpaired t test).

In contrast, Fe-NTA incubation did not affect LTP in control rats compared to control incubated only with vehicle ((126.23 ± 6.18% C Fe vs 131.29 ± 2.70% C veh, p = 0.4245 Tukey's *post-hoc* test). These results showed that the imbalance in the iron proteins observed in the hippocampus of PAE rats can be perfectly correlated with altered synaptic plasticity observed after iron addition in PAE, which does not occur in slices from control rats incubated with iron.

To analyze the effect of iron on LTP induction we quantified the area under the curve during a HFS burst as a measurement of charge transfer. Not changes were detected in PAE slices treated with vehicle versus Fe-NTA (**Supplementary Figure 4**).

Labile iron depletion with DFP impairs LTP in hippocampal slices (Muñoz et al., 2011). The two way ANOVA analysis showed a significant main differences between vehicle vs DFP treatment [$F_{(1,6)}$ = 18.16, p = 0.00581, η^2p = 0.7516). Tukey's *post-hoc* test confirm a significant difference between control and PAE slices treated with vehicle (p = 0.04) and also that DFP decreased the magnitude of LTP in control hippocampal slices compared to control slice treated with vehicle (111.74 ± 4.51 C Fe % vs

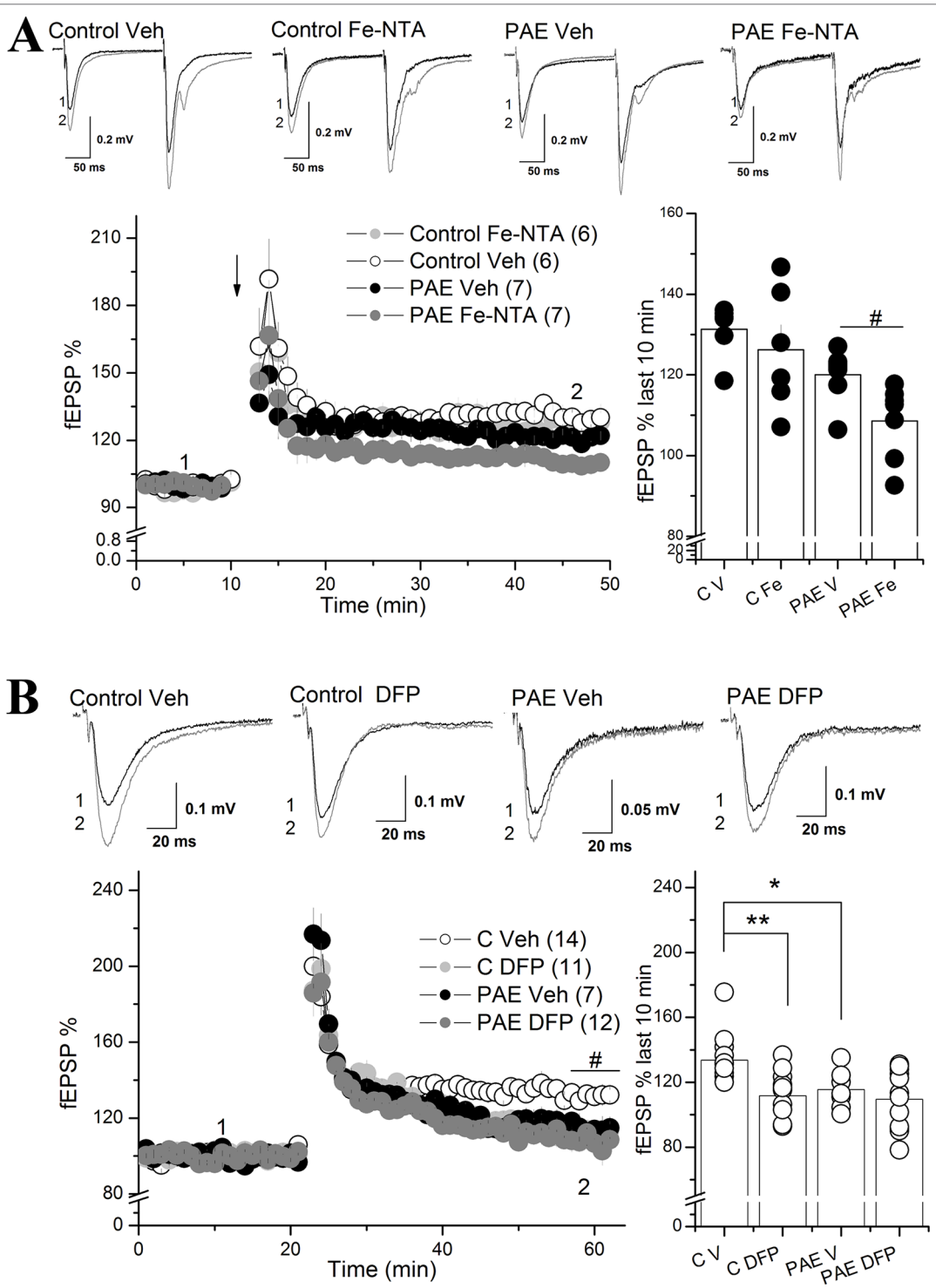

FIGURE 4 | Iron addition (Fe-NTA) and iron chelation (DFP) altered the long-term potentiation (LTP) of prenatal ethanol exposure (PAE) rats compared to controls rats. **(A)** Effect of Fe-NTA on CA1 LTP of PAE and control rats. For long-term potentiation (LTP) analysis, slices from control or PAE rats were preincubated with 20 μM Fe-NTA, or saline (vehicle), during 40 min and continually perfused during the experiment. LTP (% fEPSP) was induced by high frequency stimulation (HFS) (100 Hz, 1 s). The average % fEPSP of the last 10 min was represented by bar graphs. Note that in PAE but not in control animals, Fe-NTA produced a significant decrease of LTP. **(B)** Effect of DFP on CA1 LTP of PAE and control rats. Slices were preincubated for 40 min with DFP and were continually perfused during the experiment. LTP experiment similar to A but in the presence of 100 μM of DFP. LTP (% fEPSP) was induced by high frequency stimulation (HFS) (100 Hz, 1 s). The average % fEPSP of the last 10 min was represented by bar graphs. Note that DFP significantly affected the LTP of control rats but not PAE rats. In all panels, sample traces were taken at the times indicated by numbers on the summary plot. The number of litter is indicated in parentheses. # Two way ANOVA C vs C DFP in temporal curse graph **(B)**.**p value < 0.01, *p value < 0.05, repeated measured two way ANOVA followed Tukey's *post-hoc* test. $^{\#}p < 0.01$ unpaired t test.

133.66 ± 3.79% C Veh, p = 0.00551), **Figure 4B**); meanwhile DFP maintained the magnitude of LTP in PAE rats compared to PAE incubated with vehicle (109.57 ± 5.28% PAE Fe NTA, 115.53 ± 4.51% PAE Veh, p = 0.15697). These results showed that the remained plasticity in PAE animals does not require intracellular labile iron levels in contrast to the iron requirements of control animals. Moreover, the addition of Fe in PAE slices also is detrimental for LTP, strongly suggesting altered iron homeostasis compared to controls.

Altogether, we found for the first time that rats with prenatal alcohol exposure presented misregulated expression of genes involved in iron homeostasis at the PFC (upregulation of DMT1) and the hippocampus (upregulation of TfR, and downregulation of FT and FPN), which could be functionally correlated with a dysregulated basal transmission and plasticity in the CA1 of PAE rats compared to controls.

DISCUSSION

PAE may generate fetal alcohol spectrum disorder (FASD) characterized by cognitive alterations in learning and memory formation (Sutherland et al., 1998; Patten et al., 2014; Contreras et al., 2017). Since the mechanisms are poorly understood, some recent studies have shown that PAE alters hippocampal synaptic plasticity (Marquardt and Brigman, 2016), and affects brain iron homeostasis (Miller et al., 1995; Carter et al., 2007; Rufer et al., 2012; Huebner et al., 2016), supporting the hypothesis that PAE can dysregulates brain iron homeostasis, contributing to altered hippocampal synaptic plasticity in adolescent animals. To evaluate this, we analyzed the expression of genes involved in iron homeostasis [DMT1, TFR, H-FT, FPN, and hepcidin (HAMP)] at three areas related with cognitive processes such as the PFC, hippocampus, and VTA (Lisman and Grace, 2005), together with functional measurement of glutamatergic synaptic transmission and plasticity in the hippocampal CA1 region. We found that PAE misregulated specifically and differentially the expression of genes involved in iron homeostasis in the PFC and hippocampus, but not in the VTA. Interestingly, in adolescent hippocampus, PAE upregulated TfR, but downregulated both FT and FPN, most likely resulting in a higher levels of intracellular iron. These results are consistent with an altered glutamatergic transmission and plasticity in response to iron or iron chelation, in hippocampal CA1 slices. These evidences show for the first time that PAE affects iron homeostasis and iron-dependent synaptic transmission and plasticity at the hippocampal CA1 area, suggesting that iron homeostasis dysregulation may be a critical target for developing therapeutic strategies for offspring suffering FASD.

PAE Misregulated Genes Involved in Iron Homeostasis in the Hippocampus of Adolescent PAE Rats

Our first finding that PAE misregulated genes involved in iron homeostasis at the PFC and hippocampus, but not in the VTA, was supported by mRNA (RT-qPCR) and protein expression (Western-blotting) analysis. We found that PAE specifically upregulated the iron uptake proteins DMT1 at the PFC, and TfR at the hippocampus, while PAE downregulated both FPN mRNA at the PFC, and FT and FPN at the hippocampus, in all tested 21 day old offspring (**Figures 1** and **2**). Since, previous studies have shown that PAE present decreased iron levels at the cerebral cortex, but not at the subcortical forebrain and brainstem between P1 and P60–75 (Miller et al., 1995) our results open the question that PAE decreased the levels of LIP in specific brain areas, however still remain to be determinate. In agreement with our results, recently Huebner and coworkers showed that PAE rats, with an iron deficient diet, produced an exacerbated iron decrease and downregulation of FT in the whole brain at gestational day 20.5 (G20.5) (Huebner et al., 2016). However, contrary to our results, this group reported that PAE downregulated TfR protein and did not affect DMT1 and FPN protein expression, differences that could be explained by the age of the animal analyzed (G20.5) and/or the type of samples analyzed (total brain homogenate) (Huebner et al., 2016), meanwhile our analysis of expression levels (mRNA and protein) were performed in specific brain areas from postnatal 21-day-old rats.

Our observation of altered expression of genes involved in iron homeostasis, high TfR, and low FT and FPN, is consistent with a cellular response to low intracellular labile iron levels, which can be mediated by IRP. It is known that cells in order to uptake or release iron can coordinately modulate the expression of iron transporters (DMT1, TfR, FPN) and iron-storage proteins (FT) at the transcriptional and translational levels (Hentze and Kuhn, 1996; Kruer, 2013). In low iron level conditions, cells increase their expression of TFR and DMT1 through IRP interacting with the 3′ mRNA of TfR and DMT1 to increase their stability and translation, while decreasing the expression of FPN and FT by binding IRP with IREs located at the 5′ of these mRNAs to repress translation (Bogdan et al., 2016). These antecedents suggest that the iron/IRP mechanism could be involved in the misregulation that we observed in some genes involved in iron homeostasis at the PFC and/or hippocampus of adolescent PAE rats. However, upregulation of DMT1-1B, an isoform lacking the IRE element (**Figures 1A**, **C**), suggests that DMT1 1B isoforms expression could be activated by a mechanism independent of IRP. A possible mechanism could be mediated by HAMP, which downregulates DMT-1B (–) IRE mRNA in the PFC (Li et al., 2011), predicting that low expression of hepcidin in the PAE could upregulates DMT-1B (–) IRE mRNA. However, contrary to this prediction, previous reports have shown that PAE rats (at gestational day 20) overexpress HAMP (Huebner et al., 2016), and also our RT-qPCR results show that HAMP mRNA expression was unaffected in all brain areas analyzed (**Figure 2**). The mechanisms involved in DMT1 overexpression in PAE animals is still unknown. However it is tempted to suggest a regulation by inflammatory molecules (IL6 and TNF) as it has been described to upregulate DMT1 in brain (Urrutia et al., 2013). More studies are necessary to resolve how PAE upregulates DMT1/(–)IRE. Thus, our results show that PAE specifically and differentially misregulated the expression of genes involved in iron homeostasis (TfR, DMT1B/(–)IRE, FT, and FPN) in brain areas related with learning and memory such as the PFC and hippocampus, but not in the VTA, suggesting iron

homeostasis dysregulation as a new mechanism of maladapted neuronal plasticity in animals exposed to ethanol in utero. In addition, misregulation of genes involved in iron homeostasis observed in PAE animals could affect several mechanisms involved in synaptic transmission and plasticity that underlie cognitive alterations observed in FASD.

PAE Presented Dysregulated Basal Hippocampal Transmission and Synaptic Plasticity That Correlates With Misregulation of Genes Involved in Iron Homeostasis

Several mechanisms may be involved in how iron homeostasis dysregulation in PAE rats that could affect the offspring and induce a maladaptation to the environment. Nutritional studies have shown that iron deficiency both prenatally and perinatally are associated with intellectual disabilities and psychiatric disorders (Carlson et al., 2007; Sidrak et al., 2014). Here we observed iron homeostasis genes are differentially regulated by PAE in several regions of the brain, perhaps modulating a coordinated activation of different regions involved in cognition, in special between PFC and hippocampus, where we found the more consistent observations described above. Moreover an iron deficient diet can affect hippocampal plasticity by impairing dopaminergic-mediated synaptic plasticity (Breton et al., 2015), disruption of synaptic maturation (Jorgenson et al., 2005), or by abnormality of the CA1 apical dendrite structure (Fretham et al., 2011; Muñoz and Humeres, 2012).

Also, the hippocampal conditional knockout mice (KO) of DMT1 ($Slc11a2^{hipp/hipp}$) had a decreased energy status that promotes shorter dendrites and disorganized branching patterns in the hippocampal CA1 region compared with normal mice (Carlson et al., 2009), and also a reduced spatial memory behavior (Carlson et al., 2010). Also, iron homeostasis seems to be involved in hippocampal glutamatergic transmission, since DMT1B (mRNA and protein levels) was upregulated after NMDAR activation or spatial memory training (Haeger et al., 2010). Interestingly, recent evidence showed that iron uptake mediated by lysosomal DMT1 can negatively modulate NMDAR activity (White et al., 2016). Additionally, Liu and coworkers using a conditional KO mice for TfR, showed a dramatic reduction of basal transmission and long term plasticity (LTP) through an iron-independent mechanism involving TfR-dependent AMPAR trafficking (Liu et al., 2016). Therefore, all these studies, together with our gene expression results, suggest that this misregulation of the iron homeostasis genes could mediate altered glutamatergic transmission in the hippocampal CA1 region of PAE rats.

In agreement with this, our first electrophysiological results showed that AMPAR synaptic transmission in the hippocampal CA1 area of control rats was reduced together with decreased fiber volley and increased PPR when incubated with iron (Fe-NTA), suggesting an Iron dependent presynaptic mechanism. This evidence suggests that in controls, but not in PAE animals, Iron regulates glutamatergic transmission through a presynatic mechanism that in turn decreases neuronal excitability when exposed to excess iron. Nevertheless, this 40% of reduction in AMPAR synaptic transmission is not enough to affect the induction of long term potentiation in control animals in presence of Fe-NTA (**Figure 3A**).

Even though the mechanism affecting iron over the short term is unknown it has been described that synaptosome treated with 10 μM FeSO4 for 4 h decreases glutamate uptake (Guo et al., 2000). We can speculate that the elevated postsynaptic expression of TfR in PAE animals masks the presynaptic effect because it regulates the iron concentration in the synaptic cleft. However, deferiprone incubation slightly decreased AMPAR synaptic transmission in control as well in PAE animals denoting that the mechanism involving basal synaptic transmission is a complex process, therefore we cannot discard that other mechanisms are affecting by Iron, such as presynaptic and postsynaptic events (Vargas et al., 2007; Fioravante and Regehr, 2011; Ramaswami et al., 2016) and the complex regulation by astrocytes (Navarrete and Araque, 2011; Panatier et al., 2011). Additional studies are necessary to determine which is the putative mechanism.

Our second electrophysiological results showed that hippocampal synaptic plasticity in the CA1 was also altered by iron incubation (Fe-NTA) in adolescent PAE rats compared with controls (**Figures 4A**, **B**). Our findings showed that Fe-NTA exacerbated the impaired LTP in PAE rats compared to control animals. Since it is known that Fe-NTA can be uptake by the cell by Tf/TfR endocytic pathway and the Tf-independent mechanism (Matsuura, 1983)(Chitambar and Sax, 1992), it is tempting to suggest that the high expression of TfR and low expression of FT and FPN in the hippocampus of PAE animals allows intracellular iron levels to increase in turn impairing LTP. The changes in LIP could affect synaptic plasticity at the CA1 of PAE rats by different nonexclusive mechanisms.

One possibility is that changes in labile iron concentration affect NMDAR activity. In agreement with this, it was recently described that depletion of iron with a permeable chelator (pyridoxal isonicotinoyl hydrazine) enhances the excitability of hippocampal pyramidal cells, increasing the amount of the NR2A subunit and NMDAR activity (White et al., 2016). Interestingly, this iron-dependent NMDAR modulation requires iron release from lysosomes, which is a DMT1 mediated process (White et al., 2016). Given that an important pathway for iron uptake and release to the endosomal/lysosomal system is mediated by endocytosis of the Tf/TfR complex and lysosomal DMT1 (Fleming et al., 1998; Lawrence et al., 1999; Cheng et al., 2004), the upregulated TfR expression in the hippocampus of PAE rats could promote increased iron uptake, after incubation with Fe-NTA, compared to controls; producing the lower LTP observed in the hippocampal CA1 of PAE rats.

An additional mechanism that could be involved in impaired LTP at the CA1 of PAE rats after incubation with Fe-NTA may be mediated by oxidative stress. A controlled ROS production provides the optimal redox state necessary for synaptic plasticity (Beckhauser et al., 2016), however when high ROS is accumulated it induces oxidative stress which is associated with LTP impairment and cognitive decline as observed in neurodegenerative disorders and age-dependent decay of neuroplasticity (Massaad and Klann, 2011). Physiological intracellular iron levels can react with peroxide (H_2O_2), through the Haber–Weiss and Fenton reactions,

to produce hydroxyl radical which sensitizes ryanodine receptor, a endoplasmatic Ca^{2+} channels, to calcium induces calcium release after activation of NMDAR during induction of LTP (Muñoz et al., 2011). Additionally, the incubation of several iron-related compounds such as forms of hemoglobin, hemin, and ferrous chloride increase ROS, affecting synaptic transmission of hippocampal brain slices (Pellmar, 1986; Pellmar et al., 1991; Yip and Sastry, 2000). Thus, these evidences suggest that incubation with Fe-NTA promotes high intracellular iron levels, mediated by dysregulated expression of genes involved in iron homeostasis (TFR, FPN, and FT), favoring the Fenton reaction and oxidative stress, impairing LTP. Several oxidative stress mechanisms could affect hippocampal LTP, including ROS mediated upregulation of calcineurin, which through the activation of protein phosphatase 1 can decrease AMPAR activity, and/or ROS mediated modulation of CAMKII that can directly alters NMDA receptor function (Beckhauser et al., 2016).

It is amply known that iron-dependent ROS generation regulates NMDAR activity, favoring NMDAR-induced calcium signal (Muñoz et al., 2011) or negatively modulate NMDAR activity mediated by lysosomal iron uptake througth DMT1 (White et al., 2016). In our case, exogenous iron application, but not iron chelation, decreased LTP in PAE slices. It is tempting to suggest that mysregulated iron homeostasis in PAE animals could affect iron-dependent NMDAR activation during LTP induction. However, quantification of the area under HFS-burst does not change in the the presence of Iron (**Supplementary Figure 4**), supporting the idea that the global machinery during LTP induction is not modified. However, we can still not discard a direct and a transient effect on NMDAR activity.More studies are necessary to dissect the particular role of iron in the hippocampal plasticity of PAE animals.

Similar to the hippocampus, we detected changes in the iron transporter DMT1 and FNP in PFC at P21, but not in P70–78 or VTA. However, we did not evaluate the functional significance of the mysregulated iron homeostasis in these brain region. We speculate that PFC function could be similar to the hippocampus due to their active metabolic rate (Rice and Barone, 2000) and complementarity in memory processes (Nelson, 1995). Moreover, perinatal iron deficiency increased the expression of iron transporters in both areas, similar to that observed in this study. In contrast striatum did not have the same response as the hippocampus and cortex, suggesting different iron requirements for striatum activity (Siddappa et al., 2003). Moreover the function of the PFC and hippocampus was measured by different tasks in adolescents with chronic and severe iron deficiency during infancy. They showed impairment in the frontostriatal-mediated executive functions and in the performance of hippocampus-based recognition memory tasks (Lukowski et al., 2010) supporting similar Iron requirement in both areas.

In the VTA of PAE animals iron homeostasis genes did not change compared to age-matched controls (P21 and P70–78). However we did observe that the VTA of control animals expressed higher levels of DMT1(+), IRE, DMT1 (–) IRE y HAMP than the hippocampus, and higher levels of HAMP mRNA than the PFC, respectively (see **Supplementary Figure 1**, **Supplementary Table 1A**). These evidences complement the essential role of iron for the synthesis, metabolism, and function of dopamine (Ramsey et al., 1996; Matak et al., 2016; Yien and Paw, 2016). Regarding the function of VTA in PAE animals, we previously described that NOX2 inhibition, a synaptic enzyme that synthesizes superoxide in the VTA, restored alcohol-conditioned place preference in PAE animals (Contreras et al., 2017). Moreover we detected higher DOPAC levels, a dopamine metabolite, in the VTA terminals of nucleus accumbens of PAE animals (Plaza et al., 2019). However, the mechanism involved in iron homeostasis and the particular role of Iron in VTA function of PAE animals will be a matter to be addressed in future studies.

The present study has several limitations and caveats. Since changes in the expression of different mRNAs involved in iron homeostasis suggest reduced intracellular iron levels in the hippocampus of PAE animals, we also need to measure iron as well protein levels in different brain regions. Moreover, to understand the iron-dependent mechanism involved in glutamatergic transmission it will be important to study the role of Iron in isolated NMDAR activity and its participation in hippocampal LTP induction.

Despite these limitations, the present study showed, for the first time, that adolescents rat that were exposed to alcohol *in utero* presented a specific misregulation of iron homeostasis genes (DMT1, TFR, FT, and FPN) in the PFC and hippocampus, but not in the VTA. Moreover, in the hippocampal CA1 area of PAE rats we found a functional correlation between a misregulation of iron homeostasis genes with dysregulated synaptic transmission and plasticity of this brain area. Alterations in iron homeostasis could represent a potential mechanism that underlies the cognitive deficits associated with FASD. In addition, our study predicts that nutritional iron supplementation of postnatal PAE animals could be deleterious for neuronal activity and plasticity, since it could add to the potential increase of iron mediated by the misregulation of iron homeostasis genes. Identification of this mechanism will facilitate the development of novel therapies for fetal alcohol spectrum disorder.

DATA AVAILABILITY STATEMENT

All datasets generated for this study are included in the article/ **Supplementary Material**.

ETHICS STATEMENT

The animal study was reviewed and approved by Bioethic, Scientific, and Animal Care and Use Committee of the Universidad Católica del Norte, Chile.

AUTHOR CONTRIBUTIONS

EF-O and PH contributed to the conception and design of the study. EF-O and SV-R contributed to the acquisition and

statistical analysis of RT-qPCR experiments. WP-B and PH contributed to the acquisition of data and statistical analysis electrophysiological experiments. EF-O and PH worked on the analysis and interpretation of data and wrote the manuscript. All authors contributed to manuscript revision, read, and approved the submitted version.

FUNDING

This work was supported by Chilean Fondecyt grant no. 1140855 and from PEW Latin American postdoctoral fellowship to P.H. VRIDT-UCN, IBRO-LARC.

ACKNOWLEDGMENTS

We would like to thank Daniela Muñoz and Daniela Jara for their contribution in the pilot experiments and Dr Ricardo M. Pautassi for his advice in statistical analysis. We also thank Dr. Marco Tulio Nuñez for providing the specific DMT1 antibody and for his critical review of the manuscript.

SUPPLEMENTARY MATERIAL

The Supplementary Material for this article can be found online at: https://www.frontiersin.org/articles/10.3389/fphar.2019.01312/full#supplementary-material

REFERENCES

Aisen, P., Wessling-Resnick, M., and Leibold, E. A. (1999). Iron metabolism. *Curr. Opin. Chem. Biol.* 3, 200–206. doi: 10.1016/S1367-5931(99)80033-7

Andersen, H. S., Gambling, L., Holtrop, G., and McArdle, H. J. (2007). Effect of dietary copper deficiency on iron metabolism in the pregnant rat. *Br. J. Nutr.* 97, 239–246. doi: 10.1017/S0007114507239960

Aros, S. I., Mills, J. L., Torres, C., Henriquez, C., Fuentes, A., Capurro, T., et al. (2009). Prospective identification of pregnant women drinking four or more standard drinks (> or = 48 g) of Alcohol Per Day. *Subst. Use Misuse* 41, 183–197. doi: 10.1080/10826080500391779

Beard, J. L., and Connor, J. R. (2003). Iron status and neural functioning. *Annu. Rev. Nutr.* 23, 41–58. doi: 10.1146/annurev.nutr.23.020102.075739

Beckhauser, T. F., Francis-Oliveira, J., De Pasquale, R., Pasquale, R., De, Beckhauser, T. F., and Francis-Oliveira, J. (2016). Reactive oxygen species: physiological and physiopathological effects on synaptic plasticity. *J. Exp. Neurosci.* 10, 23–48. doi: 10.4137/JEN.S39887

Bogdan, A. R., Miyazawa, M., Hashimoto, K., and Tsuji, Y. (2016). Regulators of iron homeostasis: new players in metabolism, Cell Death, and Disease. *Trends Biochem. Sci.* 41, 274–286. doi: 10.1016/j.tibs.2015.11.012

Bond, N. W., and di Giusto, E. L. (1976). Effects of prenatal alcohol consumption on open-field behaviour and alcohol preference in rats. *Psychopharmacologia* 46, 163–165. doi: 10.1007/BF00421386

Boserup, M. W., Lichota, J., Haile, D., and Moos, T. (2011). Heterogenous distribution of ferroportin-containing neurons in mouse brain. *Biometals* 24, 357–375. doi: 10.1007/s10534-010-9405-2

Breton, A. B., Fox, J. A., Brownson, M. P., and McEchron, M. D. (2015). Postnatal nutritional iron deficiency impairs dopaminergic-mediated synaptic plasticity in the CA1 area of the hippocampus. *Nutr. Neurosci.* 18, 241–247. doi: 10.1179/1476830514Y.0000000121

Burgess, N., Maguire, E. A., and O'Keefe, J. (2002). The human hippocampus and spatial and episodic memory. *Neuron* 35, 625–641. doi: 10.1016/S0896-6273(02)00830-9

Carlson, E. S., Fretham, S. J. B., Unger, E., O'Connor, M., Petryk, A., Schallert, T., et al. (2010). Hippocampus specific iron deficiency alters competition and cooperation between developing memory systems. *J. Neurodev. Disord.* 2, 133–143. doi: 10.1007/s11689-010-9049-0

Carlson, E. S., Stead, J. D. H., Neal, C. R., Petryk, A., and Georgieff, M. K. (2007). Perinatal iron deficiency results in altered developmental expression of genes mediating energy metabolism and neuronal morphogenesis in hippocampus. *Hippocampus* 17, 679–691. doi: 10.1002/hipo.20307

Carlson, E. S., Tkac, I., Magid, R., O'Connor, M. B., Andrews, N. C., Schallert, T., et al. (2009). Iron is essential for neuron development and memory function in mouse hippocampus. *J. Nutr.* 139, 672–679. doi: 10.3945/jn.108.096354

Carter, R. C., Jacobson, S. W., Molteno, C. D., and Jacobson, J. L. (2007). Fetal alcohol exposure, iron-deficiency anemia, and infant growth. *Pediatrics* 120, 559–567. doi: 10.1542/peds.2007-0151

Carter, R. C., Senekal, M., Dodge, N. C., Bechard, L. J., Meintjes, E. M., Molteno, C. D., et al. (2017). Maternal alcohol use and nutrition during pregnancy: diet and anthropometry. *Alcohol Clin. Exp. Res.* 41, 2114–2127. doi: 10.1111/acer.13504

Cheng, Y., Zak, O., Aisen, P., Harrison, S. C., Walz, T., and York, N. (2004). Structure of the human transferrin receptor-transferrin complex Albert Einstein college of medicine. *Cell* 116, 565–576. doi: S0092867404001308

Chitambar, C. R., and Sax, D. (1992). Regulatory effects of gallium on transferrin-independent iron uptake by human leukemic HL60 cells. *Blood* 80, 505–511. Available at: http://www.ncbi.nlm.nih.gov/pubmed/1627803 [Accessed March 5, 2019].

Collins, J. F., Wessling-Resnick, M., and Knutson, M. D. (2008). Hepcidin regulation of iron transport. *J. Nutr.* 138, 2284–2288. doi: 10.3945/jn.108.096347

Contreras, M. L., de la Fuente-Ortega, E., Vargas-Roberts, S., Muñoz, D. C., Goic, C. A., and Haeger, P. A. (2017). NADPH oxidase isoform 2 (NOX2) is involved in drug addiction vulnerability in progeny developmentally exposed to ethanol. *Front. Neurosci.* 11, 3029. doi: 10.3389/fnins.2017.00338

Cuzon, V. C., Yeh, P. W. L., Yanagawa, Y., Obata, K., and Yeh, H. H. (2008). Ethanol consumption during early pregnancy alters the disposition of tangentially migrating GABAergic interneurons in the fetal cortex. *J. Neurosci.* 28, 1854–1864. doi: 10.1523/JNEUROSCI.5110-07.2008

Dong, J., Sulik, K. K., and Chen, S. (2010). The role of NOX enzymes in ethanol-induced oxidative stress and apoptosis in mouse embryos. *Toxicol. Lett.* 193, 94–100. doi: 10.1016/j.toxlet.2009.12.012

Eccles, J. C. (1986). Mechanisms of long-term memory. *J. Physiol. (Paris)* 81, 312–317. Available at: http://www.ncbi.nlm.nih.gov/pubmed/3572825 [Accessed March 29, 2019].

Eichenbaum, H. (2017). Prefrontal–hippocampal interactions in episodic memory. *Nat. Rev. Neurosci.* 18, 547–558. doi: 10.1038/nrn.2017.74

Fabio, M. C., Macchione, A. F., Nizhnikov, M. E., and Pautassi, R. M. (2015). Prenatal ethanol increases ethanol intake throughout adolescence, alters ethanol-mediated aversive learning, and affects μ but not δ or κ opioid receptor mRNA expression. *Eur. J. Neurosci.* 41, 1569–1579. doi: 10.1111/ejn.12913

Fioravante, D., and Regehr, W. G. (2011). Short-term forms of presynaptic plasticity. *Curr. Opin. Neurobiol.* 21, 269–274. doi: 10.1016/j.conb.2011.02.003

Fleming, M. D., Romano, M. A., Su, M. A., Garrick, L. M., Garrick, M. D., and Andrews, N. C. (1998). Nramp2 is mutated in the anemic Belgrade (b) rat: Evidence of a role for Nramp2 in endosomal iron transport. *Proc. Natl. Acad. Sci.* 95, 1148–1153. doi: 10.1073/pnas.95.3.1148

Fretham, S. J. B., Carlson, E. S., and Georgieff, M. K. (2011). The role of iron in learning and memory. *Adv. Nutr.* 2, 112–121. doi: 10.3945/an.110.000190

Glickstein, H., El, R., Link, G., Breuer, W., Konijn, A. M., Hershko, C., et al. (2006). Action of chelators in iron-loaded cardiac cells: accessibility to intracellular labile iron and functional consequences. *Blood* 108, 3195–3203. doi: 10.1182/blood-2006-05-020867

Guo, Z., Ersoz, A., Butterfield, D. A., and Mattson, M. P. (2000). Beneficial effects of dietary restriction on cerebral cortical synaptic terminals: Preservation of glucose and glutamate transport and mitochondrial function after exposure to amyloid β-peptide, iron, and 3-nitropropionic acid. *J. Neurochem.* 75, 314–320. doi: 10.1046/j.1471-4159.2000.0750314.x

Haeger, P., Álvarez, Á., Leal, N., Adasme, T., Núñez, M. T., and Hidalgo, C. (2010). Increased hippocampal expression of the divalent metal transporter 1 (DMT1) mRNA variants 1B and +IRE and DMT1 protein after NMDA-Receptor stimulation or spatial memory training. *Neurotox. Res.* 17, 238–247. doi: 10.1007/s12640-009-9096-z

Hentze, M. W., and Kuhn, L. C. (1996). Molecular control of vertebrate iron metabolism: mRNA-based regulatory circuits operated by iron, nitric oxide, and oxidative stress. *Proc. Natl. Acad. Sci.* 93, 8175–8182. doi: 10.1073/pnas.93.16.8175

Hentze, M. W., Muckenthaler, M. U., and Andrews, N. C. (2004). Balancing acts: molecular control of mammalian iron metabolism. *Cell* 117, 285–297. doi: 10.1016/S0092-8674(04)00343-5

Hidalgo, C., Carrasco, M. A., Muñoz, P., and Núñez, M. T. (2007). A role for reactive oxygen/nitrogen species and iron on neuronal synaptic plasticity. *Antioxid. Redox Signal.* 9, 245–255. doi: 10.1089/ars.2007.9.245

Huebner, S. M., Blohowiak, S. E., Kling, P. J., and Smith, S. M. (2016). Prenatal alcohol exposure alters fetal iron distribution and elevates hepatic hepcidin in a rat model of fetal alcohol spectrum disorders. *J. Nutr.* 146, 1180–1188. doi: 10.3945/jn.115.227983

Jorgenson, L. A., Sun, M., O'Connor, M., and Georgieff, M. K. (2005). Fetal iron deficiency disrupts the maturation of synaptic function and efficacy in area CA1 of the developing rat hippocampus. *Hippocampus* 15, 1094–1102. doi: 10.1002/hipo.20128

Ke, Y., Chang, Y. Z., Duan, X. L., Du, J. R., Zhu, L., Wang, K., et al. (2005). Age-dependent and iron-independent expression of two mRNA isoforms of divalent metal transporter 1 in rat brain. *Neurobiol. Aging* 26, 739–748. doi: 10.1016/j.neurobiolaging.2004.06.002

Kruer, M. C. (2013). The neuropathology of neurodegeneration with brain iron accumulation. *Int. Rev. Neurobiol.*, 110, 165–194. doi: 10.1016/B978-0-12-410502-7.00009-0

Kruszewski, M. (2003). Labile iron pool: the main determinant of cellular response to oxidative stress. *Mutat. Res. Mol. Mech. Mutagen.* 531, 81–92. doi: 10.1016/j.mrfmmm.2003.08.004

Lawrence, C. M., Ray, S., Babyonyshev, M., Galluser, R., Borhani, D. W., and Harrison, S. C. (1999). Crystal structure of the ectodomain of human transferrin receptor. *Science.* 286, 779–783. doi: 10.1126/science.286.5440.779

Li, L., Holscher, C., Chen, B.-B., Zhang, Z.-F., and Liu, Y.-Z. (2011). Hepcidin treatment modulates the expression of divalent metal transporter-1, ceruloplasmin, and ferroportin-1 in the rat cerebral cortex and hippocampus. *Biol. Trace Elem. Res.* 143, 1581–1593. doi: 10.1007/s12011-011-8967-3

Lisman, J. E., and Grace, A. A. (2005). The hippocampal-vta loop: controlling the entry of information into long-term memory. *Neuron* 46, 703–713. doi: 10.1016/j.neuron.2005.05.002

Liu, K., Lei, R., Li, Q., Wang, X.-X., Wu, Q., An, P., et al. (2016). Transferrin receptor controls ampa receptor trafficking efficiency and synaptic plasticity. *Sci. Rep.* 6, 21019. doi: 10.1038/srep21019

Livak, K. J., and Schmittgen, T. D. (2001). Analysis of relative gene expression data using real-time quantitative pCR and the 2–ΔΔCT method. *Methods* 25, 402–408. doi: 10.1006/meth.2001.1262

Lukowski, A. F., Koss, M., Burden, M. J., Jonides, J., Nelson, C. A., Kaciroti, N., et al. (2010). Iron deficiency in infancy and neurocognitive functioning at 19 years: evidence of long-term deficits in executive function and recognition memory. *Nutr. Neurosci.* 13, 54–70. doi: 10.1179/147683010X12611460763689

Mackenzie, E. L., Iwasaki, K., and Tsuji, Y. (2008). Intracellular iron transport and storage: from molecular mechanisms to health implications. *Antioxid. Redox Signal.* 10, 997–1030. doi: 10.1089/ars.2007.1893

Marquardt, K., and Brigman, J. L. (2016). The impact of prenatal alcohol exposure on social, cognitive and affective behavioral domains: Insights from rodent models. *Alcohol* 51, 1–15. doi: 10.1016/j.alcohol.2015.12.002

Massaad, C. A., and Klann, E. (2011). Reactive oxygen species in the regulation of synaptic plasticity and memory. *Antioxid. Redox Signal.* 14, 2013–2054. doi: 10.1089/ars.2010.3208

Matak, P., Matak, A., Moustafa, S., Aryal, D. K., Benner, E. J., Wetsel, W., et al. (2016). Disrupted iron homeostasis causes dopaminergic neurodegeneration in mice. *Proc. Natl. Acad. Sci. U. S. A.* 113, 3428–3435. doi: 10.1073/pnas.1519473113

Matsuura, R. (1983). Uptake of iron and nitrilotriacetate (NTA) in rat liver and the toxic effect of Fe-NTA. *Acta Med. Okayama* 37, 393–400. doi: 10.18926/AMO/32422

Miller, M. W., Roskams, A. J., and Connor, J. R. (1995). Iron regulation in the developing rat brain: effect of in utero ethanol exposure. *J. Neurochem.* 65, 373–380. doi: 10.1046/j.1471-4159.1995.65010373.x

Moriconi, F., Ahmad, G., Ramadori, P., Malik, I., Sheikh, N., Merli, M., et al. (2009). Phagocytosis of gadolinium chloride or zymosan induces simultaneous upregulation of hepcidin-and downregulation of hemojuvelin-and Fpn-1-gene expression in murine liver. *Lab. Investig.* 89, 1252–1260. doi: 10.1038/labinvest.2009.92

Muñoz, P., and Humeres, A. (2012). Iron deficiency on neuronal function. *BioMetals* 25, 825–835. doi: 10.1007/s10534-012-9550-x

Muñoz, P., Humeres, A., Elgueta, C., Kirkwood, A., Hidalgo, C., and Núñez, M. T. (2011). Iron mediates n -methyl-d-aspartate receptor-dependent stimulation of calcium-induced pathways and hippocampal synaptic plasticity. *J. Biol. Chem.* 286, 13382–13392. doi: 10.1074/jbc.M110.213785

Navarrete, M., and Araque, A. (2011). Basal synaptic transmission: Astrocytes rule! *Cell* 146, 675–677. doi: 10.1016/j.cell.2011.08.006

Naz, N., Malik, I. A., Sheikh, N., Ahmad, S., Khan, S., Blaschke, M., et al. (2012). Ferroportin-1 is a 'nuclear'-negative acute-phase protein in rat liver: a comparison with other iron-transport proteins. *Lab. Investig.* 92, 842–856. doi: 10.1038/labinvest.2012.52

Nelson, C. A. (1995). The ontogeny of human memory: A cognitive neuroscience perspective. *Dev. Psychol.* 31, 723–738. doi: 10.1037/0012-1649.31.5.723

Nguyen, P. V., and Kandel, E. R. (1997). Brief theta-burst stimulation induces a transcription-dependent late phase of LTP requiring cAMP in area CA1 of the mouse hippocampus. *Learn. Mem.* 4, 230–243. doi: 10.1101/lm.4.2.230

Núñez, M. T., Gaete, V., Watkins, J. A., and Glass, J. (1990). Mobilization of iron from endocytic vesicles. The effects of acidification and reduction. *J. Biol. Chem.* 265, 6688–6692. Available at: http://www.ncbi.nlm.nih.gov/pubmed/2324097.

Panatier, A., Vallée, J., Haber, M., Murai, K. K., Lacaille, J. C., and Robitaille, R. (2011). Astrocytes are endogenous regulators of basal transmission at central synapses. *Cell* 146, 785–798. doi: 10.1016/j.cell.2011.07.022

Patten, A. R., Fontaine, C. J., and Christie, B. R. (2014). A comparison of the different animal models of fetal alcohol spectrum disorders and their use in studying complex behaviors. *Front. Pediatr.* 2, 93. doi: 10.3389/fped.2014.00093

Pelizzoni, I., Zacchetti, D., Smith, C. P., Grohovaz, F., and Codazzi, F. (2012). Expression of divalent metal transporter 1 in primary hippocampal neurons: reconsidering its role in non-transferrin-bound iron influx. *J. Neurochem.* 120, 269–278. doi: 10.1111/j.1471-4159.2011.07578.x

Pellmar, T. (1986). Electrophysiological correlates of peroxide damage in guinea pig hippocampus *in vitro*. *Brain Res.* 364, 377–381. doi: 10.1016/0006-8993(86)90851-6

Pellmar, T. C., Hollinden, G. E., and Sarvey, J. M. (1991). Free radicals accelerate the decay of long-term potentiation in field CA1 of guinea-pig hippocampus. *Neuroscience* 44, 353–359. doi: 10.1016/0306-4522(91)90060-2

Pfaffl, M. W. (2001). A new mathematical model for relative quantification in real-time RT-PCR. *Nucleic Acids Res.* 29, 45e– 45. doi: 10.1093/nar/29.9.e45

Phillips, J. G., and Whitlock, R. I. (1976). The effect of an alcoholic injection for facial pain. *Br. J. Oral Surg.* 14, 173–178.

Plaza, W., Gaschino, F., Gutierrez, C., Santibañez, N., Estay-Olmos, C., Sotomayor-Zárate., et al. (2019). Pre and postnatal alcohol exposure delays, in female but not in male rats, the extinction of an auditory fear conditioned memory and increases alcohol consumption. *Dev. Psychobiol.* doi: 10.1002/dev.21925

Ramaswami, M., Krishnan, K. S., Balakrishnan, S. S., Kumar, V., Reddy-Alla, S., Thakur, R. S., et al. (2016). σ 2 -Adaptin facilitates basal synaptic transmission and is required for regenerating endo-exo cycling pool under high-frequency nerve stimulation in drosophila. *Genetics* 203, 369–385. doi: 10.1534/genetics.115.183863

Ramsey, A. J., Hillas, P. J., and Fitzpatrick, P. F. (1996). Characterization of the active site iron in tyrosine hydroxylase Redox states of the iron. *J. Biol. Chem.* 271, 24395–24400.

Ramsay, M. (2010). Genetic and epigenetic insights into fetal alcohol spectrum disorders. *Genome Med.* 2, 27. doi: 10.1186/gm148

Rice, D., and Barone, S. (2000). Critical periods of vulnerability for the developing nervous system: evidence from humans and animal models. *Environ. Health Perspect.* 108, 511–5303. doi: 10.1289/ehp.00108s3511

Rufer, E. S., Tran, T. D., Attridge, M. M., Andrzejewski, M. E., Flentke, G. R., and Smith, S. M. (2012). Adequacy of maternal iron status protects against behavioral, neuroanatomical, and growth deficits in fetal alcohol spectrum disorders. *PloS One* 7, e47499. doi: 10.1371/journal.pone.0047499

Schmittgen, T. D., and Livak, K. J. (2008). Analyzing real-time PCR data by the comparative CT method. *Nat. Protoc.* 3, 1101–1108. doi: 10.1038/nprot.2008.73

Siddappa, A. J. M., Rao, R. B., Wobken, J. D., Casperson, K., Leibold, E. A., Connor, J. R., et al. (2003). Iron deficiency alters iron regulatory protein and iron transport protein expression in the perinatal rat brain. *Pediatr. Res.* 53, 800–807. doi: 10.1203/01.PDR.0000058922.67035.D5

Sidrak, S., Yoong, T., and Woolfenden, S. (2014). Iron deficiency in children with global developmental delay and autism spectrum disorder. *J. Paediatr. Child Health* 50, 356–361. doi: 10.1111/jpc.12483

Singh, N., Haldar, S., Tripathi, A. K., Horback, K., Wong, J., Sharma, D., et al. (2014). Brain iron homeostasis: from molecular mechanisms to clinical significance and therapeutic opportunities. *Antioxid. Redox Signal.* 20, 1324–1363. doi: 10.1089/ars.2012.4931

Skorput, A. G. J., Gupta, V. P., Yeh, P. W. L., and Yeh, H. H. (2015). Persistent Interneuronopathy in the prefrontal cortex of young adult offspring exposed to ethanol in utero. *J. Neurosci.* 35, 10977–10988. doi: 10.1523/JNEUROSCI.1462-15.2015

Sutherland, R. J., McDonald, R. J., and Savage, D. D. (1998). Prenatal exposure to moderate levels of ethanol can have long-lasting effects on hippocampal synaptic plasticity in adult offspring. *Hippocampus* 7, 232–238. doi: 10.1002/(sici)1098-1063(1997)7:2<232::aid-hipo9>3.0.co;2-o

Urrutia, P., Aguirre, P., Esparza, A., Tapia, V., Mena, N. P., Arredondo, M., et al. (2013). Inflammation alters the expression of DMT1, FPN1 and hepcidin, and it causes iron accumulation in central nervous system cells. *J. Neurochem.* 126, 541–549. doi: 10.1111/jnc.12244

Valko, M., Morris, H., and Cronin, M. T. D. (2005). Metals, toxicity and oxidative stress. *Curr. Med. Chem.* 12, 1161–1208. doi: 0.2174/0929867053764635

Vargas, R., Cifuentes, F., and Morales, M. A. (2007). Differential contribution of extracellular and intracellular calcium sources to basal transmission and long-term potentiation in the sympathetic ganglion of the rat. *Dev. Neurobiol.* 67, 589–602. doi: 10.1002/dneu.20364

Wang, J., and Pantopoulos, K. (2011). Regulation of cellular iron metabolism. *Biochem. J.* 434, 365–381. doi: 10.1042/BJ20101825

White, R. S., Bhattacharya, A. K., Chen, Y., Byrd, M., McMullen, M. F., Siegel, S. J., et al. (2016). Lysosomal iron modulates NMDA receptor-mediated excitation *via* small GTPase, Dexras1. *Mol. Brain* 9, 1–14. doi: 10.1186/s13041-016-0220-8

Wu, L. J., Leenders, A. G., Cooperman, S., Meyron-Holtz, E., Smith, S., Land, W., et al. (2004). Expression of the iron transporter ferroportin in synaptic vesicles and the blood-brain barrier. *Brain Res.* 1001, 108–117. doi: 10.1016/j.brainres.2003.10.066

Yien, Y. Y., and Paw, B. H. (2016). A role for iron deficiency in dopaminergic neurodegeneration. *Proc. Natl. Acad. Sci.* 113, 3417–3418. doi: 10.1073/pnas.1601976113

Yip, S., and Sastry, B. R. (2000). Effects of hemoglobin and its breakdown products on synaptic transmission in rat hippocampal CA1 neurons. *Brain Res.* 864, 1–12. doi: 10.1016/S0006-8993(00)02067-9

Conflict of Interest: The authors declare that the research was conducted in the absence of any commercial or financial relationships that could be construed as a potential conflict of interest.

frontiers in Pharmacology

ORIGINAL RESEARCH
published: 14 November 2019
doi: 10.3389/fphar.2019.01314

Upregulation of Cortical Renin and Downregulation of Medullary (Pro) Renin Receptor in Unilateral Ureteral Obstruction

*Stefanny M. Figueroa[1,2], Mauricio Lozano[1], Carolina Lobos[1], Matthew T. Hennrikus[3], Alexis A. Gonzalez[2] and Cristián A. Amador[1]**

[1] Laboratorio de Fisiopatología Renal, Instituto de Ciencias Biomédicas, Universidad Autónoma de Chile, Santiago, Chile, [2] Instituto de Química, Pontificia Universidad Católica de Valparaíso, Valparaíso, Chile, [3] Department of Physiology, Tulane University School of Medicine, New Orleans, LA, United States

Chronic kidney disease (CKD) is characterized by renal dysfunction, which is a common feature of other major diseases, such as hypertension and diabetes. Unilateral ureteral obstruction (UUO) has been used as a model of CKD in experimental animals and consists of total obstruction of one kidney ureter. The UUO decreases renal blood flow, which promotes the synthesis of renin in the juxtaglomerular apparatus, the first step in renin–angiotensin system (RAS) cascade. RAS induces inflammation and remodeling, along with reduced renal function. However, it remains unknown whether intrarenal RAS (iRAS) is activated in early stages of CKD. Our objective was to characterize different iRAS components in the renal cortex and in the medulla in an early phase of UUO. Male C57BL/6 mice (8–12 weeks old) were subjected to UUO in the left kidney, or to sham surgery, and were euthanized after 7 days (n = 5/group). Renal function, renal inflammatory/remodeling processes, and iRAS expression were evaluated. UUO increased plasma creatinine, right renal hypertrophy (9.08 ± 0.31, $P < 0.05$ vs. Sham), and tubular dilatation in the left kidney cortex (42.42 ± 8.19μm, $P < 0.05$ vs. Sham). This correlated with the increased mRNA of IL-1β (1.73 ± 0.14, $P < 0.01$ vs. Sham, a pro-inflammatory cytokine) and TGF-β1 (1.76 ± 0.10, $P < 0.001$ vs. Sham, a pro-fibrotic marker). In the renal cortex of the left kidney, UUO increased the mRNA and protein levels of renin (in 35% and 28%, respectively, $P < 0.05$ vs. Sham). UUO decreased mRNA and protein levels for the (pro)renin receptor in the renal medulla (0.67 ± 0.036 and 0.88 ± 0.028, respectively, $P < 0.05$ vs. Sham). Our results suggest that modulation of iRAS components depends on renal localization and occurs in parallel with remodeling and pro-inflammatory/pro-fibrotic mechanisms.

Keywords: chronic kidney disease, intrarenal RAS, unilateral ureter obstruction, inflammation, pro-renin receptor

OPEN ACCESS

Edited by:
Guillermo Diaz-Araya, University of Chile, Chile

Reviewed by:
Shankar Munusamy, Drake University, United States
Kazem Zibara, Lebanese University, Lebanon
Ana Cristina Simões E. Silva, Federal University of Minas Gerais, Brazil

***Correspondence:**
Cristián A. Amador
cristian.amador@uautonoma.cl

Specialty section:
This article was submitted to Translational Pharmacology, a section of the journal Frontiers in Pharmacology

Received: *01 July 2019*
Accepted: *15 October 2019*
Published: *14 November 2019*

Citation:
Figueroa SM, Lozano M, Lobos C, Hennrikus MT, Gonzalez AA and Amador CA (2019) Upregulation of Cortical Renin and Downregulation of Medullary (Pro)Renin Receptor in Unilateral Ureteral Obstruction. Front. Pharmacol. 10:1314. doi: 10.3389/fphar.2019.01314

INTRODUCTION

Chronic kidney disease (CKD) is a worldwide health problem closely linked to other major diseases (Tonelli et al., 2015) that is difficult to diagnose and affects around 10% of the population (De Nicola and Zoccali 2016). CKD increases cardiovascular mortality and is a risk multiplier for patients with hypertension and/or diabetes mellitus (Couser et al., 2011).

CKD is defined by a sustained reduction in glomerular filtration rate (GFR) (Levey et al., 2011), which involves structural or functional anomalies of the kidneys evidenced on urine analysis (proteinuria) (Tonelli et al., 2011), biopsy, or imaging. Evidential structural abnormalities in CKD are characterized by glomerulosclerosis, tubular atrophy, and tubulo-interstitial fibrosis (Menon and Ross 2016), three conditions that drive nephrons to deterioration and to irreversible renal failure.

The unilateral ureteral obstruction (UUO) is a physiologically relevant *in vivo* model of renal inflammation that leads to fibrosis (Yang et al., 2010). UUO recapitulates the fundamental pathophysiologic mechanisms that typify all forms of human CKD in a relatively short time span (Eddy et al., 2012). It has been demonstrated that UUO increases interstitial capillary permeability (Yamaguchi et al., 2012) and the levels of IL-1-linked cytokines and transforming growth factor-β1 (TGF-β1), which correlate with the recruitment of inflammatory mononuclear cells (Eddy and Neilson 2006; Chi et al., 2017). Cao et al., 2015 described that during the first week, this pro-inflammatory phenotype is crucial for renal fibrosis consolidation observed after 4 weeks of UUO in mice (Cao et al., 2015). Thus, the UUO surgery in rodents can be used as an experimental model for studying the early (inflammatory, 7 days) (Ucero et al., 2014) and/or consolidated (fibrotic, 14 days) stage of CKD (Martínez-Klimova et al., 2019).

Ureteral constriction reduces the GFR and induces a renin release (Eide et al., 1977), which represent the first step of renin–angiotensin system (RAS) activation (Kobori et al., 2007). This effect is considered to be critical because kidneys possess an intrinsic RAS (or intrarenal RAS, iRAS) that can also regulate the water and sodium balance and blood pressure (Velez 2009). In this context, it has been demonstrated that 24 h of UUO downregulates the mRNA levels of renal angiotensin-II (AngII) type 1 receptor (AT_1R) (Pimentel et al.,1994) and increases the mRNA levels of renin from the juxtaglomerular apparatus (Pimentel et al., 1993). These changes, of which most were characterized 20 years ago, suggest that obstructive uropathy rapidly leads to hemodynamic alterations that may be implicated in the onset of CKD. Renin is also expressed in the collecting duct and is secreted by the principal cells in the renal medulla. Renin binds to the (pro)renin receptor (PRR, named also ATPase, H^+ transporting lysosomal accessory protein 2—*Atp6ap2*) (Nehme et al., 2019) at the neighboring intercalated cells (also in the medulla), thus activating pro-renin in a catalytic or non-catalytic form and increasing intratubular AngII formation while also triggering intracellular cascades related to fibrosis (Gonzalez et al., 2017).

We hypothesized that iRAS activation occurs during the early structural changes and the pro-inflammatory phase induced by UUO. This would be crucial for fibrosis consolidation and renal remodeling. Therefore, the main objective of our work was to characterize the iRAS components such as renin and PRR in the renal cortex and in the medulla at 7 days of UUO in mice.

MATERIALS AND METHODS

Animals and Experimental Protocol

For UUO, 9- to 12-week-old male C57BL/6 mice (n = 5) were anesthetized with a solution of ketamine/xylazine (80:8 mg kg^{-1}) and the left ureter was exposed by a dorsal incision. Then the ureter was obstructed by two-point ligation with silk sutures. Sham-operated mice (n = 5) underwent the same procedure, except for the obstruction of the left ureter (Ucero et al., 2014). All the experimental procedures with animals were performed according to the Committee on Animal Research and Ethics (Guidelines for Ethical Conduct in the Care and Use of Nonhuman Animals in Research, 2012) and were under the surveillance of the Ethics Committee of the Universidad Autonoma de Chile. Animals were placed in conditions of light–dark cycle (12 h), temperature of 21°C, humidity of 50%, adequate ventilation, noise-free, food and water *ad libitum*, and under continuous veterinary monitoring.

For histological and biochemical analyses, the animals were sacrificed 7 days after surgeries and the kidneys were quickly removed through a dorsal incision. Plasma was collected and stored at −20°C. Plasma creatinine and blood urine nitrogen (BUN) were analyzed using automated chemistry Jaffe assay and UV urease kit, respectively (Valtek Diagnostics, Santiago, Chile).

Histological Analysis

Sagittal sections of obstructed kidneys were fixed in Bouin (Sigma Aldrich, USA), embedded in paraffin, and 5-μm sections were prepared using a Leica RM2235 microtome (Leica Microsystems, Shanghai). The sections were washed and stained with hematoxylin–eosin (Sigma Aldrich, USA) for the assessment of tubular diameter. Images for cortices and medullas were captured with a Nikon digital sight DS-U3 digital camera, attached to a Nikon Upright Microscope ECLIPSE Ci-L (Nikon Instruments Inc., USA), and analyzed using ImageJ 1.43u software (NIH, USA).

Total RNA Isolation and qrt-PCR

Total RNA from whole kidney, cortex, and medulla was extracted with the TRIzol reagent, according to the manufacturer's instructions (ThermoFisher Scientific, USA). For whole kidney and renal cortex, cDNA was synthesized from 2 μg of RNA using M-MLV reverse transcriptase kit® (Promega, USA), while in the medulla, cDNA was synthesized from 1 μg of RNA using Superscript II reverse transcriptase kit® (ThermoFisher Scientific, USA). Real-time PCR reactions were performed in a LightCycler96® (Roche, Switzerland), and transcript levels were detected by SYBR Green method using FastStart Essential DNA Master mix (Roche, Switzerland). The following primers were used: 18S: (F) 5′-GCC GCTAGAGGTGAAATTCTTGGA-3′, (R) 5′-ATCGCCAGTGGCATCGTTTAT-3′; angiotensin-converting enzyme (ACE)1: (F) 5′-ATGAAGCCAAGGCTGACAGGTT-3′, (R) 5′-GTGATTGGAT ACCTCCGTTGCTT-3′; ACE2: (F) 5′-GGGGTGAAATTCCCAAAGAGCAGT-3′, (R) 5′-TCTGC CCAGCTTCAGTGGAATTTG-3′; AGT: (F) 5′-ACTGCTCC

AGGCTTTCGTCTAA-3′, (R) 5′-TC CACCCTGTCACAGCCT TTAT-3′; AT1Ra: (F) 5′-ACACTGCCATGCCCATAACCA-3′, (R) 5′-T AGACAGGCTTGAGTGCGACTT-3′; IL-1β: (F) 5′-ACTGGTACATCAGCACCTCACAAG-3′, (R) 5′-GCT GTCTGCTCATTCACGAAAAGG-3′; PRR (*Atp6ap2* gene): (F) 5′-GCGGGTGCTTTA GGGAATGAAT-3′, (R) 5′-TGG CCAAGACAGGTCTTCCTTT-3′; REN1: (F) 5′-AGCTCCCT GA AGTTGATCATGC-3′, (R) 5′-CTCCTGTTGGGATACTGT AGCA-3′; TGF-β1: (F) 5′-TACGCCT GAGTGGCTGTCTTTT-3′, (R) 5′-TTGGGGCTGATCCCGTTGATTT-3′. All PCR products were subjected to a melting curve program to confirm amplification specificity. Results were analyzed according to the standard curve method and mRNA level was calculated with respect to the relative amount of 18S for each sample.

Protein Analysis by Western Blot

For protein extraction, a lysis buffer containing 50 mM Tris-HCl (pH 7.5), 0.1 mM NaCl, 0.5% Triton X-100, 0.5 M EDTA, and a mixture of protease/phosphatase inhibitors (Roche, Switzerland) were used. We used a D-160 Scilogex polytron (ABC Scientific, USA) and sonication at 130 W, 20 KHz and 60% amplification (Ultrasonic Processor, USA) to homogenize the tissues. After centrifugation at 7,500×*g* for 5 min at 4°C, the supernatant was collected and total protein concentration in the sample was measured using a BCA protein assay kit (ThermoFisher Scientific, USA). Samples containing equal amounts of protein (40 μg for cortex and 10 μg for medulla/lane) were separated based on their molecular weight by 7.5% polyacrylamide gels for electrophoresis (SDS-PAGE) and transferred onto nitrocellulose membranes at a constant current of 2.5 A, 25 V for 7 min (BioRad, USA). After blocking with 5% non-fat milk in Tris-buffered saline with 0.1% Tween-20 (TBST) for 1 h at room temperature (RT), the membranes were stain with ponceau red and later incubated with primary antibodies against renin and ACE (both used at 1:200; Santa Cruz Biotechnology, USA), angiotensinogen (AGT) (1:200, Immuno-Biological Laboratory, Japan), PRR (1:250, Sigma Aldrich, USA), and α-tubulin (1:40,000, Sigma Aldrich, USA) overnight at 4°C. Subsequently, the membranes were washed with TBST and incubated with the corresponding secondary antibodies (including goat anti-mouse IgG and mouse anti-rabbit IgG, 1:3,000) for 1 h at RT, and finally visualized by enhanced chemiluminescence reagents (ThermoFisher Scientific, USA). The relative expression level of proteins was analyzed using ImageJ software.

Statistics

Results from *in vivo* studies were expressed as the mean ± SEM. Data were analyzed by one-way analysis of variance (ANOVA) test followed by Bonferroni posttest (more than two groups), by Student's *t* test, or Mann–Whitney nonparametric test (two groups), as appropriate. All analyses were performed using GraphPad Prism (GraphPad Software, USA). Values of $P < 0.05$ were considered as statistically significant.

RESULTS

UUO Induces an Increase in Plasma Creatinine and Hypertrophy in Contralateral Kidney

After 7 days of total left ureteral obstruction, mice presented with right kidney hypertrophy, as shown by the increase in right kidney weight/tibia length ratio (9.76 ± 0.42 g, $P < 0.05$; **Table 1**). No difference was detected in left kidney weight.

As an indirect way to determine GFR reduction in our model, we observed that UUO induced an increase in plasma creatinine in relation to the Sham group (0.57 ± 0.12 mg/dl, $P < 0.05$), but did not increase the BUN.

UUO Produces a Pro-Inflammatory and Pro-Fibrotic Status in the Obstructed Kidney

Since our aim was to study the UUO during the pro-inflammatory phase leading to the pro-fibrotic phenotype, we determined the levels of interleukin-1β (IL-1β) and TGF-β1, as a major pro-inflammatory cytokine involved in tubulointerstitial injury (Tesch et al., 1997) and as the main fibrosis-promoting factor (Ding et al., 2014), respectively. The analysis by quantitative RT-PCR demonstrated that IL-1β (1.7-fold change, FC, vs. Sham, $P < 0.01$) and TGF-β1 (1.9 FC vs. Sham, $P < 0.001$) were increased in the left (obstructed) kidney after 7 days of UUO (**Figures 1A**, **B**, respectively). These effects were not observed at level of the right kidney and were in concordance with previous results reported (Pimentel et al., 1995; Wang et al., 2015).

UUO Induces Tubular Remodeling in Cortex and Medulla of Obstructed Kidney

In order to explore the tubular remodeling induced by UUO in the renal cortex and in the medulla, we analyzed by light microscopy transversal sections of the left kidney stained by hematoxylin–eosin (**Figure 2**). We observed that UUO induced an increase of tubule interstitial space (**Figure 2**, black arrows) and an enlargement of diameter in cortical tubules (**Figure 2**), which has been related with the increase of the tubular lumen

TABLE 1 | UUO induces a contralateral renal hypertrophy and a rise of plasma creatinine.

Group	Sham	UUO
Total weight (g)	23.77 ± 0.45	22.28 ± 0.61
Left kidney weight/tibia length (mg/mm)	8.09 ± 0.35	8.41 ± 0.38
Right kidney weight/tibia length (mg/mm)	8.13 ± 0.26	**9.76 ± 0.42***
Blood urea nitrogen (mg/dl)	58.32 ± 1.87	59.19 ± 7.49
Creatinine (mg/dl)	0.368 ± 0.021	**0.574 ± 0.117***

*Physiological parameters at 7 days of UUO BUN blood urea nitrogen, UUO unilateral ureteral obstruction Mann–Whitney statistic test. *P < 0.05 vs. Sham group (n = 5).*

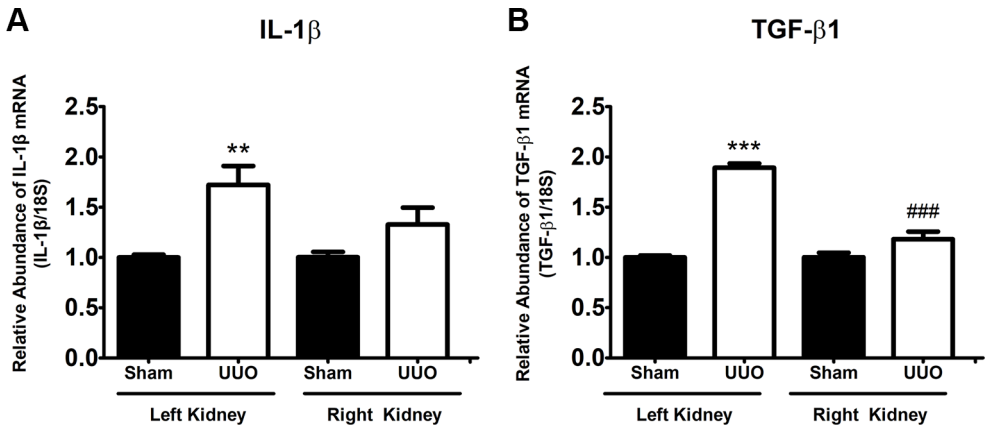

FIGURE 1 | Unilateral ureteral obstruction (UUO) induces a pro-inflammatory and pro-fibrotic phenotype at 7 days. **(A)** IL-1β and **(B)** TGF-β1 mRNA levels in the left and right kidneys. 18S mRNA was used as the housekeeping gene. One-way ANOVA test followed by Bonferroni test was performed. ***P* 0.01 and ****P* 0.001 vs. Sham group. ###*P* 0.001 vs. UUO left kidney group (*n* = 5).

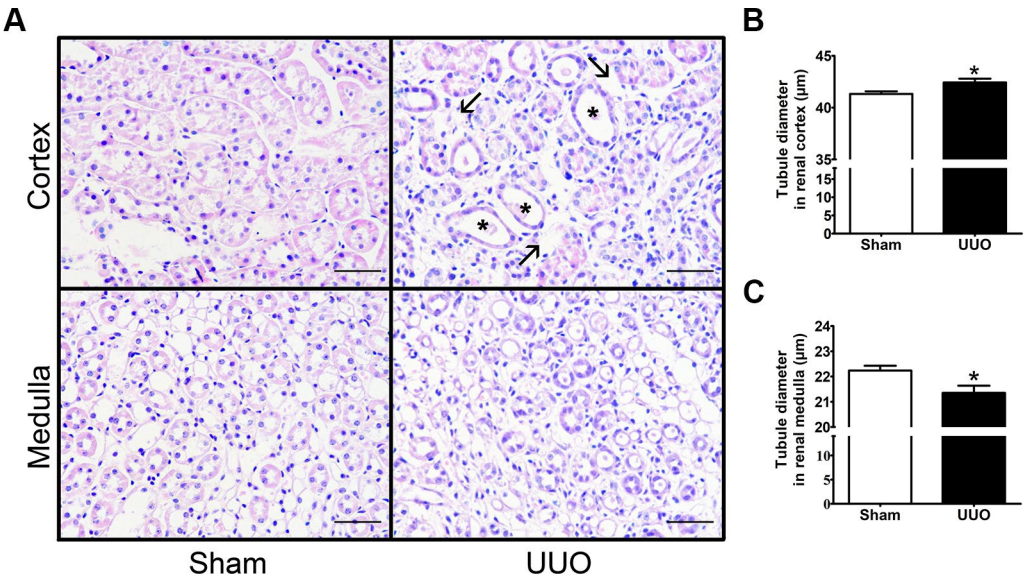

FIGURE 2 | Unilateral ureteral obstruction (UUO) induces tubular remodeling in the renal cortex and medulla after 7 days. **(A)** Haematoxylin–eosin staining in the renal cortex and medulla (*scale bar*, 100 μm). *Black arrows* show the increase of tubule interstitial space, while *black asterisks* show tubular dilation. Quantification of tubule diameter in the **(B)** cortex and **(C)** medulla of Sham and UUO groups. Mann–Whitney statistic test. **P* 0.05 vs. Sham group (*n* = 5).

area in obstructive uropathy ($P < 0.05$) (Cavaglieri et al., 2015). On the other hand, we detected a diminution in tubular diameter of kidney medulla with ureteral obstruction ($P < 0.05$) (**Figure 2**), suggesting a differential remodeling of kidney at 7 days of UUO.

UUO Induces Differential Changes of iRAS Components in Left Renal Cortex and Medulla at mRNA Level, but not at Protein Level

As the renal remodeling induced by 7 days of UUO was not equal in the renal cortex and in the medulla, we studied the levels of iRAS components separately. In the renal cortex of the left kidney, UUO promoted an induction of renin (1.4 FC vs. Sham, $P < 0.001$) and a reduction of ACE1 mRNA (0.3 FC vs. Sham, $P < 0.01$) (**Figure 3A**), suggesting a differential response of iRAS. Only the renin increase was confirmed at protein level (**Figure 3B**). No differences were detected for the mRNA levels of AGT, ACE2, PRR, or AT1R in the renal cortex (**Figure 3A**), and neither for ACE1 at protein level (**Figure 3C**).

On the other hand, UUO diminished significantly the mRNA level for AGT, for ACE2 (in both cases 0.5 FC vs. Sham, $P < 0.05$), and for PRR (0.3 FC vs. Sham, $P < 0.01$) in renal medulla of the left kidney (**Figure 4A**). In the case of protein

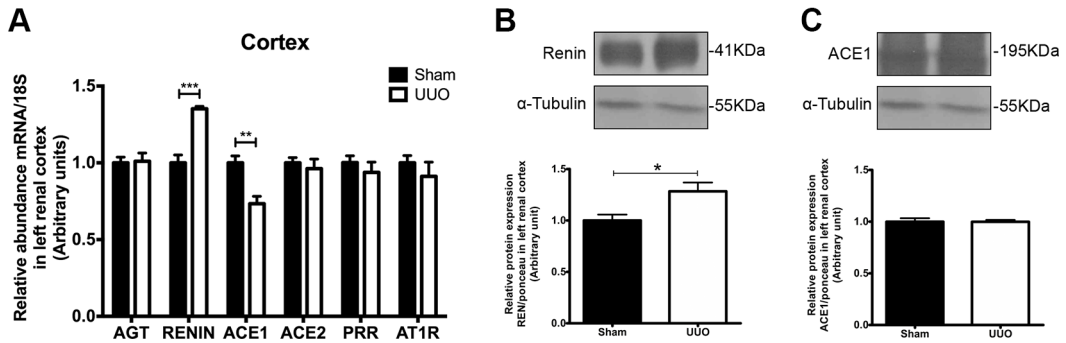

FIGURE 3 | Unilateral ureteral obstruction (UUO) induces upregulation of renin in left renal cortex. **(A)** mRNA levels for: angiotensinogen (AGT), renin, angiotensin-converting enzyme (ACE)1/2, (pro)renin receptor (PRR), and angiotensin-II receptor type 1 (AT1R) in the renal cortex. 18S mRNA was used as the housekeeping gene in qRT-PCR studies. Western blot and immunodetection of **(B)** renin and **(C)** ACE1 in the renal cortex. α-tubulin was used as internal loading control. Student's *t* test was performed. $^{**}P < 0.01$ or $^{***}P < 0.001$ vs. Sham group ($n = 5$).

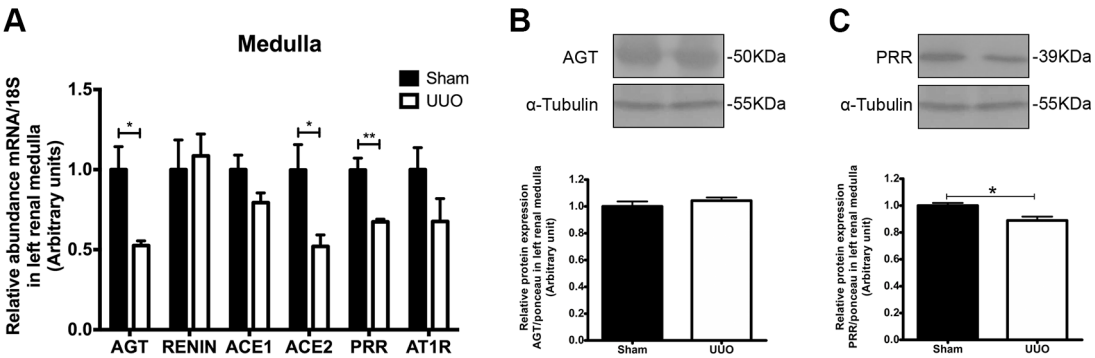

FIGURE 4 | UUO induces downregulation of (pro)renin receptor (PRR) in left renal medulla. **(A)** mRNA levels for: AGT, renin, ACE1/2, PRR, and AT1R in renal medulla. 18S mRNA was used as the housekeeping gene in qRT-PCR studies. Western blot and immunodetection of **(B)** AGT and **(C)** PRR in renal medulla. α-tubulin was used as internal loading control. Student's *t* test was performed. $^{*}P < 0.05$ or $^{**}P < 0.01$ vs. Sham group ($n = 5$).

expression, we corroborated the diminution only for PRR in renal medulla after UUO (**Figures 4B**, **C**). No differences were detected in medullary renin or ACE1 ($P = 0.09$). In the case of AT1R, we observed a modest reduction of mRNA (**Figure 4A**), which has been reported previously by Pimentel et al. at 24 h of UUO and by non-quantitative techniques (Pimentel et al.,1994).

DISCUSSION

Different mediators belonging to the RAS have been described in renal tissue for more than 30 years where their activation may promote or accelerate CKD. For instance, it has been demonstrated that in diabetes mellitus and hypertension, the two major risk factors of CKD, the urinary AGT (Hollenberg et al., 2003) and the intrarenal AngII (Navar et al., 2011), are induced. Here, by using an experimental CKD model that promotes renal inflammation driving to fibrosis, we have characterized different elements of iRAS in the cortex and in renal medulla.

Our main findings suggested that during the pro-inflammatory phase of obstructive uropathy, where the tubular remodeling is also observed, the iRAS is activated in the cortex as reflected by the increase in renin in dilated proximal tubules (**Figure 5**). This observation is in accordance with studies from Eide and collaborators, which demonstrated that ureteral constriction in dogs induces rapid renin release (Eide et al., 1977). In this study, renin upregulation was observed at mRNA and protein levels specifically in the cortex of obstructed kidneys after 7 days (**Figure 3**). An additional way for confirming an "iRAS activation" is the measurement of AngII; it has been demonstrated that 15 h of UUO in dogs increases the plasma AngII (Frøkiaer et al., 1992). However, this has not been demonstrated directly in kidney tubules of mice with ureteral obstruction due to the amount of tubular fluid necessary for AngII analysis. Alternatively, the increase of urinary AngII has been used as a marker of iRAS activation during CKD development in rats (Fang et al., 2018). In general, this iRAS activation results in hemodynamic changes with GFR reduction, observed as a plasma creatinine increase in UUO mice and in increases in the intraluminal pressure leading to

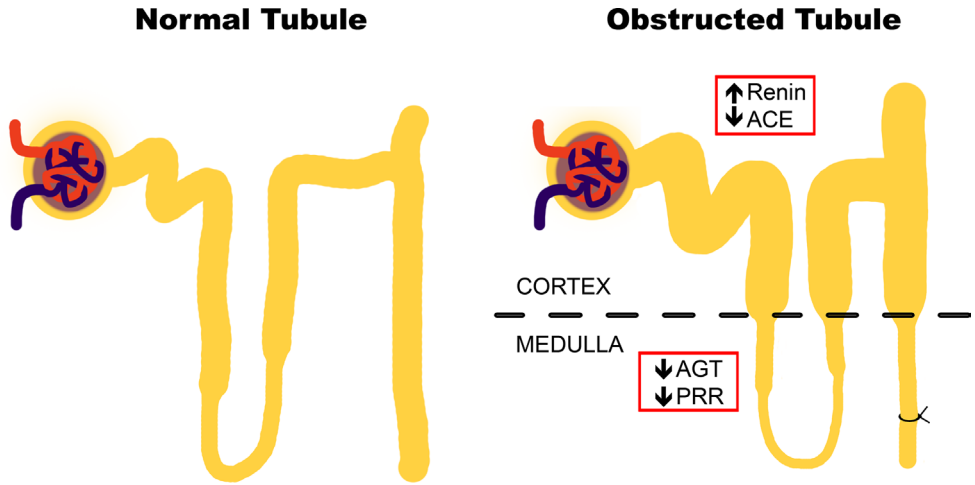

FIGURE 5 | Proposal of changes in intrarenal renin–angiotensin system (iRAS) components during the inflammatory stage of UUO. Obstructive uropathy at 7 days (recognized as "the pro-inflammatory phase") induces tubular remodeling and iRAS activation in the cortex, as reflected by the renin increase in dilated tubules. This activation may be counteracted by the iRAS components in the medulla, particularly by PRR.

tubular dilation observed in the proximal tubule (**Table 1** and **Figure 2**, respectively).

Since renin and pro-renin are synthetized by the collecting ducts cells in kidneys, it has been hypothesized that AngII production has a crucial role in renal compartments and a local biological activity (Nehme et al., 2019). The experimental evidence suggests that pro-renin and renin generation is critical for intratubular AngII formation and for interaction with PRR, promoting tubular damage and further intratubular AngII formation (Gonzalez et al., 2017). In this context, it is proposed that PRR activation contributes directly to the generation of some pro-inflammatory mediators (for instance, prostaglandin E2), as an additional mechanism for renal damage and remodeling (Carlsen et al., 2010; Gonzalez and Prieto 2015). Since renin is increased during the pro-inflammatory phase of UUO at the cortical level, we propose that the downregulation of medullary PRR, corroborated at mRNA and protein levels (**Figure 4A**), may act as a negative feedback of the axis. This represents an integrative iRAS modulation between the cortex and medulla (**Figure 5**).

Cumulative evidence supports the beneficial effects of direct renin antagonism in UUO models. It has been demonstrated that aliskiren prevents the renal aquaporin-2 downregulation (Wang et al., 2015) and prevents the interstitial fibrosis and collagen accumulation at renal level induced by 7 days of UUO (Chung et al., 2017). In addition, it has been reported that the anti-inflammatory and anti-fibrotic effects observed by aliskiren can be achieved alone or in combination with calcium channel blockers and valsartan (Wu et al., 2010). On the other hand, Fang and collaborators showed that the administration of PRO20, a decoy inhibitor of PRR, prevents renal increase of TGF-β1, oxidative stress, and interstitial fibrosis in rats with albumin overload (Fang et al., 2018). They demonstrated that PRR antagonism dramatically reduces the proteinuria, which has been recognized as an independent risk factor of CKD progression. This has not been demonstrated with other renin receptors, such as the renin-binding protein (RnBP) nor the mannose 6-phosphate/insulin-like grow factor II (M6P/IGFII) receptor (Batenburg and Danser 2012). Recently, Nehme et al. have highlighted that the regulation of PRR and other mediators of non-classical systemic RAS, such as ACE2 (called "extended RAS", and also evaluated by us in **Figures 3** and **4**) (Nehme et al., 2015; Nehme et al., 2016), can be used for the development of more effective and selective pharmaceuticals therapies.

In summary, we demonstrate that the pro-inflammatory phase of UUO involves tubular damage, with cortical upregulation of renin (juxtaglomerular) and medullary PRR downregulation. This scenario suggests a differential iRAS modulation as part of the mechanisms involved in the early stages of CKD.

DATA AVAILABILITY STATEMENT

The raw data supporting the conclusions of this manuscript will be made available by the authors, without undue reservation, to any qualified researcher.

ETHICS STATEMENT

The animal study was reviewed and approved by Ethic Commitee of the Universidad Autónoma de Chile.

AUTHOR CONTRIBUTIONS

CA and AG designed the experiments. SF conducted most of the experiments and collected and analyzed the data. ML and CL conducted specific experiments and collected

and analyzed their respective data. CA and SF wrote the manuscript, and AG contributed to its revision. MH wrote and revised the manuscript.

FUNDING

This work was supported by FONDECYT Iniciación #11150542 and DIUA157-2019 project from Vicerrectoría de Investigación y Postgrado (VRIP) (CA). In addition, SF received support from the scholarships for undergraduate (VRIEA-Pontificia Universidad Católica de Valparaíso, #039.407/2017) and PhD students (VRIP-UA).

ACKNOWLEDGMENTS

We thank Mrs. Eliana Pino and Mrs. Pamela Torres for their technical and administrative assistance, respectively.

REFERENCES

Batenburg, W. W., and Danser, A. H. (2012). (Pro)Renin and its receptors: pathophysiological implications. *Clin. Sci.* 123 (3), 121–133. doi: 10.1042/CS20120042

Cao, Q., Harris, D., and Wang, Y. (2015). Macrophages in kidney injury, inflammation, and fibrosis. *Physiol. (Bethesda Md.)* 30 (3), 183–194. doi: 10.1152/physiol.00046.2014

Carlsen, I., Donohue, K. E., Jensen, A. M., Selzer, A. L., Chen, J., Dix, P., et al. (2010). Increased cyclooxygenase-2 expression and prostaglandin e2 production in pressurized renal medullary interstitial cells. *Am. J. Physiol. Regulatory Integr. Comp. Physiol.* 299 (3), R823–R831. doi: 10.1152/ajpregu.00544.2009

Cavaglieri, R. C., Day, R. T., Feliers, D., and Abboud, H. E. (2015). Metformin prevents renal interstitial fibrosis in mice with unilateral ureteral obstruction. *Mol. Cell. Endocrinol.* 412, 116–122. doi: 10.1016/j.mce.2015.06.006

Chi, H. H., Hua, K. F., Lin, Y. C., Chu, C. L., Hsieh, C. Y., Hsu, Y. J., et al. (2017). IL-36 Signaling facilitates activation of the NLRP3 inflammasome and IL-23/IL-17 axis in renal inflammation and fibrosis. *J. Am. Soc. Nephrology: JASN* 28 (7), 2022–2037. doi: 10.1681/ASN.2016080840

Chung, S., Kim, S., Kim, M., Koh, E. S., Shin, S. J., Park, C. W., et al. (2017). Treatment combining aliskiren with paricalcitol is effective against progressive renal tubulointerstitial fibrosis *via* dual blockade of intrarenal renin. *PloS One* 12 (7), e0181757. doi: 10.1371/journal.pone.0181757

Couser, W. G., Remuzzi, G., Mendis, S., and Tonelli, M. (2011). The contribution of chronic kidney disease to the global burden of major noncommunicable diseases. *Kidney Int.* 80 (12), 1258–1270. doi: 10.1038/ki.2011.368

De Nicola, L., and Zoccali, C. (2016). Chronic kidney disease prevalence in the general population: heterogeneity and concerns. *Nephrology Dialysis Transplantation: Official Publ. Eur. Dialysis Transplant Assoc. Eur. Renal Assoc.* 31 (3), 331–335. doi: 10.1093/ndt/gfv427

Ding, Y., Kim, S. I., Lee, S. Y., Koo, J. K., Wang, Z., and Choi, M. E. (2014). Autophagy regulates tgf-β expression and suppresses kidney fibrosis induced by unilateral ureteral obstruction. *J. Am. Soc. Nephrology: JASN* 25 (12), 2835–2846. doi: 10.1681/ASN.2013101068

Eddy, A., and Neilson, E. (2006). Chronic kidney disease progression. *J. Am. Soc. Nephrology: JASN* 17 (11), 2964–2966. doi: 10.1681/ASN.2006070704

Eddy, A., López-Guisa, J., Okamura, D., and Yamaguchi, I. (2012). Investigating mechanisms of chronic kidney disease in mouse models. *Pediatr. Nephrology (Berlin Germany)* 27 (8), 1233–1247. doi: 10.1007/s00467-011-1938-2

Eide, I., Loyning, E., Langård, O., and Kiil, F. (1977). Mechanism of renin release during acute ureteral constriction in dogs. *Circulation Res.* 40 (3), 293–299. doi: 10.1161/01.res.40.3.293

Fang, H., Deng, M., Zhang, L., Lu, A., Su, J., Xu, C., et al. (2018). Role of (pro)renin receptor in albumin overload-induced nephropathy in rats. *Am. J. Physiol. Renal Physiol.* 315 (6), F1759–F1768. doi: 10.1152/ajprenal.00071.2018

Frøkiaer, J., Knudsen, L., Nielsen, A. S., Pedersen, E. B., and Djurhuus, J. C. (1992). Enhanced intrarenal angiotensin II generation in response to obstruction of the pig ureter. *Am. J. Physiol.* 263 (3 Pt 2), F527–F533. doi: 10.1152/ajprenal.1992.263.3.F527

Gonzalez, A., and Prieto, M. (2015). Renin and the (Pro)renin receptor in the renal collecting duct. *Clin. Exp. Pharmacol. Physiol.* 42 (1), 14–21. doi: 10.1111/1440-1681.12319

Gonzalez, A., Zamora, L., Reyes-Martinez, C., Salinas-Parra, N., Roldan, N., Cuevas, C., et al. (2017). (Pro)Renin receptor activation increases profibrotic markers and fibroblast-like phenotype through MAPK-Dependent ROS formation in mouse renal collecting duct cells. *Clin. Exp. Pharmacol. Physiol.* 44 (11), 1134–1144. doi: 10.1111/1440-1681.12813

Hollenberg, N. K., Price, D. A., Fisher, N. D., Lansang, M. C., Perkins, B., Gordon, M. S., et al. (2003). Glomerular hemodynamics and the renin-angiotensin system in patients with type 1 diabetes mellitus. *Kidney Int.* 63 (1), 172–178. doi: 10.1046/j.1523-1755.2003.00701.x

Kobori, H., Nangaku, M., Navar, L. G., and Nishiyama, A. (2007). The intrarenal renin-angiotensin system: from physiology to the pathobiology of hypertension and kidney disease. *Pharmacological Rev.* 59 (3), 251–287. doi: 10.1124/pr.59.3.3

Levey, A. S., de Jong, P. E., Coresh, J., El Nahas, M., Astor, B. C., Matsushita, K., et al. (2011). The definition, classification, and prognosis of chronic kidney disease: A KDIGO controversies conference Report. *Kidney Int.* 80 (1), 17–28. doi: 10.1038/ki.2010.483

Martínez-Klimova, E., Aparicio-Trejo, O. E., Tapia, E., and Pedraza-Chaverri, J. (2019). Unilateral ureteral obstruction as a model to investigate fibrosis-attenuating treatments. *Biomolecules* 9 (4), 1–28. doi: 10.3390/biom9040141

Menon, M. C., and Ross, M. J. (2016). Epithelial-to-mesenchymal transition of tubular epithelial cells in renal fibrosis: a new twist on an old tale. *Kidney Int.* 89 (2), 263–266. doi: 10.1016/j.kint.2015.12.025

Navar, L. G., Kobori, H., Prieto, M. C., and Gonzalez-Villalobos, R. A. (2011). Intratubular renin-angiotensin system in hypertension. *Hypertension* 57 (3), 355–362. doi: 10.1161/HYPERTENSIONAHA.110.163519

Nehme, A., Cerutti, C., and Zibara, K. (2016). Transcriptomic analysis reveals novel transcription factors associated with renin-angiotensin-aldosterone system in human atheroma. *Hypertension* 68 (6), 1375–1384. doi: 10.1161/HYPERTENSIONAHA.116.08070

Nehme, A., Cerutti, C., Dhaouadi, N., Gustin, M. P., Courand, P. Y., Zibara, K., et al. (2015). Atlas of tissue renin-angiotensin-aldosterone system in human: a transcriptomic meta-analysis. *Sci. Rep.* 5, 10035. doi: 10.1038/srep10035

Nehme, A., Zouein, F. A., Zayeri, Z. D., and Zibara, K. (2019). An update on the tissue renin angiotensin system and its role in physiology and pathology. *J. Cardiovasc. Dev. Dis.* 6 (2), 1–17. doi: 10.3390/jcdd6020014

Nehme, A., Marcelo, P., Nasser, R., Kobeissy, F., Bricca, G., and Zibara, K. (2016b). The kinetics of angiotensin-I metabolism in human carotid atheroma: an emerging role for angiotensin (1-7). *Vascular Pharmacol.* 85, 50–56. doi: 10.1016/j.vph.2016.08.001

Pimentel, J. L., Sundell, C. L., Wang, S., Kopp, J. B., Montero, A., and Martínez-Maldonado, M. (1995). Role of angiotensin II in the expression and regulation of transforming growth factor-beta in obstructive nephropathy. *Kidney Int.* 48 (4), 1233–1246. doi: 10.1038/ki.1995.407

Pimentel, J. L., Martinez-Maldonado, M., Wilcox, J. N., Wang, S., and Luo, C. (1993). Regulation of renin-angiotensin system in unilateral ureteral obstruction. *Kidney Int.* 44 (2), 390–400. doi: 10.1038/ki.1993.257

Pimentel, J. L., Wang, S., and Martinez-Maldonado, M. (1994). Regulation of the renal angiotensin II receptor gene in acute unilateral ureteral obstruction. *Kidney Int.* 45 (6), 1614–1621. doi: 10.1038/ki.1994.212

Tesch, G. H., Yang, N., Yu, H., Lan, H. Y., Foti, R., Chadban, S. J., et al. (1997). Intrinsic renal cells are the major source of interleukin-1 beta synthesis in normal and diseased rat kidney. *Nephrology Dialysis Transplantation: Official Publ. Eur. Dialysis Transplant Assoc. Eur. Renal Assoc.* 12 (6), 1109–1115. doi: 10.1093/ndt/12.6.1109

Tonelli, M., Wiebe, N., Guthrie, B., James, M. T., Quan, H., Fortin, M., et al. (2015). Comorbidity as a driver of adverse outcomes in people with chronic kidney disease. *Kidney Int.* 88 (4), 859–866. doi: 10.1038/ki.2015.228

Tonelli, M., Muntner, P., Lloyd, A., Manns, B. J., James, M. T., Klarenbach, S., et al. (2011). Using proteinuria and estimated glomerular filtration rate to classify risk in patients with chronic kidney disease: a cohort study. *Ann. Internal Med.* 154 (1), 12–21. doi: 10.7326/0003-4819-154-1-201101040-00003

Ucero, A. C., Benito-Martin, A., Izquierdo, M. C., Sanchez-Niño, M. D., Sanz, A. B., Ramos, A. M., et al. (2014). Unilateral ureteral obstruction: beyond obstruction. *Int. Urology Nephrology* 46 (4), 765–776. doi: 10.1007/s11255-013-0520-1

Velez, J. C. (2009). The importance of the intrarenal renin-angiotensin system. *Nat. Clin. Pract. Nephrology* 5 (2), 89–100. doi: 10.1038/ncpneph1015

Wang, W., Luo, R., Lin, Y., Wang, F., Zheng, P., Levi, M., et al. (2015). Aliskiren restores renal aqp2 expression during unilateral ureteral obstruction by inhibiting the inflammasome. *Am. J. Physiol. Renal Physiol.* 308 (8), F910–F922. doi: 10.1152/ajprenal.00649.2014

Wu, W. P., Chang, C. H., Chiu, Y. T., Ku, C. L., Wen, M. C., Shu, K. H., et al. (2010). A reduction of unilateral ureteral obstruction-induced renal fibrosis by a therapy combining valsartan with aliskiren. *Am. J. Physiol. Renal Physiol.* 299 (5), F929–F941. doi: 10.1152/ajprenal.00192.2010

Yamaguchi, I., Tchao, B. N., Burger, M. L., Yamada, M., Hyodo, T., Giampietro, C., et al. (2012). Vascular endothelial cadherin modulates renal interstitial fibrosis. *Nephron Exp. Nephrology* 120 (1), e20–e31. doi: 10.1159/000332026

Yang, H. C., Zuo, Y., and Fogo, A. (2010). Models of chronic kidney disease. *Drug Discovery Today Dis. Models* 7 (1–2), 13–19. doi: 10.1016/j.ddmod.2010.08.002

Conflict of Interest: The authors declare that the research was conducted in the absence of any commercial or financial relationships that could be construed as a potential conflict of interest.

frontiers in Pharmacology

MINI REVIEW
published: 15 November 2019
doi: 10.3389/fphar.2019.01362

The Neuronal Glutamate Transporter EAAT3 in Obsessive-Compulsive Disorder

Angélica P. Escobar[1], Jens R. Wendland[1†], Andrés E. Chávez[1] and Pablo R. Moya[1,2]**

[1] Centro Interdisciplinario de Neurociencia de Valparaíso CINV, Facultad de Ciencias, Universidad de Valparaíso, Valparaíso, Chile, [2] Instituto de Fisiología, Facultad de Ciencias, Universidad de Valparaíso, Valparaiso, Chile

Obsessive compulsive disorder (OCD) is a heterogeneous psychiatric disorder affecting 1%–3% of the population worldwide. About half of OCD afflicted individuals do not respond to currently available pharmacotherapy, which is mainly based on serotonin reuptake inhibition. Therefore, there is a critical need to search novel and improved therapeutic targets to treat this devastating disorder. In recent years, accumulating evidence has supported the glutamatergic hypothesis of OCD, and particularly pointing a potential role for the neuronal glutamate transporter EAAT3. This mini-review summarizes recent findings regarding the neurobiological basis of OCD, with an emphasis on the glutamatergic neurotransmission and EAAT3 as a key player in OCD etiology.

Keywords: EAAT3, OCD, obsessive-compulsive disorder, glutamate transporter, synaptic function, NMDAR, animal model, SLC1A1

OPEN ACCESS

Edited by:
Ramón Sotomayor-Zárate, University of Valparaíso, Chile

Reviewed by:
Marcela Julio-Pieper, Pontificia Universidad Católica de Valparaíso, Chile
Renae Ryan, University of Sydney, Australia

****Correspondence:***
Angélica P. Escobar
angelica.escobar@cinv.cl
Pablo R. Moya
pablo.moya@uv.cl

†Present address:
Jens R. Wendlend
Takeda Pharmaceuticals, Cambridge, MA, United States

Specialty section:
This article was submitted to Translational Pharmacology, a section of the journal Frontiers in Pharmacology

Received: *08 August 2019*
Accepted: *28 October 2019*
Published: *15 November 2019*

Citation:
Escobar AP, Wendland JR, Chávez AE and Moya PR (2019) The Neuronal Glutamate Transporter EAAT3 in Obsessive-Compulsive Disorder. Front. Pharmacol. 10:1362. doi: 10.3389/fphar.2019.01362

OBSESSIVE COMPULSIVE DISORDER

Obsessive compulsive disorder (OCD) is a psychiatric disorder affecting 1%–3% of the population worldwide (Grabe et al., 2000; Angst et al., 2004). It is characterized by recurrent, intrusive worries, feelings or unwanted thoughts (obsessions), and repetitive, structured, ritualistic mental acts and/or behaviors (compulsions). OCD is clinically heterogeneous, displaying a wide range of symptomatic expression (Murphy et al., 2013). Most OCD patients also have high levels of anxiety, likely due to the inability to control or stop the appearance of obsessions (Pauls et al., 2014). Both obsessions and compulsions are time consuming, causing a high impairment in social and occupational areas (American Psychiatric Association, 2013).

Current OCD treatment involves cognitive-behavioral therapy alone or combined with pharmacotherapy mainly based on serotonin reuptake inhibitors (SRI), such as fluoxetine, clomipramine or paroxetine (Bouvard et al., 2004; Cottraux et al., 2005; Skapinakis et al., 2016). However, only about half of patients achieve an adequate decrease in the severity of symptoms (Hirschtritt et al., 2017), highlighting the need for new therapeutic options to treat this devastating disorder.

CORTICO-STRIATO-THALAMO-CORTICAL LOOP MODIFICATIONS IN OCD

Since original reports, neuroimaging studies have consistently indicated that a dysfunction in the cortico-striato-thalamo-cortical (CSTC) loop is involved in OCD (Milad and Rauch, 2012; Nakao et al., 2014; Burguiere et al., 2015). In a brief and oversimplified manner, the CSTC loop

is composed of glutamatergic pyramidal cortical neurons that project onto striatal subnuclei. From here, GABAergic neurons project to basal ganglia and the thalamus throughout both direct and indirect pathways; in turn, the thalamus sends recurrent projections back to cortical areas (Alexander and Crutcher, 1990). A normal CSTC loop function is required for regulating habitual and goal-directed behaviors (Gerfen and Surmeier, 2011). Neuroimaging studies, for example, indicated changes in the volume of the anterior cingulate cortex and the thalamus in OCD patients compared to healthy controls (Atmaca et al., 2007; Radua and Mataix-Cols, 2009), an alteration that was shown to be restored in responders to SRI treatment (Atmaca et al., 2006). At the functional level, hyperactivity of the anterior cingulate, orbitofrontal cortex, and caudate (Saxena et al., 2001; Maia et al., 2008), as well as altered functional connectivity between the medial frontal cortex and striatal regions have been reported in OCD (Fitzgerald et al., 2011; Posner et al., 2014).

GLUTAMATE SYSTEM DYSFUNCTIONS IN THE PATHOGENESIS OF OCD

Multiple neurotransmitter systems have been implicated in the etiology of OCD. Since clinically efficacious pharmacotherapy targets the serotonin system, impairments in this neurotransmitter were hypothesized to be disease-causing (Insel et al., 1985; March et al., 1989; Barr et al., 1993) and probably explain certain aspects of OCD pathophysiology. However, like other neuropsychiatric entities, OCD is multifactorial and thereby additional hypotheses have been proposed (Pauls et al., 2014). For instance, some SRI-refractory OCD patients can benefit from combined therapy with antipsychotic drugs targeting dopamine D2 receptors (Dold et al., 2013; Dold et al., 2015), consistent with changes in dopaminergic system reported in OCD patients (Denys et al., 2004), including a decrease in dopamine transporter (DAT) and dopamine D2 receptors levels in basal ganglia (Denys et al., 2004; Hesse et al., 2005). Both monoamine hypotheses are supported by reports of OCD-like behaviors in animal models where modifications of serotonin or dopamine neurotransmitter systems were achieved by genetic or pharmacological intervention (Yadin et al., 1991; Szechtman et al., 1998; Chou-Green et al., 2003; Ralph-Williams et al., 2003).

Over the last decades, increasing lines of evidence support a glutamatergic hypothesis in OCD. For instance, multiple trials have reported promising results in OCD using glutamate-targeting drugs. Memantine, ketamine, and rapastinel, all drugs acting on glutamate NMDA receptors (NMDAR) have shown beneficial effects in OCD treatment (Bakhla et al., 2013; Rodriguez et al., 2016; Modarresi et al., 2018). Moreover, Riluzole, a drug that reduces glutamate synaptic levels (by acting at both presynaptically and at glial glutamate transporters) has been shown to improve OCD symptomatology in about 50% of patients when given concomitantly with SRI (Coric et al., 2005; Grant et al., 2007; Pittenger et al., 2015). Other studies have shown that the adjunctive use of N-acetyl cysteine alleviates OCD symptomatology (Lafleur et al., 2006; Lalanne et al., 2014; Ghanizadeh et al., 2017; di Michele et al., 2018). N-acetyl cysteine is a cysteine donor, precursor for glutathione (a potent antioxidant), and also increases glutamate levels by activating the glial glutamate/cysteine antiporter.

Alterations in fluid or imaging biomarkers of glutamatergic neurotransmission have been reported in OCD, including increased glutamate content in cerebrospinal fluid of OCD untreated patients (Chakrabarty et al., 2005) and a positive correlation between compulsive behavior and glutamate concentration in the anterior cingulate cortex (Naaijen et al., 2017). Interestingly, a previous study performed in child and adolescent OCD patients reported decreased, rather than increased glutamate levels in this brain region (Rosenberg et al., 2004). Higher glutamate concentration was also found in the caudate nucleus in child OCD patients that was restored after treatment with paroxetine (Rosenberg et al., 2000). Such alterations in the levels of glutamate in distinct nuclei of the CSTC loop might lead to (or reflect) functional changes that ultimately, lead to abnormal neuronal circuit activity. Consistent with this idea, three recently developed animal models of OCD display glutamatergic alterations in cortico-striatal synapses (Welch et al., 2007; Shmelkov et al., 2010; Delgado-Acevedo et al., 2019).

GENETICS OF GLUTAMATERGIC SYSTEM GENES IN OCD

Genetic studies also provide support for the glutamatergic hypothesis of OCD, including linkage and association studies. For instance, the 5072T/G variant of *GRIN2B* gene, which encodes for the NR2B subunit of NMDARs, was significantly associated with OCD in a family-based study (Arnold et al., 2004), whereas the rs1019385 polymorphism was associated with reduced glutamate levels in the anterior cingulate in drug-free pediatric OCD patients. Variants in the *GRIK2* gene encoding the kainate receptor subunit 2 have been also reported in OCD (Delorme et al., 2004; Sampaio et al., 2011). Another glutamate-related gene proposed in OCD is *DLGAP3,* which encodes for the postsynaptic scaffolding protein SAPAP3 implicated in the anchoring of glutamate receptors. As discussed below, SAPAP3 knock-out (KO) mice display OCD relevant behaviors (Welch et al., 2007). These findings prompted genetic studies where some *DLGAP3* gene variants were found to be more associated with grooming disorders than with OCD (Bienvenu et al., 2009; Zuchner et al., 2009; Boardman et al., 2011).

Genetic studies have also suggested a role for the *SLC1A1* gene, encoding the neuronal glutamate transporter 3 (EAAT3) in OCD. This gene was originally proposed in two independent genome-wide linkage OCD studies (Hanna et al., 2002; Willour et al., 2004). Subsequent family-based association and case-control studies found *SLC1A1* gene variants that are associated with OCD (Arnold et al., 2006; Dickel et al., 2006; Stewart et al., 2007; Shugart et al., 2009; Wendland et al., 2009; Samuels et al., 2011). In addition, an association between an *SLC1A1* haplotype and the appearance of atypical antipsychotic-induced OCD symptoms has been also reported (Kwon et al., 2009), reinforcing the idea that modifications of *SLC1A1* gene might underlie the generation of compulsive behavior. A recent study found

that some *SLC1A1* variants are associated with white matter microstructure modifications in child and adolescent OCD patients (Gasso et al., 2015), suggesting that they might also underlie the anatomical alterations seen in OCD. Nevertheless, a meta-analysis study found just a weak association between the *SLC1A1* variant rs301443 and OCD, while rs12682807 was modestly associated in male subjects (Stewart et al., 2013). The lack of stronger association might be attributed to inadequate sample size, distinct clinical subtypes of OCD and genetic/phenotypic heterogeneity of the subjects (Stewart et al., 2013; Rajendram et al., 2017). Two genome-wide association studies reported no *SLC1A1* variants reaching genome wide significance, potentially due to statistical power limitations given low sample size (Stewart et al., 2013; Mattheisen et al., 2015).

To date, three studies have addressed the impact of *SLC1A1* gene variants on EAAT3 expression/function. Veenstra-VanderWeele and colleagues characterized the rare *SLC1A1* coding variant T164A found in an OCD family, which was shown to have modest effects on both EAAT3 V_{max} and K_m parameters, suggesting a decrease in the number of EAAT3 available and its affinity for glutamate, respectively, which might be involved in the disorder (Veenstra-VanderWeele et al., 2012). However, no protein quantification was carried out in this work. In a second study, Bailey and colleagues characterized the EAAT3 loss-of-function variants R445W and I395del found in human dicarboxylic aminoaciduria; both mutants dramatically reduced or abolished glutamate and cysteine transport by EAAT3 and led to almost absent EAAT3 surface expression in a cell line model (Rodenas-Ruano et al., 2012). Although no psychiatric assessment was available for the subjects in this study, authors reported that one of the patients carrying R445W variants exhibited features consistent with a diagnosis of OCD (Bailey et al., 2011). In a third study, Wendland and colleagues described *SLC1A1* variants that affect mRNA expression in human dorsolateral prefrontal cortex tissue and that were associated with OCD in a large case-control study (Wendland et al., 2009). Collectively, these data suggest that gene variants impacting EAAT3 expression might underlie the pathogenesis of OCD. A more definitive answer will hopefully be provided in the near future through adequately-powered, large genome-wide association or sequencing studies that can yield statistically robust insights into the role of *SLC1A1* and other glutamatergic system genes in OCD.

THE NEURONAL GLUTAMATE TRANSPORTER EAAT3

EAAT3 belongs to the excitatory amino acid transporters family (EAAT1-5) that regulates the extracellular levels of glutamate. Although its expression is approximately 100-fold lower than other EAAT in brain (Holmseth et al., 2012), enriched EAAT3 content is found in CSTC loop, including the cerebral cortex, hippocampus, striatum, and basal ganglia (Rothstein et al., 1994; Furuta et al., 1997; Shashidharan et al., 1997; Kanai and Hediger, 2004; Holmseth et al., 2012), in glutamatergic, GABAergic, and dopaminergic neurons (Coco et al., 1997; Conti et al., 1998; Sidiropoulou et al., 2001; Underhill et al., 2014). EAAT3 is localized peri-synaptically on the postsynaptic spine (Coco et al., 1997; He et al., 2000), and several studies have indicated that its contribution to the overall glutamate uptake is much lesser compared to that of the astrocytic transporters EAAT1 and EAAT2 (Tong and Jahr, 1994; Rothstein et al., 1996; Diamond and Jahr, 1997; Tanaka et al., 1997). Nonetheless, increasing evidence indicate that EAAT3 contributes to buffer glutamate released during synaptic events and prolong the time course of astrocytic clearance in the hippocampus (Scimemi et al., 2009), and to regulate the responses of extra-synaptic glutamate NMDA and AMPA receptors (Scimemi et al., 2009; Jarzylo and Man, 2012; Underhill et al., 2014; Delgado-Acevedo et al., 2019) as well as metabotropic glutamate receptors (Otis et al., 2004; Wadiche and Jahr, 2005). As changes in EAAT3 activity can modify the trafficking of AMPARs and function of NMDARs, it is not surprising that EAAT3 has been shown to be involved in excitatory synaptic plasticity (Cao et al., 2014; Bjorn-Yoshimoto and Underhill, 2016; Delgado-Acevedo et al., 2019). EAAT3 can also control neuronal activity through a negative feedback of excitatory neurotransmission by regulating the synthesis of GABA at inhibitory terminals (Sepkuty et al., 2002; Mathews and Diamond, 2003) and by regulating the expression of D1 dopamine receptors (Bellini et al., 2018). Collectively, the evidence strongly supports the notion that EAAT3 regulates glutamate levels in the synaptic cleft and thus the function of postsynaptic receptors. Therefore, changes in EAAT3 expression and/or function at glutamatergic synapses within the CSTC loop might underlie the neurobiological basis of OCD.

EAAT3 has been also suggested to play a role on the neuronal redox balance as they also transport cysteine, the rate limiting substrate for glutathione synthesis (Himi et al., 2003; Aoyama et al., 2006; Watabe et al., 2007). Indeed, EAAT3 KO mice have reduced glutathione brain levels, which correlates with the brain atrophy and hippocampal neurodegeneration in aged mice and impaired spatial memory reported in these mice (Aoyama et al., 2006; Berman et al., 2011). Increased oxidative stress and a reduced number of dopaminergic neurons were also found in EAAT3 KO mice (Berman et al., 2011). Correspondingly, mice lacking GTRAP3-18, a reticulum protein that interacts with and retains EAAT3 on cellular compartment (Lin et al., 2001) not only showed increased EAAT3 levels at the plasma membrane, but also increased cysteine and glutathione brain content as well as improved performance in spatial memory tasks (Aoyama et al., 2012). In contrast, mice overexpressing EAAT3 have higher glutathione brain levels (Delgado-Acevedo et al., 2019), raising the possibility that alterations in redox balance might be also involved in OCD.

IMPAIRED GLUTAMATERGIC NEUROTRANSMISSION IN OCD ANIMAL MODELS

Three different genetic models, namely, the Sapap3 KO (Welch et al., 2007) mice, the Slitrk5 KO mice (Shmelkov et al., 2010), and the EAAT3 overexpressing mice (Delgado-Acevedo et al., 2019), have been reported to recapitulate OCD hallmarks including cortico-striatal glutamatergic alterations, particularly

changes in NMDAR function, and displaying OCD-like behaviors that could be rescued by chronic administration of SSRI (See **Table 1**). Mice lacking SAPAP3 (a member of SAP90/PSD-95-associated protein family (SAPAPs)) exhibit an aberrantly increased self-grooming leading to skin wounds (Welch et al., 2007). SAPAP3 KO mice also showed increased anxiety-like behavior in the open field, zero-maze, and light-dark emergence tests; both increased anxiety and hyper-grooming behaviors were alleviated by fluoxetine administration for 6 days (Welch et al., 2007). SAPAP3 KO mice also show abnormalities at cortico-striatal synapses, including a decrease in AMPAR-mediated transmission and an increase in NMDAR-mediated transmission. Such alterations were specific for cortico-striatal synapses, as they were not observed in the hippocampus (Welch et al., 2007) neither in thalamo-striatal synapses (Wan et al., 2014) and were rescued by striatal injections of a lentivirus expressing SAPAP3 (Welch et al., 2007). While the reduction in AMPAR-mediated transmission is likely due to AMPAR endocytosis, an increased activity of mGluR5 receptors was also reported and might be involved in the increase of silent synapses (Wan et al., 2011). This increased mGluR5 activity seemed not only to accompany the OCD-like phenotype but could also be a causative agent, since acute mGluR5 activation recapitulated OCD-like behavior in wildtype mice, and mGluR5 antagonism reverted the phenotype on SAPAP3 KO mice (Ade et al., 2016). Additional dysregulation in serotonin and dopamine release and/or metabolism (Wood et al., 2018) as well as deficits in behavioral inhibition have been also reported in SAPAP3 KO mice (Burguiere et al., 2013). While this evidence links SAPAP3 to compulsive behaviors, human *DLGAP3*/SAPAP3 gene variants seem to be more related to disorders belonging to the obsessive-compulsive spectrum rather than directly to OCD, as discussed above (Bienvenu et al., 2009; Zuchner et al., 2009; Boardman et al., 2011).

Similarly, the deletion of *SlitrK5* gene was found to induce compulsive and anxiety-like behaviors in mice (Shmelkov et al., 2010). The N-terminal region of SlitrK5, a transmembrane protein, is similar to Slit proteins conformed by two leucine-rich domains, whereas the C-terminal is similar to Trk neurotrophin receptor (Aruga and Mikoshiba, 2003). Like SAPAP3 KO mice, increased self-grooming leading to skin lesions and facial hair loss has been reported in SlitrK5 KO mice (Shmelkov et al., 2010). They also display compulsive-like behavior in the marble burying test and increased anxiety-like behavior in the open field and elevated plus maze tests, behavioral impairments that were restored by chronic (18 days) treatment with fluoxetine (Shmelkov et al., 2010). Importantly, SlitrK5 KO mice have selective over-activation of the orbitofrontal cortex and abnormalities in striatal glutamatergic signaling, including a reduction in the level of glutamate receptor subunits GluR1, GluR2, NR2A, and NR2B and a decrease in the amplitude of spikes in response to the cortico-striatal stimulation (Shmelkov et al., 2010). While the exact mechanism by which Slitrk5 deletion impacts glutamatergic signaling remains unclear, Slitrk5 might play an important role in neuronal development as a rare synaptogenesis-impairing

TABLE 1 | Summary of the behavioral alterations relevant to obsessive-compulsive disorder reported in the SAPAP3 KO mouse, Slitrk5 KO mouse, and EAAT3glo/CMKII mouse.

Animal Model	Grooming behavior	Reversion with SSRI	Extinction deficits	Marble burying	Locomotion	Open Field	Elevated Zero-Maze	Elevated Plus Maze	Dark-light emergence	Other behavioral tests
Sapap3 KO (Welch et al., 2007)	Very high (self-injured) starting at 6 months. Increased number of bouts and duration.	Yes, 6 days fluoxetine treatment	Not tested	Not tested	Normal	Less time in center	-Higher latency to open area. -Less time in open area	Not tested	-Higher latency to lit. -Less time in the lit chamber	Impaired behavioral inhibition (tone paired with water drop (Burguiere et al., 2015)
Slitrk5 KO (Shmelkov et al., 2010)	Very high (self-injured) starting at 3 months). Increased duration.	Yes, 21 days fluoxetine treatment	Not tested	Increased	Normal	-Less time in center. Less entries to center	Not tested	Reduced time in open arms	Not tested	–
EAAT3glo/ CMKII (Delgado-Acevedo et al., 2019)	High (no self-injured) tested at 2-3 months. Increased duration.	Yes, 21 days fluoxetine or clomipramine treatment	Greater spontaneous recovery of fear memories	Increased	Normal	-Less time in center. -Less entries to center	Not tested	Not tested	-Higher latency to lit. -Less time in the lit chamber	Unaltered cognitive flexibility in visual discrimination task

mutation in the *SLITRK5* gene has been recently associated with OCD (Song et al., 2017), suggesting that changes in the development and/or maturation of excitatory neurons in the CSTC circuit might underlie OCD pathophysiology. Consistent with this idea, SlitrK5 KO mice display decreased arbor complexity in striatal medium spiny neurons (Shmelkov et al., 2010), which might explain the decreased number of postsynaptic glutamate receptors and glutamatergic function, two hallmarks of OCD disorders.

Mouse models with altered EAAT3 expression have been useful to study OCD neurobiology. The first EAAT3 KO mouse model was reported in 1997 and indicated reduced spontaneous locomotor activity, but no other neurological dysfunctions nor OCD relevant behaviors (Peghini et al., 1997). Later, it was found that EAAT3 KO mice also display an age-dependent decrease of dopaminergic neurons number in the substantia nigra, which might explain the impaired locomotor activity (Berman et al., 2011). Similarly, changes in the volume of the hippocampal CA1 region, associated with an age-progressive decline in swim velocity and in spatial memory performance were also reported (Aoyama et al., 2006). Moreover, neurons from EAAT3 KO mice have been found to be more sensitive to oxidative stress (Aoyama et al., 2006), ischemia (Jang et al., 2012; Choi et al., 2014), and traumatic brain injury (Choi et al., 2016). Since some of the alterations in EAAT3 KO mice can be rescued by the treatment with N-acetyl cysteine (Berman et al., 2011), it is plausible to suggest that EAAT3 has a role in neuroprotection due to its cysteine donor function. In this context, increased oxidative status in OCD patients as well as a positive correlation between the severity of OCD symptoms and the level of lipid peroxidation have been reported (Chakraborty et al., 2009). Increased glutathione peroxidase levels in the plasma serum of treatment-naïve children with OCD (Simsek et al., 2016) and lower levels of glutathione in the posterior cingulate cortex have been also reported (Brennan et al., 2016). While animal and human studies indicate that SRIs can restore neuron oxidative status observed in mood disorders, to the best of our knowledge, only one study has suggested that fluoxetine treatment restores the oxidative status in OCD patients (Chakraborty et al., 2009).

After two decades of research since the first publication of an EAAT3 KO mouse model (Peghini et al., 1997), only one study has reported some behaviors reminiscent of compulsive-like behavior in EAAT3 KO mice (Bellini et al., 2018). A second EAAT3 KO mouse model was recently developed by a different research group and, in agreement with the majority of the studies, they found unaltered anxiety or compulsive-like behaviors in this model (Zike et al., 2017). Indeed, a decrease in grooming behavior and amphetamine-induced locomotor activity, as well as in D1 dopamine receptor agonist-induced stereotypy (an effect correlated with reduced dopamine release in the striatum) was reported in this second EAAT3 KO model (Quinlan et al., 1999). While genetic background (C57BL/6 vs CD1 strain) and/or the age of the animals might explain some of the differences observed in the repetitive behavior in EAAT3 KO mouse, both studies highlight the impact of EAAT3 ablation on dopamine neurotransmission (Zike et al., 2017; Bellini et al., 2018). Altogether, these data suggest that OCD susceptibility might not be related to a reduced (or absent) EAAT3 expression/function. Consistent with this idea, one of the *SLC1A1* gene variants highly replicated in OCD genetic studies is associated with increased rather than decreased EAAT3 mRNA levels in human brain tissue (Wendland et al., 2009). To explore this EAAT3 gain-of-function hypothesis, a conditional transgenic mouse line, in which EAAT3 was overexpressed under CamKIIα driver (EAAT3glo/CMKII) was recently reported (Delgado-Acevedo et al., 2019). This model exhibits increased anxiety and compulsive-like behaviors that were restored by chronic, but not acute, fluoxetine, or clomipramine treatment. Moreover, EAAT3glo/CMKII mice displayed alterations in the glutamatergic system in the striatum, including changes in NMDARs subunit composition (increased NR2B/NR2A ratio), and impaired NMDA-dependent synaptic plasticity (Delgado-Acevedo et al., 2019). Interestingly, EAAT3glo/CMKII mice also displayed higher spontaneous recovery of fear memory, suggesting impairment in long-term extinction, which has also been described in OCD patients (Milad et al., 2013) and, to the best of our knowledge, for the first time in an OCD mouse model (Delgado-Acevedo et al., 2019). In view of their high density in extinction-related brain areas, the NMDAR has been suggested to be a candidate for modulating extinction learning (for review see (Myers and Davis, 2002; Davis, 2011). However, whether changes in NMDAR subunits composition observed in the striatum of EAAT3glo/CMKII mice (Delgado-Acevedo et al., 2019) also occur in extinction-related areas remain to be determined.

CONCLUSIONS

Converging evidence from genetic, neuroanatomical, pharmacological, and preclinical studies in both humans and animal models support that glutamate dysregulations may contribute to the pathophysiology of OCD. As discussed above, the findings from genetic mouse models that are relevant of OCD not only highlight glutamatergic alterations, and particularly altered NMDAR function in the OCD etiology, but also establish EAAT3 overexpression rather than an EAAT3 reduction as an attractive model to further explore in this and other related disorders. While the exact mechanism by which altered EAAT3 levels impact NMDARs subunit composition remains unknown, the fact that they can change in the order of minutes to hours in response to neuronal activity (Barria and Malinow, 2002; Bellone and Nicoll, 2007; Matta et al., 2011), as well as in a long-lasting manner by early life experience (Quinlan et al., 1999; Rodenas-Ruano et al., 2012) strongly suggests that EAAT3 not only limits NMDARs function by rapidly binding synaptically released glutamate (Scimemi et al., 2009), but also might lead to a cascade of events that, ultimately, can modify the relative levels of NR2B to NR2A subunits composition of NMDARs in a long-lasting manner during brain development to impair function. Since redox balance also alters NMDAR function (Choi and Lipton, 2000), the EAAT3-dependent cysteine uptake might also impact glutamatergic neurotransmission by modifying the neuronal oxidative status. Further studies are warranted to better dissect

the interplay between of NMDAR and redox balance in the etiology of OCD.

AUTHOR CONTRIBUTIONS

PM conceived the work. AE, JW, AC, PM drafted the work, critically revised the work and provided important intellectual content. AE, JW, AC, PM provided approval for publication of the content and agreed to be accountable for all aspects of the work.

FUNDING

This work was supported by grants Fondecyt N° 1190833, Fondecyt N° 3190843, and ICM-MINECOM N° P09-022-F CINV.

REFERENCES

Ade, K. K., Wan, Y., Hamann, H. C., O'Hare, J. K., Guo, W., Quian, A., et al. (2016). Increased metabotropic glutamate receptor 5 signaling underlies obsessive-compulsive disorder-like behavioral and striatal circuit abnormalities in mice. *Biol. Psychiatry* 80, 522–533. doi: 10.1016/j.biopsych.2016.04.023

Alexander, G. E., and Crutcher, M. D. (1990). Functional architecture of basal ganglia circuits: neural substrates of parallel processing. *Trends Neurosci.* 13, 266–271. doi: 10.1016/0166-2236(90)90107-L

Angst, J., Gamma, A., Endrass, J., Goodwin, R., Ajdacic, V., Eich, D., et al. (2004). Obsessive-compulsive severity spectrum in the community: prevalence, comorbidity, and course. *Eur. Arch. Psychiatry Clin. Neurosci.* 254, 156–164. doi: 10.1007/s00406-004-0459-4

Aoyama, K., Suh, S. W., Hamby, A. M., Liu, J., Chan, W. Y., Chen, Y., et al. (2006). Neuronal glutathione deficiency and age-dependent neurodegeneration in the EAAC1 deficient mouse. *Nat. Neurosci.* 9, 119–126. doi: 10.1038/nn1609

Aoyama, K., Wang, F., Matsumura, N., Kiyonari, H., Shioi, G., Tanaka, K., et al. (2012). Increased neuronal glutathione and neuroprotection in GTRAP3-18-deficient mice. *Neurobiol. Dis.* 45, 973–982. doi: 10.1016/j.nbd.2011.12.016

Arnold, P. D., Rosenberg, D. R., Mundo, E., Tharmalingam, S., Kennedy, J. L., and Richter, M. A. (2004). Association of a glutamate (NMDA) subunit receptor gene (GRIN2B) with obsessive-compulsive disorder: a preliminary study. *Psychopharmacol. (Berl.)* 174, 530–538. doi: 10.1007/s00213-004-1847-1

Arnold, P. D., Sicard, T., Burroughs, E., Richter, M. A., and Kennedy, J. L. (2006). Glutamate transporter gene SLC1A1 associated with obsessive-compulsive disorder. *Arch. Gen. Psychiatry* 63, 769–776. doi: 10.1001/archpsyc.63.7.769

Aruga, J., and Mikoshiba, K. (2003). Identification and characterization of Slitrk, a novel neuronal transmembrane protein family controlling neurite outgrowth. *Mol. Cell Neurosci.* 24, 117–129. doi: 10.1016/S1044-7431(03)00129-5

American Psychiatric Association. (2013). Diagnostic and statistical manual of mental disorders (5th ed.). Arlington, VA

Atmaca, M., Yildirim, B. H., Ozdemir, B. H., Aydin, B. A., Tezcan, A. E., and Ozler, A. S. (2006). Volumetric MRI assessment of brain regions in patients with refractory obsessive-compulsive disorder. *Prog. Neuropsychopharmacol. Biol. Psychiatry* 30, 1051–1057. doi: 10.1016/j.pnpbp.2006.03.033

Atmaca, M., Yildirim, H., Ozdemir, H., Tezcan, E., and Poyraz, A. K. (2007). Volumetric MRI study of key brain regions implicated in obsessive-compulsive disorder. *Prog. Neuropsychopharmacol. Biol. Psychiatry* 31, 46–52. doi: 10.1016/j.pnpbp.2006.06.008

Bailey, C. G., Ryan, R. M., Thoeng, A. D., Ng, C., King, K., Vanslambrouck, J. M., et al. (2011). Loss-of-function mutations in the glutamate transporter SLC1A1 cause human dicarboxylic aminoaciduria. *J. Clin. Invest.* 121, 446–453. doi: 10.1172/JCI44474

Bakhla, A. K., Verma, V., Soren, S., Sarkhel, S., and Chaudhury, S. (2013). An open-label trial of memantine in treatment-resistant obsessive-compulsive disorder. *Ind. Psychiatry J.* 22, 149–152. doi: 10.4103/0972-6748.132930

Barr, L. C., Goodman, W. K., and Price, L. H. (1993). The serotonin hypothesis of obsessive compulsive disorder. *Int. Clin. Psychopharmacol.* 8 Suppl 2, 79–82. doi: 10.1097/00004850-199311002-00011

Barria, A., and Malinow, R. (2002). Subunit-specific NMDA receptor trafficking to synapses. *Neuron.* 35, 345–353. doi: 10.1016/S0896-6273(02)00776-6

Bellini, S., Fleming, K. E., De, M., McCauley, J. P., Petroccione, M. A., D'Brant, L. Y., et al. (2018). Neuronal glutamate transporters control dopaminergic signaling and compulsive behaviors. *J. Neurosci.* 38, 937–961. doi: 10.1523/JNEUROSCI.1906-17.2017

Bellone, C., and Nicoll, R. A. (2007). Rapid bidirectional switching of synaptic NMDA receptors. *Neuron.* 55, 779–785. doi: 10.1016/j.neuron.2007.07.035

Berman, A. E., Chan, W. Y., Brennan, A. M., Reyes, R. C., Adler, B. L., Suh, S. W., et al. (2011). N-acetylcysteine prevents loss of dopaminergic neurons in the EAAC1-/- mouse. *Ann. Neurol.* 69, 509–520. doi: 10.1002/ana.22162

Bienvenu, O. J., Wang, Y., Shugart, Y. Y., Welch, J. M., Grados, M. A., Fyer, A. J., et al. (2009). Sapap3 and pathological grooming in humans: Results from the OCD collaborative genetics study. *Am. J. Med. Genet. B. Neuropsychiatr. Genet.* 150B, 710–720. doi: 10.1002/ajmg.b.30897

Bjorn-Yoshimoto, W. E., and Underhill, S. M. (2016). The importance of the excitatory amino acid transporter 3 (EAAT3). *Neurochem. Int.* 98, 4–18. doi: 10.1016/j.neuint.2016.05.007

Boardman, L., van der Merwe, L., Lochner, C., Kinnear, C. J., Seedat, S., Stein, D. J., et al. (2011). Investigating SAPAP3 variants in the etiology of obsessive-compulsive disorder and trichotillomania in the South African white population. *Compr. Psychiatry* 52, 181–187. doi: 10.1016/j.comppsych.2010.05.007

Bouvard, M. A., Milliery, M., and Cottraux, J. (2004). Management of obsessive compulsive disorder. *Psychother. Psychosom.* 73, 149–157. doi: 10.1159/000076452

Brennan, B. P., Jensen, J. E., Perriello, C., Pope, H. G.Jr., Jenike, M. A., Hudson, J. I., et al. (2016). Lower posterior cingulate cortex glutathione levels in obsessive-compulsive disorder. *Biol. Psychiatry Cognit. Neurosci. Neuroimaging* 1, 116–124. doi: 10.1016/j.bpsc.2015.12.003

Burguiere, E., Monteiro, P., Feng, G., and Graybiel, A. M. (2013). Optogenetic stimulation of lateral orbitofronto-striatal pathway suppresses compulsive behaviors. *Science* 340, 1243–1246. doi: 10.1126/science.1232380

Burguiere, E., Monteiro, P., Mallet, L., Feng, G., and Graybiel, A. M. (2015). Striatal circuits, habits, and implications for obsessive-compulsive disorder. *Curr. Opin. Neurobiol.* 30, 59–65. doi: 10.1016/j.conb.2014.08.008

Cao, J., Tan, H., Mi, W., and Zuo, Z. (2014). Glutamate transporter type 3 regulates mouse hippocampal GluR1 trafficking. *Biochim. Biophys. Acta* 1840, 1640–1645. doi: 10.1016/j.bbagen.2014.01.006

Chakrabarty, K., Bhattacharyya, S., Christopher, R., and Khanna, S. (2005). Glutamatergic dysfunction in OCD. *Neuropsychopharmacology* 30, 1735–1740. doi: 10.1038/sj.npp.1300733

Chakraborty, S., Singh, O. P., Dasgupta, A., Mandal, N., and Nath Das, H. (2009). Correlation between lipid peroxidation-induced TBARS level and disease severity in obsessive-compulsive disorder. *Prog. Neuropsychopharmacol. Biol. Psychiatry* 33, 363–366. doi: 10.1016/j.pnpbp.2009.01.001

Choi, Y. B., and Lipton, S. A. (2000). Redox modulation of the NMDA receptor. *Cell Mol. Life Sci.* 57, 1535–1541. doi: 10.1007/PL00000638

Choi, B. Y., Kim, J. H., Kim, H. J., Lee, B. E., Kim, I. Y., Sohn, M., et al. (2014). EAAC1 gene deletion increases neuronal death and blood brain barrier disruption after transient cerebral ischemia in female mice. *Int. J. Mol. Sci.* 15, 19444–19457. doi: 10.3390/ijms151119444

Choi, B. Y., Kim, I. Y., Kim, J. H., Lee, B. E., Lee, S. H., Kho, A. R., et al. (2016). Decreased cysteine uptake by EAAC1 gene deletion exacerbates neuronal oxidative stress and neuronal death after traumatic brain injury. *Amino Acids* 48, 1619–1629. doi: 10.1007/s00726-016-2221-4

Chou-Green, J. M., Holscher, T. D., Dallman, M. F., and Akana, S. F. (2003). Compulsive behavior in the 5-HT2C receptor knockout mouse. *Physiol. Behav.* 78, 641–649. doi: 10.1016/S0031-9384(03)00047-7

Coco, S., Verderio, C., Trotti, D., Rothstein, J. D., Volterra, A., and Matteoli, M. (1997). Non-synaptic localization of the glutamate transporter EAAC1 in cultured hippocampal neurons. *Eur. J. Neurosci.* 9, 1902–1910. doi: 10.1111/j.1460-9568.1997.tb00757.x

Conti, F., DeBiasi, S., Minelli, A., Rothstein, J. D., and Melone, M. (1998). EAAC1, a high-affinity glutamate tranporter, is localized to astrocytes and gabaergic neurons besides pyramidal cells in the rat cerebral cortex. *Cereb. Cortex* 8, 108–116. doi: 10.1093/cercor/8.2.108

Coric, V., Taskiran, S., Pittenger, C., Wasylink, S., Mathalon, D. H., Valentine, G., et al. (2005). Riluzole augmentation in treatment-resistant obsessive-compulsive disorder: an open-label trial. *Biol. Psychiatry* 58, 424–428. doi: 10.1016/j.biopsych.2005.04.043

Cottraux, J., Bouvard, M. A., and Milliery, M. (2005). Combining Pharmacotherapy with cognitive-behavioral interventions for obsessive-compulsive disorder. *Cognit. Behav. Ther.* 34, 185–192. doi: 10.1080/16506070510043750

Davis, M. (2011). NMDA receptors and fear extinction: implications for cognitive behavioral therapy. *Dialogues Clin. Neurosci.* 13, 463–474.

Delgado-Acevedo, C., Estay, S. F., Radke, A. K., Sengupta, A., Escobar, A. P., Henriquez-Belmar, F., et al. (2019). Behavioral and synaptic alterations relevant to obsessive-compulsive disorder in mice with increased EAAT3 expression. *Neuropsychopharmacology* 44, 1163–1173. doi: 10.1038/s41386-018-0302-7

Delorme, R., Krebs, M. O., Chabane, N., Roy, I., Millet, B., Mouren-Simeoni, M. C., et al. (2004). Frequency and transmission of glutamate receptors GRIK2 and GRIK3 polymorphisms in patients with obsessive compulsive disorder. *Neuroreport* 15, 699–702. doi: 10.1097/00001756-200403220-00025

Denys, D., Zohar, J., and Westenberg, H. G. (2004). The role of dopamine in obsessive-compulsive disorder: preclinical and clinical evidence. *J. Clin. Psychiatry* 65 Suppl 14, 11–17.

Denys, D., van der Wee, N., Janssen, J., De Geus, F., and Westenberg, H. G. (2004). Low level of dopaminergic D2 receptor binding in obsessive-compulsive disorder. *Biol. Psychiatry* 55, 1041–1045. doi: 10.1016/j.biopsych.2004.01.023

di Michele, F., Siracusano, A., Talamo, A., and Niolu, C. (2018). N-Acetyl cysteine and vitamin d supplementation in treatment resistant obsessive-compulsive disorder patients: a general review. *Curr. Pharm. Des.* 24, 1832–1838. doi: 10.2174/1381612824666180417124919

Diamond, J. S., and Jahr, C. E. (1997). Transporters buffer synaptically released glutamate on a submillisecond time scale. *J. Neurosci.* 17, 4672–4687. doi: 10.1523/JNEUROSCI.17-12-04672.1997

Dickel, D. E., Veenstra-VanderWeele, J., Cox, N. J., Wu, X., Fischer, D. J., Van Etten-Lee, M., et al. (2006). Association testing of the positional and functional candidate gene SLC1A1/EAAC1 in early-onset obsessive-compulsive disorder. *Arch. Gen. Psychiatry* 63, 778–785. doi: 10.1001/archpsyc.63.7.778

Dold, M., Aigner, M., Lanzenberger, R., and Kasper, S. (2013). Antipsychotic augmentation of serotonin reuptake inhibitors in treatment-resistant obsessive-compulsive disorder: a meta-analysis of double-blind, randomized, placebo-controlled trials. *Int. J. Neuropsychopharmacol.* 16, 557–574. doi: 10.1017/S1461145712000740

Dold, M., Aigner, M., Lanzenberger, R., and Kasper, S. (2015). Antipsychotic augmentation of serotonin reuptake inhibitors in treatment-resistant obsessive-compulsive disorder: an update meta-analysis of double-blind, randomized, placebo-controlled trials. *Int. J. Neuropsychopharmacol.* 18:1-11. doi: 10.1093/ijnp/pyv047

Fitzgerald, K. D., Welsh, R. C., Stern, E. R., Angstadt, M., Hanna, G. L., Abelson, J. L., et al. (2011). Developmental alterations of frontal-striatal-thalamic connectivity in obsessive-compulsive disorder. *J. Am. Acad. Child Adolesc. Psychiatry* 50, 938–948 e3. doi: 10.1016/j.jaac.2011.06.011

Furuta, A., Rothstein, J. D., and Martin, L. J. (1997). Glutamate transporter protein subtypes are expressed differentially during rat CNS development. *J. Neurosci.* 17, 8363–8375. doi: 10.1523/JNEUROSCI.17-21-08363.1997

Gasso, P., Ortiz, A. E., Mas, S., Morer, A., Calvo, A., Bargallo, N., et al. (2015). Association between genetic variants related to glutamatergic, dopaminergic and neurodevelopment pathways and white matter microstructure in child and adolescent patients with obsessive-compulsive disorder. *J. Affect. Disord.* 186, 284–292. doi: 10.1016/j.jad.2015.07.035

Gerfen, C. R., and Surmeier, D. J. (2011). Modulation of striatal projection systems by dopamine. *Annu. Rev. Neurosci.* 34, 441–466. doi: 10.1146/annurev-neuro-061010-113641

Ghanizadeh, A., Mohammadi, M. R., Bahraini, S., Keshavarzi, Z., Firoozabadi, A., and Alavi Shoshtari, A. (2017). Efficacy of N-Acetylcysteine augmentation on obsessive compulsive disorder: a multicenter randomized double blind placebo controlled clinical trial. *Iran J. Psychiatry* 12, 134–141.

Grabe, H. J., Meyer, C., Hapke, U., Rumpf, H. J., Freyberger, H. J., Dilling, H., et al. (2000). Prevalence, quality of life and psychosocial function in obsessive-compulsive disorder and subclinical obsessive-compulsive disorder in northern Germany. *Eur. Arch. Psychiatry Clin. Neurosci.* 250, 262–268. doi: 10.1007/s004060070017

Grant, P., Lougee, L., Hirschtritt, M., and Swedo, S. E. (2007). An open-label trial of riluzole, a glutamate antagonist, in children with treatment-resistant obsessive-compulsive disorder. *J. Child Adolesc. Psychopharmacol.* 17, 761–767. doi: 10.1089/cap.2007.0021

Hanna, G. L., Veenstra-VanderWeele, J., Cox, N. J., Boehnke, M., Himle, J. A., Curtis, G. C., et al. (2002). Genome-wide linkage analysis of families with obsessive-compulsive disorder ascertained through pediatric probands. *Am. J. Med. Genet.* 114, 541–552. doi: 10.1002/ajmg.10519

He, Y., Janssen, W. G., Rothstein, J. D., and Morrison, J. H. (2000). Differential synaptic localization of the glutamate transporter EAAC1 and glutamate receptor subunit GluR2 in the rat hippocampus. *J. Comp. Neurol.* 418, 255–269. doi: 10.1002/(SICI)1096-9861(20000313)418:3<255::AID-CNE2>3.0.CO;2-6

Hesse, S., Muller, U., Lincke, T., Barthel, H., Villmann, T., Angermeyer, M. C., et al. (2005). Serotonin and dopamine transporter imaging in patients with obsessive-compulsive disorder. *Psychiatry Res.* 140, 63–72. doi: 10.1016/j.pscychresns.2005.07.002

Himi, T., Ikeda, M., Yasuhara, T., Nishida, M., and Morita, I. (2003). Role of neuronal glutamate transporter in the cysteine uptake and intracellular glutathione levels in cultured cortical neurons. *J. Neural Transm. (Vienna)* 110, 1337–1348. doi: 10.1007/s00702-003-0049-z

Hirschtritt, M. E., Bloch, M. H., and Mathews, C. A. (2017). Obsessive-compulsive disorder: advances in diagnosis and treatment. *JAMA* 317, 1358–1367. doi: 10.1001/jama.2017.2200

Holmseth, S., Dehnes, Y., Huang, Y. H., Follin-Arbelet, V. V., Grutle, N. J., Mylonakou, M. N., et al. (2012). The density of EAAC1 (EAAT3) glutamate transporters expressed by neurons in the mammalian CNS. *J. Neurosci.* 32, 6000–6013. doi: 10.1523/JNEUROSCI.5347-11.2012

Insel, T. R., Mueller, E. A., Alterman, I., Linnoila, M., and Murphy, D. L. (1985). Obsessive-compulsive disorder and serotonin: is there a connection?. *Biol. Psychiatry* 20, 1174–1188. doi: 10.1016/0006-3223(85)90176-3

Jang, B. G., Won, S. J., Kim, J. H., Choi, B. Y., Lee, M. W., Sohn, M., et al. (2012). EAAC1 gene deletion alters zinc homeostasis and enhances cortical neuronal injury after transient cerebral ischemia in mice. *J. Trace Elem. Med. Biol.* 26, 85–88. doi: 10.1016/j.jtemb.2012.04.010

Jarzylo, L. A., and Man, H. Y. (2012). Parasynaptic NMDA receptor signaling couples neuronal glutamate transporter function to AMPA receptor synaptic distribution and stability. *J. Neurosci.* 32, 2552–2563. doi: 10.1523/JNEUROSCI.3237-11.2012

Kanai, Y., and Hediger, M. A. (2004). The glutamate/neutral amino acid transporter family SLC1: molecular, physiological and pharmacological aspects. *Pflugers Arch.* 447, 469–479. doi: 10.1007/s00424-003-1146-4

Kwon, J. S., Joo, Y. H., Nam, H. J., Lim, M., Cho, E. Y., Jung, M. H., et al. (2009). Association of the glutamate transporter gene SLC1A1 with atypical antipsychotics-induced obsessive-compulsive symptoms. *Arch. Gen. Psychiatry* 66, 1233–1241. doi: 10.1001/archgenpsychiatry.2009.155

Lafleur, D. L., Pittenger, C., Kelmendi, B., Gardner, T., Wasylink, S., Malison, R. T., et al. (2006). N-acetylcysteine augmentation in serotonin reuptake inhibitor refractory obsessive-compulsive disorder. *Psychopharmacol. (Berl.)* 184, 254–256. doi: 10.1007/s00213-005-0246-6

Lalanne, L., Ayranci, G., Kieffer, B. L., and Lutz, P. E. (2014). The kappa opioid receptor: from addiction to depression, and back. *Front. Psychiatry* 5, 170. doi: 10.3389/fpsyt.2014.00170

Lin, C. I., Orlov, I., Ruggiero, A. M., Dykes-Hoberg, M., Lee, A., Jackson, M., et al. (2001). Modulation of the neuronal glutamate transporter EAAC1 by the interacting protein GTRAP3-18. *Nature* 410, 84–88. doi: 10.1038/35065084

Maia, T. V., Cooney, R. E., and Peterson, B. S. (2008). The neural bases of obsessive-compulsive disorder in children and adults. *Dev. Psychopathol.* 20, 1251–1283. doi: 10.1017/S0954579408000606

March, J. S., Gutzman, L. D., Jefferson, J. W., and Greist, J. H. (1989). Serotonin and treatment in obsessive-compulsive disorder. *Psychiatr. Dev.* 7, 1–18.

Mathews, G. C., and Diamond, J. S. (2003). Neuronal glutamate uptake Contributes to GABA synthesis and inhibitory synaptic strength. *J. Neurosci.* 23, 2040–2048. doi: 10.1523/JNEUROSCI.23-06-02040.2003

Matta, J. A., Ashby, M. C., Sanz-Clemente, A., Roche, K. W., and Isaac, J. T. (2011). mGluR5 and NMDA receptors drive the experience- and activity-dependent NMDA receptor NR2B to NR2A subunit switch. *Neuron.* 70, 339–351. doi: 10.1016/j.neuron.2011.02.045

Mattheisen, M., Samuels, J. F., Wang, Y., Greenberg, B. D., Fyer, A. J., McCracken, J. T., et al. (2015). Genome-wide association study in obsessive-compulsive disorder: results from the OCGAS. *Mol. Psychiatry* 20, 337–344. doi: 10.1038/mp.2014.43

Milad, M. R., and Rauch, S. L. (2012). Obsessive-compulsive disorder: beyond segregated cortico-striatal pathways. *Trends Cognit. Sci.* 16, 43–51. doi: 10.1016/j.tics.2011.11.003

Milad, M. R., Furtak, S. C., Greenberg, J. L., Keshaviah, A., Im, J. J., Falkenstein, M. J., et al. (2013). Deficits in conditioned fear extinction in obsessive-compulsive disorder and neurobiological changes in the fear circuit. *JAMA Psychiatry* 70, 608–618. doi: 10.1001/jamapsychiatry.2013.914

Modarresi, A., Sayyah, M., Razooghi, S., Eslami, K., Javadi, M., and Kouti, L. (2018). Memantine augmentation improves symptoms in serotonin reuptake inhibitor-refractory obsessive-compulsive disorder: a randomized controlled trial. *Pharmacopsychiatry* 51, 263–269. doi: 10.1055/s-0043-120268

Murphy, D. L., Moya, P. R., Fox, M. A., Rubenstein, L. M., Wendland, J. R., and Timpano, K. R. (2013). Anxiety and affective disorder comorbidity related to serotonin and other neurotransmitter systems: obsessive-compulsive disorder as an example of overlapping clinical and genetic heterogeneity. *Philos. Trans. R. Soc. Lond. B. Biol. Sci.* 368, 20120435. doi: 10.1098/rstb.2012.0435

Myers, K. M., and Davis, M. (2002). Behavioral and neural analysis of extinction. *Neuron.* 36, 567–584. doi: 10.1016/S0896-6273(02)01064-4

Naaijen, J., Zwiers, M. P., Amiri, H., Williams, S. C. R., Durston, S., Oranje, B., et al. (2017). Fronto-striatal glutamate in autism spectrum disorder and obsessive compulsive disorder. *Neuropsychopharmacology* 42, 2456–2465. doi: 10.1038/npp.2016.260

Nakao, T., Okada, K., and Kanba, S. (2014). Neurobiological model of obsessive-compulsive disorder: evidence from recent neuropsychological and neuroimaging findings. *Psychiatry Clin. Neurosci.* 68, 587–605. doi: 10.1111/pcn.12195

Otis, T. S., Brasnjo, G., Dzubay, J. A., and Pratap, M. (2004). Interactions between glutamate transporters and metabotropic glutamate receptors at excitatory synapses in the cerebellar cortex. *Neurochem. Int.* 45, 537–544. doi: 10.1016/j.neuint.2003.11.007

Pauls, D. L., Abramovitch, A., Rauch, S. L., and Geller, D. A. (2014). Obsessive-compulsive disorder: an integrative genetic and neurobiological perspective. *Nat. Rev. Neurosci.* 15, 410–424. doi: 10.1038/nrn3746

Peghini, P., Janzen, J., and Stoffel, W. (1997). Glutamate transporter EAAC-1-deficient mice develop dicarboxylic aminoaciduria and behavioral abnormalities but no neurodegeneration. *EMBO J.* 16, 3822–3832. doi: 10.1093/emboj/16.13.3822

Pittenger, C., Bloch, M. H., Wasylink, S., Billingslea, E., Simpson, R., Jakubovski, E., et al. (2015). Riluzole augmentation in treatment-refractory obsessive-compulsive disorder: a pilot randomized placebo-controlled trial. *J. Clin. Psychiatry* 76, 1075–1084. doi: 10.4088/JCP.14m09123

Posner, J., Marsh, R., Maia, T. V., Peterson, B. S., Gruber, A., and Simpson, H. B. (2014). Reduced functional connectivity within the limbic cortico-striato-thalamo-cortical loop in unmedicated adults with obsessive-compulsive disorder. *Hum. Brain Mapp.* 35, 2852–2860. doi: 10.1002/hbm.22371

Quinlan, E. M., Olstein, D. H., and Bear, M. F. (1999). Bidirectional, experience-dependent regulation of N-methyl-D-aspartate receptor subunit composition in the rat visual cortex during postnatal development. *Proc. Natl. Acad. Sci. U.S.A.* 96, 12876–12880. doi: 10.1073/pnas.96.22.12876

Radua, J., and Mataix-Cols, D. (2009). Voxel-wise meta-analysis of grey matter changes in obsessive-compulsive disorder. *Br. J. Psychiatry* 195, 393–402. doi: 10.1192/bjp.bp.108.055046

Rajendram, R., Kronenberg, S., Burton, C. L., and Arnold, P. D. (2017). Glutamate genetics in obsessive-compulsive disorder: a review. *J. Can. Acad. Child Adolesc. Psychiatry* 26, 205–213.

Ralph-Williams, R. J., Paulus, M. P., Zhuang, X., Hen, R., and Geyer, M. A. (2003). Valproate attenuates hyperactive and perseverative behaviors in mutant mice with a dysregulated dopamine system. *Biol. Psychiatry* 53, 352–359. doi: 10.1016/S0006-3223(02)01489-0

Rodenas-Ruano, A., Chavez, A. E., Cossio, M. J., Castillo, P. E., and Zukin, R. S. (2012). REST-dependent epigenetic remodeling promotes the developmental switch in synaptic NMDA receptors. *Nat. Neurosci.* 15, 1382–1390. doi: 10.1038/nn.3214

Rodriguez, C. I., Zwerling, J., Kalanthroff, E., Shen, H., Filippou, M., Jo, B., et al. (2016). Effect of a Novel NMDA receptor modulator, rapastinel (Formerly GLYX-13), in OCD: proof of concept. *Am. J. Psychiatry* 173, 1239–1241. doi: 10.1176/appi.ajp.2016.16080868

Rosenberg, D. R., MacMaster, F. P., Keshavan, M. S., Fitzgerald, K. D., Stewart, C. M., and Moore, G. J. (2000). Decrease in caudate glutamatergic concentrations in pediatric obsessive-compulsive disorder patients taking paroxetine. *J. Am. Acad. Child Adolesc. Psychiatry* 39, 1096–1103. doi: 10.1097/00004583-200009000-00008

Rosenberg, D. R., Mirza, Y., Russell, A., Tang, J., Smith, J. M., Banerjee, S. P., et al. (2004). Reduced anterior cingulate glutamatergic concentrations in childhood OCD and major depression versus healthy controls. *J. Am. Acad. Child Adolesc. Psychiatry* 43, 1146–1153. doi: 10.1097/01.chi.0000132812.44664.2d

Rothstein, J. D., Martin, L., Levey, A. I., Dykes-Hoberg, M., Jin, L., Wu, D., et al. (1994). Localization of neuronal and glial glutamate transporters. *Neuron.* 13, 713–725. doi: 10.1016/0896-6273(94)90038-8

Rothstein, J. D., Dykes-Hoberg, M., Pardo, C. A., Bristol, L. A., Jin, L., Kuncl, R. W., et al. (1996). Knockout of glutamate transporters reveals a major role for astroglial transport in excitotoxicity and clearance of glutamate. *Neuron.* 16, 675–686. doi: 10.1016/S0896-6273(00)80086-0

Sampaio, A. S., Fagerness, J., Crane, J., Leboyer, M., Delorme, R., Pauls, D. L., et al. (2011). Association between polymorphisms in GRIK2 gene and obsessive-compulsive disorder: a family-based study. *CNS Neurosci. Ther.* 17, 141–147. doi: 10.1111/j.1755-5949.2009.00130.x

Samuels, J., Wang, Y., Riddle, M. A., Greenberg, B. D., Fyer, A. J., McCracken, J. T., et al. (2011). Comprehensive family-based association study of the glutamate transporter gene SLC1A1 in obsessive-compulsive disorder. *Am. J. Med. Genet. B. Neuropsychiatr. Genet.* 156B, 472–477. doi: 10.1002/ajmg.b.31184

Saxena, S., Bota, R. G., and Brody, A. L. (2001). Brain-behavior relationships in obsessive-compulsive disorder. *Semin. Clin. Neuropsychiatry* 6, 82–101. doi: 10.1053/scnp.2001.21833

Scimemi, A., Tian, H., and Diamond, J. S. (2009). Neuronal transporters regulate glutamate clearance, NMDA receptor activation, and synaptic plasticity in the hippocampus. *J. Neurosci.* 29, 14581–14595. doi: 10.1523/JNEUROSCI.4845-09.2009

Sepkuty, J. P., Cohen, A. S., Eccles, C., Rafiq, A., Behar, K., Ganel, R., et al. (2002). A neuronal glutamate transporter contributes to neurotransmitter GABA synthesis and epilepsy. *J. Neurosci.* 22, 6372–6379. doi: 10.1523/JNEUROSCI.22-15-06372.2002

Shashidharan, P., Huntley, G. W., Murray, J. M., Buku, A., Moran, T., Walsh, M. J., et al. (1997). Immunohistochemical localization of the neuron-specific glutamate transporter EAAC1 (EAAT3) in rat brain and spinal cord revealed by a novel monoclonal antibody. *Brain Res.* 773, 139–148. doi: 10.1016/S0006-8993(97)00921-9

Shmelkov, S. V., Hormigo, A., Jing, D., Proenca, C. C., Bath, K. G., Milde, T., et al. (2010). Slitrk5 deficiency impairs corticostriatal circuitry and leads to obsessive-compulsive-like behaviors in mice. *Nat. Med.* 16, 598–602. doi: 10.1038/nm.2125

Shugart, Y. Y., Wang, Y., Samuels, J. F., Grados, M. A., Greenberg, B. D., Knowles, J. A., et al. (2009). A family-based association study of the glutamate transporter gene SLC1A1 in obsessive-compulsive disorder in 378 families. *Am. J. Med. Genet. B. Neuropsychiatr. Genet.* 150B, 886–892. doi: 10.1002/ajmg.b.30914

Sidiropoulou, K., Chao, S., Lu, W., and Wolf, M. E. (2001). Amphetamine administration does not alter protein levels of the GLT-1 and EAAC1 glutamate transporter subtypes in rat midbrain, nucleus accumbens, striatum, or prefrontal cortex. *Brain Res. Mol. Brain Res.* 90, 187–192. doi: 10.1016/S0169-328X(01)00110-3

Simsek, S., Gencoglan, S., and Yuksel, T. (2016). DNA damage and antioxidants in treatment naive children with obsessive-compulsive disorder. *Psychiatry Res.* 237, 133–137. doi: 10.1016/j.psychres.2016.01.054

Skapinakis, P., Caldwell, D. M., Hollingworth, W., Bryden, P., Fineberg, N. A., Salkovskis, P., et al. (2016). Pharmacological and psychotherapeutic interventions for management of obsessive-compulsive disorder in adults: a

systematic review and network meta-analysis. *Lancet Psychiatry* 3, 730–739. doi: 10.1016/S2215-0366(16)30069-4

Song, M., Mathews, C. A., Stewart, S. E., Shmelkov, S. V., Mezey, J. G., Rodriguez-Flores, J. L., et al. (2017). Rare synaptogenesis-impairing mutations in slitrk5 are associated with obsessive compulsive disorder. *PloS One* 12, e0169994. doi: 10.1371/journal.pone.0169994

Stewart, S. E., Fagerness, J. A., Platko, J., Smoller, J. W., Scharf, J. M., Illmann, C., et al. (2007). Association of the SLC1A1 glutamate transporter gene and obsessive-compulsive disorder. *Am. J. Med. Genet. B. Neuropsychiatr. Genet.* 144B, 1027–1033. doi: 10.1002/ajmg.b.30533

Stewart, S. E., Mayerfeld, C., Arnold, P. D., Crane, J. R., O'Dushlaine, C., Fagerness, J. A., et al. (2013). Meta-analysis of association between obsessive-compulsive disorder and the 3' region of neuronal glutamate transporter gene SLC1A1. *Am. J. Med. Genet. B. Neuropsychiatr. Genet.* 162B, 367–379. doi: 10.1002/ajmg.b.32137

Stewart, S. E., Yu, D., Scharf, J. M., Neale, B. M., Fagerness, J. A., Mathews, C. A., et al. (2013). Genome-wide association study of obsessive-compulsive disorder. *Mol. Psychiatry* 18, 788–798. doi: 10.1038/mp.2012.85

Szechtman, H., Sulis, W., and Eilam, D. (1998). Quinpirole induces compulsive checking behavior in rats: a potential animal model of obsessive-compulsive disorder (OCD). *Behav. Neurosci.* 112, 1475–1485. doi: 10.1037//0735-7044.112.6.1475

Tanaka, K., Watase, K., Manabe, T., Yamada, K., Watanabe, M., Takahashi, K., et al. (1997). Epilepsy and exacerbation of brain injury in mice lacking the glutamate transporter GLT-1. *Science* 276, 1699–1702. doi: 10.1126/science.276.5319.1699

Tong, G., and Jahr, C. E. (1994). Block of glutamate transporters potentiates postsynaptic excitation. *Neuron.* 13, 1195–1203. doi: 10.1016/0896-6273(94)90057-4

Underhill, S. M., Wheeler, D. S., Li, M., Watts, S. D., Ingram, S. L., and Amara, S. G. (2014). Amphetamine modulates excitatory neurotransmission through endocytosis of the glutamate transporter EAAT3 in dopamine neurons. *Neuron.* 83, 404–416. doi: 10.1016/j.neuron.2014.05.043

Veenstra-VanderWeele, J., Xu, T., Ruggiero, A. M., Anderson, L. R., Jones, S. T., Himle, J. A., et al. (2012). Functional studies and rare variant screening of SLC1A1/EAAC1 in males with obsessive-compulsive disorder. *Psychiatr. Genet.* 22, 256–260. doi: 10.1097/YPG.0b013e328353fb63

Wadiche, J. I., and Jahr, C. E. (2005). Patterned expression of Purkinje cell glutamate transporters controls synaptic plasticity. *Nat. Neurosci.* 8, 1329–1334. doi: 10.1038/nn1539

Wan, Y., Feng, G., and Calakos, N. (2011). Sapap3 deletion causes mGluR5-dependent silencing of AMPAR synapses. *J. Neurosci.* 31, 16685–16691. doi: 10.1523/JNEUROSCI.2533-11.2011

Wan, Y., Ade, K. K., Caffall, Z., Ilcim Ozlu, M., Eroglu, C., Feng, G., et al. (2014). Circuit-selective striatal synaptic dysfunction in the Sapap3 knockout mouse model of obsessive-compulsive disorder. *Biol. Psychiatry* 75, 623–630. doi: 10.1016/j.biopsych.2013.01.008

Watabe, M., Aoyama, K., and Nakaki, T. (2007). Regulation of glutathione synthesis via interaction between glutamate transport-associated protein 3-18 (GTRAP3-18) and excitatory amino acid carrier-1 (EAAC1) at plasma membrane. *Mol. Pharmacol.* 72, 1103–1110. doi: 10.1124/mol.107.039461

Welch, J. M., Lu, J., Rodriguiz, R. M., Trotta, N. C., Peca, J., Ding, J. D., et al. (2007). Cortico-striatal synaptic defects and OCD-like behaviours in Sapap3-mutant mice. *Nature* 448, 894–900. doi: 10.1038/nature06104

Wendland, J. R., Moya, P. R., Timpano, K. R., Anavitarte, A. P., Kruse, M. R., Wheaton, M. G., et al. (2009). A haplotype containing quantitative trait loci for SLC1A1 gene expression and its association with obsessive-compulsive disorder. *Arch. Gen. Psychiatry* 66, 408–416. doi: 10.1001/archgenpsychiatry.2009.6

Willour, V. L., Yao Shugart, Y., Samuels, J., Grados, M., Cullen, B., Bienvenu, O. J., et al. (2004). Replication study supports evidence for linkage to 9p24 in obsessive-compulsive disorder. *Am. J. Hum. Genet.* 75, 508–513. doi: 10.1086/423899

Wood, J., LaPalombara, Z., and Ahmari, S. E. (2018). Monoamine abnormalities in the SAPAP3 knockout model of obsessive-compulsive disorder-related behaviour. *Philos. Trans. R. Soc. Lond. B. Biol. Sci.* 373 (1742). doi: 10.1098/rstb.2017.0023

Yadin, E., Friedman, E., and Bridger, W. H. (1991). Spontaneous alternation behavior: an animal model for obsessive-compulsive disorder?. *Pharmacol. Biochem. Behav.* 40, 311–315. doi: 10.1016/0091-3057(91)90559-K

Zike, I. D., Chohan, M. O., Kopelman, J. M., Krasnow, E. N., Flicker, D., Nautiyal, K. M., et al. (2017). OCD candidate gene SLC1A1/EAAT3 impacts basal ganglia-mediated activity and stereotypic behavior. *Proc. Natl. Acad. Sci. U.S.A.* 114, 5719–5724. doi: 10.1073/pnas.1701736114

Zuchner, S., Wendland, J. R., Ashley-Koch, A. E., Collins, A. L., Tran-Viet, K. N., Quinn, K., et al. (2009). Multiple rare SAPAP3 missense variants in trichotillomania and OCD. *Mol. Psychiatry* 14, 6–9. doi: 10.1038/mp.2008.83

Conflict of Interest: The authors declare that the research was conducted in the absence of any commercial or financial relationships that could be construed as a potential conflict of interest.

The handling editor declared a shared affiliation, though no other collaboration, with the authors AE, JW, AC, PM at time of review.

frontiers in Pharmacology

ORIGINAL RESEARCH
published: 03 December 2019
doi: 10.3389/fphar.2019.01429

UFR2709, a Nicotinic Acetylcholine Receptor Antagonist, Decreases Ethanol Intake in Alcohol-Preferring Rats

Gabriel Quiroz[1†], Ramón Sotomayor-Zárate[2†], Juan Pablo González-Gutierrez[3], Franco Vizcarra[4], Felipe Moraga[4], Isabel Bermudez[5], Miguel Reyes-Parada[6,7], María Elena Quintanilla[8], Diego Lagos[9], Mario Rivera-Meza[9] and Patricio Iturriaga-Vásquez[4,10]**

[1] Programa de Doctorado en Farmacología, Facultad de Ciencias Químicas y Farmacéuticas, Universidad de Chile, Santiago, Chile, [2] Laboratorio de Neuroquímica y Neurofarmacología, Centro de Neurobiología y Fisiopatología Integrativa (CENFI), Instituto de Fisiología, Facultad de Ciencias, Universidad de Valparaíso, Valparaíso, Chile, [3] Programa de Doctorado en Química, Facultad de Ciencias, Universidad de Chile, Santiago, Chile, [4] Laboratorio de Síntesis Orgánica y Farmacología Molecular, Departamento de Ciencias Químicas y Recursos Naturales, Facultad de Ingeniería y Ciencias, Universidad de la Frontera, Temuco, Chile, [5] Deptartment of Biological & Medical Sciences, Faculty of Health & Life Sciences, Oxford Brookes University, Oxford, United Kingdom, [6] Centro de Investigación Biomédica y Aplicada (CIBAP), Escuela de Medicina, Facultad de Ciencias Médicas, Universidad de Santiago de Chile, Santiago, Chile, [7] Facultad de Ciencias de la Salud, Universidad Autónoma de Chile, Santiago, Chile, [8] Programa de Farmacología Molecular y Clínica, ICBM, Facultad de Medicina, Universidad de Chile, Santiago, Chile, [9] Departamento de Química Farmacológica y Toxicológica, Facultad de Ciencias Químicas y Farmacéuticas, Universidad de Chile, Santiago, Chile, [10] Center of Excellence in Biotechnology Research Applied to the Environment, Universidad de La Frontera, Temuco, Chile

OPEN ACCESS

Edited by:
Andrew Lawrence, University of Melbourne, Australia

Reviewed by:
Valentina Vengeliene, Vilnius University, Lithuania
Joyce Besheer, University of North Carolina at Chapel Hill, United States

***Correspondence:**
Mario Rivera-Meza
mario.rivera@ciq.uchile.cl
Patricio Iturriaga-Vásquez
patricio.iturriaga@ufrontera.cl

[†]These authors have contributed equally to this work

Specialty section:
This article was submitted to Translational Pharmacology, a section of the journal Frontiers in Pharmacology

Received: *01 July 2019*
Accepted: *08 November 2019*
Published: *03 December 2019*

Citation:
Quiroz G, Sotomayor-Zárate R, González-Gutierrez JP, Vizcarra F, Moraga F, Bermudez I, Reyes-Parada M, Quintanilla ME, Lagos D, Rivera-Meza M and Iturriaga-Vásquez P (2019) UFR2709, a Nicotinic Acetylcholine Receptor Antagonist, Decreases Ethanol Intake in Alcohol-Preferring Rats. Front. Pharmacol. 10:1429. doi: 10.3389/fphar.2019.01429

Brain nicotinic acetylcholine receptors (nAChRs), a heterogeneous family of pentameric acetylcholine-gated cation channels, have been suggested as molecular targets for the treatment of alcohol abuse and dependence. Here, we examined the effect of the competitive nAChR antagonist UFR2709 on the alcohol consumption of high-alcohol-drinking UChB rats. UChB rats were given free access to ethanol for 24-h periods in a two-bottle free choice paradigm and their ethanol and water intake were measured. The animals were i.p. injected daily for 17 days with a 10, 5, 2.5, or 1 mg/kg dose of UFR2709. Potential confounding motor effects of UFR2709 were assessed by examining the locomotor activity of animals administered the highest dose of UR2709 tested (10 mg/kg i.p.). UFR2709 reduced ethanol consumption and ethanol preference and increased water consumption in a dose-dependent manner. The most effective dose of UFR2709 was 2.5 mg/kg, which induced a 56% reduction in alcohol consumption. Administration of UFR2709 did not affect the weight or locomotor activity of the rats, suggesting that its effects on alcohol consumption and preference were mediated by specific nAChRs.

Keywords: alcohol dependence, ethanol, UChB rats, nAChR antagonism, voluntary ethanol drinking

INTRODUCTION

Alcohol is the most commonly abused legal substance and alcoholism is a serious public health problem worldwide (WHO, 2014). Several lines of evidence have identified neuronal nicotinic acetylcholine receptors (nAChRs) in the mesocorticolimbic-dopamine (DA) system as being involved in alcoholism (Madden and Heath, 2002; John et al., 2003; Dani and Harris, 2005; Falk et al.,

2006). Consistent with this view, nAChR ligands reduce ethanol consumption in various animal models and humans (Chatterjee and Bartlett, 2010; Rahman et al., 2015).

nAChRs belong to the pentameric ligand-gated ion channel superfamily. The most abundant nAChRs in the brain are the heteromeric α4β2 and homomeric α7 subtypes (Gotti et al., 2006; Albuquerque et al., 2009). Other heteromeric nAChRs present in the brain include the α4β2α5, α6β2β3, α4β2α6, α4β4, α3β4 and α3β2 subtypes, but these are less abundant and/or have a more restricted distribution (Gotti et al., 2006). Ethanol intake appears to involve a variety of nAChR subtypes (Joslyn et al., 2008; Saccone et al., 2009; Taslim and Saeed Dar, 2011). α7 (Kamens et al., 2010a) and α3β4 nAChRs (Chatterjee et al., 2011; Miller et al., 2019) have both been implicated in ethanol intake, and receptors containing the α5 nAChR subunit are thought to be associated with the sedative effects of ethanol (Santos et al., 2013). Furthermore, the α4β2 nAChR subtype may be involved in alcohol intake due to its role in the brain's reward system. Ethanol activates the mesolimbic-DA system, inducing the release of DA in the nucleus accumbens from projections that arise in the ventral tegmental area (VTA) (Gessa et al., 1985; Di Chiara and Imperato, 1988). VTA dopaminergic neurons primarily express the α4β2 nAChR subtype, but also express nAChRs exhibiting combinations of α5 and α6 subunits (Klink et al, 2001; Azam et al., 2002). These nAChRs are activated by cholinergic inputs from the laterodorsal tegmental and pedunculopontine tegmental nuclei (Oakman et al., 1995; Jerlhag et al., 2012; Xiao et al., 2016). Interestingly, voluntary ethanol consumption increases ACh levels in the VTA and promotes DA overflow in the nucleus accumbens in rats (Larsson et al., 2005). This establishes a cholinergic-dopaminergic reward axis (Xiao et al., 2016), which is affected by ethanol (Engel and Jerlhag, 2014).

Partial agonists of nAChRs such as cytisine (Papke and Heinemann, 1993; Rollema et al., 2010) and varenicline (Coe et al., 2005; Rollema et al., 2007) have been shown to decrease ethanol intake in rodents after a single dose or short-term administration (Steensland et al., 2007; Kamens et al., 2010b; Sajja and Rahman, 2011). Indeed, we confirmed the effects of varenicline and cytisine on alcohol intake in alcohol-preferring University of Chile (UChB) rats (Sotomayor-Zárate et al., 2013). These animals have been selectively bred for over 90 generations for their ethanol preference and are considered suitable models of alcohol dependence (Mardones and Segovia-Riquelme, 1983; Quintanilla et al., 2006; Tampier and Quintanilla, 2010). Given that partial agonists display competitive antagonistic effects in the presence of a full agonist, the effects of cytisine and varenicline on alcohol intake may stem from their antagonistic effects rather than from their partial activation of nAChRs. Consistent with this possibility, we showed that administration of erysodine, a competitive nAChR inhibitor, induced a marked decrease in alcohol intake in UChB rats (Quiroz et al., 2018). To further explore the efficacy of nAChR inhibitors in reducing alcohol intake, we assessed the effects of UFR2709 [(S)-1-methylpyrrolidin-2-yl) methyl benzoate], a recently described competitive nAChR antagonist (Faundez-Parraguez et al., 2013), on the maintenance of ethanol intake by alcohol-preferring UChB rats. Here, we show that UFR2709 reduces ethanol intake in a dose-dependent manner without affecting body weight or locomotor activity.

MATERIALS AND METHODS

Drugs and Drinking Solutions

UFR2709-HCl (M.W. 255.74 g/mol) was synthesized as previously reported (Faundez-Parraguez et al., 2013). The structure of UFR2709-HCl was confirmed by one- and two-dimensional ^{1}H and ^{13}C NMR analyses. Nicotine ditartrate was purchased from Sigma-Aldrich (St. Louis, MO, USA). All other reagents used were of analytical grade. The volume of injection (1 ml/kg) was adjusted to body weight to achieve the desired dose of UFR2709-HCl. Ethanol solutions (10% $^{v}/_{v}$) were prepared by mixing absolute ethanol (Merck, Darmstadt, Germany) with tap water. Ethanol concentration was chosen based on prior studies using UChB rats (Mardones and Segovia-Riquelme, 1983; Quintanilla et al., 2006).

Animals

The experiments were carried out in male Wistar-UChB rats (n = 37). The UChB rat line has been bred for over 90 generations to ingest 10% ethanol solution in preference to water (Mardones and Segovia-Riquelme, 1983; Quintanilla et al., 2006). Thus, these animals are considered suitable models of alcoholism and are used to screen medications to treat alcoholism (Quintanilla et al., 2006). UChB rats weighing between 240 and 280 g were housed individually (for ethanol consumption experiments) or in trios (for locomotor activity experiments) in polycarbonate cages in temperature- and humidity-controlled conditions under a regular 12-h light-dark cycle (lights off at 19:00 h) with free access to food and water. All alcohol consumption experiments were performed at the Faculty of Medicine, Universidad de Chile.

All animal experiments were performed in accordance with ARRIVE guidelines (Kilkenny et al., 2010) and approved by the "Animal Experimentation Ethics Committee of the Universidad de Chile".

Effect of Different Doses of UFR2709 on the Maintenance of Ethanol Intake by UChB Rats

The ethanol preference of UChB rats administered different doses of UFR2709 was assessed using a two-bottle free choice experimental paradigm, as previously described (Mardones and Segovia-Riquelme, 1983; Quintanilla et al., 2006; Tampier and Quintanilla, 2010; Sotomayor-Zárate et al., 2013). Twenty-five UChB rats were housed in individual cages and subjected to a homecage two-bottle free choice regimen between ethanol 10% $^{v}/_{v}$ and distilled water with continuous access (24 h/day). The positions of the bottles were alternated daily to avoid potential position preference. After 20 days, a stable plateau of ethanol consumption was reached, and the final three drinking days were averaged to obtain the mean voluntary ethanol consumption of each rat. The rats were then randomly divided

into five groups (n = 5 per group), and a single i.p. injection of UFR2709-HCl (1, 2.5, 5, or 10 mg/kg) or saline was administered for 17 days at 15:00 h. After the treatment period, all UChB rats were maintained under the 24-h continuous access two-bottle free choice paradigm for three additional days. The animals were allowed *ad libitum* access to food. The weight and ethanol and water intake of the animals were recorded at 14:00 h each day and expressed as g ethanol/kg/day and mL water/kg/day, respectively.

Effect of UFR2709 on Locomotor Activity

Locomotor activity was assessed using the open-field test, as previously described (Rivera-Meza et al., 2014). The open-field apparatus consisted of a black polycarbonate chamber (43 × 43 × 43 cm), the floor of which was marked with lines (length: 14.3 cm) forming a 3 × 3 grid. To study the effects of UFR2709 on locomotor activity, 12 ethanol-naïve UChB rats were randomly assigned to two groups and administered a 10 mg/kg dose (i.p.) of UFR2709 (n = 6) or an equivalent volume of saline (n = 6) (1 mL/kg). After 30 min of UFR2709 or saline administration, the animals were individually placed in the center of the open-field apparatus, and their locomotor activity was recorded for 30 min. Locomotor activity was recorded by a digital camera which was fixed above the test chamber and connected to a computer in another room. The apparatus was wiped and cleaned with water after each trial. Horizontal locomotor activity was expressed as activity units (AUs) per 5 min. An AU was defined as complete crossing from one square to another. The number of times of vertical rear per 5 min and the time (in s) spent in grooming behavior were also measured.

Determination of Octanol-Buffer Distribution Coefficient of UFR2709 At pH 7.4

Octanol-buffer distribution coefficient at pH 7.4 (Log $D_{7.4}$) values were determined using the shake-flask method (Andrés et al., 2015). Briefly, 5 mg of UFR2709-HCl and nicotine were added to 5 mL of 50 mM phosphate buffer (pH 7.4) and 5 mL of n-octanol (water saturated) in a glass vial. The sample vial was mixed by vortexing and then incubated to equilibrium for 24 h at 25°C. After equilibration, the phases were separated and the compounds were measured by UV spectroscopy at a wavelength of 232 nm for UFR2709-HCl and 257 nm for nicotine using calibration curves. The logarithm of the quotient of the concentrations in the organic and aqueous phases (Log $D_{7.4}$) was calculated. Values correspond to the mean ± SEM of five independent assays.

Statistical Analysis

Differences between UFR2709- and saline-treated animals were analyzed using two-way ANOVA with Tukey´s multiple comparison test (**Figures 1** and **2**). One-way ANOVA followed by Tukey's *post hoc* test was used to analyze the effect of 17 days of saline or UFR2709 administration on average ethanol intake (**Figure 3**). The time-course of horizontal and vertical locomotor activity and grooming behavior was recorded every 5 min throughout the 30 min test period. Data were analyzed using two-way ANOVA followed by Bonferroni's *post hoc* test to compare the effects of saline and UFR2709 (10 mg/kg, i.p.) (**Figure 4**). Data are expressed as mean ± SEM. Statistical analyses were performed using Graph Pad Prism 8.0 software (Graph Pad Software, San Diego, CA, USA), and the level of statistical significance was set at $P < 0.05$.

RESULTS

Effect of UFR2709 on the Maintenance of Ethanol Intake by UChB Rats

To determine the effect of different doses of UFR2709 on the maintenance of voluntary ethanol intake, alcohol-preferring UChB rats were given a free choice between 10% $^{v}/_{v}$ ethanol and water for 20 days. At day 20 of ethanol access, animals were administered a 1, 2.5, 5, or 10 mg/kg dose of UFR2709 or saline each day for 17 consecutive days. The baseline levels of ethanol consumption for all groups correspond to the average ethanol intake during the last 3 days before the treatment period. Two-way ANOVA with Tukey's multiple comparison test with dose and day as factors showed that all UFR2709 doses significantly reduced ethanol intake (**Figure 1**) in comparison to saline (interaction [$F_{(76,400)} = 2.992$, $P < 0.0001$]; days [$F_{(19,400)} = 10.20$, $P < 0.0001$]; doses [$F_{(4,400)} = 179.5$, $P < 0.0001$]). In addition, all UFR2709 doses significantly increased water intake (**Figure 2**) in comparison to saline (interaction [$F_{(76,400)} = 2.244$, $P < 0.0001$]; days [$F_{(19,400)} = 6.708$, $P < 0.0001$]; doses [$F_{(4,400)} = 77.82$, $P < 0.0001$]).

Figure 3 shows the total average ethanol intake across the treatment period of the groups administered different doses of UFR2709. One-way ANOVA indicated that UFR2709 treatment significantly reduced average ethanol intake [$F_{(4,80)} = 50.18$, $P < 0.0001$], and Tukey's *post hoc* test confirmed that all UFR2709 doses significantly reduced average ethanol intake compared to saline. Administration of a 2.5 mg/kg dose of UFR2709 induced a 56.9% reduction in alcohol intake. All other UFR2709 doses induced smaller reductions in alcohol intake: 1, 5, and 10 mg/kg doses induced 33.4%, 35.2%, and 31.3% reductions, respectively. Administration of UFR2709 did not affect body weight compared to saline, and the rats exhibited normal increases in body weight during the course of this study (data shown in **Supplementary Material**).

Effects of UFR2709 on Locomotor Activity

To determine if differences in alcohol consumption could be attributed to decreased locomotor activity, we assessed the locomotor activity of UFR2709- and saline-treated animals. For these experiments, animals were administered the highest dose of UFR2709 (10 mg/kg i.p) used in the aforementioned experiments. **Figure 4A** shows the time-course of horizontal locomotor activity measured every 5 min during the 30-min test period of UChB rats treated with UFR2709 (10 mg/kg) or saline. Two-way ANOVA showed that UFR2709 treatment did not affect locomotor activity compared to saline (treatment [$F_{(1,60)} = 3.77$, $P = 0.057$]). **Figure 4B** shows the time-course of vertical activity measured every 5 min during the 30-min test period of UChB rats treated with UFR2709 (10 mg/kg) or saline. Two-way

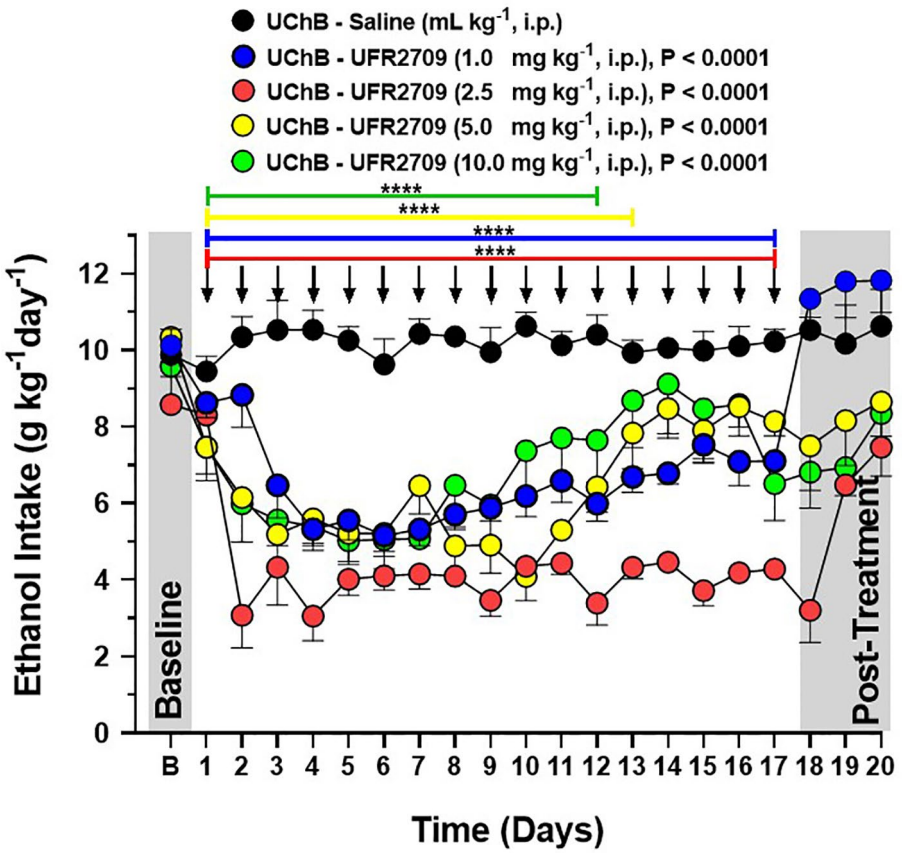

FIGURE 1 | Influence of 17 days of UFR2709 treatment on the voluntary ethanol intake of high-alcohol-drinking UChB rats under a 24-h access two-bottle free choice paradigm. The baseline ethanol consumption of each experimental group is the average ethanol intake during the last 3 days before the treatment period. For 17 consecutive days, rats (n = 5 per group) were administered a single i.p. injection of UFR2709 (1, 2.5, 5, or 10 mg/kg/day) or saline (1 mL/kg/day) at 15:00 h, and ethanol consumption was recorded at 14:00 h the next day. Ethanol consumption data are expressed as mean ± SEM (g/kg/day). Two-way ANOVA with Tukey's multiple comparison test was used to analyze the effect of UFR2709 treatment on ethanol consumption ($P < 0.0001$). Arrows indicate the time points of UFR2709 (1, 2.5, 5, or 10 mg/kg) or saline (1 mL/kg) administration *via* i.p. injection. ****0.0001.

ANOVA showed that UFR2709 treatment did not significantly affect the vertical activity of the animals (treatment [$F_{(1,60)}$ = 2.47, P = 0.121]). **Figure 4C** shows the time-course of grooming activity measured every 5 min during the 30-min test period of UChB rats treated with UFR2709 (10 mg/kg) or saline. Two-way ANOVA showed that UFR2709 treatment did not significantly affect the grooming activity of the animals (treatment [$F_{(1,60)}$ = 0.04, P = 0.845]).

Distribution Coefficient

Prior to the experimental determination of Log $D_{7.4}$, we theoretically calculated the cLogP value of UFR2709. The theoretical cLogP value for UFR2709 was 2.5, indicating that this drug should be able to access the central nervous system (CNS). As shown in **Table 1**, UFR2709 had an experimental $LogD_{7.4}$ value of 1.14 ± 0.03 (assessed by the shake-flask method), which was higher than that obtained for nicotine (0.13 ± 0.01) (Zhu et al., 2002; Andrés et al., 2015), confirming its capacity to access the CNS. We also calculated the cLogP values of molecules capable of crossing the blood-brain barrier (BBB), namely imipramine, fluoxetine, methylphenidate, mecamylamine, and erysodine, obtaining values of 4.32, 4.27, 2.16, 2.38, and 1.40, respectively.

DISCUSSION

Here, we report the effects of UFR2709, a non-selective competitive nAChR antagonist, on the ethanol consumption of high-alcohol-drinking UChB rats (Mardones and Segovia-Riquelme, 1983; Quintanilla et al., 2006; Tampier and Quintanilla, 2010). Our results show that all doses of UFR2709 tested elicited a reduction in voluntary ethanol consumption and a concomitant increase in water intake. However, the effect of UFR270 on reducing alcohol intake was bell-shaped—its efficacy increased from 1 mg/kg to 2.5 mg/kg and then reduced at higher concentrations (5 and 10 mg/kg). This gradual loss of effectiveness may be due to the development of tolerance, which we have previously observed with the partial agonists cytisine and varenicline in UChB rats (Sotomayor-Zárate et al., 2013).

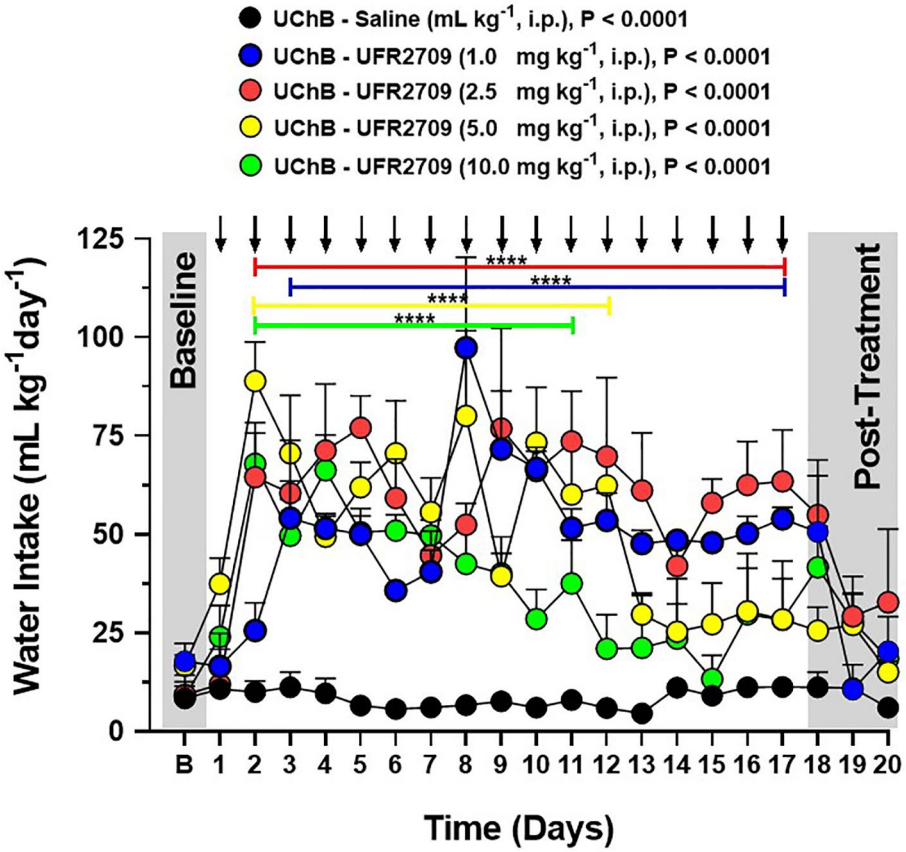

FIGURE 2 | Influence of 17 days of UFR2709 treatment on the water intake of high-alcohol-drinking UChB rats under a 24-h access two-bottle free choice paradigm. The baseline water consumption of each experimental group is the average water intake during the last three days before the treatment period. For 17 consecutive days, rats (n = 5 per group) were administered a single i.p. injection of UFR2709 (1, 2.5, 5, or 10 mg/kg/day) or saline (1 mL/kg/day) at 15:00 h, and water intake was recorded at 14:00 h the next day. Water intake data are expressed as mean ± SEM (mL/kg/day). Two-way ANOVA with Tukey's multiple comparison test was used to analyze the effect of UFR2709 treatment on water intake ($P < 0.0001$). Arrows indicate the time points of UFR2709 (1, 2.5, 5, or 10 mg/kg) or saline (1 mL/kg) administration *via* i.p. injection. ****0.0001.

The effects of UFR2709 on alcohol intake may have resulted from UFR2709 reducing locomotor activity *via* the inhibition of muscle nAChRs. This is unlikely, however, as administration of a single 10 mg/kg dose of UFR2709 to ethanol-naïve UChB rats had no effect on the time-course of horizontal, vertical, or grooming activity. Signs of discomfort or changes in body weight were not observed in the alcohol-exposed animals, suggesting that the effects of UFR2709 on alcohol intake were due to the inhibition of nAChRs in the mesocorticolimbic-DA system.

Our results support the view that nAChR inhibition in the mesocorticolimbic-DA system reduces ethanol consumption. Previous reports have indicated that systemic administration of mecamylamine, a non-competitive and non-selective nAChR antagonist that crosses the BBB (Bacher et al., 2009), reduces voluntary ethanol consumption in rodents (Blomqvist et al., 1996; Ford et al., 2009; Farook et al., 2009). Importantly, hexamethonium, a nAChR antagonist that does not cross the BBB, has no effect on ethanol intake (Blomqvist et al., 1996). Therefore, given that the Log $D_{7.4}$ value of UFR2709 is between 1 and 3, which, according to the literature, is the optimum range for CNS penetration (Andrés et al., 2015), we suggest that it acts in the CNS. Furthermore, microdialysis experiments conducted in the striatum indicated that UFR2709 did not induce DA release, but rather elicited a slight decrease in basal DA levels, although this change was not statistically significant (data shown in **Supplementary Material**).

Even though UFR2709 displays higher affinity for α4β2 nAChRs than for α7 nAChRs (Faundez-Parraguez et al., 2013), the fact that ACh-induced currents are potentiated by ethanol (Aistrup et al., 1999; Cardoso et al., 1999) indicates that some other nAChR subtype(s) may be involved in the actions of UFR2709. Inhibition of α7 nAChRs does not modify the behavioral and neurochemical effects of ethanol (Larsson et al., 2002). However, α-conotoxin-MII, an antagonist of α3β2- and α6-containing nAChRs, blocks ethanol-associated conditioned reinforcement (Löf et al., 2007), and reduces ethanol-induced DA efflux and voluntary ethanol consumption in mice and rats (Larsson et al., 2004), suggesting that these nAChR subtypes may be involved in neurochemical effects of ethanol. Moreover, α6 subunit-containing nAChRs are predominantly expressed

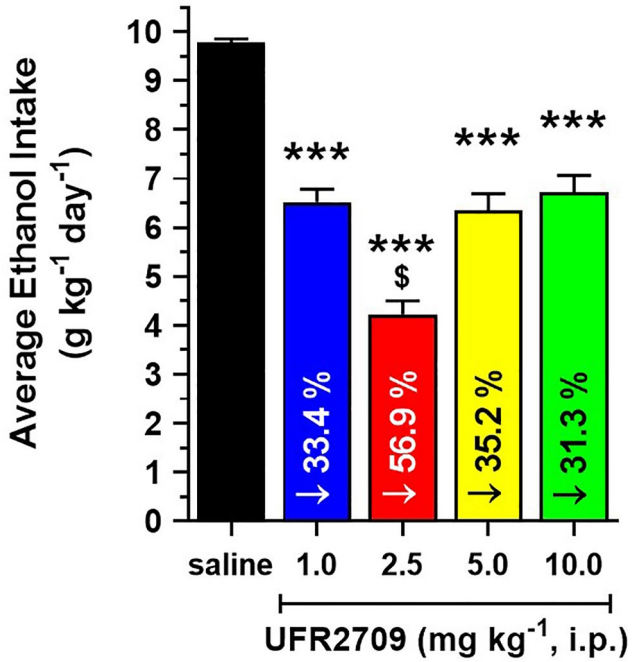

FIGURE 3 | Average reduction in ethanol intake induced by 17 consecutive days of UFR2709 (1, 2.5, 5, 10 mg/kg/day i.p.) or saline (1 mL/kg i.p.) administration. Each bar represents the average ethanol intake of high-alcohol-drinking UChB rats (n = 5 per group) during the 17-day treatment period. Data are expressed as mean ± SEM (g/kg/day). One-way ANOVA followed by Tukey's *post hoc* test was used to compare the saline and UFR2709 groups (***P < 0.001 vs. saline group; $P < 0.001 vs. 2.5 mg/kg UFR2709 group). The number inside each bar indicates the percentage reduction in ethanol intake compared to the saline group.

TABLE 1 | Theoretical (cLogP) and experimental lipophilicity of UFR2709 and Nicotine were determined using the octanol-buffer distribution coefficient at pH 7.4 (Log $D_{7.4}$).

Compound	cLogP	Log $D_{7.4}$	Reference Log $D_{7.4}$
UFR2709	2.15	1.14 ± 0.03.	–
Nicotine	0.93	0.13 ± 0.01	0.41[a]

Data represent the mean ± SEM of five experiments. [a]*Zhu et al., 2002.*

by dopaminergic neurons of the mesocorticolimbic-DA system (Klink et al., 2001; Champtiaux et al., 2002), and ethanol induces an α6 subunit-dependent increase in the firing rate of dopaminergic neurons in the VTA (Liu et al., 2013). Our study does not indicate the nAChR subtypes implicated in the effects of UFR2709, but clearly demonstrates that nAChR inhibition reduces ethanol intake. This supports the idea that nAChRs could be used as therapeutic targets for the treatment of alcohol abuse.

CONCLUSION

In summary, UFR2709 reduces ethanol consumption in a dose-dependent manner. The effects of the highest doses of UFR2709 (5 and 10 mg/kg) were less sustained than those of the lower doses, suggesting that high doses induced drug tolerance. On the other hand, the 2.5 mg/kg dose of UFR2709 was the most potent and therapeutically effective, eliciting a long-lasting effect. Remarkably, this effect continued for at least 2 days after the last administration. Additionally, our results show that UFR2709 does not affect locomotor activity or body weight. Thus, our data give further support to the idea that UFR2709, a nAChR

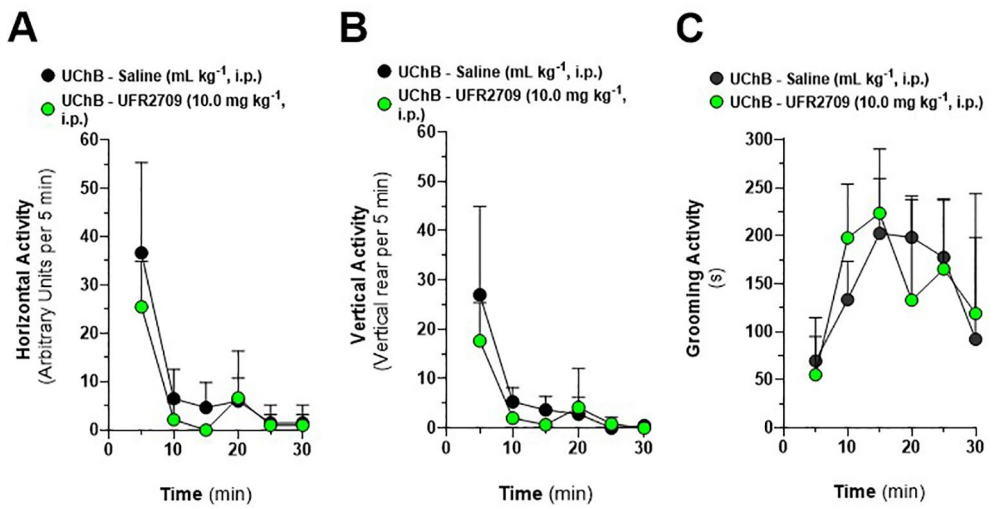

FIGURE 4 | Effect of UFR2709 (10 mg/kg i.p.) or saline (1 mL/kg i.p.) administration on the locomotor activity and grooming behavior of UChB rats. Twelve rats were administered UFR2709 (n = 6) or saline (n = 6) 30 min before locomotor activity was assessed. **(A)** Time-course of horizontal activity per 5 min, presented as the number of arbitrary units (AU) of activity per 5 min. Results are expressed as the mean ± SEM. **(B)** Time-course of vertical activity per 5 min, presented as the number of vertical rears per 5 min. Results are expressed as the mean ± SEM. **(C)** Time-course of grooming activity per 5 min, presented as the time (s) of grooming activity per 5 min. Results are expressed as the mean ± SEM. Two-way ANOVA followed by Bonferroni's *post hoc* test was used to compare the saline and UFR2709 groups.

antagonist, may be a novel therapeutic agent for the treatment of alcoholism, and highlight nAChRs as potential targets for the design of drugs aimed to reduce ethanol intake.

DATA AVAILABILITY STATEMENT

All datasets generated for this study are included in the article/ **Supplementary Material**.

ETHICS STATEMENT

The animal study was reviewed and approved by University of Chile.

AUTHOR CONTRIBUTIONS

GQ, RS-Z, MQ, MR-P, MR-M, PI-V, and IB wrote the manuscript and they designed the experiments and interpreted the results. JG-G and PI-V synthesized UFR2709 and performed its characterization by ^{1}H and ^{13}C NMR analysis. RS-Z, MR-P, IB, and MR-M performed statistical analysis of data. GQ, MR-M, and MQ performed ethanol intake assays. MR-M and DL performed locomotor activity assays. All authors review critically the manuscript and GQ and RS-Z are considered the first authors of this work.

FUNDING

This work was supported by "Fondo Nacional de Desarrollo Científico y Tecnológico" (FONDECYT) Grants 113-0012 (MQ), 117-0662 (MR-P), 115-0615 (PI-V), and 116-0398 (RS-Z). Additional funding was provided by PII2018 (MR-M). GQ and JG-G were fellows of the CONICYT National Ph.D. Scholar Fellowship.

SUPPLEMENTARY MATERIAL

The Supplementary Material for this article can be found online at: https://www.frontiersin.org/articles/10.3389/fphar.2019.01429/full#supplementary-material

REFERENCES

Aistrup, G. L., Marszalec, W., and Narahashi, T. (1999). Ethanol modulation of nicotinic acetylcholine receptor currents in cultured cortical neurons. *Mol. Pharmacol.* 55 (1), 39–49. doi: 10.1124/mol.55.1.39

Albuquerque, E. X., Pereira, E. F. R., Alkondon, M., and Rogers, S. W. (2009). Mammalian nicotinic acetylcholine receptors: from structure to function. *Physiol. Rev.* 89 (1), 73–120. doi: 10.1152/physrev.00015.2008

Andrés, A., Rosés, M., Ràfols, C., Bosch, E., Espinosa, S., Segarra, V., et al. (2015). Setup and validation of shake-flask procedures for the determination of partition coefficients (logD) from low drug amounts. *Eur. J. Pharm. Sci.* 76, 181–191. doi: 10.1016/j.ejps.2015.05.008

Azam, L., Winzer-Serhan, U. H., Chen, Y., and Leslie, M. F. (2002). Expression of neuronal nicotinic acetylcholine receptor subunit mRNAs within midbrain dopamine neurons. *J. Comp. Neurol.* 444 (3), 260–274. doi: 10.1002/cne.10138

Bacher, I., Wu, B., Shytle, D. R., and George, T. P. (2009). Mecamylamine, a nicotinic acetylcholine receptor antagonist with potential for the treatment of neuropsychiatric disorders. *Expert Opin. Pharmacother.* 10 (16), 2709–2721. doi: 10.1517/14656560903329102

Blomqvist, O., Ericson, M., Johnson, D. H., Engel, J. A., and Söderpalm, B. (1996). Voluntary ethanol intake in the rat: effects of nicotinic acetylcholine receptor blockade or subchronic nicotine treatment. *Eur. J. Pharmacol.* 314 (3), 257–267. doi: 10.1016/s0014-2999(96)00583-3

Cardoso, R. A., Brozowski, S. J., Chavez-Noriega, L. E., Harpold, M., Valenzuela, C. F., and Harris, R. A. (1999). Effects of ethanol on recombinant human neuronal nicotinic acetylcholine receptors expressed in xenopus oocytes. *J. Pharmacol. Exp. Ther.* 289 (2), 774–780.

Champtiaux, N., Han, Z., Bessis, A., Rossi, F. M., Zoli, M., Marubio, L., et al. (2002). Distribution and pharmacology of α6-containing nicotinic acetylcholine receptors analyzed with mutant mice. *J. Neurosci.* 22 (4), 1208–1217. doi: 10.1523/JNEUROSCI.22-04-01208.2002

Chatterjee, S., and Bartlett, S. E. (2010). Neuronal nicotinic acetylcholine receptors as pharmacotherapeutic targets for the treatment of alcohol use disorders. *CNS Neurol. Disord. Drug Targets* 9 (1), 60–76. doi: 10.2174/187152710790966597

Chatterjee, S., Steensland, P., Simms, J. A., Holgate, J., Coe, J. W., Hurst, R. S., et al. (2011). Partial agonists of the α3β4* neuronal nicotinic acetylcholine receptor reduce ethanol consumption and seeking in rats. *Neuropsychopharmacology* 36 (3), 603–615. doi: 10.1038/npp.2010.191

Coe, J. W., Brooks, P. R., Vetelino, M. G., Wirtz, M. C., Arnold, E. P., Huang, J., et al. (2005). Varenicline: an alpha4beta2 nicotinic receptor partial agonist for smoking cessation. *J. Med. Chem.* 48 (10), 3474–3477. doi: 10.1021/jm050069n

Dani, J. A., and Harris, R. A. (2005). Nicotine addiction and comorbidity with alcohol abuse and mental illness. *Nat. Neurosci.* 8 (11), 1465–1470. doi: 10.1038/nn1580

Di Chiara, G., and Imperato, A. (1988). Drugs abused by humans preferentially increase synaptic dopamine concentrations in the mesolimbic system of freely moving rats. *Proc. Natl. Acad. Sci. U.S.A.* 85 (14), 5274–5278. doi: 10.1073/pnas.85.14.5274

Engel, J. A., and Jerlhag, E. (2014). Alcohol: mechanisms along the mesolimbic dopamine system. *Prog. Brain Res.* 211, 201–233. doi: 10.1016/B978-0-444-63425-2.00009-X

Falk, D. E., Yi, H., and Hiller-Sturmhöfel, S. (2006). An epidemiologic analysis of co-occurring alcohol and tobacco use and disorders. *Alcohol Res. Health* 29 (3), 162–171.

Farook, J. M., Lewis, B., Gaddis, J. G., Littleton, J. M., and Barron, S. (2009). Effects of mecamylamine on alcohol consumption and preference in male C57BL/6J mice. *Pharmacology* 83 (6), 379–384. doi: 10.1159/000219488

Faundez-Parraguez, M., Farias-Rabelo, N., Gonzalez-Gutierrez, J. P., Etcheverry-Berrios, A., Alzate-Morales, J., Adasme-Carreño, F., et al. (2013). Neonicotinic analogues: Selective antagonists for α4β2 nicotinic acetylcholine receptors. *Bioorg. Med. Chem.* 21 (10), 2687–2694. doi: 10.1016/j.bmc.2013.03.024

Ford, M. M., Fretwell, A. M., Nickel, J. D., Mark, G. P., Strong, M. N., Yoneyama, N., et al. (2009). The influence of mecamylamine on ethanol and sucrose self-administration. *Neuropharmacology* 57 (3), 250–258. doi: 10.1016/j.neuropharm.2009.05.012

Gessa, G. L., Muntoni, F., Collu, M., Vargiu, L., and Mereu, G. (1985). Low doses of ethanol activate dopaminergic neurons in the ventral tegmental area. *Brain Res.* 348 (1), 201–203. doi: 10.1016/0006-8993(85)90381-6

Gotti, C., Zoli, M., and Clementi, F. (2006). brain nicotinic acetylcholine receptors: native subtypes and their relevance brain nicotinic acetylcholine receptors : native subtypes and their relevance. *Trends Pharmacol. Sci.* 27 (9), 482–491. doi: 10.1016/j.tips.2006.07.004

Jerlhag, E., Janson, A. C., Waters, S., and Engel, J. A. (2012). Concomitant release of ventral tegmental acetylcholine and accumbal dopamine by Ghrelin in rats. *PloS One* 7 (11), e49557. doi: 10.1371/journal.pone.0049557

John, U., Meyer, C., Rumpf, H. J., Schumann, A., Thyrian, J. R., and Hapke, U. (2003). Strength of the relationship between tobacco smoking, nicotine dependence and the severity of alcohol dependence syndrome criteria in a population-based sample. *Alcohol Alcohol.* 38 (6), 606–612. doi: 10.1093/alcalc/agg122

Joslyn, G., Brush, G., Robertson, M., Smith, T. L., Kalmijn, J., Schuckit, M., et al. (2008). Chromosome 15q25.1 genetic markers associated with level of response to alcohol in humans. *Proc. Natl. Acad. Sci. U. S. A.* 105 (51), 20368–20373. doi: 10.1073/pnas.0810970105

Kamens, H. M., Andersen, J., and Picciotto, M. R. (2010a). Modulation of ethanol consumption by genetic and pharmacological manipulation of nicotinic acetylcholine receptors in mice. *Psychopharmacol. (Berl).* 208 (4), 613–626. doi: 10.1007/s00213-009-1759-1

Kamens, H. M., Andersen, J., and Picciotto, M. R. (2010b). The nicotinic acetylcholine receptor partial agonist varenicline increases the ataxic and sedative-hypnotic effects of acute ethanol administration in C57BL/6J mice. *Alcohol. Clin. Exp. Res.* 34 (12), 2053–2060. doi: 10.1111/j.1530-0277.2010.01301.x

Kilkenny, C., Browne, W., Cuthill, I. C., Emerson, M., and Altman, D. G. (2010). Animal research: Reporting *in vivo* experiments: The ARRIVE guidelines. *Br. J. Pharmacol.* 160 (7), 1577–1579. doi: 10.1111/j.1476-5381.2010.00872.x

Klink, R., Kerchove, A. D., Zoli, M., and Changeux, J. (2001). Molecular and physiological diversity of nicotinic acetylcholine receptors in the midbrain dopaminergic nuclei. *J. Neurosci.* 21 (5), 1452–1463. doi: 10.1523/JNEUROSCI.21-05-01452.2001

Löf, E., Olausson, P., Stomberg, R., Mcintosh, J. M., Taylor, J. R., and Söderpalm, B. (2007). Nicotinic acetylcholine receptors in the ventral tegmental area mediate the dopamine activating and reinforcing properties of ethanol cues. *Psychopharmacol. (Berl).* 195 (3), 333–343. doi: 10.1007/s00213-007-0899-4

Larsson, A., Svensson, L., Söderpalm, B., and Engel, J. A. (2002). Role of different nicotinic acetylcholine receptors in mediating behavioral and neurochemical effects of ethanol in mice. *Alcohol* 28 (3), 157–167. doi: 10.1016/S0741-8329(02)00244-6

Larsson, A., Jerlhag, E., Svensson, L., Söderpalm, B., and Engel, J. A. (2004). Is an α-conotoxin MII – sensitive mechanism involved in the neurochemical, stimulatory, and rewarding effects of ethanol? *Alcohol* 34 (2-3), 239–250. doi: 10.1016/j.alcohol.2004.10.002

Larsson, A., Edström, L., Svensson, L., Söderpalm, B., and Engel, J. A. (2005). Voluntary ethanol intake increases extracellular acetylcholine levels in the ventral tegmental area in the rat. *Alcohol Alcohol.* 40 (5), 349–358. doi: 10.1093/alcalc/agh180

Liu, L., Zhao-Shea, R., Mcintosh, J. M., and Tapper, A. R. (2013). Nicotinic acetylcholine receptors containing the a6 subunit contribute to ethanol activation of ventral tegmental area dopaminergic neurons. *Biochem. Pharmacol.* 86 (8), 1194–1200. doi: 10.1016/j.bcp.2013.06.015

Madden, P. A. F., and Heath, A. C. (2002). shared genetic vulnerability in alcohol and cigarette use and dependence. *Alcohol. Clin. Exp. Res.* 26 (12), 1919–1921. doi: 10.1097/01.ALC.0000040960.15151.30

Mardones, J., and Segovia-Riquelme, N. (1983). Thirty-two years of selection of rats by ethanol preference: ICHA and UCHB strains. *Neurobehav. Toxicol. Teratol.* 5 (2), 171–178.

Miller, C. N., Ruggery, C., and Kamens, H. M. (2019). The α3β4 nicotinic acetylcholine receptor antagonist 18-Methoxycoronaridine decreases binge-like ethanol consumption in adult C57BL/6J mice. *Alcohol* 79, 1–6. doi: 10.1016/j.alcohol.2018.11.006

Oakman, S. A., Paris, P., Kerr, P. E., Cozzari, C., and Hartman, B. K. (1995). Distribution of pontomesencephalic cholinergic neurons projecting to substantia nigra differs significantly from those projecting to ventral tegmental area. *J. Neurosci.* 15 (9), 5859–5869. doi: 10.1523/JNEUROSCI.15-09-05859.1995

Papke, R. L., and Heinemann, S. F. (1993). Partial agonist properties of cytisine on neuronal receptors containing the beta 2 subunit. *Mol. Pharmacol.* 45 (1), 142–149.

Quintanilla, M. E., Israel, Y., Sapag, A., and Tampier, L. (2006). The UChA and UChB rat lines: metabolic and genetic differences influencing ethanol intake. *Addict. Biol.* 11 (3-4), 310–323. doi: 10.1111/j.1369-1600.2006.00030.x

Quiroz, G., Guerra-Díaz, N., Iturriaga-Vásquez, P., Rivera-Meza, M., Quintanilla, M. E., and Sotomayor-Zárate, R. (2018). Erysodine, a competitive antagonist at neuronal nicotinic acetylcholine receptors, decreases ethanol consumption in alcohol-preferring UChB rats. *Behav. Brain Res.* 349, 169–176. doi: 10.1016/j.bbr.2018.04.038

Rahman, S., Engleman, E. A., and Bell, R. L. (2015). Nicotinic receptor modulation to treat alcohol and drug dependence. *Front. Neurosci.* 8, 426. doi: 10.3389/fnins.2014.00426

Rivera-Meza, M., Quintanilla, M. E., Bustamante, D., Delgado, R., Buscaglia, M., and Herrera-Marschitz, M. (2014). Overexpression of hyperpolarization-activated cyclic nucleotide-gated channels into the ventral tegmental area increases the rewarding effects of ethanol in UChB drinking rats. *Alcohol Clin. Exp. Res.* 38 (4), 911–920. doi: 10.1111/acer.12344

Rollema, H., Chambers, L. K., Coe, J. W., Glowa, J., Hurst, R. S., Lebel, L. A., et al. (2007). Pharmacological profile of the α4β2 nicotinic acetylcholine receptor partial agonist varenicline, an effective smoking cessation aid. *Neuropharmacology* 52 (3), 985–994. doi: 10.1016/j.neuropharm.2006.10.016

Rollema, H., Shrikhande, A., Ward, K. M., Tingley, F. D., Coe, J. W., O´Neill, B. T., et al. (2010). Pre-clinical properties of the α4β2 nicotinic acetylcholine receptor partial agonists varenicline, cytisine and dianicline translate to clinical efficacy for nicotine dependence. *Br. J. Pharmacol.* 160 (2), 334–345. doi: 10.1111/j.1476-5381.2010.00682.x

Saccone, N. L., Wang, J. C., Breslau, N., Johnson, E. O., Hatsukami, D., Saccone, S. F., et al. (2009). The CHRNA5-CHRNA3-CHRNB4 nicotinic receptor subunit gene cluster affects risk for nicotine dependence in african-americans and in european-americans. *Cancer Res.* 69 (17), 6848–6856. doi: 10.1158/0008-5472.CAN-09-0786

Sajja, R. K., and Rahman, S. (2011). Lobeline and cytisine reduce voluntary ethanol drinking behavior in male C57BL/6J mice. *Progr. Neuropsychopharmacol. Biol. Psychiatry* 35 (1), 257–264. doi: 10.1016/j.pnpbp.2010.11.020

Santos, N., Chatterjee, S., Henry, A., Holgate, J., and Bartlett, S. E. (2013). The α5 neuronal nicotinic acetylcholine receptor subunit plays an important role in the sedative effects of ethanol but does not modulate consumption in mice. *Alcohol. Clin. Exp. Res.* 37 (4), 655–662. doi: 10.1111/acer.12009

Sotomayor-Zárate, R., Gysling, K., Bustos, U. E., Cassels, B. K., Tampier, L., and Quintanilla, M. E. (2013). Varenicline and cytisine: two nicotinic acetylcholine receptor ligands reduce ethanol intake in University of Chile bibulous rats. *Psychopharmacology* 227 (2), 287–298. doi: 10.1007/s00213-013-2974-3

Steensland, P., Simms, J. A., Holgate, J., Richards, J. K., and Bartlett, S. E. (2007). Varenicline, an α3β4* nicotinic acetylcholine receptor partial agonist, selectively decreases ethanol consumption and seeking. *Proc. Natl. Acad. Sci. U.S.A.* 104 (30), 12518–12523. doi: 10.1073/pnas.0705368104

Tampier, L., and Quintanilla, M. E. (2010). UChA and UChB rats: an animal model for the study of alcoholism. *Rev. La Sociedad Farmacología Chile* 3 (1), 5–11.

Taslim, N., and Saeed Dar, M. (2011). The role of nicotinic acetylcholine receptor (nAChR) α7 subtype in the functional interaction between nicotine and ethanol in mouse cerebellum. *Alcohol. Clin. Exp. Res.* 35 (3), 540–549. doi: 10.1111/j.1530-0277.2010.01371.x

WHO (2014). Global status report on alcohol and health 2014. World Health Organization.

Xiao, C., Cho, J. R., Zhou, C., Treweek, J. B., Chan, K., McKinney, S. L., et al. (2016). Cholinergic mesopontine signals govern locomotion and reward through dissociable midbrain pathways. *Neuron* 90 (2), 333–347. doi: 10.1016/j.neuron.2016.03.028

Zhu, C., Jiang, L., Chen, T., and Hwang, K. (2002). A comparative study of artificial membrane permeability assay for high throughput profiling of drug absorption potential. *Eur. J. Med. Chem.* 37 (5), 399–407. doi: 10.1016/S0223-5234(02)01360-0

Conflict of Interest: The authors declare that the research was conducted in the absence of any commercial or financial relationships that could be construed as a potential conflict of interest.

frontiers in Pharmacology

ORIGINAL RESEARCH
published: 08 January 2020
doi: 10.3389/fphar.2019.01501

Type 2β Corticotrophin Releasing Factor Receptor Forms a Heteromeric Complex With Dopamine D1 Receptor in Living Cells

Hector E. Yarur, Maria Estela Andrés and Katia Gysling**

Department of Cellular and Molecular Biology, Faculty of Biological Sciences, Pontificia Universidad Católica de Chile, Santiago, Chile

Corticotrophin releasing factor (CRF) and its related peptides differentially bind to CRF receptors to modulate stress-related behaviors. CRF receptors comprise two G-protein coupled receptors (GPCR), type-1 CRF receptors (CRF1), and type-2 CRF receptors (CRF2). CRF2 encompasses three spliced variants in humans, alpha (CRF2α), beta (CRF2β), and gamma (CRF2γ), which differ in their N-terminal extracellular domains and expression patterns. Previously, we showed that CRF2α form a heteromeric protein complex with dopamine D1 receptors (D1R), leading to changes in the signaling of D1R. Based on the high sequence identity between CRF2α and CRF2β, we hypothesized that CRF2β also heteromerize with D1R. To test the hypothesis, we compared the expression and localization of both CRF2 isoforms and whether CRF2β form stable protein complexes with D1R in HEK293 and ATR75 cell lines. We observed that the immunoreactivity for CRF2β was similar to that of CRF2α in the endoplasmic compartment but significantly higher in the Golgi compartment. Immunoprecipitation analysis showed that CRF2β forms a heteromeric protein complex with D1R. Furthermore, the protein complex formed by CRF2β and D1R was stable enough to change the sub-cellular localization of CRF2β when it was co-expressed with a construct of D1R bearing a nuclear localization signal. Immunofluorescence in A7R5 cells, which endogenously express CRF2β and D1R, shows significant colocalization of CRF2β with D1R. In conclusion, our results show that CRF2β forms a stable heteromeric protein complex with D1R, a potential new therapeutic target in tissues where both receptors are co-expressed, such as the septum in the brain, and heart, kidney, and skeletal muscle in the periphery.

Keywords: D1R (dopamine D1 receptor), heteromer, GPCR (G protein-coupled receptors, A7r5 cells, CRF2β

OPEN ACCESS

Edited by:
Ramón Sotomayor-Zárate, University of Valparaíso, Chile

Reviewed by:
Iria Gonzalez Dopeso-Reyes, UMR5535 Institut de Génétique Moléculaire de Montpellier (IGMM), France
Mario Rivera-Meza, University of Chile, Chile

****Correspondence:***
Hector E. Yarur
heyarur@uc.cl
Katia Gysling
kgysling@bio.puc.cl

Specialty section:
This article was submitted to Neuropharmacology, a section of the journal Frontiers in Pharmacology

Received: *25 July 2019*
Accepted: *20 November 2019*
Published: *08 January 2020*

Citation:
Yarur HE, Andrés ME and Gysling K (2020) Type 2β Corticotrophin Releasing Factor Receptor Forms a Heteromeric Complex With Dopamine D1 Receptor in Living Cells. Front. Pharmacol. 10:1501. doi: 10.3389/fphar.2019.01501

INTRODUCTION

Corticotrophin releasing factor (CRF) constitutes a key component in the animal stress response (Vale et al., 1981; Snyder et al., 2015). The CRF system has three additional peptides, urocortin (UCN) 1, UCN2, and UCN3 (Hillhouse and Grammatopoulos, 2006). CRF peptides signal through two G-protein coupled receptors (GPCR), type-1 (CRF1) and type-2 (CRF2) receptors (Dautzenberg and

Hauger, 2002). CRF1 and CRF2 receptors have high amino acid sequence identity but a distinct affinity for CRF peptides (Chalmers et al., 1996). CRF has a higher affinity for CRF1 than for CRF2, (Rutz et al., 2006; Deussing and Chen, 2018). UCN1 has higher affinity than CRF for CRF1 and CRF2, while UCN2 and UCN3 are highly selective for CRF2 (De Souza, 1995).

Three splice variants of CRF2 (α, β, and γ) are expressed in several human tissues (Lovenberg et al., 1995a; Kostich et al., 1998). In rodents and humans, the CRF2α splice variant presents a high density in the central nervous system, and the CRF2β splice variant is primarily expressed in peripheral tissue (Lovenberg et al., 1995b; Perrin et al., 1995). In humans, CRF2β is present in some brain regions and peripheral tissues (Kostich et al., 1998). CRF2 splice variants differ only in their N-terminal extracellular domains, which confer significant differences in their sub-cellular localization (Schulz et al., 2010; Teichmann et al., 2012; Slater et al., 2016a). It has been described that CRF and dopamine (DA) signaling contributes to responses, such as stress-related response (Orozco-Cabal et al., 2008). Thus, the understanding of the mechanisms by which DA and CRF interact could lead to reveal the mechanisms by which these neurotransmitters modulate the behavioral response.

We and other groups have shown that CRF receptors form heteromers with other GPCRs (Fuenzalida et al., 2014; Navarro et al., 2015; Hasdemir et al., 2017). Particularly, the CRF2β isoform assembles into heteromeric complexes with CRF1 (Hasdemir et al., 2017) and the CRF2α isoform assembles with the dopamine D1 receptor (D1R, Fuenzalida et al., 2014). CRF2α/D1R heteromer displays distinct signaling properties than D1R and CRF2α alone (Fuenzalida et al., 2014).

Since CRF2α and CRF2β share a high protein sequence similarity and CRF2α can interact with D1R, we decided to study whether CRF2β forms also a stable heteromeric complex with D1R. To this end, we first compared the sub-cellular localization of recombinant CRF2α and CRF2β expressed in HEK293 cells. Next, we studied if CRF2β can form a stable protein complex with D1R. To this end we used the strategy designed by O'Dowd et al. (2005) consisting in: a) the addition of a nuclear localization signal (nls) to D1R (D1Rnls) that translocate the receptor and its eventual partner CRf2o the nucleus and b) the use of butaclamol, a reverse agonist of D1R that retains D1Rnls and its partner in the plasmatic membrane. We also evaluated the degree of colocalization between D1R and CRF2β in the A7R5 cell line, derived from vascular smooth muscle, that has been shown to express D1R (Chen et al., 2018) and CRF2β (Kageyama et al., 2000; Hoare et al., 2005). Our results show, that CRF2β can form a stable protein complex with D1R and that both receptors are significantly colocalized in A7R5 cells.

MATERIAL AND METHODS

Cell Culture and Transfection

HEK293T cells and A7R5 cells (kindly donated by Dr. Mario Chiong, University of Chile) were grown with DMEM (Gibco) supplemented with 10% FBS (HyClone Labs), 1% penicillin/streptomycin 100× (Gibco), and 2 mM GlutaMax (Gibco). Plasmids were transfected using Lipofectamine 2000 (Invitrogen) according to the manufacturer's instructions and as previously described (Fuenzalida et al., 2014). Experiments were performed 48 h after plasmids transfection. The ratio of transfected plasmid was 1:1 and the amount of DNA transfected for immunofluorescence was 500 ng of total DNA and for immunoprecipitation experiments was 8 ug of total DNA.

Expression Vectors

pcDNA3.1/Myc-His/D1R, pcDNA3.1/myc-His/D1Rnls, and pcDNA3.1/HA-CRF2α were previously described (Fuenzalida et al., 2014; Slater et al., 2016b). The pcDNA3.1/HA-CRF2β was commercially obtained (GeneCopoeia). The HA epitope in both receptors is located in their N terminal.

Protein Extraction and Immunoprecipitation

After treatments, HEK293T cells were collected in ice-cold PBS (pH 7.4), centrifuged at 1500 rpm for 5 min and resuspended in lysis buffer (50 mM Tris-HCl, pH 8.0, 150 mM NaCl, 1 mM EDTA, 0.1% SDS, and 1% Triton X-100) with the Protease Inhibitor Cocktail cOmplete Mini (Roche) as described by Rutz et al. (2006). Cells were then homogenized with three pulses of 10 s using a piston sonicator (Cell Ultrasonic Disrupter) and incubated for at least 1 h at 4°C. Finally, the homogenate was centrifuged at 15,000 rpm for 15 min at 4°C. The supernatant was collected, and protein concentration determined with the Micro BCA Protein Assay Kit (Thermo Scientific). Co-immunoprecipitation assays were performed essentially as previously described (Fuenzalida et al., 2014). Seven hundred μg of protein extract were pre-cleared with TrueBlot® anti-Rabbit Ig IP Agarose Beads (Rockland) and incubated with 1 μg of rabbit anti-Myc antibody (Ab9106, Abcam). Loading buffer 2× (8 M urea, 2% SDS, 100 mM DTT, 375 mM Tris, pH 6.8) was added to each sample and heated to 37°C for 1 h to perform western blotting.

Western Blotting

Proteins were fractionated in 10% sodium dodecyl sulfate–polyacrylamide gel electrophoresis (SDS–PAGE) and then transferred into PVDF membrane (Millipore). Membranes were incubated overnight at 4°C with mouse anti-HA (1:1000, #901501, BioLegend) followed by the peroxidase-conjugated anti-mouse antibody for 2 h (1/4000, Jackson ImmunoResearch Laboratories). The membranes were revealed using SuperSignal West Pico Chemiluminescent Substrate (Pierce Biotechnology).

Heteromer Mobilization Assay

HEK293T cells were seeded at a density of 7×10^6 cells per well on a 24-well plate on coverslips coated with poly-L-lysine (Sigma). Six hours post-transfection, the cells were treated with 1 μM (+)-butaclamol (D1R antagonist) in supplemented DMEM medium for 48 h (O'Dowd et al., 2005). After washing with PBS, cells were fixed with 4% paraformaldehyde (PFA) and receptors localization analyzed by immunofluorescence.

Immunofluorescence and Confocal Microscopy

Immunofluorescence assays were done as previously described (Fuenzalida et al., 2014). Cells were incubated with primary antibodies: rabbit anti-D1R (1:500; sc-14001, Santa Cruz Biotechnology), goat anti-CRF2 (1:500; sc-20550, Santa Cruz Biotechnology), mouse anti-HA (1:1000; HA.11 Clone 16B12, Covance Inc), rat anti-KDEL (1:500; ab50601, Abcam); rabbit anti-D1R receptor (1:500; ab20066, Abcam), and rabbit anti-Giantin (1:500; ab80864, Abcam) overnight at 4°C in a wet-chamber. Cells were then washed and incubated for 2 h with the following secondary antibodies: donkey anti-rabbit AlexaFluor^{488}, donkey anti-rabbit AlexaFluor^{Cy3}, donkey anti-goat AlexaFluor^{488}, donkey anti-goat AlexaFluor^{Cy3}, and donkey anti-rat AlexaFluor^{647} at room temperature. Cells were washed and mounted with mounting media (Dako).

Images were obtained with a confocal microscope (Fluoview 1000, Olympus) And Fluoview V6.0 software. images were digitally obtained with a 100× objective (N.A. 1.4 Oil). The stacking of images was done with A Z step of 200 Nm per cell. Images were processed using the imagej software (Rsb.Info.Nih.Gov/Ij). The deconvolution analysis was performed using the "Iterative Deconvolve 3D" plugin within imagej as previously described (Blanco et al., 2011) and Manders coefficient And Van Steensel analysis was used for measure colocalization (Manders et al., 1993; Van Steensel et al., 1996). Fluorescence Intensity was used to compare the cellular distribution of the marks.

Statistical Analysis

Statistical analysis was performed with the GraphPad Prism 6 software (GraphPad Software). The data are expressed as the mean ± SEM. Statistical significance was assessed with unpaired Mann-Whitney *U* test.

RESULTS

Subcellular Localization of CRF2 Isoforms Expressed in HEK293 Cells

The residence time of GPCR in each compartment of the secretory path varies according to their protein sequence that determines specific protein-protein interactions (Chuang and Sung, 1998). To determine the localization of each CRF receptor, we used specific markers for each secretory compartment, KDEL for the endoplasmic reticular compartment, and Giantin for the Golgi compartment (**Figure 1**). As can be seen in **Figure 1**,

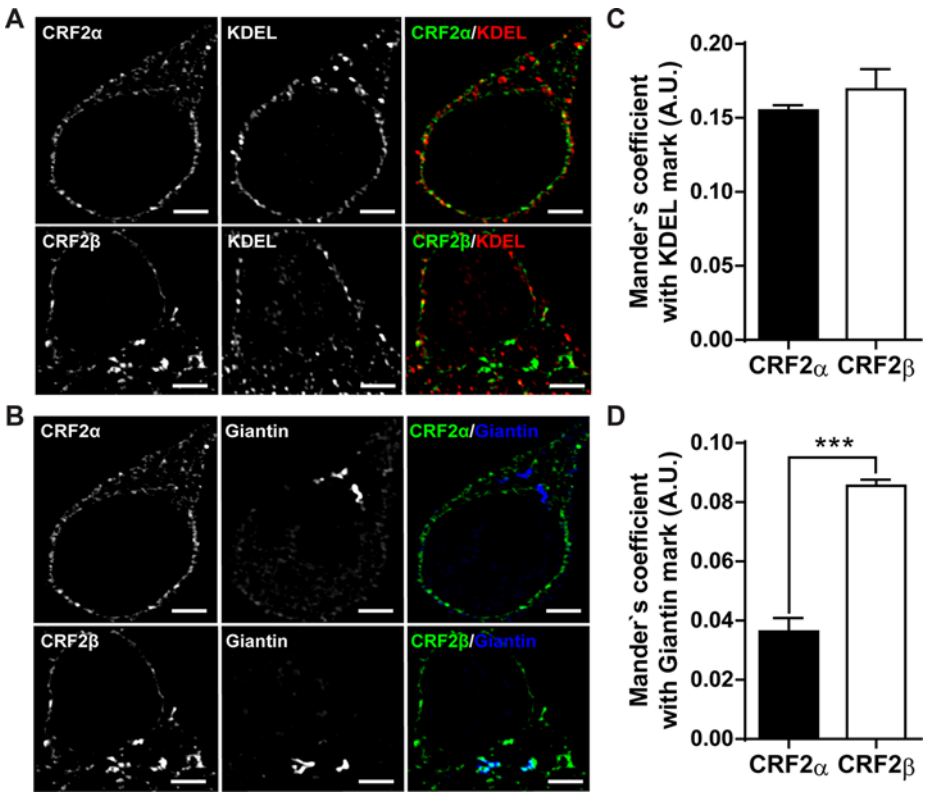

FIGURE 1 | Comparison of the subcellular distribution of CRF2 isoforms in HEK293 cells. **(A** and **B**) Confocal immunodetection of the CRF2 isoforms in a preparation of HEK293 cells (one-plane microphotographs). **(A)** Confocal immunofluorescence for CRF2α or CRF2β (green), using a mouse anti-HA antibody and KDEL (red) (scale bar: 2 μm). **(B)** Confocal immunofluorescence for CRF2α or CRF2β (green) and Giantin (blue) (scale bar: 2 μm). **(C)** Mander's analyses for co-localization in A. **(D)** Mander's analyses for co-localization in B. Unpaired Mann-Whitney *U* test compared between CRF2 isoforms (***p < 0.0005). Values are expressed as mean ± SEM, N = 3 and each N represent 7 independent cells analyzed.

CRF2α is mostly associated with the KDEL compartment (**Figures 1 A**, **B**), as previously shown (Fuenzalida et al., 2014). The presence of CRF2β in the KDEL compartment was similar to CRF2α (**Figures 1A**, **C**). In contrast, the presence of CRF2β in the Giantin compartment was significantly higher than that of CRF2α (**Figures 1B**, **D**). Overall, these results indicate that the presence of CRF2β in the secretory pathway is significantly higher than CRF2α.

CRF2β Forms a Protein Complex With D1R

To determine if CRF2β form a protein complex with D1R, we performed co-immunoprecipitation experiments using whole extracts obtained from HEK293 cells transfected with plasmids bearing human HA-CRF2β and Myc-D1R. HA-CRF2β (band of ~70 kDa) precipitated in the same immunocomplex with Myc-D1R in protein extracts from cells transiently transfected with both receptors (**Figure 2**). The specificity of this interaction is shown by control experiments in which immunoreactivity is not observed when the immunoprecipitations were performed with protein extracts from cells transfected with HA-CRF2β alone or with the empty vectors.

To evaluate the stability of the protein complex formed between CRF2β and D1R, we used the heteromer mobilization strategy described by O'Dowd et al. (2005). Through the use of immunofluorescence, we observed that CRF2β and D1R co-localize in intracellular compartments (**Figure 3**). Interestingly, the incubation with 1 μM butaclamol (BTC), specific D1R antagonist, changed the subcellular distribution of CRF2β from a central localization to an out of the center localization in HEK293 cells (**Figures 3A**, **B**) supporting the formation of a stable protein complex between the receptors.

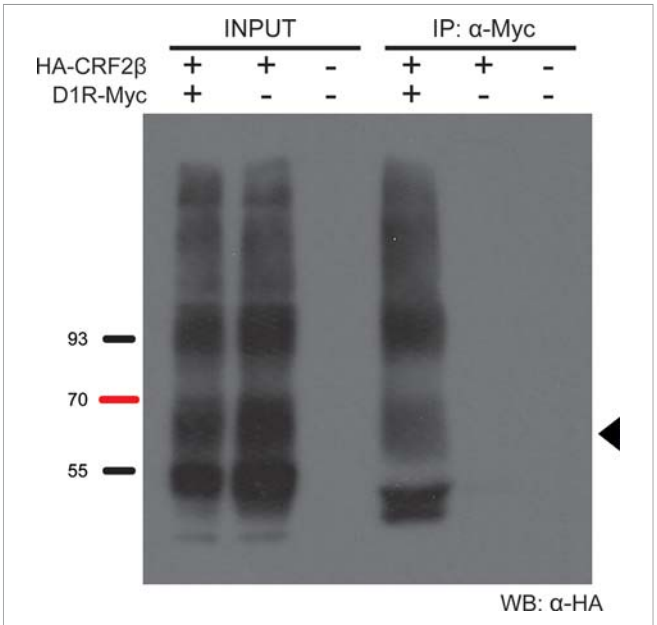

FIGURE 2 | D1R and CRF2β form a protein complex in HEK293 cells. Representative western blot of the co-immunoprecipitation of D1R and CRF2β from HEK293 cells. The protein extract from HEK293 cells expressing CRF2β plus D1R, CRF2β, or empty vector pcDNA were incubated with a rabbit anti-myc antibody for the immunoprecipitation and with a mouse anti-HA antibody for the immunoreactivity for CRF2β. The black arrow shows the estimated molecular weight for CRF2β (~70 kDa). The image was a representation of three replicated experiments. Input line is 5% of the whole protein extraction and IP line is the immunoprecipitation of the protein of interest from the whole protein extraction.

To further test the interaction and stability of the complex between D1R and CRF2β, we studied the localization of CRF2β when it is co-expressed with a mutant recombinant D1R that bears a nls (**Figures 3C**, **D**). We detected a more pronounced co-localization of the CRF2β with D1Rnls (**Figure 3**). The formation of a stable protein complex was further proven using HEK293 cells co-expressing D1Rnls and CRF2β in the presence of BTC. The presence of BTC modified the cellular distribution of CRF2β, from a central location to a peripheral localization (**Figures 3C**, **D**). Taken together, the data show that CRF2β forms a stable protein complex with D1R in HEK293 cells.

In Vivo Visualization of the CRF2β and D1R Heteromer Complex in A7R5 Cells

The previous data showing that recombinant CRF2β and D1R form a stable protein complex, prompted us to test whether endogenous proteins heteromerize. To this end, we used A7R5 cells derived from vascular smooth muscle cells from rat thoracic aorta that express both receptors (Hoare et al., 2005; Chen et al., 2018). Using immunofluorescence, we corroborated the expression of both CRF2β and D1R in A7R5 cells, which colocalize in these cells (**Figure 4A**). To quantify the extent of colocalization, we applied the method of Van Steensel et al. (1996). As can be seen in **Figure 4B**, the quantitative analysis of CRF2β and D1R labels yielded a "bell shape" curve indicating colocalization, with a colocalization index of 0.140 ± 0.006 (**Figure 4B**).

DISCUSSION

In the present study, we show that CRF2β differs in its subcellular localization pattern with CRF2α, but also form a stable protein complex with D1R. CRF2α and CRF2β were found mainly in the endoplasmic reticulum; however, CRF2β was associated with the Golgi apparatus in a significantly higher amount than CRF2α. Interestingly, equal to CRF2α, CRF2β can form a stable protein complex with D1R.

CRF2β was found mainly associated with the endoplasmic reticulum; similar to what it has been previously reported for CRF2α (Slater et al., 2016b). However, CRF2β displays a higher association than CRF2α to the Golgi apparatus. Previously, it was reported that overexpressed CRF2β localizes in the plasma membrane of HEK293 cells (Markovic et al., 2008). Our immunofluorescent assays with overexpressed CRF2α and CRF2β in HEK293 cells unequivocally show that the labeling is mainly associated with the endoplasmic reticulum for both CRF2α and CRF2β, although CRF2β is also associated with the Golgi compartment.

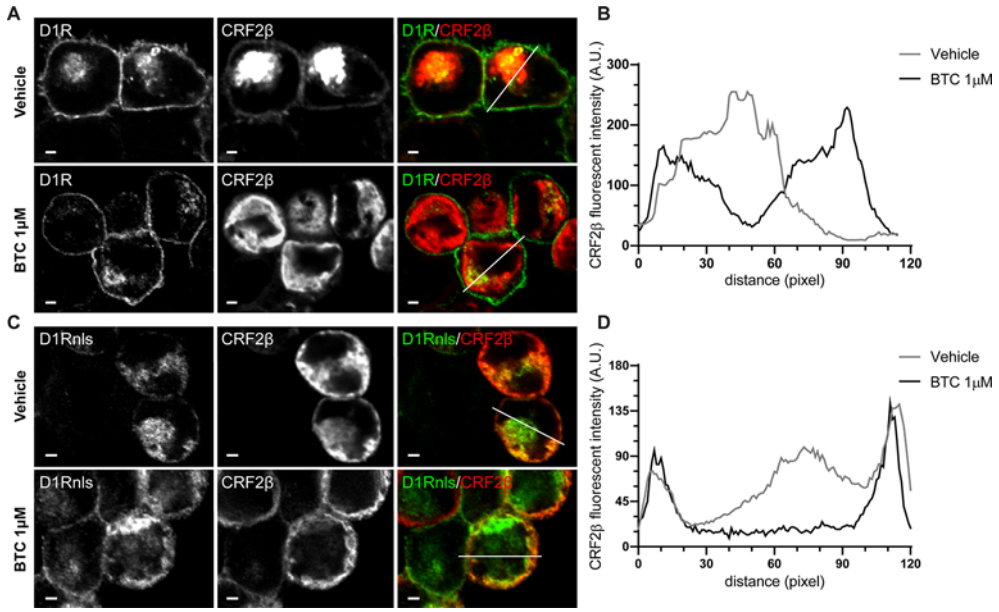

FIGURE 3 | The protein complex of D1R and CRF2β is stable to change their cellular localization. **(A** and **C)** Confocal immunodetection of the CRF2β and D1R or D1Rnls in the presence of 1 μM of Butaclamol (BTC) in HEK293 cells. **(A)** Confocal immunofluorescence for CRF2β (red), using a mouse anti-HA antibody and D1R (green) in the presence of BTC or vehicle (scale bar: 2 μm). **(C)** Confocal immunofluorescence for CRF2β (red) and D1Rnls (green) in the presence of BTC or vehicle (scale bar: 2 μm). **(B)** Quantification of the distribution of CRF2β fluorescence in A. **(D)** Quantification of the distribution of CRF2β fluorescence in C. White lines depict the zone where CRF2β fluorescence was quantified.

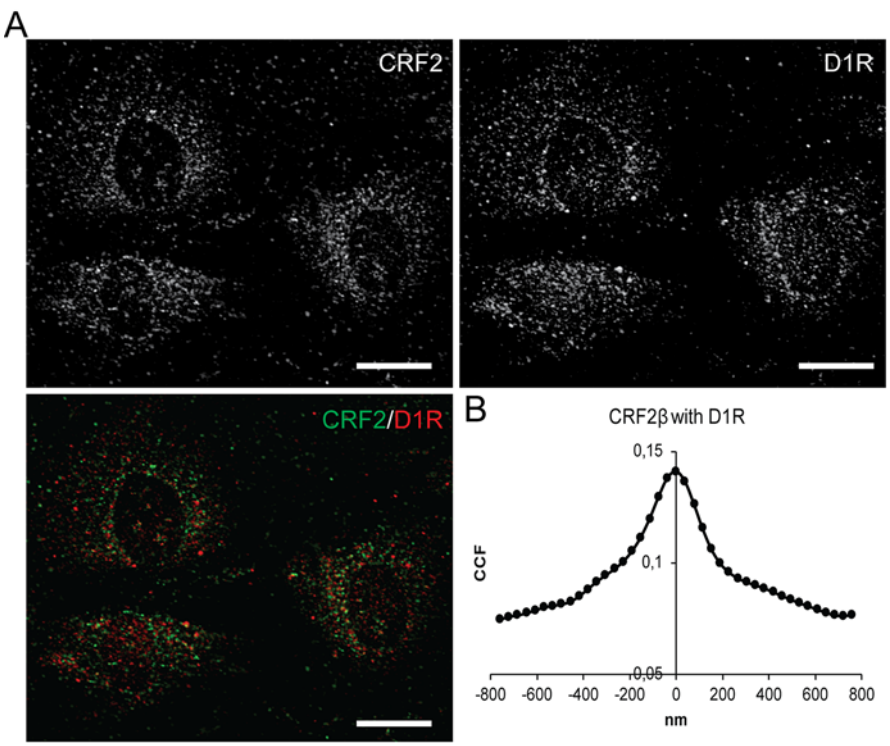

FIGURE 4 | CRF2β and D1R are endogenously express in A7R5 cells and present significant colocalization. **(A)** Confocal immunodetection of CRF2β and D1R in A7R5 cells. **(A)** Confocal immunofluorescence for CRF2β (green) and D1R (red) (scale bar: 20 μm). **(B)** Quantification of the colocalization of CRF2β with D1R by Van Steensel analysis.

CRF2α, but not CRF2β, has a non-cleavable pseudo signal peptide in the N-terminal that allows the formation of a protein complex with calnexin, an integral protein of the endoplasmic reticulum (Rutz et al., 2006; Schulz et al., 2010). Thus, it is possible that the difference in the N-terminals between both CRF2 isoforms could be responsible for the differences in their subcellular localization.

Different experimental approaches support that CRF2β forms a protein complex with D1R, like CRF2α (Fuenzalida et al., 2014). First, co-immunoprecipitation assays of recombinant proteins showed that CRF2β and D1R are in the same immunocomplex. Second, the use of the heteromer mobilization assay described by O'Dowd et al. (2005), allowed us to show that CRF2β follows the cellular distribution of D1Rnls, indicative of a stable protein complex. The stability of the protein complex is relevant for cellular functions such as signaling and endocytosis, among others (Tohgo et al., 2003).

The interaction between GPCRs is not required for ligand recognition or signaling, but may affect receptor mobilization and/or intracellular trafficking (Lohse, 2010). The formation of a heteromeric complex could change some of the GPCR properties such as the ligand affinity, intracellular signaling, desensitization, and recycling properties of the single receptors that compose the heteromeric complex. Several examples of these changes have been published (Juhasz et al., 2008; Magalhaes et al., 2010; Navarro et al., 2015). The presence of GPCRs mainly in intracellular compartments has been described before (Magalhaes et al., 2010; Chow et al., 2012). This subcellular localization of GPCRs is relevant for the assembly of a protein complex between them (Margeta-Mitrovic et al., 2000; Magalhaes et al., 2010). Further studies should evaluate how the difference in the subcellular localization between CRF2α and CRF2β impacts in their heteromerization with D1R, and how the presence of ligands influences in their assembly or disassembly with D1R (O'Dowd et al., 2011). The high identity in amino acid sequence that share both CRF2 receptors allow suggesting that a common domain could be responsible for the interaction of CRF2 with D1R.

The functional implications of the interaction between CRF2β and D1R could involve modulation of their actions in brain regions such as the septum and hippocampus, where both receptors are co-expressed and various peripheral areas such as the renal system and/or the blood circulatory system (Jose et al., 1998; Takahashi, 2012). Interestingly, the expression of both CRF2β and D1R is well documented in the kidney and the heart (Seeman and Grigoriadis, 1987; Yamaguchi et al., 1993; Ozono et al., 1997; Tezval et al., 2009; Takahashi, 2012). Dopamine controls ion transport and inflammatory response in the kidney (Armando et al., 2011) and even though the role of CRF2β is still not understood, it has been proposed that it could be implicated in vascular relaxation on renal arteries (Sanz et al., 2003). It has not been shown the presence of the D1R/CRF2beta complex in human cells. However, the presence of both receptors in the same cells in human kidney and heart tissue gives anatomical support for their eventual heteromerization.

In summary, the formation of a CRF2β and D1R protein complex may be therefore a potential therapeutic target for some brain disorders as well as cardiovascular or renal diseases. Thus, our data provide a new molecular target with new potential pharmacological properties.

DATA AVAILABILITY STATEMENT

The datasets generated for this study are available on request to the corresponding author.

AUTHOR CONTRIBUTIONS

HY, MA, and KG designed the experiments. HY performed the experiments and wrote the manuscript. HY, MA, and KG edited the manuscript.

FUNDING

This work was funded by FONDECYT grants No 1150244 and 1191274 from CONICYT. HY was recipient of a doctoral fellowship from CONICYT.

ACKNOWLEDGMENTS

We thank Dr. Mario Chiong, Universidad de Chile, for giving us access to the A7R5 cells and for his insightful comments on how to work with them.

REFERENCES

Armando, I., Villar, V. A., and Jose, P. A. (2011). Dopamine and renal function and blood pressure regulation. *Comp. Physiol.* 1, 1075–1117. doi: 10.1002/cphy.c100032

Blanco, E. H., Zúñiga, J. P., Andrés, M. E., Alvarez, A. R., and Gysling, K. (2011). Corticotropin-releasing factor binding protein enters the regulated secretory pathway in neuroendocrine cells and cortical neurons. *Neuropeptides* 45, 273–279. doi: 10.1016/j.npep.2011.05.002

Chalmers, D. T., Lovenberg, T. W., Grigoriadis, D. E., Behan, D. P., and De Souza, E. B. (1996). Corticotrophin-releasing factor receptors: from molecular biology to drug design. *Trends Pharmacol. Sci.* 17, 166–172. doi: 10.1016/0165-6147(96)81594-X

Chen, J., Shi, S., Cai, X., Li, H., Wang, L., Li, H., et al. (2018). DR1 activation reduces the proliferation of vascular smooth muscle cells by JNK/c-Jun dependent increasing of Prx3. *Mol. Cell Biochem.* 440 (1-2), 157–165. doi: 10.1007/s11010-017-3164-0

Chow, K. B., Sun, J., Chu, K. M., Tai Cheung, W., Cheng, C. H., and Wise, H. (2012). The truncated ghrelin receptor polypeptide (GHS-R1b) is localized in the endoplasmic reticulum where it forms heterodimers with ghrelin receptors (GHS-R1a) to attenuate their cell surface expression. *Mol. Cell Endocrinol.* 348, 247–254. doi: 10.1016/j.mce.2011.08.034

Chuang, J. Z., and Sung, C. H. (1998). The cytoplasmic tail of rhodopsin acts as a novel apical sorting signal in polarized MDCK cells. *J. Cell Biol.* 142 (5), 1245–1256. doi: 10.1083/jcb.142.51245

Dautzenberg, F. M., and Hauger, R. L. (2002). The CRF peptide family and their receptors: yet more partners discovered. *Trends Pharmacol. Sci.* 23, 71–77. doi: 10.1016/S0165-6147(02)01946-6

De Souza, E. B. (1995). Corticotropin-releasing factor receptors: physiology, pharmacology, biochemistry and role in central nervous system and immune disorders. *Psychoneuroendocrinology* 20, 789–819. doi: 10.1016/0306-4530(95)00011-9

Deussing, J. M., and Chen, A. (2018). The Corticotropin-Releasing Factor Family: physiology of the stress response. *Physiol. Rev.* 98, 2225–2286. doi: 10.1152/physrev.000422017

Fuenzalida, J., Galaz, P., Araya, K. A., Slater, P. G., Blanco, E. H., Campusano, J. M., et al. (2014). Dopamine D1 and corticotrophin-releasing hormone type-2α receptors assemble into functionally interacting complexes in living cells. *Br. J. Pharmacol.* 171, 5650–5664. doi: 10.1111/bph.12868

Hasdemir, B., Mahajan, S., Oses-Prieto, J., Chand, S., Woolley, M., Burlingame, A., et al. (2017). Actin cytoskeleton-dependent regulation of corticotropin-releasing factor receptor heteromers. *Mol. Biol. Cell.* 28, 2386–2399. doi: 10.1091/mbc.e16-11-0778

Hillhouse, E. W., and Grammatopoulos, D. K. (2006). The molecular mechanisms underlying the regulation of the biological activity of corticotropin-releasing hormone receptors: implications for physiology and pathophysiology. *Endocr. Rev.* 27, 260–286. doi: 10.1210/er.2005-0034

Hoare, S. R., Sullivan, S. K., Fan, J., Khongsaly, K., and Grigoriadis, D. E. (2005). Peptide ligand binding properties of the corticotropin-releasing factor (CRF) type 2 receptor: pharmacology of endogenously expressed receptors, G-protein-coupling sensitivity and determinants of CRF2 receptor selectivity. *Peptides.* 26, 457–470. doi: 10.1016/j.peptides.2004.10.019

Jose, P. A., Eisner, G. M., and Felder, R. A. (1998). Renal dopamine receptors in health and hypertension. *Pharmacol. Ther.* 80, 149–182. doi: 10.1016/S0163-7258(98)00027-8

Juhasz, J. R., Hasbi, A., Rashid, A. J., So, C. H., George, S. R., and O'Dowd, B. F. (2008). Mu-opioid receptor heterooligomer formation with the dopamine D1 receptor as directly visualized in living cells. *Eur. J. Pharmacol.* 581, 235–243. doi: 10.1016/j.ejphar.2007.11.060

Kageyama, K., Gaudriault, G. E., Bradbury, M. J., and Vale, W. W. (2000). Regulation of corticotropin-releasing factor receptor type 2b messenger ribonucleic acid in the rat cardiovascular system by urocortin, glucocorticoids, and cytokines. *Endocrinol.* 141, 2285–2293. doi: 10.1210/endo.141.77572

Kostich, W. A., Chen, A., Sperle, K., and Largent, B. L. (1998). Molecular identification and analysis of a novel human corticotropin-releasing factor (CRF) receptor: the CRF2gamma receptor. *Mol. Endocrinol.* 12, 1077–1085. doi: 10.1210/mend.12.80145

Lohse, M. J. (2010). Dimerization in GPCR mobility and signaling. *Curr. Opin. Pharmacol.* 10, 53–58. doi: 10.1016/j.coph.2009.10.007

Lovenberg, T. W., Chalmers, D. T., Liu, C., and De Souza, E. B. (1995b). CRF2 alpha and CRF2 beta receptor mRNAs are differentially distributed between the rat central nervous system and peripheral tissues. *Endocrinology* 136, 4139–4142. doi: 10.1210/endo.136.9.7544278

Lovenberg, T. W., Liaw, C. W., Grigoriadis, D. E., Clevenger., W., Chalmers, D. T., De Souza, E. B., et al. (1995a). Cloning and characterization of a functionally distinct corticotropin-releasing factor receptor subtype from rat brain. *Proc. Natl. Acad. Sci. U. S. A.* 92, 5759. doi: 10.1073/pnas.92.3.836

Magalhaes, A. C., Holmes, K. D., Dale, L. B., Comps-Agrar, L., Lee, D., Yadav, P. N., et al. (2010). CRF receptor 1 regulates anxiety behavior via sensitization of 5-HT2 receptor signaling. *Nat. Neurosci.* 13, 622–629. doi: 10.1038/nn2529

Manders, E. M., Verbeek, F. J., and Aten, J. A. (1993). Measurement of co-localization of objects in dual-colour confocal images. *J. Microsc.* 169, 375–382. doi: 10.1111/j.1365-2818.1993.tb03313.x

Margeta-Mitrovic, M., Jan, Y. N., and Jan, L. Y. (2000). A trafficking checkpoint controls GABA(B) receptor heterodimerization. *Neuron* 27, 97–106. doi: 10.1016/S0896-6273(00)00012-X

Markovic, D., Punn, A., Lehnert, H., and Grammatopoulos, D. K. (2008). Intracellular mechanisms regulating corticotropin-releasing hormone receptor-2beta endocytosis and interaction with extracellularly regulated kinase 1/2 and p38 mitogen-activated protein kinase signaling cascades. *Mol. Endocrinol.* 22, 689–706. doi: 10.1210/me.2007-0136

Navarro, G., Quiroz, C., Moreno-Delgado, D., Sierakowiak, A., McDowell, K., Moreno, E., et al. (2015). Orexin-corticotropin-releasing factor receptor heteromers in the ventral tegmental area as targets for cocaine. *J. Neurosci.* 35, 6639–6653. doi: 10.1523/JNEUROSCI.4364-142015

O'Dowd, B. F., Ji, X., Alijaniaram, M., Rajaram, R. D., Kong, M. M., Rashid, A., et al. (2005). Dopamine receptor oligomerization visualized in living cells. *J. Biol. Chem.* 280, 37225–37235. doi: 10.1074/jbc.M504562200

O'Dowd, B. F., Ji, X., Alijaniaram, M., Nguyen, T., and George, S. R. (2011). Separation and reformation of cell surface dopamine receptor oligomers visualized in cells. *Eur. J. Pharmacol.* 658, 74–83. doi: 10.1016/j.ejphar.2011.02.030

Orozco-Cabal, L., Liu, J., Pollandt, S., Schmidt, K., Shinnick-Gallagher, P., and Gallagher, J. P. (2008). Dopamine and corticotropin-releasing factor synergistically alter basolateral amygdala-to-medial prefrontal cortex synaptic transmission: functional switch after chronic cocaine administration. *J. Neurosci.* 28, 529–542. doi: 10.1523/JNEUROSCI.2666-072008

Ozono, R., O'Connell, D. P., Wang, Z. Q., Moore, A. F., Sanada, H., Felder, R. A., et al. (1997). Localization of the dopamine D1 receptor protein in the human heart and kidney. *Hypertension* 30 (3 Pt 2), 725–729. doi: 10.1161/01.HYP.30.3.725

Perrin, M., Donaldson, C., Chen, R., Blount, A., Berggren, T., Bilezikjian, L., et al. (1995). Identification of a second corticotropin-releasing factor receptor gene and characterization of a cDNA expressed in heart. *Proc. Natl. Acad. Sci. U. S A.* 92, 2969–2973. doi: 10.1073/pnas.92.72969

Rutz, C., Renner, A., Alken, M., Schulz, K., Beyermann, M., Wiesner, B., et al. (2006). The corticotropin-releasing factor receptor type 2a contains an N-terminal pseudo signal peptide. *J. Biol. Chem.* 281, 24910–24921. doi: 10.1074/jbc.M601554200

Sanz, E., Monge, L., Fernández, N., Climent, B., Diéguez, G., and Garcia-Villalón, A. L. (2003). Mechanisms of relaxation by urocortin in renal arteries from male and female rats. *Br. J. Pharmacol.* 140, 1003–1007. doi: 10.1038/sj.bjp.0705516

Schulz, K., Rutz, C., Westendorf, C., Ridelis, I., Vogelbein, S., Furkert, J., et al. (2010). The pseudo signal peptide of the corticotropin-releasing factor receptor type 2a decreases receptor expression and prevents Gi-mediated inhibition of adenylyl cyclase activity. *J. Biol. Chem.* 285, 32878–32887. doi: 10.1074/jbc.M110.129627

Seeman, P., and Grigoriadis, D. (1987). Dopamine receptors in brain and periphery. *Neurochem. Int.* 10, 1–25. doi: 10.1016/0197-0186(87)90167-7

Slater, P. G., Yarur, H. E., and Gysling, K. (2016a). Corticotropin-releasing factor receptors and their interacting proteins: functional consequences. *Mol. Pharmacol.* 90, 627–632. doi: 10.1124/mol.116.104927

Slater, P. G., Cerda, C. A., Pereira, L. A., Andrés, M. E., and Gysling, K. (2016b). CRF binding protein facilitates the presence of CRF type 2α receptor on the cell surface. *Proc. Natl. Acad. Sci. U. S. A.* 113, 4075–4080. doi: 10.1073/pnas.1523745113

Snyder, K., Barry, M., and Valentino, R. (2015). Cognitive impact of social stress and coping strategy throughout development. *Psychopharmacology* 232, 185–195. doi: 10.1007/s00213-014-3654-7

Takahashi, K. (2012). Distribution of urocortins and corticotropin-releasing factor receptors in the cardiovascular system. *Int. J. Endocrinol.* 2012, 395284. doi: 10.1155/2012/395284

Teichmann, A., Rutz, C., Kreuchwig, A., Krause, G., Wiesner, B., and Schülein, R. (2012). The Pseudo signal peptide of the corticotropin-releasing factor receptor type 2A prevents receptor oligomerization. *J. Biol. Chem.* 287, 27265–27274. doi: 10.1074/jbc.M112.360594

Tezval, H., Jurk, S., Atschekzei, F., Becker, J. U., Jahn, O., Serth, J., et al. (2009). Urocortin and corticotropin-releasing factor receptor 2 in human renal cell carcinoma: disruption of an endogenous inhibitor of angiogenesis and proliferation. *World J. Urol.* 27, 825–830. doi: 10.1007/s00345-009-0417-x

Tohgo, A., Choy, E. W., Gesty-Palmer, D., Pierce, K. L., Laporte, S., Oakley, R. H., et al. (2003). The stability of the G protein-coupled receptor-beta-arrestin interaction determines the mechanism and functional consequence of ERK activation. *J. Biol. Chem.* 278, 6258–6267. doi: 10.1074/jbc.M212231200

Vale, W., Spiess, J., Rivier, C., and Rivier, J. (1981). Characterization of a 41-residue ovine hypothalamic peptide that stimulates secretion of corticotropin and beta endorphine. *Science* 213, 1394–1397. doi: 10.1126/science.6267699

Van Steensel, B., Van Binnendijk, E. P., Hornsby, C. D., Van der Voort, H. T., Krozowski, Z. S., de Kloet, E. R., et al. (1996). Partial colocalization of glucocorticoid and mineralocorticoid receptors in discrete compartments in nuclei of rat hippocampus neurons. *J. Cell Sci.* 109 (Pt 4), 787–792.

Yamaguchi, I., Jose, P. A., Mouradian, M. M., Canessa, L. M., Monsma, F. J. Jr., Sibley, D. R., et al. (1993). Expression of dopamine D1A receptor gene in proximal tubule of rat kidneys. *Am. J. Physiol.* 264 (2 Pt 2), F280–F285. doi: 10.1152/ajprenal.1993.264.2.F280

Conflict of Interest: The authors declare that the research was conducted in the absence of any commercial or financial relationships that could be construed as a potential conflict of interest.

The handling editor declared a past co-authorship with one of the authors [MA].

frontiers in Pharmacology

REVIEW
published: 23 January 2020
doi: 10.3389/fphar.2019.01590

Amphetamine Derivatives as Monoamine Oxidase Inhibitors

Miguel Reyes-Parada[1,2]*, *Patricio Iturriaga-Vasquez*[3] *and Bruce K. Cassels*[4]

[1] Centro de Investigación Biomédica y Aplicada (CIBAP), Escuela de Medicina, Facultad de Ciencias Médicas, Universidad de Santiago de Chile, Santiago, Chile, [2] Facultad de Ciencias de la Salud, Universidad Autónoma de Chile, Talca, Chile, [3] Departamento de Ciencias Químicas y Recursos Naturales, Facultad de Ingeniería y Ciencias, Universidad de la Frontera, Temuco, Chile, [4] Departamento de Química, Facultad de Ciencias, Universidad de Chile, Santiago, Chile

Amphetamine and its derivatives exhibit a wide range of pharmacological activities, including psychostimulant, hallucinogenic, entactogenic, anorectic, or antidepressant effects. The mechanisms of action underlying these effects are usually related to the ability of the different amphetamines to interact with diverse monoamine transporters or receptors. Moreover, many of these compounds are also potent and selective monoamine oxidase inhibitors. In the present work, we review how structural modifications on the aromatic ring, the amino group and/or the aliphatic side chain of the parent scaffold, modulate the enzyme inhibitory properties of hundreds of amphetamine derivatives. Furthermore, we discuss how monoamine oxidase inhibition might influence the pharmacology of these compounds.

Keywords: monoamine oxidase, amphetamine derivatives, serotonin syndrome, serotonin transporter, dopamine transporter, norepinephrine transporter, monoamine oxidase-A

OPEN ACCESS

Edited by:
Juan J. Canales,
University of Tasmania, Australia

Reviewed by:
David Pubill,
University of Barcelona, Spain
Matthias E. Liechti,
University Hospital of Basel, Switzerland

***Correspondence:**
Miguel Reyes-Parada
miguel.reyes@usach.cl

Specialty section:
This article was submitted to Neuropharmacology, a section of the journal Frontiers in Pharmacology

Received: *14 September 2019*
Accepted: *09 December 2019*
Published: *23 January 2020*

Citation:
Reyes-Parada M, Iturriaga-Vasquez P and Cassels BK (2020) Amphetamine Derivatives as Monoamine Oxidase Inhibitors. Front. Pharmacol. 10:1590. doi: 10.3389/fphar.2019.01590

INTRODUCTION

Since its first description as "Phenisopropylamin" more than a century ago (Edeleano, 1887), amphetamine (1-phenylpropan-2-amine, phenylisopropylamine, amfetamine, alpha-methylphenethylamine; AMPH; **Figure 1**) has received considerable attention due to its multiple psychotropic effects, first noted in the early 1930s (Prinzmetal and Bloomberg, 1935). Nowadays, AMPH is indicated for the treatment of attention deficit hyperactivity disorder (Heal et al., 2013), narcolepsy (Dauvilliers and Barateau, 2017), and— in the form of its prodrug lisdexamfetamine— binge-eating disorder (Hilbert, 2019). Its psychostimulant effects are usually related to its catecholamine-releasing properties, which arise from its ability to compete with dopamine (DA) and norepinephrine (NE) for uptake into the nerve terminals, and to induce reverse transport *via* the corresponding transporter (DAT and NET, respectively). Nevertheless, its polypharmacological

Abbreviations: AMPH, amphetamine; DA, dopamine; NE, norepinephrine; DAT, dopamine transporter; NET, norepinephrine transporter; 5-HT, serotonin; SERT, serotonin transporter; MAO, monoamine oxidase; FAD, flavin adenine dinucleotide; MAOI, monoamine oxidase inhibitor; MTA, 4-methylthioamphetamine; PMA, *p*-methoxyamphetamine; MDA, 3,4-methylenedioxyamphetamine; NMMTA, 4-methylthiomethamphetamine; PMMA, *p*-methoxymethamphetamine; MDMA, 3,4-methylenedioxymethamphetamine; FLA727, *p*-methylaminoamphetamine; MSOA, *p*-methylsulfoxyamphetamine; MSO2A, *p*-methylsulfonylamphetamine; PCA, *p*-chloroamphetamine; PBA, *p*-bromoamphetamine; PFA, *p*-fluoroamphetamine; FLA289, *p*-dimethylaminoamphetamine; NIPA, 2-naphthylisopropylamine (also known as PAL-287); DOI, 4-iodo-2,5,-dimethoxyamphetamine; DOB, 4-bromo-2,5,-dimethoxyamphetamine.

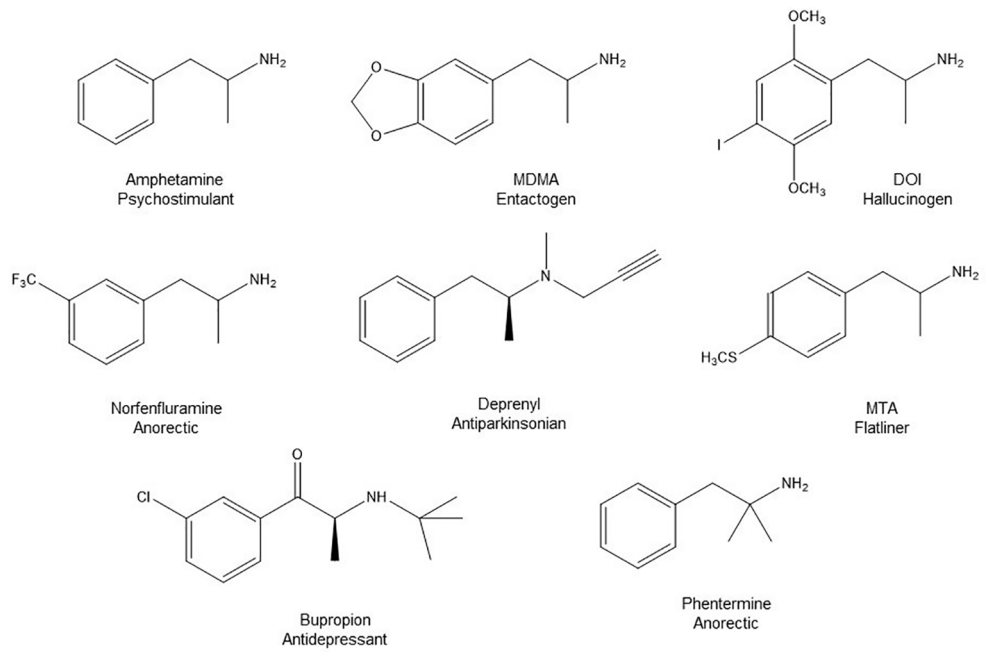

FIGURE 1 | Chemical structures of some AMPH derivatives.

profile involves actions upon other monoaminergic targets such as the serotonin (5-HT) transporter (SERT), the vesicular monoamine transporter and monoamine oxidase (MAO) (Sulzer et al., 2005; Heal et al., 2013).

A remarkable characteristic of AMPH is that subtle structural variations can produce drastic changes in its pharmacodynamics, and lead to compounds that interact differentially with several biogenic amine target proteins. Consequently, the AMPH skeleton has served as a privileged scaffold for the design and synthesis of hundreds of derivatives with many different and often useful activities, but also conveying misuse potential (Biel and Bopp, 1978; Nichols, 1994; Glennon, 1999; Rothman and Baumann, 2003; Welter-Luedeke and Maurer, 2016). Thus, the diversity of mechanisms of action of AMPH derivatives determines a many-colored palette of pharmacological activities in humans, including psychostimulant, entactogenic, psychedelic, anorectic, nootropic, and antidepressant effects. It is noteworthy that the structural changes also modify toxicological properties and abuse liability of AMPH derivatives (Fleckenstein et al., 2007; Rothman et al., 2007; Simmler et al., 2013; Barbosa et al., 2015).

MAO (monoamine oxygen oxidoreductase (deaminating) (flavin-containing); EC 1.4.3.4) is the main catabolic enzyme for biogenic monoamines such as NE, DA, 5-HT, and β-phenethylamine, and also for dietary and xenobiotic amines such as tyramine and benzylamine. MAO exists in two isoforms termed MAO-A and MAO-B. Both isozymes are outer mitochondrial membrane-bound flavoproteins, with the FAD cofactor covalently bound to the enzyme. The metabolic reaction involves the generation of an imine intermediate and the reduction of the flavin cofactor, which is reoxidized by molecular oxygen producing hydrogen peroxide. The imine intermediate is hydrolyzed, in a non-enzymatic process, generating ammonia and the corresponding aldehyde (Shih et al., 1999; Tipton et al., 2004; Edmondson et al., 2007). Although both isoforms have similar catalytic activities, they differ in their molecular genetics, physiological roles, tissue distribution, substrate preference, and inhibitor selectivity (Reyes-Parada et al., 2005). In the central nervous system, catecholaminergic neurons contain predominantly MAO-A, whereas serotonergic neurons express MAO-B (Westlund et al., 1988; Luque et al., 1995). MAO-A preferentially metabolizes 5-HT and is irreversibly inhibited by nanomolar concentrations of clorgyline, whereas MAO-B preferentially catalyzes the oxidative deamination of phenethylamine and benzylamine and is irreversibly inhibited by nanomolar concentrations of *l*-deprenyl. DA and NE are non-selective substrates of both isoforms (Youdim et al., 2006). MAO inhibitors (MAOI) are currently used in the treatment of diverse neuropsychiatric and neurological disorders, including depression and Parkinson's disease (Cesura and Pletscher, 1992; Youdim et al., 2006; Finberg and Rabey, 2016; Kumar et al., 2017). In 2002, Binda and colleagues (Binda et al., 2002) published a seminal article showing the high-resolution structure of human MAO-B. Subsequent structures of this enzyme (Binda et al., 2003; Binda et al., 2004), as well as that of rat (Ma et al., 2004) and human MAO-A (De Colibus et al., 2005; Son et al., 2008), have allowed detailed comparison of the overall structures of both isoforms and their active sites (Binda et al., 2011;

Iacovino et al., 2018). Thus, the substrate/inhibitor binding site of both isozymes (see **Figure 2**) can be described as a pocket lined by the isoalloxazine ring and several aliphatic and aromatic residues. A critical role of Y444, Y407, G215, and I180 of MAO-A (Y435, Y398, G206, and L171 being the corresponding residues in MAO-B) in the orientation and stabilization of the substrate/inhibitor binding can be inferred from the X-ray diffraction data. The availability of MAO crystal structures has allowed a quicker pace in the rational design of novel MAOIs and in the understanding of catalytic and inhibitory mechanisms. Thus, a vast number of studies in which molecular simulation approaches have been used to rationalize and/or to predict the functional interactions between the proteins and their substrates or inhibitors have been reported recently (Ferino et al., 2012; Vianello et al., 2016; Dhiman et al., 2017; Dhiman et al., 2018).

In the following pages, we review the effects of several dozen AMPH derivatives upon MAOs and describe, through the analysis of a set of representative examples, how structural

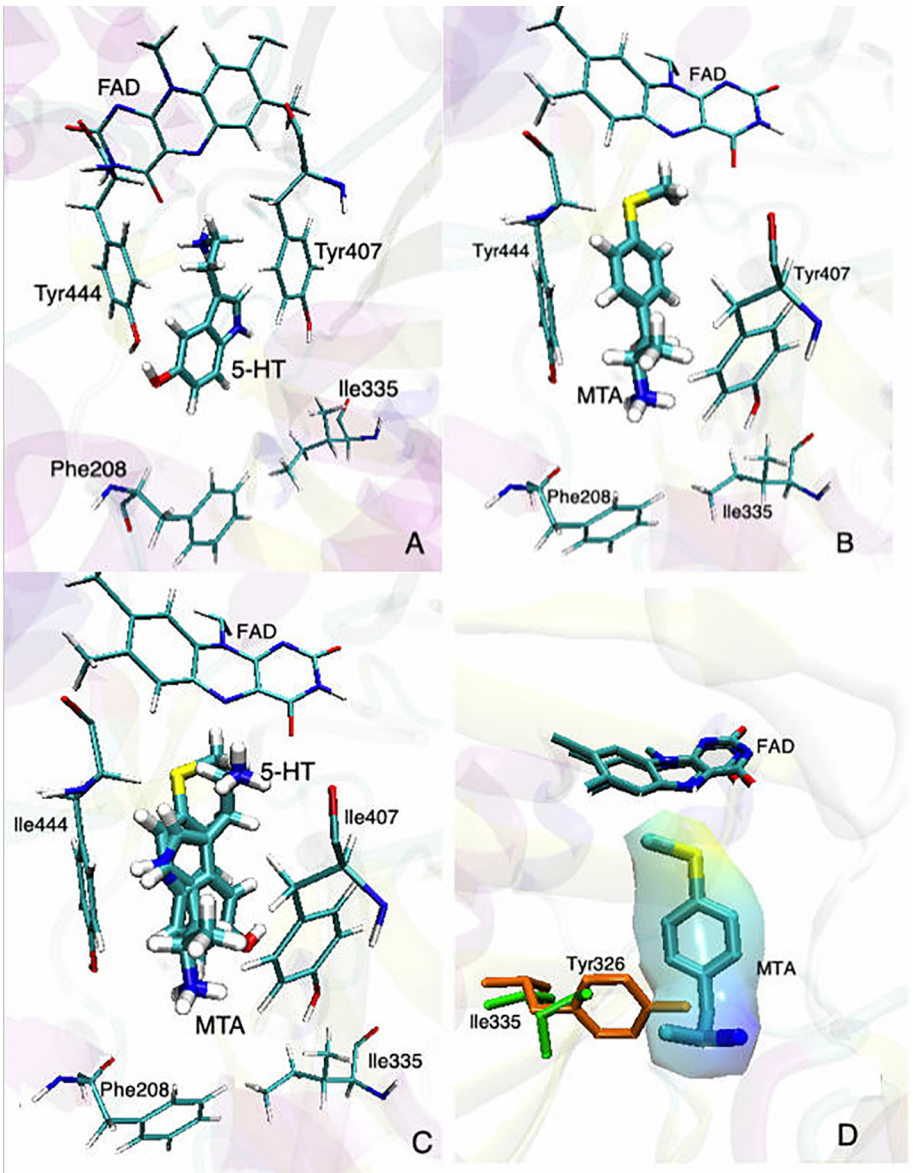

FIGURE 2 | Binding modes of **(A)** 5-HT and **(B)** MTA to MAO-A (PDB: 2BXS). **(C)** Superimposed structures of 5-HT and MTA docked into the active site of MAO-A. **(D)** Superimposed binding sites of MAO-A (green residues) and MAO-B (orange residues) with MTA already docked into the active site of MAO-A; the "wrapper" around MTA represents the solvent accessible surface area (SASA). In all cases, for the sake of clarity, only the most relevant residues are shown. Docking conditions were as in Fierro et al., 2007.

modifications on the aromatic ring, the amino group and/or the aliphatic side chain of the parent scaffold, modulate the enzyme inhibitory properties of this type of compounds.

GENERAL NATURE OF MAO INHIBITION BY AMPH DERIVATIVES

Since the first pharmacological study more than 50 years ago proving the existence of the two enzyme isoforms (Johnston, 1968), hundreds of AMPH derivatives have been tested as MAOIs. **Tables 1–5** summarize the effects of a subset of these compounds. It should be noted that, as expected for results obtained from different laboratories over a long period of time, the methodological approaches used to assess MAO inhibition are diverse. Thus, a variety of biochemical assays to follow MAO activities (e.g. radiometric, luminometric, spectrophotometric, electrochemical, fluorometric), substrates (e.g. 5-HT, kynuramine, β-phenethylamine, benzylamine, 4-dimethylaminophenethylamine), inhibition parameters (e.g. IC_{50}, K_i), tissue sources (e.g. brain, lung, liver), and species (e.g. rat, mouse, human from fresh tissue, human recombinant heterologously expressed in yeast), have been employed in these experiments. Therefore, although we made an effort to consider results obtained under relatively similar conditions for comparative analysis, the reader should bear in mind this limitation when evaluating the data presented below.

Despite these considerations, some general conclusions about the MAO inhibitory activity of AMPH derivatives can be established. Thus, in the vast majority of the cases in which a relevant inhibitory activity was detected, this effect shows a clear selectivity towards MAO-A (e.g. Mantle et al., 1976; Green and el Hait, 1980; Ask et al., 1982a and Ask et al., 1982b; Ask et al., 1985; Florvall et al., 1986; Scorza et al., 1997; Gallardo-Godoy et al., 2005; Matsumoto et al., 2014; **Tables 1–5**). In addition, when assessed, AMPH derivatives produce in all cases a competitive and reversible[1] inhibition of MAO (e.g. Mantle et al., 1976; Fowler and Oreland, 1981; Arai et al., 1990; Leonardi and Azmitia, 1994; Ulus et al., 2000; Fierro et al., 2007). Even though no crystal structure of MAO-A in complex with AMPH derivatives has been reported yet, docking simulations have shed light on the molecular mechanism underlying both the MAO-A inhibitory activity and the selectivity exhibited by these compounds (Vallejos et al., 2005; Fierro et al., 2007; Vilches-Herrera et al., 2009 and Vilches-Herrera et al., 2016). **Figure 2** summarizes our current view in this regard. Thus, when a substrate, in this case 5-HT, is docked at the catalytic site, it locates in a pose where the amino group is in close proximity to the isoalloxazine ring of the FAD cofactor (**Figure 2A**). This would favor the abstraction of the pro-*R* α-proton of the amine by the N5 atom of the flavin ring, which is a critical step of MAO-catalyzed amine oxidation. On the other hand, AMPH derivatives (exemplified in this case by 4-methylthioAMPH; MTA) docked at the same site, exhibit binding modes where the amino group points away from the FAD ring system (**Figure 2B**) but with the aromatic ring positioned almost identically to that of the substrate (**Figure 2C**). Indeed, such a binding mode provides a rationale for the observed inhibitory activity, since while blocking the access of any substrate to the active site, AMPH derivatives could avoid deamination by adopting a pose where the amino group is remote from the influence of the flavin ring. Furthermore, in **Figure 2D** the active site of MAO-B was superimposed on the corresponding site of MAO-A already docked with MTA. As shown, the presence of Y326 in MAO-B (I335 being the corresponding residue in MAO-A), could prevent the close fit of MTA into the active site of MAO-B. Thus, our docking experiments suggest a possible explanation for the MAO-A selectivity exhibited by most AMPH derivatives. It is worth pointing out that fragments I335 and Y326 in MAO-A and MAO-B, respectively, have been regarded as major determinants of selectivity for both substrates and inhibitors (Edmondson et al., 2007; Binda et al., 2011; Iacovino et al., 2018).

[1] It should be noted that we do not review here irreversible inhibitors such as deprenyl or tranylcypromine. These compounds and their analogues can also be considered as AMPH derivatives, but due to particular structural characteristics (the presence either of a propargyl moiety on the amino group or a cyclopropyl ring involving the α and β carbons of the side chain, respectively), they are suicide substrates that can form covalent adducts with the flavin ring of the enzyme's cofactor. This characteristic leads to an irreversible mode of inhibition and generates completely different structure-activity relationships. These have been analyzed elsewhere (e.g. Magyar, 1994; Yoshida et al., 2004; Malcomson et al., 2015) and the reader is also referred to the literature (Binda et al., 2003; De Colibus et al., 2005) to have insights regarding the actual structural characteristics of the MAO-drug adducts formed by these compounds.

STRUCTURE-ACTIVITY RELATIONSHIPS OF AMPH DERIVATIVES AS MAOI

Modifications of the Side Chain

The presence of a methyl group on the α-carbon atom of phenethylamine transforms this compound, which is a selective MAO-B substrate, into AMPH which is a selective MAO-A inhibitor. This substrate-to-inhibitor change has also been reported for other phenethylamine/AMPH derivative pairs (e.g. Edwards, 1978; Yu, 1986; Fagervall et al., 1988; Reyes-Parada et al., 1994a and Reyes-Parada et al., 1994b; **Tables 1–2**. **Figure 3**). Considering that the α-C-H bond cleavage is likely the rate-limiting step in the catalytic cycle of both MAO isozymes (Miller and Edmondson, 1999), it seems reasonable that impeding/altering the feasibility of this step results in MAO inhibitory properties. Although stereospecific abstraction of the pro-*R*-hydrogen has been demonstrated with several substrates (Yu et al., 1986; Yu, 1988), it is noteworthy that both isomers of chiral AMPH derivatives inhibit MAOs, regardless of whether the pro-*R*- or the pro-*S*-hydrogen is the substituted atom (see **Tables 1–4** and references therein). This supports our idea that MAOI properties of AMPH derivatives are not necessarily due to the hindrance of hydrogen abstraction, but that the introduction of alkyl substituents at the α-carbon atom of the phenethylamine results in its adopting a different binding mode in the catalytic site (**Figure 2**). Nevertheless, extension of the alkyl substituent on the α-carbon atom or the introduction of a second methyl

TABLE1 | MAO inhibitory activity of AMPH derivatives and amiflamine analogues.

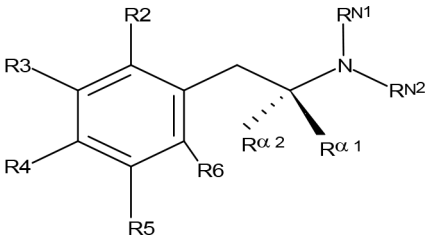

Compound[b]	R2	R3	R4	R5	R6	$R^{\alpha1}$	$R^{\alpha2}$	R^{N1}	R^{N2}	MAOI Activity IC_{50}(Ki)[a] (μM) MAO-A	MAO-B
(+)-Amphetamine	H	H	H	H	H	CH_3	H	H	H	20.0[c];4.9[d];33.8[e]	770[c];118[d];161[e]
Amphetamine	H	H	H	H	H	HCH_3		H	H	11.0[f](5.3[g])	236[g]
(-)-Amphetamine	H	H	H	H	H	H	CH_3	H	H	70.0[c];203[e]	600[c];180[e]
Methamphetamine	H	H	H	H	H	HCH_3		CH_3	H	41[h](17.2[g])	> 200[h](297)[g]
Phentermine	H	H	H	H	H	CH_3	CH_3	H	H	143[i](88[d];196[g])	285[i](310[d];138[g])
AEPEA	H	H	H	H	H	HCH_2CH_3		H	H	14.0[g]	234[g]
N,α-DEPEA	H	H	H	H	H	HCH_2CH_3		CH_2CH_3	H	251[g]	159[g]
Amiflamine/(+)-FLA336	CH_3	H	$N(CH_3)_2$	H	H	CH_3	H	H	H	0.8[j];2.0[f]	> 1000[j]
FLA336	CH_3	H	$N(CH_3)_2$	H	H	HCH_3		H	H	2.7[k]	440[k]
(-)-FLA336	CH_3	H	$N(CH_3)_2$	H	H	H	CH_3	H	H	3.0[j]	125[l]
FLA289	H	H	$N(CH_3)_2$	H	H	HCH_3		H	H	3.7[l];2.0[m]	400[l]
FLA727	H	H	$NHCH_3$	H	H	HCH_3		H	H	0.55[l]-1.2[m]	1500[l]
(+)-FLA788	CH_3	H	$NHCH_3$	H	H	CH_3	H	H	H	0.13[j]	> 1000[j]
FLA558	F	H	$N(CH_3)_2$	H	H	HCH_3		H	H	1.2[k]	120[k]
FLA314	Cl	H	$N(CH_3)_2$	H	H	HCH_3		H	H	0.21[k]	80[k]
FLA405	Br	H	$N(CH_3)_2$	H	H	HCH_3		H	H	0.22[k]	100[k]
FLA365	Cl	H	$N(CH_3)_2$	H	Cl	HCH_3		H	H	0.013[l]	180[l]
FLA450	Cl	H	$N(CH_3)_2$	H	H	HCH_2CH_3		H	H	0.38[k]	75[k]
FLA463	Cl	H	$N(CH_3)_2$	H	H	CH_3	CH_3	H	H	1.2[k]	700[k]
FLA717	CH_3	H	$N(CH_3)_2$	H	H	CH_3	CH_3	H	H	12.0[k]	2100[k]
FLA384	H	CH_3	$N(CH_3)_2$	H	H	HCH_3		H	H	8.0[l]	650[l]
(+)NBF003	CH_3	H	$N(CH_3)_2$	Br	H	CH_3	H	H	H	1.1[l]	480[l]

[a]IC_{50} and/or Ki are reported, depending on the reference considered. [b]Chemical name and/or common acronym and/or common name is given. When not indicated, the compound is the racemic mixture. [c]Mantle et al., 1976. [d]Ulus et al., 2000. [e]Robinson, 1985. [f]Scorza et al., 1997.[g]Santillo, 2014. [h]Matsumoto et al., 2014. [i]Kilpatrick et al., 2001. [j]Ask et al., 1982b. [k]Ask et al., 1982a. [l]Ask et al., 1985. [m]Reyes-Parada et al., 1994a.

group at this position, lead to a decrease of MAOI-A potency compared with the parent compounds (**Figure 4**). Moreover, cyclization of the side chain to generate 2-aminoindan or 2-aminotetraline analogues results in a marked decrease of the affinity of these compounds for MAOs (Feenstra et al., 1983; Scorza et al., 1999). Such reductions of inhibitory activity would presumably reflect impediments to binding in the enzyme's active site.

As shown in **Tables 1**, **2**, and **4**, in most of the instances in which the dependence of enzyme inhibition on the chirality of the α-carbon atom has been tested, it has been found that the (*S*)-(+)-AMPH derivatives are the eutomers as MAOI-A (Mantle et al., 1976; Fowler and Oreland, 1981; Ask et al., 1982b; Robinson, 1985; Leonardi and Azmitia, 1994; Hurtado-Guzmán et al., 2003; **Figure 5**). As stated before, the difference in MAO-A inhibitory potency between optical isomers of AMPH derivatives is, in general, not remarkable (**Tables 1**–**4**). This suggests that stereoselectivity may not be as influential in the pharmacodynamics of these compounds as has been shown to be for the effects of AMPH derivatives upon other monoaminergic target proteins such as monoamine transporters or 5-HT receptors (Nichols, 1994; Nichols, 2018).

Given the notoriety that the recreational use of cathinone derivatives has reached in the last few years (Simmler et al., 2013; Paillet-Loilier et al., 2014; Angoa-Pérez et al., 2017), it is somewhat surprising that MAOI properties of this type of compounds (as an example of β-substituted AMPH derivatives) have not been extensively studied. Nevertheless, Osorio-Olivares et al. (2004) reported that cathinone is almost completely devoid of activity as a MAOI, whereas some derivatives with alkylthio or alkoxy groups at the *para* position of the aromatic ring have IC_{50} values in the low micromolar range (**Table 3**). These results indicate that β-keto substitution of AMPH may lead to a decrease in MAOI-A potency (**Figure 6**). Nevertheless, some of these compounds showed an interesting MAO-B inhibiting activity (**Table 3**), which suggests that selectivity can be effectively modulated by side-chain substituents. In addition, β-keto substitution seems to diminish the enantioselectivity for MAO inhibition, since in some cases in which it was evaluated, the *R(-)*-derivatives were the eutomers

TABLE 2 | MAO inhibitory activity of AMPH derivatives monosubstituted in the aromatic ring.

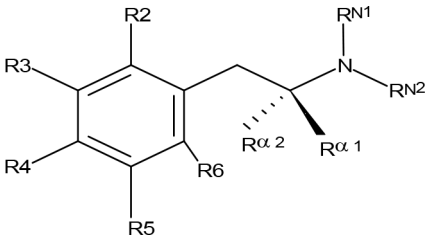

Compound[b]	R2	R3	R4	R5	R6	$R^{\alpha1}$	$R^{\alpha2}$	R^{N1}	R^{N2}	MAOI Activity IC_{50}(Ki)[a] (μM) MAO-A	MAO-B
PMA/4-MeOA	H	H	OCH_3	H	H	HCH_3		H	H	0.3[c];0.6[d](0.2[e])	45[d](530[e])
2-MeOA	OCH_3	H	H	H	H	HCH_3		H	H	9.0[e]	350[e]
3-MeOA	H	OCH_3	H	H	H	HCH_3		H	H	23[e]	1940[e]
PMMA	H	H	OCH_3	H	H	HCH_3		CH_3	H	1.7[d]	58[d]
4-EtOA	H	H	OCH_2CH_3	H	H	HCH_3		H	H	0.22[f]	> 100[f]
4-PrOA	H	H	$O(CH_2)_2CH_3$	H	H	HCH_3		H	H	0.13[f]	> 100[f]
4-BuOA	H	H	$O(CH_2)_3CH_3$	H	H	HCH_3		H	H	0.32[f]	> 100[f]
4-BzOA	H	H	OCH_2Phe	H	H	HCH_3		H	H	3.42[f]	0.71[f]
MTA	H	H	SCH_3	H	H	HCH_3		H	H	0.25[g]	NE[g]
(+)-MTA	H	H	SCH_3	H	H	CH_3	H	H	H	0.13[h]	NE[h]
(-)-MTA	H	H	SCH_3	H	H	H	CH_3	H	H	2.04[g]	NE[g]
NMMTA	H	H	SCH_3	H	H	HCH_3		CH_3	H	0.89[g]	NE[g]
DMMTA	H	H	SCH_3	H	H	HCH_3		CH_3	CH_3	2.10[g]	NE[g]
NEMTA	H	H	SCH_3	H	H	HCH_3		CH_2CH_3	H	1.80[g]	NE[g]
DEMTA	H	H	SCH_3	H	H	HCH_3		CH_2CH_3	CH_2CH_3	6.45[g]	NE[g]
NPMTA	H	H	SCH_3	H	H	HCH_3		$(CH_2)_2CH_3$	H	2.41[g]	> 10[g]
DPMTA	H	H	SCH_3	H	H	HCH_3		$(CH_2)_2CH_3$	$(CH_2)_2CH_3$	> 10[g]	NE[g]
NBzMTA	H	H	SCH_3	H	H	HCH_3		CH_2Phe	H	> 100[f]	> 100[f]
MTAB	H	H	SCH_3	H	H	HCH_2CH_3		H	H	0.84[g]	NE[g]
ETA	H	H	SCH_2CH_3	H	H	HCH_2CH_3		H	H	0.10[c]	29[c]
(+)-ETA	H	H	SCH_2CH_3	H	H	CH_3	H	H	H	0.075[h]	> 100[h]
(+)-PTA	H	H	$S(CH_2)_2CH_3$	H	H	CH_3	H	H	H	0.030[h]	14.0[h]
ITA	H	H	$SCH(CH_3)_2$	H	H	HCH_3		H	H	0.40[c]	8.1[c]
(+)-BTA	H	H	$S(CH_2)_3CH_3$	H	H	HCH_3		H	H	0.022[h]	4.6[h]
MSOA	H	H	$SOCH_3$	H	H	HCH_3		H	H	> 100[i]	NT
MSO2A	H	H	SO_2CH_3	H	H	HCH_3		H	H	> 100[i]	NT
PCA/*p*-Chloroamphetamine	H	H	Cl	H	H	HCH_3		H	H	4.0[c];1.9[j]	NE[c]
PBA/*p*-Bromoamphetamine	H	H	Br	H	H	HCH_3		H	H	1.5[j]	NT
PFA/*p*-Fluoroamphetamine	H	H	F	H	H	HCH_3		H	H	16[j]	NT
POHA	H	H	OH	H	H	HCH_3		H	H	24.0[k]	NE[k]
(+)-Fenfluramine	H	CF_3	H	H	H	CH_3	H	CH_2CH_3	H	256[l]	800[l]
Fenfluramine	H	CF_3	H	H	H	HCH_3		CH_2CH_3	H	440[m]	720[m]
(-)-Fenfluramine	H	CF_3	H	H	H	H	CH_3	CH_2CH_3	H	115[l]	685[l]
(+)-Norfenfluramine	H	CF_3	H	H	H	CH_3	H	H	H	36[l]	160[l]

[a]IC_{50} and/or Ki are reported, depending on the reference considered. [b]Chemical name and/or common acronym and/or common name is given. When not indicated the compound is the racemic mixture. [c]Scorza et al., 1997. [d]Matsumoto et al., 2014. [e]Green and el Hait, 1980. [f]Vilches-Herrera et al., 2009. [g]Hurtado-Guzmán et al., 2003. [h]Fierro et al., 2007. [i]Vallejos et al., 2002. [j]Fuller et al., 1975. [k]Arai et al., 1990. [l]Kilpatrick et al., 2001. [m]Leonardi and Azmitia, 1994. NE, No effect at 100 μM; NT, Not tested.

against MAO-A. Furthermore, when the β-keto substituent was replaced by a hydroxyl group, the compounds lost their activity on MAO-B while retaining MAOI-A inhibitory properties, although with lower potencies than their AMPH counterparts (Osorio-Olivares et al., 2004; **Table 3**).

N-Substitution

Relatively few amino group substituents have been studied in AMPH derivatives regarding their influence upon MAOI potency. In general terms, any *N*-substitution leads to a decrease in the activity of the compound as a MAOI-A. Thus, the *N*-methyl derivatives of AMPH, MTA, *p*-methoxyAMPH (PMA), and 3,4-methylenedioxyAMPH (MDA)— i.e. methamphetamine, NMMTA, PMMA, and MDMA respectively— have about one-third the inhibitory potency of their corresponding primary amine congeners (Scorza et al., 1997; Hurtado-Guzmán et al., 2003; Matsumoto et al., 2014; Santillo, 2014; **Tables 1**, **2**, **4**). In addition, enlargement of the amine substituent to *N*-ethyl, *N*-*n*-propyl, or *N*-allyl seems to cause a further decrease in MAO-A affinity, correlated with the length of the substituent (Kilpatrick et al., 2001; Hurtado-Guzmán et al., 2003; Santillo, 2014; **Figure 7**). Even larger substituents such as *N*-benzyl can lead to a complete loss of MAOI properties (Vilches-Herrera et al., 2009). Furthermore,

TABLE 3 | MAO inhibitory activity of β-substituted AMPH derivatives.

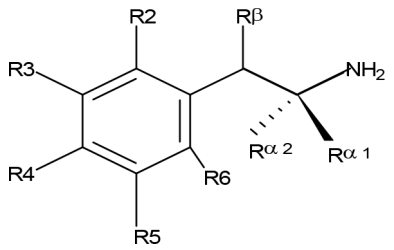

Compound[b]	R^{β}	R2	R3	R4	R5	R6	$R^{\alpha1}$	$R^{\alpha2}$	MAOI Activity IC_{50}[a] (μM) MAO-A	MAO-B
Cathinone	=O	H	H	H	H	H		HCH_3	NE	NE
4-MetOCat	=O	H	H	OCH_3	H	H		HCH_3	77.0	NE
4-EtOCat	=O	H	H	OCH_2CH_3	H	H		HCH_3	37.0	> 100
4-PropOCat	=O	H	H	$O(CH_2)_2CH_3$	H	H		HCH_3	7.2	8.9
4-ButOCat	=O	H	H	$O(CH_2)_3CH_3$	H	H		HCH_3	14.4	6.0
(+)4-ButOCat	=O	H	H	$O(CH_2)_3CH_3$	H	H	CH_3	H	29.5	5.6
(-)4-ButOCat	=O	H	H	$O(CH_2)_3CH_3$	H	H	H	CH_3	6.8	6.4
4-MetSCat	=O	H	H	SCH_3	H	H		HCH_3	45.0	> 100
(+)4-MetSCat	=O	H	H	SCH_3	H	H	CH_3	H	44.5	> 100
(-)4-MetSCat	=O	H	H	SCH_3	H	H	H	CH_3	38.9	NT
4-EtSCat	=O	H	H	S CH_2CH_3	H	H		HCH_3	15.1	> 100
(+)4-EtSCat	=O	H	H	S CH_2CH_3	H	H	CH_3	H	12.9	> 100
(-)4-EtSCat	=O	H	H	S CH_2CH_3	H	H	H	CH_3	38.0	NT
4-MetONEPhe	OH	H	H	OCH_3	H	H		HCH_3	9.8	NE
4-EtONEPhe	OH	H	H	O CH_2CH_3	H	H		HCH_3	7.0	NE
4-PropONEPhe	OH	H	H	O $(CH_2)_2CH_3$	H	H		HCH_3	2.8	100
4-ButONEPhe	OH	H	H	O $(CH_2)_3CH_3$	H	H		HCH_3	4.7	65
4-OHNEPhe	OH	H	H	OH	H	H		HCH_3	220.0[c]	NE[c]
4-MetSNEPhe	OH	H	H	SCH_3	H	H		HCH_3	7.3	NE
4-EtSNEPhe	OH	H	H	S CH_2CH_3	H	H		HCH_3	1.9	> 100
4-PropSNEPhe	OH	H	H	S $(CH_2)_2CH_3$	H	H		HCH_3	1.7	> 100
BMetOA	OCH_3	H	H	H	H	H		HCH_3	> 100	> 100
B,4DMetOA	OCH_3	H	H	OCH_3	H	H		HCH_3	77.5	> 100
BMetSA	OCH_3	H	H	SCH_3	H	H		HCH_3	50.6	> 100

[a]Unless stated, IC_{50} values are from Osorio-Olivares et al., 2004. [b]Chemical name and/or common acronym and/or common name is given. When not indicated the compound is the racemic mixture. [c]Arai et al., 1990. NE, No effect at 100 μM; NT, Not tested.

tertiary amines (i.e. derivatives with a second group upon the amino moiety) are even less potent as MAOI-A than their secondary or primary analogues (Hurtado-Guzmán et al., 2003). These structure-activity relationships are very similar to those observed for AMPH derivatives regarding their interactions with DAT, NET, and SERT (Nichols, 1994), which agrees with a recent report that demonstrates a remarkable structural similarity between the ligand binding sites of MAOs and monoamine transporters (Nuñez-Vivanco et al., 2018).

Aromatic Ring Substitution

Even though some aliphatic MAO substrates and inhibitors have been identified (Yu et al., 1994; Yu et al., 1995; Kalgutkar et al., 2001), most studies have shown that the presence of an aromatic ring is essential for potent MAOI activity (Wouters, 1998; Kalgutkar et al., 2001; Tripathi et al., 2018; Dhiman et al., 2018). In the specific case of AMPH derivatives, docking simulations indicate that the benzene ring of these compounds binds to MAO-A mainly *via* interactions with π-systems of the catalytic site residues such as Y407, Y444 (both of which form part of the so called "aromatic cage"), Y69, F208, and/or F352 (Vallejos et al., 2005; Fierro et al., 2007; Vilches-Herrera et al., 2009; Fresqui et al., 2013; Vilches-Herrera et al., 2016; **Figure 2**). Accordingly, a handful of QSAR studies have shown that electronic features of the benzene ring (e.g. CHELPG atomic charges, HOMO energies) are the most important factors to determine the affinity of AMPH derivatives for MAO-A, and hence that their variation caused by substituents can greatly modulate their potency as enzyme inhibitors (Norinder et al, 1994; Vallejos et al., 2002; Fresqui et al., 2013). In this respect, the presence of a single substituent with electron-donor properties (e.g. alkoxy, alkylthio, alkylamino) at the *para* position of the aromatic ring seems to be the most influential substitution favoring potency toward MAO-A. Thus, MTA, PMA, and *p*-methylaminoAMPH (FLA727) are 20-50-fold more potent than the parent compound (Ask et al., 1985; Scorza et al., 1997; **Tables 1**, **2**, **Figure 8**). The importance of the electron-donor character of the substituent at the *para* position is substantiated by the significant decrease of potency observed when the *p*-methylthio group is replaced by electron-withdrawing moieties such as *p*-

TABLE 4 | MAO inhibitory activity of AMPH derivatives polysubstituted in the aromatic ring.

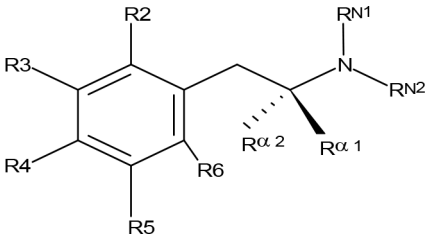

Compound[b]	R2	R3	R4	R5	R6	$R^{\alpha1}$	$R^{\alpha2}$	R^{N1}	R^{N2}	MAOI Activity IC_{50}(Ki)[a] (μM) MAO-A	MAO-B
2,4-DMA	OCH_3	H	OCH_3	H	H	HCH_3		H	H	0.6[c]	NE[c]
3,4-DMA	H	OCH_3	OCH_3	H	H	HCH_3		H	H	20[c]	NE[c]
2,5-DMA	OCH_3	H	H	OCH_3	H	HCH_3		H	H	> 100[f]	NE[f]
3,4,5-TMA	H	OCH_3	OCH_3	OCH_3	H	HCH_3		H	H	NE[c];NI[d]	NE[c];NI[d]
2,4,5-TMA	OCH_3	H	OCH_3	OCH_3	H	HCH_3		H	H	NE[c]	NE[c]
2,4,6-TMA	OCH_3	H	OCH_3	H	OCH_3	HCH_3		H	H	0.4[e]	NE[e]
2-Br-DMA	Br	H	OCH_3	OCH_3	H	HCH_3		H	H	9.3[c]	NE[c]
5-Br-DMA	OCH_3	H	OCH_3	Br	H	HCH_3		H	H	13.0[c]	NE[c]
2-NO_2-DMA	NO_2	H	OCH_3	OCH_3	H	HCH_3		H	H	NE[c]	NE[c]
6-Cl-DMA	OCH_3	H	OCH_3	H	Cl	HCH_3		H	H	0.07[e]	NE[e]
ALEPH-1	OCH_3	H	SCH_3	OCH_3	OCH_3	HCH_3		H	H	5.1[c]	NE[c]
ALEPH-2	OCH_3	H	SCH_2CH_3	OCH_3	H	HCH_3		H	H	3.2[c]	NE[c]
4-PrS-DMA	OCH_3	H	$S(CH_2)_2CH_3$	OCH_3	H	HCH_3		H	H	2.4[e]	NE[e]
4-BuS-DMA	OCH_3	H	$S(CH_2)_3CH_3$	OCH_3	H	HCH_3		H	H	2.9[e]	NE[e]
4-PentS-DMA	OCH_3	H	$S(CH_2)_4CH_3$	OCH_3	H	HCH_3		H	H	14.3[e]	NE[e]
2,5-DM-MTAB	OCH_3	H	SCH_3	OCH_3	H	HCH_2CH_3		H	H	30.9[e]	NE[e]
2,5-DM-ETAB	OCH_3	H	SCH_2CH_3	OCH_3	H	HCH_2CH_3		H	H	11.8[e]	NE[e]
2,6-DM-MTA	OCH_3	H	SCH_3	H	OCH_3	HCH_3		H	H	0.30[e]	NE[e]
2,6-DM-ETA	OCH_3	H	SCH_2CH_3	H	OCH_3	HCH_3		H	H	0.08[e]	NE[e]
4-ESO-2,5-DMA	OCH_3	H	$SOCH_3$	OCH_3	H	HCH_3		H	H	> 100[f]	NT
4-ESO2-2,5-DMA	OCH_3	H	SO_2CH_3	OCH_3	H	HCH_3		H	H	NE[f]	NT
DOM	OCH_3	H	CH_3	OCH_3	H	HCH_3		H	H	24.0[c]	NE[c]
DOI	OCH_3	H	I	OCH_3	H	HCH_3		H	H	24[c];37[d]	NE[c]
DOB	OCH_3	H	Br	OCH_3	H	HCH_3		H	H	100[c]	NE[c]
DON	OCH_3	H	NO_2	OCH_3	H	HCH_3		H	H	NE[c]	NE[c]
DOTFM	OCH_3	H	CF_3	OCH_3	H	HCH_3		H	H	NE[c]	NE[c]
MDA	H	CH_2-O-CH_2		H	H	HCH_3		H	H	9.3[c](8.5[g])	NE[c]
2Br-MDA	Br	H	CH_2-O-CH_2		H	HCH_3		H	H	13.0[c]	64.0[c]
2Cl-MDA	Cl	H	CH_2-O-CH_2		H	HCH_3		H	H	6.3[c]	38.0[c]
2NO_2-MDA	NO_2	H	CH_2-O-CH_2		H	HCH_3		H	H	NE[c]	NE[c]
MDMA	H	CH_2-O-CH_2		H	H	HCH_3		CH_3	H	30[c](24.7[g])	NE[c]
(+)-MDMA	H	CH_2-O-CH_2		H	H	CH_3	H	CH_3	H	44[h](22[h])	370[h]
(-)-MDMA	H	CH_2-O-CH_2		H	H	H	CH_3	CH_3	H	56[h](28.3[h])	378[h]

[a]IC_{50} and/or Ki are reported, depending on the reference considered. [b]Chemical name and/or common acronym and/or common name is given. When not indicated the compound is the racemic mixture. [c]Scorza et al., 1997. [d]Matsumoto et al., 2014. [e]Gallardo-Godoy et al., 2005. [f]Vallejos et al., 2002. [g]Steuer et al., 2016. [h]Leonardi and Azmitia, 1994. NE, No effect at 100 μM; NI, No inhibition at 200 μM; NT, Not tested.

methylsulfoxy or *p*-methylsulfonyl (i.e. MSOA or MSO2A, respectively; Vallejos et al., 2002; **Table 2**, **Figure 8**). It is worth pointing out that *para*-halogenated AMPHs (PCA, PBA, and PFA) are also fairly potent MAOI-A, with their potencies negatively correlated with their electron-withdrawing character, that is, PBA and PCA being about 7- and 4-fold more potent, and PFA being slightly less potent than AMPH (Fuller et al., 1975; Scorza et al., 1997; **Table 2**, **Figure 8**). Modestly increasing the size of the *para*-sulfur/oxygen substituent with linear aliphatic chains (i.e. ethyl-, propyl-, butyl-) leads to an increase in potency, while larger or branched substituents generate less potent compounds (Scorza et al., 1997; Gallardo-Godoy et al., 2005; Fierro et al., 2007; Vilches-Herrera et al., 2009 and Vilches-Herrera et al., 2016; **Figure 9**). It has been suggested (Fierro et al., 2007) that the increase in potency might be related to steric parameters of the *para* substituent (van der Waals volume and/or Taft steric parameter E_s) which would be optimal for alkyl chains containing up to four carbon atoms. Longer chains, however, might oblige the compound to adopt a more folded conformation, which would disfavor their interaction with the residues at the binding site. Interestingly, cycloalkyl analogues of pentylthioAMPH and hexylthioAMPH showed higher rat MAOI-A potencies than their *n*-alkyl counterparts, which was attributed to a better fit within the binding site due to the entropic advantage conferred by their "precoiled" conformations (Vilches-Herrera et al., 2016; **Figure 9**). In contrast, the presence of substituents at the *ortho* or *meta* positions in *para*-unsubstituted compounds had no effect or

TABLE 5 | MAO inhibitory activity of some AMPH derivatives containing aromatic systems larger than benzene.

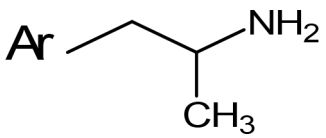

Compound[b]	Ar	MAOI Activity $IC_{50}(Ki)$[a] (μM) MAO-A	MAO-B
NIPA/PAL-287	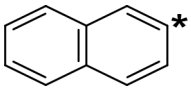	0.42[c]	> 100[c]
6-MeO-NIPA	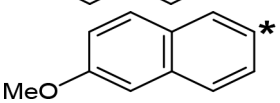	0.18[c]	16.3[c]
6-EtO-NIPA	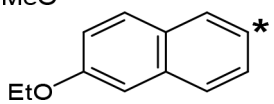	0.45[c]	13.6[c]
6-PrO-NIPA	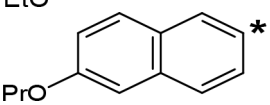	0.68[c]	13.5[c]
6-BuO-NIPA	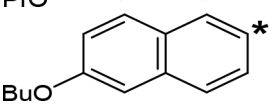	1.53[c]	NT
6-MeS-NIPA	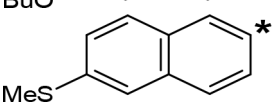	0.50[c]	NT
2-Benzofuryl-IPA	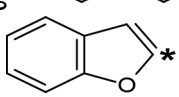	0.80[d]	> 100[d]
AMT	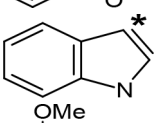	0.38[e]	> 10[e]
4-MeO-AMT	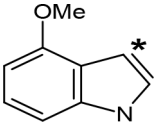	1.4[e]	> 10[e]
5-MeO-AMT	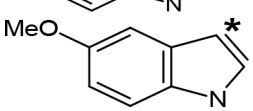	31[e]	> 10[e]
5-Me-AMT	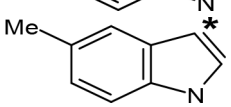	1.5[e]	> 10[e]
5-F-AMT	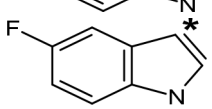	0.45[e](0.032[f])	376[e](575[f])
5-Cl-AMT	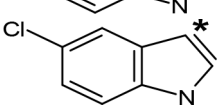	0.25[e]	82[e]
7-Me-AMT	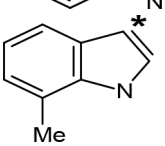	0.049[e]	> 10[e]

*[a]IC_{50} and/or K_i are reported, depending on the reference considered. [b]Chemical name and/or common acronym and/or common name is given. [c]Vilches-Herrera et al., 2009. [d]Vallejos et al., 2005. [e]Wagmann et al., 2017. [f]Kinemuchi et al., 1988. NT, Not tested. Ar, Aromatic ring. *: This symbol denotes where, in the aromatic ring, the aliphatic side chain is linked. Me, Methyl; Et, Ethyl; Pr, Propyl; Bu, Butyl.*

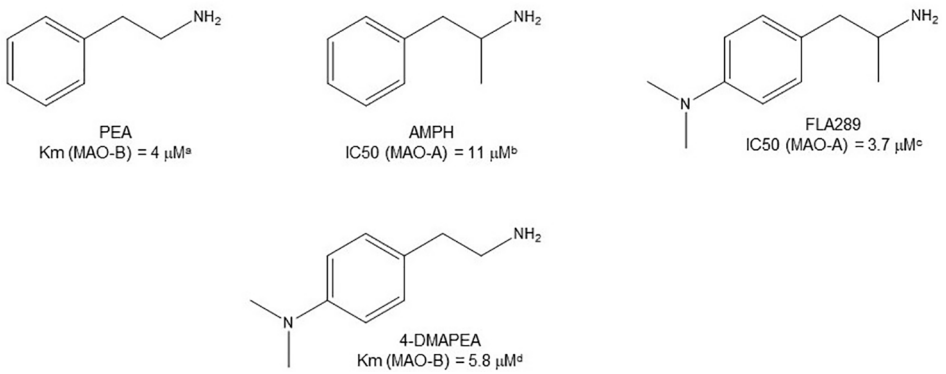

FIGURE 3 | Chemical structures and MAO parameters of some phenethylamine/AMPH derivative pairs. [a]Youdim et al., 2006. [b]Scorza et al., 1997. [c]Reyes-Parada et al., 1994b. [d]Reyes-Parada et al., 1994a.

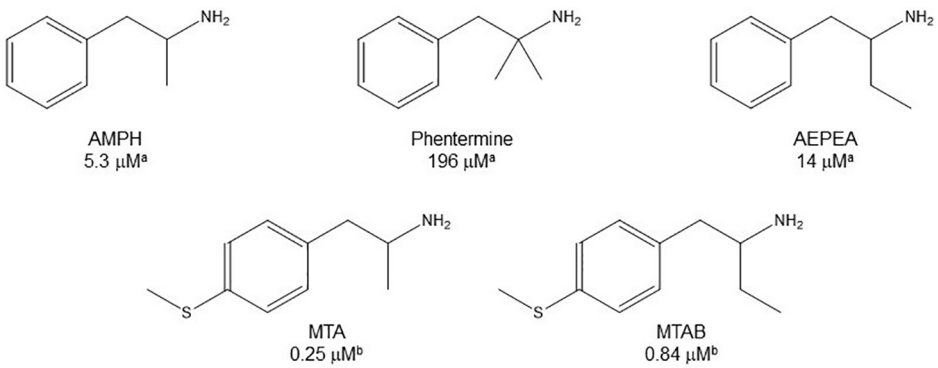

FIGURE 4 | Chemical structures and MAO-A IC_{50} of some α-substituted AMPH derivatives. [a]Santillo, 2014. [b]Hurtado-Guzmán et al., 2003.

led to a decrease of the potency as MAOI-A as compared with AMPH (Green and el Hait, 1980; Scorza et al., 1997; Kilpatrick et al., 2001; **Tables 2** and **4**). Moreover, the addition of bulky groups adjacent to the *para*-substituted position induces a decrease in potency. Thus, the presence of one or two substituents at the *meta* position(s) of PMA produce compounds that are respectively 60-fold less potent or completely inactive (Scorza et al., 1997; **Figure 10**). Nonetheless, the introduction of substituents at more distant positions has less detrimental effects on potency, and even in some cases a marked increase of activity (and selectivity) has been reported. Thus, the addition of a methyl group at the *ortho* position of *p*-dimethylaminoAMPH (FLA289) to yield FLA336 produced a slight increase in potency, which was more evident (along with a remarkable increase in MAO-A/B selectivity) in the case of amiflamine, the (*S*)-(+)-isomer of FLA336 (Ask et al., 1985; **Table 1**). Indeed, the introduction of one or two halogen atoms (Cl or Br) at the *ortho* position(s), generates some of the most potent MAOI-A AMPH derivatives described until now (Ask et al., 1985; Gallardo-Godoy et al., 2005; **Tables 1** and **4**).

The expansion of the aromatic ring of AMPH is an additional modification that has yielded interesting results and potent and selective MAOIs-A (**Table 5**). This could have been anticipated considering that: a) the structure of 5-HT, one of the natural substrates of MAO-A, contains an indolyl moiety instead a simple benzene ring and; b) the electron-richness of the aromatic ring seems to be an important molecular determinant for MAO-A affinity (Vallejos et al., 2002), and therefore aromatic systems larger than benzene might establish stronger π-type interactions with aromatic and non-aromatic residues present in the active site of the protein. Accordingly, for example 2-naphthylisopropylamine (NIPA, also known as PAL-287; Rothman et al., 2005) and its methoxylated or methylthio derivatives (Vilches-Herrera et al., 2009), 2-benzofurylisopropylamine (Vallejos et al., 2005) or several α-methyltryptamine derivatives (Kinemuchi et al., 1988; Wagmann et al., 2017) have been shown to be highly selective

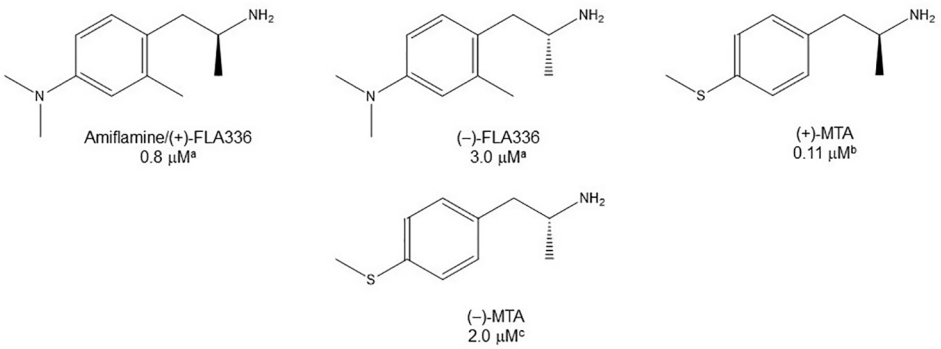

FIGURE 5 | Chemical structures and MAO-A IC_{50} of some enantiomerically pure AMPH derivatives. [a]Ask et al., 1982b. [b]Fierro et al., 2007. [c]Hurtado-Guzmán et al., 2003.

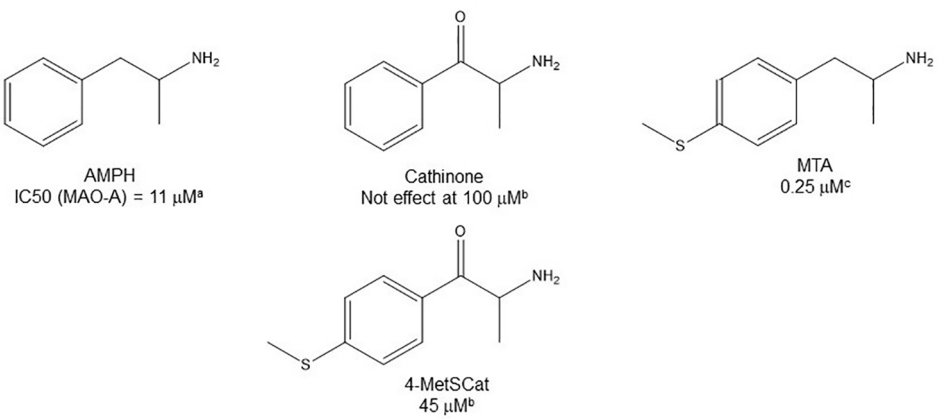

FIGURE 6 | Chemical structures and MAO-A IC_{50} of some β-keto substituted AMPH derivatives. [a]Scorza et al., 1997. [b]Osorio-Olivares et al., 2004. [c]Hurtado-Guzmán et al., 2003.

MAOI-A, much more potent than AMPH (**Table 5**). Both electronic and steric factors have been invoked to explain the higher activity of AMPH derivatives containing aromatic rings larger than benzene (Vallejos et al., 2005; Vilches-Herrera et al., 2009). Thus, π systems with an increased electron-donating capacity, softer and/or more polarizable as compared with benzene, might favor charge-transfer (Vallejos et al., 2002) and/or π-stacking interactions (Fresqui et al., 2013) with aromatic fragments in the active site. In addition, docking simulations have shown that AMPH derivatives containing large aromatic rings, can establish interactions not only with the aromatic residues forming the so-called aromatic cage (i.e. Y407 and Y444), but also with aminoacids located more distantly, such as F208, Y69, and F352 (Vallejos et al., 2005; Vilches-Herrera et al., 2009). Therefore, the higher potency of AMPH derivatives containing condensed aromatic systems could be explained by an increased probability of establishing dispersive short length interactions and also a greater number of interactions.

SUMMARY OF STRUCTURE-ACTIVITY RELATIONSHIPS AND IMPLICATIONS OF MAOI PROPERTIES FOR THE OVERALL PHARMACOLOGY OF AMPH DERIVATIVES

Potent, selective, and competitive MAO-A inhibitory properties are found in many AMPH derivatives. This is likely due to the structural similarity of this type of compounds with physiological

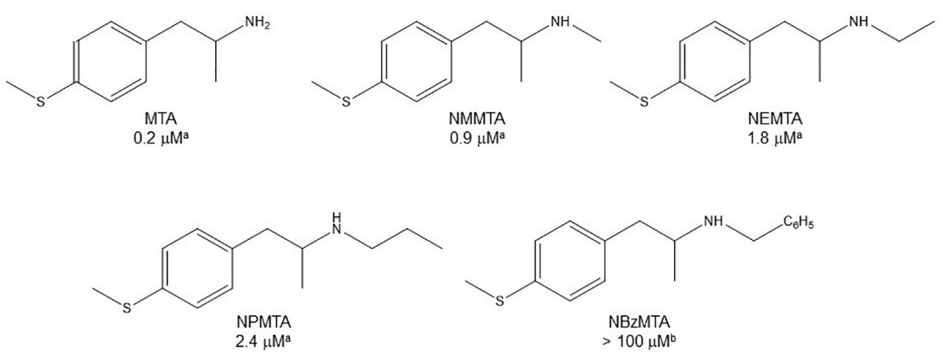

FIGURE 7 | Chemical structures and MAO-A IC_{50} of some *N*-substituted AMPH derivatives. [a]Hurtado-Guzmán et al., 2003. [b]Vilches-Herrera et al., 2009.

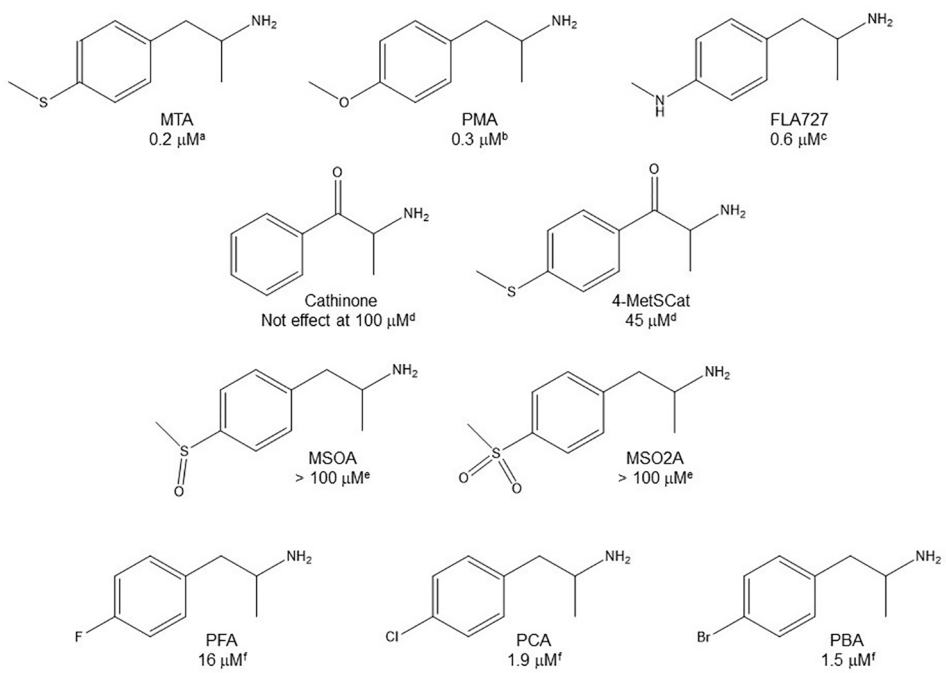

FIGURE 8 | Chemical structures and MAO-A IC_{50} of some *p*-substituted AMPH derivatives. [a]Hurtado-Guzmán et al., 2003. [b]Scorza et al., 1997. [c]Reyes-Parada et al., 1994a. [d]Osorio-Olivares et al., 2004. [e]Vallejos et al., 2002. [f]Fuller et al., 1975.

substrates, which allows AMPH derivatives to occupy, and consequently block the access of any substrate into the active site of the enzyme.

Although not extensively studied, in general the introduction of diverse substituents on either the amino group or the side chain of the basic AMPH skeleton leads to compounds with lower affinity as compared with the parent counterparts. Furthermore, several studies have shown that (*S*)-(+)-AMPH derivatives are the eutomers for MAO inhibition. Besides, as aromatic interactions in the active site of the enzyme seem to be critical for inhibition, substituents at this portion of the AMPH structure greatly modulate its potency. In general, electron-donor substituents at the *para* position of the aromatic ring generate potent MAOI-A, while substituents adjacent to this position decrease activity. In addition, replacement of the benzene ring by larger π systems exhibiting an increased electron-donating capacity, generates compounds with higher MAOI potency.

Even though MAO inhibition has been demonstrated for several AMPH derivatives, this is often considered not relevant for their global effect, since their affinity for MAO is usually weak compared to affinity for their main pharmacological targets (i.e. monoamine transporters or receptors). This is most likely true in the case of compounds such as the anti-obesity agents

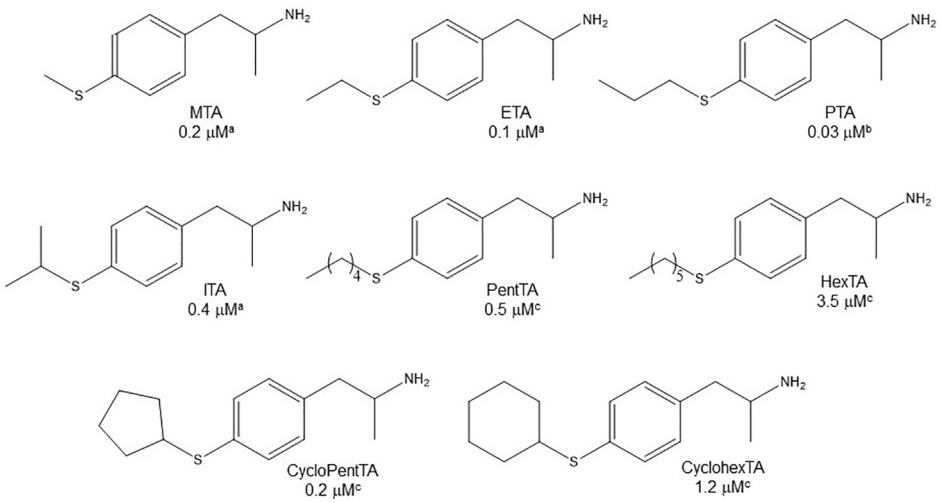

FIGURE 9 | Chemical structures and MAO-A IC_{50} of some *p*-alkylthio AMPH derivatives. [a]Scorza et al., 1997. [b]Fierro et al., 2007. [c]Vilches-Herrera et al., 2016.

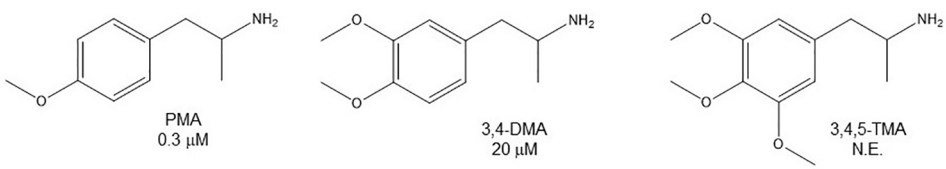

FIGURE 10 | Chemical structures and MAO-A IC_{50} of some *p*-methoxy AMPH derivatives. IC_{50} values are from Scorza et al., 1997. NE, No effect.

phentermine and fenfluramine (Kilpatrick et al., 2001; Nandigama et al., 2002), or the hallucinogenic drugs DOI and DOB (Nichols, 2018), whose ability either to evoke monoamine release or to activate 5-HT receptors exceeds by several orders of magnitude their potency as MAOIs. However, in the case of monoamine releasing agents such as PMA or MTA, their potency upon their main protein targets (i.e. SERT and DAT) is remarkably similar to that reported for MAO-A (Green and el Hait, 1980; Nichols et al., 1993; Scorza et al., 1997; Callaghan et al., 2005; Gobbi et al., 2008; Sotomayor-Zárate et al., 2012; Matsumoto et al., 2014). Thus, one may assume that the cases of severe toxicity reported after recreational use of these drugs (e.g. Elliott, 2000; De Letter et al., 2001; Martin, 2001; Lamberth et al., 2008), which resemble "serotonin syndrome" symptoms (Lapoint et al., 2013), are related to a sustained increase of synaptic 5-HT and DA resulting from both monoamine reverse transport and MAO-A inhibition. Furthermore, as many AMPH derivatives are monoamine transporter substrates (Simmler et al., 2013; Sitte and Freissmuth, 2015), even in those cases in which relatively weak MAOI activity is demonstrated, these drugs might be concentrated in presynaptic nerve terminals or glial cells, and some enzyme inhibition could occur (Heal et al., 2013). In this sense, accumulation and pronounced inhibition of MAO in monoaminergic neurons has been consistently reported for amiflamine and its analogues (Ask et al., 1983; Ask et al., 1985; Ask et al., 1986; Ask and Ross, 1987). In addition, especially after relatively prolonged use, antidepressant and/or anxiolytic effects derived from MAO-A inhibition might influence the global pharmacological effect of AMPH derivatives. Thus, for example, considering the high overlap between depression and drug abuse (Markou et al., 1998; Bruijnzeel et al., 2004), it is enticing to suggest that at least part of the antiaddictive potential of PAL-287 (NIPA; **Table 5**), which has been attributed to its DA and 5-HT releasing properties (Rothman et al., 2005; Rothman et al., 2007; Rothman et al., 2008), might be related also to its MAOI-A activity (Vilches-Herrera et al., 2009). Moreover, subtle differences in the subjective experience generated by hallucinogenic AMPH derivatives such as DOI or DOB as compared with sulfur containing analogues (Shulgin and Shulgin, 1991), might be associated with the much more pronounced MAOI-A activity of the latter (**Table 4**, Scorza et al., 1997; Gallardo-Godoy et al., 2005). Thus, these and other examples highlight the notion that MAOI properties should be considered when assessing the overall pharmacology of AMPH derivatives.

CONCLUDING REMARKS

Although many AMPH derivatives have been tested as MAOI, the structural diversity of such compounds is relatively limited. This calls for a broader exploration of the chemical space around the parent scaffold in the search of compounds with novel properties, in which MAOI properties might or might not be pursued. As known and unknown AMPH derivatives are usually attractive for illicit purposes (production, marketing, and/or consumption), it seems very relevant to evaluate in every case the possible MAOI activity of these drugs, since it may convey dangerous consequences for uninformed users.

Regarding the mechanism of enzyme inhibition, insofar as a crystal structure of MAO in complex with some AMPH derivative is not available, molecular simulation appears as one of the most reliable tools to study this issue. Nevertheless, most of current information has been obtained through docking studies, without resorting to molecular dynamics simulations that consume much more computer time, and therefore models generated still require a further validation. In addition, several reports indicate that MAOI profiles differ if enzymes from human or other species are used (not only for AMPH derivatives). Hence, inferences regarding possible effects in humans should be most cautious when data are obtained initially in animal models. Moreover, in comparison to recent characterizations of the monoamine transporter and receptor interactions of amphetamines (Simmler et al., 2013; Luethi and Liechti, 2018), the MAO inhibiting properties have not been investigated using the same assays across a larger range of substances. Therefore, comparative analyses should be done cautiously when considering results obtained under different experimental conditions

Beyond these considerations, in our view it is clear that AMPH derivatives can act as MAOI and that this activity should be taken into account when analyzing the overall pharmacodynamics of these structurally versatile compounds.

AUTHOR CONTRIBUTIONS

All authors equally contributed to the writing of this manuscript.

FUNDING

The constant support of FONDECYT, in particular grants 1170662 (MR-P), 1150615 (PI-V), and 1150868 (BKC), is gratefully acknowledged.

ACKNOWLEDGMENTS

The authors are grateful to all the colleagues who have contributed over the years to the studies carried out in our laboratories on the MAOI properties of AMPH derivatives. We also thank Dr. Patricia Möller-Acuña for her valuable help in doing measurements and preparing **Figure 2**.

REFERENCES

Angoa-Pérez, M., Anneken, J. H., and Kuhn, D. M. (2017). Neurotoxicology of Synthetic Cathinone Analogs. *Curr. Top. Behav. Neurosci.* 32, 209–230. doi: 10.1007/7854_2016_21

Arai, Y., Kim, S. K., Kinemuchi, H., Tadano, T., Satoh, S. E., Satoh, N., et al. (1990). Inhibition of brain type A monoamine oxidase and 5-hydroxytryptamine uptake by two amphetamine metabolites, p-hydroxyamphetamine and p-hydroxynorephedrine. *J. Neurochem.* 55, 403–408. doi: 10.1111/j.1471-4159.1990.tb04151.x

Ask, A. L., and Ross, S. B. (1987). Inhibition of 5-hydroxytryptamine accumulation and deamination by substituted phenylalkylamines in hypothalamic synaptosomes from normal and reserpine-pretreated rats. *Naunyn Schmiedebergs Arch. Pharmacol.* 336, 591–596. doi: 10.1007/bf00165748

Ask, A. L., Hellström, W., Norrman, S., Ögren, S. O., and Ross, S. B. (1982a). Selective inhibition of the A form of monoamine oxidase by 4-dimethylamino-alpha-methylphenylalkylamine derivatives in the rat. *Neuropharmacology*21, 299–308. doi: 10.1016/0028-3908(82)90092-2

Ask, A. L., Högberg, K., Schmidt, L., Kiessling, H., and Ross, S. B. (1982b). (+)-4-Dimethylamino-2,alpha-dimethylphenethylamine (FLA 336(+)), a selective inhibitor of the A form of monoamine oxidase in the rat brain. *Biochem. Pharmacol.* 31, 1401–1406. doi: 10.1016/0006-2952(82)90035-1

Ask, A. L., Fagervall, I., and Ross, S. B. (1983). Selective inhibition of monoamine oxidase in monoaminergic neurons in the rat brain. *Naunyn-Schmiedebergs Arch. Pharmacol.* 324, 79–87. doi: 10.1007/bf00497011

Ask, A. L., Fagervall, I., Florvall, L., Ross, S. B., and Ytterborn, S. (1985). Inhibition of monoamine oxidase in 5-hydroxytryptaminergic neurones by substituted p-aminophenylalkylamines. *Br. J. Pharmacol.* 85, 683–690. doi: 10.1111/j.1476-5381.1985.tb10564.x

Ask, A. L., Fagervall, I., Florvall, L., Ross, S. B., and Ytterborn, S. (1986). Selective inhibition of monoamine oxidase by p-aminosubstituted phenylalkylamines in catecholaminergic neurones. *Neuropharmacology* 25, 33–40. doi: 10.1016/0028-3908(86)90055-9

Barbosa, D. J., Capela, J. P., Feio-Azevedo, R., Teixeira-Gomes, A., Bastos, Mde, L., and Carvalho, F. (2015). Mitochondria: key players in the neurotoxic effects of amphetamines. *Arch. Toxicol.* 89, 1695–1725. doi: 10.1007/s00204-015-1478-9

Biel., J. H., and Bopp, B. A. (1978). "Amphetamines: structure–activity relationships," in *Handbook of Psychopharmacology*. Eds. L. L. Iversen, S. D. Iversen and S. H. Snyder (New York, NY: Stimulants. Plenum), 1–40.

Binda, C., Newton-Vinson, P., Hubálek, F., Edmondson, D. E., and Mattevi, A. (2002). Structure of human monoamine oxidase B, a drug target for the treatment of neurological disorders. *Nat. Struct. Biol.* 9, 22–26. doi: 10.1038/nsb732

Binda, C., Li, M., Hubálek, F., Restelli, N., Edmondson, D. E. , and Mattevi, A. (2003). Insights into the mode of inhibition of human mitochondrial monoamine oxidase B from high-resolution crystal structures. *Proc. Natl. Acad. Sci. U. S. A.* 100 8755–9759. doi: 10.1073/pnas.1633804100

Binda, C., Hubálek, F., Li, M., Herzig, Y., Sterling, J., Edmondson, D. E., et al. (2004). Crystal structures of monoamine oxidase B in complex with four inhibitors of the N-propargylamino-indan class. *J. Med. Chem.* 47, 1767–1774. doi: 10.1021/jm031087c

Binda, C., Mattevi, A., and Edmondson, D. E. (2011). Structural properties of human monoamine oxidases A, and B. *Int. Rev. Neurobiol.* 100, 1–11. doi: 10.1016/B978-0-12-386467-3.00001-7

Bruijnzeel., A. W., Repetto, M., and Gold, M. S. (2004). Neurobiological mechanisms in addictive and psychiatric disorders. *Psychiatr. Clin. North Am.* 27, 661–674. doi: 10.1016/j.psc.2004.06.005

Callaghan, P. D., Irvine, R. J., and Daws, L. C. (2005). Differences in the *in vivo* dynamics of neurotransmitter release and serotonin uptake after acute para-

methoxyamphetamine and 3,4-methylenedioxymethamphetamine revealed by chronoamperometry. *Neurochem. Int.* 47, 350–361. doi: 10.1016/j.neuint.2005.04.026

Cesura, A. M., and Pletscher, A. (1992). The new generation of monoamine oxidase inhibitors. *Prog. Drug Res.* 38, 171–297. doi: 10.1007/978-3-0348-7141-9_3

Dauvilliers, Y., and Barateau, L. (2017). Narcolepsy and Other Central Hypersomnias. Continuum (Minneapolis, MN). *Sleep Neurol.* 23:l, 989–1004. doi: 10.1212/CON.0000000000000492

De Colibus, L., Li, M., Binda, C., Lustig, A., Edmondson, D. E., and Mattevi, A. (2005). Three-dimensional structure of human monoamine oxidase A (MAO A): Relation to the structures of rat MAO A and human MAO B. *Proc. Natl. Acad. Sci. U. S. A.* 102, 12684–12689. doi: 10.1073/pnas.0505975102

De Letter, E. A., Coopman, V. A., Cordonnier, J. A., and Piette, M. H. (2001). One fatal and seven non-fatal cases of 4-methylthioamphetamine (4-MTA) intoxication: clinico-pathological findings. *Int. J. Legal Med.* 114, 352–356. doi: 10.1007/s004140100204

Dhiman, P., Malik, N., and Khatkar, A. (2017). Docking-Related Survey on Natural-Product-Based New Monoamine Oxidase Inhibitors and Their Therapeutic Potential. *Comb. Chem. High Throughput Screen.* 20, 474–491. doi: 10.2174/1386207320666170414102814

Dhiman, P., Malik, N., and Khatkar, A. (2018). 3D-QSAR and in-silico Studies of Natural Products and Related Derivatives as Monoamine Oxidase Inhibitors. *Curr. Neuropharmacol.* 16, 881–900. doi: 10.2174/1570159X15666171128143650

Edeleano, L. (1887). Ueber einige derivate der phenylmethacrylsäure und der phenylisobuttersaure. *Ber. Deut. Chem. Ges.* 20, 616–622. doi: 10.1002/cber.188702001142

Edmondson, D. E., Binda, C., and Mattevi, A. (2007). Structural insights into the mechanism of amine oxidation by monoamine oxidases A, and B. *Arch. Biochem. Biophys.* 464, 269–276. doi: 10.1016/j.abb.2007.05.006

Edwards, D. J. (1978). Phenylethanolamine is a specific substrate for type B monoamine oxidase. *Life Sci.* 23, 1201–1207. doi: 10.1016/0024-3205(78)90355-7

Elliott, S. P. (2000). Fatal poisoning with a new phenylethylamine: 4-methylthioamphetamine (4-MTA). *J. Anal. Toxicol.* 24, 85–89. doi: 10.1093/jat/24.2.85

Fagervall, I., Kelder, D., and Ross, S. B. (1988). Selective inhibition by 4,alpha-dimethyl-m-tyramine (H77/77) and 4-methyl-alpha-ethyl-m-tyramine (H75/12) of the monoamine oxidase within serotonergic and noradrenergic neurons in the rat brain. *Naunyn-Schmiedebergs Arch. Pharmacol.* 338, 143–147. doi: 10.1007/bf00174862

Feenstra, M. G., van der Velden, T., Dijkstra, D., Hommes, O. R., and Horn, A. S. (1983). Inhibition of rat brain monoamine oxidase type A by 2-aminotetralin and tetrahydroisoquinoline analogues of dopamine. *Pharm. Weekbl. Sci.* 5, 131–133. doi: 10.1007/bf01961468

Ferino, G., Vilar, S., Matos, M. J., Uriarte, E., and Cadoni, E. (2012). Monoamine oxidase inhibitors: ten years of docking studies. *Curr. Top. Med. Chem.* 12, 2145–2162. doi: 10.2174/156802612805220048

Fierro, A., Osorio-Olivares, M., Cassels, B. K., Edmondson, D. E., Sepúlveda-Boza, S., and Reyes-Parada, M. (2007). Human and rat monoamine oxidase-A are differentially inhibited by (S)-4-alkylthioamphetamine derivatives: insights from molecular modeling studies. *Bioorg. Med. Chem.* 15, 5198–5206. doi: 10.1016/j.bmc.2007.05.021

Finberg, J. P., and Rabey, J. M. (2016). Inhibitors of MAO-A and MAO-B in Psychiatry and Neurology. *Front. Pharmacol.* 7, 340. doi: 10.3389/fphar.2016.00340

Fleckenstein, A. E., Volz, T. J., Riddle, E. L., Gibb, J. W., and Hanson, G. R. (2007). New insights into the mechanism of action of amphetamines. *Annu. Rev. Pharmacol. Toxicol.* 47, 681–698. doi: 10.1146/annurev.pharmtox.47.120505.105140

Florvall, L., Fagervall, I., Ask, A. L., and Ross, S. B. (1986). Selective monoamine oxidase inhibitors. 4. 4-Aminophenethylamine derivatives with neuron-selective action. *J. Med. Chem.* 29, 2250–2256. doi: 10.1021/jm00161a020

Fowler, C. J., and Oreland, L. (1981). Substrate- and stereoselective inhibition of human brain monoamine oxidase by 4-dimethylamino-alpha,2-dimethylphenethylamine (FLA 336). *J. Pharm. Pharmacol.* 33, 403–406. doi: 10.1111/j.2042-7158.1981.tb13819.x

Fresqui, M. A., Ferreira, M. M., and Trsic, M. (2013). The influence of R and S configurations of a series of amphetamine derivatives on quantitative structure-activity relationship models. *Anal. Chim. Acta* 759, 43–52. doi: 10.1016/j.aca.2012.11.004

Fuller, R. W., Baker, J. C., Perry, K. W., and Molloy, B. B. (1975). Comparison of 4-chloro-, 4-bromo- and 4-fluoroamphetamine in rats: drug levels in brain and effects on brain serotonin metabolism. *Neuropharmacology* 14, 739–746. doi: 10.1016/0028-3908(75)90099-4

Gallardo-Godoy, A., Fierro, A., McLean, T. H., Castillo, M., Cassels, B. K., Reyes-Parada, M., et al. (2005). Sulfur-substituted alpha-alkyl phenethylamines as selective and reversible MAO-A inhibitors: biological activities, CoMFA analysis, and active site modeling. *J. Med. Chem.* 48, 2407–2419. doi: 10.1021/jm0493109

Glennon, R. A. (1999). Arylalkylamine drugs of abuse: an overview of drug discrimination studies. *Pharmacol. Biochem. Behav.* 64, 251–256. doi: 10.1016/s0091-3057(99)00045-3

Gobbi, M., Funicello, M., Gerstbrein, K., Holy, M., Moya, P. R., Sotomayor, R., et al. (2008). N,N-dimethyl-thioamphetamine and methyl-thioamphetamine, two non-neurotoxic substrates of 5-HT transporters, have scant *in vitro* efficacy for the induction of transporter-mediated 5-HT release and currents. *J. Neurochem.* 105, 1770–1780. doi: 10.1111/j.1471-4159.2008.05272.x

Green, A. L., and el Hait, M. A. S. (1980). *p*-Methoxyamphetamine, a potent reversible inhibitor of type-A monoamine oxidase *in vitro* and *in vivo*. *J. Pharm. Pharmacol.* 32 262–266. doi: 10.1111/j.2042-7158.1980.tb12909.x.

Heal, D. J., Smith, S. L., Gosden, J., and Nutt, D. J. (2013). Amphetamine, past and present - a pharmacological and clinical perspective. *J. Psychopharmacol.* 27, 479–496. doi: 10.1177/0269881113482532

Hilbert, A. (2019). Binge-eating disorder. *Psychiatr. Clin. North Am.* 42, 33–43. doi: 10.1016/j.psc.2018.10.011

Hurtado-Guzmán, C., Fierro, A., Iturriaga-Vásquez, P., Sepúlveda-Boza, S., Cassels, B. K., and Reyes-Parada, M. (2003). Monoamine oxidase inhibitory properties of optical isomers and *N*-substituted derivatives of 4-methylthioamphetamine. *J. Enzyme Inhib. Med. Chem.* 18, 339–347. doi: 10.1080/1475636031000118437

Iacovino, L. G., Magnani, F., and Binda, C. (2018). The structure of monoamine oxidases: past, present, and future. *J. Neural Transm (Vienna).* 125, 1567–1579. doi: 10.1007/s00702-018-1915-z

Johnston, J. P. (1968). Some observations upon a new inhibitor of monoamine oxidase in brain tissue. *Biochem. Pharmacol.* 17, 1285–1297. doi: 10.1016/0006-2952(68)90066-x

Kalgutkar, A. S., Dalvie, D. K., Castagnoli., N.Jr., and Taylor, T. J. (2001). Interactions of nitrogen-containing xenobiotics with monoamine oxidase (MAO) isozymes A and B: SAR studies on MAO substrates and inhibitors. *Chem. Res. Toxicol.* 14, 1139–1162. doi: 10.1021/tx010073b

Kilpatrick, I. C., Traut, M., and Heal, D. J. (2001). Monoamine oxidase inhibition is unlikely to be relevant to the risks associated with phentermine and fenfluramine: a comparison with their abilities to evoke monoamine release. *Int. J. Obes. Relat. Metab. Disord.* 25, 1454–1458. doi: 10.1038/sj.ijo.0801732

Kinemuchi, H., Arai, Y., Toyoshima, Y., Tadano, T., and Kisara, K. (1988). Studies on 5-fluoro-alpha-methyltryptamine and p-chloro-beta-methylphenethylamine: determination of the MAO-A or MAO-B selective inhibition *in vitro*. *Jpn. J. Pharmacol.* 46 197–199. doi: 10.1254/jjp.46.197

Kumar, B., Gupta, V. P., and Kumar, V. A. (2017). Perspective on monoamine oxidase enzyme as drug target: challenges and opportunities. *Curr. Drug Targets.* 18, 87–97. doi: 10.2174/1389450117666151209123402

Lamberth, P. G., Ding, G. K., and Nurmi, L. A. (2008). Fatal paramethoxy-amphetamine (PMA) poisoning in the Australian Capital Territory. *Med. J. Aust.* 188, 426. doi: 10.5694/j.1326-5377.2008.tb01695.x

Lapoint, J., Dargan, P. I., and Hoffman, R. S. (2013). "Synthetic Amphetamine Derivatives," in *Novel Psychoactive Substances*. Eds. P. I. Dargan and D. M. Wood (Boston, MA: Academic Press), 161–178.

Leonardi, E. T., and Azmitia, E. C. (1994). MDMA (ecstasy) inhibition of MAO type A and type B: comparisons with fenfluramine and fluoxetine (Prozac). *Neuropsychopharmacology* 10, 231–238. doi: 10.1038/npp.1994.26

Luethi, D., and Liechti, M. E. (2018). Monoamine transporter and receptor interaction profiles in vitro predict reported human doses of novel psychoactive stimulants and psychedelics. *Int. J. Neuropsychopharmacol.* 21, 926–931. doi: 10.1093/ijnp/pyy047

Luque, J. M., Kwan, S. W., Abell, C. W., Da Prada, M., and Richards, J. G. (1995). Cellular expression of mRNAs encoding monoamine oxidases A and B in the rat central nervous system. *J. Comp. Neurol.* 363, 665–680. doi: 10.1002/cne.903630410

Ma, J., Masato, Y., Yamashita, E., Nakagawa, A., Ito, A., and Tsukihara, T. (2004). Structure of rat monoamine oxidase and its specific recognitions for substrates and inhibitors. *J. Mol. Biol.* 338, 103–114. doi: 10.1016/j.jmb.2004.02.032

Magyar, K. (1994). Behaviour of (-)-deprenyl and its analogues. *J. Neural Transm. Suppl.* 41, 167–175. doi: 10.1007/978-3-7091-9324-2_23

Malcomson, T., Yelekci, K., Borrello, M. T., Ganesan, A., Semina, E., De Kimpe, N., et al. (2015). cis-Cyclopropylamines as mechanism-based inhibitors of monoamine oxidases. *FEBS J.* 282, 3190–3198. doi: 10.1111/febs.13260

Mantle, T. J., Tipton, K. F., and Garrett, N. J. (1976). Inhibition of monoamine oxidase by amphetamine and related compounds. *Biochem. Pharmacol.* 25, 2073–2077. doi: 10.1016/0006-2952(76)90432-9

Markou, A., Kosten, T. R., and Koob, G. F. (1998). Neurobiological similarities in depression and drug dependence: a self-medication hypothesis. *Neuropsychopharmacology* 18, 135–174. doi: 10.1016/S0893-133X(97)00113-9

Martin, T. L. (2001). Three cases of fatal paramethoxyamphetamine overdose. *J. Anal. Toxicol.* 25, 649–651. doi: 10.1093/jat/25.7.649

Matsumoto, T., Maeno, Y., Kato, H., Seko-Nakamura, Y., Monma-Ohtaki, J., Ishiba, A., et al. (2014). 5-Hydroxytryptamine- and dopamine-releasing effects of ring-substituted amphetamines on rat brain: a comparative study using *in vivo* microdialysis. *Eur. Neuropsychopharmacol.* 24, 1362–1370. doi: 10.1016/j.euroneuro.2014.04.009

Miller, J. R., and Edmondson, D. E. (1999). Structure-activity relationships in the oxidation of para-substituted benzylamine analogues by recombinant human liver monoamine oxidase A. *Biochemistry*38, 13670–13683. doi: 10.1021/bi990920y

Núñez-Vivanco, G., Fierro, A., Moya, P., Iturriaga-Vásquez, P., and Reyes-Parada, M. (2018). 3D similarities between the binding sites of monoaminergic target proteins. *PloS One* 13, e0200637. doi: 10.1371/journal.pone.0200637

Nandigama, R. K., Newton-Vinson, P., and Edmondson, D. E. (2002). Phentermine inhibition of recombinant human liver monoamine oxidases A, and B. *Biochem. Pharmacol.* 63, 865–869. doi: 10.1016/s0006-2952(02)00840-7

Nichols, D. E., Marona-Lewicka, D., Huang, X., and Johnson, M. P. (1993). Novel serotonergic agents. *Drug Des. Discov.* 9, 299–312.

Nichols, D. E. (1994). "Medicinal Chemistry and Structure-Activity Relationships," in *Amphetamine and Its Analogues: Psychopharmacology, Toxicology, and Abuse*. Eds. A. K. Cho and D. S. Segal (San Diego, CA: Academic Press), 3–41.

Nichols, D. E. (2018). Chemistry and Structure-Activity Relationships of Psychedelics. *Curr. Top. Behav. Neurosci.* 36, 1–43. doi: 10.1007/7854_2017_475

Norinder, U., Florvall, L., and Ross, S.B. (1994). A PLS quantitative structure-activity relationship study of some monoamine oxidase inhibitors of the phenyl alkylamine type. *Eur. J. Med. Chem.* 29, 191–195. doi: 10.1016/0223-5234(94)90037-X

Osorio-Olivares, M., Rezende, M. C., Sepúlveda-Boza, S., Cassels, B. K., and Fierro, A. (2004). MAO inhibition by arylisopropylamines: the effect of oxygen substituents at the beta-position. *Bioorg. Med. Chem.* 12, 4055–4066. doi: 10.1016/j.bmc.2004.05.033

Paillet-Loilier, M., Cesbron, A., Le Boisselier, R., Bourgine, J., and Debruyne, D. (2014). Emerging drugs of abuse: current perspectives on substituted cathinones. *Subst. Abuse Rehabil.* 5, 37–52. doi: 10.2147/SAR.S37257

Prinzmetal, M., and Bloomberg, W. (1935). The use of benzedrine for the treatment of narcolepsy. *J. Am. Med. Assoc.* 105, 2051–2054. doi: 10.1001/jama.1935.02760510023006

Reyes-Parada, M., Scorza, M. C., Silveira, R., Dajas, F., Costa, G., Tipton, K. F., et al. (1994a). Monoamine oxidase inhibitory effects of some 4-aminophenethylamine derivatives. *Biochem. Pharmacol.* 47, 1365–1371. doi: 10.1016/0006-2952(94)90335-2

Reyes-Parada, M., Scorza, M. C., Silveira, R., Dajas, F., and Cassels, B. K. (1994b). 4-Dimethylaminophenethylamine, a sensitive, specific, electrochemically detectable monoamine oxidase-B substrate. *Life Sci.* 54, 1955–1963. doi: 10.1016/0024-3205(94)90130-9

Reyes-Parada, M., Fierro, A., Iturriaga-Vásquez, P., and Cassels, B. K. (2005). Monoamine oxidase inhibition in the light of new structural data. *Curr. Enz. Inhib.* 1, 85–95. doi: 10.2174/1573408052952711

Robinson, J. B. (1985). Stereoselectivity and isoenzyme selectivity of monoamine oxidase inhibitors. Enantiomers of amphetamine, *N*-methylamphetamine and deprenyl. *Biochem. Pharmacol.* 34, 4105–4108. doi: 10.1016/0006-2952(85)90201-1

Rothman, R. B., and Baumann, M. H. (2003). Monoamine transporters and psychostimulant drugs. *Eur. J. Pharmacol.* 479, 23–40. doi: 10.1016/j.ejphar.2003.08.054

Rothman, R. B., Blough, B. E., Woolverton, W. L., Anderson, K. G., Negus, S. S., Mello, N. K., et al. (2005). Development of a rationally designed, low abuse potential, biogenic amine releaser that suppresses cocaine self-administration. *J. Pharmacol. Exp. Ther.* 313, 1361–1369. doi: 10.1124/jpet.104.082503

Rothman, R. B., Blough, B. E., and Baumann, M. H. (2007). Dual dopamine/serotonin releasers as potential medications for stimulant and alcohol addictions. *AAPS J.* 9, E1–E10. doi: 10.1208/aapsj0901001

Rothman, R. B., Blough, B. E., and Baumann, M. H. (2008). Dual dopamine/serotonin releasers: potential treatment agents for stimulant addiction. *Exp. Clin. Psychopharmacol.* 16, 458–474. doi: 10.1037/a0014103

Santillo, M. F. (2014). Inhibition of monoamine oxidase (MAO) by α-ethylphenethylamine and N,α-diethylphenethylamine, two compounds related to dietary supplements. *Food Chem. Toxicol.* 74, 265–269. doi: 10.1016/j.fct.2014.10.009

Scorza, M. C., Carrau, C., Silveira, R., Zapata-Torres, G., Cassels, B. K., and Reyes-Parada, M. (1997). Monoamine oxidase inhibitory properties of some methoxylated and alkylthio amphetamine derivatives: structure-activity relationships. *Biochem. Pharmacol.* 54, 1361–1369. doi: 10.1016/s0006-2952(97)00405-x

Scorza, C., Silveira, R., Nichols, D. E., and Reyes-Parada, M. (1999). Effects of 5-HT-releasing agents on the extracellular hippocampal 5-HT of rats. Implications for the development of novel antidepressants with a short onset of action. *Neuropharmacology*38, 1055–1061. doi: 10.1016/s0028-3908(99)00023-4

Shih, J. C., Chen, K., and Ridd, M. (1999). Monoamine oxidases: from genes to behavior. *Ann. Rev. Neurosci.* 22, 197–217. doi: 10.1146/annurev.neuro.22.1.197

Shulgin, A. T., and Shulgin, A. (1991). *Phenethylamines I Have Known And Loved* (Berkeley: Transform Press).

Simmler, L., Buser, T., Donzelli, M., Schramm, Y., Dieu, L. H., Huwyler, J., et al. (2013). Pharmacological characterization of designer cathinones *in vitro*. *Br. J. Pharmacol.* 168458–470. doi: 10.1111/j.1476-5381.2012.02145.x

Sitte, H. H., and Freissmuth, M. (2015). Amphetamines, new psychoactive drugs and the monoamine transporter cycle. *Trends Pharmacol. Sci.* 36, 41–50. doi: 10.1016/j.tips.2014.11.006

Son, S. Y., Ma, J., Kondou, Y., Yoshimura, M., Yamashita, E., and Tsukihara, T. (2008). Structure of human monoamine oxidase A at 2.2-Å resolution: the control of opening the entry for substrates/inhibitors. *Proc. Natl. Acad. Sci. U. S. A.* 105, 5739–5744. doi: 10.1073/pnas.0710626105

Sotomayor-Zárate, R., Quiroz, G., Araya, K. A., Abarca, J., Ibáñez, M. R., Montecinos, A., et al. (2012). 4-Methylthioamphetamine increases dopamine in the rat striatum and has rewarding effects *in vivo*. *Basic Clin. Pharmacol. Toxicol.* 111371–379. doi: 10.1111/j.1742-7843.2012.00926.x

Steuer, A. E., Boxler, M. I., Stock, L., and Kraemer, T. (2016). Inhibition potential of 3,4-methylenedioxymethamphetamine (MDMA) and its metabolites on the *in vitro* monoamine oxidase (MAO)-catalyzed deamination of the neurotransmitters serotonin and dopamine. *Toxicol. Lett.* 243, 48–55. doi: 10.1016/j.toxlet.2015.12.001

Sulzer, D., Sonders, M. S., Poulsen, N. W., and Galli, A. (2005). Mechanisms of neurotransmitter release by amphetamines: a review. *Prog. Neurobiol.* 75, 406–433. doi: 10.1016/j.pneurobio.2005.04.003

Tipton, K. F., Boyce, S., O'Sullivan, J., Davey, G. P., and Healy, J. (2004). Monoamine oxidases: certainties and uncertainties. *Curr. Med. Chem.* 11, 1965–1982. doi: 10.2174/0929867043364810

Tripathi, A. C., Upadhyay, S., Paliwal, S., and Saraf, S. K. (2018). Privileged scaffolds as MAO inhibitors: Retrospect and prospects. *Eur. J. Med. Chem.* 145, 445–497. doi: 10.1016/j.ejmech.2018.01.003

Ulus, I. H., Maher, T. J., and Wurtman, R. J. (2000). Characterization of phentermine and related compounds as monoamine oxidase (MAO) inhibitors. *Biochem. Pharmacol.* 59, 1611–1621. doi: 10.1016/s0006-2952(00)00306-3

Vallejos, G., Rezende, M. C., and Cassels, B. K. (2002). Charge-transfer interactions in the inhibition of MAO-A by phenylisopropylamines – a

QSAR study. *J. Comput. Aided Mol. Des.* 16, 95–103. doi: 10.1023/a:1016344030772

Vallejos, G., Fierro, A., Rezende, M. C., Sepúlveda-Boza, S., and Reyes-Parada, M. (2005). Heteroarylisopropylamines as MAO inhibitors. *Bioorg. Med. Chem.* 13, 4450–4457. doi: 10.1016/j.bmc.2005.04.045

Vianello, R., Domene, C., and Mavri, J. (2016). The use of multiscale molecular simulations in understanding a relationship between the structure and function of biological systems of the brain: the application to monoamine oxidase enzymes. *Front. Neurosci.* 10, 327. doi: 10.3389/fnins.2016.00327

Vilches-Herrera, M., Miranda-Sepúlveda, J., Rebolledo-Fuentes, M., Fierro, A., Lühr, S., Iturriaga-Vasquez, P., et al. (2009). Naphthylisopropylamine and N-benzylamphetamine derivatives as monoamine oxidase inhibitors. *Bioorg. Med. Chem.* 17, 2452–2460. doi: 10.1016/j.bmc.2009.01.074

Vilches-Herrera, M., Fierro, A., Lühr, S., Miranda-Sepúlveda, J., Iturriaga-Vasquez, P., Reyes-Parada, M., et al. (2016). Cycloalkylthiophenylisopropylamine derivatives are better monoamine oxidase inhibitors than their open chain analogues. *Rev. Farmacol. Chile.* 9, 39–42.

Wagmann, L., Brandt, S. D., Kavanagh, P. V., Maurer, H. H., and Meyer, M. R. (2017). In vitro monoamine oxidase inhibition potential of alpha-methyltryptamine analog new psychoactive substances for assessing possible toxic risks. *Toxicol. Lett.* 272, 84–93. doi: 10.1016/j.toxlet.2017.03.007

Welter-Luedeke, J., and Maurer, H. H. (2016). New Psychoactive Substances: Chemistry, Pharmacology, Metabolism, and Detectability of Amphetamine Derivatives With Modified Ring Systems. *Ther. Drug Monit.* 38, 4–11. doi: 10.1097/FTD.0000000000000240

Westlund, K. N., Denney, R. M., Rose, R. M., and Abell, C. W. (1988). Localization of distinct monoamine oxidase A and monoamine oxidase B cell populations in human brainstem. *Neuroscience*25, 439–456. doi: 10.1016/0306-4522(88)90250-3

Wouters, J. (1998). Structural aspects of monoamine oxidase and its reversible inhibition. *Curr. Med. Chem.* 5, 137–162.

Yoshida, S., Rosen, T. C., Meyer, O. G., Sloan, M. J., Ye, S., Haufe, G., et al. (2004). Fluorinated phenylcyclopropylamines. Part 3: Inhibition of monoamine oxidase A, and B. *Bioorg. Med. Chem.* 12, 2645–2652. doi: 10.1016/j.bmc.2004.03.010

Youdim, M. B. H., Edmondson, D., and Tipton, K. F. (2006). The therapeutic potential of monoamine oxidase inhibitors. *Nat. Rev. Neurosci.* 7, 295–309. doi: 10.1038/nrn1883

Yu, P. H., Bailey, B. A., Durden, D. A., and Boulton, A. A. (1986). Stereospecific deuterium substitution at the alpha-carbon position of dopamine and its effect on oxidative deamination catalyzed by MAO-A and MAO-B from different tissues. *Biochem. Pharmacol.* 35, 1027–1036. doi: 10.1016/0006-2952(86)90094-8

Yu, P. H., Davis, B. A., Boulton, A. A., and Zuo, D. M. (1994). Deamination of aliphatic amines by type B monoamine oxidase and semicarbazide-sensitive amine oxidase; pharmacological implications. *J. Neural Transm.* Suppl. 41, 397–406. doi: 10.1007/978-3-7091-9324-2_53

Yu, P. H., Davis, B. A., and Boulton, A. A. (1995). Aliphatic propargylamines, a new series of potent selective, irreversible non-amphetamine-like MAO-B inhibitors. Their structures, function and pharmacological implications. *Adv. Exp. Med. Biol.* 363, 17–23. doi: 10.1007/978-1-4615-1857-0_3

Yu, P. H. (1986). Inhibition of monoamine oxidase activity by phenylpropanolamine, an anorectic agent. *Res. Commun. Chem. Pathol. Pharmacol.* 51, 163–171.

Yu, P. H. (1988). Three types of stereospecificity and the kinetic deuterium isotope effect in the oxidative deamination of dopamine as catalyzed by different amine oxidases. *Biochem. Cell Biol.* 66, 853–861. doi: 10.1139/o88-097

Conflict of Interest: The authors declare that the research was conducted in the absence of any commercial or financial relationships that could be construed as a potential conflict of interest.

frontiers in Pharmacology

MINI REVIEW
published: 31 January 2020
doi: 10.3389/fphar.2019.01679

Exploring the Multi–Target Neuroprotective Chemical Space of Benzofuran Scaffolds: A New Strategy in Drug Development for Alzheimer's Disease

Jaime R. Cabrera-Pardo[1,2,3]*, *Jorge Fuentealba*[4]*, *Javiera Gavilán*[4], *Daniel Cajas*[2], *José Becerra*[2] and *Mariola Napiórkowska*[5]

[1] Departamento de Química, Facultad de Ciencias, Universidad del Bio-Bio, Concepción, Chile, [2] Departamento de Botánica, Facultad de Ciencias Naturales y Oceanográficas, Universidad de Concepción, Concepción, Chile, [3] Department of Chemistry, University of Utah, Salt Lake City, Utah, United States, [4] Departamento de Fisiología, Facultad de Ciencias Biológicas, Universidad de Concepción, Concepción, Chile, [5] Chair and Department of Biochemistry, Medical University of Warsaw, Warsaw, Poland

OPEN ACCESS

Edited by:
Ashok Kumar,
University of Florida,
United States

Reviewed by:
Aida Karachi,
University of Florida,
United States
Ranganath Keri,
Jain University, India
Luis Gandía,
Autonomous University of
Madrid, Spain

***Correspondence:**
Jaime R. Cabrera-Pardo
jacabrera@ubiobio.cl
Jorge Fuentealba
jorgefuentealba@udec.cl

Specialty section:
This article was submitted to Neuropharmacology, a section of the journal Frontiers in Pharmacology

Received: 19 August 2019
Accepted: 23 December 2019
Published: 31 January 2020

Citation:
Cabrera-Pardo JR, Fuentealba J, Gavilán J, Cajas D, Becerra J and Napiórkowska M (2020) Exploring the Multi–Target Neuroprotective Chemical Space of Benzofuran Scaffolds: A New Strategy in Drug Development for Alzheimer's Disease. Front. Pharmacol. 10:1679. doi: 10.3389/fphar.2019.01679

Alzheimer's disease (AD) is an irreversible and progressive neurodegenerative disorder that slowly destroys memory. The precise mechanism of AD is still not entirely understood and remains under discussion; it is believed to be a multifactorial disease in which a number of mechanisms are involved in its pathogenesis. Worldwide, near 37 million people suffer from the effects of AD. As a cause of death for elderly, it is predicted that AD will rank third in the coming years, just behind cancer and heart disease. Unfortunately, AD remains an incurable condition. Despite the devastating problems associated with AD, there are only four FDA approved drugs for palliative treatment of this pathology. Hence, renewed scientific efforts are required not only to uncover more insights into the AD process but also to develop more efficient pharmacological tools against this disease. Due to the complexity and multiple mechanisms at play in the progression of AD, the development of drugs by rational design is extremely difficult. The existing drugs to fight against Alzheimer's have had limited success, mainly due to their ability to modulate only one of the mechanisms involved in AD. As opposed to single-targeted strategies, the identification of small molecules able to affect multiple pathways involved in Alzheimer's is a promising strategy to develop more efficient medicines against this disease. Central to existing efforts to develop pharmaceuticals controlling AD is the discovery of new chemicals displaying strong neuroactivity. Benzofurans are privileged oxygen containing heterocycles that have a strong neuroprotective behavior, inhibiting several of the important events involved in the AD process. In this review, an approach is presented that relies on expanding the neuroprotective chemical space of benzofuran scaffolds by accessing them from Andean–Patagonian fungi and synthetic sources (chemical libraries). The exploration of the neuroprotective chemical space of these scaffolds has the potential to allow the discovery of substitution patterns that display multi-target neuroactivity

against multiple events involved in AD. This benzofuran chemical framework will establish a multi-target chemical space that could set the basis for the development of super drugs against AD.

Keywords: Alzheimer's disease, benzofuran, natural products, chemical libraries, Andean-Patagonian fungi

INTRODUCTION

Alzheimer's disease (AD), the most common cause of dementia, is a neurodegenerative disorder that affects areas of the cerebral cortex and hippocampus (Hane et al., 2017). Abnormalities, usually first detected in the frontal and temporal lobes, then slowly and unremittingly progress to other areas of the neocortex (Masters et al., 2015). The precise mechanism of AD is still not entirely understood and it is believed to be a multifactorial disease in which a number of mechanisms are involved in its pathogenesis (Robinson et al., 2017). Since the initial report identifying an amyloid protein in postmortem patients and the amyloid cascade hypothesis in the early 1990's, efforts to investigate AD have grown exponentially. Currently, studies regarding AD reach over 20,000 articles (Hane et al., 2017). While all these studies have certainly contributed to understanding AD, there is still a long path ahead and much to uncover in order to fully comprehend this multifactorial and devastating disease.

Improvements in medical care and life style have led to a substantial growth in the elderly population (Wimo et al., 2003). Due to increasing lifespans and the close association of AD with aging, this disease may become an intractable problem on a global scale in the near future. Worldwide, nearly 37 million people are currently affected by dementia and the majority is AD related (Wimo et al., 2003; Qiu et al., 2009). This figure is already increasing at a disturbing pace; around 6 million new cases of AD are diagnosed per year in the geriatric population. In 2013, nearly 85,000 deaths from AD were recorded, positioning AD as the sixth leading cause of death in the United States (Wimo et al., 2003; Qiu et al., 2009). Globally, costs related to AD treatment reached approximately US$315 billion back in 2005 (Qiu et al., 2009). These costs are expected to double by 2040 (Hurd et al., 2013).

Unfortunately, AD remains an incurable condition. Existing drugs approved by the U.S. Food and Drug Administration (FDA) against AD only ameliorate its symptoms. Despite the devastating problems associated with AD, there are only four FDA approved drugs for the treatment of this disorder (donepezil, galantamine, rivastigmine, and memantine). Shockingly, the pace of production of new drugs to control Alzheimer's is stagnating, without any new entity incorporated into the pharmacological arsenal during the last 15 years (Casey et al., 2010; Mullard, 2012; Becker et al., 2014; Cummings et al., 2017). Hence, scientific efforts are required not only to uncover more insights into the AD process but also to develop more efficient pharmaceuticals against this disease. Central to existing efforts to develop medicines controlling AD is the identification of chemical cores displaying strong neuroactivity (Aziz et al., 2014). Due to the complexity of the AD process, involving a number of different mechanisms, the development of drugs by rational design has proved cumbersome (Crews and Masliah, 2010). As opposed to single-targeted strategies, the identification of small molecules able to modulate multiple pathways involved in Alzheimer's can result in the development of more efficient medicines against this disease (Bajda et al., 2011; Leon et al., 2013; Dias et al., 2014; Prati et al., 2016; Unzeta et al., 2016). Thus, taking into consideration the chemical space that is relevant in biological systems, herein we present an approach for the identification and investigation of a region of this space with neuroprotective bioactivity, potentially leading to the discovery of molecules displaying a multi-target behavior. We envision that this could be achieved by taking advantage of the rich chemistry provided by natural and synthetic sources.

NEUROPROTECTIVE CHEMICAL SPACE

Organic molecules are defined by a number of variables including connectivity, type, number, and stereochemistry of the atoms described in the structural formula. Taking into account these descriptors, plus the molecular weight and fundamental laws of physical organic chemistry, there is a definable number of small organic molecules that can be synthesized. This is the chemical space, which is an important concept in cheminformatics, and refers to the set of all small organic molecules from natural or synthetic origins (Reymond, 2015). Some have estimated chemical space to reach beyond 10^{60}; a number that despite being finite, is preposterously high and inaccessible to explore by existing synthetic methods. The development of small molecules that control protein function is at the center of chemical biology research and the pharmaceutical industry. Crucial to the discovery of these important compounds is the identification of the biologically relevant chemical space, which is defined as the set of chemical cores that are required for biological systems to operate (Dobson, 2004; Koch et al., 2005; Reymond et al., 2010; Deng et al., 2013). For instance, the total number of small organic molecules present in the human body reaches a few thousand. As a consequence, the biologically relevant chemical space represents only a fraction of the total chemical space and is of great importance for the identification of molecules with interesting biological activity.

While the biologically relevant chemical space refers to the ensemble of small molecules crucial for biological systems to function, it is important to identify a subset of this space that

displays a given biological activity. In living organisms, the continuing evolution of biosynthetic routes has equipped natural products with scaffolds that act as modulators of biochemical pathways by effectively binding to proteins. Alternatively, in the laboratory, synthetic methodology has grown tremendously during the last century, allowing practitioners of medicinal chemistry to assemble biomimetic cores able to modulate biological systems. Taking into consideration these sources of bioactive molecules, the ensemble of compounds originating from both natural and synthetic origins displaying a particular biological effect is defined as the bioactive chemical space (Klenner et al., 2012; Von Salm et al., 2015; Zhang et al., 2015; Bajorath, 2016; Prati et al., 2016; Mei et al., 2017). As part of the drug development process, it is paramount to identify and explore this biologically active space since it narrows the universe of potentially active molecules, accelerating the pace of the discovery of new medicines. Thus, identifying and exploring parts of the biologically active chemical space with neurological effects could lead to the discovery of compounds displaying neuroprotective and multi-target bioactivities.

BENZOFURAN SCAFFOLDS ARE PROMISING TARGETS TO EXPLORE THE NEUROPROTECTIVE CHEMICAL SPACE

Benzofurans are privileged oxygen containing heterocycles that are present in a number of biologically important molecules. This class of chemical motifs have been shown to display antibacterial, antifungal, antioxidant, antitumoral, antiinflammatory, anticonvulsant, and anti-HIV bioactivities (Hiremathad et al., 2015; Khanam, 2015; Nevagi et al., 2015). Interestingly, benzofurans have also been found to have neuroprotective activity, inhibiting the important events involved in the AD process (Howlett et al., 1999; Allsop et al., 2001; Ono et al., 2002; Ono et al., 2006; Rizzo et al., 2008; Rizzo et al., 2012; Sashidhara et al., 2014; Ha et al., 2017; González-Ramírez et al., 2018; Kumar et al., 2018). Our research group has also investigated the role of natural fungal benzofurans in synaptic failure, decay of intracellular Ca^{2+} transients and synaptic disorganization (González-Ramírez et al., 2018). Although several factors are involved in the development of AD, it has been established that the production of toxic Aβ is crucial for the genesis of AD. Indeed, benzofuran scaffolds have been reported to play an important role as inhibitors of Aβ fibril formation (**Figure 1A**). Despite the promising neuroactivity displayed by benzofuran derivatives, their bioactivity still remains single-targeted in nature and a systematic study exploring the neuroprotective chemical space of these interesting heterocycles has not been carried out (González-Ramírez et al., 2018). This investigation is essential to find the chemical fundamentals that would provide the knowledge necessary to develop multi-target AD drugs based on benzofuran scaffolds. Existing reports show that the neuroprotective bioactivity of benzofuran derivatives falls into the μM range (Howlett et al., 1999; Allsop et al., 2001; Ono et al., 2002; Ono et al., 2006; Rizzo et al., 2008; Rizzo et al., 2012; Sashidhara et al., 2014; Ha et al., 2017; González-Ramírez et al., 2018). Thus, chemical probes containing benzofuran cores have yet to become approved drugs to control AD, mainly due to their modest potency. The lack of drug development could be attributed to the limited knowledge of protein-ligand interactions between benzofurans and important protein targets involved in AD progression (Howlett et al., 1999; Allsop et al., 2001; Kumar et al., 2018). In order to increase their efficacy, chemical transformation can be employed to tune their biological properties. Such chemical modifications could be achieved either by hemi-synthesis or total synthesis of natural benzofuran cores. In addition to blocking the Aβ fibril formation process, benzofuran compounds have proven to be efficient inhibitors of butyrylcholinesterase (Kumar et al., 2018), which is another important target for drug development to control AD. Given the importance of developing multitarget probes to control AD (Bajda et al., 2011; Leon et al., 2013; Prati et al., 2016; Unzeta et al., 2016), the dual activity displayed by benzofuran scaffolds against different mechanisms of AD make them worthwhile ligand targets for drug development. Thus, synthetic efforts in conjunction with the development of benzofuran based chemical libraries would provide the necessary collection of molecules to efficiently explore the multi-target neuroprotective chemical space of this scaffold, facilitating the discovery of effective pharmaceuticals against AD.

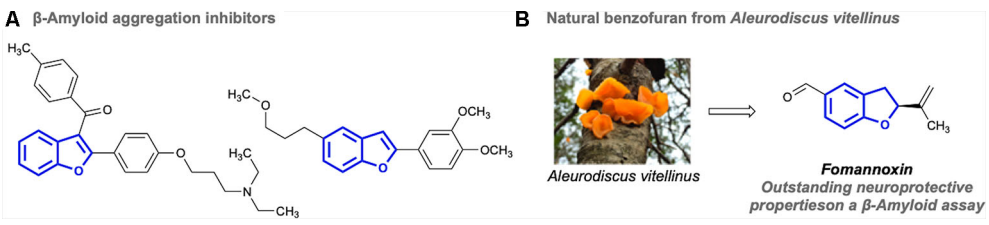

FIGURE 1 | Some benzofuran scaffolds with neuroprotective AD bioactivities. **(A)** Examples of synthetic benzofurans with inhibitory properties against beta-amyloid. **(B)** A natural benzofuran isolated from Aleurodiscus vitellinus.

Chemical libraries, which can be inspired by natural products or synthetic scaffolds, are collections of chemicals often used in high-throughput screening (Shelat and Guy, 2007; Grabowski et al., 2008; Quinn et al., 2008; Galloway et al., 2010; Gu et al., 2013; Saleeb et al., 2018). The development of chemical libraries relies on well-known and robust chemical transformations in which practitioners of organic chemistry can generate a number of variations on a defined molecular scaffold or backbone. In the drug discovery process, a range of small molecules are synthesized and tested against biological assays. Efficient screening requires the synthesis of chemical libraries covering a desired biologically relevant chemical space. More specifically, the development of a collection of molecules focused on a bioactive chemical space delivers a number of variations on pharmaceutically privileged scaffolds, accelerating the drug discovery process.

FUNGAL BENZOFURAN NATURAL PRODUCTS ARE A PROLIFIC SOURCE OF CHEMICAL PROBES TO EXPLORE THE NEUROPROTECTIVE CHEMICAL SPACE

Natural products display unique biological activities and are still the main source of medicines that propels the drug discovery field (Cragg and Newman, 2013; Newman and Cragg, 2016). Fungi represent one of the largest groups of organisms. They are widely distributed across mild and extreme ecosystems on our planet (Choi and Kim, 2017). In addition, these organisms are entirely heterotrophic as they are unable to perform photosynthesis. Consequently, they have developed a unique metabolic plasticity allowing them to rapidly adapt and survive through the biosynthesis of an array of fascinating natural products (Calvo et al., 2002). Recent analysis of fungal genomes has revealed a vast number of secondary metabolite pathways that can be tuned or modified, allowing the production of novel and useful chemical scaffolds (Nielsen et al., 2017). Fungi-derived natural products are pharmaceutically prolific, having been developed into a number of important biological applications ranging from highly potent toxins to approved drugs (Schueffler and Anke, 2014). Over the last decades, several natural products showing encouraging biological activities have been isolated from fungi. For example, in the course of the long–standing research program of natural product chemistry at the University of Concepcion (Chile), we have recently investigated the secondary metabolites of *Aleurodiscus vitellinus*, isolated from Chilean Patagonia (González-Ramírez et al., 2018). We discovered that fomannoxin, a natural benzofuran compound, showed outstanding neuroprotective properties according to an amyloid-β peptide model (**Figure 1B**). The importance of this finding lies in the fact that anti-amyloid therapies are considered to be a promising alternative to existing AD medicines. Considering that amyloid species, especially the oligomers, have been associated with early synaptic toxicity, controlling the aggregation process could represent an interesting approach to develop new pharmacological tools (Lal et al., 2007).

The multifactorial nature of AD requires treatment with molecules able to target multiple pathogenic events. The discovery of multi-target probes would enable the development of effective AD drugs that, to date, are not available. Given the promising potential of Andean-Patagonian fungi from our previous studies on *A. vitellinus*, the neuroprotective chemical space of benzofurans may be able to be effectively expanded by isolating more of these scaffolds from other fungi. This scientific exercise would potentially enable the discovery of fungal benzofurans displaying similar bioactivity as in our previous work: positive effects on neuronal functionality (González-Ramírez et al., 2018).

While the Andean-Patagonian ecosystem displays a high chemical and biological diversity, mycological studies in this environment have been limited mainly due to challenges in accessibility and extreme weather conditions (Gamundí, 2003). This ecosystem displays unique microclimate and terrain conditions promoting high levels of endemism (Cowling et al., 1994). Thus, investigating the chemical diversity of fungi from Andean-Patagonian environments could lead to the discovery of highly diverse benzofuran scaffolds, expanding the neuroprotective chemical space of this heterocycle from natural sources (Youdim et al., 2014, **Figure 2A**).

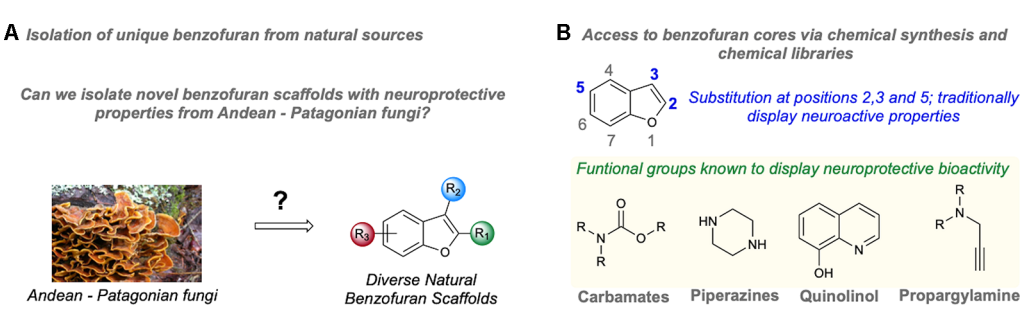

FIGURE 2 | Strategies to expand the neuroprotective chemical space of benzofurans. **(A)** Schematic for the isolation of benzofuran scaffolds from natural fungal sources. **(B)** Schematic of synthetic strategies to access benzofurans.

CHEMICAL LIBRARIES BASED ON BENZOFURAN SCAFFOLDS OFFER AN EFFICIENT PLATFORM TO INVESTIGATE THE NEUROPROTECTIVE CHEMICAL SPACE

Studies investigating the neuroprotective activity of synthetic benzofurans have shown that chemical substitution at positions 2, 3, and 5 on this heterocycle results in compounds displaying neuroactivity (Howlett et al., 1999; Allsop et al., 2001; Ono et al., 2002; Ono et al., 2006; Rizzo et al., 2008; Rizzo et al., 2012; Sashidhara et al., 2014; Ha et al., 2017; González-Ramírez et al., 2018). Despite the ability of benzofuran cores to control important events in AD development, structure-activity relation studies on neuroprotection are limited (Wakabayashi et al., 2016), making the drug development process to control AD lengthy and cumbersome. To our knowledge, a systematic chemical study exploring the neuroprotective chemical space of benzofurans has not been carried out. In the development of other chemicals as treatments for neurological diseases, several chemical functionalities have been described that display strong neuroprotective behavior (**Figure 2B**). For instance, carbamates are the main player responsible for the bioactivity of rivastigmine, which is an acetylcholinesterase inhibitor used for the treatment of Alzheimer's and Parkinson's disease (Youdim et al., 2014). Piperazines have also displayed a range of biological activities including neuroprotective effects (Varadaraju et al., 2013; Modi et al., 2014; Wang et al., 2016). The quinolinol moiety is a strong radical scavenger present in Tacrine, the first drug approved for the treatment of AD (FernáNdez-Bachiller et al., 2010). Propargylamines are also neuroprotective functional groups by inhibiting MAO (Gal et al., 2005; Zheng et al., 2005). Thus, an interesting strategy would be the preparation of benzofuran hybrids containing the neuroactive functional groups identified in these studies, hoping to obtain benzofurans displaying positive synergistic effects on neuroprotective multi-target biological assays. This represents a rational strategy to achieve compounds displaying multi-target neuroprotective activity because it combines a neuroactive core linked to neuroactive functional groups, increasing the chances to access single molecules modulating multiple factors responsible for AD.

MAIN MECHANISMS INVOLVED IN ALZHEIMER'S DISEASE: TARGET TO DEVELOP MULTITARGET CHEMICAL PROBES

Approved FDA drugs to control AD are often ineffective since they target only one of the many possible routes that cause Alzheimer's. Classic single-target chemical probes include: Acetylcholinesterase (AChase) (i.e. galantamine from *galantus sp*), NMDA receptors (memantine), oxidative stress (polyphenols: reseveratrol, catequins, antocianidins, etc), modulators of neuronal Acetylcholine receptors (nAChR, quinolizidinc alkaloids), or molecules that can interfere with the main event involved in the pathogenesis of disease, the amyloid β-peptide (βA) (Sala Frigerio and De Strooper, 2016; Cummings et al., 2017; Sharma et al., 2018). Moreover, during the last 15 years, no new drugs have been approved by the FDA for AD (Casey et al., 2010; Mullard, 2012; Becker et al., 2014; Cummings et al., 2017). Taking into consideration the stagnating production of therapeutics to control AD, the development of new targets against this disease is a valuable scientific niche that ought to be explored. It is important to note that chemicals developed to control targets for AD should reach promising levels of neuroprotective bioactivities so that they stand a chance to reach clinical use. Thus, new approaches to drug design are imperative, and the development of chemical probes capable of simultaneously targeting multiple mechanisms leading to AD is a highly promising route to effectively control this devastating disease. Several molecular mechanisms can be responsible for AD (Leon et al., 2013): deposition and aggregation of β-amyloid (oligomers and plaques); oxidative stress; cholinergic impairment; deregulation of calcium metabolism and metal dys-homeostasis; neuroinflammation; mitochondrial damage and hyperphosphorylated and β-folded tau proteins. Therefore, the development of chemical probes able to target multiple mechanisms involved in Alzheimer´s disease represents a distinct strategy to control this devastating disease.

CONCLUSION

AD is a condition that still demands extensive efforts to understand its pathogenesis. Despite its devastating nature, AD is not curable and its symptoms can only be partially treated. Hence, the development of efficient pharmaceuticals against AD is in urgent need. The mode of action of existing FDA drugs relies on controlling single mechanisms of this pathology. While single-targeted approaches have been effective in certain pathologies, overall the use of this strategy to tackle multifactorial disease such as AD renders poor outcomes. For this reason, the development of drugs to control AD has stalled over the last decade. Current efforts to produce AD medicines have shifted towards the development of agents with multi-target activity in order to produce more effective pharmaceuticals. However, the generation of therapeutics that combine the biological effects of different AD drugs in a super molecule, modulating multiple events responsible for Alzheimer's is extremely difficult. Nevertheless, benzofurans are heterocycles with promising neuroactive properties. We suggest that one promising approach is to expand the neuroprotective chemical space of benzofuran scaffolds by accessing these molecules from Andean–Patagonian fungi and synthetic sources. Exploring the neuroprotective chemical space of benzofuran scaffolds represents a distinct venue that could lead to the discovery of new substitution patterns displaying multi-target neuroactivity against multiple events involved in AD. This benzofuran chemical framework can establish a multi-target chemical

space, setting the basis for the development of super drugs against AD.

AUTHOR CONTRIBUTIONS

JC-P conceived, designed and wrote the manuscript. JF and JG provided useful suggestions regarding the neuroprotective assays. DC and JB participated in the mycology aspect of the manuscript. MN gave input on the chemistry aspect of benzofurans.

FUNDING

JC-P was kindly supported by FONDECYT regular 1190652. JF acknowledges the support of FONDECYT regular 1161078.

ACKNOWLEDGMENTS

We thank Dr. Ellen Leffler for the critical reading of our manuscript.

REFERENCES

Allsop, D., Gibson, G., Martin, I. K., Moore, S., Turnbull, S., and Twyman, L. J. (2001). 3-p-toluoyl-2-[4'-(3-diethylaminopropoxy)-phenyl]-benzofuran and 2-[4'-(3-diethylaminopropoxy)-phenyl]-benzofuran do not act as surfactants or micelles when inhibiting the aggregation of ß-amyloid peptide. *Bioorg. Med. Chem. Lett.* 11, 255–257. doi: 10.1016/S0960-894X(00)00645-4

Aziz, O., Bürli, R. W., Fischer, D. F., Frearson, J., and Wall, M. D. (2014). "Towards small molecules as therapies for alzheimer's disease and other neurodegenerative disorders," in *Drug Design and Discovery in Alzheimer's Disease*, 4, 199–290. (Elsevier). doi: 10.1016/B978-0-12-803959-5.50004-0

Bajda, M., Guzior, N., Ignasik, M., and Malawska, B. (2011). Multi-target-directed ligands in Alzheimer's disease treatment. *Curr. Med. Chem.* 18, 4949–4975. doi: 10.2174/092986711797535245

Bajorath, J. (2016). Extending accessible chemical space for the identification of novel leads. *Expert Opin. Drug Discov.* 11, 825–829. doi: 10.1080/17460441.2016.1210126

Becker, R. E., Greig, N. H., Giacobini, E., Schneider, L. S., and Ferrucci, L. (2014). A new roadmap for drug development for Alzheimer's disease. *Nat. Rev. Drug Discovery* 13, 156. doi: 10.1038/nrd3842-c2

Calvo, A. M., Wilson, R. A., Bok, J. W., and Keller, N. P. (2002). Relationship between secondary metabolism and fungal development. *Microbiol. Mol. Biol. Rev.* 66, 447–459. doi: 10.1128/MMBR.66.3.447-459.2002

Casey, D. A., Antimisiaris, D., and O'brien, J. (2010). Drugs for Alzheimer's disease: are they effective? *Pharm. Ther.* 35, 208.

Choi, J., and Kim, S.-H. (2017). A genome tree of life for the fungi kingdom. *Proc. Nat. Acad. Sci.* 114, 9391–9396. doi: 10.1073/pnas.1711939114

Cowling, R., Witkowski, E., Milewski, A., and Newbey, K. (1994). Taxonomic, edaphic and biological aspects of narrow plant endemism on matched sites in mediterranean South Africa and Australia. *J. Biogeogr.* 21, 651–664. doi: 10.2307/2846038

Cragg, G. M., and Newman, D. J. (2013). Natural products: a continuing source of novel drug leads. *Biochim. Biophys. Acta (BBA)-General Subj.* 1830, 3670–3695. doi: 10.1016/j.bbagen.2013.02.008

Crews, L., and Masliah, E. (2010). Molecular mechanisms of neurodegeneration in Alzheimer's disease. *Hum. Mol. Genet.* 19, R12–R20. doi: 10.1093/hmg/ddq160

Cummings, J., Lee, G., Mortsdorf, T., Ritter, A., and Zhong, K. (2017). Alzheimer's disease drug development pipeline: 2017. *Alzheimer's Dementia: Transl. Res. Clin. Interventions* 3, 367–384. doi: 10.1016/j.trci.2017.05.002

Deng, Z.-L., Du, C.-X., Li, X., Hu, B., Kuang, Z.-K., Wang, R., et al. (2013). Exploring the biologically relevant chemical space for drug discovery. *J. Chem. Inf. Model.* 53, 2820–2828. doi: 10.1021/ci400432a

Dias, I. H., Polidori, M. C., Li, L., Weber, D., Stahl, W., Nelles, G., et al. (2014). Plasma levels of HDL and carotenoids are lower in dementia patients with vascular comorbidities. *J. Alzheimer's Dis.* 40, 399–408. doi: 10.3233/JAD-131964

Dobson, C. M. (2004). Chemical space and biology. *Nature* 432, 824–828. doi: 10.1038/nature03192

Ferna´Ndez-Bachiller, M.a.I., Pérez, C., González-Munoz, G. C., Conde, S., López, M. G., Villarroya, M., et al. (2010). Novel tacrine– 8-hydroxyquinoline hybrids as multifunctional agents for the treatment of Alzheimer's disease, with neuroprotective, cholinergic, antioxidant, and copper-complexing properties. *J. Med. Chem.* 53, 4927–4937. doi: 10.1021/jm100329q

Gal, S., Zheng, H., Fridkin, M., and Youdim, M. B. (2005). Novel multifunctional neuroprotective iron chelator-monoamine oxidase inhibitor drugs for neurodegenerative diseases. in vivo selective brain monoamine oxidase inhibition and prevention of MPTP-induced striatal dopamine depletion. *J. Neurochem.* 95, 79–88. doi: 10.1111/j.1471-4159.2005.03341.x

Galloway, W. R., Isidro-Llobet, A., and Spring, D. R. (2010). Diversity-oriented synthesis as a tool for the discovery of novel biologically active small molecules. *Nat. Commun.* 1, 80. doi: 10.1038/ncomms1081

Gamundí, I. J. (2003). Discomycetes (Fungi, Ascomycota) de Chile Austral. *I. Darwiniana* 41, 29–36.

González-Ramírez, M., Gavilán, J., Silva-Grecchi, T., Cajas-Madriaga, D., Triviño, S., Becerra, J., et al. (2018). A natural benzofuran from the patagonic aleurodiscus vitellinus fungus has potent neuroprotective properties on a cellular model of amyloid-ß peptide toxicity. *J. Alzheimer's Dis.* 61, 1463–1475. doi: 10.3233/JAD-170958

Grabowski, K., Baringhaus, K.-H., and Schneider, G. (2008). Scaffold diversity of natural products: inspiration for combinatorial library design. *Nat. Prod. Rep.* 25, 892–904. doi: 10.1039/b715668p

Gu, J., Gui, Y., Chen, L., Yuan, G., Lu, H.-Z., and Xu, X. (2013). Use of natural products as chemical library for drug discovery and network pharmacology. *PloS one* 8, e62839. doi: 10.1371/journal.pone.0062839

Ha, H.-J., Kang, D. W., Kim, H.-M., Kang, J.-M., Ann, J., Hyun, H. J., et al. (2017). Discovery of an orally bioavailable benzofuran analogue that serves as a ß-amyloid aggregation inhibitor for the potential treatment of Alzheimer's disease. *J. Med. Chem.* 61, 396–402. doi: 10.1021/acs.jmedchem.7b00844

Hane, F. T., Lee, B. Y., and Leonenko, Z. (2017). Recent progress in Alzheimer's disease research, part 1: Pathology. *J. Alzheimer's Dis.* 57, 1–28. doi: 10.3233/JAD-160882

Hiremathad, A., Patil, M. R., Chethana, K., Chand, K., Santos, M. A., and Keri, R. S. (2015). Benzofuran: an emerging scaffold for antimicrobial agents. *RSC Adv.* 5, 96809–96828. doi: 10.1039/C5RA20658H

Howlett, D. R., Perry, A. E., Godfrey, F., Swatton, J. E., Jennings, K. H., Spitzfaden, C., et al. (1999). Inhibition of fibril formation in beta-amyloid peptide by a novel series of benzofurans. *Biochem. J.* 340, 283. doi: 10.1042/bj3400283

Hurd, M. D., Martorell, P., Delavande, A., Mullen, K. J., and Langa, K. M. (2013). Monetary costs of dementia in the United States. *New Engl. J. Med.* 368, 1326–1334. doi: 10.1056/NEJMsa1204629

Khanam, H. (2015). Bioactive Benzofuran derivatives: a review. *Eur. J. Med. Chem.* 97, 483–504. doi: 10.1016/j.ejmech.2014.11.039

Klenner, A., Hähnke, V., Geppert, T., Schneider, P., Zettl, H., Haller, S., et al. (2012). From virtual screening to bioactive compounds by visualizing and clustering of chemical space. *Mol. Inf.* 31, 21. doi: 10.1002/minf.201100147

Koch, M. A., Schuffenhauer, A., Scheck, M., Wetzel, S., Casaulta, M., Odermatt, A., et al. (2005). Charting biologically relevant chemical space: a structural classification of natural products (SCONP). *Proc. Nat. Acad. Sci.* 102, 17272–17277. doi: 10.1073/pnas.0503647102

Kumar, A., Pintus, F., Di Petrillo, A., Medda, R., Caria, P., Matos, M. J., et al. (2018). Novel 2-pheynlbenzofuran derivatives as selective butyrylcholinesterase inhibitors for Alzheimer's disease. *Sci. Rep.* 8, 4424. doi: 10.1038/s41598-018-22747-2

Lal, R., Lin, H., and Quist, A. P. (2007). Amyloid beta ion channel: 3D structure and relevance to amyloid channel paradigm. *Biochim. Biophys. Acta (BBA)-Biomembranes* 1768, 1966–1975. doi: 10.1016/j.bbamem.2007.04.021

Leon, R., Garcia, A. G., and Marco-Contelles, J. (2013). Recent advances in the multitarget-directed ligands approach for the treatment of Alzheimer's disease. *Med. Res. Rev.* 33, 139–189. doi: 10.1002/med.20248

Masters, C. L., Bateman, R., Blennow, K., Rowe, C. C., Sperling, R. A., and Cummings, J. L. (2015). Alzheimer's disease. *Nat. Rev. Dis. Primers* 1, 15056. doi: 10.1038/nrdp.2015.56

Mei, X., Yan, X., Zhang, H., Yu, M., Shen, G., Zhou, L., et al. (2017). Expanding the bioactive chemical space of anthrabenzoxocinones through engineering the highly promiscuous biosynthetic modification steps. *ACS Chem. Biol.* 13, 200–206. doi: 10.1021/acschembio.7b00743

Modi, G., Antonio, T., Reith, M., and Dutta, A. (2014). Structural Modifications of Neuroprotective Anti-Parkinsonian (–)-N 6-(2-(4-(Biphenyl-4-yl) piperazin-1-yl)-ethyl)-N 6-propyl-4, 5, 6, 7-tetrahydrobenzo [d] thiazole-2, 6-diamine (D-264): An Effort toward the Improvement of in vivo efficacy of the parent molecule. *J. Med. Chem.* 57, 1557–1572. doi: 10.1021/jm401883v

Mullard, A. (2012). Sting of Alzheimer's failures offset by upcoming prevention trials. *Nat. Rev. Drug. Discov.* 11, 657–660. doi: 10.1038/nrd3842

Nevagi, R. J., Dighe, S. N., and Dighe, S. N. (2015). Biological and medicinal significance of benzofuran. *Eur. J. Med. Chem.* 97, 561–581. doi: 10.1016/j.ejmech.2014.10.085

Newman, D. J., and Cragg, G. M. (2016). Natural products as sources of new drugs from 1981 to 2014. *J. Nat. Prod.* 79, 629–661. doi: 10.1021/acs.jnatprod.5b01055

Nielsen, J. C., Grijseels, S., Prigent, S., Ji, B., Dainat, J., Nielsen, K. F., et al. (2017). Global analysis of biosynthetic gene clusters reveals vast potential of secondary metabolite production in Penicillium species. *Nat. Microbiol.* 2, 17044. doi: 10.1038/nmicrobiol.2017.44

Ono, M., Kung, M.-P., Hou, C., and Kung, H. F. (2002). Benzofuran derivatives as Aß-aggregate-specific imaging agents for Alzheimer's disease. *Nucl. Med. Biol.* 29, 633–642. doi: 10.1016/S0969-8051(02)00326-8

Ono, M., Kawashima, H., Nonaka, A., Kawai, T., Haratake, M., Mori, H., et al. (2006). Novel benzofuran derivatives for PET imaging of ß-amyloid plaques in Alzheimer's disease brains. *J. Med. Chem.* 49, 2725–2730. doi: 10.1021/jm051176k

Prati, F., Cavalli, A., and Bolognesi, M. L. (2016). Navigating the chemical space of multitarget-directed ligands: from hybrids to fragments in Alzheimer's disease. *Molecules* 21, 466. doi: 10.3390/molecules21040466

Qiu, C., Kivipelto, M., and Von Strauss, E. (2009). Epidemiology of Alzheimer's disease: occurrence, determinants, and strategies toward intervention. *Dialogues Clin. Neurosci.* 11, 111.

Quinn, R. J., Carroll, A. R., Pham, N. B., Baron, P., Palframan, M. E., Suraweera, L., et al. (2008). Developing a drug-like natural product library. *J. Nat. Prod.* 71, 464–468. doi: 10.1021/np070526y

Reymond, J.-L., Van Deursen, R., Blum, L. C., and Ruddigkeit, L. (2010). Chemical space as a source for new drugs. *MedChemComm* 1, 30–38. doi: 10.1039/c0md00020e

Reymond, J.-L. (2015). The chemical space project. *Accounts Chem. Res.* 48, 722–730. doi: 10.1021/ar500432k

Rizzo, S., Rivie`Re, C. L., Piazzi, L., Bisi, A., Gobbi, S., Bartolini, M., et al. (2008). Benzofuran-based hybrid compounds for the inhibition of cholinesterase activity, ß amyloid aggregation, and Aß neurotoxicity. *J. Med. Chem.* 51, 2883–2886. doi: 10.1021/jm8002747

Rizzo, S., Tarozzi, A., Bartolini, M., Da Costa, G., Bisi, A., Gobbi, S., et al. (2012). 2-Arylbenzofuran-based molecules as multipotent Alzheimer's disease modifying agents. *Eur. J. Med. Chem.* 58, 519–532. doi: 10.1016/j.ejmech.2012.10.045

Robinson, M., Lee, B. Y., and Hane, F. T. (2017). Recent progress in Alzheimer's disease research, part 2: genetics and epidemiology. *J. Alzheimer's Dis.* 57, 317–330. doi: 10.3233/JAD-161149

Sala Frigerio, C., and De Strooper, B. (2016). Alzheimer's disease mechanisms and emerging roads to novel therapeutics. *Ann. Rev. Neurosci.* 39, 57–79. doi: 10.1146/annurev-neuro-070815-014015

Saleeb, M., Mojica, S., Eriksson, A. U., Andersson, C. D., Gylfe, Å., and Elofsson, M. (2018). Natural product inspired library synthesis-Identification of 2, 3-diarylbenzofuran and 2, 3-dihydrobenzofuran based inhibitors of Chlamydia trachomatis. *Eur. J. Med. Chem.* 143, 1077–1089. doi: 10.1016/j.ejmech.2017.11.099

Sashidhara, K. V., Modukuri, R. K., Jadiya, P., Dodda, R. P., Kumar, M., Sridhar, B., et al. (2014). Benzofuran–chalcone hybrids as potential multifunctional agents against Alzheimer's disease: Synthesis and *in vivo* studies with transgenic Caenorhabditis elegans. *ChemMedChem* 9, 2671–2684. doi: 10.1002/cmdc.201402291

Schueffler, A., and Anke, T. (2014). Fungal natural products in research and development. *Nat. Prod. Rep.* 31, 1425–1448. doi: 10.1039/C4NP00060A

Sharma, P., Srivastava, P., Seth, A., Tripathi, P. N., Banerjee, A. G., and Shrivastava, S. K. (2018). Comprehensive review of mechanisms of pathogenesis involved in Alzheimer's disease and potential therapeutic strategies. *Prog. Neurobiol.* 174, 53–89. doi: 10.1016/j.pneurobio.2018.12.006

Shelat, A. A., and Guy, R. K. (2007). Scaffold composition and biological relevance of screening libraries. *Nat. Chem. Biol.* 3, 442. doi: 10.1038/nchembio0807-442

Unzeta, M., Esteban, G., Bolea, I., Fogel, W. A., Ramsay, R. R., Youdim, M. B., et al. (2016). Multi-target directed donepezil-like ligands for Alzheimer's disease. *Front. Neurosci.* 10, 205. doi: 10.3389/fnins.2016.00205

Varadaraju, K. R., Kumar, J. R., Mallesha, L., Muruli, A., Mohana, K. N. S., Mukunda, C. K., et al. (2013). Virtual screening and biological evaluation of piperazine derivatives as human acetylcholinesterase inhibitors. *Int. J. Alzheimer's Dis.* 2, 653962. doi: 10.1155/2013/653962

Von Salm, J., Santiago, D., Wilson, N., Calcul, L., Kyle, D., Guida, W., et al. (2015). Targeting bioactive chemical space with a small natural products library: Expanding diversity and predictability. *Planta Med.* 81, CL11. doi: 10.1055/s-0035-1556174

Wakabayashi, T., Tokunaga, N., Tokumaru, K., Ohra, T., Koyama, N., Hayashi, S., et al. (2016). Discovery of benzofuran derivatives that collaborate with insulin-like growth factor 1 (IGF-1) to promote neuroprotection. *J. Med. Chem.* 59, 5109–5114. doi: 10.1021/acs.jmedchem.6b00191

Wang, W.-Y., Shen, C.-W., Weng, Z.-J., Wang, T.-C., Zhang, C., Jin, X.-Q., et al. (2016). Design, synthesis and biological evaluation of novel dicarbonylalkyl piperazine derivatives as neuroprotective agents. *Chin. Chem. Lett.* 27, 387–390. doi: 10.1016/j.cclet.2015.11.002

Wimo, A., Winblad, B., Aguero-Torres, H., and Von Strauss, E. (2003). The magnitude of dementia occurrence in the world. *Alzheimer Dis. Associated Disord.* 17, 63–67. doi: 10.1097/00002093-200304000-00002

Youdim, M. B., Kupershmidt, L., Amit, T., and Weinreb, O. (2014). Promises of novel multi-target neuroprotective and neurorestorative drugs for Parkinson's disease. *Parkinsonism Related Disord.* 20, S132–S136. doi: 10.1016/S1353-8020(13)70032-4

Zhang, B., Vogt, M., Maggiora, G. M., and Bajorath, J. (2015). Comparison of bioactive chemical space networks generated using substructure-and fingerprint-based measures of molecular similarity. *J. Comput-aided Mol. Des.* 29, 595–608. doi: 10.1007/s10822-015-9872-1

Zheng, H., Gal, S., Weiner, L. M., Bar-Am, O., Warshawsky, A., Fridkin, M., et al. (2005). Novel multifunctional neuroprotective iron chelator-monoamine oxidase inhibitor drugs for neurodegenerative diseases: *in vitro* studies on antioxidant activity, prevention of lipid peroxide formation and monoamine oxidase inhibition. *J. Neurochem.* 95, 68–78. doi: 10.1111/j.1471-4159.2005.03340.x

Conflict of Interest: The authors declare that the research was conducted in the absence of any commercial or financial relationships that could be construed as a potential conflict of interest.

frontiers in Pharmacology

REVIEW
published: 18 February 2020
doi: 10.3389/fphar.2020.00057

Crosstalk Between Kappa Opioid and Dopamine Systems in Compulsive Behaviors

Angélica del Pilar Escobar[1], *José Patricio Casanova*[2,3], *María Estela Andrés*[4] *and José Antonio Fuentealba*[5*†]

[1] Centro Interdisciplinario de Neurociencias de Valparaíso, Faculty of Sciences, Universidad de Valparaíso, Valparaíso, Chile, [2] Departamento de Neurociencia, Facultad de Medicina, Universidad de Chile, Santiago, Chile, [3] Núcleo Milenio NUMIND Biology of Neuropsychiatric Disorders, Universidad de Valparaíso, Valparaíso, Chile, [4] Department of Cellular and Molecular Biology, Faculty of Biological Sciences, Pontificia Universidad Católica de Chile, Santiago, Chile, [5] Department of Pharmacy and Interdisciplinary Center of Neuroscience, Faculty of Chemistry, Pontificia Universidad Católica de Chile, Santiago, Chile

OPEN ACCESS

Edited by:
Gonzalo E. Yevenes, University of Concepcion, Chile

Reviewed by:
Luis Gerardo Aguayo, University of Concepcion, Chile
Hugo Tejeda, National Institute on Drug Abuse (NIDA), United States
Cecilia Scorza, Instituto de Investigaciones Biológicas Clemente Estable (IIBCE), Uruguay

***Correspondence:**
José Antonio Fuentealba
jfuentea@uc.cl

†ORCID:
José Antonio Fuentealba
orcid.org/0000-0003-0775-0675

Specialty section:
This article was submitted to Translational Pharmacology, a section of the journal Frontiers in Pharmacology

Received: 16 October 2019
Accepted: 22 January 2020
Published: 18 February 2020

Citation:
Escobar AdP, Casanova JP, Andrés ME and Fuentealba JA (2020) Crosstalk Between Kappa Opioid and Dopamine Systems in Compulsive Behaviors. Front. Pharmacol. 11:57. doi: 10.3389/fphar.2020.00057

The strength of goal-oriented behaviors is regulated by midbrain dopamine neurons. Dysfunctions of dopaminergic circuits are observed in drug addiction and obsessive-compulsive disorder. Compulsive behavior is a feature that both disorders share, which is associated to a heightened dopamine neurotransmission. The activity of midbrain dopamine neurons is principally regulated by the homeostatic action of dopamine through D2 receptors (D2R) that decrease the firing of neurons as well as dopamine synthesis and release. Dopamine transmission is also regulated by heterologous neurotransmitter systems such as the kappa opioid system, among others. Much of our current knowledge of the kappa opioid system and its influence on dopamine transmission comes from preclinical animal models of brain diseases. In 1988, using cerebral microdialysis, it was shown that the acute activation of the Kappa Opioid Receptors (KOR) decreases synaptic levels of dopamine in the striatum. This inhibitory effect of KOR opposes to the facilitating influence of drugs of abuse on dopamine release, leading to the proposition of the use of KOR agonists as pharmacological therapy for compulsive drug intake. Surprisingly, 30 years later, KOR antagonists are instead proposed to treat drug addiction. What may have happened during these years that generated this drastic change of paradigm? The collected evidence suggested that the effect of KOR on synaptic dopamine levels is complex, depending on the frequency of KOR activation and timing with other incoming stimuli to dopamine neurons, as well as sex and species differences. Conversely to its acute effect, chronic KOR activation seems to facilitate dopamine neurotransmission and dopamine-mediated behaviors. The opposing actions exerted by acute versus chronic KOR activation have been associated with an initial aversive and a delayed rewarding effect, during the exposure to drugs of abuse. Compulsive behaviors induced by repeated activation of D2R are also potentiated by the sustained co-activation of KOR, which correlates with decreased synaptic levels of

dopamine and sensitized D2R. Thus, the time-dependent activation of KOR impacts directly on dopamine levels affecting the tuning of motivated behaviors. This review analyzes the contribution of the kappa opioid system to the dopaminergic correlates of compulsive behaviors.

Keywords: kappa opioid receptor, dopamine, compulsivity, amphetamine, quinpirole, locomotor sensitization

INTRODUCTION

Dopaminergic System in Compulsive Behaviors

Compulsion is the impossibility of self-stopping to execute a habitual action with known outcome, despite adverse consequences (Robbins et al., 2012). Compulsive behaviors are hallmarks of obsessive-compulsive disorder (OCD) and drug addiction, among other psychiatric diseases. Checking behavior is very common in obsessive-compulsive spectrum disorders being characterized by the constant repetition of a certain routine, in a stereotyped or ritualistic way (Williams et al., 2013). A wide range of normal behaviors (e.g., checking, cleaning, hands washing, etc.) can turn into compulsive in OCD patients and in general, arises in response to obsessive and distressing thoughts inducing anxiety. Similarly, seeking and consuming drugs of abuse become compulsive in drug addicts As in OCD, anxiety plays a key role triggering compulsive drug consumption in experienced drug abusers. The same impairments in reward and punishment processing are observed in both conditions (Figee et al., 2016), which has led some authors to discuss OCD as a behavioral addiction (Holden, 2001).

One possible mechanism leading to compulsive behavior is framed within the incentive-sensitization theory of addiction which is that an amplified motivation ("wanting") for the drug develops during addiction without developing an amplified pleasurable ("liking") effect (Berridge et al., 1989; Berridge and Robinson, 2016). Enduring sensitization of the reward/motivation circuit is involved in the induction of incentive-sensitization associated to drug seeking. The reward/motivation circuit is composed of midbrain dopamine neurons of the *substantia nigra* (SN) and ventral tegmental area (VTA), which target the dorsal and ventral tiers of the striatum, respectively. Dopamine neurons that project to the ventral striatum or nucleus accumbens (NAc) have been traditionally related to goal-oriented behaviors, whereas dopamine neurons that project to the dorsal striatum have been associated with habits acquisition (Everitt and Robbins, 2005; Wise, 2009; Yager et al., 2015; Volkow et al., 2017).

Sensitization of the reward/motivation circuit is observed in rodents as the gradual increase in locomotor activity induced by repeated administration of a potentially addictive drug fixed dose (Pierce and Kalivas, 1997; Robinson and Berridge, 2001). Locomotor sensitization is an endurable phenomenon as it is observable after weeks, months and even a year after drug withdrawal (Robinson and Berridge, 1993). It was early suggested that sensitization of the reward/motivation circuit contributes to the compulsive drug seeking (Robinson and Berridge, 1993). Accordingly, locomotor sensitization facilitates self-administration cocaine seeking reinstatement (De Vries et al., 2002). Moreover, rats with extended access to cocaine self-administration show greater locomotor response to cocaine than rats with limited access (Ferrario et al., 2005). In addition, the neurochemical changes underlying locomotor sensitization to psychostimulants are also observed in compulsive drug seeking (Steketee and Kalivas, 2011; Giuliano et al., 2019). These data support the early proposed correspondence between locomotor sensitization and compulsive drug seeking observed in humans (Robinson and Berridge, 1993; Vanderschuren and Kalivas, 2000). Mechanistically, repeated administration of drugs of abuse sensitizes mesolimbic dopamine circuits increasing dopaminergic neurotransmission. Psychostimulants, like cocaine or amphetamines, that block the plasma membrane dopamine transporter (DAT), induce a large increase of dopamine in the synaptic space in the striatum and NAc, thus activating locomotion (Steketee and Kalivas, 2011). As in drug addiction, sensitization of the dopamine reward/motivation circuit contribute to compulsive behaviors seen in OCD. Indeed, the repeated activation of dopamine D2 receptors (D2Rs) is enough to induce locomotor sensitization and checking behavior in both rats and mice (Szechtman et al., 1998; Szechtman et al., 1999; Sun et al., 2019). Repeated administration of quinpirole, a D2R/D3R agonist, is an accepted model of OCD as it recapitulates face validity, through an increment of compulsive checking and stereotyped behavior, predictive validity, as seen by a decrease of compulsive behaviors after chronic treatment with serotonin reuptake inhibitors (SRI) and construct validity as brain structures involved in this model are shared with those in the pathology (Stuchlik et al., 2016; Szechtman et al., 2017). In summary, repeated activation of dopamine transmission, either by pre-synaptic (dopamine release) or post-synaptic (activation of D2R) mechanisms lead to locomotor sensitization and compulsive behaviors.

The kappa opioid system is one of the most preponderant systems controlling dopamine transmission in the reward/motivation circuit. Evidence shows that kappa-opioid transmission opposes to the effects of dopamine; the acute activation of kappa opioid receptors (KORs) counteracts the locomotor activity induced by psychostimulants (Gray et al., 1999). Conversely, repeated KOR activation maintains and enhances compulsive and habitual drug seeking (Koob, 2013). Consumption of drugs of abuse induce a homeostatic enhanced

kappa opioid transmission, probably contributing to the negative emotional states of dysphoria (Koob, 2013) triggering compulsive drug use (Chavkin and Koob, 2016). In fact, the blockade of KOR prevented stress- but not drug-induced reinstatement of nicotine (Jackson et al., 2013), cocaine (Beardsley et al., 2005) and ethanol (Sperling et al., 2010). In line with this finding, KOR blockade reverts dopaminergic changes in the dorsolateral striatum of amphetamine sensitized rats, without modifying their enhanced locomotor response to the drug (Azocar et al., 2019). Thus, KOR system seems to enhance negative reinforcement increasing drug-value. In OCD, negative reinforcement is triggered by obsessions, which strengthen a given compulsion in order to avoid that obsession. Although it has not been directly tested, negative reinforcing could play a role on quinpirole sensitization. Indeed, D2R are involved in the generation of negative reinforcement. For example, place avoidance to a morphine- withdrawal-paired area was not developed in mice lacking the long isoform of D2R (Smith et al., 2002) and repeated quinpirole treatment during abstinence period reinstates cocaine and heroin seeking in an auto-administration paradigm, an effect related to sensitized locomotion to quinpirole (De Vries et al., 2002), suggesting shared mechanisms between psychostimulant and quinpirole-induced sensitization. Moreover, the introduction of the home cage, but not a novel cage, to the open-field arena reduces locomotor sensitization and compulsive checking behavior (Szechtman et al., 2001), indicating that safety/familiar cues might compete with negative environmental cues that favor sensitization. Similarly to psychostimulant-induced sensitization, the repeated activation of KOR facilitates locomotor sensitization (Escobar et al., 2017) and compulsive checking behavior (Perreault et al., 2007) induced by repeated administration of quinpirole. Whether this potentiating effect is a consequence of enhanced negative reinforcement remains to be elucidated.

The thorough analysis carried out recently shows that the effect of the kappa-opioid system on dopaminergic transmission is complex: it depends on the dopamine pathway involved (Margolis et al., 2006; Margolis et al., 2008), and on the timing between the activation of the KOR receptor and the activation of the dopamine receptor (Chartoff et al., 2016). Consistent with this complexity, the potential therapeutic use of KOR ligands has been widely discussed. It has been proposed that KOR agonist may be clinically useful during the drug use phase, attenuating the drug induced hyperdopaminergia (Shippenberg et al., 2007). On the other hand, a KOR antagonist may be useful in treating withdrawal syndrome induced by an increase in dynorphin expression after repeated drug consumption (Wee and Koob, 2010). Accordingly, it has been proposed that KOR partial agonist (Béguin et al., 2012) could be a therapeutic option to treat both the compulsive drug intake and withdrawal symptoms in addicted individuals (Chartoff et al., 2016; Callaghan et al., 2018). In this review, we analyze the time/context-dependent modulation of dopaminergic correlates of behavioral sensitization and compulsivity.

Anatomical and Functional Crosstalk Between Kappa Opioid and Dopaminergic Systems in Striatal and Midbrain Regions

Striatal Regions

KORs are Gi/o protein-coupled receptors highly expressed in the midbrain dopamine system (Mansour et al., 1996). These receptors belong to the family of opioid receptors composed by mu (MOR), delta (DOR) and kappa (KORs). The endogenous agonists for these receptors are endorphins, enkephalin and dynorphin, respectively. In the striatum, dynorphin is synthetized by dopamine D1receptor (D1R)-containing medium-sized neurons (MSNs) that have recurrent axons activating KORs from the same nuclei (Mansour et al., 1995). Electron microscopy images of rat NAc shows that KORs are found predominantly in DAT-containing presynaptic structures while a minor proportion of KORs localizes on dendrites in apposition to DAT (Svingos et al., 2001; Kivell et al., 2014). Immunofluorescent studies characterizing presynaptic-synaptosomal preparations from NAc show that KORs and D2Rs preferentially coexist in synaptosomes containing the dopamine synthetizing enzyme, tyrosine hydroxylase (TH) (Escobar et al., 2017). Moreover, KORs are abundant in cell bodies of the NAc and striatum, and colocalize with D2Rs in a cell subpopulation (Escobar et al., 2017). With genetic and molecular insights, it has been suggested that a 20% of total KOR binding in the striatum is observed in DA terminals (Van't Veer et al., 2013). Moreover, Tejeda et al. (2017) showed that both D1R and D2R MSNs express KOR with a higher preference for D1R containing MSNs (Tejeda et al., 2017). This anatomical data indicates that KORs are present pre and postsynaptically, regulating dopamine neurotransmission in the reward/motivation circuit.

Several experimental approaches show that the activation of KORs inhibits dopamine release. The acute activation of KORs by a systemic injection or the local infusion of agonists decreases the extracellular levels of dopamine in the NAc (Di Chiara and Imperato, 1988; Spanagel et al., 1992; Fuentealba et al., 2006) and dorsal striatum (Gehrke et al., 2008). Supporting a tonic inhibitory action of KORs over dopamine neurotransmission, the direct infusion of the long-lasting and selective KOR antagonist nor-binaltorphimine (nor-BNI) (Broadbear et al., 1994) increases basal levels of dopamine in the NAc (Spanagel et al., 1992) and dopamine release in the dorsal striatum (Azocar et al., 2019). Final evidence of KOR tonic inhibition of dopamine was shown in KOR knockout mice, which displayed increased extracellular levels of dopamine in the striatum and NAc (Chefer et al., 2005). The mechanisms responsible for KOR inhibition of dopamine release are not completely elucidated. However, it is well known that the activation of KORs leads to the increase of K + and decrease of Ca2+ conductances, thus inducing cell hyperpolarization and blockade of vesicular neurotransmitter release (Bruchas and Chavkin, 2010; Margolis and Karkhanis, 2019).

Additionally, *in vitro* and *in vivo* functional data suggests that KORs modify dopamine extracellular levels by modulating the

activity of DAT. For instance, the activation of KORs in EM4 cells that co-express KORs and DAT, lead to an increased uptake of dopamine measured by voltammetry (Kivell et al., 2014). An *ex vivo* analysis also using voltammetry in disaggregated tissues, showed that a systemic injection of KOR agonist U-69593 increased dopamine uptake in the NAc (Thompson et al., 2000). A similar recent article shows that nor-BNI blocks the increase of dopamine uptake in the ventral and dorsal striatum, induced by an acute systemic injection of MP1104, a mixed Kappa/Delta opioid receptor agonist (Atigari et al., 2019). Nevertheless, the effect of KOR activation on dopamine uptake has yet not been not fully elucidated. The systemic administration of the KOR partial agonist nalmefene decreased striatal dopamine uptake dose dependently, quantified by fast scan cyclic voltammetry (FSCV) (Rose et al., 2016). Using a no-net flux microdialysis in adult male rats, blocking of KOR was accompanied by an increase in extraction fraction (Ed), which is an indirect measure of dopamine uptake (Chefer et al., 2006; Azocar et al., 2019), suggesting that tonic activation of KOR exerts an inhibitory control on DAT activity (dopamine uptake). These results highlight the complex role of endogenous KOR activity on dopamine uptake to control dopamine extracellular levels. Higher temporal resolution approaches such as FSCV have failed to show an effect of KOR on dopamine uptake (Ebner et al., 2010; Ehrich et al., 2015; Hoffman et al., 2016), suggesting that KOR enhancing DAT activity in striatal regions needs an incubation period., KOR-mediated enhancement of DAT activity could be explained by an increase in the number of DAT on cell membranes induced by KOR activation, as reported in striatal synaptosomes and cell lines (Kivell et al, 2014).

Midbrain Regions

Autoradiographic assays performed in the rat midbrain show significant binding for KORs on the rostrocaudal axis of the SN and VTA (Speciale et al., 1993). On the other hand, electron microscopy data show that dynorphin-containing terminals synapse directly on TH positive dendrites in the SN and the VTA (Sesack and Pickel, 1992), suggesting that KORs localize in somatodendritic compartments of dopamine neurons. Striatal D1R-containing MSNs are one of the dynorphin inputs to midbrain dopamine neurons. Interestingly, blockage of KORs does not modify the inhibitory effect of D1R-MSNs to VTA dopamine neurons, indicating that this inhibition is mediated by GABA (Edwards et al, 2017). KORs modulate somatodendritic responses of dopamine midbrain neurons. Electrophysiological studies show that the activation of KORs in the VTA hyperpolarizes and decreases the spontaneus firing rate of dopamine neurons (Margolis et al., 2003). Consequently, the infusion of KOR agonists decreases somatodendritic dopamine efflux (Smith et al., 1992; Dalman and O'Malley, 1999). However, this inhibitory effect of KORs on dopamine neurons seems to be circuit dependent. The infusion of kappa-opioid agonists in the VTA decreases dopamine release in the medial prefrontal cortex (mPFC) (Margolis et al., 2006) but not in the NAc (Devine et al., 1993; Margolis et al, 2006). Moreover, Margolis et al. (2006) found that KORs inhibit VTA dopamine neurons that project to the mPFC and basolateral amygdala, but not those that project to the NAc. In that same year, Ford et al. (2006) showed that bath application of KOR agonists in mouse VTA slices induced a higher outward current in dopamine neurons that project to the NAc compared to those that project to the basolateral amygdala, indicating that KORs exert a greater inhibition of dopamine neurons that project to the NAc than to the amygdala. Furthermore, the activation of KOR decreases the amplitude of excitatory (Margolis et al., 2005) and inhibitory (Ford et al., 2007) postsynaptic currents into midbrain dopamine neurons. Differences between species and the complex efferents proyections of VTA to mPFC and NAc (Van Bockstaele and Pickel, 1995; Carr and Sesack, 2000) make it challenging to establish whether KORs inhibit selectively some of the neuronal dopamine populations in VTA. Nevertheless, the data summarized here indicates that KORs are in the soma and terminals of dopamine neurons, as well as in the inputs that regulate them, thus exquisitely positioned to control the synaptic activity of midbrain dopamine neurons.

Role of KORs Controlling Dopamine Neurotransmission in Psychostimulants-Induced Sensitization and Compulsive Behaviors

Drug addiction is a process that involves initially impulsive drug seeking associated with their positive-reinforcing effects. On the other hand, compulsivity is a personality trait observable in drug addicts. Several neuroadaptations in dopaminergic pathways have been proposed to account for compulsive drug seeking and intake following repeated exposure to drugs of abuse (Everitt and Robbins, 2005; Koob and Volkow, 2016). One of the proposed hypotheses driving compulsive drug intake is the sensitization of its negative-reinforcing effects (Koob, 2013). The inhibitory control of kappa opioid system on dopamine release could contribute to the negative-reinforcing properties of drugs of abuse. However, the consequences of KOR activation on dopamine neurotransmission and compulsive drugs seeking seems to be complex and apparently contradictory. Indeed, dopamine release induced by amphetamine and cocaine is attenuated by concomitant administration of KOR agonists (Heidbreder and Shippenberg, 1994; Maisonneuve et al., 1994; Thompson et al., 2000) and even decrease cocaine self-administration (Negus et al., 1997). Moreover, KORs exert an inhibitory feedback on dopamine release of the mesolimbic pathway in response to the sustained activation of post-synaptic D1R as occurs with repeated exposure to psychostimulants (Cole et al., 1995; Nestler, 2001). Paradoxically, the activation of KORs can also facilitate dopamine release in the reward/motivation pathway (Fuentealba et al., 2006; Fuentealba et al., 2007) and psychostimulants consumption (Wee et al., 2009). Fuentealba et al. (2007) showed that after four days administering U69593, a KOR agonist, increased amphetamine induced dopamine release in the NAc. Recently, it was shown that blocking KORs reverses the changes in dopamine release and uptake in dorsal striatum that takes place during the locomotor sensitization induced by amphetamine (Azocar et al., 2019). Altogether, these data suggest

that the activation of KORs might also contribute to positive-reinforcing properties of drug of abuse (Chartoff et al., 2016).

In addition, KORs activation also seem to contribute to compulsive drug seeking; KORs blockade reduces cocaine (Wee et al., 2009), heroin (Schlosburg et al., 2013) and methamphetamine (Whitfield et al., 2015) intake in rats with unlimited access to the drug (Wee et al, 2009). This effect is also evidenced in stress-induced drug seeking. For instance, the KOR knockout mice did not show cocaine place preference after forced swimming stress (McLaughlin et al., 2006a). The blocking of KORs attenuates the nicotine place preference induced by forced swim stress exposure (Smith et al., 2012). Interestingly, the blocking of KOR attenuates the cocaine and nicotine seeking induced by stress but did not affect seeking induced by a drug challenge (Beardsley et al., 2005; Jackson et al., 2013). This facilitator KOR effect induced by stress seems to be mediated by the reward/motivation circuit (Shippenberg et al., 2007; Wee and Koob, 2010). In an elegant study performed by Dr. Kauer and her group, it was shown that blocking KORs in the VTA, either previously or after an acute stress, inhibits the reinstaintment of cocaine-seeking, an effect associated to the rescue of long-term-potentiation of inhibitory synapses in dopamine neurons (Graziane et al., 2013; Polter et al., 2014).

The facilitation of psychostimulants intake exerted by KORs seems to depend on a time-window regarding drug exposure. The administration of the KOR agonist U50488 1 h before cocaine exposure potentiates both cocaine place preference and the relative dopamine release evoked by cocaine in the NAc, while the opposite effects are observed when given 15 min before (McLaughlin et al., 2006a; Ehrich et al., 2014). Using intracranial self-stimulation Chartoff et al. (2016) observed that the KOR agonist Salvinorin A, has an initial aversive and a delayed rewarding effect, accompanied by a decrease and an increase in stimulated dopamine release in the NAc, respectively. All together these data indicate a time-dependent effect of KOR activation on the rewarding properties of cocaine, and points to the stress-mediated KOR activation as a key player for the development of compulsive drug-seeking.

Quinpirole-Induced Locomotor Sensitization and Compulsive Behavior

The facts that the dopamine system is involved in the generation of sensitization and compulsivity is strengthened by the behavior observed in rodents treated with the D2R agonist, quinpirole. Briefly, D2Rs are Gi coupled receptors widely expressed in the reward/motivation circuit; they are expressed somatodendritically and on axon terminals of dopamine neurons (Sesack et al., 1994), and its activation decreases dopamine extracellular levels (Imperato and Di Chiara, 1988). In the striatum, D2Rs are also located postsynaptically on medium spiny neurons (Sesack et al., 1994) and its activation inhibits the indirect pathway allowing locomotor activity.

Dr. Henry Szechtman began studying the effects of quinpirole on the behavior of rats ending the decade of 1980. Their initial findings showed that the acute administration of quinpirole has dose-dependent effect on locomotor activity. At low doses (0.03 mg/kg) it decreases locomotor activity, while at higher doses (>0.5 mg/kg), it increments. (Eilam and Szechtman, 1989). These effects are associated with the activation of high-affinity presynaptic D2Rs and low-affinity postsynaptic D2Rs, respectively (Usiello et al., 2000). Unexpectedly, the repeated (every other day) administration of quinpirole induces a gradual and sustained increase in locomotion, resembling the locomotor sensitization induced by psychostimulants (Szechtman et al., 1993; Szechtman et al., 1994). The locomotor sensitizing effect was shown to depend on D2Rs, since mice deficient for this receptor do not develop locomotor sensitization to quinpirole (Escobar et al., 2015).

At the beginning of the 90's, Szechtman and Eilam reported that along with locomotor sensitization, rats developed a stereotyped behavior, which is reinforced with each administration of quinpirole (Eilam and Szechtman, 1989; Szechtman et al., 1993). Today, quinpirole repeated administration is a validated model for OCD (Szechtman et al., 1999; Szechtman et al., 2001; Eilam and Szechtman, 2005; Stuchlik et al., 2016; Szechtman et al., 2017), based on the observation that the behavior of rats becomes increasingly structured and inflexible, reminiscent of the ritual behavior characteristic of compulsive checking behavior (Szechtman et al., 1998; Szechtman et al., 2017). Recent studies show that repeated quinpirole also induces compulsive behaviors in mice, such as compulsive checking (Sun et al., 2019), behavioral inflexibility and compulsive chewing (Asaoka et al., 2019), the latter reverted by D2Rs blockade in the striatum, further supporting that repeated D2Rs activation is needed to induce compulsive behaviors. Together the data points to a crucial role of D2Rs within the midbrain dopamine pathways to induce locomotor sensitization and compulsivity. Repeated quinpirole administration primes cocaine-induced stereotyped behavior (Thompson et al., 2010) and the locomotor effects of amphetamine (Cope et al., 2010), strengthening the idea that D2Rs activation underlie psychostimulant-induced sensitization and suggesting a shared mechanism between quinpirole and psychostimulants-induced sensitization. Interestingly, the sensitizing effect of repeated D2Rs activation seems to be stronger than that induced by psychostimulants, since every rat treated with quinpirole develop locomotor sensitization (Escobar et al., 2015), while around sixty percent of rats sensitize to amphetamine (Escobar et al., 2012; Casanova et al., 2013).

Behavioral sensitization induced by repeated activation of D2Rs is accompanied by adaptations in the reward/motivation circuit. Rats sensitized with quinpirole have lower dopaminergic tone in the NAc, observed as decreased basal (Koeltzow et al., 2003) and stimulated tonic and phasic dopamine release (Escobar et al., 2015), indicating decreased dopamine release capacity of dopamine midbrain circuit. Synaptic dopamine levels in the NAc are controlled by the activity of both, DAT and dopamine neurons activity (Goto and Grace, 2008), which *in vivo* consists of tonic and burst firing (Wilson et al., 1977; Grace and Bunney, 1980). Previous reports show that quinpirole-sensitized rats display a smaller number of dopamine neurons in tonic and burst firing in the VTA (Sesia et al., 2013). Together

these data indicate that the decrease in dopamine release seen after quinpirole sensitization is a result of a decrease in the overall activity of dopamine neurons. The compulsive behavior and sensitized locomotor activity induced by the repeated treatment with quinpirole could be a consequence of sensitization of D2Rs, due to decreased dopaminergic tone in the NAc. Indeed, quinpirole-sensitized rats show an increase in the binding of dopamine D2R (Culver et al., 2008) and an increase in the affinity state of these receptors (Perreault et al., 2007), supporting this hypothesis.

KOR-Dopamine Interactions in Quinpirole-Induced Compulsive Behaviors

Initial studies regarding the role of KOR in D2R-induced compulsive behaviors also came from Szechtman's lab. This group examined the concomitant administration of the KOR agonist U69593 with quinpirole on locomotor activity. Specifically, the authors administered subcutaneous injections to rats with a mixture U69593 and quinpirole, until 8 to 10 injections were completed. Contrary to the hypolocomotor effect of U69593 alone, hyperlocomotion was observed when administered concomitantly with low (presynaptic) and high (postsynaptic) doses of quinpirole. U69593 changed the hypolocomotor effect of a presynaptic dose of quinpirole to hyperlocomotion and enhanced the hyperlocomotor effect of a postsynaptic dose of quinpirole (Perreault et al., 2006). Co-activation of KORs also accelerated the induction of locomotor sensitization and potentiated the effect of D2Rs activation, since the maximum locomotion achieved by the double treatment duplicates the locomotor effect induced by quinpirole alone (Perreault et al., 2006; Escobar et al., 2017). Co-activation of KORs also accelerates the acquisition of compulsive checking behavior (Perreault et al., 2007). These potentiating effects of KORs on quinpirole-induced behaviors require KORs repeated activation. In fact, acute injection of the KOR agonist U69593 did not further modify the locomotor activity in rats sensitized with quinpirole (Escobar et al., 2017). The mechanism of KOR potentiating D2R-induced sensitization is unknown. One possibility is that the endogenous kappa opioid system itself is mediating D2R-dependent sensitization. However, this possibility was discarded by showing that pre-administration of norBNI did not modify locomotor sensitization to quinpirole, suggesting that dynorphin is not released downstream D2R activation (Escobar et al., 2017). This data does not rule out that dynorphin might have a role in sensitizing compulsive behaviors, for example, stress induces the release of dynorphin and activation of KORs which facilitates compulsive behaviors (McLaughlin et al., 2003; McLaughlin et al., 2006a; McLaughlin et al., 2006b).

The crosstalk between D2Rs and KORs is complex and it seems to depend on whether the activation of both receptors is coincident or temporally separated. Anatomical data indicate that the crosstalk between D2Rs and KORs can occur presynaptically in axons and soma of dopamine neurons, as well as postsynaptically in MSNs of the striatum. Although it does not rule out a role for KORs located on axons of other neurochemical systems, the anatomical data strongly points to a direct role of KORs regulating D2Rs. Either acute or repeated, the activation of KORs decreases the inhibitory D2Rs function on dopamine neurons. Electrophysiology studies showed that the acute activation of KOR in dopamine neurons of the VTA and SN inhibits D2R-mediated inhibitory postsynaptic current, an effect mediated by pre and postsynaptic mechanisms as KOR decreases dopamine release and dynorphin blocks the inhibitory effect of bath applied dopamine (Ford et al., 2007). Neurochemical studies showed that the repeated activation of KORs blocks D2R-induced inhibition of dopamine release in the NAc (Fuentealba et al., 2006). Moreover, coincident D2Rs and KORs acute activation decreases the inhibition of dopamine release in the NAc compared to the effect of each receptor alone (Escobar et al., 2017). Thus, presynaptic KORs do not act additively or in synergy with presynaptic D2Rs, conversely, KORs either inhibit or occlude D2R inhibitory effect. This mechanism could explain the locomotor activating effect of an acute dose of KOR agonists concomitant to a low dose of quinpirole (Perreault et al., 2006).

A recent study shows that KOR activation in the VTA mediates compulsive behavior measured as behavioral inhibition and marble burying (Abraham et al., 2017), reinforcing the idea that KORs activation is indeed a trigger for compulsivity. Data published by Margolis et al. (2006; 2008) indicate that KORs and D2Rs interaction should take place on dopamine neurons targeting the mPFC (Margolis et al., 2006; Margolis et al., 2008). Notwithstanding, Ford et al. (2006; 2007) found that KORs inhibition of D2R mediated IPSC takes place on dopamine neurons targeting the NAc (Ford et al., 2006; Ford et al., 2007). Together these data show that KOR interaction with D2R at the somatodendritic compartment of dopamine neurons could arise as a result of a crosstalk in the same dopamine neuron. Whether this happens in the mesolimbic or mesocortical projections is still controversial.

Remarkably, KOR was found in MSNs of the NAc (Escobar et al., 2017; Tejeda et al., 2017), thus indicating that the potentiation of D2R-induced compulsive behavior can also arise by direct actions on the target cells of dopamine neurons. In this regard, it is worth mentioning that repeated administration of U69593 increases the amount of D2Rs in the high affinity state (Perreault et al., 2007). Neurochemical data indicate that decreased dopamine extracellular levels is associated to D2Rs sensitization. KORs co-activation does not decrease further the extracellular levels of dopamine in the NAc already decreased by the repeated activation of D2Rs (Escobar et al., 2017), ruling out a role for presynaptic KORs accelerating or potentiating the sensitization of D2Rs in the NAc through this mechanism. Therefore, KORs trigger slow molecular mechanisms that further sensitize the neurochemical and behavioral effects of D2Rs, suggesting that the locomotion sensitization enhancement could be due to an adaptive postsynaptic rather than a presynaptic effect. In this regard repeated activation of KORs can trigger the inhibition of D2R indirect striatal pathway switching D1R/D2R balance to D1R inducing compulsivity (**Figure 1**).

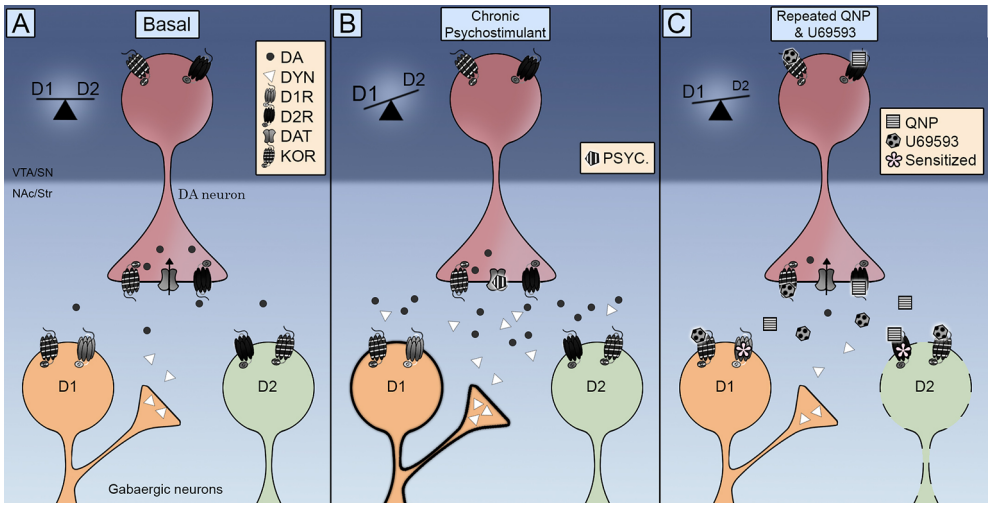

FIGURE 1 | Integrative scheme of Kappa Opioid Receptors (KOR) control on direct (D1R) and indirect (D2R) striatal phatways. **(A)** KOR are located pre-sinaptically on dopamine terminals and post sinaptically in medium-sized neurons (MSNs). Its activation controls dopamine extracellular levels and its localization promotes the interaction with dopamine transporter (DAT) and dopamine D2 receptors. **(B)** The repeated exposure to a psychostimulant is accompanied by an increase in both dopamine extracellular levels and dynorphin. The activation of D1 and D2 receptors switch the balance to the D1R direct pathway promoting locomotor sensitization. **(C)** The co-administration of quinpirole and U69593 is accompanied by a decrease in dopamine extracellular levels. The concomitant activation of KOR and D2 receptors debilitates the D2 indirect pathway inducing compulsive behavior.

Sex Differences of KOR-Dopamine Interactions in Compulsive Behaviors

Clinical studies have shown sex differences in compulsive behavior including compulsive drug seeking. An earlier onset of OCD symptoms is observed in men compared with women (Mathis et al., 2011), with women showing more prevalence of contamination and cleaning symptoms (Labad et al., 2008). Regarding sex differences in drug addiction, clinical evidence indicates that while the use of drugs is more prevalent in men, women exhibit a faster progression than men into compulsive drug seeking (Hernandez-Avila et al., 2004; Fattore and Melis, 2016).

Lately, pre-clinical evidence has strongly highlighted the neurobiological bases underpinning the sex differences in drug abuse observed in clinical studies (Becker and Chartoff, 2019). Early observations using no-net flux microdialysis showed that dopamine extracellular concentration in the dorsal striatum varies during the estrous cycle with higher levels in proestrus and estrus compared with diestrus. Moreover, while ovariectomy decreases striatal dopamine extracellular concentration in female rats, the castration of male rats does not modify dopamine striatal extracellular concentration (Xiao and Becker, 1994), suggesting an important role of ovary hormones on dopamine activity. In addition, female hormones regulate the response to psychostimulants. Early *in vitro* experiments showed that estradiol plus progesterone restore amphetamine-induced dopamine release from striatal tissue obtained of ovariectomized female rats (Becker and Ramirez, 1981). More recently, fast scan cyclic voltammetry studies have shown that females exhibit greater electrically-stimulated dopamine release and uptake compared to males (Walker et al., 2000). These sex differences in dopamine neurotransmission can account for the higher cocaine and amphetamine seeking observed in females. (Roberts et al., 1989; Cox et al., 2013).

The regulation of KOR on dopamine extracellular levels also shows sex differences (Chartoff and Mavrikaki, 2015). Using intracranial self-stimulation and cyclic voltammetry, Conway et al. (2019) showed that the lower sensitivity to the acute anhedonic effect of a KOR agonist observed in female rats compared to male rats, is accompanied by an attenuated inhibition of stimulated dopamine release in the NAc (Conway et al., 2019). It has been suggested that estradiol contributes to the blunted inhibition of dopamine release observed in female rats after KOR activation (Abraham et al., 2018). While the crosstalk between KORs and dopamine signaling has been studied in males (Tejeda and Bonci, 2019), research on this interaction and its impact in the addiction process in females is lacking (Chartoff and Mavrikaki, 2015). In female rats, the acute administration of the KOR agonist U69593 attenuated cocaine-induced hyperlocomotion in both, control and ovariectomized rats. Interestingly, U69593 repeated administration attenuated cocaine-induced hyperlocomotion in an estradiol-dependent manner (Puig-Ramos et al., 2008). These data suggest that estradiol primes KOR actions in female rats, an effect that could be related to sex differences in stress response (Puig-Ramos et al., 2008). Whether in female rats the repeated activation of KORs facilitates striatal dopamine release as observed in male is an unanswered question.

Although a facilitation in psychostimulant induced dopamine release is observed in female compared to male rats, sex

differences in the dopamine mechanisms underlying amphetamine locomotor sensitization have not been fully elucidated (Becker, 1999). The repeated exposure to amphetamine induces a greater locomotor activity in both, adolescent (Mathews and McCormick, 2007) and adult female rats (Milesi-Hallé et al., 2007), with female adolescent rats showing a more robust locomotor sensitization after repeated exposure to amphetamine. The neonatal activation of D2 receptor potentiated the amphetamine induced behavioral sensitization only in female rats (Brown et al., 2011). As mentioned before, it has been observed in male rats the repeated exposure to D2 agonist induces locomotor sensitization and compulsive-like behavior (Dvorkin et al., 2006). Moreover, the co-activation of KOR potentiates the locomotor sensitization induced by repeated exposure to quinpirole, facilitating the inhibitory control of D2 receptors on DA release in the NAc (Escobar et al., 2017). Sex differences such as the observed lower sensitivity to the inhibitory effect of KOR on dopamine release in females (Conway et al., 2019) may account for a differential contribution of KOR on compulsive drug seeking.

CONCLUSIONS

How do KORs modulate dopamine signaling to elaborate motivated behaviors and when does it result in a sensitized compulsive behavior? Anatomical data shows that KORs are exquisitely positioned to control the synaptic activity of midbrain dopamine neurons. Functional data indicate that KORs control DAT and D2R functioning as well as dopamine neurons firing rate. Initial evidence showing that the acute activation of KORs decreases dopamine release induced by drugs of abuse has been complemented with data indicating that the repeated activation of KOR facilitates dopamine release and compulsive drug-seeking. Dopamine signaling balance direct and indirect output pathways from striatal areas (**Figure 1A**). Either chronic stimulation with psychostimulants that increases dopamine release activating both D1R and D2R (**Figure 1B**) or quinpirole that activate only D2R (**Figure 1C**) results in locomotor sensitization and compulsive behaviors by a debilitated D2R indirect pathway, thus switching the balance to the D1R direct pathway. KOR transmission is enhanced during chronic psychostimulant intake by the increase of dynorphin in striatal D1 neurons (**Figure 1B**). An enhanced KOR transmission is emulated in the pharmacological model of OCD by administering U69593. This concomitant KOR activation further debilitates the D2 indirect pathway (**Figure 1C**). Future research should be carried out to fully elucidate the consequences of KOR activation on the DAT activity, understand the role of endogeous KOR system in the quinpirole induced compulsivity and determine the contribution of KOR system to the sex diffences observed in compulsive behaviors.

AUTHOR CONTRIBUTIONS

AE, MA, and JF contributed to the conception of the manuscript. AE and JF wrote the first draft of the manuscript with input from MA. MA and JC contributed to the critical review and editing of the manuscript. All the authors approved it for publication.

FUNDING

The work of the authors cited in this review has been supported by FONDECYT grant numbers: 1110352 and 1150200 to MA; 1141088 to JF; DIPOG grant 391340281 to JF; FONDECYT Postdoctoral fellow 3170497 to JC and 3190843 to AE.

REFERENCES

Abraham, A. D., Fontaine, H. M., Song, A. J., Andrews, M. M., Baird, M. A., Kieffer, B. L., et al. (2017). Kappa opioid receptor activation in dopamine neurons disrupts behavioral inhibition. *Neuropsychopharmacology* 43 (2), 362–372. doi: 10.1038/npp.2017.133

Abraham, A. D., Schattauer, S. S., Reichard, K. L., Cohen, J. H., Fontaine, H. M., Song, A. J., et al. (2018). Estrogen regulation of GRK2 inactivates kappa opioid receptor signaling mediating analgesia, but not aversion. *J. Neurosci.* 38 (37), 8031–8043. doi: 10.1523/JNEUROSCI.0653-18.2018

Asaoka, N., Nishitani, N., Kinoshita, H., Nagai, Y., Hatakama, H., Nagayasu, K., et al. (2019). An adenosine A2A receptor antagonist improves multiple symptoms of repeated quinpirole-induced psychosis. *eNeuro* 6 (1), 1–16. ENEURO.0366-18.2019. doi: 10.1523/ENEURO.0366-18.2019

Atigari, D. V., Uprety, R., Pasternak, G. W., Majumdar, S., and Kivell, B. M. (2019). MP1104, a mixed kappa-delta opioid receptor agonist has anti-cocaine properties with reduced side-effects in rats. *Neuropharmacology* 150, 217–228. doi: 10.1016/j.neuropharm.2019.02.010

Azocar, V. H., Sepúlveda, G., Ruiz, C., Aguilera, C., Andrés, M. E., and Fuentealba, J. A. (2019). The blocking of kappa-opioid receptor reverses the changes in dorsolateral striatum dopamine dynamics during the amphetamine sensitization. *J. Neurochem.* 148, 348–358. doi: 10.1111/jnc.14612

Béguin, C., Potuzak, J., Xu, W., Liu-Chen, L. Y., Streicher, J. M., Groer, C. E., et al. (2012). Differential signaling properties at the kappa opioid receptor of 12-epi-salvinorin A and its analogues. *Bioorg. Med. Chem. Lett.* 15;22 (2), 1023–1026. doi: 10.1016/j.bmcl.2011.11.128

Beardsley, P. M., Howard, J. L., Shelton, K. L., and Carroll, F. I. (2005). Differential effects of the novel kappa opioid receptor antagonist, JDTic, on reinstatement of cocaine-seeking induced by footshock stressors vs cocaine primes and its antidepressant-like effects in rats. *Psychopharmacol. (Berl)* 183, 118–126. doi: 10.1007/s00213-005-0167-4

Becker, J. B., and Chartoff, E. (2019). Sex differences in neural mechanisms mediating reward and addiction. *Neuropsychopharmacology* 44, 166–183. doi: 10.1038/s41386-018-0125-6

Becker, J. B., and Ramirez, V. D. (1981). Sex differences in the amphetamine stimulated release of catecholamines from rat striatal tissue in vitro. *Brain Res.* 204, 361–372. doi: 10.1016/0006-8993(81)90595-3

Becker, J. B. (1999). Gender differences in dopaminergic function in striatum and nucleus accumbens. *Pharmacol. Biochem. Behav.* 64, 803–812. doi: 10.1016/S0091-3057(99)00168-9

Berridge, K. C., and Robinson, T. E. (2016). Liking, wanting, and the incentive-sensitization theory of addiction. *Am. Psychol.* 71, 670–679. doi: 10.1037/amp0000059

Berridge, K. C., Venier, I. L., and Robinson, T. E. (1989). Taste reactivity analysis of 6-hydroxydopamine-induced aphagia: implications for arousal and

anhedonia hypotheses of dopamine function. *Behav. Neurosci.* 103, 36–45. doi: 10.1037/0735-7044.103.1.36

Broadbear, J. H., Negus, S. S., Butelman, E. R., de Costa, B. R., and Woods, J. H. (1994). Differential effects of systemically administered nor- binaltorphimine (nor-BNI) on kappa-opioid agonists in the mouse writhing assay. *Psychopharmacology* 115, 311–319. doi: 10.1007/BF02245071

Brown, R. W., Perna, M. K., Noel, D. M., Whittemore, J. D., Lehmann, J., and Smith, M. L. (2011). Amphetamine locomotor sensitization and conditioned place preference in adolescent male and female rats neonatally treated with quinpirole. *Behav. Pharmacol.* 22, 374–378. doi: 10.1097/FBP.0b013e328348737b

Bruchas, M. R., and Chavkin, C. (2010). Kinase cascades and ligand-directed signaling at the kappa opioid receptor. *Psychopharmacol. (Berl)* 210, 137–147. doi: 10.1007/s00213-010-1806-y

Callaghan, C. K., Rouine, J., and O'Mara, S. M. (2018). Potential roles for opioid receptors in motivation and major depressive disorder. *Prog. Brain Res.* 239, 89–119. doi: 10.1016/bs.pbr.2018.07.009

Carr, D. B., and Sesack, S. R. (2000). GABA-containing neurons in the rat ventral tegmental area project to the prefrontal cortex. *Synapse* 38 (2), 114–123. doi: 10.1002/1098-2396(200011)38:2<114::AID-SYN2>3.0.CO;2-R

Casanova, J. P., Velis, G. P., and Fuentealba, J. A. (2013). Amphetamine locomotor sensitization is accompanied with an enhanced high K+-stimulated Dopamine release in the rat medial prefrontal cortex. *Behav. Brain Res.* 237, 313–317. doi: 10.1016/j.bbr.2012.09.052

Chartoff, E. H., and Mavrikaki, M. (2015). Sex differences in kappa opioid receptor function and their potential impact on addiction. *Front. Neurosci.* 9, 466. doi: 10.3389/fnins.2015.00466

Chartoff, E. H., Ebner, S. R., Sparrow, A., Potter, D., Baker, P. M., Ragozzino, M. E., et al. (2016). Relative timing between kappa opioid receptor activation and cocaine determines the impact on reward and dopamine release. *Neuropsychopharmacology* 41, 989–1002. doi: 10.1038/npp.2015.226

Chavkin, C., and Koob, G. F. (2016). Dynorphin, dysphoria, and dependence: the stress of addiction. *Neuropsychopharmacology* 41, 373–374. doi: 10.1038/npp.2015.258

Chefer, V. I., Czyzyk, T., Bolan, E. A., Moron, J., Pintar, J. E., and Shippenberg, T. S. (2005). Endogenous kappa-opioid receptor systems regulate mesoaccumbal dopamine dynamics and vulnerability to cocaine. *J. Neurosci.* 25, 5029–5037. doi: 10.1523/JNEUROSCI.0854-05.2005

Chefer, V. I., Zapata, A., Shippenberg, T. S., and Bungay, P. M. (2006). Quantitative no-net-flux microdialysis permits detection of increases and decreases in dopamine uptake in mouse nucleus accumbens. *J. Neurosci. Methods* 155, 187–193. doi: 10.1016/j.jneumeth.2005.12.018

Cole, R. L., Konradi, C., Douglass, J., and Hyman, S. E. (1995). Neuronal adaptation to amphetamine and dopamine: molecular mechanisms of prodynorphin gene regulation in rat striatum. *Neuron* 14, 813–823. doi: 10.1016/0896-6273(95)90225-2

Conway, S. M., Puttick, D., Russell, S., Potter, D., Roitman, M. F., and Chartoff, E. H. (2019). Females are less sensitive than males to the motivational- and dopamine-suppressing effects of kappa opioid receptor activation. *Neuropharmacology* 146, 231–241. doi: 10.1016/j.neuropharm.2018.12.002

Cope, Z. A., Huggins, K. N., Sheppard, A. B., Noel, D. M., Roane, D. S., and Brown, R. W. (2010). Neonatal quinpirole treatment enhances locomotor activation and dopamine release in the nucleus accumbens core in response to amphetamine treatment in adulthood. *Synapse* 64, 289–300. doi: 10.1002/syn.20729

Cox, B. M., Young, A. B., See, R. E., and Reichel, C. M. (2013). Sex differences in methamphetamine seeking in rats: impact of oxytocin. *Psychoneuroendocrinology* 38, 2343–2353. doi: 10.1016/j.psyneuen.2013.05.005

Culver, K. E., Szechtman, H., and Levant, B. (2008). Altered dopamine D2-like receptor binding in rats with behavioral sensitization to quinpirole: effects of pre-treatment with Ro 41-1049. *Eur. J. Pharmacol.* 592, 67–72. doi: 10.1016/j.ejphar.2008.06.101

Dalman, F. C., and O'Malley, K. L. (1999). kappa-Opioid tolerance and dependence in cultures of dopaminergic midbrain neurons. *J. Neurosci.* 19, 5750–5757. doi: 10.1523/JNEUROSCI.19-14-05750.1999

De Vries, T. J., Schoffelmeer, A. N., Binnekade, R., Raasø, H., and Vanderschuren, L. J. (2002). Relapse to cocaine- and heroin-seeking behavior mediated by dopamine D2 receptors is time-dependent and associated with behavioral sensitization. *Neuropsychopharmacology* 26, 18–26. doi: 10.1016/S0893-133X(01)00293-7

Devine, D. P., Leone, P., Pocock, D., and Wise, R. A. (1993). Differential involvement of ventral tegmental mu, delta and kappa opioid receptors in modulation of basal mesolimbic dopamine release: in vivo microdialysis studies. *J. Pharmacol. Exp. Ther.* 266, 1236–1246.

Di Chiara, G., and Imperato, A. (1988). Opposite effects of mu and kappa opiate agonists on dopamine release in the nucleus accumbens and in the dorsal caudate of freely moving rats. *J. Pharmacol. Exp. Ther.* 244, 1067–1080. doi: 10.1073/pnas.85.14.5274

Dvorkin, A., Perreault, M. L., and Szechtman, H. (2006). Development and temporal organization of compulsive checking induced by repeated injections of the dopamine agonist quinpirole in an animal model of obsessive-compulsive disorder. *Behav. Brain Res.* 169, 303–311. doi: 10.1016/j.bbr.2006.01.024

Ebner, S. R., Roitman, M. F., Potter, D. N., Rachlin, A. B., and Chartoff, E. H. (2010). Depressive-like effects of the kappa opioid receptor agonist salvinorin A are associated with decreased phasic dopamine release in the nucleus accumbens. *Psychopharmacol. (Berl)* 210, 241–252. doi: 10.1007/s00213-010-1836-5

Edwards, N. J., Tejeda, H. A., Pignatelli, M., Zhang, S., McDevitt, R. A., Wu, J., et al. (2017). Circuit specificity in the inhibitory architecture of the VTA regulates cocaine-induced behavior. *Nat. Neurosci.* 20 (3), 438–448. doi: 10.1038/nn.4482

Ehrich, J. M., Phillips, P. E. M., and Chavkin, C. (2014). Kappa opioid receptor activation potentiates the cocaine-induced increase in evoked dopamine release recorded in vivo in the mouse nucleus accumbens. *Neuropsychopharmacology* 39, 3036–3048. doi: 10.1038/npp.2014.157

Ehrich, J. M., Messinger, D. I., Knakal, C. R., Kuhar, J. R., Schattauer, S. S., Bruchas, M. R., et al. (2015). Kappa Opioid Receptor-Induced Aversion Requires p38 MAPK Activation in VTA Dopamine Neurons. *J. Neurosci.* 35, 12917–12931. doi: 10.1523/JNEUROSCI.2444-15.2015

Eilam, D., and Szechtman, H. (1989). Biphasic effect of D-2 agonist quinpirole on locomotion and movements. *Eur. J. Pharmacol.* 161, 151–157. doi: 10.1016/0014-2999(89)90837-6

Eilam, D., and Szechtman, H. (2005). Psychostimulant-induced behavior as an animal model of obsessive-compulsive disorder: an ethological approach to the form of compulsive rituals. *CNS Spectr.* 10, 191–202. doi: 10.1017/S109285290001004X

Escobar, A. P., Cornejo, F. A., Andrés, M. E., and Fuentealba, J. A. (2012). Repeated treatment with the kappa opioid receptor agonist U69593 reverses enhanced K + induced dopamine release in the nucleus accumbens, but not the expression of locomotor sensitization in amphetamine-sensitized rats. *Neurochem. Int.* 60 (4), 344–349. doi: 10.1016/j.neuint.2012.01.014

Escobar, A. P., Cornejo, F. A., Olivares-Costa, M., González, M., Fuentealba, J. A., Gysling, K., et al. (2015). Reduced dopamine and glutamate neurotransmission in the nucleus accumbens of quinpirole-sensitized rats hints at inhibitory D2 autoreceptor function. *J. Neurochem.* 134, 1081–1090. doi: 10.1111/jnc.13209

Escobar, A. P., González, M. P., Meza, R. C., Noches, V., Henny, P., Gysling, K., et al. (2017). Mechanisms of kappa opioid receptor potentiation of dopamine D2 receptor function in quinpirole-induced locomotor sensitization in rats. *Int. J. Neuropsychopharmacol.* 20, 660–669. doi: 10.1093/ijnp/pyx042

Everitt, B. J., and Robbins, T. W. (2005). Neural systems of reinforcement for drug addiction: from actions to habits to compulsion. *Nat. Neurosci.* 8, 1481–1489. doi: 10.1038/nn1579

Fattore, L., and Melis, M. (2016). Sex differences in impulsive and compulsive behaviors: a focus on drug addiction. *Addict. Biol.* 21 (5), 1043–1051. doi: 10.1111/adb.12381

Ferrario, C. R., Gorny, G., Crombag, H. S., Li, Y., Kolb, B., and Robinson, T. E. (2005). Neural and behavioral plasticity associated with the transition from controlled to escalated cocaine use. *Biol. Psy.* 58 (9), 751–9.

Figee, M., Pattij, T., Willuhn, I., Luigjes, J., van den Brink, W., Goudriaan, A., et al. (2016). Compulsivity in obsessive–compulsive disorder and addictions. *Eur. Neuropsychopharmacol.* 26, 856–868. doi: 10.1016/j.euroneuro.2015.12.003

Ford, C. P., Mark, G. P., and Williams, J. T. (2006). Properties and opioid inhibition of mesolimbic dopamine neurons vary according to target location. *J. Neurosci.* 26, 2788–2797. doi: 10.1523/JNEUROSCI.4331-05.2006

Ford, C. P., Beckstead, M. J., and Williams, J. T. (2007). Kappa opioid inhibition of somatodendritic dopamine inhibitory postsynaptic currents. *J. Neurophysiol.* 97, 883–891. doi: 10.1152/jn.00963.2006

Fuentealba, J. A., Gysling, K., Magendzo, K., and Andrés, M. E. (2006). Repeated administration of the selective kappa-opioid receptor agonist U-69593 increases stimulated dopamine extracellular levels in the rat nucleus accumbens. *J. Neurosci. Res.* 84, 450–459. doi: 10.1002/jnr.20890

Fuentealba, J. A., Gysling, K., and Andrés, M. E. (2007). Increased locomotor response to amphetamine induced by the repeated administration of the selective kappa-opioid receptor agonist U-69593. *Synapse* 61, 771–777. doi: 10.1002/syn.20424

Gehrke, B. J., Chefer, V. I., and Shippenberg, T. S. (2008). Effects of acute and repeated administration of salvinorin A on dopamine function in the rat dorsal striatum. *Psychopharmacol. (Berl)* 197, 509–517. doi: 10.1007/s00213-007-1067-6

Giuliano, C., Belin, D., and Everitt, B. J. (2019). Compulsive alcohol aeeking results from a failure to disengage dorsolateral striatal control over behavior. *J. Neurosci.* 39 (9), 1744–1754. doi: 10.1523/JNEUROSCI.2615-18.2018

Goto, Y., and Grace, A. A. (2008). Limbic and cortical information processing in the nucleus accumbens. *Trends Neurosci.* 31, 552–558. doi: 10.1016/j.tins.2008.08.002

Grace, A. A., and Bunney, B. S. (1980). Nigral dopamine neurons: intracellular recording and identification with L-dopa injection and histofluorescence. *Science* 210, 654–656. doi: 10.1126/science.7433992

Gray, A. M., Rawls, S. M., Shippenberg, T. S., and McGinty, J. F. (1999). The κ-opioid agonist, U-69593, decreases acute amphetamine-evoked behaviors and calcium-dependent dialysate levels of dopamine and glutamate in the ventral striatum. *J. Neurochem.* 73, 1066–1074. doi: 10.1046/j.1471-4159.1999.0731066.x

Graziane, N. M., Polter, A. M., Briand, L. A., Pierce, R. C., and Kauer, J. A. (2013). Kappa opioid receptors regulate stress-induced cocaine seeking and synaptic plasticity. *Neuron* 77, 942–954. doi: 10.1016/j.neuron.2012.12.034

Heidbreder, C. A., and Shippenberg, T. S. (1994). U-69593 prevents cocaine sensitization by normalizing basal accumbens dopamine. *Neuroreport* 5, 1797–1800. doi: 10.1097/00001756-199409080-00028

Hernandez-Avila, C. A. 1., Rounsaville, B. J., and Kranzler, H. R. (2004). Opioid-, cannabis- and alcohol-dependent women show more rapid progression to substance abuse treatment. *Drug Alcohol Depend.* 74 (3), 265–272. doi: 10.1016/j.drugalcdep.2004.02.001

Hoffman, A. F., Spivak, C. E., and Lupica, C. R. (2016). Enhanced dopamine release by dopamine transport inhibitors described by a restricted diffusion model and fast-scan cyclic voltammetry. *ACS Chem. Neurosci.* 7, 700–709. doi: 10.1021/acschemneuro.5b00277

Holden, C. (2001). "Behavioral" addictions: do they exist? *Science* 294, 980–982. doi: 10.1126/science.294.5544.980

Imperato, A., and Di Chiara, G. (1988). Effects of locally applied D-1 and D-2 receptor agonists and antagonists studied with brain dialysis. *Eur. J. Pharmacol.* 156, 385–393. doi: 10.1016/0014-2999(88)90284-1

Jackson, K. J., McLaughlin, J. P., Carroll, F. I., and Damaj, M. I. (2013). Effects of the kappa opioid receptor antagonist, norbinaltorphimine, on stress and drug-induced reinstatement of nicotine-conditioned place preference in mice. *Psychopharmacol. (Berl)* 226, 763–768. doi: 10.1007/s00213-012-2716-y

Kivell, B., Uzelac, Z., Sundaramurthy, S., Rajamanickam, J., Ewald, A., Chefer, V., et al. (2014). Salvinorin A regulates dopamine transporter function via a kappa opioid receptor and ERK1/2-dependent mechanism. *Neuropharmacology* 86, 228–240. doi: 10.1016/j.neuropharm.2014.07.016

Koeltzow, T. E., Austin, J. D., and Vezina, P. (2003). Behavioral sensitization to quinpirole is not associated with increased nucleus accumbens dopamine overflow. *Neuropharmacology* 44, 102–110. doi: 10.1016/S0028-3908(02)00328-3

Koob, G. F., and Volkow, N. D. (2016). Neurobiology of addiction: a neurocircuitry analysis. *Lancet Psychiatry* 3, 760–773. doi: 10.1016/S2215-0366(16)00104-8

Koob, G. F. (2013). Addiction is a reward deficit and stress surfeit disorder. *Front. Psychiatry* 4, 72. doi: 10.3389/fpsyt.2013.00072

Labad, J. 1., Menchon, J. M., Alonso, P., Segalas, C., Jimenez, S., Jaurrieta, N., et al. (2008). Gender differences in obsessive-compulsive symptom dimensions. *Depress Anxiety.* 25 (10), 832–838. doi: 10.1002/da.20332

Maisonneuve, I. M., Archer, S., and Glick, S. D. (1994). U50,488, a kappa opioid receptor agonist, attenuates cocaine-induced increases in extracellular dopamine in the nucleus accumbens of rats. *Neurosci. Lett.* 181, 57–60. doi: 10.1016/0304-3940(94)90559-2

Mansour, A., Fox, C. A., Akil, H., and Watson, S. J. (1995). Opioid-receptor mRNA expression in the rat CNS: anatomical and functional implications. *Trends Neurosci.* 18 (1), 22–29. doi: 10.1016/0166-2236(95)93946-U

Mansour, A., Burke, S., Pavlic, R. J., Akil, H., and Watson, S. J. (1996). Immunohistochemical localization of the cloned kappa 1 receptor in the rat CNS and pituitary. *Neuroscience* 71, 671–690. doi: 10.1016/0306-4522(95)00464-5

Margolis, E. B., and Karkhanis, A. N. (2019). Dopaminergic cellular and circuit contributions to kappa opioid receptor mediated aversion. *Neurochem. Int.* 129, 104504. doi: 10.1016/j.neuint.2019.104504

Margolis, E. B., Hjelmstad, G. O., Bonci, A., and Fields, H. L. (2003). Kappa-opioid agonists directly inhibit midbrain dopaminergic neurons. *J. Neurosci.* 23, 9981–9986. doi: 10.1523/JNEUROSCI.23-31-09981.2003

Margolis, E. B., Hjelmstad, G. O., Bonci, A., and Fields, H. L. (2005). Both Kappa and Mu Opioid Agonists Inhibit Glutamatergic Input to Ventral Tegmental Area Neurons. *J. Neurophysiol.* 93, 3086–3093. doi: 10.1152/jn.00855.2004

Margolis, E. B., Lock, H., Chefer, V. I., Shippenberg, T. S., Hjelmstad, G. O., and Fields, H. L. (2006). Kappa opioids selectively control dopaminergic neurons projecting to the prefrontal cortex. *Proc. Natl. Acad. Sci. U. S. A.* 103, 2938–2942. doi: 10.1073/pnas.0511159103

Margolis, E. B., Mitchell, J. M., Ishikawa, J., Hjelmstad, G. O., and Fields, H. L. (2008). Midbrain dopamine neurons: projection target determines action potential duration and dopamine D(2) receptor inhibition. *J. Neurosci.* 28, 8908–8913. doi: 10.1523/JNEUROSCI.1526-08.2008

Mathews, I. Z., and McCormick, C. M. (2007). Female and male rats in late adolescence differ from adults in amphetamine-induced locomotor activity, but not in conditioned place preference for amphetamine. *Behav. Pharmacol.* 18, 641–650. doi: 10.1097/FBP.0b013e3282effbf5

Mathis, M. A. 1., Pd, A., Funaro, G., RC, T., Moraes, I., AR, T., et al. (2011). Gender differences in obsessive-compulsive disorder: a literature review. *Braz. J. Psychiatry* 33 (4), 390–399. doi: 10.1590/S1516-44462011000400014

McLaughlin, J. P., Marton-Popovici, M., and Chavkin, C. (2003). Kappa opioid receptor antagonism and prodynorphin gene disruption block stress-induced behavioral responses. *J. Neurosci.* 23 (13), 5674–5683. doi: 10.1523/JNEUROSCI.23-13-05674.2003

McLaughlin, J. P., Land, B. B., Li, S., Pintar, J. E., and Chavkin, C. (2006a). Prior activation of kappa opioid receptors by U50,488 mimics repeated forced swim stress to potentiate cocaine place preference conditioning. *Neuropsychopharmacology* 31, 787–794. doi: 10.1038/sj.npp.1300860

McLaughlin, J. P., Li, S., Valdez, J., Chavkin, T. A., and Chavkin, C. (2006b). Social defeat stress-induced behavioral responses are mediated by the endogenous kappa opioid system. *Neuropsychopharmacology* 31 (6), 1241–1248. doi: 10.1038/sj.npp.1300872

Milesi-Hallé, A., McMillan, D. E., Laurenzana, E. M., Byrnes-Blake, K. A., and Owens, S. M. (2007). Sex differences in (+)-amphetamine- and (+)-methamphetamine-induced behavioral response in male and female Sprague-Dawley rats. *Pharmacol. Biochem. Behav.* 86, 140–149. doi: 10.1016/j.pbb.2006.12.018

Negus, S. S., Mello, N. K., Portoghese, P. S., and Lin, C. E. (1997). Effects of kappa opioids on cocaine self-administration by rhesus monkeys. *J. Pharmacol. Exp. Ther.* 282, 44–55.

Nestler, E. J. (2001). Molecular basis of long-term plasticity underlying addiction. *Nat. Rev. Neurosci.* 2, 119–128. doi: 10.1038/35053570

Perreault, M. L., Graham, D., Bisnaire, L., Simms, J., Hayton, S., and Szechtman, H. (2006). Kappa-opioid agonist U69593 potentiates locomotor sensitization to the D2/D3 agonist quinpirole: pre- and postsynaptic mechanisms. *Neuropsychopharmacology* 31, 1967–1981. doi: 10.1038/sj.npp.1300938

Perreault, M. L., Seeman, P., and Szechtman, H. (2007). Kappa-opioid receptor stimulation quickens pathogenesis of compulsive checking in the quinpirole sensitization model of obsessive-compulsive disorder (OCD). *Behav. Neurosci.* 121, 976–991. doi: 10.1037/0735-7044.121.5.976

Pierce, R. C., and Kalivas, P. W. (1997). A circuitry model of the expression of behavioral sensitization to amphetamine-like psychostimulants. *Brain Res. Brain Res. Rev.* 25, 192–216. doi: 10.1016/S0165-0173(97)00021-0

Polter, A. M., Bishop, R. A., Briand, L. A., Graziane, N. M., Pierce, R. C., and Kauer, J. A. (2014). Poststress Block of Kappa Opioid Receptors Rescues Long-Term Potentiation of Inhibitory Synapses and Prevents Reinstatement of Cocaine Seeking. *Biol. Psychiatry* 76, 785–793. doi: 10.1016/j.biopsych.2014.04.019

Puig-Ramos, A., Santiago, G. S., and Segarra, A. C. (2008). U-69593, a kappa opioid receptor agonist, decreases cocaine-induced behavioral sensitization in female rats. *Behav. Neurosci.* 122, 151–160. doi: 10.1037/0735-7044.122.1.151

Robbins, T. W., Gillan, C. M., Smith, D. G., de Wit, S., and Ersche, K. D. (2012). Neurocognitive endophenotypes of impulsivity and compulsivity: towards dimensional psychiatry. *Trends Cognit. Sci.* 16, 81–91. doi: 10.1016/j.tics.2011.11.009

Roberts, D. C. S., Bennett, S. A. L., and Vickers, G. J. (1989). The estrous cycle affects cocaine self-administration on a progressive ratio schedule in rats. *Psychopharmacol. (Berl)* 98, 408–411. doi: 10.1007/BF00451696

Robinson, T. E., and Berridge, K. C. (1993). The neural basis of drug craving: an incentive-sensitization theory of addiction. *Brain Res. Brain Res. Rev.* 18, 247–291. doi: 10.1016/0165-0173(93)90013-P

Robinson, T. E., and Berridge, K. C. (2001). Incentive-sensitization and addiction. *Addiction* 96, 103–114. doi: 10.1046/j.1360-0443.2001.9611038.x

Rose, J. H., Karkhanis, A. N., Steiniger-Brach, B., and Jones, S. R. (2016). Distinct effects of nalmefene on dopamine uptake rates and kappa opioid receptor activity in the nucleus accumbens following chronic intermittent ethanol exposure. *Int. J. Mol. Sci.* 17, 1216. doi: 10.3390/ijms17081216

Schlosburg, J. E., Whitfield, T. W. Jr., Park, P. E., Crawford, E. F., George, O., Vendruscolo, L. F., et al. (2013). Long-term antagonism of κ opioid receptors prevents escalation of and increased motivation for heroin intake. *J. Neurosci.* 33 (49), 19384–19392. doi: 10.1523/JNEUROSCI.1979-13.2013

Sesack, S. R., and Pickel, V. M. (1992). Dual ultrastructural localization of enkephalin and tyrosine hydroxylase immunoreactivity in the rat ventral tegmental area: multiple substrates for opiate-dopamine interactions. *J. Neurosci.* 12, 1335–a1350. doi: 10.1523/JNEUROSCI.12-04-01335.1992

Sesack, S. R., Aoki, C., and Pickel, V. M. (1994). Ultrastructural localization of D2 receptor-like immunoreactivity in midbrain dopamine neurons and their striatal targets. *J. Neurosci.* 14, 88–106. doi: 10.1523/JNEUROSCI.14-01-00088.1994

Sesia, T., Bizup, B., and Grace, A. A. (2013). Evaluation of animal models of obsessive-compulsive disorder: correlation with phasic dopamine neuron activity. *Int. J. Neuropsychopharmacol.* 16, 1295–1307. doi: 10.1017/S146114571200154X

Shippenberg, T. S., Zapata, A., and Chefer, V. I. (2007). Dynorphin and the pathophysiology of drug addiction. *Pharmacol. Ther.* 116, 306–321. doi: 10.1016/j.pharmthera.2007.06.011

Smith, J. A., Loughlin, S. E., and Leslie, F. M. (1992). kappa-Opioid inhibition of [3H]dopamine release from rat ventral mesencephalic dissociated cell cultures. *Mol. Pharmacol.* 42.

Smith, J. W., Fetsko, L. A., Xu, R., and Wang, Y. (2002). Dopamine D2L receptor knockout mice display deficits in positive and negative reinforcing properties of morphine and in avoidance learning. *Neuroscience* 113 (4), 755–765. doi: 10.1016/S0306-4522(02)00257-9

Smith, J. S., Schindler, A. G., Martinelli, E., Gustin, R. M., Bruchas, M. R., and Chavkin, C. (2012). Stress-induced activation of the dynorphin/κ-opioid receptor system in the amygdala potentiates nicotine conditioned place preference. *J. Neurosci.* 32, 1488–1495. doi: 10.1523/JNEUROSCI.2980-11.2012

Spanagel, R., Herz, A., and Shippenberg, T. S. (1992). Opposing tonically active endogenous opioid systems modulate the mesolimbic dopaminergic pathway. *Proc. Natl. Acad. Sci.* 89, 2046–2050. doi: 10.1073/pnas.89.6.2046

Speciale, S. G., Manaye, K. F., Sadeq, M., and German, D. C. (1993). Opioid receptors in midbrain dopaminergic regions of the rat. II. Kappa and delta receptor autoradiography. *J. Neural Transm. Gen. Sect.* 91, 53–66. doi: 10.1007/BF01244918

Sperling, R. E., Gomes, S. M., Sypek, E. I., Carey, A. N., and McLaughlin, J. P. (2010). Endogenous kappa-opioid mediation of stress-induced potentiation of ethanol-conditioned place preference and self-administration. *Psychopharmacol. (Berl)* 210 (2), 199–209. doi: 10.1007/s00213-010-1844-5

Steketee, J. D., and Kalivas, P. W. (2011). Drug Wanting: behavioral sensitization and relapse to drug-seeking behavior sibley DR, ed. *Pharmacol. Rev.* 63, 348–365. doi: 10.1124/pr.109.001933

Stuchlik, A., Radostová, D., Hatalova, H., Vales, K., Nekovarova, T., Koprivova, J., et al. (2016). Validity of quinpirole sensitization rat model of OCD: linking evidence from animal and clinical studies. *Front. Behav. Neurosci.* 10, 209. doi: 10.3389/fnbeh.2016.00209

Sun, T., Song, Z., Tian, Y., Tian, W., Zhu, C., Ji, G., et al. (2019). Basolateral amygdala input to the medial prefrontal cortex controls obsessive-compulsive disorder-like checking behavior. *Proc. Natl. Acad. Sci. U. S. A.* 116, 3799–3804. doi: 10.1073/pnas.1814292116

Svingos, A. L., Chavkin, C., Colago, E. E. O., and Pickel, V. M. (2001). Major coexpression of ??-opioid receptors and the dopamine transporter in nucleus accumbens axonal profiles. *Synapse* 42, 185–192. doi: 10.1002/syn.10005

Szechtman, H., Talangbayan, H., and Eilam, D. (1993). Environmental and behavioral components of sensitization induced by the dopamine agonist quinpirole. *Behav. Pharmacol.* 4, 405–410. doi: 10.1097/00008877-199308000-00014

Szechtman, H., Talangbayan, H., Canaran, G., Dai, H., and Eilam, D. (1994). Dynamics of behavioral sensitization induced by the dopamine agonist quinpirole and a proposed central energy control mechanism. *Psychopharmacol. (Berl)* 115, 95–104. doi: 10.1007/BF02244757

Szechtman, H., Sulis, W., and Eilam, D. (1998). Quinpirole induces compulsive checking behavior in rats: a potential animal model of obsessive-compulsive disorder (OCD). *Behav. Neurosci.* 112, 1475–1485. doi: 10.1037/0735-7044.112.6.1475

Szechtman, H., Culver, K., and Eilam, D. (1999). Role of dopamine systems in obsessive-compulsive disorder (OCD): implications from a novel psychostimulant-induced animal model. *Pol. J. Pharmacol.* 51, 55–61.

Szechtman, H., Eckert, M. J., Tse, W. S., Boersma, J. T., Bonura, C a, JZ, M., et al. (2001). Compulsive checking behavior of quinpirole-sensitized rats as an animal model of Obsessive-Compulsive Disorder (OCD): form and control. *BMC Neurosci.* 2, 4. doi: 10.1186/1471-2202-2-4

Szechtman, H., Ahmari, S. E., Beninger, R. J., Eilam, D., Harvey, B. H., Edemann-Callesen, H., et al. (2017). Obsessive-compulsive disorder: Insights from animal models. *Neurosci. Biobehav. Rev.* 76, 254–279. doi: 10.1016/j.neubiorev.2016.04.019

Tejeda, H. A., and Bonci, A. (2019). Dynorphin/kappa-opioid receptor control of dopamine dynamics: Implications for negative affective states and psychiatric disorders. *Brain Res.* 1713, 91–101. doi: 10.1016/j.brainres.2018.09.023

Tejeda, H. A., Wu, J., Kornspun, A. R., Pignatelli, M., Kashtelyan, V., Krashes, M. J., et al. (2017). Pathway- and cell-specific kappa-opioid receptor modulation of excitation-inhibition balance differentially gates d1 and d2 accumbens neuron activity. *Neuron* 93 (1), 147–163. doi: 10.1016/j.neuron.2016.12.005

Thompson, A. C., Zapata, A., Justice, J. B., Vaughan, R. A., Sharpe, L. G., and Shippenberg, T. S. (2000). Kappa-opioid receptor activation modifies dopamine uptake in the nucleus accumbens and opposes the effects of cocaine. *J. Neurosci.* 20, 9333–9340. doi: 10.1523/JNEUROSCI.20-24-09333.2000

Thompson, D., Martini, L., and Whistler, J. L. (2010). Altered ratio of D1 and D2 dopamine receptors in mouse striatum is associated with behavioral sensitization to cocaine. *PloS One* 5, e11038. doi: 10.1371/journal.pone.0011038

Usiello, A., Baik, J.-H., Rougé-Pont, F., Picetti, R., Dierich, A., LeMeur, M., et al. (2000). Distinct functions of the two isoforms of dopamine D2 receptors. *Nature* 408, 199–203. doi: 10.1038/35041572

Van Bockstaele, E. J., and Pickel, V. M. (1995). GABA-containing neurons in the ventral tegmental area project to the nucleus accumbens in rat brain. *Brain Res.* 682 (1-2), 215–221. doi: 10.1016/0006-8993(95)00334-M

Van't Veer, A., Bechtholt, A. J., Onvani, S., Potter, D., Wang, Y., Liu-Chen, L. Y., et al. (2013). Ablation of kappa-opioid receptors from brain dopamine neurons has anxiolytic-like effects and enhances cocaine-induced plasticity. *Neuropsychopharmacology* 38 (8), 1585–1597. doi: 10.1038/npp.2013.58

Vanderschuren, L. J., and Kalivas, P. W. (2000). Alterations in dopaminergic and glutamatergic transmission in the induction and expression of behavioral sensitization: a critical review of preclinical studies. *Psychopharmacol. (Berl)* 151 (2-3), 99–120. doi: 10.1007/s002130000493

Volkow, N. D., Wise, R. A., and Baler, R. (2017). The dopamine motive system: implications for drug and food addiction. *Nat. Rev. Neurosci.* 18, 741–752. doi: 10.1038/nrn.2017.130

Walker, Q. D., Rooney, M. B., Wightman, R. M., and Kuhn, C. M. (2000). Dopamine release and uptake are greater in female than male rat striatum as measured by fast cyclic voltammetry. *Neuroscience* 95, 1061–1070. doi: 10.1016/S0306-4522(99)00500-X

Wee, S., and Koob, G. F. (2010). The role of the dynorphin–κ opioid system in the reinforcing effects of drugs of abuse. *Psychopharmacol. (Berl)* 210, 121–135. doi: 10.1007/s00213-010-1825-8

Wee, S., Orio, L., Ghirmai, S., Cashman, J. R., and Koob, G. F. (2009). Inhibition of kappa opioid receptors attenuated increased cocaine intake in rats with extended access to cocaine. *Psychopharmacol. (Berl)* 205, 565–575. doi: 10.1007/s00213-009-1563-y

Whitfield, T. W. Jr., Schlosburg, J. E., Wee, S., Gould, A., George, O., Grant, Y. , et al. (2015). κ Opioid receptors in the nucleus accumbens shell mediate escalation of methamphetamine intake. *J. Neurosci.* 35 (10), 4296–4305. doi: 10.1523/JNEUROSCI.1978-13.2015

Williams, M. T., Mugno, B., Franklin, M., and Faber, S. (2013). Symptom dimensions in obsessive-compulsive disorder: phenomenology and treatment outcomes with exposure and ritual prevention. *Psychopathology* 46, 365–376. doi: 10.1159/000348582

Wilson, C. J., Young, S. J., and Groves, P. M. (1977). Statistical properties of neuronal spike trains in the substantia nigra: cell types and their interactions. *Brain Res.* 136, 243–260. doi: 10.1016/0006-8993(77)90801-0

Wise, R. A. (2009). Roles for nigrostriatal—not just mesocorticolimbic—dopamine in reward and addiction. *Trends Neurosci.* 32, 517–524. doi: 10.1016/j.tins.2009.06.004

Xiao, L., and Becker, J. B. (1994). Quantitative microdialysis determination of extracellular striatal dopamine concentration in male and female rats: effects of estrous cycle and gonadectomy. *Neurosci. Lett.* 180, 155–158. doi: 10.1016/0304-3940(94)90510-X

Yager, L. M., Garcia, A. F., Wunsch, A. M., and Ferguson, S. M. (2015). The ins and outs of the striatum: role in drug addiction. *Neuroscience* 301, 529–541. doi: 10.1016/j.neuroscience.2015.06.033

Conflict of Interest: The authors declare that the research was conducted in the absence of any commercial or financial relationships that could be construed as a potential conflict of interest.

The handling editor is currently organizing a Research Topic with one of the authors JF, and confirms the absence of any other collaboration.

frontiers in Pharmacology

REVIEW
published: 28 February 2020
doi: 10.3389/fphar.2019.01641

Dexmedetomidine Improves Cardiovascular and Ventilatory Outcomes in Critically Ill Patients: Basic and Clinical Approaches

Rodrigo L. Castillo[1,2], Mauricio Ibacache[3], Ignacio Cortínez[3], Catalina Carrasco-Pozo[4], Jorge G. Farías[5], Rodrigo A. Carrasco[6], Patricio Vargas-Errázuriz[2,7,8], Daniel Ramos[1], Rafael Benavente[1], Daniela Henríquez Torres[1] and Aníbal Méndez[1]*

[1] Departamento de Medicina Interna Oriente, Facultad de Medicina, Universidad de Chile, Santiago, Chile, [2] Unidad de Paciente Crítico, Hospital del Salvador, Santiago, Chile, [3] Programa de Farmacología y Toxicología & División de Anestesiología, Facultad de Medicina, Pontificia Universidad Católica de Chile, Santiago, Chile, [4] Discovery Biology, Griffith Institute for Drug Discovery, Griffith University, Nathan, QLD, Australia, [5] Departmento de Ingeniería Química, Facultad de Ingeniería y Ciencias, Universidad de La Frontera, Francisco Salazar, Chile, [6] Departamento de Cardiología, Clínica Alemana-Universidad del Desarrollo, Santiago, Chile, [7] Unidad de Paciente Crítico Adulto, Clínica Universidad de Los Andes, Santiago, Chile, [8] Unidad de Paciente Crítico, Clínica Alemana-Universidad del Desarrollo, Santiago, Chile

Dexmedetomidine (DEX) is a highly selective α2-adrenergic agonist with sedative and analgesic properties, with minimal respiratory effects. It is used as a sedative in the intensive care unit and the operating room. The opioid-sparing effect and the absence of respiratory effects make dexmedetomidine an attractive adjuvant drug for anesthesia in obese patients who are at an increased risk for postoperative respiratory complications. The pharmacodynamic effects on the cardiovascular system are known; however the mechanisms that induce cardioprotection are still under study. Regarding the pharmacokinetics properties, this drug is extensively metabolized in the liver by the uridine diphosphate glucuronosyltransferases. It has a relatively high hepatic extraction ratio, and therefore, its metabolism is dependent on liver blood flow. This review shows, from a basic clinical approach, the evidence supporting the use of dexmedetomidine in different settings, from its use in animal models of ischemia-reperfusion, and cardioprotective signaling pathways. In addition, pharmacokinetics and pharmacodynamics studies in obese subjects and the management of patients subjected to mechanical ventilation are described. Moreover, the clinical efficacy of delirium incidence in patients with indication of non-invasive ventilation is shown. Finally, the available evidence from DEX is described by a group of Chilean pharmacologists and clinicians who have worked for more than 10 years on DEX.

Keywords: dexmedetomidine, cardiac, preconditioning, pharmacokinetics, non-invasive mechanical ventilation, sedative and analgesic properties

OPEN ACCESS

Edited by:
Ramón Sotomayor-Zárate, University of Valparaíso, Chile

Reviewed by:
Ventura Simonovich, Italian Hospital of Buenos Aires, Argentina
Romina Andrea Rojas-Ponce, University of Concepcion, Chile
Raúl Vinet, University of Valparaíso, Chile

****Correspondence:***
Rodrigo L. Castillo
rcastillo@med.uchile.cl;
rodrigouch@gmail.com

Specialty section:
This article was submitted to Translational Pharmacology, a section of the journal Frontiers in Pharmacology

Received: *17 August 2019*
Accepted: *16 December 2019*
Published: *28 February 2020*

Citation:
Castillo RL, Ibacache M, Cortínez I, Carrasco-Pozo C, Farías JG, Carrasco RA, Vargas-Errázuriz P, Ramos D, Benavente R, Torres DH and Méndez A (2020) Dexmedetomidine Improves Cardiovascular and Ventilatory Outcomes in Critically Ill Patients: Basic and Clinical Approaches. Front. Pharmacol. 10:1641. doi: 10.3389/fphar.2019.01641

INTRODUCTION

Dexmedetomidine (DEX), a pharmacological alpha 2-adrenergic agonist, which induces sympatholytic mechanism on the brain with anxiolytic and sedative effects (Cormack et al., 2005). DEX triggers the sedative pathways, causing a type of mild sedation and minimizing the risk of respiratory depression. This drug is mainly used in two settings: (1) in intensive care for moderate sedation, although it is not recommended for long-term sedation; and (2) in anesthesia as a stand-alone sedative or as co-adjuvant for general anesthesia. In both settings, DEX has shown interesting cardiovascular, respiratory, anti-inflammatory, and organ protective properties. In clinic, it is used in perioperative sedation and intensive care, due to its analgesic and anxiolytics effects. The drug is commonly administered intravenously, either as a single bolus of approximately 1 μg/kg or as a bolus plus a continuous infusion ranging between 0.2 and 1 μg/kg/h. The stimulus of the different subtypes of α2-adrenergic receptors (α2A, α2B, α2C) and its location in the nervous system (pre or postsynaptic), will determine the different effects observed during use. Currently, many biological functions of DEX have been demonstrated in different animal models, through several signaling pathways.

Currently, the biological functions of DEX have been demonstrated in different animal models through several signaling pathways. Some studies demonstrate the beneficial effects of DEX against ischemia–reperfusi0on (I/R) injury (Riquelme et al., 2016; Deng et al., 2019), activating the eNOS/NO cardioprotective signaling pathways. *In vivo* mechanistic studies are needed to determine the effects of DEX in clinical events that are associated with I/R. This review shows that DEX may be a pharmacological agent that modulates the organ I/R injury responses in humans.

PHARMACOKINETIC PROPERTIES

DEX is an imidazole derivative with a 236.7 g/mol molecular mass and a 2.89 octanol/water partition coefficient (Reel, 2019). Loading doses and infusion rates are determined on a milligram per kilogram total body weight (TBW). In general, linear pharmacokinetics adequately describes the body disposition of the drug, even after prolonged high dose administration in critically ill patients (Iirola et al., 2011a; Välitalo et al., 2013). However, patients with severe hepatic failure or obstructive jaundice have shown a reduction of metabolic clearance (CL) and significant changes in the volume of distribution (VD) (Cunningham et al., 1999; Song et al., 2018). DEX CL remains stable with dose increments within the therapeutic range and decreases with the administration of supratherapeutic doses (Dutta et al., 2000; Iirola et al., 2012).

Even though DEX was developed for intravenous use, it has been administered by different routes with variable bioavailability. Intramuscular administration has shown bioavailability of 103.6% with a time to peak of 1.7 ± 1.8 h (Anttila et al., 2003). Nasal or buccal (submucosal) administration has been successfully used in patients without available venous access, avoiding high plasma peak levels. The bioavailability and time to peak of the nasal approach is 65% (35–93%) and 38 (15–60) min, respectively (Iirola et al., 2011b; Yoo et al., 2015). The bioavailability and time to peak of the buccal route is 81.8% (72.6–92.1%) and 1.5 ± 0.2 h, respectively. Due to an extensive first-pass effect, the bioavailability of the drug reaches only 15.6% after oral administration (Anttila et al., 2003). DEX has a high protein binding (94%) with an extensive VD and easily crosses the blood-brain barrier (Bhana et al., 2000). In non-compartmental kinetics, the administration of a single bolus has a 6.5 ± 3.4 min distribution half-life (Anttila et al., 2003). The drug has a described steady state VD of 80–194 l, which is related to patient weight (Dyck et al., 1993; Khan et al., 1999; Välitalo et al., 2013). ICU patients tend to have greater variability of this parameter (109–223 l), and hypoalbuminemia has been shown to increase the VD in these patients (Iirola et al., 2012; Hodiamont et al., 2017).

The drug is extensively metabolized in the liver with a determined extraction ratio of 0.7, and less than 1% of the drug eliminated without changes (Anttila et al., 2003). DEX undergoes N-glucuronidation (34%) by uridine diphosphate glucuronosyltransferases (UGT2B10, UGT1A4) and is also hydroxylated in a smaller proportion by the P450 enzyme system, specifically CYP2A6 (Adams and Murphy, 2000; Jorden and Tung, 2002; Kohli et al., 2012). The generated metabolites are approximately 100 times less potent than the original administered drug and are considered inactive. These metabolites are finally eliminated *via* the kidneys (95%). The CL is 36–42 l/h in average adult patients (Dyck et al., 1993; Khan et al., 1999). In ICU patients, CL has been defined at 31.8–57 l/h (Venn et al., 2002; Zhang et al., 2015). In healthy volunteers, the elimination half-life is 2.1–3.1 h, and in ICU patients, the half-life slightly increases to 2.2–3.7 h (Karol and Maze, 2000; Venn et al., 2002; Zhang et al., 2015). In this context, the presence of hypoalbuminemia decreases or increases half-life times (Iirola et al., 2011a; Zhang et al., 2015). However, as a drug with a high hepatic extraction ratio, DEX CL would depend more on the blood flow to the liver (cardiac output) than on protein binding (Benet, 2002). It has been reported that a 19% cardiac output reduction decreases DEX CL by 12% (Dutta et al., 2000).

Numerous factors influencing the DEX dosage have been reported in the literature. Conditions such as hypoalbuminemia, liver dysfunction, reduced cardiac output, and hemodynamic alterations significantly affect both the VD and CL (Karol and Maze, 2000; Dutta et al., 2000; Zhang et al., 2015). Several pharmacokinetic models developed in different populations show that observed inter-individual variability of DEX body disposition is explained by the influence of the aforementioned covariates on pharmacokinetic parameters and patient dose requirements. Other covariates, such as ethnicity and polymorphisms of metabolic enzymes, are less relevant contributors to the described variability (Karol, 1996; Karol and Maze, 2000; Kurnik et al., 2008; Kohli et al., 2012).

In adults, the majority of these experimental models were derived from four trials of critically ill patients or healthy volunteers in which different DEX continuous infusions with

varying durations were used. In most studies, a 2-compartment model adequately describes the disposition and elimination of DEX (Khan et al., 1999; Venn et al., 2002; Zhang et al., 2015; Cortinez et al., 2015). Fewer trials have described models of 1 and 3 compartments (Dyck et al., 1993; Dutta et al., 2000; Lin et al., 2011; Hannivoort et al., 2015). In these models, the VD has been correlated with patient age, TBW, free-fat mass (FFM), albuminemia, and the intercurrence of surgery. The CL varies according to patient height, TBW, FFM, albuminemia, and alanine aminotransferase metabolic activity. The review article by Weerink et al. evaluated the impact of different covariates on the DEX plasma concentration-time profile by means of comprehensive simulations (Weerink et al., 2017). For this purpose, a DEX 35 μg loading dose infused over 10 min, followed by a 35 μg/h maintenance dose was simulated supporting the different published pharmacokinetic simulations. In a 2h DEX simulated infusion the authors found: 1) DEX reached concentrations after a bolus dose was directly dependent on patient albuminemia and inversely related to patient height, with a less significant influence of age on the observed maximum concentration; 2) the accomplished concentration during DEX infusion (steady state) was influenced by patient age, albuminemia, height, and body weight. These findings are in agreement with previously published data where age-associated metabolic CL reduction increases DEX plasma concentration in patients (Iirola et al., 2012). Albuminemia and height may also influence DEX concentrations, but their impact is less clear compared to other more relevant covariates (Lin et al., 2011; Lee et al., 2012; Zhang et al., 2015). For instance, available evidence suggests that DEX CL is significantly influenced by hepatic blood flow and cardiac output, but since DEX likely has a high hepatic extraction ratio, this influence is difficult to establish in all populations. However, the non-linear behavior of DEX CL has been described in non-compartmental and compartmental analyses where DEX concentration increments reduce the drug CL by reducing cardiac output (Dutta et al., 2000; Iirola et al., 2012). At present, changes in TBW or FFM have a significant impact on concentrations after a bolus and during the infusion of DEX and should be considered when dosing adult patients (Cortinez et al., 2015; Hannivoort et al., 2015; Kuang et al., 2016).

As previously mentioned, TBW emerges as a significant covariate that influences the concentrations of DEX. Infusion schemes using mass units of drug per kilogram of TBW do not seem appropriate for the obese individual, as they result in increased plasma levels than those observed in lean subjects. In a pharmacokinetic modeling analysis by Cortinez et al., lean tissues showed as fat-free mass (FFM) accounted for size-dependent changes in VD of DEX (Cortinez et al., 2015). In addition, they also showed that for any lean body mass, total CL decreased associated with major fat mass. In a second trial by the same study group, authors confirmed that lean body mass was an appropriate dosing scalar for size in obese patients and showed that decreased hepatic blood had a significant effect on the CL of DEX (Rolle et al., 2018). The observed CL reduction in this population is most probably explained by a relative overdose of obese patients caused by TBW-based dosing schemes. In this setting, scaling doses to FFM or allometric TBW seems more relevant (Cortinez et al., 2015; Hannivoort et al., 2015; Rolle et al., 2018).

Although the drug is not approved for clinical administration in the pediatric population, its off-label use is widely extended in these patients (Mahmoud and Mason, 2015). DEX pharmacokinetics in children has been studied in ICU patients and in patients undergoing cardiac and non-cardiac surgery (Potts et al., 2009; Su et al., 2010; Wiczling et al., 2016; Su F. et al., 2016; Liu et al., 2017). A 2-compartment model, using TBW scaled to 1 for the VD and 0.75 for the CL (Equation 1), adequately describes the disposition of the drug in pediatric populations.

$$y = a \; [\![\; TBW \;]\!] \; \wedge PWR \tag{1}$$

where y is the variable of interest (e.g., Cl or V), a is the allometric coefficient, and PWR is the allometric exponent.

In children, 93% of DEX is protein bound with a rapid redistribution half-life of approximately 7 min and elimination half-life of 2 h (Petroz et al., 2006; Mason and Lerman, 2011). Weight appears as a significant covariate influencing DEX CL in children older than 2 years with nearby levels (within 30–40%) to those reported in adults (Petroz et al., 2006). Several studies report the influence of the maturation of neonatal enzymatic activity on CL, but the available data are very dissimilar. At birth, a full-term neonate has a DEX CL of 43–54% adult values, and in a variable period (1 month–1 year) reaches adult values (Potts et al., 2009; Wiczling et al., 2016). Overall, allometric scaling can be used to predict DEX concentrations in children older than 1 year of age. In children younger than 1 year, inter-individual variability significantly influences the CL and is substantially greater than the impact of maturation on this parameter. Thus, despite considering maturation and patient age, it is difficult to achieve a certain predicted concentration in very small children.

PHARMACODYNAMIC PROPERTIES

In terms of the pharmacodynamic properties of DEX, it shows a high affinity and selectivity for the α2-adrenoceptors, this pharmacological characteristic determines a typical biphasic hemodynamic response. After infusion, DEX induces sympatholytic effect, such as a lower mean arterial blood pressure (MAP) and heart rate (HR) through activation of presynaptic α2-adrenoceptors in the central nervous system. In addition, DEX induces vasodilation through activation of α2-adrenoceptors in endothelial cells (Figueroa et al., 2001; Talke et al., 2003). At higher concentrations, vasoconstrictive effects of DEX are attributable to activation of α2-adrenoceptors in vascular smooth muscle, resulting clinically in an increase in MAP and diminution of HR (Snapir et al., 2006). The pharmacokinetic and pharmacodynamic effects of DEX have been extensively studied in animal models, however its role in critical patients' arterial pressure and heart rate has been scarcely addressed (Ebert et al., 2000; Snapir et al., 2006; Potts et al., 2010).

Adverse Effects

Adverse effects of dexmedetomidine are mainly restricted to hemodynamic alterations. These include hypertension, bradycardia, and hypotension owing to pre- and postsynaptic α2-receptor activation, which causes vasoconstriction, vasodilatation, and reflex bradycardia (Ebert et al., 2000). Long-term use of dexmedetomidine leads to super sensitization and upregulation of receptors. With abrupt discontinuation, a withdrawal syndrome of nervousness, agitation, headaches, and hypertensive crisis can occur.

Common adverse effects for organ systems (1 to 10%) are: respiratory, Atelectasis, hypoxia, pulmonary edema, pleural effusion, respiratory failure, acute respiratory distress syndrome, bradypnea, pneumonia, pharyngolaryngeal pain, gastrointestinal, dry mouth, vomiting, constipation, abdominal distension, abdominal pain, diarrhea, hematologic, anemia, metabolic, hyperglycemia, hypoglycemia, hypocalcemia, acidosis, hypokalemia, hypomagnesemia, hypernatremia, hypophosphatemia, acute renal failure, and oliguria (Cheung et al., 2014).

Dexmedetomidine is not recommended in patients with advanced heart block and ventricular dysfunction. FDA has classified it as a category C pregnancy risk, therefore the drug should be used with extreme caution in women who are pregnant (Morgan et al., 2006).

Two major limitations regarding dexmedetomidine use, are its long-lasting effects and its hemodynamic side effects. A safe and quick reversal of these effects would benefit clinical practice, presumably leading to more widespread use of dexmedetomidine. The selective α2-antagonist atipamezole can effectively reverse dexmedetomidine's hemodynamic and sedative effects (Karhuvaara et al., 1991). The reduction in heart rate and blood pressure caused by dexmedetomidine is quickly reversed after IV administration of 15–150 μg/kg atipamezole. Higher doses of atipamezole (150 μg/kg) also reverse sedation. Transient orthosympathic activation, with a 10-fold increase in plasma norepinephrine levels, is seen with higher doses or fast infusion rates (Scheinin et al., 1998).

Effects on Cardiovascular and Ventilatory Physiology

The US Food and Drug Administration (FDA) originally approved DEX for use in "initially intubated, mechanically ventilated patients," that is, in ventilated patients requiring sedation throughout and after extubation. Then Hanna and Milap, (2008) approved its use for the sedation of non-invasive intubated critical patients (Panzer et al., 2009; Keating et al., 2012). Since DEX's appearance on the market as a sedative drug, cardiovascular and ventilatory effects have been extensively characterized (Deutsch and Tobias, 2007).

The effects of DEX on the cardiovascular system are a consequence of the pharmacological modulation of the α-2 adrenergic receptor. The stimulation of the different subtypes of α2 adrenergic receptors (α2A, α2B α2C) and their location in the nervous system (pre or postsynaptic), will determine the different cardiovascular effects observed during its use. An intravenous bolus of DEX in healthy individuals determines a biphasic blood pressure response. DEX infusion induces an initial transient increase vasoconstriction in vascular smooth musculature (by activation of postsynaptic α2B receptors), followed by a decrease in blood pressure and heart rate (by the activation of α2A receptors in the central nervous system). This apparent dual action of the drug becomes evident when its effect is considered in sympathetically denervated territories, such as when an anesthetic blockade of peripheral nerve exists (Talke et al., 2003) or when high doses of the drug are used. In these situations, the peripheral vasoconstrictor effect of the drug predominates. The opposite effect, vasodilation associated with central sympatholysis is observed when low doses are used in subjects with a non-intervened sympathetic system. The omission of the DEX loading bolus prevents initial hypertension and reflex bradycardia (Ickeringill et al., 2004). In addition, stimulation of postsynaptic α2-adrenergic receptors in endothelial cells would also induce vasodilation. In this context, the correct infusion rate of the drug, appropriate volume administration and clinical indication, make DEX a substance with a wide security therapeutic range (Kamibayashi and Maze, 2000). The central inhibition of the sympathetic system could minimize patient stress and instability in blood pressure during and after cardiac surgery (Gong et al., 2017). Evidence suggests that induced autonomic nervous system modulation during perioperative administration of DEX is associated with a trend towards improved cardiac outcomes following noncardiac surgery (Biccard et al., 2008; Wijeysundera et al., 2009). In addition, this central inhibition of sympathetic discharge could prevent the sympathetic reservoir from being depleted, and therefore the Dex group has higher blood pressure compared to the control group. Mukhtar et al. used a dosage of 0.5 μg/kg/h by infusion, which was effective in diminishing the hemodynamic response to surgery without deleterious vasodepressor effects (Mukhtar, 2006).

Despite the deep sedative effects, DEX is associated with minor respiratory depression, even when it is dosed in plasma levels up to 15 times with those usually obtained during administration, offering a higher level of safety, compared with other sedative agents (Venn et al., 2000; Filbey et al., 2014). Hypercapnic stimulation is preserved and limits apnea or attenuates the stimulatory effect of CO2 levels. In volunteers, DEX infusions preserved the hypercapnic ventilatory response, the respiratory rate was significantly increased, and the overall apnea/hypopnea index was significantly decreased. The distribution of inspiratory time/ventilatory cycle time showed an increased peak. More importantly, DEX exhibited a hypercapnic arousal phenomenon similar to that which has been described during natural sleep (Hsu et al., 2004). Compared with opioid infusions, DEX can be infused by a tracheal tube in a safe manner (Panzer et al., 2009).

DEX Molecular Pathways

DEX modulates some intracellular pathways such as G protein-coupled receptors, protein kinase C (PKC) activity, and inositol triphosphate (IP3) levels in renal cells. Protein kinase C is relevant as an ischemic preconditioning trigger providing organ protection, the opening mitochondrial ATP-sensitive K+ channels, and the

induction of protective gene transcription (Curtis et al., 2011). DEX determines the *in vitro* activation of the adenylyl cyclase-cyclic adenosine monophosphate (cAMP), suggesting that DEX may have a protective effect through the modulation of PKC activation-induced HSP27 phosphorylation (Tanabe et al., 2008; Tanabe et al., 2010). The α2-AR-focal adhesion kinase-Src-phosphatidylinositol 3-kinase (PI3K)-protein kinase B (Akt) (Girault et al., 1999; Parcellier et al., 2008), and the mitochondrial ATP-sensitive K+ channel pathways are involved in the preconditioning and postconditioning mechanisms induced by DEX against hippocampal oxidative damage (Dahmani et al., 2008; Dahmani et al., 2010). Treatment with DEX reduces central nervous injury in rats subjected to focal I/R, which is mediated by the activation of the PI3K/Akt and ERK1/2 pathways (Zhu et al., 2013). Moreover, DEX attenuates hippocampal CA1 long-term potentiation. α2-ARs and imidazoline I2 receptors are modulated by DEX (Takamatsu et al., 2008). Regarding the neuroprotective effects, epidermal growth factor receptor activation in astrocytes *in vivo* represents an important process secondary to α2-AR activation (Du et al., 2009). Moreover, the α2-ARs also activate the mitogen-activated protein kinase pathway and thus determine the proliferation of tubular cells derived from the human intestinal epithelium in rats. (Schaak et al., 2000; Cussac et al., 2002; Karkoulias et al., 2006).

Previous animal experiments have shown benefits and cardioprotective effects of DEX administration in the ischemic heart (Roekaerts et al., 1996; Willigers et al., 2003; Okada et al., 2007). Furthermore, it has been shown that DEX administration causes activation of signaling pathways associated with cardiac survival. The DEX pretreatment of rat hearts induces Erk 1/2, Akt and eNOS activation, improves myocardial function and reduces myocardial infarction size after regional ischemia-reperfusion (I/R) of the heart in the *in vivo* and *ex vivo* models (Ibacache et al., 2012). In this study, the three isotypes of α2-adrenergic receptors were detected in the whole cardiac tissue and the α2A and α2C adrenergic receptors were detected only in isolated cardiomyocytes. The authors concluded that independently from autonomic nervous system modulation, DEX cardioprotective effects are mediated by activation of pro-survival PI3K/Akt signaling pathway after cardiac α2-adrenergic receptor stimulation. More recent studies have demonstrated the role of endothelial α2-adrenergic receptors with beneficial effects on DEX against I/R injury (Riquelme et al., 2016; Deng et al., 2019), activating the eNOS/NO cardioprotective signaling pathways (Kim et al., 2009).

Molecular Mechanisms of Dexmedetomidine Effects on Heart and Lung

The mitochondria are critical coordinators of cellular life through their function on bioenergetics, producing energy, and their role in apoptosis, regulating cell death (Wang and Youle, 2009). The mitochondria supply 90% of the cardiomyocyte ATP, which is necessary to support contraction, metabolism, and ion homeostasis, and thus have a critical role in cardiac function (Harris and Das, 1991; Pohjoismäki and Goffart, 2017). Mitochondrial dysfunction has been involved in the pathophysiology of cardiovascular disease, including ischemia/reperfusion (I/R) injury, arrhythmogenesis, and left ventricular dysfunction (Lesnefsky et al., 2001; Chen et al., 2018a; Chen et al., 2018b). It has been shown that DEX preconditioning rat cardiomyocytes through mitochondrial protection diminishes reactive oxygen species (ROS)-induced apoptosis (Liu et al., 2018; Weng et al., 2018). Dexmedetomidine prevented the increase in the oxygen consumption rate and ROS levels induced by H2O2. It improved the coupling efficiency of the mitochondria potentially by preserving mitochondrial membrane potential (MMP) in the presence of mitochondrial uncouplers (Liu et al., 2018; Weng et al., 2018). Moreover, dexmedetomidine decreased the H2O2-induced activity of caspase 12, and the mRNA levels of Grp78 (glucose regulated protein 78 kDa) and IRE1α (serine/threonine protein kinase/endoribonuclease), three signaling pathways that determine ER stress mediated cell death (Liu et al., 2018). The cardioprotective effect of DEX has also been evidenced in isolated rat hearts, in which DEX preconditioning (10 nmol/l before ischemia for 15 min) had protective effects against I/R injury. The agonist attenuates myocardial cell death and improves cardiac function through mechanisms that involve the inhibition of the mitochondrial permeability transition pore (mPTP) opening at reperfusion time (Jiang et al., 2013). The opening of the mPTP results in respiratory chain uncoupling, mitochondrial ATP synthesis reduction, mitochondrial swelling and cell death (Hunter and Haworth, 1979; Halestrap, 2009). Thus, the mPTP is a selective pharmacological target for cell death prevention in pathophysiological conditions. Cyclophilin D, a regulator of the mPTP, protects against cell death in response to different injuries (Millay et al., 2008; Martin et al., 2009; Ramachandran et al., 2011). The protection of the mitochondrial function, by inhibiting the mPTP opening and thus preserving the MMP, is a plausible mechanism by which DEX exerts its cardioprotective effects.

As an anesthesia co-adjuvant, dexmedetomidine can improve hemodynamic stability and reduce the doses of anesthetics and analgesics during surgery, and it may contribute to the prevention of postoperative cognitive dysfunction (POCD) (Carr et al., 2018). In patients undergoing elective surgery under general anesthesia induced by remifentanil (0.5–1 μg/kg/h) and propofol (3–10 mg/kg/h), the addition of dexmedetomidine (0.2 μg/kg/h) during induction and maintenance periods improved POCD, through the mechanism involving mitochondrial function protection. Dexmedetomidine attenuated the decrease in postoperative National Institutes of Health Stroke Scale (NIHSS) and Auditory Verbal Learning Test (AVLT) scores and the increase in the Beck Depression Inventory (BDI) score. In terms of mitochondrial function, dexmedetomidine alleviated the postoperative decrease in mitochondrial membrane potentials and the activities of the mitochondrial respiratory complexes I–IV in leukocyte cells (Chen et al., 2018a; Chen et al., 2018b). Moreover, dexmedetomidine has been shown to have neuroprotective effects against apoptosis through mechanisms involving mitochondrial functions (Flatters and Bennett, 2006).

Apoptosis is a major pathway in I/R-induced neuronal and cardiac insults (Borgens and Liu-Synder, 2012). Dexmedetomidine prevented apoptosis induced by I/R by protecting against MMP reduction, Bax and cytochrome c release as well as caspase activation in neuro-2a and NB41A3 neuronal cells (Wu et al., 2017). Dexmedetomidine also protected PC12 cells from lidocaine-induced apoptosis, diminished the mRNA levels of COL3A1, increasing Bcl2, and inhibiting caspase 3 activation (Wang et al., 2017). Interestingly, this effect was reversed by the miR-let-7b inhibitor, indicating that dexmedetomidine exerts neuroprotection *via* miR-let-7b, a recognized modulator of mitochondrial function (Barrey et al., 2011; Wang et al., 2017). Dexmedetomidine protected PC12 cells against glutamate-induced cytotoxicity through its mitochondrial protective effect, stabilizing MMP and Ca2+ homeostasis, and through its antioxidant properties, reducing malondialdehyde and augmenting superoxide dismutase activity (Zhang et al., 2016).

In addition, DEX has demonstrated neuroprotective effects against ischemia or tissular hypoxia. In an *in vivo* neuroprotection model, DEX prevented the brain damage induced by cerebral ischemia-reperfusion in rats by activating mitochondrial ATP-sensitive potassium channel (mitoKATP) (Yuan et al., 2017). Dexmedetomidine (50 μg/kg injected intraperitoneally before ischemia and after onset of reperfusion) prevented the I/R-induced increase in the neurological deficit score, pro-oxidant enzyme activity (such as myeloperoxidase and malondialdehyde) in the brain and pro-inflammatory cytokine levels in plasma (like IL-6 and TNF-α) (Yuan et al., 2017). The neuroprotective mechanism by DEX was not observed in the presence of 5-hydroxydecanoate, a mito-KATP channel blocker, which suggests that its pharmacological target involves mitochondrial components (Yuan et al., 2017).

Acute lung injury (ALI) is a common condition in critical patients, and lipopolysaccharide (LPS) is the most important pathogen that determines the development of ALI in sepsis (Gonzales et al., 2014). Dexmedetomidine has been reported to attenuate LPS-induced ALI in rats (Hanci et al., 2012; Fu et al., 2017). Specifically, DEX (50 μg/l 30 min prior to LPS cell treatment) diminished LPS-induced mitochondrial dysfunction by preventing the reduction in cellular ATP levels and MMP in rat type I alveolar epithelial cells (AECs) (Fu et al., 2017). In addition, the same concentration of DEX markedly reduced the LPS-induced mitochondrial-dependent apoptotic pathway in AECs, as the 2α-adrenoreceptor agonist decreased the cytosolic cytochrome c and caspase 3 activity (Liu et al., 2018). *In vivo* dexmedetomidine (50 ug/kg, 30 min prior LPS administration) also decreased LPS-induced apoptosis, as demonstrated by attenuating DNA fragmentation, activation of caspase 3, Bax upregulation and Bcl-2 downregulation in lungs. Furthermore, DEX markedly diminished LPS-induced oxidative stress, as evidenced by the downregulation of cellular ROS in AECs and lipidperoxidation levels in serum (Fu et al., 2017). Moreover, dexmedetomidine treatment inhibited hyperoxia or the LPS/ATP-induced decrease of MMP and mitochondrial ROS production in RAW264.7 cells; therefore, through this mechanism, dexmedetomidine restrained the NLRP3 inflammasome activation-mediated increased release of IL-1β, IL-18, and TNF-α (Zhang et al., 2017). Dexmedetomidine may contribute to reducing ALI, by preventing the activation of macrophages through a mechanism that involves mitochondrial protections or by inducing neutrophil cell death, also by targeting the mitochondria (Kishikawa et al., 2008). Dexmedetomidine (100 ng/ml, 24 h incubation) has been shown to induce apoptosis in neutrophils through mechanisms involving caspase cascade activation and mitochondrial intrinsic pathway triggered by decreasing the MMP (Kishikawa et al., 2008). In the intrinsic pathway, loss of MMP induces the mitochondrial disruption, and mitochondrial pro-apoptotic proteins are released into the cytosol, triggering the activation of caspase-9 (Wang and Youle, 2009). Interestingly, DEX-induced apoptosis is unlikely to be 2α-adrenoreceptor-mediated, as yohimbine, a 2α-adrenoreceptor antagonist, did not attenuate its pro-apoptotic effects (Kishikawa et al., 2008). As the pro-apoptotic effect of dexmedetomidine is evidenced at a concentration 100-times greater than is considered clinically relevant (1 ng/ml), the clinical administration is safe for ICU patients.

The molecular signaling pathways trigger by DEX, and pathophysiological effects are shown in **Figure 1**.

CLINICAL EFFICACY FOR THE USE OF DEX IN DIFFERENT CLINICAL SETTINGS

Diverse effects of DEX include sedation, analgesia, anxiolysis, sympatholysis, cardiovascular stabilization and reduction of anesthetic requirements with preservation of respiratory function (Bhana et al., 2000; Kaur and Singh, 2011; Mahmoud and Mason, 2015). Although labeled for short-term sedation only (24 h or less), its use has been demonstrated to be safe for long-term sedation in critically ill patients (Ozaki et al., 2014), in whom pharmacokinetics is often unpredictable (Weerink et al., 2017). Other important benefits are its easy dosage titration (reducing oversedation risk), its several routes of administration, and minimal clinical impact of its metabolites (Devlin, 2008; Gerlach et al., 2009). These features have given DEX an advantage over other sedatives, such as opioids and benzodiazepines. Its clinical use has been focused on two major scenarios: periprocedural sedation in anesthesia and "light to mild" sedation in the ICU (Arcangeli et al., 2009).

DEX as Peri-Procedural Sedation in Anesthesia

The unique properties of DEX make it suitable for sedation and analgesia during the entire perioperative state in a wide range of procedures (**Table 1**). DEX can be used as premedication, as an anesthetic adjunct for anesthesia or as a postoperative sedative process. This versatility is further enhanced by the property of being compatible with practically all administration routes used in usual perioperative care (**Table 2**). This is particularly useful in pediatrics, non-collaborative patients, or those with insufficient

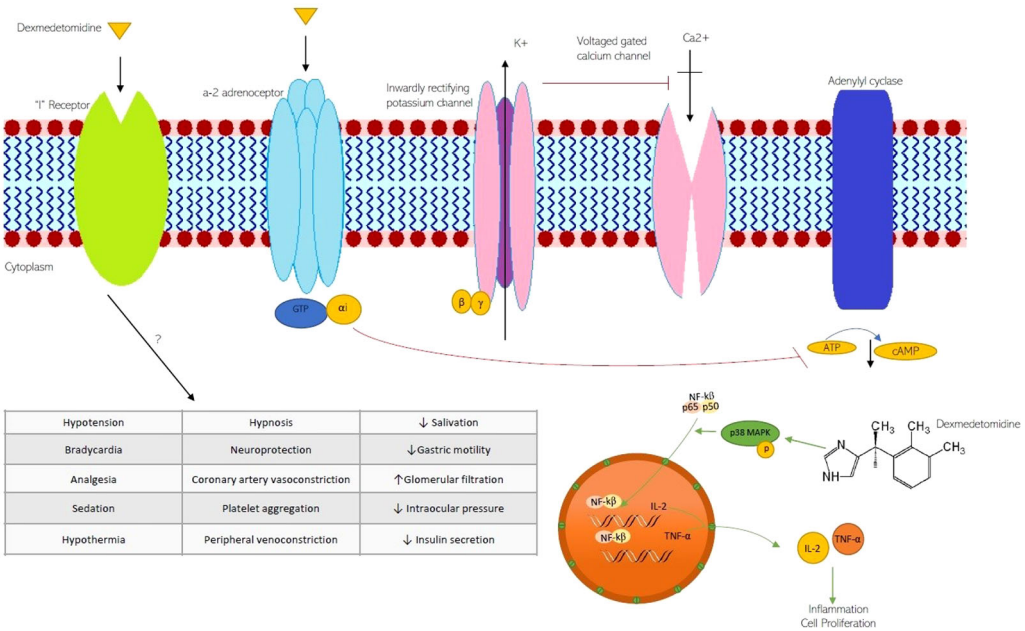

FIGURE 1 | The molecular signaling pathways trigger by DEX and pathophysiological effects on ion channels and G-protein-coupled receptors. K^+, potassium channel; Ca^{2+} calcium channel; GTP guanosine triphosphate; αi alpha inhibitory unit; cAMP c- adenosine monophosphate; NF-κB nuclear factor kappaB; MAPK, Mitogen-Activated Protein Kinases.

TABLE 1 | Reported use of DEX in several settings of perioperative care.

Epidural anesthesia	Schnaider et al., 2005
Spinal anesthesia	Kanazi et al., 2006
Caudal anesthesia	El-Hennawy et al., 2009
Peripheral nerve block	Dai et al., 2018
Intraarticular use (Arthroscopic surgery)	Al-Metwalli et al., 2008
Intensive care unit sedation	Riker et al., 2009
Transesophageal echocardiography	Cooper et al., 2011
Colonoscopy	Jalowiecki et al., 2005
Awake carotid endarterectomy	Bekker et al., 2004
Awake intubation	Bergese et al., 2007
Vitreoretinal surgery	Ghali et al., 2011
Tonsillectomy/Adenoidectomy	Olutoye et al., 2010/Li et al., 2018
Shockwave lithotripsy	Kaygusuz et al., 2008
Attenuated response to tracheal intubation and extubation	Guler et al., 2005
Post-operative analgesia	Venn et al., 1999
Cardiac surgery	Wijeysundera et al., 2003
Neurosurgery	Bekker et al., 2008/Bekker et al., 2013
Sedation in obese patients	Hofer et al., 2005
Use in MRI	Mason et al., 2008
Endoscopic retrograde cholangio-pancreatography	Lu et al., 2018
Ureteroscopy	Shariffuddin et al., 2018

venous access (Scott-Warren and Sebastian, 2016; Weerink et al., 2017; Sottas, 2017).

Several meta-analyses have evaluated the use of DEX in the perioperative period. Piao and Wu (2014) focused on cardiovascular stress response to surgical injury. They found patients receiving DEX had significantly lower blood pressure and heart rate. Conversely, they also found more hypotension and bradycardia. In an earlier publication, Sun et al. (2008) found that DEX reduced the amount of intravenous and inhaled anesthetics, but did not reduce muscle relaxant dosages. Other authors have shown a reduction in postoperative delirium (see below), pain (Schnabel et al., 2013a; Schnabel et al., 2013b; Huang et al., 2015) and shivering (Lewis et al., 2015; Liu et al., 2015; Hoffman and Hamner, 2016). The effect of DEX on postoperative shivering is still not well understood (Lopez, 2018). Although some positive results have been shown in clinical trials, the evidence is still regarded as poor. Moreover, DEX is not superior to other anti-shivering agents, such as fentanyl, meperidine, tramadol or clonidine.

DEX in the ICU

Sedatives are administered to critically ill patients to alleviate discomfort, prevent agitation-related harm, decrease metabolic demand (reducing O_2 consumption and CO_2 production), and improve tolerance and adaptation to mechanical ventilation (Taittonen et al., 1997; Chlan et al., 2017). In order to reduce the adverse events associated with sedative drugs, clinical guidelines have been issued (Barr et al., 2013; Devlin et al., 2018). One of the principal indication for the use of DEX is to alleviate the pain and induce sedation in critical patients by targeting light levels of sedation. However, its administration is not recommended in acute respiratory distress syndrome (ARDS), shock or intracranial

TABLE 2 | Dosage of DEX used in several administration routes.

Route	Dosage	
Intravenous	For ICU sedation 0.2–1.4 mcg/kg/h, may start 1.0 mcg/kg bolus For Procedural sedation 0.2–1 mcg/kh/h	Riker et al., 2009
Intranasal	1–2 mcg/kg	Cimen et al., 2013
Buccal	1–2 mcg/kg	Cimen et al., 2013
Intramuscular	2.5 mcg/kg	Sun et al., 2014
Spinal	0.1–0.2 mcg/kg	Kanazi et al., 2006
Epidural	1–2 mcg/kg	Schnaider et al., 2005
Peripheral nerve block	1 mcg/kg	Obayah et al., 2010

hypertension. These recommendations match in many aspects, the pharmacological and clinical properties of DEX, explaining its increasing use in intensive care units (DeBiasi et al., 2015).

Among the main reported benefits associated with DEX use in the ICU are shorter ICU stays and mechanical ventilation duration (Chlan et al., 2017), less use of benzodiazepines, and lower incidence of delirium (Su X. et al., 2016; Nunes et al., 2018). Conversely, bradycardia and hypotension occurrence have been described in ICU patients with a minimal impact on mortality (Barr et al., 2013; Constantin et al., 2016; Devlin et al., 2018).

DEX in Invasive Mechanical Ventilation

As noted earlier, one of the main indications of sedoanalgesia in the ICU is to improve tolerance and adaptation to mechanical ventilation, as the prevalence of anxiety and agitation in ventilated patients of up to 80% has been reported (Tate et al., 2012; Chlan et al., 2017). Conversely, in the case the use of oversedation in ICU patients the deleterious effects are evidenced. In this case, the clinical effects include: increase in the occurrence of delirium, immobility, respiratory muscle atrophy, long-term mechanical ventilation duration, prolonged of ICU stays, and increased costs and even a rise in mortality (Rodrigues Júnior and do Amaral, 2004; Wunsch, 2012; Kress and Hall, 2014; Reade and Finfer, 2014). Thus, the optimal management of sedation in this scenario has been the subject of extensive debate. For a better understanding of this issue, it is essential to distinguish between two different scenarios where mechanical ventilation is frequently used. The first involves an unstable patient, where deep sedation is required, often associated with a neuromuscular blockade, and where protective ventilation is sought. This patient needs complete suppression of spontaneous respiratory effort, with the physiological objective of reducing the associated pulmonary injury (Yang and Kang, 2017), decreasing metabolic demand (Kumba and Van der Linden, 2008) or reducing intracerebral pressure (Oddo et al., 2016). Examples of this situation include ARDS, severe shock, or unstable intracranial hypertension. In these settings, the use of DEX does not seem to have a role.

In the second scenario, the patient has a less severe condition than the one previously described. Clinical stability has been reached, the cause that led to ICU admission is in clear resolution, resuscitation has been completed, or the effort for strict "pulmonary protection" has ceased. In other words, the patient has entered the "dereanimation" phase (Silversides et al., 2017), where the target is the reduction of the morbidity attributed to the interventions carried out in the ICU. In this scenario, it is highly likely that a more superficial sedation, which favors controlled spontaneous ventilatory effort, mobility, and awakening, will produce better clinical outcomes. DEX has a role in this setting and has indeed shown optimal outcomes in clinical trials (Fraser et al., 2013; Hayashida et al., 2016).

In summary, in patients undergoing mechanical ventilation in the ICU who do not require deep sedation, the use of DEX is associated with fewer days in the ICU, shorter time to extubation and a decrease in the incidence of delirium, although no differences in mortality have been shown (Reade and Finfer, 2014; Su X. et al., 2016; Nunes et al., 2018).

DEX in Non-Invasive Ventilation

Non-invasive ventilation (NIV) has shown to be beneficial in the treatment of acute respiratory failure associated with acute cardiogenic pulmonary edema, chronic obstructive pulmonary disease and postoperative care, amongst others (Jaber et al., 2010; Osadnik et al., 2017; Bello et al., 2018). These benefits are mainly explained by decreasing the need for intubation and connection to mechanical ventilation (Osadnik et al., 2017; Bello et al., 2018). One of the leading causes of NIV failure is agitation, non-tolerance, and non-cooperative patient, reaching rates of up to 22% (Carlucci et al., 2001). In these situations, light sedation has been proposed, and some series have reported its use in up to 20% of patients (Hilbert et al., 2015). DEX has been used in this setting considering its sedative and analgesic effect, without depressing the respiratory center or interfering with airway protection, in addition to its excellent safety profile (Hilbert et al., 2015). Current evidence suggests that it is a safe choice, especially in centers where there is a specialized NIV team (Hilbert et al., 2015). Regarding its effectiveness, the literature is scarce and otherwise contradictory.

DEX and Delirium

Delirium is a common problem in clinical medicine, which is defined as an acute alteration of attention and awareness, attributable to a general medical state (American Psychiatric Association, 2013). In a comprehensive review (Inouye et al., 2014), the highest incidence rates were observed in ICU and postoperative care settings, ranging between 19 and 82%. Although usually transient, it is associated with worse clinical outcomes, including longer hospital length of stay, increased costs, more days on mechanical ventilation, and long-term cognitive impairment and dependence (Pun and Ely, 2007). Moreover, patients who develop delirium in the ICU

experience a threefold increase in six-month mortality risk compared to matched, non-delirious ICU patients (Ely et al., 2004). Among the modifiable risk factors, the use of sedatives and opioid agents has been identified as one of the most relevant, conferring a relative risk of 4.5 in validated predictive models (Inouye et al., 2014). Hence, it is not surprising other drugs have been tested to provide analgesia or light sedation with a lower delirium risk. Several systematic reviews and meta-analyses have evaluated DEX versus opioids, benzodiazepines, and propofol in terms of delirium occurrence (Mo and Zimmermann, 2013; Pasin et al., 2014; Duan et al., 2018; Flükiger et al., 2018). The most recent one by Flükiger et al. (2018) included 25 trials regarding delirium prevention and three regarding its treatment. The authors found that the use of DEX was associated with significantly minor incidence of delirium when compared to the placebo group, standard sedatives, or opioids. In terms of treatment, the small sample and different comparators made it impossible to argue in favor of or against its use. Recently, prophylactic nightly use of DEX has shown to reduce delirium (Skrobik et al., 2018). The results of this industry-funded, two-center, double-blind, placebo-controlled trial have not been replicated but remain promising.

Current published clinical guidelines (Devlin et al., 2018) do not directly support the use of DEX for delirium prevention. Still, they do acknowledge the use of DEX, as a sedoanalgesia, is associated with a lower incidence of delirium compared to strategies based on benzodiazepines or opioids. No recommendations are made concerning its prophylactic nightly use. Finally, regarding delirium treatment, guidelines suggest the use of DEX in patients undergoing mechanical ventilation, in which agitation precludes weaning/extubation.

DEX in Neurological Injury

Scare evidence exists for the neuroprotective effects of DEX in children following neurological injury (Alam et al., 2017). In addition, there are no trials showing the long-term effects of DEX on memory acquisition in children; this is probably due to the inherent challenges associated with designing trials in children. As a result, clinical evidence for the neuroprotective effects of dexmedetomidine in children is limited to cases of delirium following anesthetic infusion, and sedation in critical care patients (Sottas, 2017).

Intracranial lesions or trauma-related damage activate immune inflammation and neuroendocrine responses, causing ischemic brain injury. Studies have shown that inflammatory pathways mediated by neuroendocrine hormones and proinflammatory cytokines is implicated in the pathophysiology of ischemic brain injury. Alpha2-adrenoceptor agonist, dexmedetomidine, is used as neuroprotectant in anesthetic procedures (Jiang et al., 2017). However, meta-analyses to evaluate the neuroprotection of dexmedetomidine against ischemic brain injury are still lacking.

DEX exerts protective effects on brain injury through multiple mechanisms, such as decreasing local inflammation and improving the cerebral oxygen metabolism (Oh-Nishi et al., 2009). These mechanisms underlay the effect of DEX in reducing the ischemic zona and infarct size in an animal model of brain hypoxia-ischemia injury (Ren et al., 2016). Experimental approaches indicated that DEX decreases tumor necrosis factor (TNF)-α, interleukin (IL)-6 levels; and maintains a high level of superoxide dismutase (SOD) activity (Wang et al., 2015). In addition, DEX achieves hemodynamic stability and attenuates the stress-related increase of intracranial pressure (Schomer et al., 2019). In this case, the modulation of inflammatory and stress hormones levels are all relevant predictors of clinical outcome following ischemic brain injury (Sahay et al., 2018).

DEX and Sepsis

Other effects of DEX have been shown *in vitro,* such as anti-inflammatory mechanism in sepsis. These effects are mediated by its action on adrenergic receptors that trigger NF-kB inhibition and level reduction of TNF-α, IL-6, IL-8, and HMGB1 (Kawasaki et al., 2013). Moreover, *in vivo* sepsis, the vagus nerve and α7nAChR-mediated cholinergic anti-inflammatory pathway are required for the anti-inflammatory effect of DEX (Xiang et al., 2014).

Patients that develop sepsis may have marked respiratory and cardiovascular depression. Early stages of sepsis are associated with a drop in the systemic vascular resistance, high cardiac output, and a hypercontractile state (Yuki and Murakami, 2015). The improvement of the sepsis management often requires that patients receive anesthesia as well as analgesia. This is due to the unstable cardiovascular state, changes that exacerbate the cardiac dysfunction. Anesthetic drugs in this setting, should not inhibit compensatory hemodynamic responses. Unfortunately, current intravenous drugs and inhalational pharmacological agents do not meet these considerations (Yuki and Murakami, 2015; Cata et al., 2019). However, DEX seems promising in this context, and mechanistic, pharmacodynamic, and pharmacokinetic studies with DEX in critical septic patients have increased in recent years. Recent evidence in septic shock sedated patients have shown that for a comparable level of sedation, switching from propofol to dexmedetomidine resulted in a reduction of norepinephrine requirements in septic shock patients (Morelli et al., 2019).

Table 3 shows the benefits of adding DEX in different clinical settings.

CONCLUDING REMARKS

Dexmedetomidine is a highly selective alpha-2 receptor agonist. Since its approval by the FDA for sedation in the ICU, its applications have expanded significantly because of its unique mechanism of action, minimal effect on the respiratory drive, and ideal safety profile. Its applications include premedication for pediatric and adult patient populations, procedural sedation and monitored anesthesia care, adjuvant for general and regional anesthesia, perioperative pain control, and postoperative delirium. Clinical evidence show that dexmedetomidine has

TABLE 3 | Benefits of adding DEX in different clinical settings.

Clinical scenario	Benefits of using DEX	References
Peri-procedural sedation	Effective sedation in diverse procedural scenarios. Diverse administration routes. Reduces sympathetic and stress response to surgery. Sparing effects of anesthetic agents Reduces postoperative delirium, shivering and pain	Dyck et al., 1993; Khan et al., 1999; Bhana et al., 2000; Dutta et al., 2000; Venn et al., 2002; Anttila et al., 2003; Petroz et al., 2006; Sun et al., 2008; Potts et al., 2009; Su et al., 2010; Lin et al., 2011; Iirola et al., 2011b; Schnabel et al., 2013a; Schnabel et al., 2013b; Piao and Wu, 2014; Cortinez et al., 2015; Hannivoort et al., 2015; Lewis et al., 2015; Liu et al., 2015; Mahmoud and Mason, 2015; Yoo et al., 2015; Zhang et al., 2015; Hoffman and Hamner, 2016; Scott-Warren and Sebastian, 2016; Su X. et al., 2016; Wiczling et al., 2016; Liu et al., 2017; Sottas, 2017; Weerink et al., 2017
ICU	Reduces ICU stays and duration of mechanical ventilation Sparing effects of benzodiazepines Delirium prevention	Bhana et al., 2000; Su X. et al., 2016; Chlan et al., 2017; Nunes et al., 2018; Flükiger et al., 2018
Invasive Mechanical Ventilation	Shorter Time to extubation and ICU stay. Decrease incidence of delirium	Fraser et al., 2013; Reade and Finfer, 2014; Su et al., 2016; Hayashida et al., 2016; Nunes et al., 2018
Non-invasive Ventilation	Sedation and analgesia without respiratory depression	Hilbert et al., 2015
Delirium	Reduces incidence of delirium in ICU and postoperative period	Mo and Zimmermann, 2013; Pasin et al., 2014; Mahmoud and Mason, 2015; Duan et al., 2018; Flükiger et al., 2018; Skrobik et al., 2018
Neurological Injury	Potential neuroprotection in young children. Potential neuroprotection in Ischemic brain injury	Ren et al., 2016; Alam et al., 2017; Sottas, 2017; Schomer et al., 2019
Sepsis	Anti-inflamatory effects in sepsis. Potential hemodynamic stability	Xiang et al., 2014; Morelli et al., 2019

little effect on the respiratory drive; it still can cause airway obstruction in combination with other anesthetic agents (Nguyen et al., 2017).

Preclinical studies with DEX on murine models have revealed protective effects, including the inhibition of proinflammatory cytokine production (Taniguchi et al., 2004). In *vitro* studies with human whole blood samples have shown that DEX significantly suppresses Lipopolysaccharide induced proinflammatory mediators dose-dependently (Kawasaki et al., 2013). Clinical investigations with human subjects evaluating the effects of DEX on serum inflammatory cytokines during perioperative conditions show inconsistencies in the outcomes (Liu and Qian, 2013; Liang et al., 2017)

Multiple trials and meta-analyses also suggest that DEX use is associated with less delirium and cognitive disturbance, faster weaning from mechanical ventilation, and decreased time to extubation compared with other sedative agents (Shehabi et al., 2019; Yamamoto et al., 2019). As such, DEX seems to be an ideal primary anesthetic agent in the sedation of intubated and mechanically ventilated critical patients.

Regarding their molecular effects, DEX pre-, intra- and postconditioning treatments showed neuroprotective and cardioprotective effects reduced cell necrosis, although only preconditioning showed antiapoptotic mechanisms (Ren et al., 2016; Deng et al., 2019). Dexmedetomidine treatments also reduced IL-6 and TNF-α levels, especially in the preconditioning groups. Oxidative stress is attenuated with all DEX-preconditioning treatments, but only with the higher dose in the intraconditioning group, and no effects were observed in the postconditioning (Rodriguez-Gonzalez, 2016; Cheng et al., 2018). According to these changes, conditioning strategies increased BDNF levels and attenuate mitochondrial dysfunction *in vivo* and *in vitro* models of IR injury (Huang and Jiang, 2019).

Cardiac preconditioning effects associated with DEX administration validated in animal models are shown in **Figure 2**.

Overall, evidence shows that DEX may attenuate the mortality and inhibit inflammatory processes, as it enhances the activity of the immune system while reducing its systemic reaction and lowering cytokine levels. Moreover, DEX succeeds in alleviating heart injury during sepsis, acting beneficially for microcirculation, and shows a neuroprotective role by inhibiting cell death pathways. Various molecular signaling pathways, such as mitochondria or the modulation of transcriptional factors, are under study in both *in vivo* and *in vitro* models.

Therefore, we can say with the reviewed evidence that DEX can be used as a drug for the study of translational models from the cellular and animal point of view and in clinical trials with humans which including cardiovascular and ventilator outcomes. The biological activities associated with DEX continues keep growing, and its diverse effects suggest that it may offer a novel therapeutic approach for the treatment of human diseases with I/R involvement.

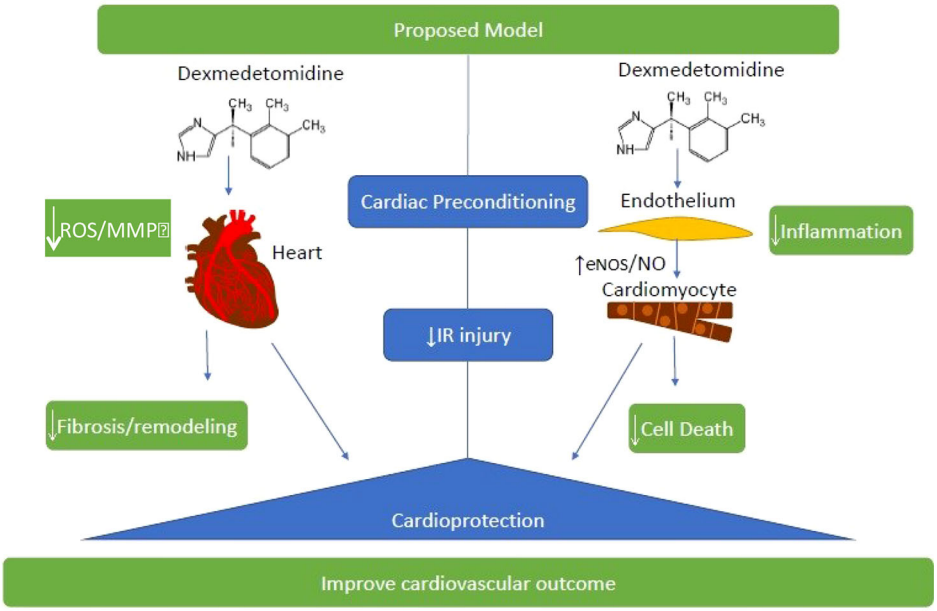

FIGURE 2 | Cardiac preconditioning effects associated with DEX administration validated in animal models. These strategies that determine an attenuation of oxidative stress and inflammation in cardiac tissue are very important to improve the clinical outcome of patients subjected to ischemia-reperfusion (IR) injury. ROS, reactive oxygen species; MMP Matrix metalloproteinases; eNOS, endothelial nitric oxide synthase; NO, nitric oxide.

AUTHOR CONTRIBUTIONS

RC: designed the manuscript and the structure of the themes and wrote about animal models and basic targets of DEX. MI and IC: wrote about human pharmacokinetics of DEX. CC-P: provided evidence of DEX on the mitochondrial protection and clinical outcomes. RC: wrote about DEX on cardioprotection. PV-E, RB, and DR: wrote about DEX in different clinical settings. DT and AM: contributed to the design of the figures and the configuration of the references. JGF: contributed to the design of the Tables, figures and the drafting of the conclusions.

FUNDING

This work was supported by "Fondo Nacional de Desarrollo Científico y Tecnológico" (FONDECYT) Grants 1180387, Gobierno de Chile (JGF). Additional funding was provided by Grant SANTANDER-UNIVERSIA 2015, Banco Santander, Chile (RC).

REFERENCES

Adams, J. P., and Murphy, P. G. (2000). Obesity in anaesthesia and intensive care. *Br. J. Anaesth.* 85, 91–108. doi: 10.1093/bja/85.1.91

Alam, A., Suen, K. C., Hana, Z., Sanders, R. D., Maze, M., and Ma, D. (2017). Neuroprotection and neurotoxicity in the developing brain: an update on the effects of dexmedetomidine and xenon. *Neurotoxicol. Teratol.* 60, 102–116. doi: 10.1016/j.ntt.2017.01.001

Al-Metwalli, R. R., Mowafi, H. A., Ismail, S. A., Siddiqui, A. K., Al-Ghamdi, A. M., Shafi, M. A., et al. (2008). Effect of intra-articular dexmedetomidine on postoperative analgesia after arthroscopic knee surgery. *Br. J. Anaesth.* 101, 395–399. doi: 10.1093/bja/aen184

American Psychiatric Association (2013). *Diagnostic and statistical manual of mental disorders: DSM-5* (Washington, D.C: American Psychiatric Association). doi: 10.1176/appi.books.9780890425596

Anttila, M., Penttila, J., Helminen, A., Vuorilehto, L., and Scheinin, H. (2003). Bioavailability of dexmedetomidine after extravascular doses in healthy subjects. *Br. J. Clin. Pharmacol.* 56, 691–693. doi: 10.1046/j.1365-2125.2003.01944.x

Arcangeli, A., D'Alo, C., and Gaspari, R. (2009). Dexmedetomidine use in general anaesthesia. *Curr. Drug Targets* 10, 687–695. doi: 10.2174/138945009788982423

Barr, J., Fraser, G. L., Puntillo, K., Ely, E. W., Gélinas, C., Dasta, J., et al. (2013). Clinical practice guidelines for the management of pain, agitation, and delirium in adult patients in the intensive care unit. *Crit. Care Med.* 41, 263–306. doi: 10.1097/CCM.0b013e3182783b72

Barrey, E., Saint-Auret, G., Bonnamy, B., Damas, D., Boyer, O., and Gidrol, X. (2011). Pre-microRNA and mature microRNA in human mitochondria. *PloS One* 6, e20220. doi: 10.1371/journal.pone.0020220

Bekker, A. Y., Basile, J., Gold, M., Riles, T., Adelman, M., Cuff, G., et al. (2004). Dexmedetomidine for awake carotid endarterectomy: efficacy, hemodynamic profile, and side effects. *J. Neurosurg. Anesthesiol.* 16, 126–135. doi: 10.1097/00008506-200404000-00004

Bekker, A., Sturaitis, M., Bloom, M., Moric, M., Golfinos, J., Parker, E., et al. (2008). The effect of dexmedetomidine on perioperative hemodynamics in patients undergoing craniotomy. *Anesth. Analg.* 107, 1340–1347. doi: 10.1213/ane.0b013e3181804298

Bekker, A., Haile, M., Kline, R., Didehvar, S., Babu, R., Martiniuk, F., et al. (2013). The effect of intraoperative infusion of dexmedetomidine on the quality of

recovery after major spinal surgery. *J. Neurosurg. Anesthesiol.* 25, 16–24. doi: 10.1097/ANA.0b013e31826318af

Bello, G., De Santis, P., and Antonelli, M. (2018). Non-invasive ventilation in cardiogenic pulmonary edema. *Ann. Transl. Med.* 6, 355. doi: 10.21037/atm.2018.04.39

Benet, L. (2002). Changes in plasma protein binding have little clinical relevance. *Clin. Pharmacol. Ther.* 71, 115–121. doi: 10.1067/mcp.2002.121829

Bergese, S. D., Khabiri, B., Roberts, W. D., Howie, M. B., McSweeney, T. D., and Gerhardt, M. A. (2007). Dexmedetomidine for conscious sedation in difficult awake fiberoptic intubation cases. *J. Clin. Anesth.* 19, 141–144. doi: 10.1016/j.jclinane.2006.07.005

Bhana, N., Goa, K. L., and McClellan, K. J. (2000). Dexmedetomidine. *Drugs* 59, 263–268. doi: 10.2165/00003495-200059020-00012

Biccard, B., Goga, S., and de Beurs, J. (2008). Dexmedetomidine and cardiac protection for non-cardiac surgery: a meta-analysis of randomised controlled trials. *Anaesthesia* 63, 4–14. doi: 10.1111/j.1365-2044.2007.05306.x

Borgens, R. B., and Liu-Snyder, P. (2012). Understanding secondary injury. *Q. Rev. Biol.* 87, 89–127. doi: 10.1086/665457

Carlucci, A., Richard, J. C., Wysocki, M., Lepage, E., and Brochard, L. (2001). Noninvasive versus conventional mechanical ventilation: an epidemiologic survey. *Am. J. Respir. Crit. Care Med.* 163, 874–880. doi: 10.1164/ajrccm.163.4.2006027

Carr, Z. J., Cios, T. J., Potter, K. F., and Swick, J. T. (2018). Does dexmedetomidine ameliorate postoperative cognitive dysfunction? A Brief Review of the Recent Literature. *Curr. Neurol. Neurosci. Rep.* 18, 64. doi: 10.1007/s11910-018-0873-z

Cata, J. P., Owusu-Agyemang, P., Kapoor, R., and Lonnqvist, P. A. (2019). Impact of anesthetics, analgesics, and perioperative blood transfusion in pediatric cancer patients: a comprehensive review of the literature. *Anesth. Analg.* 129 (6), 1653–1665. doi: 10.1213/ANE.0000000000004314

Chen, J., Shen, N., Duan, X., and Guo, Y. (2018a). An investigation of the mechanism of dexmedetomidine in improving postoperative cognitive dysfunction from the perspectives of alleviating neuronal mitochondrial membrane oxidative stress and electrophysiological dysfunction. *Exp. Ther. Med.* 15, 2037–2043. doi: 10.3892/etm.2017.5589

Chen, Q., Aluri, H., and Lesnefsky, E. J. (2018b). Cardiac protection by moving the mitochondria? *Int. J. Cardiol.* 271, 256–257. doi: 10.1016/j.ijcard.2018.06.051

Cheng, X., Hu, J., Wang, Y., Ye, H., Li, X., Gao, Q., et al. (2018). Effects of Dexmedetomidine Postconditioning on Myocardial Ischemia/Reperfusion Injury in Diabetic Rats: Role of the PI3K/Akt-Dependent Signaling Pathway. *J. Diabetes Res.* 2018, 3071959. doi: 10.1155/2018/3071959

Cheung, C. W., Qiu, Q., Ying, A. C., Choi, S. W., Law, W. L., and Irwin, M. G. (2014). The effects of intra-operative dexmedetomidine on postoperative pain, side-effects and recovery in colorectal surgery. *Anaesthesia* 69, 1214–1221. doi: 10.1111/anae.12759

Chlan, L., Skaar, D., Tracy, M., Hayes, S., Hetland, B., Savik, K., et al. (2017). Safety and acceptability of patient-administered sedation during mechanical ventilation. *Am. J. Crit. Care* 26, 288–296. doi: 10.4037/ajcc2017408

Cimen, Z. S., Hanci, A., Sivrikaya, G. U., Kilinc, L. T., and Erol, M. K. (2013). Comparison of buccal and nasal dexmedetomidine premedication for pediatric patients. *Paediatr. Anaesth.* 23, 134–138. doi: 10.1111/pan.12025

Constantin, J. M., Momon, A., Mantz, J., Payen, J. F., De Jonghe, B., Perbet, S., et al. (2016). Efficacy and safety of sedation with Dexmedetomidine in critical care patients: A meta-analysis of randomized controlled trials. *Anaesth. Crit. Care Pain Med.* 35, 7–15. doi: 10.1016/j.accpm.2015.06.012

Cooper, L., Candiotti, K., Gallagher, C., Grenier, E., Arheart, K. L., and Barron, M. E. (2011). A randomized, controlled trial on dexmedetomidine for providing adequate sedation and hemodynamic control for awake, diagnostic transesophageal echocardiography. *J. Cardiothorac. Vasc. Anesth.* 25, 233–237. doi: 10.1053/j.jvca.2010.06.006

Cormack, J. R., Orme, R. M., and Costello, T. G. (2005). The role of alpha2-agonists in neurosurgery. *J. Clin. Neurosci.* 12, 375–378. doi: 10.1016/j.jocn.2004.06.008

Cortinez, L. I., Anderson, B. J., Holford, N. H. G., Puga, V., de la Fuente, N., and Auad, H. (2015). Dexmedetomidine pharmacokinetics in the obese. *Eur. J. Clin. Pharmacol.* 71, 1501–1508. doi: 10.1007/s00228-015-1948-2

Cunningham, F. E., Baughman, V. L., Tonkovich, L., Lam, N., and Layden, T. (1999). Pharmacokinetics of dexmedetomidine in patients with hepatic failure. *Clin. Pharmacol. Ther.* 65, 128. doi: 10.1016/S0009-9236(99)80045-9

Curtis, F. G., Vianna, P. T., Viero, R. M., Fiorio, P. M., Silva, L. M., Braz, J. R., et al. (2011). Dexmedetomidine and S+-ketamine in ischemia and reperfusion injury in the rat kidney. *Acta Cir. Bras.* 26, 202–206. doi: 10.1590/S0102-86502011000300008

Cussac, D., Schaak, S., Gales, C., Flordellis, C., Denis, C., and Paris, H. (2002). Alpha(2B)-Adrenergic receptors activate MAPK and modulate proliferation of primary cultured proximal tubule cells. *Am. J. Physiol. Renal Physiol.* 282, F943–F952. doi: 10.1152/ajprenal.0108.2001

Dahmani, S., Paris, A., Jannier, V., Hein, L., Rouelle, D., and Scholz, J. (2008). Dexmedetomidine increases hippocampal phosphorylated extracellular signal-regulated protein kinase 1 and 2 content by an alpha 2-adrenoceptor-independent mechanism: evidence for the involvement of imidazoline I1 receptors. *Anesthesiology* 108, 457–466. doi: 10.1097/ALN.0b013e318164ca81

Dahmani, S., Rouelle, D., Gressens, P., and Mantz, J. (2010). Characterization of the postconditioning effect of dexmedetomidine in mouse organotypic hippocampal slice cultures exposed to oxygen and glucose deprivation. *Anesthesiology* 112, 373–383. doi: 10.1097/ALN.0b013e3181ca6982

Dai, W., Tang, M., and He, K. (2018). The effect and safety of dexmedetomidine added to ropivacaine in brachial plexus block: a meta-analysis of randomized controlled trials. *Med. (Baltimore)* 97, e12573. doi: 10.1097/MD.0000000000012573

DeBiasi, E. M., Akgün, K. M., and Pisani, M. (2015). Awake or Sedated: Trends in the Evaluation and Management of Agitation in the Intensive Care Unit. *Semin. Respir. Crit. Care Med.* 36, 899–913. doi: 10.1055/s-0035-1564875

Deng, L., Chen, H., Wei, N., Zhang, Z., and Wang, G. (2019). The cardioprotective effect of dexmedetomidine on regional ischemia/reperfusion injury in type 2 diabetic rat hearts. *Microvasc. Res.* 123, 1–6. doi: 10.1016/j.mvr.2018.08.006

Deutsch, E., and Tobias, J. D. (2007). Hemodynamic and respiratory changes following dexmedetomidine administration during general anesthesia: Sevoflurane vs. desflurane. *Paediatr. Anaesth.* 17, 438–444. doi: 10.1111/j.1460-9592.2006.02139.x

Devlin, J. W., Skrobik, Y., Gélinas, C., Needham, D. M., Slooter, A. J. C., Pandharipande, P. P., et al. (2018). Clinical practice guidelines for the prevention and management of pain, agitation/sedation, delirium, immobility, and sleep disruption in adult patients in the ICU. *Crit. Care Med.* 46, e825–e873. doi: 10.1097/CCM.0000000000003299

Devlin, J. W. (2008). The pharmacology of oversedation in mechanically ventilated adults. Curr. *Opin. Crit. Care* 14, 403–407. doi: 10.1097/MCC.0b013e32830280b3

Du, T., Li, B., Liu, S., Zang, P., Prevot, V., Hertz, L., et al. (2009). ERK phosphorylation in intact, adult brain by alpha(2)-adrenergic transactivation of EGF receptors. *Neurochem. Int.* 55, 593–600. doi: 10.1016/j.neuint.2009.05.016

Duan, X., Coburn, M., Rossaint, R., Sanders, R. D., Waesberghe, J. V., and Kowark, A. (2018). Efficacy of perioperative dexmedetomidine on postoperative delirium: systematic review and meta-analysis with trial sequential analysis of randomised controlled trials. *Br. J. Anaesth.* 121, 384–397. doi: 10.1016/j.bja.2018.04.046

Dutta, S., Lal, R., Karol, M. D., Cohen, T., and Ebert, T. (2000). Influence of cardiac output on dexmedetomidine pharmacokinetics. *J. Pharm. Sci.* 89, 519–527. doi: 10.1002/(SICI)1520-6017(200004)89:4<519::AID-JPS9>3.0.CO;2-U

Dyck, J. B., Maze, M., Haack, C., Vuorilehto, L., and Shafer, S. L. (1993). The pharmacokinetics and hemodynamic effects of intravenous and intramuscular dexmedetomidine hydrochloride in adult human volunteers. *Anesthesiology* 78, 813–820. doi: 10.1097/00000542-199305000-00002

Ebert, T. J., Hall, J. E., Barney, J. A., Uhrich, T. D., and Colinco, M. D. (2000). The effects of increasing plasma concentrations of dexmedetomidine in humans. *Anesthesiology* 93, 382–394. doi: 10.1097/00000542-200008000-00016

El-Hennawy, A. M., Abd-Elwahab, A. M., Abd-Elmaksoud, A. M., El-Ozairy, H. S., and Boulis, S. R. (2009). Addition of clonidine or dexmedetomidine to bupivacaine prolongs caudal analgesia in children. *Br. J. Anaesth.* 103, 268–274. doi: 10.1093/bja/aep159

Ely, E. W., Shintani, A., Truman, B., Speroff, T., Gordon, S. M., Harrell, F. E., et al. (2004). Delirium as a predictor of mortality in mechanically ventilated patients

in the intensive care unit. *JAMA* 291, 1753–1762. doi: 10.1001/jama.291.14.1753

Figueroa, X. F., Poblete, M. I., Boric, M. P., Mendizabal, V. E., Adler-Graschinsky, E., and Huidobro-Toro, J. P. (2001). Clonidine-induced nitric oxide-dependent vasorelaxation mediated by endothelial a2-adrenoceptor activation. *Br. J. Pharmacol.* 134, 957–968. doi: 10.1038/sj.bjp.0704320

Filbey, W. A., Sanford, D. T., Baghdoyan, H. A., Koch, L. G., Britton, S. L., and Lydic, R. (2014). Eszopiclone and dexmedetomidine depress ventilation in obese rats with features of metabolic syndrome. *Sleep* 37, 871–880. doi: 10.5665/sleep.3650

Flükiger, J., Hollinger, A., Speich, B., Meier, V., Tontsch, J., Zehnder, T., et al. (2018). Dexmedetomidine in prevention and treatment of postoperative and intensive care unit delirium: a systematic review and meta-analysis. *Ann. Intensive Care* 8, 92. doi: 10.1186/s13613-018-0437-z

Flatters, S. J., and Bennett, G. J. (2006). Studies of peripheral sensory nerves in paclitaxel-induced painful peripheral neuropathy: evidence for mitochondrial dysfunction. *Pain* 122, 245–257. doi: 10.1016/j.pain.2006.01.037

Fraser, G. L., Devlin, J. W., Worby, C. P., Alhazzani, W., Barr, J., Dasta, J. F., et al. (2013). Benzodiazepine versus nonbenzodiazepine-based sedation for mechanically ventilated, critically ill adults: a systematic review and meta-analysis of randomized trials. *Crit. Care Med.* 41, S30–S38. doi: 10.1097/CCM.0b013e3182a16898

Fu, C., Dai, X., Yang, Y., Lin, M., Cai, Y., and Cai, S. (2017). Dexmedetomidine attenuates lipopolysaccharide-induced acute lung injury by inhibiting oxidative stress, mitochondrial dysfunction and apoptosis in rats. *Mol. Med. Rep*. 15 (1), 131–138.

Gerlach, A. T., Dasta, J. F., Steinberg, S., Martin, L. C., and Cook, C. H. (2009). A new dosing protocol reduces dexmedetomidine-associated hypotension in critically ill surgical patients. *J. Crit. Care* 24, 568–574. doi: 10.1016/j.jcrc.2009.05.015

Ghali, A., Mahfouz, A. K., Ihanamäki, T., and El Btarny, A. M. (2011). Dexmedetomidine versus propofol for sedation in patients undergoing vitreoretinal surgery under sub-Tenon's anesthesia. *Saudi J. Anaesth.* 5, 36–41. doi: 10.4103/1658-354X.76506

Girault, J. A., Costa, A., Derkinderen, P., Studler, J. M., and Toutant, M. (1999). FAK and PYK2/CAKbeta in the nervous system: a link between neuronal activity, plasticity and survival? *Trends Neurosci.* 22, 257–263. doi: 10.1016/S0166-2236(98)01358-7

Gong, Z., Ma, L., Zhong, Y. L., Li, J., Lv, J., and Xie, Y. B. (2017). Myocardial protective effects of dexmedetomidine in patients undergoing cardiac surgery: A meta-analysis and systematic review. *Exp. Ther. Med.* 13, 2355–2361. doi: 10.3892/etm.2017.4227

Gonzales, J. N., Gorshkov, B., Varn, M. N., Zemskova, M. A., Zemskov, E. A., Sridhar, S., et al. (2014). Protective effect of adenosine receptors against lipopolysaccharide-induced acute lung injury. *Am. J. Physiol. Lung Cell Mol. Physiol.* 306, L497–L507. doi: 10.1152/ajplung.00086.2013

Guler, G., Akin, A., Tosun, Z., Eskitascoglu, E., Mizrak, A., and Boyaci, A. (2005). Single-dose dexmedetomidine attenuates airway and circulatory reflexes during extubation. *Acta Anaesthesiol. Scand.* 49, 1088–1091. doi: 10.1111/j.1399-6576.2005.00780.x

Halestrap, A. P. (2009). What is the mitochondrial permeability transition pore? *J. Mol. Cell. Cardiol.* 46, 821–831. doi: 10.1016/j.yjmcc.2009.02.021

Hanci, V., Yurdakan, G., Yurtlu, S., Turan, I.Ö., and Sipahi, E. Y. (2012). Protective effect of dexmedetomidine in a rat model of α-naphthylthiourea-induced acute lung injury. *J. Surg. Res.* 178, 424–430. doi: 10.1016/j.jss.2012.02.027

Hanna, P., and Milap, C. N. (2008). Clinical Uses of Dexmedetomidine in Pediatric Patient. *Paediatr Drugs* 10 (1), 49–69.

Hannivoort, L. N., Eleveld, D. J., Proost, J. H., Reyntjens, K. M., Absalom, A. R., Vereecke, H. E., et al. (2015). Development of an optimized pharmacokinetic model of dexmedetomidine using target-controlled infusion in healthy volunteers. *Anesthesiology* 123, 357–367. doi: 10.1097/ALN.0000000000000740

Harris, D. A., and Das, A. M. (1991). Control of mitochondrial ATP synthesis in the heart. *Biochem. J.* 280, 561–573. doi: 10.1042/bj2800561

Hayashida, K., Umegaki, T., Ikai, H., Murakami, G., Nishimura, M., and Imanaka, Y. (2016). The relationship between sedative drug utilization and outcomes in critically ill patients undergoing mechanical ventilation. *J. Anesth.* 30, 763–769. doi: 10.1007/s00540-016-2196-z

Hilbert, G., Navalesi, P., and Girault, C. (2015). Is sedation safe and beneficial in patients receiving NIV? *Yes Intensive Care Med.* 41, 1688–1691. doi: 10.1007/s00134-015-3935-6

Hodiamont, C. J., Juffermans, N. P., Bouman, C. S., de Jong, M. D., Mathôt, R. A., and van Hest, R. M. (2017). Determinants of gentamicin concentrations in critically ill patients: a population pharmacokinetic analysis. *Int. J. Antimicrob. Agents* 49, 204–211. doi: 10.1016/j.ijantimicag.2016.10.022

Hofer, R. E., Sprung, J., Sarr, M. G., and Wedel, D. J. (2005). Anaesthesia for a patient with morbid obesity using dexmedetomidine without narcotics. *Can. J. Anesth.* 52, 176–180. doi: 10.1007/BF03027725

Hoffman, J., and Hamner, C. (2016). Effectiveness of dexmedetomidine use in general anesthesia to prevent postoperative shivering: a systematic review. *JBI. Database Syst. Rev. Implement. Rep.* 13, 287–313. doi: 10.11124/jbisrir-2015-2257

Hsu, Y. W., Cortinez, L. I., Robertson, K. M., Keifer, J. C., Sum-Ping, S. T., and Moretti, E. W. (2004). Dexmedetomidine pharmacodynamics: part I: crossover comparison of the respiratory effects of dexmedetomidine and remifentanil in healthy volunteers. *Anesthesiology* 101, 1066–1076. doi: 10.1097/00000542-200411000-00005

Huang, J., and Jiang, Q. (2019). Dexmedetomidine protects against neurological dysfunction in a mouse intracerebral hemorrhage model by inhibiting mitochondrial dysfunction-derived oxidative stress. *J. Stroke Cerebrovasc. Dis.* 28, 1281–1289. doi: 10.1016/j.jstrokecerebrovasdis.2019.01.016

Huang, X. Z., Tu, W. F., Peng, J., Deng, R. F., Mo, K., Hu,, et al. (2015). Effect of preemptive local injection of ropivocaine with dexmedetomidine on mirror pain in rats and its mechanism. *Asian Pac. J. Trop. Med.* 8, 836–840. doi: 10.1016/j.apjtm.2015.09.010

Hunter, D. R., and Haworth, R. A. (1979). The Ca2+-induced membrane transition in mitochondria. I. The protective mechanisms. *Arch. Biochem. Biophys.* 195, 453–459. doi: 10.1016/0003-9861(79)90371-0

Ibacache, M., Sanchez, G., Pedrozo, Z., Galvez, F., Humeres, C., Echevarria, G., et al. (2012). Dexmedetomidine preconditioning activates pro-survival kinases and attenuates regional ischemia/reperfusion injury in rat heart. *Biochim. Biophys. Acta* 1822, 537–545. doi: 10.1016/j.bbadis.2011.12.013

Ickeringill, M., Shehabi, Y., Adamson,, and Ruettimann, U. (2004). Dexmedetomidine infusión without loading dose in surgical patients requiring mechanical ventilation: haemodynamic effects and efficacy. *Anaesth. Intensive Care* 32, 741–745. doi: 10.1177/0310057X0403200602

Iirola, T., Aantaa, R., Laitio, R., Kentala, E., Lahtinen, M., Wighton, A., et al. (2011a). Pharmacokinetics of prolonged infusion of high-dose dexmedetomidine in critically ill patients. *Crit. Care* 15, R257. doi: 10.1186/cc10518

Iirola, T., Vilo, S., Manner, T., Aantaa, R., Lahtinen, M., Scheinin, M., et al. (2011b). Bioavailability of dexmedetomidine after intranasal administration. *Eur. J. Clin. Pharmacol.* 67, 825–831. doi: 10.1007/s00228-011-1002-y

Iirola, T., Ihmsen, H., Laitio, R., Kentala, E., Aantaa, R., Kurvinen, J. P., et al. (2012). Population pharmacokinetics of dexmedetomidine during long-term sedation in intensive care patients. *Br. J. Anaesth.* 108, 460–468. doi: 10.1093/bja/aer441

Inouye, S. K., Westendorp, R. G., and Saczynski, J. S. (2014). Delirium in elderly people. *Lancet* 383, 911–922. doi: 10.1016/S0140-6736(13)60688-1

Jaber, S., Chanques, G., and Jung, B. (2010). Postoperative Noninvasive Ventilation. *Anesthesiology* 112, 453–61. doi: 10.1097/ALN.0b013e3181c5e5f2

Jalowiecki, P., Rudner, R., Gonciarz, M., Kawecki, P., Petelenz, M., and Dziurdzik, P. (2005). Sole use of dexmedetomidine has limited utility for conscious sedation during outpatient colonoscopy. *Anesthesiology* 103, 269–273. doi: 10.1097/00000542-200508000-00009

Jiang, C., Xia, M., Wang, M., and Chen, S. (2013). Dexmedetomidine preconditioning protects isolated rat hearts against ischemia/reperfusion injuries and its mechanism. *Zhejiang Da Xue Xue Bao Yi Xue Ban.* 42, 326–330.

Jiang, L., Hu, M., Lu, Y., Cao, Y., Chang, Y., and Dai, Z. (2017). The protective effects of dexmedetomidine on ischemic brain injury: a meta-analysis. *J. Clin. Anesth.* 40, 25–32. doi: 10.1016/j.jclinane.2017.04.003

Jorden, V., and Tung, A. (2002). Dexmedetomidine: clinical update. *Semin. Anesth. Perioperat. Med. Pain* 21, 265–274. doi: 10.1053/sane.2002.34195

Kamibayashi, T., and Maze, M. (2000). Clinical uses of alpha-2 adrenergic agonists. *Anesthesiology* 93, 1345–1349. doi: 10.1097/00000542-200011000-00030

Kanazi, G. E., Aouad, M. T., Jabbour-Khoury, S. I., Al Jazzar, M. D., Alameddine, M. M., Al-Yaman, R., et al. (2006). Effect of low-dose dexmedetomidine or clonidine on the characteristics of bupivacaine spinal block. *Acta Anaesthesiol. Scand.* 50, 222–227. doi: 10.1111/j.1399-6576.2006.00919.x

Karhuvaara, S., Kallio, A., Salonen, M., Tuominen, J., and Scheinin, M. (1991). Rapid reversal of alpha 2-adrenoceptor agonist effects by atipamezole in human volunteers. *Br. J. Clin. Pharmacol.* 1991 (31), 160–165. doi: 10.1111/j.1365-2125.1991.tb05505.x

Karkoulias, G., Mastrogianni, O., Lymperopoulos, A., Paris, H., and Flordellis, C. (2006). Alpha(2)-Adrenergic receptors activate MAPK and Akt through a pathway involving arachidonic acid metabolism by cytochrome P450-dependent epoxygenase, matrix metalloproteinase activation and subtype-specific transactivation of EGFR. *Cell Signal.* 18, 729–739. doi: 10.1016/j.cellsig.2005.06.014

Karol, M. D., and Maze, M. (2000). Pharmacokinetics and interaction pharmacodynamics of dexmedetomidine in humans. *Best Pract. Res. Clin. Anaesthesiol.* 14, 261–269. doi: 10.1053/bean.2000.0081

Karol, M. D. (1996). Pharmacokinetics of dexmedetomidine hydrochloride injection in healthy male volunteers following administration at three different rates, abbott laboratories. *Internal Rep*.

Kaur, M., and Singh, P. M. (2011). Current role of dexmedetomidine in clinical anesthesia and intensive care. *Anesth. Essays Res.* 5, 128–133. doi: 10.4103/0259-1162.94750

Kawasaki, T., Kawasaki, C., Ueki, M., Hamada, K., Habe, K., and Sata, T. (2013). Dexmedetomidine suppresses proinflammatory mediator production in human whole blood *in vitro*. *J. Trauma Acute Care Surg.* 74, 1370–1375. doi: 10.1097/TA.0b013e31828db978

Kaygusuz, K., Gokce, G., Gursoy, S., Ayan, S., Mimaroglu, C., and Gultekin, Y. (2008). A comparison of sedation with dexmedetomidine or propofol during shockwave lithotripsy: a randomized controlled trial. *Anesth. Analg.* 106, 114–119. doi: 10.1213/01.ane.0000296453.75494.64

Keating, G. M., Hoy, S. M., and Lyseng-Williamson, K. A. (2012). Dexmedetomidine: a guide to its use for sedation in the US. *Clin. Drug Investig.* 32, 561–567. doi: 10.2165/11209820-000000000-00000

Khan, Z. P., Munday, I. T., Jones, R. M., Thornton, C., Mant, T. G., and Amin, D. (1999). Effects of dexmedetomidine on isoflurane requirements in healthy volunteers. 1: pharmacodynamic and pharmacokinetic interactions. *Br. J. Anaesth.* 83, 372–380. doi: 10.1093/bja/83.3.372

Kim, H. J., Sohn, J. T., Jeong, Y. S., Cho, M. S., Kim, H. J., and Chang, K. C. (2009). Direct effect of dexmedetomidine on rat isolated aorta involves endothelial nitric oxide synthesis and activation of the lipoxygenase pathway. *Clin. Exp. Pharmacol. Physiol.* 36, 406–412. doi: 10.1111/j.1440-1681.2008.05082.x

Kishikawa, H., Kobayashi, K., Takemori, K., Okabe, T., Ito, K., and Sakamoto, A. (2008). The effects of dexmedetomidine on human neutrophil apoptosis. *BioMed. Res.* 29, 189–194. doi: 10.2220/biomedres.29.189

Kohli, U., Pandharipande, P., Muszkat, M., Sofowora, G. G., Friedman, E. A., and Scheinin, M. (2012). CYP2A6 genetic variation and dexmedetomidine disposition. *Eur. J. Clin. Pharmacol.* 68, 937–942. doi: 10.1007/s00228-011-1208-z

Kress, J. P., and Hall, J. B. (2014). ICU-Acquired weakness and recovery from critical illness. *N. Engl. J. Med.* 370, 1626–1635. doi: 10.1056/NEJMra1209390

Kuang, Y., Xiang, Y., Guo, C. X., Zhang, R. R., Yang, G., Hou, G. F., et al. (2016). Population pharmacokinetics study of dexmedetomidine in Chinese adult patients during spinal anesthesia. *Int. J. Clin. Pharmacol. Ther.* 54, 200–207. doi: 10.5414/CP202521

Kumba, C., and Van der Linden, P. (2008). Effects of sedative agents on metabolic demand. *Ann. Fr. Anesth. Reanim.* 27, 574–580. doi: 10.1016/j.annfar.2008.04.010

Kurnik, D., Muszkat, M., Sofowora, G. G., Friedman, E. A., Dupont, W. D., and Scheinin, M. (2008). Ethnic and genetic determinants of cardiovascular response to the selective 2-adrenoceptor agonist dexmedetomidine. *Hypertension* 51, 406–411. doi: 10.1161/HYPERTENSIONAHA.107.098939

Lee, S., Kim, B. H., Lim, K., Stalker, D., Wisemandle, W., Shin, S. G., et al. (2012). Pharmacokinetics and pharmacodynamics of intravenous dexmedetomidine in healthy Korean subjects. *J. Clin. Pharm. Ther.* 37, 698–703. doi: 10.1111/j.1365-2710.2012.01357.x

Lesnefsky, E. J., Moghaddas, S., Tandler, B., Kerner, J., and Hoppel, C. L. (2001). Mitochondrial dysfunction in cardiac disease: ischemia–reperfusion, aging, and heart failure. *J. Mol. Cell. Cardiol.* 33, 1065–1089. doi: 10.1006/jmcc.2001.1378

Lewis, S. R., Nicholson, A., Smith, A. F., and Alderson, P. (2015). Alpha-2 adrenergic agonists for the prevention of shivering following general anaesthesia. *Cochrane Database Syst. Rev.* 8, CD011107. doi: 10.1002/14651858.CD011107.pub2

Li, L. Q., Wang, C., Xu, H. Y., Lu, H. L., and Zhang, H. Z. (2018). Effects of different doses of intranasal dexmedetomidine on preoperative sedation and postoperative agitation in pediatric with total intravenous anesthesia undergoing adenoidectomy with or without tonsillectomy. *Med. (Baltimore)* 97, e12140. doi: 10.1097/MD.0000000000012140

Liang, H., Liu, H. Z., Wang, H. B., Zhong, J. Y., Yang, C. X., and Zhang, B. (2017). Dexmedetomidine protects against cisplatin-induced acute kidney injury in mice through regulating apoptosis and inflammation. *Inflammation Res.* 66, 399–411. doi: 10.1007/s00011-017-1023-9

Lin, L., Guo, X., Zhang, M. Z., Qu, C. J., Sun, Y., and Bai, J. (2011). Pharmacokinetics of dexmedetomidine in Chinese post-surgical intensive care unit patients. *Acta Anaesthesiol. Scand.* 55, 359–367. doi: 10.1111/j.1399-6576.2010.02392.x

Liu, H. L., and Qian, Y. N. (2013). Effects of dexmedetomidine on perioperative inflammatory response in patients undergoing valve replacement. *Zhongguo Ying Yong Sheng Li Xue Za Zhi.* 29, 316–317.

Liu, Z. X., Xu, F. Y., Liang, X., Zhou, M., Wu, L., Wu, J. R., et al. (2015). Efficacy of dexmedetomidine on postoperative shivering: a meta-analysis of clinical trials. *Can. J. Anaesth.* 62, 816–829. doi: 10.1007/s12630-015-0368-1

Liu, H. C., Lian, Q. Q., Wu, F. F., Wang, C. Y., Sun, W., Zheng, L. D., et al. (2017). Population pharmacokinetics of dexmedetomidine after short intravenous infusion in Chinese children. *Eur. J. Drug Metab. Pharmacokinet.* 42, 201–211. doi: 10.1007/s13318-016-0333-6

Liu, X. R., Li, T., Cao, L., Yu, Y. Y., Chen, L. L., Fan, X. H., et al. (2018). Dexmedetomidine attenuates H2O2-induced neonatal rat cardiomyocytes apoptosis through mitochondria- and ER-medicated oxidative stress pathways. *Mol. Med. Rep.* 17, 7258–7264. doi: 10.3892/mmr.2018.8751

Lopez, M. B. (2018). Postanaesthetic shivering - from pathophysiology to prevention. *Rom. J. Anaesth. Intensive Care* 25, 73–81. doi: 10.21454/rjaic.7518.251.xum

Lu, Z., Li, W., Chen, H., and Qian, Y. (2018). Efficacy of a dexmedetomidine-remifentanil combination compared with a midazolam-remifentanil combination for conscious sedation during therapeutic endoscopic retrograde cholangio-pancreatography: a prospective, randomized, single-blinded preliminary trial. *Dig. Dis. Sci.* 63, 1633–1640. doi: 10.1007/s10620-018-5034-3

Mahmoud, M., and Mason, K. (2015). Dexmedetomidine: review, update, and future considerations of paediatric perioperative and periprocedural applications and limitations. *Br. J. Anaesth.* 115 (2), 171–182. doi: 10.1093/bja/aev226

Martin, L. J., Gertz, B., Pan, Y., Price, A. C., Molkentin, J. D., and Chang, Q. (2009). The mitochondrial permeability transition pore in motor neurons: involvement in the pathobiology of ALS mice. *Exp. Neurol.* 218, 333–346. doi: 10.1016/j.expneurol.2009.02.015

Mason, K., and Lerman, J. (2011). Dexmedetomidine in children: current knowledge and future applications. *Anesth. Analg.* 113, 1129–1142. doi: 10.1213/ANE.0b013e31822b8629

Mason, K. P., Zurakowski, D., Zgleszewski, S. E., Robson, C. D., Carrier, M., Hickey, P. R., et al. (2008). High dose dexmedetomidine as the sole sedative for pediatric MRI. *Paediatr. Anaesth.* 18, 403–411. doi: 10.1111/j.1460-9592.2008.02468.x

Millay, D. P., Sargent, M. A., Osinska, H., Baines, C. P., Barton, E. R., Vuagniaux, G., et al. (2008). Genetic and pharmacologic inhibition of mitochondrial-dependent necrosis attenuates muscular dystrophy. *Nat. Med.* 14, 442–447. doi: 10.1038/nm1736

Mo, Y., and Zimmermann, A. E. (2013). Role of dexmedetomidine for the prevention and treatment of delirium in intensive care unit patients. *Ann. Pharmacother.* 47, 869–876. doi: 10.1345/aph.1AR708

Morelli, A., Sanfilippo, F., Arnemann, P., Hessler, M., Kampmeier, T. G., D'Egidio, A., et al. (2019). The effect of propofol and dexmedetomidine sedation on norepinephrine requirements in septic shock patients: a crossover trial. *Crit. Care Med.* 47, e89–e95. doi: 10.1097/CCM.0000000000003520

Morgan, G. E., Mikhail, M. S., and Murray, M. J. (2006). *In: Preoperative Medication in Clinical Anaethesia. 4th ed.* (New York: Mc graw Hill), 248.

Mukhtar, A. M., Obayah, E. M., and Hassona, A. M. (2006). The use of dexmedetomidine in pediatric cardiac surgery. *Anesth. Analg.* 103, 52–56. doi: 10.1213/01.ane.0000217204.92904.76

Nguyen, V., Tiemann, D., Park, E., and Salehi, A. (2017). Alpha-2 Agonists. *Anesthesiol. Clin.* 35, 233–245. doi: 10.1016/j.anclin.2017.01.009

Nunes, S. L., Forsberg, S., Blomqvist, H., Berggren, L., Sörberg, M., Sarapohja, T., et al. (2018). Effect of sedation regimen on weaning from mechanical ventilation in the intensive care unit. *Clin. Drug Investig.* 38, 535–543. doi: 10.1007/s40261-018-0636-2

Obayah, G. M., Refaie, A., Aboushanab, O., Ibraheem, N., and Abdelazees, M. (2010). Addition of dexmedetomidine to bupivacaine for greater palatine nerve block prolongs postoperative analgesia after cleft palate repair. *Eur. J. Anaesthesiol.* 27, 280–284. doi: 10.1097/EJA.0b013e3283347c15

Oddo, M., Crippa, I., Mehta, S., Menon, D., Payen, J. F., Taccone, F., et al. (2016). Optimizing sedation in patients with acute brain injury. *Crit. Care* 20, 128. doi: 10.1186/s13054-016-1294-5

Oh-Nishi, A., Saji, M., Satoh, S. Z., Ogata, M., and Suzuki, N. (2009). Late phase of long-term potentiation induced by co-application of N-methyl-d-aspartic acid and the antagonist of NR2B-containing N-methyl-d-aspartic acid receptors in rat hippocampus. *Neuroscience* 159 (1), 127–135. doi: 10.1016/j.neuroscience.2008.10.037

Okada, H., Kurita, T., Mochizuki, T., Morita, K., and Sato, S. (2007). The cardioprotective effect of dexmedetomidine on global ischaemia in isolated rat hearts. *Resuscitation* 74 (2007), 538–545. doi: 10.1016/j.resuscitation.2007.01.032

Olutoye, O. A., Glover, C. D., Diefenderfer, J. W., McGilberry, M., Wyatt, M. M., Larrier, D. R., et al. (2010). The effect of intraoperative dexmedetomidine on dostoperative analgesia and sedation in pediatric patients undergoing tonsillectomy and adenoidectomy. *Anesth. Analg.* 111, 490–495. doi: 10.1213/ANE.0b013e3181e33429

Osadnik, C. R., Tee, V. S., Carson-Chahhoud, K. V., Picot, J., Wedzicha, J. A., and Smith, B. J. (2017). Non-invasive ventilation for the management of acute hypercapnic respiratory failure due to exacerbation of chronic obstructive pulmonary disease. *Cochrane Database Syst. Rev.* 7, CD004104. doi: 10.1002/14651858.CD004104.pub4

Ozaki, M., Takeda, J., Tanaka, K., Shiokawa, Y., Nishi, S., Matsuda, K., et al. (2014). Safety and efficacy of dexmedetomidine for long-term sedation in critically ill patients. *J. Anesth.* 28, 38–50. doi: 10.1007/s00540-013-1678-5

Panzer, O., Moitra, V., and Sladen, R. N. (2009). Pharmacology of sedative-analgesic agents: dexmedetomidine, remifentanil, ketamine, volatile anesthetics, and the role of peripheral mu antagonists. *Crit. Care Clin.* 25, 451–469. doi: 10.1016/j.ccc.2009.04.004

Parcellier, A., Tintignac, L. A., Zhuravleva, E., and Hemmings, B. A. (2008). PKB and the mitochondria: AKTing on apoptosis. *Cell Signal* 20, 21–30. doi: 10.1016/j.cellsig.2007.07.010

Pasin, L., Landoni, G., Nardelli, P., Belletti, A., Di Prima, A. L., Taddeo, D., et al. (2014). Dexmedetomidine reduces the risk of delirium, agitation and confusion in critically Ill patients: a meta-analysis of randomized controlled trials. *J. Cardiothorac. Vasc. Anesth.* 28, 1459–1466. doi: 10.1053/j.jvca.2014.03.010

Petroz, G., Sikich, N., James, M., van Dyk, H., Shafer, S. L., Schily, M., et al. (2006). A Phase I, two-center study of the pharmacokinetics and pharmacodynamics of dexmedetomidine in children. *Anesthesiology* 105, 1098–1110. doi: 10.1097/00000542-200612000-00009

Piao, G., and Wu, J. (2014). Systematic assessment of dexmedetomidine as an anesthetic agent: a meta-analysis of randomized controlled trials. *Arch. Med. Sci.* 10, 19–24. doi: 10.5114/aoms.2014.40730

Pohjoismäki, J. L., and Goffart, S. (2017). The role of mitochondria in cardiac development and protection. *Free Radic. Biol. Med.* 106, 345–354. doi: 10.1016/j.freeradbiomed.2017.02.032

Potts, A. L., Anderson, B. J., Warman, G. R., Lerman, J., Diaz, S. M., and Vilo, S. (2009). Dexmedetomidine pharmacokinetics in pediatric intensive care: a pooled analysis. *Paediatr. Anaesth.* 19, 1119–1129. doi: 10.1111/j.1460-9592.2009.03133.x

Potts, A. L., Anderson, B. J., Holford, N. H., Vu, T. C., and Warman, G. R. (2010). Dexmedetomidine hemodynamics in children after cardiac surgery. *Paediatr. Anaesth.* 20, 425–433. doi: 10.1111/j.1460-9592.2010.03285.x

Pun, B. T., and Ely, E. W. (2007). The importance of diagnosing and managing ICU delirium. *Chest* 132, 624–636. doi: 10.1378/chest.06-1795

Ramachandran, A., Lebofsky, M., Baines, C. P., Lemasters, J. J., and Jaeschke, H. (2011). Cyclophilin D deficiency protects against acetaminophen-induced oxidant stress and liver injury. *Free Radical Res.* 45, 156–164. doi: 10.3109/10715762.2010.520319

Reade, M., and Finfer, S. (2014). Sedation and delirium in the intensive care unit. *N. Engl. J. Med.* 370, 444–454. doi: 10.1056/NEJMra1208705

Reel, B. (2019). "Dexmedetomidine" n: *StatPearls*. ed. C. V Maani (Treasure Island (FL): StatPearls Publishing).

Ren, X., Ma, H., and Zuo, Z. (2016). Dexmedetomidine postconditioning reduces brain injury after brain hypoxia-ischemia in neonatal rats. *J. Neuroimmune. Pharmacol.* 11, 238–247. doi: 10.1007/s11481-016-9658-9

Riker, R. R., Shehabi, Y., Bokesch, P. M., Ceraso, D., Wisemandle, W., Koura, F., et al. (2009). Dexmedetomidine vs midazolam for sedation of critically ill patients: a randomized trial. *JAMA* 301, 489–499. doi: 10.1001/jama.2009.56

Riquelme, J. A., Westermeier, F., Hall, A. R., Vicencio, J. M., Pedrozo, Z., Ibacache, M., et al. (2016). Dexmedetomidine protects the heart against ischemia-reperfusion injury by an endothelial eNOS/NO dependent mechanism. *Pharmacol. Res.* 103, 318–327. doi: 10.1016/j.phrs.2015.11.004

Rodrigues Júnior, G. R., and do Amaral, J. L. (2004). Influence of sedation on morbidity and mortality in the intensive care unit. *Sao Paulo Med. J.* 122, 8–11. doi: 10.1590/S1516-31802004000100003

Rodríguez-González, R., Sobrino, T., Veiga, S., López, P., Rodríguez-García, J., Veiras del Río, S., et al. (2016). Neuroprotective Effects of Dexmedetomidine Conditioning Strategies: Evidences From an in Vitro Model of Cerebral Ischemia. *Life Sci* 144, 162–9. doi: 10.1016/j.lfs.2015.12.007

Roekaerts, P., Prinzen, F., and De Lange, S. (1996). Beneficial effects of dexmedetomidine on ischaemic myocardium of anaesthetized dogs. *Br. J. Anaesth.* 77, 427–429. doi: 10.1093/bja/77.3.427

Rolle, A., Paredes, S., Cortinez, L., Anderson, B. J., Quezada, N., Solari, S., et al. (2018). Dexmedetomidine metabolic clearance is not affected by fat mass in obese patients. *Br. J. Anaesth.* 120, 969–977. doi: 10.1016/j.bja.2018.01.040

Sahay, N., Bhadani, U. K., Guha, S., Himanshu, A., Sinha, C., Bara, M., et al. (2018). Effect of dexmedetomidine on intracranial pressures during laparoscopic surgery: a randomized, placebo-controlled trial. *J. Anaesthesiol. Clin. Pharmacol.* 34, 341–346. doi: 10.4103/joacp.JOACP_171_17

Schaak, S., Cussac, D., Cayla, C., Devedjian, J. C., Guyot, R., Paris, H., et al. (2000). Alpha(2) adrenoceptors regulate proliferation of human intestinal epithelial cells. *Gut* 47, 242–250. doi: 10.1136/gut.47.2.242

Scheinin, H., Aantaa, R., Anttila, M., Hakola, P., Helminen, A., and Karhuvaara, S. (1998). Reversal of the sedative and sympatholytic effects of dexmedetomidine with a specific alpha2-adrenoceptor antagonist atipamezole: a pharmacodynamic and kinetic study in healthy volunteers. *Anesthesiology* 89, 574–584. doi: 10.1097/00000542-199809000-00005

Schnabel, A., Meyer-Frießem, C. H., Reichl, S. U., Zahn, P. K., and Pogatzki-Zahn, E. M. (2013a). Is intraoperative dexmedetomidine a new option for postoperative pain treatment? *A meta-analysis Randomized Controlled Trials Pain* 154, 1140–1149. doi: 10.1016/j.pain.2013.03.029

Schnabel, A., Reichl, S. U., Poepping, D. M., Kranke, P., Pogatzki-Zahn, E. M., and Zahn, P. K. (2013b). Efficacy and safety of intraoperative dexmedetomidine for acute postoperative pain in children: a meta-analysis of randomized controlled trials. *Paediatr. Anaesth.* 23, 170–179. doi: 10.1111/pan.12030

Schnaider, T. B., Vieira, A. M., Brandao, A. C., and Lobo, M. V. (2005). Intraoperative analgesic effect of epidural ketamine, clonidine or dexmedetomidine for upper abdominal surgery. *Rev. Bras. Anestesiol.* 55, 525–531. doi: 10.1590/s0034-70942005000500007

Schomer, K. J., Sebat, C. M., Adams, J. Y., Duby, J. J., Shahlaie, K., and Louie, E. L. (2019). Dexmedetomidine for refractory intracranial hypertension. *J. Intensive Care Med.* 34, 62–66. doi: 10.1177/0885066616689555

Scott-Warren, V. L., and Sebastian, J. (2016). Dexmedetomidine: its use in intensive care medicine and anaesthesia. *BJA Educ.* 16, 242–246. doi: 10.1093/bjaed/mkv047

Shariffuddin, I. I., Teoh, W. H., Wahab, S., and Wang, C. Y. (2018). Effect of single-dose dexmedetomidine on postoperative recovery after ambulatory ureteroscopy and ureteric stenting: a double blind randomized controlled study. *BMC Anesthesiol.* 18, 3. doi: 10.1186/s12871-017-0464-6

Shehabi, Y., Howe, B. D., Bellomo, R., Arabi, Y. M., Bailey, M., Bass, F. E., et al. (2019). anzics clinical trials group; spice iii investigators; anzics clinical trials group and the SPICE III Investigators. early sedation with dexmedetomidine in critically Ill patients. *N. Engl. J. Med.* 380, 2506–2517. doi: 10.1056/NEJMoa1904710

Silversides, J. A., Major, E., Ferguson, A. J., Mann, E. E., McAuley, D. F., Marshall, J. C., et al. (2017). Conservative fluid management or deresuscitation for patients with sepsis or acute respiratory distress syndrome following the resuscitation phase of critical illness: a systematic review and meta-analysis. *Intensive Care Med.* 43, 155–170. doi: 10.1007/s00134-016-4573-3

Skrobik, Y., Duprey, M., Hill, N. S., and Devlin, J. W. (2018). Low-dose nocturnal dexmedetomidine prevents ICU delirium. a randomized, placebo-controlled trial. *Am. J. Respir. Crit. Care Med.* 197, 1147–1156. doi: 10.1164/rccm.201710-1995OC

Snapir, A., Posti, J., Kentala, E., Koskenvuo, J., Sundell, J., Tuunanen, H., et al. (2006). Effects of low and high plasma concentrations of dexmedetomidine on myocardial perfusion and cardiac function in healthy male subjects. *Anesthesiology* 105, 902–910. doi: 10.1097/00000542-200611000-00010

Song, J. C., Gao, H., Qiu, H. B., Chen, Q. B., Cai, M. H., and Zhang, M. Z. (2018). The pharmacokinetics of dexmedetomidine in patients with obstructive jaundice: a clinical trial. *PloS One* 13, e0207427. doi: 10.1371/journal.pone.0207427

Sottas, C. E. (2017). Anderson B.J. Dexmedetomidine: the new all-in-one drug in paediatric anaesthesia? *Curr. Opin. Anaesthesiol.* 30, 441–451. doi: 10.1097/ACO.0000000000000488

Su, F., Nicolson, S. C., Gastonguay, M. R., Barrett, J. S., Adamson, P. C., Kang, D. S., et al. (2010). Population pharmacokinetics of dexmedetomidine in infants after open heart surgery. *Anesth. Analg.* 110, 1383–1392. doi: 10.1213/ANE.0b013e3181d783c8

Su, F., Gastonguay, M. R., Nicolson, S. C., DiLiberto, M., Ocampo-Pelland, A., and Zuppa, A. F. (2016). Dexmedetomidine pharmacology in neonates and infants after open heart surgery. *Anesth. Analg.* 122, 1556–1566. doi: 10.1213/ANE.0000000000000869

Su, X., Meng, Z. T., Wu, X. H., Cui, F., Li, H. L., Wang, D. X., et al. (2016). Dexmedetomidine for prevention of delirium in elderly patients after non-cardiac surgery: a randomised, double-blind, placebo-controlled trial. *Lancet* 388, 1893–1902. doi: 10.1016/S0140-6736(16)30580-3

Sun, J. H., Han, N., and Wu, X. Y. (2008). Dexmedetomidine in the general anesthesia: a meta-analysis of randomized controlled trials. *Chin. J. Evidence-Based Med.* 8, 773–780.

Sun, Y., Liu, C., Zhang, Y., Luo, B., She, S., Xu, L., et al. (2014). Low-Dose Intramuscular Dexmedetomidine as Premedication: A Randomized Controlled Trial. *Med. Sci. Monit.* 20, 2714–2719. doi: 10.12659/MSM.891051

Taittonen, M. T., Kirvela, O. A., Aantaa, R., and Kanto, J. H. (1997). Effect of clonidine and dexmedetomidine premedication on perioperative oxygen consumption and haemodynamic state. *Br. J. Anaesth.* 78, 400–406. doi: 10.1093/bja/78.4.400

Takamatsu, I., Iwase, A., Ozaki, M., Kazama, T., Wada, K., and Sekiguchi, M. (2008). Dexmedetomidine reduces long-term potentiation in mouse hippocampus. *Anesthesiology* 108, 94–102. doi: 10.1097/01.anes.0000296076.04510.e1

Talke, P., Lobo, E., and Brown, R. (2003). Systemically administered α2 agonist-induced peripheral vasoconstriction in humans. *Anesthesiology* 99, 65–70. doi: 10.1097/00000542-200307000-00014

Tanabe, K., Takai, S., Matsushima-Nishiwaki, R., Kato, K., Dohi, S., and Kozawa, O. (2008). Alpha2 adrenoreceptor agonist regulates protein kinase C-induced heat shock protein 27 phosphorylation in C6 glioma cells. *J. Neurochem.* 106, 519–528. doi: 10.1111/j.1471-4159.2008.05389.x

Tanabe, K., Matsushima-Nishiwaki, R., Dohi, S., and Kozawa, O. (2010). Phosphorylation status of heat shock protein 27 regulates the interleukin-1β-induced interleukin-6 synthesis in C6 glioma cells. *Neuroscience* 170, 1028–1034. doi: 10.1016/j.neuroscience.2010.08.014

Taniguchi, T., Kidani, Y., Kanakura, H., Takemoto, Y., and Yamamoto, K. (2004). Effects of dexmedetomidine on mortality rate and inflammatory responses to endotoxin-induced shock in rats. *Crit. Care Med.* 32, 1322–1326. doi: 10.1097/01.CCM.0000128579.84228.2A

Tate, J. A., Devito Dabbs, A., Hoffman, L. A., Milbrandt, E., and Happ, M. B. (2012). Anxiety and Agitation in Mechanically Ventilated Patients. *Qual. Health Res.* 22, 157–173. doi: 10.1177/1049732311421616

Välitalo, P. A., Ahtola-Sät;ilä, ,. T., Wighton, A., Sarapohja, T., Pohjanjousi, P., and Garratt, C. (2013). Population pharmacokinetics of dexmedetomidine in critically ill patients. *Clin. Drug Invest.* 33, 579–587. doi: 10.1007/s40261-013-0101-1

Venn, R. M., Bradshaw, C. J., Spencer, R., Brealey, D., Caudwell, E., Naughton, C., et al. (1999). Preliminary UK experience of dexmedetomidine, a novel agent for postoperative sedation in the intensive care unit. *Anaesthesia* 54, 1136–1142. doi: 10.1046/j.1365-2044.1999.01114.x

Venn, R. M., Hell, J., and Grounds, R. M. (2000). Respiratory effects of dexmedetomidine in the surgical patient requiring intensive care. *Crit. Care* 4, 302–308. doi: 10.1186/cc712

Venn, R. M., Karol, M. D., and Grounds, R. M. (2002). Pharmacokinetics of dexmedetomidine infusions for sedation of postoperative patients requiring intensive care. *Br. J. Anaesth.* 88, 669–675. doi: 10.1093/bja/88.5.669

Wang, C., and Youle, R. J. (2009). The role of mitochondria in apoptosis. *Annu. Rev. Genet.* 43, 95–118. doi: 10.1146/annurev-genet-102108-134850

Wang, X. W., Cao, J. B., Lv, B. S., Mi, W. D., Wang, Z. Q., Zhang, C., et al. (2015). Effect of perioperative dexmedetomidine on the endocrine modulators of stress response: a meta-analysis. *Clin. Exp. Pharmacol. Physiol.* 42, 828–836. doi: 10.1111/1440-1681.12431

Wang, Q., She, Y., Bi, X., Zhao, B., Ruan, X., and Tan, Y. (2017). Dexmedetomidine Protects PC12 Cells from Lidocaine-Induced Cytotoxicity Through Downregulation of COL3A1 Mediated by miR-let-7b. *DNA Cell Biol.* 36, 518–528. doi: 10.1089/dna.2016.3623

Weerink, M., Struys, M., Hannivoort, L., Barends, C. R. M., Absalom, A. R., and Colin, P. (2017). Clinical Pharmacokinetics and Pharmacodynamics of Dexmedetomidine. *Clin. Pharmacokinet.* 56, 893–913. doi: 10.1007/s40262-017-0507-7

Weng, X., Zhang, X., Lu, X., Wu, J., and Li, S. (2018). Reduced mitochondrial response sensitivity is involved in the antiapoptotic effect of dexmedetomidine pretreatment in cardiomyocytes. *Int. J. Mol. Med.* 41, 2328–2338. doi: 10.3892/ijmm.2018.3384

Wiczling, P., Bartkowska-S´niatkowska, ,. A., Szerkus, O., Siluk, D., Rosada-Kurasińska, J., Warzybok, J., et al. (2016). The pharmacokinetics of dexmedetomidine during long-term infusion in critically ill pediatric patients: a Bayesian approach with informative priors. *J. Pharmacokinet. Pharmacodyn.* 43, 315–324. doi: 10.1007/s10928-016-9474-0

Wijeysundera, D. N., Naik, J. S., and Beattie, W. S. (2003). Alpha-2 adrenergic agonists to prevent perioperative cardiovascular complications: a meta-analysis. *Am. J. Med.* 114, 742–752. doi: 10.1016/S0002-9343(03)00165-7

Wijeysundera, D., Bender, J., and Beattie, W. (2009). Alpha-2 adrenergic agonists for the pre-vention of cardiac complications among patients undergoing surgery. *CochraneDatabase Syst. Rev.* 4, CD004126. doi: 10.1002/14651858.CD004126.pub2

Willigers, H., Prinzen, F., Roekaerts, P., De Lange, S., and Durieux, M. (2003). Dexmedetomidine decreases perioperative myocardial lactate release in dogs, Anesth. *Analg* 96, 657–664. doi: 10.1213/01.ANE.0000048708.75957.FF

Wu, G. J., Chen, J. T., Tsai, H. C., Chen, T. L., Liu, S. H., and Chen, R. M. (2017). Protection of dexmedetomidine against ischemia/reperfusion-induced apoptotic insults to neuronal cells occurs via an intrinsic mitochondria-dependent pathway. *J. Cell. Biochem.* 118, 2635–2644. doi: 10.1002/jcb.25847

Wunsch, H. (2012). Weighing the costs and benefits of a sedative. *JAMA* 307, 1195–1197. doi: 10.1001/jama.2012.319

Xiang, H., Hu, B., Li, Z., and Li, J. (2014). Dexmedetomidine controls systemic cytokine levels through the cholinergic anti-inflammatory pathway. *Inflammation* 37, 1763–1770. doi: 10.1007/s10753-014-9906-1

Yamamoto, T., Mizobata, Y., Kawazoe, Y., Miyamoto, K., Ohta, Y., Morimoto, T., et al. (2019). Incidence, risk factors, and outcomes for sepsis-Associated delirium in patients with mechanical ventilation: a sub-analysis of a multicenter randomized controlled trial. *J. Crit. Care.* 56, 140–144.

Yang, J., and Kang, Y. (2017). Effect of sedation on respiratory function of patients undergoing mechanical ventilation. *Zhonghua Wei Zhong Bing Ji Jiu Yi Xue* 29, 857–860. doi: 10.3760/cma.j.issn.2095-4352.2017.09.019

Yoo, H., Iirola, T., Vilo, S., Manner, T., Aantaa, R., Lahtinen, M., et al. (2015). Mechanism based population pharmacokinetic and pharmacodynamic modeling of intravenous and intranasal dexmedetomidine in healthy subjects. *Eur. J. Clin. Pharmacol.* 71, 1197–1207. doi: 10.1007/s00228-015-1913-0

Yuan, F., Fu, H., Sun, K., Wu, S., and Dong, T. (2017). Effect of dexmedetomidine on cerebral ischemia-reperfusion rats by activating mitochondrial ATP-sensitive potassium channel. *Metab. Brain Dis.* 32, 539–546. doi: 10.1007/s11011-016-9945-4

Yuki, K., and Murakami, N. (2015). Sepsis pathophysiology and anesthetic consideration. *Cardiovasc. Hematol. Disord. Drug Targets* 15, 57–69. doi: 10.2174/1871529X15666150108114810

Zhang, T., Deng, Y., He, P., He., Z., and Wang, X. (2015). Effects of mild hypoalbuminemia on the pharmacokinetics and pharmacodynamics of dexmedetomidine in patients after major abdominal or thoracic surgery. *J. Clin. Anesth.* 27, 632–637. doi: 10.1016/j.jclinane.2015.06.002

Zhang, W. D., Zhang, H., Wang, H., Zhang, N., Du, C. Y., Yu, J., et al. (2016). Protective effect of dexmedetomidine against glutamate-induced cytotoxicity in PC12 cells and its mechanism. *Nan Fang Yi Ke Da Xue Xue Bao.* 37, 150–156.

Zhang, Q., Wu, D., Yang, Y., Liu, T., and Liu, H. (2017). Dexmedetomidine alleviates hyperoxia-induced acute lung injury *via* inhibiting NLRP3 inflammasome activation. *Cell Physiol. Biochem.* 42, 1907–1919. doi: 10.1159/000479609

Zhu, Y. M., Wang, C. C., Chen, L., Qian, L. B., Ma, L. L., and Yu, J. (2013). Both PI3K/Akt and ERK1/2 pathways participate in the protection by dexmedetomidine against transient focal cerebral ischemia/reperfusion injury in rats. *Brain Res.* 1494, 1–8. doi: 10.1016/j.brainres.2012.11.047

Conflict of Interest: The authors declare that the research was conducted in the absence of any commercial or financial relationships that could be construed as a potential conflict of interest.

frontiers in Pharmacology

MINI REVIEW
published: 03 March 2020
doi: 10.3389/fphar.2020.00211

Therapeutic Use of Vitamin C in Cancer: Physiological Considerations

Francisco J. Roa[1], Eduardo Peña[1], Marcell Gatica[1], Kathleen Escobar-Acuña[2], Paulina Saavedra[2], Mafalda Maldonado[1], Magdalena E. Cuevas[2], Gustavo Moraga-Cid[2], Coralia I. Rivas[1] and Carola Muñoz-Montesino[2]**

[1] Departamento de Fisiopatología, Facultad de Ciencias Biológicas, Universidad de Concepción, Concepción, Chile,
[2] Departamento de Fisiología, Facultad de Ciencias Biológicas, Universidad de Concepción, Concepción, Chile

Since the early studies of William J. McCormick in the 1950s, vitamin C has been proposed as a candidate for the treatment of cancer. A number of reports have shown that pharmacological concentrations of vitamin C selectively kill cancer cells *in vitro* and decrease the growth rates of a number of human tumor xenografts in immunodeficient mice. However, up to the date there is still doubt regarding this possible therapeutic role of vitamin C in cancer, mainly because high dose administration in cancer patients has not showed a clear antitumor activity. These apparent controversial findings highlight the fact that we lack information on the interactions that occurs between cancer cells and vitamin C, and if these transformed cells can uptake, metabolize and compartmentalize vitamin C like normal human cells do. The role of SVCTs and GLUTs transporters, which uptake the reduced form and the oxidized form of vitamin C, respectively, has been recently highlighted in the context of cancer showing that the relationship between vitamin C and cancer might be more complex than previously thought. In this review, we analyze the state of art of the effect of vitamin C on cancer cells *in vitro* and *in vivo*, and relate it to the capacity of cancer cells in acquiring, metabolize and compartmentalize this nutrient, with its implications on the potential therapeutic role of vitamin C in cancer.

Keywords: vitamin C, cancer therapy, cancer, SVCT2, GLUT, vitamin C transporters

OPEN ACCESS

Edited by:
Ramón Sotomayor-Zárate, University of Valparaíso, Chile

Reviewed by:
Claudio Acuña-Castillo, Universidad de Santiago de Chile, Chile
Rodrigo L. Castillo, University of Chile, Chile

***Correspondence:**
Coralia I. Rivas
corivas@udec.cl
Carola Muñoz-Montesino
carmunozm@udec.cl

Specialty section:
This article was submitted to Translational Pharmacology, a section of the journal Frontiers in Pharmacology

Received: *29 November 2019*
Accepted: *14 February 2020*
Published: *03 March 2020*

Citation:
Roa FJ, Peña E, Gatica M, Escobar-Acuña K, Saavedra P, Maldonado M, Cuevas ME, Moraga-Cid G, Rivas CI and Muñoz-Montesino C (2020) Therapeutic Use of Vitamin C in Cancer: Physiological Considerations. Front. Pharmacol. 11:211. doi: 10.3389/fphar.2020.00211

INTRODUCTION

Vitamin C is an essential nutrient for humans, acting as an antioxidant and a cofactor for several enzymatic reactions. These reactions involve dioxygenase enzymes which participate in a number of physiological processes, such as collagen synthesis, carnitine synthesis, norepinephrine and serotonin synthesis, hypoxia-inducible transcription factor (HIF) regulation and histone demethylation (Verrax and Calderon, 2008; Du et al., 2012).

Humans, unlike most mammalian species, are unable to synthesize vitamin C, hence it is an essential dietary component and humans need to acquire this vitamin from external sources, such as vegetables and fruits (Rivas et al., 2008). The recommended dose for an adult is around 100 mg per day, which has shown to maintain plasmatic concentration of 50 μM. However, when intracellular content is measured, differential concentrations of vitamin C are found depending on the tissue. Circulating leucocytes, pituitary gland, adrenal glands and brain, among others, accumulate largely higher concentrations than plasma reaching millimolar range (Rose, 1988).

Vitamin C, which performs most of its functions inside the cells, must enter through the plasma membrane of specific cells in a process that requires the participation of transporters. Vitamin C exists in two molecular forms with different chemical stability, half-life *in vivo*, and transport mechanism. The oxidized form, dehydroascorbic acid (DHA) is transported from extracellular medium into the cell by glucose transporters (GLUTs), while the reduced form, ascorbic acid (AA), is transported by sodium-vitamin C co-transporters (SVCT) (Vera et al., 1993; Tsukaguchi et al., 1999).

After more than 50 years of research focused in the role of vitamin C in cancer, it still remains unclear the ways that this nutrient specifically affects cancer cells. And, until recently, there was a lack of information on the physiological aspects of their interaction: it was practically unknown how cancer cells acquire vitamin C, and how it is metabolized or compartmentalized inside these cells.

VITAMIN C TRANSPORT AND COMPARTMENTALIZATION IN CANCER CELLS

As we addressed before, the knowledge on vitamin C uptake capacity and the organelle requirements of this nutrient in the context of cancer is still incomplete. Most of what is known comes from the analysis of GLUTs, which even if they have been mainly studied in the context of glucose uptake capacities in cancer, have direct implications in DHA uptake. In this context, it has been well described that cancer tissues overexpress GLUTs, which leads to an increased capacity to acquire glucose (Adekola et al., 2012; Ancey et al., 2018).

SVCTs on the other hand have been poorly studied. Meanwhile SVCT1 does not appear to have relevance in cancer (Pena et al., 2019), different studies have proposed that SVCT2 has a major function in tumors. The first of them showed that breast tumors have higher levels of SVCT2 expression compared to normal cells (Hong et al., 2013). In fact, overexpression of this transporter led to an increased chemosensitivity to high dose of ascorbate, which resulted in augmented reactive oxygen species (ROS) production and ulterior cell death. Oppositely, siRNA against SVCT2 render the cancer cells resistant to this treatment (Hong et al., 2013). Therefore, SVCT2 might be implicated in the ascorbate induced cancer cell death phenomena. Similar results were observed by two groups in cholangiocarcinoma cells (Wang et al., 2017), hepatocellular carcinoma (Lv et al., 2018) and colon cancer cells (Cho et al., 2018), where SVCT2 expression determines the susceptibility to pharmacological ascorbate-induced cell death.

A comprehensive study on this matter, focused on breast cancer cells mechanisms to acquire vitamin C was recently published (Pena et al., 2019; Roa et al., 2019). This work has shown that most (if not all) of the vitamin C that is capture by breast cancer cells is in the oxidized form. These cells are not able to uptake AA at physiological concentrations. Interestingly, SVCT2 is expressed in cancer cells, and as it was shown before by Hong et al. (2013) its expression is restricted to breast cancer cells, but not normal breast tissue. The lack of AA transport was due to the fact that SVCT2 is absent at the cell surface, with most of the protein distributed within the inner membrane of the mitochondria. Mitochondrial SVCT2 was previously described in U937 cells (Azzolini et al., 2013) and HEK293 cells (Munoz-Montesino et al., 2014) and it was also observed in various cancer derived cell lines from different origin, where the presence of SVCT2 is always link to the mitochondria (Pena et al., 2019). Considering these data, at least under physiological conditions, the external source of vitamin C for cancer cells must be DHA and the transport mechanism implied is through GLUTs. Since DHA is not the most abundant form of vitamin C *in vivo*, Pena et al. (2019), developed an experimental system to check if AA could be oxidized locally by PMA-activated neutrophil like cells, which are producing ROS. Co-culture experiments in the presence of AA showed that cancers cells were able to acquire vitamin C in a process inhibited by cytochalasin B, a glucose transporter inhibitor, and by glucose, indicating that they were able to acquire DHA through GLUTs by bystander effect (Nualart et al., 2003). In this regard, it is important to emphasize that the main form of vitamin C found after this co-culture was AA, meaning cancer cells are able to efficiently reduce DHA once inside the cell (Pena et al., 2019).

On the other hand, the observation that a vitamin C transporter is located in an organelle membrane is not new. Other groups have reported the relevance of organelle vitamin C transporters in a number of cellular systems, including plants, mammals and other organisms (Banhegyi et al., 2014). In this context, organelle requirements for vitamin C in cancer cells have not been previously described. Therefore, the observation that the mitochondrial form of SVCT2 (mitSVCT2) is linked to cancer pathology (Pena et al., 2019), and absent in normal cells, it may have unforeseen implications: mitochondrial vitamin C could be relevant for cancer cell development or survival.

VITAMIN C IN THE TREATMENT OF CANCER: AN HISTORICAL PERSPECTIVE

Based in the known role of vitamin C in collagen synthesis, about six decades ago, William J. McCormick hypothesized that cancer metastasis could be related to a vitamin C deficiency, due to a poor collagen formation and connective tissue degeneration. Hence, the maintenance of collagen synthesis at optimal levels by using vitamin C was proposed to limit metastasis process (McCormick, 1954, 1959). Since this first assumption until now, the possible benefit of vitamin C in the treatment of cancer has been controversial.

McCormick's hypothesis was extended in the 1970s by Ewan Cameron et al. Cameron proposed that vitamin C inhibited the enzyme hyaluronidase, which reduces tissue disruption and cancer cell proliferation (Cameron and Rotman, 1972). For this, Cameron performed the first clinical studies analyzing the anti-cancer effect of ascorbate, initially together with Allan Campbell (Cameron and Campbell, 1974; Cameron et al., 1975) and then with the Nobel Prize winner Linus Pauling. In two retrospective

studies, Cameron and Pauling suggested a therapeutic effect of high-dose vitamin C treatment in advanced cancer. Terminal cancer patients receiving intravenous (IV) followed by oral doses of ascorbate, showed increased survival times and symptomatic relief compared to control patients (Cameron and Pauling, 1976, 1978). These studies created a controversy and the results were criticized, among other things, for the lack of blinding inherent to a retrospective trial and the possibility of a placebo effect.

Studies performed at the Mayo Clinic tried to evaluate Cameron and Pauling's results, analyzing the efficacy of vitamin C in randomized double-blind placebo-controlled trials. Prospective studies from Creagan et al. (1979) and Moertel et al. (1985) found no effect of oral ascorbate treatment in the survival of patients with advanced cancer, compared to patients receiving placebo. These results silenced for many years the initial attempt to determine the use of vitamin C as an anti-cancer agent.

None of the above-mentioned studies measured plasmatic levels of AA, a fundamental issue to understand the real effect of the vitamin C administration in patients. This was clarified in studies performed by the National Institute of Health (NIH), in order to establish dietary recommendations for AA (Levine et al., 1996, 2001). Physiological analyses in healthy young subjects showed that ascorbic acid pharmacokinetics differ depending on the way of administration. When subjects received oral doses, low plasma ascorbate concentrations were achieved (around 100–200 μM), while IV doses resulted in concentrations 100-fold higher than oral (around 15 mM) (Padayatty et al., 2004). This is a consequence of a limited intestinal absorption, renal reabsorption and excretion in oral administration. Unlike oral, IV administration eludes this tight control and produces high plasmatic concentrations that are safe or tolerable for humans (Padayatty et al., 2004).

Thus, high ("pharmacologic") concentrations of AA are achieved only with IV, not with oral administration ("physiologic"). Based in this evidence, it was proposed that only pharmacologic ascorbate concentrations could act as a drug, and the interest for using vitamin C as an anti-cancer agent reemerged.

EFFECT OF PHARMACOLOGIC VITAMIN C IN CANCER CELLS

Since the basic knowledge regarding vitamin C pharmacokinetics was established, several studies analyzing the effect of pharmacologic ascorbate in cancer cells have been reported. Initially, *in vitro* studies in a number of human and mice cancer cell lines showed that ascorbic acid at concentrations around 20 mM selectively kill cancer cells, without effect in normal cell lines. In addition, the authors proposed that the cancer cell death inducing mechanism was dependent on hydrogen peroxide (H_2O_2) formation with ascorbate radical as an intermediate (Chen et al., 2005). The same research group later confirmed in rats that ascorbic acid at pharmacologic levels, achieved by IV or parenteral administration, induced ascorbate radical and H_2O_2 formation in the extracellular medium (Chen et al., 2007).

Regarding *in vivo* studies, Chen et al. (2008) showed that intraperitoneal administration of pharmacologic ascorbate decreased growth rates of human ovarian, mouse pancreatic and rat glioblastoma tumors causing a prooxidant effect. Similarly, Verrax and Calderon (2009) showed that intraperitoneal administration of ascorbate decreased the growth rate of a murine hepatoma in mice. The mechanism of cytotoxicity is linked to the production of extracellular H_2O_2 and involves intracellular transition metals (Chen et al., 2008; Verrax and Calderon, 2009). In the same line, several reports support the induction of ROS achieved by high concentrations of vitamin C in cancer cells as a mechanism for cancer cell death induction: in human pancreatic tumor (Du et al., 2010), in human mesothelioma (Takemura et al., 2010), in human breast cancer (Hong et al., 2013), among others.

Experiments performed *in vitro* to test compatibility with other anti-carcinogenic substances revealed that AA can have a synergistic effect with some of them (Espey et al., 2011; Ma et al., 2014; Hatem et al., 2018; O'Leary et al., 2018; Graczyk-Jarzynka et al., 2019). For instance, Gemcitabine in combination with AA (Espey et al., 2011) have a synergistic cytotoxic effect in eight pancreatic cancer cell lines, which is mediated by the pro-oxidant effect of ascorbate, again with an increase in the production of H_2O_2. In addition, mice bearing pancreatic tumor xenografts showed a higher inhibition in tumor growth when treated with the mixture of Gemcitabine and AA, compared to mice treated only with the drug (Espey et al., 2011). A synergistic effect of AA and two of the chemotherapeutic drugs used in the treatment of ovarian cancer was also observed: carboplatin and paclitaxel, which inhibited tumor growth in models of mice with ovarian cancer and decreased the adverse effects of chemotherapy in patients with this disease. In triple negative breast cancer (TNBC), a new combination with AA was tested using Auranofin (AUF), which targets thioredoxin reductase (TRXR) (Hatem et al., 2018). In combination, these molecules also act in a synergistic way, inducing extracellular production of H_2O_2 and cytotoxicity against MDA-MB-231 (a breast cancer derived cell line) in cell culture and in xenografts in mice. Proteomic and functional analyses in this model suggested that prostaglandin reductase 1 expression was linked with the breast cancer sensitivity to AUF/AA combination (Hatem et al., 2018).

The synergistic effect of ascorbate in the treatment of various types of cancer has been observed not only in combination with chemotherapeutic drugs but also in treatments with ionizing radiation (Du et al., 2015). *In vitro*, AA has been shown to potentiate the cytotoxic effect of ionizing radiation in various pancreatic cancer cell lines, but not in non-tumorigenic cell lines. This synergistic effect is attributed to an increase in oxidative stress within the tumor cells, which causes substantial oxidative damage. Murine models of pancreatic cancer, subjected to both radiotherapy and AA treatment showed a reduction in tumor growth without observing damage to their gastrointestinal system, with an increase in survival time. It can be proposed that AA can be used as a complementary therapy to radiotherapy in patients with pancreatic cancer (Du et al., 2015).

Vitamin C toxicity could also be associated with its oxidation byproducts. Lu et al. (2018) reported that DHA, which is

transporter by GLUTs and no SVCTs enhance the efficacy of oxaliplatin through redox modulation in a gastric cancer model (Lu et al., 2018). The question whether AA or DHA is the most cytotoxic vitamin C species in cancer was addressed recently in breast cancer derived cell lines. AA showed higher toxicity in TNBC cells than DHA, increasing H_2O_2 in the extracellular medium and in intracellular compartments (El Banna et al., 2019).

AA antitumoral effect is not only restricted to the promotion of ROS. Ge et al. (2018) suggests that vitamin C analogs may play a role in cell reprogramming and growth regulation by enhancing the catalytic activity of ten-eleven translocation (TET) enzymes responsible for the oxidation of 5-methylcytosine (5 mC) a well-known differentiation promoting agent. Loss of 5 mC expression correlates with the development of several aggressive form of cancer. Therefore, AA dependent restoration underlines the role of AA and its analogs in cancer epigenetics, inducing an alteration in the differentiation potential of cancer stem cells, playing a role avoiding cancer metastasis (Ge et al., 2018; Satheesh et al., 2020).

Undoubtedly, the data in the last 15 years showing an anti-cancer effect of high doses of AA represent an interesting opportunity for the field of therapeutic use of vitamin C. However, as described below, these results have not been clearly replicated in humans. An important reason is the difference in vitamin C metabolism between mouse models and human. While humans need to acquire vitamin C from the diet, mice synthesize its own. This essential difference should be considered when interpreting the results from xenograft models.

VITAMIN C ADMINISTRATION IN CLINICAL STUDIES

Since the early 2000s, several studies including case reports and clinical trials, have been analyzed the effect of IV vitamin C in patients with different types of cancer. Two initial reports showed that treatment with high-dose IV ascorbate is well tolerated for cancer patients (Padayatty et al., 2006; Hoffer et al., 2008). However, although one study analyzing three cases showed long survival times of patients (Padayatty et al., 2006), the second study analyzing 24 cases failed to demonstrate anticancer activity of vitamin C (Hoffer et al., 2008). A study considering 125 breast cancer patients showed that IV ascorbate reduces chemotherapy-related side effects, such as nausea, fatigue and dizziness (Vollbracht et al., 2011). Similar results were obtained in a study with 60 patients with different types of cancer, where IV ascorbate improved their quality of life (Takahashi et al., 2012). In addition, vitamin C administrated alone also improved quality of life in a study including 17 patients with different solid tumors, although no patient showed an objective antitumor response (Stephenson et al., 2013).

Two studies evaluated the effect of IV ascorbate in the survival of patients with stage IV pancreatic cancer under standard chemotherapy treatment. Both studies reported reduction of tumor mass and possible improvements of survival in 14 (Monti et al., 2012) and nine patients (Welsh et al., 2013) analyzed. Another study analyzed 14 patients with different types of cancer receiving chemotherapy, and reported that IV ascorbate administration produces an increased energy and functional improvement in patients (Hoffer et al., 2015). A randomized controlled trial performed in 27 patients with ovarian cancer showed that IV ascorbate treatment reduced the chemotherapy-associated toxicity, however, minimal effect on survival of patients was observed (Ma et al., 2014).

A study performed in 23 patients with metastatic castration-resistant prostate cancer showed that IV ascorbate administration did not result in disease remission or anticancer effect (Nielsen et al., 2017). On the other hand, a study analyzing 13 glioblastoma patients receiving radiotherapy and 14 non-small-cell lung cancer patients receiving chemotherapy, showed that IV ascorbate treatment extended survival of patients (Schoenfeld et al., 2017). Similarly, a report analyzing 14 pancreatic cancer patients receiving IV ascorbate and chemotherapy showed the possibility to prolong survival of patients (Polireddy et al., 2017). Another report performed in 73 patients with acute myeloid leukemia showed that IV ascorbate treatment combined with chemotherapy produced a higher complete remission and prolonged survival compared to patients who received only chemotherapy (Zhao et al., 2018). In a retrospective study in 613 hepatocellular carcinoma patients, it was shown that IV ascorbate administration improved disease-free survival of patients after surgery (Lv et al., 2018). Finally, a phase I metastatic colorectal and gastric cancer study in 36 patients applying high-dose AA in combination with mFOLFOX6 or FOLFIRI, showed potential clinical efficacy in these patients (Wang et al., 2019).

In general, most of the studies described above reported that vitamin C treatment could improve quality of life or reduce chemotherapy-related side effects in cancer patients. However, only a few works showed a clear antitumor effect of vitamin C or the consequent prolongation of patients' survival, especially when vitamin C is applied as an adjuvant. The differential results could be due to the disparities between the studies, such as doses, number of patients, types of cancer, methodologies, and parameters studied, issue that has been previously analyzed by several reviews (Fritz et al., 2014; Jacobs et al., 2015; Carr and Cook, 2018; Nauman et al., 2018). Even more important, components involved in cell transport and compartmentalization of vitamin C should be considered in each particular case to interpret these clinical results and understand the role of vitamin C in cancer.

THE CANCER-VITAMIN C PARADOX: PHYSIOLOGICAL CONSIDERATIONS

In this review, we have briefly gathered together more than 6 decades of studies focused on unraveling the relationship between vitamin C and cancer. Contradictory effects of this nutrient in cancer have been reported: on one hand the evidence showing anti-cancer activity with differential results depending on a number of factors; and, on the other hand, some evidence from *in vitro* studies showing that certain cancer cells exposed to vitamin C inhibited apoptosis or DNA damage (Perez-Cruz et al., 2007; Heaney et al., 2008).

The first important element to consider when analyzing cancer-vitamin C connection is the administration route, which has been well established in humans: limited by the intestinal barrier, oral administration, no matter the dose, in plasma will reach only in the μM range of concentration. Therefore, to achieve "pharmacological" or therapeutic plasmatic concentrations in the mM range, intravenous administration is required. The effect that vitamin C has on tumor cells will also depend on the dose. Meanwhile physiological doses do not induce cell death, pharmacological doses are able to specifically kill cancer cells *in vitro* and in xenograft mice *in vivo*.

The second consideration is regarding the specific abilities of each cancer to acquire this nutrient and metabolize it (**Figure 1**). The role of SVCT2 and GLUTs, partly addressed by the studies performed so far, must be studied in each case in particular,

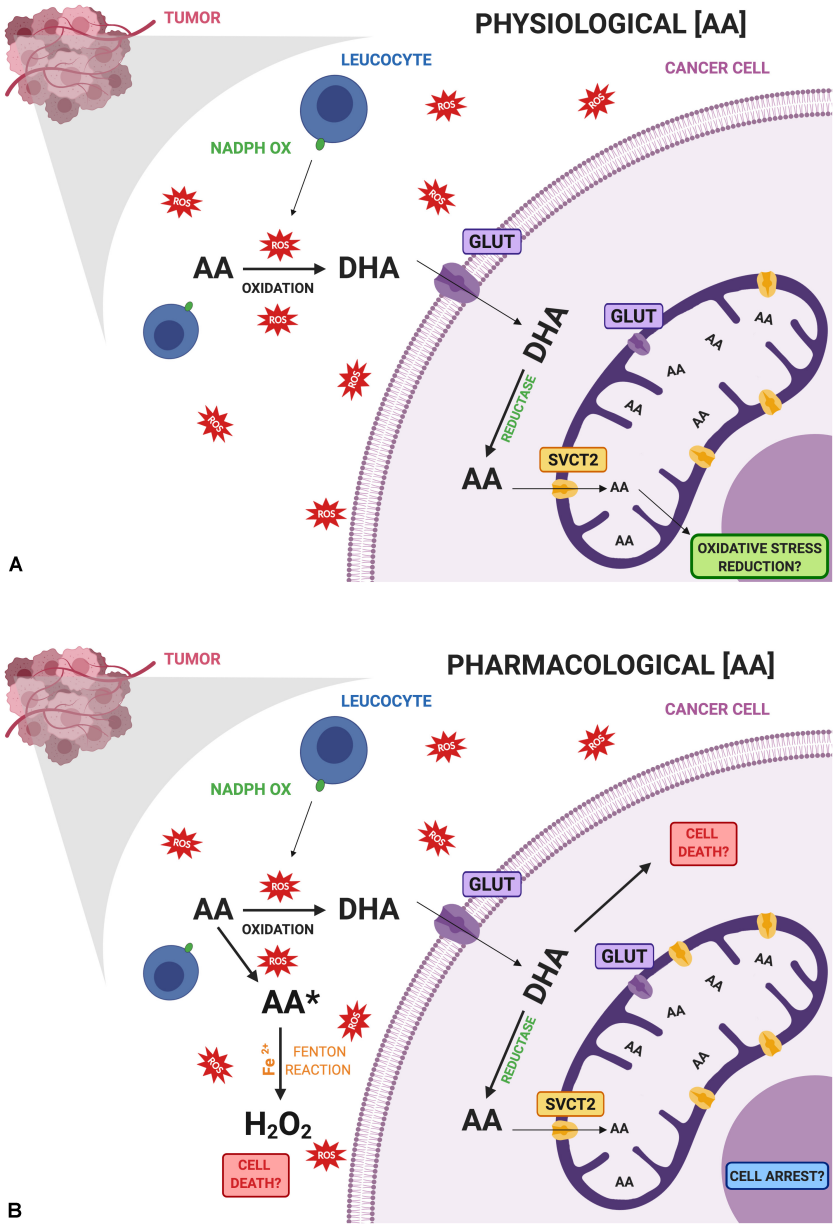

FIGURE 1 | Comparative diagram of vitamin C doses and its possible effects on cancer cells. **(A)** Physiological doses of ascorbic acid (AA) are oxidized with the help of activated leucocytes that are infiltrating the tumor, producing dehydroascorbic acid (DHA), which is the main form transported by cancer cells. Once inside the cell, DHA is rapidly reduced to AA where it can enter mitochondria via SVCT2 reducing oxidative stress at this level. **(B)** Pharmacological doses of AA may induce the production of ascorbate radical (AA*) and hydrogen peroxide (H_2O_2) inducing cell death. On the other hand, increased amounts of DHA entering cancer cells through GLUTs may participate in cell death due to an increase in oxidative stress. Role of mitochondrial GLUTs must be further studied in cancer. Finally, intracellular vitamin C could contribute to cell arrest. All these events are related to the cytotoxic effects of vitamin C in cancer cells. Created with BioRender.com.

considering their intracellular distribution. In this context, breast cancer cell lines have shown a strong capacity to acquire only the oxidized form of vitamin C and an efficient machinery to reduce it to AA. Even more, they overexpress mitochondrial SVCT2 that could be related to oxidative stress resistance. Nevertheless, when studied in pharmacological doses, the same or similar cancer cell lines showed to be sensitive to vitamin C treatment. We proposed a model considering the vitamin C transporters present in breast cancer cells, and how this can affect their capacity to interact with vitamin C (**Figure 1**). At physiological doses (**Figure 1A**), DHA byproduct from AA could enter the cancer cell, be reduced and enter the mitochondria, which could be related with the protective effect of vitamin C. However, at pharmacological doses (**Figure 1B**), extracellular accumulation of AA is able to induce H_2O_2 production, being one possible mechanism inducing cancer cell death. In addition, the direct effect of an increased DHA uptake by cancer cells when high concentrations of AA are available must be studied. Since cancer cells efficiently reduce DHA, this might be another mechanism that could promote cell death by glutathione depletion. Finally, vitamin C uptake capacity is directly influencing its epigenetic role that has relevance avoiding metastasis.

In conclusion, the knowledge on the capacities of cancer cells in acquiring and compartmentalize vitamin C is crucial and has direct implications for rational development of new vitamin C intervention procedures in human cancer, with plasma membrane glucose/dehydroascorbic acid transporters and mitochondrial ascorbic acid transporters as novel primary targets.

AUTHOR CONTRIBUTIONS

EP, FR, GM-C, CR, and CM-M: conceptualization. KE-A and PS: figure design. GM-C and CR: funding acquisition. FR, EP, MM, MG, MC, and CM-M: article reviewing. FR, GM-C, CR, and CM-M: resources, supervision, and writing – review and editing. FR, EP, MG, MC, MM, GM-C, CR, and CM-M: writing – original draft.

FUNDING

This work was supported in part by grants 1130842 (Juan Carlos Vera) and 1140429 (CR) from the Fondo Nacional de Investigación Científica y Tecnológica (FONDECYT, Chile) and grant VRID 2019.033.111-INV (GM-C) from Universidad de Concepción.

ACKNOWLEDGMENTS

In memory of our mentor Juan Carlos Vera, who passed away on August 14, 2015.

REFERENCES

Adekola, K., Rosen, S. T., and Shanmugam, M. (2012). Glucose transporters in cancer metabolism. *Curr. Opin. Oncol* 24, 650–654. doi: 10.1097/CCO.0b013e328356da72

Ancey, P. B., Contat, C., and Meylan, E. (2018). Glucose transporters in cancer - from tumor cells to the tumor microenvironment. *Febs J.* 285, 2926–2943. doi: 10.1111/febs.14577

Azzolini, C., Fiorani, M., Cerioni, L., Guidarelli, A., and Cantoni, O. (2013). Sodium-dependent transport of ascorbic acid in U937 cell mitochondria. *IUBMB Life* 65, 149–153. doi: 10.1002/iub.1124

Banhegyi, G., Benedetti, A., Margittai, E., Marcolongo, P., Fulceri, R., Nemeth, C. E., et al. (2014). Subcellular compartmentation of ascorbate and its variation in disease states. *Biochim. Biophys. Acta* 1843, 1909–1916. doi: 10.1016/j.bbamcr.2014.05.016

Cameron, E., and Campbell, A. (1974). The orthomolecular treatment of cancer. II. Clinical trial of high-dose ascorbic acid supplements in advanced human cancer. *Chem Biol Interact* 9, 285–315. doi: 10.1016/0009-2797(74)90019-2

Cameron, E., Campbell, A., and Jack, T. (1975). The orthomolecular treatment of cancer. III. Reticulum cell sarcoma: double complete regression induced by high-dose ascorbic acid therapy. *Chem. Biol .Interact* 11, 387–393.

Cameron, E., and Pauling, L. (1976). Supplemental ascorbate in the supportive treatment of cancer: prolongation of survival times in terminal human cancer. *Proc. Natl. Acad. Sci. U.S.A.* 73, 3685–3689. doi: 10.1073/pnas.73.10.3685

Cameron, E., and Pauling, L. (1978). Supplemental ascorbate in the supportive treatment of cancer: reevaluation of prolongation of survival times in terminal human cancer. *Proc. Natl. Acad. Sci. U.S.A.* 75, 4538–4542. doi: 10.1073/pnas.75.9.4538

Cameron, E., and Rotman, D. (1972). Ascorbic acid, cell proliferation, and cancer. *Lancet* 1:542. doi: 10.1016/s0140-6736(72)90215-2

Carr, A. C., and Cook, J. (2018). Intravenous Vitamin C for Cancer therapy - identifying the current gaps in our knowledge. *Front. Physiol.* 9:1182. doi: 10.3389/fphys.2018.01182

Chen, Q., Espey, M. G., Krishna, M. C., Mitchell, J. B., Corpe, C. P., Buettner, G. R., et al. (2005). Pharmacologic ascorbic acid concentrations selectively kill cancer cells: action as a pro-drug to deliver hydrogen peroxide to tissues. *Proc. Natl. Acad. Sci. U.S.A.* 102, 13604–13609. doi: 10.1073/pnas.0506390102

Chen, Q., Espey, M. G., Sun, A. Y., Lee, J. H., Krishna, M. C., Shacter, E., et al. (2007). Ascorbate in pharmacologic concentrations selectively generates ascorbate radical and hydrogen peroxide in extracellular fluid in vivo. *Proc. Natl. Acad. Sci. U.S.A.* 104, 8749–8574.

Chen, Q., Espey, M. G., Sun, A. Y., Pooput, C., Kirk, K. L., Krishna, M. C., et al. (2008). Pharmacologic doses of ascorbate act as a prooxidant and decrease growth of aggressive tumor xenografts in mice. *Proc. Natl. Acad. Sci. U.S.A.* 105, 11105–11109. doi: 10.1073/pnas.0804226105

Cho, S., Chae, J. S., Shin, H., Shin, Y., Song, H., Kim, Y., et al. (2018). Hormetic dose response to L-ascorbic acid as an anti-cancer drug in colorectal cancer cell lines according to SVCT-2 expression. *Sci. Rep./* 8, 11372. doi: 10.1038/s41598-018-29386-7

Creagan, E. T., Moertel, C. G., O'fallon, J. R., Schutt, A. J., O'connell, M. J., Rubin, J., et al. (1979). Failure of high-dose vitamin C (ascorbic acid) therapy to benefit patients with advanced cancer. A controlled trial. *N. Engl. J. Med.* 301, 687–690. doi: 10.1056/nejm197909273011303

Du, J., Cieslak, J. A. III, Welsh, J. L., Sibenaller, Z. A., Allen, B. G., Wagner, B. A., et al. (2015). Pharmacological Ascorbate Radiosensitizes Pancreatic Cancer. *Cancer Res.* 75, 3314–3326. doi: 10.1158/0008-5472.CAN-14-1707

Du, J., Cullen, J. J., and Buettner, G. R. (2012). Ascorbic acid: chemistry, biology and the treatment of cancer. *Biochim. Biophys. Acta* 1826, 443–457. doi: 10.1016/j.bbcan.2012.06.003

Du, J., Martin, S. M., Levine, M., Wagner, B. A., Buettner, G. R., Wang, S. H., et al. (2010). Mechanisms of ascorbate-induced cytotoxicity in pancreatic cancer. *Clin. Cancer Res* 16, 509–520. doi: 10.1158/1078-0432.CCR-09-1713

El Banna, N., Hatem, E., Heneman-Masurel, A., Leger, T., Baille, D., Vernis, L., et al. (2019). Redox modifications of cysteine-containing proteins, cell cycle arrest and translation inhibition: involvement in vitamin C-induced breast cancer cell death. *Redox Biol.* 26:101290. doi: 10.1016/j.redox.2019.101290

Espey, M. G., Chen, P., Chalmers, B., Drisko, J., Sun, A. Y., Levine, M., et al. (2011). Pharmacologic ascorbate synergizes with gemcitabine in preclinical models of pancreatic cancer. *Free Radic. Biol. Med.* 50, 1610–1619. doi: 10.1016/j.freeradbiomed.2011.03.007

Fritz, H., Flower, G., Weeks, L., Cooley, K., Callachan, M., Mcgowan, J., et al. (2014). Intravenous Vitamin C and cancer: a systematic review. *Integr. Cancer Ther.* 13, 280–300. doi: 10.1177/1534735414534463

Ge, G., Peng, D., Xu, Z., Guan, B., Xin, Z., He, Q., et al. (2018). Restoration of 5-hydroxymethylcytosine by ascorbate blocks kidney tumour growth. *EMBO Rep.* 19:e45401. doi: 10.15252/embr.201745401

Graczyk-Jarzynka, A., Goral, A., Muchowicz, A., Zagozdzon, R., Winiarska, M., Bajor, M., et al. (2019). Inhibition of thioredoxin-dependent H2O2 removal sensitizes malignant B-cells to pharmacological ascorbate. *Redox Biol.* 21:101062. doi: 10.1016/j.redox.2018.11.020

Hatem, E., Azzi, S., El Banna, N., He, T., Heneman-Masurel, A., Vernis, L., et al. (2018). Auranofin/Vitamin C: a novel drug combination targeting triple-negative breast cancer. *J. Natl. Cancer Inst.* 111, 597–608. doi: 10.1093/jnci/djy149

Heaney, M. L., Gardner, J. R., Karasavvas, N., Golde, D. W., Scheinberg, D. A., Smith, E. A., et al. (2008). Vitamin C antagonizes the cytotoxic effects of antineoplastic drugs. *Cancer Res.* 68, 8031–8038. doi: 10.1158/0008-5472.CAN-08-1490

Hoffer, L. J., Levine, M., Assouline, S., Melnychuk, D., Padayatty, S. J., Rosadiuk, K., et al. (2008). Phase I clinical trial of i.v. ascorbic acid in advanced malignancy. *Ann. Oncol.* 19, 1969–1974. doi: 10.1093/annonc/mdn377

Hoffer, L. J., Robitaille, L., Zakarian, R., Melnychuk, D., Kavan, P., Agulnik, J., et al. (2015). High-dose intravenous vitamin C combined with cytotoxic chemotherapy in patients with advanced cancer: a phase I-II clinical trial. *PLoS One* 10:e0120228. doi: 10.1371/journal.pone.0120228

Hong, S. W., Lee, S. H., Moon, J. H., Hwang, J. J., Kim, D. E., Ko, E., et al. (2013). SVCT-2 in breast cancer acts as an indicator for L-ascorbate treatment. *Oncogene* 32, 1508–1517. doi: 10.1038/onc.2012.176

Jacobs, C., Hutton, B., Ng, T., Shorr, R., and Clemons, M. (2015). Is there a role for oral or intravenous ascorbate (vitamin C) in treating patients with cancer? A systematic review. *Oncologist* 20, 210–223. doi: 10.1634/theoncologist.2014-0381

Levine, M., Conry-Cantilena, C., Wang, Y., Welch, R. W., Washko, P. W., Dhariwal, K. R., et al. (1996). Vitamin C pharmacokinetics in healthy volunteers: evidence for a recommended dietary allowance. *Proc. Natl. Acad. Sci. U.S.A.* 93, 3704–3709. doi: 10.1073/pnas.93.8.3704

Levine, M., Wang, Y., Padayatty, S. J., and Morrow, J. (2001). A new recommended dietary allowance of vitamin C for healthy young women. *Proc. Natl. Acad. Sci. U.S.A.* 98, 9842–9846. doi: 10.1073/pnas.171318198

Lu, Y. X., Wu, Q. N., Chen, D. L., Chen, L. Z., Wang, Z. X., Ren, C., et al. (2018). Pharmacological ascorbate suppresses growth of gastric cancer cells with GLUT1 overexpression and enhances the efficacy of oxaliplatin through redox modulation. *Theranostics* 8, 1312–1326. doi: 10.7150/thno.21745

Lv, H., Wang, C., Fang, T., Li, T., Lv, G., Han, Q., et al. (2018). Vitamin C preferentially kills cancer stem cells in hepatocellular carcinoma via SVCT-2. *NPJ Precis. Oncol.* 2:1. doi: 10.1038/s41698-017-0044-8

Ma, Y., Chapman, J., Levine, M., Polireddy, K., Drisko, J., and Chen, Q. (2014). High-dose parenteral ascorbate enhanced chemosensitivity of ovarian cancer and reduced toxicity of chemotherapy. *Sci. Transl. Med.* 6:222ra218. doi: 10.1126/scitranslmed.3007154

McCormick, W. J. (1954). Cancer: the preconditioning factor in pathogenesis; a new etiologic approach. *Arch. Pediatr.* 71, 313–322.

McCormick, W. J. (1959). Cancer: a collagen disease, secondary to a nutritional deficiency. *Arch. Pediatr.* 76, 166–171.

Moertel, C. G., Fleming, T. R., Creagan, E. T., Rubin, J., O'connell, M. J., and Ames, M. M. (1985). High-dose vitamin C versus placebo in the treatment of patients with advanced cancer who have had no prior chemotherapy. A randomized double-blind comparison. *N. Engl. J. Med.* 312, 137–141. doi: 10.1056/nejm198501173120301

Monti, D. A., Mitchell, E., Bazzan, A. J., Littman, S., Zabrecky, G., Yeo, C. J., et al. (2012). Phase I evaluation of intravenous ascorbic acid in combination with gemcitabine and erlotinib in patients with metastatic pancreatic cancer. *PLoS One* 7:e29794. doi: 10.1371/journal.pone.0029794

Munoz-Montesino, C., Roa, F. J., Pena, E., Gonzalez, M., Sotomayor, K., Inostroza, E., et al. (2014). Mitochondrial ascorbic acid transport is mediated by a low-affinity form of the sodium-coupled ascorbic acid transporter-2. *Free Radic. Biol. Med.* 70, 241–254. doi: 10.1016/j.freeradbiomed.2014.02.021

Nauman, G., Gray, J. C., Parkinson, R., Levine, M., and Paller, C. J. (2018). Systematic review of intravenous ascorbate in cancer clinical trials. *Antioxidants* 7:89. doi: 10.3390/antiox7070089

Nielsen, T. K., Hojgaard, M., Andersen, J. T., Jorgensen, N. R., Zerahn, B., Kristensen, B., et al. (2017). Weekly ascorbic acid infusion in castration-resistant prostate cancer patients: a single-arm phase II trial. *Transl. Androl. Urol.* 6, 517–528. doi: 10.21037/tau.2017.04.42

Nualart, F. J., Rivas, C. I., Montecinos, V. P., Godoy, A. S., Guaiquil, V. H., Golde, D. W., et al. (2003). Recycling of vitamin C by a bystander effect. *J. Biol. Chem.* 278, 10128–10133. doi: 10.1074/jbc.m210686200

O'Leary, B. R., Houwen, F. K., Johnson, C. L., Allen, B. G., Mezhir, J. J., Berg, D. J., et al. (2018). Pharmacological ascorbate as an adjuvant for enhancing radiation-chemotherapy responses in gastric adenocarcinoma. *Radiat Res* 189, 456–465. doi: 10.1667/RR14978.1

Padayatty, S. J., Riordan, H. D., Hewitt, S. M., Katz, A., Hoffer, L. J., and Levine, M. (2006). Intravenously administered vitamin C as cancer therapy: three cases. *CMAJ* 174, 937–942. doi: 10.1503/cmaj.050346

Padayatty, S. J., Sun, H., Wang, Y., Riordan, H. D., Hewitt, S. M., Katz, A., et al. (2004). Vitamin C pharmacokinetics: implications for oral and intravenous use. *Ann. Intern. Med.* 140, 533–537.

Pena, E., Roa, F. J., Inostroza, E., Sotomayor, K., Gonzalez, M., Gutierrez-Castro, F. A., et al. (2019). Increased expression of mitochondrial sodium-coupled ascorbic acid transporter-2 (mitSVCT2) as a central feature in breast cancer. *Free Radic. Biol. Med.* 135, 283–292. doi: 10.1016/j.freeradbiomed.2019.03.015

Perez-Cruz, I., Carcamo, J. M., and Golde, D. W. (2007). Caspase-8 dependent TRAIL-induced apoptosis in cancer cell lines is inhibited by vitamin C and catalase. *Apoptosis* 12, 225–234. doi: 10.1007/s10495-006-0475-0

Polireddy, K., Dong, R., Reed, G., Yu, J., Chen, P., Williamson, S., et al. (2017). High dose parenteral ascorbate inhibited pancreatic cancer growth and metastasis: mechanisms and a Phase I/IIa study. *Sci. Rep.* 7, 17188. doi: 10.1038/s41598-017-17568-8

Rivas, C. I., Zuniga, F. A., Salas-Burgos, A., Mardones, L., Ormazabal, V., and Vera, J. C. (2008). Vitamin C transporters. *J. Physiol. Biochem.* 64, 357–375.

Roa, F. J., Pena, E., Inostroza, E., Sotomayor, K., Gonzalez, M., Gutierrez-Castro, F. A., et al. (2019). Data on SVCT2 transporter expression and localization in cancer cell lines and tissues. *Data Brief* 25, 103972. doi: 10.1016/j.dib.2019.103972

Rose, R. C. (1988). Transport of ascorbic acid and other water-soluble vitamins. *Biochim. Biophys. Acta* 947, 335–366. doi: 10.1016/0304-4157(88)90014-7

Satheesh, N. J., Samuel, S. M., and Busselberg, D. (2020). Combination therapy with Vitamin C could eradicate cancer stem cells. *Biomolecules* 10, 79. doi: 10.3390/biom10010079

Schoenfeld, J. D., Sibenaller, Z. A., Mapuskar, K. A., Wagner, B. A., Cramer-Morales, K. L., Furqan, M., et al. (2017). O2(-) and H2O2-mediated disruption of fe metabolism causes the differential susceptibility of NSCLC and GBM cancer cells to pharmacological ascorbate. *Cancer Cell* 31, e488.

Stephenson, C. M., Levin, R. D., Spector, T., and Lis, C. G. (2013). Phase I clinical trial to evaluate the safety, tolerability, and pharmacokinetics of high-dose intravenous ascorbic acid in patients with advanced cancer. *Cancer Chemother. Pharmacol.* 72, 139–146. doi: 10.1007/s00280-013-2179-9

Takahashi, H., Mizuno, H., and Yanagisawa, A. (2012). High-dose intravenous vitamin C improves quality of life in cancer patients. *Personal. Med. Univ.* 1, 49–53. doi: 10.1016/j.pmu.2012.05.008

Takemura, Y., Satoh, M., Satoh, K., Hamada, H., Sekido, Y., and Kubota, S. (2010). High dose of ascorbic acid induces cell death in mesothelioma cells. *Biochem. Biophys. Res. Commun.* 394, 249–253. doi: 10.1016/j.bbrc.2010.02.012

Tsukaguchi, H., Tokui, T., Mackenzie, B., Berger, U. V., Chen, X. Z., Wang, Y., et al. (1999). A family of mammalian Na+-dependent L-ascorbic acid transporters. *Nature* 399, 70–75. doi: 10.1038/19986

Vera, J. C., Rivas, C. I., Fischbarg, J., and Golde, D. W. (1993). Mammalian facilitative hexose transporters mediate the transport of dehydroascorbic acid. *Nature* 364, 79–82. doi: 10.1038/364079a0

Verrax, J., and Calderon, P. B. (2008). The controversial place of vitamin C in cancer treatment. *Biochem. Pharmacol.* 76, 1644–1652. doi: 10.1016/j.bcp.2008.09.024

Verrax, J., and Calderon, P. B. (2009). Pharmacologic concentrations of ascorbate are achieved by parenteral administration and exhibit antitumoral effects. *Free Radic. Biol. Med.* 47, 32–40. doi: 10.1016/j.freeradbiomed.2009.02.016

Vollbracht, C., Schneider, B., Leendert, V., Weiss, G., Auerbach, L., and Beuth, J. (2011). Intravenous vitamin C administration improves quality of life in breast cancer patients during chemo-/radiotherapy and aftercare: results of a retrospective, multicentre, epidemiological cohort study in Germany. *In Vivo* 25, 983–990.

Wang, C., Lv, H., Yang, W., Li, T., Fang, T., Lv, G., et al. (2017). SVCT-2 determines the sensitivity to ascorbate-induced cell death in cholangiocarcinoma cell lines and patient derived xenografts. *Cancer Lett.* 398, 1–11. doi: 10.1016/j.canlet.2017.03.039

Wang, F., He, M. M., Wang, Z. X., Li, S., Jin, Y., Ren, C., et al. (2019). Phase I study of high-dose ascorbic acid with mFOLFOX6 or FOLFIRI in patients with metastatic colorectal cancer or gastric cancer. *BMC Cancer* 19:460. doi: 10.1186/s12885-019-5696-z

Welsh, J. L., Wagner, B. A., Van't Erve, T. J., Zehr, P. S., Berg, D. J., Halfdanarson, T. R., et al. (2013). Pharmacological ascorbate with gemcitabine for the control of metastatic and node-positive pancreatic cancer (PACMAN): results from a phase I clinical trial. *Cancer Chemother. Pharmacol.* 71, 765–775. doi: 10.1007/s00280-013-2070-8

Zhao, H., Zhu, H., Huang, J., Zhu, Y., Hong, M., Zhu, H., et al. (2018). The synergy of Vitamin C with decitabine activates TET2 in leukemic cells and significantly improves overall survival in elderly patients with acute myeloid leukemia. *Leuk. Res.* 66, 1–7. doi: 10.1016/j.leukres.2017.12.009

Conflict of Interest: The authors declare that the research was conducted in the absence of any commercial or financial relationships that could be construed as a potential conflict of interest.

frontiers in Pharmacology

MINI REVIEW
published: 03 March 2020
doi: 10.3389/fphar.2020.00167

Pentameric Ligand-Gated Ion Channels as Pharmacological Targets Against Chronic Pain

César O. Lara[1], *Carlos F. Burgos*[1], *Gustavo Moraga-Cid*[1], *Mónica A. Carrasco*[2*] *and Gonzalo E. Yévenes*[1*]

[1] Department of Physiology, Faculty of Biological Sciences, University of Concepcion, Concepcion, Chile, [2] Department of Biomedical Sciences, Faculty of Health Sciences, University of Talca, Talca, Chile

Chronic pain is a common detrimental condition that affects around 20% of the world population. The current drugs to treat chronic pain states, especially neuropathic pain, have a limited clinical efficiency and present significant adverse effects that complicates their regular use. Recent studies have proposed new therapeutic strategies focused on the pharmacological modulation of G-protein-coupled receptors, transporters, enzymes, and ion channels expressed on the nociceptive pathways. The present work intends to summarize recent advances on the pharmacological modulation of pentameric ligand-gated ion channels, which plays a key role in pain processing. Experimental data have shown that novel allosteric modulators targeting the excitatory nicotinic acetylcholine receptor, as well as the inhibitory $GABA_A$ and glycine receptors, reverse chronic pain-related behaviors in preclinical assays. Collectively, these evidences strongly suggest the pharmacological modulation of pentameric ligand-gated ion channels is a promising strategy towards the development of novel therapeutics to treat chronic pain states in humans.

Keywords: pentameric ligand-gated ion channels, chronic pain, allosteric modulation, analgesia, drug development, preclinical research

OPEN ACCESS

Edited by:
Ashok Kumar,
University of Florida, United States

Reviewed by:
Vinod Tiwari,
Indian Institute of Technology (BHU), India
Petra Scholze,
Medical University of Vienna, Austria
Antoine Taly,
Centre National de la Recherche Scientifique (CNRS), France

***Correspondence:**
Mónica A. Carrasco
mocarrasco@utalca.cl
Gonzalo E. Yévenes
gyevenes@udec.cl

Specialty section:
This article was submitted to Neuropharmacology, a section of the journal Frontiers in Pharmacology

Received: *18 October 2019*
Accepted: *07 February 2020*
Published: *03 March 2020*

Citation:
Lara CO, Burgos CF, Moraga-Cid G, Carrasco MA and Yévenes GE (2020) Pentameric Ligand-Gated Ion Channels as Pharmacological Targets Against Chronic Pain. Front. Pharmacol. 11:167. doi: 10.3389/fphar.2020.00167

OVERVIEW OF CHRONIC PAIN STATES

Chronic pain is defined as pain that persists after a normal healing time (Treede et al., 2015). Chronic pain can be originated by injury to the somatosensory system (neuropathic pain), degenerative processes, chronic inflammation (e.g., osteoarthritis and rheumatoid arthritis), disease (e.g., cancer pain), or by poorly managed acute pain (e.g., post-surgical and post-traumatic pain). In addition, several genetic conditions (e.g., primary erythromelalgia, paroxysomal extreme pain disorder) may generate persistent chronic pain (Drenth and Waxman, 2007; Basbaum et al., 2009; Skerratt and West, 2015; Yekkirala et al., 2017). Epidemiological studies have shown that chronic pain is a prominent health care issue, affecting around 19% of the adult European population (Breivik et al., 2006). Furthermore, these studies also have shown that a major part of these patients received inadequate pain management. Chronic pain is characterized by an increased responsiveness to innocuous (allodynia) and to nociceptive stimuli (hyperalgesia), together with episodes of spontaneous pain. Diverse peripheral and central mechanisms

contribute to the development and the maintenance of these pain hypersensitivity manifestations [reviewed in (Basbaum et al., 2009; Zeilhofer et al., 2012a; Zeilhofer et al., 2012b; Yekkirala et al., 2017)].

CURRENT PHARMACOLOGICAL STRATEGIES

The current pharmacological therapeutics to manage chronic pain mainly includes non-opioid analgesics and opioids [reviewed in (Varrassi et al., 2010; Labianca et al., 2012)]. Weak opioids, such as codeine and tramadol, are used for moderate pain, while severe pain is treated with strong opioids such as morphine and fentanyl (Varrassi et al., 2010; Labianca et al., 2012). Other groups of commonly used drugs are the anticonvulsants, such as gabapentin and pregabalin (Varrassi et al, 2010). Tricyclic antidepressants and neurotransmitter reuptake inhibitors (e.g., duloxetine and venlafaxine) are also used in neuropathic pain (Varrassi et al., 2010).

A major issue of the long-term use of both non-opioid and opioid analgesics is that pain relief is often achieved at the expense of unwanted adverse events (AEs) (Labianca et al., 2012). Constipation is the most frequent AE associated with long-term opioid therapy. Other AEs associated with the use of opioids includes effects on the CNS such as delirium, reduced cognition, sedation, respiratory depression, tolerance, addiction, and physical dependence (Labianca et al., 2012). On the other hand, the prolonged use of tricyclic antidepressants and reuptake inhibitors generates several AEs, such as dry mouth, disturbed vision, constipation, orthostatic hypotension, dizziness, sedation, nausea, and vomiting (Varrassi et al., 2010; Labianca et al., 2012).

In addition to the AEs described above, the clinical efficacy of the current treatments against chronic pain, particularly those directed to neuropathic pain, is significantly limited (Finnerup et al., 2015). This scenario highlights the imperative need to develop novel effective and safe analgesics. Coincidentally, the expanding knowledge regarding the neurophysiology of the nociceptive pathways in acute and chronic pain conditions have revealed new protein targets to develop such novel analgesics. These targets proteins mainly include G-protein-coupled receptors (GPCRs), enzymes, transporters, and ion channels, including the members of the pentameric ligand-gated ion channels [reviewed in (Yekkirala et al., 2017)].

PENTAMERIC LIGAND-GATED ION CHANNELS

Pentameric ligand-gated ion channels (pLGICs), a family of channels previously known as Cys-loop receptors, are main players of the chemical neurotransmission on the central nervous system (Zeilhofer et al., 2012a; Nys et al., 2013; Gielen and Corringer, 2018). Mammalian pLGICs comprises nicotinic acetylcholine (nAChR), type 3 serotonin (5-HT_3R), γ-aminobutyric type A ($GABA_A$R), and glycine receptors (GlyR) (Nys et al., 2013). pLGICs are integral membrane protein complexes composed of five subunits arranged around a central pore. The ion fluxes through pLGICs generate transient changes in the membrane potential, allowing the dynamic control of the neuronal excitability. Recent structural data has revealed a conserved cylinder-shape architecture for all pLGICs, in which five subunits are arranged around a central five-fold axis. Each subunit comprises a large extracellular domain (ECD) which contains the agonist-binding site, four transmembrane domains (TM1–4) which shape the ion pore, a large intracellular domain (ICD) between TM3 and TM4, and a short extracellular C-terminal region (**Figure 1**) (Nys et al., 2013; Burgos et al., 2016; Gielen and Corringer, 2018). The binding of the agonist to the orthosteric site within the ECD triggers a rapid isomerization (i.e., gating) that results

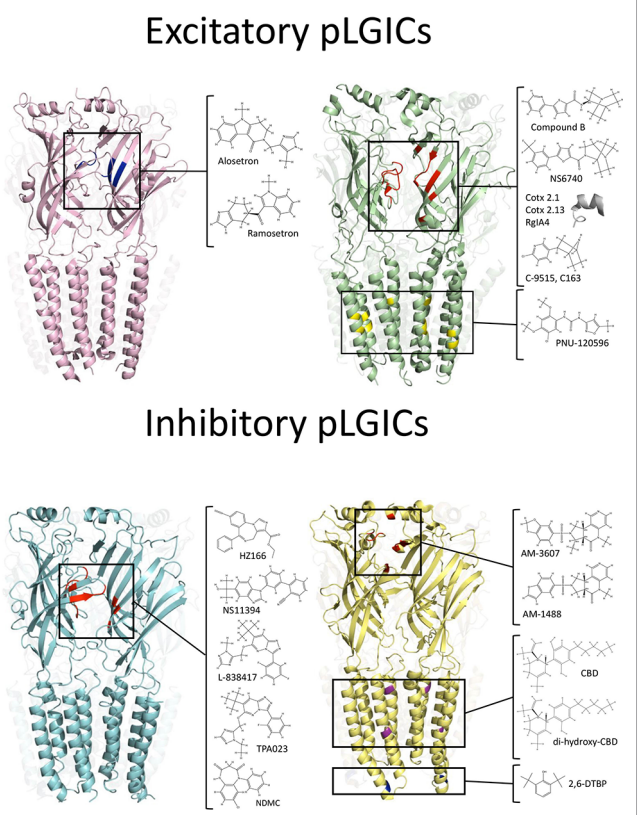

FIGURE 1 | Binding sites of analgesic compounds on pLGIC structures. *Top*: The purple structure represent the 5-HT3R (PDB:6HIQ). The black square highlight the tropeine binding site described within the orthosteric site (blue). The green structure represents nAChRs (PDB: 4AQ9). The black squares show two different binding sites for analgesic molecules (ECD and TMD). The binding site within the ECD correspond to the orthosteric binding site. The inset show chemical compounds and toxins-derivate peptides that may interact with residues on the orthosteric site (red). Conversely, the PAM PNU-120596 binds to an intra-subunit cavity in the TMD (yellow). *Bottom*: The cyan structure represents $GABA_A$Rs (PDB: 6HUO). The black square shows the binding site of BDZ at the ECD, in the interphase between α and γ subunits. The yellow structure represent GlyRs (PDB: 5TIO). The black squares show three putative binding sites for analgesic compounds. The tricyclic sulfonamides AM-1488 and AM-3607 binds to ECD, in the interphase between two adjacent α subunits. The binding site for DH-CBD has been described within the TMD. The compound 2,6-DTBP has been proposed to interact with α3GlyRs in an ICD a putative binding site.

TABLE 1 | Compounds targeting pLGICs with analgesic effects.

Receptor targeted	Molecule	Model	Dose and administration	Reference
α7nAChR	PNU-120596	Carrageenan	0.3–30 mg kg^{-1} (sc)	Munro et al., 2012
		CFA	10–30 mg kg^{-1} (sc)	
	Comp B	Formalin	45–60 mg kg^{-1} (sc)	Munro et al., 2012
		Carrageenan	3–30 mg kg^{-1} (sc)	
		CFA	10–30 mg kg^{-1} (sc)	
	Comp 111	CFA	10 mg kg^{-1} (iv)	Balsera et al., 2014
	Comp 31	CFA	10 mg kg^{-1} (iv)	Criado et al., 2016
	Comp 19	CFA	10 mg kg^{-1} (iv)	Balsera et al., 2018
	Comp 21			
	NS6740	CCI	1–9 mg kg^{-1} (ip)	Papke et al., 2015
		Formalin	0.1–9 mg kg^{-1} (ip)	
	Cotx 2.1	PIPN	1.5 mg kg^{-1} (ip)	Liu et al., 2019
	Cotx 2.13	PIPN	2 mg kg^{-1} (ip)	
	Cotx 1.1	PIPN	1 mg kg^{-1} (ip)	
α4β2nAChR	C-9515	Formalin	0.003–0.03 mg kg^{-1} (ip)	Li et al., 2018
		CCI	0.003 mg kg^{-1} (ip)	
	C163	Formalin	1–10 mg kg^{-1} (ip)	
	Cris-104	STZ-IN	35 mg kg^{-1} (po)	Debom et al., 2014
		Formalin	10–100 mg kg^{-1} (po)	Sudo et al., 2018
		SNL	10–100 mg kg^{-1} (po)	
α9 α10 nAChR	RgIA4	Oxaliplatin-induced neuropathy	0.128–80 μg kg^{-1} (sc)	Romero et al., 2017
α2/α3 GABAAR	HZ166	CCI	5–480 mg kg^{-1} (ip)	Di Lio et al., 2011
		Zymosan A	16 mg kg^{-1} (ip)	
	NS11394	Formalin	0.3–30 mg kg^{-1} (po)	Munro et al., 2008; Hofmann et al., 2012
		SNI	3–30 mg kg^{-1} (po)	
		CFA	1–10 mg kg^{-1} (po)	
		CCI	5–30 mg kg^{-1} (po)	
	L-838417	Formalin	1–10 mg kg^{-1} (ip)	Knabl et al., 2008; Nickolls et al., 2011; Hofmann et al., 2012
		Zymozan	0.1–10 mg kg^{-1} (ip)	
		CFA	1–10 mg kg^{-1} (po)	
		CCI	10 mg kg^{-1} (po)	
		SNI	10 mg kg^{-1} (ip)	
		SNL	10 mg kg^{-1} (po)	
	TPA023	CCI	1 mg kg^{-1} (po)	Nickolls et al., 2011
		SNL	10–30 mg kg^{-1} (po)	
	NDMC	CCI	3–30 mg kg^{-1} (po)	Ralvenius et al., 2016
	MP-III-024	Zymozan A	10–32 mg kg^{-1} (ip)	Fischer et al., 2017
	KRM-II-81	Formalin	30 mg kg^{-1} (ip)	Witkin et al., 2019
		SNL	50 mg kg^{-1} (ip)	
α1/α3GlyR	CBD	CFA	50 mg kg^{-1}(ip)	Xiong et al., 2012; Lu et al., 2018
	DH-CBD		50 μg (it)	
		SNL	100 μg (it)	
	AM-1488	SNI	20 mg kg^{-1} (po)	Bregman et al., 2017
	AM-3607			Huang et al., 2017
α3 GlyR	2,6-DTBP	CFA	90 mg kg^{-1} (it)	Acuna et al., 2016
		Zymozan A	90 mg kg^{-1} (it)	
		CCI	90 mg kg^{-1} (it)	

nAChR, nicotinic acetylcholine receptor; $GABA_AR$, γ-aminobutyric acid type A receptor; GlyR, glycine receptor; NDMC, N-desmethyl clobazam; CBD, cannabidiol; DH-CBD, dehydroxyl-cannabidiol; 2,6-DTBP, 2,6-di-tert-butylphenol; CFA, Complete Freund's Adjuvant; CCI, chronic constriction injury; SNI, spared-nerve injury; SNL, spinal nerve ligation; PIPN, paclitaxel-induced peripheral neuropathy; STZ-IN, streptozotocin-induced neuropathy; po, oral administration; ip, intraperitoneal administration; it, intrathecal administration; sc, subcutaneous administration.

on the transient structural rearrangements of the TM2 and TM3, allowing the passive diffusion of ions through the ion channel pore (Alexander et al., 2017). The structural transitions involved in the gating process are able to be modified by allosteric modulators, which for example, can reversibly stabilize the open state of the ion channel, potentiating the ionic currents in an agonist-dependent manner (Corringer et al., 2012).

The dysfunction of the neurotransmitter systems associated with the pLGICs has been associated with several CNS disorders, such as schizophrenia, epilepsy, and Alzheimer's disease (Sparling and DiMauro, 2017). Additional genetic, electrophysiological, biochemical, and pharmacological studies have linked chronic pain states with the dysfunction of cholinergic, GABAergic, and glycinergic neurotransmission (Harvey et al., 2004; Miraucourt et al., 2007; Bagdas et al., 2018; Vuilleumier et al., 2018). The prominent role of the pLGICs in chronic pain have been further highlighted by recent evidences showing that several allosteric modulators of nAChRs, $GABA_ARs$, and GlyRs display analgesic effects in behavioral models of chronic pain (summarized in **Table 1**).

The present work intends to offer a systematic summary of the current state of the pLGIC pharmacology with focus on advances in preclinical chronic pain research.

5-HT$_3$RS

5-HT$_3$Rs are cation-selective pLGICs which mediate neuronal depolarization within the central and peripheral nervous systems (Barnes et al., 2009; Cortes-Altamirano et al., 2018). The effects of drugs modulating 5-HT$_3$Rs on behavioral assays of chronic pain have not been systemically investigated on preclinical assays in rodent models of chronic pain. However, clinical studies have revealed that the treatment with several 5-HT$_3$ antagonists (e.g., alosetron, ondansetron) displayed effective pain management on intestinal bowel syndrome (Camilleri and Boeckxstaens, 2017; Binienda et al., 2018; Cortes-Altamirano et al., 2018) and fibromyalgia (Ablin and Hauser, 2016).

nAChRs

nAChRs are cation-selective ion channels expressed in both peripheral and central nervous system (Alexander et al., 2017; Bagdas et al., 2018). A total of 17 nAChR subunits (α1–10, β1–4, γ, δ and ϵ) have been identified. The first molecules displaying nAChR-mediated analgesia were nicotine, epibatine, and ABT-594. However, the evaluation of these compounds on clinical trials reported important AEs [reviewed in (Taly et al., 2009; Lemoine et al., 2012)]. Novel compounds targeting three specific subunit combinations of nAChRs (α7,α4β2 and α9α10) have displayed analgesic effects on behavioral chronic pain models with improved AEs profiles in preclinical models. Munro and coworkers showed that the α7-selective agonist (i.e., compound B) and PNU-120596, a selective positive allosteric modulator (PAM) of α7 nAChR, showed analgesic effects in inflammatory pain models (Munro et al., 2012). Both compounds dose-dependently reversed the pain hypersensitivity produced by Complete Freund's Adjuvant (CFA) injection. The maximal efficacy obtained with both molecules was similar to that produced by diclofenac (Munro et al., 2012). Other authors have shown that NS6740, a silent agonist selective for α7nAChR (i.e., a ligand that binds to the orthosteric site but more effectively promotes the conformational changes associated with desensitization than activation), reduced pain hypersensitivity elicited by the paw injection of formalin and by chronic constriction of the sciatic nerve (CCI). Interestingly, these effects were not observed in α7 nAChR knock-out mice and were blocked by the α7nAChR antagonist MLA (Papke et al., 2015). A systematic screening of a library of small natural molecules (Greenpharma Natural compound library, Prestwick Chemical, France) combined with structure–activity relationship analysis lead to the discovery of hydroxylated chalcones as new PAMs targeting α7nAChRs (Balsera et al., 2014; Criado et al., 2016; Balsera et al., 2018). The compound 111 was characterized as a selective α7nAChR PAM (EC_{50} ≈3 μM) by using two-electrode voltage-clamp (TEVC) recordings in *Xenopus* oocytes. Interestingly, compound 111 exerted analgesic activity in CFA-injected rats (Balsera et al., 2014). Further work studied the compound 31, which displayed an improved potentiation (≈666%, 10 μM of compound) of α7nAChRs-mediated currents (Criado et al., 2016). In CFA-injected rats, the compound 31 displayed analgesic effects similar to those obtained with PNU-120596 (Criado et al., 2016). However, these chalcone-derivate compounds have low aqueous solubility and short time of action *in vivo* (Balsera et al., 2018). To solve this issue, Balsera and collaborators reported the characterization of peptide-based carrier prodrugs of these compounds (Balsera et al., 2018). Despite the electrophysiological evidences showing inhibitory actions on the ACh-evoked currents, two peptide derivatives (i.e., comp19 and comp21) carrying the compound 31 showed a recovery of the mechanical hyperalgesia with a prolonged effect (Balsera et al., 2018). Conversely, other authors have studied the actions of peptides directly targeting α7nAChRs. For example, cotx2.1, cotx2.13, and coxt1.1 are peptides originated from optimizations of the cone snail toxin BuIA (Liu et al., 2019). *In silico* approaches and binding assays have shown that these peptides have a higher affinity for α7nAChRs over other nAChRs conformations. These peptides displayed analgesic effects on models of chemotherapy-induced neuropathy, alleviating the paclitaxel-induced hyperalgesia (Liu et al., 2019).

Additional efforts have directed attention to other nAchR subunit combinations. Recently, epibatine analogs with high affinity for α4β2 nAChRs were evaluated in chronic pain models (Debom et al., 2014; Li et al., 2018; Sudo et al., 2018). The analogs C-9515 and C-163 dose-dependently reduced the formalin and the CCI-induced hyperalgesia (Li et al., 2018). Further chemical modifications originated the compound Cris-104, a selective α4β2 ligand with an improved ADME profile (Debom et al., 2014). Cris-104 exerted analgesic effects in diverse chronic pain models, such as diabetes-induced neuropathy, spared nerve ligation (SNL), and formalin test (Debom et al., 2014; Sudo et al., 2018). Open field performances showed that the analgesic doses of Cris-104 does not produce significant alterations on the locomotor activity (Debom et al., 2014; Sudo et al., 2018).

On the other hand, nAChRs composed by the subunits α9α10 have shown to be important in the generation of chemotherapy-induced pain. Through the optimization of cone snail venoms toxins, Romero and coworkers generated the peptide RgIA4, which displayed a high potency (IC_{50} ≈ 1 nM) as an antagonist for both human and rodent α9α10nAChRs (Romero et al., 2017). RgIA4 has selectivity over other nAChRs conformations, such as α2/3β2/4nAChRs (EC50 > 10 μM) (Romero et al., 2017). Interestingly, repeated subcutaneous injections of RgIA4 prevented the progressive oxaliplatin-induced cold allodynia in rats (Romero et al., 2017).

GABA$_A$RS

GABA$_A$Rs are anion-permeable pLGICs. Activation of GABA$_A$Rs hyperpolarizes the membrane potential, contributing to the control of neuronal excitability across the whole CNS (Michels and Moss, 2007). Pentameric GABA$_A$Rs

are composed by any of 19 different subunits (α1-α6, β1-β3, γ1-3, δ, ϵ, ρ, ο). However, a large proportion of $GABA_AR$s are composed by two α-subunits, two β-subunits, and one γ-subunit (Michels and Moss, 2007). $GABA_AR$ PAMs such as diazepam, a classical benzodiazepine (BDZ), attenuate nociceptive transmission in animal models of chronic pain (Hwang and Yaksh, 1997; Kaneko and Hammond, 1997). However, the use of classical BDZs is hampered by sedation and other side effects occurring mainly as a consequence of the modulation of $GABA_AR$s containing the α1 subunit (Rudolph et al., 1999; McKernan et al., 2000). Interestingly, an increasing number of reports have shown that a new generation of BDZ-site ligands, with higher selectivity over α2/α3-containing $GABA_AR$s, alleviate inflammatory and neuropathic pain with less adverse effects than classical BDZs (Ralvenius et al., 2015; Zeilhofer et al., 2015). For example, NS11394 is a BDZ-site agonist which have superior efficacy at α3$GABA_AR$ compared to α1$GABA_AR$ (Mirza et al., 2008). NS11394 showed analgesic effects on the formalin test, CFA, and CCI model. However, the administration of the compound also showed a reduction on the locomotor activity and motor performance (Munro et al., 2008; Hofmann et al., 2012). Similar studies have shown that non-sedative BDZ-site agonist L-838417 displayed analgesic effects on formalin, Zymozan A, CCI, CFA, and spared nerve injury (SNI) models in rats (Knabl et al., 2008; Nickolls et al., 2011; Hofmann et al., 2012). Nevertheless, L-838417 possesses low bioavailability and a short half-life in mice (Knabl et al., 2008; Hofmann et al., 2012). Other studies have characterized additional BDZ-site ligands with improved AE profiles. Studies with TPA023, a BDZ-site agonist which has no α1$GABA_AR$s activity, low levels of α2/3$GABA_AR$s efficacy, and minimal activity at α5$GABA_AR$s significantly increased the paw withdraw threshold in CCI and SNL models of neuropathic pain (Nickolls et al., 2011). Analgesic doses TPA023 did not affect the rotarod performance (Atack et al., 2006). HZ166, a BDZ-site ligand with preferentially targeting α2- and α3-$GABA_AR$, showed dose-dependent anti-hyperalgesic effects in Zymozan A and CCI models (Di Lio et al., 2011). HZ166 did not generate neither locomotor impairment, sedation, nor tolerance (Di Lio et al., 2011). A newer BDZ-type drug, MP-III-024, is a α2/α3$GABA_AR$ PAM that displayed analgesic effects in inflamed mice without significant effects on the open field performance (Fischer et al., 2017). In the same line, KRM-II-81 is another α2/α3-selective $GABA_AR$ BDZ-site ligand that displayed anti-nociceptive effects in rodents with reduced motor side effects (Lewter et al., 2017; Witkin et al., 2019). An intriguing case is N-desmethyl clobazam (NDMC), which was found to be a human metabolite of the clinically used BDZ Clobazam (CBZ). Electrophysiological recordings have shown that NDMC potentiated α2 and α3GABAARs to a considerably higher degree than α1 and α2$GABA_AR$s (Ralvenius et al., 2016). Behavioral studies showed that NDMC dose-dependently reduced both thermal and mechanical hyperalgesia in neuropathic animals with no impact on the locomotor activity (Ralvenius et al., 2016). Noteworthy, clinical trials performed on chronic lower-back pain patients have shown that CBZ and their metabolites are able to generate analgesia in humans (Besson et al., 2015; Schliessbach et al., 2017).

GlyRs

GlyRs are chloride-permeable ion channels that mediates inhibitory neurotransmission mainly in the spinal cord and brainstem (Lynch, 2009). The human genome encodes four GlyR subunits (α1, α2, α3 and β)(Lynch, 2009; Zeilhofer et al., 2018). Genetic, electrophysiological, and behavioral experiments have shown the presence of dysfunctional α3-containing GlyRs in chronic pain of inflammatory origin (Harvey et al., 2004). Thus, the selective potentiation of α3GlyR activity through PAMs has emerged as a rational approach to restore glycinergic inhibition (Cioffi, 2018; Zeilhofer et al., 2018). One of the first evidences showing a GlyR-dependent analgesia comes from studies using the synthetic phytocannabinoid derivative de-hydroxyl-cannabidiol (DH-CBD). Systemic application of DH-CBD generated a dose-dependent analgesia on the CFA model in mice (Xiong et al., 2012). DH-CBD was characterized as a PAM targeting α1/α3GlyRs without psychoactive effects (Xiong et al., 2012). Interestingly, the analgesic effects of DH-CBD were significantly reduced in α3GlyR knock-out mice (Xiong et al., 2012). However, Lu and co-workers recently reported that α1GlyR is also involved in the DH-CBD-induced analgesia (Lu et al., 2018). These studies characterized a genetically modified mice carrying a mutation in α1GlyR (i.e., S296A), that render the receptor resistant to DH-CBD. Behavioral studies showed that the DH-CBD-induced analgesia in the CFA model was suppressed in the α1S296A GlyR mice (Lu et al., 2018).

Other compound targeting GlyRs is 2,6-di-tertbutylphenol (2,6-DTBP), a non-sedative analog of propofol (Ahrens et al., 2009). 2,6-DTBP enhanced the glycine-evoked current of α1/α3GlyRs (Acuna et al., 2016). In models of inflammatory pain, 2,6-DTBP reduced inflammatory hyperalgesia in an α3GlyR-dependent manner (Acuna et al., 2016). Interestingly, 2,6-DTBP was able to enlarge the decay time kinetics of glycinergic synaptic currents in dorsal horn neurons from inflamed animals or after the activation of EP2 receptors with PGE2, suggesting the recovery of the spinal glycinergic inhibition as a main mechanism of action (Acuna et al., 2016). The first glycinergic PAM generated by rational drug design is AM-1488, which is a tricyclic sulfonamide that enhance the GlyR function in recombinant and native systems (Bregman et al., 2017). The oral administration of AM-1488 reversed the tactile allodynia in SNI model (Bregman et al., 2017). Noteworthy, these authors achieved the first crystal structure of α3GlyRs bound to a PAM. This seminal study showed the binding of AM-3607, an AM-1488 analog, to the interphase of two α subunits at the ECD (**Figure 1**) (Huang et al., 2017).

CONCLUSIONS

The data summarized here allow us to conclude that the search of novel pLGICs modulators may originate chemical templates for the design and development of clinically relevant analgesics. However, it is important to note that only few studies investigated the molecular sites involved in the allosteric modulation of these new molecules (see **Figure 1**). The combination of functional (e.g., electrophysiology) with structural (e.g., X-ray crystallography or cryo-electron microscopy) studies likely will boost the optimization of these novel compounds, allowing the generation of PAMs with improved potency, efficacy, and subunit-selectivity. Additionally, the generation of translational techniques that ensure a successful transition from *in vitro/in vivo* laboratory experiments to human clinical trials is still a critical issue. The recent development of new stem-cells and gene editing technologies may offer a viable alternative for the study of allosteric modulators using neurons derived from human-induced pluripotent stem cells (hiPSC) of specific patients (Boer, 1999; Okita et al., 2007). Recent evidences have reported that human neurons derived from iPSCs expresses ion channels, including pLGICs. Immunocytochemical and qRT-PCR studies performed on human neurons have shown the expression of genes related with voltage-gated ion channels and some pLGICs, such as $GABA_A$Rs and nAChRs. In addition, Ca^{2+} imaging studies and electrophysiological techniques have shown that iPSCs-derived neurons expresses functional pLGICs, providing a suitable platform to study endogenous neuronal ion channels in human neurons for pharmacological studies (Haythornthwaite et al., 2012; Dage et al., 2014; Stanslowsky et al., 2014; Chatzidaki et al., 2015; Yuan et al., 2016; Antonov et al., 2019). Moreover, the development of new gene editing techniques (such as CRISPRs/Cas9) may allow the genetic manipulation of these human-derived neurons, making possible the study of PAMs on mutated pLGICs or to directly examine potential off-targets (Santos et al., 2016). However, neurons derived from iPSCs displayed a neonatal expression profile (Dage et al., 2014; Stanslowsky et al., 2014; Yuan et al., 2016). Thus, future investigations with focus on the generation of iPSCs-neurons of the nociceptive pathway (i.e., sensory neurons, spinal cord neurons) having an adult gene-expression profile may provide an excellent platform to further explore the pharmacological modulation of pLGICs and other ion channels by novel allosteric modulators.

AUTHOR CONTRIBUTIONS

CL, GM-C, MC, and GY participated in the conception of the review and wrote the manuscript. CL and CB design and develop the figure and the table. MC and GY edited the manuscript.

FUNDING

This work was supported by grant FONDECYT 1170252 (to GY), FONDECYT 1161014 (to MC), FONDECYT 3170108 (to CB), and VRID 219.033.111-INV (to GM-C). CL was supported by CONICYT doctoral fellowship 21171549.

REFERENCES

Ablin, J. N., and Hauser, W. (2016). Fibromyalgia syndrome: novel therapeutic targets. *Pain Manage.* 6 (4), 371–381. doi: 10.2217/pmt-2016-0007

Acuna, M. A., Yevenes, G. E., Ralvenius, W. T., Benke, D., Di Lio, A., Lara, C. O., et al. (2016). Phosphorylation state-dependent modulation of spinal glycine receptors alleviates inflammatory pain. *J. Clin. Invest.* 126 (7), 2547–2560. doi: 10.1172/JCI83817

Ahrens, J., Leuwer, M., de la Roche, J., Foadi, N., Krampfl, K., and Haeseler, G. (2009). The non-anaesthetic propofol analogue 2,6-di-tert-butylphenol fails to modulate GABA(A) receptor function. *Pharmacology* 83 (2), 95–98. doi: 10.1159/000180125

Alexander, S. P., Peters, J. A., Kelly, E., Marrion, N. V., Faccenda, E., Harding, S. D., et al. (2017). The concise guide to pharmacology 2017/18: ligand-gated ion channels. *Br. J. Pharmacol.* 174 Suppl 1, S130–S159. doi: 10.1111/bph.13879

Antonov, S. A., Novosadova, E. V., Kobylyansky, A. G., Illarioshkin, S. N., Tarantul, V. Z., and Grivennikov, I. A. (2019). Expression and functional properties of NMDA and GABAA receptors during differentiation of human induced pluripotent stem cells into ventral mesencephalic neurons. *Biochem. Biokhimiia* 84 (3), 310–320. doi: 10.1134/S0006297919030131

Atack, J. R., Wafford, K. A., Tye, S. J., Cook, S. M., Sohal, B., Pike, A., et al. (2006). TPA023 [7-(1,1-dimethylethyl)-6-(2-ethyl-2H-1,2,4-triazol-3-ylmethoxy)-3-(2-fluorophenyl)-1,2,4-triazolo[4,3-b]pyridazine], an agonist selective for alpha2- and alpha3-containing GABAA receptors, is a nonsedating anxiolytic in rodents and primates. *J. Pharmacol. Exp. Ther.* 316 (1), 410–422. doi: 10.1124/jpet.105.089920

Bagdas, D., Gurun, M. S., Flood, P., Papke, R. L., and Damaj, M. I. (2018). New insights on neuronal nicotinic acetylcholine receptors as targets for pain and inflammation: a focus on alpha7 nAChRs. *Curr. Neuropharmacol.* 16 (4), 415–425. doi: 10.2174/1570159X15666170818102108

Balsera, B., Mulet, J., Fernandez-Carvajal, A., de la Torre-Martinez, R., Ferrer-Montiel, A., Hernandez-Jimenez, J. G., et al. (2014). Chalcones as positive allosteric modulators of alpha7 nicotinic acetylcholine receptors: a new target for a privileged structure. *Eur. J. Med. Chem.* 86, 724–739. doi: 10.1016/j.ejmech.2014.09.039

Balsera, B., Mulet, J., Sala, S., Sala, F., de la Torre-Martinez, R., Gonzalez-Rodriguez, S., et al. (2018). Amino acid and peptide prodrugs of diphenylpropanones positive allosteric modulators of alpha7 nicotinic receptors with analgesic activity. *Eur. J. Med. Chem.* 143, 157–165. doi: 10.1016/j.ejmech.2017.10.083

Barnes, N. M., Hales, T. G., Lummis, S. C., and Peters, J. A. (2009). The 5-HT3 receptor—the relationship between structure and function. *Neuropharmacology* 56 (1), 273–284. doi: 10.1016/j.neuropharm.2008.08.003

Basbaum, A. I., Bautista, D. M., Scherrer, G., and Julius, D. (2009). Cellular and molecular mechanisms of pain. *Cell* 139 (2), 267–284. doi: 10.1016/j.cell.2009.09.028

Besson, M., Matthey, A., Daali, Y., Poncet, A., Vuilleumier, P., Curatolo, M., et al. (2015). GABAergic modulation in central sensitization in humans: a randomized placebo-controlled pharmacokinetic-pharmacodynamic study comparing clobazam with clonazepam in healthy volunteers. *Pain* 156 (3), 397–404. doi: 10.1097/01.j.pain.0000460331.33385.e8

Binienda, A., Storr, M., Fichna, J., and Salaga, M. (2018). Efficacy and safety of serotonin receptor ligands in the treatment of irritable bowel syndrome: a

review. *Curr. Drug Targets* 19 (15), 1774–1781. doi: 10.2174/1389450119666171227225408

Boer, G. J. (1999). Ethical issues in neurografting of human embryonic cells. *Theor. Med. Bioethics* 20 (5), 461–475. doi: 10.1023/A:1009985223158

Bregman, H., Simard, J. R., Andrews, K. L., Ayube, S., Chen, H., Gunaydin, H., et al. (2017). The discovery and hit-to-lead optimization of tricyclic sulfonamides as potent and efficacious potentiators of glycine receptors. *J. Med. Chem.* 60 (3), 1105–1125. doi: 10.1021/acs.jmedchem.6b01496

Breivik, H., Collett, B., Ventafridda, V., Cohen, R., and Gallacher, D. (2006). Survey of chronic pain in Europe: prevalence, impact on daily life, and treatment. *Eur. J. Pain* 10 (4), 287–333. doi: 10.1016/j.ejpain.2005.06.009

Burgos, C. F., Yevenes, G. E., and Aguayo, L. G. (2016). Structure and pharmacologic modulation of inhibitory glycine receptors. *Mol. Pharmacol.* 90 (3), 318–325. doi: 10.1124/mol.116.105726

Camilleri, M., and Boeckxstaens, G. (2017). Dietary and pharmacological treatment of abdominal pain in IBS. *Gut* 66 (5), 966–974. doi: 10.1136/gutjnl-2016-313425

Chatzidaki, A., Fouillet, A., Li, J., Dage, J., Millar, N. S., Sher, E., et al. (2015). Pharmacological characterisation of nicotinic acetylcholine receptors expressed in human iPSC-derived neurons. *PloS One* 10 (4), e0125116. doi: 10.1371/journal.pone.0125116

Cioffi, C. L. (2018). Modulation of glycine-mediated spinal neurotransmission for the treatment of chronic pain. *J. Med. Chem.* 61 (7), 2652–2679. doi: 10.1021/acs.jmedchem.7b00956

Corringer, P. J., Poitevin, F., Prevost, M. S., Sauguet, L., Delarue, M., and Changeux, J. P. (2012). Structure and pharmacology of pentameric receptor channels: from bacteria to brain. *Structure* 20 (6), 941–956. doi: 10.1016/j.str.2012.05.003

Cortes-Altamirano, J. L., Olmos-Hernandez, A., Jaime, H. B., Carrillo-Mora, P., Bandala, C., Reyes-Long, S., et al. (2018). Review: 5-HT1, 5-HT2, 5-HT3 and 5-HT7 receptors and their role in the modulation of pain response in the central nervous system. *Curr. Neuropharmacol.* 16 (2), 210–221. doi: 10.2174/1570159X15666170911121027

Criado, M., Balsera, B., Mulet, J., Sala, S., Sala, F., de la Torre-Martinez, R., et al. (2016). 1,3-Diphenylpropan-1-ones as allosteric modulators of alpha7 nACh receptors with analgesic and antioxidant properties. *Future Med. Chem.* 8 (7), 731–749. doi: 10.4155/fmc-2015-0001

Dage, J. L., Colvin, E. M., Fouillet, A., Langron, E., Roell, W. C., Li, J., et al. (2014). Pharmacological characterisation of ligand- and voltage-gated ion channels expressed in human iPSC-derived forebrain neurons. *Psychopharmacology* 231 (6), 1105–1124. doi: 10.1007/s00213-013-3384-2

Debom, R. C., Trachez, M. M., Sudo, G. Z., da Silva, J. S., Oliveira, K. M., Garcia, A. L., et al. (2014). Novel nicotinic receptor agonist reduces hyperalgesia and allodynia of neuropathic pain in diabetic rats. *J. Diabetes Metab.* 5, 396. doi: 10.4172/2155-6156.1000396

Di Lio, A., Benke, D., Besson, M., Desmeules, J., Daali, Y., Wang, Z. J., et al. (2011). HZ166, a novel GABAA receptor subtype-selective benzodiazepine site ligand, is antihyperalgesic in mouse models of inflammatory and neuropathic pain. *Neuropharmacology* 60 (4), 626–632. doi: 10.1016/j.neuropharm.2010.11.026

Drenth, J. P., and Waxman, S. G. (2007). Mutations in sodium-channel gene SCN9A cause a spectrum of human genetic pain disorders. *J. Clin. Invest.* 117 (12), 3603–3609. doi: 10.1172/JCI33297

Finnerup, N. B., Attal, N., Haroutounian, S., McNicol, E., Baron, R., Dworkin, R. H., et al. (2015). Pharmacotherapy for neuropathic pain in adults: a systematic review and meta-analysis. *Lancet Neurol.* 14 (2), 162–173. doi: 10.1016/S1474-4422(14)70251-0

Fischer, B. D., Schlitt, R. J., Hamade, B. Z., Rehman, S., Ernst, M., Poe, M. M., et al. (2017). Pharmacological and antihyperalgesic properties of the novel alpha2/3 preferring GABAA receptor ligand MP-III-024. *Brain Res. Bull.* 131, 62–69. doi: 10.1016/j.brainresbull.2017.03.001

Gielen, M., and Corringer, P. J. (2018). The dual-gate model for pentameric ligand-gated ion channels activation and desensitization. *J. Physiol.* 596 (10), 1873–1902. doi: 10.1113/JP275100

Harvey, R. J., Depner, U. B., Wassle, H., Ahmadi, S., Heindl, C., Reinold, H., et al. (2004). GlyR alpha3: an essential target for spinal PGE2-mediated inflammatory pain sensitization. *Science* 304 (5672), 884–887. doi: 10.1126/science.1094925

Haythornthwaite, A., Stoelzle, S., Hasler, A., Kiss, A., Mosbacher, J., George, M., et al. (2012). Characterizing human ion channels in induced pluripotent stem cell-derived neurons. *J. Biomol. Screening* 17 (9), 1264–1272. doi: 10.1177/1087057112457821

Hofmann, M., Kordas, K. S., Gravius, A., Bolcskei, K., Parsons, C. G., Dekundy, A., et al. (2012). Assessment of the effects of NS11394 and L-838417, alpha2/3 subunit-selective GABA(A) [corrected] receptor-positive allosteric modulators, in tests for pain, anxiety, memory and motor function. *Behav. Pharmacol.* 23 (8), 790–801. doi: 10.1097/FBP.0b013e32835a7c7e

Huang, X., Shaffer, P. L., Ayube, S., Bregman, H., Chen, H., Lehto, S. G., et al. (2017). Crystal structures of human glycine receptor alpha3 bound to a novel class of analgesic potentiators. *Nat. Struct. Mol. Biol.* 24 (2), 108–113. doi: 10.1038/nsmb.3329

Hwang, J. H., and Yaksh, T. L. (1997). The effect of spinal GABA receptor agonists on tactile allodynia in a surgically-induced neuropathic pain model in the rat. *Pain* 70 (1), 15–22. doi: 10.1016/S0304-3959(96)03249-6

Kaneko, M., and Hammond, D. L. (1997). Role of spinal gamma-aminobutyric acid a receptors in formalin-induced nociception in the rat. *J. Pharmacol. Exp. Ther.* 282 (2), 928–938.

Knabl, J., Witschi, R., Hosl, K., Reinold, H., Zeilhofer, U. B., Ahmadi, S., et al. (2008). Reversal of pathological pain through specific spinal GABAA receptor subtypes. *Nature* 451 (7176), 330–334. doi: 10.1038/nature06493

Labianca, R., Sarzi-Puttini, P., Zuccaro, S. M., Cherubino, P., Vellucci, R., and Fornasari, D. (2012). Adverse effects associated with non-opioid and opioid treatment in patients with chronic pain. *Clin. Drug Invest.* 32 Suppl 1, 53–63. doi: 10.2165/11630080-000000000-00000

Lemoine, D., Jiang, R., Taly, A., Chataigneau, T., Specht, A., and Grutter, T. (2012). Ligand-gated ion channels: new insights into neurological disorders and ligand recognition. *Chem. Rev.* 112 (12), 6285–6318. doi: 10.1021/cr3000829

Lewter, L. A., Fisher, J. L., Siemian, J. N., Methuku, K. R., Poe, M. M., Cook, J. M., et al. (2017). Antinociceptive effects of a novel alpha2/alpha3-subtype selective GABAA receptor positive allosteric modulator. *ACS Chem. Neurosci.* 8 (6), 1305–1312. doi: 10.1021/acschemneuro.6b00447

Li, W., Cai, J., Wang, B. H., Huang, L., Fan, J., and Wang, Y. (2018). Antinociceptive effects of novel epibatidine analogs through activation of alpha4beta2 nicotinic receptors. *Sci. China Life Sci.* 61 (6), 688–695. doi: 10.1007/s11427-017-9062-3

Liu, C., Wu, P., Zhu, H., Grieco, P., Yu, R., Gao, X., et al. (2019). Rationally designed alpha-conotoxin analogues maintained analgesia activity and weakened side effects. *Molecules* 24 (2). doi: 10.3390/molecules24020337

Lu, J., Fan, S., Zou, G., Hou, Y., Pan, T., Guo, W., et al. (2018). Involvement of glycine receptor alpha1 subunits in cannabinoid-induced analgesia. *Neuropharmacology* 133, 224–232. doi: 10.1016/j.neuropharm.2018.01.041

Lynch, J. W. (2009). Native glycine receptor subtypes and their physiological roles. *Neuropharmacology* 56 (1), 303–309. doi: 10.1016/j.neuropharm.2008.07.034

McKernan, R. M., Rosahl, T. W., Reynolds, D. S., Sur, C., Wafford, K. A., Atack, J. R., et al. (2000). Sedative but not anxiolytic properties of benzodiazepines are mediated by the GABA(A) receptor alpha1 subtype. *Nat. Neurosci.* 3 (6), 587–592. doi: 10.1038/75761

Michels, G., and Moss, S. J. (2007). GABAA receptors: properties and trafficking. *Crit. Rev. In Biochem. Mol. Biol.* 42 (1), 3–14. doi: 10.1080/10409230601146219

Miraucourt, L. S., Dallel, R., and Voisin, D. L. (2007). Glycine inhibitory dysfunction turns touch into pain through PKCgamma interneurons. *PloS One* 2 (11), e1116. doi: 10.1371/journal.pone.0001116

Mirza, N. R., Larsen, J. S., Mathiasen, C., Jacobsen, T. A., Munro, G., Erichsen, H. K., et al. (2008). NS11394 [3′-[5-(1-hydroxy-1-methyl-ethyl)-benzoimidazol-1-yl]-biphenyl-2-carbonitrile], a unique subtype-selective GABAA receptor positive allosteric modulator: *in vitro* actions, pharmacokinetic properties and *in vivo* anxiolytic efficacy. *J. Pharmacol. Exp. Ther.* 327 (3), 954–968. doi: 10.1124/jpet.108.138859

Munro, G., Lopez-Garcia, J. A., Rivera-Arconada, I., Erichsen, H. K., Nielsen, E. O., Larsen, J. S., et al. (2008). Comparison of the novel subtype-selective GABAA receptor-positive allosteric modulator NS11394 [3′-[5-(1-hydroxy-1-methyl-ethyl)-benzoimidazol-1-yl]-biphenyl-2-carbonitrile] with diazepam, zolpidem, bretazenil, and gaboxadol in rat models of inflammatory and neuropathic pain. *J. Pharmacol. Exp. Ther.* 327 (3), 969–981. doi: 10.1124/jpet.108.144568

Munro, G., Hansen, R., Erichsen, H., Timmermann, D., Christensen, J., and Hansen, H. (2012). The alpha7 nicotinic ACh receptor agonist compound B

and positive allosteric modulator PNU-120596 both alleviate inflammatory hyperalgesia and cytokine release in the rat. *Br. J. Pharmacol.* 167 (2), 421–435. doi: 10.1111/j.1476-5381.2012.02003.x

Nickolls, S., Mace, H., Fish, R., Edye, M., Gurrell, R., Ivarsson, M., et al. (2011). A comparison of the alpha2/3/5 selective positive allosteric modulators L-838,417 and TPA023 in preclinical models of inflammatory and neuropathic pain. *Adv. In Pharmacol. Sci.* 2011, 608912. doi: 10.1155/2011/608912

Nys, M., Kesters, D., and Ulens, C. (2013). Structural insights into Cys-loop receptor function and ligand recognition. *Biochem. Pharmacol.* 86 (8), 1042–1053. doi: 10.1016/j.bcp.2013.07.001

Okita, K., Ichisaka, T., and Yamanaka, S. (2007). Generation of germline-competent induced pluripotent stem cells. *Nature* 448 (7151), 313–317. doi: 10.1038/nature05934

Papke, R. L., Bagdas, D., Kulkarni, A. R., Gould, T., AlSharari, S. D., Thakur, G. A., et al. (2015). The analgesic-like properties of the alpha7 nAChR silent agonist NS6740 is associated with non-conducting conformations of the receptor. *Neuropharmacology* 91, 34–42. doi: 10.1016/j.neuropharm.2014.12.002

Ralvenius, W. T., Benke, D., Acuna, M. A., Rudolph, U., and Zeilhofer, H. U. (2015). Analgesia and unwanted benzodiazepine effects in point-mutated mice expressing only one benzodiazepine-sensitive GABAA receptor subtype. *Nat. Commun.* 6, 6803. doi: 10.1038/ncomms7803

Ralvenius, W. T., Acuna, M. A., Benke, D., Matthey, A., Daali, Y., Rudolph, U., et al. (2016). The clobazam metabolite N-desmethyl clobazam is an alpha2 preferring benzodiazepine with an improved therapeutic window for antihyperalgesia. *Neuropharmacology* 109, 366–375. doi: 10.1016/j.neuropharm.2016.07.004

Romero, H. K., Christensen, S. B., Di Cesare Mannelli, L., Gajewiak, J., Ramachandra, R., Elmslie, K. S., et al. (2017). Inhibition of alpha9alpha10 nicotinic acetylcholine receptors prevents chemotherapy-induced neuropathic pain. *Proc. Natl. Acad. Sci. U States America* 114 (10), E1825–E1832. doi: 10.1073/pnas.1621433114

Rudolph, U., Crestani, F., Benke, D., Brunig, I., Benson, J. A., Fritschy, J. M., et al. (1999). Benzodiazepine actions mediated by specific gamma-aminobutyric acid(A) receptor subtypes. *Nature* 401 (6755), 796–800. doi: 10.1038/44579

Santos, D. P., Kiskinis, E., Eggan, K., and Merkle, F. T. (2016). Comprehensive protocols for CRISPR/Cas9-based gene editing in human pluripotent stem cells. *Curr. Protoc. In Stem Cell Biol.* 38, 5B 6 1–5B 6 60. doi: 10.1002/cpsc.15

Schliessbach, J., Vuilleumier, P. H., Siegenthaler, A., Butikofer, L., Limacher, A., Juni, P., et al. (2017). Analgesic effect of clobazam in chronic low-back pain but not in experimentally induced pain. *Eur. J. Pain* 21 (8), 1336–1345. doi: 10.1002/ejp.1032

Singla, N. K., Skobieranda, F., Soergel, D. G., Salamea, M., Burt, D. A., Demitrack, M. A., et al. (2019). APOLLO-2: a randomized, placebo and active-controlled phase III study investigating oliceridine (TRV130), a G protein-biased ligand at the mu-opioid receptor, for management of moderate to severe acute pain following abdominoplasty. *Pain Practice Off. J. World Institute Pain* 19 (7), 715–731. doi: 10.1111/papr.12801

Skerratt, S. E., and West, C. W. (2015). Ion channel therapeutics for pain. *Channels* 9 (6), 344–351. doi: 10.1080/19336950.2015.1075105

Sparling, B. A., and DiMauro, E. F. (2017). Progress in the discovery of small molecule modulators of the cys-loop superfamily receptors. *Bioorg. Med. Chem. Lett.* 27 (15), 3207–3218. doi: 10.1016/j.bmcl.2017.04.073

Stanslowsky, N., Haase, A., Martin, U., Naujock, M., Leffler, A., Dengler, R., et al. (2014). Functional differentiation of midbrain neurons from human cord blood-derived induced pluripotent stem cells. *Stem Cell Res. Ther.* 5 (2), 35. doi: 10.1186/scrt423

Sudo, R. T., Hayashida, K., Santos, A. N., Kawatani, M., Monteiro, C. E., Moreira, R. D., et al. (2018). Novel agonist of alpha4beta2* neuronal nicotinic receptor with antinociceptive efficacy in rodent models of acute and chronic pain. *J. Pain Res.* 11, 2453–2462. doi: 10.2147/JPR.S169637

Taly, A., Corringer, P. J., Guedin, D., Lestage, P., and Changeux, J. P. (2009). Nicotinic receptors: allosteric transitions and therapeutic targets in the nervous system. *Nat. Rev. Drug Discovery* 8 (9), 733–750. doi: 10.1038/nrd2927

Treede, R. D., Rief, W., Barke, A., Aziz, Q., Bennett, M. I., Benoliel, R., et al. (2015). A classification of chronic pain for ICD-11. *Pain* 156 (6), 1003–1007. doi: 10.1097/j.pain.0000000000000160

Varrassi, G., Muller-Schwefe, G., Pergolizzi, J., Oronska, A., Morlion, B., Mavrocordatos, P., et al. (2010). Pharmacological treatment of chronic pain—the need for CHANGE. *Curr. Med. Res. Opin.* 26 (5), 1231–1245. doi: 10.1185/03007991003689175

Vuilleumier, P. H., Fritsche, R., Schliessbach, J., Schmitt, B., Arendt-Nielsen, L., Zeilhofer, H. U., et al. (2018). Mutations affecting glycinergic neurotransmission in hyperekplexia increase pain sensitivity. *Brain A J. Neurol.* 141 (1), 63–71. doi: 10.1093/brain/awx289

Witkin, J. M., Cerne, R., Davis, P. G., Freeman, K. B., do Carmo, J. M., Rowlett, J. K., et al. (2019). The alpha2,3-selective potentiator of GABAA receptors, KRM-II-81, reduces nociceptive-associated behaviors induced by formalin and spinal nerve ligation in rats. *Pharmacol. Biochem. Behav.* 180, 22–31. doi: 10.1016/j.pbb.2019.02.013

Xiong, W., Cui, T., Cheng, K., Yang, F., Chen, S. R., Willenbring, D., et al. (2012). Cannabinoids suppress inflammatory and neuropathic pain by targeting alpha3 glycine receptors. *J. Exp. Med.* 209 (6), 1121–1134. doi: 10.1084/jem.20120242

Yekkirala, A. S., Roberson, D. P., Bean, B. P., and Woolf, C. J. (2017). Breaking barriers to novel analgesic drug development. *Nat. Rev. Drug Discovery* 16 (8), 545–564. doi: 10.1038/nrd.2017.87

Yuan, N. Y., Poe, M. M., Witzigmann, C., Cook, J. M., Stafford, D., and Arnold, L. A. (2016). Characterization of GABAA receptor ligands with automated patch-clamp using human neurons derived from pluripotent stem cells. *J. Pharmacol. Toxicol. Methods* 82, 109–114. doi: 10.1016/j.vascn.2016.08.006

Zeilhofer, H. U., Benke, D., and Yevenes, G. E. (2012a). Chronic pain states: pharmacological strategies to restore diminished inhibitory spinal pain control. *Annu. Rev. Pharmacol. Toxicol.* 52, 111–133. doi: 10.1146/annurev-pharmtox-010611-134636

Zeilhofer, H. U., Wildner, H., and Yevenes, G. E. (2012b). Fast synaptic inhibition in spinal sensory processing and pain control. *Physiol. Rev.* 92 (1), 193–235. doi: 10.1152/physrev.00043.2010

Zeilhofer, H. U., Ralvenius, W. T., and Acuna, M. A. (2015). Restoring the spinal pain gate: GABA(A) receptors as targets for novel analgesics. *Adv. Pharmacol.* 73, 71–96. doi: 10.1016/bs.apha.2014.11.007

Zeilhofer, H. U., Acuna, M. A., Gingras, J., and Yevenes, G. E. (2018). Glycine receptors and glycine transporters: targets for novel analgesics? *Cell. Mol. Life Sci.: CMLS* 75 (3), 447–465. doi: 10.1007/s00018-017-2622-x

Conflict of Interest: The authors declare that the research was conducted in the absence of any commercial or financial relationships that could be construed as a potential conflict of interest.

frontiers in Pharmacology

ORIGINAL RESEARCH
published: 25 March 2020
doi: 10.3389/fphar.2020.00355

Noninvasive 40-Hz Light Flicker Rescues Circadian Behavior and Abnormal Lipid Metabolism Induced by Acute Ethanol Exposure *via* Improving SIRT1 and the Circadian Clock in the Liver-Brain Axis

Youli Yao[1,2], Wenjiang Zhang[2], Ruibo Ming[2], Qiyu Deng[1], Along Zuo[3], Shengli Zhang[2], Ying Ying[1], Yingying Zhao[1] and Junxian Ma[2]**

[1] Department of Physiology, School of Basic Medical Sciences, Shenzhen University Health Sciences Center, Shenzhen University, Shenzhen, China, [2] School of Information Engineering, Shenzhen University, Shenzhen, China, [3] Key Laboratory for Natural Resource of Changbai Mountain and Functional Molecules, Ministry of Education, Yanbian University, Yanji, China

OPEN ACCESS

Edited by:
Gonzalo E. Yevenes,
University of Concepcion, Chile

Reviewed by:
Tao Zeng,
Shandong University, China
Mario Rivera-Meza,
University of Chile, Chile

***Correspondence:**
Yingying Zhao
zhaoyingying@szu.edu.cn
Junxian Ma
majx@szu.edu.cn

Specialty section:
This article was submitted to Gastrointestinal and Hepatic Pharmacology, a section of the journal Frontiers in Pharmacology

Received: 09 September 2019
Accepted: 10 March 2020
Published: 25 March 2020

Citation:
Yao Y, Zhang W, Ming R, Deng Q, Zuo A, Zhang S, Ying Y, Zhao Y and Ma J (2020) Noninvasive 40-Hz Light Flicker Rescues Circadian Behavior and Abnormal Lipid Metabolism Induced by Acute Ethanol Exposure via Improving SIRT1 and the Circadian Clock in the Liver-Brain Axis. Front. Pharmacol. 11:355. doi: 10.3389/fphar.2020.00355

Sirtuin 1 (SIRT1) is a protein deacetylase with important cellular functions, as it regulates numerous processes, including the circadian rhythm in peripheral tissues. Efforts are ongoing to reveal how Sirt1 can be used to treat diseases, such as alcoholic liver disease (ALD), Alzheimer's disease, and liver fibrosis. We have recently shown that noninvasive exposure to 40-Hz light flicker activates hypothalamic SIRT1 gene expression, thereby regulating the central circadian clock. This study investigated the effects of 40-Hz light flicker in a mouse model of ALD. RNA sequencing (RNA-seq) analysis was performed to explore the potential pathways affected by 40-Hz light flicker. We found that 40-Hz light flicker significantly decreased the acute ethanol-induced increases in serum alanine aminotransferase (ALT) and serum triglyceride (TG) levels and reduced fat-droplet accumulation in mouse livers. Additionally, 40-Hz light flicker significantly suppressed ethanol-induced increases in sterol regulatory element binding protein 1 (SREBP-1) and fatty acid synthase (Fasn) levels. Furthermore, the ethanol induced significant decreases in both Sirt1 levels and phosphorylation of adenosine monophosphate-activated protein kinase subunit (AMPKα), compared with those in the control group. Strikingly, pretreatment with 40-Hz light flicker ameliorated such ethanol-induced decreases in SIRT1 levels and AMPKα phosphorylation. In addition, ethanol-induced increases in levels of brain and muscle arnt-like protein-1 (BMAL1), circadian locomotor output cycles kaput (CLOCK), and period 2 (PER2) were reversed by 40-Hz light flicker. RNA-seq analysis revealed significant differences in expression of genes related to the AMPK signalling. Moreover, ethanol consumption altered mRNA levels of Sirt1 and circadian genes in the suprachiasmatic nucleus (SCN), indicating that ethanol influenced central pacemaker

genes; however, 40-Hz light flicker reversed these ethanol-induced changes. Taken together, our findings demonstrate that 40-Hz light flicker rapidly influence the SCN and exhibits inhibitory properties on hepatic lipogenesis, indicating that 40-Hz light flicker has therapeutic potential for preventing alcoholic liver steatosis.

Keywords: 40-Hz light flicker, sirtuin 1, circadian clock, alcoholic liver steatosis, suprachiasmatic nucleus

INTRODUCTION

The number of patients with chronic liver disease has increased rapidly in recent years (Llorente et al., 2017). Chronic liver diseases, such as cirrhosis and liver cancer, are among the top causes of deaths worldwide (Kim et al., 2014). Approximately 50% of all liver-related deaths are related to alcohol (Rehm et al., 2013). Acute alcoholic liver disease (ALD) is caused by excessive intake of alcohol (Gustot and Jalan, 2019). Ethanol consumption disrupts lipid metabolism, leading to excessive accumulation of triglycerides in the liver, which aggravates damage to hepatocytes (Wang et al., 2016b). If drinking continues, acute alcoholic fatty liver will develop to hepatic fibrosis, cirrhosis, or even hepatic cancer. Unfortunately, there have been no effective treatments for ALD other than alcohol withdrawal. Therefore, discovery and development of safe and effective therapies are urgently needed.

Sirtuin 1 (SIRT1) is a histone deacetylase that modulates the activity of a number of transcription factors (Rahman and Islam, 2011). In cellular metabolism, SIRT1 couples with circadian machinery to modulate cellular activity and stability. Brain and muscle arnt-like protein-1 (BMAL1) is an important component of the circadian clock. Ethanol-diet-fed mice with liver-specific knockout of BMAL1 develop more severe liver steatosis and injury, as well as a simultaneous suppression of both *de novo* lipogenesis and fatty acid oxidation (Zhang et al., 2018a). The activation of BMAL1 regulates cyclic variation in levels of various metabolic genes that drive the metabolism of lipid, glucose, and cholesterol (Asher and Sassone-Corsi, 2015). SIRT1 promotes the deacetylation and degradation of period 2 (PER2) by binding to BMAL1: circadian locomotor output cycles kaput (CLOCK) heterodimers (Asher et al., 2008). PER2 is a member of the period family of genes and regulates daily rhythms of metabolism, locomotor activity, and other behaviors. The degradation of PER proteins prevents the formation of large protein complexes, thereby inhibiting the transcriptional activity of the BMAL1: CLOCK heterodimer (Nakahata et al., 2008).

SIRT1 relies on nicotinamide adenine dinucleotide (NAD^+) histone deacetylase to regulate energy metabolism, stress responses, aging, and maintenance of genomic integrity. Adenosine monophosphate-activated protein kinase (AMPK) is a metabolic sensor that regulates cellular energy homeostasis and interacts with SIRT1. The overexpression of SIRT1 causes serine/threonine kinase 11 (also known as liver kinase B1, LKB1) translocation from the nucleus to the cytoplasm, resulting in LKB1 activation (Lan et al., 2008). LKB1 is constitutively active and functions as an upstream kinase for Thr172 of AMPK (Alexander and Walker, 2011). Activated LKB1 then activates AMPK through phosphorylation. AMPK activates SIRT1 by transcription of nicotinamide phosphoribosyl transferase. SIRT1 inhibits transcription factor activity, thereby regulating lipid-metabolism signaling pathways. Sterol regulatory element binding protein 1 (SREBP-1) is a master transcription factor that regulates lipogenic enzymatic expression, including fatty acid synthase, acetyl-CoA carboxylase (ACC), and stearoyl-CoA desaturase-1 (Purohit et al., 2009) (You et al., 2002). Peroxisome proliferator-activated receptor-α (PPARα) is a key transcriptional regulator of lipolytic enzymes and uncoupling proteins (Mandard et al., 2004). Phosphorylation of AMPK inhibits lipogenesis and accelerates fatty acid oxidation by modulating the activities of SREBP1 and PPARα. Therefore, this study postulated that SIRT1/AMPK and BMAL1 may represent key therapeutic targets for reducing disease progression.

Cyclic variation in molecular rhythms are self-sustaining and self-generating (Nagoshi et al., 2004). However, mammalian central peripheral clocks respond to light/dark changes through diverse pathways. Among the mechanisms involved are photic inputs transduced by retinal neurons. These inputs are transmitted to the suprachiasmatic nucleus (SCN) through the retinohypothalamic tract (Takahashi, 2017). The SCN cells process these inputs and convey this information to neurocircuitry that ensure peripheral regulation of metabolic activity (Panda, 2016). Light innervation alters behavioral and metabolic outputs—including feeding patterns, energy expenditure, and corticosterone secretion—*via* changes in the expression of clock genes within ventromedial hypothalamic (VMH) neurons, as well as within liver and brown tissues (del Río-Martín et al., 2019).

Long-term clinical observations have demonstrated that bright light therapy can significantly improve mood, sleep, and daily activities in patients with Alzheimer's disease, and its application is noninvasive, affordable, and convenient (Perusini et al., 2017) (Iaccarino et al., 2016). Tsai et al. found that light therapy at a frequency of 40 Hz can inhibit the production of amyloid beta (Aβ) and activate microglia to accelerate the removal of existing Aβ (Iaccarino et al., 2016). Other studies have found that light can restore memory in a model of Alzheimer's disease. However, little is known about the efficacy of 40-Hz light flicker on circadian parameters, and it remains unclear whether 40-Hz light flicker protects the liver from acute alcoholic hepatic injury. Hence, the aim of this study was to

Abbreviations: ALD, alcoholic liver disease; ALT, alanine aminotransferase; AMPK, AMP-activated protein kinase; BMAL1, brain and muscle arnt-like protein-1; CLOCK, circadian locomotor output cycles kaput; PER, period; SCN, suprachiasmatic nuclei; SIRT1, Sirtuin 1; SREBP1, sterol regulatory element binding protein-1; TG, triglycerides.

investigate the hepatoprotective effects of 40-Hz light flicker on the regulation of lipid accumulation and circadian clocks *via* SIRT1/AMPK and BMAL1 in mice with acute alcohol exposure.

MATERIALS AND METHODS

Animals

Ten-week-old male C57BL/6 mice (22–25 g) were obtained from the Guangdong Medical Laboratory Animal Center (Guangzhou, China) (SPF, SCXK (Yue) 2018-0002, Guangzhou, China). The experiment procedures were approved by the Institutional Animal Care and Use Committee of Shenzhen University (Resolution number, 2019005). All efforts were made to reduce animal suffering. Mice were randomly divided into the following four groups (n = 10 per group): a control group, ethanol group (ETOH), 40-Hz light flicker group (40 Hz) and an ETOH plus 40-Hz light flicker group (ETOH + 40Hz). In this study, a light source device was fabricated using the following spectrum (**Figure S1A**). The four sides of the exposure boxes were wrapped with black cloth or plastic as shown in **Figure S1B**. This strategy blocked unwanted light from other sources and, hence, ensured that light was only from the LED. The LED source was placed above the box. Mice were acclimatized to the lab for 1 h. Thereafter, ETOH mice were subjected to ETOH (5 g/kg body weight) three times within 24 h, whereas control mice and 40-Hz group mice were administrated (by gavage) with an equal volume of saline. The 40-Hz group and ETOH + 40-Hz group were exposed to 40-Hz light flicker for 1 h (**Figure S1C**) at 8:00 (defined as zeitgeber time zero [ZT0]) from ZT0 to ZT1 two times within 24 h. During stimulation, mice were allowed to freely explore or rest around the exposure box. The mice were euthanized at 4 h after the last ethanol dosing. The brain, blood, and liver tissue were collected from each euthanized mouse. All animal experiments and maintenance were approved by the Laboratory Animal Ethics Committee of Shenzhen University.

Ten-week-old male C57BL/6 mice (n = 4) were used for recording. Ethovision XT is the applied video tracking software and used to record and analyze locomotor behavior. Spontaneous locomotor activity was defined as the moving distance per unit time (3 min). Mice were videotaped for 4 days as basal measurements. For the following 24 h, all mice were given ETOH (5 g/kg body weight), and they were divided into "ETOH groups" and "ETOH + 40-Hz groups" based on whether a 40-Hz light flicker treatment was given. The mice were continuously recorded for 5 days.

Antibodies and Reagents

Anti-SREBP1 (ab28481), anti-GAPDH (ab8245), anti-CLOCK (ab3517), anti-BMAL1 (ab228594), and anti-SIRT1 (ab110304) were purchased from Abcam (Cambridge, MA, USA). Antibodies against AMPKα (cs5831) and p-AMPKα (cs2535) were purchased from Cell Signaling Technology (Beverly, MA, USA). Antibodies against PER2 (AB2202) was purchased from Millipore (Billerica, MA, USA). Horseradish peroxidase (HRP)-conjugated goat anti-rabbit and goat anti-mouse antibodies were purchased from Abcam.

Serum Aminotransferase and Triglyceride Measurements

Blood samples were separated by centrifugation at 3,000 rpm for 30 min and levels of alanine aminotransferase (ALT) and triglycerides (TGs) in blood sera were measured using an Automatic Chemistry analyzer (SPOTCHEM, sp-235 4430, Japan).

Immunofluorescent Staining

Immunofluorescent staining for p-AMPKα (cs2535), SIRT1 (ab110304), SREBP1 (ab28481), CLOCK (ab3517), BMAL1 (ab228594), and PER2 (AB2202) were performed on frozen sections. Frozen sections were fixed in acetone/methanol (1:1), dried, dehydrated, and blocked with normal goat serum for 1 h to reduce nonspecific binding. The tissue sections were incubated with primary antibodies (1:200) overnight at 4°C. Subsequently, the slides were incubated with secondary antibodies (1:200) for 1 h. After counterstaining with DAPI, fluorescence was viewed and imaged *via* ultra-high resolution confocal microscopy (LSM880, CARL ZEISS, Germany).

RNA-Sequencing Analysis

Isolated RNA was subsequently used for RNA-seq analysis. cDNA library construction and sequencing were performed by the BGI-Shenzhen using the BGISEQ-500 platform. We identified differentially expressed genes (DEGs) between samples and performed clustering analysis and functional annotation. Genes with ≥ twofold change and a false discovery rate (FDR) of ≤ 0.001 were considered to be statistically significant.

Western Blot Analysis

The liver was lysed by RIPA buffer (Sigma) with the presence of protease and phosphatase inhibitors. The supernatants were collected and protein concentrations were measured by BCA Protein Assay Kit (BIO RAD). Equal amounts of protein were separated by SDS/PAGE and then transferred to PVDF membranes (GE healthcare, Freibury, Germany). The membranes were incubated with specific primary antibodies, at 4°C overnight. HRP-conjugated secondary antibodies (1:8,000) were from Abcam. Immunoreactive bands were revealed by enhanced chemiluminescence (Clarity Western ECL Subs kits, BIO RAD) and then stripped and reprobed with anti-GAPDH for the loading control. Band intensities were quantified by densitometry using Quantity One software (BIO RAD).

Quantitative Real-Time PCR

The extraction of total RNA from hepatic tissue, reverse transcription of total RNA was performed using commercial reagent kit (TaKaRa, Dalian, China). The relative gene expression was determined by real-time PCR with Power SYBR® Green PCR Master Mix (Bio-Rad, Hercules, CA, USA) on an Analytik Jena QPCR System. The relative expression of genes was analyzed by method of $2^{-\Delta\Delta Ct}$. The specific primers used for the gene expression analysis are shown in **Table 1**.

TABLE 1 | Primer sequences used for quantitative real-time PCR analysis.

Genes	Forward (5'-3')	Reverse (5'-3')
mSrebp1	5'-CTTAGCCTCTACACCAACTG-3'	5'-AGGAATACCCTCCTCATAGC-3'
mFasn	5'-ATTGTGGATGGAGGTATCAAC-3'	5'-CTGGTAGGCATTCTGTAGTG-3'
mClock	5'-TCACCACGTTCACTCAGGACA-3'	5'-AAGGATTCCCATGGAGCAA-3'
mBmal1	5'-ACAATGAGCCAGACAACG-3'	5'-TTCCCATCTATTGCGTGT-3'
mPer2	5'-CACTTGCCTCCGAAATAA-3'	5'-ACTACTGCCTCTGGACTGG-3'
mSirt1	5'-TGATTGGCACCGATCCTCG-3'	5'-CCACAGCGTCATATCATCCAG-3
mGAPDH	5'-CTTGTGCAGTGCCAGCC-3'	5'-GCCCAATACGGCCAAATCC-3'

Statistical Analyses

All data were expressed as the mean ± SD. Statistical significance was analyzed by one-way ANOVA followed by a Student's *t* test. Data were considered significant when $P < 0.05$. Calculations were performed using GraphPad Prism (GraphPad Software, San Diego, CA, USA).

RESULTS

40-Hz Light Flicker Ameliorates Ethanol-Induced Liver Injury

Serum ALT and TG levels were used to evaluate the effects of ethanol and/or 40-Hz light flicker in the liver. As shown in **Figures 1A, B** ethanol significantly increased serum ALT and TG, which were reversed by 40-Hz light flicker. Structurally, the liver tissues of control mice were reddish-brown, and their surfaces were soft, smooth, elastic, and not easily broken (**Figure 1C**). However, the liver tissues in ethanol-treated mice were yellowish, greasy, easily broken, and weak in elasticity. With 40-Hz light flicker treatment, the livers of ethanol-treated mice were reddish brown, normal in color, and elastic. Application of 40-Hz light flicker alone did not induce any significant changes compared with parameters in the control group.

Next, hematoxylin and eosin (H&E) staining was performed to assess the extent of histopathological injury (**Figure 1D**). Acute ethanol exposure resulted in massive fat vacuoles compared with those of the control group. These changes were significantly reversed by 40-Hz light flicker pretreatment. To further evaluate hepatic steatosis, liver sections were subjected to Oil-Red-O staining. Substantial fat droplets formed in the ethanol group but exposure to 40-Hz light flicker antagonized such ethanol-induced hepatic steatosis (**Figure 1E**). Unexpectedly, the lipid droplets of alone 40-Hz pretreated mouse livers were much smaller and less abundant

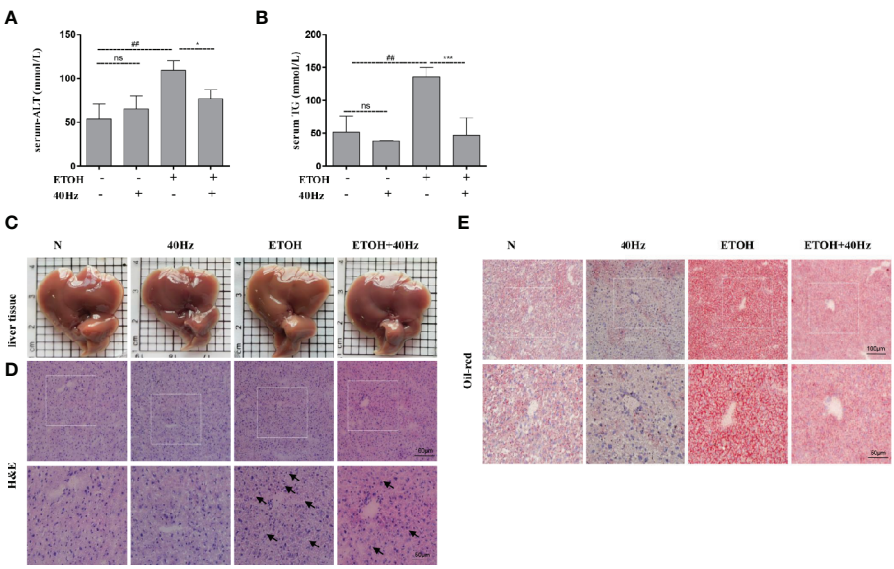

FIGURE 1 | Forty-hertz light flicker reduces the features of ethanol-induced liver injury. Serum alanine aminotransferase (ALT) **(A)** and triglyceride (TG) **(B)** contents. Each value is expressed as the mean ± SD (n = 6 in each group). Liver appearance pictures **(C)**, Hematoxylin and Eosin (H&E) **(D)** and Oil Red O staining **(E)** were performed with samples obtained at 4 h after the last ethanol administration (200 × original magnification). $^{\#\#}P < 0.01$ significantly different from normal group; $^{*}P < 0.05$, $^{***}P < 0.001$, significantly different from ethanol alone group; one-way ANOVA followed by Tukey's test. All histograms represent the mean ± SD of five independent assays. NS, nonsignificant.

(**Figure 1E**). These results reveal that 40-Hz light flicker suppressed the effects of ethanol on hepatic steatosis and lipid metabolism.

Effects of 40-Hz Light Flicker and Acute Ethanol on SIRT1 Signaling

After receiving various treatments, the mice were euthanized and their livers were harvested. We then compared liver RNA levels from the ETOH group with those of the control, 40-Hz, and ETOH + 40-Hz groups (**Figure 2A**). RNA sequencing (RNA-seq) analysis showed significant changes in 311 mRNA levels in the ethanol group compared with the ETOH + 40-Hz group **(Figure 2A)**. Kyoto Encyclopedia of Genes and Genomes (KEGG) pathway analysis identified 19 significant signaling pathways, including those involved in fat absorption/digestion, protein absorption/digestion, pancreatic secretion, and AMPK signaling **(Figures 2B, C)**.

The development of fatty liver following ethanol uptake is regulated by lipid homeostasis, a process in which SIRT1 plays a role. **Figure 3** shows that the protein expression of SIRT1 was decreased following ethanol exposure. Furthermore, 40-Hz light flicker increased SIRT1 protein and mRNA levels, especially from single 40-Hz light flicker administration, indicating that 40-Hz light flicker may act as a SIRT1 activator (**Figure 3** and **Figure S3**). AMPK participates in glucose and lipid metabolism by interacting with SIRT1. We found that ethanol exposure markedly decreased p-AMPKα levels in the liver compared with those in the control group, whereas 40-Hz light flicker promoted p-AMPKα expression relative to that in ETOH group. Similar to the Western blot results, decreases of SIRT1 and p-AMPKα levels caused by acute alcohol-induced liver injury were prevented by 40-Hz light flicker, as examined by immunofluorescence (**Figure 3B**).

40-Hz Light Flicker Prevents Ethanol-Induced Increases in SREBP-1

RNA-seq analysis revealed significant differences in Srebp1 and Fasn between mice that received 40-Hz light flicker treatment and those treated with ethanol (**Figure 4A**). It has been reported that SREBP-1 is a key driver of fatty acid synthesis. We, therefore investigated the impact of 40-Hz light flicker on SREBP-1. Alcohol promoted the expression of SERBP-1 at both mRNA and protein levels (**Figures 4B, C**). In contrast, 40-Hz light flicker significantly reversed these effects. However, treatment with only 40-Hz light flicker had no effect on SREBP-1. In addition, liver histological sections were analyzed by immunofluorescence to assess the distribution of SREBP-1 in the liver. SREBP-1 showed positive staining in liver sections from

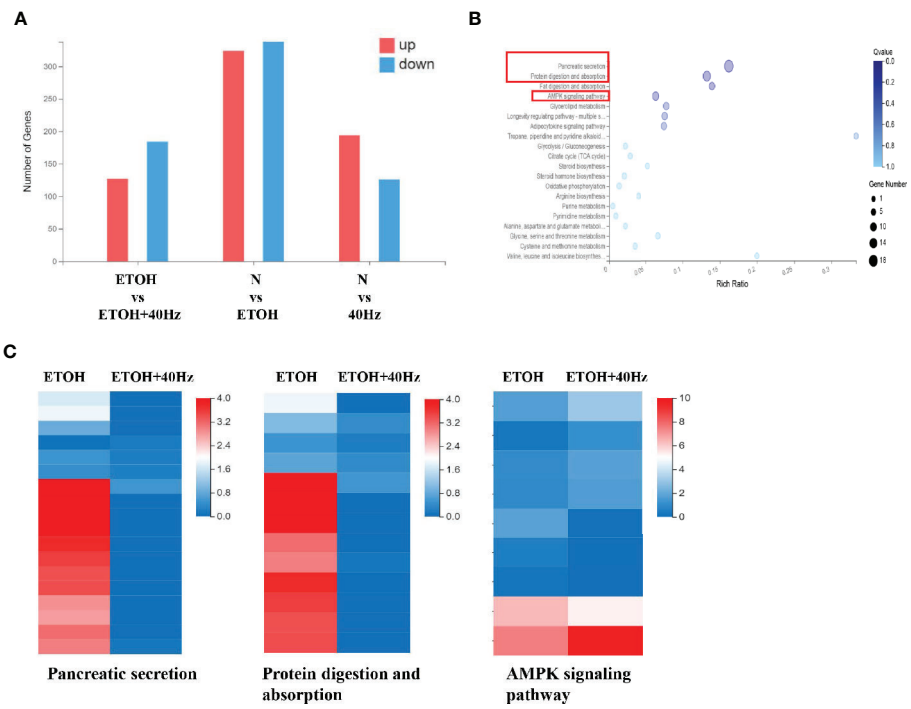

FIGURE 2 | Effects of 40-Hz light flicker and acute ethanol challenge on gene expression. **(A)** Differentially expressed genes of livers treated with ethanol and/or 40-Hz light flicker, as indicated by RNA-seq analysis (n = 3). **(B)** Gene ontology (GO) analysis of target genes, showing biological processes affected by 40-Hz light flicker treatment (n = 3). The *x*-axis is the enrichment ratio (Rich Ratio = Term Candidate Gene Num/Term Gene Num). The *y*-axis represents the GO terms. The size of each bubble indicates the number differentially expressed genes annotated to a GO Term. The color represents the enriched Q value. The darker the color, the smaller the Q value. **(C)** Heatmap of genes upregulated or downregulated from 40-Hz light flicker and/or ethanol treatment in liver tissue (n = 3). The horizontal axis is the log2 (expression value +1) of the sample, and the vertical axis represents the corresponding gene. Patches that have a redder color denote higher expression, whereas patches with bluer colors denote lower expression.

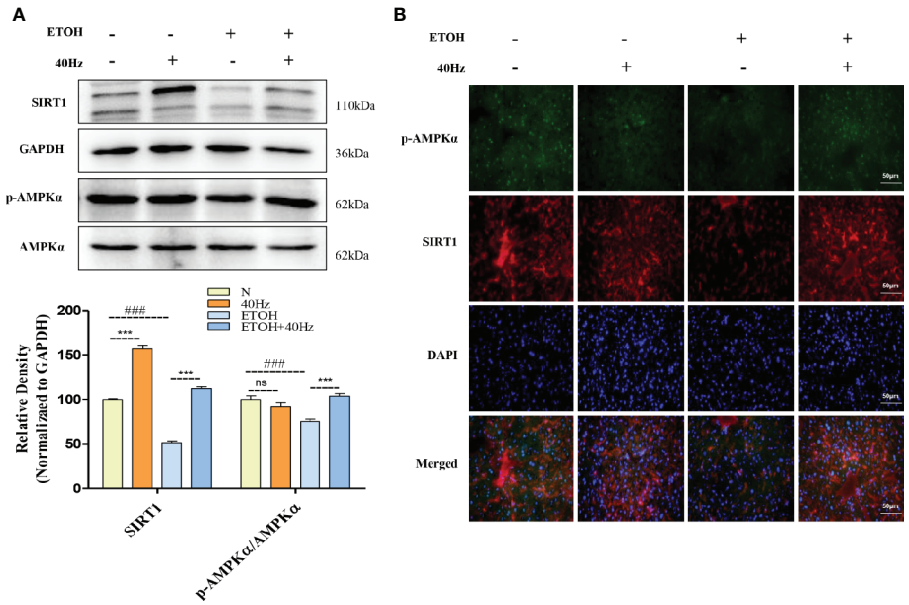

FIGURE 3 | Effects of 40-Hz light flicker and acute ethanol challenge on the Sirtuin 1(SIRT1)–adenosine monophosphate-activated protein kinase subunit (AMPKα) signalling. **(A)** Protein expression levels of SIRT1, AMPKα, and phospho-AMPKα of mice liver were determined at 4 h after the last ethanol administration by five independent Western blots. **(B)** SIRT1 (red), phospho-AMPKα staining (green) and nuclei with DAPI (blue) are shown (400× original magnification, n = 6). $^{###}P < 0.001$ significantly different from normal group; $^{***}P < 0.001$, significantly different from ethanol alone group; one-way ANOVA followed by Tukey's test.

the ethanol group (**Figure 4D**), whereas the staining was weakened by 40-Hz light-flicker treatment (**Figure 4D**). FASN plays an important role in lipogenesis by synthesizing saturated long-chain fatty acids. Therefore, we assessed whether 40-Hz light-flicker treatment was related to FASN inhibition. **Figure 4B** shows that ethanol challenge enhanced Fasn mRNA levels, but 40-Hz light flicker treatment decreased its expression of ethanol-treated mice. These results demonstrate that 40-Hz light flicker blocked lipogenesis by inhibiting SREBP-1 and FASN expression in the liver after ethanol exposure.

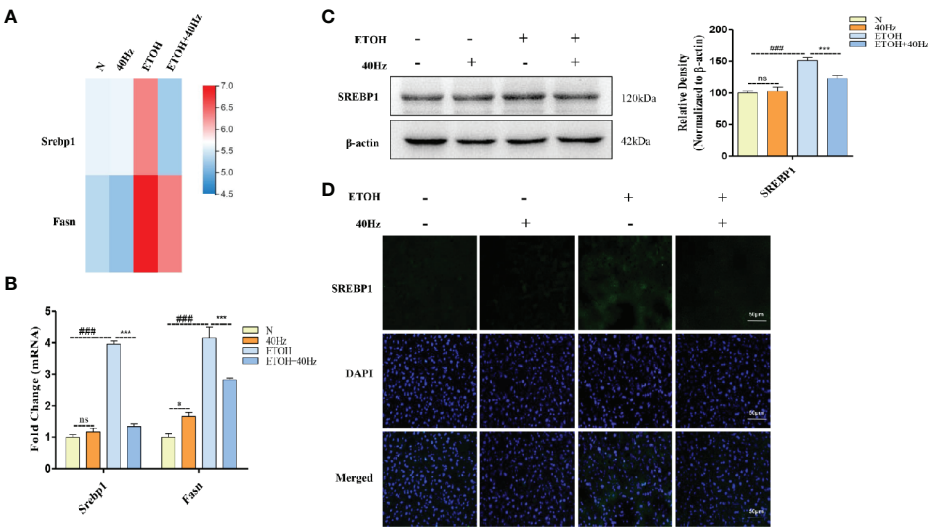

FIGURE 4 | Forty-hertz light flicker suppressed sterol regulatory element binding protein 1 (SREBP-1) activations induced by acute ethanol challenge. **(A)** Heatmap of srebp1 and fatty acid synthase (Fasn) with 40 Hz light-flickering or ethanol treatment of mice liver tissue (n = 3). **(B)** The mRNA expression of srebp1 and Fasn. **(C)** Protein expression of SREBP1 was determined by five independent Western blots. **(D)** SREBP1 staining (green) and nuclei with DAPI (blue) are shown. $^{###}P < 0.001$ significantly different from normal group; $^{*}P < 0.005$, $^{***}P < 0.001$, significantly different from ethanol alone group; one-way ANOVA followed by Tukey's test. NS, nonsignificant.

40-Hz Light Flicker Resets the Circadian Rhythm in Mice Receiving Acute Alcohol Exposure

In other experiments, we assessed patterns of spontaneous locomotor activity under control light-dark conditions (12-h light/12-h dark). Compared with that during the light period, wild-type mice were more active during the dark period, displaying occasional activity bouts during the light (**Figure 5A**); this result is consistent with the nocturnal nature of mice. Under control light-dark conditions, daily diurnal locomotion rhythms were stable. We further explored whether circadian clock patterns were altered in ethanol-treated mice. We found that ethanol-treated mice displayed activity bouts during the light and low activity during the dark (**Figure 5A**). Furthermore, 40-Hz light stimulation suppressed the activity of ethanol-treated mice during the light whereas ethanol exposure suppressed feeding frequency during the dark (**Figure 5B**). As expected, 40-Hz light stimulation increased feeding frequency of ethanol-treated mice. Despite the few striking differences compared with parameters in wild-type mice, the distribution of locomotor activity of ETOH + 40-Hz groups were similar throughout the 8-day recording period.

40-Hz Light Flicker Attenuates Ethanol-Induced Disruption of the Circadian Clock Pathway

It is well documented that ethanol alters the circadian system in the liver (Zhang et al., 2018a). To explore the molecular mechanisms of this phenomenon, RNA-seq was performed to detect changes in mRNA levels in control and ETOH mice *via* a BGISEQ-500 platform (**Figure 6A**). The RNA-seq results provided information on the genes involved in the circadian pathway (**Figure 6A**). Bmal1 and Clock mRNA levels were decreased in the ethanol group (**Figure 6A**). To further evaluate the protein expression patterns of BMAL1 and CLOCK, we performed Western blotting and immunofluorescent analyses (**Figures 6B, C**). In the ethanol group, acute ethanol administration downregulated BMAL1 and CLOCK protein levels (**Figures 6B, C**). In contrast, 40-Hz light-licker treatment significantly increased protein expressions of BMAL1 and CLOCK in comparison with those in ethanol-group mice.

It has been demonstrated that SIRT1 interacts with CLOCK/BMAL1 to promote deacetylation and degradation of PER2 in the liver (Wang et al., 2016a). Therefore, we next measured changes in PER2 expression. Acute exposure to ethanol caused a marked upregulation of liver PER2 protein levels, as determined by Western blotting and immunofluorescent assays (**Figures 6B, C**). In contrast, 40-Hz light-flicker treatment downregulated PER2 levels in comparison with those in ethanol-treated mice. Taken together, these results show that 40-Hz light flicker is sufficient to correct circadian gene disruption in the liver from ethanol-induced hepatosteatosis.

Effects of 40-Hz Light Flicker on mRNA Levels of Clock Genes in the SCN

To determine if ethanol-dependent alterations in the liver circadian clock were due to dysregulation of the central

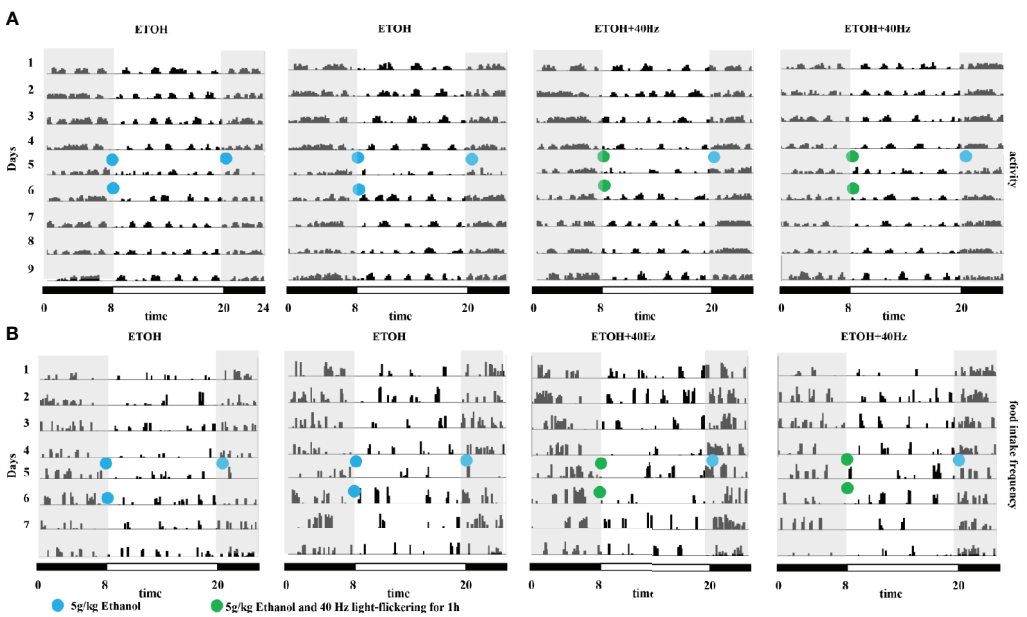

FIGURE 5 | Effects of 40-Hz light flicker on average locomotor activity and food intake in mice provided with acute alcohol exposure. **(A)** Representative average locomotor activity records. Locomotor activity was defined as the moving distance per unit time (3 min) of each group. **(B)** Representative frequencies of food intake. Food-intake frequency was defined as the number of episodes of food intake per unit time (3 min) of each group. Blue circles represent gavage of 5 g/kg of alcohol; green circles represent gavage of 5 g/kg of alcohol and 40-Hz light flicker for 1 h. Double-plotted actograms are shown; black and white bars on the bottom indicate dark and light periods, respectively. Gray shading indicates dark periods.

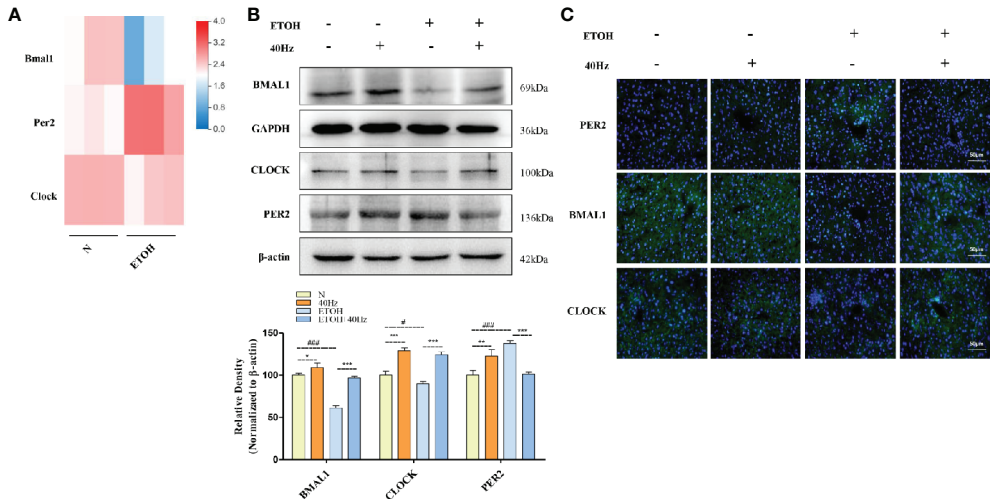

FIGURE 6 | Forty-hertz light flicker attenuates dysregulation of the circadian clock pathway in alcohol exposure mice. **(A)** Heatmap of brain and muscle arnt-like protein-1 (Bmal1), period 2 (Per2), and circadian locomotor output cycles kaput (Clock) with ethanol treatment of mice liver tissue (n=3). **(B)** Protein expression levels of PER2, BMAL1, and CLOCK of mice liver were determined at 4 h after the last 40-Hz light flicker administration by five independent Western blots. **(C)** Expression of PER2, BMAL1, and CLOCK in mouse livers were evaluated by immunofluorescence staining (400× original magnification) (n = 6). $^{\#}P < 0.05$, $^{\#\#\#}P < 0.001$ significantly different from pair-fed group; $^{*}P < 0.05$, $^{**}P < 0.01$, $^{***}P < 0.001$, significantly different from ethanol group; one-way ANOVA followed by Tukey's test.

circadian clock in the SCN, we next examined mRNA levels of Bmal1, Clock, and Per2 in SCN samples. We observed reductions in the mRNA levels of key clock regulators, including Bmal1, Clock, and Per2 in ethanol-treated mice, whereas 40-Hz light flicker treatment activated the circadian pathway by elevating these mRNA levels (**Figure 7A**). In addition, the gene expression of Sirt1 was downregulated from ethanol exposure, where this ethanol-induced inhibitory effect was ameliorated *via* 40-Hz light flicker treatment (**Figure 7B**). Immunofluorescent analysis also demonstrated a positive regulation of 40-Hz light flicker on Sirt1 in the SCN (**Figure 7C**). These results suggested that 40-Hz light flicker activated Sirt1 and corrected ethanol-induced disruption of the central circadian rhythm in SCN, suggesting that 40-Hz light flicker may reset liver clock by first affecting the function of the central pacemaker.

DISCUSSION

ALD is comprised of a broad spectrum of disorders, ranging from steatosis, alcoholic hepatitis and fibrosis, and even to hepatocellular caner. Management of ALD is currently at a limited pharmacotherapy stage (Addolorato et al., 2009). The recommended drugs by the FDA for ALD include pentoxifylline, prednisolone, disulfiram, and naltrexone (M Edwards et al., 2011) (Vuittonet et al., 2014). Despite their modest success in controlling the symptoms of ALD, the survival rate and curative effects for severe ALD cases are low. Thus, first-line therapeutic interventions include nutritional optimization and abstinence from alcohol.

In this study, we show, for the first time, that 40-Hz light flicker activates SIRT1 in the SCN to regulate central circadian control in the mouse brain to reset the liver clock and lipid metabolism. We found that 40-Hz light flicker directly activated BMAL1 transcription by SIRT1 to regulate the magnitude of SCN gene expression of BMAL1 and other circadian regulatory proteins. Our findings on the liver-protective effect induced by alteration of SIRT1 are congruent with the reported effects of SIRT1 on liver function (by SIRT1 knockout or overexpression) (Timmers et al., 2011) (Purushotham et al., 2009). Thus, our results reveal that 40-Hz light flicker is a promising therapeutic intervention for linking changes in SIRT1 expression with modulation of the circadian clock.

The pathogenesis of alcoholic fatty liver begins with the development of hepatic steatosis (Zhang et al., 2018b). Alcohol exposure can increase fat production by directly or indirectly regulating SIRT1 and disrupting fatty acid β-oxidation, thereby promoting liver fat accumulation. SIRT1 is known as a longevity gene, since it regulates the longevity effect induced by caloric restriction, and it enhances DNA-base-excision repair and produces unique metabolites (Rahman and Islam, 2011). To investigate whether and how 40-Hz light flicker may improve alcoholic fatty liver degeneration *in vivo*, we employed a mouse model of acute alcoholic steatosis *via* triple intragastric administration of ethanol to the stomach. We investigated the effects of 40-Hz light flicker on SIRT1 and p-AMPKα. Our data demonstrated that 40-Hz light flicker remarkably increased the activities of SIRT1 and p-AMPKα. AMPK regulates the balance of lipid metabolism, and the p-AMPK activation increases lipid β-oxidation (Woods et al., 2017). SIRT1 deacetylates and activates the upstream kinase of AMPK, LKB1 (Yao et al., 2017). LKB1 activates AMPK through phosphorylation. In addition, activated AMPK can activate nicotinamide phosphoribosyl transferase through transcription, which in turn activates SIRT1. SIRT1 regulates lipid homeostasis and mediates fatty acid-β oxidation

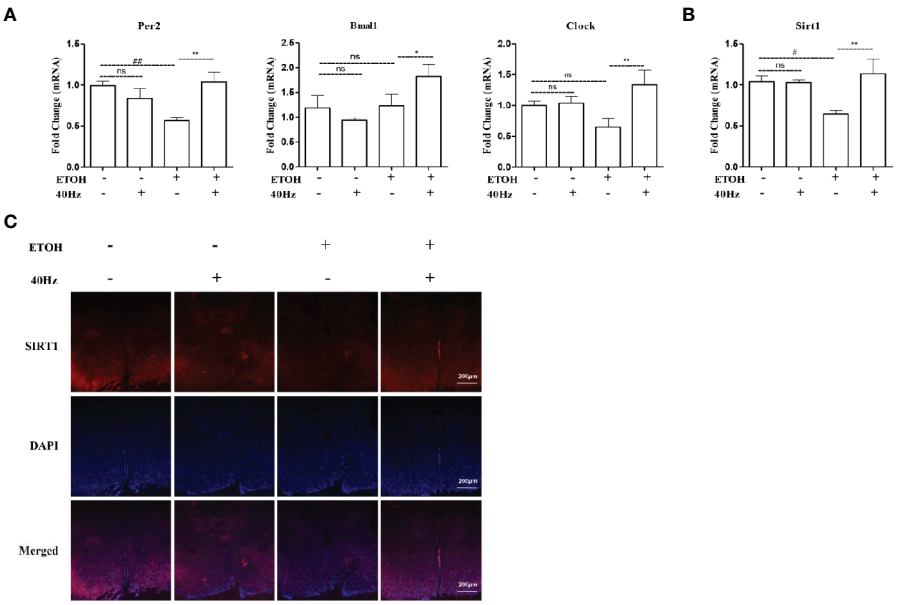

FIGURE 7 | Effects of 40-Hz light flicker on clock genes in the suprachiasmatic nucleus (SCN). **(A)** The mRNA expression of Per2, Bmal1, and Clock (n = 6). **(B)** The mRNA expression of Sirt1 (n = 6). **(C)** SIRT1 (red) and nuclei with DAPI (blue) are shown (100 × original magnification). $^{\#}P < 0.05$, $^{\#\#}P < 0.01$ significantly different from normal group; $^{*}P < 0.005$, $^{**}P < 0.01$, significantly different from ethanol alone group; one-way ANOVA followed by Tukey's test. All histograms represent the mean ± SD of five independent assays. NS, nonsignificant.

through interaction with peroxisome proliferator-activated receptor alpha (PPARα) (Sharples et al., 2015). The expression of PPARα positively correlates with the expression of SIRT1 (Avila et al., 2016). In alcohol-exposed mice, we found that 40-Hz light flicker enhanced liver SIRT1 expression; therefore, we speculate that 40-Hz light flicker also increased PPARα expression. Ethanol inhibits SIRT1, which leads to inhibition of AMPKα phosphorylation. However, AMPKα also regulates SREBP1 activity, which controls lipid synthesis. In our present study, 40-Hz light flicker suppressed SREBP1 expression and stimulated p-AMPKα in alcohol-induced steatotic livers, suggesting that 40-Hz light flicker modulated lipid metabolism by inhibiting lipid biosynthesis and promoting lipid β-oxidation.

Several processes play a role in coordinating the expression of circadian-associated genes—such as those involved in fatty acid synthesis/oxidation, glucose metabolism, mitochondrial function, and tricarboxylic acid cycle (Panda et al., 2002)—which precipitate diurnal variations in many metabolites (Eckel-Mahan et al., 2012). There are many key transcriptional regulators of lipid metabolism. These transcriptional regulators are present in both adipose and liver tissues and are controlled by the circadian clock. Peripheral circadian rhythms are critical for maintaining organ physiology and function. Research has shown that circadian rhythm disorders can lead to lipid metabolism disorders, obesity, as well as metabolic diseases. It has been shown that a high-fat diet significantly inhibits the hepatic circadian clock, even before the development of obesity (Kohsaka et al., 2007). Additionally, acute alcohol exposure disrupts the molecular clock of the liver. Activated SIRT1 is directly phosphorylated by AMPK kinase-associated cryptochrome 1 and is involved in the regulation of lipid biosynthesis. Therefore, we were intrigued whether 40-Hz light flicker regulated alcoholic liver steatosis *via* the circadian clock. As expected, ethanol decreased BMAL1 and CLOCK protein levels, which were suppressed by 40-Hz light-flicker administration and was accompanied by PER2 degradation in the liver, suggesting that 40-Hz light flicker may correct circadian gene disruption in alcoholic liver injury. SIRT1 triggers high transcription of some clock-related genes, thereby participating in the control of circadian rhythms. SIRT1 expression exhibits circadian oscillations (Asher et al., 2008) (Nakahata et al., 2008) (Nakahata et al., 2009). In this study, we focused on the inhibition of alcoholic liver injury and its possible molecular mechanisms. In particular, it is possible that 40-Hz light flicker modulates alcoholic liver injury *via* activation of SIRT1 and BMAL1. As expected, 40-Hz light flicker increased the expression levels of circadian-related proteins in the SCN. Interestingly, alcohol did not influence Per2 mRNA in the SCN as it did in the liver, indicating that further studies are needed to determine the effect of 40-Hz light flicker on PER2 protein in the SCN.

The discovery of mechanisms for protecting against ethanol-induced liver injury is an important step towards the development of effective treatments for liver fibrosis, before overt clinical symptoms develop. It was previously reported that stimulation of 40-Hz neural activity *via* noninvasive administration of 40-Hz light flicker triggered the transformation of microglia into an engulfing state and inhibited Aβ, the latter of which contributes to neurotoxicity in Alzheimer's disease (Singer et al., 2018).

In this study, 40-Hz light flicker prevented alcoholic hepatosteatosis through activating SIRT1 and resetting the circadian clock. To the best of our knowledge, this is the first report to provide evidence that 40-Hz light flicker can reprogram the circadian clock to improve alcohol-induced liver injury. RNA-seq analysis indicated significant changes in expression levels of genes related to AMPK signaling. Therefore, we speculate that 40-Hz light flicker exerts its protective effects on ethanol-induced liver injury by activating SIRT1.

In conclusion, our study demonstrates that 40-Hz light flicker modulated central circadian control in the brain by modulating the activity of SIRT1 (**Figure S2**). This effect suppressed alcohol-induced lipid accumulation in mice liver. Furthermore, 40-Hz light flicker decreased SREBP1 activation following alcohol administration, indicating that 40-Hz light flicker may be an effective therapy for alcoholic liver steatosis.

DATA AVAILABILITY STATEMENT

The raw data supporting the conclusions of this manuscript will be made available by the authors, without undue reservation, to any qualified researcher.

ETHICS STATEMENT

The animal study was reviewed and approved by the Institutional Animal Care and Use Committee of Shenzhen University.

AUTHOR CONTRIBUTION

YZ and YYa are the primary investigators in this study. RM, WZ, and QD participated in part of animal experiments. YYi, AZ and SZ participated in part of data analysis. JM and YZ designed this study and wrote the manuscript as corresponding authors. JM prepared all the light irradiation devices needed for the experiment.

ACKNOWLEDGMENT

This work was supported by the grants from the Shenzhen Science Technology and Innovation Commission (JCYJ20160427174443407), Natural Science Foundation of Guangdong Province (2016A030310037). YYa was supported by Guangdong Basic and Applied Basic Research Fund (submission sequential number: 19201910240000031). We also thank the Instrumental Analysis Center of Shenzhen University (Xili Campus) for their assistance in our experiments.

SUPPLEMENTARY MATERIAL

The Supplementary Material for this article can be found online at: https://www.frontiersin.org/articles/10.3389/fphar.2020.00355/full#supplementary-material

FIGURE S1 | Schematic of the experimental setting. (A) The following parameters of light were used during the experiment: central wavelength of 462.6 nm and a color temperature of Tc ≥ 25,000 K. (B) Diagram of sample stimulus conditions (40 Hz) and intensity of light (3 mW/cm^2). (C) Animal experimental procedures.

FIGURE S2 | A schematic representation showing the partial prevention of ethanol-induced liver lipid deposition and inflammation *via* 40-Hz light flicker.

FIGURE S3 | Effect of 40-Hz light flicker on Sirt1 mRNA. The mRNA levels of Sirt1. $^{\#}P < 0.05$ significantly different from control group; $^{*}P < 0.005$, $^{**}P < 0.01$, significantly different from ethanol-alone group; one-way ANOVA followed by Tukey's test. All of the histograms represent the mean ± SD of five independent assays.

REFERENCES

Addolorato, G., Russell, M., Albano, E., Haber, P. S., Wands, J. R., and Leggio, L. (2009). Understanding and treating patients with alcoholic cirrhosis: An update. *Alcohol. Clin. Exp. Res.* 33, 1136–1144. doi: 10.1111/j.1530-0277.2009.00956.x

Alexander, A., and Walker, C. L. (2011). The role of LKB1 and AMPK in cellular responses to stress and damage. *FEBS Lett.* 585 (7), 952–957. doi: 10.1016/j.febslet.2011.03.010

Asher, G., and Sassone-Corsi, P. (2015). Time for food: the intimate interplay between nutrition, metabolism, and the circadian clock. *Cell* 161, 84–92. doi: 10.1016/j.cell.2015.03.015

Asher, G., Gatfield, D., Stratmann, M., Reinke, H., Dibner, C., Kreppel, F., et al. (2008). SIRT1 regulates circadian clock gene expression through PER2 deacetylation. *Cell* 134, 317–328. doi: 10.1016/j.bbrc.2019.01.143

Avila, D. V., Barker, D. F., Zhang, J. W., McClain, C. J., Barve, S., and Gobejishvili, L. (2016). Dysregulation of hepatic cAMP levels via altered Pde4b expression plays a critical role in alcohol-induced steatosis. *J. Pathol.* 240 (1), 96–107. doi: 10.1002/path.4760

del Río-Martín, A., Pérez-Taboada, I., Fernández-Pérez, A., Moratalla, R., de la Villa, P., and Vallejo, M. (2019). Hypomorphic Expression of Pitx3 Disrupts Circadian Clocks and Prevents Metabolic Entrainment of Energy Expenditure. *Cell Rep.* 29 (11), 3678–3692. e4. doi: 10.1016/j.celrep.2019.11.027

Eckel-Mahan, K. L., Patel, V. R., Mohney, R. P., Vignola, K. S., Baldi, P., and Sassone-Corsi, P. (2012). Coordination of the transcriptome and metabolome by the circadian clock. *Proc. Natl. Acad. Sci.* 109, 5541–5546. doi: 10.1073/pnas.1118726109

Edwards, S., Kenna, G. A., Swift, R. M., and Leggio, L. (2011). Current and promising pharmacotherapies, and novel research target areas in the treatment of alcohol dependence: a review. *Curr. Pharm. Des.* 17, 1323–1332. doi: 10.2174/138161211796150765

Gustot, T., and Jalan, R. (2019). Acute-on-chronic liver failure in patients with alcohol-related liver disease. *J. Hepatol.* 70, 319–327. doi: 10.1016/j.jhep.2018.12.008

Iaccarino, H. F., Singer, A. C., Martorell, A. J., Rudenko, A., Gao, F., Gillingham, T. Z., et al. (2016). Gamma frequency entrainment attenuates amyloid load and modifies microglia. *Nature* 540, 230. doi: 10.1038/nature20587

Kim, Y., Ejaz, A., Tayal, A., Spolverato, G., Bridges, J. F. P., Anders, R. A., et al. (2014). Temporal trends in population-based death rates associated with chronic liver disease and liver cancer in the United States over the last 30 years. *Cancer* 120, 3058–3065. doi: 10.1002/cncr.28843

Kohsaka, A., Laposky, A. D., Ramsey, K. M., Estrada, C., Joshu, C., Kobayashi, Y., et al. (2007). High-fat diet disrupts behavioral and molecular circadian rhythms in mice. *Cell Metab.* 6, 414–421. doi: 10.1016/j.cmet.2007.09.006

Lan, F., Cacicedo, J. M., Ruderman, N., and Ido, Y. (2008). SIRT1 modulation of the acetylation status, cytosolic localization, and activity of LKB1: Possible role

in AMP-activated protein kinase activation. *J. Biol. Chem*. 283 (41), 27628–27635. doi: 10.1074/jbc.M805711200

Llorente, C., Jepsen, P., Inamine, T., Wang, L., Bluemel, S., Wang, H. J., et al. (2017). Gastric acid suppression promotes alcoholic liver disease by inducing overgrowth of intestinal Enterococcus. *Nat. Commun.* 8 (1), 1–15. doi: 10.1038/s41467-017-00796-x

Mandard, S., Müller, M., and Kersten, S. (2004). Peroxisome proliferator-activated receptor α target genes. *Cell. Mol. Life Sci.* 61 (4), 393–416. doi: 10.1007/s00018-003-3216-3

Nagoshi, E., Saini, C., Bauer, C., Laroche, T., Naef, F., and Schibler, U. (2004). Circadian gene expression in individual fibroblasts: cell-autonomous and self-sustained oscillators pass time to daughter cells. *Cell* 119, 693–705. doi: 10.1016/j.cell.2004.11.015

Nakahata, Y., Kaluzova, M., Grimaldi, B., Sahar, S., Hirayama, J., Chen, D., et al. (2008). The NAD+-dependent deacetylase SIRT1 modulates CLOCK-mediated chromatin remodeling and circadian control. *Cell* 134, 329–340. doi: 10.1016/j.cell.2008.07.002

Nakahata, Y., Sahar, S., Astarita, G., Kaluzova, M., and Sassone-Corsi, P. (2009). Circadian control of the NAD+ salvage pathway by CLOCK-SIRT1. *Sci. (80-.).* 324, 654–657. doi: 10.1126/science.1170803

Panda, S.. (2016). Circadian physiology of metabolism. *Science*. 354 (6315), 1008–1015. doi: 10.1126/science.aah4967

Panda, S., Antoch, M. P., Miller, B. H., Su, A. I., Schook, A. B., Straume, M., et al. (2002). Coordinated transcription of key pathways in the mouse by the circadian clock. *Cell* 109, 307–320. doi: 10.1016/s0092-8674(02)00722-5

Perusini, J. N., Cajigas, S. A., Cohensedgh, O., Lim, S. C., Pavlova, I. P., Donaldson, Z. R., et al. (2017). Optogenetic stimulation of dentate gyrus engrams restores memory in Alzheimer's disease mice. *Hippocampus* 27, 1110–1122. doi: 10.1002/hipo.22756

Purohit, V., Gao, B., and Song, B. J. (2009). Molecular mechanisms of alcoholic fatty liver. *Alcohol. Clin. Exp. Res.* 33 (2), 191–205. doi: 10.1111/j.1530-0277.2008.00827.x

Purushotham, A., Schug, T. T., Xu, Q., Surapureddi, S., Guo, X., and Li, X. (2009). Hepatocyte-specific deletion of SIRT1 alters fatty acid metabolism and results in hepatic steatosis and inflammation. *Cell Metab.* 9, 327–338. doi: 10.1016/j.cmet.2009.02.006

Rahman, S., and Islam, R. (2011). Mammalian Sirt1: Insights on its biological functions. *Cell Commun. Signal.* 9 (1), 11. doi: 10.1186/1478-811X-9-11

Rehm, J., Samokhvalov, A. V., and Shield, K. D. (2013). Global burden of alcoholic liver diseases. *J. Hepatol.* 59, 160–168. doi: 10.1016/j.jhep.2013.03.007

Sharples, A. P., Hughes, D. C., Deane, C. S., Saini, A., Selman, C., and Stewart, C. E. (2015). Longevity and skeletal muscle mass: The role of IGF signalling, the sirtuins, dietary restriction and protein intake. *Aging Cell.* 14 (4), 511–523. doi: 10.1111/acel.12342

Singer, A. C., Martorell, A. J., Douglas, J. M., Abdurrob, F., Attokaren, M. K., Tipton, J., et al. (2018). Noninvasive 40-Hz light flicker to recruit microglia and reduce amyloid beta load. *Nat. Protoc.* 13, 1850. doi: 10.1038/s41596-018-0021-x

Takahashi, J. S. (2017). Transcriptional architecture of the mammalian circadian clock. *Nat. Rev. Genet.* 18, 164. doi: 10.1038/nrg.2016.150

Timmers, S., Konings, E., Bilet, L., Houtkooper, R. H., van de Weijer, T., Goossens, G. H., et al. (2011). Calorie restriction-like effects of 30 days of resveratrol supplementation on energy metabolism and metabolic profile in obese humans. *Cell Metab.* 14, 612–622. doi: 10.1016/j.cmet.2011.10.002

Vuittonet, C. L., Halse, M., Leggio, L., Fricchione, S. B., Brickley, M., Haass-Koffler, C. L., et al. (2014). Pharmacotherapy for alcoholic patients with alcoholic liver disease. *Am. J. Heal. Pharm.* 71, 1265–1276. doi: 10.2146/ajhp140028

Wang, R.-H., Zhao, T., Cui, K., Hu, G., Chen, Q., Chen, W., et al. (2016a). Negative reciprocal regulation between Sirt1 and Per2 modulates the circadian clock and aging. *Sci. Rep.* 6, 28633. doi: 10.1038/srep28633

Wang, S., Pacher, P., De Lisle, R. C., Huang, H., and Ding, W. (2016b). A mechanistic review of cell death in alcohol-induced liver injury. *Alcohol. Clin. Exp. Res.* 40, 1215–1223. doi: 10.1111/acer.13078

Woods, A., Williams, J. R., Muckett, P. J., Mayer, F. V., Liljevald, M., Bohlooly-Y, M., et al. (2017). Liver-Specific Activation of AMPK Prevents Steatosis on a High-Fructose Diet. *Cell Rep.* 18 (13), 3043–3051. doi: 10.1016/j.celrep.2017.03.011

Yao, Y.-L., Han, X., Li, Z.-M., Lian, L.-H., Nan, J.-X., and Wu, Y.-L. (2017). Acanthoic Acid Can Partially Prevent Alcohol Exposure-Induced Liver Lipid Deposition and Inflammation. *Front. Pharmacol.* 8, 134. doi: 10.3389/fphar.2017.00134

You, M., Fischer, M., Deeg, M. A., and Crabb, D. W. (2002). Ethanol induces fatty acid synthesis pathways by activation of sterol regulatory element-binding protein (SREBP). *J. Biol. Chem.* 277 (32), 27635–29347. doi: 10.1074/jbc.M202411200

Zhang, D., Tong, X., Nelson, B. B., Jin, E., Sit, J., Charney, N., et al. (2018a). The hepatic BMAL1/AKT/lipogenesis axis protects against alcoholic liver disease in mice via promoting PPARα pathway. *Hepatology* 68, 883–896. doi: 10.1002/hep.29878

Zhang, Y., Jin, Q., Li, X., Jiang, M., Cui, B.-W., Xia, K.-L., et al. (2018b). Amelioration of Alcoholic Liver Steatosis by Dihydroquercetin through the Modulation of AMPK-Dependent Lipogenesis Mediated by P2X7R–NLRP3-Inflammasome Activation. *J. Agric. Food Chem.* 66, 4862–4871. doi: 10.1021/acs.jafc.8b00944

Conflict of Interest: The authors declare that the research was conducted in the absence of any commercial or financial relationships that could be construed as a potential conflict of interest.

frontiers in Pharmacology

PERSPECTIVE
published: 24 April 2020
doi: 10.3389/fphar.2020.00429

Mifepristone for Treatment of Metabolic Syndrome: Beyond Cushing's Syndrome

Francisco Díaz-Castro[1], *Matías Monsalves-Álvarez*[1,2], *Leonel E. Rojo*[3,4], *Andrea del Campo*[5] *and Rodrigo Troncoso*[1,2]*

[1] Laboratorio de Investigación en Nutrición y Actividad Física (LABINAF), Instituto de Nutrición y Tecnología en Alimentos (INTA), Universidad de Chile, Santiago, Chile, [2] Advanced Center for Chronic Diseases (ACCDIS), Universidad de Chile, Santiago, Chile, [3] Departamento de Biología, Facultad de Química y Biología, Universidad de Santiago de Chile, Santiago, Chile, [4] Centro de Biotecnología Acuícola, Universidad de Santiago de Chile, Santiago, Chile, [5] Departamento de Farmacia, Facultad de Química y de Farmacia, Pontificia Universidad Católica de Chile, Santiago, Chile

A growing body of research indicates that cortisol, the glucocorticoid product of the activation of the hypothalamic-pituitary-adrenal axis, plays a role in the pathophysiology of metabolic syndrome. In this regard, chronic exposure to cortisol is associated with risk factors related to metabolic syndrome like weight gain, type 2 diabetes, hypertension, among others. Mifepristone is the only FDA-approved drug with antiglucocorticoids properties for improved the glycemic control in patients with type 2 patients secondary to endogenous Cushing's syndrome. Mifepristone also have been shown positive effects in rodents models of diabetes and patients with obesity due to antipsychotic treatment. However, the underlying molecular mechanisms are not fully understood. In this perspective, we summarized the literature regarding the beneficial effects of mifepristone in metabolic syndrome from animal studies to clinical research. Also, we propose a potential mechanism for the beneficial effects in insulin sensitivity which involved the regulation of mitochondrial function in muscle cells.

Keywords: RU486, insulin resistance, skeletal muscle, mitochondria, glycaemia

OPEN ACCESS

Edited by:
Gonzalo E. Yevenes, University of Concepcion, Chile

Reviewed by:
Chin Moi Chow, University of Sydney, Australia
Christopher Stuart Walker, The University of Auckland, New Zealand

***Correspondence:**
Rodrigo Troncoso
rtroncoso@inta.uchile.cl

Specialty section:
This article was submitted to Translational Pharmacology, a section of the journal Frontiers in Pharmacology

Received: *29 November 2019*
Accepted: *19 March 2020*
Published: *24 April 2020*

Citation:
Díaz-Castro F, Monsalves-Álvarez M, Rojo LE, del Campo A and Troncoso R (2020) Mifepristone for Treatment of Metabolic Syndrome: Beyond Cushing's Syndrome. Front. Pharmacol. 11:429. doi: 10.3389/fphar.2020.00429

INTRODUCTION

Mifepristone, also known as RU486, was the result of the biomedical revolution forced by the wave of women´s movements in the 20th century seeking to control their reproductive life (Spitz, 2010). This drug is a synthetic hormone with antiprogestogen receptor blocker and glucocorticoid receptor (GR) antagonism activity. However, their first and most common use is as an emergency contraceptive or abortion-inducing pill during the first month of pregnancy (Rodger and Baird, 1987; Silvestre et al., 1990). Mifepristone had also demonstrated to display antiproliferative and antimetastasis effects in several cancer cell lines such as breast, endometrium, cervix, prostate, gastrointestinal tract, brain, bone, and ovary (Chen et al., 2014).

Regarding the antiglucocorticoid properties, mifepristone has three and 10 times higher relative binding affinity for the GR than dexamethasone and cortisol, respectively (Castinetti et al., 2012). In

general terms, glucocorticoids regulate numerous physiological processes that maintain the organism's homeostasis (Ramamoorthy and Cidlowski, 2013). However, chronic exposition to endogenous and exogenous glucocorticoids is associated with the appearance of several signs or diseases such as hyperglycemia, weight gain, hypertension, type 2 diabetes, muscle weakness, osteoporosis, depression, and decreased immune function (Schäcke et al., 2002). Due to the several effects caused by chronic glucocorticoids exposure, mifepristone is being investigated as a potential therapeutic drug for the treatment of psychiatric disorders such as psychotic depression, alcohol and cocaine dependence, schizophrenia, and bipolar disorder (Howland, 2013). There has also been reported one successful case of mifepristone use is the control of glycaemia in patients with Cushing's syndrome (Fleseriu et al., 2012). Due to the favorable results found in glycaemia control in these patients, the U.S. Food and Drug Administration (FDA) approved in 2012 the use of mifepristone for glycaemia control in patients with Cushing's syndrome who have developed type 2 diabetes (Korlym®). Moreover, since 1995 to date several studies in rodents and humans with metabolic syndrome had shown beneficial effects of mifepristone (see **Table 1**). Despite the accumulative evidence, little is known about the mechanisms involved in the hypoglycemic effects of mifepristone. Here, in this perspective article, we briefly summarize the available evidence on the beneficial effects of mifepristone in Cushing's syndrome and metabolic syndrome and, propose a feasible mode of action that involves the regulation of mitochondrial function, which could explain mifepristone insulin-sensitizing effects.

TABLE 1 | Mifepristone effects in model of metabolic syndrome.

Reference	Model	Mifepristone doses/via administration/treatment time	Insulin sensivity effect	Glycemic effect	Weight Changes	Other effects	Comments
Kusunoki et al., 1995	High fat diet and high starch diet (rats)	30 mg • kg-1 • day-1/In the food/25 days	↑	=	=	N/A	Mifepristone reverse the insulin resistance induced by HFD. In skeletal muscle, mifepristone produced the major effect.
Gettys et al., 1997	ob/ob mice	30 mg • kg • day/ subcutaneously injection/21 days	N/A	↓	=	N/A	Mifepristone reduce fasting glucose amd insulin levels in ob/ob mice.
Taylor et al., 2009	ob/ob mice	30 mg • kg • day/ subcutaneously injection/28 days	↑	↓	=	N/A	–
Gross et al., 2009	Olanzapine traetment (human)	600 mg • day/oral/14 days	=	=	↓	↓ Waist circumference ↓ BMI	Mifepristone reduced weight gain.
Gross et al., 2010	Risperidone traetment (human)	600 mg • day/oral/28 days	↑	N/A	↓	↓Triglycerides ↓Food consumption	Mifepristone reduced HOMA-IR.
Hashimoto et al., 2013	High fat diet (mice)	0.1 - 1.0 and 30 mg • kg • day/Orally/22 weeks	↑	↓	=	↑ adiponectin secretion ↓ Liver weight ↓ Adipocity area ↓ Aspartate aminotransferase	The higher effects were seen with a dose of 30mg • kg • day of mifepristone
Nikolic et al., 2013	MIF-KO mice	20 mg • kg • day/N/A/7 days	↑	↓	N/A	N/A	Mifepristone increased the phosphorylation induced by insulin in liver.
van den Heuvel et al., 2016	High fat fructose diet (mice)	60 mg • kg • day/in the food/4 weeks	N/A	↓	↓	↓ fat mass	Mifepristone reduced the inhibition of lipolysis by insulin
Priyadarshini and Anuradha, 2017	High fructose diet (mice)	20 mg • kg • day/oral gavage/18 days	N/A	↓	↓	↓ Liver weight ↓Viceral adipose tissue ↑ Liver triglycerides ↓ Total cholesterol ↓ Free fatty acids	Mifepristone reduced GC-target genes in liver.
Bernal-Sore et al., 2018	L6 myotubes (rat)	10 μM/24 h	↑	↓	N/A	↓Oxygen consumption ↓Intracellular ATP ↓ROS production	The RU486 increase insulin sensitivity through AMPK activation

↑ *increase;* ↓ *decrease;* = *not change; N/A not assessed.*

MIFEPRISTONE IN CUSHING'S SYNDROME

Cushing's syndrome (CS) is a condition where cortisol plasma levels are high for a long period of time, developing different signs and symptoms, such as weight gain (especially in the upper body), rounded face, insulin resistance, hypertension, osteoporosis and/or muscle weakness (Newell-Price et al., 2006). This deregulation may be produced by endogenous or exogenous factors. The less common is the endogenous CS, which is usually caused by a tumor that produces an excess of cortisol or ACTH depending on its anatomical location (adrenal or pituitary gland) (Allolio and Fassnacht, 2006). The most common cause for CS is the treatment with exogenous glucocorticoids, such as prednisone, for asthma, rheumatoid arthritis, and immunosuppression organ transplantation (Lacroix et al., 2015).

During 2011 the results from the clinical trial "A Study of the Efficacy and Safety of CORLUX (now registered as Korlym®) for the Treatment of Endogenous Cushing's Syndrome (SEISMIC)" (NCT00569582) were published. This study enrolled 50 patients for 24 weeks with endogenous CS. The results showed that subjects treated with mifepristone had improvement of physical parameters such as body weight, fat mass, waist circumference and also improvement of insulin sensitivity in 87% of patients. In subjects with diabetes mellitus or glucose intolerance, the improvement in glucose profiles was of 60% (Fleseriu et al., 2012). Before that, other works reported benefits of mifepristone use in patients with CS. In 1985, Neiman et al., treated successfully a patient with CS due to ectopic ACTH secretion. The patient improved somatic features as buffalo hump, central obesity and moon face, and sensitive glucocorticoid parameters such as fasting blood glucose (Nieman et al., 1985). Other cases of patients with CS treated with mifepristone have been summarized in a previous retrospective study. The authors concluded that treatment with mifepristone produced a reduction in signs of hypercortisolism, half-reduced blood pressure and half of the patients with diabetes improved blood glucose levels (Castinetti et al., 2010). In 2015, the follow-up and long-term extension of the SEISMIC clinical trial (NCT00936741) was published. In this report, the weight loss achieved during the treatment of 24-week in SEISMIC, persisted for two additional years in patients who remained on therapy (Fein et al., 2015). Due to the results obtained in SEISMIC, Korlym® was FDA-approved for their use in patients with type 2 diabetes or glucose intolerance secondary to endogenous CS. In addition, to the beneficial effects on glycaemia control in patients with CS, several works have reported beneficial effects of mifepristone in metabolic syndrome (see **Table 1**).

MIFEPRISTONE IN METABOLIC SYNDROME

The metabolic syndrome is a group of physiologic, biochemical and metabolic factors that lead to increased risk for type 2 diabetes, stroke and cardiovascular diseases (Eckel et al., 2005). These factors (visceral obesity, dyslipidemia, hyperglycemia and hypertension) are associated with changes in lifestyle, mainly in dietary preferences and sedentary behavior (Dalle Grave et al., 2010). Insulin resistance is a major underlying mechanism of metabolic syndrome, which affects different organs such as the brain, liver, pancreas, vascular endothelium, adipose tissue, heart and skeletal muscle, which contribute to development of metabolic syndrome (Guo, 2014). People with metabolic syndrome may have abnormal levels of cortisol, as in Cushing patients, but without developing CS (Pasquali and Vicennati, 2000). Whereby the deregulation of cortisol action could have an important role in the development of metabolic syndrome, but this is still uncertain (Paredes and Ribeiro, 2014). Mifepristone, being the only antiglucocorticoid drug clinically available, has been used to investigate this hypothesis and has promise as a potential insulin sensitizer (see **Table 1**). In 1995, Kusunoki et al. showed the first approximation in the metabolic effects of mifepristone independently of CS, where animals fed with a high-fat diet and treated with mifepristone showed an improvement in insulin sensitivity without changes in body weight (Kusunoki et al., 1995). Moreover, mifepristone enhances insulin-dependent glucose uptake, improving insulin sensitivity in obese animals (Hashimoto et al., 2013). In addition, mifepristone ameliorates diabetes symptoms in ob/ob mice (Gettys et al., 1997), improves glucose tolerance in knockout mice for the macrophage migration inhibitory factor (Nikolic et al., 2013), decreases lipid abnormalities and reduces insulin resistance in mice fed with high fructose diet (Priyadarshini and Anuradha, 2017). Moreover, mifepristone ameliorates obesity and metabolic perturbations in patients with antipsychotic medication (Gross et al., 2009; Gross et al., 2010). All of these reports pointed that mifepristone could be useful in the treatment of metabolic syndrome not associated with CS, however the mechanisms of the beneficial action of mifepristone in metabolic syndrome are far from being elucidated.

As is known, one of the most important tissues in glycemic control is the skeletal muscle, where approximately 80% of the glucose uptake is carried out and used in postprandial state (Otto Buczkowska and Dworzecki, 2003). Skeletal muscle insulin response is one of the mayor processes altered in metabolic syndrome, thus leading to high plasmatic levels of glucose and insulin resistance (Guo, 2014). In this regard, we recently reported a potential mechanism the beneficial effects of mifepristone associated with skeletal muscle physiology. We demonstrated that mifepristone increases insulin-dependent glucose uptake through a mitochondrial-AMPK pathway (Bernal-Sore et al., 2018).

MITOCHONDRIAL FUNCTION AS A TARGET OF MIFEPRISTONE

Mitochondria are known as the powerhouse of the cell by its main role in ATP production, but it is also important for other

processes, such as signaling pathways (Goldenthal and Marín-García, 2004), cell cycle regulation (Finkel and Hwang, 2009), oxidative stress (Orrenius et al., 2007), and apoptosis (Xiong et al., 2014) among others. This organelle is able to synthesize ATP through oxidative phosphorylation (OXPHOS) which uses reducing agents (NADH-$FADH_2$) from the oxidation of glucose, fatty acids, and ketone bodies on Krebs's cycle, counting for almost 90% of the energy produced by the cell (Senior, 1988).

Mitochondrial function and response to stimuli are highly dependent on their structure and dynamics. Mitochondria can modulate their morphology in response to stressors to create an elongated mitochondrial network or fragmented mitochondria depending on energy demands (Eisner et al., 2018). These changes on shape and distribution of mitochondria are known as mitochondrial dynamics and are controlled by fusion events, that depend on Mitofusins (MFN1 and MFN2), which catalyze the outer membrane fusion, and the optic atrophy 1 gene (OPA1) in charge of the inner membrane fusion, and by fission, which needs the recruitment of Dynamin-related protein 1 (DRP1), by fission 1 homolog 1 (FIS1), and mitochondrial fission factor (MFF), to the outer membrane to constrict the mitochondria and divide into two uneven daughters mitochondria (Sebastián et al., 2017).

Mitochondrial dysfunction has gained attention as an important player in the development of type 2 diabetes, obesity, dyslipidemia, and cardiovascular diseases. Excess in ROS production or nutrient supply led to a decrease of mitochondrial protein levels, changes in substrate oxidation and modifications on the shape and size of the mitochondria (Joseph et al., 2012). In addition, changes on the expression of mitochondrial dynamics related proteins in type 2 diabetes have been reported, particularly a downregulation of MFN2 and an increase on DRP1, favoring mitochondrial fission (Joseph et al., 2012).

Our recent research demonstrated that mifepristone enhances insulin-stimulated glucose uptake on L6 skeletal muscle cells through a mechanism that reduces oxygen consumption, ROS levels and ATP production, promoting AMPK activation (Bernal-Sore et al., 2018). The activation of AMPK, subsequent to the decrease of ATP production, has been previously documented as a possible mechanism of several compounds that promote insulin sensitivity (Smith and Steinberg, 2017). These compounds include berberine, a herb-derived drug widely used in China for the treatment of type 2 diabetes (Yin et al., 2008), metformin which inhibits the respiratory chain complex I (Brunmair et al., 2004; Martineau, 2012) and resveratrol, which inhibits the mitochondrial ATP synthase (Zang et al., 2006). In the case of mifepristone, the mechanism associated with the regulation of mitochondrial function is not yet elucidated.

To gain insight into how mifepristone affects mitochondrial function, we evaluated the changes in mitochondrial morphology. To assess this, we incubated L6 myoblast with Mitotracker Orange after incubation with mifepristone 10 µm for 6 and 24 h and fixed with PFA 4% to subsequently mount them in a coverslip. Confocal images stack of the mitochondrial network were captured with a Nikon C2 Confocal microscope. The number and volume of individual mitochondria were quantified using ImageJ software (NIH) as described previously (del Campo et al., 2014). Our results show that mifepristone induces an increase in the number and a decrease in the volume of mitochondria at 6 and 24 h of treatment when compared to control cells, which determine a fragmented phenotype (**Figure 1A**). Then, we evaluate the protein levels of MFN2 and DRP1. Our results show that mifepristone induces a non-statistical increase in DRP1 without changes in MFN2 protein levels, which could be associate with an increase in mitochondrial fragmentation (**Figure 1B**) (Sebastián et al., 2017). These results suggest that mifepristone regulates mitochondrial

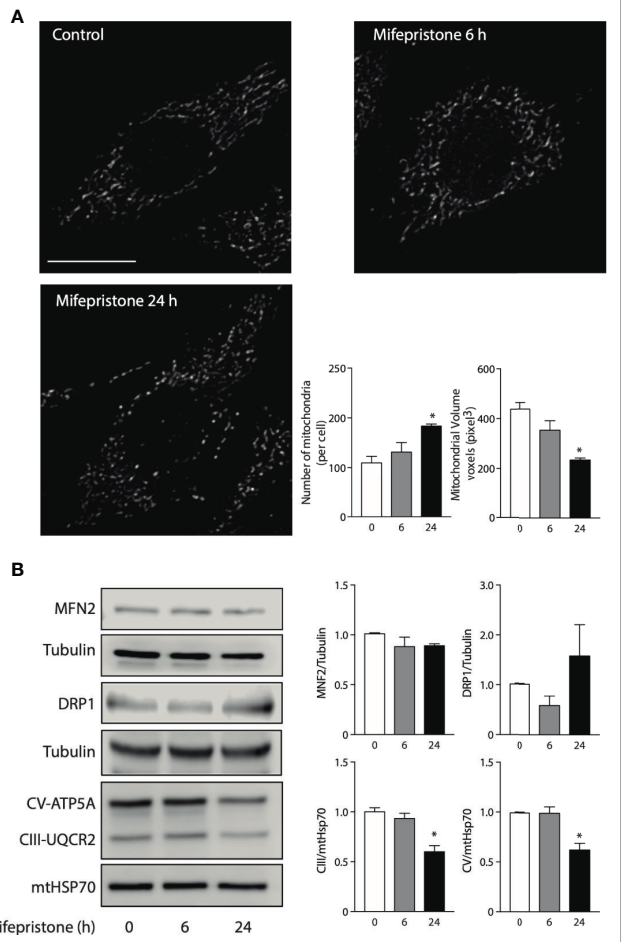

FIGURE 1 | Mifepristone targets mitochondria. **(A)** Time course of mifepristone on mitochondrial morphology. Cells were incubated with mifepristone (10 uM) at indicated times and then loaded with MitoTracker Orange. Multislice imaging reconstitution was obtained by confocal microscopy. The scale bar is 10 µm. The individual mitochondrial volume and number of mitochondria per cell were determined. **(B)** Left panel: Representative immunoblot of the effect of mifepristone treatment in MNF2, DRP1, CV-ATP5A, CIII-UQCR2, mtHSP70, and tubulin protein levels; Right panel: Densitometry analysis. (mean ± SEM; n 4). *$p < 0.05$ versus control.

morphology toward a fragmented state, which correlates with the decrease in mitochondrial function that we previously reported (Bernal-Sore et al., 2018). Fusion and fission processes are part of the mitochondria life cycle, which allow the mitochondria to respond to cell stressors adapting ATP production efficiency (Liesa and Shirihai, 2013). To further elucidate whether changes in mitochondrial morphology correlate with mitochondrial function, we examined the modification in OXPHOS proteins levels. Our results show that mifepristone reduces the protein levels of mitochondrial respiratory chain complexes III and V (**Figure 1B**). Thus, it is possible that mifepristone-induced OXPHOS reduction leads to fragmentation of the mitochondrial network due to a compensatory effect triggered by the reduction in ATP levels and an increase in AMPK activity (Toyama et al., 2016). However, how mifepristone is affecting mitochondria is still unknown, the aforementioned results point this could be through a direct effect on mitochondria, just as metformin or resveratrol, without discarding the effects of its antagonist activity over the GR. Regarding the latter, it is known that glucocorticoids regulate mitochondrial RNA synthesis (Mansour and Nass, 1970). Moreover, GR localized inside the mitochondria can regulate OXPHOS by binding to mitochondrial DNA and activating mitochondrial gene expression in HepG2 cells (Psarra and Sekeris, 2011). The above, open the possibility that mifepristone may regulate mitochondrial function through the control of mitochondrial gene expression.

CONCLUDING REMARKS

The beneficial effects of mifepristone in the control of glycaemia in patients with CS had been proven. In addition, several clinical and basic research works have reported its potential use as an insulin sensitizer in different models of metabolic syndrome (**Table 1**). However, the mechanisms of these beneficial effects are not completely elucidated. Here, we propose a new perspective to explore the mechanism of mifepristone-induced insulin sensitization based on the regulation of OXPHOS and mitochondrial dynamics, which could explain the reduction in ATP levels and the activation of AMPK. In this regard, mifepristone improves glycemic control through the regulation of mitochondrial function in skeletal muscle, but its feasible to propose that mifepristone also could control insulin resistance in other organs. Moreover, in patients with CS mifepristone decreases body weight, fasting glucose and blood pressure which suggests that other tissues, like brain, liver and endothelium could be involved in the beneficial effects of mifepristone (Fleseriu et al., 2012). It is important to note, that the consequences of mifepristone in glycemic control are similar to approved drug for diabetes such as pioglitazone and metformin, which mechanism of action also is related in regulation of AMPK activity and mitochondrial function, but mifepristone may have a subtly different mechanism of action or side-effects profile that could be helpful in pool of patients with different base pathology, risk factors or response to treatment.

Nonetheless, the first use of mifepristone was as a contraceptive drug. Therefore, the use of this drug should be restricted in some populations, including pregnant women and women who wish to get pregnant. Mifepristone's other potential side-effects should also be considered. Furthermore, effects in fertility and endocrine system after a short and long-term treatment should be studied to determine the potential patients of this drug and thus be able to determine the potential advantages of mifepristone or mifepristone-derived drugs over currently available treatments for metabolic disorders.

DATA AVAILABILITY STATEMENT

The datasets generated for this study are available on request to the corresponding author.

AUTHOR CONTRIBUTIONS

FD-C performed experiments, data analysis, and contributed to the manuscript writing. MM -Á performed experiments and data analysis. LR and AC designed experiments and contributed to the manuscript writing. RT outlined the manuscript, overviewed the experiments, analyzed data, and wrote the manuscript.

ACKNOWLEDGMENTS

This work was supported by grants from Enlace FONDECYT-VID: EN29/18 to RT, FONDECYT 1191078 to RT and 11190756 to AC, and FONDAP 15130011 to RT.

REFERENCES

Allolio, B., and Fassnacht, M. (2006). Clinical review: Adrenocortical carcinoma: clinical update. *J. Clin. Endocrinol. Metab.* 91, 2027–2037. doi: 10.1210/jc.2005-2639

Bernal-Sore, I., Navarro-Marquez, M., Osorio-Fuentealba, C., Díaz-Castro, F., Del Campo, A., Donoso-Barraza, C., et al. (2018). Mifepristone enhances insulin-stimulated Akt phosphorylation and glucose uptake in skeletal muscle cells. *Mol. Cell Endocrinol.* 461, 277–283. doi: 10.1016/j.mce.2017.09.028

Brunmair, B., Staniek, K., Gras, F., Scharf, N., Althaym, A., Clara, R., et al. (2004). Thiazolidinediones, like metformin, inhibit respiratory complex I: a common mechanism contributing to their antidiabetic actions? *Diabetes* 53, 1052–1059. doi: 10.2337/diabetes.53.4.1052

Castinetti, F., Conte-Devolx, B., and Brue, T. (2010). Medical treatment of Cushing's syndrome: glucocorticoid receptor antagonists and mifepristone. *Neuroendocrinology* 92 Suppl 1, 125–130. doi: 10.1159/000314224

Castinetti, F., Brue, T., and Conte-Devolx, B. (2012). The use of the glucocorticoid receptor antagonist mifepristone in Cushing's syndrome. *Curr. Opin. Endocrinol. Diabetes Obes.* 19, 295–299. doi: 10.1097/MED.0b013e32835430bf

Chen, J., Wang, J., Shao, J., Gao, Y., Xu, J., Yu, S., et al. (2014). The unique pharmacological characteristics of mifepristone (RU486): from terminating

pregnancy to preventing cancer metastasis. *Med. Res. Rev.* 34, 979–1000. doi: 10.1002/med.21311

Dalle Grave, R., Calugi, S., Centis, E., Marzocchi, R., El Ghoch, M., and Marchesini, G. (2010). Lifestyle modification in the management of the metabolic syndrome: achievements and challenges. *Diabetes Metab. Syndr. Obes.* 3, 373–385. doi: 10.2147/DMSOTT.S13860

del Campo, A., Parra, V., Vásquez-Trincado, C., Gutiérrez, T., Morales, P. E., López-Crisosto, C., et al. (2014). Mitochondrial fragmentation impairs insulin-dependent glucose uptake by modulating Akt activity through mitochondrial Ca2+ uptake. *Am. J. Physiol. Endocrinol. Metab.* 306, E1–E13. doi: 10.1152/ajpendo.00146.2013

Eckel, R. H., Grundy, S. M., and Zimmet, P. Z. (2005). The metabolic syndrome. *Lancet* 365, 1415–1428. doi: 10.1016/S0140-6736(05)66378-7

Eisner, V., Picard, M., and Hajnóczky, G. (2018). Mitochondrial dynamics in adaptive and maladaptive cellular stress responses. *Nat. Cell Biol.* 20, 755–765. doi: 10.1038/s41556-018-0133-0

Fein, H. G., Vaughan, T. B., Kushner, H., Cram, D., and Nguyen, D. (2015). Sustained weight loss in patients treated with mifepristone for Cushing's syndrome: a follow-up analysis of the SEISMIC study and long-term extension. *BMC Endocr. Disord.* 15, 63. doi: 10.1186/s12902-015-0059-5

Finkel, T., and Hwang, P. M. (2009). The Krebs cycle meets the cell cycle: mitochondria and the G1-S transition. *Proc. Natl. Acad. Sci. U.S.A.* 106, 11825–11826. doi: 10.1073/pnas.0906430106

Fleseriu, M., Biller, B. M. K., Findling, J. W., Molitch, M. E., Schteingart, D. E., Gross, C., et al. (2012). Mifepristone, a glucocorticoid receptor antagonist, produces clinical and metabolic benefits in patients with Cushing's syndrome. *J. Clin. Endocrinol. Metab.* 97, 2039–2049. doi: 10.1210/jc.2011-3350

Gettys, T. W., Watson, P. M., Taylor, I. L., and Collins, S. (1997). RU-486 (Mifepristone) ameliorates diabetes but does not correct deficient beta-adrenergic signalling in adipocytes from mature C57BL/6J-ob/ob mice. *Int. J. Obes. Relat. Metab. Disord.* 21, 865–873. doi: 10.1038/sj.ijo.0800479

Goldenthal, M. J., and Marín-García, J. (2004). Mitochondrial signaling pathways: a receiver/integrator organelle. *Mol. Cell Biochem.* 262, 1–16. doi: 10.1023/b:mcbi.0000038228.85494.3b

Gross, C., Blasey, C. M., Roe, R. L., Allen, K., Block, T. S., and Belanoff, J. K. (2009). Mifepristone treatment of olanzapine-induced weight gain in healthy men. *Adv. Ther.* 26, 959–969. doi: 10.1007/s12325-009-0070-1

Gross, C., Blasey, C. M., Roe, R. L., and Belanoff, J. K. (2010). Mifepristone reduces weight gain and improves metabolic abnormalities associated with risperidone treatment in normal men. *Obes. (Silver Spring)* 18, 2295–2300. doi: 10.1038/oby.2010.51

Guo, S. (2014). Insulin signaling, resistance, and the metabolic syndrome: insights from mouse models into disease mechanisms. *J. Endocrinol.* 220, T1–T23. doi: 10.1530/JOE-13-0327

Hashimoto, T., Igarashi, J., Hasan, A. U., Ohmori, K., Kohno, M., Nagai, Y., et al. (2013). Mifepristone promotes adiponectin production and improves insulin sensitivity in a mouse model of diet-induced-obesity. *PloS One* 8, e79724. doi: 10.1371/journal.pone.0079724

Howland, R. H. (2013). Mifepristone as a therapeutic agent in psychiatry. *J. Psychosoc. Nurs. Ment. Health Serv.* 51, 11–14. doi: 10.3928/02793695-20130513-01

Joseph, A.-M., Joanisse, D. R., Baillot, R. G., and Hood, D. A. (2012). Mitochondrial dysregulation in the pathogenesis of diabetes: potential for mitochondrial biogenesis-mediated interventions. *Exp. Diabetes Res.* 2012, 642038. doi: 10.1155/2012/642038

Kusunoki, M., Cooney, G. J., Hara, T., and Storlien, L. H. (1995). Amelioration of high-fat feeding-induced insulin resistance in skeletal muscle with the antiglucocorticoid RU486. *Diabetes* 44, 718–720. doi: 10.2337/diab.44.6.718

Lacroix, A., Feelders, R. A., Stratakis, C. A., and Nieman, L. K. (2015). Cushing's syndrome. *Lancet* 386, 913–927. doi: 10.1016/S0140-6736(14)61375-1

Liesa, M., and Shirihai, O. S. (2013). Mitochondrial dynamics in the regulation of nutrient utilization and energy expenditure. *Cell Metab.* 17, 491–506. doi: 10.1016/j.cmet.2013.03.002

Mansour, A. M., and Nass, S. (1970). In vivo cortisol action on RNA synthesis in rat liver nuclei and mitochondria. *Nature* 228, 665–667. doi: 10.1038/228665a0

Martineau, L. C. (2012). Large enhancement of skeletal muscle cell glucose uptake and suppression of hepatocyte glucose-6-phosphatase activity by weak uncouplers of oxidative phosphorylation. *Biochim. Biophys. Acta* 1820, 133–150. doi: 10.1016/j.bbagen.2011.11.012

Newell-Price, J., Bertagna, X., Grossman, A. B., and Nieman, L. K. (2006). Cushing's syndrome. *Lancet* 367, 1605–1617. doi: 10.1016/S0140-6736(06)68699-6

Nieman, L. K., Chrousos, G. P., Kellner, C., Spitz, I. M., Nisula, B. C., Cutler, G. B., et al. (1985). Successful treatment of Cushing's syndrome with the glucocorticoid antagonist RU 486. *J. Clin. Endocrinol. Metab.* 61, 536–540. doi: 10.1210/jcem-61-3-536

Nikolic, I., Vujicic, M., Saksida, T., Berki, T., Stosic-Grujicic, S., and Stojanovic, I. (2013). The role of endogenous glucocorticoids in glucose metabolism and immune status of MIF-deficient mice. *Eur. J. Pharmacol.* 714, 498–506. doi: 10.1016/j.ejphar.2013.06.037

Orrenius, S., Gogvadze, V., and Zhivotovsky, B. (2007). Mitochondrial oxidative stress: implications for cell death. *Annu. Rev. Pharmacol. Toxicol.* 47, 143–183. doi: 10.1146/annurev.pharmtox.47.120505.105122

Otto Buczkowska, E., and Dworzecki, T. (2003). [The role of skeletal muscle in the regulation of glucose homeostasis]. *Endokrynol. Diabetol. Chor. Przemiany Mater. Wieku Rozw* 9, 93–97. doi: 10.1002/iub.1293

Paredes, S., and Ribeiro, L. (2014). Cortisol: the villain in metabolic syndrome? *Rev. Assoc. Med. Bras (1992)* 60, 84–92. doi: 10.1590/1806-9282.60.01.017

Pasquali, R., and Vicennati, V. (2000). The abdominal obesity phenotype and insulin resistance are associated with abnormalities of the hypothalamic-pituitary-adrenal axis in humans. *Horm. Metab. Res.* 32, 521–525. doi: 10.1055/s-2007-978680

Priyadarshini, E., and Anuradha, C. V. (2017). Glucocorticoid Antagonism Reduces Insulin Resistance and Associated Lipid Abnormalities in High-Fructose-Fed Mice. *Can. J. Diabetes* 41, 41–51. doi: 10.1016/j.jcjd.2016.06.003

Psarra, A.-M. G., and Sekeris, C. E. (2011). Glucocorticoids induce mitochondrial gene transcription in HepG2 cells: role of the mitochondrial glucocorticoid receptor. *Biochim. Biophys. Acta* 1813, 1814–1821. doi: 10.1016/j.bbamcr.2011.05.014

Ramamoorthy, S., and Cidlowski, J. A. (2013). "Exploring the Molecular Mechanisms of Glucocorticoid Receptor Action from Sensitivity to Resistance," in *Endocrine Development*. Eds. M. Maghnie, S. Loche, M. Cappa, L. Ghizzoni and R. Lorini (Basel: S. KARGER AG), 41–56. doi: 10.1159/000342502

Rodger, M. W., and Baird, D. T. (1987). Induction of therapeutic abortion in early pregnancy with mifepristone in combination with prostaglandin pessary. *Lancet* 2, 1415–1418. doi: 10.1016/s0140-6736(87)91126-3

Schäcke, H., Döcke, W. D., and Asadullah, K. (2002). Mechanisms involved in the side effects of glucocorticoids. *Pharmacol. Ther.* 96, 23–43. doi: 10.1016/s0163-7258(02)00297-8

Sebastián, D., Palacín, M., and Zorzano, A. (2017). Mitochondrial Dynamics: Coupling Mitochondrial Fitness with Healthy Aging. *Trends Mol. Med.* 23, 201–215. doi: 10.1016/j.molmed.2017.01.003

Senior, A. E. (1988). ATP synthesis by oxidative phosphorylation. *Physiol. Rev.* 68, 177–231. doi: 10.1152/physrev.1988.68.1.177

Silvestre, L., Dubois, C., Renault, M., Rezvani, Y., Baulieu, E. E., and Ulmann, A. (1990). Voluntary interruption of pregnancy with mifepristone (RU 486) and a prostaglandin analogue. A large-scale French experience. *N. Engl. J. Med.* 322, 645–648. doi: 10.1056/NEJM199003083221001

Smith, B. K., and Steinberg, G. R. (2017). AMP-activated protein kinase, fatty acid metabolism, and insulin sensitivity. *Curr. Opin. Clin. Nutr. Metab. Care* 20, 248–253. doi: 10.1097/MCO.0000000000000380

Spitz, I. M. (2010). Mifepristone: where do we come from and where are we going? Clinical development over a quarter of a century. *Contraception* 82, 442–452. doi: 10.1016/j.contraception.2009.12.012

Taylor, A. I., Frizzell, N., McKillop, A. M., Flatt, P. R., and Gault, V. A. (2009). Effect of RU486 on hepatic and adipocyte gene expression improves diabetes control in obesity-type 2 diabetes. *Hom. Metab. Res. Hom. Stoffwechselforschung Hom. Metab.* 41, 899–904. doi: 10.1055/s-0029-1234071

Toyama, E. Q., Herzig, S., Courchet, J., Lewis, T. L., Losón, O. C., Hellberg, K., et al. (2016). Metabolism. AMP-activated protein kinase mediates mitochondrial fission in response to energy stress. *Science* 351, 275–281. doi: 10.1126/science.aab4138

van den Heuve, J. K., Boon, M. R., van Hengel, I., Peschier-van der Put, E., van Beek, L., van Harmelen, V., et al (2016). Identification of a selective

glucocorticoid receptor modulator that prevents both diet-induced obesity and inflammation. *Br. J. Pharmacol.* 173, 1793–1804. doi: 10.1111/bph.13477

Xiong, S., Mu, T., Wang, G., and Jiang, X. (2014). Mitochondria-mediated apoptosis in mammals. *Protein Cell* 5, 737–749. doi: 10.1007/s13238-014-0089-1

Yin, J., Gao, Z., Liu, D., Liu, Z., and Ye, J. (2008). Berberine improves glucose metabolism through induction of glycolysis. *Am. J. Physiol. Endocrinol. Metab.* 294, E148–E156. doi: 10.1152/ajpendo.00211.2007

Zang, M., Xu, S., Maitland-Toolan, K. A., Zuccollo, A., Hou, X., Jiang, B., et al. (2006). Polyphenols stimulate AMP-activated protein kinase, lower lipids, and inhibit accelerated atherosclerosis in diabetic LDL receptor-deficient mice. *Diabetes* 55, 2180–2191. doi: 10.2337/db05-1188

Conflict of Interest: The authors declare that the research was conducted in the absence of any commercial or financial relationships that could be construed as a potential conflict of interest.

frontiers in Pharmacology

MINI REVIEW
published: 08 May 2020
doi: 10.3389/fphar.2020.00655

New Pharmacological Strategies for the Treatment of Non-Infectious Uveitis. A Minireview

Rodrigo A. Valenzuela[1,2†], Iván Flores[1†], Beatriz Urrutia[3], Francisca Fuentes[1], Pablo E. Sabat[4,5], Carolina Llanos[6], Loreto Cuitino[1,7] and Cristhian A. Urzua[1,4,8*]*

[1] Laboratory of Ocular and Systemic Autoimmune Diseases, Faculty of Medicine, University of Chile, Santiago, Chile, [2] Department of Chemical and Biological Sciences, Faculty of Health, Universidad Bernardo O Higgins, Santiago, Chile, [3] Rheumatology Service, Department of Medicine, Hospital Clinico Universidad de Chile, Santiago, Chile, [4] Department of Ophthalmology, University of Chile, Santiago, Chile, [5] Department of Ophthalmology, Clínica las Condes, Santiago, Chile, [6] Departamento de Inmunología Clínica y Reumatología, Escuela de Medicina, Pontificia Universidad Católica de Chile, Santiago, Chile, [7] Servicio de Oftalmología, Hospital Clínico Universidad de Chile, Santiago, Chile, [8] Faculty of Medicine, Clinica Alemana-Universidad del Desarrollo, Santiago, Chile

OPEN ACCESS

Edited by:
Roberto Paganelli,
Università degli Studi G. d'Annunzio Chieti e Pescara, Italy

Reviewed by:
Karthik Babu Mallilankaraman, National University of Singapore, Singapore
Sudheer Kumar Ravuri, Steadman Philippon Research Institute, United States

***Correspondence:**
Loreto Cuitino
cuitinole@gmail.com
Cristhian A. Urzua
cristhian.urzua@uchile.cl

[†]These authors have contributed equally to this work

Specialty section:
This article was submitted to Translational Pharmacology, a section of the journal Frontiers in Pharmacology

Received: 04 December 2019
Accepted: 22 April 2020
Published: 08 May 2020

Citation:
Valenzuela RA, Flores I, Urrutia B, Fuentes F, Sabat PE, Llanos C, Cuitino L and Urzua CA (2020) New Pharmacological Strategies for the Treatment of Non-Infectious Uveitis. A Minireview. Front. Pharmacol. 11:655. doi: 10.3389/fphar.2020.00655

Non-infectious uveitis (NIU) is a group of disorders characterized by intraocular inflammation at different levels of the eye. NIU is a leading cause of irreversible blindness in working-age population in the developed world. The goal of uveitis treatment is to control inflammation, prevent recurrences, and preserve vision, as well as minimize the adverse effects of medications. Currently, the standard of care for NIU includes the administration of corticosteroids (CS) as first-line agents, but in some cases a more aggressive therapy is required. This includes synthetic immunosuppressants, such as antimetabolites (methotrexate, mycophenolate mofetil, and azathioprine), calcineurinic inhibitors (cyclosporine, tacrolimus), and alkylating agents (cyclophosphamide, chlorambucil). In those patients who become intolerant or refractory to CS and conventional immunosuppressive treatment, biologic agents have arisen as an effective therapy. Among the most evaluated treatments, TNF-α inhibitors, IL blockers, and anti-CD20 therapy have emerged. In this regard, anti-TNF agents (infliximab and adalimumab) have shown the strongest results in terms of favorable outcomes. In this review, we discuss latest evidence concerning to the effectiveness of biologic therapy, and present new therapeutic approaches directed against immune components as potential novel therapies for NIU.

Keywords: uveitis, intraocular inflammation, biologics, anti-tumor necrosis factor, treatment

INTRODUCTION

Uveitis included a group of heterogeneous diseases characterized by inflammation of the uveal tract. It is an important cause of vision loss accounting for approximately 25% of total blindness in developed countries, particularly among the working-age population (Thorne et al., 2016). Uveitis may be generally classified by the etiology of inflammation as infectious or non-infectious (autoimmune disorders), which could be related or not to a systemic disease. If after a

comprehensive investigation there is no a clear cause of inflammation, it is considered as idiopathic (Nussenblatt, 1990). The differential diagnosis for autoimmune uveitis includes systemic inflammatory diseases—such as spondyloarthropathies (SPA), inflammatory bowel disease (IBD), rheumatoid arthritis (RA), Behçet's disease (BD), sarcoidosis, or juvenile idiopathic arthritis (JIA)-, and autoimmune diseases that preferentially affect ocular tissues—such as Vogt-Koyanagi-Harada (VKH), white dot syndromes, sympathetic ophthalmia, and birdshot chorioretinopathy (BCR). In addition, uveitis can be anatomically classified as anterior, intermediate, posterior or panuveitis, and they may have an acute, chronic or recurrent course. The clinical presentation is variable, the symptoms may include blurred vision, photophobia, ocular pain and significant visual impairment (Keino et al., 2017). The etiology of uveitis depends on environmental, cultural, and genetic factors (Chan et al., 1985). In a recently published work by our group, uveitis was found to be secondary to a non-infectious autoimmune disease in 42% of cases. Infectious agents cause another 16.8%, while the condition remains idiopathic in the remaining 41% (Liberman et al., 2015).

Pathophysiology of Uveitis

The pathophysiology understanding of intraocular inflammation is limited. The eye has immunological properties known as "immune privilege," in which conventional immune response in not evoked by foreign antigens placed in those tissues. The haemato-ocular barriers, the lack of cell expression of both MHC-I and MHC-II, and the presence of immune modulators, such as TGF-β, among others, give this feature to the eye (Liberman et al., 2015).

It is thought that most non-infectious uveitis (NIU) are mediated by T cells, predominantly CD4+ T cells that exhibit a Th1 phenotype. Although the exact pathogenesis of uveitis is not completely understood, cytokines such as IL-2, TNF-α, INF-γ, IL-12, and IL-17 have been detected in patients with active disease, and it is believed that they would be key players in the pathogenesis (Durrani et al., 2004; Levy-Clarke et al., 2014; Dunn, 2015). Thus, these cytokines may be therapeutic targets for new treatments of NIU, whose management represents a challenge, given the broad variability in its nature and pathophysiology.

Treatment of Non-Infectious Uveitis

The first line of treatment for NIU corresponds to corticosteroids (CS), particularly due to their high efficacy and rapid control of acute inflammation. Depending on the severity of the condition and the type of ocular involvement, CS can be administered topically, periocularly, intraocularly, or systemically (Poetker and Reh, 2010; Knickelbein et al., 2017; Rossi et al., 2019). However, systemic CS have been associated not only with a significant number of systemic adverse effects with long-term therapy—including diabetes, Cushing's syndrome, hypercholesterolemia, and osteoporosis—but also cataracts and glaucoma, which can ultimately result in visual impairment and blindness (Rothova et al., 1996; Poetker and Reh, 2010; Multicenter et al., 2011). The most studied and used CS is prednisolone, having the greatest clinical evidence supporting its use (Jabs et al., 2000; Biswas et al., 2004; Hedayatfar et al., 2014; Sheppard et al., 2014). In some clinical scenarios, immunosuppressant therapy (IMT)—such as antimetabolites (methotrexate, mycophenolate mofetil, azathioprine), calcineurinic inhibitors (cyclosporine, tacrolimus), and alkylating agents (cyclophosphamide, chlorambucil)—is required to treat uncontrolled inflammation (Knickelbein et al., 2017; Hassan et al., 2019; Rossi et al., 2019). In addition, these drugs are the standard of care in some clinical entities, such as BD, BCR, or pediatric uveitis, due to the higher prevalence of chronic disease (e.g., JIA-associated uveitis) in this last subset of patients (Knickelbein et al., 2017; Sood and Angeles-Han, 2017; Cann et al., 2018).

Biological therapy has emerged as a new therapeutic approach in pediatric and adulthood uveitis, based on targeting relevant immunological pathways involved in disease pathogenesis, particularly tumor necrosis factor alpha (TNF-α) (Knickelbein et al., 2017; Sood and Angeles-Han, 2017; Cann et al., 2018; Hassan et al., 2019).

Anti TNF-α Drugs

TNF-α is a pro-inflammatory cytokine that participates in the pathophysiology of autoimmune and inflammatory diseases, and thus, it has become an important therapeutic target (Kuiper et al., 2017). TNF-α blockers have been used for the treatment of rheumatic diseases since 1999 and have dramatically changed the clinical course of invalidating diseases, such as RA and SPAs (Maini et al., 1999). Noteworthy, several trials and case series have already demonstrated the effectiveness of anti-TNF-α for treating refractory uveitis (**Table 1**) (Kruh et al., 2014; Vallet et al., 2016), showing a reduction of inflammatory signs and relapses, as well as an increase of the likelihood of visual acuity preservation (more than 90% in some cases) and the quality of life of uveitis patients (Fabiani et al., 2019a; Leal et al., 2019; Sharma et al., 2019). If uveitis is refractory to systemic CS and IMT or patients become intolerant to such therapies, a good sight-saving measure is the use of biological agents (Mercier et al., 2018; Trivedi and Katelaris, 2018).

Adalimumab

Adalimumab (Humira®) is an entirely humanized monoclonal antibody against TNF-α which is may be subcutaneously self-administered. It is the most used and studied biologic medication for the treatment of adulthood NIU since its approval in 2016 (Borrás-Blasco et al., 2015; Humira (R), (adalimumab), 2016).

The first report of adalimumab's role in the treatment of NIU was in 2008 (Diaz-Llopis et al., 2008). Subsequently, large multicenter randomized clinical trials (Visual I, II, and III) have showed this drug is effective in non-anterior NIU for inflammation control and as steroid-sparing agent (Diaz-Llopis et al., 2008; Jaffe et al., 2016; Nguyen et al., 2016; Leal et al., 2018; Lee et al., 2018; Suhler et al., 2018; Goto et al., 2019). The Visual I study was a multinational phase 3 trial where adalimumab given fortnightly, was used to treat active non-infectious intermediate, posterior, and panuveitis. The authors showed the rate of treatment failure was slashed to 50% in the adalimumab group

TABLE 1 | Current anti-TNF-α available treatments in non-infectious uveitis.

Therapy	Description	Study type	References
Adalimumab	Anti TNF-α humanized antibody	Clinical trial	(Diaz-Llopis et al., 2008)
		Systematic review	(Borrás-Blasco et al., 2015)
		Clinical trial	(Jaffe et al., 2016)
		Clinical trial	(Goto et al., 2019)
		Prospective study	(Sharma et al., 2019)
		Meta-analysis	(Leal et al., 2019)
		Systematic review	(Leal et al., 2018)
		Clinical trial	(Suhler et al., 2018)
		Clinical trial	(Lee et al., 2018)
		Retrospective study	(Mercier et al., 2018)
		Clinical trial	(Nguyen et al., 2016)
Infliximab	Anti TNF-α chimeric antibody	Systematic review	(Borrás-Blasco et al., 2015)
		Prospective study	(Sharma et al., 2019)
		Meta-analysis	(Leal et al., 2019)
		Systematic review	(Leal et al., 2018)
		Retrospective study	(Mercier et al., 2018)
Golimumab	Anti TNF-α humanized antibody	Systematic review	(Borrás-Blasco et al., 2015)
		Meta-analysis	(Leal et al., 2019)
		Systematic review	(Leal et al., 2018)
Etanercept	Anti TNF-α dimeric protein, act as a decoy for TNF-α Receptor	Meta-analysis	(Leal et al., 2019)
		Systematic review	(Leal et al., 2018)
Certolizumab	Anti TNF-α antibody	Systematic review	(Leal et al., 2019)
		Systematic review	(Leal et al., 2018)

compared with placebo (Jaffe et al., 2016). In the Visual II multicenter, randomized trial, adalimumab also lowered the risk of uveitis recurrence or vision loss, upon steroids withdrawal, in patients with inactive, non-infectious intermediate, posterior, and panuveitis, controlled by moderate systemic steroids dose. Treatment failure occurred in 55% of patients in the placebo group compared with 39% of patients in the adalimumab group (Nguyen et al., 2016). Noteworthy, although the good efficacy shown in these trials, further studies have found up to 40% of therapeutic failure after 12 months of treatment (Suhler et al., 2018).

In pediatric patients, adalimumab was approved in 2017 (Humira (R), (adalimumab), 2016; Shahab et al., 2018; Suhler et al., 2018). The combination of adalimumab with CS has been described as beneficial in terms of lowering therapeutic failure rate (Simonini et al., 2014). Ramanan et al. published a randomized trial that compared efficacy of adalimumab in children with active JIA-related uveitis despite methotrexate. In their work, patients assigned to the adalimumab arm had a significant lower treatment failure compared with placebo (27% vs 60%; $p < 0.0001$) (Ramanan et al., 2017). However, drug-induced remission of JIA-associated uveitis did not persist when the drug was withdrawn after 1 to 2 years of treatment (Horton et al., 2019). In addition, it has been showed that adalimumab is more effective for controlling inflammation and lowering relapses in pediatric NIU, in comparison with infliximab and etanercept (Simonini et al., 2011; Simonini et al., 2014).

Pediatric doses are started with a minimum of 24 mg/m^2, and a maximum of 40 mg weekly. Adult scheme doses are started with a loading dose of 80 mg, and then maintenance of 40 mg every 2 weeks (Simonini et al., 2014; Sood and Angeles-Han, 2017).

Importantly, a bimodal agent of adalimumab (SB5) has been recently approved for the treatment of NIU and other autoimmune entities, such as RA, JIA, IBD, among others (Frampton, 2018).

Infliximab

Infliximab (Remicade®) is a chimeric monoclonal antibody used since 2001 (Sfikakis et al., 2001). It has 25% murine and 75% humanized domains. Its use is FDA-approved for RA, psoriatic arthritis (PsA), IBD, and AS, but not for NIU. It is only intravenously administered, usually in conjunction with methotrexate to prevent the generation of antibodies against the drug (Maini et al., 1999; Sood and Angeles-Han, 2017).

There is great evidence of its efficacy in NIU, mainly BD (Sfikakis et al., 2001; Vallet et al., 2016; Fabiani et al., 2018). Maleki et al., in a small retrospective case series, achieved remission in 19 of 23 patients with active intermediate NIU refractory to at least one IMT (Maleki et al., 2017). Along the same line, Baughman et al. showed a remarkable improvement in 13 out of 14 patients with several underlying causes of ocular inflammation, who were treated with infliximab after failure of classical IMT (Baughman et al., 2005) In other retrospective study, Bodaghi et al. achieved a rapid control of uveitis in all 12 patients refractory to CS and IMT (Bodaghi et al., 2005). Suhler et al. conducted a prospective non-comparative trial of infliximab therapy for refractory uveitis, in which 18 out of 23 patients met criteria for clinical success at week 10 (Suhler et al., 2005).

Nevertheless, despite these good results, some studies have indicated that the rate of therapeutic failure at 12 months of treatment is around 60% (Bodaghi et al., 2005; Simonini et al., 2011; Simonini et al., 2013a), which puts it at a disadvantage compared to adalimumab. However, infliximab presents a rapid onset of action, which is why it is recommended in severe exacerbations (Sfikakis et al., 2001; Markomichelakis et al., 2011).

The posology is very variable. In adults, the dose and frequency depend on the disease, which can be between 3 and 5 mg/kg every 6 to 8 weeks. The pediatric dose begins with a loading dose between 3 and 5 mg/kg at weeks 0, 2, and 6, and continues with a maintenance dose of at least 7.5 mg/kg/dose every 4 to 8 weeks; the dose is adjusted according to the clinical response and the patient's tolerance to the medication, with a evaluated maximum dose of 20 mg/kg (Sukumaran et al., 2012; Sood and Angeles-Han, 2017).

Golimumab

Golimumab (Simponi®) is a fully humanized monoclonal antibody, subcutaneously administered with a dose of 50 mg every 4 weeks. Its use has been approved for the treatment of AS, RA, PsA, and UC (Sukumaran et al., 2012; Calvo-Río et al., 2016). There is little evidence, but it has been described its

efficacy in patients with NIU refractory to adalimumab or infliximab, and thus golimumab is usually reserved as treatment for this subset of non-responders (Miserocchi et al., 2014; Calvo-Río et al., 2016; Fabiani et al., 2019b). In that sense, this medication would present a higher affinity for the receptor, being able to improve clinical signs of inflammation in refractory patients (Tosi et al., 2019). Tosi et al. published a retrospective study of 21 uveitis patients treated with Golimumab (10 patients) or Certolizumab pegol (11 patients). They showed a significant reduction in ocular flares from 128.6 events/100 patients-year to 24.9 events/100 patients-years, although no specific results were published for each group. All patients in the Golimumab group had received another anti-TNF drug previously (Tosi et al., 2019). Additionally, Palmou-Fontana et al. showed complete remission of four of seven patients with JIA-associated uveitis treated with golimumab (Palmou-Fontana et al., 2018).

Etanercept

The mechanism of action of etanercept (Enbrel®) differs from the other anti-TNF-α agents. It is a dimeric protein that has an Fc portion of human IgG and a portion of the ligand-binding site of the TNF receptor p75 (Scott, 2005). Etanercept is subcutaneously administrated at a dose of 50 mg once per week or 25 mg twice a week. In children over 2 years old, etanercept is approved for the treatment of JIA at the dose of 0.4 mg/kg (up to a maximum of 25 mg/dose) twice a week or 0.8 mg/kg (maximum 50 mg) once weekly (Guillot et al., 2017).

There is little evidence about this medication, and case reports indicate that although patients with BD respond to therapy, this effect is not sustained (Simonini et al., 2014). Etanercept is no longer prescribed for uveitis given its low distribution in ocular tissue, and its lower efficacy compared to adalimumab and infliximab (Foster et al., 2003; Tynjälä et al., 2007; Touhami et al., 2019).

Certolizumab

Certolizumab (Cimzia®) is a recombinant humanized monoclonal antibody administered subcutaneously at an initial dose of 400 mg at weeks 0, 2, and 4 and then 200 mg per week. It is approved for the treatment of AS, PsA, RA, and Crohn's disease (Llorenç et al., 2016). It has been little studied in NIU, and in general, it has been evaluated in small case series. However, it has shown positive results, and no major adverse effects have been reported during its use (Rudwaleit et al., 2016; Lopalco et al., 2017a). It seems to have a better and higher distribution toward inflamed tissues than adalimumab and infliximab (Llorenç et al., 2016). A recent study has indicated that both golimumab and certolizumab represent effective and safe options for patients with uveitis even if the result with other anti-TNF-α drugs has not been successful (Tosi et al., 2019).

Adverse Effects of Anti TNF-α Drugs

As adalimumab and golimumab are fully humanized antibodies, they have less immunogenic potential than chimeric antibodies (Simonini et al., 2014). The main adverse effects of anti-TNF-α agents include development of autoimmune diseases, increased risk of infection, where tuberculosis and histoplasmosis stand out, among others. Reactions at the injection site have been also described. In addition, anti-TNF-α blockers have been associated with an increased risk of malignancy, mainly lymphomas (Diak et al., 2010), although further studies have ruled this out (Shelton et al., 2016) and with debut or worsening of demyelinating disorders, such as multiple sclerosis (Magnano et al., 2004).

Adverse effects of adalimumab also include arthralgias, nasopharyngitis, and headaches. Side effects of infliximab may include the development of mild or severe lupus-like symptoms (9% and 1% respectively) (Levy-Clarke et al., 2014). Golimumab may cause nausea, fever, and anemia (Diak et al., 2010). In the case of etanercept, uveitis, IBD flares, and granulomatous diseases have been shown to be more prevalent compared to other TNF blockers (Scott, 2005; Guillot et al., 2017). Certolizumab has been little studied in NIU, and in general, it has been evaluated in small case series, showing positive results and mild or moderate adverse effects during its use (Rudwaleit et al., 2016; Lopalco et al., 2017b), with infections being the most common (Bykerk et al., 2015), and in fewer cases it has been reported a generalized skin reaction (in the third administration), anaphylactic reactions, and a lupus-like episodes (Bykerk et al., 2015).

A significant proportion of patients experiences loss of response during maintenance treatment with anti-TNF-α, due to the development of an immune response directed at the drug itself, leading to lower concentration of anti-TNF-α and the presence of anti-anti TNF-α antibodies in serum (Guerra et al., 2011; Touhami et al., 2019). The measurement of drug concentrations and probably, the measurement of anti-infliximab or anti-adalimumab antibodies, might be useful for improving the selection of patients who would benefit from the maintenance treatment with infliximab or adalimumab, avoiding inappropriate treatments, and helping to decide which procedure to follow in case of loss of response (Guerra et al., 2011). However, there is no enough evidence to recommend level or antibody measurements as standard of care in uveitis patients.

IMT are added in order to reduce the immunogenicity against anti-TNF-α drugs. Although there is no solid evidence-based data regarding their use, the use of an immunosuppressant together, such as methotrexate, is suggested in case of pathologies-associated uveitis (e.g. BD, JIA, etc.) (Touhami et al., 2019).

Other Biologics Therapies

When conventional IMT and/or anti-TNF-α therapies fail, other biological agents are recommended. Some of the newest therapies have focused on blocking interleukin actions (**Table 2**).

Anti-IL-6 Therapies

Interleukin-6 (IL-6) is a proinflammatory cytokine implicated in various immune-mediated diseases. Its produced by monocytes, macrophages, B cells, and T cells mainly. In some pathologies, such as central retinal vein occlusion, diabetes, or uveitis, intraocular concentrations of IL-6 are increased (Petrinović-Doresić et al., 1999). The recombinant human monoclonal antibody tocilizumab (Actemra®) is an IL-6 receptor blocker and has shown a good effect in the treatment of NIU (Lopalco

TABLE 2 | Current available non–anti-TNF Biologics treatments in non-infectious uveitis.

Therapy	Description	Study type	References
Tocilizumab	Anti-IL-6 humanized antibody	Systematic review	(Lopalco et al., 2017a)
		Clinical trial	(Papo et al., 2014)
		Systematic review	(Cann et al., 2018)
		Systematic review	(Sharma et al., 2018)
		Retrospective study	(Silpa-Archa et al., 2016)
Secukinumab	Anti-IL-17A monoclonal antibody	Clinical trial	(Dick et al., 2013)
		Review	(Sanford and McKeage, 2015)
Canakinumab	Anti-IL-1β	Case report	(Simonini et al., 2013b)
		Systematic review	(Simonini et al., 2015)
Anakinra	IL-1 receptor antagonist	Systematic review	(Simonini et al., 2015)
Rituximab	Anti CD20 antibody	Systematic review	(Simonini et al., 2015)
		Retrospective study	(Miserocchi et al., 2016)
		Clinical trial	(Davatchi et al., 2010)

IL, interleukin; CD, cluster of differentiation.

et al., 2017a), particularly in BD patients with refractory uveitis (Atienza-Mateo et al., 2018). FDA approved the use of tocilizumab for the management of RA, including refractory patients (Hassan et al., 2019). In general, tocilizumab, presents minor adverse effects such as chest tightness, fatigue, nausea, and blisters on the hands and limbs (Silpa-Archa et al., 2016; Sharma et al., 2018), non-serious bronchitis, leukopenia, and thrombocytopenia in which the drug was not suspended (Papo et al., 2014). However, cases with more severe manifestations such as neutropenia, unacceptable dizziness and nausea, severe infusion reaction, severe angioedema, and severe abdominal pain have been reported, requiring discontinuation of the medication (Silpa-Archa et al., 2016; Atienza-Mateo et al., 2018). There is a reported case of probable association of anxiety, sweating, and flushing with the infusion (Sepah et al., 2017).

Anti-IL-1 Therapies

Anti-IL-1 treatment includes antagonist of the IL-1 receptor, anakinra (Kineret®), and anti-IL-1β antibody, canakinumab (Ilaris®). Both anti-IL-1s were evaluated in a multicenter retrospective study that included 19 BD-associated uveitis patients. In this study, both treatments were effective in the management of uveitis, providing a good control of inflammation and steroid-sparing effect, in refractory and long-lasting cases (Fabiani et al., 2017). IL-1 blockers have shown mild adverse effects, confirming their excellent safety profile (Fabiani et al., 2017). In the case of anakinra the most reported manifestations are headaches and arthralgias (Kullenberg et al., 2016; Cavalli and Dinarello, 2018). There is only a reported case of reactivation of pulmonary TB, but in an elderly patient with RA and record of pulmonary TB (Cavalli and Dinarello, 2018).

Anti-CD20 Therapies

Rituximab (Rituxan®/MabThera®) is a chimeric (human and murine portion) monoclonal antibody directed against the CD20 antigen present on the B-cells surface. In 1997 it was approved to treat lymphoma, and its use has continued to control other diseases, such as RA (Davatchi et al., 2010). In a retrospective study with JIA-related uveitis patients, all achieved complete control of uveitis within 5 months of first infusion over a mean follow up of 44 months, demonstrating the long-term efficacy of rituximab for anti-TNF-α refractory cases (Miserocchi et al., 2016). In addition, rituximab was effective for treating resistant ANCA-positive vasculitis, with no significant adverse effects (Eriksson, 2005). Regarding adverse effects, there are minor cases of hives and flushing, and others more severe that have required the suspension of the infusion. Infection-like pneumonia and herpes zoster have been also reported (Davatchi et al., 2010).

Anti-CD25 Therapies

Daclizumab is a monoclonal antibody targeted to 2α subunit of the IL-2 receptor on activated T-cells, blocking the conventional T-cells immune responses (Sen et al., 2009; Giovannoni et al., 2016). In this case, mild adverse effects are more frequent than serious. The most frequently reported adverse effects have been on the one hand herpes zoster, rash, and palpitations, and the other liver disorders and elevated transaminases, although mainly asymptomatic and self-limited (Sen et al., 2009; Giovannoni et al., 2016).

Anti-IL-17A Therapies

Secukinumab is a monoclonal antibody (fully humanized) that binds and neutralizes the IL-17A (Dick et al., 2013; Sanford and McKeage, 2015). Some problems in the upper respiratory tract (nasopharyngitis) and headache has been reported as adverse effects, and it has been seen cases of reactivation of uveitis, as well as arthralgias (Dick et al., 2013).

CONCLUSIONS

Biologic agents have revolutionized the immunological treatment of NIU in the past 20 years. The most newly published guidelines for uveitis management suggest a step-ladder approach, starting with topical, periocular, and systemic CS, followed by IMT, and finally the use of biologic therapy (preferably a TNF-α inhibitor). In this sense, despite the well-known side effects of CS, they remain as the cornerstone of treatment for acute diseases and exacerbations. Furthermore, the use of new therapies is still limited due to their high cost, and all the aspects that remain to be studied, such as follow-up regimens and monitoring. Nevertheless, it would not be a surprise that, with the availability of new data, biological agents may be recommended as first-line therapy in the management of some causes of uveitis. Furthermore, new insights have emerged to present new therapeutic approaches directed against immune components as potential novel therapies for NIU.

AUTHOR CONTRIBUTIONS

RV and IF wrote the manuscript. RV and FF made the tables. RV, IF, BU, FF, PS, CL, LC, and CU read, discussed, and revised the manuscript. All authors listed have made a substantial, direct and intellectual contribution to the work and approved it for publication.

FUNDING

This study was supported by Fondo de Fomento al Desarrollo Científico y Tecnológico (FONDEF) grant No. IT17I0087 (to CU) and National Agency for Research and Development (ANID) grant Fondecyt de Iniciación en Investigación No. 11191215 (to LC).

REFERENCES

Atienza-Mateo, B., Calvo-Río, V., Beltrán, E., Martínez-Costa, L., Valls-Pascual, E., Hernández-Garfella, M., et al. (2018). Anti-interleukin 6 receptor tocilizumab in refractory uveitis associated with Behçet's disease: multicentre retrospective study. *Rheumatol. (Oxford).* 57, 856–864. doi: 10.1093/rheumatology/kex480

Baughman, R. P., Bradley, D. A., and Lower, E. E. (2005). Infliximab in chronic ocular inflammation. *Int. J. Clin. Pharmacol. Ther.* 43, 7–11. doi: 10.5414/cpp43007

Biswas, J., Ganeshbabu, T. M., Raghavendran, S. R., Raizada, S., Mondkar, S. V., and Madhavan, H. N. (2004). Efficacy and safety of 1% rimexolone versus 1% prednisolone acetate in the treatment of anterior uveitis–a randomized triple masked study. *Int. Ophthalmol.* 25, 147–153. doi: 10.1007/s10792-004-5195-2

Bodaghi, B., Bui Quoc, E., Wechsler, B., Tran, T. H., Cassoux, N., Le Thi Huong, D., et al. (2005). Therapeutic use of infliximab in sight threatening uveitis: retrospective analysis of efficacy, safety, and limiting factors.[letter]. *Ann. Rheum. Dis.* 64 (6), 962–964. doi: 10.1136/ard.2004.025882

Borrás-Blasco, J., Casterá, D. E., Cortes, X., Abad, F. J., Rosique-Robles, J. D., and Mallench, L. G. (2015). Effectiveness of infliximab, adalimumab and golimumab for non-infectious refractory uveitis in adults. *Int. J. Clin. Pharmacol. Ther.* 53, 377–390. doi: 10.5414/CP202171

Bykerk, V. P., Cush, J., Winthrop, K., Calabrese, L., Lortholary, O., de Longueville, M., et al. (2015). Update on the safety profile of certolizumab pegol in rheumatoid arthritis: an integrated analysis from clinical trials. *Ann. Rheum. Dis.* 74, 96–103. doi: 10.1136/annrheumdis-2013-203660

Calvo-Río, V., Blanco, R., Santos-Gómez, M., Rubio-Romero, E., Cordero-Coma, M., Gallego-Flores, A., et al. (2016). Golimumab in refractory uveitis related to spondyloarthritis. Multicenter study of 15 patients. *Semin. Arthritis Rheumatol.* 46, 95–101. doi: 10.1016/j.semarthrit.2016.03.002

Cann, M., Ramanan, A. V., Crawford, A., Dick, A. D., Clarke, S. L. N., Rashed, F., et al. (2018). Outcomes of non-infectious Paediatric uveitis in the era of biologic therapy. *Pediatr. Rheumatol. Online J.* 16, 51. doi: 10.1186/s12969-018-0266-5

Cavalli, G., and Dinarello, C. A. (2018). Anakinra Therapy for Non-cancer Inflammatory Diseases. *Front. Pharmacol.* 9, 1157. doi: 10.3389/fphar.2018.01157

Chan, C. C., Palestine, A. G., Nussenblatt, R. B., Roberge, F. G., and Benezra, D. (1985). Anti-retinal auto-antibodies in Vogt-Koyanagi-Harada syndrome, Behcet's disease, and sympathetic ophthalmia. *Ophthalmology.* 92, 1025–1028. doi: 10.1016/S0161-6420(85)33911-8

Davatchi, F., Shams, H., Rezaipoor, M., Sadeghi-Abdollahi, B., Shahram, F., Nadji, A., et al. (2010). Rituximab in intractable ocular lesions of Behcet's disease; randomized single-blind control study (pilot study). *Int. J. Rheum. Dis.* 13, 246–252. doi: 10.1111/j.1756-185X.2010.01546.x

Diak, P., Siegel, J., La Grenade, L., Choi, L., Lemery, S., and McMahon, A. (2010). Tumor necrosis factor alpha blockers and malignancy in children: forty-eight cases reported to the Food and Drug Administration. *Arthritis Rheumatol.* 62, 2517–2524. doi: 10.1002/art.27511

Diaz-Llopis, M., García-Delpech, S., Salom, D., Udaondo, P., Hernández-Garfella, M., Bosch-Morell, F., et al. (2008). Adalimumab therapy for refractory uveitis: a pilot study. *J. Ocul. Pharmacol. Ther.* 24, 351–361. doi: 10.1089/jop.2007.0104

Dick, A. D., Tugal-Tutkun, I., Foster, S., Zierhut, M., Melissa Liew, S. H., Bezlyak, V., et al. (2013). Secukinumab in the treatment of noninfectious uveitis: results of three randomized, controlled clinical trials. *Ophthalmology.* 120, 777–787. doi: 10.1016/j.ophtha.2012.09.040

Dunn, J. P. (2015). Uveitis. *Prim. Care* 42, 305–323. doi: 10.1016/j.pop.2015.05.003

Durrani, O. M., Meads, C. A., and Murray, P. I. (2004). Uveitis: a potentially blinding disease. *Ophthalmologica.* 218, 223–236. doi: 10.1159/000078612

Eriksson, P. (2005). Nine patients with anti-neutrophil cytoplasmic antibody-positive vasculitis successfully treated with rituximab. *J. Intern Med.* 257, 540–548. doi: 10.1111/j.1365-2796.2005.01494.x

Fabiani, C., Vitale, A., Emmi, G., Lopalco, G., Vannozzi, L., Guerriero, S., et al. (2017). Interleukin (IL)-1 inhibition with anakinra and canakinumab in Behçet's disease-related uveitis: a multicenter retrospective observational study. *Clin. Rheumatol.* 36, 191–197. doi: 10.1007/s10067-016-3506-4

Fabiani, C., Vitale, A., Rigante, D., Emmi, G., Lopalco, G., Sota, J., et al. (2018). Predictors of sustained clinical response in patients with Behçet's disease-related uveitis treated with infliximab and adalimumab. *Clin. Rheumatol.* 37, 1715–1720. doi: 10.1007/s10067-018-4092-4

Fabiani, C., Vitale, A., Rigante, D., Emmi, G., Lopalco, G., Sota, J., et al. (2019a). Efficacy of anti-tumour necrosis factor-α monoclonal antibodies in patients with non-infectious anterior uveitis. *Clin. Exp. Rheumatol.* 37, 301–305.

Fabiani, C., Sota, J., Rigante, D., Vitale, A., Emmi, G., Vannozzi, L., et al. (2019b). Rapid and Sustained Efficacy of Golimumab in the Treatment of Multirefractory Uveitis Associated with Behçet's Disease. *Ocul. Immunol. Inflamm.* 27, 58–63. doi: 10.1080/09273948.2017.1351573

Foster, C. S., Tufail, F., Waheed, N. K., Chu, D., Miserocchi, E., Baltatzis, S., et al. (2003). Efficacy of etanercept in preventing relapse of uveitis controlled by methotrexate. *Arch. Ophthalmol.* 121, 437–440. doi: 10.1001/archopht.121.4.437

Frampton, J. E. (2018). SB5: An Adalimumab Biosimilar. *BioDrugs.* 32, 507–510. doi: 10.1007/s40259-018-0307-0

Giovannoni, G., Kappos, L., Gold, R., Khatri, B. O., Selmaj, K., Umans, K., et al. (2016). Safety and tolerability profile of daclizumab in patients with relapsing-remitting multiple sclerosis: An integrated analysis of clinical studies. *Mult. Scler Relat. Disord.* 9, 36–46. doi: 10.1016/j.msard.2016.05.010

Goto, H., Zako, M., Namba, K., Hashida, N., Kaburaki, T., Miyazaki, M., et al. (2019). Adalimumab in Active and Inactive, Non-Infectious Uveitis: Global Results from the VISUAL I and VISUAL II Trials. *Ocul. Immunol. Inflamm.* 27, 40–50. doi: 10.1080/09273948.2018.1491605

Guerra, I., Chaparro, M., Bermejo, F., and Gisbert, J. P. (2011). Utility of measuring serum concentrations of anti-TNF agents and anti-drug antibodies in inflammatory bowel disease. *Curr. Drug Metab.* 12, 594–598. doi: 10.2174/138920011795713689

Guillot, X., Prati, C., Sondag, M., and Wendling, D. (2017). Etanercept for treating axial spondyloarthritis. *Expert Opin. Biol. Ther.* 17, 1173–1181. doi: 10.1080/14712598.2017.1347156

Hassan, M., Karkhur, S., Bae, J. H., Halim, M. S., Ormaechea, M. S., Onghanseng, N., et al. (2019). New therapies in development for the management of non-infectious uveitis: A review. *Clin. Exp. Ophthalmol.* 47, 396–417. doi: 10.1111/ceo.13511

Hedayatfar, A., Hashemi, H., Asgari, S., and Chee, S. P. (2014). Comparison of efficacy and ocular surface toxicity of topical preservative-free methylprednisolone and preserved prednisolone in the treatment of acute anterior uveitis. *Cornea.* 33, 366–372. doi: 10.1097/ICO.0000000000000039

Horton, S., Jones, A. P., Guly, C. M., Hardwick, B., Beresford, M. W., Lee, R. W. J., et al. (2019). Adalimumab in juvenile-idiopathic arthritis-associated uveitis (JIA-U): 5-year follow-up of the Bristol participants of the SYCAMORE trial. *Am. J. Ophthalmol* 207, 170–174. doi: 10.1016/j.ajo.2019.06.007

Humira (R), (adalimumab) (2016). *Full Prescribing Information* (North Chicago, IL: AbbVie Inc.).

Jabs, D. A., Rosenbaum, J. T., Foster, C. S., Holland, G. N., Jaffe, G. J., Louie, J. S., et al. (2000). Guidelines for the use of immunosuppressive drugs in patients

with ocular inflammatory disorders: recommendations of an expert panel. *Am. J. Ophthalmol.* 130, 492–513. doi: 10.1016/S0002-9394(00)00659-0

Jaffe, G. J., Dick, A. D., Brézin, A. P., Nguyen, Q. D., Thorne, J. E., Kestelyn, P., et al. (2016). Adalimumab in Patients with Active Noninfectious Uveitis. *N Engl. J. Med.* 375, 932–943. doi: 10.1056/NEJMoa1509852

Keino, H., Watanabe, T., Taki, W., Nakayama, M., Nakamura, T., Yan, K., et al. (2017). Clinical features of uveitis in children and adolescents at a tertiary referral centre in Tokyo. *Br. J. Ophthalmol.* 101, 406–410. doi: 10.1136/bjophthalmol-2015-308194

Knickelbein, J. E., Kim, M., Argon, E., Nussenblatt, R. B., and Sen, N. H. (2017). Comparative efficacy of steroid-sparing therapies for non-infectious uveitis. *Expert Rev. Ophthalmol.* 12, 313–319. doi: 10.1080/17469899.2017.1319762

Kruh, J. N., Yang, P., Suelves, A. M., and Foster, C. S. (2014). Infliximab for the treatment of refractory noninfectious Uveitis: a study of 88 patients with long-term follow-up. *Ophthalmology.* 121, 358–364. doi: 10.1016/j.ophtha.2013.07.019

Kuiper, J. J., Beretta, L., Nierkens, S., van Leeuwen, R., Ten Dam-van Loon, N. H., Ossewaarde-van Norel, J., et al. (2017). An Ocular Protein Triad Can Classify Four Complex Retinal Diseases. *Sci. Rep.* 7, 41595. doi: 10.1038/srep41595

Kullenberg, T., Löfqvist, M., Leinonen, M., Goldbach-Mansky, R., and Olivecrona, H. (2016). Long-term safety profile of anakinra in patients with severe cryopyrin-associated periodic syndromes. *Rheumatol. (Oxford).* 55, 1499–1506. doi: 10.1093/rheumatology/kew208

Leal, I., Rodrigues, F. B., Sousa, D. C., Romão, V. C., Duarte, G. S., Carreño, E., et al. (2018). Efficacy and safety of intravitreal anti-tumour necrosis factor drugs in adults with non-infectious uveitis—a systematic review. *Acta Ophthalmol.* 96, e665–e675. doi: 10.1111/aos.13699

Leal, I., Rodrigues, F. B., Sousa, D. C., Duarte, G. S., Romão, V. C., Marques-Neves, C., et al. (2019). Anti-TNF Drugs for Chronic Uveitis in Adults-A Systematic Review and Meta-Analysis of Randomized Controlled Trials. *Front. Med. (Lausanne).* 6, 104. doi: 10.3389/fmed.2019.00104

Lee, J. T., Yates, W. B., Rogers, S., Wakefield, D., McCluskey, P., and Lim, L. L. (2018). Adalimumab for the treatment of refractory active and inactive non-infectious uveitis. *Br. J. Ophthalmol.* 102, 1672–1678. doi: 10.1136/bjophthalmol-2017-311234

Levy-Clarke, G., Jabs, D. A., Read, R. W., Rosenbaum, J. T., Vitale, A., and Van Gelder, R. N. (2014). Expert panel recommendations for the use of anti-tumor necrosis factor biologic agents in patients with ocular inflammatory disorders. *Ophthalmology.* 121, 785–96.e3. doi: 10.1016/j.ophtha.2013.09.048

Liberman, P., Gauro, F., Berger, O., and Urzua, C. A. (2015). Causes of Uveitis in a Tertiary Center in Chile: A Cross-sectional Retrospective Review. *Ocul. Immunol. Inflamm.* 23, 339–345. doi: 10.3109/09273948.2014.981548

Llorenç, V., Mesquida, M., Sainz de la Maza, M., Blanco, R., Calvo, V., Maíz, O., et al. (2016). Certolizumab Pegol, a New Anti-TNF-α in the Armamentarium against Ocular Inflammation. *Ocul. Immunol. Inflamm.* 24, 167–172. doi: 10.3109/09273948.2014.967779

Lopalco, G., Fabiani, C., Sota, J., Lucherini, O. M., Tosi, G. M., Frediani, B., et al. (2017a). IL-6 blockade in the management of non-infectious uveitis. *Clin. Rheumatol.* 36, 1459–1469. doi: 10.1007/s10067-017-3672-z

Lopalco, G., Emmi, G., Gentileschi, S., Guerriero, S., Vitale, A., Silvestri, E., et al. (2017b). Certolizumab Pegol treatment in Behcet's disease with different organ involvement: A multicenter retrospective observational study. *Mod Rheumatol.* 27, 1031–1035. doi: 10.1080/14397595.2017.1285857

Magnano, M. D., Robinson, W. H., and Genovese, M. C. (2004). Demyelination and inhibition of tumor necrosis factor (TNF). *Clin. Exp. Rheumatol.* 22, S134–S140.

Maini, R., St Clair, E. W., Breedveld, F., Furst, D., Kalden, J., Weisman, M., et al. (1999). Infliximab (chimeric anti-tumour necrosis factor alpha monoclonal antibody) versus placebo in rheumatoid arthritis patients receiving concomitant methotrexate: a randomised phase III trial. ATTRACT Study Group. *Lancet.* 354, 1932–1939. doi: 10.1016/s0140-6736(99)05246-0

Maleki, A., Sahawneh, H. F., Ma, L., Meese, H., He, Y., and Foster, C. S. (2017). Infliximab therapy in patients with noninfectious intermediate uveitis resistant to conventional immunomodulatory therapy. *Retina.* 37, 836–843. doi: 10.1097/IAE.0000000000001269

Markomichelakis, N., Delicha, E., Masselos, S., Fragiadaki, K., Kaklamanis, P., and Sfikakis, P. P. (2011). A single infliximab infusion vs corticosteroids for acute panuveitis attacks in Behçet's disease: a comparative 4-week study. *Rheumatol. (Oxford).* 50, 593–597. doi: 10.1093/rheumatology/keq366

Mercier, A. E., Ribeiro, E., Korobelnik, J. F., Delyfer, M. N., and Rougier, M. B. (2018). Efficacy of Anti-TNF-α Therapy for the Treatment of Non-infectious Uveitis: A Retrospective Study of 21 Patients. *Ocul. Immunol. Inflamm.* 26, 477–484. doi: 10.1080/09273948.2016.1236968

Miserocchi, E., Modorati, G., Pontikaki, I., Meroni, P. L., and Gerloni, V. (2014). Long-term treatment with golimumab for severe uveitis. *Ocul. Immunol. Inflamm.* 22, 90–95. doi: 10.3109/09273948.2013.844265

Miserocchi, E., Modorati, G., Berchicci, L., Pontikaki, I., Meroni, P., and Gerloni, V. (2016). Long-term treatment with rituximab in severe juvenile idiopathic arthritis-associated uveitis. *Br. J. Ophthalmol.* 100, 782–786. doi: 10.1136/bjophthalmol-2015-306790

Multicenter, USTMUSTTRG, Kempen, J. H., Altaweel, M. M., Holbrook, J. T., Jabs, D. A., Louis, T. A., et al. (2011). Randomized comparison of systemic anti-inflammatory therapy versus fluocinolone acetonide implant for intermediate, posterior, and panuveitis: the multicenter uveitis steroid treatment trial. *Ophthalmology.* 118, 1916–1926. doi: 10.1016/j.ophtha.2011.07.027

Nguyen, Q. D., Merrill, P. T., Jaffe, G. J., Dick, A. D., Kurup, S. K., Sheppard, J., et al. (2016). Adalimumab for prevention of uveitic flare in patients with inactive non-infectious uveitis controlled by corticosteroids (VISUAL II): a multicentre, double-masked, randomised, placebo-controlled phase 3 trial. *Lancet.* 388, 1183–1192. doi: 10.1016/S0140-6736(16)31339-3

Nussenblatt, R. B. (1990). The natural history of uveitis. *Int. Ophthalmol.* 14, 303–308. doi: 10.1007/BF00163549

Palmou-Fontana, N., Calvo-Río, V., Martín-Varillas, J. L., Fernández-Díaz, C., Mesquida, M., Adán, A., et al. (2018). Golimumab in refractory uveitis associated to juvenile idiopathic arthritis: multicentre study of 7 cases and literature review. *Clin. Exp. Rheumatol.* 36, 652–657.

Papo, M., Bielefeld, P., Vallet, H., Seve, P., Wechsler, B., Cacoub, P., et al. (2014). Tocilizumab in severe and refractory non-infectious uveitis. *Clin. Exp. Rheumatol.* 32, S75–S79.

Petrinović-Doresić, J., Mazuran, R., Henc-Petrinović, L., Kuzmanović, B., and Jovicić, A. (1999). Interleukin 6 and its soluble receptor are elevated in aqueous humor of patients with uveitis. *Ocul. Immunol. Inflamm.* 7, 75–84. doi: 10.1076/ocii.7.2.75.4017

Poetker, D. M., and Reh, D. D. (2010). A comprehensive review of the adverse effects of systemic corticosteroids. *Otolaryngol Clin. North Am.* 43, 753–768. doi: 10.1016/j.otc.2010.04.003

Ramanan, A. V., Dick, A. D., Jones, A. P., McKay, A., Williamson, P. R., Compeyrot-Lacassagne, S., et al. (2017). Adalimumab plus Methotrexate for Uveitis in Juvenile Idiopathic Arthritis. *N Engl. J. Med.* 376, 1637–1646. doi: 10.1056/NEJMoa1614160

Rossi, D. C., Ribi, C., and Guex-Crosier, Y. (2019). Treatment of chronic non-infectious uveitis and scleritis. *Swiss Med. Wkly.* 149, w20025. doi: 10.4414/smw.2019.20025

Rothova, A., Suttorp-van Schulten, M. S., Frits Treffers, W., and Kijlstra, A. (1996). Causes and frequency of blindness in patients with intraocular inflammatory disease. *Br. J. Ophthalmol.* 80, 332–336. doi: 10.1136/bjo.80.4.332

Rudwaleit, M., Rosenbaum, J. T., Landewé, R., Marzo-Ortega, H., Sieper, J., van der Heijde, D., et al. (2016). Observed Incidence of Uveitis Following Certolizumab Pegol Treatment in Patients With Axial Spondyloarthritis. *Arthritis Care Res. (Hoboken).* 68, 838–844. doi: 10.1002/acr.22848

Sanford, M., and McKeage, K. (2015). Secukinumab: first global approval. *Drugs.* 75, 329–338. doi: 10.1007/s40265-015-0359-0

Scott, D. L. (2005). Etanercept in arthritis. *Int. J. Clin. Pract.* 59, 114–118. doi: 10.1111/j.1742-1241.2005.00380.x

Sen, H. N., Levy-Clarke, G., Faia, L. J., Li, Z., Yeh, S., Barron, K. S., et al. (2009). High-dose daclizumab for the treatment of juvenile idiopathic arthritis-associated active anterior uveitis. *Am. J. Ophthalmol.* 148, 696–703.e1. doi: 10.1016/j.ajo.2009.06.003

Sepah, Y. J., Sadiq, M. A., Chu, D. S., Dacey, M., Gallemore, R., Dayani, P., et al. (2017). Primary (Month-6) Outcomes of the STOP-Uveitis Study: Evaluating the Safety, Tolerability, and Efficacy of Tocilizumab in Patients With Noninfectious Uveitis. *Am. J. Ophthalmol.* 183, 71–80. doi: 10.1016/j.ajo.2017.08.019

Sfikakis, P. P., Theodossiadis, P. G., Katsiari, C. G., Kaklamanis, P., and Markomichelakis, N. N. (2001). Effect of infliximab on sight-threatening

panuveitis in Behcet's disease.[letter]. *Lancet* 358 (9278), 295–296. doi: 10.1016/s0140-6736(01)05497-6

Shahab, M. A., Mir, T. A., and Zafar, S. (2018). Optimising drug therapy for non-infectious uveitis. *Int. Ophthalmol.* 39, 1633–1650. doi: 10.1007/s10792-018-0984-1

Sharma, S. M., Fu, D. J., and Xue, K. (2018). A Review of the Landscape of Targeted Immunomodulatory Therapies for Non-Infectious Uveitis. *Ophthalmol. Ther.* 7, 1–17. doi: 10.1007/s40123-017-0115-5

Sharma, S. M., Damato, E., Hinchcliffe, A. E., Andrews, C. D., Myint, K., Lee, R., et al. (2019). Long-term efficacy and tolerability of TNFα inhibitors in the treatment of non-infectious ocular inflammation: an 8-year prospective surveillance study. *Br. J. Ophthalmol.* doi: 10.1007/s00417-015-3140-x

Shelton, E., Laharie, D., Scott, F. I., Mamtani, R., Lewis, J. D., Colombel, J. F., et al. (2016). Cancer Recurrence Following Immune-Suppressive Therapies in Patients With Immune-Mediated Diseases: A Systematic Review and Meta-analysis. *Gastroenterology.* 151, 97–109.e4. doi: 10.1053/j.gastro.2016.03.037

Sheppard, J. D., Toyos, M. M., Kempen, J. H., Kaur, P., and Foster, C. S. (2014). Difluprednate 0.05% versus prednisolone acetate 1% for endogenous anterior uveitis: a phase III, multicenter, randomized study. *Invest. Ophthalmol. Vis. Sci.* 55, 2993–3002. doi: 10.1167/iovs.13-12660

Silpa-Archa, S., Oray, M., Preble, J. M., and Foster, C. S. (2016). Outcome of tocilizumab treatment in refractory ocular inflammatory diseases. *Acta Ophthalmol.* 94, e400–e406. doi: 10.1111/aos.13015

Simonini, G., Taddio, A., Cattalini, M., Caputo, R., De Libero, C., Naviglio, S., et al. (2011). Prevention of flare recurrences in childhood-refractory chronic uveitis: an open-label comparative study of adalimumab versus infliximab. *Arthritis Care Res. (Hoboken).* 63, 612–618. doi: 10.1002/acr.20404

Simonini, G., Taddio, A., Cattalini, M., Caputo, R., de Libero, C., Parentin, F., et al. (2013a). Superior efficacy of Adalimumab in treating childhood refractory chronic uveitis when used as first biologic modifier drug: Adalimumab as starting anti-TNF-α therapy in childhood chronic uveitis. *Pediatr. Rheumatol. Online J.* 11, 16. doi: 10.1186/1546-0096-11-16

Simonini, G., Xu, Z., Caputo, R., De Libero, C., Pagnini, I., Pascual, V., et al. (2013b). Clinical and transcriptional response to the long-acting interleukin-1 blocker canakinumab in Blau syndrome-related uveitis. *Arthritis Rheumatol.* 65, 513–518. doi: 10.1002/art.37776

Simonini, G., Druce, K., Cimaz, R., Macfarlane, G. J., and Jones, G. T. (2014). Current evidence of anti-tumor necrosis factor α treatment efficacy in childhood chronic uveitis: a systematic review and meta-analysis approach of individual drugs. *Arthritis Care Res. (Hoboken).* 66, 1073–1084. doi: 10.1002/acr.22214

Simonini, G., Cimaz, R., Jones, G. T., and Macfarlane, G. J. (2015). Non-anti-TNF biologic modifier drugs in non-infectious refractory chronic uveitis: The current evidence from a systematic review. *Semin. Arthritis Rheumatol.* 45, 238–250. doi: 10.1016/j.semarthrit.2015.05.006

Sood, A. B., and Angeles-Han, S. T. (2017). An Update on Treatment of Pediatric Chronic Non-Infectious Uveitis. *Curr. Treat. Opt Rheumatol.* 3, 1–16. doi: 10.1007/s40674-017-0057-z

Suhler, E. B., Smith, J. R., Wertheim, M. S., Lauer, A. K., Kurz, D. E., Pickard, T. D., et al. (2005). A prospective trial of infliximab therapy for refractory uveitis: preliminary safety and efficacy outcomes. *Arch. Ophthalmol.* 123, 903–912. doi: 10.1001/archopht.123.7.903

Suhler, E. B., Adán, A., Brézin, A. P., Fortin, E., Goto, H., Jaffe, G. J., et al. (2018). Safety and Efficacy of Adalimumab in Patients with Noninfectious Uveitis in an Ongoing Open-Label Study: VISUAL III. *Ophthalmology.* 125, 1075–1087. doi: 10.1016/j.ophtha.2017.12.039

Sukumaran, S., Marzan, K., Shaham, B., and Reiff, A. (2012). High dose infliximab in the treatment of refractory uveitis: does dose matter. *ISRN Rheumatol.* 2012, 765380. doi: 10.5402/2012/765380

Thorne, J. E., Skup, M., Tundia, N., Macaulay, D., Revol, C., Chao, J., et al. (2016). Direct and indirect resource use, healthcare costs and work force absence in patients with non-infectious intermediate, posterior or panuveitis. *Acta Ophthalmol.* 94, e331–e339. doi: 10.1111/aos.12987

Tosi, G. M., Sota, J., Vitale, A., Rigante, D., Emmi, G., Lopalco, G., et al. (2019). Efficacy and safety of certolizumab pegol and golimumab in the treatment of non-infectious uveitis. *Clin. Exp. Rheumatol.* 37, 680–683.

Touhami, S., Diwo, E., Sève, P., Trad, S., Bielefeld, P., Sène, D., et al. (2019). Expert opinion on the use of biological therapy in non-infectious uveitis. *Expert Opin. Biol. Ther.* 19, 477–490. doi: 10.1080/14712598.2019.1595578

Trivedi, A., and Katelaris, C. (2018). The Use of Biologic Agents in the Management of Uveitis. *Intern Med. J.* 49, 1352–1363. doi: 10.1111/imj.14215

Tynjälä, P., Lindahl, P., Honkanen, V., Lahdenne, P., and Kotaniemi, K. (2007). Infliximab and etanercept in the treatment of chronic uveitis associated with refractory juvenile idiopathic arthritis. *Ann. Rheum. Dis.* 66, 548–550. doi: 10.1136/ard.2006.058248

Vallet, H., Seve, P., Biard, L., Baptiste Fraison, J., Bielefeld, P., Perard, L., et al. (2016). Infliximab Versus Adalimumab in the Treatment of Refractory Inflammatory Uveitis: A Multicenter Study From the French Uveitis Network. *Arthritis Rheumatol.* 68, 1522–1530. doi: 10.1002/art.39667

Conflict of Interest: The authors declare that the research was conducted in the absence of any commercial or financial relationships that could be construed as a potential conflict of interest.

frontiers in Pharmacology

ORIGINAL RESEARCH
published: 08 May 2020
doi: 10.3389/fphar.2020.00566

Magnesium Salt, a Simple Strategy to Improve Methadone Analgesia in Chronic Pain: An Isobolographic Preclinical Study in Neuropathic Mice

Valeria González[1], *Teresa Pelissier*[1], *Victoria Cazanga*[1], *Alejandro Hernández*[1] *and Luis Constandil*[1,2]*

[1] Laboratory of Neurobiology, Department of Biology, Faculty of Chemistry and Biology, University of Santiago of Chile, Santiago, Chile, [2] Center for the Development of Nanoscience and Nanotechnology (CEDENNA), Santiago, Chile

OPEN ACCESS

Edited by:
Gonzalo E. Yevenes, University of Concepcion, Chile

Reviewed by:
Hugo F. Miranda, University of Chile, Chile
Luis Gandía, Autonomous University of Madrid, Spain

***Correspondence:**
Luis Constandil
luis.constandil@usach.cl

Specialty section:
This article was submitted to Neuropharmacology, a section of the journal Frontiers in Pharmacology

Received: *19 November 2019*
Accepted: *14 April 2020*
Published: *08 May 2020*

Citation:
González V, Pelissier T, Cazanga V, Hernández A and Constandil L (2020) Magnesium Salt, a Simple Strategy to Improve Methadone Analgesia in Chronic Pain: An Isobolographic Preclinical Study in Neuropathic Mice. Front. Pharmacol. 11:566. doi: 10.3389/fphar.2020.00566

Analgesic efficacy of methadone in cancer and chronic non-cancer pains is greater than that of other opioids, probably because of its unique pharmacokinetics properties and also because it targets glutamatergic receptors in addition to μ-opioid receptors. However, methadone has drawbacks which are clearly related to dosing and treatment duration. The authors hypothesized that the antinociceptive efficacy of methadone could be synergistically potentiated by magnesium and copper salts in a preclinical mouse model of chronic pain, using the intraplantar formalin test as algesimetric tool. The spared nerve injury mice model was used to generate mononeuropathy. A low dose (0.25%) formalin was injected in the neuropathic limb in order to give rise only to Phase I response, resulting from direct activation by formalin of nociceptive primary afferents. Licking/biting of the formalin-injected limb was evaluated as nociceptive behavior during a 35-min observation period. Dose-response curves for intraperitoneal magnesium sulfate (10, 30, 100, and 300 mg/kg i.p.), copper sulfate (0.1, 0.3, 1, and 3 mg/kg i.p.) and methadone (0.1, 0.3, 1, and 3 mg/kg i.p.) allowed to combine them in equieffective doses and to determine their interaction by isobolographic analysis. Magnesium sulfate, copper sulfate and methadone dose-dependently decreased the nociceptive response evoked by formalin injection, the respective ED_{50} being 76.38, 1.18, and 0.50 mg/kg i.p. Isobolographic analysis showed a superadditive interaction for magnesium and methadone. Indeed, despite that both ED_{50} are obviously equieffective, the ED_{50} for the MgSO4/methadone combination contained less than one third of the methadone having the ED_{50} for methadone alone. For the $CuSO_4$/methadone combination, the interaction was only additive. Extrapolated to clinical settings, the results suggest that magnesium salts might be used to improve synergistically the efficacy of methadone in neuropathy, which would allow to reduce the dose of methadone and its associated side effects.

Keywords: neuropathic pain, magnesium, isobolographic study, methadone, pain treatment

INTRODUCTION

Among the variety of opioid drugs currently used to manage cancer and chronic non-cancer pains, methadone is well positioned because: (i) methadone has no known active metabolites, it is well absorbed by oral and rectal routes, suffers less first pass metabolization and has a lesser interindividual variation in bioavailability than oral morphine (Gourlay et al., 1986); (ii) analgesic efficacy during chronic dosing is greater (Davis and Walsh, 2001) and opioid escalation is lesser (Mercadante et al., 1998) in patients treated with methadone than those treated with morphine; (iii) methadone displays antagonistic properties at the *N*-methyl-D-aspartate (NMDA) receptor (Ebert et al., 1995; Gorman et al., 1997), which is known to be involved in chronic pain; and (iv) methadone acts as an inhibitor of 5-hydroxytryptamine and norepinephrine uptake (Codd et al., 1995), a mechanism classically associated to pain control by tricyclic antidepressants, particularly important in the case of neuropathic pain.

Nevertheless, besides to those adverse effects that are common for all opioids (i.e., addiction, sedation, nausea, and respiratory depression), methadone has some drawbacks. First, its long and variable half-life can lead to accumulation and associated side effects in some patients, such as respiratory arrest in patients without prior opioid treatment and in those with a history of sleep apnea, severe asthma or respiratory failure (Bruera and Sweeney, 2002; Brown et al., 2004). Second, methadone interacts with other drugs that inhibit or activate the cytochrome P450 system, which is involved in the methadone metabolism (Iribarne et al., 1996; Herrlin et al., 2000). Third, weight gain (Dyer and White, 1997) and sexual dysfunction (Spring et al., 1992) are commonly reported among patients on methadone maintenance. Although these drawbacks may discourage the use of methadone for chronic non-cancer pain, therapeutic methadone use has increased 167.0% from 2000 to 2014 globally and 205.2% in the United States (Manchikanti et al., 2018). The drawbacks of chronic methadone administration are clearly related to dosing and treatment duration both for cancer (McPherson et al., 2018) and non-cancer (Els et al., 2017) pain. Consequently, the possibility of enhancing the analgesic effect of methadone (and therefore of reducing its dose) by combining it with other non-opioid antinociceptive drugs could significantly help to reduce the side effects and risks associated with the therapeutic use of this drug. Combination of methadone with tricyclic antidepressants (Banks et al., 2010; Schreiber et al., 2014), methylphenidate (Schreiber et al., 2017), delta9-tetrahydrocannabinol (Cichewicz et al., 1999) and ketamine (Pelissier et al., 2003) have already been reported, but almost in acute preclinical pain models. Methadone/ketamine (de Godoy et al., 2013) and methadone/ibuprofen (Ferrer-Brechner and Ganz, 1984) combinations have been used as antinociceptive agents in the clinic, but controlled studies reported that ketamine alone is more effective than the methadone/ketamine combination (Rigo et al., 2017) and that at the long-term nonsteroidal anti-inflammatory drugs (NSAIDs) can result in increased risk of gastrointestinal and cardiovascular side-effects (Wehling, 2014; Ho et al., 2018).

Here, we propose to study whether the antinociceptive efficacy of methadone could be potentiated by magnesium and copper salts in a preclinical model of chronic pain. Magnesium ions are coactivators of the activity of many enzymes and regulate the conductance of the NMDA receptor channel in the central nervous system (Swaminathan, 2003; Seo and Park, 2008), which play a crucial role in the mechanisms of chronic pain. Clinical trials showed that systemic Mg^{2+}, used as adjuvant medication of opioids (mostly morphine, but also fentanyl and tramadol), significantly reduced opioid consumption in acute intraoperative and post-operative pain complaints (Bujalska-Zadrożny et al., 2017), but no similar data exist regarding chronic pain syndromes (Kreutzwiser and Tawfic, 2019). On the other hand, copper has demonstrated antinociceptive properties against various pain modalities in preclinical studies hot plate, tail flick tests, and in the writhing test (Tamba et al., 2013), formalin test (Cazanga et al., 2018), adjuvant arthritic rat pain model (Okuyama et al., 1987), and that it may enhance the peripheral analgesic effect of fenoprofen (Gumilar et al., 2012)) and the central analgesic effect of ketamine (Cazanga et al., 2018), but copper has not yet been tested as antinociceptive agent in humans *via* systemic route.

Thus, the aim of the present study was to evaluate the antinociceptive effect of magnesium and copper salts in a neuropathic mice model using the intraplantar formalin test, and to examine whether their effects may interact synergistically with methadone-induced antinociception using isobolographic analysis.

MATERIALS AND METHODS

Animals

Naïve outbred CF1 male adult mice weighing 28–33 g were used for the study. Animals were housed 6 per cage and maintained with controlled temperature (21 ± 1°C) and light conditions (12:12 h light-dark cycle, lights on at 7:00 am). In total, one hundred and five mice were used in the experiments. Animals had *ad libitum* access to food and water and were allowed to habituate to the housing facility for one week before the beginning of experiments. The experimental procedure was achieved during the light phase, between 9:00 am and 12:00 am, in a quiet room. The housing conditions and experimental procedures were approved by the Bioethics Committee of the University of Santiago de Chile, and were in agreement with the ethical guidelines published by the International Association for the Study of Pain and with the Guide for the Care and Use of Laboratory Animals of NIH (National Research Council, 2011). To determine the number of required mice in each experimental group, we conducted a sample size power analysis by using the G*Power 3 Software (Faul et al., 2007). All the experimental measurements were performed in blinded condition. Each

mouse was sacrificed at the end of the experiment by a carbon dioxide overdose.

Neuropathy

Neuropathy was induced by using the spared nerve injury mice model proposed by Omori et al. (2009), which is a modification of the spared nerve injury rat model described by Decosterd and Woolf (2000) resulting in early, prolonged, and robust changes in mechanical sensitivity and thermal responsiveness that closely mimic many features of clinical neuropathic pain. In the original rat model of Decosterd and Woolf (2000), two of the three terminal distal branches of the sciatic nerve were axotomized (the tibial and common peroneal nerves), sparing only one (the sural nerve), whereas in the present mice version of the model only the sural nerve was transected, sparing the tibial and common peroneal nerves. Since the sural nerve contains almost no motor fibers (Peyronnard and Charron, 1982; Schmalbruch, 1986), this procedure allowed to generate a neuropathic pain model in mice (Omori et al., 2009) and rats (Bravo et al., 2014) in which the posture and motor functions of the hindpaw are preserved, without affecting the evaluation of pain-like responses of the paw. Briefly, animals were anesthetized with 400 mg/kg i.p. of 7% chloral hydrate solution (w/v) and a skin incision approximately 10 mm long was made in the right hindpaw at the level of sciatic nerve. The subcutaneous tissue was dissected, and the biceps femoris muscle was freed from the pelvic and vertebral heads to expose the sciatic nerve. The nerve path was then followed until its split into three branches: the sural, common peroneal, and tibial nerves. The sural nerve was cut 2 mm from its emergence, and the overlying tissues were sutured in layers. During the following 2 days after surgery, animals were daily given 3 mg/kg s.c. of the analgesic ketoprofen and 5 mg/kg s.c. of the antimicrobial agent enrofloxacin. The neural lesion described above resulted in thermal hyperalgesia of the mouse hindpaw, as measured in the hot-plate test, that persisted for at least 28 days (data not shown).

Drugs

Magnesium sulfate heptahydrate (Fresenius Kabi, Santiago, Chile) and copper sulfate pentahydrate (Winkler, Santiago, Chile) were dissolved in physiological saline (0.9% NaCl) and administered *via* i.p. route, in a volume 0.5 ml. Doses of magnesium sulfate were 10, 30, 100, and 300 mg/kg (four groups of five mice each) and doses of copper sulfate were 0.1, 0.3, 1, and 3 mg/kg (four groups of five mice each). Methadone chlorhydrate (Laboratorio Biosano, Santiago, Chile) was administered i.p. (0.5 ml) at doses of 0.1, 0.3, 1, and 3 mg/kg (four groups of five mice each). Controls groups (five mice) received 0.5 ml of 0.9% NaCl. Thus, each mouse was given only one injection of a determined drug dose or of the solvent used.

Behavioral Assessment: Formalin Test

The intraplantar formalin test was chosen instead mechanical or thermal pain testing, because these later are mostly based on evoked withdrawal responses that do not measure pain itself but the threshold of hyperactive reflexes that accompany pain. To run the formalin test in mice with spared nerve injury, it was used a lower formalin concentration (0.25%) than those regularly utilized for formalin testing in healthy mice (2 to 5%). This low formalin concentration gives rise only to Phase I response (direct activation by formalin of the transient receptor potential ankyrin 1, TRPA1, existing in nociceptive primary afferents) but not to Phase II response (secondary activation of nociceptive primary afferents by molecules released by neighboring injured cells, *via* formalin covalent crosslinks to proteins that disrupt cells membranes) when applied to neuropathic mice (see below in *Results*, and also see Abe et al., 2011), thereby minimizing interaction during pain testing with the neurogenic inflammation process that occurs in most models of experimental neuropathy with peripheral lesion (Meacham et al., 2017). Therefore, with this paradigm of low formalin concentration, the pain response is mostly due to direct nociceptor stimulation, as occurs with mechanical and thermal nociceptive stimuli, but with the advantage of measuring the pain response itself to nociceptor activation and not merely the threshold for eliciting a pain response as usually occurs with mechanical and thermal testing.

The animals were acclimatized in the experimental room 2 h before beginning of experiments. Fifteen min before the behavioral evaluation, mice were given a single injection either of saline (controls), $MgSO_4$ alone, $CuSO_4$ alone, methadone alone, $MgSO_4$ plus methadone, or $CuSO_4$ plus methadone. Behavioral testing was carried out by a researcher who was blind to the particular drug treatment given to each animal. For this, mice were situated into an acrylic cylinder (25 cm high x 25 cm in diameter) enclosed by two mirrors placed perpendicularly to each other. Previous to testing, each mouse was positioned into the cylinder for 10 min to acclimatize and minimize stress. Mice were then gently restrained and 20 µl of 0.25% formalin solution were injected either into the plantar surface of the right hindlimb. The intraplantar formalin test was performed as described by Cazanga et al. (2018). The nociceptive behavior evaluated was the licking/biting of the injected limb and the test was run during a 35-min observation period starting from the time of formalin administration, which was divided into seven blocks of 5-min each. A nociceptive score was determined for each block by measuring the number of seconds that the animals spent the nociceptive behavior (licking/biting the formalin-injected limb).

As it is known (e.g., Zhao et al., 2003), the time course of the nociceptive response to formalin is usually studied by plotting the individual nociceptive scores obtained during the first 10 min following intraplantar formalin injection (the so-called Phase I) and between 10 and 35 min after formalin (the so-called Phase II). Since no Phase II response could be observed with the intraplantar injection of 0.25% formalin (see the time-course of nociceptive scores in **Figures 1** and **2**), in the present study the data was analyzed as compiled for the 35-min total time of observation. By summating the seven individual nociceptive scores (NS) recorded during the total time of observation, a global nociceptive score (ΣNS) was obtained. This was

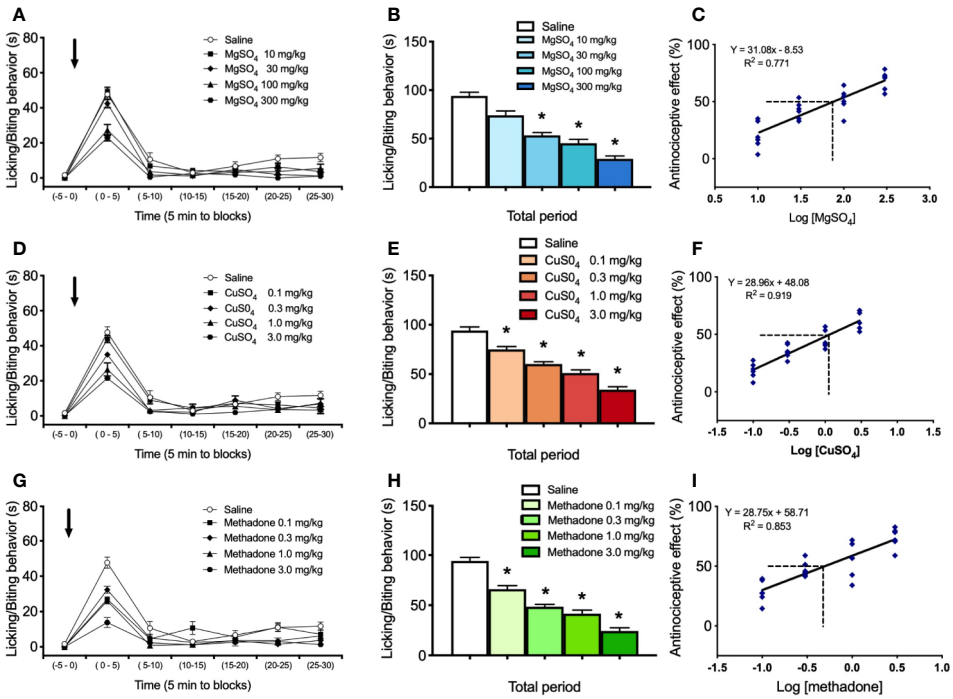

FIGURE 1 | Effect of i.p. administration of saline, $MgSO_4$, $CuSO_4$, or methadone on licking/biting behavior elicited by intraplantar administration of 0.25% formalin in the neuropathic hindlimb of mice. Saline, $MgSO_4$, $CuSO_4$, or methadone were administered as a single i.p. injection 15 min before intraplantar formalin administration. **(A)** Time-course of effects of saline and 10, 30, 100, and 300 mg/kg of $MgSO_4$ in nociceptive response, expressed as seconds spending licking/biting activity. **(B)** Global nociceptive score (∑NS) of licking/biting behavior for Total time of observation in intraplantar formalin test after i.p. administration of saline or increasing doses of $MgSO_4$. **(C)** Dose-response data representing the antinociceptive effect (%) of $MgSO_4$, expressed as dose logarithm. The ED_{50} was calculated from the regression line and is shown with segmented line. **(D)** Time-course of effects of saline and 0.1, 0.3, 1, and 3 mg/kg of $CuSO_4$ in nociceptive response, expressed as seconds spending licking/biting activity. **(E)** Global nociceptive score (∑NS) of licking/biting behavior for Total time of observation in intraplantar formalin test after i.p. administration of saline or increasing doses of $CuSO_4$. **(F)** Dose-response data representing the antinociceptive effect (%) of $CuSO_4$, expressed as dose logarithm. The ED_{50} was calculated from the regression line and is shown with segmented line. **(G)** Time-course of effects of saline and 0.1, 0.3, 1, and 3 mg/kg of methadone in nociceptive response, expressed as seconds spending licking/biting activity. **(H)** Global nociceptive score (∑NS) of licking/biting behavior for Total time of observation in intraplantar formalin test after i.p. administration of saline or increasing doses of methadone. **(I)** Dose-response data representing the antinociceptive effect (%) of methadone, expressed as dose logarithm. The ED_{50} was calculated from the regression line and is shown with segmented line. For **(A, D, G)**: Arrows indicate formalin injection. For **(B, E, H)**: Each bar represents the mean ± SEM of 5 independent determinations. Intergroup statistics were compared by One-way ANOVA followed by Bonferroni's multiple comparison *post hoc* test (*$p < 0.01$). For **(C, F, I)**: The equation for linear regression and the goodness of fit (R^2) are shown in each graph.

subsequently used to calculate the antinociceptive effect of each dose of drug, as:

$$\text{Antinociceptive effect (\%)} = [(\Sigma\text{NSsaline} - \Sigma\text{NSdrug})/\Sigma\text{NSsaline}] \times 100$$

where ∑NSsaline is the algebraic sum of the scores under saline and ∑NSdrug is the algebraic sum of the scores under drug. Plotting the Antinociceptive effect (%) against log dose allowed for obtaining the ED_{50} (effective dose that produce the 50% of the maximal effect) by linear regression analysis.

Isobolographic Analysis

Evaluation of the interactions of $MgSO_4$ and $CuSO_4$ with methadone was performed by using isobolographic analysis (Tallarida, 2000; Tallarida, 2006). The isobologram is a graphic method that involves calculating the theoretical additive dose for each level of effect and their statistical comparison with the combination dose that causes the same effect experimentally. Equieffective doses of the drugs alone are necessary to calculate the expected dose in a combination. To this end, for each drug we defined the dose that produces 50% of maximal effect (ED_{50}) by using a linear regression analysis from the dose-response curve of four increasing doses of $MgSO_4$, $CuSO_4$, or methadone, as stated above. Once the ED_{50} of each of the three drugs was obtained, a graph was constructed by placing in the x-axis the ED_{50} of $MgSO_4$ or that of $CuSO_4$, and on the y-axis the ED_{50} of methadone. The union of the two points by a straight line (isobole), also known as line of additivity, allowed establishing the expected theoretical additivity ED50 of each ion salt with methadone in the middle of the isobole. Then, a dose–response curve for the co-administration of $MgSO_4$ with methadone (four groups of five mice each) or CuSO4 with methadone (four groups of five mice each) was carried out, by administering the combination in fixed ratios of 1/2, 1/4, 1/8,

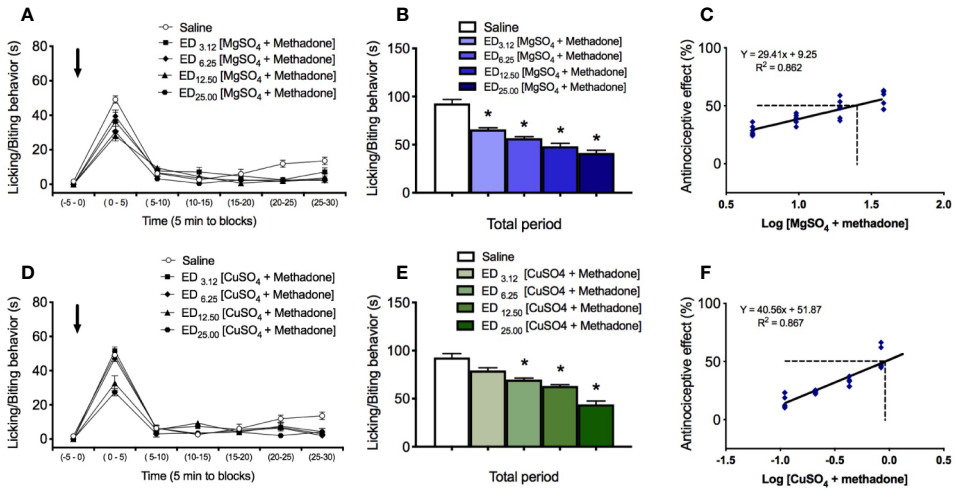

FIGURE 2 | Effect of i.p. administration of saline and of the combinations of either magnesium sulfate or copper sulfate with methadone, on licking/biting behavior elicited by intraplantar administration of 0.25% formalin in the neuropathic hindlimb of mice. Saline and combinations $MgSO_4$/methadone or $CuSO_4$/methadone, were administered as a single i.p. injection 15 min before intraplantar formalin administration. **(A)** Time course of effects of saline and $MgSO_4$/methadone combinations administered in fixed ratios of 1/2, 1/4, 1/8, and 1/16 of their respective ED_{50}, expressed as seconds spending licking/biting activity. **(B)** Global nociceptive score (∑NS) of licking/biting behavior for Total time of observation in intraplantar formalin test after i.p. administration of saline or increasing equieffective doses of $MgSO_4$/ketamine combination. **(C)** Dose-response data representing the antinociceptive effect (%) of $MgSO_4$/methadone combination, expressed as dose logarithm. The respective ED_{50} were calculated from the regression lines and are shown in each figure with segmented line. **(D)** Time course of effects of saline and $CuSO_4$/methadone combinations administered in fixed ratios of 1/2, 1/4, 1/8, and 1/16 of their respective ED_{50}, expressed as seconds spending licking/biting activity. **(E)** Global nociceptive score (∑NS) of licking/biting behavior for Total time of observation in intraplantar formalin test after i.p. administration of saline or increasing equieffective doses of $CuSO_4$/ketamine combination. **(F)** Dose-response data representing the antinociceptive effect (%) of $CuSO_4$/methadone combination, expressed as dose logarithm. The respective ED_{50} were calculated from the regression lines and are shown in each figure with segmented line. For **(A, D)**: Arrows indicate formalin injection. For **(B, E)**: Each bar represents the mean ± SEM of five independent determinations. Intergroup statistics were compared by One-way ANOVA followed by Bonferroni's multiple comparison *post hoc* test (*$p < 0.01$). For **(C, F)**: The equation for linear regression and the goodness of fit (R^2) are shown in each graph.

and 1/16 of their respective ED_{50}. Each combination of each ion salt with methadone was administered as a single i.p. injection, 15 min before the intraplantar formalin injection. The relation between the experimental value (experimental ED_{50}) of the combination with to the theoretical value (theoretical additivity ED_{50}) determines the type of interaction: if the value is located under the line of additivity and it is statistically different from the theoretical value, the interaction is synergistic or superadditive (effect greater than the sum of the individual effects of drugs); if it is not statistically different from the theoretical value, the interaction is simple additivity (equal effect than the sum of each drug); conversely, if the experimental value is located above the line of additivity and is statistically different from the theoretical value, it is a subadditive or antagonistic interaction. This relation can be calculated by the interaction index (γ = experimental ED_{50}/theoretical additive ED_{50}) between the drugs tested. This index, when smaller than 1 corresponds to a synergistic interaction, when equal to 1 corresponds to an additive interaction, and when greater than 1 is an antagonistic interaction.

Analysis of Results

The results of scores obtained were expressed as means ± S.E.M., while the computed ED_{50} values included the 95% confidence intervals. To characterize the interaction between the drugs studied, an isobolographic analysis was performed using a custom Microsoft Excel macro program based on the method described by Ronald J. Tallarida (2000; 2006; 2016), and the interaction index calculated. The results were examined using Student's *t*-test for unpaired data. To compare the effect of the different doses of each drug or their combinations, the results were examined using one-way analysis of variance (ANOVA) followed by the Bonferroni *post hoc* multiple comparisons test. The statistical analyses were made by using Prism 7.0 Software (GraphPad Software Inc, San Diego, CA). Significance was accepted at an alpha level of 0.05.

RESULTS

Antinociceptive Effect of Magnesium Sulfate, Copper Sulfate, and Methadone in Neuropathic Mice

Intraplantar administration of 0.25% formalin in the neuropathic hindpaw of mice under drug-free condition (saline controls) induced a score of nociceptive licking/biting behavior amounting to 91.9 ± 4.1 s for the total time of observation (n=5; **Figure 1B**). Administration of magnesium sulfate i.p. induced a dose-dependent reduction of the nociceptive response induced by 0.25% formalin (**Figure 1A**). Indeed, the licking/biting behavior

scores amounted to 74.0 ± 5.8 s, 55.8 ± 3.7 s, 45.6 ± 4.6 s, and 32.1 ± 3.5 s, for doses of 10, 30, 100, and 300 mg/kg of $MgSO_4$, respectively (n=5 for each group; **Figure 1B**), all the nociceptive scores being significantly lower to that obtained after saline administration (*$p < 0.01$). The calculated value of ED_{50} for $MgSO_4$ was 76.38 mg/kg with a 95% confidence interval (95% CI) of 55.21 mg/kg to 105.66 mg/kg (**Figure 1C**).

Administration of copper sulfate i.p. dose-dependently reduced the formalin-induced nociceptive response (**Figure 1D**), the licking/biting behavior scores amounting to 75.1 ± 3.7 s, 59.8 ± 3.3 s, 49.6 ± 4.1 s, and 34.1 ± 3.4 s, for doses of 0.1, 0.3, 1, and 3 mg/kg of $CuSO_4$, respectively (n=5 for each group; **Figure 1E**). All these nociceptive scores were significantly lower to that obtained after saline administration (*$p < 0.01$). The calculated ED_{50} for $CuSO_4$ was 1.18 mg/kg with a 95% CI of 0.98 mg/kg to 1.42 mg/kg (**Figure 1F**).

Methadone i.p. administration induced a dose-dependent reduction of the nociceptive licking/biting scores induced by formalin administration (**Figure 1G**). Nociceptive scores were 67.4 ± 4.9 s, 49.0 ± 2.6 s, 41.2 ± 4.2 s, and 25.2 ± 3.2 s, for doses of 0.3, 1, 1, and 3 mg/kg of methadone, respectively (n=5 for each group; **Figure 1H**). All doses of methadone produced significantly lower nociceptive scores compared to saline (*$p < 0.01$). The ED_{50} value for methadone was 0.50 mg/kg with a 95% confidence interval (95% CI) of 0.33 mg/kg to 0.75 mg/kg (**Figure 1I**).

Antinociceptive Effect of the Combinations of Either Magnesium Sulfate or Copper Sulfate With Methadone in Neuropathic Mice

The administration of the combination of magnesium sulfate and methadone, in equieffective proportions of their respective ED_{50}, induced a dose-dependent reduction of the rubbing/scratching behavior scores in the intraplantar formalin test (**Figure 2A**). For the total period of observation after formalin injection, association of $MgSO_4$ and methadone administered in fixed ratios of 1/2, 1/4, 1/8, and 1/16 of their respective ED_{50}, produced nociceptive licking/biting scores of 67.1 ± 2.8 s, 58.2 ± 2.6 s, 47.6 ± 3.3 s, and 38.0 ± 3.8 s, respectively (n=5 for each group; **Figure 2B**). All these nociceptive scores were significantly lower than the obtained under saline administration (*$p < 0.001$). The experimental ED_{50} for the $MgSO_4$/methadone association was 24.29 mg/kg (with 95% CI from 18.20 mg/kg to 32.41 mg/kg, **Figure 2C**), which can be decomposed in 24.13 mg/kg $MgSO_4$ plus 0.16 mg/kg methadone. Isobolographic analysis for the administration of $MgSO_4$/methadone combination showed that the experimental ED_{50} was significantly lower than the theoretical additive ED_{50} ($p < 0.05$, two-tailed Student's *t*-test), with an interaction index $\gamma = 0.632$, which means a superadditive effect (**Figure 3A**).

The administration of the combination of copper sulfate and methadone, in fixed ratios of 1/2, 1/4, 1/8, and 1/16 of their respective ED_{50}, produced nociceptive licking/biting scores of 67.1 ± 4.8 s, 58.2 ± 3.6 s, 47.6 ± 3.3 s, and 38.0 ± 4.8 s, respectively (n=5 for each group; **Figure 2E**). The three higher doses of combined copper sulfate and methadone administered led to significantly lower nociceptive scores, compared to saline administration (*$p < 0.01$), and the calculated experimental ED_{50} for the $CuSO_4$/methadone association was 0.90 mg/kg (with 95% CI from 0.68 mg/kg to 1.32 mg/kg, **Figure 2F**), which can be decomposed in 0.63 mg/kg $CuSO_4$ plus 0.27 mg/kg methadone. Isobolographic analysis for the administration of $MgSO_4$/methadone combination showed that the experimental ED_{50} did not significantly differ from the theoretical additive ED_{50} (two-tailed Student's *t*-test), with an interaction index $\gamma = 1.148$, which means simple additivity (**Figure 3B**).

DISCUSSION

The present results showed that both magnesium sulfate and copper sulfate produced dose-dependent antinociceptive effects in the intraplantar formalin test. This is in agreement with

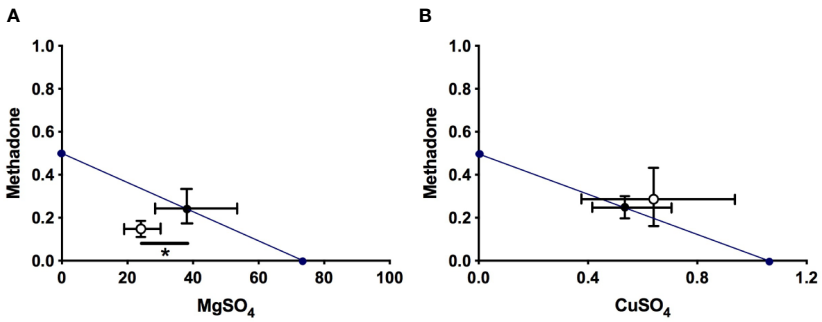

FIGURE 3 | Isobolograms of interaction for $MgSO_4$/methadone **(A)** and $CuSO_4$/methadone **(B)** combinations in neuropathic mice, for total observation period in the intraplantar formalin test. The black circle on the straight line represents the point of theoretical additivity of the combination, whereas the white circle corresponds to the experimental point. In **(A)**: The experimental point was significantly different from the theoretical point (mean ± SEM; *$p < 0.05$, two-tailed Student *t* test), indicating superadditive interaction. The standard errors for $MgSO_4$ and methadone are resolved into $MgSO_4$ (abscissa scale) and methadone (ordinate scale) components and shown by horizontal and vertical bars, respectively. In **(B)**: The experimental point was not significantly different from the theoretical point (mean ± SEM; not significant, two-tailed Student *t* test), indicating an additive interaction of both drugs. The standard errors for $CuSO_4$ and methadone are resolved into $CuSO_4$ (abscissa scale) and methadone (ordinate scale) components and shown by horizontal and vertical bars, respectively.

expectations since magnesium and copper salts have been found to induce dose-dependent antinociception in the hot-plate, tail-flick, and writhing tests (Tamba et al., 2013). Besides, the antinociceptive effects showed by magnesium and copper ions also coincide with those obtained in other studies using formalin-induced pain, where systemic magnesium improved the antinociceptive effect of ketamine (Vujović et al., 2017) and copper-NSAIDs complexes exhibited higher antinociceptive effect than NSAIDs alone (Gumilar et al., 2012). The foregoing results also showed that the $MgSO_4$/methadone and $CuSO_4$/methadone combinations produced higher antinociception than methadone alone, an opiate agonist that has proven to be effective in thermal and mechanical pain models (Lemberg et al., 2006), as well as in chemonociception (Miranda et al., 2014) and different models of neuropathic pain (Erichsen et al., 2005).

The main and most important result of the present study was that $MgSO_4$ and methadone interacted synergistically in the intraplantar formalin pain model, which means that there was a potentiation of the antinociceptive effect of the drugs when given in combination. In fact, the ED_{50} of methadone alone was 0.50 mg/kg while the equieffective dose of the $MgSO_4$/methadone combination only contained 0.16 mg/kg methadone, which means that the addition of $MgSO_4$ allowed the methadone content of the dose to be reduced to less than one third. If extrapolated to humans, this might be an important finding because the side-effects of methadone in clinical settings are related to dosing and treatment duration, both for cancer (McPherson et al., 2018) and non-cancer (Els et al., 2017) pains. Indeed, according to the guidelines from the American Pain Society (Chou et al., 2014) and from the experts group of the Hospice and Palliative Care (McPherson, 2016), rotation to methadone of opioid-tolerant patients with cancer pain should be based on dose calculations, as exact opioid/methadone ratios. The same apply to chronic non-cancer pain, where the risk for addiction increases with increasing opioid doses (Huffman et al., 2015), and sleep-disordered breathing and respiratory depression may result in opioid-associated deaths demonstrating a clear relationship to dose (Walker et al., 2007; Jungquist et al., 2012).

It seems worth to remark that the superadditive interaction between $MgSO_4$ and methadone, detected by isobolographic analysis upon intraplantar formalin testing, originated from parallel regression lines obtained in the dose-response plots of the individual drugs, meaning that the potency ratio for these two drugs remained constant during testing of formalin-induced pain in neuropathic rats (Tallarida, 2000; Tallarida, 2006; Tallarida, 2016). Theoretically, superadditivity in the effect of two simultaneously administered antinociceptive drugs implies that the combined molecules act on anatomically and/or functionally different substrates for nociceptive processing, which may represent different neurons, different receptors in the same neuron, or even different sites of binding in the same receptor. In this regard, it is well known that magnesium induce antinociception by antagonistic binding to NMDA receptors (Traynelis et al., 2010), while the antinociceptive effect of methadone can be explained by both agonism at μ opiate receptors and antagonism on NMDA receptors (Gorman et al., 1997).

Methadone is a potent inhibitor of [^{3}H]MK-801 binding, a specific uncompetitive NMDA receptor antagonist, with a K_i of 0.85 ± 0.31 μM (Ebert et al., 1995). Gorman et al. (1997) reported moderate affinity, but still in the low μM range, for the displacement of [^{3}H]MK-801 by *l*-, *d*-, and *dl*-methadone (K_i of 3.4 ± 0.3, 7.4 ± 1.2, and 8.3 ± 1.2, respectively) from non-competitive NMDA receptor sites in the rat forebrain. More recently, Matsui and Williams (2010) showed that the NMDA current induced by iontophoretic application of L-aspartate in locus coeruleus neurons was dose-dependently inhibited by *l/d* methadone with an IC50 value for *l/d*-methadone of 3.5 ± 0.3 μM, which was statistically similar to the IC50 of *d*-and *l*-methadone enantiomers. Since methadone blocked the inward but not the outward current in the NMDA channel, it can be concluded that, in addition to μ-opioid receptor binding, at low μM concentration methadone could act as a non stereoselective, uncompetitive, voltage-dependent pore blocker of the NMDA receptor. Despite that the $MgSO_4$/methadone combination reported here was synergistic, it seems apparent that the effects of Mg^{2+} and methadone were redundant at the NMDA receptor, because both magnesium ions (Traynelis et al., 2010) and methadone (Gorman et al., 1997; Matsui and Williams, 2010) are open channel blockers that act as voltage-dependent uncompetitive NMDA receptor antagonists in the same site of the NMDA channel. In such a case, one drug substitutes for the other and only additivity should be expected when the two drugs are given simultaneously. Thus, it is likely that the synergy of the $MgSO_4$/methadone combination reported here arose from the interaction between the blocking properties of magnesium ions in the NMDA receptor channels and the agonistic properties of methadone in μ opioid receptors. With regard to this, it has been reported that binding of opioid agonists and antagonists in brain homogenates is allosterically promoted by Mg^{2+} in a concentration-dependent manner (Rodriguez et al., 1992), which could be at the base of the synergistic effect of magnesium on methadone-induced antinociception. A rather similar synergistic interaction between methadone and ketamine in neuropathic rats has previously been reported (Pelissier et al., 2003), but the translational potential of such a combination is likely to be impaired by the well-known undesirable psychomimetic effects of ketamine (Persson, 2013). In contrast, magnesium is cheap and well tolerated by oral route, as children have been safely treated from chronic constipation with 2 ml/kg daily of milk of magnesia, i.e., 160 mg magnesium hydroxide/kg/day (Loening-Baucke and Pashankar, 2006).

As it is known, subcutaneously injected formalin into the mouse paw gives rise to phase I response by direct activation of nociceptive primary afferents *via* TRPA1 channels (McNamara et al., 2007), and to phase II response (or inflammatory phase) corresponding to a secondary activation of nociceptive primary afferents by histamine, bradykinin, cytokines, and substance P, among others mediators released by inflammatory cells (Zouikr et al., 2015). Various forms of experimental neuropathy induced by peripheral injury (Kingery et al., 1999; Botz et al., 2013; Gallo et al., 2017) have

been associated to neurogenic inflammation, eliciting the release of substance P, calcitonin gene-related peptide, neurokinin A, endothelin-3, cytokines, among others cellular mediators of inflammation. Since both formalin administration and the neuropathic process upregulate rather similar inflammatory mediators, this makes difficult the interpretation of nociceptive data during phase II response. Therefore, we utilized a paradigm of low formalin concentration, as proposed by Abe et al., 2011, where only phase I pain response can be observed.

Unlike the superadditive interaction between magnesium salt and methadone, copper ions give rise only to an additive effect in the intraplantar formalin test when administered together with methadone. This different interaction, obtained through isobologram analysis of data, could be related to the already reported different mode of binding of Cu^{2+} on NMDA channels, where copper acts as a high-affinity NMDA receptor antagonist characterized by a voltage-independent mechanism of action (Herrlin et al., 2000).

Although it remains yet uncertain the mechanism underlying the ability of magnesium sulfate to exert a synergistic action upon the methadone antinociceptive effect, this issue could constitute a potential basis for future clinical applications addressed to lower methadone dosing together with a lowering of its side-effects. As pointed out elsewhere (Erichsen et al., 2005), it is not possible to determine synergism in humans due to scientific, practical and ethical reasons, and thus prior to testing drug interaction in clinical trials, studies on preclinical drug combinations should be carried out in animals to obtain the basis and rationale for further studies in humans. Among opioids, methadone should be well positioned for treat neuropathic pain because of its unique ability to target NMDA receptors in addition to its well-known effect on μ opioid receptors. However, therapeutic guidelines relegate strong opioids, including methadone, to third-line therapy in neuropathic pain mainly because of safety concerns (Finnerup et al., 2015). Drug combination strategies aimed to reduce methadone dosing—and therefore its side-effects—could be a promising therapeutic approach to optimize opioid analgesia under neuropathic pain conditions, provided the drug co-administered with methadone does not give rise to important side-effects by its own. To this end, magnesium salts probably represent the best alternative, since the European Food Safety Authority (EFSA) of the European Union states that the upper limit for magnesium (i.e., the daily dose that does not produce any observable adverse effect in healthy adult humans) is as high as 350 mg, while toxic hypermagnesemia is only seen at oral doses greater than 2500 mg daily (Scientific Committee on Food, Scientific Panel on Dietetic Products, Nutrition and Allergies, 2006). Although further studies are necessary to examine in detail the mechanism underlying the synergistic interaction between magnesium ions and methadone, it can be concluded that this association could represent a potential therapeutic strategy aimed to treat some forms of chronic pain in humans, which deserves more investigation in clinical settings.

DATA AVAILABILITY STATEMENT

The datasets generated for this study are available on request to the corresponding author.

ETHICS STATEMENT

The animal study was reviewed and approved by Bioethics Committee of the University of Santiago de Chile.

AUTHOR CONTRIBUTIONS

TP and LC provided ideas or concepts for definition of intellectual context, particularly designed and performed the experiments. VG, VC, and TP performed research. AH, TP, and LC contributed new reagents/analytic tools. VG, AH, TP, and LC analyzed data. AH and LC wrote the paper. All authors of this paper have read and approved the final version of the manuscript.

FUNDING

This work was supported by the Fondecyt Project (grant 1181622) and the Centers of Excellence with Basal/Conicyt financing, CEDENNA (grant AFB180001).

ACKNOWLEDGMENTS

We thank Ms. Cristina Arenas and Mr José López for technical support and animal care.

REFERENCES

Abe, K., Fujii, Y., and Nojima, H. (2011). Evaluation of hyperalgesia in spared nerve injury model using mechanical, thermal, and chemical stimuli in the mouse. *Neurol. Res.* 33, 656–662. doi: 10.1179/1743132810Y.0000000019

Banks, M. L., Rice, K. C., and Negus, S. S. (2010). Antinociceptive interactions between mu-opioid receptor agonists and the serotonin uptake inhibitor clomipramine in rhesus monkeys: role of mu agonist efficacy. *J. Pharmacol. Exp. Ther.* 335, 497–505. doi: 10.1124/jpet.110.169276

Botz, B., Imreh, A., Sándor, K., Elekes, K., Szolcsányi, J., Reglődi, D., et al. (2013). Role of Pituitary Adenylate-Cyclase Activating Polypeptide and Tac1 gene derived tachykinins in sensory, motor and vascular functions under normal and neuropathic conditions. *Peptides* 43, 105–112. doi: 10.1016/j.peptides.2013.03.003

Bravo, D., Ibarra, P., Retamal, J., Pelissier, T., Laurido, C., Hernandez, A., et al. (2014). Pannexin 1: a novel participant in neuropathic pain signaling in the rat spinal cord. *Pain* 155, 2108–2115. doi: 10.1016/j.pain.2014.07.024

Brown, R., Kraus, C., Fleming, M., and Reddy, S. (2004). Methadone: applied pharmacology and use as adjunctive treatment in chronic pain. *Postgrad. Med. J.* 80, 654–659. doi: 10.1136/pgmj.2004.022988

Bruera, E., and Sweeney, C. (2002). Methadone use in cancer patients with pain: a review. *J. Palliat. Med.* 5, 127–138. doi: 10.1089/10966210252785097

Bujalska-Zadrożny, M., Tatarkiewicz, J., Kulik, K., Filip, M., and Naruszewicz, M. (2017). Magnesium enhances opioid-induced analgesia - What we have learnt in the past decades? *Eur. J. Pharm. Sci.* 99, 113–127. doi: 10.1016/j.ejps.2016.11.020

Cazanga, V., Hernandez, A., Morales, B., Pelissier, T., and Constandil, L. (2018). Antinociception induced by copper salt revisited: Interaction with ketamine in formalin-induced intraplantar and orofacial pain in mice. *J. Oral. Facial Pain Headache* 32, 247–257. doi: 10.11607/ofph.1961

Chou, R., Cruciani, R. A., Fiellin, D. A., Compton, P., Farrar, J. T., Haigney, M. C., et al. (2014). Methadone safety: a clinical practice guideline from the American Pain Society and College of Problems on Drug Dependence, in collaboration with the Heart Rhythm Society. *J. Pain* 15, 321–337. doi: 10.1016/j.jpain.2014.01.494

Cichewicz, D. L., Martin, Z. L., Smith, F. L., and Welch, S. P. (1999). Enhancement mu opioid antinociception by oral Δ^9-tetrahydrocannabinol: dose-response analysis and receptor identification. *J. Pharmacol. Exp. Ther.* 289, 859–867.

Codd, E., Shank, R., Schupsky, J., and Raffa, R. (1995). Serotonin and norepinephrine uptake inhibiting activity of centrally acting analgesics: structural determinants and role in antinociception. *J. Pharmacol. Exp. Ther.* 274, 1263–1270.

Davis, M. P., and Walsh, D. (2001). Methadone for relief of cancer pain: a review of pharmacokinetics, pharmacodynamics, drug interactions and protocols of administration. *Support Care Cancer* 9, 73–83. doi: 10.1007/s005200000180

de Godoy, M. C., Dalmolin, G. D., Rigo, F. K., Rossato, M. F., de Menezes, M. S., Alvarez, M. A., et al. (2013). Management of chronic neuropathic pain of different causes with the combination of oral methadone along with ketamine: A report of 18 cases. *Eur. J. Anaesthesiol.* 30, 638–640. doi: 10.1097/EJA.0b013e32835f9a3b

Decosterd, I., and Woolf, C. J. (2000). Spared nerve injury: an animal model of persistent peripheral neuropathic pain. *Pain* 87, 149–158. doi: 10.1016/s0304-3959(00)00276-1

Dyer, K. R., and White, J. M. (1997). Patterns of symptom complaints in methadone maintenance patients. *Addiction* 92, 1445–1455. doi: 10.1111/j.1360-0443.1997.tb02866.x

Ebert, B., Andersen, S., and Krogsgaard-Larsen, P. (1995). Ketobemidone, methadone and pethidine are non-competitive N-methyl-D-aspartate (NMDA) antagonists in the rat cortex and spinal cord. *Neurosci. Lett.* 187, 165–168. doi: 10.1016/0304-3940(95)11364-3

Els, C., Jackson, T. D., Kunyk, D., Lappi, V. G., Sonnenberg, B., Hagtvedt, R., et al. (2017). Adverse events associated with medium- and long-term use of opioids for chronic non-cancer pain: an overview of Cochrane Reviews. *Cochrane Database Syst. Rev.* 10, CD012509. doi: 10.1002/14651858.CD012509.pub2

Erichsen, H. K., Hao, J. X., Xu, X. J., and Blackburn-Munro, G. (2005). Comparative actions of the opioid analgesics morphine, methadone and codeine in rat models of peripheral and central neuropathic pain. *Pain* 116, 347–358. doi: 10.1016/j.pain.2005.05.004

Faul, F., Erdfelder, E., Lang, A. G., and Buchner, A. (2007). G*Power 3: a flexible statistical power analysis program for the social, behavioral, and biomedical sciences. *Behav. Res. Methods* 39, 175–191. doi: 10.3758/bf03193146

Ferrer-Brechner, T., and Ganz, P. (1984). Combination therapy with ibuprofen and methadone for chronic cancer pain. *Am. J. Med.* 77, 78–83. doi: 10.1016/s0002-9343(84)80023-6

Finnerup, N. B., Attal, N., Haroutounian, S., McNicol, E., Baron, R., Dworkin, R. H., et al. (2015). Pharmacotherapy for neuropathic pain in adults: A systematic review and meta-analysis. *Lancet Neurol.* 14, 162–173. doi: 10.1016/S1474-4422(14)70251-0

Gallo, A., Leerink, M., Michot, B., Ahmed, E., Forget, P., Mouraux, A., et al. (2017). Bilateral tactile hypersensitivity and neuroimmune responses after spared nerve injury in mice lacking vasoactive intestinal peptide. *Exp. Neurol.* 293, 62–73. doi: 10.1016/j.expneurol.2017.03.019

Gorman, A. L., Elliott, K. J., and Inturrisi, C. E. (1997). The d- and l-isomers of methadone bind to the non-competitive site on the N-methyl-D-aspartate (NMDA) receptor in rat forebrain and spinal cord. *Neurosci. Lett.* 223, 5–8. doi: 10.1016/s0304-3940(97)13391-2

Gourlay, G. K., Cherry, D. A., and Cousins, M. J. (1986). A comparative study of the efficacy and pharmacokinetics of oral methadone and morphine in the treatment of severe pain in patients with cancer. *Pain* 25, 297–312. doi: 10.1016/0304-3959(86)90234-4

Gumilar, F., Agotegaray, M., Bras, C., Gandini, N. A., Minetti, A., and Quinzani, O. (2012). Anti-nociceptive activity and toxicity evaluation of Cu(II)-fenoprofenate complexes in mice. *Eur. J. Pharmacol.* 675, 32–39. doi: 10.1016/j.ejphar.2011.11.049

Herrlin, K., Segerdahl, M., Gustafsson, L. L., and Kalso, E. (2000). Methadone, ciprofloxacin, and adverse drug reactions. *Lancet* 356, 2069–2070. doi: 10.1016/S0140-6736(00)03409-7

Ho, K. Y., Gwee, K. A., Cheng, Y. K., Yoon, K. H., Hee, H. T., and Omar, A. R. (2018). Nonsteroidal anti-inflammatory drugs in chronic pain: implications of new data for clinical practice. *J. Pain Res.* 11, 1937–1948. doi: 10.2147/JPR.S168188

Huffman, K. L., Shella, E. R., Sweis, G., Griffith, S. D., Scheman, J., and Covington, E. C. (2015). Nonopioid substance use disorders and opioid dose predict therapeutic opioid addiction. *J. Pain* 16, 126–134. doi: 10.1016/j.jpain.2014.10.011

Iribarne, C., Berthou, F., Baird, S., Dreano, Y., Picart, D., Bail, J. P., et al. (1996). Involvement of cytochrome P450 3A4 enzyme in the N-demethylation of methadone in human liver microsomes. *Chem. Res. Toxicol.* 9, 365–973. doi: 10.1021/tx950116m

Jungquist, C. R., Flannery, M., Perlis, M. L., and Grace, J. T. (2012). Relationship of chronic pain and opioid use with respiratory disturbance during sleep. *Pain Manage. Nurs.* 13, 70–79. doi: 10.1016/j.pmn.2010.04.003

Kingery, W. S., Castellote, J. M., and Maze, M. (1999). Methylprednisolone prevents the development of autotomy and neuropathic edema in rats, but has no effect on nociceptive thresholds. *Pain* 80, 555–566. doi: 10.1016/s0304-3959(98)00251-6

Kreutzwiser, D., and Tawfic, Q. A. (2019). Expanding role of NMDA receptor antagonists in the management of pain. *CNS Drugs* 33, 347–374. doi: 10.1007/s40263-019-00618-2

Lemberg, K., Kontinen, V. K., Viljakka, K., Kylänlahti, I., Yli-Kauhaluoma, J., and Kalso, E. (2006). Morphine, oxycodone, methadone and its enantiomers in different models of nociception in the rat. *Anesth. Analg.* 102, 1768–1774. doi: 10.1213/01.ane.0000205751.88422.41

Loening-Baucke, V., and Pashankar, D. S. (2006). A randomized, prospective, comparison study of polyethylene glycol 3350 without electrolytes and milk of magnesia for children with constipation and fecal incontinence. *Pediatrics* 118, 528–535. doi: 10.1542/peds.2006-0220

Manchikanti, L., Kaye, A. M., Knezevic, N. N., McAnally, H., Slavin, K., Trescot, A. M., et al. (2018). Responsible, safe, and effective prescription of opioids for chronic non-cancer pain: American Society of Interventional Pain Physicians (ASIPP) Guidelines. *Pain Physician* 20 (2S), S3–S92.

Matsui, A., and Williams, J. T. (2010). Activation of μ-opioid receptors and block of Kir3 potassium channels and NMDA receptor conductance by L- and D-methadone in rat locus coeruleus. *Br. J. Pharmacol.* 161, 1403–1413. doi: 10.1111/j.1476-5381.2010.00967.x

McNamara, C. R., Mandel-Brehm, J., Bautista, D. M., Siemens, J., Deranian, K. L., Zhao, M., et al. (2007). TRPA1 mediates formalin-induced pain. *Proc. Natl. Acad. Sci. U.S.A.* 104, 13525–13530. doi: 10.1073/pnas.0705924104

McPherson, M. L., Costantino, R. C., and McPherson, A. L. (2018). Methadone: Maximizing Safety and Efficacy for Pain Control in Patients with Cancer. *Hematol. Oncol. Clin. North Am.* 32, 405–415. doi: 10.1016/j.hoc.2018.01.004

McPherson, M. L. (2016). Methadone safety guidelines for hospice and palliative care. *AAHPM Q.* 17, 8–9. doi: 10.1016/j.jpainsymman.2018.12.001

Meacham, K., Shepherd, A., Mohapatra, D. P., and Haroutounian, S. (2017). Neuropathic pain: Central vs. peripheral mechanisms. *Curr. Pain Headache Rep.* 21, 28–28. doi: 10.1007/s11916-017-0629-5

Mercadante, S., Casuccio, A., Agnello, A., Serretta, R., Calderone, L., and Barresi, L. (1998). Morphine versus methadone in the pain treatment of advanced-cancer patients followed up at home. *J. Clin. Oncol.* 16, 3656–3661. doi: 10.1200/JCO.1998.16.11.3656

Miranda, H. F., Noriega, V., Zanetta, P., Prieto, J. C., Prieto-Rayo, J. C., Aranda, N., et al. (2014). Isobolographic analysis of the opioid-opioid interactions in a tonic and a phasic mouse model of induced nociceptive pain. *J. BioMed. Sci.* 21, 62–62. doi: 10.1186/s12929-014-0062-6

National Research Council (2011). *Guide for the Care, and Use of Laboratory Animals. 8th Edn.* (Washington DC: The National Academies Press).

Okuyama, S., Hashimoto, S., Aihara, H., Willingham, W. M., and Sorenson, J. R. (1987). Copper complexes of nonsteroidal antiinflammatory agents: analgesic activity and possible opioid receptor activation. *Agents Actions* 21, 130–144. doi: 10.1007/bf01974933

Omori, Y., Kagaya, K., Enomoto, R., Sasaki, A., Andoh, T., Nojima, H., et al. (2009). A mouse model of sural nerve injury-induced neuropathy: gabapentin inhibits pain-related behaviors and the hyperactivity of wide-dynamic range neurons in the dorsal horn. *J. Pharmacol. Sci.* 109, 532–539. doi: 10.1254/jphs.08319fp

Pelissier, T., Laurido, C., Kramer, V., Hernández, A., and Paeile, C. (2003). Antinociceptive interactions of ketamine with morphine or methadone in mononeuropathic rats. *Eur. J. Pharmacol.* 477, 23–28. doi: 10.1016/s0014-2999(03)02192-7

Persson, J. (2013). Ketamine in pain management. *CNS Neurosci. Ther.* 19, 396–402. doi: 10.1111/cns.12111

Peyronnard, J. M., and Charron, L. (1982). Motor and sensory neurons of the rat sural nerve: a horseradish peroxidase study. *Muscle Nerve* 5, 654–660. doi: 10.1002/mus.880050811

Rigo, F. K., Trevisan, G., Godoy, M. C., Rossato, M. F., Dalmolin, G. D., Silva, M. A., et al. (2017). Management of neuropathic chronic pain with methadone combined with ketamine: A randomized, double blind, active-controlled clinical trial. *Pain Physician* 20, 207–215.

Rodriguez, F. D., Bardaji, E., and Traynor, J. R. (1992). Differential effects of Mg^{2+} and other divalent cations on the binding of tritiated opioid ligands. *J. Neurochem.* 59, 467–472. doi: 10.1111/j.1471-4159.1992.tb09393.x

Schmalbruch, H. (1986). Fiber composition of the rat sciatic nerve. *Anat. Rec.* 215, 71–81. doi: 10.1002/ar.1092150111

Schreiber, S., Barak, Y., Hostovsky, A., Baratz-Goldstein, R., Volis, I., Rubovitch, V., et al. (2014). Interaction of different antidepressants with acute and chronic methadone in mice, and possible clinical implications. *J. Mol. Neurosci.* 52, 598–604. doi: 10.1007/s12031-013-0115-4

Schreiber, S., Bader, M., Rubovitch, V., and Pick, C. G. (2017). Interaction between methylphenidate, methadone and different antidepressant drugs on antinociception in mice, and possible clinical implications. *World J. Biol. Psychiatry* 18, 300–307. doi: 10.3109/15622975.2015.1086492

Scientific Committee on Food, Scientific Panel on Dietetic Products, Nutrition and Allergies (2006). *Tolerable upper intake levels for vitamins and minerals* (European Food Safety Authority (EFSA), European Union), 107–116.

Seo, J. W., and Park, T. J. (2008). Magnesium metabolism. *Electrolyte Blood Press* 6, 86–95. doi: 10.5049/EBP.2008.6.2.86

Spring, W. D.Jr., Willenbring, M. L., and Maddux, T. L. (1992). Sexual dysfunction and psychological distress in methadone maintenance. *Int. J. Addict.* 27, 1325–1334. doi: 10.3109/10826089209047354

Swaminathan, R. (2003). Magnesium metabolism and its disorders. *Clin. Biochem. Rev.* 24, 47–66.

Tallarida, R. J. (2000). *Drug Synergism and Dose-Effect Data Analysis* (Chapman & Hall/CRC: Boca Raton).

Tallarida, R. J. (2006). An overview of drug combination analysis with isobolograms. *J. Pharmacol. Exp. Ther.* 319, 1–7. doi: 10.1124/jpet.106.104117

Tallarida, R. J. (2016). Drug combinations: Tests and analysis with isoboles. *Curr. Protoc. Pharmacol.* 72, 9.19.1–9.19.9. doi: 10.1002/0471141755.ph0919s72

Tamba, B. I., Leon, M. M., and Petreus, T. (2013). Common trace elements alleviate pain in an experimental mouse model. *J. Neurosci. Res.* 91, 554–561. doi: 10.1002/jnr.23191

Traynelis, S. F., Wollmuth, L. P., McBain, C. J., Menniti, F. S., Vance, K. M., Ogden, K. K., et al. (2010). Glutamate receptor ion channels: structure, regulation, and function. *Pharmacol. Rev.* 62, 405–496. doi: 10.1124/pr.109.002451

Vujović, K. S., Vučković, S., Vasović, D., Medić, B., Knežević, N., and Prostran, M. (2017). Additive and antagonistic antinociceptive interactions between magnesium sulfate and ketamine in the rat formalin test. *Acta Neurobiol. Exp. (Wars)* 77, 137–146. doi: 10.21307/ane-2017-046

Walker, J. M., Farney, R. J., Rhondeau, S. M., Boyle, K. M., Valentine, K., Cloward, T. V., et al. (2007). Chronic opioid use is a risk factor for the development of central sleep apnea and ataxic breathing. *J. Clin. Sleep Med.* 3, 455–461. doi: 10.5664/jcsm.26908

Wehling, M. (2014). Non-steroidal anti-inflammatory drug use in chronic pain conditions with special emphasis on the elderly and patients with relevant comorbidities: management and mitigation of risks and adverse effects. *Eur. J. Clin. Pharmacol.* 70, 1159–1172. doi: 10.1007/s00228-014-1734-6

Zhao, C. S., Tao, Y. X., Tall, J. M., Donovan, D. M., Meyer, R. A., and Raja, S. N. (2003). Role of μ-opioid receptors in formalin-induced pain behavior in mice. *Exp. Neurol.* 184, 839–845. doi: 10.1016/S0014-4886(03)00346-7

Zouikr, I., Ahmed, A. F., Horvat, J. C., Beagley, K. W., Clifton, V. L., Ray, A., et al. (2015). Programming of formalin-induced nociception by neonatal LPS exposure: Maintenance by peripheral and central neuroimmune activity. *Brain Behav. Immun.* 44, 235–246. doi: 10.1016/j.bbi.2014.10.014

Conflict of Interest: The authors declare that the research was conducted in the absence of any commercial or financial relationships that could be construed as a potential conflict of interest.

frontiers in Pharmacology

ORIGINAL RESEARCH
published: 21 May 2020
doi: 10.3389/fphar.2020.00709

Changes in PGC-1α/SIRT1 Signaling Impact on Mitochondrial Homeostasis in Amyloid-Beta Peptide Toxicity Model

*Jessica D. Panes[1], Pamela A. Godoy[1], Tiare Silva-Grecchi[1], María T. Celis[1], Oscar Ramirez-Molina[1], Javiera Gavilan[1], Carola Muñoz-Montecino[2], Patricio A. Castro[2], Gustavo Moraga-Cid[2], Gonzalo E. Yévenes[2], Leonardo Guzmán[2], Jeffrey L. Salisbury[3], Eugenia Trushina[3] and Jorge Fuentealba[1,4]**

[1] Laboratory of Screening of Neuroactive Compound, Physiology Department, Faculty of Biological Sciences, Universidad de Concepción, Concepción, Chile, [2] Physiology Department, Faculty of Biological Sciences, Universidad de Concepción, Concepción, Chile, [3] Neurology Research, Mayo Clinic Foundation, Rochester, MN, United States, [4] Center for Advanced Research on Biomedicine (CIAB-UdeC), Physiology Department, Faculty of Biological Sciences, Universidad de Concepción, Concepción, Chile

OPEN ACCESS

Edited by:
Carlos M. Opazo, University of Melbourne, Australia

Reviewed by:
Darius John Rowland Lane, University of Melbourne, Australia
Nibaldo C. Inestrosa, Pontificia Universidad Católica de Chile, Chile

***Correspondence:**
Jorge Fuentealba
jorgefuentealba@udec.cl

Specialty section:
This article was submitted to Neuropharmacology, a section of the journal Frontiers in Pharmacology

Received: *25 September 2019*
Accepted: *29 April 2020*
Published: *21 May 2020*

Citation:
Panes JD, Godoy PA, Silva-Grecchi T, Celis MT, Ramirez-Molina O, Gavilan J, Muñoz-Montecino C, Castro PA, Moraga-Cid G, Yévenes GE, Guzmán L, Salisbury JL, Trushina E and Fuentealba J (2020) Changes in PGC-1α/SIRT1 Signaling Impact on Mitochondrial Homeostasis in Amyloid-Beta Peptide Toxicity Model. Front. Pharmacol. 11:709. doi: 10.3389/fphar.2020.00709

Alzheimer's disease (AD) is a neurodegenerative disorder characterized by cognitive impairment that increasingly afflicts the elderly population. Soluble oligomers (AβOs) has been implicated in AD pathogenesis: however, the molecular events underlying a role for Aβ are not well understood. We studied the effects of AβOs on mitochondrial function and on key proteins that regulate mitochondrial dynamics and biogenesis in hippocampal neurons and PC-12 cells. We find that AβOs treatment caused a reduction in total Mfn1 after a 2 h exposure (42 ± 11%); while DRP1 increased at 1 and 2 h (205 ± 22% and 198 ± 27%, respectively), correlating to changes in mitochondrial morphology. We also observed that SIRT1 levels were reduced after acute and chronic AβOs treatment (68 ± 7% and 77 ± 6%, respectively); while PGC-1α levels were reduced with the same time treatments (68 ± 8% and 67 ± 7%, respectively). Interestingly, we found that chronic treatment with AβOs increased the levels of pSIRT1 (24 h: 157 ± 18%), and we observed changes in the PGC-1α and p-SIRT1 nucleus/cytosol ratio and SIRT1-PGC-1α interaction pattern after chronic exposure to AβOs. Our data suggest that AβOs induce important changes in the level and localization of mitochondrial proteins related with the loss of mitochondrial function that are mediated by a fast and sustained SIRT1/PGC-1α complex disruption promoting a "non-return point" to an irreversible synaptic failure and neuronal network disconnection.

Keywords: mitochondrial dysfunction, Alzheimer's disease, amyloid beta oligomers, PGC-1α, SIRT1, DRP1, Mfn1

INTRODUCTION

Alzheimer's disease (AD) is a type of dementia characterized as a progressive brain disorder with high prevalence in elderly people. The etiology of AD has not been completely determined. The time course of the disease involves the loss of cognitive abilities and behavioral changes related to progressive neuronal failure and death, mainly in the hippocampus and cortex (Castellani et al., 2010). There are

two classical histopathological biomarkers detected in AD: neurofibrillary tangles and amyloid plaques that are intracellular aggregates of hyperphosphorylated microtubule-associated protein tau (Kosik et al., 1986) are insoluble and extracellular aggregates of the β-amyloid peptide (Aβ), respectively (Glenner and Wong, 1984). Aβ monomers aggregate forming soluble oligomers composed of 3–24 monomers, known as soluble oligomers (AβOs), these can produce alterations in dendrite spine morphology in hippocampal neurons (Shankar et al., 2007; Parodi et al., 2010). AβOs provide a unifying mechanism for initiation of AD pathogenesis. It has a preference for central nervous system (CNS) (Ferreira and Klein, 2011), especially in the synapses zones (Gong et al., 2003). AβOs could be the responsible for initiation and the main agent of chronic neurotoxic effects, rather than monomers and fibrils, that do not correspond to neuroactive forms of Aβ able to depress synaptic transmission (Parodi et al., 2010). Additionally, it was found that AβOs treatments on different scales emulated the main aspects of the disease, i.e. neuronal loss, calcium dyshomeostasis, synaptic failure, and particularly ATP leakage and P2XR overexpression (Fuentealba et al., 2011; Saez-Orellana et al., 2016).

It has been found that the consequences of Aβ peptide on mitochondrial function could promote early synaptic loss (Manczak et al., 2006; Schmitt et al., 2011). One of the main proposed mechanisms for Aβ toxicity is the formation of a non-specific pore in the cell membrane (Lal et al., 2007) that allows the passage of molecules and ions (Näslund, 2000; Parodi et al., 2010). Thus, Ca2+ influx through this pore has been suggested as one of the main causes of excitotoxicity in AD (Sepulveda et al., 2010), mitochondrial Ca^{2+} overload and dysfunction; this could be as consequence of plasma membrane pore formation or by direct interaction of AβOs to mitochondrial cristae (Manczak et al., 2006; Arrazola et al., 2017; Toglia et al., 2018), issue that are still under discussion. A correlation between progressive reduction in brain glucose metabolism and a decreased expression of either nuclear or mitochondrial genes related to oxidative phosphorylation (Chandrasekaran et al., 1996; Zolezzi et al., 2017; Terada et al., 2020) and mitochondrial size (Zhu et al., 2006) has been described on AD patients. These defects in mitochondrial dynamic proteins lead to impaired mitochondrial function in neurons (Liesa et al., 2009; Lee et al., 2012; Pham et al., 2012). The events of fusion and fission are highly coordinated by proteins like Mfn1, Mfn2 (mitofusin 1, 2), and OPA1 (mitochondrial dynamin like GTPase) involved in cristae fusion, while DRP1 (dynamin-related protein) and Fis1 (mitochondrial fission 1 protein) have been related with the constriction of mitochondrial cristae which lead to mitochondrial fission (Wang et al., 2014).

For example, the levels of OPA1, Mfn1, and Mfn2 were significantly reduced, whereas the levels of Fis1 were significantly increased in AD hippocampus (Wang et al., 2009). Defects in the fission process lead to an accumulation of mitochondria in the cell body and reduced dendritic and synaptic mitochondrial content (Li et al., 2004). Alterations in mitochondrial morphology, particularlyfragmented mitochondria, were found in fibroblasts and brain tissue from AD patients (Wang et al., 2008), by the interaction of Aβ with DRP1 (Reddy et al., 2011; Zhang et al., 2016).

It has been postulated that the loss of mitochondrial biogenesis is key to understanding how mitochondrial dysfunction in AD patients occurs (Hirai et al., 2001). This process is controlled by PGC-1α (peroxisome proliferator-activated receptor-γ coactivator-1α), a fasting-induced transcriptional coactivator recruited during PPAR stimulation (Viswakarma et al., 2010). SIRT1 (silent information regulator 2 homolog 1), a NAD +-dependent histone deacetylases (HDAC) deacetylase, can interact and deacetylate PGC-1α, and this deacetylation results in the upregulation of its transcriptional function (Lehman et al., 2000; Rodgers et al., 2005; Qin et al., 2009). SIRT1 is essential for maintaining cellular survival, cognitive function, and synaptic plasticity (Feng et al., 2009). Particularly in oxidative stress environments, SIRT1 regulates diverse processes such as apoptosis, cellular senescence, glucose homeostasis, and aging (Haigis and Sinclair, 2010). Importantly, it has been described that PGC-1α and SIRT1 require changes on its localization in response to stimuli (Anderson et al., 2008; Bai and Zhang, 2016). While the PGC1α-NRF-TFAM pathway was found to be downregulated in animal model of AD (Sheng et al., 2012) showing a decreased expression level in PGC-1α (Lehman et al., 2000), as changes on SIRT1 activity (Bonda et al., 2010; Godoy et al., 2014).

In this work, we assessed the effects of AβOs on early mitochondrial dysfunction and the impact on the main mitochondrial homeostasis controllers. We hypothesized that AβOs downregulate PGC-1α and the downstream mitochondrial biogenesis and dynamic process. To test this hypothesis, we used PC-12 cells, cultured mice hippocampal neurons, and hippocampal slices as models to study the effects of soluble oligomers of Aβ1–40 on mitochondrial biogenesis by measuring the expression of the SIRT1-PGC-1α pathway. Using cellular and molecular approaches, we evaluated the effects of AβOs on proteins involved in mitochondrial health and how that impacts neuronal and synaptic function.

Abbreviations: AD, Alzheimer's disease; AMPK, AMP-activated kinase; APP, Amyloid precursor protein; Aβ, β-amyloid peptide; AβOs, Solubles Oligomers of Aβ peptide; CaMK, calmodulin-dependent kinase; CN, calcineurin; DRP1, Dynamin-related protein; FCCP, Uncoupler p-trifluoromethoxyphenyl-hydrazone; Fis1, Mitochondrial fission 1 protein; GCN5, N-acetyltransferases; HDAC, Histone Deacetylases; JNK1, C-Jun N-terminal kinases; Mfn1, Mitofusin 1; NRF, Nuclear respiratory factor; OPA1, Mitochondrial dynamin like GTPase; PGC-1α, Peroxisome proliferator-activated receptor gamma coactivator 1-alpha; PPARγ, Peroxisome proliferator-activated receptor gamma; RXR, retinoid X receptor; SIRT1, silent information regulator 2 homolog 1; TFAM, transcription factor A; TOM20, Mitochondrial import receptor subunit TOM20.

MATERIALS AND METHODS

Cell Culture

A PC-12 rat pheochromocytoma cell line was cultured in DMEM with glutamine (Dulbecco's modified Eagle medium, Invitrogen, Grand Island, NY, USA), supplemented with 5% fetal bovine serum, 5% serum horse (HyClone, South Logan, UT, USA), and 1% streptomycin-penicillin (Invitrogen, Grand Island, NY, USA). The

cells were plated in 12-well plates at a density of 2.5x105 cells/ml. Cultures were maintained at 37°C with 5% CO_2. The cells were used when 70–80% confluence was achieved. All experiments are performed in triplicate for three independent experiments.

Primary Hippocampal Cultures

Eighteen to nineteen days pregnant C57BL/J6 mice were treated in accordance with regulations recommended by NIH (National Institute of Health, USA) and the ethics committee at the University of Concepción. Mice were deeply anesthetized by CO2 inhalation before being sacrificed by cervical dislocation. Primary cultures of embryonic hippocampi were prepared as previously published (Fuentealba et al., 2011) and plated at 320,000 cells/ml on coverslips coated with poly-L-lysine (Trevigen, Gaithersburg, MD). Cultures were maintained at 37° C with 5% CO_2. All experiments are performed in triplicate for three independent experiments.

Mice Brain Slices and Immunohistochemistry

Brain slices were obtained from C57BL/6J mice (animals were manipulated in accordance with the ethical regulations established by NIH and University of Concepción). Brain slices (120 μM) were obtained on a Leica VT1200S vibratome following the Káradóttir & Attwell method (Karadottir and Attwell, 2006). Once cut, the slices were incubated for 1 h in oxigenated ACSF solution (95% O2–5% CO2) at 34–37°C. The slices were transferred to a culture plate containing ACSF solution and treated with AβOs (0.5 μM) for 1 and 5 h. All steps in the immunohistochemistry protocol were done at ice-cold temperature and constant agitation. Slices were fixed with 500 μl 4% paraformaldehyde for 35 min. Once fixed, slices were washed five times with PBS (5 min per wash) and then incubated in blocking/permeabilization solution (0.3–0.5% Triton X-100 + 10% horse serum + PBS) for 1 h. Then, slices were incubated with the primary antibodies at ice cold temperature for 3 h (or overnight at 4° C). Antibodies used were PGC1α (rabbit, 1:400, Novus Biologicals, NBP1-04676) and MAP2 (mouse, 1:400, Santa Cruz, A-4) prepared in a solution containing 0.3% Triton X-100 + 10% horse serum + PBS. Subsequently, slices were washed five times for 3 min each and incubated with the corresponding secondary antibody (conjugated with either Cy3 or AlexaFluor488) for 90 min. After incubation, nuclear staining was performed with DAPI 300 nM for 15 min. Afterwards, slices were washed five times for 3 min each and mounted with DAKO fluorescent mounting media. Stack images were acquired on a LSM780 NLO Zeiss confocal microscope using a 63X/1.4NA objective (oil immersion). Images were processed using both ZEN software (Carl Zeiss MicroImaging GmbH) and Image J (NIH, USA). Immunoreactivity was quantified with ImageJ for both primary antibodies using 15 regions of interest in each slice within each stack for each experimental condition. PGC1α immunoreactivity was normalized for each stack of 15 ROIs were randomly selected.

Data was analyzed with GraphPad Prism Software (GraphPad Software, Inc.) where all statistical calculations (one way ANOVA with Kruskal-Wallis test, Dunn's multiple comparison test for stack quantification, and one way ANOVA with Dunnet's multiple comparisons test for single plane quantification) were done. All experiments a performed in triplicate for three independent experiments.

$A\beta_{1-40}$ Aggregation

A lyophilized stock of $A\beta_{1-40}$ (rPeptide, Bogart, GA, USA) was reconstituted in DMSO at a concentration of 2.3 mM. 2 μl of this solution was diluted in sterile distilled water to reach a concentration of 80 μM. Subsequently, the peptide was aggregated at 500 rpm for 4 h at room temperature. Soluble Aβ oligomers (AβOs) were used to treat the cells and tissues for 1, 2, 5, and 24 h at a final concentration of 0.5 μM. The identity of oligomeric Aβ species (AβOs) were checked by silver staining and electronic microscopy (were performed as previously published (Sáez-Orellana et al., 2018)).

Transmission Electron Microscopy

Ten microliters of $A\beta_{1-40}$ at a concentration of 80 μM was applied to carbon-coated Formvar grids. Samples were fixed with a 2% glutaraldehyde solution for 5 min was exposure to colloidal beta amyloid antibody (MOAB-2, 1:50, 1 h) and gold particles (10 nm) conjugated with a secondary antibody (mouse, 1:500). The aggregates were stained with 5 μl of 0.2% (w/v) phosphotungstic acid (PTA) and the grid was air-dried. Samples were examined using a JEOL 1200 EX II electron microscope.

Western Blot

To study the expression of mitochondrial biogenesis and dynamics proteins, we prepared whole cell lysates with a buffer containing 10 mM Tris, 10 mM EDTA, 100 mM NaCl, 0.5% Triton, 10% glycerol, and protease inhibitors. Culture lysates were mixed with 4X loading buffer and denatured at 95°C for 10 min. Then, samples were subjected to SDS-PAGE in 10% acrylamide gels at 100 V for 100 min and transferred to nitrocellulose membranes at 250 mA for 120 min. Membranes were blocked with 5% non-fat milk in TBS 1X-Tween for 1 h. The primary antibodies SIRT1 (mouse, 1:1,000, Novus Biologicals, 1F3), PGC-1α (rabbit, 1:500, Novus Biologicals, NBP1-04676), DRP1 (rabbit, 1:2,000, Novus Biologicals, NB110-55288), Mfn1 (rabbit, 1:1,000, NBP1-51841), and β-actin (mouse, 1:1000, Santa Cruz Biotechnology, AC-15) were incubated overnight. Anti-rabbit-HRP (1:5,000, Santa Cruz, Biotechnology, sc-2004) and anti-mouse-HRP (1:5,000 Santa Cruz, Biotechnology, sc-2005) were used as secondary antibodies and were incubated for 1 h. Immunoreactive signals were detected using the Western Lighting kit (Perkin Elmer, USA) andquantified with an Odyssey imaging system (Li-Cor, Lincoln, NE, USA).

Co-Immunoprecipitation (Co-IP)

To evaluate the interaction between SIRT1 and PGC-1α, we prepared lysates from PC12 cells control and treated 24 h with AβOs. Protein concentration was normalized for the different samples. Then, the lysates were precleared with 10 µl of Protein A/G PLUS Agarose Immunoprecipitation Reagent (Santa Cruz Biotechnology Y, INC. sc-2003) and the resulting mixture was incubated at 4°C for 1 h. Subsequently, the precleared samples were incubated for 1 h with 1 µg of an anti-PGC-1α rabbit monoclonal antibody (Novus Biologicals, NBP1-04676) or a rabbit control IgG (Sigma-Aldrich, 12–370), per mg of protein. Finally, we added 50 µl of Protein A/G PLUS Agarose Immunoprecipitation Reagent to each sample and incubated the mixture overnight. Proteins were eluted in 2X loading buffer at 100°C for 8 min, analyzed by SDS-PAGE, and visualized by western blot using anti-PGC-1α and anti-SIRT1 antibodies (Novus Biologicals).

Immunocytochemistry

To study $A\beta_{1-40}$ toxic effects on mitochondrial biogenesis, dynamics proteins, organization, and distribution, PC-12 cell cultures were treated with 0.5 µM AβOs 1–40 for 1, 2, and 24 h. The cells were washed with PBS1X and fixed with 4% paraformaldehyde for 10 min at room temperature (RT). Later, cells were permeabilized with 0.1% Triton X-100 and blocked with 10% horse serum for 30 min at RT. Samples were incubated for 1 h at RT with the following primary antibodies: SIRT1 (mouse 1:300, Novus Biologicals, IF3), PGC-1α (rabbit 1:400, Novus Biologicals, NBP1-04676), Ser-46 SIRT1 (Sigma 1:200, SAB4301426), DRP1 (rabbit 1:200, Novus Biologicals, NB 110-55288), and Mfn1 (rabbit 1:200, Novus Biologicals, NBP1-51841). Subsequently, the corresponding Cy3 or Alexa Fluor 488 conjugated were incubated for 45 min. Then, samples were incubated with 300 nM DAPI nuclear staining for 10 min and mounted using DAKO immunofluorescence mounting media (Dako, Glostrup, Denmark). Images were acquired using a LSM780 NLO confocal microscope (Carl Zeiss Microscopy, Jena, Germany), a Nikon Eclipse TE2000-U epifluorescence microscope, and Zeiss SR-SIM equipment (Elyra S1 model), which was equipped with a DPSS Diode laser (488 and 561 nm of excitation). The 63X/1.4 NA oil immersion objective with an additional 1.6X lens was used which explains why the total increase was 1008X. Images were processed, and quantification was performed using Image J (NIH, Bethesda, MD, USA). Images were deconvolved considering the following parameters: immersion oil refractive index (1.518), objective numerical aperture (1.4), and wavelength (510 nm). Immunoreactivity for mitochondrial biogenesis and dynamics proteins was quantified. Additionally, nuclear and cytoplasmic immunoreactivity was analyzed using three aleatory areas in both cases and quantifying the mean intensity for each cell in three independent experiments.

Digital Imaging Processing of Mitochondria Morphology Analyses

To study AβOs1–40 toxic effects on mitochondrial morphology, PC-12 cells and hippocampal neurons were stained with a specific primary antibody for TOM 20 (sc-17764, mouse monoclonal, F-10, outer mitochondria membrane). Images were acquired using a LSM780 NLO confocal microscope (Carl Zeiss Microscopy, Jena, Germany) or superresolution microscopy (see above). After acquisition, images were processed with Image Processing and 3D reconstructions were performed using BitPlane IMARIS 9.1 software to evaluate the shape and area of MTG-stained cells. Briefly, binary objects were obtained by image segmentation, and subsequently an automatic measurement tool was used to calculate the volume and elongation of each mitochondrion.

Superresolution Microscopy

Images by structured illumination were obtained using a Zeiss SRSIM model Elyra S1 superresolution microscope equipped with a DPSS diode laser (561 nm excitation). An oil immersion 63x/1.4 NA objective was used with an additional 1.6x lens for a total magnification of 1008x. The emission filters used were a BP570-650 and LP750 for the fluorophores FITC and Cy3, respectively. For all captured images a configuration with five grid positions was used (28 µm for the 488 nm laser and 34 µm for the 561 laser), with a z-stack spacing of 110 nm between each plane captured. Images were processed using Image J software (NIH, Bethesda, MD, USA).

Data Analysis

The obtained data was analyzed using GraphPad Prism 6 Software. Normality was verified using the Kolmogorov-Smirnov test or Shapiro-Wilk normality test depending on sample size. In the case of normal data, statistical significance was determined using unpaired Student's t-test (for two groups) orone-way ANOVA followed by the Dunnett's multiple comparisons test (for multiple group comparisons). In the case of non-normal data, statistical significance was determined using Mann-Whitney test (for two groups) or Kruskal-Wallis test followed by the Dunn's multiple comparisons test (for multiple group comparisons). All experimental data are expressed as the mean ± SEM (unless otherwise indicated). P-values < 0.05 were considered statistically significant. Exact n for each experiment is reported in Figure legends.

Animal Manipulations

All procedures related with animal management and tissue isolation were done following NIH (USA) and CONICYT guidelines and with protocols approved by the bioethical committee of the Universidad de Concepcion. 297

RESULTS

AβOs Induced an Imbalance in Mitochondrial Fission/Fusion Proteins in PC-12 Cells

To characterize the $A\beta_{1-40}$ aggregates, we performed transmission electron microscopy and silver staining experiments to confirm the presence of $A\beta_{1-40}$ oligomers (preparations used in this study, **Figure 1**). The data showed

that the soluble oligomers of $A\beta_{1-40}$ were principally low molecular weight structures (**Figure 1A**). Moreover, these AβOs (**Figure 1B**) displayed similar than toxic effects mitochondrial uncoupler FCCP (10 μM). With these experimental approaches, we confirm that the Aβ species used in this were mainly toxic oligomers. We decided the use of $A\beta_{1-40}$ instead of $A\beta_{1-42}$, because $A\beta_{1-42,}$ aggregation process is difficult to control which usually promote the formation of less active aggregates (Pauwels et al., 2012). Furthermore, we have characterized β-amyloid effects of different Aβ species (monomers, soluble oligomers, or protofibrils), and we observed that monomeric species of Aβ have a neurotrophic-like effects (Cuevas et al., 2011); while soluble oligomeric species of Aβ effects were compared with insoluble fibrillar species (Parodi et al., 2010; Sepulveda et al., 2010); taken together, we corroborated that the soluble oligomers, have the active toxicity related to synaptic failure described by our group previously.

After AβOs characterization, we used PC-12 cells to compare the effects of acute AβOs treatments (1–2 h) on two of the most important proteins related with mitochondrial dynamics: DRP1 and Mfn1 with chronic AβOs treatments (24 h). Using western blot, we evaluated total protein levels of Mfn1 (**Figure 2A**) and DRP1 (**Figure 2B**) in PC12 cells after 1 and 2 h treatments with AβOs (0.5 μM). Western blot analyses showed that Mfn1 protein levels were significantly reduced (**Figure 2C**) after 2 h of acute AβOs treatments compared to control cells (42 ± 11%); while DRP1 (**Figure 2D**) were significantly increased after acute treatments, reaching two-fold increased (1 h: 205 ± 2%, 2 h: 198 ± 3%, **Figure 1D**) but were not seen after prolonged times (24 h) of AβOs treatments (**Supplementary Figure 1**). These results were compared with the effects of FCCP (10 μM, 2 h), which caused a significant increase in the levels of DRP1 (193 ± 27%, **Figure 2D**). Initially, these results suggest that, during mitochondrial dynamics, the fission process could be potentiated by acute exposure to AβOs, and this effect was maintained under chronic conditions. To corroborate these results, we performed immunocytochemistry experiments to evaluate the immunoreactivity of Mfn1 (**Figure 3A**) and DRP1 (**Figure 3B**). Using epifluorescence microscopy, we quantified the total immunoreactivity levels for Mfn1 (48 ± 7%, **Figure 3C**) and found that the fluorescence intensity was significantly reduced at 2 h in line with western blot results. DRP1 immunoreactivity (**Figure 3D**), on the other hand, showed a significantly increase in the fluorescence intensity at 2 h (139 ± 8%, **Figure 3D**), also in line with the observations on western blot. Therefore, these results suggest that acute exposure to AβOs (0.5 μM), induced a fast activation of the fission process as an early event to restore mitochondrial homeostasis, and thus separate the defective mitochondrial population from the functional ones for the maintenance of their vital functions. These changes in the balance of mitochondrial fission and fusion proteins were not seen after prolonged times (6 or 24 h) of AβOs treatments (**Supplementary Figure 1**), suggesting that AβOs could promote fast changes in the mitochondrial network causing and early impact mitochondrial dynamic processes leading to a no-return point in the pathway to cell death.

Changes in Mitochondrial Network Morphology After AβOs Treatments

To confirm our previous observations, we studied the morphology of the mitochondrial network, based on our previous work, where we observed that ATP leakage induced by AβOs causes a decrease on neuronal energetic availability (Saez-Orellana et al., 2016). We evaluated mitochondrial morphometric parameters using a TOM20 marker with confocal and superresolution microscopy to examine if changes in the size and distribution of mitochondria are a consequence of changes in the dynamic's proteins. First, we evaluated

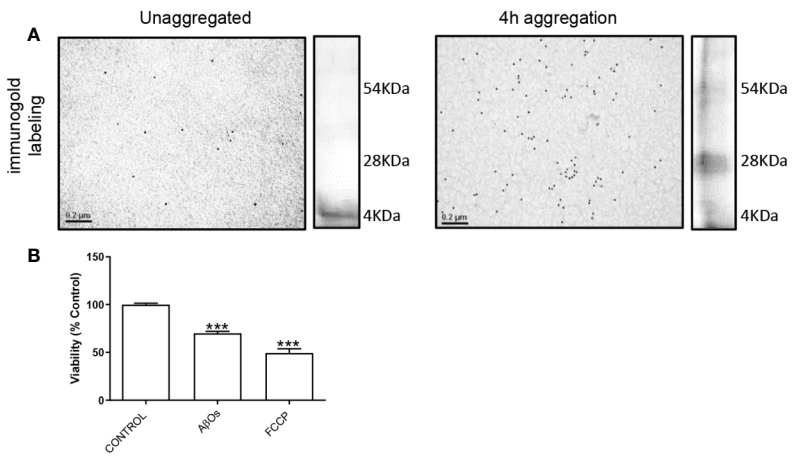

FIGURE 1 | Characterization of AβOs. **(A)** Microscopy electronic of $A\beta_{1-40}$ peptide. $A\beta_{1-40}$ peptide was aggregated 4 h and was exposure to colloidal gold particles (10 nm) conjugated with a β amyloid Antibody (MOAB-2). $A\beta_{1-40}$ peptide aggregation is visualized by silver staining to the right side of each panel. **(B)** PC-12 cells were incubated with AβOs 0.5 μM for 24 h and FCCP (10 μM). Data are represented as mean ± SEM. ***$p < 0.001$ compared between the control group. One-way ANOVA used for all statistical analyses. FCCP, Carbonyl cyanide-4-trifluoromethoxy) phenylhydrazone. (n=3–5 for each group).

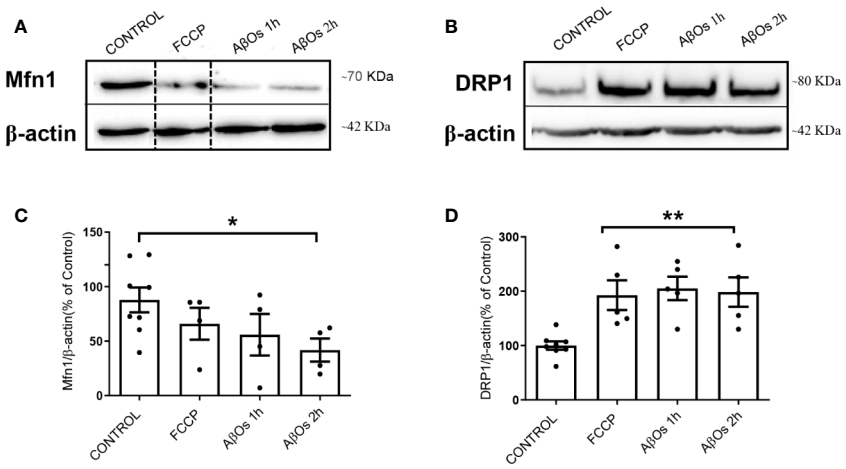

FIGURE 2 | Acute effects of AβOs on total levels of proteins that regulate mitochondrial dynamics. **(A)** Mfn1 and **(B)** DRP1 western blot of lysates from PC12 cells treated with FCCP (10 μM, 2 h) and AβOs (0.5 μM, 1 and 2 h). A dotted line on the western blot indicates different regions of the same gel. **(C, D)** Quantification of Mfn1 and DRP1 levels normalized to beta actin. Data are represented as mean ± SEM. *$p < 0.05$, **$p < 0.01$ compared between the control group. One-way ANOVA with the Dunnett's multiple comparisons test was used for all statistical analyses. Mfn1, mitofusin 1; DRP1, dynamin-related protein 1. (n = 4–5 for each group) (original gel blot are provided on **Supplementary Figure 2**).

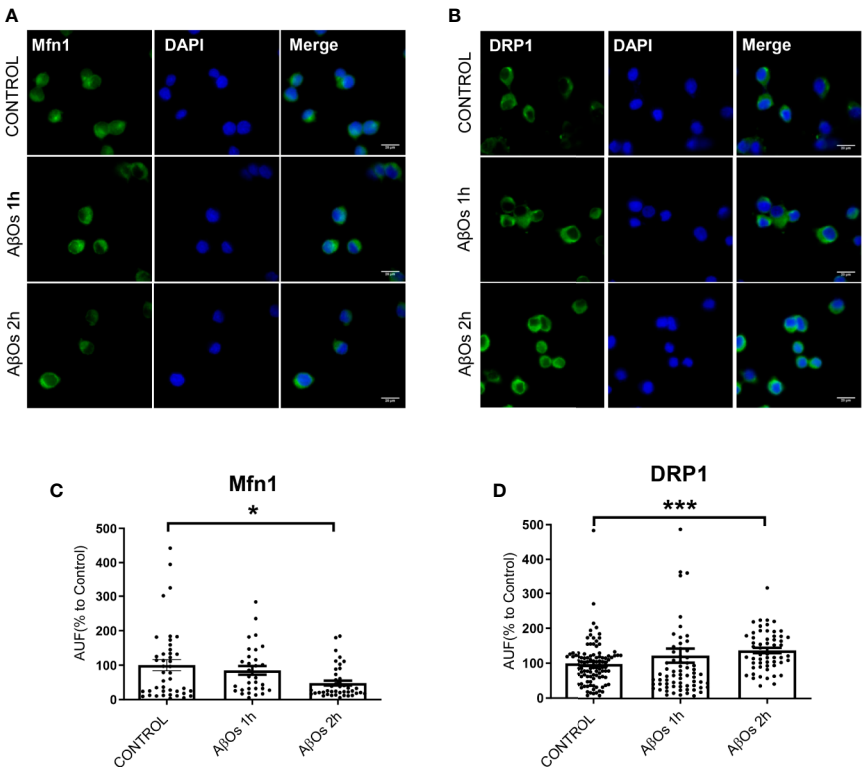

FIGURE 3 | Acute effects of AβOs on immunoreactivity of proteins that regulate mitochondrial dynamics. Representative epifluorescence images of **(A)** Mfn1 and **(B)** DRP1 immunoreactivity in PC-12 cells control and treated with AβOs (0.5 μM) for 1 and 2 h. Quantification of **(C)** Mfn1 and **(D)** DRP1 immunoreactivity (intensity), under the same experimental conditions. Scale bars: 20 μm. Data are represented as mean ± SEM. *$p < 0.05$, ***$p < 0.001$ compared between the control group. One-way ANOVA with the Dunn's multiple comparisons test was used for all statistical analyses. Mfn1, mitofusin 1; DRP1, dynamin-related protein 1. (n=3–6 for each group, N= 56–103) (entire inmunocytochemistry for Mfn1 and DRP1 with control are provided on **Supplementary Figure 3**).

morphometric changes in mitochondrial size induced by acute (1 h) and chronic (24 h) AβOs treatments on PC-12 cells using confocal microscopy (**Figure 4A**). We found a significantly reduction in the size of mitochondrial bodies compared to control conditions (C: 2.4 ± 0.04, 1 h: 0.76 ± 0.02, **Figure 4B**), and this fragmented phenotype was also seen significant after chronic treatment with AβOs (24 h: 1.2 ± 0.03, **Figure 4C**) where the mitochondria remained very small and the populations exhibited a granular appearance, instead to the more fibrillary phenotype in control conditions. Next, we evaluated mitochondrial morphometric parameters using a superresolution microscopy in hippocampal neurons (**Figure 5A**), followed by a digital image analysis capable of measuring the area and length of each mitochondria (see digital imaging processing for details) under chronic AβOs treatment. Representative images of zoom regions from 2D and 3D reconstructions of the mitochondrial network by superresolution technique in control (left) and treated (right) conditions are showed on **Figure 5B**, respectively. We evaluated three parameters from these reconstructions: volume (**Figure 5C**), length (**Figure 5D**), and mitochondrial number (**Figure 5E**). We observed that the mitochondria number in AβOs treatment conditions were significantly increased at 24 h (219 ± 9%, **Figure 5E**), which was associated with a significant increase of mitochondrial volume in the smaller mitochondria population (24 h: 112 ± 3%; < 0.3 μm^3).

Additionally, mitochondria with shorter size were significantly increased with chronic Aβ treatment (24 h), compared to control conditions (24 h:127 ± 5%; < 2 μm, **Figure 5D**, left graph), while largest mitochondria were significantly decreased with chronic Aβ treatment (24 h), compared to control conditions (24 h:83 ± 3%; > 2 μm, **Figure 5D**, right graph). We observed a similar mitochondrial phenotype under acute AβOs treatments (data not shown). Taken together, our hypothesis is that earlier predominance of granular mitochondrial phenotype is associated with an early imbalance in mitochondrial dynamics proteins which appears to be the crucial point to initiate deficits in neuronal metabolism that finally produces synaptic failure and cell death. Curiously, loss of the normal mitochondrial phenotype network after chronic exposure to AβOs did not cause additional changes in the levels of mitochondrial dynamics proteins (data no shown), suggesting that acute loss of these proteins leads to an irreversible mitochondrial fragmented phenotype and could represent a point of no return for the recovery of its function full stop.

Acute and Chronic AβOs Treatments Induced Changes in Mitochondrial Biogenesis Proteins

As rescue mechanism, the neurons to protect themselves against AβOs toxicity, are able to activate a biogenesis mechanism to restore the mitochondrial population which is necessary to support key

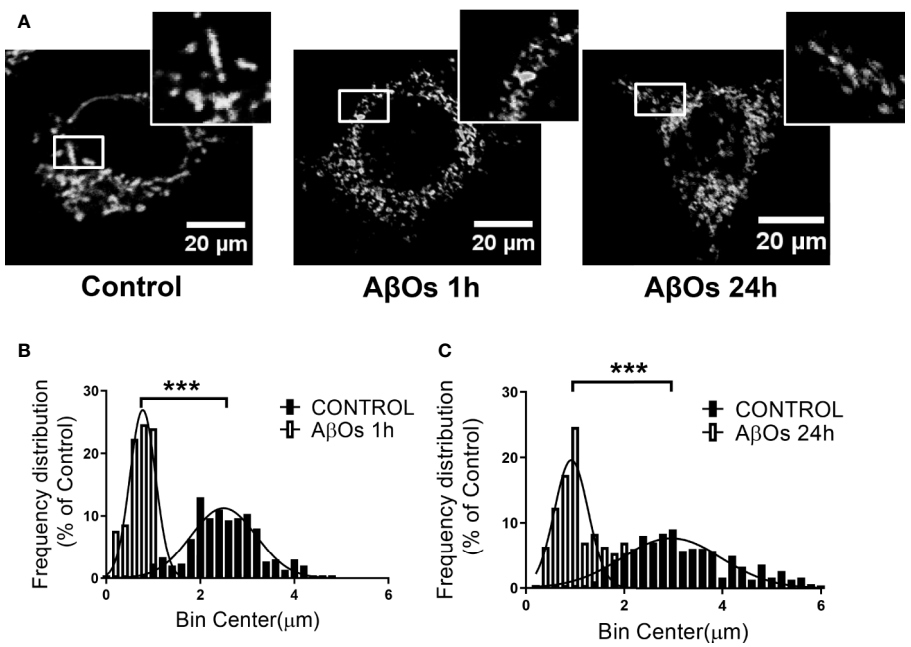

FIGURE 4 | Changes in mitochondrial network size after acute and chronic exposure to AβOs in PC12-cells. **(A)** Confocal images of PC-12 cells showing immunoreactivity of the specific primaryantibody for TOM 20 (white) in control conditions (left panel) and after AβOs treatments (0.5 μM) during 1 and 24 h of incubation (middle panel and right panel, respectively). White squares show a magnification of the soma region of the cell). **(B)** Histogram shows the mitochondrial size distribution after acute and **(C)** chronic treatments with AβOs. Data are represented as mean ± SEM. ***p < 0.001 compared between the control group. Student's t-test followed by Mann-Whitney test was used for all statistical analyses. TOM20, translocase of outer membrane. (n=3, N=18–23) (complete inmunocytochemistry for TOM20 with control are provided on **Supplementary Figure 4**).

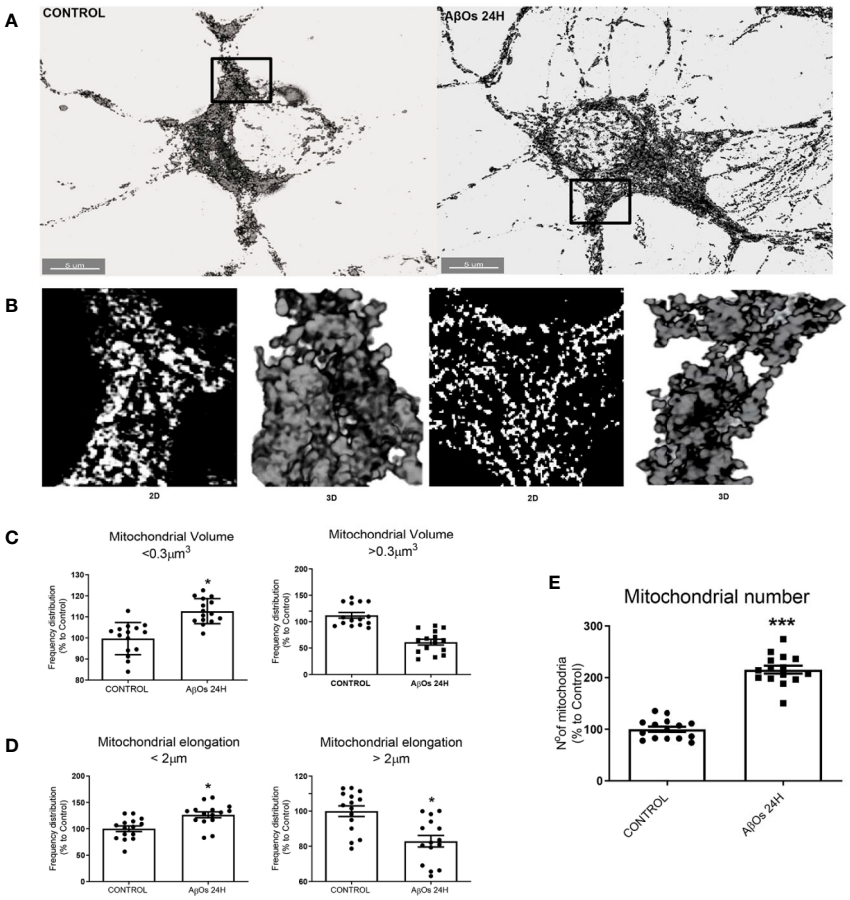

FIGURE 5 | Changes in mitochondrial network size after acute and chronic exposure to AβOs in hippocampal neurons. **(A)** Super-resolution images of hippocampal neurons showing the immunoreactivity for the specific primary antibody for TOM 20 (white) in control condition (left panel) and after 24 h of incubation with AβOs (0.5 μM; right panel). **(B)** Representative 2D and 3D images of mitochondrial population in figure A. **(C)** The data were analyzed as the percentages of number for volume (> and < 0.3 μm3, **C**), length (> and < 2 μm, **D**), and number **(E)** of mitochondrial population in AβOs treated cells compared with untreated cells. Scale bars: 5 μm. Data are represented as mean ± SEM. *p < 0.05, ***p < 0.001 compared between the control group. Student's t-test followed by unpaired t-test was used for all statistical analyses. TOM20, translocase of outer membrane. (n=3, N=15) (complete inmunocytochemistry for TOM20 with controls are provided on **Supplementary Figure 5**).

function as synaptic activity (in the case of neurons) or metabolic activity (in the case of common cells). Thus, there is a possibility that the irreversible effects of AβOs could be associated with an impediment of the mitochondria to repair and/or restore their intracellular network. Therefore, to evaluate this aspect we examined the status of the key mitochondrial biogenesis regulators: PGC-1α (**Figure 6A**) and SIRT1 (**Figure 6B**). Changes in the total levels of these proteins were evaluated to determine if the cells could activate the generation of new functional mitochondria after AβOs treatment in response to the toxic action of Aβ and avoid the generation of the fragmented phenotype seen previously. However, after acute and chronic AβOs exposure in PC12 cells (1–24 h), western blot studies showed a significantly decreased in PGC-1α levels (1 h: 68 ± 8%; 24 h: 67 ± 7%, **Figure 6C**). Similarly, SIRT1 were decreased (**Figure 6B**) after acute and chronic treatments with AβOs compared to control cells (1 h: 68 ± 7%; 24 h: 77 ± 6%, **Figure 6D**). This data is in line with immunocytochemistry and confocal microscopy results that informed changes in the intracellular distribution and immunoreactivity of PGC-1α and SIRT1 in PC12 cells (**Figure 7A**). Interestingly, after 24 h of AβOs exposure, nucleus/cytosol ratio(N/C) of PGC-1α were significantly decreased compared to control conditions (24 h ± 4%, **Figure 7B**, lower graph), with a change in their spatial distribution of immunoreactivity (x,y) (**Figure 7C**, surface plots and plot profiles), suggesting that in cells exposed to AβOs the mechanisms for repair and maintenance of mitochondrial population and functions are defective. However, we did not find any statistically significant changes in SIRT1 total levels or distribution after acute or chronic treatment with AβOs (**Figure 7B**, upper graph).

We replicated the same experimental conditions in hippocampal neurons to evaluate the effects of AβOs exposure at 24 h (**Figure 8A**). Using confocal microscopy images, observed a significantly decreased on the nucleus/cytosolic ratio of PGC-1α

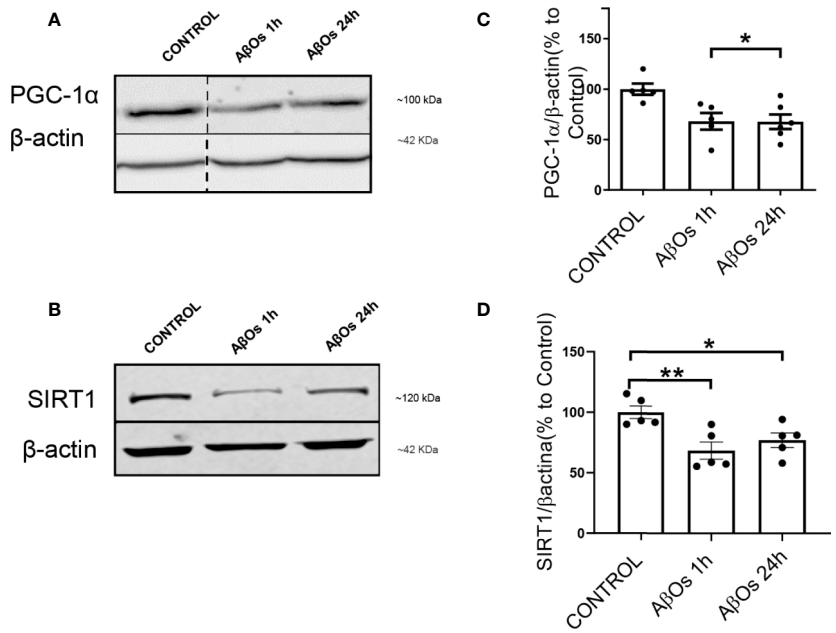

FIGURE 6 | Changes in SIRT1 and PGC-1α levels after exposure to AβOs. **(A)** PGC-1α western blot of PC12 lysates control and treated with AβOs (0.5 μM) for 1 and 24 h. **(B)** SIRT1 western blot of PC12 lysates in the same conditions as A. **(C)** Quantification of PGC-1α protein levels normalized to β actin levels, and **(D)** SIRT1 protein levels under similar conditions as C. Data are represented as mean ± SEM. *p < 0.0, **p < 0.01, compared between the control group. One-way ANOVA with the Dunn's multiple comparisons test was used for all statistical analyses. PGC-1, Peroxisome proliferator-activated receptor gamma coactivator 1-alpha; SIRT1, silent information regulator 2 homolog 1. (n=5–6/group). A dotted line on the western blot indicates different regions of the same gel (original gel blot are provided on **Supplementary Figure 6**).

in AβOs-treated neurons (24 h: 51 ± 8%, **Figure 8B**). The analysis of the distribution of immunofluorescence with plot profile tools, shown that the fluorescence profile for PGC-1α that overlaps with the fluorescence profile for DAPI nuclear stain in control conditions (**Figure 8C** left graph); while, in the treatment with AβOs the fluorescence profile for PGC-1α shown increased fluorescence intensities in non-DAPI areas (**Figure 8C**, right graph) suggesting that after AβOs treatment this protein is no longer available in the nucleus to support mitochondrial biogenesis. To complement these results, we wanted to evaluate the effects of AβOs on a more physiological and conserved matrix.

These results suggest that mitochondrial dysfunction and consequent neuronal failure and synaptic silencing could be associated mainly to changes in PGC-1α more than SIRT-1. Even though our western blot data showed a significantly decrease in SIRT1 at 1 and 24 h, we did not observe any changes regarding SIRT1 nucleus/cytosol ratio in PC-12 cells (**Figure 7**; **Supplementary Figure 7**). However, as mentioned previously, the interaction between PGC-1α and SIRT-1 is fundamental to the biogenesis process. Thus, we studied if the accumulation of PGC-1α in the cytosol was related to changes in the interaction with SIRT1 that could alter the activation of mitochondrial biogenesis. Using co-immunoprecipitation, we observed that the interaction between both proteins was lost after 24 h of AβOs treatment (**Figure 9A**), confirming that PGC-1α is unable to access to the nucleus and activate the mitochondrial biogenesis process, which agrees with our previous results. Additionally, we evaluated the mechanism by which AβOs reduced the level of SIRT1 proteins. To do this, we exposed PC-12 cells and hippocampal neurons to AβOs and evaluated the phosphorylation status of SIRT1 at its serine 47 residue, since this phosphorylation induces ubiquitination and proteasome-dependent degradation in SIRT1 (Gao et al., 2011). Western blot analysis (**Figure 9B**) showed that the levels of pSIRT1 were significantly increased in PC-12 cells treated with AβOs compared to control (157 ± 18%, **Figure 9C**).

Using immunocytochemistry, we studied the changes on p-SIRT1 in PC12 Cells (**Figure 10A**) and hippocampal neurons (**Figure 10B**). We found that despite the increase on p-SIRT1 fluorescence intensity (**Figure 10C**), the nucleus/cytoplasm ratio of p-SIRT1 decreased in a time-dependent manner with respect to control in PC12 cells (**Figure 10D**) (24 h: 47 ± 5%). In parallel, hippocampal neurons (**Figure 10B**), also shown a moderate increase fluorescence intensity (**Figure 10E**), and a significantly decrease of nucleus/cytoplasm ratio of p-SIRT1 under the same AβOs treatment (24 h: 73 ± 8%, **Figure 10F**). Taken together, our data suggest that p-47 phosphorylation induce a SIRT1 structural change that may precludes its translocation to the nucleus to carry out its function.

Finally, we obtained hippocampal slices from 9 months old mice, exposed them to AβOs for 1–5 h and then performed immunohistochemistry (**Figure 11A**). Using confocal microscopy, we observed similar phenomena than in cultured

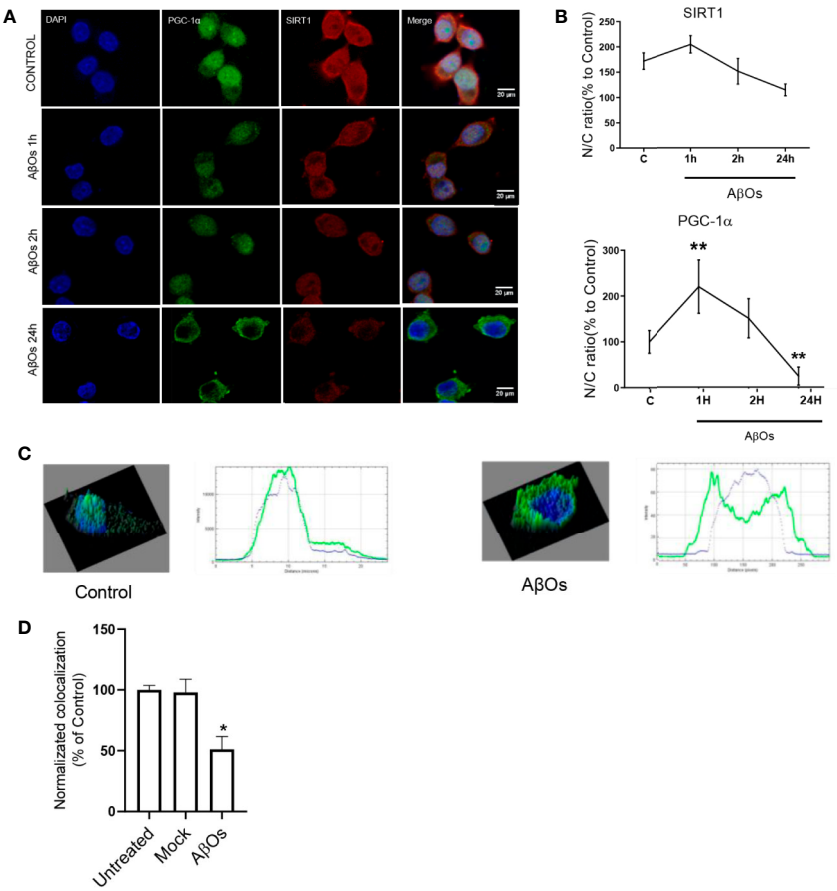

FIGURE 7 | Immunocytochemistry of SIRT1 and PGC-1α in PC12 cells treated with AβOs. **(A)** Representative confocal images of PC 12 cells stained with specific primary antibodies for PGC-1α (Green),SIRT1 (red), and DAPI (blue) in control condition (upper panel), and after AβOs treatments (0.5 μM) during different incubation times (1 and 24 h, lower panels). **(B)** Quantification of the nucleus/cytosol ratio (N/C) for SIRT1 (upper graph) and PGC-1α (lower graph) from images shown in A. **(C)** Surface plot of a representative cell shown in A, correlating spatial distribution (x,y) with fluorescence intensity (z) for DAPI and PGC-1α in control condition (left panel) and after 24 h of treatment with AβOs (right panel). Scale bars: 20 μm. **(D)** Manders colocalization coefficient (MCC) values quantify the different levels of colocalization between PGC-1α and SIRT1. Data are represented as mean ± SEM. *p < 0.05, **p < 0.01, compared between the control group. One-way ANOVA with the Dunn's multiple comparisons test was used for all statistical analyses. PGC-1, Peroxisome proliferator-activated receptor gamma coactivator 1-alpha; SIRT1, silent information regulator 2 homolog 1. (n=3, N=37).

cells (see **Figure 6**), i.e. a significant decrease in PGC-1α immunoreactivity after AβOs treatments. To further examine this result, we analyzed a stack of images for each condition to evaluate the immunoreactivity of PGC-1α in several planes of the same tissue (**Figure 11B**). The results showed that PGC1α immunoreactivity was reduced by AβOs treatments at 5 h 407 (**Figure 11C**, **Supplementary Figure 11**, and **Supplementary Figure 12**).

DISCUSSION

The neuronal mitochondrial network is regulated by a dynamic process to support high metabolic activity of the brain cells, especially the ATP demand and Ca^{2+} handling (Alonso et al., 1999) that support relevant processes such as synaptic communication, neurotransmitter synthesis and others (Kann and Kovács, 2007). Mitochondrial function depends on the correct performance of mitochondrial dynamics and mitochondrial biogenesis, which coordinates the formation of new functional mitochondria, and is an important defense mechanism for cells to survive from mitochondrial damage (Hackenbrock et al., 1971; LC et al., 2011), then the loss of functional mitochondria could be a very sensitive problem to the neurons. It has been observed that mitochondrial dysfunction is one of the earliest and most prominent features of AD (Schmitt et al., 2011). Mitochondrial cascade hypothesis in AD proposes that a mitochondrial perturbation precede the synaptic damage, the neuronal cell death, and the deficits in learning/memory ability in AD (Swerdlow et al., 2010; Swerdlow, 2018). A new approach for the treatment of AD based on the preservation of the mitochondrial structure as a target (Course and Wang, 2016; Arrazola et al., 2017)

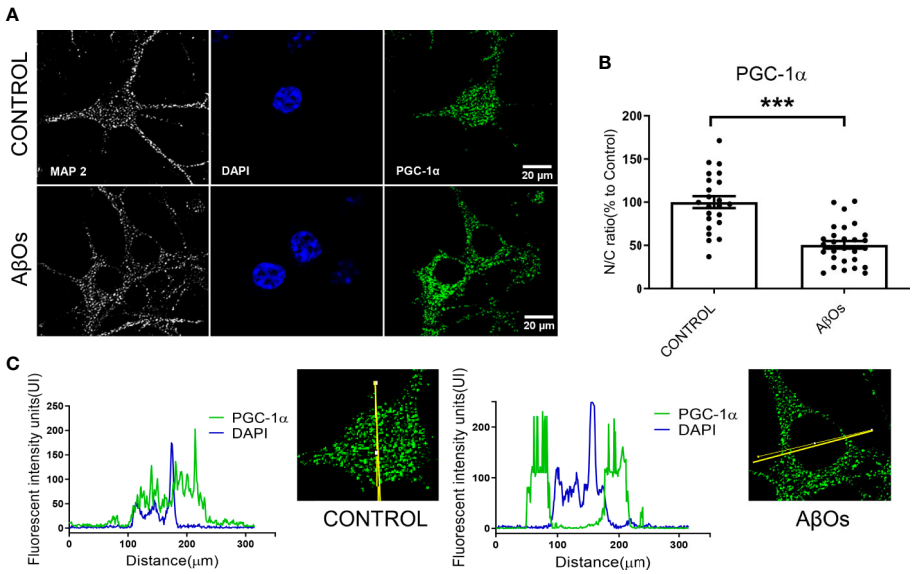

FIGURE 8 | Immunocytochemistry to evaluate the PGC-1α distribution in hippocampal neurons treated with AβOs. **(A)** Representative confocal images of immunoreactivity for specific primary antibodies for PGC-1α (Green) and DAPI (blue) in PC-12 cells in control condition (upper panel) and after 24 h of AβOs treatment (0.5 μM, lower panel). **(B)** Quantification of the nucleus/cytosol (N/C) ratio for images shown in A. **(C)** Plot profiles for images showing the intensity of fluorescence in control condition (left panel) and after 24 h treatment with AβOs (right panel) of images obtained in A. Scale bars: 20 μm. Data are represented as mean ± SEM. ***p < 0.001 compared between the control group. One-way ANOVA with the Dunnett's multiple comparisons test was used for all statistical analyses. PGC-1α, Peroxisome proliferator-activated receptor gamma coactivator 1-alpha; SIRT1, silent information regulator 2 homolog 1. (n=3, N=23–28) (hinmunocytochemistry with controls ares provided in **Supplementary Figure 8**).

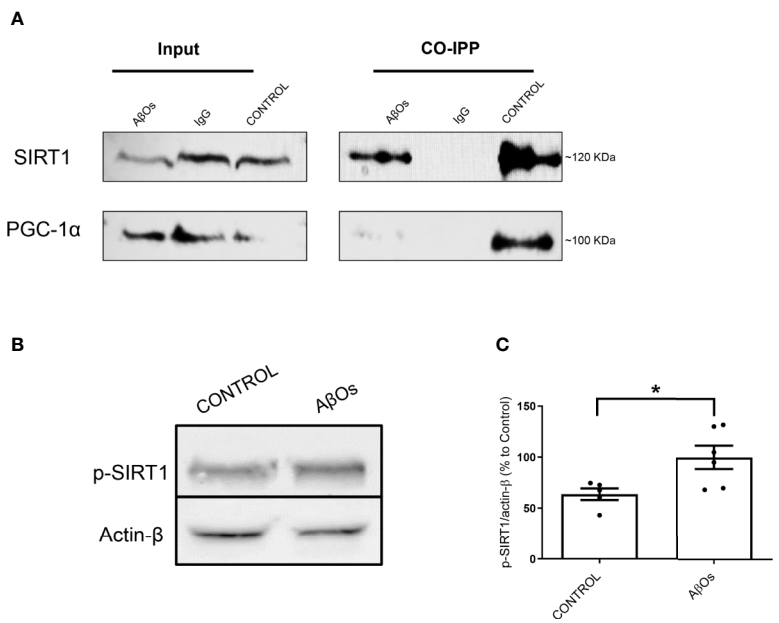

FIGURE 9 | Changes in interaction between the PGC-1α/SIRT1 and association with the levels of p- SIRT1 after chronic treatment with AβOs. **(A)** Representative western blot for PGC-1α (91 kDa) and SIRT1 (120 kDa) in PC-12 cells in control condition (lane 1) and after chronic treatment with AβOs (0.5 μM; lane 3). Lane 2 is the IgG control. Co-immunoprecipitation of SIRT1 with PGC-1α are shown in lanes 4, where we can see untreated cells, lane 5 corresponds a IgG control, and lane 6 corresponds to AβOs treatment **(B)** western blot of whole cell lysates of PC12 cells treated with AβOs (0.5 μM) for 24 h showing p-SIRT1 levels. **(C)** Quantification of p-SIRT1 levels normalized to β actin. Data are represented as mean ± SEM. *p < 0.05, compared between the control group. Student's t-test followed by unpaired t-test was used for all statistical analyses. PGC-1α, Peroxisome proliferator- activated receptor gamma coactivator 1-alpha; SIRT1, silent information regulator 2 homolog 1 (n=3/group) (Original blots are provided in **Supplementary Figure 9**).

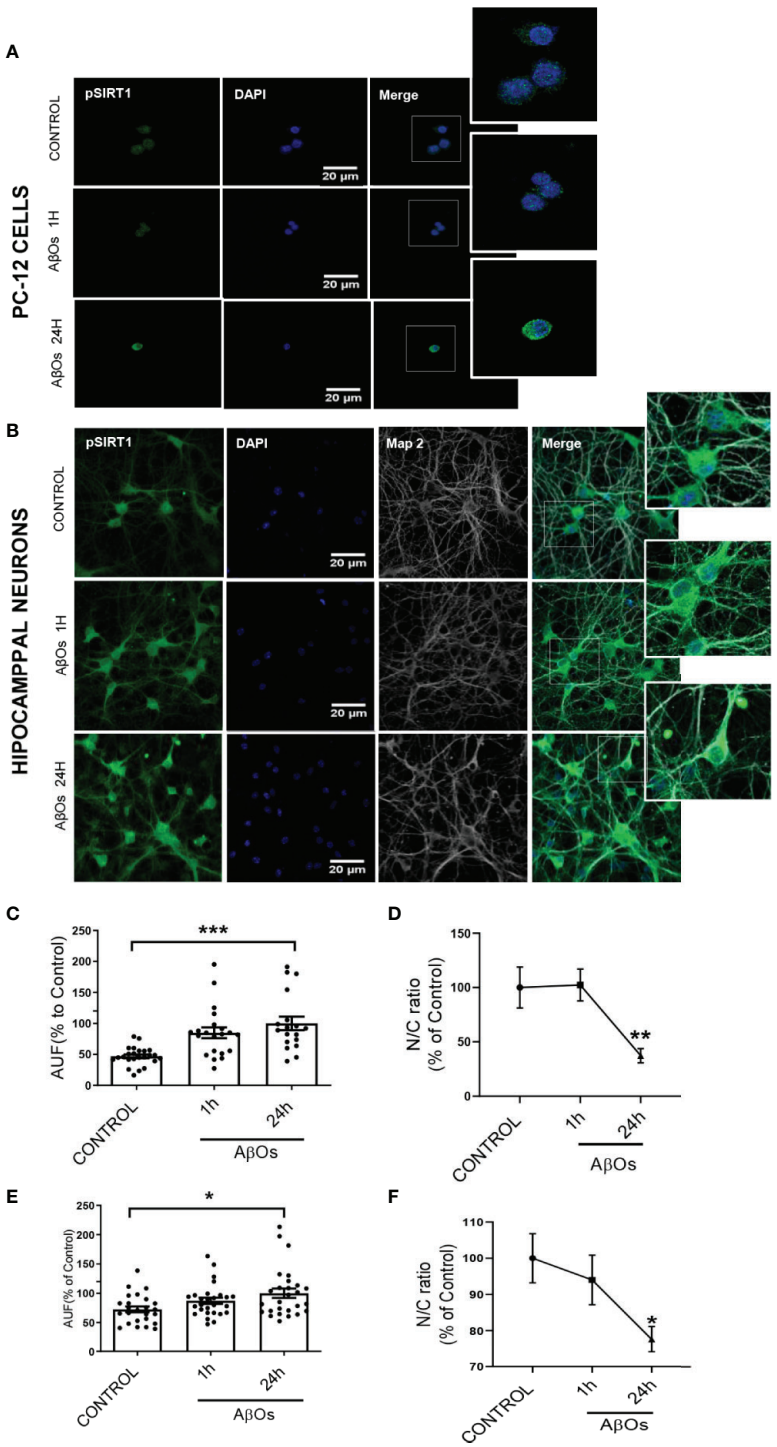

FIGURE 10 | Immunocytochemistry to evaluate p-SIRT1 distribution in PC12 cells and hippocampal neurons treated with AβOs. Representative confocal images of **(A)** PC12 cells and **(B)** hippocampal neurons showing the immunoreactivity of specific primary antibodies for ph-SIRT1 (green) and DAPI (blue) in control condition (upper panel) and after AβOs treatment (0.5 µM) during different incubation times (1, 24 h lower panels). **(C)** Quantification of the total levels of ph-SIRT1 (lower left panel) and Quantification of the relation of nuclear and cytosolic (N/C) of p-SIRT1 in PC-12 cells **(D)**. **(E)** Quantification of the total levels of ph-SIRT1 (left corner panel) and quantification of the relation of nuclear and cytosolic (N/C) of p-SIRT1 in hippocampal neurons **(F)** expressed as percentage of control. Scale bars: 20 µm. Data are represented as mean ± SEM. *p< 0.05, **p < 0.01 ***p < 0.001 compared between the control group. One-way ANOVA with the Dunnett's multiple comparisons test was used for all statistical analyses. SIRT1, silent information regulator 2 homolog 1. [n=3, N=18–27 (Complete inmunocytochemistry with controls are provided in **Supplementary Figure 10**)].

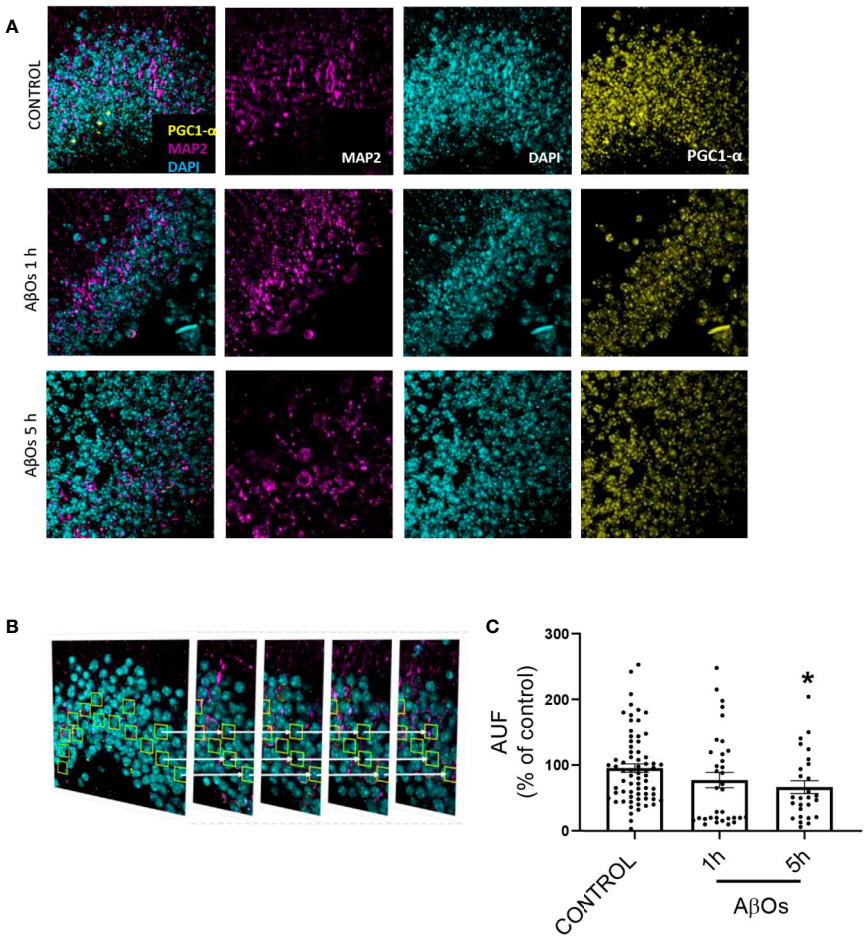

FIGURE 11 | Immunohistochemistry of PGC-1α after acute and sub-chronic treatments of AβOs in mice hippocampal slices. **(A)** Maximum intensity projections of confocal images showing neurons from the granular layer of the dentate gyrus in mice hippocampus stained for: PGC-1α (yellow), MAP2 (violet, for neurons), and DAPI (cyan, for nucleus). **(B)** Maximum intensity projections of stacked confocal images showed in **(A)**. **(C)** Normalized quantification of the fluorescence intensity for PGC-1α normalized with respect to MAP2 immunofluorescence in control condition and after AβOs (0.5 μM) exposure for 1 or 5 h. Scale bars: 5 μm. Data analyzed using one way ANOVA with Kruskall-Wallis test and Dunn's Multiple Comparison test. (*$p < 0.05$ vs control nroi: 462/nslices: 75, AβOs 1H nroi: 664/nslices: 37, AβOs 5H nroi: 977/nslices: 30/per each independent experiment, n=3).

opens a new line of study, and according with our data PGC1-α could be a interesting candidate.

Several studies postulate that mitochondrial failure may occur from a dysfunction in the mechanisms involved in mitochondrial turnover (the balance between organelle biogenesis and dynamics), which may also help delineate the underlying causes in age-related dysregulation of mitochondria in damaged neurons that are not available to support the metabolic demand of the synapse (Bonda et al., 2010). In the AD case, the lost on neuronal connectivity and synaptic failure mediated mainly by AβOs toxicity (Ferreira and Klein, 2011; Saez-Orellana et al., 2016), has been correlated with an early mitochondrial function loss (Eckert et al., 2010; Mendoza et al., 2014), cell damage (Reddy et al., 2012), and cognitive failure (Kimata et al., 2012). However, the mechanisms by which AβOs signaling promotes neuronal cell death and mitochondrial dysfunction are unclear (Swerdlow, 2018). The property of PGC-1α to interact with multiple DNA-binding transcription factors (TFs) to regulate the mitochondrial biogenesis and dynamic it allows maintenance of mitochondrial protein levels and other relevant proteins such as calmodulin-dependent kinase (CaMK), calcineurin (CN), PPARs, AMP-activated kinase (AMPK), SIRT1, ERR regulator in muscle 1, and retinoid X receptor (RXR) (Dorn et al., 2015), reinforce our idea about the consideration as new molecular target for modulation. During PPAR/PGC-1α interaction, the stimulation can rescue mitochondrial dysfunction and induces improvement in mitochondrial dynamic events (Fuenzalida et al., 2007). In this context expression of several nuclear and mitochondrial genes, Drp1, Mfn1 and mitochondrial transcription factor A (TFAM), is necessary for mitochondrial biogenesis (Westermann, 2010). Indeed, agonists for both PPARγ and α can prevent Aβ-associated mitochondrial dysfunction through a PGC-1α-dependent mechanism (Zolezzi et al., 2017),

and it's able to promote axonal growth, reduce oxidative stress, and improve brain clearance of toxic Aβ peptide (Puigserver et al., 1998; Zolezzi et al., 2017).

Taken together, any alterations on its role as fine tuner of mitochondrial biogenesis could be crucial for neuronal functions. Therefore the possibility to understand the early changes in this factor that can induce the loss of balance between fusion and fission may be considered as early market of neuronal damage by toxic agents, in this case amyloid β peptide. Several studies have reported that the level of PGC-1α evidently decreases in association with diminished mitochondrial density in the brains of AD patients (Qin et al., 2009). Indeed PGC-1α able to preserve synaptic function in animal models of AD (Halagappa et al., 2007), acting as a possible target for therapeutic intervention in AD (Sweeney and Song, 2016).

Upon the occurrence of cellular metabolic stress conditions, NAD^+/NADH ratio increases, promoting SIRT1 activation and transcriptional activity of PGC-1α by deacetylating at least one of its 13 acetylated lysine residues (Nogueiras et al., 2012). SIRT1 deacetylase activity has been linked to a neuroprotective effect in murine models of AD (Kim et al., 2007). Specifically, activation of SIRT1 manages to improve dendritic branching and neuronal function by inactivating the RhoA/ROCK pathway (Codocedo et al., 2012; Godoy et al., 2014). Indeed, positive modulation of the expression levels and activity of SIRT1 successfully improved energy expenditure in several animal models for neurodegenerative diseases associated with mitochondrial dysfunction (Donmez, 2012), and in case of AD it is able to diminish the memory deficits (Kim et al., 2007), but the mechanism that confers neuroprotection is still poorly understood.

In our work, we provide evidence about a biphasic behavior of PGC-1α/SIRT1 in a time-depend Aβ toxicity. Our first experimental evidence, as consequences of acute AβOs exposure, was the imbalance in the fission/fusion proteins (**Figures 2** and **3**) that induced a shift in the equilibrium to granular or fractioned mitochondrial phenotype (**Figures 4** and **5**), suggesting that the energetic pathway into the neurons it was interrupted. We expected that mitochondrial phenotype promotes an increase in the activation of signaling molecules for mitochondrial biogenesis as compensatory biological response to produce more functional and healthy mitochondria (a quantitative increase to overcome a qualitative deficiency, due to alterations in mitochondrial proteins that are either nuclear or mitochondrial encoded). However, we found that PGC-1α changed its subcellular distribution from predominant nuclear distribution in control conditions, to cytosolic distribution of PGC-1α (**Figures 7C** and **8C**), after chronic treatment with AβOs. The options to explain that PGC-1α was unable to translocated to the nucleus could be linked with changes on the levels of the protein, but without apparent differences on its immunoreactivity, the possibility that the changes from the acetylated form to deacetylated form, suggest that the option of an alteration with other elements in the signaling pathway like SIRT1. When attempting to elucidate this phenomenon, we evaluated the phosphorylated form of p-SIRT (Ser 46, 47 in humans) that regulates the SIRT1 availability. Phosphorylation of SIRT1 by JNK1 as a result of cell stress induced a brief activation of the SIRT1 function, followed by the degradation of SIRT1 by the proteasome due to its ubiquitination (Gao et al., 2011).

Under chronic treatments of AβOs, total levels of pSIRT1 were increased (**Figure 9C**), and there was a significant decrease in its nucleus/cytosol ratio (**Figure 10**) presenting a behavior like cytosolic PGC-1α (**Figure 7B**), was not observed for total SIRT1 distribution (**Figure 7B**). We have found that an increased in p-SIRT1(Ser 46), could be related with a novel mechanism induced by chronic treatments of AβOs, which also altered SIRT1 interaction with PGC-1α. We propose that this pathway could be directly associated to overactivation upon JNK1, and SIRT1 ubiquitination and degradation according with the evidence provided by Okazawa and Gadhave groups (Okazawa and Estus, 2002; Gadhave et al., 2016).

We performed morphologic analyses of the mitochondrial network in PC-12 cells, to corroborate our findings and the data showed that there were early alterations in mitochondria shape after treatment with AβOs (**Figures 4** and **5**). There was a clear granular phenotype that persisted even at chronic exposure times. At the chronic times, the total levels of Drp1 and Mfn1 did not change (**Supplementary Figure 1**). These findings are in line with the study that identify a previously unknown mitochondrial fission arrest phenotype that resulted in elongated interconnected organelles called "mitochondria-on-a-string" (MOAS) (Zhang et al., 2016). However, after chronic AβOs treatment (**Figures 6** and **11**), we found a significantly reduction in the total levels of both PGC-1α and SIRT1, but only PGC-1α presented an alteration in the nucleus/cytosol ratio showing an increase in its cytosolic distribution, reinforcing the idea that PGC-1α it has been "sequestered" in the cytosol, and this could be explained by a significant decrease on the interaction between SIRT1 and PGC-1α after chronic exposure to AβOs (**Figures 9A** and **12**). Several evidence suggest the existence of an orchestration between mitochondrial biogenesis and mitochondrial dynamics. For instance, these findings described above indicate that mitochondrial dynamics can affect mitochondrial biogenesis. PGC-1α-deficient mice showed an altered mitochondrial morphology including fragmentation and elongation and defects in proper mitochondrial dynamics in which the levels of Mfn1 were downregulated (Uittenbogaard and Chiaramello, 2014). In summary, recent data have implicated the existence of cross-regulatory circuits that coordinate both mitochondrial dynamics and mitochondrial biogenesis (Martin et al., 2014; Dorn et al., 2015; Song et al., 2015).

In this study we describe an important link between SIRT1/PGC-1α downregulation and the fast-morphological changes observed on mitochondria networks, promoting by a misbalance on DRP1/Mfn1 in a Aβ toxicity model (**Figure 12**). The "sequestered" PGC-1α in the cytosol could represent the non-return point for the neuron on the amyloid β toxicity. This study suggests a possible new approach for the treatment of AD, based on the preservation of the mitochondrial structure which open a new space of study centered on the modulation of PGC-1α/SIRT1 signaling, by PGC-1α deacetylation promotors, as new pharmacological tools to promote neuroprotection.

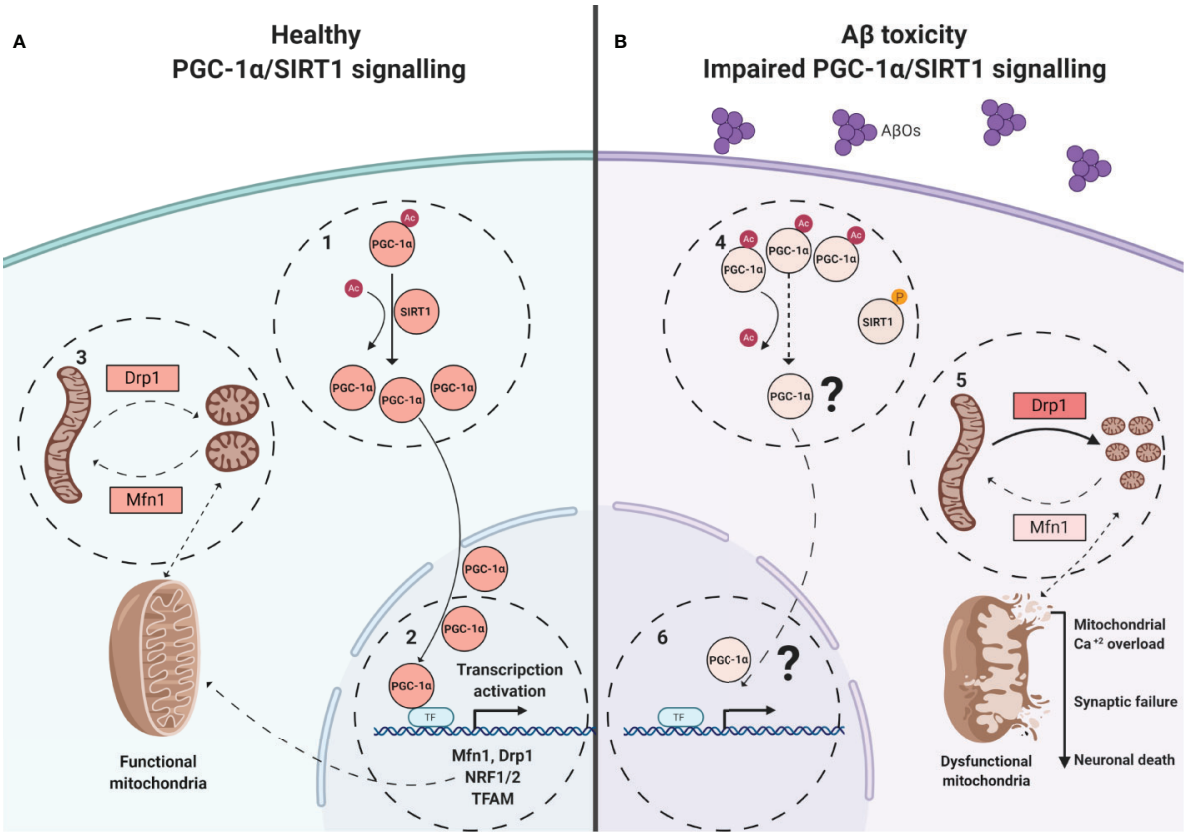

FIGURE 12 | Model of alterations induced on SIRT1/PGC-1α pathway by AβOs. **(A)**. Healthy neuronal conditions were energy depletion and/or decreased catabolic rates can be sensed by SIRT1 promoting the PGC-1α deacetylation (1). Transcription and co-activates of factors like NRF- 1/2 for the expression of nuclear-encoded mitochondrial genes and dynamic mitochondrial proteins, requires of PGC-1α translocation (2). Coordinated mitochondrial dynamics (3, fission/fusion), depends of adequate expression of Mfn1, Drp1. **(B)**. In AβOs treated neurons, the PGC-1α is unable to be deacetylated and to translocate to the nucleus (4). The expression of key genes is loss (5), and imbalance between fusion and fission to promote the granular mitochondrial phenotype (6) and neuronal death.

DATA AVAILABILITY STATEMENT

All datasets generated for this study are included in the article/ **Supplementary Material**.

ETHICS STATEMENT

All procedures related with animal management and tissue isolation were done following NIH (USA) and CONICYT guidelines and with protocols approved by the Bioethical Committee of the Universidad de Concepcion

AUTHOR CONTRIBUTIONS

JP and JF designed the study. JP, PG, OR-M and JG contributed to the sample preparation, data collection and analysis. JP, JF, CM-M, GY, GM-C, PC, LG, JS, and ET contributed to write the manuscript. JP, TS-G, and MC directed the experiments. All authors reviewed the manuscript.

FUNDING

This work was supported by Fondecyt 1161078 (JF), 1200908 (JF), and Conicyt 21141247 (JP).

ACKNOWLEDGMENTS

We thank Mrs. L. J. Aguayo, Ms. Ixia Cid, and Ms Pilar Vasquez for technical assistance and editing the manuscript. We thanks Centro de Microscopia Avanzada Bio-Bio, Universidad de Concepcion (CMA-BioBio).

SUPPLEMENTARY MATERIAL

The Supplementary Material for this article can be found online at: https://www.frontiersin.org/articles/10.3389/fphar.2020.00709/full#supplementary-material

REFERENCES

Alonso, M. T., Barrero, M. J., Michelena, P., Carnicero, E., Cuchillo, I., García, A. G., et al. (1999). Ca2+-induced Ca2+ release in chromaffin cells seen from inside the ER with targeted aequorin. *J. Cell Biol.* 144, 241–254. doi: 10.1083/jcb.144.2.241

Anderson, R. M., Barger, J. L., Edwards, M. G., Braun, K. H., O'connor, C. E., Prolla, T. A., et al. (2008). Dynamic regulation of PGC-1α localization and turnover implicates mitochondrial adaptation in calorie restriction and the stress response. *Aging Cell* 7, 101–111. doi: 10.1111/j.1474-9726.2007.00357.x

Arrazola, M. S., Ramos-Fernandez, E., Cisternas, P., Ordenes, D., and Inestrosa, N. C. (2017). Wnt Signaling Prevents the Abeta Oligomer-Induced Mitochondrial Permeability Transition Pore Opening Preserving Mitochondrial Structure in Hippocampal Neurons. *PloS One* 12, e0168840. doi: 10.1371/journal.pone.0168840

Bai, W., and Zhang, X. (2016). Nucleus or cytoplasm? The mysterious case of SIRT1's subcellular localization. *Cell Cycle* 15, 3337–3338. doi: 10.1080/15384101.2016.1237170

Bonda, D. J., Wang, X., Perry, G., Smith, M. A., and Zhu, X. (2010). Mitochondrial dynamics in Alzheimer's disease: opportunities for future treatment strategies. *Drugs Aging* 27, 181–192. doi: 10.2165/11532140-000000000-00000

Castellani, R. J., Rolston, R. K., and Smith, M. A. (2010). Alzheimer disease. *Dis. Mon.* 56, 484–546. doi: 10.1016/j.disamonth.2010.06.001

Chandrasekaran, K., Hatanpaa, K., Brady, D. R., and Rapoport, S. I. (1996). Evidence for physiological down-regulation of brain oxidative phosphorylation in Alzheimer's disease. *Exp. Neurol.* 142, 80–88. doi: 10.1006/exnr.1996.0180

Codocedo, J. F., Allard, C., Godoy, J. A., Varela-Nallar, L., and Inestrosa, N. C. (2012). SIRT1 regulates dendritic development in hippocampal neurons. *PloS One* 7, e47073–e47073. doi: 10.1371/journal.pone.0047073

Course, M. M., and Wang, X. (2016). Transporting mitochondria in neurons. *F1000Research* 5, 1–10. doi: 10.12688/f1000research.7864.1

Cuevas, M. E., Haensgen, H., Sepulveda, F. J., Zegers, G., Roa, J., Opazo, C., et al. (2011). Soluble Abeta(1-40) peptide increases excitatory neurotransmission and induces epileptiform activity in hippocampal neurons. *J. Alzheimers. Dis.* 23, 673–687. doi: 10.3233/JAD-2011-091717

Donmez, G. (2012). The effects of SIRT1 on Alzheimer's disease models. *Int. J. Alzheimers. Dis.* 2012, 4–7. doi: 10.1155/2012/509529

Dorn, G., Vega, R. B., and Kelly, D. P. (2015). Mitochondrial biogenesis and dynamics in the developing and diseased heart. *Genes Dev.* 29, 1981–1991. doi: 10.1101/gad.269894.115

Eckert, A., Schulz, K. L., Rhein, V., and Götz, J. (2010). Convergence of amyloid-beta and tau pathologies on mitochondria in vivo. *Mol. Neurobiol.* 41, 107–114. doi: 10.1007/s12035-010-8109-5

Feng, Y., Wang, X. P., Yang, S. G., Wang, Y. J., Zhang, X., Du, X. T., et al. (2009). Resveratrol inhibits beta-amyloid oligomeric cytotoxicity but does not prevent oligomer formation. *Neurotoxicology* 30, 986–995. doi: 10.1016/j.neuro.2009.08.013

Ferreira, S. T., and Klein, W. L. (2011). The Aβ oligomer hypothesis for synapse failure and memory loss in Alzheimer's disease. *Neurobiol. Learn. Mem.* 96, 529–543. doi: 10.1016/j.nlm.2011.08.003

Fuentealba, J., Dibarrart, A. J., Fuentes-Fuentes, M. C., Saez-Orellana, F., Quinones, K., Guzman, L., et al. (2011). Synaptic failure and adenosine triphosphate imbalance induced by amyloid-beta aggregates are prevented by blueberry-enriched polyphenols extract. *J. Neurosci. Res.* 89, 1499–1508. doi: 10.1002/jnr.22679

Fuenzalida, K., Quintanilla, R., Ramos, P., Piderit, D., Fuentealba, R. A., Martinez, G., et al. (2007). Peroxisome proliferator-activated receptor gamma up-regulates the Bcl-2 anti-apoptotic protein in neurons and induces mitochondrial stabilization and protection against oxidative stress and apoptosis. *J. Biol. Chem.* 282, 37006–37015. doi: 10.1074/jbc.M700447200

Gadhave, K., Bolshette, N., Ahire, A., Pardeshi, R., Thakur, K., Trandafir, C., et al. (2016). The ubiquitin proteasomal system: a potential target for the management of Alzheimer's disease. *J. Cell. Mol. Med.* 20, 1392–1407. doi: 10.1111/jcmm.12817

Gao, Z., Zhang, J., Kheterpal, I., Kennedy, N., Davis, R. J., and Ye, J. (2011). Sirtuin 1 (SIRT1) protein degradation in response to persistent c-Jun N-terminal kinase 1 (JNK1) activation contributes to hepatic steatosis in obesity. *J. Biol. Chem.* 286, 22227–22234. doi: 10.1074/jbc.M111.228874

Glenner, G. G., and Wong, C. W. (1984). Alzheimer's disease: initial report of the purification and characterization of a novel cerebrovascular amyloid protein. *Biochem. Biophys. Res. Commun.* 120, 885–890. doi: 10.1016/S0006-291X(84)80190-4

Godoy, J. A., Zolezzi, J. M., Braidy, N., and Inestrosa, N. C. (2014). Role of Sirt1 during the ageing process: relevance to protection of synapses in the brain. *Mol. Neurobiol.* 50, 744–756. doi: 10.1007/s12035-014-8645-5

Gong, Y., Chang, L., Viola, K. L., Lacor, P. N., Lambert, M. P., Finch, C. E., et al. (2003). Alzheimer's disease-affected brain: presence of oligomeric A beta ligands (ADDLs) suggests a molecular basis for reversible memory loss. *Proc. Natl. Acad. Sci. U. S. A.* 100, 10417–10422. doi: 10.1073/pnas.1834302100

Hackenbrock, C. R., Rehn, T. G., Weinbach, E. C., and Lemasters, J. J. (1971). Oxidative phosphorylation and ultrastructural transformation in mitochondria in the intact ascites tumor cell. *J. Cell Biol.* 51, 123–137. doi: 10.1083/jcb.51.1.123

Haigis, M. C., and Sinclair, D. A. (2010). Mammalian sirtuins: biological insights and disease relevance. *Annu. Rev. Pathol.* 5, 253–295. doi: 10.1146/annurev.pathol.4.110807.092250

Halagappa, V. K. M., Guo, Z., Pearson, M., Matsuoka, Y., Cutler, R. G., Laferla, F. M., et al. (2007). Intermittent fasting and caloric restriction ameliorate age-related behavioral deficits in the triple-transgenic mouse model of Alzheimer's disease. *Neurobiol. Dis.* 26, 212–220. doi: 10.1016/j.nbd.2006.12.019

Hirai, K., Aliev, G., Nunomura, A., Fujioka, H., Russell, R. L., Atwood, C. S., et al. (2001). Mitochondrial abnormalities in Alzheimer's disease. *J. Neurosci.* 21, 3017–3023. doi: 10.1523/JNEUROSCI.21-09-03017.2001

Kann, O., and Kovács, R. (2007). Mitochondria and neuronal activity. *Am. J. Physiol. Physiol.* 292, C641–C657. doi: 10.1152/ajpcell.00222.2006

Karadottir, R., and Attwell, D. (2006). Combining patch-clamping of cells in brain slices with immunocytochemical labeling to define cell type and developmental stage. *Nat. Protoc.* 1, 1977–1986. doi: 10.1038/nprot.2006.261

Kim, D., Nguyen, M. D., Dobbin, M. M., Fischer, A., Sananbenesi, F., Rodgers, J. T., et al. (2007). SIRT1 deacetylase protects against neurodegeneration in models for Alzheimer's disease and amyotrophic lateral sclerosis. *EMBO J.* 26, 3169–3179. doi: 10.1038/sj.emboj.7601758

Kimata, T., Sasakura, H., Ohnishi, N., Nishio, N., and Mori, I. (2012). Thermotaxis of C. elegans as a model for temperature perception, neural information processing and neural plasticity. *Worm* 1, 31–41. doi: 10.4161/worm.19504

Kosik, K. S., Joachim, C. L., and Selkoe, D. J. (1986). Microtubule-associated protein tau (tau) is a major antigenic component of paired helical filaments in Alzheimer disease. *Proc. Natl. Acad. Sci. U. S. A.* 83, 4044–4048. doi: 10.1073/pnas.83.11.4044

Lal, R., Lin, H., and Quist, A. P. (2007). Amyloid beta ion channel: 3D structure and relevance to amyloid channel paradigm. *Biochim. Biophys. Acta* 1768, 1966–1975. doi: 10.1016/j.bbamem.2007.04.021

LC, G., G, D. B., and Scorrano, L. (2011). During autophagy mitochondria elongate, are spared from degradation and sustain cell viability. *Nat. Cell Biol.* 13, 589–598. doi: 10.1038/ncb2220

Lee, S., Sterky, F. H., Mourier, A., Terzioglu, M., Cullheim, S., Olson, L., et al. (2012). Mitofusin 2 is necessary for striatal axonal projections of midbrain dopamine neurons. *Hum. Mol. Genet.* 21, 4827–4835. doi: 10.1093/hmg/dds352

Lehman, J. J., Barger, P. M., Kovacs, A., Saffitz, J. E., Medeiros, D. M., and Kelly, D. P. (2000). Peroxisome proliferator-activated receptor gamma coactivator-1 promotes cardiac mitochondrial biogenesis. *J. Clin. Invest.* 106, 847–856. doi: 10.1172/JCI10268

Li, Z., Okamoto, K.-I., Hayashi, Y., and Sheng, M. (2004). The importance of dendritic mitochondria in the morphogenesis and plasticity of spines and synapses. *Cell* 119, 873–887. doi: 10.1016/j.cell.2004.11.003

Liesa, M., Palacin, M., and Zorzano, A. (2009). Mitochondrial dynamics in mammalian health and disease. *Physiol. Rev.* 89, 799–845. doi: 10.1152/physrev.00030.2008

Manczak, M., Anekonda, T. S., Henson, E., Park, B. S., Quinn, J., and Reddy, P. H. (2006). Mitochondria are a direct site of A beta accumulation in Alzheimer's disease neurons: implications for free radical generation and oxidative damage in disease progression. *Hum. Mol. Genet.* 15, 1437–1449. doi: 10.1093/hmg/ddl066

Martin, O. J., Lai, L., Soundarapandian, M. M., Leone, T. C., Zorzano, A., Keller, M. P., et al. (2014). A role for peroxisome proliferator-activated receptor

gamma coactivator-1 in the control of mitochondrial dynamics during postnatal cardiac growth. *Circ. Res.* 114, 626–636. doi: 10.1161/CIRCRESAHA.114.302562

Mendoza, E., Miranda-Barrientos, J. A., Vazquez-Roque, R. A., Morales-Herrera, E., Ruelas, A., De la Rosa, G., et al. (2014). In vivo mitochondrial inhibition alters corticostriatal synaptic function and the modulatory effects of neurotrophins. *Neuroscience* 280, 156–170. doi: 10.1016/j.neuroscience.2014.09.018

Näslund, J. (2000). Correlation Between Elevated Levels of Amyloid β-Peptide in the Brain and Cognitive Decline. *Jama* 283, 1571. doi: 10.1001/jama.283.12.1571

Nogueiras, R., Habegger, K. M., Chaudhary, N., Finan, B., Banks, A. S., Dietrich, M. O., et al. (2012). Sirtuin 1 and sirtuin 3: physiological modulators of metabolism. *Physiol. Rev.* 92, 1479–1514. doi: 10.1152/physrev.00022.2011

Okazawa, H., and Estus, S. (2002). The JNK/c-Jun cascade and Alzheimer's disease. *Am. J. Alzheimers. Dis. Other Demen.* 17, 79–88. doi: 10.1177/153331750201700209

Parodi, J., Sepulveda, F. J., Roa, J., Opazo, C., Inestrosa, N. C., and Aguayo, L. G. (2010). Beta-amyloid causes depletion of synaptic vesicles leading to neurotransmission failure. *J. Biol. Chem.* 285, 2506–2514. doi: 10.1074/jbc.M109.030023

Pauwels, K., Williams, T. L., Morris, K. L., Jonckheere, W., Vandersteen, A., Kelly, G., et al. (2012). Structural basis for increased toxicity of pathological abeta42: abeta40 ratios in Alzheimer disease. *J. Biol. Chem.* 287, 5650–5660. doi: 10.1074/jbc.M111.264473

Pham, A. H., Meng, S., Chu, Q. N., and Chan, D. C. (2012). Loss of Mfn2 results in progressive, retrograde degeneration of dopaminergic neurons in the nigrostriatal circuit. *Hum. Mol. Genet.* 21, 4817–4826. doi: 10.1093/hmg/dds311

Puigserver, P., Wu, Z., Park, C. W., Graves, R., Wright, M., and Spiegelman, B. M. (1998). A cold-inducible coactivator of nuclear receptors linked to adaptive thermogenesis. *Cell* 92, 829–839. doi: 10.1016/S0092-8674(00)81410-5

Qin, W., Haroutunian, V., Katsel, P., Cardozo, C. P., Ho, L., Buxbaum, J. D., et al. (2009). PGC-1alpha expression decreases in the Alzheimer disease brain as a function of dementia. *Arch. Neurol.* 66, 352–361. doi: 10.1001/archneurol.2008.588

Reddy, P. H., Reddy, T. P., Manczak, M., Calkins, M. J., Shirendeb, U., and Mao, P. (2011). Dynamin-related protein 1 and mitochondrial fragmentation in neurodegenerative diseases. *Brain Res. Rev.* 67, 103–118. doi: 10.1016/j.brainresrev.2010.11.004

Reddy, P. H., Tripathi, R., Troung, Q., Tirumala, K., Reddy, T. P., Anekonda, V., et al. (2012). Abnormal mitochondrial dynamics and synaptic degeneration as early events in Alzheimer's disease: implications to mitochondria-targeted antioxidant therapeutics. *Biochim. Biophys. Acta* 1822, 639–649. doi: 10.1016/j.bbadis.2011.10.011

Rodgers, J. T., Lerin, C., Haas, W., Gygi, S. P., Spiegelman, B. M., and Puigserver, P. (2005). Nutrient control of glucose homeostasis through a complex of PGC-1alpha and SIRT1. *Nature* 434, 113–118. doi: 10.1038/nature03354

Sáez-Orellana, F., Fuentes-Fuentes, M. C., Godoy, P. A., Silva-Grecchi, T., Panes, J. D., Guzmán, L., et al. (2018). P2X receptor overexpression induced by soluble oligomers of amyloid beta peptide potentiates synaptic failure and neuronal dyshomeostasis in cellular models of Alzheimer's disease. *Neuropharmacology* 128, 366–378. doi: 10.1016/j.neuropharm.2017.10.027

Saez-Orellana, F., Godoy, P. A., Bastidas, C. Y., Silva-Grecchi, T., Guzman, L., Aguayo, L. G., et al. (2016). ATP leakage induces P2XR activation and contributes to acute synaptic excitotoxicity induced by soluble oligomers of beta-amyloid peptide in hippocampal neurons. *Neuropharmacology* 100, 116–123. doi: 10.1016/j.neuropharm.2015.04.005

Schmitt, K., Grimm, A., Kazmierczak, A., Strosznajder, J. B., Götz, J., and Eckert, A. (2011). Insights into Mitochondrial Dysfunction: Aging, Amyloid-β, and Tau–A Deleterious Trio. *Antioxid. Redox Signal.* 16, 1456–1466. doi: 10.1089/ars.2011.4400

Sepulveda, F. J., Parodi, J., Peoples, R. W., Opazo, C., and Aguayo, L. G. (2010). Synaptotoxicity of Alzheimer beta amyloid can be explained by its membrane perforating property. *PloS One* 5, e11820. doi: 10.1371/journal.pone.0011820

Shankar, G. M., Bloodgood, B. L., Townsend, M., Walsh, D. M., Selkoe, D. J., and Sabatini, B. L. (2007). Natural oligomers of the Alzheimer amyloid-beta protein induce reversible synapse loss by modulating an NMDA-type glutamate receptor-dependent signaling pathway. *J. Neurosci.* 27, 2866–2875. doi: 10.1523/JNEUROSCI.4970-06.2007

Sheng, B., Wang, X., Su, B., Lee, H., Casadesus, G., Perry, G., et al. (2012). Impaired mitochondrial biogenesis contributes to mitochondrial dysfunction in Alzheimer's disease. *J. Neurochem.* 120, 419–429. doi: 10.1111/j.1471-4159.2011.07581.x

Song, M., Mihara, K., Chen, Y., Scorrano, L., and Dorn, G. (2015). Mitochondrial fission and fusion factors reciprocally orchestrate mitophagic culling in mouse hearts and cultured fibroblasts. *Cell Metab.* 21, 273–286. doi: 10.1016/j.cmet.2014.12.011

Sweeney, G., and Song, J. (2016). The association between PGC-1α and Alzheimer's disease. *Anat. Cell Biol.* 49, 1–6. doi: 10.5115/acb.2016.49.1.1

Swerdlow, R. H., Burns, J. M., and Khan, S. M. (2010). The Alzheimer's Disease Mitochondrial Cascade Hypothesis. *J. Alzheimer's Dis.* 20, S265–S279. doi: 10.3233/JAD-2010-100339

Swerdlow, R. H. (2018). Mitochondria and Mitochondrial Cascades in Alzheimer's Disease. *J. Alzheimers. Dis.* 62, 1403–1416. doi: 10.3233/JAD-170585

Terada, T., Obi, T., Bunai, T., Matsudaira, T., Yoshikawa, E., Ando, I., et al. (2020). In vivo mitochondrial and glycolytic impairments in patients with Alzheimer disease. *Neurology* 94 (15), e1592–e1604. doi: 10.1212/WNL.0000000000009249

Toglia, P. T., Demuro, A., Parker, I., and Ullah, G. (2018). Mitochondrial Dysfunction due to Intracellular Beta Amyloid Oligomers. *Biophys. J.* 114, 660a–661a. doi: 10.1016/j.bpj.2017.11.3567

Uittenbogaard, M., and Chiaramello, A. (2014). Mitochondrial biogenesis: a therapeutic target for neurodevelopmental disorders and neurodegenerative diseases. *Curr. Pharm. Des.* 20, 5574–5593. doi: 10.2174/1381612820666140305224906

Viswakarma, N., Jia, Y., Bai, L., Vluggens, A., Borensztajn, J., Xu, J., et al. (2010). Coactivators in PPAR-Regulated Gene Expression. *PPAR Res.* 2010, 1–21. doi: 10.1155/2010/250126

Wang, X., Su, B., Fujioka, H., and Zhu, X. (2008). Dynamin-like protein 1 reduction underlies mitochondrial morphology and distribution abnormalities in fibroblasts from sporadic Alzheimer's disease patients. *Am. J. Pathol.* 173, 470–482. doi: 10.2353/ajpath.2008.071208

Wang, X., Su, B., Lee, H.-g., Li, X., Perry, G., Smith, M. A., et al. (2009). Impaired Balance of Mitochondrial Fission and Fusion in Alzheimer's Disease. *J. Neurosci.* 29, 9090–9103. doi: 10.1523/JNEUROSCI.1357-09.2009

Wang, I. H., Chen, H. Y., Wang, Y. H., Chang, K. W., Chen, Y. C., and Chang, C. R. (2014). Resveratrol modulates mitochondria dynamics in replicative senescent yeast cells. *PloS One* 9, 1–8. doi: 10.1371/journal.pone.0104345

Westermann, B. (2010). Mitochondrial fusion and fission in cell life and death. *Nat. Rev. Mol. Cell Biol.* 11, 872–884. doi: 10.1038/nrm3013

Zhang, L., Trushin, S., Christensen, T. A., Bachmeier, B. V., Gateno, B., Schroeder, A., et al. (2016). Altered brain energetics induces mitochondrial fission arrest in Alzheimer's Disease. *Sci. Rep.* 6, 18725. doi: 10.1038/srep18725

Zhu, X., Perry, G., Moreira, P. I., Aliev, G., Cash, A. D., Hirai, K., et al. (2006). Mitochondrial abnormalities and oxidative imbalance in Alzheimer disease. *J. Alzheimers. Dis.* 9, 147–153. doi: 10.3233/JAD-2006-9207

Zolezzi, J. M., Santos, M. J., Bastias-Candia, S., Pinto, C., Godoy, J. A., and Inestrosa, N. C. (2017). PPARs in the central nervous system: roles in neurodegeneration and neuroinflammation. *Biol. Rev. Camb. Philos. Soc* 92, 2046–2069. doi: 10.1111/brv.12320

Conflict of Interest: The authors declare that the research was conducted in the absence of any commercial or financial relationships that could be construed as a potential conflict of interest.

frontiers in Pharmacology

ORIGINAL RESEARCH
published: 18 June 2020
doi: 10.3389/fphar.2020.00920

Dietary Potassium Downregulates Angiotensin-I Converting Enzyme, Renin, and Angiotensin Converting Enzyme 2

Carlos P. Vio[1,2*], *Pedro Gallardo*[3], *Carlos Cespedes*[1,2], *Daniela Salas*[1], *Jessica Diaz-Elizondo*[1] and *Natalia Mendez*[4]

[1] Center for Aging and Regeneration CARE UC, Department of Physiology, Facultad de Ciencias Biológicas, Pontificia Universidad Católica de Chile, Santiago, Chile, [2] Facultad de Medicina y Ciencia, Universidad San Sebastian, Santiago, Chile, [3] Facultad de Medicina, Escuela de Medicina, Universidad Finis Terrae, Santiago, Chile, [4] Facultad de Medicina, Institute of Anatomy, Histology and Pathology, Universidad Austral de Chile, Valdivia, Chile

OPEN ACCESS

Edited by:
Guillermo Diaz-Araya,
University of Chile, Chile

Reviewed by:
Chin Moi Chow,
University of Sydney, Australia
Ana Cristina Simões E. Silva,
Federal University of Minas Gerais, Brazil
Dulce Elena Casarini,
Universidade Federal de São Paul, Brazil

***Correspondence:**
Carlos P. Vio
cvio@uc.cl;
carlos.vio@uss.cl

Specialty section:
This article was submitted to Translational Pharmacology, a section of the journal Frontiers in Pharmacology

Received: 02 November 2019
Accepted: 05 June 2020
Published: 18 June 2020

Citation:
Vio CP, Gallardo P, Cespedes C, Salas D, Diaz-Elizondo J and Mendez N (2020) Dietary Potassium Downregulates Angiotensin-I Converting Enzyme, Renin, and Angiotensin Converting Enzyme 2. Front. Pharmacol. 11:920. doi: 10.3389/fphar.2020.00920

Background: The importance of dietary potassium in health and disease has been underestimated compared with that placed on dietary sodium. Larger effort has been made on reduction of sodium intake and less on the adequate dietary potassium intake, although natural food contains much more potassium than sodium. The benefits of a potassium-rich diet are known, however, the mechanism by which it exerts its preventive action, remains to be elucidated. With the hypothesis that dietary potassium reduces renal vasoconstrictor components of the renin-angiotensin system in the long-term, we studied the effect of high potassium diet on angiotensin-I converting enzyme, renin, and angiotensin converting enzyme 2.

Methods: Sprague Dawley male rats on a normal sodium diet received normal potassium (0.9%, NK) or high potassium diet (3%, HK) for 4 weeks. Urine was collected in metabolic cages for electrolytes and urinary volume measurement. Renal tissue was used to analyze angiotensin-I converting enzyme, renin, and angiotensin converting enzyme 2 expression. Protein abundance analysis was done by Western blot; gene expression by mRNA levels by RT-qPCR. Renal distribution of angiotensin-I converting enzyme and renin was done by immunohistochemistry and morphometric analysis in coded samples.

Results: High potassium diet (4 weeks) reduced the levels of renin, angiotensin-I converting enzyme, and angiotensin converting enzyme 2. Angiotensin-I converting enzyme was located in the brush border of proximal tubules and with HK diet decreased the immunostaining intensity ($P < 0.05$), decreased the mRNA ($P < 0.01$) and the protein levels ($P < 0.01$). Renin localization was restricted to granular cells of the afferent arteriole and HK diet decreased the number of renin positive cells ($P < 0.01$) and renin mRNA levels ($P < 0.01$). High potassium intake decreased angiotensin converting enzyme 2 gene expression and protein levels ($P < 0.01$). No morphological abnormalities were observed in renal tissue during high potassium diet.The reduced expression of angiotensin-I converting enzyme, renin, and angiotensin converting enzyme 2 during

potassium supplementation suggest that high dietary potassium intake could modulate these vasoactive enzymes and this effects can contribute to the preventive and antihypertensive effect of potassium.

Keywords: dietary potassium intake, renin, angiotensin converting enzyme 2 (ACE2), immunohistochemistry, angiotensin-I converting enzyme (ACE)

INTRODUCTION

Sodium and potassium ions are important for life. Body sodium content maintains extracellular volume and plasma sodium concentration determines plasma osmolality (Slotki and Skorecki, 2016). Body potassium content resides mainly in the intracellular space and a small fraction in the extracellular space. The ratio of intracellular to extracellular potassium concentration determines the membrane potential, which is critical for maintaining normal excitability in nerve and cardiac muscle (Blaustein et al., 2012). Cardiovascular and kidney disease are major causes of mortality worldwide. The kidney is involved in the pathophysiology of arterial hypertension, which in turn is a major risk factor in cardiovascular diseases. High chronic daily sodium intake is a major factor determining endothelial dysfunction and arterial hypertension.

Several epidemiological and meta-analysis studies demonstrate that high dietary sodium intake is associated with high risk of cardiovascular disease including high systolic and diastolic blood pressure and many other cardiovascular and kidney disease (Aaron and Sanders, 2013). High dietary potassium intake reduced systolic and diastolic blood pressure (Tobian, 1997). The reduction of blood pressure associated with high dietary potassium intake was observed only in hypertensive population (Aaron and Sanders, 2013; Mente et al., 2014). Furthermore, it was demonstrated that in hypertensive people, the increase in potassium intake had no adverse effects (Agurto et al., 2013).

The mechanisms responsible for the beneficial effects of a high dietary potassium on the cardiovascular system are incompletely understood. Epidemiological studies demonstrate that there is a negative correlation between potassium excretion and systolic pressure; the relationship is steeper in hypertensive people (Mente et al., 2014). These results suggest that at least the beneficial effect of a high potassium diet on systolic blood pressure is related to the kidneys through renal potassium excretion. Potassium secretion by distal convoluted tubule 2, connecting and principal cells of the distal nephron is the major process involved in potassium excretion (McDonough and Youn, 2017). On the other hand, the distal nephron is also involved in the regulation of extracellular volume and blood pressure through the fine tuning of sodium reabsorption and, at the same level, sodium reabsorption and potassium secretion are intimately related (Penton et al., 2015). A high potassium diet also stimulates the renal kallikrein-kinin system. Kallikrein, secreted by the connecting tubule cells, is an enzyme that mediates the synthesis of bradykinin. This peptide mediates vasodilation and natriuresis by binding to B2K receptors, which in turn stimulates NO and prostaglandin synthesis (Vio and Figueroa, 1987). Therefore, the kidneys seem to be an important target through which a high potassium intake lowers arterial blood pressure.

Several vasoactive systems may contribute to arterial hypertension. The systemic renin-angiotensin system increases arterial blood pressure in several ways. Angiotensin II increases total peripheral resistance (Touyz and Schiffrin, 2000); increases NaCl reabsorption (Gamba, 2012) and stimulates aldosterone synthesis, which in turn increases NaCl reabsorption in the aldosterone-sensitive distal nephron (Féraille and Doucet, 2001). The intrarenal renin-angiotensin system may also contribute to hypertension. Renin enzyme can reach the proximal tubule that express angiotensinogen, angiotensin-I converting enzyme (ACE), and AT1 receptors in the apical domain of proximal tubule and distal convoluted tubule producing angiotensin II that contributes to hypertension through the stimulation of NaCl reabsorption in the proximal and distal convoluted tubule (Velez, 2009; Gurley et al., 2011; Li et al., 2018).

Plasma potassium plays an important role in the regulation of intrarenal vasoactive systems. It was demonstrated in rats, that hypokalemia maintained for 12 weeks increases the expression of cortical ACE and endothelin-1. This protocol of hypokalemia also induced renal injury that was most prominent in the cortex. All these findings favor the development of salt sensitivity and hypertension (Suga et al., 2001). On the other hand, salt sensitivity requires the expression of renal ACE as in mouse models lacking ACE where salt sensitivity in response to renal injury was completely absent (Giani et al., 2015). The cellular mechanisms underlying the effects of hypokalemia on ACE expression are unclear. The intrarenal mechanisms by which a high potassium diet reduces arterial blood pressure, increases natriuresis and diuresis, are incompletely understood. Since the intrarenal renin-angiotensin system favors sodium retention, the inhibition of this system could contribute to the potassium induced natriuretic response. With the hypothesis that a high potassium diet could down regulate the components of the intrarenal renin-angiotensin system, the aim of this research was to study the effect of a chronic high potassium diet on the expression of cortical renin, ACE, and angiotensin converting enzyme 2 (ACE2) in rat kidney.

METHODS

Animals and Experimental Procedures

Adult male Sprague-Dawley rats (180 to 200 g, n = 11 for each group) were housed under controlled temperature (18–20°C) and a 12 h light/dark cycle. All animals received food and water

ad-libitum and kept at the animal care facilities of the Pontificia Universidad Catolica de Chile. All experiments were carried out following the directions of the "Manual de Normas de Bioseguridad" version 2008, FONDECYT-CONICYT, and the Guide for the Care and Use of Laboratory Animals of the Institute for Laboratory Animal Research of the National Research Council, and approved by the Institutional Ethical Committee (Fondecyt 1130741).

Rats were randomly assigned to a control group (NK, 0.26% sodium and 0.91% potassium in chow, tap water) or a supplemented potassium diet (HK, 0.26% sodium and 2% potassium in chow, 2% KCl in water), with free access to food and water for 4 weeks. During the first week of treatment, the HK group received 1% KCl in drinking water. Then, KCl was raised to 2% from week 2 until the end of the treatment. Normal (Prolab RMH 3000) or potassium supplemented chow (Prolab RMH 3000 supplemented with potassium to a final concentration of 2% potassium) were purchased from Purina LabDiet. The sodium and potassium content were verified at the Laboratory of Food Analysis at the Instituto de Ciencia y Tecnologia de los Alimentos, Universidad Austral de Chile, Valdivia, Chile.

For urine collection, rats were placed in metabolic cages (Tecniplast, Buguggiate, Italy) for 16 h (from 5 pm to 9 am) during the last day of the 4 week period; water and food were supplied *ad libitum*. Urine samples were obtained, measured, and pelleted at 1,000 g for 10 min and stored at −20°C. After the sampling period, rats were anesthetized with isoflurane (isoflurane + O_2, induction 4–5% and maintenance 1–2%). A blood sample was obtained from Vena Cava in heparin-tubes, both kidneys were removed, isoflurane was increased until breathing stopped and death of the animals was confirmed. Pneumothorax was performed as a secondary physical method of euthanasia.

Kidney capsule was rapidly removed. Whole kidney sections were obtained for immunohistochemistry, Western blot, and qRT-PCR. The samples for Western blot and qRT-PCR were rapidly frozen in liquid nitrogen and stored at −80°C until processing. Serum concentration and urinary excretion of potassium and sodium were determined using an ion selective electrolyte analyzer 9180 (Roche Diagnostic).

Source of Antisera and Chemicals

Antibodies. Anti-α-tubulin antibody (T-5168) were purchased from Sigma Chemical; anti-ACE antibody (SC-12187), anti-goat IgG-HRP (SC-2020) were from Santa Cruz Biotechnology (Santa Cruz, CA); secondary antibody and corresponding peroxidase-anti-peroxidase (PAP) complex were from MP Biomedicals (Santa Ana, CA). Anti-renin antibody for immunohistochemistry was a gift from Dr. Pierre Corvol (College de France, Paris, France), ACE2 antibody for Western blot was from Abcam (Cambridge, UK).

Reagents. MMLV, DNAse I, TRIzol reagent and phosphatase inhibitor were from Invitrogen (Carlsbad, CA); dNTPs, random primers, FAST SYBR Green Master Mix, from Thermo Fisher Scientific (Waltham, MA). ECL Western blotting substrate was from Pierce (Waltham, MA).

Tissue Processing and Immunohistochemical Analysis

Renal tissue samples (3-mm thick) were fixed by immersion in Bouin's solution for 24 h at room temperature, dehydrated, embedded in paraffin (Paraplast Plus, Sigma-Aldrich), and serially sliced at 5 μm thickness with a Leica rotary microtome. The samples were mounted on glass slides and stored for immunohistochemistry. Renin and ACE immunostaining was performed using an indirect immunoperoxidase technique in randomly selected kidney samples (Vio et al., 2012; Vio et al., 2018). Briefly, kidney sections were dewaxed, rehydrated, and rinsed in 0.05 M Tris-phosphate-saline (TPS) buffer pH 7.6. The kidney sections were incubated overnight at 22°C with a primary antiserum raised against renin or ACE. After rinsing in TPS buffer, the secondary antibody and corresponding PAP complex were applied for 30 min each at 22°C. The immunoreactive sites were revealed after incubating the sections in 0.1% (wt/vol) diaminobenzidine and 0.03% hydrogen peroxide. The sections were rinsed with TPS buffer, counterstained with hematoxylin, dehydrated, and cleared with xylene. Controls for the immunostaining procedure were prepared by omission of the first antibody. The kidney sections were examined with conventional light microscopy and acquired using a Nikon Eclipse E600 microscope and Nikon DS-Ri1 digital camera. For renin and ACE, the stained area in each image was quantified using Simple PCI, a computer-assisted image-analysis software, Hamamatsu Corporation (Sewickley, PA). The values corresponding to total immunostained area, were averaged and expressed as fold change *versus* control.

Western Blotting

Western blotting was performed as described previously (Vio et al., 2012; Vio et al., 2018). In brief, kidney sections weighing 100 mg were homogenized in lysis buffer (150 mM NaCl, 50 mM Tris·HCl, 0.5% deoxycholate, 0.1% SDS, NP40) containing protease and phosphatase inhibitors (phosphatase inhibitor cocktail 1 and 2) with an Ultra-Turrax. After centrifugation at 14,000 rpm for 10 min, protein concentration was determined using the BCA method. Equal amount of protein extract (50 μg total) was mixed with sample buffer (100 mM Tris·HCl, pH 6.8, 200 mM dithiotreitol, 4% SDS, 0.2% bromophenol blue, and 20% glycerol) and heated at 75°C for 10 min. The protein samples were separated in 10% Tris-glycine SDS-PAGE and transferred to a PVDF membrane. The membrane was soaked in blocking solution 5% skim milk in TTBS (Tris-buffered saline and Tween 20) for 1 h at room temperature and incubated with a primary antibody against ACE or ACE2 overnight at 4°C. The membranes were washed in TTBS, and incubated with the horseradish peroxidase (HRP)-conjugated secondary antibody for 1 h at room temperature. Immunoreactivity in the membrane was detected with SuperSignal West Dura Extended Duration Substrate (Thermo Fisher Scientific) and stored with ChemiDoc-It Imaging System (UVP, Upland, CA).

Quantitative RT-PCR

Total RNA was extracted from frozen kidney samples using TRIzol reagent according to the manufacturer instructions. RNA integrity was determined in 1% agarose gel electrophoresis. Total RNA concentration was determined by measuring the absorbance at 260/280 nm. cDNA synthesis was carried out with 2.5 μg of total RNA incubated with MMLV reverse transcriptase, dNTPs, and random primers according to instructions provided by the manufacturer. After incubation, samples were treated with DNAse I. For quantitative PCR, the primer sequences used were the following:

ACE, forward primer: 5'-AACACGGCTCGTGCAGAAG-3',

ACE, reverse primer: 5'-CCTGCTGTGGTTCCAGGTACA-3';

ACE2, forward primer: 5'-ACCCTTCTTACATCAGCCCTACTG-3',

ACE2, reverse primer 5'-TGTCCAAAACCTACCCCACTAT-3';

Renin, forward primer: 5'-GCTACATGGAGAATGGGACTGAA-3',

Renin, reverse primer: 5'-ACCACATCTTGGCTGAGGAAAC-3'.

Quantitative PCR was performed in duplicate in a StepOnePlus Real-Time PCR System (Applied Biosystems) using FAST SYBR Green Master Mix for amplification. Results were normalized by glyceraldehyde 3 phosphate dehydrogenase (GAPDH) forward primer: 5'-CACGGCAAGTTCAACGGC-3' reverse primer 5'-GGTGGTGAAGACGCCAGTA-3'. Mathematical quantification was carried out using the $2^{-\Delta\Delta CT}$ method (Livak and Schmittgen, 2001).

Statistics

All data are presented as mean ± SEM. Statistical analyses were performed using an unpaired Student's t-test and GraphPad Prism software (La Jolla, CA). Differences with $P < 0.05$ were considered statistically significant.

RESULTS

The effect of a chronic high potassium diet (HK) on serum potassium and sodium concentration, and urinary excretion of sodium and potassium are shown in **Table 1**. As expected, plasma sodium concentration did not change between both groups and plasma potassium concentration was slightly increased in the HK diet group compared to control group (3.80 ± 0.08 mEq/L *versus* 4.46 ± 0.26 mEq/L; $P < 0.05$). The effect of a high potassium diet on sodium excretion is shown in **Table 1**. Compared to control rats, the HK group increased significantly its urinary sodium (0.92 ± 0.08 *versus* 1.87 ± 0.31; $P < 0.01$) and urinary potassium (3.60 ± 0.23 *versus* 30.30 ± 4.32; $P < 0.01$) excretion.

In this study immunohistochemical staining was used to characterize the protein expression at tissue level and the distribution of the vasoactive enzymes ACE and renin in the kidney.

Renal tissue samples were examined in coded fashion by two of us (C.Cespedes and C.Vio), and systematic analysis of kidney tissue samples was done focusing on the overall morphological aspect, and on cortical and medullary tubules, glomeruli, blood vessels, interstitial space, and intratubular spaces as previously done (Vio et al., 2018).

An overall and detailed examination of renal tissue with immunostaining and hematoxylin of kidneys from animals from both groups showed no signs of pathological alterations in the cortex or the medulla. No vascular changes were observed, tubules were normally shaped in terms of diameter and cell size, and no signs of cell infiltration or inflammation were observed in the tubulointerstitial space. Glomeruli from cortical or juxtamedullary nephrons had a normal aspect (**Figures 1** and **4**).

Vasoactive Enzyme Expression and Distribution

Angiotensin-I Converting Enzyme

The immunolocalization of ACE is shown in **Figure 1**. In the kidneys from control rats (**Figures 1A, B**), ACE was localized in proximal straight tubules. The immunoperoxidase signal was mainly present in the apical domain; scarce or none immunostaining was seen in the cytoplasm and no staining was observed at the basolateral domain, as reported previously (Vio and Jeanneret, 2003). The immunoperoxidase signal was markedly reduced in the high potassium diet group (**Figures 1C, D**) compared to the control diet group. In the HK group, localization of ACE immunostaining remained in the proximal straight tubules. The subcellular localization of the immunoperoxidase signal was also conserved compared to control group. However, the morphometric analysis of the ACE immunostained area (**Figure 1E**), showed a significant decrease in the HK group compared to control group. The reduction of the ACE immunoperoxidase signal found in the experimental group suggest a reduction in ACE protein abundance. To investigate if the reduction in ACE immunostaining observed in the HK group was accompanied by a reduction of protein abundance, we performed Western blot analysis with total kidney protein

TABLE 1 | Serum and urinary electrolytes.

Group (diet)	Serum concentration (mEq/L)		Urinary excretion (mEq/16 h)	
	Na^+	K^+	Na^+	K^+
NK	**140.80 ± 1.07**	**3.80 ± 0.08**	**0.92 ± 0.08**	**3.60 ± 0.23**
HK	**139.80 ± 0.66**	**4.46 ± 0.26***	**1.87 ± 0.31****	**30.30 ± 4.32****

*Effect of a chronic high potassium diet on serum electrolytes and urinary excretion in adult male rats. The potassium supplementation diet (HK) did not alter significantly the serum Na^+ concentration. Serum K^+ concentration was increased significantly. In the HK group, urinary sodium excretion was doubled compared to control diet. Urinary potassium excretion was also significantly increased. Data are expressed as mean ± SEM; n = 11; *P < 0.05, **P < 0.01.*

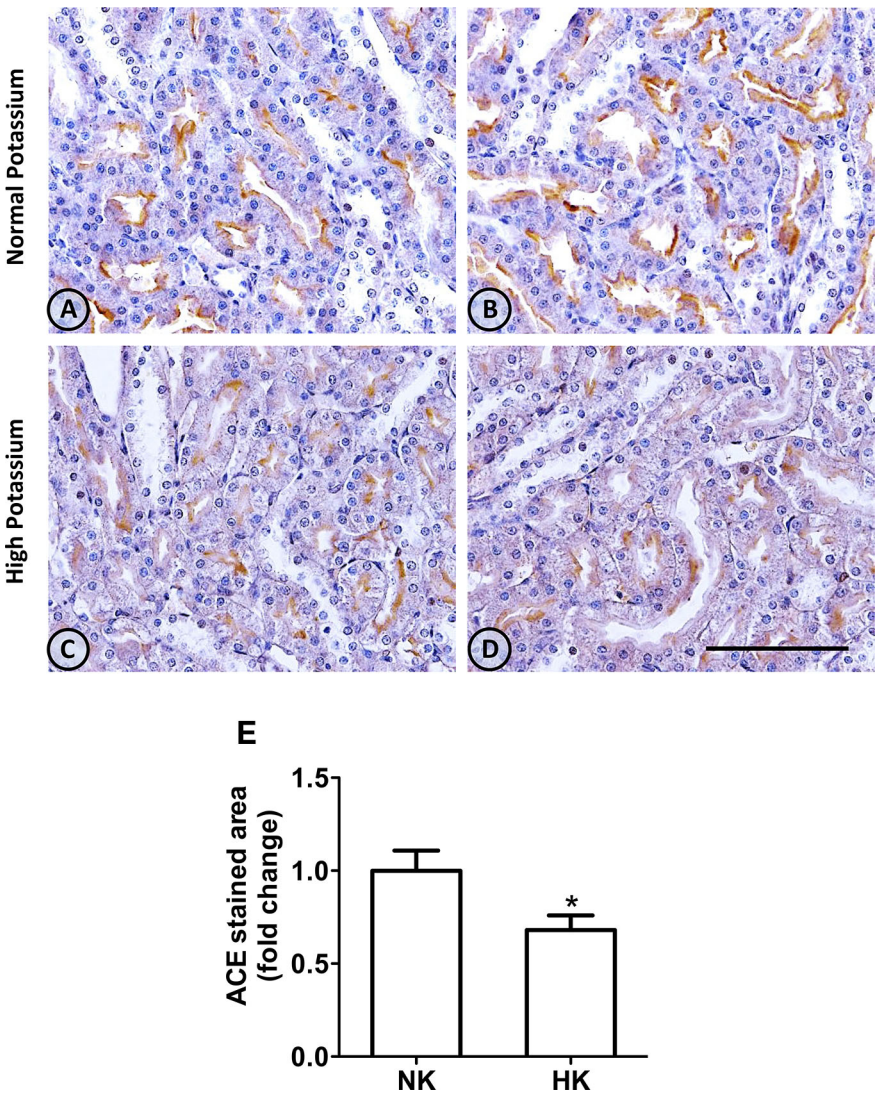

FIGURE 1 | ACE immunolocalization in normal (NK) and high potassium (HK) diet. **(A, B)** Light micrographs of kidneys from different rats on normal potassium diet group. ACE immunoperoxidase signal is restricted to the apical domain of proximal straight tubules. **(C, D)** Light micrographs from kidneys of rats on the high potassium diet show the reduction in ACE immunoperoxidase signal. **(E)** Morphometric analysis of the stained area in micrographs of kidneys of both groups. The high potassium diet decreased significantly the immunostained area compared to control diet (mean ± SEM; n = 11; *P < 0.05). Scale bar for all micrographs = 100 μm.

(**Figure 2A**). The densitometric analysis of bands (**Figure 2B**) showed that ACE protein abundance was significantly reduced in the HK group. Quantitative RT-PCR was used to determine if the high potassium diet induced changes of ACE at mRNA level. As shown in **Figure 3**, the ACE mRNA abundance is markedly reduced in the HK group. Therefore, the high potassium diet supplementation produced significant reductions in ACE mRNA and protein abundance, which could also be observed as a reduction in ACE immunoperoxidase signal in the proximal tubules.

Renin

The effect of HK diet on renin localization was investigated through immunohistochemistry. The renin immunoperoxidase signal was detected only in renal cortex. Specific localization of renin immunoperoxidase signal was restricted, in both groups, to juxtaglomerular cells located in the afferent arterioles (**Figure 4**). The HK diet reduced the number of juxtaglomerular cells positive for renin in the wall of afferent arterioles, as evidenced by the significant reduction in the renin stained areas showed in the morphometric analysis (**Figure 4E**). The HK diet did not modify the localization of the renin immunoperoxidase signal. Quantitative RT-PCR was performed to determine if the HK diet affected renin mRNA abundance. As shown in **Figure 5**, a significant reduction in renin mRNA abundance was found in the HK group. We performed Western blot analysis to determine if the HK diet affected renin protein abundance. However, our results did not

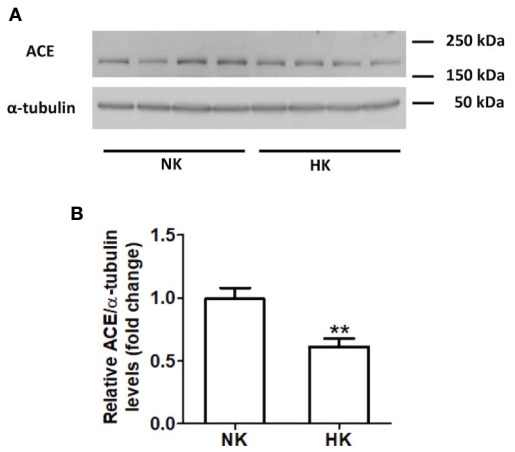

FIGURE 2 | ACE protein abundance in normal (NK) and high potassium diet (HK). **(A)** Immunoblot for ACE using total renal protein; **(B)** densitometric analysis of ACE immunoblot shows a significant reduction in ACE protein abundance in the high potassium diet group compared to control group (mean ± SEM; n = 11; **P < 0.01).

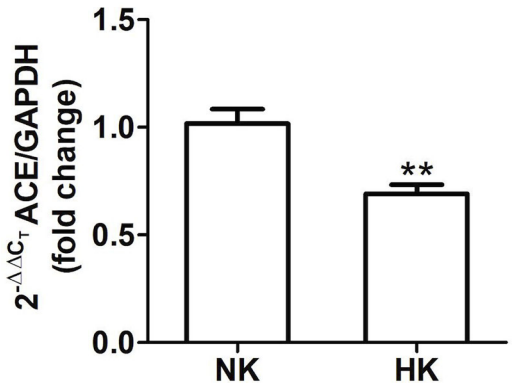

FIGURE 3 | Quantitative real time PCR for ACE mRNA in control (NK) and high potassium (HK) diet group. Potassium supplementation in the diet markedly reduces the mRNA abundance of ACE compared to the control group (mean ± SEM; n = 11; **P < 0.01).

clarify whether renin protein abundance was reduced by a high potassium diet. Therefore, our results show that a high potassium diet reduced renin mRNA level. This finding could explain the reduction of the renin immunoperoxidase signal observed in afferent arterioles of animals fed a HK diet.

Angiotensin Converting Enzyme 2

We also investigated the effect of HK diet on ACE homolog ACE2 at the protein and mRNA level. The effect of the chronically HK diet on ACE2 protein abundance was investigated through Western blot analysis (**Figures 6A, B**), showing that ACE2 protein abundance was markedly reduced. Quantitative RT-PCR also revealed a significant reduction in ACE2 mRNA abundance (**Figure 7**). In contrast with the results obtained with ACE and renin, no positive immunostaining for ACE2 was observed in renal structures, despite the use of several commercial antibodies.

DISCUSSION

There is a large body of evidence showing that potassium supplementation reduces blood pressure, but the mechanisms are still not fully understood. The main findings of the present study are that chronic potassium supplementation reduces the abundance of mRNA and protein of ACE and ACE2 and also reduces the number of renin-positive cells and its mRNA, with no signs of pathologic lesions in the kidney.

The experiment to demonstrate the effect of a high potassium diet was set for 4 weeks. During the first week the rat were fed with 2% potassium in chow plus 1% KCl in drinking water and increased to 2% KCl by the second week. Control rats received 0.91% potassium in chow and tap water. Measurements of electrolyte urinary excretion as well as plasma Na^+ and K^+ were done in the last day of the treatment. Therefore, during the 4-week period, the kidneys of the HK group undergone potassium adaptation. This phenomenon allowed a higher urinary potassium excretion to compensate a higher potassium ingestion and the maintenance of potassium balance. Physiological and morphometric studies carried out in control and potassium loaded rats for 4 weeks demonstrated that chronic renal potassium adaptation and high urinary potassium excretion is supported by increased potassium secretion and basolateral membrane area in connecting and principal cells of the distal nephron (Stanton et al., 1981). Although not evaluated directly, we can assume that our HK group is in steady state in relation to potassium since an increased ingestion was accompanied with an increased urinary excretion.

As previously stated, all measurements were carried out under steady state rather than acute conditions. The high potassium diet produced an increase in natriuresis and potassium urinary excretion. These results are consistent with other chronic experiment, where rats were fed for 8 days with a high potassium diet and K^+-induced natriuresis was also doubled (van der Lubbe et al., 2013). Potassium-induced natriuresis was also demonstrated in acute experiments. In mice receiving an oral KCl load through a gastric gavage, K^+-induced natriuresis increased 30–60 min after the administration (Sørensen et al., 2013).

The functioning of the high potassium diet induced natriuresis depends on coordinated action of several mechanisms. The increase in dietary K^+ produces a small increase in plasma K^+ concentration that is sensed by Kir 4.1/5.1 potassium channel at the basolateral membrane (Su et al., 2019; Wu et al., 2019). The potassium channel inhibition closes a basolateral chloride channel. The increase in intracellular chloride concentration inhibits the WNK/SPAK/OSRI signal cascade and the activation of apical NCC (Terker et al., 2015).

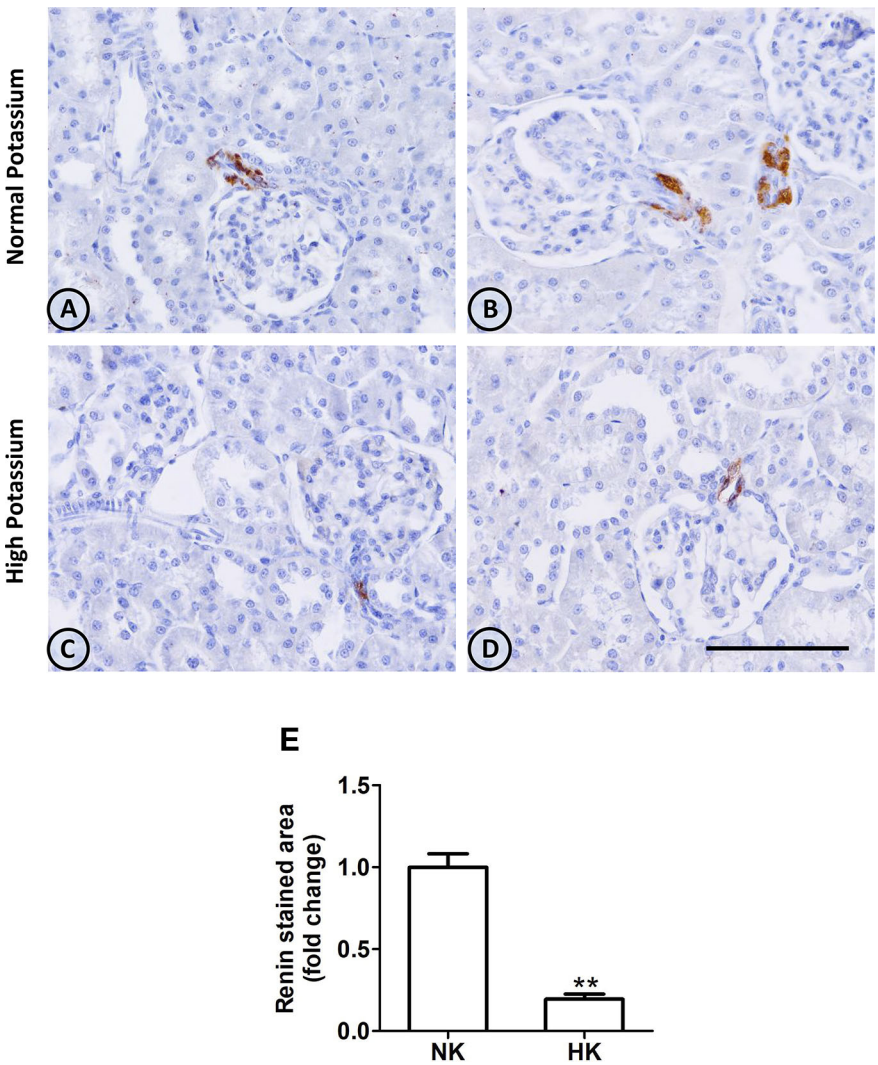

FIGURE 4 | Renin immunolocalization in control (NK) and high potassium (HK) diet. **(A, B)** Light micrographs of two different normal kidneys showing renin immunoperoxidase signal only in afferent arterioles. **(C, D)** Images from different kidneys of rats in a high potassium diet. Renin immunolocalization is conserved, but the number of positive immunostained cells is reduced. **(E)** Morphometric analysis of the immunostained area for renin shows a marked decrease in the high potassium diet group (mean ± SEM; n = 11; **P < 0.01). Scale bar for all micrographs = 100 μm.

This latter inhibition increases NaCl delivery to the connecting and cortical collecting tubule.

It has been stated that that the preceding mechanism is not enough to enhance K^+ secretion in connecting cells and principal cells. Kir 4.1 is expressed in the basolateral membrane of connecting and principal cells (Sørensen et al., 2019). An increase in plasma K^+ inhibits the channel and increases intracellular K^+ concentration. Recently it was demonstrated that cell K^+ activates mTORC2, which in turn phosphorylates SGK1. Activated SGK1 inhibits ENaC retrieval from apical membrane, this increasing the driving force for K^+ secretion. This novel local mechanism stimulates K^+ secretion necessary to maintain K^+ homeostasis in the presence of a high dietary potassium.

Angiotensin-I converting enzyme plays a key role in intrarenal vasoactive peptide systems. The enzyme transforms angiotensin I into angiotensin II inducing vasoconstriction and also inactivates bradykinin, a vasodilator peptide (Li et al., 2018). In our experiments, ACE immunolocalization was mainly present in the brush border of epithelial cells of proximal straight tubules although ACE had been localized also in mesangial cells and collecting duct (Redublo Quinto et al., 2007). In our experiments, chronic potassium supplementation did not modify the subcellular localization of the enzyme but ACE immunostaining and protein abundance were reduced. The reduction in protein abundance was also accompanied by a decrease in ACE mRNA levels. Therefore, the potassium supplementation reduced both ACE mRNA and protein

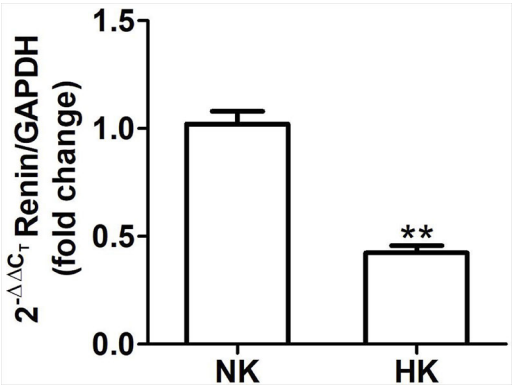

FIGURE 5 | Renin mRNA abundance in control (NK) and high potassium (HK) diet. Renin mRNA abundance is reduced in rats with chronic high potassium diet compared to control rats (mean ± SEM; n = 11; **P < 0.01).

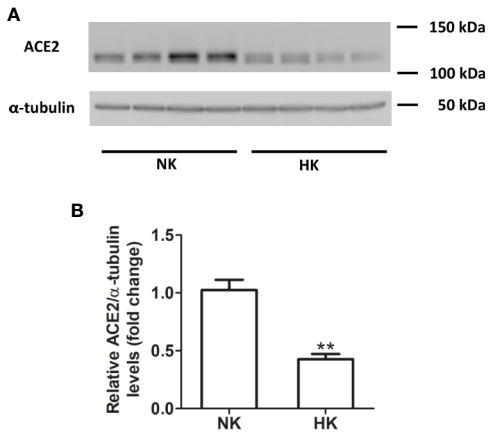

FIGURE 6 | ACE2 protein abundance in normal (NK) and high potassium diet (HK) **(A)**: ACE2 immunoblot using total renal proteins of control (NK) and high potassium (HK) diet. **(B)**: Densitometry of bands show a significant decrease in ACE2 protein abundance in the HK group (mean ± SEM; n = 11; **P < 0.01).

abundance. As a consequence, there should be a reduction in the conversion rate of angiotensin I into its active peptide angiotensin II. This peptide is a very important stimulator of proximal tubule Na^+ reabsorption by enhancing apical NHE3 exchanger activity (Geibel et al., 1990). Thus, less formation of intratubular angiotensin II could explain the increased natriuresis induced by high potassium in addition to the described dephosphorylation of the renal sodium chloride cotransporter in response to oral potassium intake (Sørensen et al., 2013; Penton et al., 2015).

The mechanisms responsible for the decrease in ACE mRNA and protein are incompletely understood, but could be attributed to a decrease in the transcription rate, mRNA stability, or an increase in mRNA degradation. There is little information regarding ACE regulation. Studies carried out in human cardiac fibroblast showed that dexamethasone increased ACE abundance by transcriptional and post-transcriptional mechanisms (Barretto-Chaves et al., 2001). In endothelial cells, it was demonstrated that ACE expression is under the control of β-adrenergic stimulation. The effect was reproduced by Gs protein stimulation, adenylyl cyclase stimulation, cAMP analogs and was blocked by propranolol and PKA inhibitors (Xavier-Neto et al., 1999). Our results cannot elucidate if one of these mechanisms is operating under our experimental conditions. Further experiments need to be done in order to understand the mechanism behind ACE mRNA and protein reduction induced by high potassium diet.

In contrast to our observation of ACE reduction with a high potassium diet, low potassium diet increases ACE expression (Suga et al., 2001). Given the importance of ACE in the generation of angiotensin II (the main pro-hypertensive peptide), it seems logical that both low and high potassium regulate its abundance. It remains to be elucidated whether ACE reduction and overexpression share the same molecular mechanisms.

Juxtaglomerular cells are the source of cortical renin in the normal kidney (Castrop et al., 2010). In both normal and high potassium diet groups, renin immunolocalization was restricted to cells at the glomerular end of the afferent arterioles. However, in the high potassium group the number of renin positive cells in afferent arterioles was reduced. The morphometric analysis showed a reduction of the renin immunostaining in the afferent arterioles area in the high potassium group. In the same group, the reduction in renin immunoperoxidase signal was accompanied by a significant decrease in renin mRNA levels. The reduction in renin positive cells in immunohistochemistry studies and the reduction of mRNA abundance in high potassium group suggest a reduction in the renin protein abundance. It has been shown that a high salt diet decreases cortical renin and its abundance (Castrop et al., 2010). The reduction of renin found in the high potassium diet group could not be attributed to high sodium intake, since in both groups the amount of sodium in pellet was the same. We could not demonstrate, through Western blot, if the chronic high potassium diet affects renin protein abundance. Problems with Western blots to identify cortical renin seem a common technical issue and might explain the scarcity of published cortical renin Western blots in the literature.

Even though we did not measure plasma renin activity, the reduction of plasma renin activity has been demonstrated in acute and chronic potassium loading protocols. In an acute K^+-loading protocol carried out in dogs, Vander demonstrated a reduction of plasma renin activity in venous blood of dogs that received a KCl infusion through the renal artery (Vander, 1970). Chronic experiments carried out in rats that received a high potassium diet for 8 days, also showed a reduction in plasma renin activity (van der Lubbe et al., 2013). Therefore, either an acute or chronic potassium loading results in a reduction of plasma renin activity. Since renin can be filtered in the glomerular barrier (Li et al., 2018), a decrease in filtered renin implies a decrease in formation of angiotensin I from angiotensinogen, which can be secreted by

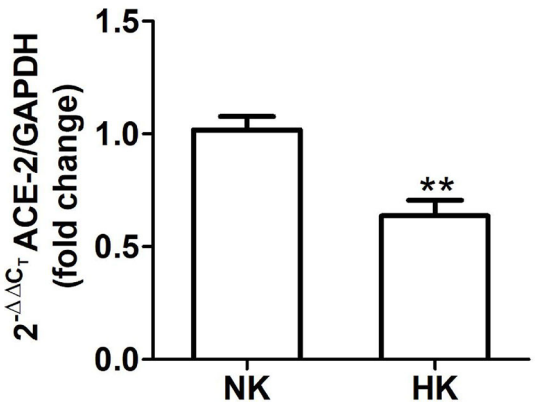

FIGURE 7 | ACE2 mRNA abundance in normal (NK) and high potassium (HK) diet. ACE2 mRNA abundance is reduced in the high potassium group (mean ± SEM; n = 11; **P < 0.01).

proximal straight tubules (Navar et al., 2011). Therefore, a reduction in the number of renin positive cells could be related to the observed reduction in plasma renin activity in animal models of potassium loading.

As stated above, the reduction in ACE and renin expression induced by high potassium diet could imply a reduced rate of intratubular angiotensin II formation, which in turn is a key stimulator of NHE3 exchanger in the proximal tubule brush border (Geibel et al., 1990). Since NHE3 mediates one third of proximal Na^+ reabsorption, a reduction in its activity or abundance might be one of the mechanisms involved in potassium-induced natriuresis. Experiments carried out in male and female mice submitted to a 7 day period of a high potassium diet showed a gender-independent significant reduction in NHE3 protein abundance in the high potassium group. This effect could not be explained by changes in NHE3 gene expression since no change was observed in the NHE3 mRNA abundance in high potassium and control group (Yang et al., 2018). The mechanism responsible for NHE3 protein down regulation in the high potassium group remains unknown.

The apical sodium chloride cotransporter (NCC) cotransporter of the distal tubule is another target of angiotensin II through a WNK4-SPAK dependent pathway. SPAK-dependent NCC phosphorylation increases cotransporter activity in the apical membrane (Gamba, 2012). Thus, a reduced formation of angiotensin II could account for the marked reduction in NCC phosphorylation that was reported in mice after an acute oral potassium load (Sørensen et al., 2013). In chronic potassium loading experiments, total NCC and phosphorylated NCC protein abundance were drastically reduced in the high potassium group (Yang et al., 2018). Therefore, the reported reduction of protein abundance of proximal tubule NHE3 and distal convoluted NCC could explain the increased natriuresis found in the high potassium group in our experiments.

As stated above, ACE also mediates bradykinin degradation to inactive peptides, therefore a reduction in ACE could lead to an increase of intrarenal bradykinin (Rhaleb et al., 2011). Furthermore, it is recognized that a high potassium diet increases kallikrein synthesis and secretion in the connecting cells (Vio and Figueroa, 1987). Thus, a high potassium diet generates a setting in which ACE is reduced and kallikrein is increased. Both conditions favor intrarenal bradykinin formation. Recent studies demonstrate that the activation of B2 bradykinin receptors in the distal tubule results in the inhibition of NCC and Kir4.1 mediated potassium conductance (Zhang et al., 2018). Taken together, the phenomenon of potassium-induced natriuresis could be explained not only by the reduction of the activity of the intratubular renin-angiotensin system but also by the upregulation of the kallikrein-kinin system.

ACE2 is an ACE homolog expressed in the kidney and many other organs (Soler et al., 2013; Santos et al., 2018). ACE2 mRNA expression was studied in microdissected nephron segments; the highest abundance was found in proximal straight tubule (Li et al., 2005). Western blot and immunohistochemical studies revealed that ACE2 protein has a wide tubular and vascular distribution in the renal tissue. However, the immunohistochemistry did not clarify the exact subcellular localization of ACE2 protein. Mass spectrometry studies carried out with isolated proximal straight tubules from rat kidney suggest that ACE2 converts angiotensin I to angiotensin 1-7 and angiotensin 1-9; the latter is converted to angiotensin 1-7 by ACE (Li et al., 2005).

In our study, ACE2 mRNA abundance was reduced in kidney from rats exposed to high potassium diet. Consistently, the same group exhibited a reduction in ACE2 protein abundance. Unfortunately, none of the several primary antibodies tested were useful to visualize the cellular localization and subcellular distribution of ACE2. Therefore, we could not demonstrate any possible effect of the chronic high potassium diet on ACE2 tissue distribution and subcellular localization. There are few studies with the localization of ACE2 in the kidney (proximal tubules and podocytes) and they are in mice kidneys (Ye et al., 2006), perhaps species differences could explain our lack of visualization of ACE2 in rat kidneys. The effect of the high potassium diet on ACE2 mRNA and protein abundance could imply a reduction in intrarenal angiotensin 1-7 formation. Since the proximal straight tubule has the highest ACE2 expression, it is possible that a high potassium diet could reduce angiotensin 1-7 formation in this tubular segment. It has been shown that intrarenal ACE2 expression and activity has beneficial effects that could be eliminated in the HK group due to the reduction of intrarenal ACE2. However, the histology of renal cortex of HK group is preserved compared to control group. On the other hand, studies of arterial pressure under the same diet protocol revealed that rats were normal (Gonzalez et al., 2019).

The effects of angiotensin 1-7 on tubular NaCl and water reabsorption are conflicting. Micropuncture studies carried out in rat kidney showed a lack of effect of physiological concentrations of intratubular angiotensin 1-7 on proximal tubule fluid reabsorption, loop of Henle and distal tubule (Vallon et al., 1997). In other study carried out in rat isolated microperfused proximal straight tubules, 1 pM angiotensin 1-7, added to the bath, stimulated fluid and bicarbonate reabsorption.

This stimulatory effect was reduced at higher concentration of the peptide in the bath (Garcia and Garvin, 1994). Since the effect of angiotensin 1-7 on tubular NaCl and water reabsorption in unclear, it is very difficult to envision a mechanism involving angiotensin 1-7 in the potassium induced natriuretic effect.

In summary, our experiments demonstrate that a chronic high potassium diet down regulates key components of intratubular renin-angiotensin system. This down regulation could be a novel mechanism involved in the potassium induced natriuresis that is beneficial for blood pressure and cardiovascular health. Further experiments should be carried out to determine the mechanisms that mediate the reduction in the expression of the intrarenal renin-angiotensin system.

DATA AVAILABILITY STATEMENT

The datasets generated for this study are available on request to the corresponding author.

ETHICS STATEMENT

The animal study was reviewed and approved by Comite Etico Cientifico of PontificiaUniversidad Catolica of Chile.

AUTHOR CONTRIBUTIONS

CV, DS, and CC designed the study. DS performed gene expression. JD-E performed protein expression. CC performed immunohistochemical studies. CC and NM were responsible for carrying experiment in animals. PG, DS, CC, and JD-E analyzed data and made the figures. PG and CV analyzed data, drafted and revised the paper. All authors contributed to the article and approved the submitted version.

FUNDING

This research was funded by Grants PIA CONICYT AFB170005 to CARE-UC and Fondecyt 11170245 to NM, and a donation of SQM to the Pontificia Universidad Catolica de Chile.

ACKNOWLEDGMENTS

The authors are grateful to Maria Alcoholado for the technical assistance in tissue sections. DS, JD-E, and NM were postdoctoral fellows from the Center CARE UC and CONICYT. The UC CINBIOT Animal Facility is funded by PIA CONICYT ECM-07.

REFERENCES

Aaron, K. J., and Sanders, P. W. (2013). Role of the dietary salt and potassium intake in cardiovascular health and disease: A review of evidence. *Mayo Clin. Proc.* 88, 987–995. doi: 10.1016/j.mayocp.2013.06.005

Agurto, N. J., Hanson, S., Gutierrez, H., Hooper, L., Elliot, P., and Cappucio, F. P. (2013). Effect of increased potassium intake on cardiovascular risk factors and disease: systematic review and meta-analyses. *BMJ* 346, f 1378. doi: 10.1136/bmj.f1378

Barretto-Chaves, M. L., Aneas, I., and Krieger, J. E. (2001). Glucocorticoid regulation of angiotensin-converting enzyme in primary culture of adult cardiac fibroblasts. *Am. J. Physiol. Regul. Integr. Comp. Physiol.* 280, R25–R32. doi: 10.1152/ajpregu.2001.280.1.R25

Blaustein, M. P., Kao, J. P., and Matteson, D. R. (2012). "Electrical consequences of ionic gradients," in *Cellular Physiology and Neurophysiology* (USA: Elsevier Philadelphia), 33–46.

Castrop, H., Höcherl, K., Kurtz, A., Schweda, F., Todorov, V., and Wagner, C. (2010). Physiology of kidney renin. *Physiol. Rev.* 90, 607–673. doi: 10.1152/physrev.00011.2009

Féraille, E., and Doucet, A. (2001). Sodium-potassium-adenosinetriphosphatase-dependent sodium transport in the kidney: hormonal control. *Physiol. Rev.* 81, 345–418. doi: 10.1152/physrev.2001.81.1.345

Gamba, G. (2012). Regulation of the renal Na^+-Cl^- cotransporter by phosphorylation and ubiquitylation. *Am. J. Physiol. Renal Physiol.* 303, F1573–F1583. doi: 10.1152/ajprenal.00508.2012

Garcia, N. H., and Garvin, J. L. (1994). Angiotensin 1-7 has a biphasic effect on fluid absorption in the proximal straight tubule. *J. Am. Soc Nephrol.* 5, 1133–1138.

Geibel, J., Giebisch, G., and Boron, W. F. (1990). Angiotensin II stimulates both Na (+)-H+ exchange and Na+/HCO3- cotransport in the rabbit proximal tubule. *Proc. Natl. Acad. Sci. U.S.A.* 87, 7917–7920. doi: 10.1073/pnas.87.20.7917

Giani, J. F., Bernstein, K. E., Janjulia, T., Han, J., Toblli, J. E., Shen, X. Z., et al. (2015). Salt sensitivity in response to renal injury requires renal angiotensin-converting enzyme. *Hypertension* 66, 534–542. doi: 10.1161/HYPERTENSIONAHA.115.05320

Gonzalez, A. A., Gallardo, M., Cespedes, C., and Vio, C. P. (2019). Potassium intake prevents the induction of the renin-angiotensin system and increases renal medullary ACE2 and COX-2 in the kidney of angiotensin II-dependent hypertensive rats. *Front. Pharmacol.* 10 1212. doi: 10.3389/fpharmacol.2019.01212. article 1212.

Gurley, S. B., Riquier-Brison, A. D. M., Schnermann, J., Sparks, M. A., Allen, A. M., Haase, V. H., et al. (2011). AT1A angiotensin receptors in the renal proximal tubule regulate blood pressure. *Cell. Metab.* 13, 469–475. doi: 10.1016/j.cmet.2011.03.001

Li, N., Zimpelmann, J., Cheng, K., Wilkins, J. A., and Burns, K. D. (2005). The role of angiotensin converting enzyme 2 in the generation of angiotensin 1-7 by rat proximal tubules. *Am. J. Physiol. Renal. Physiol.* 288, F353–F362. doi: 10.1152/ajprenal.00144.2004

Li, X. C., Zhu, D., Zheng, X., Zhang, J., and Zhuo, J. L. (2018). Intratubular and intracellular renin-angiotensin system in the kidney: a unifying perspective in blood pressure control. *Clin. Sci. (Lond.)* 132, 1383–1401. doi: 10.1042/CS20180121

Livak, K. J., and Schmittgen, T. D. (2001). Analysis of relative gene expression data using real-time quantitative PCR and the 2-ΔΔCT method. *Methods* 25, 402–408. doi: 10.1006/meth.2001.1262

McDonough, A. A., and Youn, J. H. (2017). Potassium homeostasis: the knowns, the unknowns, and the health benefits. *Physiol. (Bethesda)* 32, 100–111. doi: 10.1152/physiol.00022.2016

Mente, A., O'Donnell, M. J., Rangarajan, S., McQueen, M. J., Poirier, P., Wielgosz, A., et al. (2014). Association of urinary sodium and potassium excretion with blood pressure. *N. Engl. J. Med.* 371, 601–611. doi: 10.1016/S0140-6736(18)31376-X

Navar, L. G., Kobori, H., Prieto, M. C., and Gonzalez-Villalobos, R. A. (2011). Intratubular renin-angiotensin system in hypertension. *Hypertension* 57, 355–362. doi: 10.1161/HYPERTENSIONAHA.110.163519

Penton, D., Czogalla, J., and Loffing, J. (2015). Dietary potassium and the renal control of salt balance and blood pressure. *Pflugers Arch.* 467, 513–530. doi: 10.1007/s00424-014-1673-1

Redublo Quinto, M. B., Camargo, M. C., Ronchi, F., Santos, E., Alves, S., Shimuta, S., et al. (2007). Expression of angiotensin-converting enzymes and bradykinin

B2 receptors in mouse inner collecting duct cells. *Int. Immunopharmacol.* 8, 254–260. doi: 10.1016/j.intimp.2007.09.013

Rhaleb, N. E., Yang, X. P., and Carretero, O. A. (2011). The kallikrein-kinin system as a regulator of cardiovascular and renal function. *Compr. Physiol.* 1, 971–993. doi: 10.1002/cphy.c100053

Sørensen, M. V., Grossmann, S., Roensinger, M., Gresko, N., Todkar, A. P., Barmettler, G., et al. (2013). Rapid dephosphorylation of the renal sodium chloride cotransporter in response to oral potassium intake in mice. *Kidney Int.* 83, 811–824. doi: 10.1038/ki.2013.14

Sørensen, M. V., Saha, B., Jensen, I. S., Wu, P., Ayasse, N., Gleason, C. E., et al. (2019). Potassium acts through mTOR to regulate its own secretion. *JCI Insight* 5, pii: 126910. doi: 10.1172/jci.insight.126910

Santos, R. A. S., Sampaio, W. O., Alzamora, A. C., Motta-Santos, D., Alenina, N., Bader, M., et al. (2018). The ACE2/angiotensin-(1–7)/MAS axis of the renin-angiotensin system: focus on angiotensin-(1–7). *Physiol. Rev.* 98, 505–553. doi: 10.1152/physrev.00023.2016

Slotki, I. N., and Skorecki, K. L. (2016). "Disorders of sodium balance," in *The Kidney, Brenner and Rector"s* (USA: Elsevier Philadelphia), 390–459.

Soler, M. J., Wysocki, J., and Batlle, D. (2013). ACE2 alterations in kidney disease. *Nephrol. Dial Transpl.* 28, 2687–2697. doi: 10.1093/ndt/gft320

Stanton, B. A., Biemederfer, D., Wade, J. B., and Giebisch, G. H. (1981). Structural study of the rat distal nephron: effect of potassium adaptation and depletion. *Kidney Int.* 19, 36–48. doi: 10.1038/ki.1981.5

Su, X. T., Ellison, D. H., and Wang, W. H. (2019). Kir4.1/Kir5.1 in the DCT plays a role in the regulation of renal K^+ excretion. *Am. J. Physiol. Renal Physiol.* 316 (3), F582–F586. doi: 10.1152/ajprenal.00412.2018

Suga, S. I., Phillips, M. I., Ray, P. E., Raleigh, J. A., Vio, C. P., Kim, Y. G., et al. (2001). Hypokalemia induces renal injury and alterations in vasoactive mediators that favor salt sensitivity. *Am. J. Physiol. Renal Physiol.* 281, F620–F629. doi: 10.1152/ajprenal.2001.281.4.F620

Terker, A. S., Zhang, C., McCormick, J. A., Lazelle, R. A., Zhang, C., and Meermeier, N. P. (2015). Potassium modulates electrolyte balance and blood pressure through effects on distal cell voltage and chloride. *Cell Metab.* 21 (1), 39–50. doi: 10.1016/j.cmet.2014.12.006

Tobian, L. (1997). Dietary sodium chloride and potassium have effects on the pathophysiology of hypertension in humans and animals. *Am. J. Clin. Nutr.* 65, 606S–611S. doi: 10.1093/ajcn/65.2.606S

Touyz, R. M., and Schiffrin, E. L. (2000). Signal transduction mechanisms mediating the physiological and pathophysiological actions of angiotensin II in vascular smooth muscle cells. *Pharmacol. Rev.* 52, 639–672.

Vallon, V., Richter, K., Heyne, N., and Osswald, H. (1997). Effect of intratubular application of angiotensin 1-7 on nephron function. *Kidney Blood Press Res.* 20, 233–239. doi: 10.1159/000174151

van der Lubbe, N., Moes, A. D., Rosenbaeck, L. L., Schoep, S., Meima, M. E., Danser, A. H., et al. (2013). K+-induced natriuresis is preserved during Na+ depletion and accompanied by inhibition of the Na+-Cl- cotransporter. *Am. J. Physiol. Renal Physiol.* 305, F1177–F1188. doi: 10.1152/ajprenal.00201.2013

Vander, A. J. (1970). Direct effects of potassium on renin secretion and renal function. *Am. J. Physiol.* 219, 455–459. doi: 10.1152/ajplegacy.1970.219.2.455

Velez, J. C. (2009). The importance of the intrarenal renin-angiotensin system. *Nat. Clin. Pract. Nephrol.* 5, 89–100. doi: 10.1038/ncpneph1015

Vio, C. P., and Figueroa, C. D. (1987). Evidence for a stimulatory effect of high potassium diet on renal kallikrein. *Kidney Int.* 31, 1327–1334. doi: 10.1038/ki.1987.146

Vio, C. P., and Jeanneret, V. (2003). Local induction of angiotensin-converting enzyme in the kidney as a mechanism of progressive renal diseases. *Kidney Int.* 64, S57–S63. doi: 10.1046/j.1523-1755.64.s86.11.x

Vio, C. P., Quiroz-Munoz, M., Cuevas, C. A., Cespedes, C., and Ferreri, N. R. (2012). Prostaglandin E2 EP3 receptor regulates cyclooxygenase-2 expression in the kidney. *Am. J. Physiol. Renal Physiol.* 303, F449–F457. doi: 10.1152/ajprenal.00634.2011

Vio, C. P., Salas, D., Cespedes, C., Diaz-Elizondo, J., Mendez, N., Alcayaga, J., et al. (2018). Imbalance in renal vasoactive enzymes induced by mild hypoxia: angiotensin-converting enzyme increases while neutral endopeptidase decreases. *Front. Physiol.* 9, 1791. doi: 10.3389/fphys.2018.01791

Wu, P., Gao, Z. X., Su, X. T., Wang, M. X., Wang, W. H., and Lin, D. H. (2019). Kir4.1/Kir5.1 activity is essential for dietary sodium intake-induced modulation of Na-Cl cotransporter. *J. Am. Soc. Nephrol.* 30 (2), 216–227. doi: 10.1681/ASN.2018080799

Xavier-Neto, J., Pereira, A. C., Junqueira, M. L., Carmona, R., and Krieger, J. E. (1999). Rat angiotensin-converting enzyme promoter regulation by beta-adrenergics and cAMP in endothelium. *Hypertension* 34, 31–38. doi: 10.1161/01.HYP.34.1.31

Yang, L., Xu, S., Guo, X., Uchida, S., Weinstein, A. M., Wang, T., et al. (2018). Regulation of renal Na transporters in response to dietary K. *Am. J. Physiol. Renal Physiol.* 315, F1032–F1041. doi: 10.1152/ajprenal.00117.2018

Ye, M., Wysocki, J., William, J., Soler, M. J., Cokic, I., and Batlle, D. (2006). Glomerular localization and expression of angiotensin-converting enzyme 2 and angiotensin-converting enzyme: implications for albuminuria in diabetes. *J. Am. Soc Nephrol.* 17, 3067–3075. doi: 10.1681/ASN.2006050423

Zhang, D. D., Gao, Z. X., Vio, C. P., Xiao, Y., Wu, P., Zhang, H., et al. (2018). Bradykinin stimulates renal Na+ and K+ excretion by inhibiting the K+ channel (Kir 4.1) in the distal convoluted tubule. *Hypertension* 72, 361–369. doi: 10.1161/HYPERTENSIONAHA.118.11070

Conflict of Interest: The authors declare that the research was conducted in the absence of any commercial or financial relationships that could be construed as a potential conflict of interest.

frontiers in Pharmacology

BRIEF RESEARCH REPORT
published: 19 June 2020
doi: 10.3389/fphar.2020.00900

Altered Glutaminase 1 Activity During Neurulation and Its Potential Implications in Neural Tube Defects

*Camila Benavides-Rivas[1], Lina Mariana Tovar[1], Nicolás Zúñiga[1], Ingrid Pinto-Borguero[1], Claudio Retamal[1], Gonzalo E. Yévenes[2], Gustavo Moraga-Cid[2], Jorge Fuentealba[2], Leonardo Guzmán[2], Claudio Coddou[3], Luisa Bascuñán-Godoy[4] and Patricio A. Castro[1]**

[1] Laboratory of Physiology and Pharmacology for Neural Development, LAND, Departamento de Fisiología, Facultad de Ciencias Biológicas, Universidad de Concepción, Concepción, Chile, [2] Departamento de Fisiología, Facultad de Ciencias Biológicas, Universidad de Concepción, Concepción, Chile, [3] Departamento de Ciencias Biomédicas, Facultad de Medicina, Universidad Católica del Norte, Coquimbo, Chile, [4] Departamento de Botánica, Facultad de Ciencias Naturales y Oceanográficas, Universidad de Concepción, Concepción, Chile

OPEN ACCESS

Edited by:
Francisco Ciruela, University of Barcelona, Spain

Reviewed by:
José A. Campos-Sandoval, University of Malaga, Spain
Yunlong Huang, University of Nebraska Medical Center, United States

***Correspondence:**
Patricio A. Castro
pacastrom@gmail.com

Specialty section:
This article was submitted to Neuropharmacology, a section of the journal Frontiers in Pharmacology

Received: *29 November 2019*
Accepted: *02 June 2020*
Published: *19 June 2020*

Citation:
Benavides-Rivas C, Tovar LM, Zúñiga N, Pinto-Borguero I, Retamal C, Yévenes GE, Moraga-Cid G, Fuentealba J, Guzmán L, Coddou C, Bascuñán-Godoy L and Castro PA (2020) Altered Glutaminase 1 Activity During Neurulation and Its Potential Implications in Neural Tube Defects. Front. Pharmacol. 11:900. doi: 10.3389/fphar.2020.00900

The neurulation process is regulated by a large amount of genetic and environmental factors that determine the establishment, folding, and fusion of the neural plate to form the neural tube, which develops into the main structure of the central nervous system. A recently described factor involved in this process is glutamate. Through NMDA ionotropic receptor, glutamate modifies intracellular Ca^{2+} dynamics allowing the oriented cell migration and proliferation, essentials processes in neurulation. Glutamate synthesis depends on the mitochondrial enzyme known as glutaminase 1 (GLS1) that is widely expressed in brain and kidney. The participation of GLS 1 in prenatal neurogenic processes and in the adult brain has been experimentally established, however, its participation in early stages of embryonic development has not been described. The present investigation describes for the first time the presence and functionality of GLS1 in *Xenopus laevis* embryos during neurulation. Although protein expression levels remains constant, the catalytic activity of GLS1 increases significantly (~66%) between early (stage 12) and middle to late (stages 14–19) neurulation process. Additionally, the use of 6-diazo-5-oxo-L-norleucine (L-DON, competitive inhibitor of glutamine-depend enzymes), reduced significantly the GLS1 specific activity during neurulation (~36%) and induce the occurrence of neural tube defects involving its possible participation in the neural tube closure in *Xenopus laevis* embryos.

Keywords: neurulation, neural tube defects, glutamate, glutaminase 1, DON

INTRODUCTION

The neurulation process corresponds to a series of complex morphogenetic events which begin around the third week and extends until the fourth week of pregnancy in humans (Blom, 2009). During neurulation, the neural plate cells differentiate, fold, and fuse to form a tubular structure. This structure, called the neural tube, will eventually develop into the brain and spinal cord (Davidson and Keller, 1999; Copp and Greene, 2010; Nikolopoulou et al., 2017). Neurulation

disturbances prevent normal neural tube closure and cause neural tube defects (NTDs) (Stottmann et al., 2006; Wallingford et al., 2013). NTDs are one of the most common birth malformations in the human population with a prevalence of 1 per 1,000 births worldwide (Stottmann et al., 2006; Ybot-Gonzalez et al., 2007; Copp and Greene, 2010). Despite the clinical relevance of these diseases, their molecular and cellular causes remain poorly understood (Wallingford et al., 2013). Therefore, an understanding of the neurulation mechanism is essential to explain the embryonic pathogenesis of NTDs.

It is well described that Wnt ligand and Bone Morphogenic protein (BMP) regulates essential processes for neural tube closure, such as planar cell polarity (PCP), convergent extension and formation, apposition, and fusion of neural folds (Reichert et al., 2013; Nikolopoulou et al., 2017). A recent study showed that, in addition to these molecules glutamate also plays an important role in neural tube closure (Sequerra et al., 2018). Thus, the presence of glutamate in early stages of development has already been described (Root et al., 2008), as well as the presence of transcripts for proteins involved in neurotransmission such as the vesicular glutamate transporter (VGluT1), vesicle-associated membrane protein (VAMP1), syntaxin 1 (Stx1), and synaptosome-associated protein 25 (SNAP25) (Sequerra et al., 2018). In addition, different types of glutamate receptors have been found during the neural plate stage and early neurulation (Lujan et al., 2005; Root et al., 2008). Particularly, Sequerra et al. demonstrated that knocking down the expression of the GluN1 subunit from the NMDA receptor increases the number of mitotic neural plate cells and perturbs the lateral-medial migration. Taken together, this data suggests the existence of a glutamate-mediated signaling before synaptic communication. This pathway is capable of regulating neural plate cell proliferation and migration during neurulation (Sequerra et al., 2018).

In adult neural tissue, the main glutamate synthesis depends on the mitochondrial enzyme called glutaminase 1 (GLS1) encoded by the GLS1 gene and widely expressed in kidney and brain tissue (Masson et al., 2006; Li et al., 2016). In its inactive state, GLS1 exists as dimers and needs to be oligomerized to form tetramers or higher oligomers with catalytic activity (Li et al., 2016). The active tetramer deamidates glutamine and produces stoichiometric amounts of glutamate and ammonia (Stalnecker et al., 2017). Since it is activated by phosphate, it is commonly known as a phosphate-activated glutaminase (PAG) (Schousboe et al., 2013). The binding of inorganic phosphate is not only important for ensuring that the proper orientation of the catalytic residues occurs, but also ensures optimal product release (Li et al., 2016; Stalnecker et al., 2017).

In addition to its role in excitatory synapses, it has been shown that GLS1 participates in tumoral (Lukey et al., 2016) and endothelial tissue proliferation (Peyton et al., 2018). In the nervous system, GLS1 has also been reported to participate in migration, proliferation, and differentiation of neural stem progenitor cells (NPCs) in neurogenic areas from the adult brain (Wang et al., 2014). However, the role of GLS1 in early stages of neurulation remains unknown. Since GLS1 is the main pathway to synthesize glutamate and this neurotransmitter is expressed in early stages of development, we aimed to investigate the expression and function of GLS1 enzyme during neurulation. Using *Xenopus laevis* embryos, we demonstrate that GLS1 is present during neurulation and is able to transform glutamine to glutamate. We also show that GLS inhibition, using L-DON, a glutamine analog, could be related with alterations in normal neural tube closure and associated to neural tube defects.

MATERIALS AND METHODS

Xenopus laevis embryos

According Sive et al. (2007), embryos were generated by *in vitro* fertilization. Adult females from *Xenopus laevis* were injected once (pre-prime) with 50U of human chorionic gonadotropin hormone (hCG) 1–4 days before egg collection. Later, females were injected again (prime) with 300-400U of hCG 24 h before egg collection. Eggs collected were fertilized with a small piece of minced testis. This was considered time 0 of fertilization. Fertilized oocytes were kept in a 10% Marc's Modified Ringer's (MMR) saline solution containing (in mM): 10 NaCl, 0.2 KCl, 0.1 $MgSO_4$, 0.5 HEPES, 5 EDTA, and 0.2 $CaCl_2$. Dejellying of embryos was performed by briefly swirling fertilized eggs in 2% cysteine solution. After dejellying embryos were kept in 10% MMR solution (pH 8) and collected in stages of neurulation: stage 12.5 (early neurulation), stage 14 (middle neurulation) and stage 19 (late neurulation). Developmental stages were recorded according to Nieuwkoop and Faber (1994). Animals were handled according to the Institutional Animal Care and Use Committee guidelines and under an approved animal protocol using humane procedures.

RT-PCR Conventional and RT-qPCR Assay

Total RNA Extraction

Total mRNA extraction was performed using E.Z.N.A®HP total RNA kit according to manufacturer's instructions. *Xenopus laevis* embryos in neurulation stages and adult brain tissue were used in this assay. Samples (30 mg) (15 embryos) were homogenized in 700 µl of GTC lysis buffer. Centrifugation cycles were performed according the Kit's instructions. Samples were washed with 500 µl of ethanol (70% v/v) and centrifuged at 10,000 rpm during 5 min. Total RNA was suspended in 30 µl of RNase-Free water and quantified by absorbance at 260 nm (NanoQuant infinite 200 PRO, Tekan). RNA purity was measured according to 260/280 relation. Samples with a ratio inferior to 1.9 were discarded. The RNA Integrity was determined by visualization of 18S and 28S ribosomal subunits bands in a denaturing formaldehyde/agarose gel electrophoresis. RNA was stored at −80°C for further use.

Total RNA Reverse Transcription (RT)

DNA synthesis was performed using the reverse transcriptase M-MuLV Enzyme Mix from ProtoScript® II First Strand cDNA Synthesis Kit. In a final volume of 20 µl, 1 µg of total RNA was incubated with 0.5 µg of oligo-$(dT)_{15}$, denatured at 70°C during 5 min and placed on ice for 2 min. Later, 400U of M-MuLV

Enzyme Mix were added. The samples were incubated during 1 h at 42°C. Last incubation was carried out at 70°C during 5 min. Same transcription protocol was applied to negative controls, but no oligo-dT or M-MuLV Enzyme Mix was added.

cDNA Amplification by PCR

cDNA amplification was carried out in a BioRad thermocycler (Icycler) implementing the Biolabs PCR kit (New England BioLabs). A final volume of 25 µl was prepared using 1× of ThermoPol or Standard Taq Reaction Buffer, 0.2 mM from each dNTPs, a set of specific primers, 0.625 U of DNA Taq-polymerase (New England BioLabs) and 1 µl of RT product. The incubation program was 95°C for 5 min, followed by 35 cycles of 95°C for 30 s, 57°C for 30s, 72°C for 30s, and a final extension of 72°C for 5 min. The following specific primers were used: GLS1 forward 5′-GGAGGTGACCAGAGGGTGAA-3′ and reverse 5′-CTACGTGCAAGGCTGTACGA-3′; GeneBank accession no. XM_018239036.1. Primers were designed using Primer-Blast NCBI software (https://www.ncbi.nlm.nih.gov/tools/primer-blast/) to have melting temperature of 58–60°C and generate PCR products of 90–150 bp. The transcription factor Sub-1 was used as endogenous (housekeeping) gene (Mughai et al., 2018) in order to normalize experimental results (Bustin et al., 2009). This assay was performed four times using different batches of embryos samples. Every measure was made in duplicates o triplicates. Sequencing of PCR product was performed using the same primers mentioned before (**Supplementary Figure S3E**).

Agarose Gel Electrophoresis

DNA fragments were separated using agarose gels (1%). Agarose gels were prepared with electrophoresis buffer TAE (Tris-acetic acid EDTA; 40 mM Tris-HCl, 30 mM acetic acid, 1 mM EDTA; pH 7.6) and ethidium bromide at 0.5µg/ml (APEX). Molecular weight marker was 100 bp DNA ladder (GeneRuler, Thermo Scientific). To visualize DNA bands in agarose gel a transilluminator equipment was used.

RT-qPCR Assay

RT-qPCR reaction was prepared with Brilliant II SYBR Green qPCR Master Mix (Agilent Technologies, Santa Clara, CA, USA). A final volume of 20 µl was prepared with 2 µl of cDNA and 500nM of each primer set. Mx3000P thermocycler (Agilent Technologies, Inc.) was used with the following program: 5 min at 95°C; 40 cycles 95°C for 30s; 55°C during 30s, 72°C for 30s, and a final extension of 72°C during 5 min. After the PCR cycles, the purity of the PCR products was checked by analysis of the corresponding melting curve. Quantification was calculated comparing the number of cycles required to amplify each gene over the threshold cycle (Ct) in relation to the reference gene (Bustin et al., 2009). Mughai et al. (2018) evaluated several genes in developmental stages and they determined that sub-1 is the most appropriate control because its constant level of expression in this specific type of samples. After first quantification, the ΔΔCt was determined by normalization against stage 12.5. Experiments included four biological replicates (embryos from different batches) and three technical replicates for each biological replicate were performed. The following primer was used: Sub-1 forward 5′-AGCAGGAGAAATGAAGCCAGG-3′ reverse 5′-CCGACATCTGCTCCTTCAGT-3′ GeneBank accession no. XM_018235664.1; GLS1 primers used in this assay were the same as for RT-PCR.

Western Blot Assay

Total Protein Extract

Xenopus laevis embryos in neurulation stages and adult brain tissue were used in this assay. Total protein extracts were homogenized using protease inhibitor (ROCHE) and sonicated three times on ice at 300 W. Concentration of lysed protein was normalized using Bradford technique and Nanoquat equipment (M200, Infinite).

Polyacrylamide Gel Electrophoresis and Electrotransfer

Denaturing gel of acrylamide 12% (SDS-PAGE) were used to separate the protein of interest. Samples were incubated at 95°C during 5 min with loading buffer (62.5 mM Tris-HCl pH 6.8, 2% SDS, 10% glycerol, 0.01% bromophenol blue) and 100 mM DTT. Approximately, 125 µg of total protein were loaded on gel next to the protein standard (Spectra Multicolor, Broad Range Protein Ladder, Thermo Scientific), and run at 100 V in run solution (25 mM Tris, 250 mM glycine, and 0.1% SDS). Protein were transfer to Immobilon-P membrane (0.45 µm pore, Merck Millipore, Tullagreen, Carrigtwohill, Irlanda) with transfer solution (25 mM Tris, 192 mM glycine, 20% methanol) at 250 mM during 2 h.

Protein Immunodetection

Several washes with TBS-Tween (150 mM NaCl, 10 mM Tris, 0.05% Tween20) were performed. Membrane was blocked with 5% milk in TBS-Tween during 1 h. Overnight incubation at 4°C using primary antibodies was carried out. Primary antibodies: GLS (1:250, Novusbio), N-cadherin (1:1,000, SySy), and β-actin (1:300, SySy). Secondary antibody incubation was performed during 1 h using anti-mouse and anti-rabbitt peroxidase conjugated antibodies (1:1,000; Jackson ImmunoResearch Laboratories, Inc.). Membrane was washed with TBS-Tween for 10 min three times. Finally, membrane was revealed with chemiluminescent solution (Western Lightening Plus-ECL", Perkin Elmer) in the chemiluminescent and fluorescent equipment (Licor).

Mitochondrial Enrichment

To improve the yield of GLS1, a mitochondrial enrichment protocol (Frezza et al., 2007) was applied before enzyme activity measurement. Samples were homogenized using 400 µl of IBc buffer containing: 10 mM Tris-MOPS (0.1 M Tris using MOPS to adjust pH to 7.4), 1 mM EGTA/Tris (0.1 M EGTA using Tris to adjust pH to 7.4), 200 mM sucrose at pH 7.4, and then centrifuged at 600g for 10 min at 4°C. The supernatant was removed and samples were centrifuged again at 7,000g for 10 min at 4°C. The resultant pellet was suspended in 400 µl of IBc buffer and then centrifuged at 7,000g for 10 min at 4°C. Finally, each pellet was homogenized in a 40 µl homogenization buffer

(0.1 M EDTA-TRIS (0.1 M EDTA using Tris to adjust pH to 7.4) and 1 unit of protease inhibitor, Roche).

Enzymatic Activity Measurement

A two-step protocol was used to assay glutaminase activity (Botman et al., 2014; Lukey et al., 2016). In the first reaction, GLS1 transforms glutamine to glutamate, then in a second reaction, the enzyme glutamate dehydrogenase (GDH) catalyses the oxidative deamination of glutamate to form a-ketoglutarate and NADH. In general, one mole of glutamate produces the same amount of NADH, which can be measured through its absorbance at 340 nm at 25°C. For the first reaction assay, 35 µl from homogenized mitochondrial enrichment embryos samples [approximately ~40 µg of total protein (38.8 ± 2.8)] were added to 105 µl of reaction mixture 1 containing: 20 mM glutamine, 0.2 mM EDTA, 50 mM Tris-acetate at pH 8.6. Samples were rocked at 37°C for 45 min. The reaction was then quenched by adding 10 µl of 3 M HCl, and samples were placed on ice. Next, 45 µl of reaction mixture 1 was added to 200 µl of reaction mixture 2 containing 1 unit bovine liver GDH, 80 mM Tris-HCl, 200 mM hydrazine, 0.25 mM of ADP (adenosine diphosphate), 2 mM NAD (Nicotinamide adenine dinucleotide) at pH 9.4. Then, the changes in Absorbance associated with NADH production was measured at 340 nm at 25°C to final point (1 h). We used the endpoint register to calculate the amount of glutamate produced. The values of GLS activity are expressed as nmol of NADH production per min^{-1} per mg^{-1} total protein. Enzymatic activity assay without substrate glutamine (gln) and without the incubation period (45 min at 37°C) was used as blank to evaluate the basal level and glutamate formation independent of GLS *in vitro* activity. These value were substracted to the total activity and the contribution of these blanks to the total activity were always less than 20%

We determined the effect of competitive inhibitor 6-diazo-5-oxo-L-norleucine (also known as L-DON) over GLS1 obtained from *X. laevis*. After mitochondrial enrichment, embryo samples at stage 12.5 were incubated with different concentrations of L-DON (0, 1, and 5mM) during 40 min. A two-step protocol for enzymatic activity was then applied. Enzyme and reagents were acquired from Sigma-Aldrich.

Protein Quantification

Quantification of total protein obtained from *X. laevis* embryos and kidney samples was carried out using a Micro BCA™ kit following the manufacturer's instructions. A standard curve was also prepared by adding known amounts of Bovine serum albumin (BSA) (0, 2.5, 5, and 10 µg) to reaction mix. This allowed to determine the protein mass contained in *X. laevis* samples. The absorbance was measured at 560 nm at 37°C.

Pharmacological Assay

Embryos were incubated with L-DON at different concentrations (1 µM, 3 µM, 10 µM, 30 µM, 100 µM, 300 µM, and 1 mM) and 10% Marc's Modified Ringer's (MMR) saline solution was used as control. The incubation started at stage 12.5 (early neurulation) until stage 20. Afterward, embryos were removed from treatment and suspended in 10% MMR solution. The anterior-posterior measure of embryo length was performed at tadpole stage 45-50.

Data Analysis

Results are expressed as mean ± s.e.m. Statistical analyses were performed using one-way analysis of variance (ANOVA). $P < 0.05$ was considered statistically significant. All experiments were performed at least six times in duplicate for each trial. Embryos of both sexes were included in this study.

RESULTS

To examine the expression of GLS1 during neurulation, samples from *Xenopus laevis* were collected at different stages of development: early neurulation (stg 12.5), middle neurulation (stg 14), and late neurulation (stg 19–20). GLS1 expression was measured using conventional PCR, RT-qPCR and western blot assays. Our data showed the presence of transcripts for GLS1 at all neurulation stages (**Figure 1A**). The transcript quantification did not show significant differences between the neurulation stages (**Figure 1B**) (stg 12.5: 1.1 ± 0.2; stg 14: 0.8 ± 0.1; stg 19: 1.1 ± 0.04). To confirm protein expression using the western blot assay, we used β-actin, a cytoskeleton protein, as control, and N-cadherin, an adhesion protein preferentially expressed in neural tissue. The results revealed expression of GLS1 proteins during neurulation (**Figure 1C**), and similar to qPCR data, the protein level did not change significantly during the process (**Figure 1D**) (GLS1: stg 12.5: 1 ± 0.2, stg 14: 1.1 ± 0.1, stg 19: 1.2 ± 0.01; β-actin: stg 12.5: 1 ± 0.1, stg 14: 1 ± 0.1, stg 19: 1 ± 0.04 and N-cadherin: stg12.5: 1 ± 0.006, stg 14: 1.4 ± 0.1, stg 19: 2.2 ± 0.3). Taken together, these results demonstrate that GLS1 is expressed during neural tube formation.

To confirm that GLS1 is a catalytically active enzyme, embryos in neurulation stages were collected and evaluated using an enzymatic assay (see *Materials and Methods*). Again, whole embryos were used. Since GLS1 is widely expressed in kidney we used these samples from adult *X. laevis* as positive control. Our data revealed the presence of glutamate in all the samples analyzed, thereby demonstrating the functionality of GLS1. The activity values of neurulation samples oscillate in the activity range obtained from control groups Glu 0 mM and Glu 0.25 mM (See **Supplementary Figure S1A**).

These results show a significant increase in the activity of GLS1 from the samples at stage 14. This activity remained the same at stage 19, but in both cases was lower than GLS1 activity obtained from kidney samples (**Figure 1E**) (stg 12.5: 18.0 ± 2.1; stg 14: 29.9 ± 1.5; stg 19: 28.9 ± 2.7; and kidney: 39.2 ± 2.03). From these data, we concluded that GLS1 is able to synthesize glutamate from glutamine, and its activity increases during neurulation.

Finally, the effect of GLS inhibition on embryos phenotype was evaluated. Through *in vitro* assays, we first examined the efficacy of the competitive inhibitor 6-diazo-5-oxo-L-norleucine (L-DON) in *Xenopus laevis* embryos in early and late neurulation. After homogenization process, samples were

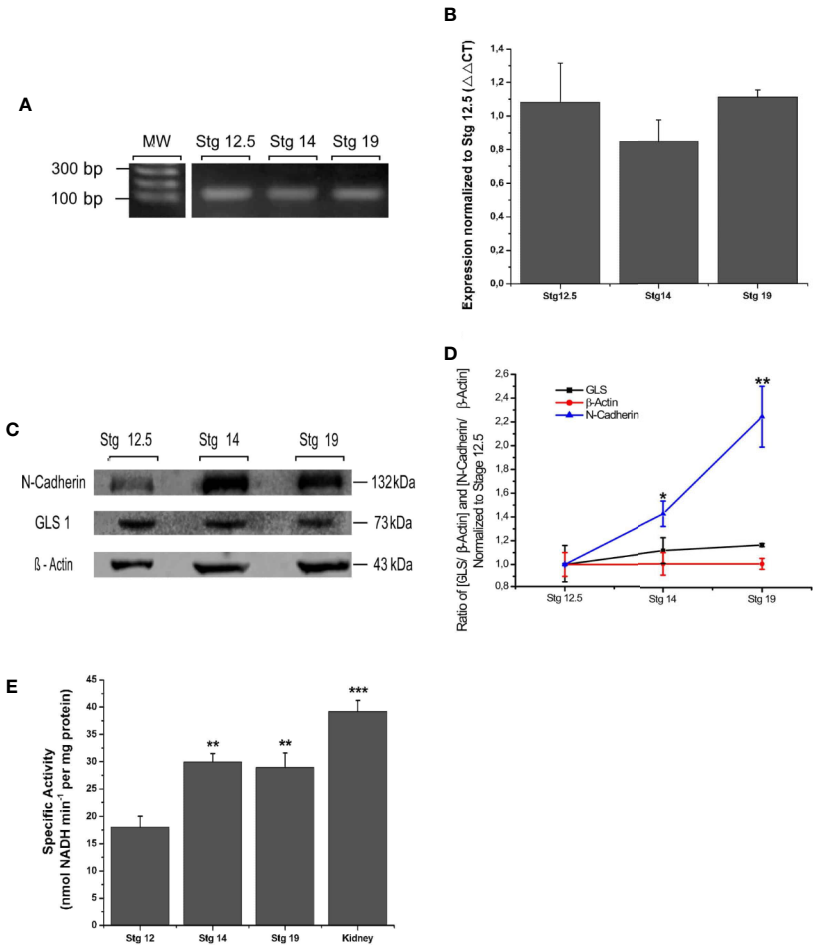

FIGURE 1 | Expression and functionality of GLS1 during neurulation. **(A)** PCR assay revealed the presence of GLS transcripts at all neurulation stages and also in the adult brain (n = 5). **(B)** Transcript quantification using the qPCR assay was normalized to early neurulation. The graph does not show significant differences between stages (n = 6). **(C)** Protein samples obtained from embryos at stg 12.5, stg 14, and stg 19 were analyzed using the western blot assay to determine GLS1 expression (1:250), using β-actin as a loading control (1:300) and N-cadherin (1:1,000) as a neural tissue positive control. The results revealed the presence of protein in all samples (n = 6). **(D)** Quantification of western blot results as ratio [GLS/β-actine] and [N-cadherin/β-actin] demonstrate that GLS1 levels are constant during neurulation. **(E)** GLS1 specific activity expressed as nmol NADH min^{-1} per protein mass (mg). The graph indicates that GLS1 activity increases in stg 14 and remains the same in stg 19, in both cases the activity is significantly lower than kidney, used as a positive control (n = 8). Results expressed as mean ± SEM, *p < 0.05; **p < 0.01; ***p < 0.001. PCR and WB original results were added to **Supplementary Figure S3**.

incubated with 0, 1, and 5 mM of DON during 40 min. The samples were later evaluated with the same enzymatic activity assay. The results showed that DON statistically inhibited GLS activity in embryos on early neurulation (**Figure 2A**) (stg 12.5: DON 0 mM: 18.4 ± 1.7, DON 1 mM: 11.7± 3.02, and DON 5 mM: 10.7 ± 2.1; stg 19: DON 0mM: 25.1 ± 2.6, DON 1 mM: 15.9 ± 2.9 and DON 5 mM: 13.7 ± 1.2). Later, pharmacological assays were carried out incubating embryos at stage 12 with increasing concentrations of DON and 10% MMR solution for controls until stage 20. The severity of NTDs was determined measuring the horizontal opening of the neural tube (**Figure 2B**). The dose-response curve analysis displayed an EC_{50} of 25 ± 15 μM. The maximal effect was obtained with concentrations of 1 mM of DON (0.18 mm opening) (**Figure 2C**). Subsequent analyses showed that DON also altered the anterior-posterior length of embryos at tadpole 45–50 stage (IC_{50} of 124 ± 35 μM) and the curvature of the tail (IC_{50} of 598 ± 221 μM) (**Supplementary Figure S2**).

DISCUSSION

Neurulation is a critical period in the vertebrate's development because it determines the establishment of the central nervous system (Christodoulou and Skourides, 2015). This process is the result of highly regulated interactions between growth factors, local gradient concentration, receptor expression, and the presence of morfogenetic neurotransmitters (Luk and Sadikot,

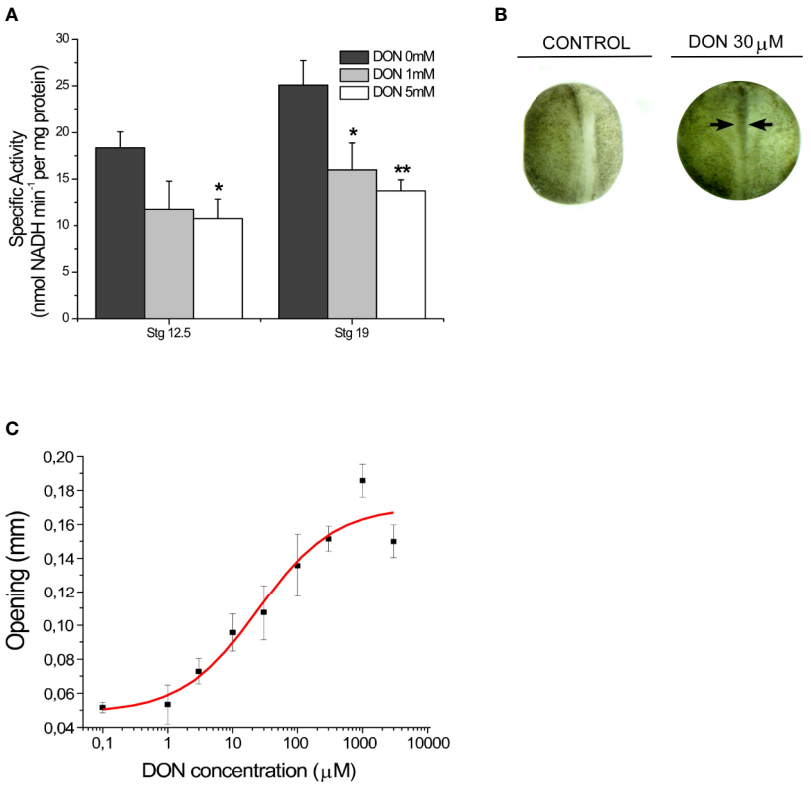

FIGURE 2 | GLS1 inhibition results in a NTDs phenotype in *Xenopus laevis* embryos. **(A)** Inhibition of enzymatic activity of GLS1 using DON in embryo samples at stage 12.5 and stage 19. GLS1 activity is significantly reduced with DON concentrations of 1 and 5 mM (n = 6). DON inhibition in kidney samples was also performed (**Supplementary Figure S1**). **(B)** Sample phenotypes obtained at stg 20 after DON incubation during neurulation, using 0 and 30 μM of DON. Controls were established using a 10% MMR saline solution. After incubation embryos were washed and placed in a 10% MMR saline solution. (n = 6) **(C)** NTDs severity was measured by examining the horizontal opening of the neural tube (black arrows from **B**) after incubation with different concentrations of DON (1 μM, 3 μM, 10 μM, 30 μM, 100 μM, 300 μM, 1 mM, 3 mM, and 10 mM). Controls were established using a 10% MMR saline solution. The maximal severity was obtained with 1mM of DON (0.18 mm opening) (n = 6; EC_{50} of 25 ± 15 μM). (Results expressed as mean ± SEM, *p < 0.05; **p < 0.01.

2004). Prenatal exposure to medications that modulate glutamatergic or GABAergic mechanisms, including sedatives, anticonvulsants, and anesthetics, have been associated with aberrations in the proliferation and development of the brain (Luk and Sadikot, 2004). Particularly, the study conducted by Sequerra et al. (2018) showed that glutamate-mediated signaling is essential for neural tube closure and alterations in this pathway result in NTDs in *Xenopus laevis* embryos. Here, we evaluated the presence and functionality of an important component in glutamate-mediated signaling: the GLS1 enzyme. This protein is widely expressed in brain tissue (Masson et al., 2006) and represents the main pathway to synthesize glutamate in neurons (Schousboe et al., 2013). In our experiments, we demonstrated the presence of mRNA and GLS1 protein during neurulation stages in *Xenopus laevis* embryos. However, GLS1 expression remained constant during neural tube closure. Later, the presence of glutamate in *Xenopus laevis* samples revealed the catalytic activity of GLS1. The enzymatic activity assay includes an incubation period which glutamine is transformed into glutamate. Samples without this incubation period produces lower concentration of glutamate. This suggests that the presence of glutamate in neurulation is related with the catalytic activity of GLS and not only come from TCA (tricarboxylic acid cycle) intermediaries. Even when protein expression remains constant during neurulation the catalytic activity of GLS increases significantly (~66%) during the process. Several molecules are able to increase GLS1 activity, one of the most important is inorganic phosphate. This allosteric activator allows the pairing of dimers to form an active tetramer, ensure the proper orientation of the catalytic residues and the optimal product release (Li et al., 2016). In addition to phosphate, ADP is also considered a GLS regulator increasing the affinity with substrate glutamine. This effect is enhanced by the presence of ATP (Massola and Ngubone, 2010).

How GLS1 participates in neurulation is still unclear. However, the most likely alternative is through the immediate product of catalytic activity: glutamate. On one hand, glutamate is transformed into α-ketoglutarate, a TCA intermediary, regulating energy metabolism and promoting cell proliferation, an essential event in neurulation (Lukey et al., 2016; Rumping et al., 2019). Moreover, it was recently discovered that glutamate plays an important role in neurulation, acting through NMDA

receptors (Sequerra et al., 2018). NMDA receptors are necessary for normal Ca^{+2} signaling and this ion regulates biomechanical processes and epithelial remodeling during neurulation. Ca^{+2} is also associated with proliferation and migration of neural plate cells (Sequerra et al., 2018) and apical constriction necessary for the elevation of neural folds (Christodoulou and Skourides, 2015; Suzuki et al., 2017). Therefore, GLS1 synthesizes glutamate that participates in neural tube closure.

The GLS loss of function seems to have profound consequences for both construction and maintenance of brain structures (Rumping et al., 2019). Furthermore, a study by Wang et al. (2014) demonstrated for the first time that GLS1 inhibition is detrimental for proliferation, differentiation, and survival of neural precursor cells, but there is no evidence of GLS1 inhibition in early stages of development. Here, we demonstrate that L-DON, a well-documented GLS1 inhibitor, reduce GLS1 specific activity and could participate in the alterations of the neural tube closure. L-DON is a non-selective glutamine analog a capable of interacting with other enzymes such as NAD-synthase, cytidine triphosphate (CTP)-synthetase, and some aminotransferases (Stalnecker et al., 2015; Xu et al., 2019). Consequently, these phenotypic results can be the summary of several inhibitions mediated by L-DON, including GLS1. Fortunately, the establishment of GLS1 as an oncogene (Zhang et al., 2019) has allowed the discovery of more specific inhibitors for the enzyme. It would be interesting to evaluate the effect of these new inhibitors during neurulation in further investigations. Here, we demonstrated that GLS1 is present in early stages of neural development as an active enzyme, but future investigations are needed to elucidate how GLS1 participates in neurulation and how alterations in its activity modify normal neural tube closure.

CONCLUSIONS

Our investigation describes for the first time the presence and functionality of GLS1 at early stages of neural development. Furthermore, pharmacological inhibition with L-DON prevents neural tube closure showing the possible participation of GLS1 in neurulation. Notwithstanding, further investigations using additional strategies will be necessary to understand the fine mechanism of action of this pathway.

DATA AVAILABILITY STATEMENT

The datasets generated for this study are available on request to the corresponding author.

ETHICS STATEMENT

The animal study was reviewed and approved by Universidad de Concepción.

AUTHOR CONTRIBUTIONS

CB-R, LT, NZ, IP-B, CR, and PC performed the research. JF, LG, LB-G, CC, GM-C, GY, and PC designed the research and contributed with analytical tools. CB-R, LT, NZ, IP-B, CR, and PC analyzed the data. CB-R and PC wrote the manuscript. All authors contributed to the article and approved the submitted versión.

FUNDING

This work was funded by FONDECYT 11160562 and VRID 220.033.112-4 (PAC). CB-R, LT, and NZ were supported by the Universidad de Concepción postgraduate fellowships (MSc Program in Biochemistry and Bioinformatics).

ACKNOWLEDGMENTS

The authors thank Susana Rojas, Jocelyn Gonzalez, Alejandra Ilabaca and Laurie Aguayo for their outstanding technical assistance.

SUPPLEMENTARY MATERIAL

The Supplementary Material for this article can be found online at: https://www.frontiersin.org/articles/10.3389/fphar.2020.00900/full#supplementary-material

SUPPLEMENTARY FIGURE S1 | (A) Temporal register of enzymatic activity assay. Absorbance was measured at 340nm (as NADH production) for embryo samples (stg 12.5, stg14 and stg 19) and kidney from adult X. laevis (n = 6). Controls were established with different amounts of glutamate (0 and 0.25 mM). The curve shows activity in all embryo samples and higher activity in adult kidney. **(B)** Specific GDH activity of glutamate controls 0 (0.9 ± 0.4) and 0.25 mM (42.9 ± 4.7). **(C)** Inhibition of enzymatic activity of GLS1 using DON in kidney tissue. GLS1 specific activity is significantly reduced with DON concentrations of 1 and 5 mM (n = 6) (0 mM: 37.8 ± 2.1; 1 mM: 23.4 ± 8.2; 5 mM: 21.5 ± 9.7).

SUPPLEMENTARY FIGURE S2 | GLS1 inhibition alters the phenotype of *Xenopus laevis* tadpoles. **(A)** Phenotypes obtained at tadpole stage after DON inhibition during neurulation using 3 μM, 30 μM, 300 μM and 3 mM DON concentration. **(B)** Higher concentrations of DON result in a shortening of tadpole length. The maximal effect was obtained with 1 mM of DON (IC_{50} of 124 ± 35 μM). **(C)** GLS inhibition also alters the tail curvature in a dose-response manner with a maximal effect obtained with 10 mM (IC_{50} of 598 ± 221 μM). (Results expressed as mean ± SEM; n = 6).

SUPPLEMENTARY FIGURE S3 | (A) PCR original results. Lane 1 corresponds to molecular weight; lanes 10, 11 and 12 correspond to transcripts from GLS1 obtained from embryo samples at stg 12.5, 14, 19, respectively. All samples were obtained from Xenopus laevis. Lanes 2 to 9 and 13 to 28 correspond to transcripts from other proteins irrelevant to this study. **(B)** Western blot original results for GLS1. Lane 1 corresponds to page ruler; lanes 2, 3 and 4 correspond to GLS1 protein obtained from embryos at stg 12.5, 14 and 19, respectively. **(C)** Western blot original results for β-actin. Lane 1 corresponds to page ruler; Lanes 2, 3 and 4 correspond to β-actin obtained from embryos at stg 12.5, 14 and 19. **(D)** Western blot original results for N-cadherin. Lanes 1 and 5 corresponds to page ruler; Lanes 2, 3 and 4 corresponds to N-cadherin obtained from embryos at stg 12.5, 14 and 19 respectively. **(E)** Chromatogram of Sanger sequencing. A region of PCR product sequence presents a 100% identity with GLS1 mRNA from *Xenopus laevis*. Results were obtained through local alignment of sequences (BLAST Pubmed and Xenbase).

REFERENCES

Avagliano, L., Massa, V., George, T., Qureshy, S., Bulfamante, G., and Finell, R. (2018). Overview on neural tube defects: From development to physical characteristics. *Birth Defects Res*. 111, 1455–1467. doi: 10.1002/bdr2.1380

Blom, H. (2009). Folic acid, methylation and neural tube closure in humans. *Birth Defects Res. A Clin. Mol. Teratol.* 85 (4), 295–302. doi: 10.1002/bdra.20581

Botman, D., Tigchelaar, W., and Van Noorden, V. (2014). Determination of phosphate-activated glutaminase activity and its kinetics in mouse tissues using metabolic mapping. *J. Histochem Cytochem.* 62 (11), 813–826. doi: 10.1369/0022155414551177

Bustin, S. A., Benes, V., Garson, J. A., Hellemans, J., Huggett, J., Kubista, M., et al. (2009). The MIQE guidelines: minimum information for publication of quantitative real-time PCR experiments. *Clin. Chem.* 55 (4), 611–622. doi: 10.1373/clinchem.2008.112797

Christodoulou, N., and Skourides, P. (2015). Cell-autonomous Ca2+ flashes elicit pulsed contractions of an apical actin network to drive apical constriction during neural tube closure. *Cell Reports.* 13 (10), 2189–2202. doi: 10.1016/j.celrep.2015.11.017

Copp, A., and Greene, N. (2010). Genetics and development of neural tube defects. *J. Pathol.* 220 (2), 217– 230. doi: 10.1002/path.2643

Davidson, L. A., and Keller, R. E. (1999). Neural tube closure in Xenopus laevis involves medial migration, directed protrusive activity, cell intercalation and convergent extension. *Development* 126 (20), 4547–4556.

Frezza, C., Cipolat, S., and Scorrano, L. (2007). Organelle isolation: functional mitochondria from mouse liver, muscle and cultured filroblasts. *Nat. Protoc.* 2 (2), 287–295. doi: 10.1038/nprot.2006.478

Li, Y., Erickson, J. W., Stalnecker, C. A., Katt, W. P., Huang, Q., Cerione, R., et al. (2016). Mechanistic basis of glutaminase activation: A key enzyme that promotes glutamine metabolism in cancer cells. *J. Bio Chem.* 291 (40), 20900–20910. doi: 10.1074/jbc.M116.72026

Lujan, R., Shigemoto, R., and Lopez-Bendito, G. (2005). Glutamate and GABA receptor signaling in the developing brain. *Neuroscience* 10 (3), 567–580. doi: 10.1016/j.neuroscience.2004.09.042

Luk, K., and Sadikot, A. (2004). Glutamate and regulation of proliferation in the developing mammalian telencephalon. *Dev. Neurosci.* 26 (2-4), 218–228. doi: 10.1159/000082139

Lukey, M., Greene, S., Erickson, J. W., Wilson, K., and Cerione, R. (2016). The oncogenic transcription factor c-Jun regulates glutaminase expression and sensitizes cells to glutaminase-targeted therapy. *Nat. Commun.* 18 (7), 1–14. doi: 10.1038/ncomms11321

Massola, B., and Ngubone, N. P. (2010). The activity of phosphate-dependent glutaminase from the rat small intestine. is modulated by ADP and is dependent on integrity of mitochondria. *Arch. Biochem. Biophys.* 504, 197–203. doi: 10.1016/j.abb.2010.09.002

Masson, J., Darmon, M., Conjard, A., Chuhma, N., Ropert, N., Thoby-Brisson, M., et al. (2006). Mice lacking brain/kidney phosphate-activated glutaminase have impaired glutamatergic synaptic transmission, altered breathing, disorganized goal-directed behavior and die shortly after Birth. *J. Neurosci.* 26 (17), 4660–4671. doi: 10.1523/JNEUROSCI.4241-05.2006

Mughai, B. B., Leemans, M., Spirhanzlova, P., Demeneix, B., and Fini, J. B. (2018). Reference gene identification and validation for quantitative real-time PCR studies in developing Xenopus laevis. *Sci. Rep.* 8 (1), 1–9. doi :10.1038/s41598-017-18684-1

Nieuwkoop, P. D., and Faber, J. (1994). *Normal table of Xenopus laevis (Daudin): A systematical and chronological survey of the development from the fertilized egg till the end of metamorphosis* (New York: Garland Pub.).

Nikolopoulou, E., Galea, G., Rolo, A., Greene, N., and Copp, A. (2017). Neural tube closure: cellular, molecular and biomechanical mechanisms. *Development* 144 (4), 552–566. doi: 10.1242/dev.145904

Peyton, K., Liu, X., Yu, Y., Yates, B., Behnammanesh, G., and Durante, W. (2018). Glutaminase-1 stimulates the proliferation, migration, and survival of human endothelial cells. *Biochem. Pharmacol.* 156, 204–214. doi: 10.1016/j.bcp.2018.08.032

Reichert, S., Randall, R., and Hill, C. (2013). A BMP regulatory network controls ectodermal cell fate decision at the neural plate border. *Development* 140 (21), 4435–4444. doi: 10.1242/dev.098707

Root, C., Velazquez-Ulloa, N., Monsalve, G., Minakova, E., and Spitzer, N. (2008). Embryonically expressed GABA and glutamate drive electrical activity regulating neurotransmitter specification. *J. Neurocis.* 28 (18), 4777–4784. doi: 10.1523/JNEUROSCI.4873-07.2008

Rumping, L., Buttner, B., Maier, O., Rehmann, H., Lequin, M., Schlump, J., et al. (2019). Identification of a loss-of-function mutation in the context of glutaminase deficiency and Neonatal Epileptic Encephalopathy. *JAMA Neurol.* 76 (3), 342–350. doi: 10.1001/jamaneurol.2018.2941

Schousboe, A., Bak, L., and Waagepetersen, H. (2013). Astrocytic control of biosynthesis and turnover of the neurotransmitters glutamate and GABA. *Front. Endocrinol. (Lausanne).* 15; 4, 102. doi: 10.3389/fendo.2013.00102

Sequerra, E., Goyal, R., Castro, P., Levi, J. B., and Borodinsky, L. N. (2018). NMDA receptor signaling is important for neural tube formation and for preventing antiepileptic drug-induced neural tube defects. *J. Neurosci.* 38 (20), 4762–4773. doi: 10.1523/JNEUROSCI.2634-17.2018

Sive, H. L., Grainer, R. M., and Harland, R. M. (2007). Inducing Ovulation in Xenopus laevis. *Cold Spring Harb Protoc.* 2007 (5), 1–157. doi: 10.1101/pdb.prot4734

Stalnecker, C., Ulrich, S., Lia, Y., Ramachandrana, S., McBrayer, M., DeBerardini, R., et al. (2015). Mechanism by which a recently discovered allosteric inhibitor blocks glutamine metabolism in transformed cells. *Proc. Natl. Acad. Sci. U S A.* 13112 (2), 394–399. doi: 10.1073/pnas.1414056112

Stalnecker, C. A., Erickson, J. W., and Cerione, R. A. (2017). Conformational changes in the activation loop of mitochondrial glutaminase C: A direct fluorescence readout that distinguishes the binding of allosteric inhibitors from activators. *J. Bio Chem.* 292 (15), 6095–6107. doi: 10.1074/jbc.M116.758219

Stottmann, R., Berrong, M., Matta, K., Choi, M., and Klingensmith, J. (2006). The BMP antagonist Noggin promotes cranial and spinal neurulation by distinct mechanism. *Dev. Biol.* 295 (2), 647–663. doi: 10.1016/j.ydbio.2006.03.051

Suzuki, M., Sato, M., Komaya, H., Hara, Y., Hayashi, K., Yasue, N., et al. (2017). Distinct intracellular Ca^{2+} dynamics regulate apical constriction and differentially contribute to neural tube closure. *Development* 144, 1307–1316. doi: 10.1242/dev.141952

Wallingford, J. B., Niswander, L. A., Shaw, G. M., and Finell, R. H. (2013). The continuing challenge of understanding, preventing, and treating neural tube defects. *Science* 339 (6123), 1222002. doi: 10.1126/science.1222002

Wang, Y., Huang, Y., Zhao, L., Li, Y., and Zheng, J. (2014). Glutaminase 1 Is essential for the differentiation, proliferation, and survival of human neural progenitor cells. *Stem Cells Dev.* 23 (22), 2782–2790. doi: 10.1089/scd.2014.0022

Xu, X., Meng, Y., Li, L., Xu, P., Wang, J., Li, Z., et al. (2019). Overview of the Development of Glutaminase Inhibitors: Achievements and Future Directions. *J. Med. Chem.* 2019 62 (3), 1096–1115. doi: 10.1021/acs.jmedchem.8b00961

Ybot-Gonzalez, P., Gaston-Masuet, C., Girdler, G., Klingensmith, J., Arkell, R., Greene, N., et al. (2007). Neural plate morphogenesis during mouse neurulation is regulated by antagonism of Bmp signaling. *Development* 134 (17), 3203–3211. doi: 10.1242/dev.008177

Zhang, J., Mao, S., Guo, Y., Wu, Y., Yao, X., and Huang, Y. (2019). Inhibition of GLS suppresses proliferation and promotes apoptosis in prostate cancer. *Biosci Rep.* 39 (6), BSR20181826. doi: 10.1042/BSR20181826

Conflict of Interest: The authors declare that the research was conducted in the absence of any commercial or financial relationships that could be construed as a potential conflict of interest.

Advantages of publishing in Frontiers

OPEN ACCESS
Articles are free to read for greatest visibility and readership

FAST PUBLICATION
Around 90 days from submission to decision

HIGH QUALITY PEER-REVIEW
Rigorous, collaborative, and constructive peer-review

TRANSPARENT PEER-REVIEW
Editors and reviewers acknowledged by name on published articles

Frontiers
Avenue du Tribunal-Fédéral 34
1005 Lausanne | Switzerland

Visit us: www.frontiersin.org
Contact us: info@frontiersin.org | +41 21 510 17 00

REPRODUCIBILITY OF RESEARCH
Support open data and methods to enhance research reproducibility

DIGITAL PUBLISHING
Articles designed for optimal readership across devices

FOLLOW US
@frontiersin

IMPACT METRICS
Advanced article metrics track visibility across digital media

EXTENSIVE PROMOTION
Marketing and promotion of impactful research

LOOP RESEARCH NETWORK
Our network increases your article's readership